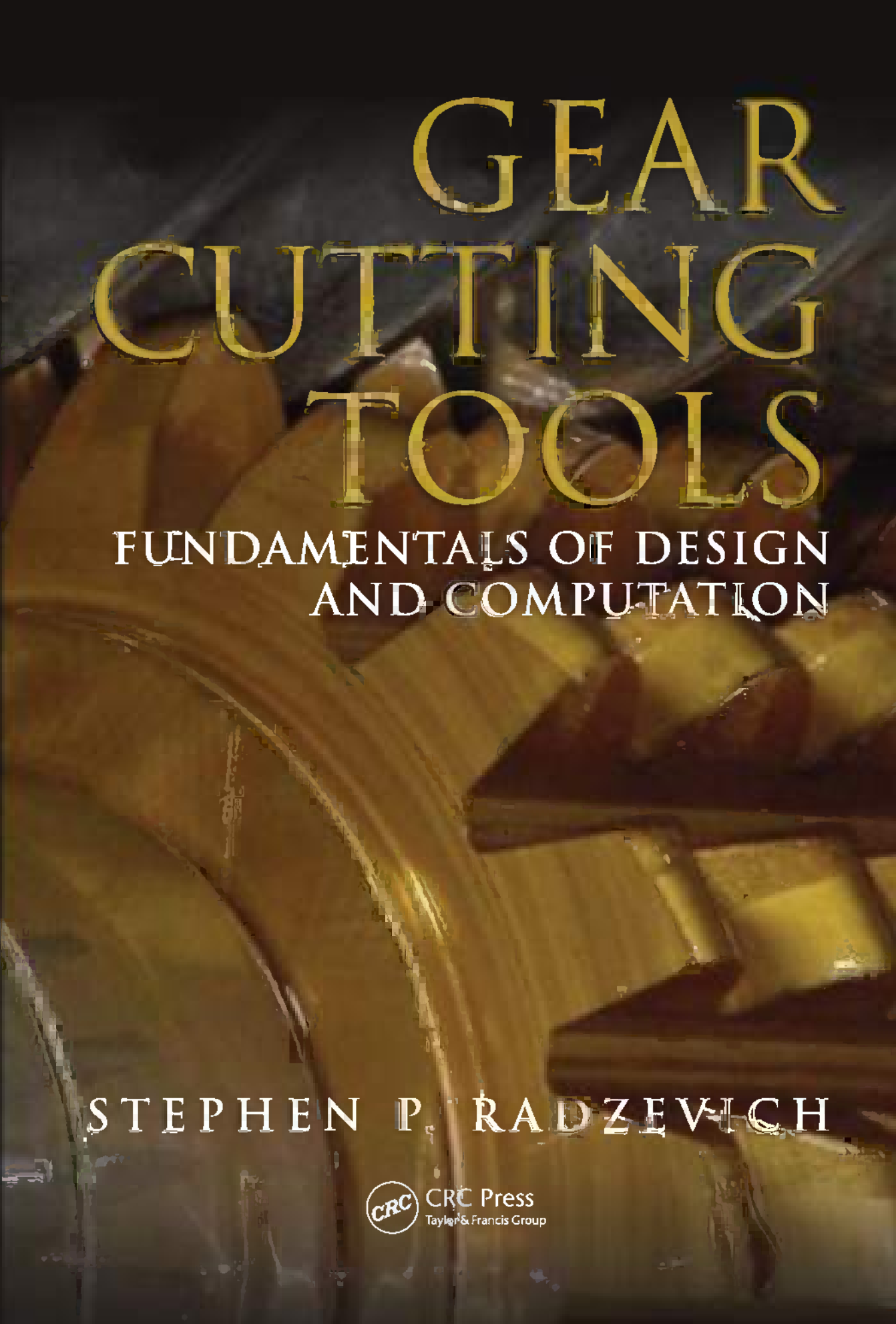
GEAR
CUTTING
TOOLS
FUNDAMENTALS OF DESIGN
AND COMPUTATION
STEPHEN P. RADZEVICH
CRC Press
Taylor & Francis Group

GEAR CUTTING TOOLS

FUNDAMENTALS OF DESIGN AND COMPUTATION

GEAR CUTTING TOOLS

FUNDAMENTALS OF DESIGN AND COMPUTATION

STEPHEN P. RADZEVICH

CRC Press
Taylor & Francis Group
Boca Raton London New York

CRC Press is an imprint of the
Taylor & Francis Group, an **informa** business

CRC Press
Taylor & Francis Group
6000 Broken Sound Parkway NW, Suite 300
Boca Raton, FL 33487-2742

© 2010 by Taylor and Francis Group, LLC
CRC Press is an imprint of Taylor & Francis Group, an Informa business

No claim to original U.S. Government works

Printed in the United States of America on acid-free paper
10 9 8 7 6 5 4 3 2 1

International Standard Book Number: 978-1-4398-1967-8 (Hardback)

This book contains information obtained from authentic and highly regarded sources. Reasonable efforts have been made to publish reliable data and information, but the author and publisher cannot assume responsibility for the validity of all materials or the consequences of their use. The authors and publishers have attempted to trace the copyright holders of all material reproduced in this publication and apologize to copyright holders if permission to publish in this form has not been obtained. If any copyright material has not been acknowledged please write and let us know so we may rectify in any future reprint.

Except as permitted under U.S. Copyright Law, no part of this book may be reprinted, reproduced, transmitted, or utilized in any form by any electronic, mechanical, or other means, now known or hereafter invented, including photocopying, microfilming, and recording, or in any information storage or retrieval system, without written permission from the publishers.

For permission to photocopy or use material electronically from this work, please access www.copyright.com (http://www.copyright.com/) or contact the Copyright Clearance Center, Inc. (CCC), 222 Rosewood Drive, Danvers, MA 01923, 978-750-8400. CCC is a not-for-profit organization that provides licenses and registration for a variety of users. For organizations that have been granted a photocopy license by the CCC, a separate system of payment has been arranged.

Trademark Notice: Product or corporate names may be trademarks or registered trademarks, and are used only for identification and explanation without intent to infringe.

Library of Congress Cataloging-in-Publication Data

Radzevich, S. P. (Stepan Pavlovich)
Gear cutting tools : fundamentals of design and computation / by Stephen P. Radzevich.
p. cm.
Includes bibliographical references and index.
ISBN 978-1-4398-1967-8
1. Gear-cutting machines. 2. Gearing--Design and construction. 3. Metal-cutting tools--Design and construction--Mathematical models. 4. Machinery, Kinematics of--Mathematical models. I. Title.

TJ187.R34 2010
621.9'44--dc22 2009031422

Visit the Taylor & Francis Web site at
http://www.taylorandfrancis.com

and the CRC Press Web site at
http://www.crcpress.com

This book is dedicated to my family.

Contents

Preface xix
Acknowledgments xxi
Introduction xxiii
Syntax xxxi

Section I Basics

1. Gears: Geometry of Tooth Flanks 3
1.1 Basic Types of Gears 3
1.2 Analytical Description of Gear Tooth Flanks 6
1.2.1 Tooth Flank of an Involute Spur Gear 9
1.2.2 Tooth Flank of an Involute Helical Gear 10
1.2.3 Tooth Flank of a Bevel Gear 14
1.2.4 Tooth Flank of a Helical Bevel Gear 15
1.3 Gear Tooth for Surfaces That Allow Sliding 16

2. Principal Kinematics of a Gear Machining Process 19
2.1 Relative Motions in Gear Machining 19
2.1.1 Elementary Relative Motions of the Work Gear and the Gear Cutting Tool 20
2.1.2 Feasible Relative Motions of the Work Gear and the Gear Cutting Tool 21
2.2. Rolling of the Conjugate Surfaces 23

3. Kinematics of Continuously Indexing Methods of Gear Machining Processes 25
3.1 Vector Representation of the Gear Machining Mesh 25
3.2 Kinematic Relationships for the Gear Machining Mesh 32
3.3 Configuration of the Vectors of Relative Motions 37
3.3.1 Principal Features of Configuration of the Rotation Vectors 37
3.3.2 Classification of Gear Machining Meshes 39
3.4 Kinematics of Gear Machining Processes 42

4. Elements of Coordinate Systems Transformations 43
4.1 Coordinate System Transformation 43
4.1.1 Introduction 43
4.1.2 Translations 44
4.1.3 Rotation about Coordinate Axis 46
4.1.4 Resultant Coordinate System Transformation 47
4.1.5 Screw Motion about a Coordinate Axis 48
4.1.6 Rolling Motion of a Coordinate System 50
4.1.7 Rolling of Two Coordinate Systems 52

4.2 Conversion of the Coordinate System Orientation 54
4.3 Direct Transformation of Surfaces Fundamental Forms 55

Section II Form Gear Cutting Tools

5. Gear Broaching Tools 59
5.1 Kinematics of the Gear Broaching Process 59
5.2 Generating Surface of a Gear Broach 60
5.3 Cutting Edges of the Gear Broaching Tools 61
5.3.1 Rake Surface of Finishing Teeth of a Gear Broach 61
5.3.2 Clearance Surface of Gear Broach Teeth 64
5.4 Chip Removal Diagrams 65
5.5 Sharpening of Gear Broaches 66
5.6 A Concept of Precision Gear Broaching Tool for Machining Involute Gears 70
5.7 Application of Gear Broaching Tools 72
5.7.1 Broaching Internal Gears 73
5.7.2 Broaching External Gears 73
5.8 Shear-Speed Cutting 74
5.8.1 Principle of Shear-Speed Cutting of Gears 74
5.8.2 Profiling of Form Tools for Shear-Speed Cutting of Gears 76
5.8.3 Application of Shear-Speed Cutting 79
5.9 Rotary Broaches: Slater Tools 80
5.10 Broaching Bevel Gear Teeth 81
5.10.1 Principle of the Revacycle Process of Cutting of Gear Teeth 82
5.10.2 Revacycle Cutting Tools 83
5.10.3 Profiling of a Cutter for Machining Bevel Gears Using the Revacycle Process 85
5.10.4 Application of the Revacycle Process of Cutting of Gear Teeth 90

6. End-Type Gear Milling Cutters 91
6.1 Kinematics of Gear Cutting with End-Type Milling Cutter 91
6.2 Generating Surface of the End-Type Gear Milling Cutter 92
6.2.1 Equation for the Generating Surface of an End-Type Milling Cutter for Machining Spur Involute Gears 92
6.2.2 Equation for the Generating Surface of an End-Type Milling Cutter for Machining Helical Involute Gears 96
6.2.3 Elements of Intrinsic Geometry of the Generating Surface of End-Type Milling Cutters 100
6.3 Cutting Edges of the End-Type Gear Milling Cutter 101
6.3.1 Rake Surface of the Milling Cutter for Machining of Involute Gears 101
6.3.2 Clearance Surface of the Milling Cutter for Machining of Involute Gears 105
6.3.3 Cutting Edge Geometry of the End-Type Milling Cutter 108
6.4 Accuracy of Machining of Gear Tooth Flanks with End-Type Milling Cutters 115

6.4.1 Cusps on Tooth Flanks of Spur Gear 115
6.4.2 Cusps on the Tooth Flanks of a Helical Gear 117
6.5 Application of Gear Milling Cutters 119

7. Disk-Type Gear Milling Cutters 123
7.1 Kinematics of Gear Cutting with Disk-Type Milling Cutter 123
7.2 Generating Surface of the Disk-Type Gear Milling Cutter 124
7.2.1 Equation for the Generating Surface of Disk-Type Milling Cutters for Machining Spur Involute Gears 125
7.2.2 Equation for the Generating Surface of the Disk-Type Milling Cutter for Machining Helical Involute Gears 127
7.2.3 Elements of the Intrinsic Geometry of the Generating Surface of Disk-Type Milling Cutters 130
7.3 Cutting Edges of the Disk-Type Gear Milling Cutter 132
7.3.1 Rake Surface of the Milling Cutter for Machining Involute Gears 132
7.3.2 Clearance Surface of the Milling Cutter for Machining Involute Gears 134
7.4 Profiling of the Disk-Type Gear Milling Cutters 136
7.4.1 Use of the Descriptive Geometry–Based Method of Profiling 136
7.4.2 Analytical Profiling of Disk-Type Gear Milling Cutters 138
7.5 Cutting Edge Geometry of the Disk-Type Milling Cutter 143
7.6 Disk-Type Milling Cutters for Roughing of Gears 147
7.7 Accuracy of Gear Tooth Flanks Machined with Disk-Type Milling Cutters 152
7.8 Application of Disk-Type Gear Milling Cutters 154

8. Nontraditional Methods of Gear Machining with Form Cutting Tools 163
8.1 Plurality of Single Parametric Motions 163
8.2 Implementation of the Single Parametric Motions for Designing of Form Gear Cutting Tool 166
8.2.1 End-Type Gear Milling Cutter 166
8.2.2 Disk-Type Gear Milling Cutter 167
8.2.3 Face Gear Milling Cutter 168
8.2.4 Internal Round Broach for Cutting Spur and Helical Gears 169
8.2.5 Internal Round Broach for Machining Straight Bevel Gears 170
8.3 Diversity of Form Tools for Machining a Given Gear 172
8.3.1 Machining of an Involute Worm on a Lathe 172
8.3.2 Milling of an Involute Worm 175
8.3.3 Thread Whirling 177
8.3.4 Grinding of an Involute Worm 178
8.4 Classification of Form Gear Tools 181

Section III Cutting Tools for Gear Generating: Parallel-Axis Gear Machining Mesh

9. Rack Cutters for Planing of Gears 187
9.1 Generating Surface of a Rack Cutter 187
9.2 On the Variety of Feasible Tooth Profiles of Rack Cutters 191

9.3 Cutting Edges of the Rack Cutter 193
9.3.1 Rake Surface of a Rack Cutter 194
9.3.2 Clearance Surface of a Rack Cutter 195
9.4 Profiling of Rack Cutters 196
9.4.1 Profiling of Rack Cutters Using *DG*-Based Methods 197
9.4.2 Analytical Profiling of Rack Cutters 198
9.5 Cutting Edge Geometry of the Rack Cutter 199
9.5.1 Computation of the Cutting Edge Geometry for Lateral Cutting Edges 200
9.5.2 Possible Improvements in the Geometry of Lateral Cutting Edges 203
9.6 Chip Thickness Cut by Cutting Edges of the Rack Cutter Tooth 207
9.7 Accuracy of the Machined Gear 212
9.7.1 Satisfaction of the Fifth Condition of Proper *PSG* 212
9.7.2 Satisfaction of the Sixth Condition of Proper *PSG* 215
9.8 Application of Rack Cutters 218
9.9 Potential Methods of Gear Cutting and Designs of Rack-Type Gear Cutting Tools 220

10. Gear Shaper Cutters I: External Gear Machining Mesh 223
10.1 Kinematics of Gear Shaping Operation 223
10.2 Generating Surface of a Gear Shaper Cutter 225
10.3 Cutting Edges of the Shaper Cutter 229
10.3.1 Rake Surface of a Shaper Cutter 229
10.3.2 Clearance Surface of a Shaper Cutter Tooth 232
10.4 Profiling of Gear Shaper Cutters 233
10.5 Critical Distance to the Nominal Cross Section of the Gear Shaper Cutter 236
10.6 Cutting Edge Geometry of a Gear Shaper Cutter Tooth 239
10.6.1 Angle of Inclination of the Lateral Cutting Edge 240
10.6.2 Rake Angle of the Lateral Cutting Edge 241
10.6.3 Clearance Angle of the Lateral Cutting Edge 243
10.6.4 Improvement in the Geometry of Lateral Cutting Edges 245
10.7 Desired Corrections to the Gear Shaper Cutter Tooth Profile 248
10.8 Thickness of Chip Cut by Gear Shaper Cutter Tooth 251
10.9 Accuracy of Gears Cut with the Gear Shaper Cutter 255
10.9.1 Satisfaction of the Fifth Condition of Proper *PSG* 255
10.9.2 Satisfaction of the Sixth Condition of Proper *PSG* 258
10.10 Application of Gear Shaper Cutters 260
10.10.1 Design of Shaper Cutters 261
10.10.2 Special Features of the Shaper Cutter Tooth Profile 263
10.10.3 Shaper Cutters for Machining of Helical and Herringbone Gears 264
10.10.4 Special Designs of Gear Shaper Cutters 265
10.10.5 Typical Gear Shaping Operations 273
10.10.6 Grinding of Shaper Cutters 274

11. Gear Shaper Cutters II: Internal Gear Machining Mesh 281
11.1 Kinematics of Shaping Operation of an Internal Gear 281
11.2 Design of Shaper Cutters 283
11.2.1 Generating Surface of Gear Shaper Cutters 283

11.2.2 Profiling of Gear Shaper Cutters 283
11.2.3 Cutting Edge Geometry of Gear Shaper Cutters 285
11.3 Thickness of Chip Cut by the Gear Shaper Cutter Tooth 286
11.4 Accuracy of Shaped Internal Gears 290
11.5 Enveloping Gear Shaper Cutters 293
11.6 Application of Gear Shaper Cutters 293

Section IV Cutting Tools for Gear Generating: Intersecting-Axis Gear Machining Mesh

12. Gear Shapers with a Tilted Axis of Rotation 301
12.1 Kinematics of Gear Shaper Operation with the Shaper Cutters Having a Tilted Axis of Rotation 301
12.2 Determination of the Generating Surface of a Gear Shaper Cutter Having a Tilted Axis of Rotation 304
12.3 Illustration of Capabilities of the External Intersecting-Axis Gear Machining Mesh 311
12.3.1 Shaping of Conical Involute Gears 311
12.3.2 Shaping of Face Gears 311

13. Gear Cutting Tools for Machining Bevel Gears 315
13.1 Principal Elements of the Kinematics of Bevel Gear Generation 315
13.2 Geometry of Interacting Tooth Surfaces 317
13.2.1 Principal Elements of the Geometry of the Involute Straight Bevel Gear Tooth Flank 318
13.2.2 Generating Surface of the Gear Cutting Tool 319
13.2.3 Geometry of Tooth Flanks of the Generated Gear 323
13.3 Peculiarities of Generation of Straight Bevel Gears with Offset Teeth 325
13.3.1 Generating Surface of the Gear Cutting Tool 326
13.3.2 Generating Surface of the Gear Cutting Tool 326
13.4 Generation of Straight Bevel Gear Teeth 328
13.4.1 Generation of the Plane T_a by Straight Motion of the Cutting Edge 328
13.4.2 Machining of Straight Bevel Gears 329
13.4.3 Gear Cutting Tools for Machining Straight Bevel Gears 330
13.5 Peculiarities of Straight Bevel Gear Cutting 333
13.6 Milling of Straight Bevel Gears 334
13.6.1 Peculiarities of the Gear Machining Operation 334
13.6.2 Design of Milling Cutters 335
13.6.3 Specific Features of the Shape of Finished Bevel Gear Flanks 336
13.7 Machining of Bevel Gears with Curved Teeth 337
13.7.1 Peculiarities of the Gear Machining Operation 338
13.7.2 Design of Cutters 340

14. Gear Shaper Cutters Having a Tilted Axis of Rotation: Internal Gear Machining Mesh 343
14.1 Principal Kinematics of Internal Gear Machining Mesh 343
14.2 Peculiarities of the Gear Cutting Tool Design 344

14.2.1 Shaping of Internal Gear 344
14.2.2 Shaping a Spur Gear with Enveloping Shaper Cutter 346
14.2.3 Shaping of External Recessed Tooth Forms with Enveloping Shaper Cutter 347

Section V Cutting Tools for Gear Generating: Spatial Gear Machining Mesh

Section V-A Design of Gear Cutting Tools: External Gear Machining Mesh

15. Generating Surface of the Gear Cutting Tool 353
15.1 Kinematics of External Spatial Gear Machining Mesh 353
15.2 Auxiliary Generating Surface of the Gear Cutting Tool 357
15.3 Examples of Possible Types of Auxiliary Generating Surfaces of Gear Cutting Tools 363
15.4 Generation of Generating Surface of a Gear Cutting Tool 363
15.4.1 Design Parameters of the Generating Surface of the Gear Cutting Tool 365
15.4.2 Equation of the Generating Surface of the Gear Cutting Tool 371
15.4.3 Setting Angle of the Gear Cutting Tool 374
15.4.4 Complementary Equations 376
15.5 Use of the *DG*-Based Methods for Determining the Design Parameters of the Generating Surfaces of the Gear Cutting Tools 378
15.5.1 Base Helix Angle $\psi_{b.c}$ of the Generating Surface of the Gear Cutting Tool 378
15.5.2 Base Diameter $d_{b.c}$ of the Generating Surface of the Gear Cutting Tool 380
15.6 Possible Types of Generating Surfaces of Gear Cutting Tools 381
15.6.1 Generating Surface of the Gear Cutting Tool with a Zero Profile Angle 381
15.6.2 Conical Generating Surface of the Gear Cutting Tool 383
15.6.3 Generating Surface of a Gear Cutting Tool with an Asymmetric Tooth Profile 389
15.6.4 Generating Surfaces of the Gear Cutting Tools Featuring Torus-Shaped Pitch Surfaces 390
15.7 Constraints on the Design Parameters of the Generating Surface of a Gear Cutting Tool 392

16. Hobs for Machining Gears 395
16.1 Transformation of the Generating Surface into a Workable Gear Cutting Tool 395
16.2 Geometry and Generation of Rake Surface of a Gear Hob 399
16.2.1 Geometry of the Rake Surface 399
16.2.2 Generation of the Rake Surface 403
16.2.2.1 Generation of a Rake Surface in the Form of a Plane 403
16.2.2.2 Generation of a Screw Rake Surface 405

16.2.2.3 Peculiarities of Generation of a Screw Rake Surface of a Multistart Hob 407
16.2.2.4 Methods for Generation of an Intermittent Rake Surface of the Special-Purpose Gear Hob 409
16.3 Geometry and Generation of Clearance Surfaces of Gear Hobs 411
16.3.1 Equation of the Desired Clearance Surface of the Hob Tooth 411
16.3.2 Generation of the Clearance Surface of the Hob Tooth 415
16.3.2.1 Cutting of the Relieved Clearance Surfaces of the Hob Teeth 415
16.3.2.2 Grinding of the Relieved Clearance Surfaces of the Hob Teeth 423
16.4 Accuracy of Hobs for Machining of Involute Gears 433
16.4.1 Preliminary Remarks 433
16.4.2 Accuracy of an Involute Gear Hob as a Function of Its Design Parameters 435
16.4.2.1 Analytical Description of the Desired Lateral Cutting Edge 436
16.4.2.2 Analytical Description of the Actual Lateral Cutting Edge 436
16.4.2.3 Machining Surface of an Involute Hob 437
16.4.2.4 Deviation of the Actual Machining Surface from the Desired Generating Surface of an Involute Hob 438
16.4.3 Impact of Pitch Diameter on the Accuracy of a Gear Hob 445
16.4.3.1 Peculiarities of the Relative Motion of the Work Gear and the Hob 446
16.4.3.2 Principal Design Parameters of an Involute Hob 449
16.4.3.3 Elements of Kinematic Geometry of an Involute Hob 454
16.5 Design of Gear Hobs 462
16.5.1 Design Parameters of a Gear Hob 462
16.5.2 Tooth Profile of the Gear Hob 465
16.5.3 Precision Involute Hobs with Straight Lateral Cutting Edges 468
16.5.3.1 Principal Design Parameters of the Precision Involute Hob 470
16.5.3.2 A Method for Resharpening the Precision Involute Hob 477
16.5.3.3 An Involute Hob for Machining Gear with a Modified Tooth Profile 481
16.5.4 Examples of Nonstandard Designs of Involute Hobs 487
16.5.4.1 Cylindrical Hobs of Nonstandard Design 487
16.5.4.2 Conical Gear Hobs 493
16.5.4.3 Toroidal Gear Hobs 497
16.6 The Cutting Edge Geometry of a Gear Hob Tooth 498
16.6.1 The Penetration Curve and the Machining Zone in a Gear Hobbing Operation 500
16.6.1.1 Parameters of the G/H_{pc} Penetration Curve 501
16.6.1.2 Partitioning of the Machining Zone 503
16.6.2 The Cutting Edge Geometry of a Hob Tooth in the Tool-in-Use Reference System 505
16.6.2.1 The Tool-in-Use Reference System in a Gear Hobbing Operation 505

16.6.2.2 Geometrical Parameters of the Hob Cutting Edge in the Tool-in-Use Reference System 508
16.6.2.3 The Possibility of Improving a Hob Design on the Premise of the Results of Investigating the Cutting Edge Geometry 514
16.7 Constraints on the Parameters of Modification of the Hob Tooth Profile 515
16.7.1 The Applied Reference Systems 516
16.7.2 Kinematics of the Elementary Gear Drive 517
16.7.3 Computation of the Maximum Allowed Value of the Modification of the Tooth Profile of an Involute Hob 518
16.7.4 Normalized Deviation Δ_m of the Tooth Profile of the Hobbed Gear 522
16.7.5 Peculiarities of Involute Hobs with Reduced Addendum 524
16.7.6 Illustrative Examples of the Computation 527
16.8 Application of Hobs for Machining Gears 528
16.8.1 Peculiarities of a Gear Hobbing Operation 528
16.8.2 Cycles of Gear Hobbing Operations 534
16.8.3 Minimum Hob Travel Distance 536
16.8.3.1 Hobbing Time as a Function of the Hob Total Travel Distance 536
16.8.3.2 Impact of the Hob's Idle Distance on the Minimal Neck Width of the Hobbed Cluster Gear 537
16.8.3.3 Selection of a Proper Value of the Setting Angle of the Hob 538
16.8.3.4 Computation of the Shortest Allowed Hob Idle Distance 540
16.8.3.5 Impact of Tolerance onto the Shortest Possible Hob Idle Distance 545
16.8.3.6 Computation of the Shortest Allowable Approach Distance of the Hob 552
16.8.3.7 Designing a Hob Featuring a Prescribed Value of the Setting Angle 555

17. Gear Shaving Cutters 559
17.1 Transforming the Generating Surface into a Workable Gear Shaving Cutter 559
17.1.1 Generating Surface of a Shaving Cutter 559
17.1.2 Rake Surface of the Cutting Teeth of a Shaving Cutter 560
17.1.3 Clearance Surface of the Cutting Teeth of a Shaving Cutter 562
17.1.4 Inclination Angle of the Cutting Edges of a Shaving Cutter 562
17.2 Design of the Gear Shaving Cutters 566
17.2.1 Design Parameters of a Shaving Cutter 567
17.2.2 Serrations on the Tooth Flanks of a Shaving Cutter 568
17.2.3 Resharpening of a Shaving Cutter 571
17.3 Axial Method of the Gear Shaving Process 576
17.3.1 Kinematics of the Axial Method of the Gear Shaving Process 576
17.3.2 Cutting Speed in the Axial Method of Rotary Shaving of the Gear 578
17.3.2.1 Impact of the Crossed-Axis Angle 578
17.3.2.2 Impact of the Traverse Motion 579

17.3.2.3 Impact of Profile Sliding 580
17.3.2.4 A Resultant Formula for Cutting Speed in Axial Gear Shaving 587
17.4 Diagonal Method of the Gear Shaving Process 587
17.4.1 Kinematics of the Diagonal Method of the Gear Shaving Process 588
17.4.2 Traverse Angle in Diagonal Method of the Rotary Shaving of a Gear 589
17.4.3 Cutting Speed in the Diagonal Method of the Rotary Shaving of a Gear 590
17.4.4 Optimization of the Kinematics in the Diagonal Method of the Rotary Shaving of a Gear 592
17.4.4.1 The Concept of the Optimization 592
17.4.4.2 Local Topology of the Contacting Tooth Flanks 595
17.4.4.3 Applied Coordinate Systems 596
17.4.4.4 Geometry of Contact of the Tooth Flanks $\mathcal{G}$ and T 598
17.4.4.5 Optimal Design Parameters of a Shaving Cutter and Optimal Parameters of the Kinematics of the Rotary Shaving Operation 602
17.5 Tangential Method of the Gear Shaving Process 603
17.5.1 Kinematics of the Tangential Method of the Gear Shaving Process 603
17.5.2 Cutting Speed in the Tangential Method of the Rotary Shaving of a Gear 604
17.5.3 Tangential Shaving of Shoulder Gear: Descriptive Geometry–Based Approach 605
17.5.3.1 Maximum Allowed Outer Diameter of a Shaving Cutter 606
17.5.3.2 Minimum Required Overlap of the Work Gear and the Shaving Cutter 608
17.5.3.3 Minimum Required Face Width of a Shaving Cutter 612
17.5.4 Tangential Shaving of Shoulder Gear: Analytical Approach 612
17.5.4.1 Optimal Design Parameters of a Shaving Cutter 612
17.5.4.2 Influence of the Overlap of a Shaving Cutter over the Work Gear onto the Accuracy of the Finished Tooth Flanks 615
17.6 Plunge Method of the Gear Shaving Process 619
17.6.1 Kinematics of the Plunge Method of the Gear Shaving Process 619
17.6.2 Cutting Speed in the Plunge Method of the Rotary Shaving of a Gear 620
17.6.3 Plunge Gear Shaving Process 620
17.6.4 Plunge Shaving of Topologically Modified Gears 621
17.6.4.1 Geometry of a Topologically Modified Gear Tooth Flank 621
17.6.4.2 Geometry of the Desired Topologically Modified Tooth Flank of a Shaving Cutter 624
17.6.4.3 Grinding a Topologically Modified Tooth Flank of the Shaving Cutter 625

17.6.5 Satisfaction of Conditions of Proper Part Surface Generation When Designing a Shaving Cutter for Plunge Shaving of Gears 628
17.6.5.1 Circular Mapping of Tooth Flanks of a Work Gear and the Shaving Cutter 629
17.6.5.2 Shaving Cutter of a Special Design for Plunge Shaving of Precision Gears 631
17.7 Advances in the Design of the Shaving Cutter 633
17.7.1 Elements of the Geometry of the Cutting Edges 633
17.7.2 Utilization of Features of the Generating Surface of a Shaving Cutter 636
17.8 Peculiarities of the Gear Shaving Process 638
17.8.1 Shaving Cutter Selection 639
17.8.2 Requirements for Preshaved Work Gear 639
17.8.3 Manufacturing Aspects of Gear Shaving Operation 640
17.8.4 Modification of Tooth Form and Shape 641
17.8.5 Shaving of Worm Gear 641

18. Examples of Implementation of the Classification of the Gear Machining Meshes 643
18.1 A Hob for Tangential Gear Hobbing 643
18.2 A Hob for Plunge Gear Hobbing 644
18.3 Hobbing of a Face Gear 645
18.4 A Worm-Type Gear Cutting Tool with a Continuous Helix-Spiral Cutting Edge 646
18.5 Cutting Tools for Scudding Gears 649
18.5.1 Essentials of the Gear Scudding Process 649
18.5.2 A Design Concept of a Precision Cutting Tool for the Gear Scudding Process 649
18.5.3 Applications of the Gear Scudding Process 651
18.6 A Shaper Cutter with a Tilted Axis of Rotation for Shaping Cylindrical Gears 651
18.6.1 The Kinematics of Shaping a Helical Gear with the Straight-Tooth Shaper Cutter 651
18.6.2 Principal Elements of Design of the Gear Cutting Tool 652
18.6.3 A Possible Application for the Gear Shaper Cutter with a Tilted Axis of Rotation 652
18.7 A Gear Cutting Tool for Machining a Worm in the Continuously Indexing Method 653
18.8 Rack Shaving Cutters 654
18.8.1 Rack-Type Shaving Cutter 655
18.8.2 Kinematics of the Rack Shaving Process 655
18.9 A Tool for Gear Reinforcement by Surface Plastic Deformation 657
18.10 Conical Hob for the Palloid Method of Gear Cutting 658
18.10.1 Preamble 659
18.10.2 Design of the Conical Hob 659
18.10.3 Kinematics of the Palloid Gear Hobbing Process 660
18.10.4 Peculiarities of Design of a Conical Hob for Machining a Work Gear with Crowned Teeth 662

Section V-B Design of Gear Cutting Tools: Quasi-Planar Gear Machining Mesh

19. Gear Cutting Tools for Machining of Bevel Gears 665
19.1 Design of a Gear Cutting Tool for the Plunge Method of Machining of Bevel Gears 665
19.1.1 Kinematics 665
19.1.2 Possible Designs of Tools for Machining Bevel Gears 667
19.2 Face Hob for Cutting Bevel Gear 668
19.3 More Possibilities for Designing Gear Cutting Tools Based on Quasi-Planar Gear Machining Meshes 669

Section V-C Design of Gear Cutting Tools: Internal Gear Machining Mesh

20. Gear Cutting Tools with an Enveloping Generating Surface 673
20.1 Gear Cutting Tools with a Cylindrical Generating Surface 673
20.1.1 Generating Surface of an Internal Cylindrical Gear Cutting Tool 673
20.1.2 Solution to the Inverse Problem of Part Surface Generation 674
20.1.3 Examples of Gear Cutting Tools with an Enveloping Cylindrical Generating Surface 676
20.2 Gear Cutting Tools with a Conical Generating Surface 679
20.2.1 Generating Surface of an Enveloping Conical Gear Cutting Tool 679
20.2.2 Examples of Gear Cutting Tools with an Enveloping Conical Generating Surface 680
20.3 Gear Cutting Tools with a Toroidal Generating Surface 681
20.3.1 Generating Surface of an Enveloping Toroidal Gear Cutting Tool 681
20.3.2 Examples of Gear Cutting Tools with an Enveloping Toroidal Generating Surface 684

21. Gear Cutting Tools for Machining Internal Gears 687
21.1 Principal Design Parameters of a Gear Cutting Tool for Machining an Internal Gear 687
21.1.1 Geometry of an Internal Gear 687
21.1.2 Kinematics of Machining an Internal Gear 687
21.1.3 Determination of the Generating Surface of a Gear Cutting Tool for Machining an Internal Gear 689
21.2 Examples of Gear Cutting Tools for Machining an Internal Gear 689

Conclusion 693

Appendix A: Engineering Formulae for the Specification of Gear Tooth 695

Appendix B: Conditions of Proper Part Surface Generation 699

Appendix C: Change of Surface Parameters 703

Appendix D: Cutting Edge Geometry: Definition of the Major Parameters 705

Notation 719

References 723

Index 733

Preface

Gear Cutting Tools: Fundamentals of Design and Computation is intended for mechanical engineers and manufacturing engineers who are interested in the scientific basis as well as the practical aspects of the advances in gear machining.

This book is neither a textbook nor a manual. It combines science and practice. The reader will find enough material to understand the geometry of gear cutting tools and the kinematics of a gear machining process.

This book deals with the science of surface generation. The investigation of surface generation process offers an excellent context and motivation for exploring the pervasive ties between *geometry* and *kinematics*.

The discussion in the book is based on the *DG/K*-based approach of surface generation, which is derived from the terms *differential geometry* (*DG*) and "*kinematics* (K) of multiparametric motion in Euclidean E_3 space." The *DG/K* approach was developed by the author and disclosed in more detail in some of his previous books ([125, 136, 138, 143, 153], etc.).

To the author's knowledge, this book represents the first attempt to disclose the details of designing optimal gear cutting tools based on the fundamental scientific theory. Most, but not all, important topics in the field of gear cutting tool design are covered in this book. However, this area of gear engineering is too broad, and there remains plenty of room for further improvements in this field.

Special-purpose gear cutting tools for machining noncircular gears are not considered in this monograph. However, the approach discussed in this work can be extended into the area of mechanical engineering as well.

Acknowledgments

I would like to share the credit for any research success with my numerous doctoral students with whom I have tested the proposed ideas and applied them in the industry. The contributions of many friends, colleagues, and students in overwhelming numbers cannot be acknowledged individually, and as much as our benefactors have contributed to this work, even their kindness and help must go unrecorded. Thanks are also due to a number of experts, whose suggestions have greatly improved portions of the book.

Introduction

"*Simplex sigillum veri.*" (Simplicity is the seal of truth.)

Latin proverb

This book deals with cutting tools used for machining of gears. Gears are produced in enormous amounts—billions of gears are produced every year. While the automotive industry ranks as the primary consumer of gears, numerous other industries also require huge amounts of gears: construction machinery, agricultural machinery, aerospace industry, to name a few.

The gear cutting process is costly. Cost of the gear cutting tools exceeds 50% of the total cost of the gear machining operation. If we place cost savings in the production of every gear in the range of just 10 cents, the total cost savings could reach hundreds of millions of dollars. This constitutes an appealing incentive for engineers and scientists to turn their attention to the gear machining process and the design of gear cutting tools used in the machining of gears.

In writing this book, the author has tried to expand the theory and fill various gaps.

The approach used in the text is mainly analytical. However, geometric interpretations are given, and in places synthetic reasoning is also applied. Furthermore, the author has largely limited himself to the mathematics of algebraic geometry, vector and matrix algebra, and elementary calculus. Special mathematical methods are avoided even in the final chapters.

The use of powerful computers makes it reasonable not to derive equations in their final form (as they are often bulky), but just to outline the major steps with which a problem can be solved.

At this point, it is fitting to recall the old Chinese proverb: "The beginning of wisdom is to call things by their right names." Unfortunately, even among gear specialists there is some ambiguity in the terms used to describe gears and gear-related parameters. In this work, to the extent possible, we follow the conventional terminology. When necessary, definition of new terms is provided.

The development of the scientific classification of kinematic schemes of gear machining process, as well as illustration of the classification with practical designs of gear cutting tools and advanced methods of gear machining are the two reasons, among others, that highly motivated the author to write this text.

The development of the scientific classification of kinematic schemes of gear machining is among the major goals to be disclosed in the book. Identification of the proper place of all known gear cutting tool designs in the developed classification is another important goal of the book. Ultimately, identification of areas where there is plenty of room for further developments in the field of designing optimal gear cutting tools is the third major goal of the book. However, the primary aims of this book are not just limited to these goals.

Historical Background

This study surveys and assesses the considerable body of research on gears and gear machining processes that has accumulated to date. It is not the aim of the author, who has been actively involved in this field of research for more than 30 years, to develop all possible designs of gear cutting tools. That huge task is not within the scope of this text. However, the potential disclosure of all possible conceptual designs of gear cutting tools is another major goal of this book.

Uniqueness of this Publication

This book is unique for many reasons.

Most of the material used in this book is new and cannot be found elsewhere.

This is the first work in English dedicated solely to the optimal design of gear cutting tools. The treatment is rigorous and elegant, focusing on the mathematical development of the subject apart from any particular applications. This book is also unique in the sense that most of the material was developed by the author.

The discussion starts with the general concepts and problems, and then specializes gradually to more simple cases. The kinematics of the gear machining mesh is the key point for the proper understanding of the disclosed approach. Eventually it can be understood that by just playing with two rotation vectors one can develop a novel method of gear machining as well as a novel gear cutting tool design for this purpose (playing with two rotation vectors, $\boldsymbol{\omega}_g$ and $\boldsymbol{\omega}_c$, along with one or two additional vectors of prime motion, feed motion, etc).

Numerous examples and an extensive bibliography further enhance the usefulness of the book.

Because of its generality and lucid style, this classic work will be invaluable not only to specialists in gear cutting tool design but also to those working in general areas of mechanical/manufacturing engineering.

Intended Audience

Since a perusal of the table of contents may leave the reader wondering as to whether this volume was intended as a textbook, a research monograph, or a historical treatise, some explanatory remarks are perhaps in order. There was, in fact, no conscious intent to aim for any of these—but what has transpired seems to bear the fact it is a combination of all three. Gear experts working in various industries and in academia, as well as university students (senior graduate, graduate, and postgraduate students) are the intended audience of the book.

Organization of this Book

For the readers' convenience, the book is divided into five parts. Each part is composed of about five chapters. Part V, which is large enough, is subdivided into three sections, each of which relates to gear cutting tools designed on the basis of: (a) external gear machining mesh, (b) quasi-planar gear machining mesh, and (c) internal gear machining mesh.

The content of each chapter is briefly outlined below.

Section I. Basics

Fundamental issues of gear cutting tools are covered in this section of the book. The discussion encompasses types of gears to be machined, the analytical representation of the gear tooth flanks, types of relative motions of the work gear, and the gear cutting tool in the gear machining process. The section ends with a brief consideration of the linear transformations methods that are practical in designing gear cutting tools. This part of the book is composed of four chapters.

Chapter 1. The geometry of tooth flanks of common types of gears is discussed in this chapter. Along with numerous practical examples of gear designs, equations for the tooth flanks of spur, helical, straight bevel, and helical bevel gears are derived here. The derived equations illustrate the powerful method that can be used to derive an equation for the tooth flank of a gear of any given design. An analytical description of the desired gear tooth flank is a good starting point for the gear cutting tool designer.

Chapter 2. General aspects of the kinematics of gear machining processes are considered in Chapter 2. The analysis is focused mostly on two issues: (a) possible types of relative motions in the gear machining process, including, but not limited to, elementary relative motions of the work gear and the gear cutting tool, and (b) rolling of the conjugate surfaces over each other. In particular, the readers' attention is drawn to the practical applications of special types of motions under which a surface allows sliding over itself.

Chapter 3. This chapter focuses on the kinematics of special methods of gear machining processes. The methods are referred to as the *continuously indexing methods* of gear machining processes. Vector representation of the gear machining mesh and the kinematic relationships for the gear machining mesh are covered in this chapter. Based on the in-depth analysis of the principal features of configuration of the rotation vectors that specify the gear machining mesh, a scientific classification of types of gear machining meshes is developed. The classification is the key for the development of novel designs of gear cutting tools and new methods of machining gears. Major steps for transforming the kinematics of the gear machining mesh into the corresponding kinematics of the gear machining process are considered.

Chapter 4. Practical methods of the coordinate system transformation are discussed in Chapter 4. Translations and rotations of coordinate systems are considered as particular cases of linear transformations. This chapter illustrates how operators of resultant coordinate system transformations can be composed using the operators of elementary coordinate system transformations. In addition to conventional operations of coordinate system transformations, new operators of linear transformations are introduced: (a) operator of screw motion about a coordinate axis, (b) operator of rolling motion of a coordinate system, and (c) operator of rolling of two coordinate systems. Formulae for the conversion of coordinate system orientation as well as methods for direct transformation of surface fundamental forms are also covered in this chapter.

Section II. Form Gear Cutting Tools

Gear cutting tools featuring the generating surface that is congruent to tooth surfaces of the gear to be machined are discussed in this part of the book. The kinematics of the gear machining processes used for the purpose of form gear cutting tools is the simplest possible. However, simple kinematics of surface machining often entails cutting tools of very complex designs.

Chapter 5. Design of cutting tools for broaching gears is the subject of this chapter. The discussion begins with the analysis of the kinematics of the gear broaching process, and is followed by generation of the generating surface of the gear cutting tool, transformation of the generating surface into a workable gear cutting tool, cutting edge geometry, and by chip removal diagrams. Both analytical methods and *DG*-based methods of analysis are widely used in this chapter. Sharpening of gear broaches is an issue of particular consideration. The discussion of gear broaching tools ends with a detailed disclosure of the concept of precision gear broaching tools for machining involute gears and with application issues of gear broaching tools.

The concept of broaching is the cornerstone of other methods of gear cutting. These methods include, but not limited to, (a) Shear-Speed cutting of gears, (b) rotary broaching with slater tools, (c) Revacycle method of gear cutting, etc. The principles of gear cutting tool designs for these methods of gear machining are also covered in this chapter.

Chapter 6. Design methods of end-type milling cutters for machining spur and helical gears are discussed in this chapter. At the outset, the kinematics of the gear cutting process with end-type milling cutter is discussed. This is followed by an analytical description of the secondary generating surface of the end-type milling cutter, and by an investigation of the cutting edge geometry. The analysis makes it possible to compute the cutting wedge angles at any point of interest within the cutting edge. Accuracy of the milled gears is discussed from the perspective of the geometry of interacting surfaces and the kinematics of the gear cutting process. Application of the end-type milling cutters is considered at the end of the chapter.

Chapter 7. Disk-type milling cutters as well as their design and analysis are discussed in this chapter. Analysis of the kinematics of the gear milling operation allows for determining the secondary generating surface of the milling cutter. This is followed by an analytical description of the generating surfaces of milling cutters designed for machining spur and helical gears. Next, the intrinsic geometry of the generating surfaces of the milling cutters is investigated. Considered together, an equation of the secondary generating surface of the milling cutter, an equation of the rake surface, and an equation of the clearance surface of the milling cutter tooth allow for the analytical representation of the cutting edge of the cutting tool. Profiling of milling cutters is considered from the perspective of implementing both *DG*-based methods and analytical methods in profiling of form cutting tools. The cutting edge geometry of the disk-type milling cutter is analyzed using elements of vector algebra and calculus. The peculiarities of milling cutter designs for roughing of gears are considered. Accuracy issues are investigated from the perspective of satisfaction/violation of conditions of proper part surface generation. The chapter ends with a discussion of the principal features of the practical application of disk-type milling cutters for cutting spur and helical gears.

Chapter 8. Investigation of the kinematics of gear machining operations makes it possible to develop novel gear machining methods as well as novel gear cutting tool designs. All possible methods of gear cutting are referred to as *nontraditional* methods of gear machining with form cutting tools.

The consideration begins with the systematic investigation of all possible types of single-parametric motions. Analysis reveals that novel schematics of gear cutting with (a) end-type milling cutters, (b) disk-type milling cutters, (c) face gear milling cutters, (d) with rotary broaches, etc., can be developed. In particular, various methods and cutting tools of various designs intended for machining worms are considered. In closing, a possibility of classifying form gear cutting tools is discussed.

Section III. Cutting Tools for Gear Generating: Parallel-Axis Gear Machining Mesh

Gear cutting tool designs and gear cutting methods featuring parallel axes of the work gear and the gear cutting tool are investigated in this part of the book. This section begins with a discussion of the kinematics of the parallel-axis gear machining mesh, which is the key issue for the proper understanding of the design and operation of gear cutting tools of many designs.

Chapter 9. Rack cutters for planing gears are the simplest example of generating gear cutting tools featuring parallel-axis gear machining mesh. The geometry and kinematics of machining of gears with rack cutters are analyzed. For profiling of rack cutters, use of the graphical method that is based on the wide implementation of *DG*-based methods and analytical methods is recommended. Methods of vector algebra are used to investigate the cutting edge geometry of rack cutters. Based on the results of the analysis, improvements are made in the geometry of the lateral cutting edges. Chip thickness cut by cutting edges of the rack cutter tooth is analyzed. Accuracy of the tooth flanks of machined gears is analyzed from the perspective of using the approach that is commonly referred to as the *kinematic geometry of surface machining*. Application of rack cutters as well as potential gear cutting methods and rack-type gear cutting tool designs are discussed in the final two sections.

Chapter 10. Design of gear shaper cutters and methods of shaping of external gears are investigated in Chapter 10. The external parallel-axis gear machining mesh is complemented with the cutting motion. In this way, the kinematics of the gear shaping process is derived. Analytical description of the generating surface of the gear shaper cutter, types of the rake surface, and geometry of the clearance surface are discussed. Methods of vector algebra are used to investigate the cutting edge geometry of gear shaper cutters. Valuable improvements in the cutting edge geometry are discovered based on the results of the research. Elements of the kinematics of gear meshing are used for the analytical description of thickness of chip cut by the gear shaper cutter tooth, as well as for the analytical description of the deviations of the machined gear tooth surface from the desired geometry of the gear tooth flanks. The analysis is focused on verifying whether the fifth and sixth conditions of proper part surface generation are satisfied. Issues relating to the application of gear shaper cutters cover both conventional and special-purpose designs of gear shaper cutters for machining spur and helical gears. As an example, typical operations of gear shaping are briefly described. Methods of grinding of the rake and clearance surfaces of gear shaper cutters are discussed at the end of the chapter.

Chapter 11. The design of gear cutting tools using the parallel-axis internal gear machining mesh is discussed in this chapter. The gear machining mesh is complemented with the primary motion. Design procedure encompasses (1) generation of the generating surface of the cutting tool, (2) profiling of the gear shaper cutters, and (3) exploration of the cutting edge geometry of the gear shaper cutter. Computation of thickness of chip cut by the gear shaper cutter tooth and accuracy of the shaped internal gears are also covered in this chapter. Because the same parallel-axis internal gear machining mesh is not limited to the

shaping of internal gears, but can also be applied for the design purposes of enveloping shaper cutters for machining external gears, the related issues are briefly discussed in this chapter. Some important issues relating to the practical applications of the gear shaper cutters are discussed at the end of the chapter.

Section IV. Cutting Tools for Gear Generating: Intersecting-Axis Gear Machining Mesh

Gear cutting tool designs and gear cutting methods featuring intersecting axes of the work gear and the gear cutting tool are investigated in this part of the book. The discussion starts with the investigation of the kinematics of the intersecting-axis gear machining mesh, which is the key issue for the proper understanding of the design and operation of gear cutting tools of many designs.

Chapter 12. Gear shaper cutters with a tilted axis of rotation are examples of gear cutting tools designed based on the principle of the external intersecting axis gear machining mesh. The kinematics of the intersecting-axis gear machining mesh is complemented with an additional primary motion (motion of cut) of the cutting tool to be designed. In this way, the kinematics of the gear machining process using gear shaper cutters with a tilted axis of rotation is derived. For the particular kinematics of gear cutting, the generating surface of the gear shaper cutter with a tilted axis of rotation is derived. Capabilities of the external gear machining mesh are illustrated with several cases of its applications in gear cutting tool design.

Chapter 13. Design of gear cutting tools for machining bevel gears is discussed in this chapter. Gear cutting tools are designed using a round rack that is properly meshing with the gear to be machined. The discussion begins with the analysis of the principal elements of the kinematics of bevel gear generation. Geometry of the interacting surfaces, namely, the involute straight bevel gear flank and the generating surface of the gear cutting tool, along with the geometry of tooth flanks of the generated gears, is analyzed. Generation of straight bevel gears with offset teeth is also covered in this chapter. The discussed geometrical and kinematical aspects are used for the comprehensive investigation of methods of planing and milling of straight bevel gears, and milling of bevel gears with curved teeth. The design of gear cutting tools used for this purpose is discussed along with the corresponding methods of gear machining. It is stressed here that most bevel gears are a type of practical approximation to the desired tooth geometry.

Chapter 14. The possibility of designing gear cutting tools based on an internal intersecting-axis gear machining mesh is discussed in this chapter. Shaping of internal gears using the gear shaper cutter with a tilted axis of rotation, as well as cutting of external gears with enveloping gear shaper cutters with a tilted axis of rotation are good examples in this concern. Shaping of external recessed tooth forms using an enveloping gear shaper cutter is one more opportunity to utilize an internal intersecting-axis gear machining mesh for the purpose of designing gear cutting tools. However, gear machining meshes of this type have not been subjected to a comprehensive investigation as yet.

Section V. Cutting Tools for Generating of Gears: Spatial Gear Machining Mesh

Most gear cutting tool designs are based on the generating principle. Spatial gear machining mesh is simulated when machining a gear using these gear cutting tools. The huge numbers of known as well as possible designs of gear cutting tools result in the decision

to consider them in three sections, each of which is devoted to: (a) external gear machining mesh, (b) quasi-planar gear machining mesh, and (c) internal gear machining mesh.

Section V-A. Design of Gear Cutting Tools: External Gear Machining Mesh

Gear cutting tool designs based on the principle of external spatial gear machining mesh are considered in this section. The section starts with the investigation of the possible types of generating surfaces of the gear cutting tools. Designs of gear hobs, shaver cutters, etc., are considered in consequent chapters.

Chapter 15. The generation principles of the generating surfaces of gear cutting tools are investigated in this chapter. The discussion begins with the analysis of the kinematics of the external spatial gear machining mesh. Possible types of auxiliary generating surfaces together with practical methods of their generation are considered. Generation of the generating surface of the gear cutting tool is based on the possible types of auxiliary generating surfaces. Equations of generating surfaces are derived and design parameters of the surfaces are computed. For the analysis, *DG*-based methods and analytical methods are used. Next, various types of generating surfaces are constructed. They include, but are not limited to, conventional cylindrical generating surface, cylindrical generating surface with a zero profile angle, conical generating surfaces, generating surfaces featuring an asymmetrical tooth profile, as well as surfaces with a torus-shaped pitch surface. The chapter ends with a brief discussion of the geometrical and kinematical constraints on the design parameters of the generating surface of gear cutting tools.

Chapter 16. Hobs are a perfect example of gear cutting tool design based on the external spatial gear machining mesh. The geometry of the generating surface of gear hobs along with geometry of the rake and clearance surfaces are analyzed. Generation methods for the rake and clearance surfaces of hob teeth are also considered. The derived equations for the working surfaces of the gear hob enable an in-depth analysis of the accuracy of hobs for machining of involute gears. Numerous advanced designs of hobs for machining gears are discussed as examples of implementation. The cutting edge geometry of gear hobs is analytically described in the tool-in-use reference system. To satisfy the necessary conditions of proper part surface generation in a gear machining process, constraints on the parameters of modification of the hob tooth profile are investigated. The discussion is followed by several numerical examples of computation of the design parameters of the hobs. The obtained results can be enhanced for application in the area of designing of hobs for machining noninvolute profiles. Applications of hobs for machining gears are discussed from the perspective of the analytical research on the geometry and kinematics of the gear hobbing process.

Chapter 17. Gear shaving cutters represent another type of gear cutting tool designed on the premise of spatial external gear machining mesh. The procedure of designing a shaving cutter begins with the transformation of the generating surface into the workable gear shaving cutter. Peculiarities of the geometry of the rake surface, the clearance surface, and the cutting edge geometry are discussed. Issues on the design parameters of a shaving cutter, design features of the serrations, and resharpening of shaving cutters are considered. Four basic methods for gear shaving—(1) axial shaving, (2) diagonal shaving, (3) tangential shaving, and (4) plunge shaving—are discussed from the perspective of the kinematic geometry of surface machining. The discussion ends with an analysis of the advanced designs of gear shaving cutters and practical issues relating to the implementation of gear shaving processes for shaving precision gears.

Chapter 18. Examples illustrating the capabilities of the external crossed-axis gear machining mesh are discussed in this chapter. These examples can be divided into two sections. Design of gear cutting tools and methods for machining cylindrical gears are considered in the first section. Hobs for tangential hobbing, hobs for plunge hobbing, hobs for machining face gears, continuous generating cutting of worms, gear cutting tools for the scudding process, and gear shaper cutters with a tilted axis of rotation for machining cylindrical gears along with rack-type shaper cutters are also discussed in the first section. Design of gear cutting tools and methods for machining conical gears are discussed in the second section. Discussion in this section is limited to special-purpose tools for reinforcement of gears by surface plastic deformation and conical hobs for the Palloid method of gear cutting.

Section V-B. Design of Gear Cutting Tools: Quasi-Planar Gear Machining Mesh

Design of gear cutting tools based on the principle of the kinematics of *quasi-planar* gear machining mesh is discussed in this section. The section begins with a detailed analysis of the vector representation of the kinematics of quasi-planar gear machining mesh.

Chapter 19. This chapter is devoted to cutting tools for machining bevel gears. Gear cutting tool designs for novel gear cutting methods are discussed. Topics include cutting tools for plunge cutting of bevel gears, face hobs for continuously indexing method of gear cutting, as well as possible directions for further development.

Section V-C. Design of Gear Cutting Tools: Internal Gear Machining Mesh

This final section of the book deals with designs of gear cutting tools that use internal spatial gear machining mesh. Again, the consideration begins with a detailed analysis of the kinematics of the internal spatial gear machining mesh. For this purpose, vector representation of internal spatial gear machining mesh is widely used.

Chapter 20. Designs of gear cutting tools with an enveloping generating surface are discussed in this chapter. Gear cutting tools with cylindrical, conical, and toroidal generating surfaces are covered in this chapter. The discussion includes the analytical determination of the generating surface itself, as well as some aspects relating to the accuracy of the machined gears. This is followed by examples of gear cutting tool designs relating to this group of gear cutting tools.

Chapter 21. The kinematics and design of gear cutting tools are briefly discussed in this chapter. The principal design parameters of gear cutting tools are determined. The discussion is followed by examples of novel designs of gear cutting tools for machining internal gears.

It took the author years to bring this book to completion.

It is inevitable that a study of this nature will lean toward greater emphasis on the author's own contributions, if only because they share his perspective on the subject matter. Nevertheless, an effort has been made to summarize the key ideas (if not the technical details) of the most significant developments in the field, and give pointers to many others.

A book of this size is likely to contain omissions and errors. If you have any constructive suggestions, please communicate them to Dr. S. Radzevich (radzevich@gmail.com).

Stephen P. Radzevich
Sterling Heights, MI

Syntax

Each paragraph is identified first by the chapter number and then by a serial number with the chapter. For example, the second paragraph of chapter 3 is called §3.2. Any such number inserted suddenly online and within parentheses, for example, (§3.2), is an invitation to turn to that paragraph for parallel reading. These internal references may be casting either forward to material yet to be encountered, or backward to material that might require a second reading. Appendices appear at the end of the book. They are consequently lettered A, B, C, and D for easy identification.

A list of references appears at the end of the book. These entries are referenced by means of consecutive numbers within square brackets. I have sometimes enlarged this device to refer to specific paragraphs within a quoted work. For example, [1] [§12.13] specifically refers the reader to §12.13 in [1]. The many interconnected themes of the book cannot be reduced, one by one, each to a simple number. Developing as they go, they run interwoven throughout.

No quoted statements or data are made in cases where well-known results are discussed within the text. This is the major reason why the list of references does not contain numerous works.

Algebraic symbols are listed separately in the Notation section (p. 719). Many of the drawn figures and much of the written argument are variously based on or bolstered by numerical examples. For the reader interested in reproducing the CAD calculations, most numerical values are given either directly online with the text (but isolated there within square brackets) or, more often, among the Appendices.

Section I

Basics

Gear-cutting tools are used for machining of gear teeth. When machining a gear, both the gear and the gear-cutting tool are performing a motion relative to each other. Under such motion, the work gear and the gear-cutting tool often comprise a virtual gear pair. This means that (1) the gear tooth shape, (2) the parameters of the kinematics of the relative motion of the gear and of the gear-cutting tool, and (3) the design parameters of the gear cutting tool are interdependent. Therefore, any change in the gear tooth shape immediately entails corresponding changes to the shape of the gear-cutting tool teeth, the kinematics of the gear machining process, or both.

When machining a gear, the interaction of the work gear and the gear-cutting tool closely resembles the interaction of gear tooth flanks in a gear pair. A gear pair serves the purpose of transforming the given input motion into the required output motion. Gear pairs have three principal components: (1) tooth shape of the input gear, (2) tooth shape of the conjugate output gear, and (3) motion of the output gear axis relative to the input gear axis. An infinite number of tooth shape combinations are capable of ensuring the desired motion transformation.

A similar situation is also observed in gear-machining operations. Generally speaking, a gear machining operation also features three principal components: (1) tooth shape of the gear-cutting tool to be applied, (2) tooth shape of the gear to be machined, and (3) a certain motion of the gear-cutting tool and the work gear relative to each other.

Machining of a desired gear tooth shape is the major goal of the gear machining process. An infinite number of combinations of (1) shape of the gear-cutting tool teeth and (2) kinematics of the relative motion of the work gear and the gear-cutting tool can ensure the machining of the desired gear tooth shape.

Before one begins to design a gear-cutting tool, major design parameters of the gear need to be determined. Certain kinematics of the gear machining process can be chosen among feasible relative motions of the work gear and the gear-cutting tool. Ultimately, one can conclude that for machining of a given gear, a gear-cutting tool can be designed only if the kinematics of the gear machining process is somehow specified.

Two issues can be drawn up from these considerations.

First, before designing a gear-cutting tool, it is necessary to specify the geometry of the tooth flanks of the gear to be machined. Answering the question, "What are the specific features of geometry of gear tooth surface to be machined?" is a must.

Second, we have to know exactly how the work gear and the gear-cutting tool move with respect to each other when machining the gear teeth. Investigation and analysis of all feasible relative motions of the work gear and the gear-cutting tool is of critical importance. Parameters of the optimal kinematics of the gear machining process should be predetermined before the design stage. In most practical cases, not the optimal kinematics, but the suitable/reasonable kinematics of the gear machining process is often implemented instead.

Both issues are critically important to the gear cutting tool designer.

Determination of the parameters of the geometry of the generating surface of the gear-cutting tool on the premise of (1) the known geometry of the tooth flank of the gear to be machined and (2) the predetermined kinematics of the gear machining process comprises the so-called *direct problem of gear-cutting tool design*. Another problem relates to determining the geometry of the tooth flank of the gear that is machined with a given gear-cutting tool. Often, a problem of this type is referred to as an *inverse problem of gear-cutting tool design*.

The inverse problem of gear-cutting tool design arises in two cases. First, when an approximation of the tooth profile of the designed gear-cutting tool has been implemented, then for the purpose of computing the actual accuracy of the gear-cutting tool, the inverse problem of gear-cutting tool design is analyzed. The second case ensues when a gear-cutting tool is given, and it is necessary to determine the geometry of the tooth flank of the gear that is machined with the given gear-cutting tool.

The following discussion begins with an investigation of the possible options to solve the direct problem of gear-cutting tool design.

1

Gears: Geometry of Tooth Flanks

Gears are used as elements of gear trains for transmission and transformation of motion from one shaft to another. A large number of gears are used in the automotive industry (Figure 1.1). It is commonly understood that a gear is a machine element having gear teeth. Usually, but not necessarily, the gear is round.* There is a large variety of gear forms, as well as tooth forms in lengthwise direction. Gear teeth are also available in a wide variety of profiles.

The performance of a gear transmission depends strongly on the accuracy of the gears comprising the gear transmission. Precision gears can be mainly produced by cutting with gear-cutting tools. For the purposes of gear machining and designing gear-cutting tools, the gear teeth flanks to be machined are accurately specified.

1.1 Basic Types of Gears

Although the number of gear forms, shapes of gear teeth, and teeth profiles is large, only several basic types of gear design are commonly recognized. For illustrative purposes, several basic types of gears are considered in this chapter. The following discussion aims to provide an overview of the geometry of gear tooth flanks, both a qualitative as well as quantitative understanding of how complex the geometry of gear tooth flanks can be, and the types of problems that often arise when machining gear teeth.

A *spur gear* is the simplest type of gear. Straight teeth of a spur gear are uniformly distributed around the cylindrical body of the gear. Both external spur gears (Figure 1.2) as well as internal spur gears (Figure 1.3) are recognized. In particular cases, when the pitch diameter of a spur gear approaches infinity, the gear transforms into a *spur rack*.

A *helical gear* features helical teeth (Figure 1.4). When gear teeth are shaped in the form of a helix that wraps around a cylinder, they are referred to as helical. Helix angles ranging from only a few degrees up to about 45° are practical. Helical gears may be made either with external or internal teeth.

A *helical rack* has a plane pitch surface and straight teeth that are oblique to the face surfaces.

Double-helical (Figure 1.5) and *herringbone* gears are composed of two helical gears facing in opposite directions to the helix. When two helical gears are separated, and are at a certain distance from each other, they are often referred to as a double-helical gear. The separation distance for herringbone gears is equal to zero. Again, external as well as internal double-helical and herringbone gears are recognized. In particular cases, a double-helical or herringbone rack can be formed.

* Noncircular gears, scroll gears, and special-purpose elements of mechanical transmissions are not considered in this book.

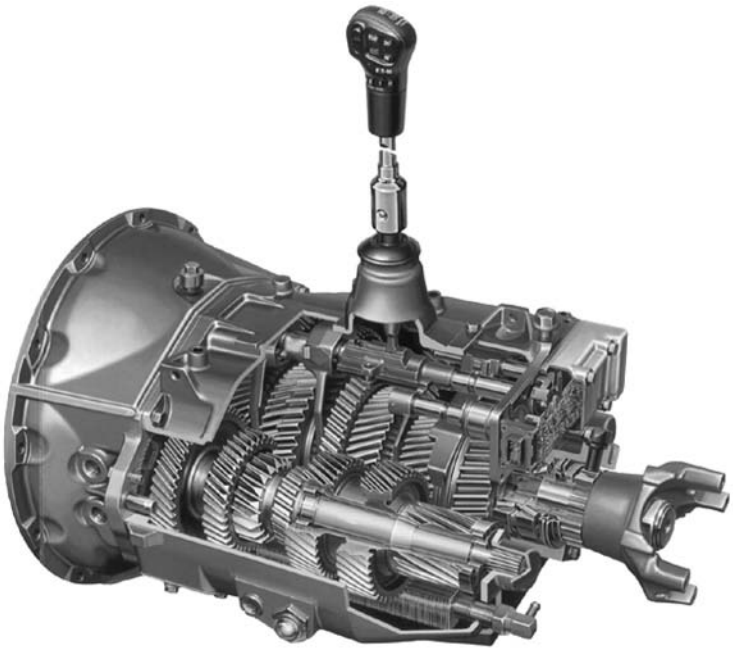

FIGURE 1.1
Gears of various types are used in the design of automobile transmission.

FIGURE 1.2
Spur gears.

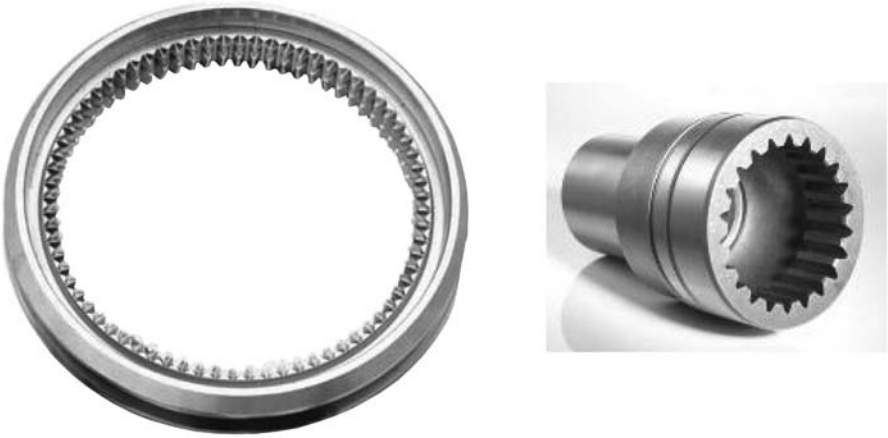

FIGURE 1.3
Internal gears.

Cluster gears (Figure 1.6) are composed of two gears that not only have different helices but different other design parameters as well.

When the helix angle of a helical gear is large, for example, when it exceeds 90° by just a few degrees up to about 45°, then the helical gear transforms into a worm (Figure 1.7). Worms can make proper mesh with ordinary spur and helical gears as well as with worm gears (Figure 1.8) of an appropriate design. In particular cases, double-enveloping worms are used. The elementary gear drive comprising a worm gear and a double-enveloping worm is commonly referred to as a *double-enveloping worm gear drive* or simply, a *Cone drive*.

Straight bevel gears (Figure 1.9) are used as machine elements of gear drives whose main purpose is the transmission of motion between shafts that are not parallel to each other. For this purpose, spiral bevel gears (Figure 1.10) can be used as well.

FIGURE 1.4
A helical gear.

FIGURE 1.5
A double-helical gear.

Face gears (Figure 1.11) are capable of transmitting rotation either between the intersecting axes of rotation or between the crossing axes of rotation. The capacity to make proper mesh with cylindrical pinion is an important advantage of face gearing.

Only designs of some of the most commonly-used gears are briefly considered here. It is not the goal of this chapter to cover a large number of gear designs widely used in industry. The interested reader may wish to read numerous special texts on gearing where various gear designs are discussed in more detail.

1.2 Analytical Description of Gear Tooth Flanks

In designing gear-cutting tools, an accurate specification of gear tooth flanks is of critical importance. The analytical description of gear tooth flanks is preferred from many

FIGURE 1.6
A cluster gear.

FIGURE 1.7
A worm.

standpoints. Although the variety of gear tooth shapes is rather large, commonly-used gear tooth forms in the lengthwise direction of the teeth are usually limited to just a few forms, including: (1) straight, (2) helical, (3) herringbone and double helical, (4) circular, (5) cycloidal, and (6) palloid. The number of tooth profiles satisfying the condition of meshing is infinitely large. However, commonly-used tooth profiles in industry are limited to: (1) involute, (2) double circular arc profile or Novikov's tooth profile, (3) spherical involute, (4) cycloidal profile, (5) rectangular splines, and (6) modified and special tooth profiles.

FIGURE 1.8
A worm gear.

FIGURE 1.9
A straight bevel gear.

The cited tooth shapes, as well as most other practical shapes of gear tooth flanks, can be described analytically.

A comprehensive analysis of the geometry of gear tooth forms is not within the scope of this text, and is discussed elsewhere in more detail. Only a few illustrative examples of the derivation of the equation for gear tooth flanks are presented. The examples show the capabilities of one of the approaches for deriving such an equation.

A set of design parameters of a gear is usually indicated on the gear blueprint. The indicated data could be sufficient for the specification of the geometry of the gear tooth flank, and are usually used for design purposes. This approach is referred to as the *engineering approach* for gear tooth flank specification.

The analytical representation of gear tooth flanks is another means of specifying the geometry of the gear tooth flank. This method of specification is preferred for analysis, development, and research. The analytical representation of a gear tooth flank is referred to as the *scientific approach* for gear tooth flank specification.

The engineering and scientific approaches are equivalent to each other and each one can be derived from the other. For this purpose, basic gear formulae can be used [10, 190]. For convenience, the equations, those necessary for this purpose are summarized in Appendix A.

The analytical description of gear tooth flanks can be easily obtained by the use of the "scientific approach."

FIGURE 1.10
A spiral bevel gear.

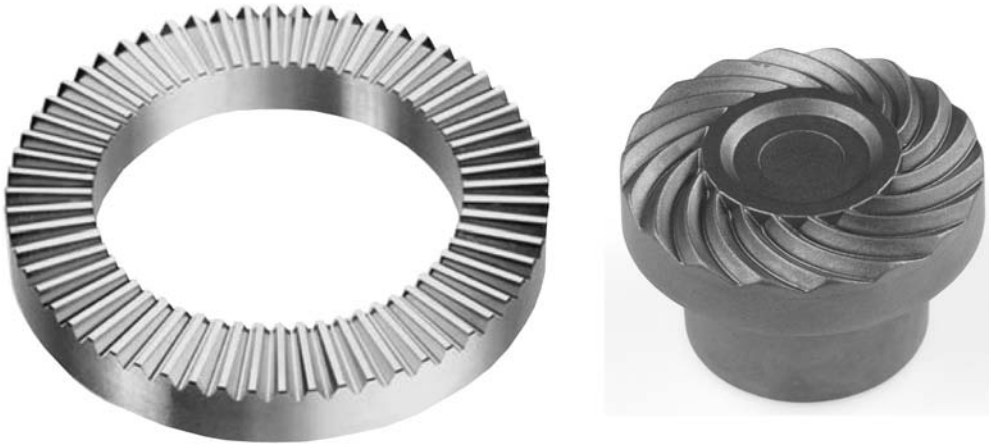

FIGURE 1.11
Face gears.

1.2.1 Tooth Flank of an Involute Spur Gear

Consider a spur gear having an involute tooth profile (Figure 1.2). The generation of the involute tooth profile is illustrated in Figure 1.12. In the coordinate system X_gY_g, position vector $\mathbf{r}_{inv}(V_g)$ of a point of an involute tooth profile allows matrix representation in the form:

$$\mathbf{r}_{inv}(V_g) = \begin{bmatrix} r_{b.g}(\sin V_g - V_g \cos V_g) \\ r_{b.g}(\cos V_g + V_g \sin V_g) \\ 0 \\ 1 \end{bmatrix}, \qquad V_g^{(l)} \le V_g \le V_g^{(a)} \tag{1.1}$$

Here, $V_g^{(l)}$ and $V_g^{(a)}$ are the values of parameter V_g, those that correspond to the start of active profile (*SAP*) point of the tooth profile and the point in the tooth profile that is located on the major diameter of the gear.

The tooth flank of an involute spur gear can be presented as the locus of consecutive positions of the involute tooth profile $\mathbf{r}_{inv}(V_g)$ that is moving in the direction of the gear axis Z_g. Let us denote the parameter of the motion of the tooth profile as U_g. Equation (1.1) immediately yields the expression for position vector $\mathbf{r}_g(U_g, V_g)$ of a point of the tooth flank of the involute spur gear:

$$\mathbf{r}_g(U_g, V_g) = \begin{bmatrix} r_{b.g}(\sin V_g - V_g \cos V_g) \\ r_{b.g}(\cos V_g + V_g \sin V_g) \\ U_g \\ 1 \end{bmatrix}, \qquad \begin{matrix} V_g^{(l)} \le V_g \le V_g^{(a)} \\ 0 \le U_g \le B_g \end{matrix} \tag{1.2}$$

The current value of parameter U_g is within the gear face width B_g.

It is possible to see that, for the chosen type of parameterization of the flank surface of the involute spur gear, the identity $U_g \equiv Z_g$ is observed.

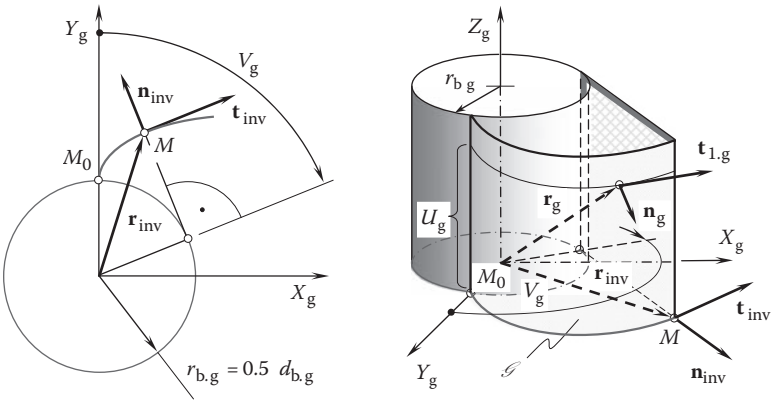

FIGURE 1.12
Derivation of the equation for the tooth flank of an involute spur gear.

1.2.2 Tooth Flank of an Involute Helical Gear

The tooth flanks of helical gears having an involute tooth profile are shaped in the form of a screw involute surface. Figure 1.13 illustrates a method to generate a screw involute surface by a straight line that rolls with no sliding over the base cylinder of the gear.

When performing a screw motion, the straight line generates a screw involute surface $\mathscr{G}$, which is represented as a locus of successive positions of the straight line. The generating line is tangent to the helix on the base cylinder of radius $r_{b.g}$. The helix in question is traced out on the base cylinder by point of tangency of the generating straight line with the cylinder. The generating line forms base lead angle $\lambda_{b.g}$ with the plane perpendicular to the Z_g axis of the Cartesian coordinate system $X_gY_gZ_g$.

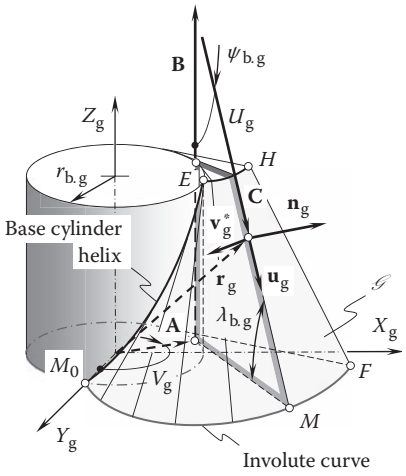

FIGURE 1.13
Screw involute surface of a helical gear tooth. (From Radzevich, S.P., *ASME Journal of Mechanical Design*, 124, 772–786, 2002. With permission.)

Position vector $\mathbf{r}_g$ of a point of the screw involute surface yields representation in the form of summa of three vectors $\mathbf{r}_g = \mathbf{A} + \mathbf{B} + \mathbf{C}$. Here, $|\mathbf{A}|$ is the base cylinder radius (i.e., the equality $|\mathbf{A}| = r_{b.g}$ is observed). Vector $\mathbf{A}$ makes roll angle V_g with the Y_g axis. $|\mathbf{B}| = p_g \cdot V_g$ is the axial displacement in screw motion corresponding to the rotation angle V_g, and p_g is the screw parameter of the flank surface $\mathscr{G}$. Ultimately, $|\mathbf{C}| = U_g$ is the segment of the generating straight line measured from the tangency point on the base cylinder to the current point on the screw involute surface $\mathscr{G}$.

Projecting vectors **A**, **B**, and **C** onto the coordinate axes yields an equation of the screw involute surface of the tooth flank. After the necessary formulae transformations are performed, equation of the screw involute surface $\mathscr{G}$ can be represented in matrix form:

$$\mathbf{r}_g(U_g, V_g) = \begin{bmatrix} r_{b.g}\cos V_g + U_g \cos\lambda_{b.g}\sin V_g \\ r_{b.g}\sin V_g - U_g \sin\lambda_{b.g}\sin V_g \\ r_{b.g}\tan\lambda_{b.g} - U_g \sin\lambda_{b.g} \\ 1 \end{bmatrix} \quad \begin{matrix} V_g^{(l)} \le V_g \le V_g^{(a)} \\ 0 \le U_g \le [U_g] \end{matrix} \tag{1.3}$$

Here, $[U_g]$ denotes the maximum allowed value of parameter U_g. Actually, the value of $[U_g]$ can be expressed in terms of the base diameter $d_{b.g} = 2r_{b.g}$ of the gear, base lead angle $\lambda_{b.g}$, and the gear face width B_g. The interested reader is referred to refs. [112, 131, 138] for more details on the derivation of Equation (1.3).

A brief analysis of the local topology of the screw involute surface $\mathscr{G}$ follows.

Equation (1.3) yields computation of two tangent vectors, $\mathbf{U}_g(U_g, V_g)$ and $\mathbf{V}_g(U_g, V_g)$, that are correspondingly equal:

$$\mathbf{U}_g(U_g, V_g) = \frac{\partial \mathbf{r}_g}{\partial U_g}(U_g, V_g) = \begin{bmatrix} \cos\lambda_{b.g}\sin V_g \\ -\cos\lambda_{b.g}\cos V_g \\ -\sin\lambda_{b.g} \\ 1 \end{bmatrix} \tag{1.4}$$

$$\mathbf{V}_g(U_g, V_g) = \frac{\partial \mathbf{r}_g}{\partial V_g}(U_g, V_g) = \begin{bmatrix} -r_{b.g}\sin V_g + U_g \cos\lambda_{b.g}\cos V_g \\ r_{b.g}\cos V_g + U_g \cos\lambda_{b.g}\sin V_g \\ r_{b.g}\tan\lambda_{b.g} \\ 1 \end{bmatrix} \tag{1.5}$$

Accordingly, the corresponding unit tangent vectors $\mathbf{u}_g$ and $\mathbf{v}_g$ are equal.

$$\mathbf{u}_g(U_g, V_g) = \frac{\mathbf{U}_g}{|\mathbf{U}_g|} \quad \text{and} \quad \mathbf{v}_g(U_g, V_g) = \frac{\mathbf{V}_g}{|\mathbf{V}_g|} \tag{1.6}$$

Unit vector $\mathbf{u}_g$ specifies the direction of the tangent to the U_g coordinate curve through the given point on the gear tooth flank $\mathscr{G}$. Similarly, unit vector $\mathbf{v}_g$ specifies the direction of the tangent to the V_g coordinate curve through that same point on surface $\mathscr{G}$.

The computed vectors, $\mathbf{U}_g$ and $\mathbf{V}_g$, can be used for the computation of the fundamental magnitudes of the first order:

$$E_g = \mathbf{U}_g \cdot \mathbf{U}_g \tag{1.7}$$

$$F_g = \mathbf{U}_g \cdot \mathbf{V}_g \tag{1.8}$$

$$G_g = \mathbf{V}_g \cdot \mathbf{V}_g \tag{1.9}$$

For a screw involute surface $\mathscr{G}$, Equations (1.7) through (1.9) return:

$$E_g = 1, \tag{1.10}$$

$$F_g = -\frac{r_{b.g}}{\cos\lambda_{b.g}} \tag{1.11}$$

$$G_g = \frac{U_g^2 \cos^4\lambda_{b.g} + r_{b.g}^2}{\cos^2\lambda_{b.g}} \tag{1.12}$$

These equations yield an expression for the first fundamental form:

$$\Phi_{1.g} \quad \Rightarrow \quad dU_g^2 - 2\frac{r_{b.g}}{\cos\lambda_{b.g}} dU_g dV_g + \frac{U_g^2 \cos^4\lambda_{b.g} + r_{b.g}^2}{\cos^2\lambda_{b.g}} dV_g^2 \tag{1.13}$$

The discriminant $H_g = \sqrt{E_g G_g - F_g^2}$ of the first fundamental form $\Phi_{1.g}$ of the surface $\mathscr{G}$ can be computed as:

$$H_g = U_g \cos\lambda_{b.g} \tag{1.14}$$

To derive an equation for the second fundamental form $\Phi_{2.g}$ of the gear tooth surface $\mathscr{G}$, the second derivatives of $\mathbf{r}_g(U_g, V_g)$ with respect to U_g and V_g are necessary. Equations (1.4) and (1.5) for vectors $\mathbf{U}_g$ and $\mathbf{V}_g$ yield the expressions:

$$\frac{\partial \mathbf{U}_g}{\partial U_g}(U_g, V_g) = \begin{bmatrix} 0 \\ 0 \\ 0 \\ 1 \end{bmatrix} \tag{1.15}$$

$$\frac{\partial \mathbf{U}_g}{\partial V_g}(U_g, V_g) \equiv \frac{\partial \mathbf{V}_g}{\partial U_g}(U_g, V_g) = \begin{bmatrix} \cos\lambda_{b.g}\cos V_g \\ \cos\lambda_{b.g}\sin V_g \\ 0 \\ 1 \end{bmatrix} \tag{1.16}$$

$$\frac{\partial \mathbf{V}_g}{\partial V_g}(U_g, V_g) = \begin{bmatrix} -r_{b.g}\cos V_g - U_g\cos\lambda_{b.g}\sin V_g \\ -r_{b.g}\sin V_g + U_g\cos\lambda_{b.g}\cos V_g \\ 0 \\ 1 \end{bmatrix} \tag{1.17}$$

for the derivatives of vectors $\mathbf{U}_g$ and $\mathbf{V}_g$ with respect to U_g and V_g.

By definition, the fundamental magnitudes of the second order can be presented in the form:

$$L_g = \frac{\frac{\partial \mathbf{U}_g}{\partial U_g} \times \mathbf{U}_g \cdot \mathbf{V}_g}{H_g} \tag{1.18}$$

$$M_g = \frac{\frac{\partial \mathbf{U}_g}{\partial V_g} \times \mathbf{U}_g \cdot \mathbf{V}_g}{H_g} \tag{1.19}$$

$$N_g = \frac{\frac{\partial \mathbf{V}_g}{\partial V_g} \times \mathbf{U}_g \cdot \mathbf{V}_g}{H_g} \tag{1.20}$$

Equations (1.18) through (1.20) allow for the computation of the second fundamental magnitudes of the helical gear tooth flank surface $\mathscr{G}$:

$$L_g = 0 \quad M_g = 0 \quad \text{and} \quad N_g = -U_g \sin\lambda_{b.g} \cos\lambda_{b.g} \tag{1.21}$$

Ultimately, the equation to compute for the second fundamental form of surface $\mathscr{G}$:

$$\boldsymbol{\Phi}_{2.g} \quad \Rightarrow \quad -\mathrm{d}\mathbf{r}_g \cdot \mathrm{d}\,\mathbf{N}_g = -U_g \sin\lambda_{b.g} \cos\tau\lambda_{b.g} \mathrm{d}V_g^2 \tag{1.22}$$

can be composed.

Discriminant T_g of the second fundamental form $\Phi_{2.g}$ of surface $\mathscr{G}$ is determined as:

$$T_g = \sqrt{L_g M_g - N_g^2} = 0 \tag{1.23}$$

Equations (1.13) and (1.22) are helpful for solving geometrical problems pertaining to the design of gear-cutting tools. For example, to compute for the actual value of radius R_g of the normal curvature of gear tooth flank $\mathscr{G}$, a simple expression, $R_g = \Phi_{1.g}/\Phi_{2.g}$, can be used. Many other parameters of the geometry of the gear tooth flank can be expressed in terms of the first ($\Phi_{1.g}$) and second ($\Phi_{2.g}$) fundamental forms of surface $\mathscr{G}$.

The set of six equations for the computation of the fundamental magnitudes of the first $\Phi_{1.g}$ and second $\Phi_{2.g}$ fundamental forms (Table 1.1) is known as the *natural parameterization* of the gear tooth flank surface $\mathscr{G}$.

TABLE 1.1

Fundamental Magnitudes of a Screw Involute Surface $\mathscr{G}$

First Order, $\Phi_{1.g}$	**Second Order, $\Phi_{2.g}$**
$E_g = 1$	$L_g = 0$
$F_g = -\dfrac{r_{b.g}}{\cos\lambda_{b.g}}$	$M_g = 0$
$G_g = \dfrac{U_g^2 \cos^4\lambda_{b.g} + r_{b.g}^2}{\cos^2\lambda_{b.g}}$	$N_g = -U_g \sin\lambda_{b.g} \cos\lambda_{b.g}$

In a similar manner, a corresponding equation of the tooth flank surface can be derived for a gear of any design.

1.2.3 Tooth Flank of a Bevel Gear

Generation of the gear tooth surface $\mathscr{G}$ can be presented as rolling with no sliding of a plane over the gear base cone (Figure 1.14). Position vector $\mathbf{r}_g$ of a point of tooth surface $\mathscr{G}$ allows for representation as summa $\mathbf{r}_g = \mathbf{A} + \mathbf{B} + \mathbf{C}$, where:

$$\mathbf{A} = -\mathbf{k} \cdot U_g \tag{1.24}$$

$$\mathbf{B} = \mathbf{i} \cdot U_g \tan\theta_g \sin\varphi_g + \mathbf{j} \cdot U_g \tan\theta_g \cos\varphi_g \tag{1.25}$$

$$\mathbf{C} = -\mathbf{i} \cdot \varphi_g U_g \tan\theta_g \cos\varphi_g + \mathbf{j} \cdot \varphi_g U_g \tan\theta_g \sin\varphi_g \tag{1.26}$$

By substituting vectors **A**, **B**, and **C** into $\mathbf{r}_g = \mathbf{A} + \mathbf{B} + \mathbf{C}$, one can come up with an equation of surface $\mathscr{G}$ for a bevel gear in matrix representation:

$$\mathbf{r}_g = \begin{bmatrix} U_g \tan\theta_g \sin\varphi_g - \varphi_g U_g \tan\theta_g \cos\varphi_g \\ U_g \tan\theta_g \cos\varphi_g + \varphi_g U_g \tan\theta_g \sin\varphi_g \\ -U_g \\ 1 \end{bmatrix} \tag{1.27}$$

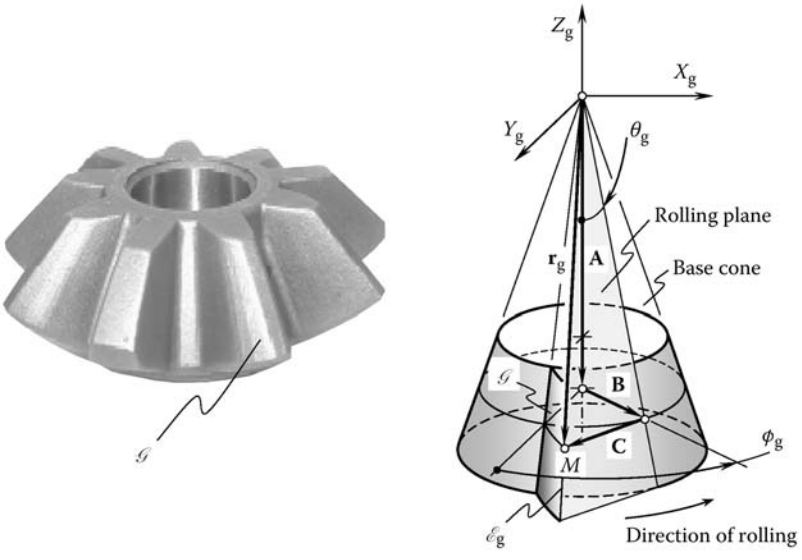

FIGURE 1.14
Tooth flank of a straight bevel gear.

Evidently, the presented approach to derive the equation for bevel gear tooth flank $\mathscr{G}$ is not the only possible one. There is plenty of room to explore other approaches.

1.2.4 Tooth Flank of a Helical Bevel Gear

For a bevel gear having helical teeth (Figure 1.15), position vector $\mathbf{r}_g$ of a point M can be expressed in terms of vectors **A**, **B**, **D**, and **E**, which comprise $\mathbf{r}_g$:

$$\mathbf{r}_g = \mathbf{A} + \mathbf{B} + \mathbf{D} + \mathbf{E} \tag{1.28}$$

Here, vectors **A** and **B** are those vectors comprising the vector $\mathbf{r}_g$ for a spur bevel gear. Vectors **D** and **E** are required to be expressed in terms of the geometrical parameters of the gear tooth surface $\mathscr{G}$.

Let us denote the magnitudes of vectors **D** and **E** as $d = |\mathbf{D}| = |\mathbf{C}| \cdot \tan \psi_{b.g}$ and $e = |\mathbf{E}| = \dfrac{|\mathbf{C}|}{\cos \psi_{b.g}}$. Here, $|\mathbf{C}| = \Phi_g U_g \tan \theta_g$. Then, one can come up with the following expression for vector **D**:

$$\mathbf{D} = -\mathbf{i} \cdot d \sin\theta_g \sin\varphi_g - \mathbf{j} \cdot d \sin\theta_g \cos\varphi_g + \mathbf{k} \cdot d \cos\theta_g \tag{1.29}$$

Vector **E** yields representation in the form of $\mathbf{E} = \mathbf{C} - \mathbf{D}$. Therefore,

$$\begin{aligned}\mathbf{E} = {} & \mathbf{i} \cdot (\varphi_g U_g \tan\theta_g \cos\varphi_g - d \sin\theta_g \sin\varphi_g) \\ & + \mathbf{j} \cdot (\varphi_g U_g \tan\theta_g \sin\varphi_g + d \sin\theta_g \cos\varphi_g) \\ & - \mathbf{k} \cdot d \cos\theta_g\end{aligned} \tag{1.30}$$

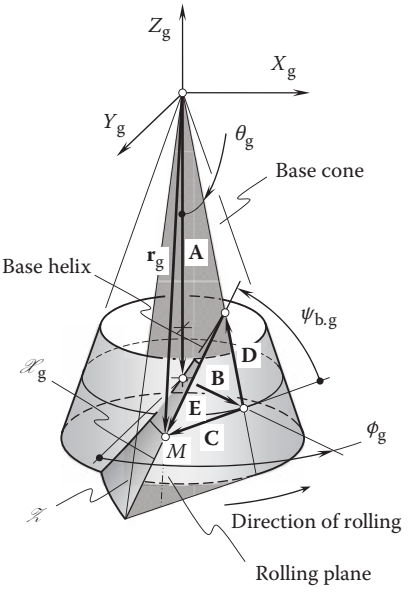

FIGURE 1.15
Tooth flank of a helical bevel gear.

Substituting $d = \varphi_g U_g \tan\theta_g \tan\psi_{b.g}$ to the equations for **D** and **E**, one can obtain the following expressions:

$$\mathbf{D} = -\mathbf{i}\cdot(\varphi_g U_g \tan\theta_g \tan\psi_{b.g} \sin\theta_g \sin\varphi_g) - \mathbf{j}\cdot(\varphi_g U_g \tan\theta_g \tan\psi_{b.g} \sin\theta_g \cos\varphi_g) + \mathbf{k}\cdot(\varphi_g U_g \tan\theta_g \tan\psi_{b.g} \cos\theta_g) \tag{1.31}$$

$$\mathbf{E} = \mathbf{i}\cdot(\varphi_g U_g \tan\theta_g \cos\varphi_g - \varphi_g U_g \tan\theta_g \tan\psi_{b.g} \sin\theta_g \sin\varphi_g) + \mathbf{j}\cdot(\varphi_g U_g \tan\theta_g \sin\varphi_g + \varphi_g U_g \tan\theta_g \tan\psi_{b.g} \sin\theta_g \cos\varphi_g) - \mathbf{k}\cdot\varphi_g U_g \tan\theta_g \tan\psi_{b.g} \cos\theta_g \tag{1.32}$$

Ultimately, an expression for the position vector $\mathbf{r}_g$ of a point of the tooth flank of the helical bevel gear is represented in matrix form:

$$\mathbf{r}_g = \begin{bmatrix} (\sin\varphi_g - 2\varphi_g \tan\psi_{b.g} \sin\theta_g \sin\varphi_g)(U_g \tan\theta_g) \\ [\cos\varphi_g + 2\varphi_g \sin\varphi_g - \tan\psi_{b.g} \sin\theta_g \cos\varphi_g(\tan\theta_g - \varphi_g)](U_g \tan\theta_g) \\ -U_g \\ 1 \end{bmatrix} \tag{1.33}$$

In a similar manner to that described in Section 1.2.2, analysis of the local topology of tooth flanks for both bevel gear and helical bevel gear can be performed.

1.3 Gear Tooth for Surfaces That Allow Sliding

Another type of surface used for the design of gear teeth comprises those surfaces that allow sliding. As will be discussed later in this text, this particular surface type is also widely used for the design of gear-cutting tools.

The property of a surface that allows sliding over it means that, for a certain surface $\mathscr{G}$, there exists a special type of motion. When this motion occurs, the enveloping surface to successive positions of the moving surface $\mathscr{G}$ is congruent to surface $\mathscr{G}$ itself. Generally speaking, this type of motion can be: (1) single parametric, (2) biparametric, or (3) triparametric.

The screw surface of constant pitch* (p_x = Const) is the most general type of surface that allows sliding. While performing a screw motion of that same pitch p_x, surface $\mathscr{G}$ is sliding over itself similar to a pair "bolt-and-nut." Surfaces of this type are found in the design of helical gears (Figure 1.4). If the involute gear performs the screw motion about its axis, and the parameter of the screw motion is equal to the parameter of the involute tooth surface, then the enveloping surface to successive positions of the moving tooth flank $\mathscr{G}$ is congruent to itself. This means that during such motion, the gear tooth flank is sliding over itself.

* *General helicoid* in other terminology.

FIGURE 1.16
A spur gear with modified (barreled) teeth.

The same is true with respect to the surface of a cylindrical worm (Figure 1.7). However, neither double-helical gears (Figure 1.5) nor cluster gears (Figure 1.6) allow sliding.

For cylinders of the general type,* the pitch of the screw surface inflates to an infinitely large value. Surfaces of this type allow straight motion along the straight generating lines of the surface. Tooth flanks of spur gears (Figures 1.2 and 1.3) are shaped in the form of cylinders of the general type. When the spur gear performs a straight motion along its axis, then the enveloping surface to successive positions of the moving tooth flank is congruent to itself. This means that as a motion of this type occurs, the teeth flanks of the spur gear are sliding over them.

Finally, the pitch of the screw surface could be equal to zero ($p_x = 0$), in which case the screw surface reduces to a surface of revolution. Every surface of revolution is sliding over itself when it is rotated about its axis. For example, the tooth flank of the modified (*barreled* or *crowned*) spur gear (Figure 1.16) could be shaped in the form of a surface of revolution. A schematic layout of how the tooth flank of a modified spur gear can be shaped in the form of a surface of revolution is shown in Figure 1.17.

Screw surfaces of constant pitch, p_x = Const, cylinders of the general type, and surfaces of rotation are the only surfaces allowing a monoparametric motion that causes the surface to slide over it.

Surfaces such as a circular cylinder allow rotation as well as straight motion along the axis of the cylinder. In this case, the surface motion is biparametric (rotation and translation can be performed independently).

A sphere allows rotations about three axes independently. A plane surface allows straight motion in two different directions as well as a rotation about an axis that is orthogonal to the plane. The surface motion in these two cases is triparametric.

Ultimately, one can summarize that surfaces allowing sliding are limited to: (1) screw surfaces of constant pitch, (2) cylinders of the general type, (3) surfaces of revolution, (4) circular cylinders, (5) spheres, and (6) plane.

It has been proven [136, 138, 153, 172] that no other types of surfaces share this particular property.

A brief look at the gears shown in Figures 1.8 through 1.11 reveals that none of these tooth flanks allow sliding.

* *Surface of translation* in other terminology.

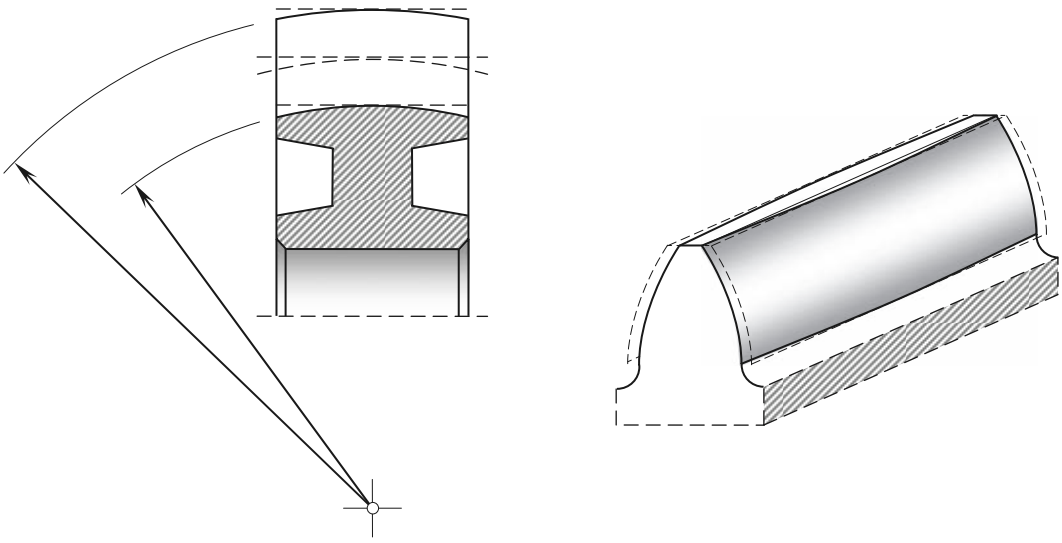

FIGURE 1.17
A spur gear with modified (crowned) teeth (tooth flanks of the gear are shaped in the form of a surface of revolution).

Surfaces that allow sliding have very convenient uses in manufacturing as well as in other engineering applications. Most of the surfaces being machined in various industries are surfaces of this nature, and many gear machining processes are utilizing this particular surface property. Almost all designs of gear-cutting tools are also developed on the premise of surfaces that allow sliding.

2

Principal Kinematics of a Gear Machining Process

Geometry of the generating surface of the gear cutting tool is the solution to the direct problem of the theory of surface generation [30, 138, 143]. In this chapter, the generating surface of the gear cutting tool T is viewed in the sense of an enveloping surface to successive positions of the gear tooth flank $\mathscr{G}$ in the motion of the work gear relative to a reference system at which the generating surface T will be analytically described. The generating surface of the gear cutting tool is conjugate to the work gear tooth flank. In particular cases, surface T can be congruent to the work gear tooth surface $\mathscr{G}$.

Most of the major elements of the geometry of gear cutting tools can be computed as a solution to the direct problem of the theory of surface generation.

Geometry of the gear tooth flank is the first major component that is necessary for solving the direct problem. Gear tooth surface can be uniquely specified based on the data available from the gear blueprint. Illustrative examples in this regard are briefly discussed in Chapter 1.

Kinematics of the gear machining process is the second major component that is also necessary for solving this problem.

The development of the generalized theory of surface generation on machine tools can be traced back to the middle of the twentieth century [20, 53, 177, 178]. Results from various research activities on surface generation were later significantly enhanced by Radzevich [125, 136, 138, 143, 153], the principal developer of the *DG/K*-based approach to surface generation. In the following discussion, the kinematics of gear machining process with focus on gear cutting tool design is largely based on the research results obtained by the author.

2.1 Relative Motions in Gear Machining

Every gear machining process features a certain kinematics of surface machining. For example, when grinding a helical involute gear with an abrasive worm (Figure 2.1), the work gear is rotating about its axis with a certain rotation ω_g. A grinding worm is rotating about its axis with a rotation ω_c. Rotations ω_g and ω_c are properly timed with each other. When spur gears are machined, the required ratio $\omega_g N_g = \omega_c N_c$ must be satisfied. Here, N_g denotes the work gear tooth number and N_c is the number of starts of the abrasive worm. In addition, the work gear and the gear cutting tool move relative to each other with a certain feed F_c in the axial direction of the gear. No kinematical restrictions are imposed on feed F_c when spur gears are machined. If a helical gear is machined, then the parameters of the kinematics of the gear machining operation ω_g, N_g and ω_c, N_c have to be satisfied not just with each other but also taking into account the pitch helix angle ψ_g of the work gear.

The example shown in Figure 2.1 illustrates that relative motions of the work gear and the gear cutting tool are critical elements in every gear machining process. It also reveals that

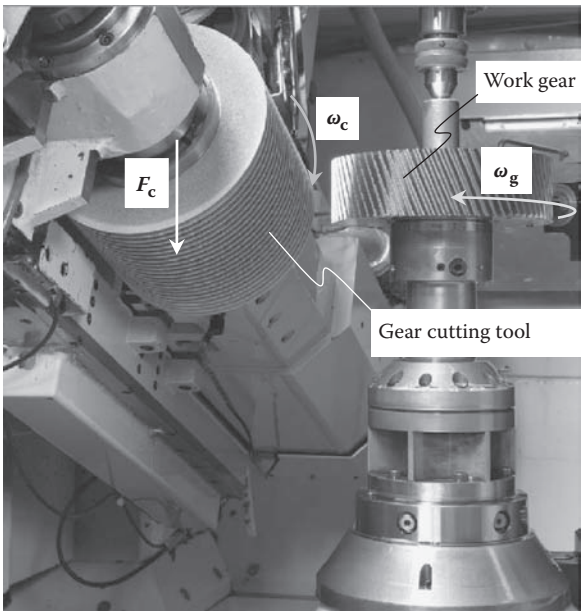

FIGURE 2.1
Elements of the kinematics of a gear machining process.

the actual variety of feasible relative motions of the work gear blank and the gear cutting tool is not limited to just a few motions. It is strongly recommended to take into account all feasible motions of the gear cutting tool with respect to the work gear if one aims to develop gear cutting tools of optimal design. Only on the basis of a profound analysis of the kinematics of the gear machining process should an optimal design be developed.

2.1.1 Elementary Relative Motions of the Work Gear and the Gear Cutting Tool

Geometry of the work gear tooth flank is the only information available when one embarks on designing a gear cutting tool. Consider a Cartesian coordinate system $X_gY_gZ_g$ that is associated with the work gear as shown in Figure 2.2. In the coordinate system $X_gY_gZ_g$, the gear tooth flanks can be described analytically, for example, by Equation (1.3).

Geometry of the generating surface of the gear cutting tool for machining of the given work gear at this point is not yet known. Therefore, it is not a gear cutting tool, but a certain coordinate system $X_cY_cZ_c$ that can be considered instead. Later, after it has been designed, the gear cutting tool will be represented in this coordinate system ($X_cY_cZ_c$).

Let us assume that any desired motion of the gear cutting tool with respect to the work gear can be performed on the machine tool. Any motion of the gear cutting tool relative to the work gear can be substituted with the corresponding motion of the coordinate system $X_cY_cZ_c$ with respect to the coordinate system $X_gY_gZ_g$. This is because the coordinate system $X_gY_gZ_g$ is rigidly connected to the work gear and the coordinate system $X_cY_cZ_c$ is rigidly connected to the gear cutting tool.

Without loss of generality, the coordinate system $X_gY_gZ_g$ can be assumed as stationary. Under this scenario, the principle of inversion of relative motions can be implemented. Following the principle of inversion, in addition to original motions, the coordinate system $X_cY_cZ_c$ performs all the motions that the coordinate system $X_gY_gZ_g$ originally performed.

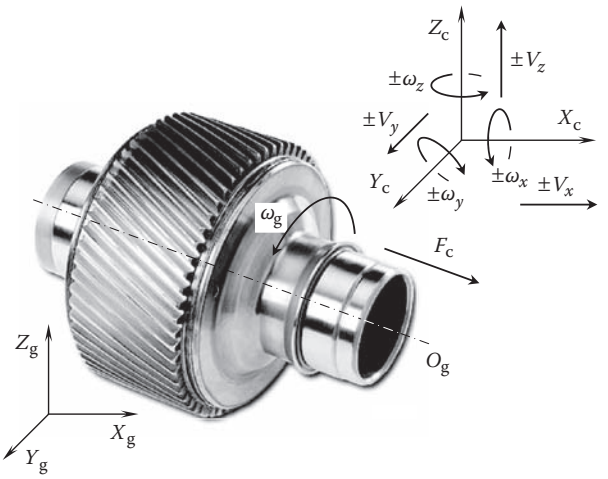

FIGURE 2.2
Elementary relative motions of the work gear and the gear cutting tool.

However, all the additional motions of the coordinate system $X_cY_cZ_c$ are performed in a direction directly opposite their original direction.

Any resultant relative motion of the gear cutting tool relative to the work gear can be decomposed into (1) translations along and (2) rotations about axes of the coordinate system $X_cY_cZ_c$. The total number of elementary translations is limited to three translations: $\pm V_x$, $\pm V_y$, and $\pm V_z$. Similarly, the total number of elementary rotations is limited to three rotations: $\pm\omega_x$, $\pm\omega_y$, and $\pm\omega_z$.

A brief look at the schematic shown in Figure 2.2 makes it clear that not all elementary translations, elementary rotations, and their combinations are feasible when machining a given work gear. Some motions and their combinations are feasible, whereas others are not. Motions of the gear cutting tool relative to the work gear that were not feasible were eliminated from further consideration. For this purpose, it is necessary to distinguish the relative motions of the gear cutting tool that are feasible for machining of a given gear from those that are not. The relative motions of the gear cutting tool relative to the work gear have to be considered in close connection with the geometry of the work gear tooth surfaces [126, 136, 138]. Peculiarities of the geometry of tooth flanks to be machined entail the corresponding peculiarities in the kinematics of surface machining.

2.1.2 Feasible Relative Motions of the Work Gear and the Gear Cutting Tool

Generally speaking, the relative motion of the work gear and the gear cutting tool is a type of spatial relative motion. When machining a gear, the gear cutting tool is moving with respect to the work gear. While moving, the gear cutting tool removes the stock from the gear blank. The machining of a gear is accomplished when the whole stock is removed from the work gear teeth.

To distinguish the feasible relative motions of the gear cutting tool relative to the work gear from those that are not, it is necessary to undertake a comprehensive analysis of the spatial motion of the gear cutting tool with respect to the machined gear. However, when only the qualitative analysis of the relative motion is required, for simplicity, a

two-dimensional (2D)—and not 3D—analysis can be performed instead. With no principal restrictions, results of a 2D analysis could be extended to the 3D case.

Generally speaking, three phases can be distinguished in a motion of the gear cutting tool with respect to the work gear: (1) roughing phase of the relative motion is observed when a tooth of the gear cutting tool approaches the work gear tooth surface; (2) when the motion of the tooth of the gear cutting tool is tangent to the work gear tooth flank, then generation of the tooth surface occurs; (3) when a tooth of the gear cutting tool breaks contact with the machined tooth surface of the work gear, neither roughing nor surface generation occurs.

The analysis in this book is based on particular locations of vector $\mathbf{V}_{c/w} \equiv \mathbf{V}_\Sigma$ of the relative motion of the generating surface T of the gear cutting tool relative to the work gear.

The gear cutting tool performs a certain motion relative to the work gear. The gear tooth surface $\mathcal{G}$ is generated as an enveloping surface to successive positions of the generating surface T of the gear cutting tool. At a certain instant, three different types of points can be distinguished on generating surface T.

At a certain point A (Figure 2.3), the vector of the resultant motion of the gear cutting tool with respect to the work gear is designated as $\mathbf{V}_\Sigma^{(A)}$. Projection $\mathrm{Pr}_\mathbf{n}\mathbf{V}_\Sigma^{(A)}$ of vector $\mathbf{V}_\Sigma^{(A)}$ onto the unit normal vector $\mathbf{n}_T^{(A)}$ to the generating surface T is pointed to the interior of the body of the work gear. Therefore, in the vicinity of point A, the gear cutting tool penetrates the body of the work gear. In this manner, the roughing cutting edges of the cutting tool cut out the stock. No geometrical or kinematical restrictions are imposed on the direction of vector $\mathbf{V}_\Sigma^{(A)}$. Point A is an example of points of the first type.

Relative motions of the type $\mathbf{V}_\Sigma^{(A)}$ are of critical importance when designing roughing teeth of gear cutting tools.

At contact point B (Figure 2.3), the vector of the resultant motion of the gear cutting tool with respect to the work gear is designated as $\mathbf{V}_\Sigma^{(B)}$. Projection $\mathrm{Pr}_\mathbf{n}\mathbf{V}_\Sigma^{(B)}$ of vector $\mathbf{V}_\Sigma^{(B)}$ onto the unit normal vector $\mathbf{n}_T^{(B)}$ to the generating surface T is perpendicular to this unit normal vector, that is, it is tangential to the work gear tooth flank $\mathcal{G}$ ($\mathrm{Pr}_\mathbf{n}\mathbf{V}_\Sigma^{(B)} = 0$). Therefore, in the vicinity of point B the cutting tool does not penetrate the body of the work gear. Cutting edges of the gear cutting tool do not cut out the stock. Generating surface T of the gear cutting tool generates the work gear tooth surface $\mathcal{G}$ in the vicinity of point B. At point B, the motion of the gear cutting tool toward the machined tooth surface $\mathcal{G}$ is not allowed. Vector $\mathbf{V}_{c/w} \equiv \mathbf{V}_\Sigma$ is located within the common tangent plane to surfaces $\mathcal{G}$ and T at point B. This means that only two types of motion are feasible for the moving surface T and the

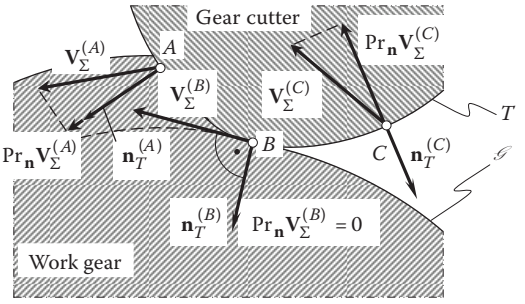

FIGURE 2.3
Various types of elementary motions of the gear cutting tool with respect to the work gear tooth surface.

enveloping surface $\mathcal{G}$. The surfaces can roll and slide over each other. The component of the resultant relative motion $\mathbf{V}_{\Sigma}^{(B)}$ in the direction of the common perpendicular to the surfaces is always equal to zero (Figure 2.3). Point *B* is an example of points of the second type.

Relative motions of the type $\mathbf{V}_{\Sigma}^{(B)}$ are investigated in this text in detail. They are of critical importance when designing finishing teeth of gear cutting tools.

At a certain point *C* (Figure 2.3), the vector of the resultant motion of the gear cutting tool with respect the work gear is designated as $\mathbf{V}_{\Sigma}^{(C)}$. Projection $\mathrm{Pr}_{\mathbf{n}}\mathbf{V}_{\Sigma}^{(C)}$ of vector $\mathbf{V}_{\Sigma}^{(C)}$ onto the unit normal vector $\mathbf{n}_{T}^{(C)}$ to the generating surface *T* is pointed outside of the gear body. Therefore, in the vicinity of point *C*, the cutting edges of the gear cutting tool leave the machined gear tooth surface $\mathcal{G}$. Point *C* is an example of points of the third type.

Evidently, in the vicinity of points of the third type, the tool cutting edges do not cut out the stock and the generating surface *T* of the gear cutting tool does not generate the work gear tooth surface $\mathcal{G}$.

Relative motions of the type $\mathbf{V}_{\Sigma}^{(C)}$ are not covered in this discussion.

When analyzing possible motions of the gear cutting tool relative to the work gear (Figure 2.2), the results derived from the analysis in Figure 2.3 are useful.

2.2 Rolling of the Conjugate Surfaces

Two types of relative motions are of particular interest to the designer of gear cutting tools. The sliding motion over surfaces $\mathcal{G}$ and *T* is one of these motions. Very few types of surfaces allow for a motion of this sort. Surfaces of this type are briefly discussed in Section 1.3. The interested reader is referred to refs. [151, 172] and other sources for more details on this subject.

Rolling of the generating surface *T* of the gear cutting tool over the work gear tooth surface $\mathcal{G}$ is the second type of feasible relative motions. Satisfaction of the condition of contact $\mathbf{n} \cdot \mathbf{V}_{\Sigma} = 0$ is the analytical requirement for rolling motion. In most cases of rolling, sliding of surfaces $\mathcal{G}$ and *T* is also observed. Therefore, pure rolling is distinguished from rolling with sliding. In the first case, no sliding of surfaces $\mathcal{G}$ and *T* is observed ($\mathbf{V}_{\Sigma} = 0$). In the second ($\mathbf{V}_{\Sigma} \neq 0$), surfaces $\mathcal{G}$ and *T* move with respect to each other in a direction that is within the common tangent plane.

When tooth surface $\mathcal{G}$ of the work gear and generating surface *T* of the cutting tool are rolling over each other, with or without sliding, two auxiliary surfaces can be rigidly associated with them. In a particular case, auxiliary surfaces have a property that allows surfaces to roll over each other with no sliding between them. Auxiliary surfaces of this particular geometry are referred to as *axodes*. The axode of the gear tooth surface is rigidly connected to the tooth flank $\mathcal{G}$. The axode of the generating surface *T* of the gear cutting tool is rigidly connected to the gear cutting tool itself. Thus, the relative motion of the work gear and the gear cutting tool can be viewed as rolling of one axode over another axode.

Depending on the actual configuration of axes of rotation of the axodes, the instant relative motion of the axodes can be interpreted as a type of instant screw motion. Instant screw motion of the axodes features a certain axis of the instant screw motion, as well as a screw parameter of the motion. Relative motion of the general type of axodes is of interest to the designer of gear cutting tools. However, specific types of relative motion can also be of particular interest.

First, the relative screw motion of axodes can occur about the axis of the screw motion, location, and orientation of which are fixed in space. This type of relative motion of axodes is referred to as the ordinary screw motion of axodes. The ordinary screw motion of axodes can be decomposed into two elementary motions—translation could be one of these motions and rotation could be another. Furthermore, the speed of one of these two elementary motions can be equal to zero. If the speed of the translation motion becomes zero, then the ordinary screw motion reduces to the corresponding rotation. Conversely, when the speed of the rotation is equal to zero, the elementary screw motion reduces to the corresponding translation. In this manner, rolling of axodes in the form of ordinary screw surfaces reduces to rolling of axodes of a simpler shape. Rolling of two circular cylinders with parallel axes is a perfect example of this setup.

3

Kinematics of Continuously Indexing Methods of Gear Machining Processes

Methods of gear machining featuring continuous indexing are widely used in industry. Gear hobbing, gear shaping, gear shaving, etc., are good examples of gear machining operations of this type.

Numerous efforts had been undertaken to investigate the surface generation process using continuously indexing methods of surface machining (e.g., [4, 18, 138, 143, 180, 181, 186]).

Meshing of two toothed bodies is imitated when machining a gear using a continuously indexing method. Under such a scenario, the work gear and the gear cutting tool perform motions in a properly timed manner. Interaction of the imaginary gear to be machined and of the generating surface of the gear cutting tool (which also is a phantom surface) can be interpreted as a type of virtual gear mesh. Virtual mesh of the imaginary gear to be machined and the generating surface of the gear cutting tool is referred to as the *gear machining mesh*. Gear machining mesh allows for interpretation in the form of a *work gear to generation surface* mesh, or briefly, $\mathcal{G}$ to T mesh.

The tooth ratio of the gear machining mesh is constant when ordinary gears are machining (see Section 1.1). Tooth ratio can be expressed in terms of the angle of rotation of the work gear when machining a noncircular gear. This issue, however, is not within the scope of this book.

Gear machining mesh plays an important role in the investigation and design of gear cutting tools. Any particular type of a gear cutting tool is designed on the premise of a certain gear machining mesh. Because of this, investigation of all types of gear machining meshes having a constant tooth ratio is of critical importance to researchers and gear cutting tool designers.

An analytical study of the gear machining mesh that is discussed in the following sections, is based on the vector representation of the gear machining mesh.

3.1 Vector Representation of the Gear Machining Mesh

Relative motions of the work gear and the generating surface of the gear cutting tool, which take place when the gear is being machined, are a type of uniform motions. This means that the rotation of the work gear ω_g and the rotation of the generating surface of the gear cutting tool ω_c are synchronized so that the ratio ω_g/ω_c is constant in time.

A uniform translation and a uniform rotation are good examples of uniform motions. Under certain circumstances, a uniform translation and a uniform rotation can be combined so that the resultant motion is a type of uniform screw motion. Screw motion is the most general type of uniform motions.

A uniform screw motion allows for representation in the form of summa of two motions: translation and rotation. The translation vector is designated as **V**, whereas rotation vector is denoted by **ω**.

The translation vector **V** and the rotation vector **ω** are sliding vectors. This means that a gear cutting tool designer is free to choose an appropriate point at which vectors **V** and **ω** are applied.

Both vectors **ω** and **V**, which comprise the uniform screw motion, are collinear vectors. They are acting along axis O_{sc} of the screw motion. Axis O_{sc} of the screw motion aligns with axis O of rotation **ω**.

In reality, vectors **ω** and **V** are pointed either in the same direction or in opposite directions. Depending on the actual configuration of vectors **ω** and **V**, the resultant uniform screw motion is recognized either as the left-hand–oriented or the right-hand–oriented screw motion. When vectors **ω** and **V** are pointed in the same direction, the resultant screw motion is known as a left-hand–oriented screw motion. Conversely, when vectors **ω** and **V** are in opposite directions, the resultant screw motion is a right-hand–oriented screw motion.

Theoretically, a screw motion can be simultaneously performed by the work gear and the gear cutting tool. The kinematics of the gear machining process of this type is physically feasible. However, this case has no practical importance. Machine tools of complex, and thus impractical, kinematics are required for this purpose. Further analysis is limited to the kinematics of the gear machining mesh composed just of two rotations about skew axis. Results of the analysis obtained in this manner will cover all known methods of gear machining. They also will cover all known and possible shapes of generating surfaces of gear cutting tools. This makes the theory complete and self-consistent.

In a gear machining mesh, the work gear and the gear cutting tool rotate about their axis, O_g and O_c, respectively. Rotation of the work gear is denoted by $\boldsymbol{\omega}_g$, and $\boldsymbol{\omega}_c$ is the rotation of the gear cutting tool. The inequalities $\boldsymbol{\omega}_g \neq 0$ and $\boldsymbol{\omega}_c \neq 0$ are commonly observed. Only in particular cases, for example, when machining a gear with the rack cutter, etc., the cutting tool rotation is equal to zero ($\boldsymbol{\omega}_c = 0$).

Rotation vector $\boldsymbol{\omega}_g$ of the gear is aligned with axis O_g of the rotation of the gear. Vector $\boldsymbol{\omega}_g$ is pointed in a direction that corresponds to the right screw (Figure 3.1). Magnitude ω_g of the rotation vector $\boldsymbol{\omega}_g$ is proportional to the revolutions per minute (RPM) of the gear. A point at which vector $\boldsymbol{\omega}_g$ is applied is discussed below.

In Figure 3.1, the rotation vector $\boldsymbol{\omega}_c$ is assigned to the gear hob. Vector $\boldsymbol{\omega}_c$ is very much similar to rotation vector $\boldsymbol{\omega}_g$. Vector $\boldsymbol{\omega}_c$ is aligned with the axis of rotation O_c of the hob. The direction of vector $\boldsymbol{\omega}_c$ corresponds to the hand of the screw of the generating surface of the hob. The magnitude $\boldsymbol{\omega}_c$ of the rotation vector $\boldsymbol{\omega}_c$ is proportional to the hob rotation. A point at which vector $\boldsymbol{\omega}_c$ is applied is discussed below.

Rotations $\boldsymbol{\omega}_g$ and $\boldsymbol{\omega}_c$ relate to each other in compliance with the proportion $\boldsymbol{\omega}_g N_g = \boldsymbol{\omega}_c N_c$. Here, N_g denotes the number of teeth of the work gear, N_c is the number of teeth/threads of the gear cutting tool, and the equalities $\boldsymbol{\omega}_g = |\boldsymbol{\omega}_g|$ and $\boldsymbol{\omega}_c = |\boldsymbol{\omega}_c|$ are observed.

Axes O_g and O_c of rotations $\boldsymbol{\omega}_g$ and $\boldsymbol{\omega}_c$ are at a certain distance $C_{g/c}$. The distance $C_{g/c}$ is measured along the centerline and is referred to as *center distance*. The length of the center distance is equal to the closest distance of approach of the crossing axes O_g and O_c.

The angle between the crossing axes O_g and O_c is an important consideration.

As shown in Figure 3.2, the angle between two skew straight lines L_1 and L_2 is usually measured between one of the lines, say line L_1, and some other straight line that intersects line L_1 and is parallel to line L_2. In this case, either the acute angle Σ or the obtuse angle

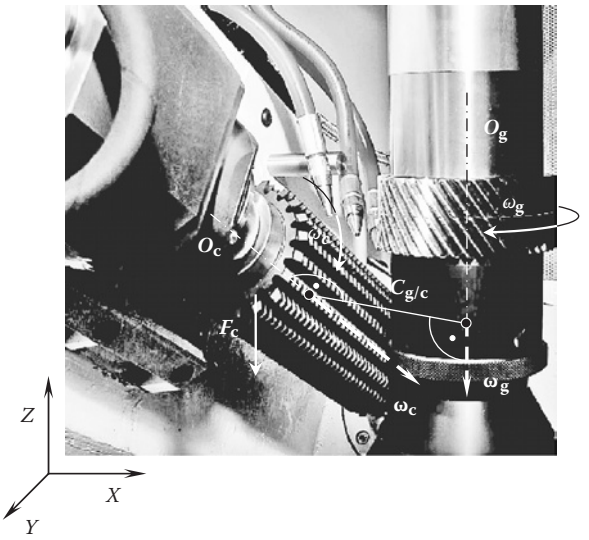

FIGURE 3.1
Configuration of the rotation vectors $\boldsymbol{\omega}_g$ and $\boldsymbol{\omega}_c$ of the work gear and the gear cutting tool in the gear machining mesh.

Σ^* can be used for the purpose of specifying the crossed angle between two skew lines, L_1 and L_2 (Figure 3.2a). Both cases are equivalent to each other.

When vectors $\mathbf{s}_1$ and $\mathbf{s}_2$ are associated with straight lines L_1 and L_2, the crossed-axis angle between the lines is uniquely specified. Depending on the actual directions of vectors $\mathbf{s}_1$ and $\mathbf{s}_2$, the crossed-axis angle Σ is either acute (Figure 3.2b) or obtuse (Figure 3.2c). No ambiguities are observed with the crossed-axis angle Σ if the vectors are assigned to crossing straight lines.

The crossing angle of axes O_g and O_c in the gear machining mesh is designated as Σ. The crossed-axis angle Σ is the angle that rotation vectors $\boldsymbol{\omega}_g$ and $\boldsymbol{\omega}_c$ make with each other $[\Sigma = \angle(\boldsymbol{\omega}_g, \boldsymbol{\omega}_c)]$. For a crossed-axis angle having an acute value, $\Sigma < 90°$, the value is equal to that which is commonly understood under the term *crossed-axis angle*. For obtuse angles, $\Sigma > 90°$, the equality $\overline{\Sigma} = 180° - \Sigma$ is observed. Here, $\overline{\Sigma}$ denotes the crossed-axis angle in the common meaning of the term.

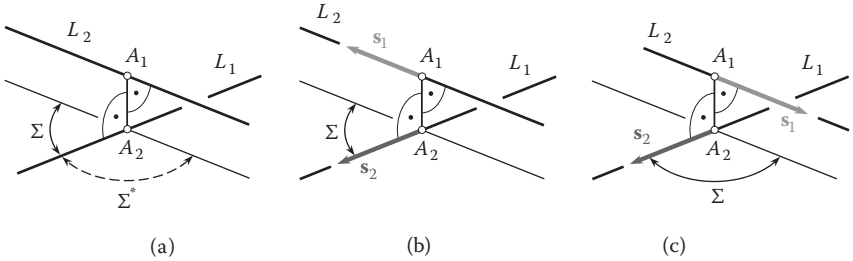

FIGURE 3.2
Crossed-axis angle Σ between two skew straight lines L_1 and L_2.

The kinematics of most gear machining methods is not limited to the motions required for gear machining meshes. In the example shown in Figure 3.1, in addition to rotations $\boldsymbol{\omega}_g$ and $\boldsymbol{\omega}_c$, one more motion is taking place when a gear is being machined. This motion is the axial feed F_c of the cutter. The feed motion F_c is occurring in the axial direction of the work gear. Depending on the design peculiarities of the hobber, either the hob moves with respect to the work gear or the worktable of the hobber is moving relative to the rotating hob.

The feed motion F_c of the cutter causes sliding of the gear tooth surface $\mathcal{G}$ over it. When analyzing the kinematics of a gear machining operation, feed motions of this type can be omitted from consideration.

The kinematics of the gear machining process shown in Figure 3.1 is widely used in conventional hobbers for machining cylindrical gears, and also spur gears and helical gears. It is easy to see that in nature (see Figure 3.1) the kinematics of the gear machining process is an invertible one. The invertibility of the kinematics of the gear machining process means that the work gear can be replaced with the gear cutting tool and vice versa. For example, in Figure 3.1, the work gear can be replaced with the gear shaper, whereas the hob can be replaced with the blank of a worm. Under such a scenario, the worm can be machined when performing the same rotations $\boldsymbol{\omega}_g$ and $\boldsymbol{\omega}_c$, and moving the cutter in the axial direction of the work gear axis O_g with feed motion F_c. In this case, the feed motion F_c causes the sliding of the worm surface over it. Machining operation of this type is physically possible; however, it is not yet used in practice. A conversion similar to what has just been discussed is valid to all types of kinematics of gear machining processes. When converting a principal kinematics of the gear machining process into a practical version, it is recommended to keep in mind the possibility of both principal kinematics of gear machining, that is, the original and the converted kinematics of the gear machining process.

Relative motion of the work gear and the gear cutting tool can be specified by the vector $\boldsymbol{\omega}_{pl}$ of instant rotation. For the determination of the rotation vector $\boldsymbol{\omega}_{pl}$, implementation of the principle of inversion is convenient. This principle is illustrated in Figure 3.3.

In reality, the work gear and the gear cutting tool rotate about their axes. The rotations are specified by rotation vectors $\boldsymbol{\omega}_g$ and $\boldsymbol{\omega}_c$ as shown in Figure 3.3a. To make the work gear stationary, the work gear must undergo one more rotation, $-\boldsymbol{\omega}_g$. Summa of the initial rotation $\boldsymbol{\omega}_g$ and of the additional rotation in the opposite direction $-\vec{\boldsymbol{\omega}}_g$ is equal to zero, $\boldsymbol{\omega}_g + (-\boldsymbol{\omega}_g) \equiv 0$. In this manner, the work gear is rendered stationary. To avoid making any changes to the rest of the elements of the gear machining mesh, the gear cutting tool must also perform an additional rotation $-\boldsymbol{\omega}_g$ (Figure 3.3b). Under this scenario, the resultant rotation of the gear cutting tool relative to the motionless work gear is specified by the vector of instant rotation

$$\boldsymbol{\omega}_{c/g} = \boldsymbol{\omega}_c + (-\boldsymbol{\omega}_g) \tag{3.1}$$

Vector $\boldsymbol{\omega}_{c/g}$ of the instant rotation of the gear cutting tool with respect to the work gear is applied at pitch point P (Figure 3.3b).

In the manner similar to that just discussed, vector $\boldsymbol{\omega}_{g/c}$ of the instant rotation of the work gear with respect to the gear cutting tool can be constructed (Figure 3.3c). This rotation vector can be calculated as

$$\boldsymbol{\omega}_{g/c} = \boldsymbol{\omega}_g + (-\boldsymbol{\omega}_c) \tag{3.2}$$

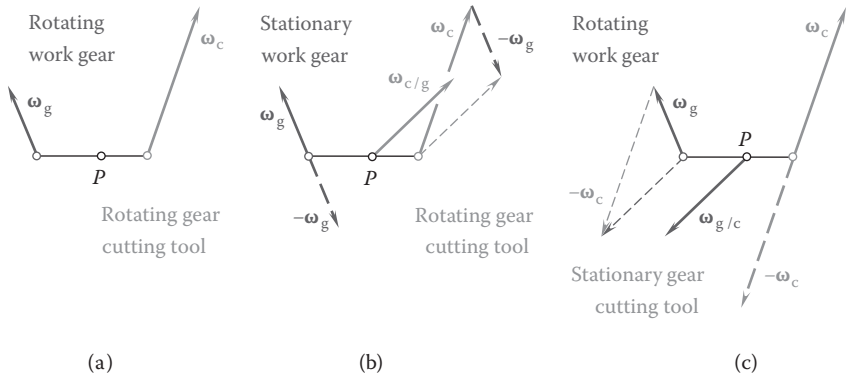

FIGURE 3.3
The principle of the inversion of two rotations.

Evidently, rotation vectors $\boldsymbol{\omega}_{c/g}$ and $\boldsymbol{\omega}_{g/c}$ are of the same magnitude [$|\boldsymbol{\omega}_{c/g}| = |\boldsymbol{\omega}_{g/c}|$] and are pointed opposite to each other.

Assume that the work gear and the gear cutting tool together are rotated about the work gear axis O_g. This rotation is specified by the rotation vector $-\boldsymbol{\omega}_g$. As the rotation $-\boldsymbol{\omega}_g$ is applied, the work gear becomes stationary

$$\boldsymbol{\omega}_g + (-\boldsymbol{\omega}_g) \equiv 0 \tag{3.3}$$

The resultant rotation of the gear cutting tool can be specified by the vector $\boldsymbol{\omega}_c + (-\boldsymbol{\omega}_g)$, which is equal to the vector $\boldsymbol{\omega}_{pl}$ of instant rotation of the gear cutting tool relative to the work gear

$$\boldsymbol{\omega}_{pl} = \boldsymbol{\omega}_c + (-\boldsymbol{\omega}_g) \tag{3.4}$$

Similarly, the rotation vector of the work gear relative to the gear cutting tool can be determined. Evidently, this rotation vector is equal to $-\boldsymbol{\omega}_{pl}$.

The rotation vector $\boldsymbol{\omega}_{pl}$ is aligned with the instant axis of rotation P_{ln}. Axis of instant rotation is often called the *pitch line* P_{ln}. Once the configuration of rotation vectors $\boldsymbol{\omega}_g$ and $\boldsymbol{\omega}_c$ is known, say rotation vectors $\boldsymbol{\omega}_g$ and $\boldsymbol{\omega}_c$ are specified in a certain reference system, the vector $\boldsymbol{\omega}_{pl}$ of the instant rotation as well as the pitch line P_{ln} can be obtained following the common rules known from vector algebra.

As an example, consider two rotation vectors, $\boldsymbol{\omega}_g$ and $\boldsymbol{\omega}_c$, as shown in Figure 3.4. The configuration of the rotation vectors is initially given in the system of two planes of projections, π_1 and π_2. Vectors $\boldsymbol{\omega}_g$ and $\boldsymbol{\omega}_c$ are the principal elements of the gear machining mesh. The rest of the important elements of the kinematics of the gear machining process can be drawn up from the *vector diagram of the gear machining mesh*. The diagram is constructed based on the rotation vectors $\boldsymbol{\omega}_g$ and $\boldsymbol{\omega}_c$ of the work gear and the gear cutting tool, respectively.

Generally speaking, vectors $\boldsymbol{\omega}_g$ and $\boldsymbol{\omega}_c$ can occupy an arbitrary location and orientation in the reference system $\pi_1\pi_2$. For convenience of the analysis, vectors $\boldsymbol{\omega}_g$ and $\boldsymbol{\omega}_c$ are shown parallel to the plane of projections π_1. The crossed-axis angle Σ is projected onto the horizontal plane of projections π_1 with no distortion. Similarly, the center distance $C_{g/c}$ is projected onto the vertical plane of projections π_2 with no distortion.

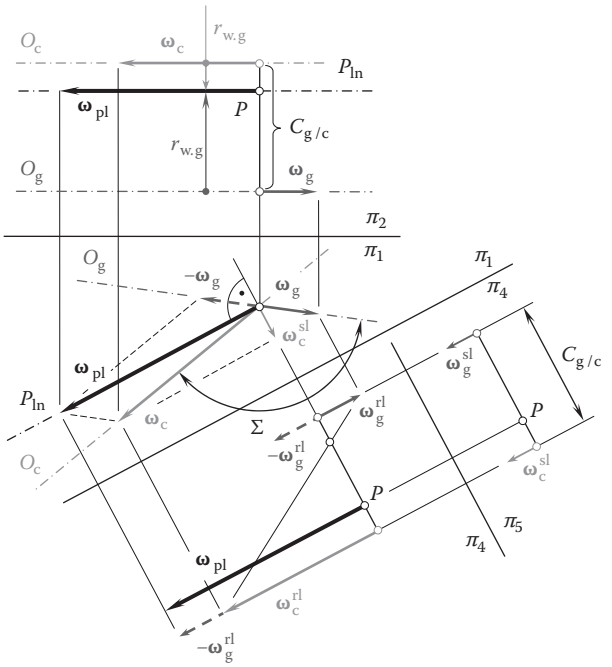

FIGURE 3.4
Vector diagram of a gear machining mesh.

In the plane of projections π_1, vector $\boldsymbol{\omega}_{pl}$ of the instant rotation is determined in terms of rotation vectors $\boldsymbol{\omega}_g$ and $\boldsymbol{\omega}_c$ [see Equation (3.4)]. Vector $\boldsymbol{\omega}_{pl}$ is applied at pitch point P, the location of which is not specified yet. It is known only that pitch point P is located within the straight-line segment $C_{g/c}$.

An additional plane of projections, π_4, is constructed for the purpose of determining the location of pitch point P. Within the plane of projections π_1, the axis of projections π_1/π_4 is passing parallel to the vector of instant rotation $\boldsymbol{\omega}_{pl}$. Because of this, the components $\boldsymbol{\omega}_g^{rl}$ and $\boldsymbol{\omega}_c^{rl}$ of rotation vectors $\boldsymbol{\omega}_g$ and $\boldsymbol{\omega}_c$ are projected with no distortions onto the plane of projections π_4. Both $\boldsymbol{\omega}_g^{rl}$ and $\boldsymbol{\omega}_c^{rl}$ are parallel to the vector of instant rotation $\boldsymbol{\omega}_{pl}$

$$\boldsymbol{\omega}_g^{rl} \left\| \boldsymbol{\omega}_c^{rl} \right\| \boldsymbol{\omega}_{pl} \tag{3.5}$$

Magnitudes ω_g^{rl} and ω_c^{rl} of the components $\boldsymbol{\omega}_g^{rl}$ and $\boldsymbol{\omega}_c^{rl}$ relate to each other the way that equality

$$\omega_g^{rl} r_{w.g} = \omega_c^{rl} r_{w.c} \tag{3.6}$$

is observed. Here, $r_{w.g}$ and $r_{w.c}$ denote distances of pitch point P from gear axis O_g and from gear cutting tool axis O_c, respectively.

The distances $r_{w.g}$ and $r_{w.c}$ are signed values. Their algebraic summa is equal to the center distance $C_{g/c}$

$$r_{w.g} + r_{w.c} = C_{g/c} \tag{3.7}$$

Ultimately, components $\boldsymbol{\omega}_g^{rl}$ and $\boldsymbol{\omega}_c^{rl}$ result in pure rolling of the axodes of the work gear and the gear cutting tool over each other.

It is important to point out that vectors $\boldsymbol{\omega}_g^{rl}$ and $\boldsymbol{\omega}_c^{rl}$ represent instant rotations, whereas vectors $\boldsymbol{\omega}_g$ and $\boldsymbol{\omega}_c$ describe continuous rotations.

Within the plane of projections π_4, rotation vectors $\boldsymbol{\omega}_g$ and $\boldsymbol{\omega}_c$ are constructed following the conventional rules developed in descriptive geometry. The location of pitch point P within the center distance $C_{g/c}$ becomes evident immediately after the projections of vectors $\boldsymbol{\omega}_g$ and $\boldsymbol{\omega}_c$ are constructed within the plane of projections π_4. Furthermore, the projection of pitch point P can be constructed within the plane of projections π_2.

Two other components, $\boldsymbol{\omega}_g^{sl}$ and $\boldsymbol{\omega}_c^{sl}$, of the rotation vectors $\boldsymbol{\omega}_g$ and $\boldsymbol{\omega}_c$ are perpendicular to the vector of instant rotation $\boldsymbol{\omega}_{pl}$

$$\boldsymbol{\omega}_g^{sl} \perp \boldsymbol{\omega}_{pl} \quad \text{and} \quad \boldsymbol{\omega}_c^{sl} \perp \boldsymbol{\omega}_{pl} \tag{3.8}$$

With no distortions, components $\boldsymbol{\omega}_g^{sl}$ and $\boldsymbol{\omega}_c^{sl}$ are projected onto the plane of projections π_5. The axis of projections π_4/π_5 is erected perpendicular to the axis of projections π_1/π_4. Vectors $\boldsymbol{\omega}_g^{sl}$ and $\boldsymbol{\omega}_c^{sl}$ are equal to each other; therefore, the equality $\boldsymbol{\omega}_g^{sl} = \boldsymbol{\omega}_c^{sl}$ is valid. Components $\boldsymbol{\omega}_g^{sl}$ and $\boldsymbol{\omega}_c^{sl}$ cause pure sliding of the axodes of the work gear and the gear cutting tool relative to each other.

It is important to point out that, similar to vectors $\boldsymbol{\omega}_g^{rl}$ and $\boldsymbol{\omega}_c^{rl}$, vectors $\boldsymbol{\omega}_g^{sl}$ and $\boldsymbol{\omega}_c^{sl}$ also represent instant rotations, whereas vectors $\boldsymbol{\omega}_g$ and $\boldsymbol{\omega}_c$ describe continuous rotations.

The $\boldsymbol{\omega}_g^{rl} = \boldsymbol{\omega}_c^{rl}$ equality should not be confusing. Aside from the fact that components $\boldsymbol{\omega}_g^{sl}$ and $\boldsymbol{\omega}_c^{sl}$ are pointed in the same direction, the corresponding linear sliding velocities $\mathbf{V}_g^{sl}$ and $\mathbf{V}_c^{sl}$ have the following properties: (a) vectors $\mathbf{V}_g^{sl}$ and $\mathbf{V}_c^{sl}$ are pointed in opposite directions and (b) they are of different magnitudes. The first is because the pitch point is located within the center distance $C_{g/c}$ and not outside this straight-line segment. The second is attributed to the fact that usually distances $r_{w.g}$ and $r_{w.c}$ are not equal to each other ($r_{w.g} \neq r_{w.c}$).

In some cases, axodes of the rotating work gear and the gear cutting tool are used for the analysis of the gear machining mesh. Axodes are two surfaces, one of which is associated with the work gear and the other with the gear cutting tool. When a continuously indexing method of machining is used for machining a work gear, the axodes roll over each other. It is commonly understood that axodes are rolling with no sliding between them. It is noteworthy that components $\boldsymbol{\omega}_g^{rl}$ and $\boldsymbol{\omega}_c^{rl}$ of rotations $\boldsymbol{\omega}_g$ and $\boldsymbol{\omega}_c$ result in pure rolling (with no sliding) of the axodes. However, components $\boldsymbol{\omega}_g^{sl}$ and $\boldsymbol{\omega}_c^{sl}$ always cause sliding of the axodes when rotation vectors $\boldsymbol{\omega}_g$ and $\boldsymbol{\omega}_c$ are crossed. This type of sliding is unavoidable in nature when rotations take place about crossing axes.

Components $\boldsymbol{\omega}_g^{sl}$ and $\boldsymbol{\omega}_c^{sl}$ usually are strongly undesired when designing an elementary gear drive. It is common practice for gear designers to reduce the sliding velocity to its lowest possible range. Components $\boldsymbol{\omega}_g^{sl}$ and $\boldsymbol{\omega}_c^{sl}$ result in sliding of the axodes of the work gear and the gear cutting tool. Sliding of the axodes unavoidably entails the corresponding sliding of the tooth flanks in the lengthwise direction of the gear tooth. In this way, sliding components $\boldsymbol{\omega}_g^{sl}$ and $\boldsymbol{\omega}_c^{sl}$ reduce the performance of the elementary gear drive.

On the other hand, components $\boldsymbol{\omega}_g^{sl}$ and $\boldsymbol{\omega}_c^{sl}$ of rotation vectors $\boldsymbol{\omega}_g$ and $\boldsymbol{\omega}_c$ can also be useful when designing a gear cutting tool. Relative sliding of the axodes can be used as the primary (cutting) motion. Under this scenario, it is highly desirable to increase the sliding velocity to its highest possible range. In this way, the efficiency of the gear machining process can be significantly improved.

The analysis shown in Figure 3.4 makes it possible to conclude that pure rolling of the axodes of the work gear and the gear cutting tool occurs if and only if rotation vectors $\boldsymbol{\omega}_g$ and $\boldsymbol{\omega}_c$ are located within a common plane. Otherwise, sliding of the axodes is unavoidable in nature. For gear machining mesh having either parallel or intersecting axes of rotation, axes O_g and O_c are located within a common plane by definition. Therefore, no sliding occurs in these cases. Sliding of axodes occurs if and only if the work gear and the gear cutting tool are rotating about skew axis O_g and O_c, or in other words, only rotations about skew axes allow for relative sliding of the axodes.

Sliding of the gear tooth flanks is proportional to the sliding rotation $\omega^{sl} = \omega_g^{sl} \equiv \omega_c^{sl}$. For a given point of interest within the line of contact of the axodes, gear teeth sliding is also proportional to the distance of the point from the pitch line P_{ln}. Keep in mind that configuration of the pitch line P_{ln} is a function of the center distance $C_{g/c}$.

The following conclusions can be drawn from the preceding analysis:

1. No sliding of axodes is observed when axes of rotation of the work gear and the gear cutting tool are located within a common plane.
2. Only rotations about skew axes allow for the relative sliding of axodes.
3. For rotations about skew axes, sliding of axodes of the gear machining mesh becomes more significant as the crossed-axis angle Σ increases. Thus, the condition $\Sigma \to 180°$ can be interpreted as the condition for maximal sliding of axodes of the gear machining mesh.
4. For rotations about skew axes, sliding of axodes of the gear machining mesh becomes smaller as the crossed-axis angle Σ decreases. Thus, the condition $\Sigma \to 0°$ can be interpreted as the condition for minimum sliding of axodes of the gear machining mesh.

In reality, a gear machining mesh can be specified just by two rotation vectors, $\boldsymbol{\omega}_g$ and $\boldsymbol{\omega}_c$, and by center distance $C_{g/c}$. The rest of the vectors used for analyzing the kinematics of the gear machining mesh can be expressed in terms of vectors $\boldsymbol{\omega}_g$ and $\boldsymbol{\omega}_c$ and center distance $C_{g/c}$.

3.2 Kinematic Relationships for the Gear Machining Mesh

Consider two rotations about skew axes as schematically illustrated in Figure 3.5. From the geometrical/kinematical standpoint, two rotations about skew axes O_g and O_c can be interpreted as the rolling of a hyperboloid of one sheet over another hyperboloid of one sheet. The one-sheet hyperboloids of rotation serve as axodes of the gear machining mesh. Axes of rotation of the axodes align with the vectors of rotations $\boldsymbol{\omega}_g$ and $\boldsymbol{\omega}_c$. The straight generating line of the axodes aligns with the vector of instant rotation $\boldsymbol{\omega}_{pl}$. Vector $\boldsymbol{\omega}_{pl}$ describes the instant rotation of axodes about pitch line P_{ln}.

Two rotation vectors, $\boldsymbol{\omega}_g$ and $\boldsymbol{\omega}_c$, are crossing at a certain crossed-axis angle Σ. Axes of rotations $\boldsymbol{\omega}_g$ and $\boldsymbol{\omega}_c$ are remote from each other at a center distance $C_{g/c}$, as shown in Figure 3.5. For the given configuration of rotation vectors $\boldsymbol{\omega}_g$ and $\boldsymbol{\omega}_c$, the corresponding vector of instant rotation $\boldsymbol{\omega}_{pl}$ is constructed in Figure 3.5a.

Consider the projections of rotation vectors $\boldsymbol{\omega}_g$, $\boldsymbol{\omega}_c$, and $\boldsymbol{\omega}_{pl}$ onto a plane that is orthogonal to the straight line segment $C_{g/c}$. Projections of rotation vectors $\boldsymbol{\omega}_g$ and $\boldsymbol{\omega}_c$ onto pitch

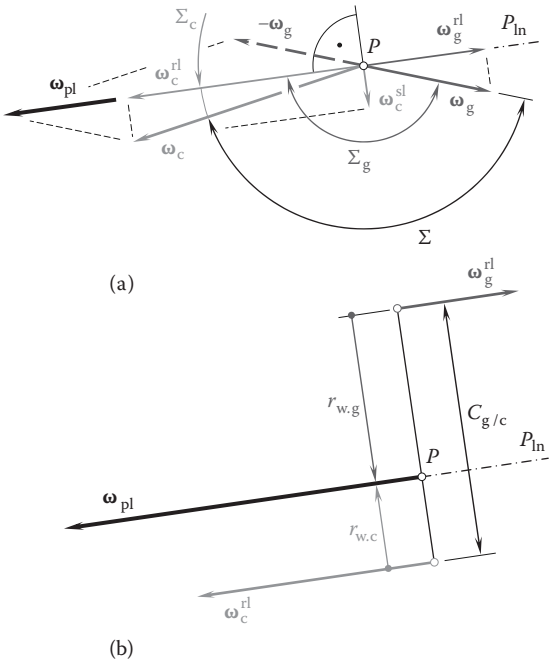

FIGURE 3.5
Derivation of the principal kinematic relationships for the gear machining mesh.

line P_{ln} are designated as $\boldsymbol{\omega}_g^{rl}$ and $\boldsymbol{\omega}_c^{rl}$, respectively. These components cause pure rotation of the axodes. Projections of rotation vectors $\boldsymbol{\omega}_g$ and $\boldsymbol{\omega}_c$ onto a direction that is perpendicular to pitch line P_{ln} are designated as $\boldsymbol{\omega}_g^{sl}$ and $\boldsymbol{\omega}_c^{sl}$. These components cause sliding of the axodes. It can be proven that components $\boldsymbol{\omega}_g^{sl}$ and $\boldsymbol{\omega}_c^{sl}$ always have the same magnitude and direction. Therefore, the equality $\boldsymbol{\omega}_g^{sl} = \boldsymbol{\omega}_c^{sl}$ is observed.

The components $\boldsymbol{\omega}_g^{rl}$ and $\boldsymbol{\omega}_c^{rl}$ are within a common plane through the straight-line segment $C_{g/c}$. The location of pitch point P within the straight-line segment $C_{g/c}$ is specified by the ratio $\boldsymbol{\omega}_g^{rl} r_g = \boldsymbol{\omega}_c^{rl} r_c$ [see Equation (3.6)] and is presented in Figure 3.4.

It is noteworthy that in particular applications, it is convenient to represent Equation (3.4) in the form

$$\frac{r_{w.g}}{(\omega_g^{rt})^{-1}} = \frac{r_{w.c}}{(\omega_c^{rt})^{-1}} \tag{3.9}$$

where it is not the rotations ω_g^{rl} and ω_c^{rl} themselves, but the inverse values $(\omega_g^{rl})^{-1}$ and $(\omega_c^{rl})^{-1}$, are used instead. The inverse values $(\omega_g^{rl})^{-1}$ and $(\omega_c^{rl})^{-1}$ are often referred to as *rotation frequencies*.

Because $r_{w.g} + r_{w.c} = C_{g/c}$ [see Equation (3.7)], for the radius $r_{w.c}$ the expression

$$r_{w.c} = C_{g/c} - r_{w.g} \tag{3.10}$$

is valid. After substitution of the last expression for $r_{w.c}$, Equation (3.6) can be cast into

$$\omega_g^{rl} r_{w.g} = \omega_c^{rl} (C_{g/c} - r_{w.g}) \tag{3.11}$$

Elementary formulae transformations yield the expression

$$r_{w.g} = \frac{1 + \omega_c - \omega_g}{1 + \omega_c} \cdot C_{g/c} \tag{3.12}$$

for the computation of radius $r_{w.g}$ (Figure 3.5b).

After the actual value of radius $r_{w.g}$ is computed, for the computation of radius $r_{w.c}$ the formula $r_{w.c} = C_{g/c} - r_{w.g}$ can be used.

When solving particular problems relating to generation of gear tooth flanks, in addition to vectors $\boldsymbol{\omega}_g^{rl}$ and $\boldsymbol{\omega}_c^{rl}$, it is often convenient to use the corresponding normalized vectors $\bar{\boldsymbol{\omega}}_g^{rl}$ and $\bar{\boldsymbol{\omega}}_c^{rl}$. Vectors $\boldsymbol{\omega}_g^{rl}$ and $\boldsymbol{\omega}_c^{rl}$ are normalized by the value of ω_c^{rl}. In this case, the normalized velocity $\bar{\boldsymbol{\omega}}_c^{rl}$ of the gear cutting tool is equal to unit vector $\bar{\boldsymbol{\omega}}_c^{rl} = \dfrac{\boldsymbol{\omega}_c^{rl}}{\omega_c^{rl}}$, ($|\bar{\boldsymbol{\omega}}_c^{rl}| \equiv 1$). Here, ω_c^{rl} designates the magnitude of vector $\boldsymbol{\omega}_c^{rl}$. The normalized velocity $\bar{\boldsymbol{\omega}}_g^{rl}$ of the gear is equal to a certain value $\bar{\boldsymbol{\omega}}_g^{rl} = \dfrac{\boldsymbol{\omega}_g^{rl}}{\omega_c^{rl}}$, ($0 \le \bar{\boldsymbol{\omega}}_g^{rl} < 1$). The normalized value $\bar{\omega}_c^{rl}$ always exceeds or is equal to the normalized value $\bar{\omega}_g^{rl} = |\bar{\boldsymbol{\omega}}_g^{rl}|$, and the inequality $\bar{\omega}_c^{rl} \ge \bar{\omega}_g^{rl}$ is valid.

Radii $r_{w.g}$ and $r_{w.c}$ of the axodes can also be normalized by $r_{w.c}$. In this case, the normalized radius of the gear cutting tool $\bar{r}_{w.c}$ is equal to unit $\bar{r}_{w.c} = \dfrac{r_{w.c}}{r_{w.c}} \equiv 1$. Accordingly, the normalized radius of the gear $\bar{r}_{w.g}$ is equal to a certain value $\bar{r}_{w.g} = \dfrac{r_{w.g}}{r_{w.c}} \ge 1$. The normalized radius $\bar{r}_{w.c}$ is always smaller or equal to the normalized radius $\bar{r}_{w.g}$. Thus, the inequality $\bar{r}_{w.c} \le \bar{r}_{w.g}$ is observed.

A few more formulae, which are listed below, are useful for the computations.

To compute for the magnitude ω_{pl} of the vector of instant rotation $\boldsymbol{\omega}_{pl}$, the formula

$$\omega_{pl} = \sqrt{(\omega_g^{rl})^2 + (\omega_c^{rl})^2 - 2\omega_g^{rl}\omega_c^{rl}\cos\Sigma} \tag{3.13}$$

can be used.

Angle Σ_g is the angle that component $\boldsymbol{\omega}_g$ makes with vector $\boldsymbol{\omega}_{pl}$ of instant rotation [$\Sigma_g = \angle(\boldsymbol{\omega}_g, \boldsymbol{\omega}_{pl})$]. To compute for Σ_g, the formula

$$\Sigma_g = \frac{1 + \omega_c - \omega_g}{1 + \omega_c} \cdot \Sigma \tag{3.14}$$

can be used. This formula is composed similar to Equation (3.12). Equation (3.14) can be derived based on the relationship

$$\frac{\Sigma_g}{\Sigma_c} = \frac{\omega_c}{\omega_g} \tag{3.15}$$

which is evident. Following the analysis presented in Figure 3.5, for angles Σ_g and Σ_c, the equality

$$\Sigma = \Sigma_g - \Sigma_c \tag{3.16}$$

is valid.

In a particular case, angle Σ_g can be equal to the right angle. The orthogonality $\boldsymbol{\omega}_g^{rl} \perp \boldsymbol{\omega}_{pl}$ occurs when the equality $\omega_{pl} = \sqrt{(\omega_c^{rl})^2 - (\omega_g^{rl})^2}$ is satisfied.

The condition under which vectors $\boldsymbol{\omega}_g$ and $\boldsymbol{\omega}_{pl}$ are orthogonal to each other can be represented in the form of dot product of these vectors

$$\boldsymbol{\omega}_g \cdot \boldsymbol{\omega}_{pl} = 0 \tag{3.17}$$

Similar to Σ_g, angle Σ_c is the angle that component $\boldsymbol{\omega}_c$ makes with the vector $\boldsymbol{\omega}_{pl}$ of instant rotation [$\Sigma_c = \angle(\boldsymbol{\omega}_c, \boldsymbol{\omega}_{pl})$]. Angle Σ_c can be computed as

$$\Sigma_c = \frac{1 + \omega_g - \omega_c}{1 + \omega_g} \cdot \Sigma \tag{3.18}$$

After Σ_g and Σ_c have been computed, it can be shown that the following formulae for projections $\boldsymbol{\omega}_g^{sl}$ and $\boldsymbol{\omega}_c^{sl}$

$$\omega_g^{sl} = \omega_g \cos(\Sigma_g - 90°) = \omega_g \sin \Sigma_g \tag{3.19}$$

$$\omega_c^{sl} = \omega_c \cos(\Sigma_c - 90°) = \omega_c \sin \Sigma_c \equiv \omega_g^{sl} \tag{3.20}$$

are valid.

Similarly, to compute for projections $\boldsymbol{\omega}_g^{rl}$ and $\boldsymbol{\omega}_c^{rl}$, the formulae

$$\omega_g^{rl} = \omega_g \cos \Sigma_g \tag{3.21}$$

$$\omega_c^{rl} = \omega_c \cos \Sigma_c \tag{3.22}$$

$$\frac{\omega_g}{\omega_c} = \frac{\omega_g^{rl}}{\omega_c^{rl}} \frac{\cos \Sigma_c}{\cos \Sigma_g} = \frac{N_c}{N_g} \tag{3.23}$$

can be used.

Magnitudes $\omega_g^{rl} = |\boldsymbol{\omega}_g^{rl}|$ and $\omega_c^{rl} = |\boldsymbol{\omega}_c^{rl}|$ of the components $\boldsymbol{\omega}_g^{rl}$ and $\boldsymbol{\omega}_c^{rl}$ are equal (Figure 3.5a) to

$$\omega_g^{rl} = \omega_g \cos \Sigma_g \tag{3.24}$$

$$\omega_c^{rl} = \omega_c \cos \Sigma_c \tag{3.25}$$

Magnitudes $\omega_g^{sl} = |\boldsymbol{\omega}_g^{sl}|$ and $\omega_c^{sl} = |\boldsymbol{\omega}_c^{sl}|$ of the components $\boldsymbol{\omega}_g^{sl}$ and $\boldsymbol{\omega}_c^{sl}$ are equal to

$$\omega_g^{sl} = \omega_g \sin \Sigma_g \tag{3.26}$$

$$\omega_c^{sl} = \omega_c \sin \Sigma_c \tag{3.27}$$

Rotation vector $\boldsymbol{\omega}_{pl}$ is applied at pitch point P, which is within the center distance $C_{g/c}$. Location of point P satisfies the condition

$$\frac{r_{w.g}}{\omega_c \cos \Sigma_c} = \frac{r_{w.c}}{\omega_g \cos \Sigma_g} = \frac{C_{g/c}}{\omega_{pl}} \tag{3.28}$$

When the principle of inversion is applied to the rotations of the work gear $\boldsymbol{\omega}_g$ and the gear cutting tool $\boldsymbol{\omega}_c$, the work gear becomes stationary and the gear cutting tool performs the resultant instant rotation $\boldsymbol{\omega}_{pl}$ with respect to the work gear. Rotation $\boldsymbol{\omega}_{pl}$ is computed as $\boldsymbol{\omega}_{pl} = \boldsymbol{\omega}_c + (-\boldsymbol{\omega}_g)$ [see Equation (3.4)]. Sliding components ω_g^{sl} and $(-\omega_c^{sl})$ of the rotations $\boldsymbol{\omega}_c$ and $(-\boldsymbol{\omega}_g)$ have the same magnitude but opposite directions. They comprise a rotation pair. This rotation pair is equivalent to a translation motion. Vector $\mathbf{V}^{sl}$ of the translation motion is parallel to vector $\boldsymbol{\omega}_{pl}$ of the instant rotation. Magnitude V^{sl} of the speed of the translation vector $\mathbf{V}^{sl}$ is

$$V^{sl} = |\mathbf{V}^{sl}| = C_{g/c}\omega_g \sin \Sigma_g = C_{g/c}\omega_c \sin \Sigma_c \tag{3.29}$$

The translation vector $\mathbf{V}^{sl}$ is parallel to the rotation vector $\boldsymbol{\omega}_{pl}$. Superposition of two motions, rotation $\boldsymbol{\omega}_{pl}$ and translation $\mathbf{V}^{sl}$, allows for interpretation in the form of a screw motion. Parameter p_{pl} of the screw motion is computed as

$$p_{pl} = \frac{V^{sl}}{\omega_{pl}} = \frac{C_{g/c}\omega_g \sin \Sigma_g}{\omega_{pl}} = \frac{C_{g/c}\omega_c \sin \Sigma_c}{\omega_{pl}} \tag{3.30}$$

Magnitude ω_{pl} of the rotation vector $\boldsymbol{\omega}_{pl}$ is equal to

$$\omega_{pl} = \frac{C_{g/c}\omega_c \cos \Sigma_c}{r_{w.g}} = \frac{C_{g/c}\omega_g \cos \Sigma_g}{r_{w.c}} \tag{3.31}$$

Magnitude ω_{pl} computed from Equation (3.31) can be substituted into Equation (3.30), which can be recast as

$$p_{pl} = r_{w.g} \tan \Sigma_c = r_{w.c} \tan \Sigma_g \tag{3.32}$$

to compute for parameter p_{pl} of the resultant instant screw motion.

Ultimately, an expression for the ratio

$$\frac{r_{w.g}}{r_{w.c}} = \frac{\tan \Sigma_g}{\tan \Sigma_c} \tag{3.33}$$

can be derived.

The preceding analysis reveals that summa of two rotations about skew axes allows for interpretation in the form of an instant screw motion.

3.3 Configuration of the Vectors of Relative Motions

The variety of all possible types of gear machining meshes strongly depends on the feasible configurations of rotation vectors $\boldsymbol{\omega}_g$ and $\boldsymbol{\omega}_c$. Rotations $\boldsymbol{\omega}_g$ and $\boldsymbol{\omega}_c$ can be implemented to develop a scientific classification of all possible types of gear machining meshes.

3.3.1 Principal Features of Configuration of the Rotation Vectors

Two arbitrary rotation vectors, $\boldsymbol{\omega}_g$ and $\boldsymbol{\omega}_c$, are shown in Figure 3.6. Vectors $\boldsymbol{\omega}_g$ and $\boldsymbol{\omega}_c$ are at a certain center distance $C_{g/c}$. A Cartesian coordinate system XYZ is associated with the vectors $\boldsymbol{\omega}_g$ and $\boldsymbol{\omega}_c$, and with the straight-line segment $C_{g/c}$. The origin of the reference system XYZ is located at pitch point P. Axis X is aligned with the straight-line segment $C_{g/c}$; axis Z is aligned with the vector of instant rotation $\boldsymbol{\omega}_{pl}$, and axis Y complements axes X and Z to the left-hand–oriented Cartesian coordinate system XYZ.

For further analysis, it is convenient to introduce a unit vector, $\mathbf{c}$. Vector $\mathbf{c}$ is along the X-axis and pointed in the positive direction of the X-axis.

The newly introduced unit vector $\mathbf{c}$ allows for the simple analytical representation of two vectors, $\mathbf{C}_g$ and $\mathbf{C}_c$ (Figure 3.6). Vector $\mathbf{C}_g$ specifies the center distance of the axes O_g and P_{ln}

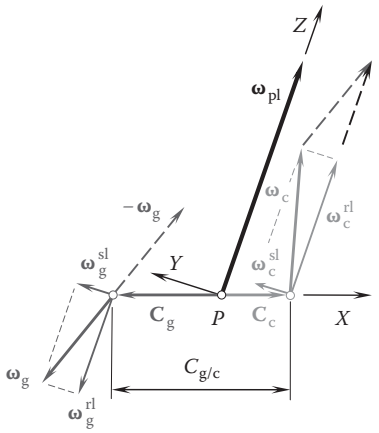

FIGURE 3.6
Specification of the principal parameters of the gear machining mesh.

of the rotations $\boldsymbol{\omega}_g$ and $\boldsymbol{\omega}_{pl}$. Vector $\mathbf{C}_c$ specifies the center distance of axes O_c and P_{ln} of the rotations $\boldsymbol{\omega}_c$ and $\boldsymbol{\omega}_{pl}$.

Vector $\mathbf{C}_c$, which is equal to $\mathbf{C}_c = r_{w.c} \cdot \mathbf{c}$, is applied at pitch point P. The normalized vector $\bar{\mathbf{C}}_c$ can be computed from the formula $\bar{\mathbf{C}}_c = \bar{r}_{w.c} \cdot \mathbf{c}$.

Vector $\mathbf{C}_g$, which is equal to $\mathbf{C}_g = -r_{w.g} \cdot \mathbf{c}$, is also applied at pitch point P. The normalized vector $\bar{\mathbf{C}}_g$ can be computed from the formula $\bar{\mathbf{C}}_g = -\bar{r}_{w.g} \cdot \mathbf{c}$.

The magnitude of vector $\mathbf{C}_g$ always exceeds or is equal to the length of vector $\mathbf{C}_c$ and thus, the inequality $|\mathbf{C}_g| \geq |\mathbf{C}_c|$ is always observed. The same is valid with respect to the normalized vectors $\bar{\mathbf{C}}_g$ and $\bar{\mathbf{C}}_c$.

Center distance $C_{g/c}$ can be expressed in terms of vectors $\mathbf{C}_g$ and $\mathbf{C}_g$. For this purpose, the expression

$$C_{g/c} = |\mathbf{C}| = |\mathbf{C}_c - \mathbf{C}_g| \tag{3.34}$$

can be used. The similar equation

$$\bar{C}_{c/g} = |\bar{\mathbf{C}}| = |\bar{\mathbf{C}}_c - \bar{\mathbf{C}}_g| \tag{3.35}$$

is valid for the normalized parameters $\bar{\mathbf{C}}_g$, $\bar{\mathbf{C}}_c$, and $\bar{C}_{g/c}$.

By definition, the normalized radius is $\bar{r}_{w.c} = 1$. Because inequality $\bar{r}_{w.g} \geq \bar{r}_{w.c}$ is always observed, the expression

$$\bar{C}_{g/c} = \bar{r}_{w.g} + \bar{r}_{w.c} \geq 2 \tag{3.36}$$

is valid for the normalized center distance $\bar{C}_{g/c}$.

Equations (3.35) and (3.36) impose strong restrictions on the configuration of axodes of the gear machining mesh.

In the general case, rotation vectors $\boldsymbol{\omega}_g$ and $\boldsymbol{\omega}_c$ cross each other at a certain crossed-axis angle Σ. For all feasible combinations of the vectors of rotations $\boldsymbol{\omega}_g$ and $\boldsymbol{\omega}_c$, the crossed-axis angle Σ is within the interval $0° \leq \Sigma \leq 180°$. Depending on the design parameters of the actual gear machining mesh, three locations of pitch point P are recognized. First, pitch point P can be located within the straight-line segment $C_{g/c}$. Second, pitch point P can be located outside the straight-line segment $C_{g/c}$. Third, pitch point P can be located at one of the two end points of the straight-line segment $C_{g/c}$. No other locations of pitch point P are feasible.

The location of pitch point P within the straight-line segment $C_{g/c}$ indicates that for a given configuration of rotation vectors $\boldsymbol{\omega}_g$ and $\boldsymbol{\omega}_c$, the corresponding axodes are externally tangent to each other. When pitch point P is located outside the straight-line segment $C_{g/c}$, the axodes are internally tangent to each other.

The third case, wherein pitch point P is located at one of the two end points of the straight-line segment $C_{g/c}$, requires a more detailed consideration. Because the configuration of the rotation vectors in the third case relates exactly to what is between the first case (external tangency of the axodes) and the second case (internal tangency of the axodes), the third case is viewed as having the *critical configuration* of rotation vectors $\boldsymbol{\omega}_g$ and $\boldsymbol{\omega}_c$.

The term "critical configuration" reflects a particular configuration of rotation vectors $\boldsymbol{\omega}_g$ and $\boldsymbol{\omega}_c$ for which pitch point P is located at one of the two ends of the straight-line segment $C_{g/c}$.

For a certain configuration of the vectors of rotations $\boldsymbol{\omega}_g$ and $\boldsymbol{\omega}_c$, vector $\boldsymbol{\omega}_g$ is orthogonal to the vector of instant rotation $\boldsymbol{\omega}_{pl}$ (Figure 3.7). In this case, pitch point P is at zero distance, $r_{w.c} = 0$, from the axis of rotation O_c of the gear cutting tool. For orthogonal vectors $\boldsymbol{\omega}_g$ and $\boldsymbol{\omega}_{pl}$, the equality $\boldsymbol{\omega}_g \cdot \boldsymbol{\omega}_{pl} = 0$ is always satisfied.

Setting in Equation (3.18) $\Sigma_c = 90°$, one can come up with the expression

$$\Sigma_{cr}^{(1)} = \frac{1+\omega_g}{1+\omega_g-\omega_c} \cdot \frac{\pi}{2} \tag{3.37}$$

to compute for the first critical value $\Sigma_{cr}^{(1)}$ of the crossed-axis angle Σ.

This case [Equation (3.37)] pertains to the scenario under which the rotation vector $\boldsymbol{\omega}_c$ of the gear cutting tool is orthogonal to the vector of instant rotation $\boldsymbol{\omega}_{pl}$.

Pitch point P can be located at the opposite end of the straight-line segment $C_{g/c}$. In the second case, setting $\Sigma_g = 90°$ in Equation (3.14), the expression

$$\Sigma_{cr}^{(2)} = \frac{1+\omega_c}{1+\omega_c-\omega_g} \cdot \frac{\pi}{2} \tag{3.38}$$

can be derived for the second critical value $\Sigma_{cr}^{(2)}$ of the crossed-axis angle Σ.

3.3.2 Classification of Gear Machining Meshes

A scientific classification of the types of gear machining meshes is developed based on the proposed vector representation of gear machining meshes. Possible types of gear machining meshes are classified as shown in Figure 3.8.

Gear machining meshes are subdivided into three groups:

1. *External gear machining meshes* are those meshes whose crossed-axis angle Σ exceeds its critical value Σ_{cr}. Pitch point P is located within the center distance $C_{g/c}$.
2. *Planar gear machining meshes* are those whose crossed-axis angle Σ is equal to its critical value Σ_{cr}. Pitch point P is located at one of the two ends of the center distance $C_{g/c}$.

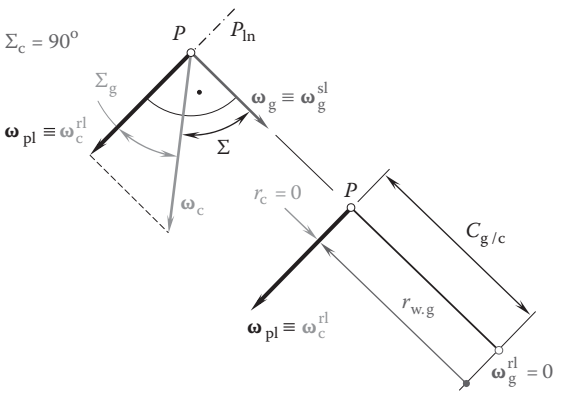

FIGURE 3.7
An example of critical configuration of rotation vectors $\boldsymbol{\omega}_g$ and $\boldsymbol{\omega}_c$.

3. *Internal gear machining meshes* are those whose crossed-axis angle Σ is smaller than its critical value Σ_{cr}. Pitch point P is located within the center distance $C_{g/c}$ beyond the end point of the center distance $C_{g/c}$.

There are five different types of gear machining meshes in total.

First, no difference is observed for the configuration of the rotation vectors $\boldsymbol{\omega}_g$ and $\boldsymbol{\omega}_c$, which represent an external gear machining mesh ($\Sigma_{cr} < \Sigma < 180°$). Any of the two rotation vectors can be associated with either the work gear or the gear cutting tool. Therefore, a vector diagram of only one type can be associated with an external gear machining mesh.

Second, for planar gear machining meshes ($\Sigma = \Sigma_{cr}$), two different types of configuration of the rotation vectors $\boldsymbol{\omega}_g$ and $\boldsymbol{\omega}_c$ are distinguished. For one of these configurations, the gear cutting tool rotation vector $\boldsymbol{\omega}_c$ is perpendicular to the vector of instant rotation $\boldsymbol{\omega}_{pl}$. For the other configuration, the work gear rotation vector $\boldsymbol{\omega}_g$ is perpendicular to the vector of instant rotation $\boldsymbol{\omega}_{pl}$.

The gear machining meshes featuring the configuration ($\Sigma = \Sigma_{cr}$) of the rotation vectors is of particular importance to designers of gear cutting tools. Values of the design parameters of the gear cutting tool, which entail the increase of components $\boldsymbol{\omega}_g^{sl}$ and $\boldsymbol{\omega}_c^{sl}$ of the rotation vectors $\boldsymbol{\omega}_g$ and $\boldsymbol{\omega}_c$, are often preferred when designing a gear cutting tool.

Third, internal gear machining meshes ($0° < \Sigma < \Sigma_{cr}$) also feature two different types of configuration of the rotation vectors $\boldsymbol{\omega}_g$ and $\boldsymbol{\omega}_c$. In one configuration, magnitude ω_g of the rotation vector $\boldsymbol{\omega}_g$ of the work gear is greater than magnitude ω_c of the rotation vector $\boldsymbol{\omega}_c$ of the gear cutting tool ($\omega_g > \omega_c$). Gear machining meshes of this type correspond to the machining processes of an external work gear with the enveloping gear cutting tool. For the other configuration, magnitude ω_g of the rotation vector $\boldsymbol{\omega}_g$ of the work gear is smaller than magnitude ω_c of the rotation vector $\boldsymbol{\omega}_c$ of the gear cutting tool ($\omega_g < \omega_c$). Gear meshes of this type correspond to the machining process of an internal work gear with the external gear cutting tool.

Three design parameters are critical for these five different types of gear machining meshes: (1) center distance $C_{g/c}$, (2) crossed-axis angle Σ, and (3) magnitude of rotation vectors $\boldsymbol{\omega}_g$ and $\boldsymbol{\omega}_c$. If one of these design parameters reaches an extremal value, then the corresponding gear machining mesh transforms into one of the particular cases of gear machining meshes.

Zero value is critical to the center distance $C_{g/c}$: When center distance vanishes ($C_{g/c} = 0$), a spatial gear machining mesh reduces to a mesh of bevel gears of the corresponding type. External spatial gear machining mesh reduces to an external mesh of bevel gears. Planar gear machining meshes reduce into two corresponding gear machining meshes, which can be imitated by axodes in the form of a cone of revolution and plane. The internal spatial gear machining mesh reduces into two corresponding gear machining meshes, which can be imitated by axodes in the form of two cones of revolution. Ultimately, if the center distance vanishes, then five spatial gear machining meshes reduce into five corresponding planar gear machining meshes.

Zero value is critical to the crossed-axis angle Σ: When the crossed-axis angle reaches zero value ($\Sigma = 0°$), a spatial gear machining mesh reduces into a mesh of gears with parallel axes of the corresponding type. Three possible types of gear machining meshes having parallel rotation vectors $\boldsymbol{\omega}_g$ and $\boldsymbol{\omega}_c$ are shown in Figure 3.8.

When the magnitude of one of the rotation vectors $\boldsymbol{\omega}_g$ and $\boldsymbol{\omega}_c$ reaches zero value, the corresponding spatial gear machining meshes reduce into two gear machining meshes, which are specified either by vectors $\boldsymbol{\omega}_g$ and $\mathbf{V}_c$ or by vectors $\mathbf{V}_g$ and $\boldsymbol{\omega}_c$. These two types of gear machining meshes are shown in Figure 3.8. In particular cases, vectors $\boldsymbol{\omega}_g$ and $\mathbf{V}_c$, as

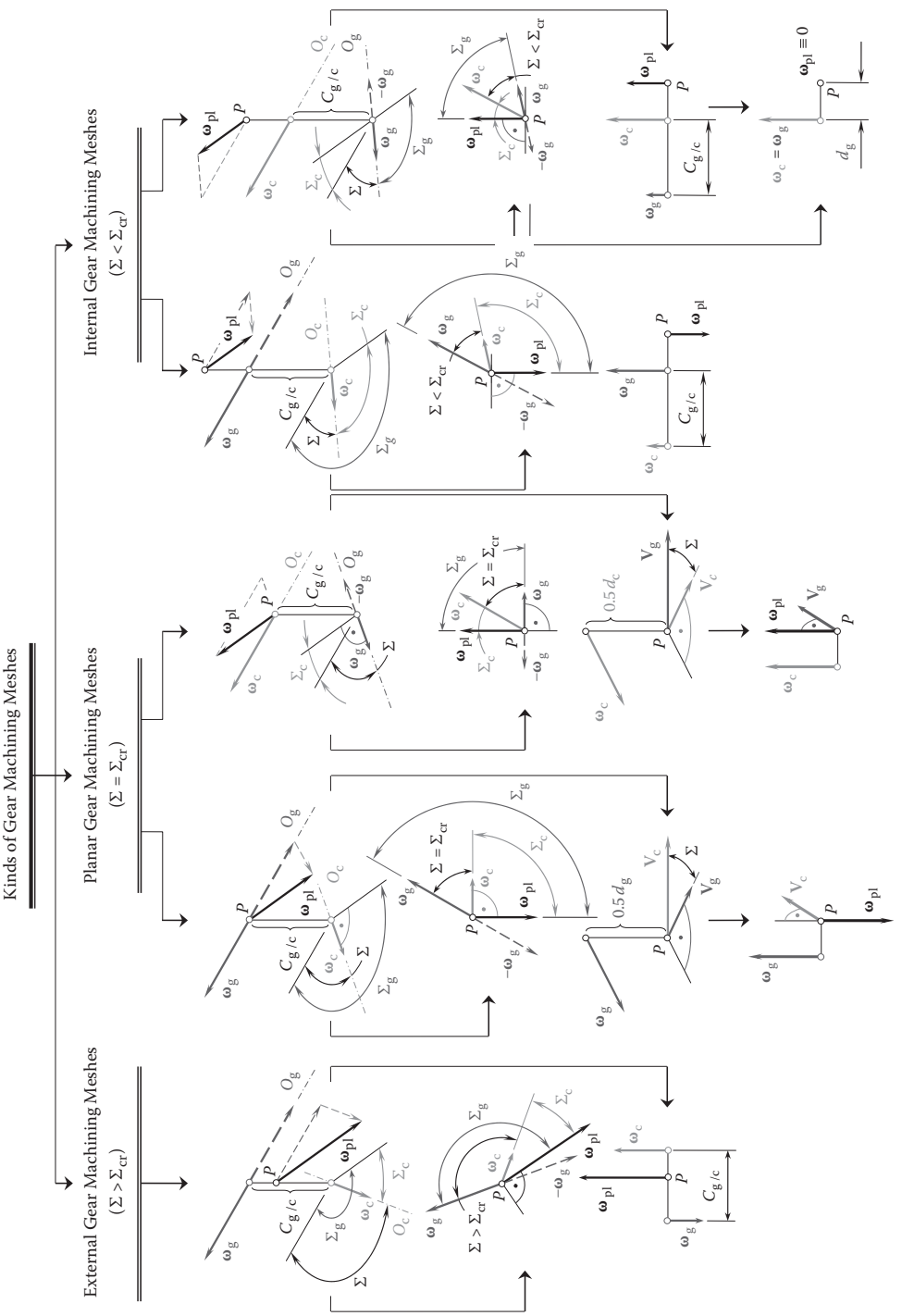

FIGURE 3.8
Classification of types of gear machining meshes.

well as vectors $\mathbf{V}_g$ and $\boldsymbol{\omega}_c$, can be perpendicular to each other ($\boldsymbol{\omega}_g \perp \mathbf{V}_c$ and $\mathbf{V}_g \perp \boldsymbol{\omega}_c$). These two types of gear machining meshes are also depicted in Figure 3.8.

In a degenerated case, not just one but two design parameters (i.e., $C_{g/c}$ and Σ) can simultaneously have zero value ($C_{g/c} = 0$ and $\Sigma = 0°$). An example of the gear machining mesh of this type is illustrated in Figure 3.8. For completeness, a few more critical combinations of the design parameters of the gear machining mesh should be noted: (a) $C_{g/c} = 0$ and either $\omega_g = 0$ or $\omega_c = 0$; (b) $\Sigma = 0°$ and either $\omega_g = 0$ or $\omega_c = 0$; and (c) $C_{g/c} = 0$, $\Sigma = 0°$, and either $\omega_g = 0$ or $\omega_c = 0$. Ultimately, the total number of possible types of gear machining meshes is limited to 21, of which 18 are depicted in Figure 3.8 and three more are specified above by critical values of the design parameters of the gear machining mesh.

The classification of possible types of gear machining meshes is the key for the development of novel designs of gear cutting tools and new methods of machining gears.

3.4 Kinematics of Gear Machining Processes

The kinematics of the gear machining mesh is the core of the kinematics of the entire gear machining process. However, the kinematics of the gear machining mesh is not always sufficient for determining the generating surface of the gear cutting tool as well as for cutting of the work gear. For these purposes, in addition to the kinematics of the gear machining mesh, the kinematics of gear machining processes also includes more relative motions of the work gear and the gear cutting tool.

Additional motions are usually those that allow for sliding over the generating surface. Through motions of this type, the gear machining mesh can be complete in most cases in terms of the kinematics of the gear machining process.

In cases where the generating surface of the gear cutting tool created via the gear machining mesh does not allow for sliding motions, a secondary generating surface is created. Secondary generating surfaces of gear cutting tools can also be implemented for the convenience of the gear manufacturer.

Ultimately, designing a gear cutting tool begins with the analysis of kinematics.

First, kinematics of the gear machining mesh is analyzed from the standpoint of whether a given work gear can be machined using only a certain gear machining mesh. If the kinematics of the gear machining mesh is sufficient for the generation of generating surface T of the gear cutting tool as well as for material removal, then the generated surface T is used for the design of the gear cutting tool.

Second, if the kinematics of no kind of the gear machining mesh is feasible for a particular gear machining operation, then those motions allow for sliding of the surface T over itself are added to the kinematics of the gear machining mesh. In this manner, the kinematics of the gear machining mesh evolves to the corresponding kinematics of the gear machining process. Motions that allow for sliding over work gear tooth surface $\mathcal{G}$ are also often incorporated into the kinematics of the gear machining process.

Third, there are cases where the generating surface of the gear cutting tool does not allow for sliding motions. Cases of this type are the most inconvenient challenge for both gear cutting tool designers and gear manufacturers. If generating surface T does not allow for sliding, then a secondary generating surface T_2 is used for the design of the gear cutting tool.

4

Elements of Coordinate Systems Transformations

Coordinate system transformation is a powerful tool for solving many geometrical and kinematical problems pertaining to the design of gear cutting tools and to the kinematics of gear machining processes.

Consequent coordinate systems transformations can easily be described analytically with the implementation of matrices. Use of matrices for the coordinate system transformation can be traced back to the late 1940s [46] and early 1950s [14, 45].

Implementation of the coordinate system transformation is necessary for representation in a common coordinate system of (1) the gear cutting tool and (2) its motion relative to the tooth flank of the work gear. At every instant of time, the configuration (position and orientation) of the gear cutting tool relative to the work gear can be analytically described with the help of a homogeneous transformation matrix corresponding to the displacement of the cutting tool from its current location to its consecutive location.

4.1 Coordinate System Transformation

In this chapter, the coordinate system transformation is briefly discussed from the standpoint of its implementation for the purposes of gear cutting tool design. For more details on this topic, the interested reader may refer to refs. [125, 136, 138, 143, 153] and other advanced sources.

4.1.1 Introduction

Homogenous coordinates utilize a mathematical trick to embed three-dimensional coordinates and transformations into a four-dimensional matrix format. As a result, inversions or combinations of linear transformations are simplified to inversion or multiplication of the corresponding matrices.

Homogenous coordinate vectors. Instead of representing each point $\mathbf{r}(x, y, z)$ in three-dimensional space with a single three-dimensional vector

$$\mathbf{r} = \begin{bmatrix} x \\ y \\ z \end{bmatrix} \tag{4.1}$$

homogenous coordinates allow each point $\mathbf{r}(x, y, z)$ to be represented by any of an infinite number of four-dimensional vectors

$$\mathbf{r} = \begin{bmatrix} Tx \\ Ty \\ Tz \\ T \end{bmatrix} \tag{4.2}$$

The three-dimensional vector corresponding to any four-dimensional vector can be computed by dividing the first three elements by the fourth element, and a four-dimensional vector corresponding to any three-dimensional vector can be created by simply adding a fourth element and setting it equal to one.

Homogenous coordinate transformation matrices of the dimension 4 × 4. Homogenous coordinate transformation matrices operate on four-dimensional homogenous vector representations of traditional three-dimensional coordinate locations. Any three-dimensional linear transformation (translation, rotation, etc.) can be represented by a 4 × 4 homogenous coordinate transformation matrix. In fact, because of the redundant representation of three-space in a homogenous coordinate system, an infinite number of different 4 × 4 homogenous coordinate transformation matrices are available to perform any given linear transformation. This redundancy can be eliminated to provide a unique representation by dividing all elements of a 4 × 4 homogenous transformation matrix by the last element (which will become equal to one). This means that the 4 × 4 homogenous transformation matrix can incorporate as many as 15 independent parameters. The generic format representation of a homogenous transformation equation for mapping the three-dimensional coordinate (x_1, y_1, z_1) to the three-dimensional coordinate (x_2, y_2, z_2) is:

$$\begin{bmatrix} T*x_2 \\ T*y_2 \\ T*z_2 \\ T* \end{bmatrix} = \begin{bmatrix} T*a & T*b & T*c & T*d \\ T*e & T*f & T*g & T*h \\ T*i & T*j & T*k & T*m \\ T*n & T*p & T*q & T* \end{bmatrix} \cdot \begin{bmatrix} Tx_2 \\ Ty_2 \\ Tz_2 \\ T \end{bmatrix} \tag{4.3}$$

If any two matrices or vectors of this equation are known, the third matrix (or vector) can be computed and then the redundant T element in the solution can be eliminated by dividing all elements of the matrix by the last element.

Various transformation models can be used to constrain the form of the matrix to transformations with fewer degrees of freedom.

4.1.2 Translations

Translation of a coordinate system is one of the major linear transformations used for the purposes of gear cutting tool design. Translations of the coordinate system $X_2Y_2Z_2$ along the axes of the coordinate system $X_1Y_1Z_1$ are illustrated in Figure 4.1. The translations can be analytically described by the homogenous transformation matrices of dimension 4 × 4.

For the analytical description of the translation along coordinate axes, the operators of translation $\mathbf{Tr}(a_x,X)$, $\mathbf{Tr}(a_y,Y)$, and $\mathbf{Tr}(a_z,Z)$ are used. The operators yield matrix representation in the form

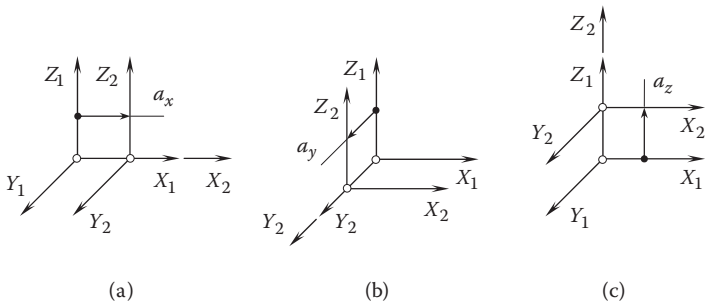

FIGURE 4.1
Analytical description of the operators of translation **Tr**(a_x,X), **Tr**(a_y,Y), and **Tr**(a_z,Z) along the coordinate axes.

$$\mathbf{Tr}(a_x, X) = \begin{bmatrix} 1 & 0 & 0 & a_x \\ 0 & 1 & 0 & 0 \\ 0 & 0 & 1 & 0 \\ 0 & 0 & 0 & 1 \end{bmatrix} \tag{4.4}$$

$$\mathbf{Tr}(a_y, Y) = \begin{bmatrix} 1 & 0 & 0 & 0 \\ 0 & 1 & 0 & a_y \\ 0 & 0 & 1 & 0 \\ 0 & 0 & 0 & 1 \end{bmatrix} \tag{4.5}$$

$$\mathbf{Tr}(a_z, Z) = \begin{bmatrix} 1 & 0 & 0 & 0 \\ 0 & 1 & 0 & 0 \\ 0 & 0 & 1 & a_z \\ 0 & 0 & 0 & 1 \end{bmatrix} \tag{4.6}$$

Here a_x, a_y, a_z are signed values denoting distances of translations along corresponding axes.

Consider two coordinate systems, $X_1Y_1Z_1$ and $X_2Y_2Z_2$, shifted along the X_1 axis on a_x (Figure 4.1a).

Let us assume that a point M in the coordinate system $X_2Y_2Z_2$ is given by the position vector $\mathbf{r}_2(M)$. In the coordinate system $X_1Y_1Z_1$, that same point M can be specified by the position vector $\mathbf{r}_1(M)$. Then, position vector $\mathbf{r}_1(M)$ can be expressed in terms of position vector $\mathbf{r}_2(M)$ by the equation $\mathbf{r}_1(M) = \mathbf{Tr}(a_x,X)\cdot\mathbf{r}_2(M)$. Equations similar to that above are valid for other operators, **Tr**(a_y,Y) and **Tr**(a_z,Z), of the coordinate system transformation (Figure 4.1b,c).

Any coordinate system transformation that does not change the orientation of a geometrical object is an *orientation-preserving transformation*, or a *direct transformation*. Therefore, transformation of translation is an example of direct transformation.

4.1.3 Rotation about Coordinate Axis

Rotation of a coordinate system about a coordinate axis is another type of major linear transformations used for the purposes of gear cutting tool design. Rotation of the coordinate system $X_2Y_2Z_2$ about the axis of the coordinate system $X_1Y_1Z_1$ is illustrated in Figure 4.2.

For an analytical description of rotation about coordinate axes, the operators of rotation $\mathbf{Rt}(\varphi_x,X)$, $\mathbf{Rt}(\varphi_y,Y)$, and $\mathbf{Rt}(\varphi_z,Z)$ are used. The operators yield representation in the form of homogenous matrices

$$\mathbf{Rt}(\varphi_x, X) = \begin{bmatrix} 1 & 0 & 0 & 0 \\ 0 & \cos\varphi_x & \sin\varphi_x & 0 \\ 0 & -\sin\varphi_x & \cos\varphi_x & 0 \\ 0 & 0 & 0 & 1 \end{bmatrix} \tag{4.7}$$

$$\mathbf{Rt}(\varphi_y, Y) = \begin{bmatrix} \cos\varphi_y & 0 & -\sin\varphi_y & 0 \\ 0 & 1 & 0 & 0 \\ \sin\varphi_y & 0 & \cos\varphi_y & 0 \\ 0 & 0 & 0 & 1 \end{bmatrix} \tag{4.8}$$

$$\mathbf{Rt}(\varphi_z, Z) = \begin{bmatrix} \cos\varphi_z & \sin\varphi_z & 0 & 0 \\ -\sin\varphi_z & \cos\varphi_z & 0 & 0 \\ 0 & 0 & 1 & 0 \\ 0 & 0 & 0 & 1 \end{bmatrix} \tag{4.9}$$

Here φ_x, φ_y, φ_z are signed values denoting angles of rotation about the corresponding axis: φ_x is rotation around the X axis (pitch); φ_y is rotation around the Y axis (roll), and φ_z is rotation around the Z axis (yaw).

Consider two coordinate systems, $X_1Y_1Z_1$ and $X_2Y_2Z_2$, turned about the X_1 axis through the angle φ_x (Figure 4.2a). In the coordinate system $X_2Y_2Z_2$, a certain point M is given by the position vector $\mathbf{r}_2(M)$. In the coordinate system $X_1Y_1Z_1$, that same point M can be specified by the position vector $\mathbf{r}_1(M)$. Then, position vector $\mathbf{r}_1(M)$ can be expressed in terms

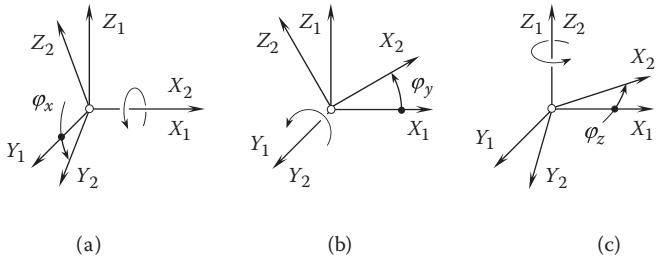

FIGURE 4.2
Analytical description of the operators of rotation $\mathbf{Rt}(\varphi_x,X)$, $\mathbf{Rt}(\varphi_y,Y)$, and $\mathbf{Rt}(\varphi_z,Z)$ about the coordinate axes.

of position vector $\mathbf{r}_2(M)$ by the equation $\mathbf{r}_1(M) = \mathbf{Rt}(\varphi_x,X) \cdot \mathbf{r}_2(M)$. Equations similar to that above are valid for other operators, $\mathbf{Rt}(\varphi_y,Y)$ and $\mathbf{Rt}(\varphi_z,Z)$, of the coordinate system transformation (Figure 4.2b,c).

4.1.4 Resultant Coordinate System Transformation

The operators of translations $\mathbf{Tr}(a_x,X)$, $\mathbf{Tr}(a_y,Y)$, and $\mathbf{Tr}(a_z,Z)$, together with the operators of rotations, $\mathbf{Rt}(\varphi_x,X)$, $\mathbf{Rt}(\varphi_y,Y)$, and $\mathbf{Rt}(\varphi_z,Z)$, are used to compose the operator $\mathbf{Rs}(1 \mapsto 2)$ of the resultant coordinate system transformation. The operator $\mathbf{Rs}(1 \mapsto 2)$ of the resultant coordinate system transformation analytically describes the transition from the initial coordinate system $X_1Y_1Z_1$ to a certain coordinate system $X_2Y_2Z_2$.

Consider three consequent translations along the coordinate axes X_1, Y_1, and Z_1. Suppose that a point P on a rigid body goes through a translation describing a straight path from P_1 to P_2 with a change of coordinates of (a_x,a_y,a_z). This motion can be described with an operator of the resultant coordinate system transformation $\mathbf{Rs}(1 \mapsto 2)$, which can be expressed in terms of the operators $\mathbf{Tr}(a_x,X)$, $\mathbf{Tr}(a_y,Y)$, and $\mathbf{Tr}(a_z,Z)$ of elementary coordinate system transformations. The operator $\mathbf{Rs}(1 \to 2)$ is equal to

$$\mathbf{Rs}(1 \to 2) = \mathbf{Tr}(a_z, Z) \cdot \mathbf{Tr}(a_y, Y) \cdot \mathbf{Tr}(a_x, X) = \begin{bmatrix} 1 & 0 & 0 & a_x \\ 0 & 1 & 0 & a_y \\ 0 & 0 & 1 & a_z \\ 0 & 0 & 0 & 1 \end{bmatrix} \tag{4.10}$$

In this particular case, the operator of the resultant coordinate system transformation $\mathbf{Rs}(1 \to 2)$ can be interpreted as the operator $\mathbf{Tr}(a,\mathbf{A})$ of translation along an $\mathbf{A}$ axis $[\mathbf{Rs}(1 \to 2) = \mathbf{Tr}(a, \mathbf{A})]$. Evidently, axis $\mathbf{A}$ is always an axis through the origin.

Similarly, three consequent rotations about coordinate axes can be described with another operator of the resultant coordinate system transformation $\mathbf{Rs}(1 \to 2)$

$$\mathbf{Rs}(1 \to 2) = \mathbf{Rt}(\varphi_z, Z) \cdot \mathbf{Rt}(\varphi_y, Y) \cdot \mathbf{Rt}(\varphi_x, X) \tag{4.11}$$

In this particular case, the operator of the resultant coordinate system transformation $\mathbf{Rs}(1 \mapsto 2)$ can be interpreted as the operator $\mathbf{Rt}(\varphi,\mathbf{A})$ of rotation about an $\mathbf{A}$ axis $[\mathbf{Rs}(1 \mapsto 2) = \mathbf{Rt}(\varphi, \mathbf{A})]$. Evidently, axis $\mathbf{A}$ is always an axis through the origin.

From a practical standpoint, it is often necessary to perform coordinate system transformations for those cases, the operator of the resultant coordinate system transformation for which is composed of translations along and rotations about coordinate axes. For example, the expression

$$\mathbf{Rs}(1 \to 5) = \mathbf{Tr}(a_x, X) \cdot \mathbf{Rt}(\varphi_z, Z) \cdot \mathbf{Rt}(\varphi_x, X) \cdot \mathbf{Tr}(a_y, Y) \tag{4.12}$$

indicates that the transition from the coordinate system $X_1Y_1Z_1$ to the coordinate system $X_5Y_5Z_5$ (Figure 4.3) is performed in the following four steps: (1) translation $\mathbf{Tr}(a_y,Y)$, (2) rotation $\mathbf{Rt}(\varphi_x,X)$, (3) second rotation $\mathbf{Rt}(\varphi_z,Z)$, and finally by (4) translation $\mathbf{Tr}(a_x,X)$. Ultimately, the equality $\mathbf{r}_1(M) = \mathbf{Rt}(5 \to 1) \cdot \mathbf{r}_5(M)$ is observed.

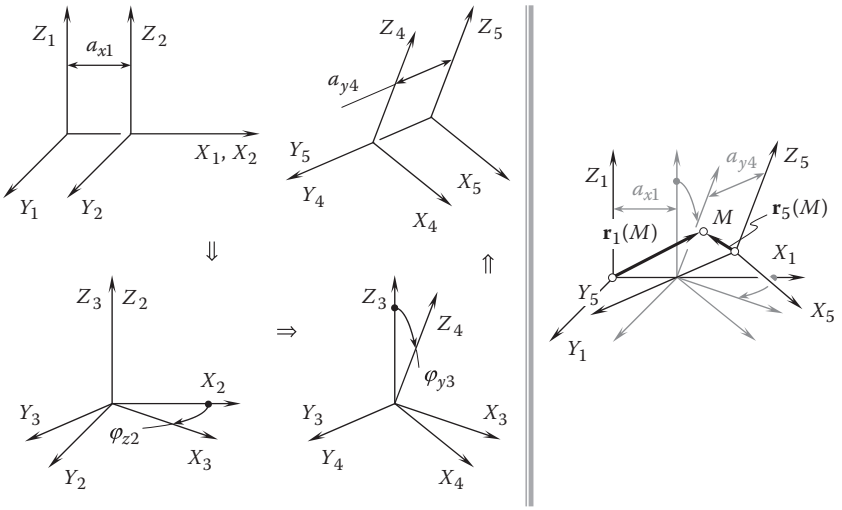

FIGURE 4.3
An example of the resultant coordinate system transformation.

When the operator $\mathbf{Rs}(1 \to t)$ of a resultant coordinate system transformation is known, the transition in the opposite direction can be performed via the operator $\mathbf{Rs}(t \to 1)$ of the inverse coordinate system transformation. The following equality

$$\mathbf{Rs}(t \to 1) = \mathbf{Rs}^{-1}(1 \to t) \tag{4.13}$$

is valid for the operator $\mathbf{Rs}(t \to 1)$ of the inverse coordinate system transformation.

4.1.5 Screw Motion about a Coordinate Axis

Operators for the analytical description of screw motions about an axis of the Cartesian coordinate system are a particular case of the operators of the resultant coordinate system transformation.

By definition (Figure 4.4), the operator $\mathbf{Sc}_x(\varphi_x, p_x)$ of a screw motion about the X axis of the Cartesian coordinate system XYZ is equal to

$$\mathbf{Sc}_x(\varphi_x, p_x) = \mathbf{Rt}(\varphi_x, X) \cdot \mathbf{Tr}(a_x, X) \tag{4.14}$$

After substituting the operator of translation $\mathbf{Tr}(a_x, X)$ [Equation (4.4)] and the operator of rotation $\mathbf{Rt}(\varphi_x, X)$ [Equation (4.7)], Equation (4.14) casts into the expression

$$\mathbf{Sc}_x(\varphi_x, p_x) = \begin{bmatrix} 1 & 0 & 0 & p_x\varphi_x \\ 0 & \cos\varphi_x & \sin\varphi_x & 0 \\ 0 & -\sin\varphi_x & \cos\varphi_x & 0 \\ 0 & 0 & 0 & 1 \end{bmatrix} \tag{4.15}$$

for the computation of the operator of the screw motion $\mathbf{Sc}_x(\varphi_x, p_x)$ about the X axis.

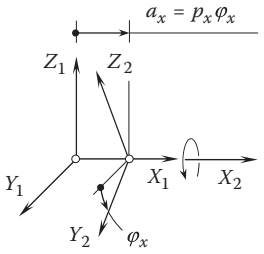

FIGURE 4.4
Analytical description of the operator of screw motion $\mathbf{Sc}_x(\varphi_x, p_x)$.

The operators of screw motions $\mathbf{Sc}_y(\varphi_y, p_y)$ and $\mathbf{Sc}_z(\varphi_z, p_z)$ about Y and Z axes are defined in a similar manner

$$\mathbf{Sc}_y(\varphi_y, p_y) = \mathbf{Rt}(\varphi_y, Y) \cdot \mathbf{Tr}(a_y, Y) \tag{4.16}$$

$$\mathbf{Sc}_z(\varphi_z, p_z) = \mathbf{Rt}(\varphi_z, Z) \cdot \mathbf{Tr}(a_z, Z) \tag{4.17}$$

Using Equations (4.5) and (4.6), together with Equations (4.8) and (4.9), one can come up with the expressions

$$\mathbf{Sc}_y(\varphi_y, p_y) = \begin{bmatrix} \cos\varphi_y & 0 & -\sin\varphi_y & 0 \\ 0 & 1 & 0 & p_y\varphi_y \\ \sin\varphi_y & 0 & \cos\varphi_y & 0 \\ 0 & 0 & 0 & 1 \end{bmatrix} \tag{4.18}$$

$$\mathbf{Sc}_z(\varphi_z, p_z) = \begin{bmatrix} \cos\varphi_z & \sin\varphi_z & 0 & 0 \\ -\sin\varphi_z & \cos\varphi_z & 0 & 0 \\ 0 & 0 & 1 & p_z\varphi_z \\ 0 & 0 & 0 & 1 \end{bmatrix} \tag{4.19}$$

to compute for the operators of the screw motion $\mathbf{Sc}_y(\varphi_y, p_y)$ and $\mathbf{Sc}_z(\varphi_z, p_z)$ about Y and Z axes.

Screw motions about a coordinate axis as well as screw surfaces are common in the design of gear cutting tools. This makes practical use of the operators of the screw motion $\mathbf{Sc}_x(\varphi_x, p_x)$, $\mathbf{Sc}_y(\varphi_y, p_y)$, and $\mathbf{Sc}_z(\varphi_z, p_z)$ when designing gear cutting tools.

In case of necessity, an operator of the screw motion about an arbitrary axis either through the origin or not through the origin of the coordinate system, can be derived following the process used for the derivation of the operators $\mathbf{Sc}_x(\varphi_x, p_x)$, $\mathbf{Sc}_y(\varphi_y, p_y)$, and $\mathbf{Sc}_z(\varphi_z, p_z)$.

4.1.6 Rolling Motion of a Coordinate System

Another practical combination of a rotation and a translation is often used when designing a gear cutting tool.

Consider a Cartesian coordinate system $X_1Y_1Z_1$ (Figure 4.5). The coordinate system $X_1Y_1Z_1$ is traveling in the direction of the X_1 axis. Speed of the translation is denoted by V. The coordinate system $X_1Y_1Z_1$ is rotating about its Y_1 axis simultaneously with the translation. Speed of the rotation is denoted by ω. Assume that the ratio V/ω is constant. Under this scenario, the resultant motion of the reference system $X_1Y_1Z_1$ to its arbitrary position $X_2Y_2Z_2$ allows for interpretation in the form of rolling with no sliding of a cylinder with radius R_w over the plane. The plane is parallel to the coordinate X_1Y_1 plane, and is remote from it at distance R_w. To compute for the radius of the rolling cylinder, the expression $R_\omega = V/\omega$ can be used.

Because rolling of the cylinder with radius R_w over the plane takes place with no sliding, a certain correspondence between the translation and the rotation of the coordinate system is established. When the coordinate system turns through a certain angle φ_y, the translation of origin of the coordinate system along the X_1 axis is $a_x = \varphi_y R_w$.

Transition from the coordinate system $X_1Y_1Z_1$ to the coordinate system $X_2Y_2Z_2$ can be analytically described by the operator of the resultant coordinate system transformation $\mathbf{Rs}(1 \mapsto 2)$, which is derived as

$$\mathbf{Rs}(1 \mapsto 2) = \mathbf{Rt}(\varphi_y, Y_1) \cdot \mathbf{Tr}(a_x, X_1) \tag{4.20}$$

where $\mathbf{Tr}(a_x, X_1)$ is the operator of the translation along the X_1 axis and $\mathbf{Rt}(\varphi_y, Y_1)$ is the operator of the rotation about the Y_1 axis.

Operators of the resultant coordinate system transformation of this type [Equation (4.20)] are referred to as operators of *rolling motion over a plane*.

When translation is performed along the X_1 axis and rotation is performed about the Y_1 axis, the operator of rolling is denoted by $\mathbf{Rl}_x(\varphi_y, Y)$. In this case, the equality $\mathbf{Rl}_x(\varphi_y, Y) = \mathbf{Rs}(1 \mapsto 2)$ [see Equation (4.20)] is valid. Based on this equality, the operator of rolling over a plane $\mathbf{Rl}_x(\varphi_y, Y)$ can be computed as

$$\mathbf{Rl}_x(\varphi_y, Y) = \begin{bmatrix} \cos\varphi_y & 0 & -\sin\varphi_y & a_x\cos\varphi_y \\ 0 & 1 & 0 & 0 \\ \sin\varphi_y & 0 & \cos\varphi_y & a_x\sin\varphi_y \\ 0 & 0 & 0 & 1 \end{bmatrix} \tag{4.21}$$

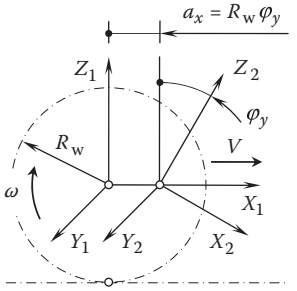

FIGURE 4.5
Illustration of the transformation of rolling $\mathbf{Rl}_x(\varphi_y, Y)$ of a coordinate system.

Although rotation remains about the Y_1 axis, translation can be performed, not along the X_1 axis, but along the Z_1 axis. For this type of rolling, the operator of rolling is

$$\mathbf{Rl}_z(\varphi_y, Y) = \begin{bmatrix} \cos\varphi_y & 0 & -\sin\varphi_y & -a_z \sin\varphi_y \\ 0 & 1 & 0 & 0 \\ \sin\varphi_y & 0 & \cos\varphi_y & a_z \cos\varphi_y \\ 0 & 0 & 0 & 1 \end{bmatrix} \tag{4.22}$$

For cases when rotation is performed about the X_1 axis, the corresponding operators of rolling are as follows

$$\mathbf{Rl}_y(\varphi_x, X) = \begin{bmatrix} 1 & 0 & 0 & 0 \\ 0 & \cos\varphi_x & \sin\varphi_x & a_y \cos\varphi_x \\ 0 & -\sin\varphi_x & \cos\varphi_x & -a_y \sin\varphi_x \\ 0 & 0 & 0 & 1 \end{bmatrix} \tag{4.23}$$

for the case of rolling along the Y_1 axis, and

$$\mathbf{Rl}_z(\varphi_x, X) = \begin{bmatrix} 1 & 0 & 0 & 0 \\ 0 & \cos\varphi_x & \sin\varphi_x & a_z \sin\varphi_x \\ 0 & -\sin\varphi_x & \cos\varphi_x & a_z \cos\varphi_x \\ 0 & 0 & 0 & 1 \end{bmatrix} \tag{4.24}$$

for the case of rolling along the Z_1 axis.

Similar expressions can be derived for the case of rotation about the Z_1 axis

$$\mathbf{Rl}_x(\varphi_z, Z) = \begin{bmatrix} \cos\varphi_z & \sin\varphi_z & 0 & a_x \cos\varphi_z \\ -\sin\varphi_z & \cos\varphi_z & 0 & a_x \sin\varphi_z \\ 0 & 0 & 1 & 0 \\ 0 & 0 & 0 & 1 \end{bmatrix} \tag{4.25}$$

$$\mathbf{Rl}_y(\varphi_z, Z) = \begin{bmatrix} \cos\varphi_z & \sin\varphi_z & 0 & a_y \sin\varphi_z \\ -\sin\varphi_z & \cos\varphi_z & 0 & a_y \cos\varphi_z \\ 0 & 0 & 1 & 0 \\ 0 & 0 & 0 & 1 \end{bmatrix} \tag{4.26}$$

Use of the operators of rolling, Equations (4.21) through (4.26), significantly simplifies the analytical description of the coordinate system transformations.

4.1.7 Rolling of Two Coordinate Systems

When designing a gear cutting tool, combinations of two rotations about parallel axes are of particular interest.

As an example, consider two Cartesian coordinate systems, $X_1Y_1Z_1$ and $X_2Y_2Z_2$, shown in Figure 4.6. Both coordinate systems $X_1Y_1Z_1$ and $X_2Y_2Z_2$ are rotated about their Z_1 and Z_2 axes. The axes of rotations are parallel to each other ($Z_1 \parallel Z_2$). Rotations ω_1 and ω_2 of the coordinate systems can be interpreted so that a circle of a certain radius R_1, which is associated with the coordinate system $X_1Y_1Z_1$, is rolling with no sliding over a circle of the corresponding radius R_2, which is associated with the coordinate system $X_2Y_2Z_2$. When the center distance C is known, radii R_1 and R_2 of the circles can be expressed in terms of the center distance C and the given rotations ω_1 and ω_2. For the computations, the following formulae

$$R_1 = C \cdot \frac{1}{1+u} \tag{4.27}$$

$$R_2 = C \cdot \frac{u}{1+u} \tag{4.28}$$

can be used. Here, the ratio ω_1/ω_2 is denoted by u.

In the initial configuration, X_1 and X_2 axes are aligned to each other, whereas Y_1 and Y_2 axes are parallel to each other. In Figure 4.6, the initial configuration of the coordinate systems $X_1Y_1Z_1$ and $X_2Y_2Z_2$ is labeled as $X_1^*Y_1^*Z_1^*$ and $X_2^*Y_2^*Z_2^*$.

When the coordinate system $X_1Y_1Z_1$ turns through a certain angle φ_1, the coordinate system $X_2Y_2Z_2$ turns through the corresponding angle φ_2. When angle φ_1 is known, the corresponding angle φ_2 is equal to $\varphi_2 = \varphi_1/u$.

Transition from the coordinate system $X_2Y_2Z_2$ to the coordinate system $X_1Y_1Z_1$ can be analytically described by the operator of the resultant coordinate system transformation $\mathbf{Rs}(1 \mapsto 2)$. Under the case being considered, the operator $\mathbf{Rs}(1 \mapsto 2)$ can be expressed in terms of the operators of the elementary coordinate system transformations

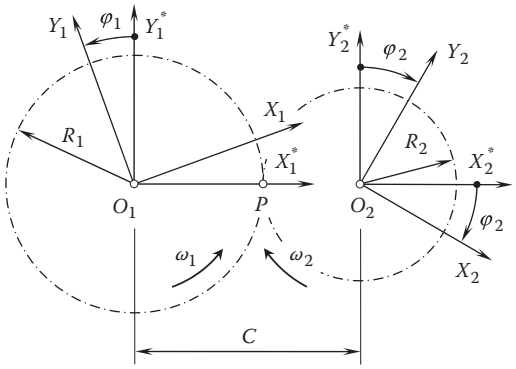

FIGURE 4.6
Derivation of the operator of rolling $\mathbf{Rr}_u(\varphi_1, Z_1)$ of two coordinate systems.

$$\mathbf{Rs}(1 \mapsto 2) = \mathbf{Rt}(\varphi_1, Z_1) \cdot \mathbf{Rt}(\varphi_1 / u, Z_1) \cdot \mathbf{Tr}(-C, X_1) \tag{4.29}$$

Other equivalent combinations of the operators of elementary coordinate system transformations can result in that same operator $\mathbf{Rs}(1 \mapsto 2)$ of the resultant coordinate system transformation. The interested reader may wish to derive his/her own equivalent expressions for the operator $\mathbf{Rs}(1 \mapsto 2)$.

The operator of the resultant coordinate system transformations of this type [see Equation (4.29)] are referred to as operators of *rolling motion over a cylinder*.

When rotations are performed about Z_1 and Z_2 axes, the operator of rolling motion over a cylinder is denoted by $\mathbf{Rr}_u(\varphi_1, Z_1)$. In this particular case, the equality $\mathbf{Rr}_u(\varphi_1, Z_1) = \mathbf{Rs}(1 \mapsto 2)$ [see Equation (4.29)] is valid. Based on this equality, the operator of rolling $\mathbf{Rr}_u(\varphi_1, Z_1)$ over a cylinder can be computed from

$$\mathbf{Rr}_u(\varphi_1, Z_1) = \begin{bmatrix} \cos\left(\varphi_1 \cdot \dfrac{u+1}{u}\right) & \sin\left(\varphi_1 \cdot \dfrac{u+1}{u}\right) & 0 & -C \\ -\sin\left(\varphi_1 \cdot \dfrac{u+1}{u}\right) & \cos\left(\varphi_1 \cdot \dfrac{u+1}{u}\right) & 0 & 0 \\ 0 & 0 & 1 & 0 \\ 0 & 0 & 0 & 1 \end{bmatrix} \tag{4.30}$$

For the inverse transformation, the inverse operator of rolling of two coordinate systems $\mathbf{Rr}_u(\varphi_2, Z_2)$ can be used. It is equal to $\mathbf{Rr}_u(\varphi_2, Z_2) = \mathbf{Rr}_u^{-1}(\varphi_1, Z_1)$. In terms of operators of the elementary coordinate system transformations, the operator $\mathbf{Rr}_u(\varphi_2, Z_2)$ can be expressed as follows

$$\mathbf{Rr}_u(\varphi_2, Z_2) = \mathbf{Rt}(\varphi_1 / u, Z_2) \cdot \mathbf{Rt}(\varphi_1, Z_2) \cdot \mathbf{Tr}(C, X_1) \tag{4.31}$$

Other equivalent combinations of the operators of elementary coordinate system transformations can result in that same operator $\mathbf{Rr}_u(\varphi_2, Z_2)$ of the resultant coordinate system transformation. The interested reader may wish to derive his/her own equivalent expressions for the operator $\mathbf{Rr}_u(\varphi_2, Z_2)$.

To compute for the operator of rolling of two coordinate systems $\mathbf{Rr}_u(\varphi_2, Z_2)$, the equation

$$\mathbf{Rr}_u(\varphi_2, Z_2) = \begin{bmatrix} \cos\left(\varphi_1 \cdot \dfrac{u+1}{u}\right) & -\sin\left(\varphi_1 \cdot \dfrac{u+1}{u}\right) & 0 & C \\ \sin\left(\varphi_1 \cdot \dfrac{u+1}{u}\right) & \cos\left(\varphi_1 \cdot \dfrac{u+1}{u}\right) & 0 & 0 \\ 0 & 0 & 1 & 0 \\ 0 & 0 & 0 & 1 \end{bmatrix} \tag{4.32}$$

can be used.

Similar to the way the expression [see Equation (4.30)] is derived for the computation of the operator of rolling $\mathbf{Rr}_u(\varphi_1, Z_1)$ around Z_1 and Z_2 axes, corresponding formulae can be

derived to compute for the operators of rolling $\mathbf{Rr}_u(\varphi_1, X_1)$ and $\mathbf{Rr}_u(\varphi_1, Y_1)$ about parallel axes X_1 and X_2, as well as about parallel axes Y_1 and Y_2.

Use of the operators of rolling about two axes, $\mathbf{Rr}_u(\varphi_1, X_1)$, $\mathbf{Rr}_u(\varphi_1, Y_1)$, and $\mathbf{Rr}_u(\varphi_1, Z_1)$, substantially simplifies the analytical description of the coordinate system transformations.

4.2 Conversion of the Coordinate System Orientation

Application of the matrix method of coordinate system transformation presumes that both coordinate systems i and $(i \pm 1)$ are of the same orientation. This means that from the very beginning, it assumed that both of them are either right-hand–oriented or left-hand–oriented Cartesian reference systems. In the event that coordinate systems i and $(i \pm 1)$ are of opposite orientations, say one of them is a right-hand–oriented coordinate system and the other is a left-hand–oriented coordinate system, then one of them should be converted to match the other system.

To convert a left-hand–oriented Cartesian coordinate system into a right-hand–oriented coordinate system or vice versa, operators of reflection are used.

To change the direction of the X_i axis of the initial coordinate system i into the opposite direction [in this case, in the new coordinate system $(i \pm 1)$ the equalities $X_{i\pm1} = -X_i$, $Y_{i\pm1} \equiv Y_i$, and $Z_{i\pm1} \equiv Z_i$ are observed], the operator of reflection $\mathbf{Rf}_x(Y_iZ_i)$ can be applied. The operator of reflection yields representation in matrix form as

$$\mathbf{Rf}_x(Y_i\, Z_i) = \begin{bmatrix} -1 & 0 & 0 & 0 \\ 0 & 1 & 0 & 0 \\ 0 & 0 & 1 & 0 \\ 0 & 0 & 0 & 1 \end{bmatrix} \tag{4.33}$$

Similarly, implementation of the operators of reflections $\mathbf{Rf}_y(X_iZ_i)$ and $\mathbf{Rf}_z(X_iY_i)$ results in the directions of Y_i and Z_i axes being reversed. Operators of reflections $\mathbf{Rf}_y(X_iZ_i)$ and $\mathbf{Rf}_z(X_iY_i)$ in this case can be analytically expressed in matrix form

$$\mathbf{Rf}_y(X_iZ_i) = \begin{bmatrix} 1 & 0 & 0 & 0 \\ 0 & -1 & 0 & 0 \\ 0 & 0 & 1 & 0 \\ 0 & 0 & 0 & 1 \end{bmatrix} \tag{4.34}$$

$$\mathbf{Rf}_z(X_iY_i) = \begin{bmatrix} 1 & 0 & 0 & 0 \\ 0 & 1 & 0 & 0 \\ 0 & 0 & -1 & 0 \\ 0 & 0 & 0 & 1 \end{bmatrix} \tag{4.35}$$

A linear transformation that reverses the direction of the coordinate axis is an *opposite transformation*. Transformation of reflection is an example of *orientation-reversing* transformations.

4.3 Direct Transformation of Surfaces Fundamental Forms

Every coordinate system transformation results in a corresponding change to the equation of the gear tooth surface $\mathcal{G}$ and/or the generating surface T of the gear cutting tool. Because of this, it is necessary to recalculate the coefficients of the first $\Phi_{1.g}$ and second $\Phi_{2.g}$ fundamental forms of the surface $\mathcal{G}$ as many times as the coordinate system transformation is being performed. This routing and time-consuming operation can be eliminated if the operators of coordinate system transformations are used directly to the fundamental forms $\Phi_{1.g}$ and $\Phi_{2.g}$. After having been computed in an initial coordinate system, the fundamental magnitudes E_g, F_g, G_g, L_g, M_g, and N_g of the forms $\Phi_{1.g}$ and $\Phi_{2.g}$ can be determined in any new coordinate system using, for this purpose, the operators of translation, rotation, and resultant coordinate system transformation. Transformations of such types of fundamental magnitudes $\Phi_{1.g}$ and $\Phi_{2.g}$ become possible due to the implementation of formulae given below.

Consider a gear tooth surface $\mathcal{G}$ given by the equation $\mathbf{r}_g = \mathbf{r}_g(U_g, V_g)$, where $(U_g, V_g) \in \mathcal{G}$.

For convenience, the first fundamental form $\Phi_{1.g}$ of the gear tooth surface $\mathcal{G}$ is represented in matrix form [128, 143]

$$\left[\Phi_{1.g}\right] = \begin{bmatrix} dU_g & dV_g & 0 & 0 \end{bmatrix} \cdot \begin{bmatrix} E_g & F_g & 0 & 0 \\ F_g & G_g & 0 & 0 \\ 0 & 0 & 1 & 0 \\ 0 & 0 & 0 & 1 \end{bmatrix} \cdot \begin{bmatrix} dU_g \\ dV_g \\ 0 \\ 0 \end{bmatrix} \tag{4.36}$$

Similarly, the equation of the second fundamental form $\Phi_{2.g}$ of the surface $\mathcal{G}$ can be given by

$$\left[\Phi_{2.g}\right] = \begin{bmatrix} dU_g & dV_g & 0 & 0 \end{bmatrix} \cdot \begin{bmatrix} L_g & M_g & 0 & 0 \\ M_g & N_g & 0 & 0 \\ 0 & 0 & 1 & 0 \\ 0 & 0 & 0 & 1 \end{bmatrix} \cdot \begin{bmatrix} dU_g \\ dV_g \\ 0 \\ 0 \end{bmatrix} \tag{4.37}$$

The coordinate system transformation with the operator of the resultant linear transformation $\mathbf{Rs}(1 \to 2)$ transfers the equation $\mathbf{r}_g = \mathbf{r}_g(U_g, V_g)$ of the gear tooth surface $\mathcal{G}$, which is initially given in $X_1Y_1Z_1$, to the equation $\mathbf{r}_g^* = \mathbf{r}_g^*(U_g^*, V_g^*)$ of that same surface P in a new coordinate system $X_2Y_2Z_2$. It is clear that the position vector of a point of the tooth flank point $\mathcal{G}$ in the first reference system $X_1Y_1Z_1$ differs from the position vector of that same point in the second reference system, $X_2Y_2Z_2$ (i.e., $\mathbf{r}_g \neq \mathbf{r}_g^*$).

The operator of the resultant linear transformation $\mathbf{Rs}(1 \to 2)$ of surface $\mathcal{G}$ having the first $\Phi_{1.g}$ and second $\Phi_{2.g}$ fundamental forms from the initial coordinate system $X_1Y_1Z_1$ to the new coordinate system $X_2Y_2Z_2$ results in a new coordinate system whose corresponding fundamental forms are expressed in the form [125, 138, 143]

$$\left[\Phi_{1.g}^*\right] = \mathbf{Rs}^T(1 \to 2) \cdot \left[\Phi_{1.g}\right] \cdot \mathbf{Rs}(1 \to 2) \tag{4.38}$$

$$\left[\Phi_{2.g}^*\right] = \mathbf{Rs}^T(1 \to 2) \cdot \left[\Phi_{2.g}\right] \cdot \mathbf{Rs}(1 \to 2) \tag{4.39}$$

Equations (4.38) and (4.39) reveal that after the coordinate system transformation is completed, the first $\Phi^*_{1.g}$ and the second $\Phi^*_{2.g}$ fundamental forms of surface $\mathcal{G}$ in the coordinate system $X_2Y_2Z_2$ are expressed in terms of the first $\Phi_{1.g}$ and the second $\Phi_{2.g}$ fundamental forms, which are initially represented in the coordinate system $X_1Y_1Z_1$. To convert the fundamental forms $\Phi_{1.g}$ and $\Phi_{2.g}$ into the new coordinate system, the corresponding fundamental form, either $\Phi_{1.g}$ or $\Phi_{2.g}$, is required to be premultiplied by $\mathbf{Rs}(1 \to 2)$ and then postmultiplied by $\mathbf{Rs}^T(1 \to 2)$.

Implementation of Equations (4.38) and (4.39) significantly simplifies formulae transformations.

The following equations

$$\left[\boldsymbol{\Phi}^*_{1.c}\right] = \mathbf{Rs}^T(1 \to 2) \cdot \left[\boldsymbol{\Phi}_{1.c}\right] \cdot \mathbf{Rs}(1 \to 2) \tag{4.40}$$

$$\left[\boldsymbol{\Phi}^*_{2.c}\right] = \mathbf{Rs}^T(1 \to 2) \cdot \left[\boldsymbol{\Phi}_{2.c}\right] \cdot \mathbf{Rs}(1 \to 2) \tag{4.41}$$

similar to Equations (4.38) and (4.39), are valid for the generating surface T of the gear cutting tool.

Section II

Form Gear Cutting Tools

The kinematics of nongenerating methods of gear machining is the simplest form possible. It is often represented by one of those motions that cause a surface to slide over it. Screw motion of constant pitch is the most general type of motions that cause surfaces to slide over them. Consider a screw surface performing a screw motion. Let us assume that the axis of the screw motion is aligned with the axis of the screw surface, and screw parameters of the surface and of the motion are identical to each other. Under such a scenario, the enveloping surface to successive positions of the screw surface in the screw motion is congruent to that same screw surface. This means that the screw motion causes the screw surface to slide over it.

When the parameter of screw motion increases, and approaches an infinite value, the screw motion reduces to a straight motion. When a cylindrical surface (a surface of translation) performs a straight motion, consequently generating a straight line, then the enveloping surface to successive positions of the cylindrical surface in a straight motion is congruent to the cylinder itself. This property of straight motions allows for interpretation in the form that motion of this kind causes cylinders to slide over them.

When the parameter of screw motion decreases and approaches zero, the screw motion reduces to a rotation. When a surface of revolution performs a rotation about its axis of rotation, the enveloping surface to successive positions of the surface of revolution in its rotational motion is congruent to the surface of revolution itself. This property of rotation motion allows for interpretation in the form that motions of this type cause surfaces of revolution to slide over them.

There are three types of motions that cause surfaces to slide: (1) screw motion of constant pitch, (2) straight motion, and (3) rotational motion.

Motions of such types are widely used when machining tooth flanks of the work gear. Tooth flanks of gears of many types allow for sliding over themselves (see Chapter 1).

5

Gear Broaching Tools

A gear broach is a cutting tool used for the rapid machining of a desired contour in a workpiece surface by moving a cutter entirely past the workpiece. Broaches are often used to cut internal and external gear teeth, racks, gear segments on small gears, and are usually designed to cut all teeth at the same time.

The broach has a long series of cutting teeth. Broach teeth are divided into two groups: roughing cutting teeth and finishing cutting teeth. Roughing cutting teeth of the broach gradually increase in height. What would be feed in other types of machining is designed into the broach and is called *chip per tooth*. The last few teeth of the broach are designed to finish the cut rather than to remove considerable amount of stock. These cutting teeth are referred to as the *finishing teeth*. Normally, finishing teeth are of uniform dimensions to take off the final increment of stock, completing the form to the major tooth shape. Cutting edges of the finishing teeth of the gear broach are located within the generating surface of the gear broach.

5.1 Kinematics of the Gear Broaching Process

In the classification of types of gear machining meshes (Figure 3.8), the gear machining mesh for the gear broaching process is reduced to the simplest type. The kinematics includes just one rotation $\boldsymbol{\omega}_g \equiv \boldsymbol{\omega}_c$, which does not affect the generation of the work gear tooth flank. The magnitude of this rotation can be of any reasonable value, and can be of zero value in particular.

To transform the gear machining mesh into the corresponding kinematics of the gear broaching process, a cutting motion is added to the gear machining mesh. In Figure 5.1, the cutting motion is represented as the superposition of the straight motion $\mathbf{V}_{cut}$ and the linear speed of the rotation $\boldsymbol{\omega}_{cut}$. Superposition of two motions, $\mathbf{V}_{cut}$ and $\boldsymbol{\omega}_{cut}$, enables the broaching of a helical work gear.

The ratio of the translation V_{cut} and the rotation ω_{cut} is specified by the pitch helix angle ψ_g of the work gear. Broaches for machining spur gears are designed on the assumption that $\omega_{cut} = 0$, and $V_{cut} \neq 0$. Physically, broaching is feasible when $\omega_{cut} \neq 0$ and $V_{cut} = 0$. Such kinematics of the machining process can be used for broaching of external and/or internal round racks. Methods of gear machining and corresponding designs of gear cutting tools based on kinematics ($\omega_{cut} \neq 0$ and $V_{cut} = 0$) have not been investigated yet.

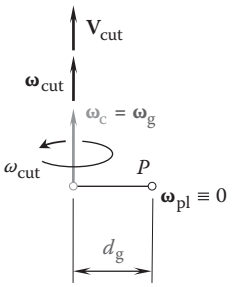

FIGURE 5.1
Kinematics of the gear broaching process.

5.2 Generating Surface of a Gear Broach

The generating surface of the gear broach is congruent to the tooth surfaces of the gear to be machined. The generating surface T of the broach for machining of spur gear is congruent to the spur gear being machined. Similarly, the generating surface of the broach for machining of helical gear is congruent to the helical gear being machined. This promptly yields an equation of the generating surface T of the gear broach

$$\mathbf{r}_c(U_c, V_c) = \begin{bmatrix} r_{b.c}\cos V_c + U_c \sin\psi_{b.c}\sin V_c \\ r_{b.c}\sin V_c - U_c \cos\psi_{b.c}\sin V_c \\ r_{b.c}\cot\psi_{b.c} - U_c\cos\psi_{b.c} \\ 1 \end{bmatrix} \tag{5.1}$$

where U_c and V_c are the curvilinear coordinates of the generating surface T, $r_{b.c}$ is the radius of the base cylinder of the generating surface T (Figure 5.2), and $\psi_{b.c}$ is the base helix angle of the surface T.

All roughing cutting edges of the gear broach are shifted inward, bounded by the generating surface T. Finishing cutting edges are located within the generating surface T of the gear broach. Theoretically, any line within the generating surface T can be used as the cutting edge of finishing teeth of the gear broach. Deviations of the finishing cutting edges from the surface T cause the corresponding deviation of the actually machined gear from its desired shape.

Based on Equation (5.1), the following expression

$$\mathbf{G}_T = \begin{bmatrix} 1 & -\dfrac{r_{b.c}}{\sin\psi_{b.c}} \\ -\dfrac{r_{b.c}}{\sin\psi_{b.c}} & \dfrac{U_c^2\sin^4\psi_{b.c} + r_{b.c}^2}{\sin^2\psi_{b.c}} \end{bmatrix} \tag{5.2}$$

can be derived for the first fundamental matrix of the generating surface T of the gear broach.

Furthermore, the second fundamental matrix of the generating surface T of the gear broach can be expressed in the form

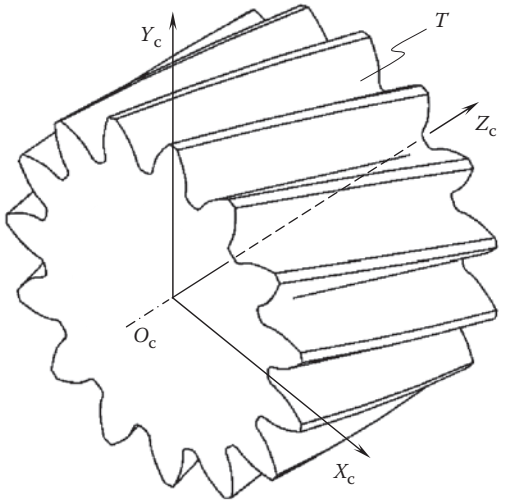

FIGURE 5.2
Geometry of generating surface T of the gear broach.

$$\mathbf{D}_T = \begin{bmatrix} 0 & 0 \\ 0 & U_c \sin\psi_{b.c} \cos\psi_{b.c} \end{bmatrix} \tag{5.3}$$

Use of the first ($\mathbf{G}_T$) and the second ($\mathbf{D}_T$) fundamental matrices simplifies the derivation of equations relating to the geometry of the generating surface T of the gear broach.

In a method largely similar to that described above, an equation for the generating surface T of the gear broach for machining noninvolute tooth profiles can be derived. Ultimately, the derived equation for surface T allows for simple formulae for the computation of many of the design parameters of the gear broach.

5.3 Cutting Edges of the Gear Broaching Tools

Cutting edges of a gear cutting tool are viewed in the sense of lines of intersection of the rake surface R_s and the clearance surface C_s. Cutting edges of roughing and semiroughing teeth are located beneath the generating surface T of the gear broach. Cutting edges of the finishing teeth of the gear broach are within the generating surface T.

There is greater freedom in designing roughing and semiroughing teeth of a gear broach. Design of finishing cutting edges is more restricted by the necessity of having to locate them within the generating surface T.

The desired cutting edges of the finishing cutting teeth of a gear broach can be specified in terms of the generating surface T of the gear broach and the rake surface R_s.

5.3.1 Rake Surface of Finishing Teeth of a Gear Broach

Designing a gear broach can be interpreted as transformation of a rigid body bounded by the generating surface T into the corresponding cutting tool capable of cutting off the

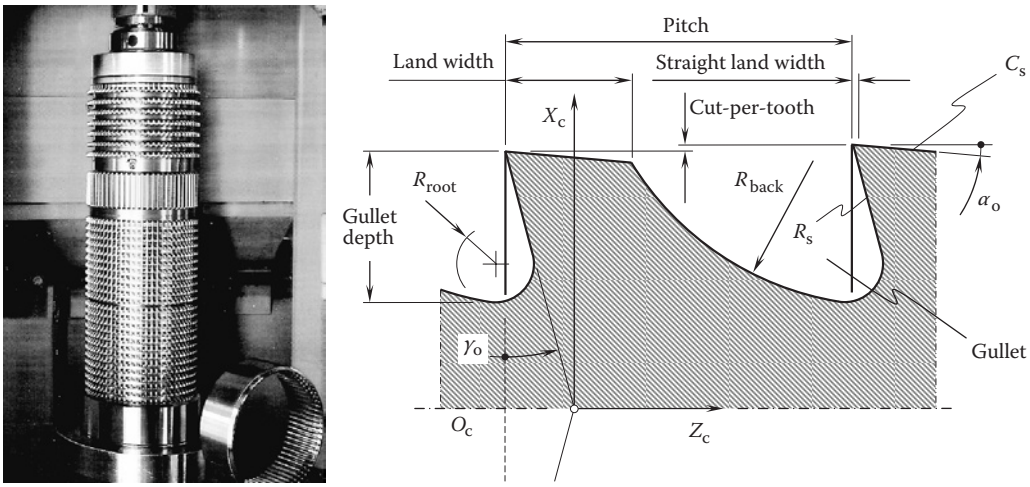

FIGURE 5.3
Principal design parameters of the cutting tooth of a gear broach.

stock. Following this concept, gullets are required to be machined. The term *gullet* is often applied to *chip space*.

The axial profile of a gear broach gullet is shown in Figure 5.3. It is shaped by: (1) axial profile of the rake surface R_s; (2) root radius R_{root}, the radius just below the cutting edge and that blends into the back of the tooth radius (and sometimes referred to as *face angle radius*); (3) back radius R_{back}, the radius on the back of the tooth in the chip space; and (4) axial profile of the clearance surface C_s, which is often referred to as *land*. For the finishing teeth of a gear broach, the cutting edge can follow by straight land, which is used for finishing teeth to retain broach size after a series of resharpenings. For the gullet depth, the term *tooth depth* is also used. The distance between two adjacent broach teeth is referred to as *pitch* of the broach teeth. Pitch is the distance from the cutting edge of one tooth to the corresponding point on the next tooth.

Chips from a broach are of necessity confined in the space between the teeth. Therefore, it is absolutely necessary to provide an adequate chip space when designing the broach. If this is not carried out, there is a chance of dulling or even breaking the tool, and roughing or tearing the surface of the work being broached. Chip space is limited by the pitch of the teeth and, in small broaches, by the diameter of the broach. Broaching in general requires the use of chip breakers.* Otherwise, an overly wide chip may be produced. Such chips are difficult to control and are usually handled by providing staggered chip breakers on successive broach teeth.

Surfaces of two major types are practically used as rake surfaces of gear broaches: (1) surface of a cone of revolution and (2) Archimedean screw surface.

Conical rake surface. Rake surface in the form of a cone of revolution is coaxial with the gear broach itself. Equation of the conical rake surface is necessary for further analysis.

A Cartesian coordinate system $X_cY_cZ_c$ is associated with the gear broach as shown in Figure 5.3. In this coordinate system, every point of the generating straight line of the rake

* *Chip-breakers* are notches in the teeth of broaches that divide the width of chips, facilitating their removal.

surface R_s satisfies the equality $Z_c = -X_c \tan \gamma_o$, where γ_o denotes the rake angle at the top cutting edge of the gear broach.*

In the case being considered, position vector of a point $\mathbf{r}_{rs}$ of the rake surface R_s can be expressed in terms of the current diameter $d_{y.c}$ of the broach, the rake angle γ_o, and the angular parameter ϑ_{rs}

$$\mathbf{r}_{rs}(d_{y.c}, \vartheta_{rs}) = \begin{bmatrix} \frac{d_{y.c}}{2} \cdot \sin \vartheta_{rs} \\ \frac{d_{y.c}}{2} \cdot \cos \vartheta_{rs} \\ -\frac{d_{y.c}}{2} \cdot \tan \gamma_o \\ 1 \end{bmatrix} \tag{5.4}$$

where current diameter $d_{y.c}$ and angular parameter ϑ_{rs} are viewed in the sense of Gaussian coordinates of the rake surface R_s.

Rake surface in the form of Archimedean screw surface. Gear broaches having the rake surface in the form of Archimedean screw surface are convenient in resharpening. The screw rake surface eliminates the necessity of indexing after sharpening of each tooth of the broach.

Screw rake surface R_s is generated by the straight line $Z_c = -X_c \tan \gamma_o$ that is performing a screw motion with a certain screw parameter p_{rs} of the screw motion. If the axial pitch of the gear broach is designated as p_c, then the screw parameter is equal to $p_{rs} = \frac{p_c}{2\pi}$. Ultimately, the matrix representation of the equation

$$\mathbf{r}_{rs}(d_{y.c}, \vartheta_{rs}) = \begin{bmatrix} \frac{d_{y.c}}{2} \cdot \sin \vartheta_{rs} \\ \frac{d_{y.c}}{2} \cdot \cos \vartheta_{rs} \\ -\frac{d_{y.c}}{2} \cdot \tan \gamma_o + p_{rs} \vartheta_{rs} \\ 1 \end{bmatrix} \tag{5.5}$$

of the Archimedean screw rake surface R_s can be derived.

In Equation (5.5), the screw parameter p_{rs} is a signed value. It is positive for the right-handed Archimedean screw rake surface, and negative for the left-handed rake surface R_s.

Rake angle γ_o for gear broaches is practically of small value and does not exceed 10 ($\gamma_o \leq 10°$). When the equality $\gamma_o = 0°$ is observed, Equation (5.5) reduces to

* The rake angle γ_o at the top cutting edge of gear broach is often referred to as the *face* angle, and sometimes also called the *hook* angle.

$$\mathbf{r}_{rs}(d_{y.c},\,\vartheta_{rs}) = \begin{bmatrix} \dfrac{d_{y.c}}{2}\cdot\sin\vartheta_{rs} \\ \dfrac{d_{y.c}}{2}\cdot\cos\vartheta_{rs} \\ p_{rs}\vartheta_{rs} \\ 1 \end{bmatrix} \tag{5.6}$$

Equations (5.4) and (5.5) make it possible to derive the first $\mathbf{G}_{rs}$ and the second $\mathbf{D}_{rs}$ fundamental matrices of the rake surface R_s of a gear broach.

5.3.2 Clearance Surface of Gear Broach Teeth

The purpose of the clearance surface is twofold. First, the clearance surface C_s provides clearance between the broach tooth and the machined surface. The clearance is necessary to reduce friction, which causes heat generation and increases tooth wear of the broach. Second, clearance surface must be of the shape that is capable of maintaining the tooth profile after every resharpening of the worn broach.

Gear broaches feature very small clearance angles.* Clearance angle α_o at the top cutting edges of roughing teeth is at the range of $\alpha_o \cong 4°$. For semifinishing cutting edges, the clearance angle is reduced to $\alpha_o \cong 2°$. Finally, the clearance angle at finishing cutting edges is in the range of $\alpha_o \cong 0.5°$.

The desired clearance surface C_s of the lateral profile of the gear broach tooth can be generated by the cutting edge that is performing a screw motion.

To derive the equation for the cutting edge CE of the gear broach tooth, the equation for the generating surface T of the broach [Equation (5.1)] is considered together with the equation for the rake surface R_s [see Equations (5.4) through (5.6)]. Without going into details of the derivation, let us assume that the equation of the cutting edge CE is derived and is presented in vector form $\mathbf{r}_{ce} = \mathbf{r}_{ce}(\xi_{ce})$, where ξ_{ce} denotes the parameter of the cutting edge of the gear broach tooth.

Furthermore, in order to generate the clearance surface C_s of the desired shape, the cutting edge $\mathbf{r}_{ce} = \mathbf{r}_{ce}(\xi_{ce})$ is performing a screw motion with a certain screw parameter p_{cs}. The value of the screw parameter p_{cs} depends on the required value of the normal clearance angle α_N at the lateral cutting edge of the gear broach tooth, and on the design parameters of the gear broach. The screw motion of the cutting edge can be analytically described either using the corresponding matrices of translation along and rotation about the axis of the gear broach or the corresponding operator of screw motion can be implemented for this purpose. Ultimately, use of the operator $\mathbf{Sc}_z(\vartheta_{cs}, p_{cs})$ [see Equation (4.19)] of screw motion yields an expression

$$\mathbf{r}_{cs}(\xi_{ce},\,\vartheta_{cs}) = \mathbf{Sc}_z(\vartheta_{cs},\,p_{cs})\cdot\mathbf{r}_{ce}(\xi_{ce}) \tag{5.7}$$

for the position vector $\mathbf{r}_{cs}$ of a point of the clearance surface C_s of the gear broach tooth.

* Clearance angle of gear broach is also referred to as *back-off angle*. This is a relief angle back of the cutting edge.

The roughing cutting teeth of a gear broach do not require an accurate profiling. This is because the final accuracy of the machined gears depends on the accuracy of the finishing teeth of the broach and not on the accuracy of its roughing teeth. Rake angle γ_o and clearance angle α_o of small values ($\gamma_o = 0°$ and $\alpha_o \cong 0.5°$) allow for simplification of the problem of profiling of the finishing cutting edges.

The generating surface T of a gear broach is congruent to the tooth flank surface of the gear to be machined. Therefore, no cusps occur on tooth flanks of the machined gear.

5.4 Chip Removal Diagrams

When broaching gears, almost the entire material found in the space between two adjacent gear teeth is removed by roughing broach teeth. Broach performance largely depends on the type of chip removal diagram that has been used in the design of the broach. Chip removal diagrams specify the shape and parameters of the cross section of stock removed by the broach teeth. Numerous chip removal diagrams are known.

Without going into details of the analysis, consider how the stock between two adjacent teeth of the gear is removed by the gear broach using a conventional cutting diagram (Figure 5.4).

A gear broach features a progressive increase in tooth height from tooth to tooth of the broach. The progressive increase in tooth height is often referred to as *cut per tooth*. Cut per tooth is also referred to by some authors as *chip per tooth*. The action of the step height produces the equivalent of feed in other types of machining.

Broaches are designed with an aim toward simple production and easy maintenance of gear cutting tools of this design.

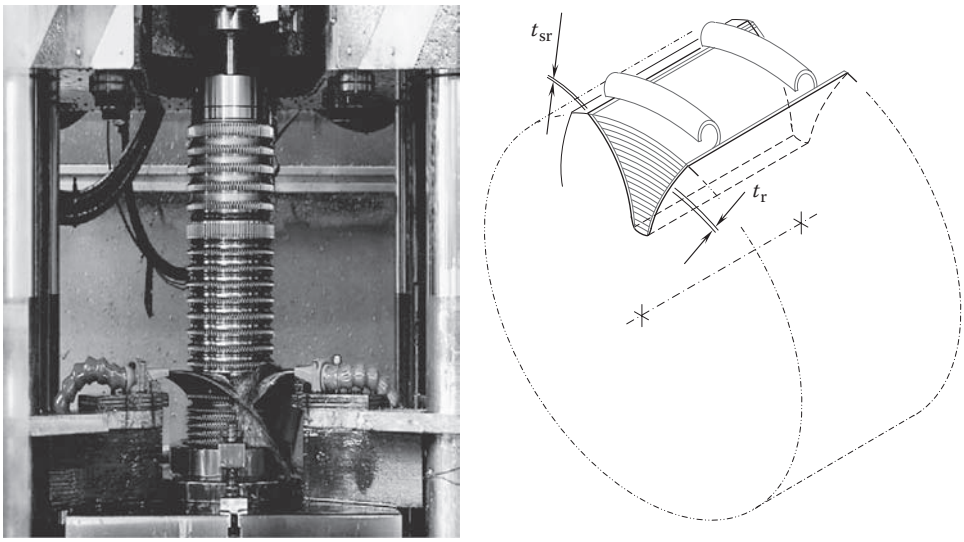

FIGURE 5.4
Chip removal diagram of an ordinary gear broach.

Production of gear broaches can be simplified if the roughing teeth of the broach are designed in the same way when they roughly *generate* the teeth flanks of the gear being machined. Cut per tooth for roughing cutting teeth of the gear broach is of a certain value, t_r. This means that every roughing cutting tooth of the gear broach is t_r higher than the previous one. Cross sections of the removed chips in this case are of almost rectangular form. The removed material easily deforms into the chip. No interference in chip flows is observed in this case, and thus it is easy to accommodate the chip in the gullet.

Cutting teeth of the semifinishing section of the gear broach are designed in the same way when they are *copying* the tooth flank of the gear being machined. Cut per tooth for semiroughing cutting teeth of the gear broach is of a certain value, t_{sr}. Every cutting tooth of the semiroughing section of the gear broach is $2t_{sr}$ wider than the previous one. Cross sections of the removed chips are slightly curved following the involute profile of the tooth flanks. However, the removed material in this case also easily deforms into the chip. No interference in chip flows is observed in this case, and it is easy to accommodate the chip in the gullet.

It has been proven practical to assign cut per tooth t_r within the roughing section of the gear broach greater than the t_{sr} for semiroughing teeth of the broach.

Teeth of the work gear are finally generated by the finishing teeth of the gear broach. Cut per tooth for finishing cutting teeth of the gear broach is of zero value.

5.5 Sharpening of Gear Broaches

Sharpening as well as resharpening of gear broach is a type of grinding operation. Gear broach resharpening is performed on the rake surface. Rake surface of roughing broach teeth is shaped in the form of an internal cone of revolution. It is grinding by external cone surface of the grinding wheel. Because of this, grinding of the rake surface of gear broaches must deal with a geometrical problem that strictly relates to the satisfaction/violation of the third necessary condition of proper part surface generation [66, 67, 124, 128, 136, 138, 143] (see Appendix B).

The rake surface R_s of a gear broach tooth is shaped in the form of an internal cone of revolution (Figure 5.5). The cone surface R_s can be specified in terms of the rake angle* γ_o of the gear broach and the broach diameter $d_c^{(min)}$. The closest point A of the straight profile of the rake surface R_s is remote from the axis of rotation O_c of the broach at the distance $0.5 \cdot d_c^{(min)}$.

The generating surface T_{gw} of the grinding wheel is shaped in the form of a cone or revolution. The cone surface T_{gw} can be specified in terms of its diameter, d_{gw}, and the angle of the cone, φ_{gw}. Diameter d_{gw} specifies the location of point A on generating surface T_{gw} of the grinding wheel.

Angle β is the angle that the axis of rotation O_{gw} of the grinding wheel makes with the axis of rotation O_c of the gear broach. Two of the three angles, γ_o, φ_{gw}, and β, are given. The third one can be expressed in terms of the two given angles. Usually, angles γ_o and β are known. In this case, the expression

* Another term is also applied for the rake angle γ_o. Sometimes, it is referred to either as the *face angle* or as the "hook" angle.

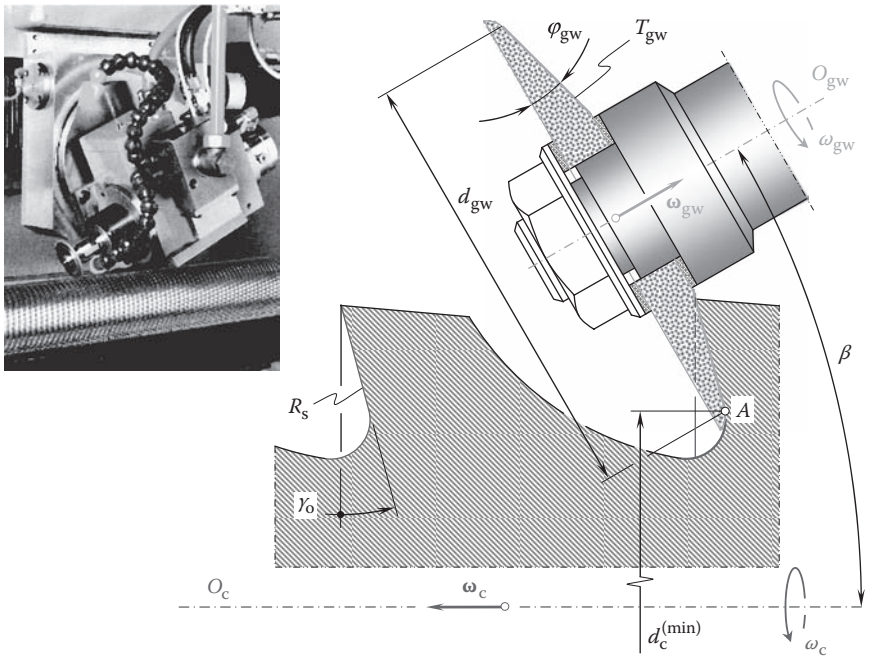

FIGURE 5.5
Geometrical constraints on the design parameters and the setup parameters of the grinding wheel for sharpening of the gear broach.

$$\varphi_{gw} = \beta - \gamma_o \tag{5.8}$$

is used to compute for the actual value of the grinding wheel angle, φ_{gw}.

A gear broach is supported at the center during resharpening. The grinding wheel is rotating about its axis O_{gw} with a certain angular velocity ω_{gw}. The rotation ω_{gw} provides the necessary speed of cut. The broach is rotating about its axis of rotation O_c with an angular velocity ω_c. Rotation ω_c serves as the feed motion.

For a gear broach, it is necessary to choose the appropriate grinding wheel size so that it does not interfere with the broach tooth.

The surfaces R_s and T_{gw} make contact along the straight line. This line is the common straight generating line for the cone surfaces R_s and T_{gw}. For the surface of internal cone R_s, all radii of normal curvature ρ_{rs} are negative ($\rho_{rs} < 0$). For the generating surface T_{gw} of the grinding wheel, all radii of normal curvature are positive ($\rho_{gw} > 0$). Magnitudes of radii of normal curvature ρ_{rs} and ρ_{gw} are not constant within the line of contact of surfaces R_s and T_{gw}. Interference of the generating surface T_{gw} into the rake surface R_s may occur if the inequality $\rho_{gw} \geq |\rho_{rs}|$ is valid. Point A is the first point at which the third necessary condition of proper part surface generation can be violated. If the third condition is satisfied at point A, then it is satisfied at all other points of the line of contact of surfaces R_s and T_{gw}.

The inequality $\rho_{gw} \geq |\rho_{rs}|$ casts into the following formula for the computation of the maximal feasible outer diameter d_{gw} of the grinding wheel

$$d_{gw} \leq d_c^{(min)} \cdot \frac{\sin(\beta - \gamma_o)}{\sin \gamma_o} \tag{5.9}$$

Details on the derivation of Equation (5.9) are available from ref. [143] and other sources.

For machining gears, gear broaches with a helical gullet* are widely used. The term *helical gullet* means chip space that wraps around a broach tool helical line (a thread†).

In a manner similar to that discussed above, a formula for the computation of maximal permissible outer diameter d_{gw} of the grinding wheel for sharpening gear broaches having helical gullet can be derived. Definitely, in the last case, the maximal diameter d_{gw} of the grinding wheel would depend on the helix angle of the grooves of the gear broach.

Another method of sharpening the gear broach on the rake surface [143] features the line of contact of the rake face R_s with the grinding wheel surface T_{gw} that splits into two branches. Generating of the rake surface R_s is performed either by the line (by the circle) or by narrow generating surface T_{gw} of the grinding wheel. The rake surface R_s is generated approximately in the first case, and accurately in the second case.

Because the rake angle γ_o of the gear broach has a positive value ($\gamma_o > 0°$), the rake surface R_s is shaped in the form of an inner cone of revolution. Grinding of the concave surface imposes constraints on the maximal permissible outer diameter of the grinding wheel. To avoid violating the third necessary condition of proper part surface generation [66, 67, 124, 128, 136, 138, 143] (see Appendix B), the outer diameter of the grinding wheel must satisfy the condition specified by the inequality (5.9). It is definitely more practical to sharpen the gear broach with a grinding wheel of the largest possible outer diameter. However, no possibilities of increasing the grinding wheel diameter have been observed in the discussed method (Figure 5.5) of sharpening of gear broaches.

A novel method of resharpening gear broaches whose concept is illustrated in Figure 5.6 resolves this issue. The generating surface T_{gw} of the grinding wheel is shaped in the form of an external cone surface of revolution. Sharpening of the broach on rake surface R_s is performed with the grinding wheel having a hole in the center. The gear broach to be sharpened is passing through the hole, as shown in Figure 5.6.

When sharpening a gear broach of outer diameter $d_{o.c}$, the broach is rotating about its axis of rotation O_c. In Figure 5.6, the rotation of the broach is designated as ω_c. The grinding wheel is rotating about its axis of rotation O_{gw}. The rotation of the grinding wheel is designated as ω_{gw}. The axis of rotation of the grinding wheel O_{gw} intersects the axis of rotation of the gear broach O_c at a certain angle δ.

To avoid violating the third necessary condition of proper part surface generation, both the design parameters of the grinding wheel as well as its setup parameters should be determined in compliance with the design parameters of the gear broach to be resharpened.

Point A of the axial profile of rake surface R_s is located at a distance of $0.5d_{f.c}$ from the axis O_c of the gear broach. This point is the critical point from the standpoint of satisfaction/violation of the third necessary condition of proper part surface generation. It is the closest point of the axial profile of rake surface R_s to axis O_c of the gear broach. If the condition is satisfied at point A, then it is satisfied at all other points of the axial profile of rake surface R_s.

---

* *Helical gullet* is also referred to as *spiral gullet*.

† Gear broaches having helical gullets also feature the so-called *shear cutting tooth*, which is specifically positioned so that it does not make a right angle with the direction of broach motion. The shear tooth cuts with a shear action, with maximum tooth overlap. The top cutting edge of the shear cutting tooth is at *shear angle* with respect to the broach axis. The shear angle is the angle between the cutting edge of a shear tooth and a line perpendicular to the broach axis or line of travel on surface broaches. In reality, the term *shear angle* is equivalent to the conventional term *angle of inclination* of the cutting edge.

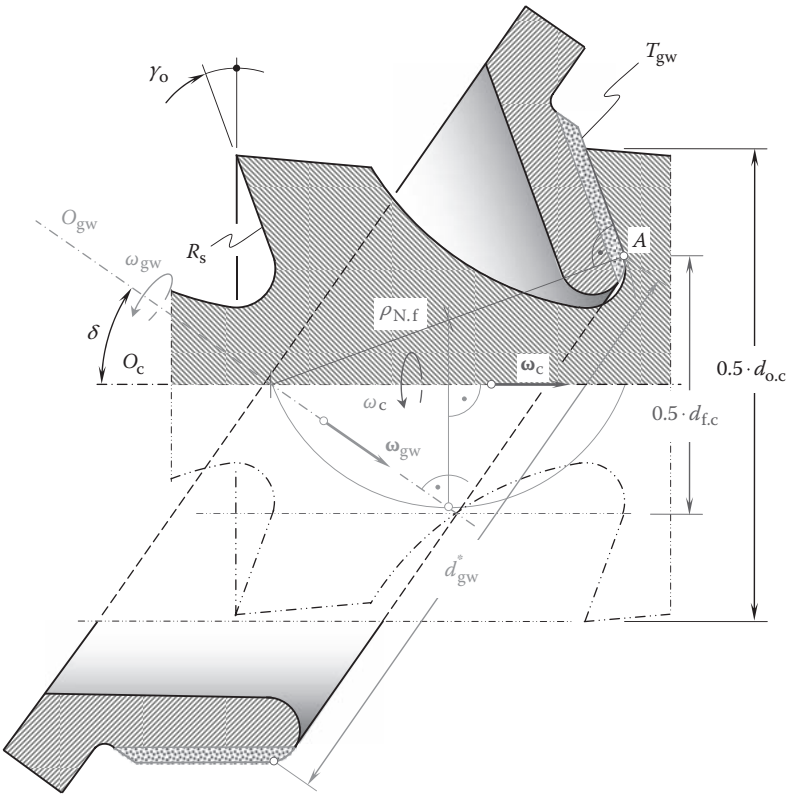

FIGURE 5.6
Schematic diagram of a method of resharpening of the gear broach.

Consider a normal cross section of surfaces R_s and T_{gw} through point A. The normal cross section is perpendicular to the line of contact of surfaces R_s and T_{gw}. The radius of curvature of rake surface R_s at this normal cross section is designated as $\rho_{N.f}$. The radius of normal curvature $\rho_{N.f}$ has a negative value ($\rho_{N.f} < 0$). This is because rake surface R_s is a concave surface. The corresponding radius of the normal curvature of the generating surface T_{gw} of the grinding wheel is designated as $\rho_{N.c}$. The radius $\rho_{N.c}$ is not shown in Figure 5.6. Because the generating surface T_{gw} is a convex surface, the radius of normal curvature $\rho_{N.c}$ has a positive value ($\rho_{N.c} > 0$).

The third necessary condition of proper part surface generation is satisfied if and only if the inequality

$$\rho_{N.c} \leq |\rho_{N.f}| \tag{5.10}$$

is satisfied.

The radii of normal curvature $\rho_{N.f}$ and $\rho_{N.c}$ can be expressed in terms of the design parameters of the gear broach and the grinding wheel, and then substituted into Equation (5.10). In this manner, the maximal permissible outer diameter d^*_{gw} of the grinding wheel and the angle δ can be determined. The diameter d^*_{gw} of the grinding wheel significantly exceeds that for the grinding wheel that is applicable in the method illustrated in Figure 5.5.

The presented method of computing for the design parameters and setup parameters of the grinding wheel can be enhanced to determine the maximal possible outer diameter d^*_{gw} of the grinding wheel. This is a particular example of the problem of optimization that can be solved using conventional methods [136, 138, 143, 153].

The method presented in Figure 5.6 can also be applied to grinding of gear broaches having helical gullets. For this case, axes O_c and O_{gw} are skewed, and are at a distance of $C_{c/gw}$ from each other. The same condition [see inequality (5.10)] should be satisfied when helical gullets are grinding.

5.6 A Concept of Precision Gear Broaching Tool for Machining Involute Gears

The finishing cutting edges of a gear broach are within the generating surface T of the broach—this is required for precision gear broaches. This requirement offers considerable freedom to the designer of the gear broach. Any line of reasonable shape that is within the generating surface T of the gear broach can be used as the finishing cutting edge. This setup is illustrated in Figure 5.7.

The finishing cutting edge *ab* can be configured so that it is inclined at a certain rake angle $\gamma_o > 0°$ at the top cutting edge. No physical restrictions are imposed on the configuration of the finishing cutting edge *ab*. As long as the finishing cutting edge *ab* is within the generating surface *T*, the accuracy of the gear broach is assured.

Because of chip, cut by the finishing cutting edges of the gear broach is thin, the rake angle γ_o does not affect the material removal process. Roundness of the cutting edge ρ_c is a more critical design parameter of the finishing cutting edges. Because of this, the fin-

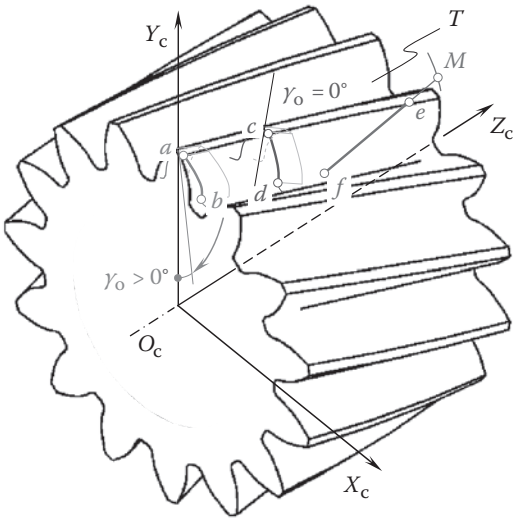

FIGURE 5.7
Feasible shapes and configurations of finishing cutting edges of an involute gear broach.

ishing cutting edge *cd* of the gear broach is configured so that the rake angle $\gamma_o = 0°$. This configuration of the finishing cutting edges is practical.

As discussed earlier, the generating surface *T* of the gear broach is a screw involute surface, which can be generated by the corresponding screw motion of a straight line. This means that a straight line can be drawn up on any screw involute surface. As an example, the straight-line segment *ef* is drawn in Figure 5.7. All points of the straight-line segment *ef* are within the generating surface *T* of the gear broach. None of others the straight lines can be located within the screw involute surface. Only a particular configuration of the straight line results in a line that is within the screw involute surface *T*. This particular configuration of the lateral cutting edge of the involute gear broach can be expressed in terms of its design parameters.

Various options are available to the designer of the involute broach in this case. Numerous configurations of straight lateral cutting edges at opposite sides of the tooth profile can be of practical importance. As an example, consider the configuration of two lateral straight cutting edges that are within a common plane. First, this particular configuration of the cutting edges of the gear broach is helpful for understanding the principal features of the geometry of the involute broach. Second, analysis of the location of straight lateral cutting edges of the involute broach can be used for the development of other practical configurations.

Without loss of generality, consider the determination of the desired configuration of just two straight lateral cutting edges of the finishing section of the precision involute broach (Figure 5.8). The descriptive geometry–based method is used for this purpose.

The involute broach is shown in the system of projective planes so that the axis O_c is perpendicular to the plane of projections π_3. The outer diameter of the broach is designated as $d_{o.c} = 2r_{o.c}$, and its base diameter is denoted by $d_{b.c} = 2r_{b.c}$. The diameter $d_{f.c} = 2r_{f.c}$ is the

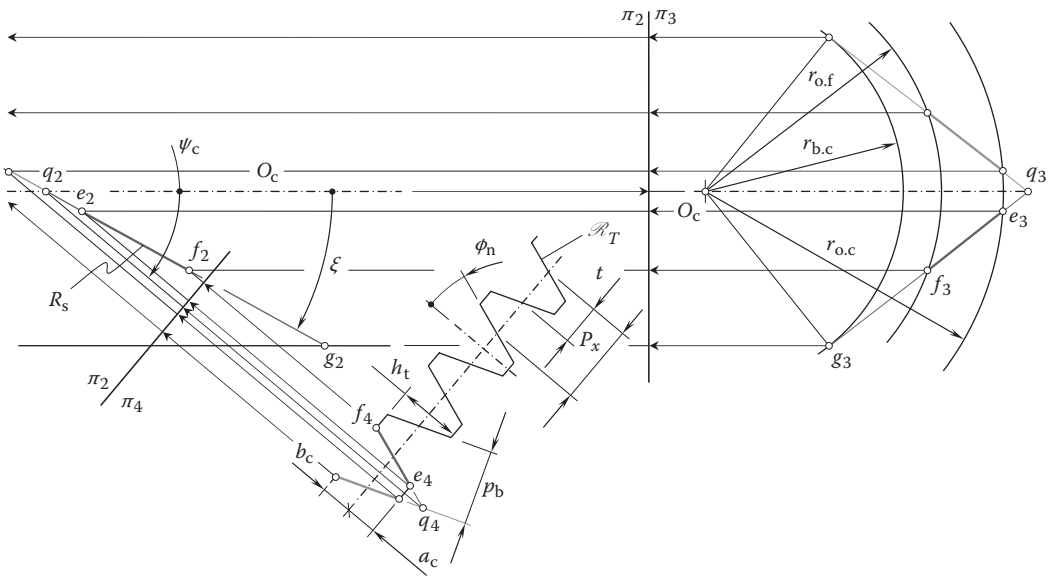

FIGURE 5.8
Determination of the configuration of straight lateral cutting edges within the rake plane R_s of the finishing tooth of a broach for involute gear.

smallest diameter of the circle, the point of the lateral cutting edge that still generates the gear tooth profile.

The normal cross section of the auxiliary rack $\mathscr{R}_T$ of the involute broach is shown in the plane of projections π_4. The location of this plane of projections is specified by the pitch helix angle ψ_c of the broach. Tooth flanks of the opposite sides of the tooth profile of the generating surface T of the broach intersect each other along a screw line. This line intersects the plane of projections π_4 at point q_4. The projections q_2 and q_3 of point q are constructed using conventional methods developed in descriptive geometry.

The straight lateral cutting edges of the involute broach align with the straight line that is tangent from the opposite sides to the base helices of the generating surface T. In the plane of projections π_3, these straight lines are tangent from the opposite sides to the base cylinder of the broach. The projection e_3f_3 of the lateral cutting edge is used for the construction of other projections e_2f_2 and e_4f_4 of the cutting edge *ef*. The cutting edge *ef* in Figure 5.8 corresponds to the cutting edge *ef* in Figure 5.7. The opposite straight lateral cutting edge is located within the rake plane R_s and is symmetrical to the cutting edge *ef*. In Figure 5.8, the opposite cutting edge is not labeled. The constructed rake plane R_s forms a certain angle ξ with the broach axis O_c. The required value of the angle ξ can be expressed in terms of the design parameters of the involute broach:

$$\xi = \tan^{-1} \frac{\cos \psi_c}{\sin \psi_c + \left(\sqrt{\dfrac{(d_c + t_c \cot \phi_n)^2}{d_{b.c}^2} - 1} \right) \tan \phi_n} \tag{5.11}$$

where

d_c = pitch diameter of the involute broach
t_c = tooth thickness
ϕ_n = normal pressure angle

For practical purposes, the straight lateral cutting edges of the opposite sides of the tooth profile can be shifted in the axial direction with respect to each other at a certain distance. The decision that the designer of the involute broach makes in this regard depends on the particular requirements that the broach is required to satisfy.

The discussed design concept of the precision gear cutting tool having straight lateral cutting edges for machining involute gears was developed by Radzevich in the late 1970s [130, 154].

5.7 Application of Gear Broaching Tools

The forming of gear teeth has traditionally been a time-consuming heavy stock removal operation for which close tooth size, shape, runout, and spacing accuracy are required.

A gear machining process in which material from a work gear is removed by pulling or pushing a broach along the axis of the work gear is called *broaching*. The actual cutting action of any single broach tooth is very much similar to that of a single form tool. Each section of the broach has as many teeth as there are tooth spaces on the gear.

Gear broaching is primarily applicable to high-volume jobs requiring high production rates. Gears can be broached accurately since a number of the elements are controlled by the accuracy of the broach. In addition, broaching can produce a fine finish on the gear tooth profile. Occasionally, it may be used in fairly small lot production to obtain an accuracy level on a critical part that cannot readily be made with a high degree of accuracy by other methods. However, a gear broach will cut only parts that have identical gear specifications.

5.7.1 Broaching Internal Gears

A broach can be used to machine almost any internal form. The part teeth can be either equally or unequally spaced, and tooth forms can be either symmetrical or asymmetrical. The tooth forms must be uniform in the direction of the broach axis, and the wall of the part must be strong enough to withstand the broaching pressure.

Small internal gears can be cut in a single pass of a broach. Large internal gears can be made by using a surface type of broaches to make several teeth at a single pass. Indexing of the gear and repeated passes of the broach can produce a complete gear. Gears as large as 1.5 m (60 in.) in diameter are made by this process.

Today, the broached internal helical running gears in automotive automatic transmissions are exclusively produced by full-form finishing high-speed steel broaches. Full-form finish broaching provides fine surface finishes, precision involute form, accurate tooth thickness and precision tooth spacing, and lead.

In some cases, broaches can be designed with a removable finishing section that finishes the complete tooth form. This "side-shaving" section of the broach finishes the entire profile of each gear tooth. A full form-finish section solves the profile problems caused by off-center drift of the broach, attributed to poor maintenance of machine alignment and perpendicularity or nonuniform tooth dulling.

In particular cases, gear broaches are designed with the so-called *burnishing button*. Burnishing button is a broach tooth without a cutting edge. A series of buttons is sometimes placed after the cutting teeth of a broach to produce a smooth surface by material compression.

Pull broaches and push broaches are used for machining gears.

Push broaches are normally short and therefore less expensive than pull broaches, which are longer. However, one pull broach can sometimes remove as much stock as several push broaches. Most internal broaching is carried out with pull broaches. Not only do they remove more stock than push broaches, they are also capable of raking much longer cuts.

Gear broaching usually requires a part with a through hole. However, blind holes can be broached if there is sufficient clearance beyond the broached section and if a series of punch-type broaches are used.

Broaching can produce close tolerances on profile, spacing, lead, and size.

5.7.2 Broaching External Gears

The fastest way to produce medium and high production external gears is by pot broaching. The basic process consists of a tool with internal teeth that are held in a pot being passed over a round part, and producing external shapes in the form of splines and involute gear teeth.

In the past, external gears were broached by either pushing the workpiece down through a stationary pot broach or mounting the workpiece on a stationary post and pushing the

pot broach down over it. This resulted in problems relating to chips packing in the chip gullets when using the push-down stationary pot broach method. Slow workpiece loading, attributed to the use of a plug-type approximate locator for each part, is a problem when broaching parts with the push-down stationary workpiece method.

Two more methods used were push-up pot broaching and pull-up broaching.

Push-up pot broaching consists of pushing the workpiece upward through a fixed pot broaching tool to produce external teeth under ideal conditions, assuring quick and complete chip removal from the broach teeth. Chips fall by gravity away from the tool and the work gear. The coolant is flushed into the tool area through a quick-disconnect coupling. Automatic loading is simplified because the part is elevated by the process and gravity is utilized to unload parts onto a conveyor [10].

Pull-up broaching is used when the part diameter and broach length are such that the required post diameter and length do not provide sufficient strength to rigidly support the workpiece. In this method, the work gear is pulled up through a stationary pot broaching tool with a pull rod. This process permits broaching parts with deeper teeth and wider faces by using longer tools.

Pot broaching tools are classified into two types: (1) the ring type for parts where tooth form and spacing are critical and (2) the lower-cost stick type, which is used where accuracy permits.

The ring-type pot broaching tool is made up of a holder with a series of individual precision ground keyed high-speed steel rings or wafers, each of whose internal cutting teeth are individually backed off. These rings can be sharpened via either the conventional face sharpening method or the progressive method, in which several face sharpenings are performed followed by inner diameter grinding of all rings. Ring-type pot broaches are used for precision running gears and splines where close tooth tolerances are required.

The stick-type pot broaching tool, which has lower-cost individual high-speed steel slab broach inserts, includes a holder that supports a series of keyed ground rings that locate the broach sticks in internal ground slots. On thin parts, the teeth in the stick inserts can have wide, long-life tooth lands, and can also be axially staggered to provide a helical pattern to balance the cutting forces.

These tools are particularly adapted to short face-width splines and gears, and are often used in combination.

5.8 Shear-Speed Cutting

With no or very little changes, the principles of profiling of gear broaching tools can be implemented for profiling of other gear cutting tools. Cutting tools for Shear-Speed®* cutting of gears is a good example in this regard.

5.8.1 Principle of Shear-Speed Cutting of Gears

The nature of the operation of shear cutting is quite similar to broaching. Form tool blades are used to shear-cut each space between the gear teeth. The same number of gear cutting

* Shear-Speed is a registered trademark of the Michigan Tool Co., Detroit, MI.

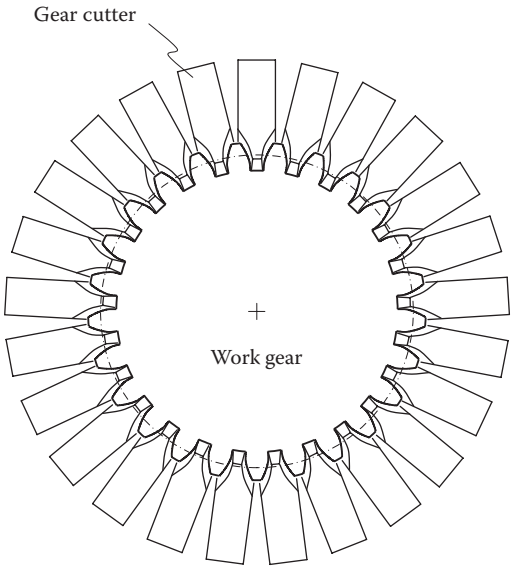

FIGURE 5.9
A set of form tools for machining a spur gear using Shear-Speed cutting principle.

tools as there are teeth in the work gear (Figure 5.9) is assembled radially in the cutting tool holder mounted at the head of the machine. The cutting tools can be compared with the teeth of the finishing section on a broach. All teeth in a gear are cut simultaneously in the Shear-Speed gear cutting process.

The principle of Shear-Speed cutting of gears is illustrated in Figure 5.10. The tool head assembly consists of three main parts: a retained housing, a radially slotted member that controls tool alignment, and a movable, double cone–shaped guiding unit that controls the feed. With the tool head being stationary, the part is reciprocated past the cutting tools. Each tool is fed radially at a predetermined distance with each stroke, until the full tooth depth is cut. All tools are retracted on each return stroke of the gear to avoid drag and are returned to their initial position at the end of each cycle.

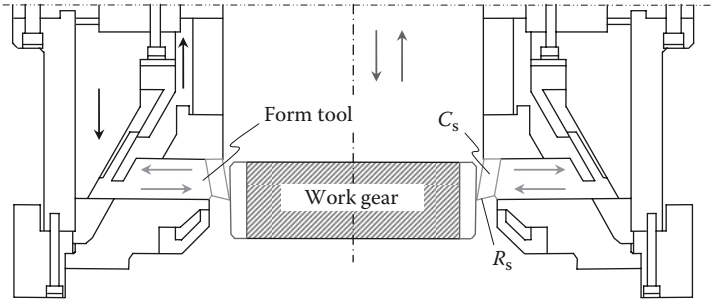

FIGURE 5.10
Kinematics of Shear-Speed cutting of spur gears.

5.8.2 Profiling of Form Tools for Shear-Speed Cutting of Gears

Cutting edges of the form tools reproduce the generating surface when the Shear-Speed gear shaper is operating. The generating surface T is congruent to the gear tooth surfaces including surfaces of the bottom lands between the gear teeth. Because form tools are designed with the rake angle $\gamma_o > 0°$, and the clearance angle α_o is always positive ($\alpha_o > 0°$), the transverse cross section of the generating surface T is not identical either to the tooth profile within the rake surface R_s of the form tool or to the normal cross section of the clearance surface C_s.

For the manufacture of form tools as well as resharpening of worn form tools, it is necessary to express the design parameters of the form tool in terms of the design parameters of the work gear. This particular problem in the design of form cutting tools can be solved either analytically or by using descriptive geometry–based methods.

Descriptive geometry–based method for profiling of the form tool. The tool heads for Shear-Speed cutting of gears (Figure 5.11) are normally designed to produce a specific part. In Figure 5.12, the generating surface T of the Shear-Speed gear cutter is the system of projective planes $\pi_2\pi_3$. For profiling of the gear cutting tool, multiple points are chosen on the transverse profile of the generating surface T. As an example, points $a, b, c, \ldots, k$ are shown. Subscript "3" is assigned to the projections of all points onto the plane of projections π_3. Corresponding projections of those same points onto the plane of projections π_2 are labeled with subscript "2."

Rake surfaces of two types are practical for the Shear-Speed cutting tool. Usually, the rake surface is shaped either in the form of a plane or in the form of a cone of revolution. As an example, the rake plane R_s is depicted in Figure 5.12. The rake plane R_s is a projective plane onto the frontal plane of projections π_3, and is inclined at the rake angle γ_o. The cutting edge CE is represented as the line of intersection of the generating surface T by the rake plane R_s. With no distortions, the cutting edge is constructed in the lower portion of Figure 5.12. Subscript "rs" is assigned to all points $a, b, c, \ldots, k$ of the cutting edge CE.

All tools are form relieved to maintain the correct form after resharpening. The clearance surface C_s, having a cylindrical shape, can be used in designing the Shear-Speed cutting tool. The clearance surface is a cylinder that passes at the clearance angle α_o through

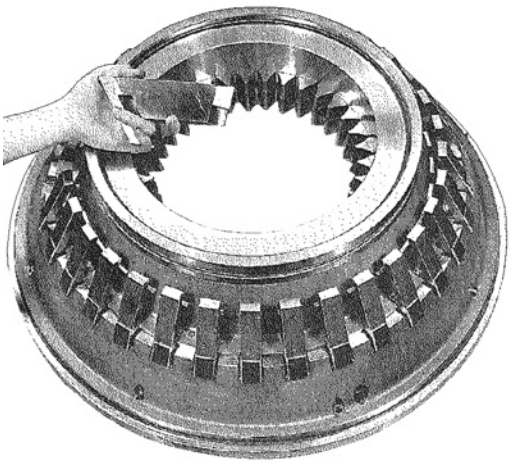

FIGURE 5.11
The tool head for Shear-Speed cutting of gears.

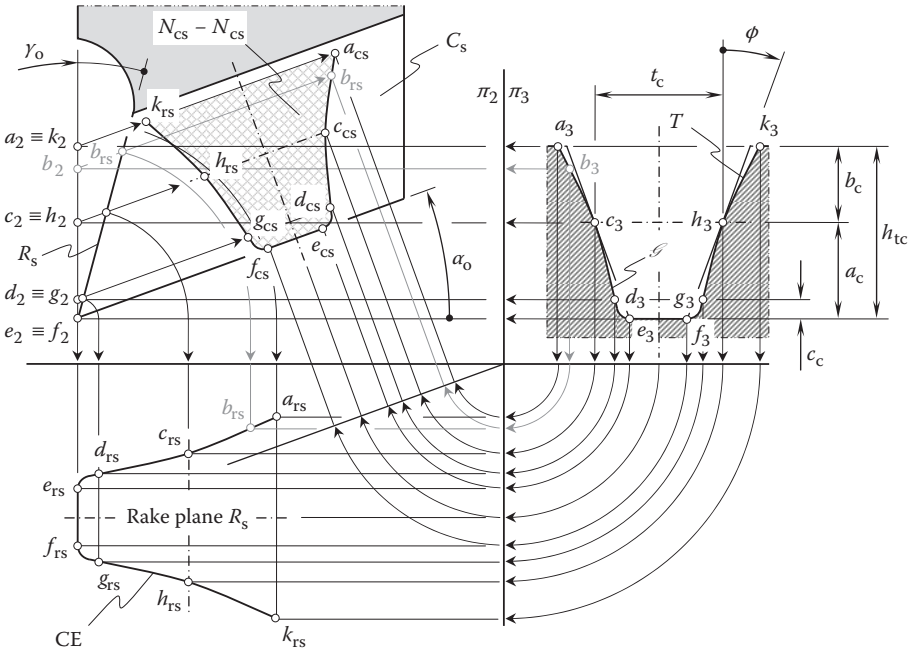

FIGURE 5.12
Descriptive geometry–based solution to the problem of profiling of the Shear-Speed cutting tool.

the cutting edge CE. The normal cross section $N_{cs} - N_{cs}$ is specified by points a, b, c, …, k to which the subscript "cs" is assigned.

The problem of profiling the Shear-Speed cutting tool is solved immediately after two profiles of the gear cutting tool are constructed. The tooth profile a_{rs}, b_{rs}, c_{rs}, …, k_{rs} within the rake plane R_s is one of them, and the normal cross section of the clearance surface a_{cs}, b_{cs}, c_{cs}, …, k_{cs} is the second one. Both profiles of the tooth are used for manufacturing, resharpening, and inspection of the gear cutting tool.

Similarly, the form cutting tools can be designed with the rake surface and with the clearance surface having any other geometry that is desired in a particular case of gear machining.

Analytical profiling of the form tool. The analytical solution to the problem of profiling of form tools for Shear-Speed cutting of gears is conceptually similar to the graphical solution.

Consider an analytical solution to the problem of profiling the form tool for machining of a spur gear having an involute tooth profile. First of all, it is necessary to analytically describe the generating surface of the form tool. In the Cartesian coordinate system $X_cY_cZ_c$ (Figure 5.13), the equation of the generating surface T can be represented in the form

$$\mathbf{r}_c(U_c, \phi_c) = \begin{bmatrix} \dfrac{r_{b.c}}{\cos\phi_c} \cdot \sin(\alpha + \text{inv}\phi_c) \\ -\dfrac{r_{b.c}}{\cos\phi_c} \cdot \cos(\alpha - \text{inv}\phi_c) \\ U_c \\ 1 \end{bmatrix} \tag{5.12}$$

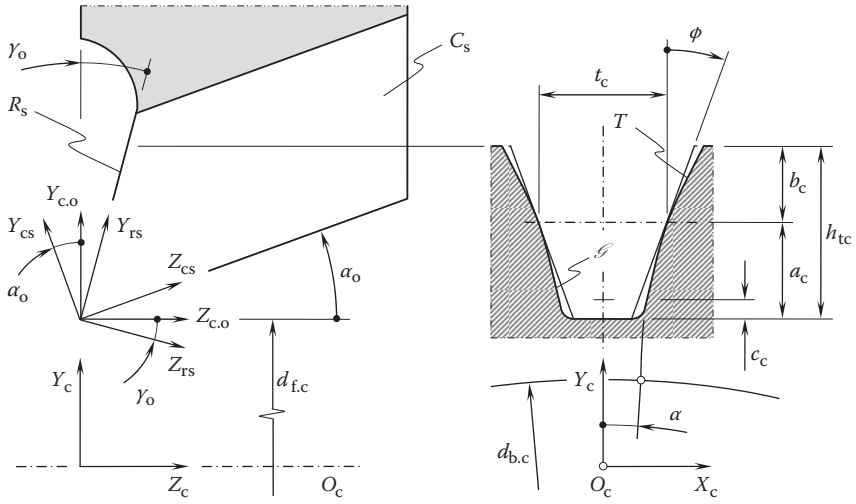

FIGURE 5.13
Cartesian coordinate systems used for the analytical profiling of the form tool.

where

$\mathbf{r}_c$ = position vector of a point of the generating surface T of the form tool
U_c, ϕ_c = Gaussian (curvilinear) coordinates on surface T
$r_{b.c}$ = base cylinder radius of involute profile of the form tool
α = angle that specifies the location of the start point of the involute curve on the base cylinder of the generating surface T of the form tool (Figure 5.13)

Equation (5.12) is based on the premise presented in Equation (1.2).

Since the generating surface T has already been determined, an equation of the cutting edge CE can be derived in the form of an equation of the line of intersection made by surface T of the form tool and the rake plane R_s. Various opportunities are available in this regard.

For example, the simplest form of analytical representation of the rake plane R_s can be derived in a particular coordinate system. A Cartesian coordinate system $X_{rs}Y_{rs}Z_{rs}$ is associated with the rake plane R_s as shown in Figure 5.13. The coordinate plane $X_{rs}Y_{rs}$ is congruent with the plane R_s. Therefore, in the reference system $X_{rs}Y_{rs}Z_{rs}$, the equation of the rake plane satisfies the equality $Z_{rs} = 0$. To derive the equation for the cutting edge CE, the generating surface T of the form tool can be represented in the coordinate system $X_{rs}Y_{rs}Z_{rs}$. Then, $Z_{rs} = 0$ is substituted into the equation for surface T. This returns an equation for the cutting edge CE.

In the reference system $X_{rs}Y_{rs}Z_{rs}$, the position vector of a point $\mathbf{r}_c^{(rs)}(U_c, \phi_c)$ of the generating surface T of the form tool can be computed from the expression

$$\mathbf{r}_c^{(rs)}(U_c, \phi_c) = \mathbf{Rt}(\gamma_o, X_{c.o}) \cdot \mathbf{Tr}(0.5\, d_{f.c}, Y_c) \cdot \mathbf{r}_c(U_c, \phi_c) \tag{5.13}$$

where $d_{f.c}$ denotes the inner diameter of the gear cutting head.

Next, the position vector of a point of the cutting edge CE of the form tool can be expressed as

$$\mathbf{r}_{ce}^{(rs)}(U_c, \phi_c) = \begin{bmatrix} X_{ce}(U_c, \phi_c) \\ Y_{ce}(U_c, \phi_c) \\ 0 \\ 1 \end{bmatrix} \tag{5.14}$$

It is important to stress here that parameters U_c and ϕ_c in Equation (5.14) are not independent, and one of them can be expressed in terms of the other in the form $U_c = U_c(\phi_c)$ or in the form $\phi_c = \phi_c(U_c)$. This means that the position vector of a point $\mathbf{r}_{ce}^{(rs)}(U_c,\phi_c)$ of the cutting edge CE depends on not two, but just one of these parameters.

Several opportunities are also available when deriving the equation for the normal cross section of the clearance surface C_s of the form tool.

The simplest analytical representation of the normal cross section of the clearance surface can be obtained in a particular reference system. A Cartesian coordinate system $X_{cs}Y_{cs}Z_{cs}$ is associated with the clearance surface C_s as shown in Figure 5.13. The coordinate plane $X_{cs}Y_{cs}$ is congruent to the plane of the normal cross section N_{cs}–N_{cs} (see Figure 5.12). Therefore, in the reference system $X_{cs}Y_{cs}Z_{cs}$, the equation for the normal plane satisfies the equality $Z_{cs} = 0$. To derive the equation for the normal cross section of the clearance surface C_s, the equation for the cutting edge CE of the form tool can be represented in the coordinate system $X_{cs}Y_{cs}Z_{cs}$. Next, the cutting edge is moved in the direction specified by clearance angle α_o. In this manner, an equation for the clearance C_s can be derived. An equation for the normal cross section of the clearance surface can be derived if $Z_{cs} = 0$ is substituted into the derived equation for the clearance surface.

In the reference system $X_{cs}Y_{cs}Z_{cs}$, position vector of a point $\mathbf{r}_{ce}^{(cs)}(U_c)$ of the cutting edge CE of the form tool can be computed from the expression

$$\mathbf{r}_{ce}^{(cs)}(U_c, V_{cs}) = \mathbf{Tr}(V_{cs}, Z_{cs}) \cdot \mathbf{Rt}[(\alpha_o + \gamma_o), X_{c.o}] \cdot \mathbf{r}_{ce}^{(rs)}[U_c, \phi_c(U_c)] \tag{5.15}$$

Equation (5.15) yields the following expression

$$\mathbf{r}_{nn}^{(cs)}(U_c, V_{cs}) = \begin{bmatrix} X_{nn}(U_c, V_{cs}) \\ Y_{nn}(U_c, V_{cs}) \\ 0 \\ 1 \end{bmatrix} \tag{5.16}$$

for the profile of the normal cross section of the clearance surface C_s of the form tool.

Again, parameters U_c and V_{cs} in Equation (5.16) are not independent, and one of them can be expressed in terms of the other, either in the form $U_c = U_c(V_{cs})$ or $V_{cs} = V_{cs}(U_c)$. This means that position vector of a point $\mathbf{r}_{nn}^{(cs)}(U_c,V_{cs})$ of the normal cross section of the clearance surface C_s depends on not two, but just one parameter.

The derived analytical descriptions of the cutting edge CE and the normal cross section of the clearance surface are the solution to the problem of profiling the form tool for Shear-Speed gear cutting head.

5.8.3 Application of Shear-Speed Cutting

The Shear-Speed process is a high-production method of producing gear teeth. The Shear-Speed cuts all teeth of external spur forms simultaneously. The production advantage is greater for gears with large numbers of teeth.

In the Shear-Speed process, it is possible to form cut involute spur gear teeth with practically any required tooth modification. This includes preshave root relief, semitopping, full fillet modifications, and modifications in the involute form.

Although some clearance on both sides of the part is required for overtravel of the form-cutting tool, parts that are integral with closely spaced flanges or shoulders, such as cluster gears, can be readily cut by the Shear-Speed process.

The number of tools depends on the number of spaces to be cut in the periphery of the work gear. All tools may have the same form, or the forms may vary depending on the part specifications. The tools may be equally or unequally spaced. The cutting tools are easily removed for sharpening and all are sharpened at one time on a surface grinder.

Although the majority of forms shaped by the Shear-Speed are external, there are cases wherein this method is most advantageous in the shaping of internal forms.

The process is limited to coarse-pitch gears having spur teeth. In addition, each model is limited to a small range of diameters and pitches.

Helical forms are not applicable to this method.

All three cutting edges of every form tool cut simultaneously. Chip flows cut by the adjusting cutting edges interfere with each other. Because of this, tool life is relatively short and normally this method is applied to semifinishing or finishing of gear teeth.

5.9 Rotary Broaches: Slater Tools

External and internal tooth forms can be produced via rotary broaches.* Cutting tools of this type are also often called *slater tools*.

The slater tool seems to be similar to one finishing section of a gear broach that is attached to the shank. The clearance angle α_o at the outer diameter of the tool is greater than that for a regular gear broach.

The kinematics of the rotary broaching process is illustrated in Figure 5.14.

When broaching, the work gear is rotated $\boldsymbol{\omega}_g$ about its axis. Because the generating surface of the slater tool is congruent to the work gear tooth surface, the generating surface T is rotated $\boldsymbol{\omega}_c$ about its axis together with the rotation of the work gear.

The shank axis is at a certain angle ϑ_{cut} with respect to the rotation vectors $\boldsymbol{\omega}_g$ and $\boldsymbol{\omega}_c$. The angle ϑ_{cut} is positive; however, it does not exceed the clearance angle α_o. Ultimately, the active value of the clearance angle in rotary broaching is equal to the difference $(\alpha_o - \vartheta_{cut})$.

When machining the work gear, the slater tool comes into contact with the work gear. The slater tool is driven by the work gear. The rotation $\boldsymbol{\omega}_{cut}$ of the slater tool is the primary motion in the rotary broaching process. While rotating, the slater tool travels $\mathbf{F}_c$ in the axial direction of the work gear. The gear is machined in only one path of the slater tool. Because of this, rotary broaching is a very fast process.

Most rotary broach tools are made of M-2 high speed steel, a material that provides the required edge toughness in an operation which, by nature, does not generate much heat. Powder metal PM4 is also used in the production of rotary broach tools. Coated with TiN or TiCN, gear slater tools have longer tool life and better cutting performance.

* Produced by Slater Tools Inc., Detroit, MI.

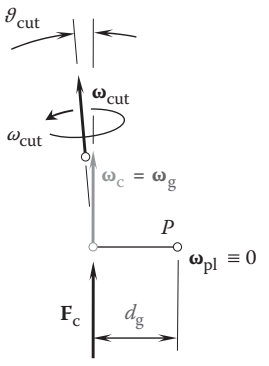

FIGURE 5.14
Kinematics of the rotary broaching process.

For rotary broaching of gear turning, milling drilling or screw machines can be used. The slater tool is installed in a *rotary broach tool holder*, which has an internal live spindle that holds an end cutting broach tool. The holder along with the end cutting broach tool is designed for producing polygon forms while the machine spindle is rotating in a forward or reverse direction.

In a turning or screw machine, the holder is mounted stationary, whereas its internal live spindle along with the end cutting broach tool rotates with and is driven by the work gear rotation. While rotating with the work gear, the end cutting broach tool's pressure and contacting points are continually changing contact points on the work gear (wobbling type action), making broached forms easily produced.

In a milling or drilling machine, the holder is mounted into and rotates with the machine spindle, whereas its internal live spindle along with the end cutting broach tool remains stationary upon contact with the work gear.

Form sizes can be broached up to 2 in. for aluminum, 1½ in. for brass, and 1 in. for steel. The practical forming length of rotary broaching is up to 1.5 times the distance across flats or the diameter of the inscribed circle of the profile to be broached.

It is required to align the end of the broach tool to the centerline of the work gear. Both internal and external forms require a pilot hole and a lead chamfer. For internal broaching, the diameter of the pilot hole should be, at minimum, equal size to the distance across the flats or the inscribed circle diameter of the form to be broached. The lead chamfer diameter must be slightly larger in diameter than the form being broached. For external broaching, the turned diameter on the work gear should be smaller than the major diameter of the form being broached. If full form is required, turn the diameter 0.0008 to 0.0015 in. larger than the final diameter. For starting the external broach tool on the work gear, a 45° chamfer should be smaller than the minor diameter and larger than the major diameter.

5.10 Broaching Bevel Gear Teeth

For broaching bevel gear teeth, the Revacycle® process is used. The Revacycle process is the fastest method for cutting straight bevel gears of commercial quality. It is primarily

used for large-volume production of gears for such applications as automotive-type differentials and agricultural implements [190].

5.10.1 Principle of the Revacycle Process of Cutting of Gear Teeth

Most Revacycle-cut gears are produced with one completing operation using a cutter continuously rotating at a uniform rate. The cutter blades, which extend radially outward from the cutter head, have concave edges that produce convex profiles on the gear teeth. During the cutting operation, the workpiece is held motionless while the cutter is moved by means of a cam in a straight line across the face of the gear and substantially parallel to its root line. This motion makes it possible to produce a straight tooth bottom, whereas the desired tooth shape is produced by the combined effect of the motion of the cutter and the shapes of the cutter blades.

There is no depthwise feed of the cutter into the work, the effective feed being obtained by making each cutter blade progressively longer than the one before it.

The completing cutter contains three types of blades: roughing, semifinishing, and finishing. One revolution of the cutter completes each tooth space, and the work is indexed in the gap between the last finishing blade and the first roughing blade.

The Revacycle process of broaching of bevel gear teeth is illustrated in Figure 5.15.

Figure 5.15 illustrates the Revacycle cutter in position at the beginning of the cut. As the cutter rotates counterclockwise, blades of gradually increasing length contact the work

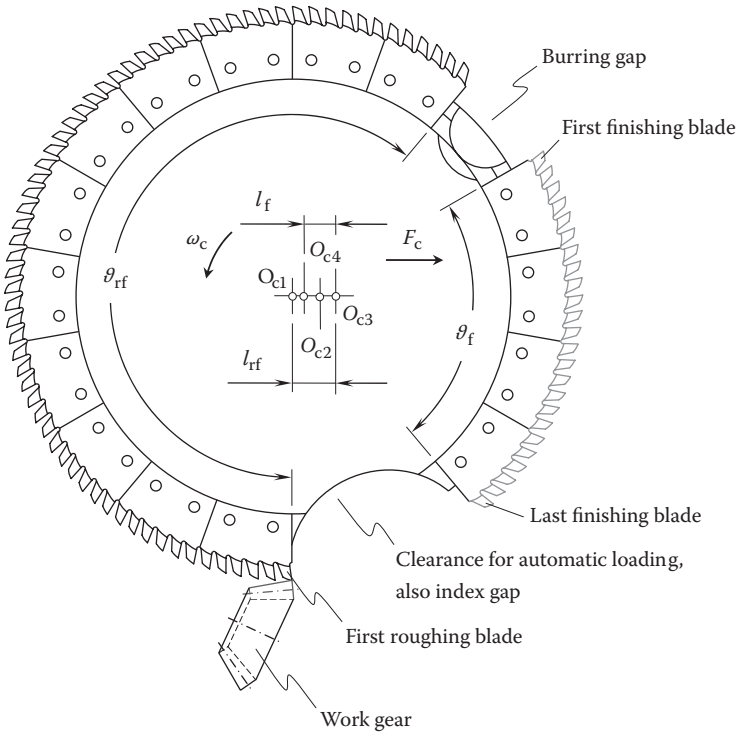

FIGURE 5.15
Kinematics of the Revacycle process of machining of bevel gear teeth.

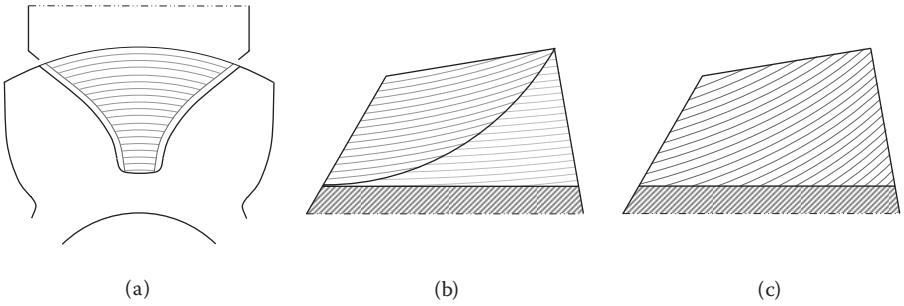

FIGURE 5.16
Tooth space generation using the Revacycle process of machining of bevel gear teeth.

gear until the root line of the tooth is reached. Figure 5.16a shows a transverse view of the tooth space as roughed to full depth. Each chip extends the full width of the slot, except for the amount of stock left for finishing. Figure 5.16b is an axial section of the same tooth showing that the roughing chips extend the full length of the tooth. During the first part of the roughing, the cutter is fed F_c from O_{c1} to O_{c2} (Figure 5.15). It then remains stationary at O_{c2} until full depth is reached.

The roughed tooth does not have the proper taper. It is substantially correct along the diagonal line in Figure 5.16b, but the portions of the tooth surface lying to the right of this line toward the heel of the tooth still have considerable stock that must be removed before finishing. This is accomplished by the semifinishing blades, which cut while the cutter center travels from O_{c2} to O_{c3} (Figure 5.15).

Finishing is carried out while the cutter center returns from O_{c3} to O_{c4} at a uniform rate. The finishing blades are given the proper shape to produce the correct tooth taper and proper profile at every point along the tooth. The blades cutting at either end of the tooth space are made slightly wider than necessary for correct taper in order to ease off the ends of the tooth and produce a crowning, which results in localized tooth bearing [190].

The resulting finished tooth surface is generated, being made up of a series of inclined cuts similar to those shown in Figure 5.16c. In general, a different cutter is required for each different gear specification.

For Revacycle work that is too deep for completing in one cut, separate roughing and finishing operations are used. Separate cutters and separate machine setups are required for each operation. The cutters and the machine cycle are similar to those described above with some slight differences. The roughing cutter has no semifinishing or finishing blades, and there is no translation of the cutter in the roughing operation. The finishing cutter, however, translates as in the completing operation, with semifinishing blades cutting on the first translation and finishing blades cutting during the return stroke.

5.10.2 Revacycle Cutting Tools

Revacycle cutter blades are relief ground when manufactured and thus require sharpening on the front face only. Blade-to-blade spacing, the angle of the plane of the front face, and surface finish of the front face must all be closely controlled during sharpening. In addition, when new segments are assembled in heads, cleanliness of assembly, accuracy of position of segment-locating keys, and close control of segment-holding bolt tension are all necessary for proper cutting results.

The lateral cutting edges of the finishing teeth of the Revacycle cutting tool are within the generating surface T. The generating surface T of the Revacycle cutting tool is tangent to the bevel gear tooth flanks $\mathcal{G}$ at every instant of cutting of the gear tooth. After it has been determined, the generating surface T is used for the analytical description of the finishing cutting edges as well as the clearance surfaces of the finishing teeth of the Revacycle cutting tool.

The generating surface of the Revacycle cutting tool is also important for profiling of roughing and semifinishing cutting blades.

Cutting edges of the roughing blades are at a certain distance t_{sr} inward of the generating surface T. The distance t_{sr} is equal to the stock thickness to be removed by the semifinishing blades. Therefore, cutting edges of the roughing blades are within a surface that is offset at the distance t_{sr} with respect to the generating surface T of the Revacycle cutting tool.

Similarly, cutting edges of the semiroughing blades are within a surface that is offset at distance t_f with respect to the generating surface T of the Revacycle cutting tool, where, t_f denotes the portion of stock to be removed by finishing blades of the cutting tool.

The brief discussion above reveals the importance of the generating surface T for the purpose of profiling of the Revacycle cutting tool.

In the case under consideration, the generating surface T of the cutting tool can be determined in the following manner.

Consider the tooth flank of the bevel gear to be machined using the Revacycle process. For the position vector of a point $\mathbf{r}_g$ of the bevel gear tooth flank, Equation (1.27) can be used

$$\mathbf{r}_g(U_g, \varphi_g) = \begin{bmatrix} U_g \tan\theta_{b.g} \sin\varphi_g - \varphi_g U_g \tan\theta_{b.g} \cos\varphi_g \\ U_g \tan\theta_{b.g} \cos\varphi_g + \varphi_g U_g \tan\theta_{b.g} \sin\varphi_g \\ -U_g \\ 1 \end{bmatrix} \tag{5.17}$$

where

U_g and φ_g = curvilinear (Gaussian) coordinates of the bevel gear tooth flank $\mathcal{G}$

$\theta_{b.g}$ = half of the base cone angle of the bevel gear

When machining bevel gear teeth, the Revacycle cutting tool is rotating and traveling in the lengthwise direction of the gear tooth. The rotation ω_c of the cutter about its axis of rotation and the translation of the cutter with a feed rate F_c are timed with each other. Within the roughing section, rotation ω_c and translation F_c are timed so that when the cutting tool turns through the angle ϑ_{rf}, it travels at a distance l_{rf}. Here, ϑ_{rf} denotes the angle that spans over the roughing section of the cutting tool and l_{rf} denotes the distance between the two consequent positions O_{c1} and O_{c3} of the axis of rotation of the Revacycle cutting tool.

Within the finishing section of the cutting tool, rotation ω_c and translation F_c are timed in a manner that is largely similar to that just discussed. When the cutting tool turns through the angle ϑ_f, it travels at a distance l_f. Here, ϑ_f denotes the angle that spans over the finishing section of the cutting tool and l_f denotes the distance between the two consequent positions O_{c3} and O_{c4} of the axis of rotation of the Revacycle cutting tool.

The analytical representation of the bevel gear tooth flank to be machined [see Equation (5.17)], along with the just outlined kinematics of the Revacycle process, makes it possible to derive the equation for both portions of the generating surface of the gear cutting tool.

5.10.3 Profiling of a Cutter for Machining Bevel Gears Using the Revacycle Process

A cutter for machining bevel gear teeth using the Revacycle process consists of a large-diameter disk (21 or 25 in., 550 or 650 mm) with the cutting blades projecting radially from the periphery, commonly arranged in groups and each blade progressively longer than the preceding one.

Most of the material from the tooth space is removed by teeth of the first group. Roughing and semiroughing teeth of the cutter are referred to as the teeth of the first group. The main purpose of the first group of teeth is to remove material from the tooth space. Teeth of the first group do not generate the bevel gear tooth flanks. Therefore, requirements to the accuracy of the gear tooth profile are not close, and can vary significantly.

Teeth of the second group are the finishing teeth. Only a small portion of the material is removed by the finishing teeth. The main purpose of the second group of teeth is to generate the bevel gear tooth flanks in compliance with the blueprint requirements. Because of this, requirements to the accuracy of the gear tooth profile are close, and can vary within very narrow intervals.

Solution to the problem of profiling of the Revacycle gear cutter can be derived in two steps.

First, profiling of the finishing teeth is considered. Next, profiling of the roughing and semiroughing teeth is performed based on the solution obtained in the first step.

Profiling of the finishing teeth of the Revacycle gear cutter. A left-hand–oriented Cartesian coordinate system $X_{bg}Y_{bg}Z_{bg}$ is associated with the bevel gear to be machined as shown in Figure 5.17. In the coordinate system $X_{bg}Y_{bg}Z_{bg}$, the bevel gear tooth flank is analytically described by Equation (5.17). See Chapter 1 for more details on the analytical description of the tooth flank of the bevel gear (Figure 1.14).

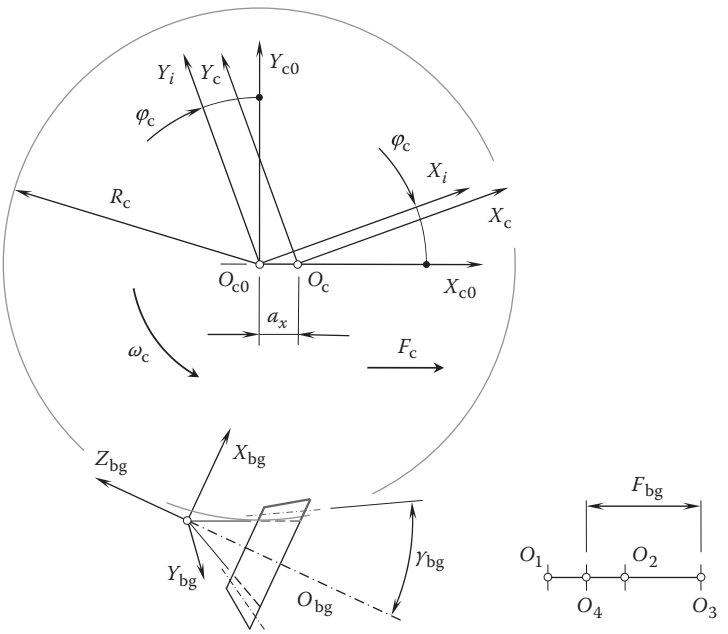

FIGURE 5.17
Reference systems used for profiling of the Revacycle cutter.

A left-hand–oriented Cartesian coordinate system $X_cY_cZ_c$ is associated to the cutter. This coordinate system is rotating ω_c together with the cutter while machining the gear. In the initial position of the cutter, the coordinate system $X_cY_cZ_c$ aligns with the coordinate system $X_{c0}Y_{c0}Z_{c0}$ as shown in Figure 5.17.

While rotating ω_c through a certain angle $\vartheta_{f.x}$ (here, the angle $\vartheta_{f.x}$ is within the range of $0° \le \vartheta_{f.x} \le \vartheta_f$), the cutter is traveling along the X_{c0} axis at a distance a_x. The angular displacement $\vartheta_{f.x}$ and the linear displacement a_x correlate with each other in the known manner $a_x = a_x(\vartheta_{f.x})$. For practicality, this relationship is reduced to the linear expression $a_x = k_{rc}\,\vartheta_{f.x}$, where k_{rc} is constant.

When deriving an equation for the generating surface T of the Revacycle gear cutter, it is necessary to represent the equation of the bevel gear tooth flank $\mathscr{G}$ in the coordinate system $X_cY_cZ_c$ associated with the gear cutter. The corresponding operators of the coordinate system transformations can be used for this purpose.

At the beginning of the machining process, configuration of the work gear and the Revacycle gear cutter is known. This statement implies that the operator $\mathbf{Rs}(\mathrm{bg} \mapsto \mathrm{c}_0)$ of the resultant coordinate system transformation, say from the bevel gear coordinate system $X_{bg}Y_{bg}Z_{bg}$ to the gear cutter coordinate system $X_{c0}Y_{c0}Z_{c0}$, is either given from the very beginning or can be composed using for this purpose the actual design parameters of the bevel gear and the Revacycle gear cutter. Consequently, the operator $\mathbf{Rs}(\mathrm{c}_0 \mapsto \mathrm{bg})$ of the inverse coordinate system transformation can be determined as well. Recall that the relationship $\mathbf{Rs}(\mathrm{c}_0 \mapsto \mathrm{bg}) = \mathbf{Rs}^{-1}(\mathrm{bg} \mapsto \mathrm{c}_0)$ for operators of the coordinate system transformations is valid. The operator $\mathbf{Rs}(\mathrm{bg} \mapsto \mathrm{c}_0)$ is used for representation of the position vector $\mathbf{r}_g$ [see Equation (5.17)] of a point of the flank surface $\mathscr{G}$ in the coordinate system $X_{c0}Y_{c0}Z_{c0}$ that corresponds to the initial configuration of the work gear and of the gear cutter. In the reference system $X_{c0}Y_{c0}Z_{c0}$, position vector of a point $\mathbf{r}_g^{(c0)}$ of the bevel gear tooth flank $\mathscr{G}$ can be computed from the expression

$$\mathbf{r}_g^{(c0)}(U_g, \varphi_g) = \mathbf{Rs}(\mathrm{bg} \mapsto \mathrm{c}_0) \cdot \mathbf{r}_g(U_g, \varphi_g) \tag{5.18}$$

Then, in the current instant of time, the coordinate system $X_cY_cZ_c$ of the Revacycle gear cutter is turned through an angle φ_c about the Z_c axis, and is shifted along the X_{c0} axis at a certain distance a_x. Recall that displacements a_x and φ_c are correlated with each other. The correlation is expressed in the form of a function $a_x = a_x(\vartheta_{f.x})$ [or in the form $\vartheta_{f.x} = \vartheta_{f.x}(a_x)$ that is equivalent to $a_x = a_x(\vartheta_{f.x})$]. In a particular case of bevel gear machining, the equality $a_x = k_{rc}\,\vartheta_{f.x}$ is observed.

The rotation of the coordinate system $X_{c0}Y_{c0}Z_{c0}$ through the angle φ_c to the position of the intermediate reference system $X_iY_iZ_i$ can be analytically described by the operator of rotation $\mathbf{Rt}(\varphi_c, Z_{c0})$. Then, for the analytical description of the translation of the intermediate coordinate system $X_iY_iZ_i$ at distance a_x to the position of the gear cutter coordinate system $X_cY_cZ_c$, the operator of translation $\mathbf{Tr}(a_x, X_i)$ can be implemented. Ultimately, the generalized expression

$$\mathbf{r}_g^{(c)}(U_g, \varphi_g, \varphi_c) = \mathbf{Tr}(a_x, X_i) \cdot \mathbf{Rt}(\varphi_c, Z_{c0}) \cdot \mathbf{Rs}(\mathrm{bg} \mapsto \mathrm{c}_0) \cdot \mathbf{r}_g(U_g, \varphi_g) \tag{5.19}$$

can be used for the analytical description of the bevel gear tooth flank $\mathscr{G}$ in the coordinate system $X_cY_cZ_c$ associated with the gear cutter.

It is instructive to note here that taking into account the direction of the translation of the Revacycle gear cutter from point O_1 through point O_2 to point O_3, and its rotation through

the angle ϑ_f (Figure 5.15), both displacements a_x and φ_c in the operators $\mathbf{Tr}(a_x, X_i)$ and $\mathbf{Rt}(\varphi_c, Z_{c0})$ of the linear transformations have negative values ($a_x < 0$ and $\varphi_c < 0°$).

At a current location of the gear cutter, position vector of a point $\mathbf{r}_g^{(c)}$ $(U_g\ \varphi_g\ \varphi_c)$ in the coordinate system $X_cY_cZ_c$ also depends on the current value of the φ_c parameter. Angle φ_c is a time-dependent parameter. It can be expressed in terms of the rotation of the cutter ω_c and time t. This relation is described by the function

$$\varphi_c = \omega_c\ t \tag{5.20}$$

With Equation (5.19), which analytically describes the current configuration of the bevel gear tooth flank $\mathcal{G}$ in the reference system $X_cY_cZ_c$, position vector of a point $\mathbf{r}_c$ of the generating surface T of the Revacycle gear cutter can be derived using Shishkov's [186] equation of contact, $\mathbf{n}_{bg} \cdot V_\Sigma = 0$ [186]. Here, $\mathbf{n}_{bg}$ denotes the unit normal vector to the bevel gear tooth flank $\mathcal{G}$ and V_Σ is the vector of the resultant motion of the surface $\mathcal{G}$ in the coordinate system $X_cY_cZ_c$. The equation for the generating surface T of the Revacycle gear cutter can be obtained as the solution to the set of two equations

$$\mathbf{r}_c \quad \Rightarrow \quad \begin{cases} \mathbf{r}_g^{(c)} = \mathbf{r}_g^{(c)}(U_g, \varphi_g, \varphi_c) \\ \begin{vmatrix} \dfrac{\partial \mathbf{r}_g^{(c)}}{\partial U_g}(U_g, \varphi_g, \varphi_c) \\ \dfrac{\partial \mathbf{r}_g^{(c)}}{\partial \varphi_g}(U_g, \varphi_g, \varphi_c) \\ \dfrac{\partial \mathbf{r}_g^{(c)}}{\partial \varphi_c}(U_g, \varphi_g, \varphi_c) \end{vmatrix} = 0 \end{cases} \tag{5.21}$$

After the second equation in Equation (5.21) is solved with respect to the parameter of relative motion φ_c, the computed solution φ_c is substituted into the first equation. Ultimately, the equation for the generating surface T of the Revacycle gear cutter can be presented as

$$T \quad \Rightarrow \quad \mathbf{r}_c = \mathbf{r}_c(U_c, V_c) \tag{5.22}$$

It is important to note here that, for the finishing group of teeth, the rotation ω_c of the reference system $X_cY_cZ_c$ is performed through the angle ϑ_c (see Figure 5.15), whereas the translation is performed at the distance O_3O_4. Theoretically, distance O_3O_4 should span over the entire face width of the tooth flank in the direction of the bottom land of the work gear tooth. However, in practice, reasonable deviations from the actual distance traveled by the coordinate system $X_cY_cZ_c$ from O_3O_4 could be allowed.

It is of critical importance to point out that the generating surface T [see Equation (5.22)] does not allow for sliding motions over itself.

Equation (5.22) makes it possible to design the precision Revacycle gear cutter. Precision of the Revacycle cut gears can even exceed the precision of generated bevel gears.

Cutting edges of the finishing teeth of the Revacycle gear cutter are within the generating surface T [see Equation (5.22)]. The total number of finishing teeth is denoted by n_c. The finishing teeth are within the angle ϑ_f that spans over the finishing section. The finishing teeth are spaced at an angular increment $\Delta\varphi_c$, which is equal to $\Delta\varphi_c = \vartheta_f/n_c$. Rake angle γ_o at the outer diameter of the gear cutter is equal to zero ($\gamma_o = 0°$). Therefore, position vector

of a point $\mathbf{r}_{rs}$ of the rake plane for each finishing tooth of the gear cutter can be presented in the form

$$\mathbf{r}_{rs}(U_{rs}, V_{rs}) = \begin{bmatrix} U_{rs} \\ U_{rs} \tan[\vartheta_f^{(0)} + \Delta\varphi_c \, (\mathrm{No} - 1)] \\ V_{rs} \\ 1 \end{bmatrix} \tag{5.23}$$

where U_{rs} and V_{rs} are the curvilinear coordinates of the rake plane R_s, which are parallel to the coordinate axes of the reference system $X_cY_cZ_c$ ($U_{rs} = X_c$ and $V_{rs} = Z_c$); $\vartheta_f^{(0)}$ is the angle at which the finishing section begins; and No denotes the number of a current finishing tooth.

Cutting edge CE of every finishing tooth satisfies both Equations (5.22) and (5.23). Therefore, an analytical description of CE can be derived as a solution to Equations (5.22) and (5.23). The solution yields representation in matrix form

$$\mathbf{r}_{ce}(V_{rs}, \mathrm{No}) = \begin{bmatrix} X(V_{rs}, \mathrm{No}) \\ Y(V_{rs}, \mathrm{No}) \\ Z(V_{rs}, \mathrm{No}) \\ 1 \end{bmatrix} \tag{5.24}$$

The actual shape of every finishing tooth depends on the parameter No. This means that the particular shape of every finishing tooth is dependent on the location of the tooth within the finishing sector. In practice, reasonable approximation is permissible for the desired shape of the finishing teeth of the Revacycle gear cutter.

Clearance surface is a type of relived surface. Clearance surface C_s is a surface through the cutting edge CE [see Equation (5.24)]. It forms the desired clearance angle α_o with the generating surface T of the gear cutter.

Shape of roughing teeth of the Revacycle gear cutter. Cutting edges of the roughing teeth are beneath the generating surface T. They are within the interior of the generating body of the Revacycle gear cutter. The purpose of the roughing teeth is twofold: (1) most of the material removal from the tooth space is performed by the roughing teeth; (2) after roughing, a little stock for finishing is left. It is desired that the stock for finishing be uniformly distributed over the bevel gear tooth flank.

Because roughing teeth do not directly affect the final tooth shape, the tolerance for accuracy of roughing teeth is not that close as it is for finishing teeth.

The desired shape of roughing teeth can be determined in the following manner.

First, let us determine a surface that is conjugate to the bevel gear tooth flank when roughing of the bevel gear teeth is performed. When roughing, the Revacycle gear cutter is rotating through angle ϑ_f and traveling from O_1 through O_2 to O_3. The kinematics of roughing is similar to that for the finishing teeth. Therefore, for the surface T_{rf} that is conjugate to the bevel gear tooth flank $\mathscr{G}$, an analytical description can be derived using the same process used for deriving the generating surface T of the Revacycle gear cutter [see Equation (5.24)]. Following this process, the following expression

$$T_{rf} \quad \Rightarrow \quad \mathbf{r}_{cr} = \mathbf{r}_{cr}(U_{cr}, V_{cr}) \tag{5.25}$$

can be derived for the position vector of a point $\mathbf{r}_{cr}$ of surface T_{rf}. If one assumes that the bevel gear tooth flanks are profiled by the roughing teeth, then their cutting edges would be within the surface T_{rf}. In reality, the roughing teeth do not make contact with the bevel gear tooth flanks. The closest distance of approach of the roughing teeth to the bevel gear tooth flank is equal to the stock thickness t_{rf} left for the finishing teeth. The stock thickness is measured along the perpendicular direction to the gear tooth flank $\mathscr{G}$. This immediately yields an equation for the position vector $\mathbf{r}_{cr}^{(a)}$ of the surface within which location of the cutting edges of the roughing teeth is desired

$$T_{rf}^{(a)} \quad \Rightarrow \quad \mathbf{r}_{cr}^{(a)}(U_{cr}, V_{cr}) = \mathbf{r}_{cr}(U_{cr}, V_{cr}) - \mathbf{n}_{bg} \cdot t_{rf} \tag{5.26}$$

where $\mathbf{n}_{bg}$ denotes the unit normal vector to the tooth flank $\mathscr{G}$. After the necessary formula transformation is accomplished, the surface $T_{rf}^{(a)}$ for the roughing teeth can be analytically described by the expression

$$T_{rf}^{(a)} \quad \Rightarrow \quad \mathbf{r}_{cr}^{(a)} = \mathbf{r}_{cr}^{(a)}(U_{cr}, V_{cr}) \tag{5.27}$$

Reasonable deviations in the actual location of the roughing cutting edges from those specified by Equation (5.27) are allowed.

Similar to the finishing group of teeth, for the roughing group of teeth the rotation ω_c of the reference system $X_cY_cZ_c$ is performed through the angle ϑ_{rf} (see Figure 5.15), whereas translation is performed at distance O_1O_3. The distance O_1O_3 correlates with the face width of the bevel gear to be machined.

The total number of roughing teeth is denoted by n_{rc}.

The first roughing tooth is the shortest one, and the last roughing tooth is of full tooth height $h_{rc} = h_{bg}$ of the tallest bevel gear tooth. The roughing tooth increment Δh_{bg} in this case can be computed as

$$\Delta h_{rc} = \frac{h_{rc}}{n_{rc} - 1} \tag{5.28}$$

To compute the tooth height of a current roughing tooth of the Revacycle gear cutter, one can use the following expression

$$h_{rc}^{(i)} = \Delta h_{rc} \, \mathrm{No}_r \tag{5.29}$$

where No_r denotes the number of the current roughing cutting tooth.

The roughing teeth are within the angle ϑ_{rf}, which spans over the roughing section. The finishing teeth are located at the angular increment $\Delta\varphi_{rc}$. The increment is equal to $\Delta\varphi_{rc} = \vartheta_{rf}/n_{rc}$. In practical terms, the increments $\Delta\varphi_c$ and $\Delta\varphi_{rc}$ are equal to each other ($\Delta\varphi_{rc} = \Delta\varphi_c$); however, this is not a required condition. Rake angle γ_{ro} at the outer cutting edges of the gear cutter is positive ($\gamma_{ro} > 0°$). Therefore, position vector of a point $\mathbf{r}_{rrf}$ of the rake plane for each finishing tooth of the gear cutter can take the form

$$\mathbf{r}_{rsr}(U_{rsr}, V_{rsr}) = \begin{bmatrix} U_{rsr} \\ U_{rsr} \tan[\vartheta_{rf}^{(0)} + \Delta\varphi_{rc} \, (\mathrm{No}_r - 1)] + 0.5 \, d_{o.c} - (h_{rc} - h_{rc}^{(i)}) \\ V_{rsr} \\ 1 \end{bmatrix} \tag{5.30}$$

where U_{rsr} and V_{rsr} denote the curvilinear coordinates of the rake plane R_{rs} and are parallel to the coordinate axes of the reference system $X_cY_cZ_c$ ($U_{rsr} = X_c$ and $V_{rsr} = Z_c$); $\vartheta_{rf}^{(0)}$ denotes the angle at which the roughing section begins.

The cutting edge of every roughing cutting tooth should satisfy both Equations (5.27) and (5.30). Therefore, an analytical description of the roughing cutting edge CE_r can be derived as a solution to Equations (5.27) and (5.30). The solution yields representation in matrix form

$$\mathbf{r}_{rce}(V_{rsr}, No_r) = \begin{bmatrix} X(V_{rsr}, No_r) \\ Y(V_{rsr}, No_r) \\ Z(V_{rsr}, No_r) \\ 1 \end{bmatrix} \tag{5.31}$$

The actual shape of every roughing tooth depends on the parameter No_r. This means that the particular shape of every roughing tooth is dependent on the location of the roughing tooth within the roughing sector of the Revacycle gear cutter.

Clearance surface C_{rs} is a type of relived surface. The clearance surface is a surface through the cutting edge CE_r [see Equation (5.31)] and forms the desired clearance angle α_{ro} with surface $T_{rf}^{(a)}$ of the gear cutter.

5.10.4 Application of the Revacycle Process of Cutting of Gear Teeth

The Revacycle process provides the quickest method of machining tooth spaces in straight bevel pinions generally intended for automotive differential units. For broaching of bevel gear teeth, large-diameter (53 or 64 cm, or 20 or 25 in.) cutters are used. In one revolution of the cutter, utilizing roughing, semifinishing, and finishing cutters, a tooth space is completely cut. The center of rotation of the cutter is changed as different operations are performed. This provides a constant root clearance in the work gear and the concave finishing cutters give the correct tooth profile. Between the finishing and the starting cutting blades, a space is provided that permits the work gear to be indexed to the next tooth space while the tool continues to rotate at a uniform rate.

In common with all high-production-rate machines, the cutting cycle is entirely automatic and ceases after the last tooth space in a blank has been completed. It is often combined with automatic loading and unloading devices so that the production process is continuous. The quality of Revacycle cut gears is inferior to that of the generated types, but the produced pinions are suitable for specific purposes. Naturally, the standard of maintenance for the machine and cutting tools is of considerable importance when the quality of the finished gear is being considered. Tooth proportions differ from the usual standards and special blanks are required.

Although the initial tooling cost is greater than for other types of straight bevel gear machines, the extremely fast production rate results in lowest overall cost for large-scale production. Revacycle cut gears are truly conjugate but are not interchangeable with gears produced by other methods. Revacycle tooth proportions differ from those of other straight bevel gears [190].

6

End-Type Gear Milling Cutters

End-type gear milling cutters are widely used in roughing and finishing external spur gears and in roughing external helical gears. Worms and racks may also be cut by end-type milling cutters. Use of end-type milling cutter does not require special gear cutting machines. Cutting of spur and helical gears with end-type milling cutters can be done in universal milling machines.

Before designing an end-type gear milling cutter, geometry of the generating surface of the gear cutting tool must be predetermined. Two critical issues should be considered when determining the generating surface of the end-type gear milling cutter. The first of these issues is geometry of the tooth flank of the work gear. Geometry of tooth flanks of spur and helical gears allows for the analytical representation of spur gears [Equation (1.2)] and helical gear tooth flanks [Equation (1.3)]. The second issue is the kinematics of the gear milling process with end-type milling cutter.

6.1 Kinematics of Gear Cutting with End-Type Milling Cutter

The kinematics of the gear machining mesh when cutting a gear with an end-type milling cutter is the simplest among those shown for various types of *gear machining meshes* (Figure 3.8). To increase the speed of cut, the sliding motion of the generating surface is not used as the primary motion (as it is occurred in gear broaching); instead, an additional rotation is used for this purpose. The motion that enables the work gear tooth flank to allow sliding over itself is used as the feed motion. Generally speaking, the feed motion in this case is a type of screw motion. The parameter of screw motion is identical to the screw parameter of the work gear.

The kinematics of gear machining with end-type milling cutter is composed of the kinematics of the gear machining mesh and the introduced rotation and feed motion. The rotations $\boldsymbol{\omega}_g$ and $\boldsymbol{\omega}_c$ are not utilized when cutting a gear with an end-type milling cutter. For such cases, the equality $\boldsymbol{\omega}_g = \boldsymbol{\omega}_c = 0$ is observed.

The kinematics of machining a work gear using an end-type milling cutter is illustrated in Figure 6.1.

The vector of the additional rotation $\boldsymbol{\omega}_{cut}$ is perpendicular to the axis of rotation O_g of the work gear. Screw feed motion is shown in Figure 6.1 as a superposition of the rotation $\boldsymbol{\omega}_{fc}$ about the work gear axis O_g and the translation $\mathbf{F}_c$ along the axis O_g. The parameter of the screw motion p_{fc} is equal to $p_{fc} = |\mathbf{F}_c|/|\boldsymbol{\omega}_{fc}|$, and is identical to the reduced pitch p_g of the tooth flank of the helical work gear ($p_{fc} \equiv p_g$). For spur gears, the screw motion reduces to straight motion $\mathbf{F}_c$.

Once the geometry of the tooth flank of the gear to be machined is known [see Equation (1.2) for spur gear and Equation (1.3) for helical gear tooth flank] and the kinematics of the gear machining process is predetermined (Figure 6.1), the generating surface of the gear cutting tool can be determined.

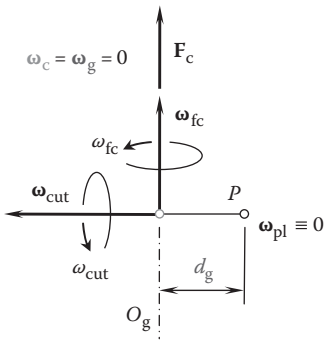

FIGURE 6.1
Kinematics of gear machining process with the end-type milling cutter.

6.2 Generating Surface of the End-Type Gear Milling Cutter

When a gear cutting tool is specifically designed so as to implement the kinematics of the gear machining mesh alone, then in the case under consideration, the generating surface of the gear cutting tool is congruent to the tooth surfaces of the gear being machined. Aside from the fact that this type of kinematics is practical and used for designing gear cutting tools, it is important to consider other possibilities, especially from the standpoint of possibly increasing the speed of the primary motion.

The rotation $\boldsymbol{\omega}_{cut}$ allows for an increase in speed of the primary motion. Moreover, there is no kinematic correlation between the newly introduced rotation $\boldsymbol{\omega}_{cut}$ and the other components of the kinematics of the gear machining process using an end-type milling cutter.

Because of the additional rotation $\boldsymbol{\omega}_{cut}$, the generating surface of the end-type gear milling cutter differs from that initially derived on the basis of just the kinematics of the gear machining mesh alone [see Equation (6.1)]. To distinguish the generating surface T that is derived based on the kinematics of the gear mesh from that derived using an additionally introduced motion(s), the generating surface of the gear cutting tool in the second case is referred to as the *secondary generating surface* T_2.

6.2.1 Equation for the Generating Surface of an End-Type Milling Cutter for Machining Spur Involute Gears

Gear tooth profiles are commonly symmetrical. For material removal from tooth spaces between two neighboring teeth having a symmetrical profile, end-type milling cutters are used.

Spur gears can be formed by milling one slot at a time and indexing to the next slot. The end-type milling cutter is specifically designed so that its axial cross section has an involute curve matching that of the gear tooth. As shown in Figure 6.2, the axial cross section of the milling cutter is the same as that through the space between two adjacent gear teeth. This observation is helpful when deriving an equation for the generating surface of the end-type gear milling cutter.

Deriving an equation for the generating surface T_2 of the end-type milling cutter for machining spur involute gears can be divided onto three steps. First, it is necessary to derive an equation for the tooth profile of the spur work gear. Second, it is required to

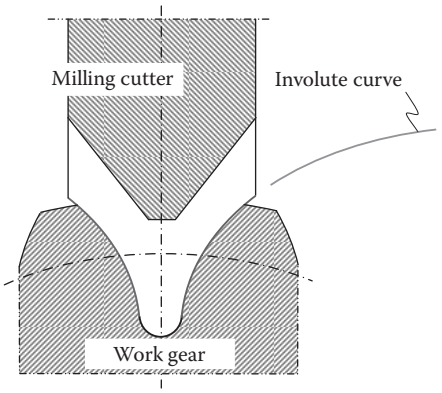

FIGURE 6.2
Correspondence between the spur gear tooth profile and the milling cutter tooth profile.

represent the equation of the spur gear tooth profile in a reference system associated with the milling cutter. In the third step, the generated surface of the end-type milling cutter is presented as the locus of successive positions of the involute gear tooth profile when it is rotating about the milling cutter axis of rotation.

A Cartesian coordinate system $X_{inv}Y_{inv}$ is associated with the work gear as shown in Figure 6.3. The involute tooth profile of the work gear is analytically described in this reference system by the vector equation

$$\mathbf{r}_{inv}(\phi_g) = \frac{d_{b.g}}{2\cos\phi_g} \cdot [\mathbf{i} \cdot \sin(\text{inv}\phi_g) + \mathbf{j} \cdot \cos(\text{inv}\phi_g)] \tag{6.1}$$

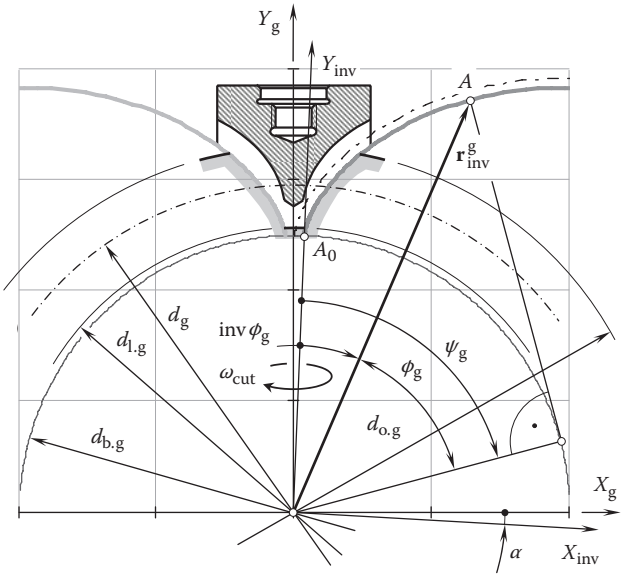

FIGURE 6.3
Determination of the shape of the generating surface T_2 of the end-milling cutter.

$$\text{inv}\phi_g = \tan\phi_g - \phi_g \tag{6.2}$$

where $d_{b.g}$ denotes the base diameter of the work gear and ϕ_g (expressed in radians) is the profile angle at a current point of the involute tooth profile.

Another form of analytical presentation of the involute tooth profile is convenient for particular applications

$$\mathbf{r}_{inv}(\psi_g) = r_{b.g}[\mathbf{i}\cdot(\sin\psi_g - \psi_g\cos\psi_g) + \mathbf{j}\cdot(\cos\psi_g + \psi_g\sin\psi_g)] \tag{6.3a}$$

Here, the equality $d_{b.g} = 2r_{b.g}$ is observed.

The angle ψ_g is correlated to the tooth profile angle ϕ_g as (see Figure 6.3)

$$\psi_g = \text{inv}\phi_g + \phi_g \tag{6.3b}$$

Next, the involute tooth profile [either Equations (6.1) and (6.2) or Equation (6.3a)] should be represented in a reference system associated with the milling cutter. For this purpose, a Cartesian coordinate system X_gY_g is introduced. Axis Y_g of the reference system X_gY_g is aligned with the line of symmetry of the gear space width. The coordinate system X_gY_g is turned about the axis of the gear rotation with respect to the coordinate system $X_{inv}Y_{inv}$ through a certain angle α. Angle α is the angle between the corresponding axes of the coordinate systems X_gY_g and $X_{inv}Y_{inv}$. To compute for the actual value of α, the following formula can be used

$$\alpha = \frac{2\pi}{N_g}\cdot\frac{\breve{s}_{w.g}}{\breve{t}_{t.g}} - \text{inv}\phi_g \tag{6.4}$$

where N_g denotes the tooth number, $\breve{s}_{w.g}$ is the space width, and $\breve{t}_{t.g}$ is the arc tooth thickness. For gears having a standard tooth profile, the equality $\breve{t}_{t.g} = \breve{s}_{w.g}$ applies. In this particular case, Equation (6.4) can be reduced to

$$\alpha = \frac{\pi}{N_g} - \text{inv}\phi_g \tag{6.5}$$

The required coordinate system transformation can be implemented by using the operator of rotation $\mathbf{Rt}(\alpha, Z_g)$ (see Chapter 4 for details).

The following equation

$$\mathbf{r}^g_{inv}(\phi_g) = \mathbf{Rt}(\alpha, Z_g)\cdot\mathbf{r}_{inv}(\phi_g) \tag{6.6}$$

is valid for the analytical description of the involute gear tooth profile in the coordinate system X_gY_g.

Equation (6.1) allows for representation in matrix form as

$$\mathbf{r}_{inv}(\phi_g) = \begin{bmatrix} \dfrac{r_{b.g}}{\cos\phi_g}\cdot\sin(\text{inv}\phi_g) \\ \dfrac{r_{b.g}}{\cos\phi_g}\cdot\cos(\text{inv}\phi_g) \\ 0 \\ 1 \end{bmatrix} \tag{6.7}$$

After $\mathbf{r}_{inv}(\phi_g)$ has been multiplied at left by

$$\mathbf{Rt}(\alpha, Z_g) = \begin{bmatrix} \cos\alpha & \sin\alpha & 0 & 0 \\ -\sin\alpha & \cos\alpha & 0 & 0 \\ 0 & 0 & 1 & 0 \\ 0 & 0 & 0 & 1 \end{bmatrix} \tag{6.8}$$

Equation (6.6) casts into

$$\mathbf{r}_{inv}^{g}(\phi_g) = \begin{bmatrix} \frac{r_{b.g}}{\cos\phi_g} \cdot \sin(\alpha + \text{inv}\phi_g) \\ -\frac{r_{b.g}}{\cos\phi_g} \cdot \cos(\alpha - \text{inv}\phi_g) \\ 0 \\ 1 \end{bmatrix} \tag{6.9}$$

of the involute gear tooth profile in the coordinate system $X_g Y_g Z_g$.

Ultimately, generating surface T_2 of the end-type milling cutter for machining spur involute gears can be represented as a locus of successive positions of the involute gear tooth profile [see Equation (6.9)] when the profile is rotating ω_{cut} about the milling cutter axis of rotation. When deriving the equation for the generating surface T_2, it is convenient to use the operator of rotation $\mathbf{Rt}(\theta, Y_g)$ about the Y_g axis—this coordinate axis is aligned with the axis of rotation of the milling cutter. In this manner, the equation for the generating surface T_2 can be presented in a generalized form as the product

$$\mathbf{r}_T^g(\phi_g, \theta) = \mathbf{Rt}(\theta, Y_g) \cdot \mathbf{r}_{inv}^g(\phi_g) \tag{6.10}$$

Multiplying $\mathbf{r}_{inv}^g(\theta_g)$ [see Equation (6.9)] at left by

$$\mathbf{Rt}(\theta, Y_g) = \begin{bmatrix} \cos\theta & 0 & \sin\theta & 0 \\ 0 & 1 & 0 & 0 \\ -\sin\theta & 0 & \cos\theta & 0 \\ 0 & 0 & 0 & 1 \end{bmatrix} \tag{6.11}$$

returns the equation

$$\mathbf{r}_T^g(\phi_g, \theta) = \begin{bmatrix} \frac{r_{b.g}}{\cos\phi_g} \cdot \sin(\alpha + \text{inv}\phi_g)\cos\theta \\ -\frac{r_{b.g}}{\cos\phi_g} \cdot \cos(\alpha - \text{inv}\phi_g) \\ \frac{r_{b.g}}{\cos\phi_g} \cdot \sin(\alpha + \text{inv}\phi_g)\sin\theta \\ 1 \end{bmatrix} \tag{6.12}$$

of the generating surface T_2 of the end-type milling cutter for machining spur gears.

The generating surface T_2 of the end-type milling cutter [Equation (6.12)] is a type of surface of revolution. Axis of rotation O_{c2} of the cutter is aligned with the $Y_{c2} \equiv Y_g$ axis of the reference system $X_{c2}Y_{c2}Z_{c2}$. Here, Y_{c2} denotes the axis of the coordinate system $X_{c2}Y_{c2}Z_{c2}$ associated with the end-type milling cutter.

The generating surface of the end-type milling cutter for machining spur gears is expressed in terms of two parameters: profile angle ϕ_g of the involute gear tooth profile at a current point of the gear tooth and angle θ of rotation of the involute tooth profile about the axis of the milling cutter ($-\infty < \theta < +\infty$).

6.2.2 Equation for the Generating Surface of an End-Type Milling Cutter for Machining Helical Involute Gears

When milling helical gears, the line of contact between the helical gear tooth flank $\mathcal{G}$ and the generating surface T_2 of the end-type milling cutter is a 3D spatial curve. No analytical description of the spatial line of contact is known at this point. Because of this, the earlier implemented approach (see Section 5.1.1) cannot be used in deriving the equation for the generating surface of the end-type milling cutter for machining helical involute gears.

To solve the problem of profiling of the end-type milling cutter, use of methods developed in the theory of enveloping surfaces is helpful. To solve this problem, two main reference systems are applied. The first coordinate system is associated with the helical gear to be machined. The second coordinate system is the one which the milling cutter will be associated with. It should be stressed that, at this point, the milling cutter does not exist yet. Therefore, we are only operating with a coordinate system that the milling cutter will be associated with.

When milling a helical gear, the milling cutter is performing two motions: (1) rotation $\boldsymbol{\omega}_{cut}$ of the milling cutter about its axis of rotation and (2) screw motion of the milling cutter with respect to the work gear. The screw relative motion is composed of the translation $\mathbf{F}_c$ and the rotation $\boldsymbol{\omega}_{fc}$ (Figure 6.1).

The screw relative motion causes sliding of a surface. Under the screw relative motion the helical gear tooth flank is sliding over it. This relative motion does not affect the shape and parameters of the generating surface of the milling cutter. Therefore, this motion can be eliminated from the list of considerations when deriving an equation for the generating surface T_2 of the end-type milling cutter. Ultimately, the generating surface of the end-type milling cutter can be interpreted as the enveloping surface to successive positions of the helical gear tooth flank that is rotating relative to the milling cutter axis of rotation.

The equation for the generating surface of the end-type milling cutter can be derived in three steps.

First, it is necessary to analytically describe the helical gear tooth surface $\mathcal{G}$ in an appropriate coordinate system. For this purpose, the equation derived earlier for the screw involute surface [see Equation (1.3)] can be used.

Second, it is necessary to derive an equation for the gear tooth flank $\mathcal{G}$ in its current location with respect to the coordinate system associated with the milling cutter. In this step, as well as in the previous step, implementation of the operators of coordinate system transformations (see Chapter 4) is convenient.

Third, the set of two equations specifying the enveloping surface has to be composed. The solution to the set of two equations returns an equation for the generating surface T_2 of the end-type milling cutter for machining helical gears.

Similar to the way the equation for the generating surface T_2 of the end-type milling cutter for machining spur gears (see Figure 6.3) has been derived, the screw involute tooth flank surface $\mathcal{G}$ should be analytically described [see Equation (1.3)]

$$\mathbf{r}_{\mathrm{g}}(U_{\mathrm{g}}, V_{\mathrm{g}}) = \begin{bmatrix} r_{\mathrm{b.g}} \cos V_{\mathrm{g}} + U_{\mathrm{g}} \cos \lambda_{\mathrm{b.g}} \sin V_{\mathrm{g}} \\ r_{\mathrm{b.g}} \sin V_{\mathrm{g}} - U_{\mathrm{g}} \sin \lambda_{\mathrm{b.g}} \sin V_{\mathrm{g}} \\ r_{\mathrm{b.g}} \tan \lambda_{\mathrm{b.g}} - U_{\mathrm{g}} \sin \lambda_{\mathrm{b.g}} \\ 1 \end{bmatrix} \qquad \begin{matrix} V_{\mathrm{g}}^{(l)} \le V_{\mathrm{g}} \le V_{\mathrm{g}}^{(a)} \\ 0 \le U_{\mathrm{g}} \le [U_{\mathrm{g}}] \end{matrix} \tag{6.13}$$

in a certain coordinate system $X_{\mathrm{g}}Y_{\mathrm{g}}Z_{\mathrm{g}}$. The Y_{g} axis of the coordinate system $X_{\mathrm{g}}Y_{\mathrm{g}}Z_{\mathrm{g}}$ is aligned with the line of symmetry of the transverse profile of the gear face.

Use of the operator of rotation $\mathbf{Rt}(\alpha_{\mathrm{t}}, Z_{\mathrm{g}})$ makes it possible to derive an equation for the tooth flank $\mathcal{G}$ with respect to the reference system conveniently associated with the work gear. The angle α_{t} used in the operator of rotation $\mathbf{Rt}(\alpha_{\mathrm{t}}, Z_{\mathrm{g}})$ is measured in the transverse section of the helical gear. This angle is analogous to angle α in the linear transformation $\mathbf{Rt}(\alpha, Z_{\mathrm{g}})$ [see Equation (6.8)].

The following equation

$$\mathbf{r}_{g}^{*}(U_{\mathrm{g}}, V_{\mathrm{g}}) = \mathbf{Rt}(\alpha_{\mathrm{t}}, Z_{\mathrm{g}}) \cdot \mathbf{r}_{\mathrm{g}}(U_{\mathrm{g}}, V_{\mathrm{g}}) \tag{6.14}$$

describes the gear tooth flank $\mathcal{G}$ in the required reference system $X_{\mathrm{g}}Y_{\mathrm{g}}Z_{\mathrm{g}}$.

Equation (6.14) is the solution to the first step of the routing of the derivation of the equation for the generating surface T_2 of the end-type milling cutter.

To derive an expression that describes the gear tooth flank $\mathcal{G}$ in its current location with respect to the coordinate system associated with the milling cutter, the Cartesian reference system $X_{\mathrm{c2}}Y_{\mathrm{c2}}Z_{\mathrm{c2}}$ is introduced (Figure 6.4). The coordinate system $X_{\mathrm{c2}}Y_{\mathrm{c2}}Z_{\mathrm{c2}}$ is turned through a certain angle θ about the Y_{g} axis of the coordinate system $X_{\mathrm{g}}Y_{\mathrm{g}}Z_{\mathrm{g}}$. The angle θ

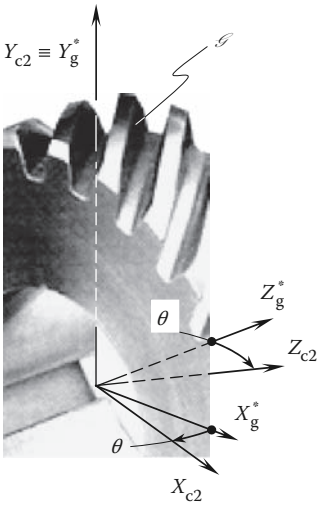

FIGURE 6.4
Configuration of the reference system $X_{\mathrm{c2}}Y_{\mathrm{c2}}Z_{\mathrm{c2}}$ associated with the end-type milling cutter relative to the helical work gear.

allows for interpretation in the form $\theta = \omega_{cut} t$, where ω_{cut} denotes the rotation of the milling cutter about its axis when machining the work gear and t denotes time.

After it has been designed, the end-type milling cutter will be associated with the coordinate system $X_{c2}Y_{c2}Z_{c2}$.

When designing the milling cutter, only the relative motion of the coordinate systems is important. It makes no difference if the milling cutter coordinate system $X_{c2}Y_{c2}Z_{c2}$ is rotating about its axis $O_{c2} \equiv Y_g$ or if the tooth flank $\mathscr{G}$ of the helical gear is rotating about the Y_g axis.

The work gear tooth flank in its current location can be analytically described by

$$\mathbf{r}_g^{c2}(U_g, V_g, \theta) = \mathbf{Rt}(\theta, Y_g) \cdot \mathbf{r}_g^*(U_g, V_g) \tag{6.15}$$

Equation (6.15) presents the solution to the second step of the routing of the derivation of the equation for the generating surface T_2 of the end-type milling cutter.

The third step in deriving the equation can be carried out in two ways: (1) based on elements of the theory of enveloping surfaces, (2) based on the kinematic properties of a moving surface.

The first (traditional) method is developed in the differential geometry of surfaces. Following this method, the equation for the generating surface T_2 of the end-type milling cutter can be derived as the solution to the set of two equations

$$\mathbf{r}_g^{c2} = \mathbf{r}_g^{c2}(U_g, V_g, \theta) \tag{6.16}$$

$$\begin{vmatrix} \dfrac{\partial \mathbf{r}_g^{c2}}{\partial U_g} & \dfrac{\partial \mathbf{r}_g^{c2}}{\partial U_g} & \dfrac{\partial \mathbf{r}_g^{c2}}{\partial U_g} \\ \dfrac{\partial \mathbf{r}_g^{c2}}{\partial V_g} & \dfrac{\partial \mathbf{r}_g^{c2}}{\partial V_g} & \dfrac{\partial \mathbf{r}_g^{c2}}{\partial V_g} \\ \dfrac{\partial \mathbf{r}_g^{c2}}{\partial \theta} & \dfrac{\partial \mathbf{r}_g^{c2}}{\partial \theta} & \dfrac{\partial \mathbf{r}_g^{c2}}{\partial \theta} \end{vmatrix} = 0 \tag{6.17}$$

Equations (6.16) and (6.17) have three unknowns: U_g, V_g, and θ. Two parameters alone are sufficient for an analytical description of a surface. To eliminate parameter θ, it is necessary to solve Equation (6.17) with respect to θ. Next, the derived expression for parameter θ is substituted into Equation (6.16). After all necessary formula transformations are performed, the equation for the generating surface T_2 of the end-type milling cutter for machining involute gears can be presented as

$$\mathbf{r}_{c2} = \mathbf{r}_{c2}(U_{c2}, V_{c2}) \tag{6.18}$$

The second method of deriving an equation for the generating surface of the milling cutter is based on implementation of Shishkov's equation of contact for moving surfaces [186]

$$\mathbf{n} \cdot \mathbf{V} = 0 \tag{6.19}$$

where $\mathbf{n}$ is the common perpendicular to the moving surfaces and $\mathbf{V}$ is the vector of the resultant relative motion of the moving surfaces.

Shishkov's equation of contact is the core equation of the so-called *kinematic method* of surface generation. In compliance with the kinematic method, at the points of contact of two surfaces, which move with respect to each other, the vector of the common perpendicular **n** and the vector of the relative motion **V** of the surfaces must be orthogonal to each other.

When the tooth flank of the helical gear is rotating about the milling cutter axis, only those points of surface $\mathscr{G}$ generate the surface T_2, at which the equation of contact is satisfied.

Equation (6.15) allows for the computation of the unit normal vector $\mathbf{n}_g$ at a current point of the helical gear tooth flank $\mathscr{G}$

$$\mathbf{n}_g(U_g, V_g, \theta) = \frac{\mathbf{U}_g \times \mathbf{V}_g}{\left|\mathbf{U}_g \times \mathbf{V}_g\right|} = \mathbf{u}_g \times \mathbf{v}_g \tag{6.20}$$

For the given parameterization of Equation (6.15), vector $\mathbf{V}_\Sigma$ of the resultant motion of a point of the tooth flank $\mathscr{G}$ can be computed from the formula $\mathbf{r}_g^{c2}(U_g, V_g, \theta)$

$$\mathbf{V}_\Sigma(U_g, V_g, \theta) = \frac{\partial \mathbf{r}_g^{c2}}{\partial \theta} \tag{6.21}$$

Equations (6.20) and (6.21) yield the equation of contact in the form

$$\mathbf{u}_g \times \mathbf{v}_g \cdot \frac{\partial \mathbf{r}_g^{c2}}{\partial \theta} = 0 \tag{6.22}$$

The solution to Equations (6.16) and (6.22)

$$\mathbf{r}_g^{c2} = \mathbf{r}_g^{c2}(U_g, V_g, \theta) \tag{6.23}$$

$$\mathbf{u}_g \times \mathbf{v}_g \cdot \frac{\partial \mathbf{r}_g^{c2}}{\partial \theta} = 0 \tag{6.24}$$

returns an equation for the generating surface T_2 of the end-type milling cutter for machining helical involute gears.

After all the necessary formulae transformations have been performed, equation for the surface T_2 can be presented in the form

$$\mathbf{r}_{c2} = \mathbf{r}_{c2}(U_{c2}, V_{c2}) \tag{6.25}$$

which is identical to the earlier derived Equation (6.18).

This method is referred to as the *kinematic method* of determining the enveloping surfaces.

The generating surface of the end-type milling cutter [see Equations (6.18) and (6.25)] is a type of surface of revolution. Axis of rotation O_{c2} of the milling cutter is aligned with the $Y_{c2} \equiv Y_g$ axis of the reference system $X_{c2}Y_{c2}Z_{c2}$. Here, Y_{c2} denotes the axis of the coordinate system $X_{c2}Y_{c2}Z_{c2}$ associated with the milling cutter.

Very similar to what has just been discussed, corresponding equations for generating surfaces of end-type milling cutters for machining spur and helical gears having noninvolute tooth profiles can be derived. Various tooth profiles can be machined with end-type milling cutters except of those having an asymmetrical tooth profile.

6.2.3 Elements of Intrinsic Geometry of the Generating Surface of End-Type Milling Cutters

Formulae for computation of the major elements of the local topology of the generating surface of the gear cutting tool can be significantly simplified if they are expressed in terms of fundamental magnitudes of the first and second order of the generating surface T_2.

Generating surface T_2 of the gear cutting tool can be initially specified via the vector equation $\mathbf{r}_{c2} = \mathbf{r}_{c2}(U_{c2}, V_{c2})$. Two tangent vectors, $\mathbf{U}_{c2} = \partial\mathbf{r}_{c2}/\partial U_{c2}$ and $\mathbf{V}_{c2} = \partial\mathbf{r}_{c2}/\partial V_{c2}$, can be computed for surface T_2. Vectors $\mathbf{U}_{c2}$ and $\mathbf{V}_{c2}$ are used to compute for the fundamental magnitudes of the first order

$$E_{c2} = \mathbf{U}_{c2} \cdot \mathbf{U}_{c2} \tag{6.26}$$

$$F_{c2} = \mathbf{U}_{c2} \cdot \mathbf{V}_{c2} = \mathbf{V}_{c2} \cdot \mathbf{U}_{c2} \tag{6.27}$$

$$G_{c2} = \mathbf{V}_{c2} \cdot \mathbf{V}_{c2} \tag{6.28a}$$

Vectors $\mathbf{U}_{c2}$ and $\mathbf{V}_{c2}$ allow users to compose matrix $\mathbf{A}_{c2}$ of the first derivatives

$$\mathbf{A}_{c2} = \left[\mathbf{U}_{c2} \middle| \mathbf{V}_{c2}\right] \tag{6.28b}$$

Use of this matrix leads to the following expression for the first fundamental matrix $\mathbf{G}_{c2}$

$$\mathbf{G}_{c2} = \mathbf{A}_{c2}^{T} \cdot \mathbf{A}_{c2} = \begin{bmatrix} E_{c2} & F_{c2} \\ F_{c2} & G_{c2} \end{bmatrix} \tag{6.28c}$$

The importance of this matrix is explained in the following discussion.

By definition, fundamental magnitudes of the second order can be presented in the form

$$L_{c2} = \frac{\dfrac{\partial \mathbf{U}_{c2}}{\partial U_{c2}} \times \mathbf{U}_{c2} \cdot \mathbf{V}_{c2}}{H_{c2}} \tag{6.29}$$

$$M_{c2} = \frac{\dfrac{\partial \mathbf{U}_{c2}}{\partial V_{c2}} \times \mathbf{U}_{c2} \cdot \mathbf{V}_{c2}}{H_{c2}} = \frac{\dfrac{\partial \mathbf{V}_{c2}}{\partial U_{c2}} \times \mathbf{U}_{c2} \cdot \mathbf{V}_{c2}}{H_{c2}} \tag{6.30}$$

$$N_{c2} = \frac{\dfrac{\partial \mathbf{V}_{c2}}{\partial V_{c2}} \times \mathbf{U}_{c2} \cdot \mathbf{V}_{c2}}{H_{c2}} \tag{6.31a}$$

Similar to Equation (6.28c), an expression for the second fundamental matrix can be composed

$$\mathbf{D}_{c2} = \begin{bmatrix} \mathbf{n}_{c2} \cdot \dfrac{\partial \mathbf{U}_{c2}}{\partial U_{c2}} & \mathbf{n}_{c2} \cdot \dfrac{\partial \mathbf{U}_{c2}}{\partial V_{c2}} \\ \mathbf{n}_{c2} \cdot \dfrac{\partial \mathbf{V}_{c2}}{\partial U_{c2}} & \mathbf{n}_{c2} \cdot \dfrac{\partial \mathbf{V}_{c2}}{\partial V_{c2}} \end{bmatrix} \tag{6.31b}$$

Since $\partial \mathbf{U}_{c2}/\partial V_{c2} = \partial \mathbf{V}_{c2}/\partial U_{c2}$ for all the surfaces we shall be concerned with, matrix $\mathbf{D}_T$ will be symmetric

$$\mathbf{D}_{c2} = \begin{bmatrix} L_{c2} & M_{c2} \\ M_{c2} & N_{c2} \end{bmatrix} \tag{6.31c}$$

Computed values of the fundamental magnitudes of the first and the second order allow for significant simplification in the analysis of the generating surface of the gear cutting tool.

6.3 Cutting Edges of the End-Type Gear Milling Cutter

End-type milling cutter can be considered as a type of form milling cutters. Determination of the generating surface of the milling cutter is just a prerequisite for designing an end-type milling cutter for machining either an involute gear or a gear with a noninvolute tooth profile. Determination of the cutting edges is the next step.

Cutting edges of a precision milling cutter are located within the generating surface T_2. Any deviation of the cutting edge from the generating surface T_2 causes a corresponding deviation in the machined gear tooth profile.

On the other hand, the cutting edge is an element of the cutting wedge formed by the rake surface and the clearance surface. The cutting edge can be interpreted as the line of intersection of the rake surface R_s of the milling cutter tooth and the clearance surface C_s of the milling cutter tooth. In addition, this line of intersection has to be located within the generating surface T_2. Ultimately, three surfaces—rake surface R_s, clearance surface C_s, and generating surface T_2—are passing through the cutting edge. Physically, the cutting edge aligns with the line of intersection of surfaces R_s and C_s. However, virtually it must be located with surface T_2.

The brief discussion above reveals the importance of geometry of the rake surface and the clearance surface to the cutting tool designer.

6.3.1 Rake Surface of the Milling Cutter for Machining of Involute Gears

Location of the cutting edges of the milling cutter within the generating surface T_2 is one of the major requirements that a milling cutter must comply with. Any curve within surface

T_2 is capable of precisely generating the involute gear tooth profile. However, the shape of the cutting edge must be reasonable for technological reasons. The rake surface and the clearance surface that physically form the cutting edge have to be machined somehow. Accuracy of the machining of surfaces R_s and C_s must be inspected, and regrinding of the worn milling cutter must be simple. Because of these reasons as well as other factors, it is not practical to include all cutting edges of every shape and geometry. Only the shapes of the cutting edge formed by surfaces R_s and C_s are practical because they are simple to machine and inspect.

Two surfaces are practical to use as rake surfaces of end-type milling cutters: a plane and an Archimedean screw surface. Implementation of both surfaces provides the milling cutter with a zero rake angle. In regrinding of worn cutting tools, milling cutters having a zero rake angle are simpler to machine. The cutting edge of the milling cutter for machining of spur gear is identical to the involute tooth profile of the gear to be machined, which significantly simplifies inspection of the milling cutter. However, in terms of cutting performance and length of tool life, milling cutters with a zero rake angle do not offer the maximum rate possible.

The rake surface is a plane. The rake surface of a precision milling cutter for finishing of an involute gear is a plane. For the milling cutter with a zero rake angle, the rake plane is a plane through the axis of rotation O_T of the cutter (Figure 6.5). Any plane through the axis O_T could serve as the rake plane of the milling cutter. As an example, the coordinate plane X_TY_T of the coordinate system $X_TY_TZ_T$, that is, the plane given by the equation $Z_T = 0$, can be used for this purpose. Under such a scenario, the cutting edge of the milling cutter can be determined as the line of intersection of the generating surface T of the milling cutter [see either Equation (6.12) for milling cutters for machining spur gears or Equation (6.18) for milling cutters for machining helical gears] by the rake plane $Z_T = 0$.

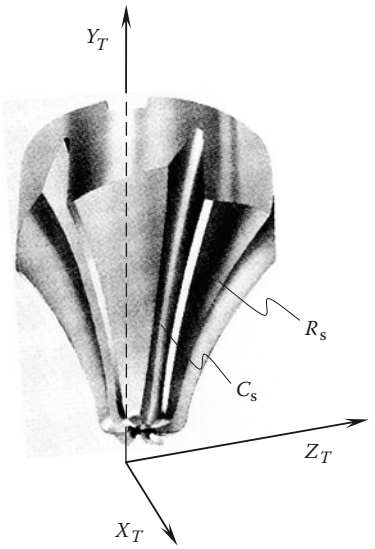

FIGURE 6.5
Rake surface R_s and clearance surface C_s of the precision milling cutter for finishing of involute gears.

In deriving the equation for the cutting edge of the gear milling cutter, the format of the analytical representation of the rake plane R_s must be the same as that for the generating surface T of the milling cutter. For this reason, the equation $Z_T = 0$ is required to be presented in matrix form

$$R_s \quad \Rightarrow \quad \mathbf{r}_{rs}(X_{rs}, Y_{rs}) = \begin{bmatrix} X_{rs} \\ Y_{rs} \\ 0 \\ 1 \end{bmatrix} \tag{6.32}$$

where coordinates of the points of rake plane R_s are expressed in terms of X_{rs} and Y_{rs}.

Parameterizations of surfaces T and R_s have to be compatible with each other when aiming for mutual consideration of the generating surface T [see Equations (6.12) and (6.18)] together with the rake plane R_s [see Equation (6.32)]. Usually, reparameterization either of surface T or surface R_s is often required (see Appendix C). As an example, parameters X_{rs} and Y_{rs} can be expressed in terms of U_T and V_T parameters as functions $X_{rs} = X_{rs}$ (U_T, V_T) and $Y_{rs} = Y_{rs}$ (U_T, V_T).

The rake surface is a screw Archimedean surface. The rake surface of a roughing milling cutter for machining of involute gear is often a screw Archimedean surface (Figure 6.6). In the coordinate system $X_T Y_T Z_T$ associated with the milling cutter, the equation for the rake surface R_s allows matrix representation in the form

$$R_s \quad \Rightarrow \quad \mathbf{r}_{rs}(\rho_{rs}, \theta) = \begin{bmatrix} \rho_{rs} \cos\theta \\ p_{rs}\theta \\ \rho_{rs} \sin\theta \\ 1 \end{bmatrix} \tag{6.33}$$

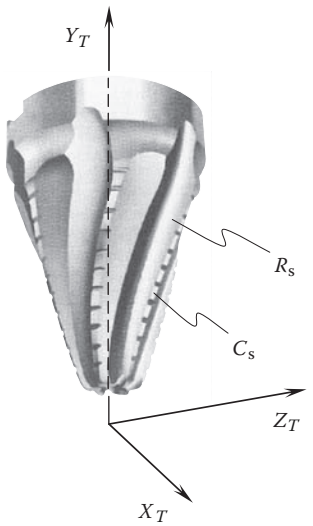

FIGURE 6.6
Rake surface R_s and clearance surface C_s of the roughing milling cutter for machining of involute gears.

where ρ_{rs} denotes the distance of a point of the rake surface R_s from the axis of rotation of the milling cutter, θ is the polar angle, and p_{rs} is the helical parameter of the screw Archimedean surface.

For the computation of the fundamental magnitudes of the first order of the rake surface given by Equation (6.33), Equations (6.26) through (6.28) can be used. In compliance with Equation (6.28c), one can derive the first fundamental matrix

$$\mathbf{G}_T = \begin{bmatrix} 1 & p_{rs} \\ p_{rs} & \rho_{rs} + p_{rs} \end{bmatrix} \tag{6.34}$$

for rake surface R_s.

Similarly, for the computation of the fundamental magnitudes of the second order of the rake surface given by Equation (6.33), Equations (6.29) through (6.31a) can be used. Using Equation (6.31c), one can derive the second fundamental matrix

$$\mathbf{D}_T = \begin{bmatrix} 0 & \dfrac{p_{rs}}{\sqrt{p_{rs}^2 + \rho_{rs}^2}} \\ \dfrac{p_{rs}}{\sqrt{p_{rs}^2 + \rho_{rs}^2}} & 0 \end{bmatrix} \tag{6.35}$$

for rake surface R_s.

Parameterizations of surfaces T and R_s have to be compatible with each other when aiming for mutual consideration of the generating surface T [see Equations (6.12) and (6.18)] and the screw Archimedean rake plane R_s [see Equation (6.33)]. Because of this, for a current point of the surface R_s the polar angle θ in Equation (6.33) is of the same value as for the generating surface T of the milling cutter [see Equation (6.12)]. The polar distance ρ_{rs} can be expressed in terms of parameters ϕ_g and θ of the generating surface T by the expression

$$\rho_{rs}(\phi_g, \theta) = \frac{r_{b.g}}{\cos\phi_g} \tag{6.36}$$

After substitution of the expression for ρ_{rs}, Equation (6.33) casts into

$$R_s \quad \Rightarrow \quad \mathbf{r}_{rs}(\phi_g, \theta) = \begin{bmatrix} \dfrac{r_{b.g}}{\cos\phi_g} \cdot \cos\theta \\ p_{rs}\theta \\ \dfrac{r_{b.g}}{\cos\phi_g} \cdot \sin\theta \\ 1 \end{bmatrix} \tag{6.37}$$

Equations (6.12) and (6.37) can be solved together. The solution to Equations (6.12) and (6.37) analytically describes the 3D spatial cutting edge of the milling cutter. Equation for the cutting edge of the end-type milling cutter can be presented in matrix form as

$$\mathbf{r}_{ce}(\vartheta_{ce}) = \begin{bmatrix} X(\vartheta_{ce}) \\ Y(\vartheta_{ce}) \\ Z(\vartheta_{ce}) \\ 1 \end{bmatrix} \tag{6.38}$$

where ϑ_{ce} is a parameter of the cutting edge of the milling cutter.

When the generating surface T of the milling cutter and the rake surface R_s are expressed in terms of common parameters, one of the parameters can be expressed in terms of another parameter. In this manner, the parameter ϑ_{ce} of the cutting edge of the milling cutter can be identified.

6.3.2 Clearance Surface of the Milling Cutter for Machining of Involute Gears

Clearance surface of the precision milling cutter is a surface through the cutting edge that makes a clearance angle with the surface of cut. For end-type milling cutters, the generating surface of the milling cutter is a perfect local approximation of the surface of cut. Therefore, two clearance angles can be distinguished: (1) the actual clearance angle α^{ac}, which is the angle between the clearance surface and the surface of cut, and (2) the computed clearance angle α, which is the angle between the clearance surface and the generating surface of the milling cutter. In most practical cases of milling of involute gears, the difference between α^{ac} and α is negligibly small ($\Delta\alpha = \alpha^{ac} - \alpha \cong 0$). Thus, the generating surface T of the milling cutter—and not the surface of cut—is used as the reference surface for the computation of the rake angle.

As noted above, the cutting edge of the milling cutter can be interpreted as the line of intersection of three surfaces: (1) generating surface T, (2) rake surface R_s, and (3) clearance surface C_s. Using the equation for cutting edge [see Equation (6.38)] allows us to construct the clearance surface C_s of the end-type milling cutter. In this method, the clearance surface is presented as a locus of consecutive positions of the cutting edge that is performing a certain motion.

In deriving the equation for clearance surface C_s, it is convenient to decompose the resultant instant motion $\mathbf{v}_{ce}$ of the cutting edge into three components (Figure 6.7a)

$$\mathbf{v}_{ce} = \mathbf{v}_t + \mathbf{v}_n + \mathbf{v}_{ax} \tag{6.39}$$

Component $\mathbf{v}_t$ is tangent to the generating surface T of the milling cutter. This component is the linear velocity of rotation $\boldsymbol{\omega}_{ce}$ of the cutting edge about the axis of rotation O_T of the milling cutter. For an arbitrary point m within the cutting edge AB, the component $\mathbf{v}_t$ can be expressed in terms of two parameters: distance r_m, which represents the distance of point m from the axis of rotation of the milling cutter, and angle θ_{ce}, the angle at which the cutting edge turns through in a certain time t. Angle θ_{ce} is equal to $\theta_{ce} = \omega_{ce}t$. Ultimately, the expression

$$\mathbf{v}_t(\theta_{ce}) = \begin{bmatrix} \omega_{ce} r_m \cos\theta_{ce} \\ 0 \\ \omega_{ce} r_m \sin\theta_{ce} \\ 1 \end{bmatrix} \tag{6.40}$$

can be obtained for the tangential component $\mathbf{v}_t$.

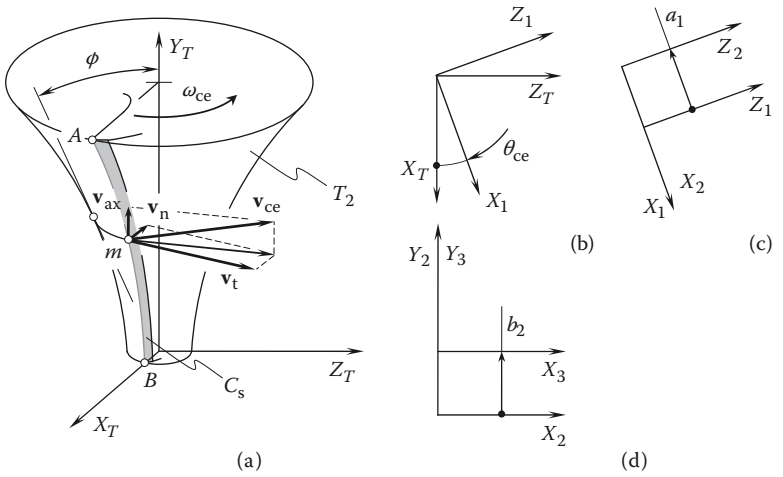

FIGURE 6.7
Construction of the clearance surface C_s of the end-type milling cutter.

The normal component $\mathbf{v}_n$ is in the radial direction of the generating surface T of the milling cutter. At point m, magnitude $|\mathbf{v}_n|$ of the component correlates to magnitude $|\mathbf{v}_t|$ of component $\mathbf{v}_t$ as

$$|\mathbf{v}_n| = |\mathbf{v}_t| \cdot \tan \alpha_{xz} \tag{6.41}$$

where α_{xz} denotes the rake angle of the milling cutter in the transverse cross section through m.

For point m, an expression for component $\mathbf{v}_n$ yields representation in matrix form as

$$\mathbf{v}_n(\theta_{ce}) = \begin{bmatrix} -\omega_{ce} r_m \sin\theta_{ce} \tan\alpha_{xz} \\ 0 \\ -\omega_{ce} r_m \cos\theta_{ce} \tan\alpha_{xz} \\ 1 \end{bmatrix} \tag{6.42}$$

Component $\mathbf{v}_{ax}$ is in the axial direction of the milling cutter. Magnitude $|\mathbf{v}_{ax}|$ of the axial component $\mathbf{v}_{ax}$ somehow correlates to magnitude $|\mathbf{v}_n|$ of the normal component $\mathbf{v}_n$. It has been proven practical to establish this correlation in the form

$$|\mathbf{v}_{ax}| = |\mathbf{v}_n| \tan\phi \tag{6.43}$$

where ϕ denotes the pressure angle on the pitch diameter of the gear to be machined. If so, point m has to be located at the cutting edge point that is tangent to the axial profile of the surface T, which forms pressure angle ϕ with the cutter axis of rotation O_t.

Equation (6.43) yields the relation

$$\mathbf{v}_{ax} = \begin{bmatrix} 0 \\ \omega_{ce} r_m \tan\alpha_{xz} \tan\phi \\ 0 \\ 1 \end{bmatrix} \tag{6.44}$$

for the axial component $\mathbf{v}_{ax}$ of the resultant motion $\mathbf{v}_{ce}$ of the cutting edge.

Consider the resultant motion of the cutting edge AB with respect to the coordinate system $X_T Y_T Z_T$ associated with the milling cutter body. Assume that the cutting edge is analytically described in a coordinate system $X_{ce} Y_{ce} Z_{ce}$. Initially, the coordinate system $X_{ce} Y_{ce} Z_{ce}$ is congruent to the coordinate system $X_T Y_T Z_T$.

In compliance with Equation (6.39), the resultant motion of the coordinate system $X_{ce} Y_{ce} Z_{ce}$ with respect to the coordinate system $X_T Y_T Z_T$ can be decomposed into three components: $\mathbf{v}_t$, $\mathbf{v}_n$, and $\mathbf{v}_{ax}$.

The tangential component $\mathbf{v}_t$ is caused by rotation ω_{ce} of the cutting edge about the axis of rotation O_T of the milling cutter. After being turned through angle θ_{ce} about the Y_{ce} axis, the coordinate system $X_{ce} Y_{ce} Z_{ce}$ occupies the first intermediate location $X_1 Y_1 Z_1$ (Figure 6.7b). Coordinate transformation of this type can be analytically described by the operator of rotation $\mathbf{Rt}(\theta_{ce}, Y_{c2})$. In the case being considered, the operator $\mathbf{Rt}(\theta_{ce}, Y_T)$

$$\mathbf{Rt}(\theta_{ce}, Y_T) = \begin{bmatrix} \cos\theta_{ce} & 0 & -\sin\theta_{ce} & 0 \\ 0 & 1 & 0 & 0 \\ \sin\theta_{ce} & 0 & \cos\theta_{ce} & 0 \\ 0 & 0 & 0 & 1 \end{bmatrix} \tag{6.45}$$

The normal component $\mathbf{v}_n$ causes the coordinate system $X_1 Y_1 Z_1$ to shift along its X_1 axis at a certain distance a_1 to the position of the second intermediate location $X_2 Y_2 Z_2$ (Figure 6.7c). The current value of distance a_1 can be obtained as

$$a_1 = \theta_{ce} r_m \tan\alpha_{xz} \tag{6.46}$$

Therefore, translation of the coordinate system $X_1 Y_1 Z_1$ to the position of the coordinate system $X_2 Y_2 Z_2$ can be analytically described by the operator of translation $\mathbf{Tr}(a_1, X_1)$. For the end-type milling cutter, the operator of translation $\mathbf{Tr}(a_1, X_1)$ is obtained as

$$\mathbf{Tr}(a_1, X_1) = \begin{bmatrix} 1 & 0 & 0 & \theta_{ce} r_m \tan\alpha_{xz} \\ 0 & 1 & 0 & 0 \\ 0 & 0 & 1 & 0 \\ 0 & 0 & 0 & 1 \end{bmatrix} \tag{6.47}$$

Ultimately, the axial component $\mathbf{v}_{ax}$ results in the shift of the coordinate system $X_2 Y_2 Z_2$ along its Y_2 axis at a certain distance b_2 to the position of the third coordinate system $X_3 Y_3 Z_3$ (Figure 6.7d). To compute for the current value of distance b_2, the expression

$$b_2 = \theta_{ce} r_m \tan\alpha_{xz} \tan\phi \tag{6.48}$$

can be used.

For the analytical description of the translation of the coordinate system $X_2 Y_2 Z_2$ to the position of the coordinate system $X_3 Y_3 Z_3$, the operator of translation $\mathbf{Tr}(b_2, Y_2)$ can be composed. For the case under consideration, this operator of linear transformation can be presented as

$$\mathbf{Tr}(b_2, Y_2) = \begin{bmatrix} 1 & 0 & 0 & 0 \\ 0 & 1 & 0 & -\theta_{ce} r_m \tan\alpha_{xz} \tan\phi \\ 0 & 0 & 1 & 0 \\ 0 & 0 & 0 & 1 \end{bmatrix} \tag{6.49}$$

Equation for the clearance surface C_s of the end-type milling cutter yields representation in the form of dot product of two expressions. To come up with an equation for the position vector $\mathbf{r}_{cs}(\vartheta_{ce}, \theta_{ce})$ of the current point of clearance surface C_s, it is necessary to multiply at left the position vector $\mathbf{r}_{ce}(\vartheta_{ce})$ of a point of the cutting edge [see Equation (6.38)] by the operator $\mathbf{Rs}(3 \mapsto T)$ of the resultant coordinate system transformation

$$\mathbf{r}_{cs}(\vartheta_{ce}, \theta_{ce}) = \mathbf{Rs}(3 \mapsto T) \cdot \mathbf{r}_{ce}(\vartheta_{ce}) \tag{6.50}$$

The operator of the resultant linear transformation $\mathbf{Rs}(3 \mapsto T)$ can be presented as the product of the operators of elementary coordinate systems transformations

$$\mathbf{Rs}(3 \mapsto T) = \mathbf{Tr}(b_2, Y_2) \cdot \mathbf{Tr}(a_1, X_1) \cdot \mathbf{Rt}(\theta_{ce}, Y_T) \tag{6.51}$$

Finally, the equation for the clearance surface C_s [see Equation (6.50)] is expressed in terms of two independent parameters, ϑ_{ce} and θ_{ce}. Parameter ϑ_{ce} specifies the location of a current point within the cutting edge AB, whereas parameter θ_{ce} specifies the current location of the cutting edge within the clearance surface.

6.3.3 Cutting Edge Geometry of the End-Type Milling Cutter

The cutting wedge of the end-type milling cutter is somehow oriented with respect to the surface of cut. Configuration of the cutting wedge relative to the surface of cut is specified by geometrical parameters of the cutting edge. Rake angle γ, clearance angle α, and angle of inclination λ are of prime importance to end-type milling cutters for machining of involute gears.

To achieve the best possible performance of the milling cutter, all the geometrical parameters of the cutting edge must be equal to their optimal values. Performance of the gear cutting tool, for example, tool life (TL) of the end-type milling cutter strongly depends on the actual values of the geometrical parameters of the cutting edge. Functionality of the gear cutting tool performance versus the actual value of the geometrical parameters of the cutting edge is at maximum as shown in Figure 6.8. This means that there always exists an optimal value of each geometrical parameter under which tool performance of the gear cutting tool reaches its maximal possible rate. For example, if the clearance angle of the milling cutter is equal to its optimal value α_{opt}, this corresponds to a maximum of the function TL = TL(α). In designing an end-type milling cutter—or any type of cutting tool, for that matter—it is highly desirable when all geometrical parameters are equal to their optimal values.

Unfortunately, because of numerous constraints, actual values of the geometrical parameters of cutting tools are too far from their optimal values. Therefore, gear cutting tools are designed not with optimal values of the clearance angle α, but with the angle α within certain interval $a_1 < \alpha < \alpha_2$, where the inequality $\alpha_2 \ll \alpha_{opt}$ is usually observed. As a result,

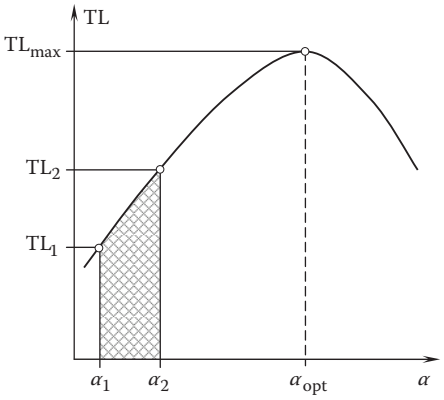

FIGURE 6.8
Qualitative relation "a gear cutting tool performance vs. clearance angle α."

the actual tool life of the gear milling cutter is within a certain range $TL_1 < TL < TL_2$. The commonly achieved tool life TL_2 is often much shorter compared to the maximal possible tool life TL_{max}.

Without going into details of optimality of the geometrical parameters of gear cutting tools, it is necessary to stress that: (1) the optimal combination of geometrical parameters of the cutting edge can be determined for a gear cutting tool of any type, and (2) in designing the most economical gear cutting tool, actual values of geometrical parameters of cutting edges must either be equal to their optimal values or their deviation from optimal values must be the smallest possible. For this purpose, it is necessary to compute the actual values of geometrical parameters at every point of the cutting edge of the gear cutting tool.

In computing the geometrical parameters at the current point of the cutting edge of the end-type milling cutter, an infinitesimally short portion of the cutting edge is considered. This assumption allows us to neglect the curvature within the differential dl of the actually curved cutting edge.

Rake surface is a plane. The geometry of the end-type milling cutter having a rake surface in the form of a plane through the axis of rotation of the milling cutter can be specified by three angles:

Rake angle $\gamma = 0°$
Angle of inclination $\lambda = 0°$
Clearance angle $\alpha > 0°$

Because both rake angle γ and angle of inclination λ have zero values ($\gamma = 0°$ and $\lambda = 0°$), no analysis of the geometry of the rake surface of the end-type milling cutter is necessary. To predict the performance of the milling cutter, only the geometry of the clearance surface needs to be investigated.

It has been proven convenient to use a method of investigation of cutting tool geometry that is based on the implementation of elements of vector algebra. To the best of the author's knowledge, Mozhayev [46] was the first to use elements of vector calculus for solving problems relating to the geometry of the active part of cutting tools. The interested reader may check other sources [138, 143, 153] for details on the method.

Consider the cutting edge of the end-type milling cutter (Figure 6.9a). The actual value of the normal rake angle α_{ce} at point m is given. It is required to derive an equation for the computation of the normal rake angle α_n at a current point m within the cutting edge of the milling cutter.

A local Cartesian coordinate system $x_m y_m z_m$ is associated with the cutting edge AB. The origin of the reference system $x_m y_m z_m$ is located at a current point m within the cutting edge AB. Axis x_m is along the assumed direction of speed of cut; axis y_m is tangent to the cutting edge and axis z_m is perpendicular to the surface of cut. The surface of cut is not determined yet. However, generation surface of the milling cutter is a perfect local approximation of the surface of cut. Therefore, the z_m axis can be constructed perpendicular to the surface T of the milling cutter.

To derive the equation, three vectors, **a**, **B** and **c**, are constructed. Here and below, unit vectors are denoted by lowercase characters, whereas vectors magnitude exceeding unit are denoted by uppercase characters. In reality, only the directions of vectors are of critical importance. Vectors can be chosen of arbitrary length. For the convenience of derivation of equations, magnitudes of some vectors were chosen equal to unit, whereas magnitudes of other vectors of another length were chosen for specific cases.

Unit vector **a** is tangent to the line of intersection of the clearance surface C_s by the normal plane. In the local coordinate system $x_m y_m z_m$, vector **a** can be expressed as (Figure 6.9b)

$$\mathbf{a} = \mathbf{i} \cdot \cos\alpha_n + \mathbf{k} \cdot \sin\alpha_n \tag{6.52}$$

The magnitude of vector **B** is chosen as the length for which the projection of **B** onto the coordinate plane $y_m z_m$ is equal to unit ($\text{pr}_{yz}\,\mathbf{B} = 1$)). Hence, the following expression

$$\mathbf{B} = \mathbf{i} \cdot \cot\alpha_{ce} + \mathbf{j} \cdot \sin(\phi - \phi_m) + \mathbf{k} \cdot \cos(\phi - \phi_m) \tag{6.53}$$

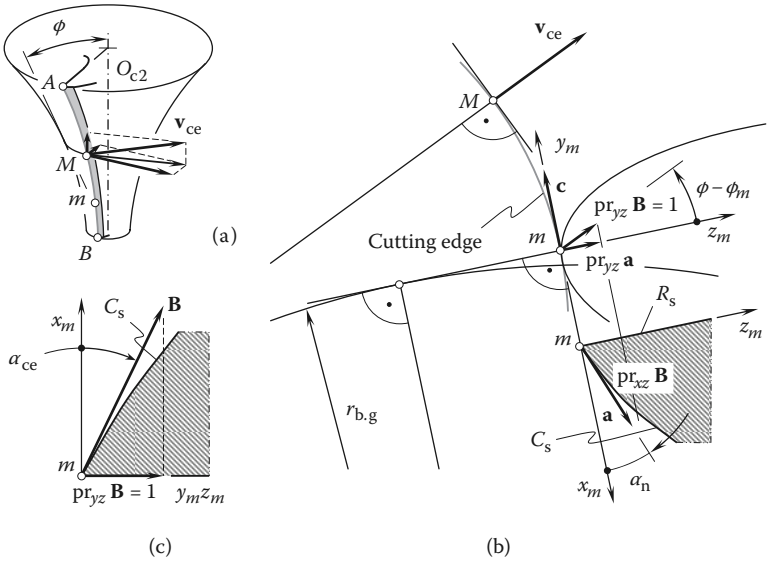

FIGURE 6.9
Analysis of the geometry of the clearance surface of the finishing milling cutter.

where a_{ce} denotes the clearance angle in the direction of $\mathbf{v}_{ce}$ [see Equation (6.39)] (α_{ce} is equal to the normal clearance angle at point M of the cutting edge); ϕ is the pressure angle of the gear to be machined; and ϕ_m is the pressure angle at point m. Angle ϕ_m can be easily expressed in terms of the design parameters of the gear to be machined.

Unit vector $\mathbf{c}$ aligns with the y_m axis of the coordinate system $x_m y_m z_m$, and is simply expressed as

$$\mathbf{c} = \mathbf{i} \tag{6.54}$$

By construction, vectors $\mathbf{a}$, $\mathbf{B}$, and $\mathbf{c}$ are within a common plane. Therefore, their triple scalar product is identical to zero $\mathbf{a} \times \mathbf{B} \cdot \mathbf{c} \equiv 0$. The triple scalar product of the vectors can be expressed in the form of a determinant. This immediately yields the following equation

$$\mathbf{a} \times \mathbf{B} \cdot \mathbf{c} = \begin{vmatrix} \cos\alpha_n & 0 & \sin\alpha_n \\ \cot\alpha_{ce} & \sin(\phi - \phi_m) & \cos(\phi - \phi_m) \\ 0 & 1 & 0 \end{vmatrix} = 0 \tag{6.55}$$

Equation (6.55) casts into

$$\alpha_n(\phi_m) = \tan^{-1}[\tan\alpha_{ce}\cos(\phi - \phi_m)] \tag{6.56}$$

where the normal clearance angle α_n is expressed in terms of pressure angle ϕ_m at a current point m within the cutting edge. The actual value of α_n can be expressed in terms of any desired design parameter of the gear to be machined. For this purpose, the equations listed in Appendix A can be used. For convenience, pressure angle ϕ_m can be expressed in terms of the design parameters of the gear to be milled. For this purpose, the following formula can be used

$$\phi_m = \cos^{-1}\left(\frac{r_{b.g}}{r_{m.g}}\right) \tag{6.57}$$

where $r_{b.g}$ is the radius of the base cylinder of the gear to be machined and $r_{m.g}$ is the radius of the circle through point m of the gear tooth profile.

Figure 6.10 illustrates an example of the variation of the normal clearance angle α_n within the tooth height of the gear to be machined. The computations are performed for the end-type milling cutter having a clearance angle $\alpha_{ce} = 12°$. The shape of the distribution curves depends on the number of teeth of the gear. Involute gears having a smaller number of teeth are subject to more severe changes in normal clearance angle. In Figure 6.10, the plot "normal clearance angle vs. height of gear tooth" does not cover the portion of the gear tooth within the transient curve at the bottom of the gear tooth space. This is because the shape of the fillet significantly differs from the true involute form of the gear tooth.

Rake surface is a screw surface. Consider a roughing end-type milling cutter having rake surface shaped in the form of a screw surface. At point m, the helix angle ψ of the rake face is given. It is necessary to derive an equation to compute for the angle of inclination λ at a current point m within the cutting edge AB of the milling cutter.

By definition [138, 143, 153], the angle of inclination λ of the cutting edge (1) is measured within the surface of cut and (2) the angle of inclination is equal to the angle that the vector of speed of cut $\mathbf{V}_\Sigma$ makes with the perpendicular to the cutting edge $\mathbf{n}_{ce}$ at the point of

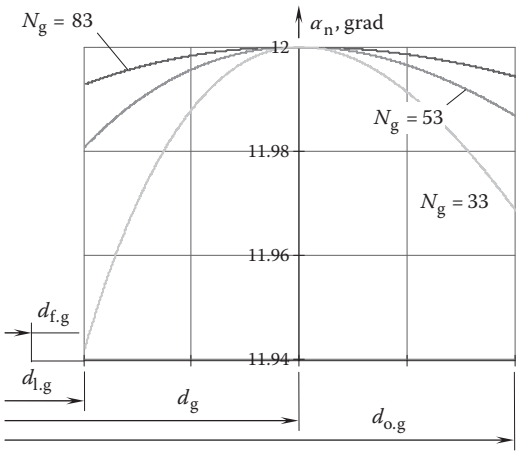

FIGURE 6.10
Normal clearance angle α_n at a current point m of the cutting edge of the end-type milling cutter (normal clearance angle α_{ce} at point M is 12°).

interest [$\lambda = \angle (\mathbf{V}_{\text{å}}\, \mathbf{n}_{ce})$]. As viewed from the end of the unit normal vector $\mathbf{n}_{se}$ to the surface of cut, the angle of inclination has a positive value when the motion from $\mathbf{V}_\Sigma$ toward $\mathbf{n}_{ce}$ is in counterclockwise direction. Otherwise, the angle of inclination has a negative value.

To derive a formula for the actual value of the angle of inclination λ at a current point m of the cutting edge of the roughing end-type milling cutter, a system of three coplanar vectors **A**, **b** and **c** through m is constructed. For the analytical description of the vectors **A**, **b** and **c**, see the local Cartesian reference system $x_m y_m z_m$ (Figure 6.11a). The coordinate system $x_m y_m z_m$ is the coordinate system that has been used earlier (see Figure 6.9).

The family of screw lines can be drawn up on the screw rake surface of the milling cutter. One of the screw lines is passing through point m. Vector **A** is tangent to the screw line through m. Vector **A** is of a magnitude under which the projection of **A** onto the coordinate plane $y_m z_m$ is equal to unit, say $\text{pr}_{yz}\,\mathbf{A} = 1$ (Figure 6.11b). Under such an assumption, vector **A** (Figure 6.11c) can be expressed analytically by the formula

$$\mathbf{A} = \mathbf{i} \cdot \tan \psi_m + \mathbf{j} \cdot \cos \phi_m - \mathbf{k} \cdot \sin \phi_m \tag{6.58}$$

where ψ_m is the helix angle of the screw rake surface and ϕ_m is the pressure angle at the local point m within the cutting edge.

The unit vector **b** is tangent to the rake surface of the milling cutter and is directed along the z_m axis towards axis of rotation O_T of the milling cutter (Figure 6.11b). Therefore,

$$\mathbf{b} = -\mathbf{k} \tag{6.59}$$

Finally, the unit vector **c** is tangent to the cutting edge and therefore, also tangent to the surface of cut. For vector **c**, the following expression can be composed (Figure 6.11d).

$$\mathbf{c} = -\mathbf{i} \sin \lambda + \mathbf{j} \cos \lambda \tag{6.60}$$

Because by construction, vectors **A**, **b** and **c** are coplanar vectors, their triple scalar product is identical to zero ($\mathbf{A} \times \mathbf{B} \cdot \mathbf{c} \equiv 0$). The triple scalar product of the vectors yields interpretation in the form of the determinant

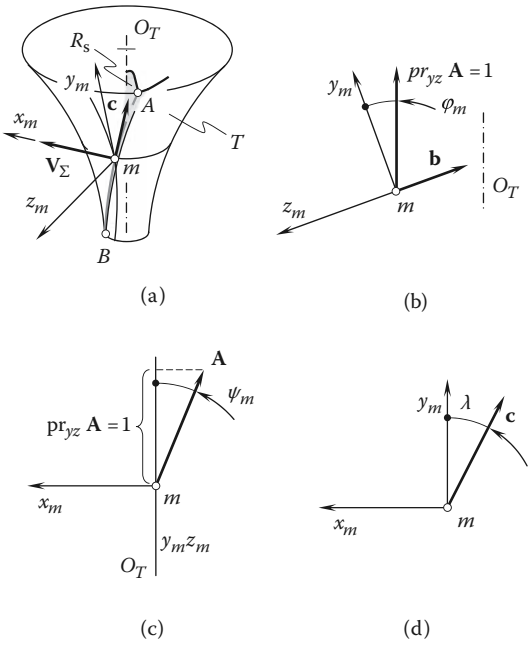

FIGURE 6.11
Analysis of the geometry of the cutting edge within the surface of cut of the roughing milling cutter.

$$\mathbf{A} \times \mathbf{b} \cdot \mathbf{c} \equiv \begin{vmatrix} \tan\psi_m & \cos\phi_m & \sin\phi_m \\ 0 & 0 & -1 \\ -\sin\lambda & \cos\lambda & 0 \end{vmatrix} = 0 \tag{6.61}$$

After the determinant has been expanded, Equation (6.61) casts into the formula

$$\lambda = \tan^{-1}\left(-\frac{\tan\psi_m}{\cos\phi_m}\right) \tag{6.62}$$

for the computation of the angle of inclination λ of the cutting edge of the roughing end-type milling cutter.

For the readers' convenience, both parameters ψ_m and ϕ_m in Equation (6.61) are necessarily expressed in terms of the design parameters of the milling cutter.

Helix angle ψ_m at a current point within the cutting edge can be expressed in terms of its known value ψ at point m. It is common practice that point m corresponds to the pitch diameter d_T of the milling cutter. Outer diameter of the cross section through point m of the end-type milling cutter is denoted by $d_{T.m}$. For the case under consideration, the following expression

$$\psi_m = \tan^{-1}\left(\frac{d_T}{d_{T.m}} \cdot \tan\psi\right) \tag{6.63}$$

can be derived for the computation of angle ψ_m.

To compute for the milling cutter geometry, it can be assumed that the outer diameter of the cross section through point m of the end-type milling cutter is equal $d_T = \pi m$ (where m is the module of the milling cutter).

To compute for diameter $d_{T.m}$ the following equality

$$\pi m - \frac{d_{T.m}}{d_{g.m}} + \text{inv}\phi_m = \frac{d_T}{d_g} + \text{inv}\phi \tag{6.64}$$

can be used.

In the case of milling cutters for machining of internal involute gears, the equality

$$\frac{d_{T.m}}{d_{g.m}} + \text{inv}\phi_m = \frac{d_T}{d_g} + \text{inv}\phi \tag{6.65}$$

is valid.

Pressure angle ϕ_m at a current point within the cutting edge can be determined using Equation (6.57).

We can compute for the inclination angle λ at a current point m within the cutting edge of the roughing end-type milling cutter using the equations derived above. An example of the computations is shown in Figure 6.12. It is common practice in gear-related texts to designate the lead angle as λ. It is also common practice to designate the angle of inclination as λ. To avoid confusion, the inclination angle is expressed in terms of the helix angle, and not in terms of the lead angle. Lead angle and helix angle complement each other to 90°. Therefore, the screw rake surface of the roughing end-type milling cutter can be specified not by the lead angle (20°) but by the helix angle ($\psi = 70°$) instead.

It is common practice to grind rake surfaces, both plane rake surfaces as well as screw rake surfaces, for sharpening and resharpening of worn end-type milling cutters. Clearance surfaces are ground on relieving operations. Commonly, clearance surfaces of worn milling cutters are not reground by users.

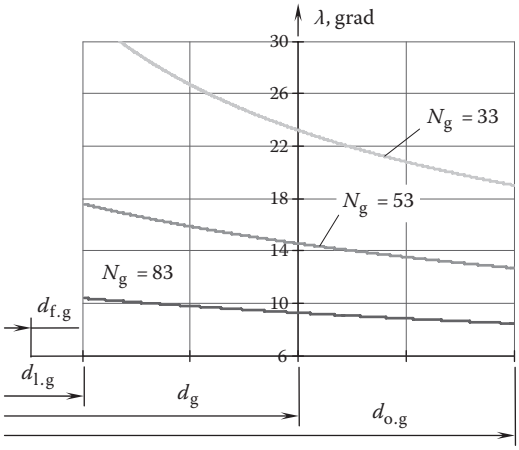

FIGURE 6.12
Angle of inclination λ at a current point m of the cutting edge of the end-type milling cutter (lead angle at point m is 20°).

6.4 Accuracy of Machining of Gear Tooth Flanks with End-Type Milling Cutters

Accuracy of machining of gears is a very complicated problem. This problem definitely deserves to be investigated, and has been discussed in a separate volume. In this text, only particular problems relating to accuracy of machining of gears are reported. This particular problem of gear machining could be referred to as accuracy of *generation* of gear tooth flanks. The major difference between accuracy of gear machining and accuracy of gear generation is as follows.

Gear machining itself causes errors of the machined gears due to the impact of physical, geometrical, kinematical, etc., factors of the machining operation. This includes, but is not limited to, the impact of (1) dynamics of the gear machining, (2) tool wear, (3) heat generation and thermal extension of the elements of the machine tool, (4) elastic deformation of the elements of the machine tool, etc. In contrast, gear generation encompasses errors of the machined gear due to just the geometrical and kinematical factors of the gear machining operation. Thus, the process of gear generation can be interpreted as a simplified model of the actual gear machining operation. As shown below, numerous useful results can be drawn up using the gear generation process as the simplified model of gear machining operation.

The line of contact of the gear tooth flank $\mathcal{G}$ and the generating surface T of the milling cutter is observed when machining a gear using an end-type milling cutter. The line of contact of surfaces $\mathcal{G}$ and T is referred to as *characteristic E*. When the milling cutter is traveling in the axial direction of the gear from one face of the gear toward the opposite face, the characteristic E travels together with the milling cutter. The gear tooth flank is generated as a family of consecutive positions of the characteristic E. No deviations between the (actual) machined tooth flank and the desired tooth flank is observed if the generating surface T is a continuous surface, that is, when the cutting tool reproduces the entire surface T. One can imagine a grinding wheel having a generating surface T that is identical to that of the end-type milling cutter. Finishing of the gear with the grinding wheel of such design produces a precision tooth flank with no deviations between the actual machined tooth flank and its desired shape.

In designing an end-type milling cutter, the entire generating surface T is not reproduced. In reality, surface T is represented not continuously, but discretely by a certain number of distinct curves—the cutting edges. Therefore, despite the fact that surfaces $\mathcal{G}$ and T are in line of contact, cusps on the milled tooth flanks of the gear are unavoidable.

6.4.1 Cusps on Tooth Flanks of Spur Gear

The end-type milling cutter shown in Figure 6.13 is spun about its axis of rotation O_c while being fed simultaneously in the direction of the feed $\mathbf{F}_r$ parallel to the axis O_g of the gear blank in a milling process. After each pass of the milling cutter, the path cut by the milling cutter is the resulting shape of the tooth profile. The gear blank is indexed one transverse pitch ($2\pi/N_g$ radians) and the cutting process is repeated. Accurate indexing of the gear blank "exactly" one transverse pitch is required when using this method for fabricating gears.

The number of teeth of the end-type milling cutter is limited. When machining a spur gear, residual cusps are generated on the gear tooth flanks due to the limited number of

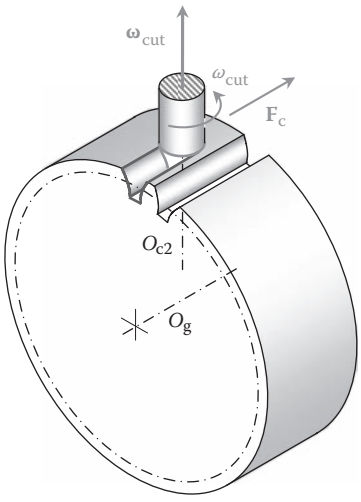

FIGURE 6.13
Schematic of the machining process of a spur gear with the end-type milling cutter.

teeth of the milling cutter (Figure 6.14). Cusps of this type are often referred to as *waviness* of the machined tooth flank. Length *ab* of cusps is equal to the feed per tooth F_r of the milling cutter. The straight-line segment *ab* is a portion of the straight generating line that is parallel to the gear axis of rotation (Figure 1.12). The waviness height *cd* is designated as h_w. The actual profile of the waviness is shaped in the form of epitrochoid. Because the length F_r of the waviness is much smaller compared to the radius of the curvature of the epitrochoid at any point within the length F_r, this allows for reasonable approximation of the epitrochoid by a circular arc. Radius of the circular arc R_w is equal to the radius of the curvature of the epitrochoid at its apex, that is, at point *a*. Under this assumption, the

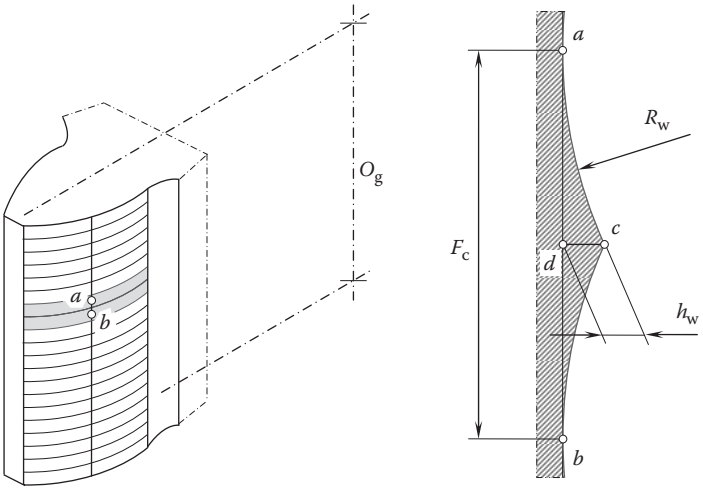

FIGURE 6.14
Deviation of the actual tooth flank from the desired tooth flank of a spur gear machined with the end-type milling cutter.

maximal deviation h_w between the actual machined tooth flank and its desirable surface $\mathcal{G}$ can be computed as

$$h_w = R_w - \sqrt{R_w^2 - 0.25F_r^2} \tag{6.66}$$

In this equation, the radius of the approximating circular arc has not been determined yet. To compute for R_w, Mensnier's formula [136, 138, 143, 153] is used. Implementation of Mensnier's formula allows an expression of the radius R_w in terms of the design parameters of the milling cutter

$$R_w = \frac{d_{c.m}}{2\cos\phi_m} \tag{6.67}$$

In this equation, diameter of the milling cutter $d_{c.m}$ at a current point m within the cutting edge is computed on the premise of the equality [see Equation (6.64)] for the cases of machining of external involute gears, or on the premises of the equality [see Equation (6.65)] for the cases of machining of internal gears.

The derived equations allow for the computation of the deviation h_w within the tooth height of the spur involute gear machined with an end-type milling cutter. Figure 6.15 illustrates an example of the computations. Deviation h_w varies in relation with the tooth height. Its value is bigger at smaller diameters of the gear and becomes progressively smaller for those points of the gear tooth profile closer to the outer diameter. Variation in the milling cutter diameter is the major reason for the variation in the values of h_w.

6.4.2 Cusps on the Tooth Flanks of a Helical Gear

The curved shape of the tooth flank of the helical gear is the main reason for the deviation between the actual and the desired gear tooth flank of the helical involute gear. In the direction of the feed $\mathbf{F}_r$, the tooth flank of a spur gear is straight. The shape of the helical

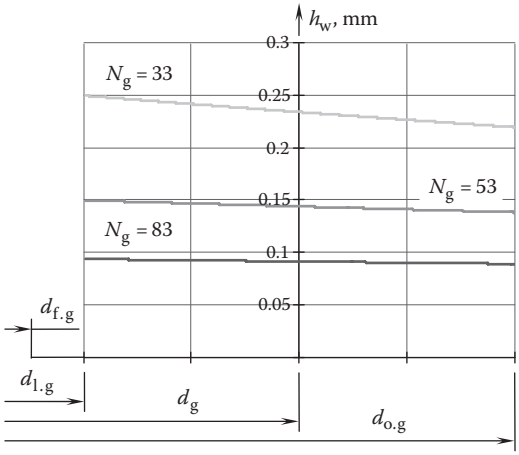

FIGURE 6.15
Deviation of the actual tooth flank from the desired tooth flank within the tooth height of a spur gear machined with the end-type milling cutter.

gear in the direction of the feed $\mathbf{F}_r$ is curved. The curvedness of the tooth flank of the helical gear should be computed and accounted for when computing the deviations between the actual and the desired gear tooth flank.

Normal curvature of the helical gear tooth flank in the direction of the feed $\mathbf{F}_r$. Similar to the generation of the tooth flank of spur gears, the tooth flank of helical gears can also be generated with a straight line (see Figure 1.13). However, in this case, the straight generating line is not parallel to the axis of rotation of the gear but makes a base helix angle $\psi_{b.g}$ with the axis O_g. In the direction of feed of the milling cutter, the normal cross section is not straight but curved. The radius of curvature R_g of this cross section can be obtained using Euler's formula

$$R_g = \frac{1}{\dfrac{R_{1.g}}{\cos^2 \psi_{b.g}} + \dfrac{R_{2.g}}{\sin^2 \psi_{b.g}}} \tag{6.68}$$

where $R_{1.g}$ and $R_{2.g}$ denote the principal radii of the curvature of the gear tooth flank $\mathscr{G}$. To compute for the actual values of the radii of curvature $R_{1.g}$ and $R_{2.g}$, the following formulae

$$R_{1.g} = \frac{\sqrt{d_{g.m}^2 - d_{b.g}^2}\cos\psi_{b.g}}{2\sin^2\psi_{b.g}} \quad \text{and} \quad R_{2.g} \to \infty \tag{6.69}$$

are derived. For details regarding the derivation of Equations (6.68) and (6.69), the interested reader is referred to refs. [92, 138, 143, 158].

Finally, one can come up with the equation

$$R_g = \frac{R_{1.g}}{\cos^2 \psi_{b.g}} \tag{6.70}$$

to compute for the actual values of the required normal radius of curvature R_g of the gear tooth flank $\mathscr{G}$.

Computation of the deviation of the machined tooth flank of the helical gear from its desired shape. The computed value of the normal radius of curvature R_g can be substituted into the approximate expression

$$h_w \cong \frac{R_g(R_g + R_w)\left(1 - \cos\dfrac{\breve{F}_w}{2R_g}\right)}{R_g - (R_g + R_w)\cos\dfrac{\breve{F}_w}{2R_g}} \tag{6.71}$$

for the computation of the cusp height h_w [136, 138, 143, 153].

In Equation (6.71), the radius of normal curvature R_g is computed via formula (6.70), and Equation (6.67) is used to compute for the milling cutter radius R_w. Feed per tooth $\breve{F}_w$ of the milling cutter is equal to the length of the arc segment *ab* in Figure 6.16.

Another expression can be implemented for the computation of the cusp height h_w. Consider two straight lines. One of them is the straight line through points *c* and *d* (Figure 6.16). The second one (not shown in Figure 6.16) is the straight line through the

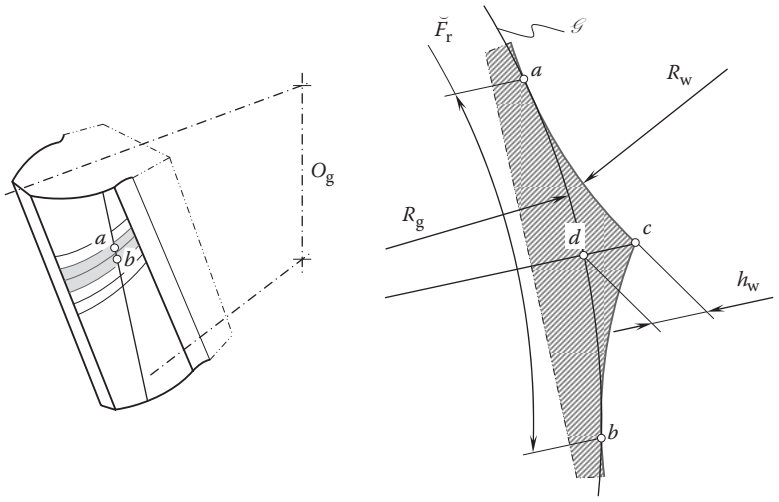

FIGURE 6.16
Deviation of the actual tooth flank from the desired tooth flank of a helical gear machined with the end-type milling cutter.

centers of curvature of the circular arcs of radii R_g and R_w. The angle between these two straight lines is denoted be φ. The value of angle φ (in radians) is known or can be computed; next, for the computation of the cusps height h_w the approximate equation [136, 138, 143, 153]

$$h_w \cong \frac{\varphi^2}{2R_w} \cdot R_g(R_g + R_w) \tag{6.72}$$

can be used.

Consider a cylinder having an arbitrary diameter $d_{y.g}$. The axis of the cylinder aligns with the axis of the gear O_g. The diameter $d_{y.g}$ is within the outer diameter of the gear $d_{o.g}$ and the limit diameter $d_{l.g}$, that is, the inequality $d_{l.g} \le d_{y.g} \le d_{o.g}$ is observed. The gear tooth flank deviation h_w is smaller for the bigger diameter $d_{y.g}$ (see Figure 6.15).

The deviation depends on the number of teeth of the machined gear, and its value is larger for gears with fewer teeth.

The deviation of tooth flanks for helical gears machined with an end-type milling cutter differs from that of tooth flanks for spur gears. The deviation h_w of tooth flanks for external helical gears is larger compared to that of spur gear, whereas the deviation h_w of tooth flanks for internal helical gears is smaller compared to that of spur gears.

6.5 Application of Gear Milling Cutters

Gear milling cutters are universal in application. Gear milling finds its widest application in roughing and finishing external spur gears, and in roughing external helical gears. Although it is usually applied to external tooth forms, internal tooth forms can also be produced by milling. The milling process is practically suitable for making racks, especially

large racks. Worms may also be produced by the milling process (Figure 6.17). Straight bevel gears are often roughed out by milling prior to generating; in some cases, these gears are finished by milling.

Most present-day uses of gear milling cutters are in coarse-pitch applications. A common application in coarse-pitch gears is the roughing operation, leaving stock for finish hobbing or shaving.

In practice, however, gear milling cutters are usually confined to producing replacement gears or small-lot gears with special tooth forms.

Gear teeth may be milled in one cut, or they may be given a rough cut almost to size and then finish-milled.

Parts to be milled must allow room for the run-out of the cutter at each end of the tooth. Wide face widths can be milled, and it is usually possible to have fairly long shaft extension on the gear.

The end-type gear milling cutter is a type of a form milling cutter. In the case of spur gears, the form on the milling cutter teeth is reproduced on the gear. When helical gears are milled, the milling cutter tooth form is not reproduced on the gear.

Gear cutters are not universal for a complete range of teeth. To produce theoretically correct gear teeth, the cutter tooth must be designed for a specific number of teeth. However, where a small error in tooth form is acceptable, cutters that are designed for a range of teeth can be used.

For spur gears, a gear cutter will produce a tooth space that has the same form as the cutter teeth. Since the cutter axis is at 90° of the gear axis, the axis of the cutter is contained in the transverse plane of the gear. Under these conditions, the gear tooth profiles are finished when the cutter teeth pass through this plane. Therefore, the form on the cutter teeth is reproduced in the gear.

The form of helical gear tooth spaces will not be the same as the cutter tooth form. In milling helical teeth, the cutter axis is usually set at the helix angle of the gear. At this setting, the axis of the cutter is contained in the normal plane through the center of the gear tooth space. Under these conditions, only one point on the finished profile is produced in this normal plane. All other points on the finished profile are produced in different planes. Therefore, the form on the cutter teeth is not reproduced in the gear. In addition to the setting angle, the diameter of the cutter affects the gear tooth form and must be considered in designing the proper cutter.

In practice, standard cutters are sometimes used to cut helical gears. The range of the cutter to be used can be determined by finding the equivalent number of spur teeth. For

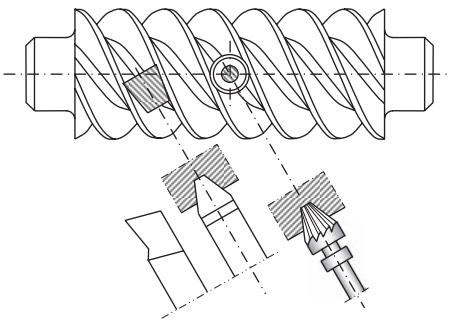

FIGURE 6.17
Machining of an involute gear with the multiple end-type milling cutters.

small helix angles, a standard cutter for the proper range of teeth will produce a close approximation to the desired gear tooth form. However, gear cutters for gears with large helix angles are usually designed specifically to produce the desired form.

Standard involute gear cutters are designed to cut a range of gear tooth numbers. For each pitch, eight cutters are made as follows:

TABLE 6.1

Standard Set of Milling Cutter for Machining of Involute Gears

Cutter No.	Will Cut Gears From
1	135 teeth to rack
2	55 to 134 teeth
3	35 to 54 teeth
4	26 to 34 teeth
5	21 to 25 teeth
6	17 to 20 teeth
7	14 to 16 teeth
8	12 to 13 teeth

The cutters are made in either 14.5° or 20° pressure angles, and a "backed-off" unground form. The cutter is designed for the lowest number of teeth in the range.

As higher accuracy of tooth form is frequently required, the "half number" gear milling cutters are used. These provide a better tooth form for the high end of each tooth range.

TABLE 6.2

Standard Set of Milling Cutter for Machining of Precision Involute Gears

Cutter No.	Will Cut Gears From
1½	80 to 114 teeth
2½	42 to 54 teeth
3½	30 to 34 teeth
4½	23 to 25 teeth
5½	19 to 20 teeth
6½	15 to 16 teeth
7½	13 teeth

The form on the cutter is made correct for the lowest number of teeth in that particular range. Thus, all teeth within the range are provided with sufficient tip relief. The same form is produced on all tooth spaces within that range. If close accuracy is desired in form-milled teeth, it is necessary to use a cutter with a curvature that is appropriate for the exact number of teeth. This can be done by purchasing a special single-purpose cutter.

Theoretically, a special cutter is required to mill a helical gear of a specific tooth form and helix angle. Determination of the equivalent number of spur teeth provides an approximation that is often used to find the standard-range cutter required. The equivalent number of spur teeth is found by dividing the actual number of gear teeth by the cosine of the helix angle cubed.

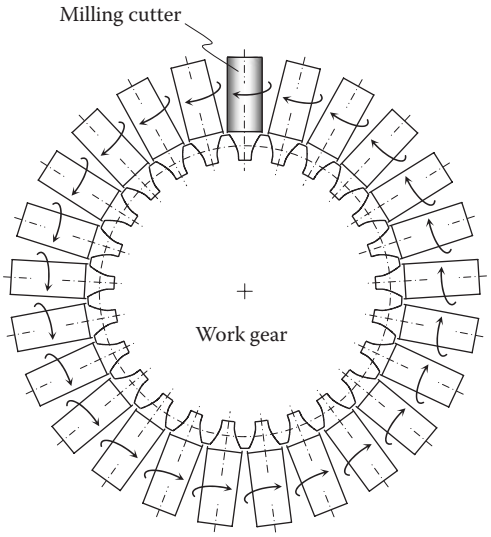

FIGURE 6.18
Machining of an involute gear with the multiple end-type milling cutters.

Milling gear teeth is primarily a form-milling operation to which the general techniques of milling apply. Except for the addition of an indexing mechanism, and the determination of lead gears and setup for helical teeth, machine operation is comparable with conventional milling practice.

Conventional milling machines equipped with a dividing head may be used to mill gear teeth. The cutter tooth form is centered correctly with the gear axis so that a symmetrical tooth space is produced. After each tooth space is milled, the gear blank is indexed to the next cutting position.

Depending on the size of the gear and the capacity of the machine, standard milling machines are used with either manual or automatic indexing mechanisms. On a production basis, where milling is used to produce large coarse-pitch gears, special automatic indexing gear cutting machines are used. Small automatic gear cutting machines are applied to the volume production of fine-pitch gears having special tooth forms.

Whether the machine is hand-operated or automatic, the accuracy of tooth spacing depends on the indexing mechanism. Impact of the indexing on the accuracy of the milled gear can be eliminated when the multiple end-type milling cutters are used (Figure 6.18).

Since milling gear teeth is a form-cutting operation in which the cutter tooth produces the complete gear tooth profile, fine surface finish can be obtained.

The number of teeth of an end-type gear milling cutter is usually even, and it is assigned in the range of 2–8 teeth for the milling cutter of diameter in the range of 40–220 mm.

Relieving of the end-type gear milling cutter is performing at the angle of 10–15° to the cutter axis of rotation.

7

Disk-Type Gear Milling Cutters

Disk-type milling cutters are widely used in roughing and finishing external spur and helical gears. Worms and racks may also be cut by disk-type milling cutters. Use of disk-type milling cutters does not require the use of special gear cutting machines.

Geometry of the generating surface of the gear cutting tool must be predetermined before a disk-type milling cutter is designed. Two issues are of critical importance when determining the generating surface of the disk-type milling cutter. Geometry of the tooth flank of the work gear is one of the issues to be considered. Geometry of tooth flanks of spur and helical gears allows for analytical representation [see Equation (1.2) for spur gears and Equation (1.3) for helical gear tooth flanks]. Kinematics of the gear milling process using an end-type milling cutter is another issue to be considered.

7.1 Kinematics of Gear Cutting with Disk-Type Milling Cutter

The kinematics of the gear machining mesh when cutting a gear using a disk-type milling cutter is simple. In fact, it is the simplest among those shown for various types of *gear machining meshes* (see Figure 3.8).

The kinematics of the gear machining process using disk-type milling cutters resembles that of milling gears with end-type milling cutters (see Figure 6.1). To increase the speed of cut, the sliding motion of the generating surface is not used as the primary motion (as this is occurred in gear broaching); instead, an additional rotation is used for this purpose. The motion that enables the work gear tooth flank to allow sliding over itself is used as the feed motion. Generally speaking, this feed motion is a type of screw motion. This parameter of screw motion is identical to the screw parameter of the work gear.

The kinematics of the gear machining process with a disk-type milling cutter is composed of the kinematics of the gear machining mesh and the introduced rotation and feed motion. The rotations $\boldsymbol{\omega}_g$ and $\boldsymbol{\omega}_c$ are not used when cutting a gear with a disk-type milling cutter. In this case, the equality $\boldsymbol{\omega}_g = \boldsymbol{\omega}_c = 0$ is observed.

The kinematics of machining of a work gear with a disk-type milling cutter is illustrated in Figure 7.1.

The rotation vector $\boldsymbol{\omega}_{cut}$ is at a certain center distance $C_{g/c}$ from the work gear axis O_g (Figure 7.1a). The vector of the additional rotation $\boldsymbol{\omega}_{cut}$ is crossing at right angle with the axis O_g of the work gear. Straight feed motion $\mathbf{F}_c$ is along the work gear axis O_g. Kinematics of the gear machining process of this type is used when machining a spur work gear.

When a helical gear is machined with the disk-type milling cutter (Figure 7.1b), the rotation vector $\boldsymbol{\omega}_{cut}$ is crossing with the axis O_g of the work gear. The crossed-axis angle is equal to the pitch helix angle ψ_g of the work gear. Feed motion is a type of screw motion. The screw feed motion is represented in Figure 7.1b as a superposition of the rotation $\boldsymbol{\omega}_{fc}$ about the work gear axis O_g and the translation $\mathbf{F}_c$ along the axis O_g. The parameter of the

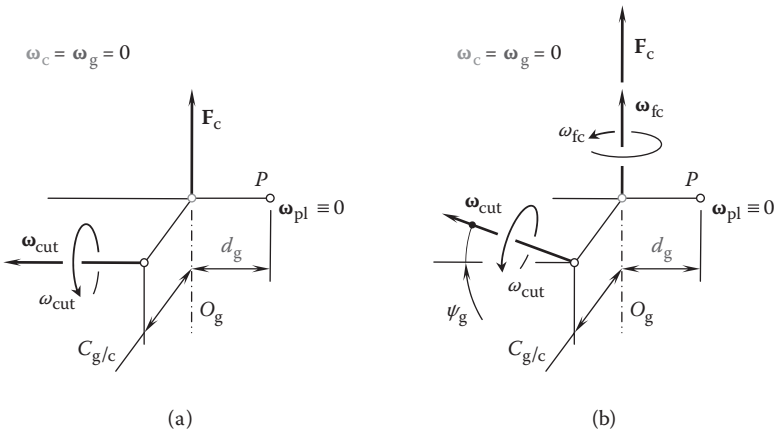

FIGURE 7.1
Kinematics of gear machining process with the disk-type milling cutter.

screw feed motion p_{fc} is equal to $p_{fc} = |\mathbf{F}_c| / |\boldsymbol{\omega}_{fc}|$, and is identical to the reduced pitch p_g of the tooth flank of the helical work gear ($p_{fc} \equiv p_g$). For a given work gear, the reduced pitch p_g is given as

$$p_g = \frac{L_g}{2\pi} \tag{7.1}$$

where L_g denotes lead of the work gear teeth.

Reduced pitch can be expressed in terms of pitch diameter d_g and pitch helix angle ψ_g of the work gear

$$p_g = \frac{d_g}{2} \cot \psi_g \tag{7.2}$$

Once the geometry of the tooth flank of the gear to be machined is known [see Equation (1.2) for spur gears and Equation (1.3) for helical gear tooth flanks] and the kinematics of the gear machining process has been predetermined (see Figure 7.1), the generating surface of the gear cutting tool can be determined.

7.2 Generating Surface of the Disk-Type Gear Milling Cutter

When designing a disk-type gear milling cutter, the secondary generating surface of the gear cutting tool must be determined. This is because the kinematics of the gear machining process with a disk-type milling cutter consists of an additional rotation $\boldsymbol{\omega}_{cut}$ of the milling cutter.

7.2.1 Equation for the Generating Surface of Disk-Type Milling Cutters for Machining Spur Involute Gears

In the case of spur gears, the translation motion $\mathbf{F}_c$ causes the gear tooth flank to slide over it. This motion does not affect the shape of the generating surface of the milling cutter. This motion can be omitted when determining the secondary generating surface T_2 of the milling cutter.

Disk-type gear milling cutters can be used for machining of both symmetrical (Figure 7.2a) and asymmetrical tooth profiles (Figure 7.2b).

Derivation of an equation for the secondary generating surface of the disk-type milling cutter for machining spur involute gears can be divived into three steps. (1) It is necessary to derive an equation for the tooth profile of the spur gear to be machined. (2) The derived equation of the spur gear tooth profile is required to be represented in a reference system associated with the milling cutter. (3) The generating surface of the disk-type milling cutter is represented as the locus of successive positions of the involute gear tooth profile when it is rotating about the axis of rotation of the milling cutter.

To derive an equation for the secondary generating surface T_2 of the disk-type gear milling cutter, the earlier derived analytical description of the involute gear tooth profile [see Equations (6.1) and (6.2)]

$$\mathbf{r}_{\text{inv}}(\phi_g) = \frac{d_{b.g}}{2\cos\phi_g} \cdot [\mathbf{i} \cdot \sin(\text{inv}\phi_g) + \mathbf{j} \cdot \cos(\text{inv}\phi_g)] \tag{7.3}$$

$$\text{inv}\phi_g = \tan\phi_g - \phi_g \tag{7.4}$$

can be used.

Equations (7.3) and (7.4) represent the solution to the first step of the problem under consideration.

In the second step, the operator of rotation $\mathbf{Rt}(a, Z_g)$ about the gear axis Z_g is composed. The operator $\mathbf{Rt}(a, Z_g)$ is implemented for transferring of the gear tooth profile [see Equations (7.3) and (7.4)] into the properly oriented Cartesian coordinate system $X_gY_gZ_g$

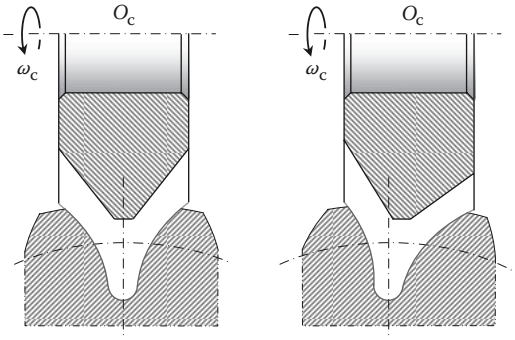

FIGURE 7.2
Tooth profile of disk-type milling cutters for machining (a) symmetrical gear tooth profile and (b) asymmetrical gear tooth profile.

(Figure 7.3). This allows us to account for the space width of the work gear. Next, the operator of translation **Tr** (C, Y_g) is used for the purpose of representing the tooth profile in the appropriate reference system that the milling cutter will be associated with.

Ultimately, the equation for the involute tooth profile in the coordinate system $X_cY_cZ_c$ allows for matrix representation

$$\mathbf{r}_{\text{inv}}^{c}(\phi_g) = \mathbf{Tr}(C, Y_g) \cdot \mathbf{Rt}(\alpha, Z_g) \cdot \mathbf{r}_{inv}(\phi_g) \tag{7.5}$$

In the third step, the generating surface T_2 of the disk-type gear milling cutter is constructed as the locus of successive positions of the involute tooth profile [see Equation (7.5)] that is rotating ω_{cut} about the milling cutter axis O_c (Figure 7.3). For this purpose, it is convenient to implement the operator of rotation **Rt**(θ, X_c) of the involute tooth profile $\mathbf{r}_{\text{inv}}^{c}(\phi_g)$ about the X_c axis. The X_c coordinate axis is aligned with the axis of rotation O_c of the milling cutter

$$\mathbf{r}_{T}^{c}(\phi_g, \theta) = \mathbf{Rt}(\theta, X_c) \cdot \mathbf{r}_{\text{inv}}^{c}(\phi_g) \tag{7.6}$$

In this equation, the operator of rotation **Rt**(θ, X_c) allows for matrix representation

$$\mathbf{Rt}(\theta, X_c) = \begin{bmatrix} 1 & 0 & 0 & 0 \\ 0 & \cos\theta & \sin\theta & 0 \\ 0 & -\sin\theta & \cos\theta & 0 \\ 0 & 0 & 0 & 1 \end{bmatrix} \tag{7.7}$$

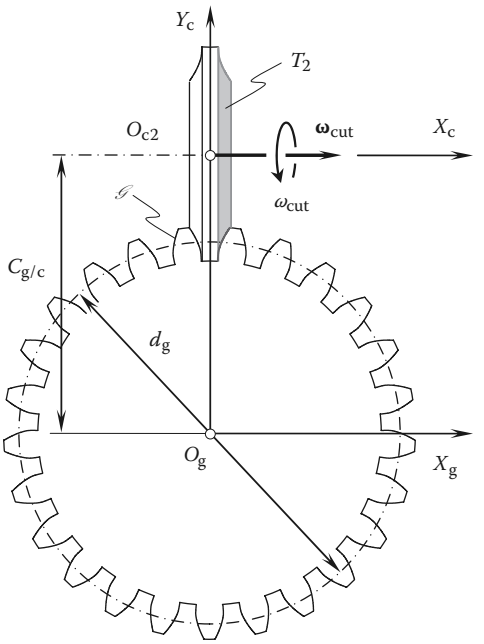

FIGURE 7.3
Reference systems used in the derivation of an equation for the secondary generating surface T_2 of the disk-type gear milling cutter for machining spur gears.

After the position vector $\mathbf{r}^{c}_{inv}(\phi_g)$ is multiplied at left by the operator $\mathbf{Rt}(\theta, X_c)$, the equation

$$\mathbf{r}^{c}_{T}(\phi_g, \theta) = \begin{bmatrix} \dfrac{r_{b.g}}{\cos\phi_g} \cdot \sin(\alpha + \text{inv}\phi_g) \\ \left(C - \dfrac{r_{b.g}}{\cos\phi_g} \cdot \cos(\alpha - \text{inv}\phi_g)\right)\cos\theta \\ -\left(C - \dfrac{r_{b.g}}{\cos\phi_g} \cdot \cos(\alpha - \text{inv}\phi_g)\right)\sin\theta \\ 1 \end{bmatrix} \tag{7.8}$$

can be derived for the secondary generating surface T_2 of the disk-type milling cutter for machining of spur involute gears.

The generating surface T_2 [see Equation (7.8)] is a surface of revolution. It is expressed in terms of two parameters: the profile angle ϕ_g of the involute at a current point of the gear tooth profile and the angle θ of rotation of the involute profile about the axis of rotation of the milling cutter ($-\infty < \theta < +\infty$).

Equation (7.8) is the solution to the problem of profiling of a disk-type milling cutter for machining spur gears.

7.2.2 Equation for the Generating Surface of the Disk-Type Milling Cutter for Machining Helical Involute Gears

When helical gears are machined, the line of contact of the helical gear tooth flank $\mathcal{G}$ and the secondary generating surface of the disk-type milling cutter is not a planar curve, but a spatial curve. This is the major reason for why the implementation of elements of the theory of enveloping surfaces is helpful for solving this particular problem in the design of disk-type milling cutters. Following this approach, two main reference systems are used. The first coordinate system is associated with the helical gear to be machined, and the second one is the coordinate system that the designed milling cutter will be associated with. It should be stressed that, at this point, the milling cutter does not exist yet. Therefore, we are operating with a coordinate system that the milling cutter will be associated with.

When milling a helical gear, the milling cutter is performing two motions: (1) rotation of the milling cutter about its axis of rotation and (2) screw motion of the milling cutter with respect to the work gear. Under the screw relative motion the helical gear tooth flank slides over itself. This relative motion does not affect the shape and parameters of the generating surface of the milling cutter. Therefore, this motion can be eliminated from the list of considerations when deriving an equation for the generating surface T_2 of the disk-type milling cutter. Ultimately, the generating surface of the disk-type milling cutter can be interpreted as the enveloping surface to successive positions of the helical gear tooth flank that is rotating relative to the milling cutter axis of rotation.

Equation for the generating surface of the disk-type milling cutter can be derived in three steps.

First, it is necessary to analytically describe the helical gear tooth surface $\mathcal{G}$ in an appropriate coordinate system. For this purpose, the earlier derived equation for a screw involute surface [see Equation (1.3)]

$$\mathbf{r}_g^* = \mathbf{r}_g^*(U_g, V_g) \tag{7.9}$$

can be used.

Second, it is necessary to derive an equation for the gear tooth flank $\mathscr{G}$ in its current location with respect to the coordinate system associated with the milling cutter.

For this purpose, consider a helical involute gear shown in Figure 7.4. A Cartesian coordinate system $X_g^* Y_g^* Z_g^*$ is associated with the gear. After it has been designed, the milling cutter will be associated with the reference system $X_{c2}Y_{c2}Z_{c2}$. The coordinate system $X_{c2}Y_{c2}Z_{c2}$ is shifted with respect to the coordinate system $X_g^* Y_g^* Z_g^*$ at the center distance $C_{g/c}$, and turned about the Y_g^* axis through the gear pitch helix angle ψ_g.

Translation of the coordinate system $X_g^* Y_g^* Z_g^*$ along the Y_g^* axis at the center distance $C_{g/c}$ can be analytically described by the operator of translation, $\mathbf{Tr}(C, Y_g^*)$. After it has been translated, the coordinate system $X_g^* Y_g^* Z_g^*$ occupies the position of the intermediate coordinate system $X_1Y_1Z_1$.

Rotation of the coordinate system $X_1Y_1Z_1$ about the Y_1 axis through the pitch helix angle ψ_g can be analytically described by the operator of rotation $\mathbf{Rt}(\psi_g, X_1)$. After it has been rotated, the coordinate system $X_1Y_1Z_1$ occupies the position of the milling cutter coordinate system $X_{c2}Y_{c2}Z_{c2}$.

Resultant coordinate system transformation from the work gear coordinate system $X_g^* Y_g^* Z_g^*$ to the milling cutter coordinate system $X_{c2}Y_{c2}Z_{c2}$ is performed by the operator $\mathbf{Rs}(g^* \mapsto c)$ of the resultant coordinate system transformation. In the case under consideration, the operator $\mathbf{Rs}(g^* \mapsto c)$ is computed from the formula

$$\mathbf{Rs}(g^* \mapsto c) = \mathbf{Rt}(\psi_g, Y_1) \cdot \mathbf{Tr}(C_{g/c}, Y_g^*) \tag{7.10}$$

To derive an equation for the gear tooth flank $\mathscr{G}$ in its current location with respect to the coordinate system $X_{c2}Y_{c2}Z_{c2}$, it is convenient to introduce one more reference system. As shown in Figure 7.4, the Cartesian coordinate system $X_2Y_2Z_2$ is turned about the X_{c2} axis through a certain angle θ. The angle θ allows for interpretation in the form $\theta = \omega_{cut}t$, where ω_{cut} is the rotation of the milling cutter about its axis of rotation O_{c2} and t denotes time.

Rotation of the coordinate system $X_{c2}Y_{c2}Z_{c2}$ about the X_{c2} axis through angle θ can be analytically described by the operator of rotation $\mathbf{Rt}(\theta, X_c)$. After it has been rotated, the coordinate system $X_{c2}Y_{c2}Z_{c2}$ occupies the position of the milling cutter coordinate system $X_2Y_2Z_2$.

When designing a disk-type gear milling cutter, only the relative motion of the coordinate systems is important. It makes no difference if the coordinate system $X_{c2}Y_{c2}Z_{c2}$ of the milling cutter is rotating about its axis $O_{c2} \equiv X_{c2}$ or if the gear tooth flank $\mathscr{G}$ is rotating about that same axis of rotation.

At a certain instant in time, the gear tooth flank $\mathscr{G}$ in its current location with respect to the coordinate system $X_{c2}Y_{c2}Z_{c2}$ can be analytically described by

$$\mathbf{r}_g^c(U_g, V_g, \theta) = \mathbf{Rt}(\theta, X_c) \cdot \mathbf{Rs}(g^* \mapsto c) \cdot \mathbf{r}_g^*(U_g, V_g) \tag{7.11}$$

Equation (7.11) represents the solution to the second step of deriving the equation for the generating surface T_2 of the disk-type gear milling cutter.

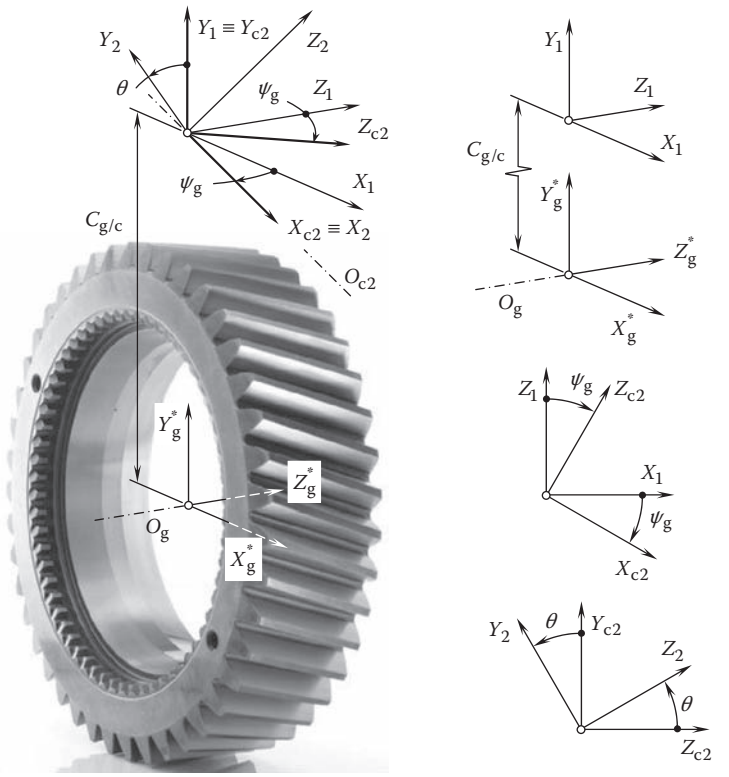

FIGURE 7.4
Reference systems for the derivation of an equation for the secondary generating surface T_2 of the disk-type gear milling cutter for machining helical gears.

Third, the kinematic method [186] of determining the enveloping surface can be applied in the derivation of an equation for the secondary generating surface T_2 of the disk-type milling cutter.

The unit normal vector $\mathbf{n}_g^c$ to the gear tooth flank $\mathcal{G}$ in its current position with respect to the coordinate system $X_{c2}Y_{c2}Z_{c2}$ can be computed as

$$\mathbf{n}_g^c(U_g, V_g, \theta) = \mathbf{u}_g^c \times \mathbf{v}_g^c \tag{7.12}$$

Equation (7.11) yields computation of the unit tangent vectors $\mathbf{u}_g^c$ and $\mathbf{v}_g^c$.

To compute for vector $\mathbf{V}_\Sigma$ of the resultant motion of a point of the tooth flank $\mathcal{G}$, Equation (7.11) is used. Therefore,

$$\mathbf{V}_\Sigma(U_g, V_g, \theta) = \frac{\partial \mathbf{r}_g^c(U_g, V_g, \theta)}{\partial \theta} \tag{7.13}$$

Solution to the set of two equations

$$\mathbf{r}_g^c = \mathbf{r}_g^c(U_g, V_g, \theta) \tag{7.14}$$

$$\mathbf{n}_g^c(U_g, V_g, \theta) \cdot \mathbf{V}_\Sigma(U_g, V_g, \theta) = 0 \tag{7.15}$$

returns an equation of the generating surface T_2 of the disk-type gear milling cutter for machining helical involute gears. After all the necessary formula transformations are performed, the equation for surface T_2 can be presented as

$$\mathbf{r}_T = \mathbf{r}_T(U_T, V_T) \tag{7.16}$$

When the pitch helix angle of a helical gear is equal to zero ($\psi_g = 0°$), the helical gear transforms into a spur gear. Under such a scenario, Equation (7.16) for the generating surface T_2 of the disk-type milling cutter for machining of helical gears reduces to Equation (7.8) for the generating surface T_2 of the disk-type milling cutter for machining of spur gears.

Very similar to what has just been discussed, corresponding equations for generating surfaces of disk-type milling cutters for machining spur and helical gears having noninvolute tooth profiles can also be derived. Various tooth profiles can be machined with disk-type milling cutters, including, but not limited to, ratchets, gears with asymmetrical involute tooth profiles, etc., especially those that cannot be machined with end-type milling cutters of conventional design.

7.2.3 Elements of the Intrinsic Geometry of the Generating Surface of Disk-Type Milling Cutters

The derived equation for the generating surface of the disk-type gear milling cutter [see Equation (7.16)] allows us to compute for the first ($\mathbf{G}_{c2}$) and second ($\mathbf{D}_{c2}$) fundamental matrices of surface T_2. To compute for the fundamental matrices $\mathbf{G}_{c2}$ and $\mathbf{D}_{c2}$, the equations

$$\mathbf{G}_{c2} = \begin{bmatrix} E_{c2} & F_{c2} \\ F_{c2} & G_{c2} \end{bmatrix} \tag{7.17}$$

$$\mathbf{D}_{c2} = \begin{bmatrix} L_{c2} & M_{c2} \\ M_{c2} & N_{c2} \end{bmatrix} \tag{7.18}$$

are used.

Formulae (6.27) through (6.29) can be used for the computation of the fundamental magnitudes of the first order (E_{c2}, F_{c2}, and G_{c2}) of the generating surface of the disk-type gear milling cutter. To compute for the fundamental magnitudes of the second order (L_{c2}, M_{c2}, and N_{c2}) of the milling cutter surface T_2, formulae (6.32) through (6.34) are used.

As an example of the implementation of elements of intrinsic geometry, consider the following practical gear machining problem. An involute helical gear to be machined is given, and you are required to determine a particular number of the milling cutter that is appropriate for machining the gear.

Standard milling cutters (see Table 6.1) are designed for machining spur gears. When machining a helical gear with a milling cutter, an appropriate approximation of the helical

gear tooth profile with the axial profile of the milling cutter is required. In other words, the problem under consideration can be formulated as follows: What is the radius of the normal curvature of the milling cutter having a number that is closest to the radius of the normal curvature of the helical gear?

Principal radii of curvature $R_{1.g}$ and $R_{2.g}$ of the tooth flank of the helical gear to be machined are the roots of square equation

$$\begin{vmatrix} L_g - \dfrac{E_g}{R_g} & M_g - \dfrac{F_g}{R_g} \\ M_g - \dfrac{F_g}{R_g} & N_g - \dfrac{G_g}{R_g} \end{vmatrix} = 0 \tag{7.19}$$

This equation casts into

$$R_g = \frac{(E_g N_g - 2F_g M_g + G_g L_g) \pm \sqrt{(E_g N_g - 2F_g M_g + G_g L_g)^2 - 4(E_g G_g - F_g^2)(L_g N_g - M_g^2)}}{2(L_g N_g - M_g^2)} \tag{7.20}$$

Omitting intermediate formulae transformations, the expressions [92, 136, 138, 143, 158]

$$R_{1.g} = \frac{\sqrt{d_g^2 - d_{b.g}^2}\,\cos\psi_{b.g}}{2\sin^2\psi_{b.g}} \tag{7.21}$$

$$R_{2.g} \to \infty \tag{7.22}$$

for the computation of the principal radii of curvature $R_{1.g}$ and $R_{2.g}$ of the helical gear tooth flank $\mathcal{G}$ can be derived. The second principal radius of curvature $R_{2.g}$ of the work gear tooth flank $\mathcal{G}$ is not of importance in solving the problem under consideration.

In Equation (7.21), d_g denotes the pitch diameter of the helical gear, $d_{b.g}$ is the base diameter of the work gear, and $\psi_{b.g}$ is the base helix angle. Parameters $d_{b.g}$ and $\psi_{b.g}$ can be expressed in terms of the design parameters of the helical gear to be machined (see Appendix A).

Furthermore, to compute for the first principal radius of curvature $R_{1.c2}$ of the generating surface T_2 of a standard milling cutter, the following expression can be used

$$R_{1.c2} = \frac{m\,N_{eq}}{2} \cdot \sin\phi \tag{7.23}$$

where m denotes the module of the work gear, ϕ is the helical gear profile angle, and N_{eq} denotes the equivalent tooth number to be determined. In reality, the equivalent tooth number N_{eq} corresponds to a phantom gear, which physically does not exist. Therefore, there should be no confusion when the computed value of N_{eq} is represented with a number with fractions.

Ideally, the error of approximation of the principal radius of curvature $R_{1.g}$ of the helical work gear by the principal radius of curvature $R_{1.c2}$ of the generating surface of the milling cutter is the minimal possible. Under such a scenario, the equality $R_{1.c2} = R_{1.g}$ is valid. This equality, together with Equations (7.21) and (7.23), yields the expression

$$N_{eq} = \frac{\sqrt{d_g^2 - d_{b.g}^2}\ \cos\psi_{b.g}}{m \sin\phi \sin^2 \psi_{b.g}} \tag{7.24}$$

for the computation of the equivalent tooth number N_{eq} for the identification of the required milling cutter.

Next, the computed value of N_{eq} is compared to the data shown in Table 6.1. In this way, the appropriate number of the milling cutter is determined. For example, if the computed number of N_{eq} is 67.375, then for machining of the given helical gear the milling cutter #2 is required.

There are numerous practical examples of the implementation of elements of the intrinsic geometry of the generating surface of disk-type milling cutters.

7.3 Cutting Edges of the Disk-Type Gear Milling Cutter

The cutting edge of a disk-type gear milling cutter is physically formed by the rake surface R_s and the clearance surface C_s. For geometrical and kinematical analysis, the cutting edge CE is interpreted as the line of intersection of surfaces R_s and C_s (Figure 7.5).

Cutting edges of a finishing gear milling cutter are located within the generating surface T_2 of the cutting tool. Therefore, three surfaces—rake surface R_s, clearance surface C_s, and generating surface T_2 of the gear milling cutter, are through the cutting edge CE. For roughing and semiroughing gear milling cutters, reasonable deviations of the cutting edge from the generating surface of the milling cutter T_2 are permissible.

7.3.1 Rake Surface of the Milling Cutter for Machining Involute Gears

The rake surface of finishing gear milling cutters of most practical designs is a plane through the axis of rotation of the cutting tool. Because of this, the rake angle is equal to

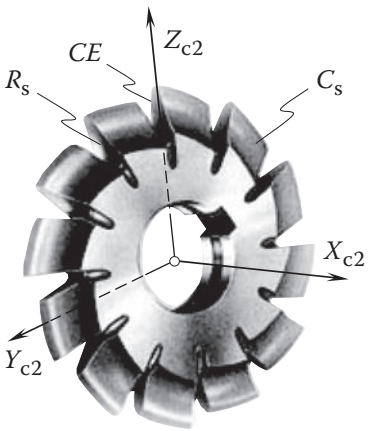

FIGURE 7.5
Rake surface R_s, clearance surface C_s, and cutting edge CE of a disk-type gear milling cutter.

zero ($\gamma_o = 0°$). After regrinding, the accuracy of the worn finishing milling cutters is less vulnerable to diameter alteration of the reground milling cutters if the rake angle $\gamma_o = 0°$.

Equation for the rake surface R_s of the finishing gear milling cutter can be presented in the form $Y_{c2} = 0$. This equation can be converted to matrix representation

$$\mathbf{r}_{rs} = \begin{bmatrix} X_{c2} \\ 0 \\ Z_{c2} \\ 1 \end{bmatrix} \tag{7.25}$$

where the position vector of a point of the rake surface R_s is denoted by $\mathbf{r}_{rs}$.

Disk-type gear milling cutters for roughing and semifinishing of gears are manufactured with a positive rake angle $\gamma_o > 0°$. For semifinishing and finishing of hardened gears, gear milling cutters with a negative rake angle at the top cutting edge ($\gamma_o < 0°$) can be applied.

Equation for the rake plane R_s of gear milling cutters having either a positive or a negative rake angle allows for matrix representation (Figure 7.6)

$$\mathbf{r}_{rs}(X_{c2}, d_{y.c}) = \begin{bmatrix} X_{c2} \\ \dfrac{d_{y.c}}{2} \cdot \cos(\upsilon - \gamma_o) \\ \dfrac{d_{y.c}}{2} \cdot \sin(\upsilon - \gamma_o) \\ 1 \end{bmatrix} \tag{7.26}$$

where angle υ is computed as

$$\upsilon = \sin^{-1}\left(\frac{d_{o.c}}{d_{y.c}} \cdot \sin\gamma_o\right) \tag{7.27}$$

and where $d_{o.c}$ denotes the outer diameter of the milling cutter, $d_{y.c}$ is the diameter through a current point of the surface R_s, and γ_o is the rake angle at the outer diameter of the milling cutter.

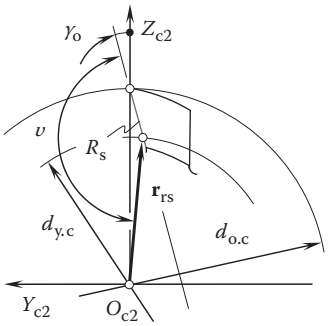

FIGURE 7.6
Rational parameterization of the rake plane R_s of the gear milling cutter having nonzero rake angle γ_o.

Equation (7.16) for the generating surface T_2 and Equation (7.26) for the rake plane R_s can be solved together. The solution to Equations (7.16) and (7.26) analytically describes the planar cutting edge of the milling cutter. Equation for the cutting edge of the disk-type gear milling cutter can be presented in matrix form as

$$\mathbf{r}_{ce}(\vartheta_{ce}) = \begin{bmatrix} X(\vartheta_{ce}) \\ Y(\vartheta_{ce}) \\ Z(\vartheta_{ce}) \\ 1 \end{bmatrix} \tag{7.28}$$

where ϑ_{ce} denotes the parameter of the cutting edge CE of the milling cutter.

When the generating surface T_2 of the milling cutter and the rake surface R_s are expressed in terms of common parameters, one of the parameters can be expressed in terms of another parameter. In this way, the parameter ϑ_{ce} of the cutting edge CE of the milling cutter can be identified.

Possible shapes of the rake surface of the disk-type gear milling cutter are not limited to the plane surface. In particular cases, rake surfaces of special geometry are also used.

7.3.2 Clearance Surface of the Milling Cutter for Machining Involute Gears

The purpose of the clearance surface is twofold. First, shape of the clearance surface provides the required clearance between the cutting wedge and the machined surface. The clearance reduces friction and wear of the milling cutter. Second, the clearance surface is designed so as to allow for no alterations in the shape of the cutting edge after each regrinding of the milling cutter.

In most practical cases, the Archimedean spiral curve is used in the design of the clearance surface of the gear milling cutter. In this case, equation for the clearance surface can be derived in the following manner.

A Cartesian coordinate system $X_{c2}Y_{c2}Z_{c2}$ is associated with the milling cutter as shown in Figure 7.7. This reference system is identical to that used in Figure 7.5. In the coordinate

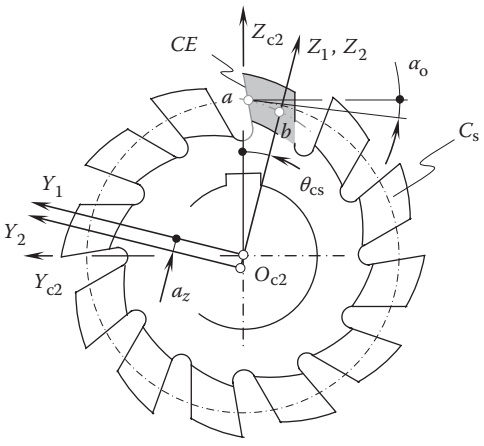

FIGURE 7.7
Cartesian coordinate systems used for the analytical description of the clearance surface C_s of the disk-type gear milling cutter.

system $X_{c2}Y_{c2}Z_{c2}$, the cutting edge CE is analytically described by Equation (7.28). The clearance surface C_s of the milling cutter yields interpretation in the form of successive positions of the cutting edge CE that is performing a certain motion in $X_{c2}Y_{c2}Z_{c2}$. When the Archimedean spiral curve is applied, the motion of the cutting edge is a superposition of two motions. One of the motions is a uniform rotation of the cutting edge about the axis of rotation O_{c2} through a certain angle. In Figure 7.7, current value of the angle is designated as θ_{cs}. The straight motion toward the axis of rotation O_{c2} through a certain distance is the second motion of the cutting edge. Current value of the distance is designated as a_z. Because of Archimedean spiral curve, both motions are uniform, therefore, current value of the angle of rotation θ_{cs} and current value of the displacement a_z correlate with each other linearly, that is, $a_z = k\theta_{cs}$, where k is a coefficient of proportionality.

The coefficient of proportionality k can be expressed in terms of the clearance angle α_o and the design parameters of the gear milling cutter. For a milling cutter with an outer diameter $d_{o.c}$ having N_c teeth, the angle θ_{cs} between every two consequent teeth is

$$\theta_{cs} = \frac{2\pi}{N_c} \tag{7.29}$$

For this specific value of the central angle θ_{cs}, the coefficient of proportionality k is designated as K. To compute for K, the expression

$$K = \frac{\pi d_{o.c}}{N_c} \cdot \tan\alpha_o \tag{7.30}$$

is used.

K is an important design parameter of the gear milling cutter, particularly for manufacturers of gear cutting tools.

Under the resultant motion, an Archimedean spiral curve is the trajectory of every point of the cutting edge CE. In Figure 7.7, the arc segment *ab* represents an example of such a trajectory. The trajectory of every point of the cutting edge CE is equidistant to the arc segment *ab*.

We introduce a coordinate system $X_{ce}Y_{ce}Z_{ce}$ that the cutting edge is rigidly connected to. When generating the clearance surface C_s, the cutting edge CE coordinate system $X_{ce}Y_{ce}Z_{ce}$ is traveling together with the cutting edge itself.

In the initial position, axes of the coordinate system $X_{ce}Y_{ce}Z_{ce}$ align with corresponding axes of the milling cutter coordinate system $X_{c2}Y_{c2}Z_{c2}$. Because of this, the cutting edge coordinate system $X_{ce}Y_{ce}Z_{ce}$ in its initial position is not shown in Figure 7.7. When the cutting edge turns through a certain angle θ_{cs}, the coordinate system $X_{ce}Y_{ce}Z_{ce}$ turns to the position of the coordinate system $X_1Y_1Z_1$. Furthermore, when the cutting edge is translated at a certain distance a_z, the cutting edge coordinate system travels to the position of the coordinate system $X_2Y_2Z_2$. In the last position of the coordinate system $X_2Y_2Z_2$ associated with the cutting edge, the equation for the cutting edge CE remains the same [see Equation (7.28)]. Therefore, in order to derive an equation for the clearance surface C_s, it is necessary to analytically describe the final position of the cutting edge CE in the coordinate system $X_{c2}Y_{c2}Z_{c2}$ associated with the milling cutter.

The operator of translation $\mathbf{Tr}(a_z, Z_2)$ can be used for the analytical description of the transition from the coordinate system $X_2Y_2Z_2$ to the coordinate system $X_1Y_1Z_1$. Furthermore, rotation from the coordinate system $X_2Y_2Z_2$ to the coordinate system $X_{c2}Y_{c2}Z_{c2}$ associated

with the milling cutter can be analytically described by the operator of rotation $\mathbf{Rt}(\theta_{cs}, X_1)$. Ultimately, use of the operators of linear transformations $\mathbf{Tr}(a_z, Z_2)$ and $\mathbf{Rt}(\theta_{cs}, X_1)$ yields an equation for the clearance surface C_s of the disk-type gear milling cutter

$$\mathbf{r}_{cs}(\theta_{cs}, \vartheta_{ce}) = \mathbf{Tr}(a_z, Z_2) \cdot \mathbf{Rt}(\theta_{cs}, X_1) \cdot \mathbf{r}_{ce}(\vartheta_{ce}) \tag{7.31}$$

where the clearance surface C_s is described in terms of two parameters, angle θ_{cs} and parameter ϑ_{ce} of the cutting edge [see Equation (7.28)].

Similarly, corresponding equations of the clearance surface C_s, which is shaped with the help of (a) a logarithmic spiral curve and (b) a circular arc and/or other appropriate curve, can be derived. For this purpose, it is sufficient to just enter an appropriate function $a_z = a_z(\theta_{cs})$ into the operator of translation $\mathbf{Tr}(a_z, Z_2)$. The function $a_z = a_z(\theta_{cs})$ establishes the appropriate correspondence between displacement a_z and angle θ_{cs}. Finally, the operator of translation could be presented in the form $\mathbf{Tr}[a_z(\theta_{cs}), Z_2]$. No other alterations to Equation (7.31) are required to be introduced at this point.

7.4 Profiling of the Disk-Type Gear Milling Cutters

When machining a spur work gear, the axial profile of the secondary generating surface of the milling cutter is identical to the normal cross section of the space width of the gear being machined. Neither face surface nor clearance surface of the gear milling cutter coincides with the normal cross section of the space width of the gear. This causes distortions in the tooth profile within the face surface of the milling cutter and the tooth profile in the normal cross section of the clearance surface. Tooth profile within the face surface of the milling cutter is used for inspection, whereas tooth profile in the normal cross section of the clearance surface of the milling cutter tooth is used for manufacturing of gear cutting tools.

7.4.1 Use of the Descriptive Geometry–Based Method of Profiling

When the spur gear tooth profile is given, the milling cutter tooth profile within the face surface as well as the normal profile of the clearance surface can be determined on the premise of descriptive geometry–based methods of profiling of form cutting tools. In the remainder of this chapter, these methods of profiling of gear cutting tools are referred to as *DG*-based methods. The high efficiency of implementation of *DG*-based methods is practically proven and widely recognized ([92, 136, 138, 143], etc.).

Consider an example of profiling of a disk-type gear milling cutter using a *DG*-based method. In Figure 7.8, the spur work gear is depicted in the system of the projective plane π_2 and π_3. Axis of rotation O_g of the work gear is parallel to the axis of projections π_1/π_2. Tooth space of the work gear is projected onto the frontal plane of projections π_3 with no distortions.

For profiling of the gear milling cutter, the gear tooth profile is subdivided by points *a*, *b*, *c*,..., into a number of reasonably short segments. It is assumed below that the linear approximation of the every short segment of the gear tooth profile in π_2 is allowed. For illustrative purposes, only point *a* of the gear tooth profile is depicted in Figure 7.8. Within

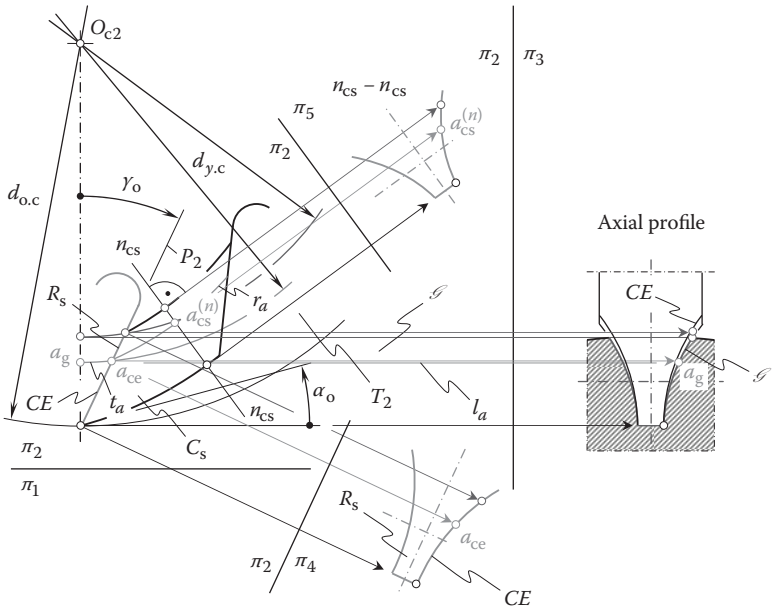

FIGURE 7.8
An example of implementation of the descriptive geometry–based method for profiling of a disk-type gear milling cutter.

the plane of projections π_2, point a of the gear tooth profile is designated as a_g. The rest of the points are treated similarly.

Within the vertical plane of projections π_2, the gear tooth flank $\mathscr{G}$ is depicted by the set of straight lines l_a, l_b, l_c, ... These lines pass through points $a, b, c, \ldots$, and all are parallel to the axis of projections π_1/π_2.

The secondary generating surface T_2 of the milling cutter can be interpreted as an enveloping surface to consecutive positions of the gear tooth flank $\mathscr{G}$ if one assumes that surface $\mathscr{G}$ is rotating about the milling cutter axis O_{c2}. In Figure 7.8, surface T_2 is represented by a set of circular arcs, t_a, t_b, t_c, ...

For profiling of the gear milling cutter, an auxiliary projective plane is constructed. This plane is a projective plane onto the vertical plane of projections π_2. Within the vertical plane of projections π_2, the auxiliary projective plane is depicted as the trace P_2. By construction, the auxiliary projective plane is a plane through the top cutting edge of the milling cutter and inclined at the face angle γ_o. Therefore, the auxiliary plane is congruent to the face surface R_s of the milling cutter. Cutting edge CE of the milling cutter aligns with the line of intersection of the generating surface T_2 of the milling cutter by the auxiliary projective plane. Point a_{ce} is within the cutting edge. With no distortions, the tooth profile of the milling cutter within the rake plane is shown in the plane of projections π_4 (Figure 7.8). The axis of projections π_2/π_4 is parallel to the trace P_2. Projection of the cutting edge CE onto the frontal plane of projections π_3 is also shown.

A relieving curve is a curve r_a through point a_{ce} that makes the desired clearance angle α_o with respect to the generating surface T_2 of the milling cutter. This could be an Archimedean spiral curve, a circular arc, or another curve of appropriate geometry.

The clearance surface C_s of the milling cutter tooth is depicted in Figure 7.8 as the set of relieving curves r_a, r_b, r_c, ...

Ultimately, the clearance surface C_s is intersected by the plane $n_s - n_s$ that is orthogonal to the surface C_s. In this way, the normal cross section of the clearance surface C_s is constructed. In Figure 7.8, point a of the normal cross section of the clearance surface is denoted by $a_{cs}^{(n)}$. This projection of point a is within the plane of projections π_5. The axis of projections π_2/π_5 is parallel to the normal cross section $n_s - n_s$.

The *DG*-based approach of profiling considered above can be expanded to profiling of disk-type milling cutters having angle of inclination at the top cutting edge.

Based on the analysis shown in Figure 7.8, the configuration of an arbitrary point a remains the same in the direction of the tooth width, but alters in the direction of the tooth height.

Graphical methods of profiling lead to a clear understanding of the problem under consideration. They also return a solution to the problem that enables elimination of rough errors in the determination of the milling cutter tooth profile in various cross sections. An accurate solution to the problem of profiling of disk-type gear milling cutters can be derived on the premise of implementation of analytical methods.

7.4.2 Analytical Profiling of Disk-Type Gear Milling Cutters

Numerous approaches can be implemented that aim for an analytical solution to the problem of profiling of disk-type gear milling cutters. A convenient method for solving this particular problem uses elements of linear transformations.

Consider the analytical profiling of the disk-type gear milling cutter for machining a spur gear.

In the coordinate system $X_g Y_g Z_g$, the tooth profile of the spur involute work gear is given by Equation (6.10)

$$\mathbf{r}_{\text{inv}}^{g}(\phi_g) = \begin{bmatrix} \dfrac{r_{b.g}}{\cos\phi_g} \cdot \sin(\alpha + \text{inv}\phi_g) \\ -\dfrac{r_{b.g}}{\cos\phi_g} \cdot \cos(\alpha - \text{inv}\phi_g) \\ 0 \\ 1 \end{bmatrix} \tag{7.32}$$

The axial profile of the milling cutter is congruent with the work gear tooth profile [see Equation (7.32)].

The coordinate system $X_{c2} Y_{c2} Z_{c2}$ is associated with the milling cutter as shown in Figure 7.9. The operator of translation $\mathbf{Tr}(C_{g/c}, Y_g)$ is used for the analytical description of transition from the coordinate system $X_g Y_g Z_g$ to the coordinate system $X_{c2} Y_{c2} Z_{c2}$. Here, the center distance is designated as $C_{g/c}$.

In the reference system $X_{c2} Y_{c2} Z_{c2}$, the axial profile of the generating surface T_2 of the milling cutter is analytically described by

$$\mathbf{r}_{\text{inv}}^{c}(\phi_g) = \mathbf{Tr}(C_{g/c}, Y_g) \cdot \mathbf{r}_{\text{inv}}^{g}(\phi_g) \tag{7.33}$$

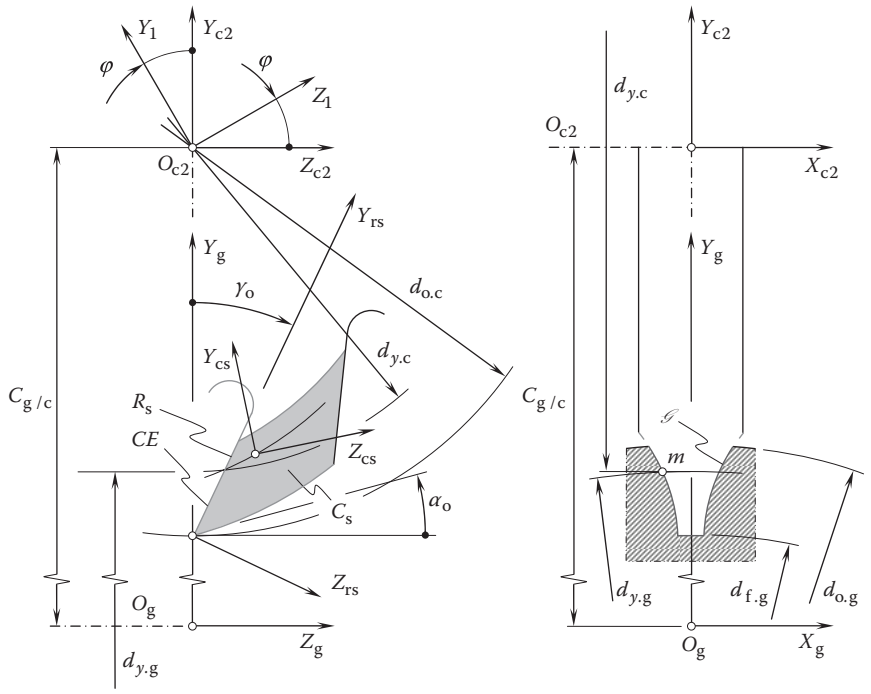

FIGURE 7.9
Analytical profiling of a disk-type gear milling cutter.

To generate the surface T_2, it is necessary to rotate the profile $\mathbf{r}^{c}_{inv}(\phi_g)$ about the axis O_{c2} of the milling cutter. For an analytical description of the rotation, the Cartesian coordinate system $X_1Y_1Z_1$ is introduced. The coordinate system $X_1Y_1Z_1$ shares axis $X_1 \equiv Z_{c2}$ with the coordinate system $X_{c2}Y_{c2}Z_{c2}$. The reference system $X_1Y_1Z_1$ is turned about the X_{c2} axis through a certain angle φ. Transition from the coordinate system $X_1Y_1Z_1$ to the coordinate system $X_{c2}Y_{c2}Z_{c2}$ can be analytically described by the operator of rotation $\mathbf{Rt}(\varphi, X_{c2})$. Position vector $\mathbf{r}_{c2}$ of a point of the generating surface T_2 of the milling cutter can be obtained by multiplying at left the position vector of a point $\mathbf{r}^{c}_{inv}(\phi_g)$ of the axial profile [see Equation (7.33)] by the operator of rotation $\mathbf{Rt}(\varphi, X_{c2})$

$$\mathbf{r}_{c2}(\phi_g, \varphi) = \mathbf{Rt}(\varphi, X_c) \cdot \mathbf{r}^{c}_{inv}(\phi_g) \tag{7.34}$$

Omitting bulky formula transformations, the following equation

$$\mathbf{r}_{c2}(\phi_{y.g}, \varphi) = \begin{bmatrix} \dfrac{r_{b.g}}{\cos\phi_{y.g}} \cdot \sin(\alpha + \mathrm{inv}\phi_{y.g}) \\ \dfrac{d_{o.c} - d_{y.c}(\phi_{y.g})}{2} \cdot \sin\phi_{y.g} \\ \dfrac{d_{o.c} - d_{y.c}(\phi_{y.g})}{2} \cdot \cos\phi_{y.g} \\ 1 \end{bmatrix} \tag{7.35}$$

can be derived for the generating surface T_2 of the gear milling cutter.

Use of Equation (7.35) for the generating surface T_2 corresponds to the grinding operation of a helical gear with the form grinding wheel as shown in Figure 7.10. In this case, the axial profile of the generating surface T_2 [see Equation (7.33)] can be used for dressing of the form grinding wheel.

The formula $C_{g/c} = 0.5 \cdot (d_{y.g} + d_{y.c})$ is used for the computation of the center distance $C_{g/c}$, were $d_{y.g}$ and $d_{y.c}$ are the diameters of the work gear and the gear cutting tool through that same current point m of the gear tooth profile, respectively (Figure 7.9). Diameter $d_{y.g}$ can be expressed in terms of the gear pressure angle $\phi_{y.g}$ at the current point of the tooth profile: $d_{y.g} = d_{y.g}(\phi_{y.g})$. For this purpose, the engineering formulae for the specification of gear tooth flank can be used (see Appendix A). Ultimately, this yields an expression, $d_{y.c} = d_{y.c}(\phi_{y.g})$, for the computation of diameter $d_{y.c}$. The last equation is used for the reparameterization in Equation (7.35).

Furthermore, in computing for the coordinates of points of the milling cutter tooth profile located within the rake plane R_s, an appropriate equation is necessary. The required equation can be derived from the following consideration.

The coordinate system $X_{rs}Y_{rs}Z_{rs}$ is associated with the rake surface R_s as shown in Figure 7.9. Transition from the milling cutter coordinate system $X_{c2}Y_{c2}Z_{c2}$ to the rake surface coordinate system $X_{rs}Y_{rs}Z_{rs}$ can be performed in two steps. First, it is necessary to translate the coordinate system $X_{c2}Y_{c2}Z_{c2}$ along its Y_{c2} axis at the distance $0.5d_{o.c}$ (Figure 7.9) to the position of the coordinate system $X_2Y_2Z_2$. Due to the lack of space, the coordinate system $X_2Y_2Z_2$ is not shown in Figure 7.9. A linear transformation of this type is analytically described by the operator of translation $\mathbf{Tr}(0.5d_{o.c}, Y_{c2})$.

Next, the coordinate system $X_2Y_2Z_2$ is turned about its axis X_2 through the rake angle γ_o to the position of the rake surface coordinate system $X_{rs}Y_{rs}Z_{rs}$. A linear transformation of this type can be analytically described by the operator of rotation $\mathbf{Rt}(\gamma_o, X_2)$.

FIGURE 7.10
Grinding of a helical gear with the form grinding wheel.

In the coordinate system $X_{rs}Y_{rs}Z_{rs}$, the equation for the secondary generating surface T_2 of the gear milling cutter [see Equation (7.35)] casts into

$$\mathbf{r}_c^{(rs)}(\phi_{y.g}, \varphi) = \mathbf{Tr}(0.5\, d_{o.c}, Y_{c2}) \cdot \mathbf{Rt}(\gamma_o, X_2) \cdot \mathbf{r}_c(\phi_{y.g}, \varphi) \tag{7.36}$$

In the coordinate system $X_{rs}Y_{rs}Z_{rs}$, the equation for the rake plane R_s of the milling cutter (Figure 7.9) allows for representation in the form $Z_{rs} = 0$. Substituting this value of Z_{rs} into Equation (7.36), we can derive

$$\mathbf{r}_{ce}^{(rs)}(\phi_{y.g}, \varphi) = \begin{bmatrix} \dfrac{r_{b.g}}{\cos\phi_{y.g}} \cdot \sin(\alpha + \text{inv}\phi_{y.g}) \\ \dfrac{d_{y.c} \sin\varphi}{\sin\gamma_o} \\ 0 \\ 1 \end{bmatrix} \tag{7.37}$$

for the computation of the coordinates of points of the milling cutter tooth profile located within the rake plane R_s, that is, coordinates of points of the cutting edge CE of the milling cutter.

It important to note that the following equality

$$\sin(\gamma_o + \varphi) = \frac{d_{o.c} \sin\gamma_o}{d_{y.c}} \tag{7.38}$$

is valid for the parameters comprising Equation (7.37).

Inverse linear transformation can be used to represent the equation for the cutting edge $\mathbf{r}_{ce}^{(rs)}$ in the coordinate system $X_{c2}Y_{c2}Z_{c2}$ associated with the milling cutter. The operator of the resultant inverse coordinate system transformation $\mathbf{Rs}(\text{rs} \mapsto \text{c})$ is equal to the dot product

$$\mathbf{Rs}(\text{rs} \mapsto \text{c}) = \mathbf{Rt}^{-1}(\gamma_o, X_2) \cdot \mathbf{Tr}^{-1}(0.5\, d_{o.c}, Y_c) \tag{7.39}$$

By multiplying at left the position vector $\mathbf{r}_{ce}^{(rs)}$ by the operator $\mathbf{Rs}(\text{rs} \mapsto \text{c})$

$$\mathbf{r}_{ce}^{(c)} = \mathbf{Rs}(\text{rs} \mapsto \text{c}) \cdot \mathbf{r}_{ce}^{(rs)} \tag{7.40}$$

the equation of the cutting edge $\mathbf{r}_{ce}^{(c)}$ that is represented in the coordinate system $X_{c2}Y_{c2}Z_{c2}$ can be derived.

To compute for the coordinates of points of the axial profile of the clearance surface of the milling cutter, it is necessary to: (1) present the formula [Equation (7.31)] for the surface C_s in an expanded form and (2) express the equation for the surface C_s in terms of parameters that are convenient for this type of analysis. For this purpose, a Cartesian coordinate system $X_{cs}Y_{cs}Z_{cs}$ is introduced. The coordinate system $X_{cs}Y_{cs}Z_{cs}$ is associated with the moving cutting edge CE that serves as the generating curve for the generation of the clearance surface C_s of the milling cutter tooth.

When the clearance surface C_s is generating, the cutting edge CE and the coordinate system $X_{cs}Y_{cs}Z_{cs}$ are performing a motion, which is commonly referred to as *relieving* motion. The relieving motion can be viewed as a superposition of two motions: (1) uniform rotation of the milling cutter about its axis O_{c2} and (2) straight motion toward the axis O_{c2}. Depending on the parameters of the straight motion—say, depending on the type of function $k = k(\theta_{cs})$ (see Section 6.2.2)—clearance surfaces of various geometries can be generated. An Archimedean clearance surface C_s is considered below as an example. For the Archimedean clearance surface, the equality $a_y = k\theta_{cs}$ is valid. When the milling cutter turns through an angle θ_{cs}, the cutting edge CE, together with the coordinate system $X_{cs}Y_{cs}Z_{cs}$, approaches the axis O_{c2} at the distance $a_y = a_y(\theta_{cs})$ (Figure 7.9). For an analytical description of the linear transformation of this type, the operator $\mathbf{Rs}(\mathrm{c} \mapsto \mathrm{cs})$ of the resultant coordinate system transformation is composed. The operator $\mathbf{Rs}(\mathrm{c} \mapsto \mathrm{cs})$ is equal to the product

$$\mathbf{Rs}(\mathrm{c} \mapsto \mathrm{cs}) = \mathbf{Tr}(a_y, Y_{cs}) \cdot \mathbf{Rt}(\theta_{cs}, X_{cs}) \tag{7.41}$$

The operator $\mathbf{Rs}(\mathrm{c} \mapsto \mathrm{cs})$ of the linear transformation is used to obtain an expanded form of the equation for the clearance surface C_s of the milling cutter tooth. By multiplying at left the position vector $\mathbf{r}_{ce}^{(c)}$ of a current point of the cutting edge by the operator $\mathbf{Rs}(\mathrm{c} \mapsto \mathrm{cs})$ of the resultant coordinate system transformation, the equation

$$\mathbf{r}_{cs}^{(cs)} = \mathbf{Rs}(\mathrm{c} \mapsto \mathrm{cs}) \cdot \mathbf{r}_{ce}^{(c)} \tag{7.42}$$

can be derived for the clearance surface C_s that is given in the local reference system $X_{cs}Y_{cs}Z_{cs}$.

Substituting $Z_{cs} = 0$ into Equation (7.42) returns an equation for the axial profile of the milling cutter tooth. The position vector of a point $\mathbf{r}_{ax}^{(cs)}$ of the axial cross section of the clearance surface C_s yields matrix representation in the form

$$\mathbf{r}_{ax}^{(cs)}(\phi_{y.g}, \theta_{cs}) = \begin{bmatrix} \dfrac{r_{b.g}}{\cos\phi_{y.g}} \cdot \sin(\alpha + \mathrm{inv}\phi_{y.g}) \\ d_{o.c} - d_{y.c} - a_y(\theta_{cs}) \\ 0 \\ 1 \end{bmatrix} \tag{7.43}$$

where the condition

$$\sin(\gamma_o + \varphi) = \frac{d_{o.c} \cdot \sin\gamma_o}{d_{y.c}} \tag{7.44}$$

is satisfied.

In a similar manner, the equation for the axial profile $\mathbf{r}_{ax}^{(cs)}$ is derived [see Equation (7.43)], and the equation for the normal cross section of the clearance surface C_s can be derived as well. To derive the equation for the position vector of a point $\mathbf{r}_{nn}^{(cs)}$ of the clearance surface C_s, it is convenient to introduce an auxiliary coordinate system $X_{nn}Y_{nn}Z_{nn}$. The coordinate plane $Z_{nn} = 0$ of the auxiliary coordinate system $X_{nn}Y_{nn}Z_{nn}$ is orthogonal to the surface C_s. The interested reader may wish to work out this partial problem on his/her own.

Results of the analysis can be generalized for the case of disk-type gear milling cutters having certain an inclination angle λ_o at the top cutting edge. Gear milling cutters of such geometry have limited use in industry. Because of this, the generalized case is not discussed in detail here.

An important intermediate conclusion. As follows from Equations (7.37), (7.38), (7.43), and (7.44), parameters of the tooth profile of the disk-type gear milling cutter depend on the outer diameter $d_{o.c}$ of the milling cutter. The outer diameter $d_{o.c}$ becomes smaller after every regrinding of the worn milling cutter. Decrease in outer diameter unavoidably entails a corresponding decrease in accuracy of the milling cutter. Reduction in accuracy is more significant for milling cutters with a larger tooth height (h)/outer diameter ($d_{o.c}$) ratio, where the tooth height is given by $h = (d_{o.c} - d_{f.c})/2$. Therefore, coarse pitch milling cutters having a small outer diameter are more subjected to the impact of regrinding, which affects the accuracy of the cutting edges.

This means that parameters of the tooth profile of the milling cutter have to be changed after every regrinding. Unfortunately, conventional methods of relieving of milling cutters do not allow for alteration of the shape of the milling cutter clearance surface. Ultimately, after every reground the accuracy of milling cutters becomes increasingly lower. To accommodate the deviations in shape of the clearance surface C_s, appropriate improvements in the relieving operation of precision disk-type gear milling cutters are of practical importance. Perfect results can be achieved when a special method of relieving of milling cutters is used. Implementation of this method [84] is efficient for relieving of green milling cutters before heat treatment and, in particular, for finish relieving of hardened milling cutters.

7.5 Cutting Edge Geometry of the Disk-Type Milling Cutter

The cutting edge geometry of the disk-type gear milling cutter can be specified in terms of (a) rake angle γ, (b) angle of inclination λ, (c) clearance angle α, (d) radius of curvature of the cutting edge R_{ce}, (e) roundness of the cutting edge ρ, and other parameters. Under particular conditions of gear machining, some of these parameters have a more severe impact on the milling cutter performance, whereas other geometrical parameters are more important under a different set of conditions.

Analytical methods can be implemented in the investigation of the cutting edge geometry of the disk-type gear milling cutter. Analysis of the geometry of the clearance surface is carried out below as an example.

A disk-type gear milling cutter is depicted in Figure 7.11. The clearance surface of the milling cutter is a type of relieved surface. It is shaped using the Archimedean spiral curve as the relieving curve. The outer diameter $d_{o.c}$ of the milling cutter and the rake angle α_o at the top cutting edge are given. The rake angle γ_o at the top cutting edge of the milling cutter tooth is equal to zero. Parameters of the involute tooth profile to be machined are also known. It is necessary to determine the normal clearance angle $\alpha_{N.y}$ at a certain point m of the cutting edge. The cutting edge point m is located in a circle of a known diameter $d_{y.c}$.

With the aim of expressing the normal clearance angle $\alpha_{N.y}$ at point m of the cutting edge in terms of the design parameters of the milling cutter, a local Cartesian coordinate system $x_m y_m z_m$ is associated with the cutting edge as shown in Figure 7.11. A set of three

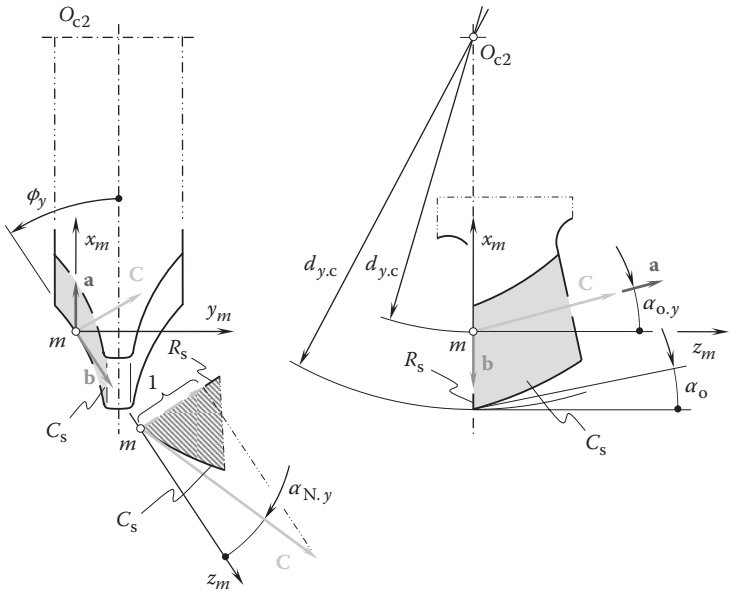

FIGURE 7.11
References system and principal vectors for the determination of the clearance angle of a disk-type milling cutter.

vectors, **a**, **b**, and **C** is constructed within the plane that is tangent at m to the clearance surface C_s.

The unit vector **a** is tangent to the relieving curve through point m. In terms of projections onto the coordinate axes, the unit vector **a** can be expressed as

$$\mathbf{a} = \mathbf{i} \cdot \sin \alpha_{o.y} + \mathbf{k} \cdot \cos \alpha_{o.y} \tag{7.45}$$

where the clearance angle $\alpha_{o.y}$ in the transverse cross section of the clearance surface C_s can be computed from the well-known formula

$$\alpha_{o.y} = \tan^{-1}\left(\frac{d_{o.c}}{d_{y.c}} \cdot \tan \alpha_o \right) \tag{7.46}$$

The unit vector **b** is tangent to the lateral cutting edge at point m. For this vector, the following expression

$$\mathbf{b} = -\mathbf{i} \cdot \cos \phi_y + \mathbf{j} \cdot \sin \phi_y \tag{7.47}$$

is valid. To compute for the profile angle ϕ_y at a current point of the cutting edge of the milling cutter, the following equation can be used

$$\phi_y = \cos^{-1}\left(\frac{d_{\mathrm{b.g}}}{d_{y.\mathrm{g}}}\right) \tag{7.48}$$

where $d_{\mathrm{b.g}}$ denotes the base diameter of the work gear and $d_{y.\mathrm{g}}$ denotes the gear diameter through point m.

Ultimately, magnitude of the vector **C** is chosen so that the length of the projection of **C** onto the coordinate plane $z_m = 0$ is equal to the unit vector. For the computation of vector **C**, the formula

$$\mathbf{C} = \mathbf{i} \cdot \sin\phi_y + \mathbf{j} \cdot \cos\phi_y + \mathbf{k} \cdot \cot\alpha_{\mathrm{N}.y} \tag{7.49}$$

can be used (Figure 7.11).

By construction, vectors **a**, **b**, and **C** are within the plane that is tangent at m to the clearance surface C_{s}. Once these vectors are within the common plane, their triple scalar product is identical to zero ($\mathbf{a} \times \mathbf{b} \cdot \mathbf{C} \equiv 0$). The triple scalar product of vectors **a**, **b**, and **C** can be expressed in the form of the determinant

$$\begin{vmatrix} \sin\alpha_{\mathrm{o}.y} & 0 & \cos\alpha_{\mathrm{o}.y} \\ -\cos\phi_y & \sin\phi_y & 0 \\ \sin\phi_y & \cos\phi_y & \cot\alpha_{\mathrm{N}.y} \end{vmatrix} = 0 \tag{7.50}$$

Equation (7.46), which is used to compute for the clearance angle $\phi_{\mathrm{o}.y}$, and Equation (7.48), used to compute for the pressure angle ϕ_y, can be substituted into Equation (7.50). After the necessary formula transformations are executed, Equation (7.50) casts into

$$\alpha_{\mathrm{N}.y} = \tan^{-1}\left(\frac{d_{\mathrm{o.c}}}{d_{y.\mathrm{c}}} \cdot \sqrt{d_{y.\mathrm{c}}^2 - d_{\mathrm{b.c}}^2}\ \tan\alpha_{\mathrm{o}}\right) \tag{7.51}$$

for the computation of the normal clearance angle $\alpha_{\mathrm{N}.y}$ at current point m of the cutting edge CE of the disk-type gear milling cutter.

An example of a graphical interpretation of Equation (7.51) is illustrated in Figure 7.12. The current value of the clearance angle $\alpha_{\mathrm{N}.y}$ is larger at points closer to the outer diameter $d_{\mathrm{o.c}}$ of the milling cutter, and becomes progressively smaller as the cutting edge point approaches the axis of rotation $O_{\mathrm{c}2}$ of the milling cutter. For portions of the cutting edge that are closer to the axis $O_{\mathrm{c}2}$, values of the normal clearance angle can reach as low as about $\alpha_{\mathrm{N}.y} \leq 2°$. The cutting performance of a gear cutting tool with an unsuitable normal clearance angle $\alpha_{\mathrm{N}.y}$ is very often insufficient from a practical standpoint. This means that appropriate improvements in the design of the gear milling cutter are needed.

Milling cutters for machining of involute gears with fewer teeth are more vulnerable to changes in the normal clearance angle $\alpha_{\mathrm{N}.y}$ within the cutting edge compared to milling cutters used for machining of gears with a larger number of teeth.

Analysis of Equation (7.51) also reveals that a particular type of relieving curve does not affect the actual value of the clearance angle $\alpha_{\mathrm{N}.y}$ at a point of the cutting edge of the milling cutter.

The same analytical method used for the investigation of the geometry of the clearance surface can also be implemented to analyze the geometry of the rake surface of the milling cutter.

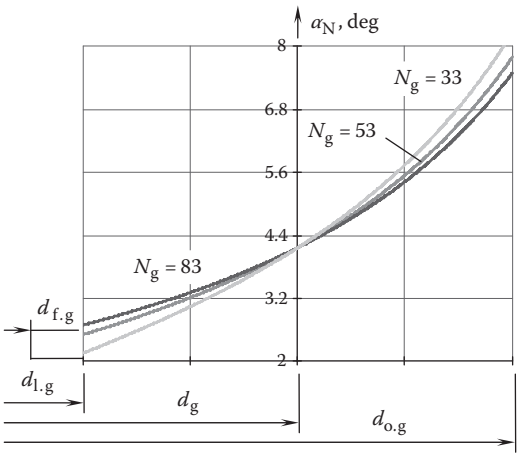

FIGURE 7.12
Alteration of the normal clearance angle $\alpha_{N.y}$ within the lateral cutting edge of the disk-type milling cutter.

Disk-type gear milling cutters are used for roughing and finishing of gears. Finishing gear milling cutters are produced with relieved teeth. The clearance surface of the finishing milling cutters is generated during the relieving operation. The clearance angle at the top cutting edges (at the outer diameter of the milling cutter) is placed in the range of α_o = 12–15°, which means that the normal clearance angle at lateral cutting edges is at the range of $\alpha_{N.y}$ = 1.5–3.0°.

Finishing milling cutters have a zero rake angle γ_o at the top cutting edge (γ_o = 0°). Therefore, both the normal rake angle $\gamma_{N.y}$ and the angle of inclination λ_y have zero values at every point of the lateral cutting edge of the milling cutter tooth ($\gamma_{N.y}$ = 0° and λ_y = 0°).

Roughing disk-type milling cutters are designed to have a rake angle of either zero (γ_o = 0°) or equal to γ_o = +10°. For these rake angle values, changes in the normal rake angle $\gamma_{N.y}$ and the angle of inclination λ_y within the lateral cutting edge are negligibly small and do not affect the cutting performance of the milling cutter.

Milling cutters for semifinishing of hardened gears (work gear tooth surface hardness at the range up to HRC = 60–62) can be designed with a negative rake angle γ_o value. For this purpose, the rake angle is increased up to γ_o = –30 to –40° (Figure 7.13). The rake angle $\gamma_{o.y}$ varies within the lateral cutting edges, and variation in angle $\gamma_{o.y}$ can reach up to $\Delta\gamma_{o.y} \cong 20°$.

Because of the increased rake angle (γ_0 = –30 to –40°), the angle of inclination λ is also approximately in that same range. Similarly, variation in the angle of inclination λ_y within the lateral cutting edges can reach up to $\Delta\lambda_{o.y} \cong 20°$.

Because of the increased negative rake angles γ_o, normal rake angles γ_N at the lateral cutting edges are also negative ($\gamma_N \cong$ –1° to –5°). It is practical to maintain the normal clearance angle at the lateral cutting edges α_N at the range α_N = 8–10°. For this purpose, clearance surfaces—and not rake surfaces—of the worn milling cutters are reground.

Top edges of the milling cutter of this design do not cut the stock. Therefore, the geometry of the top cutting edges is not a focus of interest for cutting tool designers.

The analytical method for the computation of the cutting edge geometry can also be used to analyze the geometry of the lateral cutting edges of milling cutters for semifinishing of hardened gears.

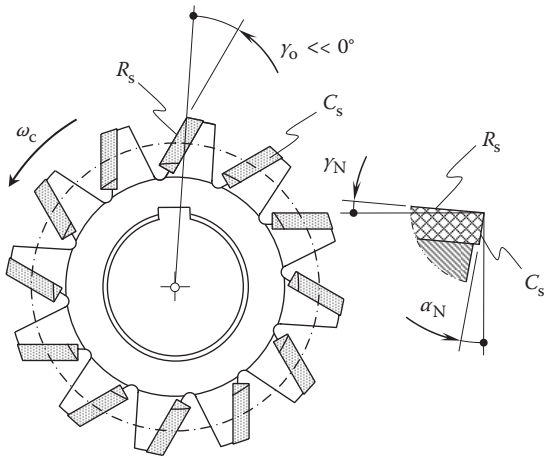

FIGURE 7.13
Milling cutter for finishing and/or semifinishing of hardened gears.

7.6 Disk-Type Milling Cutters for Roughing of Gears

Roughing milling cutters are mostly used for machining of coarse pitch gears, and are also used for machining of medium height gear teeth.

Design of roughing milling cutters is very similar to that of finishing gear milling cutters (Figure 7.14). However, accuracy requirements for roughed gears are not as strict. This allows for improvements in the design of milling cutters used only for roughing of gears.

Rake angle γ_o of roughing milling cutters is either zero ($\gamma_o = 0°$) or can be increased to $\gamma_o = 10°$ (Figure 7.14a). Clearance angle can be increased up to $\alpha_o = 15–18°$. Both the increased rake angle and the increased clearance angle result in an improved cutting performance of milling cutters.

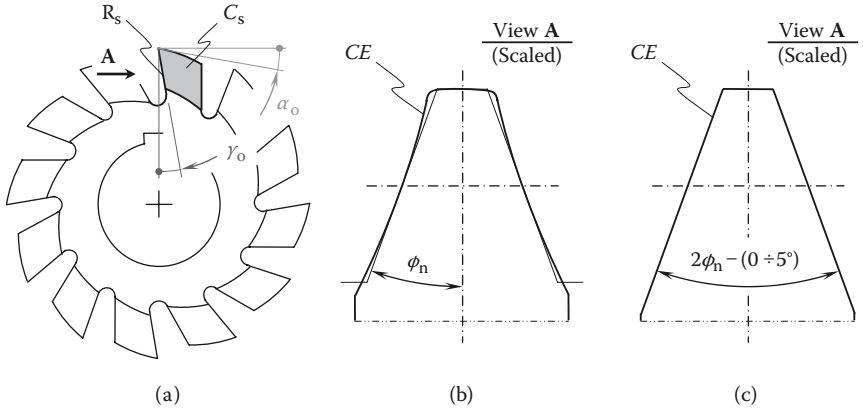

FIGURE 7.14
Design parameters of the disk-type milling cutters for roughing of involute gears.

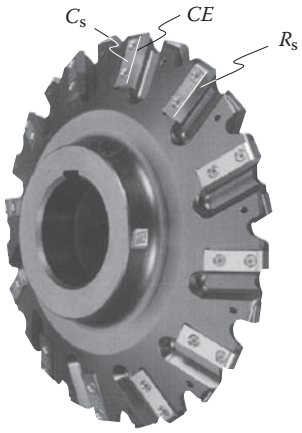

FIGURE 7.15
An assembled disk-type milling cutter for machining of coarse pitch gears.

The tooth profile of the disk-type gear milling cutter depends on the tooth number of the work gear. When the tooth number is larger than the radius of the curvature of the tooth profile of the milling cutter, is getting larger as well. When the tooth number approaches infinity, the gear transforms into a rack having straight tooth profile. This property of the gear milling cutter is used for improvements in the design of roughing milling cutters. For machining of gears having a reasonably small tooth number, milling cutters with an involute tooth profile are used (Figure 7.14b). For milling gears with large tooth number—and consequently an almost straight tooth profile, milling cutters with straight lateral cutting edges are widely used (Figure 7.14c).

When machining a coarse pitch gear, the most intensive material removal is observed during roughing of the gear. For this purpose, it is recommended to use roughing gear milling cutters having a profile angle at the range $2\phi = 35–40°$. Use of milling cutters with a slightly reduced profile angle ($2\phi = 35°$) causes good stock to be removed when finishing the gear.

Roughing gear milling cutters whose clearance surface is used for regrinding have an increased normal clearance angle on the lateral cutting edges (up to $\alpha_N = 8–10°$).

For grinding of worn gear milling cutters (Figure 7.14), conventional and special methods of grinding can be used. Both rake surfaces and clearance surfaces of milling cutters can be reground using the methods discussed elsewhere [81, 173].

For machining of coarse pitch gears, implementation of assembled disk-type gear milling cutters (Figure 7.15) is recommended. Use of carbide inserts is efficient especially for roughing of gears made of materials that are difficult to machine.

One more issue is of critical importance with respect to the design of milling cutters for roughing of gears.

Consider a disk-type roughing gear milling cutter of conventional design. Every cutting tooth of the roughing milling cutter is of trapezoidal form and has thus three cutting edges: top cutting edge and two lateral cutting edges. All three remove the stock simultaneously.

When machining a gear, the milling cutter is rotating about its axis of rotation O_{c2} (Figure 7.16). Rotation of the milling cutter is designated as ω_{cut}. Simultaneously, the milling cutter is traveling along the gear axis of rotation O_g with feed motion F_c. The major portion of the stock is removed by top cutting edges. Chip 1 from the top cutting edge flows in the direction $\mathbf{v}_1$. This direction is orthogonal to the top cutting edge. Other portions of

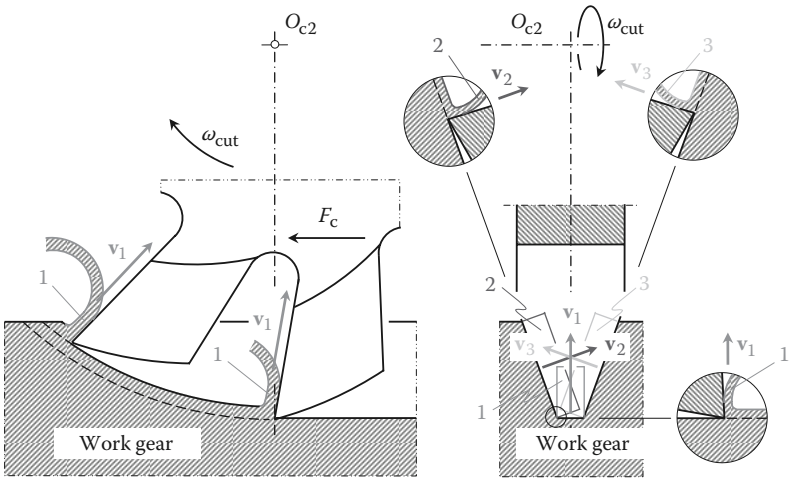

FIGURE 7.16
Interference of the chip flows from the neighboring cutting edges of the milling cutter tooth.

the stock are removed by the lateral cutting edges of the milling cutter. The desired direction of chip flow of chip 2 from the lateral cutting edge is designated as $\mathbf{v}_2$. The direction of $\mathbf{v}_2$ is perpendicular to the lateral cutting edge of the milling cutter. The opposite lateral cutting edge removes chip 3. The desired direction of chip flow of chip 3 from the lateral cutting edge is designated as $\mathbf{v}_3$. The direction of $\mathbf{v}_3$ is perpendicular to the lateral cutting edge of the milling cutter.

Vectors $\mathbf{v}_1$, $\mathbf{v}_2$, and $\mathbf{v}_3$ are within the face surface of the milling cutter. This means that chips 1, 2, and 3 are constrained to flow in the desired directions $\mathbf{v}_1$, $\mathbf{v}_2$, and $\mathbf{v}_3$. The direction $\mathbf{v}_2$ of flow of chip 2 interferes with the direction $\mathbf{v}_1$ of flow of chip 1. The direction $\mathbf{v}_3$ of flow of chip 3 interferes with the direction $\mathbf{v}_1$ of flow of chip 1. Ultimately, chips from lateral cutting edges cannot move in the directions $\mathbf{v}_2$ and $\mathbf{v}_3$. The thickest chip 1 that flows from the top cutting edge significantly affects the directions of the resultant chip flow.

As a result of the chip flow interference, an intensive deformation of the material to be removed is observed in the corners made by the top cutting edge and by the lateral cutting edges.

Interference of chip flows from neighboring cutting edges of the disk-type gear milling cutter results in an elevated cutting temperature, increased cutting forces, and intensive cutting tool wear. The interested reader may refer to Ref. [38] for details in this matter.

To improve the cutting performance of the milling cutter, it is highly desirable to eliminate the interference of chip flows from neighboring cutting edges. Modification of the milling cutter tooth profile is an effective tool for solving problems of this type. Several opportunities in this concern are known.

For example, consider the design of the disk-type gear milling cutter that removes the stock in compliance with the so-called *progressive* cutting diagram.*

Cutter teeth of milling cutters can be divided into two groups: those that are even-numbered or those that are odd-numbered (Figure 7.17a). For this purpose, all teeth are enumerated.

* USSR Pat. No. 167.118, as quoted in [38].

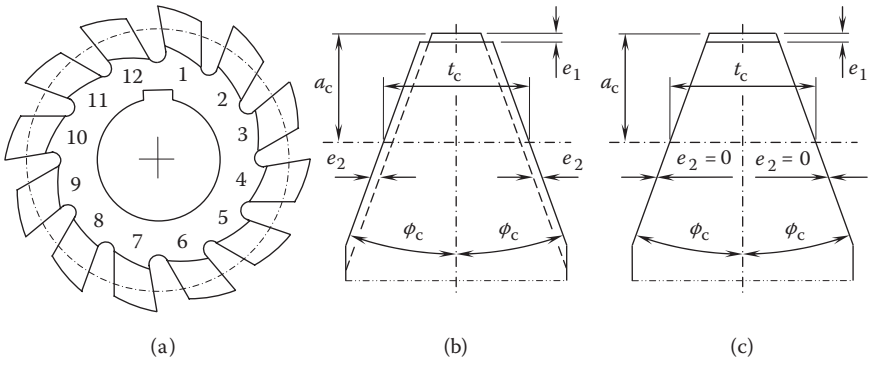

FIGURE 7.17
Cutting diagrams for roughing gear milling cutters.

Milling cutter teeth that are even-numbered form the first group. Milling cutter teeth belonging to this group are of regular tooth thickness t_c. However, they are shorter at a certain value e_1 with respect to milling cutter teeth of regular height (Figure 7.17b). Parameter e_1 is of the smallest feasible value that exceeds the thickness of the chip to be cut by the top cutting edge. Therefore, only the lateral cutting edges of the milling cutter teeth of the first group remove the stock. Top cutting edges do not cut the work gear.

Odd-numbered milling cutter teeth form the second group. Milling cutter teeth belonging to this group are of regular height. However, tooth thickness of these teeth is smaller compared to the space width of the gear to be machined at a certain value $2e_2$ (Figure 7.17b). Parameter e_2 is of the smallest feasible value that exceeds the thickness of the chip to be cut by lateral cutting edges. Therefore, only the top cutting edges of the milling cutter teeth of the second group remove the stock. Lateral cutting edges do not cut the work gear.

Practical values of parameters e_1 and e_2 can be computed using the empirical formulae [38]

$$e_1 = a_1 + 0.1 \text{ mm} \tag{7.52}$$

$$e_2 = a_{2(3)} + 0.05 \text{ mm} \tag{7.53}$$

where a_1 denotes the stock thickness to be removed by the top cutting edge and $a_{2(3)}$ denotes the stock thickness to be removed by lateral cutting edges.

The design of the gear milling cutter eliminates the possibility of chip flow interference and in this way, tool life of the milling cutter can be increased by a factor of 2 or even higher [38].

A simplified version of the design of the gear milling cutter (Figure 7.17c) is also practical. The gear milling cutter of this design removes the stock following the so-called *top-loaded* cutting diagram.* The top-loaded cutting diagram features zero value of parameter e_2.

Only lateral cutting edges of the milling cutter teeth of the first group remove the stock. Top cutting edges do not cut the work gear. Milling cutter teeth belonging to the second group cut the stock using all three cutting edges. However, the top cutting edge cuts the stock of doubled thickness. The chip flow from the top cutting edge dominates over chip

* USSR Pat. No. 181.953 as quoted in [38].

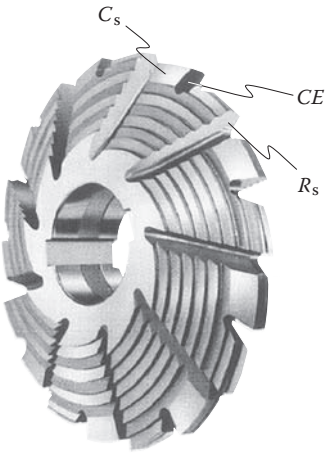

FIGURE 7.18
Stocking milling cutter for roughing of coarse pitch gears.

flows from lateral cutting edges. In this way, the cutting performance of the milling cutter can be increased by a factor of 1.5–1.8 [38].

Standard gear milling cutters can be reground in order to obtain the top-loaded milling cutters shown in Figure 7.17c. For this purpose, a special method of grinding of clearance surfaces of the milling cutter was developed by Radzevich [159].

Numerous cutting diagrams have been developed for various applications. The interested reader may refer to Refs. [39, 144] and other sources for more details on this topic.

For roughing of coarse pitch gears, use of stocking milling cutters having wavy lateral cutting edges (Figure 7.18) is preferred. These are roughing cutters designed for high-speed cutting. They are used singly and in duplex or triplex setups. Several styles of stocking milling cutters are available on the market. Wavy cutting edges subdivide wide chip into numerous narrow chips. This results in an improved cutting performance of stocking milling cutters.

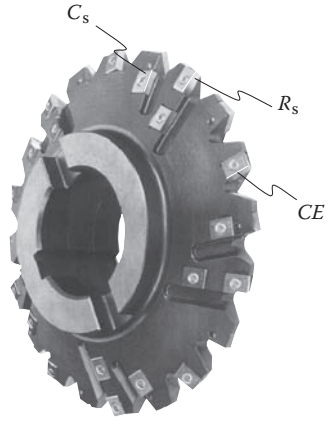

FIGURE 7.19
An assembled milling cutter for roughing.

Similarly, wide chips can be subdivided into multiple narrow chips using the assembled disk-type gear milling cutter having a special disposition of the carbide inserts (Figure 7.19).

Disk-type milling cutters of various designs for roughing of gears are currently available on the market.

7.7 Accuracy of Gear Tooth Flanks Machined with Disk-Type Milling Cutters

Line contact of the work gear tooth flank $\mathscr{G}$ and the secondary generating surface T_2 of the milling cutter is observed when machining the work gear with a disk-type milling cutter. The accuracy of the gear tooth flank $\mathscr{G}$ machined with the disk-type milling cutter is viewed here from the standpoint of satisfaction/violation of the sixth necessary condition of proper part surface generation. This means that deviations of the machined tooth surface of the work gear from the desired geometry of the tooth flank $\mathscr{G}$ are expressed in terms of (a) the design parameters of the disk-type milling cutter and (b) the parameters of the relative motions of the milling cutter and the work gear.

When the milling cutter travels in the axial direction of the work gear from one of its faces toward the opposite face, the line of contact E of surfaces $\mathscr{G}$ and T_2 travels relative to the work together with the milling cutter. The machined tooth surface of the gear is generated as the family of successive positions of the characteristic E.

In reality, not the entire generating surface T_2 is reproduced by the disk-type gear milling cutter. In fact, surface T_2 is represented not continuously, but discretely by a certain number of discrete curves—the cutting edges CE of the milling cutter. As a result, cusps occur on the machined tooth surfaces of the gear.

When machining a spur work gear, the disk-type gear milling cutter (Figure 7.20) is rotating about its axis of rotation O_{c2}. Rotation of the milling cutter is denoted as ω_{cut}. Simultaneously with the rotation ω_{cut}, the milling cutter is fed $\mathbf{F}_c$ in the axial direction of the work gear. After each pass of the milling cutter, the path cut by the milling cutter is the resulting shape of the work gear tooth profile.

The number of teeth of a disk-type gear milling cutter is limited. When machining a gear, residual waviness is generated on tooth surfaces of the machined gear.

For milled spur gears (see Figures 6.13 and 6.14) the maximal cusps height h_w on the machined gear tooth flank can be computed from the formula (6.71)

$$h_w = R_w - \sqrt{R_w^2 - 0.25\, F_c^2} \tag{7.54}$$

where R_w is the radius of the circular arc cusp profile. This parameter of the machined gear tooth surface can be computed using Mensnier's formula [136, 138, 143, 153]. For gears machined with disk-type milling cutters, implementation of Mensnier's formula yields an expression for the computation of radius R_w

$$R_w = \frac{d_{c.m}}{2 \sin \phi_m} \tag{7.55}$$

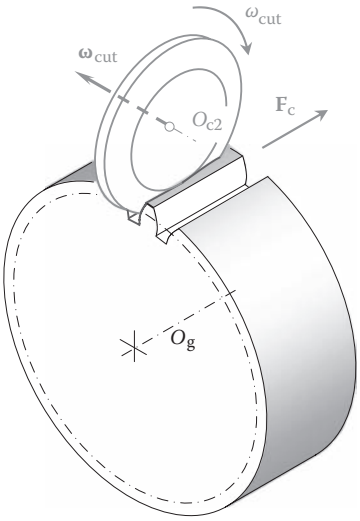

FIGURE 7.20
Schematic of machining of a spur gear with the disk-type milling cutter.

The diameter $d_{c.m}$ of the milling cutter at a current point m within the cutting edge CE is computed using either Equation (6.69) for machining of external involute gears or Equation (6.70) when internal gears are machined.

The derived equations allow for computation of the deviation h_w as well the variation in deviation h_w within the tooth height of the spur involute gear machined with the disk-type milling cutter. An example of the computations is shown in Figure 7.21. Deviation h_w varies within the tooth height. Its value is smaller for smaller diameters of the work gear and becomes larger for points of the work gear tooth profile closer to the outer diameter $d_{o.g}$. Variation in the milling cutter diameter is the major reason for the variation in deviation values h_w within the tooth height of the spur involute gear.

It is of interest to compare the waviness of the work gear tooth flank that is machined with an end-type milling cutter with that machined with the disk-type milling cutter. To make the comparison easier, results of the computations in Figure 7.21 are plotted in coordinates that are identical to that in Figure 6.15. Aside from the results of computations for both cases, which are more qualitative than quantitative, they give a clear understanding of how the deviations h_w are distributed within the machined gear teeth for both cases of gear milling.

When machining a helical gear, the curvedness of the helical gear tooth flank contributes to the resultant deviation h_w of the machined tooth flank from its desired shape.

The expression

$$R_g = \frac{R_{1.g}}{\cos^2 \psi_{b.g}} \tag{7.56}$$

can be used for the computation of the radius of the normal curvature R_g of the gear tooth surface $\mathcal{G}$ in the direction of the feed motion $\mathbf{F}_c$. Equation (7.56) is similar to the earlier derived Equation (6.75).

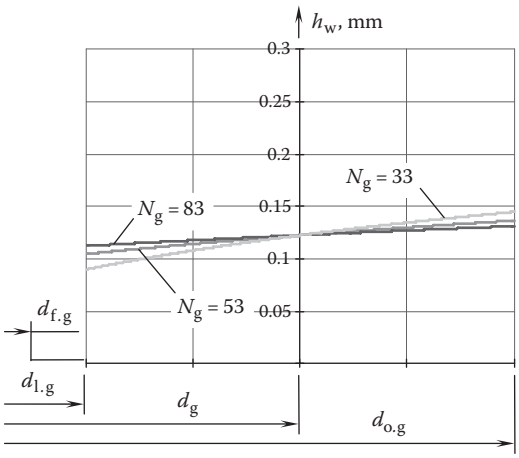

FIGURE 7.21
Deviation of the actual tooth flank from the desired tooth flank within the tooth height of a spur gear machined with the disk-type milling cutter.

To compute for the gear tooth waviness h_w, an approximate formula [see Equation (6.76)]

$$h_w = \frac{R_g(R_g + R_w)\left(1 - \cos\dfrac{F_w}{2R_g}\right)}{R_g - (R_g + R_w)\cos\dfrac{F_w}{2R_g}} \tag{7.57}$$

can be used.

The performed analysis reveals a possibility of computing for the deviation of the machined tooth flank of the work gear from its desired shape.

7.8 Application of Disk-Type Gear Milling Cutters

Most of the present-day uses of gear milling cutters are on coarse pitch applications. A common application in coarse pitch gears is the roughing operation, leaving stock for finish-hobbing or shaving. In practice, however, gear milling cutters are usually confined to producing replacement gears or small-lot gears having special tooth forms. The milling process is practically suitable for making racks, especially large racks.

The cutters have either 14.5° or 20° pressure angles, radial face sharpening, and a "backed-off" unground form.

Gear cutters are not universal for a complete range of teeth. To produce theoretically correct gear teeth, the cutter tooth form must be designed for the specific number of teeth. However, where a small error in tooth form is acceptable, cutters that are designed for a range of teeth can be used. Standard cutters are available for established ranges of teeth.

Thus, all teeth within the range are provided with sufficient tip relief. The same form is produced on all tooth spaces within that range.

Similar to end-type gear milling cutters, two types of sets of disk-type gear milling cutters are available on the market. One of them is of eight gear milling cutters (see Table 6.1). The tooth profile of the milling cutter of each number differs from that of the milling cutter of another number as shown in Figure 7.22. The form on the cutter is made correct for the lowest number of teeth in that particular range.

Another set is of 15 gear milling cutters (see Table 6.2). If close accuracy is desired in form-milled teeth, it is necessary to obtain a cutter with a curvature that is right for the exact number of teeth. This can be done by purchasing a special single-purpose cutter.

Gear teeth may be milled in one cut, or may be given a rough cut almost to size and then finish-milled.

With a single cutter, the cutter tooth form is centered correctly with the gear axis so that a symmetrical tooth space is produced. More than one tooth space can be cut by using a gang of single cutters. Normally, a roughing and a finishing cutter are ganged, with the finishing cutter being centered with respect to the gear. Gang-type milling cutters and multiple-tooth cutters are usually single-purpose cutters used only for cutting the number of teeth for which they are designed. They are made in sets to cut two or three teeth at one pass. Figure 7.23 shows milling cutters ganged together.

Gang-type milling cutters for machining of gears having a relatively small number of teeth, which can be composed of roughing milling cutters either of regular design (Figure 7.24a) or with an oblique tooth profile (Figure 7.24b), can be implemented for this purpose. In the last case, the centerline of the milling cutter tooth profile is at the angle of 10° with respect to the centerline of the milling cutter tooth of conventional design.

In the method of roughing of coarse pitch gears, the concept of the inclined tooth profile is extended to its limit. Figure 7.25 illustrates this method [176]. Two disk-type gear milling cutters are used for the machining of the work gear. The tooth profile of the milling cutters is of profile angle $2\phi_n$. One working surface of the milling cutter is flat. The opposite working surface is conical. A transient working surface is located between the flat portion of the secondary generating surface T_2 of the milling cutter and its conical portion. The

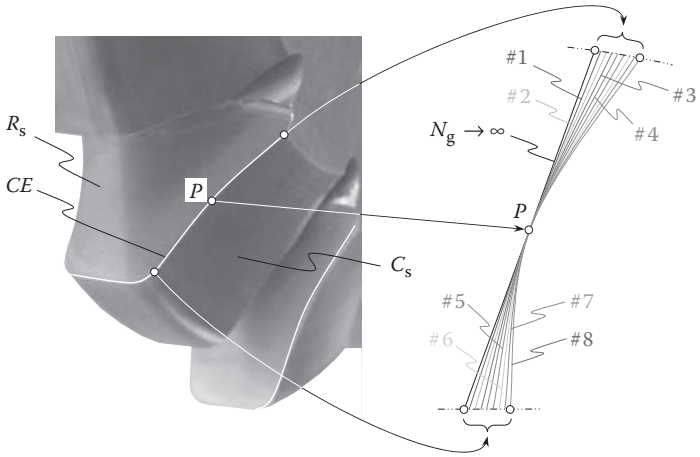

FIGURE 7.22
Tooth profiles of the standard set of eight gear milling cutters.

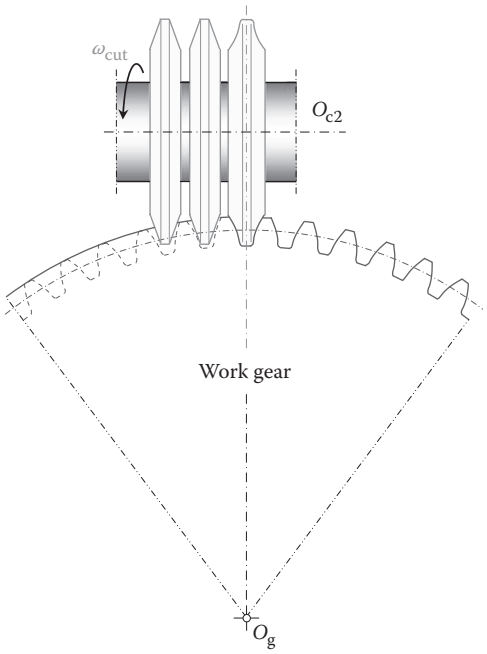

FIGURE 7.23
Gear milling cutters ganged together.

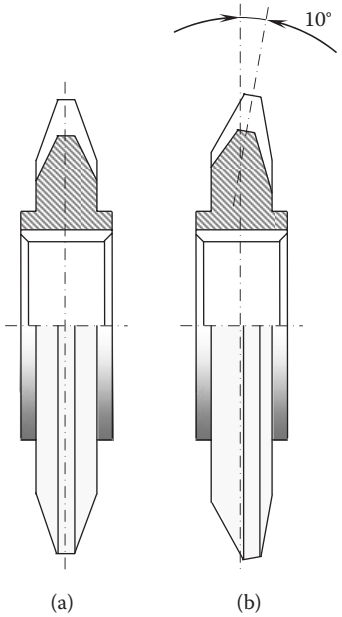

FIGURE 7.24
Roughing disk-type gear milling cutters (a) of ordinary design and (b) with an inclined tooth profile.

milling cutters are installed on a common arbor, allowing the flat working surfaces to face each other. The design and the configuration of the milling cutters create favorable clearance angles within the cutting edges, which improves the cutting performance of the gear cutting tool.

The distance between the milling cutter faces is (W + 2*t*), where *W* denotes the span measurement of the machined gear and *t* denotes the stock for finishing of the gear tooth profile. The geometry of the implemented configuration of the disk-type milling cutters (Figure 7.25) resembles that in the span measurement of an involute gear. To compute for the span measurement *W*, the following formula is derived:

$$W = d_{\text{b.g}} \frac{\tan \phi_{\text{t}}}{\sin \psi_{\text{g}}} \tag{7.58}$$

where

$d_{\text{b.g}}$= base diameter of the work gear
ϕ_{t} = transverse profile angle at the pitch diameter of the work gear
ψ_{g} = pitch helix angle of the work gear

Figure 7.26 illustrates the concept used for deriving Equation (7.58). In Figure 7.26, the normal cross-sectional view of the auxiliary generating rack $\mathscr{R}_T$ is depicted with respect

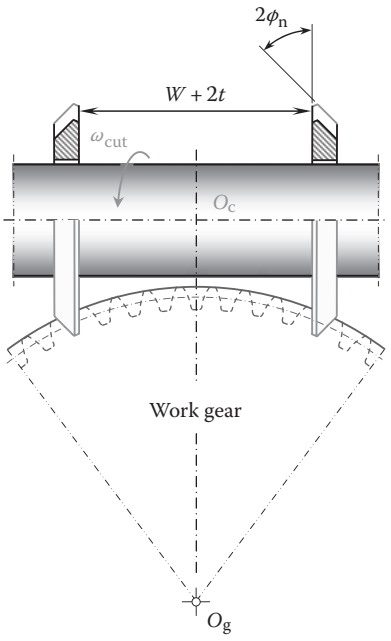

FIGURE 7.25
A method of roughing of a coarse pitch spur gear with two milling cutters having flat portions of the secondary generating surface T_2. (From Radzevich, S.P., Vinkourov, I.V., et al., USSR Patent 1815024, Int. Cl. B 23 f 5/20, 1700, Nov. 11, 1990.)

to the helical gear with an involute tooth profile. An elementary trigonometrical analysis immediately returns Equation (7.58) for the span measurement W.

Indexing after machining a space width can be executed into a certain integer number of the gear teeth N_{ind}.

When possible, it is recommended to synchronize the gear tooth number N_g, number of gear teeth within the span N_{span}, and indexing tooth number N_{ind} in such a way that all gear teeth are machined without changing the N_{ind}.

As shown in Figure 7.25, the milling cutter configuration is not limited to just roughing of coarse pitch gears. Finishing of the gears can also be done under a similar configuration (Figure 7.27).

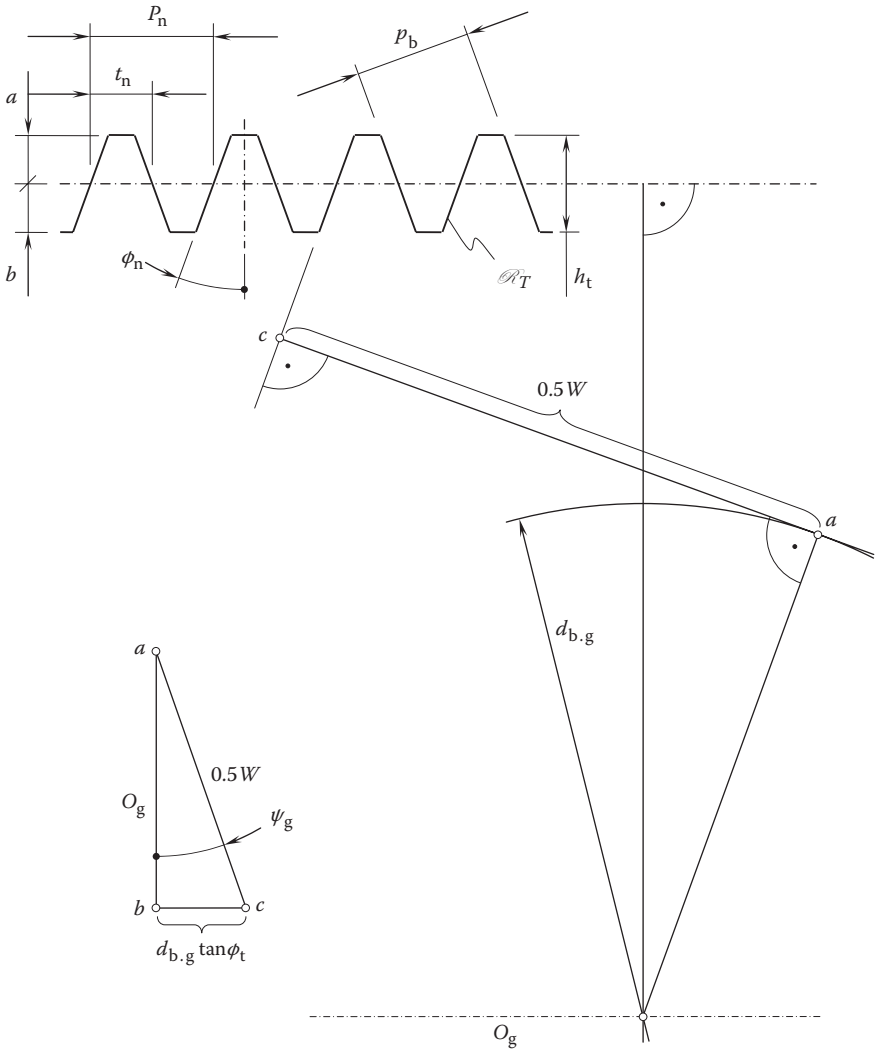

FIGURE 7.26
Computation of the span measurement W.

Profiling of the gear milling cutter (Figure 7.27) is not identical to that of ordinary disk-type gear milling cutters. The gear tooth profile that is machined in the position shown in Figure 7.25 is turned through an angle ϕ_o about the gear axis of rotation. This necessitates the use of the operator of rotation **Rt** (ϕ_o, Z_g) in addition to those used in Equation (6.3) for the position vector $\mathbf{r}^c_{inv}(\phi_g)$ of a current point of the gear tooth involute profile (see Figure 7.3).

The design of disk-type gear milling cutters (Figure 7.27) features favorable clearance angles at every point within the cutting edge. Tool life, accuracy of the machined gear, as well as other parameters of the gear machining operation, correlate with the geometry of the cutting edge of the used gear milling cutter.

For machining of extremely coarse spur gears, two circular saws can be implemented. Following this method (Figure 7.28), two reasonably narrow circular saws are ganged at the distance ($W + 2t$) on the arbor. While traveling along the gear axis O_g, each saw cuts the narrow slot. Lateral surfaces of the slots are tangent to the gear tooth profiles on the pitch diameter. When the tooth number of the gear to be machined is relatively small, the two saws can be used for roughing of the gear. When machining a gear with a large number of teeth of almost straight profiles, the method shown in Figure 7.28 is applicable for finishing of the gear.

An important feature of the method (Figure 7.28) is that not the whole material from the space width is cut in the form of chips. Large size portions of material from the space width remain solid and can be used for other purposes. This makes the method of gear machining more economical.

Multiple-tooth cutters are often used to mill rack teeth (Figure 7.29). Rack tooth gang cutters for the simultaneous machining of several tooth gaps are made up of several single-profile circular-type milling cutters. Through the continual offsetting of the gashes in

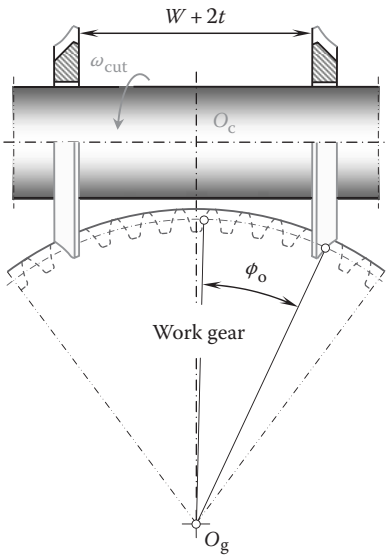

FIGURE 7.27
Finishing of a coarse pitch spur gear with two milling cutters having flat portions of the secondary generating surface T_2.

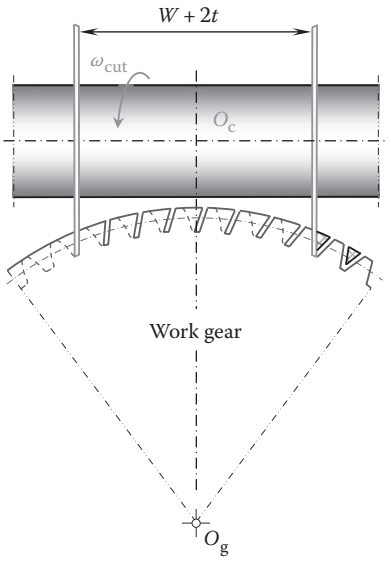

FIGURE 7.28
Implementation of two circular saws for the machining of extremely coarse pitch spur gears.

relation to the drive slot, the individual cutters are successively coming (helically) to the point of cutting addition. This feature particularly promotes quiet running of the milling machine under heavy chip loads.

To allow regrinding combined in a gang, the individual cutters are provided with an additional closely tolerated keyway (grinding slot), so that an axially parallel position of the cutting faces on the arbor is guaranteed.

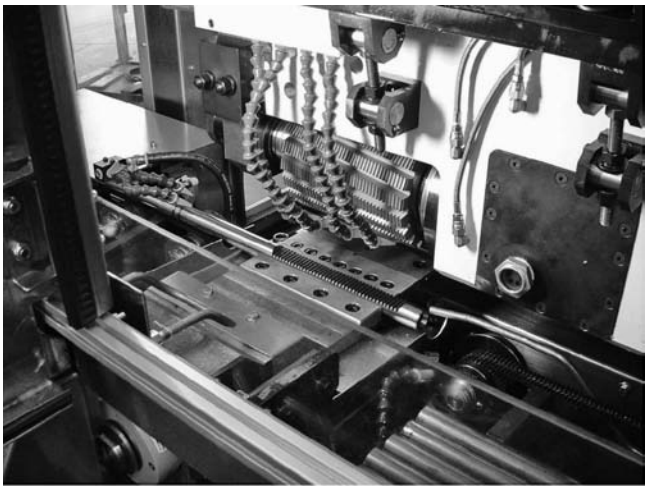

FIGURE 7.29
Milling of a rack with the rack tooth gang cutters. (Courtesy of Mr. J. Vosmik, Drake Manufacturing, Warren, OH.)

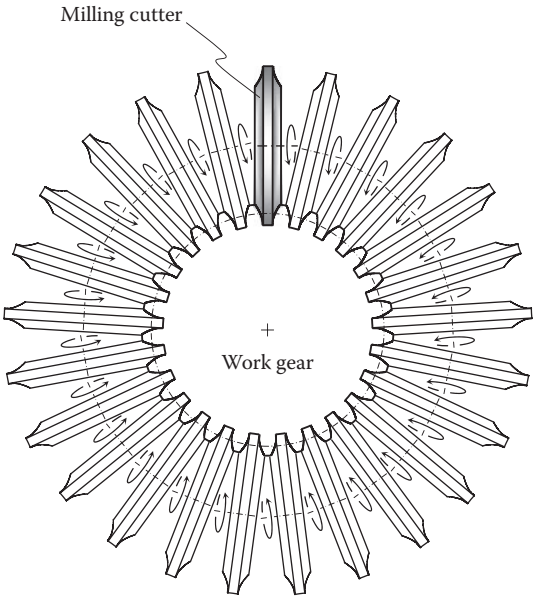

FIGURE 7.30
Machining of an involute gear with multiple disk-type milling cutters.

Rack tooth gang cutters are profile relief ground with parallel flat lapping of the contact faces.

Whether the machine is hand-operated or automatic, the accuracy of tooth spacing depends on the indexing mechanism. Impact of the indexing on the accuracy of the milled gear can be eliminated when the multiple disk-type milling cutters are used (Figure 7.30). When the work gear is passing through the set of disk-type gear milling cutters, all teeth of the gear are cut in a single path.

8

Nontraditional Methods of Gear Machining with Form Cutting Tools

The kinematics of gear machining processes with form cutting tools is simple. Only one motion is required for profiling of gear tooth flanks. This generating motion could be either a straight motion or a rotation. A combination of a translational motion with a rotational motion can also be implemented. In such a case, the translation and the rotation are timed with each other so as to comprise the screw motion. A screw motion, as well as particular types of screw motion (i.e., a translation and a rotation), represent a single parametric relative motion. Only single parametric motions are used for profiling of form tools for machining gears.

Once the kinematics of machining of a work gear with the form cutting tool is limited to just a single parametric relative motion, it becomes possible to carry out a comprehensive search for novel methods of machining of a given gear, as well as novel designs of form gear cutting tools for these purposes.

8.1 Plurality of Single Parametric Motions

Consider a work gear to be stationary. A Cartesian coordinate system $X_gY_gZ_g$ is associated with the work gear as shown in Figure 8.1. If a form gear cutting tool is considered a rigid body, then it can perform a variety of single parametric motions relative to the reference system $X_gY_gZ_g$. Generally speaking, all feasible single parametric relative motions of the form cutting tool relative to the reference system $X_gY_gZ_g$ are either a type of a screw motion or a degenerated kind of screw motion, namely, either a translation or a rotation. Under such a scenario, the secondary generating surface T_2 of the form tool makes line contact with the work gear tooth flank surface $\mathcal{G}$.

A Cartesian coordinate system $X_{c2}Y_{c2}Z_{c2}$ is the cutting tool reference system. After it has been designed, the form gear cutting tool will be represented in this reference system.

In the most general case, location and orientation of the coordinate system $X_{c2}Y_{c2}Z_{c2}$ with respect to the coordinate system $X_gY_gZ_g$ can be specified by the following parameters.

Coordinates of the origin of the coordinate system $X_{c2}Y_{c2}Z_{c2}$ are completely specified by three vectors: $\boldsymbol{a}_{gx}$, $\boldsymbol{a}_{gy}$, and $\boldsymbol{a}_{gz}$. These vectors are along the corresponding coordinate axes X_g, Y_g, and Z_g. Therefore, position vector $\boldsymbol{a}_{c2}$ of the origin of the cutting tool coordinate system $X_{c2}Y_{c2}Z_{c2}$ can be expressed in terms of vectors $\boldsymbol{a}_{gx}$, $\boldsymbol{a}_{gy}$, and $\boldsymbol{a}_{gz}$ of the elementary linear displacements

$$\boldsymbol{a}_{c2} = \boldsymbol{a}_{gx} + \boldsymbol{a}_{gy} + \boldsymbol{a}_{gz} \tag{8.1}$$

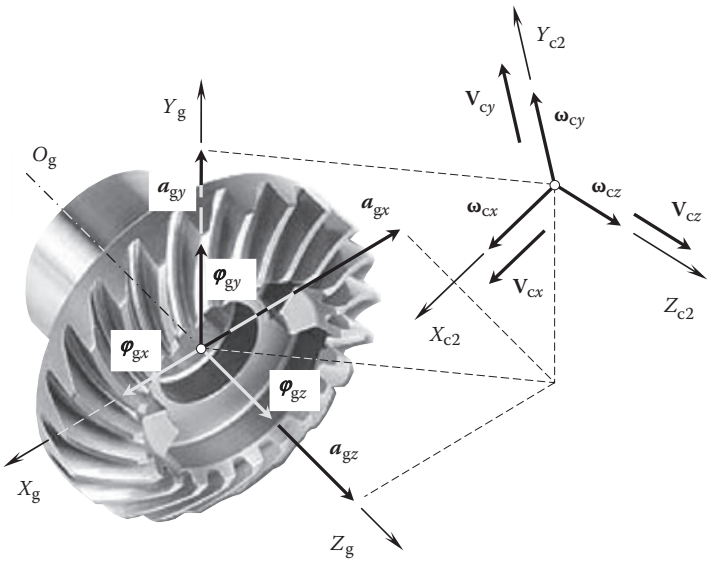

FIGURE 8.1
An arbitrary configuration of the reference system $X_{c2}Y_{c2}Z_{c2}$ associated with the form gear cutting tool with respect to the reference system $X_gY_gZ_g$ associated with the work gear.

In reality, every elementary linear displacement can be performed either along a coordinate axis or along two or even three coordinate axes simultaneously. Therefore, the total number n_a of the feasible displacements is limited to the following seven linear displacements: $\boldsymbol{a}_{gx}$, $\boldsymbol{a}_{gy}$, $\boldsymbol{a}_{gz}$, $(\boldsymbol{a}_{gx} + \boldsymbol{a}_{gy})$, $(\boldsymbol{a}_{gy} + \boldsymbol{a}_{gz})$, $(\boldsymbol{a}_{gx} + \boldsymbol{a}_{gz})$, and $(\boldsymbol{a}_{gx} + \boldsymbol{a}_{gy} + \boldsymbol{a}_{gz})$.

Orientation of the coordinate system $X_{c2}Y_{c2}Z_{c2}$ with respect to the work gear reference system $X_gY_gZ_g$ is completely specified by three rotation vectors, $\boldsymbol{\varphi}_{gx}$, $\boldsymbol{\varphi}_{gy}$, and $\boldsymbol{\varphi}_{gz}$, which are a type of angular displacements. These vectors are about the corresponding coordinate axes X_g, Y_g, and Z_g. Therefore, the resultant orientation vector $\boldsymbol{\varphi}_{c2}$ of the cutting tool coordinate system $X_{c2}Y_{c2}Z_{c2}$ can be expressed in terms of vectors $\boldsymbol{\varphi}_{gx}$, $\boldsymbol{\varphi}_{gy}$, and $\boldsymbol{\varphi}_{gz}$ of the elementary angular displacements

$$\boldsymbol{\varphi}_{c2} = \boldsymbol{\varphi}_{gx} + \boldsymbol{\varphi}_{gy} + \boldsymbol{\varphi}_{gz} \tag{8.2}$$

Each elementary angular displacement can be performed either about a coordinate axis or about two or even three coordinate axes simultaneously. Therefore, total number n_φ of the feasible displacements of this type is limited to just seven angular displacements: $\boldsymbol{\varphi}_{gx}$, $\boldsymbol{\varphi}_{gy}$, $\boldsymbol{\varphi}_{gz}$, $(\boldsymbol{\varphi}_{gx} + \boldsymbol{\varphi}_{gy})$, $(\boldsymbol{\varphi}_{gy} + \boldsymbol{\varphi}_{gz})$, $(\boldsymbol{\varphi}_{gx} + \boldsymbol{\varphi}_{gz})$, and $(\boldsymbol{\varphi}_{gx} + \boldsymbol{\varphi}_{gy} + \boldsymbol{\varphi}_{gz})$.

The total number of possible displacements $n_{a\varphi}$ of the coordinate system $X_{c2}Y_{c2}Z_{c2}$ with respect to the coordinate system $X_gY_gZ_g$ is equal to

$$n_{a\varphi} = (n_a + 1)(n_\varphi + 1) - 1 = 63 \tag{8.3}$$

The cutting tool is allowed to travel along any of the coordinate axes, X_{c2}, Y_{c2}, or Z_{c2}. Velocities of these translational motions are denoted by $\mathbf{V}_{cx}$, $\mathbf{V}_{cy}$, and $\mathbf{V}_{cz}$, respectively. Any two or even all three translations can be performed simultaneously. Without going into

details of the analysis, it is easy to see that in addition to the elementary translations, $\mathbf{V}_{cx}$, $\mathbf{V}_{cy}$, and $\mathbf{V}_{cz}$, three pairs of translations—($\mathbf{V}_{cx}$, $\mathbf{V}_{cy}$), ($\mathbf{V}_{cy}$, $\mathbf{V}_{cz}$) and ($\mathbf{V}_{cz}$, $\mathbf{V}_{cx}$), and one triple translation ($\mathbf{V}_{cx}$, $\mathbf{V}_{cy}$, $\mathbf{V}_{cz}$) are feasible. Therefore, a total of seven combinations of elementary translations are possible. All possible combinations of translations $\mathbf{V}_{cx}$, $\mathbf{V}_{cy}$, and $\mathbf{V}_{cz}$ cause the resultant motion, which is also a kind of translational motion

$$\mathbf{V}_{c\Sigma} = \mathbf{V}_{cx} + \mathbf{V}_{cy} + \mathbf{V}_{cz} \tag{8.4}$$

Ultimately, the total number $n_{\mathbf{v}}$ of possible translations of the cutting tool coordinate system $X_{c2}Y_{c2}Z_{c2}$ relative to the coordinate system $X_gY_gZ_g$ associated with the gear is limited to $n_{\mathbf{v}} = 7$ translational motions.

The cutting tool can rotate about any of the coordinate axes, X_{c2}, Y_{c2}, or Z_{c2}. Angular velocities of these rotations are respectively denoted by $\boldsymbol{\omega}_{cx}$, $\boldsymbol{\omega}_{cy}$, and $\boldsymbol{\omega}_{cz}$. Any two or three rotations can be performed simultaneously. Without going into details of the analysis, it is easy to see that in addition to the elementary rotations, $\boldsymbol{\omega}_{cx}$, $\boldsymbol{\omega}_{cy}$, and $\boldsymbol{\omega}_{cz}$, three pairs of rotations—($\boldsymbol{\omega}_{cx}$, $\boldsymbol{\omega}_{cy}$), ($\boldsymbol{\omega}_{cy}$, $\boldsymbol{\omega}_{cz}$) and ($\boldsymbol{\omega}_{cz}$, $\boldsymbol{\omega}_{cx}$)—and one triple rotation ($\boldsymbol{\omega}_{cx}$, $\boldsymbol{\omega}_{cy}$, $\boldsymbol{\omega}_{cz}$) are feasible. Therefore, seven combinations of elementary rotations in total are possible. All possible combinations of the rotations $\boldsymbol{\omega}_{cx}$, $\boldsymbol{\omega}_{cy}$, $\boldsymbol{\omega}_{cz}$ cause the resultant rotation $\boldsymbol{\omega}_{c\Sigma}$. The rotation $\boldsymbol{\omega}_{c\Sigma}$ can be expressed in terms of elementary rotations as

$$\boldsymbol{\omega}_{c\Sigma} = \boldsymbol{\omega}_{cx} + \boldsymbol{\omega}_{cy} + \boldsymbol{\omega}_{cz} \tag{8.5}$$

Similarly, the total number $n_{\boldsymbol{\omega}}$ of possible rotations of the cutting tool coordinate system $X_{c2}Y_{c2}Z_{c2}$ relative to the coordinate system $X_gY_gZ_g$ associated with the gear is limited to $n_{\boldsymbol{\omega}} = 7$ rotational motions.

Translations $\mathbf{V}_{cx}$, $\mathbf{V}_{cy}$, and $\mathbf{V}_{cz}$ and rotations $\boldsymbol{\omega}_{cx}$, $\boldsymbol{\omega}_{cy}$, and $\boldsymbol{\omega}_{cz}$ represent the components of single parametric motions.

The translations and rotations can be performed simultaneously—that is, they can be combined with one another. The total number of possible motions $n_{\mathbf{v}\boldsymbol{\omega}}$ of the coordinate system $X_{c2}Y_{c2}Z_{c2}$ with respect to the coordinate system $X_gY_gZ_g$ is equal to

$$n_{\mathbf{v}\boldsymbol{\omega}} = (n_{\mathbf{v}} + 1)(n_{\boldsymbol{\omega}} + 1) - 1 = 63 \tag{8.6}$$

Neither the linear nor angular displacements of the cutting tool reference system with respect to the work gear reference system are strictly required. They can be observed or they can be of zero value. It is the relative motion of the coordinate system $X_{c2}Y_{c2}Z_{c2}$ with respect to the coordinate system $X_gY_gZ_g$ that is essential. At least one of the possible relative motions must be observed. This means that the total number n_{cg} of all possible combinations of displacements and relative motions is limited to

$$n_{cg} = (n_{a\varphi} + 1)\, n_{\mathbf{v}\boldsymbol{\omega}} = 4032 \tag{8.7}$$

Design of a cutting tool for machining of a given gear cannot be performed in compliance with all possible combinations [see Equation (8.7)], because many of the combinations are not physically feasible.

In the most general case, the resultant translation $\mathbf{V}_{c\Sigma}$ and resultant rotation $\boldsymbol{\omega}_{c\Sigma}$ can be performed simultaneously. In this event, the motions $\mathbf{V}_{c\Sigma}$ and $\boldsymbol{\omega}_{c\Sigma}$ are timed with one another in a certain manner, and they comprise a screw motion. The actual configuration

of the resultant screw motion can be expressed in terms of the parameters of the elementary translations and elementary rotations.

8.2 Implementation of the Single Parametric Motions for Designing of Form Gear Cutting Tool

Investigation of the single parametric motions (or, similarly, investigation of all possible configurations of the resultant screw motion relative to the work gear) reveals that not all of them are feasible from the standpoint of their implementation for the design of gear cutting tools. However, potential capabilities of some of these motions sound promising.

Consider a few examples where results of the analysis of single parametric motions are used for the design of gear machining methods and gear cutting tools. The examples discussed in the following sections are aimed at illustrating the importance of the kinematical approach in the design of gear cutting tools.

8.2.1 End-Type Gear Milling Cutter

When designing a conventional end-type gear milling cutter (see Figure 6.4), it is assumed from the beginning that the axis of rotation of the milling cutter O_{c2} intersects the work gear axis of rotation O_g at right angle. This means that the milling cutter rotation vector $\boldsymbol{\omega}_c$ aligns with the rotation vector $\boldsymbol{\omega}_{cy}$. Let us assume that, in addition to the rotation $\boldsymbol{\omega}_{cy}$, the gear milling cutter is also rotating with the angular velocity $\boldsymbol{\omega}_{cz}$ (Figure 8.2). Two rotations,

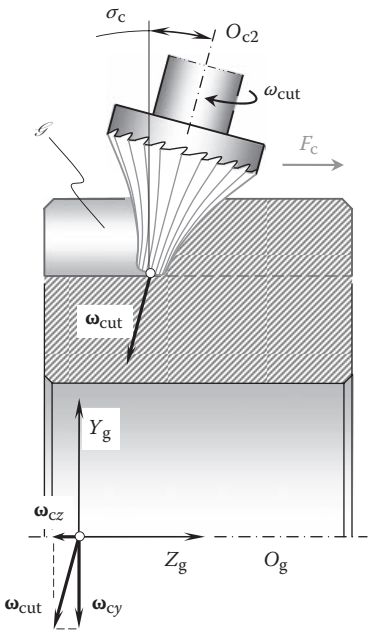

FIGURE 8.2
End-type gear milling cutter with an inclined axis of rotation.

$\boldsymbol{\omega}_{cy}$ and $\boldsymbol{\omega}_{cz}$, which are performed simultaneously, cause the resultant rotation $\boldsymbol{\omega}_{cut}$ about the axis O_{c2} ($\boldsymbol{\omega}_{cut} = \boldsymbol{\omega}_{cy} + \boldsymbol{\omega}_{cz}$). The axis O_{c2} of the resultant rotation $\boldsymbol{\omega}_{cut}$ is inclined within the coordinate plane Y_gZ_g and makes a certain angle σ_c with the Y_g axis (Figure 8.2). In determining the secondary generating surface T_2 of the milling cutter, the principle of inversion of motions can be implemented. In this case, the milling cutter surface T_2 can be generated as the enveloping surface to successive positions of the gear tooth flank $\mathscr{G}$ when it is rotating about the O_{c2} axis.

Once the generating surface T_2 of the gear milling cutter is determined, all the subsequent steps in the process of designing a gear cutting tool are quite similar to those for end-type gear milling cutters of conventional design.

Inclination of the milling cutter axis of rotation O_{c2} at an angle σ_c provides further control over the gear machining operation. In this manner, an area at which cutting speed $\mathbf{V}_{cut}$ is zero ($\mathbf{V}_{cut} = 0$) is eliminated from contact with the work gear.

8.2.2 Disk-Type Gear Milling Cutter

Milling cutters for machining gears can be designed in such a way that the work gear is located inside the form cutting tool. Figure 8.3 illustrates an example of a disk-type gear milling cutter of this kind.

The work gear is stationary when machining takes place. The milling cutter is rotating about its axis O_{c2}. Rotation of the milling cutter is denoted by ω_{cut}. The rotation vector $\boldsymbol{\omega}_{cut}$ is parallel to the X_g axis of the Cartesian coordinate system $X_gY_gZ_g$ associated with the work gear.

The work gear is fed outward of the milling cutter axis of rotation O_{c2}. The feed motion, denoted by F_c, is terminated when full depth of the tooth space is machined. After

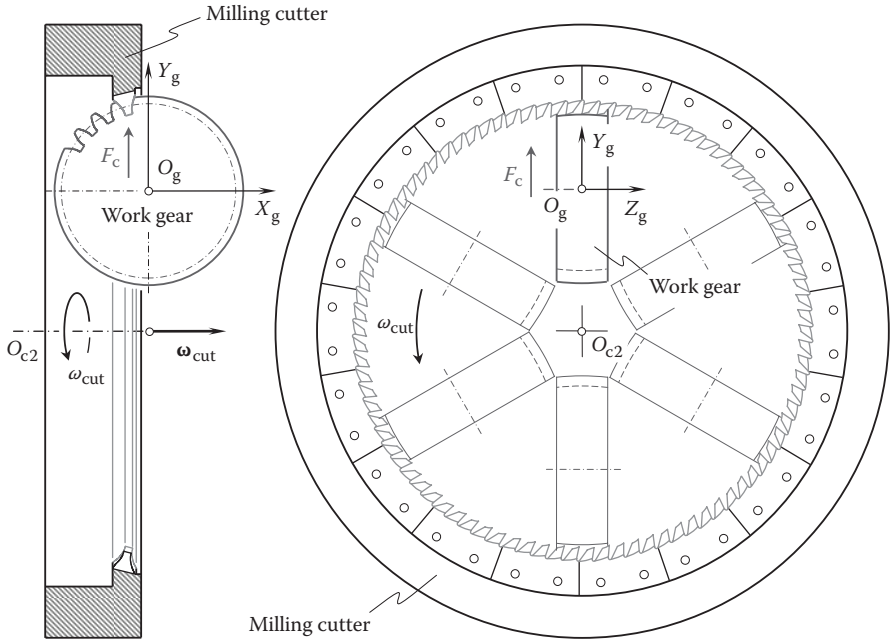

FIGURE 8.3
An enveloping form disk-type gear milling cutter. (The work gear is located inside the cutting tool.)

machining of the tooth space is accomplished, the work gear is moved toward the milling cutter axis of rotation O_{c2} for indexing. This is followed by machining of the next tooth space. Machining of the gear is finished when all tooth spaces are cut.

Because the work gear is located within the interior of the gear milling cutter, crowning of the machined gear teeth is achieved in a natural manner. For proper crowning of the gear teeth, a proper correlation between the gear face width and the inner diameter of the cutting tool is required.

Multiple gears can be simultaneously cut using the enveloping disk-type form milling cutter for which the work gears are located within the interior of the cutting tool. The productivity rate of gear machining in the last case is significantly higher.

Profiling of the milling cutter (Figure 8.3) is very similar to that for conventional disk-type gear milling cutters (see Chapter 7). The equation for generating surface T_2 of the milling cutter is of similar structure. Differences are mostly attributable to two factors: (1) different design parameters of the actual milling cutter and (2) specific location of the work gear relative to the cutting tool.

It is convenient to implement plane face surfaces of the cutting tooth of the milling cutter. The rake planes can be either through the axis of rotation of the milling cutter (in this case, the outer rake angle is zero, $\gamma_o = 0°$) can be offset at a certain distance from the axis O_{c2} (for this case, the outer rake angle is positive, $\gamma_o > 0°$).

Clearance surfaces of the milling cutter teeth are relief ground for accuracy.

8.2.3 Face Gear Milling Cutter

For machining of crowned gears, face gear milling cutters can be used. Gear milling cutters of such design feature cutting teeth located circumferentially within the face (Figure 8.4). When machining a work gear, the workpiece is stationary whereas two face form gear milling cutters are rotating about the common axis of rotation O_{c2}. In Figure 8.4, the rota-

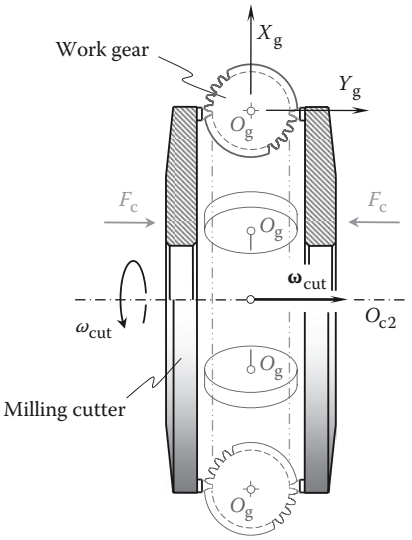

FIGURE 8.4
Face gear milling cutters for machining of crowned gears.

tion of the cutters are denoted by ω_{cut}. The rotation vector $\boldsymbol{\omega}_{cut}$ is parallel to the Y_g axis of the Cartesian coordinate system $X_gY_gZ_g$ associated with the work gear.

The milling cutters are fed along the milling cutter axis O_{c2} toward the gear being machined. The feed motion (F_c) is terminated when full depth of the tooth space is machined. After machining of the tooth space is accomplished, the milling cutters are moved out of the work gear for indexing. This is followed by machining of the next tooth space. Machining of the gear is finished when all tooth spaces are cut.

Because the work gear is located between the form milling cutters, crowning of the gear tooth flanks is achieved in a natural manner. One side of the work gear tooth profile is generated by one of two face form milling cutters. In this way, the tooth flank becomes convex in the longitudinal direction of the gear tooth. In a similar manner, the opposite side of the work gear tooth profile is generated by another face gear milling cutter. It also becomes convex in the longitudinal direction of the gear tooth.

For proper crowning of the gear teeth, a proper correlation between the work gear face width and the diameter of the cutting tool at which the cutting teeth are located is required.

Multiple work gears can be simultaneously cut using face milling cutters. Under such a scenario, the work gears are located between two face milling cutters. The productivity rate of the gear machining process in the last case is significantly higher.

Conventional methods can be used for profiling of the form milling cutter shown in Figure 8.4.

It is convenient to implement plane face surfaces of the cutting tooth of the milling cutter. The rake planes can be either through the axis of rotation of the form milling cutter (in this case, the outer rake angle is zero, $\gamma_o = 0°$) or can intersect the axis O_{c2} (for this case, the outer rake angle is positive, $\gamma_o > 0°$).

Clearance surfaces of the milling cutter teeth are relief ground for accuracy.

8.2.4 Internal Round Broach for Cutting Spur and Helical Gears

For machining gears using the earlier discussed internal disk-type gear milling cutter (see Figure 8.3), a feed motion F_c of the work gear toward the cutting tool is required. The feed motion can be eliminated from the kinematics of the gear machining process. For this purpose, the internal round broach can be used (Figure 8.5).

The work gear remains stationary when broaching is performed. The internal round gear broach is rotating ω_{cut} about its axis of rotation, designated as O_{c2} in Figure 8.5. All cutting teeth of the gear broach are divided into several sections. Roughing teeth of the broach remove most of the material from the tooth space of the work gear. Tooth height of the cutting teeth is incrementally increasing from the first roughing blade to the last cutting blade within the roughing section of the broach teeth. The roughing teeth cut chips of approximately rectangular cross section, thereby making chip curling easy. No chip interference coming from adjacent cutting edges is observed in roughing teeth. These allow for predicting high tool life of the gear broach.

The roughing teeth are followed by the semifinishing teeth, which remove a limited portion of the stock from the space width of the gear blank. The main purpose of the semifinishing teeth is to leave a uniformly distributed portion of stock for the finishing teeth.

Tooth flanks of the work gear are generated by finishing teeth. The accuracy of the finishing teeth directly affects the accuracy of the broached gears.

For automatic loading and for indexing, the internal round gear broach features a clearance between the last finishing cutting tooth and the first roughing cutting tooth.

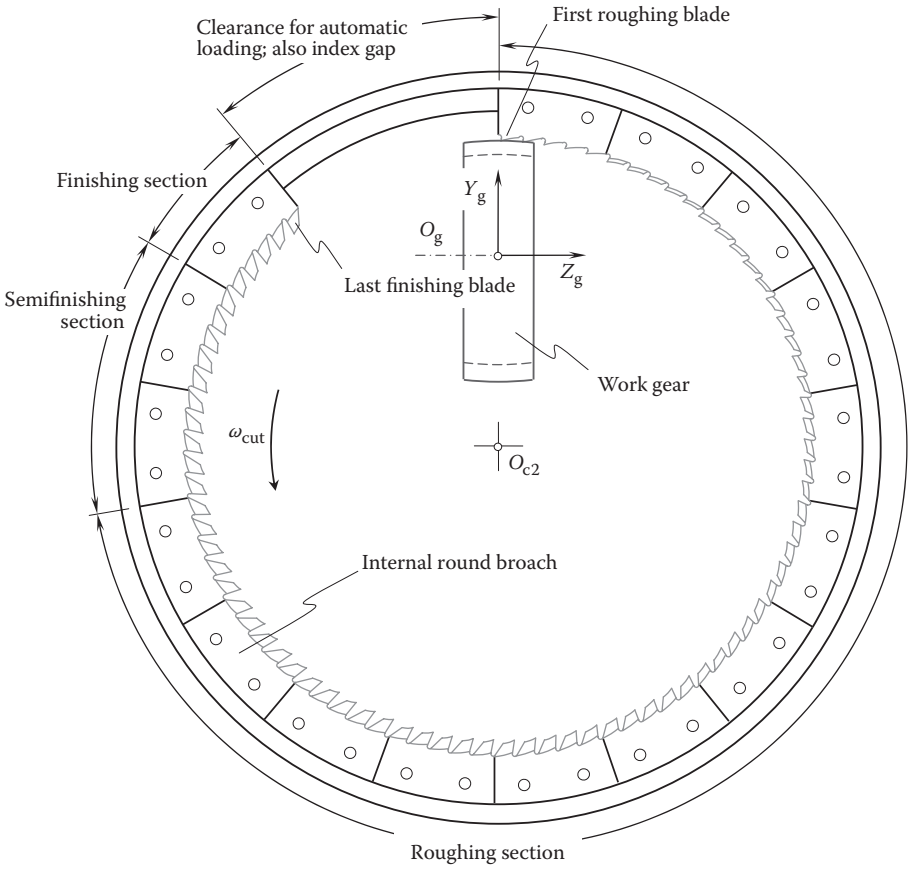

FIGURE 8.5
Internal round broach for cutting spur and helical gears.

Profiling of finishing teeth of the internal round broach is identical to that for the internal round disk-type milling cutter. Cutting edges of the roughing and semifinishing cutting teeth of the internal round gear broach are shifted inward of the generating body of the gear cutting tool.

Plane surfaces are convenient for use as rake surfaces of the internal round gear broach. The rake planes can be either through the axis of rotation of the gear broach (in this case, the outer rake angle is zero, $\gamma_o = 0°$) or can be offset at a certain distance from the axis O_{c2} (for this case, the outer rake angle is positive, $\gamma_o > 0°$).

Clearance surfaces of the round broach teeth are relief ground for accuracy.

8.2.5 Internal Round Broach for Machining Straight Bevel Gears

For cutting straight bevel gears, internal round broaches can be used (Figure 8.6).

When machining bevel gear teeth, the internal round broach is rotating about its axis of rotation. The work gear is turning about an axis O_{fr}. The O_{fr} axis is crossing at right angle with the axis of rotation O_{c2} of the broach. The rotation ω_{cut} of the broach about its axis and the rotation of the cutter with a feed rate ω_{fr} are timed with each other (Figure 8.6). The

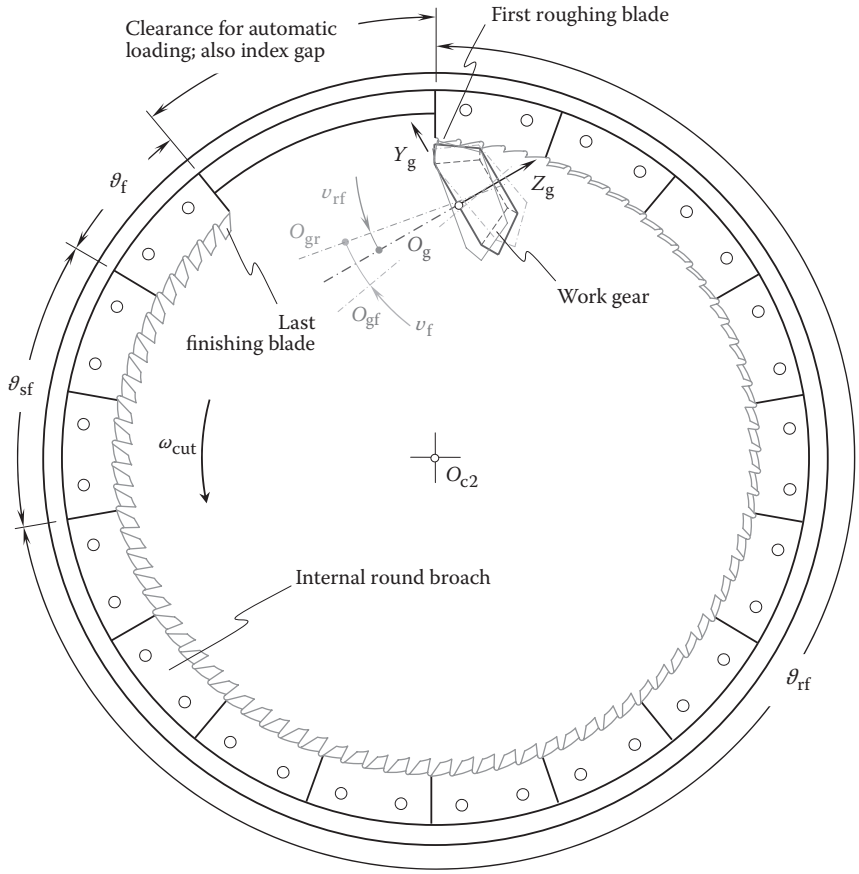

FIGURE 8.6
Internal round broach for machining straight bevel gears.

required values of the feed rate rotation ω_{fr} of the work gear, as well as the required location of the center O_{fr} of the rotation ω_{fr}, can be expressed in terms of the design parameters of the internal round broach and the bevel gear being machined.

Three sections of cutting teeth are recognized in the design of internal round broaches: (1) roughing cutting teeth, which are located within the angle ϑ_{fr}; (2) semifinishing cutting teeth, which are located within the angle ϑ_{sf}; and (3) finishing cutting teeth, which are located within the angle ϑ_f.

Roughing teeth of the broach remove most of the stock from the space width of the work gear. Tooth height of the cutting teeth is incrementally increasing from the first roughing blade to the last cutting blade within the roughing section of the broach teeth. Roughing teeth cut chips of approximately rectangular cross section, which makes chip curling easy. No chip interference coming from adjacent cutting edges is observed in roughing teeth. These allow predicting high tool life of the gear broach.

The roughing teeth are followed by the semifinishing teeth of the broach. The semifinishing teeth remove a limited portion of the stock from the tooth space of the bevel gear blank. The main purpose of the semifinishing teeth is to leave a uniformly distributed portion of stock for the finishing teeth.

The finishing teeth of the round broach generate flank surfaces of the bevel gear teeth. The accuracy of the finishing teeth directly affects the accuracy of the broached gears.

For automatic loading and for indexing, the internal round gear broach features a clearance between the last finishing cutting tooth and the first roughing cutting tooth.

Within the roughing section and the semifinishing section, the rotation ω_{cut} of the cutter and the rotation ω_g of the gear blank are appropriately timed so that when the cutting tool turns through the angle ϑ_{rf}, the gear blank simultaneously turns through the angle (υ_{rf} + υ_{sf}). Here, ϑ_{rf} denotes the angle spanning over the roughing section of the cutting tool, υ_{rf}, and υ_{sf} denotes the angles between the two consequent positions, O_g and O_{gr} and O_{gr} and O_{gf}, of the axis of the work gear. The angles of the work gear rotation υ_{rf} and υ_{sf} correspond to the roughing and semifinishing cycles of the bevel gear machining operation.

Within the finishing section of the cutting teeth, the rotation ω_{cut} and the rotation through the angle υ_f are timed in a manner that is very similar to that just discussed. When the cutting tool turns through the angle ϑ_f, the work gear turns through the angle υ_f. Here, ϑ_f denotes the angle spanning over the finishing section of the cutting tool, and υ_f denotes the angular displacement between the two consequent positions, O_{gr} and O_{gf}, of the axis of rotation of the work gear.

Profiling of the finishing teeth of the internal round broach can be performed on the premise of the known geometry of the straight bevel gear tooth flank, and the kinematics of the gear machining process we have just discussed. Use of elements of the theory of enveloping surfaces can be decisive in this matter. Cutting edges of the roughing and semiroughing cutting teeth of the internal round gear broach are shifted inward of the generating body of the gear cutting tool.

Internal round broach blades are relief ground when manufactured and thus require sharpening on the rake face only. Blade-to-blade spacing, the angle of the plane of the front face, and surface finish of the front face must all be closely controlled during sharpening. In addition, when new segments are assembled in heads, cleanliness of assembly, accuracy of position of segment-locating keys, and close control of segment-holding bolt tension are all necessary for satisfactory cutting results.

8.3 Diversity of Form Tools for Machining a Given Gear

Diversity of form tools for cutting screw involute surface of a worm is used to illustrate a possible diversity of designs of form tools for cutting of a given gear using the various kinematics of the gear machining process.

8.3.1 Machining of an Involute Worm on a Lathe

Methods of machining of a worm on a lathe represent the simplest examples of worm cutting operations. When machining a worm (Figure 8.7), the work is rotating about its axis and the form tool is traveling along the axis of the work. The rotation of the work ω_g and the translation of the form cutting tool F_c are timed with each other so that when the work makes one revolution about its axis O_g, the form tool travels at the distance that is equal to the axial pitch $P_{x.g}$ of the worm times the number of starts of the worm. Actually, the distance is equal to the lead of the screw involute surface to be machined.

Form cutters of several designs can be used for this purpose.

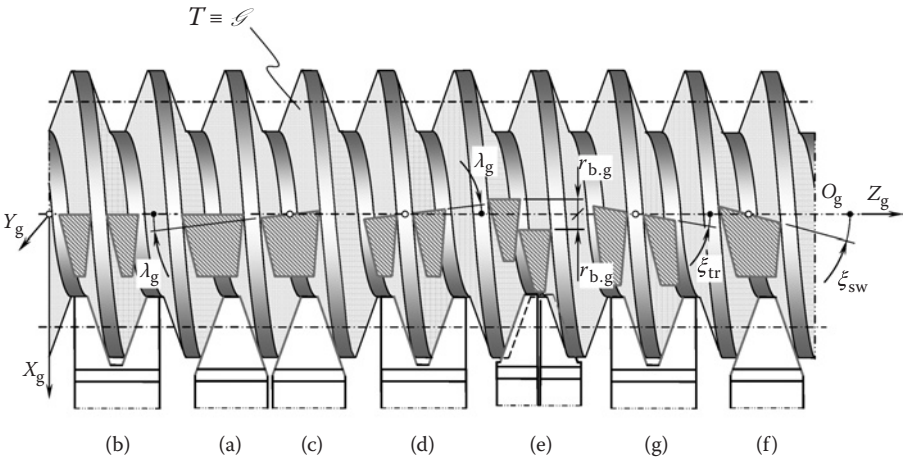

FIGURE 8.7
Form tools for cutting the screw surface of a worm on a lathe.

For turning an Archimedean worm, a form cutter having straight lateral cutting edges is used (Figure 8.7). The rake plane of the form cutter is the plane through the axis of the worm being machined. The trapezoidal profile of the form cutter within the rake plane is identical to the axial profile of the Archimedean worm.

Two designs of the form cutters are used for machining the worm. The first one features the cutter profile that coincides with the profile of the space between two adjacent threads of the worm (Figure 8.7a). The second design features the cutter profile that is congruent to the profile of threads of the worm (Figure 8.7b).

The form tool whose design is shown in Figure 8.7a is simpler in production and in resharpening after being worn. However, when cutting the worm, chip flows from all three cutting edges interfere with one another. This causes intensive wear of the form tool. The form tool featuring the design shown in Figure 8.7b is not as convenient in production and in resharpening compared to the first design. However, only two (and not three) cutting edges cut the stock. Because of this, interference of chip flows does not result in intensive wear of the form tool.

Indexing is executed when multistart worms are machined. In this case, after one thread (or after one space between two adjacent threads) is machined, indexing is performed for machining the next thread (or the next space between two adjacent threads).

Such a schematic layout of machining of worm can also be implemented for turning of involute worms. In this case, the lateral cutting edges of the form tool must not be straight but should be slightly convex. Equation for the lateral cutting edges of the form tool for turning involute worm immediately follows from the equation of the screw involute surface $\mathscr{G}$ [see Equation (1.3)]. After substituting of $Y_g = 0$, Equation (1.3) casts into

$$\mathbf{r}_g(U_g, V_g) = \begin{bmatrix} r_{b.g}\cos V_g + U_g \cos\lambda_{b.g}\sin V_g \\ 0 \\ r_{b.g}\tan\lambda_{b.g} - U_g \sin\lambda_{b.g} \\ 1 \end{bmatrix} \qquad \begin{matrix} V_g^{(l)} \le V_g \le V_g^{(a)} \\ 0 \le U_g \le [U_g] \end{matrix} \tag{8.8}$$

of the lateral cutting edge of the form tool.

Equation (8.8) is valid for both designs of the form tool: (1) when the form tool profile follows the profile of the space between two adjacent threads of the worm (Figure 8.7a) and (2) when the form cutter features the cutter profile that is congruent to the profile of threads of the worm (Figure 8.7b).

Form tools of similar design are used for turning of convolute worms. The rake plane of the form tool makes a certain angle with the axis O_g of the worm. This angle is equal to lead angle λ_g on the pitch cylinder of the worm. Again, two types of form tools are used for machining of convolute worms. The profile of one of these form tools is identical to the normal profile of the space between two adjacent threads of the worm (Figure 8.7c). The profile of the other is identical to the normal profile of the thread of the worm (Figure 8.7d).

The schematic of machining of convolute worms can be adjusted for the turning of involute worms. For this case, form tools with curved lateral cutting edges should be implemented. To derive the equation for the required geometry of lateral cutting edges of both types of form tools, implementation of Equation (1.3) would be helpful.

Two separate form tools having straight lateral cutting edges can be used for machining precision involute worms (Figure 8.7e). For this case, the rake plane of one of the cutters is shifted upward from the axis of rotation of the worm O_g, whereas the rake plane of another cutter is shifted downward from the axis of rotation of the worm. Under such a configuration of the cutters, their straight cutting edges are in tangency with the base helices of the worm threads. Use of cutters with straight profiling cutting edges offers higher accuracy in machining of involute worms.

Investigation of the geometry of involute worms has been carried out by Radzevich [155]. The performed analysis allows for the development of two designs of form tools for machining of involute worms.

A screw involute surface of one side of the thread profile of a worm can be generated by a straight line that is rolling with no sliding over the base helix within the base cylinder. The same is correct with respect to the screw involute surface of the opposite side of the thread profile of the worm. For a particular configuration, two straight generating lines could be located within a common plane. Location of two straight generating lines within a common plane is the concept for designing cutters for machining the screw involute surfaces of a worm. To take advantage of the concept, parameters of this particular configuration of two straight generating lines should be determined.

Cutters of both designs feature straight lateral cutting edges that are located in a common plane. This plane serves as the rake plane of the cutter.

To cut the worm properly, the angle that the rake plane makes with the axis of the worm O_g as well as the profile angle of the cutter should be predetermined.

The angle ξ_{tr} that the rake plane of the cutter makes with the axis of the worm O_g (Figure 8.7g) can be computed from the equation

$$\xi_{tr} = \tan^{-1}\left(\frac{\cos\psi_g \tan\nu_g}{\tan\phi_n + \sin\psi_g \tan\nu_g}\right) \tag{8.9}$$

To compute for the form tool profile angle ϕ_{rf}, the following expression

$$\phi_{rf} = \tan^{-1}\frac{\tan\nu_g}{\sin\xi_{tr}} \tag{8.10}$$

can be used.

The following expression is used to compute for the angle ν_g, which will be entered in Equations (8.9) and (8.10)

$$\nu_g = \tan^{-1} \frac{d_{b.g}}{\sqrt{(d_g + t_{n.g} \cot \phi_n)^2 - d_{b.g}^2}} \tag{8.11}$$

where [for Equations (8.9) through (8.11)]
ψ_g = pitch helix angle of the worm
ϕ_n = normal profile angle of the involute worm
$d_{b.g}$ = base diameter of the involute worm
d_g = pitch diameter of the worm
$t_{n.g}$ = normal thickness of the worm thread

Equations (8.9) and (8.10) are also valid for the computation of the design parameters of the cutter for the second type of machining of involute worms (Figure 8.7f). For this case, the formula

$$\nu_g = \tan^{-1} \frac{d_{b.g}}{\sqrt{(d_g - w_{n.g} \cot \phi_n)^2 - d_{b.g}^2}} \tag{8.12}$$

can be used to compute for angle ν_g. In Equation (8.12), $w_{n.g}$ denotes the normal width of space between two adjacent threads of the worm.

The form tools shown in Figure 8.7f and Figure 8.7g are capable of precise machining of involute worms. Both of them are easy in terms of production and resharpening.

The interested reader is referred to refs. [130, 155] for details on how Equations (8.9) through (8.12) were derived.

The cited examples illustrate some of the capabilities of the kinematical approach to designing of form cutting tools for machining gears.

8.3.2 Milling of an Involute Worm

High productivity rate can be achieved when an involute worm is machined with a form milling cutter. When machining, the worm is rotating about its axis of rotation O_g. The rotation vector of the worm $\boldsymbol{\omega}_g$ is along the O_g axis (Figure 8.8). The milling cutter is rotating about its axis of rotation O_{c2}. The rotation vector of the milling cutter $\boldsymbol{\omega}_{cut}$ aligns with the O_{c2} axis. In addition to the rotation $\boldsymbol{\omega}_{cut}$, the cutting tool is traveling along the worm axis of rotation. This motion represents the feed and is denoted by F_c. The rotation of the worm ω_g and the feed motion F_c are timed with each other. Timing of the motions $\boldsymbol{\omega}_g$ and F_c is performed in such a way that the milling cutter travels at the distance of axial pitch times the worm number of start per one revolution of the worm.

Various configurations of the rotation vectors $\boldsymbol{\omega}_g$ and $\boldsymbol{\omega}_{cut}$ are permissible when machining a worm with a milling cutter.

Machining of involute worm with an end-type milling cutter (Figure 8.8a) is a conventional means of machining a worm of coarse pitch. Axis of rotation O_{c2} of the milling cutter intersects at right angle with the axis of rotation O_g of the worm. In a particular case, the axes O_{c2} and O_g can be at a certain angle as shown in Figure 8.2. End-type milling cutter can be designed for machining of the worm when the axes O_{c2} and O_g cross each other

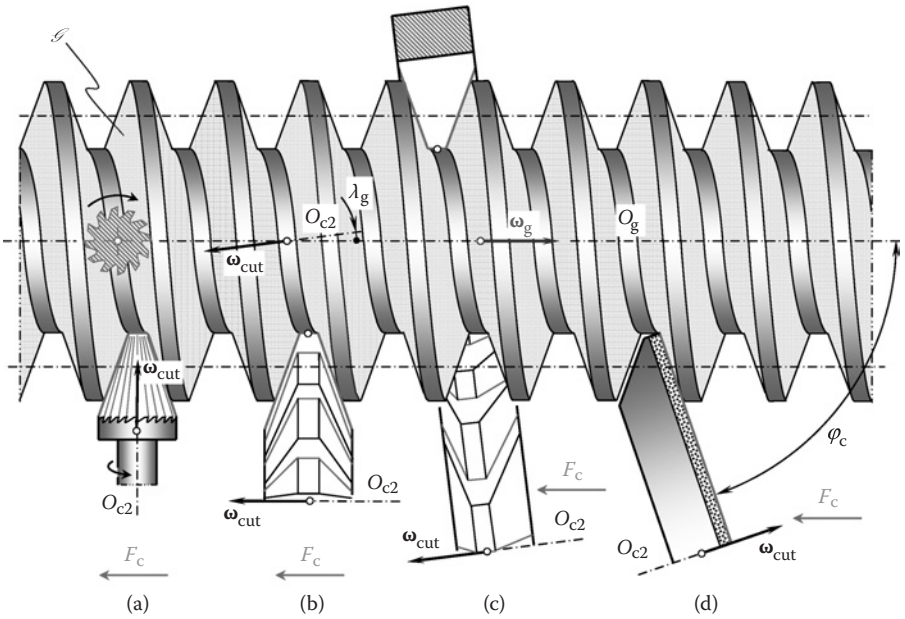

FIGURE 8.8
Form milling cutters for machining an involute worm.

either at a right angle or at a certain acute angle. No physical restrictions are imposed on such a configuration of the axes of rotation of the worm and the cutting tool.

Profiling of the end-type milling cutter for machining a worm is similar to that for machining of involute gear (see Chapter 6).

Disk-type milling cutters can also be implemented for machining of worms (Figure 8.8b). Usually, axis of rotation O_{c2} of the milling cutter crosses the axis of rotation of the worm O_g at an angle that is equal to the worm pitch lead angle λ_g. Profiling of the disk-type milling cutters of this design is similar to that considered in Chapter 7. In reality, in case of necessity a special-purpose milling cutter can be designed for machining of the worm when the axes of rotation O_g and O_{c2} form an angle that differs from the pitch lead angle λ_g of the worm. In particular, the angle that the axis of rotation O_{c2} makes with the axis of rotation O_g can be equal to zero. Under such a scenario, axes O_g and O_{c2} are parallel to each other. In this case, the gang cutter can be used for machining of the worm. This is an important advantage of the considered configuration of the axes of rotation of the worm and the milling cutter.

For milling of an involute worm, the internal round milling cutter can be used (Figure 8.8c). The angle that the rotation vector of the worm $\boldsymbol{\omega}_g$ makes with the rotation vector of the milling cutter $\boldsymbol{\omega}_{cut}$ can be either of a certain value or the rotation vectors $\boldsymbol{\omega}_g$ and $\boldsymbol{\omega}_{cut}$ can be parallel to one another. In a particular case, the angle between the rotation vectors $\boldsymbol{\omega}_g$ and $\boldsymbol{\omega}_{cut}$ can be equal to the lead angle λ_g on the pitch cylinder of the worm.

Profiling of the internal round milling cutter for machining an involute worm can be performed following the procedure of profiling of disk-type milling cutters of conventional design.

Diversity in the design of milling cutters for machining of involute worms is not limited to those considered in this discussion.

One more particular configuration of the rotation vectors $\boldsymbol{\omega}_g$ and $\boldsymbol{\omega}_{cut}$ deserves to be mentioned here. This particular configuration can be implemented for the purpose of designing a milling cutter. However, for practical reasons, it is used for grinding of involute worms.

The configuration of the rotation vectors $\boldsymbol{\omega}_g$ and $\boldsymbol{\omega}_{cut}$ under consideration relates to the case of the tangency of a plane to the screw involute surface. The approach is based on the well-known property of screw involute surfaces, according to which the screw involute surface can be generated as the enveloping surface to successive positions of a plane that is performing a screw motion. This property of screw involute surface is known from many sources (e.g., [130, 155]).

For a particular configuration, the rotation vectors $\boldsymbol{\omega}_g$ and $\boldsymbol{\omega}_{cut}$ form the base lead angle $\lambda_{b.g}$. Therefore, the plane that intersects the worm axis of rotation O_g at the angle $\varphi_g = 90° - \lambda_{b.g}$ is tangent to the surface $\mathcal{G}$ of the worm thread. This plane is used as the secondary generating surface T_2 of the grinding wheel for finishing precision involute worm (Figure 8.8d). To compute for the required angle φ_c, the following expression

$$\varphi_c = \sin^{-1}(\cos\phi_n \cos\psi_g) \tag{8.13}$$

was derived by Radzevich [130]. The angle φ_c can also be computed as

$$\varphi_c = \tan^{-1}\frac{\cos\phi_n}{\sqrt{\sin^2\phi_n + \tan^2\psi_g}} \tag{8.14}$$

which is known from many advanced sources.

In Equations (8.13) and (8.14), ϕ_n denotes the involute worm normal pressure angle and ψ_g is the worm helix angle in the pitch cylinder.

8.3.3 Thread Whirling

A version of the profile milling process used for cutting worms is provided by thread whirling [194]. Whirling shows impressive returns in producing worms for gear worm reducers. Difficult threading operations, such as very long shafts or very wide profiles, can easily be machined by whirling.

The cutter head encircles the work and is driven by a separate motor while the work is rotated at a much slower speed (Figure 8.9). During cutting, the head is swung over to the required helix angle ψ_g and the cutters are ground to suit the space profile necessary to impart the desired thread shape.

Material removal is the result of the whirling ring rotating $\boldsymbol{\omega}_{cut}$ at high speed around a slowly rotating $\boldsymbol{\omega}_g$ workpiece. The rotating workpiece, combined with the advancement of the longitudinal slide, produces the required pitch of the worm. The eccentric amount of the worm centerline to the whirling ring determines the over-pin dimension. The tangential cutting action of the whirling process leaves the tool in contact with the workpiece for a much longer time along the arc of the "cutting circle" of the insert. Subsequently, each pass of the insert removes four to six times the amount of material. In addition, the tangential cutting action also permits much higher cutting speeds, thus shortening cycle times again. The low approach angle of the insert when it first makes contact with the workpiece ensures that the whirling tools achieve a good tool life.

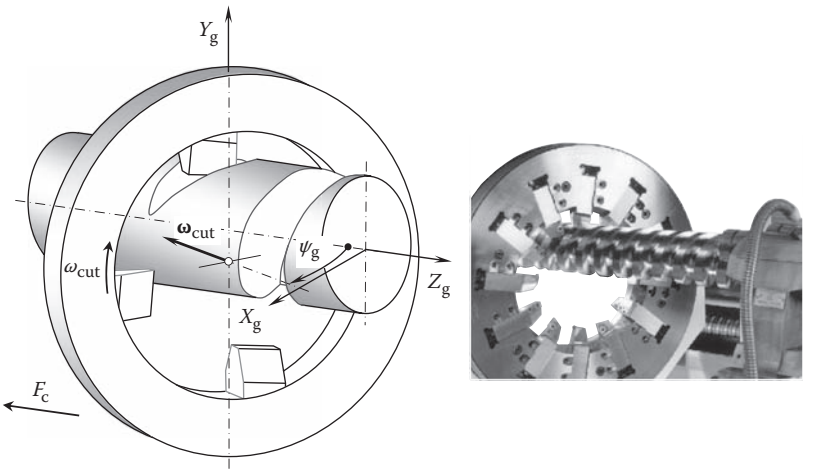

FIGURE 8.9
Concept of thread whirling.

There are limitations to the size of the worm thread that can be cut with a particular whirling head, but these are made to cut a range of sizes. Normally, single and two start worms are suitable since the maximum permissible helix angle is $\psi_g = 30°$ owing to the interference between the head and the work, but a useful range of worms can be successfully cut by the process.

Production rates of whirling, when compared to thread milling or hobbing, are at least four times faster.

Whirling of internal worms is also possible.

8.3.4 Grinding of an Involute Worm

Profiling of the form grinding wheel for finishing an involute worm can be done following the procedure used for milling cutters.

High speed of cutting is a prerequisite for grinding operations. The required speed of cutting can be easily achieved when the outer diameter of grinding tools is bigger. For this purpose, implementation of face-type form grinding tools is promising.

When machining a worm with a face-type form grinding tool, the worm is rotating about its axis of rotation O_g. The rotation vector of the worm $\boldsymbol{\omega}_g$ is along the O_g axis (Figure 8.10). The face-type grinding tool is rotating about its axis of rotation O_{c2}. The rotation vector of the form grinding tool $\boldsymbol{\omega}_{cut}$ aligns with the O_{c2} axis. In addition to the rotation $\boldsymbol{\omega}_g$, the grinding tool is traveling along the worm axis of rotation with feed F_c. Rotation of the worm ω_g and feed F_c are timed with each other. Timing of the motions $\boldsymbol{\omega}_g$ and F_c is performed in such a way that the face-type grinding tool travels at the distance of axial pitch times the worm number of start per one revolution of the worm.

When planning to use form tools for grinding of involute worms, the following types of kinematics of the worm threads can be implemented.

The rotation vector $\boldsymbol{\omega}_{cut}$ of the grinding wheel intersects the worm axis of rotation O_g at right angle. No physical restrictions are imposed on the configuration of the rotation vectors $\boldsymbol{\omega}_g$ and $\boldsymbol{\omega}_{cut}$ when they are along crossing straight lines and thus, the closest distance of approach of the straight lines is not equal to zero. A special axial profile is necessary

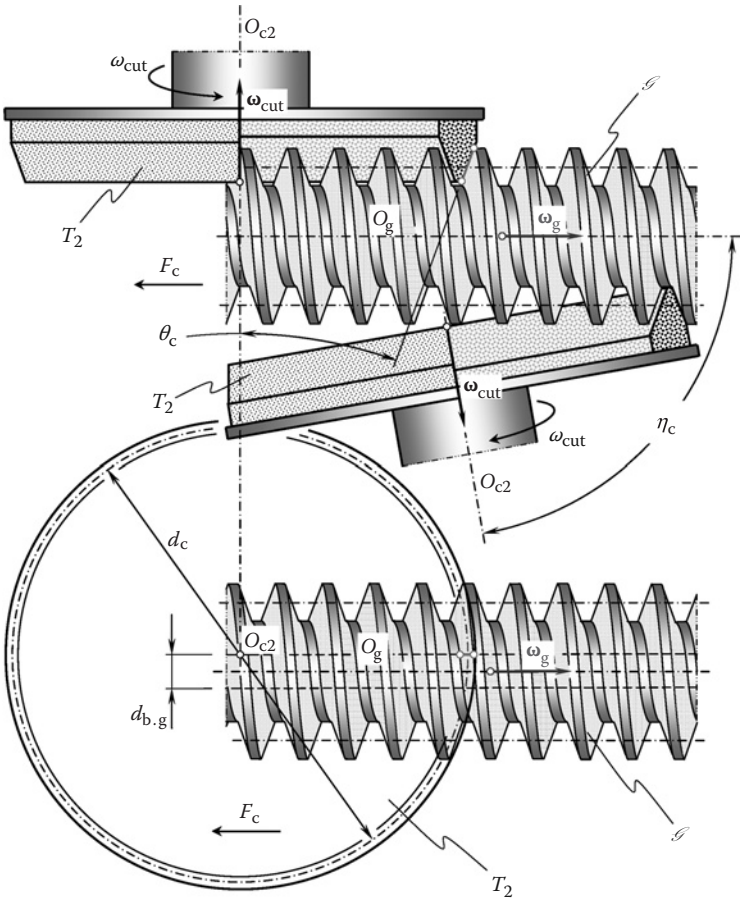

FIGURE 8.10
Grinding wheels for finishing an involute worm.

to ensure the accuracy of machining of worms in both cases. The generating surface T_2 of the form grinding wheel in this case can be determined as the enveloping surface to successive positions of the thread surface of the worm when it is rotating about the axis of rotation of the grinding wheel O_{c2}.

The necessity in profiling of the grinding wheel following the special shape can be eliminated if limited changes are introduced to the kinematics of the worm grinding process. In a particular case, when the closest distance of approach between the axes of rotation O_g and O_{c2} is equal to radius $r_{b.g} = 0.5d_{b.g}$ of the base cylinder of the worm, the grinding wheel having a straight axial profile can be used for finishing of the worm. Under such a configuration of the rotation vectors $\boldsymbol{\omega}_g$ and $\boldsymbol{\omega}_{cut}$, the cone angle θ_c of the generating surface T_2 of the grinding wheel must be equal to the base helix angle $\psi_{b.g}$ of the worm. This means that satisfaction of the equality $\theta_c = \psi_{b.g}$ is required for precision machining of the worm when axes O_g and O_{c2} are remote from each other at the distance $r_{b.g}$. Offsetting of the rotation axes O_g and O_{c2} at the prespecified distance $r_{b.g}$ is of critical importance, especially when grinding precise multistart involute worms.

Only short-length worms can be ground with a face-type grinding wheel when the rotation axes O_g and O_{c2} are at right angle to each other. The maximum feasible length of the

ground worm is limited to its length, for which there is enough room within the interior of the grinding wheel. For grinding of lengthy involute worms, say for grinding of worms theoretically of infinite length, it is recommended to implement a schematic of machining of worms when the rotation vectors $\boldsymbol{\omega}_g$ and $\boldsymbol{\omega}_{cut}$ are at a certain angle η_c (Figure 8.10). If the angle η_c is computed properly, then worms of any length can be ground with the face-type grinding wheel.

Again, axes of rotation O_g and O_{c2} can either intersect each other or they can cross each other at a certain angle. In both cases, special profiling of the form grinding wheel is required for accuracy purposes. Only at a particular configuration of the rotation vectors $\boldsymbol{\omega}_g$ and $\boldsymbol{\omega}_{cut}$ is the grinding wheel axial profile straight. For this particular configuration, the rotation O_g and O_{c2} are remote at distance $r_{b.g}$ of the radius of the base cylinder of the involute worm. To compute for the required value of cone angle θ_c of the generating surface T_2 of the grinding wheel, for which the rotation axis O_{c2} is inclined at an angle η_c with respect to the axis of rotation O_g of the worm, the following expression

$$\theta_c = \psi_{b.g} + \eta_c - 90^\circ \tag{8.15}$$

can be used.

A scenario wherein the rotation vectors $\boldsymbol{\omega}_g$ and $\boldsymbol{\omega}_{cut}$ make a certain acute angle enables machining of the internal involute worm as shown in Figure 8.11. In this case, the angle η_c and the design parameters of the grinding wheel must be computed so as to satisfy the set of conditions for proper surface generation ([128, 136, 138, 143], etc.; see Appendix B). A possibility of grinding of internal involute worms using a face-type grinding wheel having an inclined axis of rotation is an important advantage of the discussed design of the grinding wheel.

Similar to the concept of the involute worm being ground via the outer side of the conical grinding wheel (Figure 8.10), it also can be ground by the inner side of the conical grinding wheel. Two possible schematics for grinding of the involute worm using the grinding

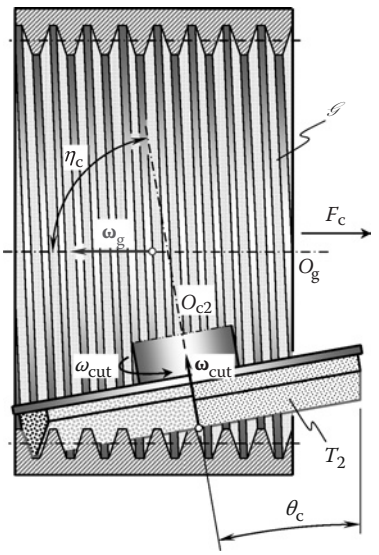

FIGURE 8.11
An example of grinding of an internal involute worm.

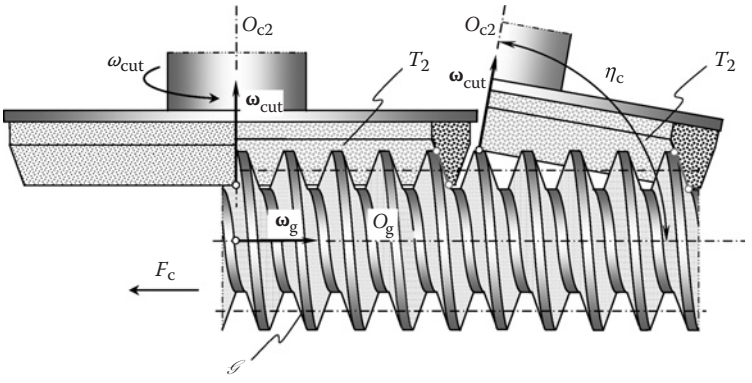

FIGURE 8.12
Grinding of an involute worm with the inner side of the conical grinding wheel.

wheel having a generating surface T_2 in the form of the inner cone of revolution are shown in Figure 8.12.

Evidently, there is much room for improvement in finishing of involute worms alternating the parameters of the schematic of worm machining.

Involute worms are not the only types of worms that can be machined by face-type grinding wheels. Worms having a thread profile of other geometries can also be machined with face-type grinding wheels. Moreover, a cutting tool of this type can be used for machining of conical worms, etc.

8.4 Classification of Form Gear Tools

Classification of all possible types of form cutting tools for machining of gears has not been developed yet. However, the need for classification is evident. It could be helpful in selecting a cutting tool design that best fits the needs of a given gear manufacturer.

It is important to bear in mind that the total number of possible configurations of the coordinate system associated with the cutting tool with respect to the coordinate system associated with the gear to be machined is not infinite, but is limited to $n_{cg} = 4032$ combinations [see Equation (8.7)]. The limited number of possible configurations makes it possible to analyze each configuration carefully, and in this way to make a decision whether a particular combination is feasible for the requirements of gear machining. Computer methods can be used for the purpose of such analyses. After all feasible configurations have been selected from the total number of combinations ($n_{cg} = 4032$), then the formal classification of all possible types of form tools for machining gears can be developed. No principal restrictions have been observed in this regard.

The development of the classification of all possible types of form tools for machining of gears is not the goal of this text. For further consideration, it is sufficient to know that: (1) the total number of possible configurations of the cutting tool relative to the work is not infinite, but is limited; (2) the total number of configurations (n_{cg}) is limited to 4032 configurations; (3) all possible configurations can be analyzed from the standpoint of their implementation in the design of gear cutting tools; (4) computers can be used to analyze the feasibility of all configurations of the coordinate systems $X_gY_gZ_g$ and $X_{c2}Y_{c2}Z_{c2}$.

Section III

Cutting Tools for Gear Generating: Parallel-Axis Gear Machining Mesh

Gear cutting tools that work on the basis of the generating principle are more sophisticated compared to form gear cutting tools. When machining a work gear with a generating gear cutting tool, rolling with no sliding of the axode of the work gear over the axode of the gear cutting tool is always observed.

In this section, we review the gear cutting tools engaged in a planar mesh with the gear.

For convenience, this review of the designs of gear cutting tools begins with the analysis of the kinematics of the parallel-axis gear machining mesh.

Kinematics of the Parallel-Axis Gear Machining Mesh

Parallel-axis gear machining mesh can be schematically depicted by two rotation vectors, which are parallel to each other—the rotation vector of the work gear $\boldsymbol{\omega}_g$ and the rotation $\boldsymbol{\omega}_c$ vector of the gear cutting tool.

The rotation vectors $\boldsymbol{\omega}_g$ and $\boldsymbol{\omega}_c$ are at a certain center distance $C_{g/c}$. They are along the axes O_g and O_c of rotation of the work gear and the gear cutting tool, respectively. Commonly, the vectors $\boldsymbol{\omega}_g$ and $\boldsymbol{\omega}_c$ are applied at the ends of the straight-line segment $C_{g/c}$ as shown in Figure III.1. However, because vectors $\boldsymbol{\omega}_g$ and $\boldsymbol{\omega}_c$ are a type of sliding vectors, in particular cases, for convenience they can be applied at other points within the corresponding axis of rotation.

Because rotation vectors $\boldsymbol{\omega}_g$ and $\boldsymbol{\omega}_c$ are parallel, the vector of instant rotation $\boldsymbol{\omega}_{pl} = \boldsymbol{\omega}_c - \boldsymbol{\omega}_g$ is also parallel to these vectors. The vector $\boldsymbol{\omega}_{pl}$ of instant rotation is applied at pitch point P. Pitch point P is located within the straight-line segment $C_{g/c}$. The ratio of the distance

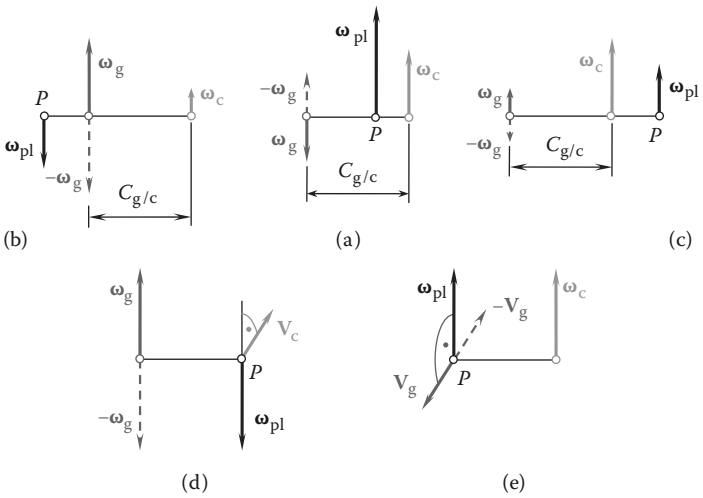

FIGURE III.1
Types of parallel-axis gear machining meshes.

r_g from the pitch point to the work gear axis O_g to the distance r_c from the pitch point to the cutting tool axis O_c is inverse to the ratio of the magnitudes of rotation vectors $\boldsymbol{\omega}_g$ and $\boldsymbol{\omega}_c$. This relationship is analytically described by the expression $r_g\omega_g = r_c\omega_c$. Evidently, the actual location of pitch point P within the straight-line segment $C_{g/c}$ depends on the ω_g/ω_c ratio. This ratio is commonly referred to as the tooth ratio of the work gear to the cutting tool mesh. Tooth ratio is designated as u. To compute for u, the expression $u = \omega_g/\omega_c \equiv r_c/r_g$ is valid.

As shown in Figure III.1a, the vector diagram corresponds to an external *work gear to cutting tool mesh*. For an external work gear to cutting tool mesh, the tooth ratio u is positive ($u > 0$).* In this particular case, the vector of instant rotation $\boldsymbol{\omega}_{pl}$ is located between the rotation vectors $\boldsymbol{\omega}_g$ and $\boldsymbol{\omega}_c$. Any alteration in the $u = \omega_g/\omega_c$ ratio immediately entails a corresponding change in the location of pitch point P within the straight-line segment $C_{g/c}$. However, as long as the ratio u is positive, the vector of instant rotation $\boldsymbol{\omega}_{pl}$ would be located between the rotation vectors $\boldsymbol{\omega}_g$ and $\boldsymbol{\omega}_c$, occupying different positions within $C_{g/c}$. Under such a scenario, pitch point P is migrating within the $C_{g/c}$ and moving closer either to the work gear axis O_g or to the cutting tool axis O_c.

If pitch point P is located beyond one of the ends of the center distance $C_{g/c}$, then the corresponding vector diagram corresponds to an internal gear machining mesh. Two types of internal gear machining meshes are recognized.

First, an external work gear can be machined with an enveloping gear cutting tool. A vector diagram for this particular case of gear machining is shown in Figure III.1b. Second, an internal work gear can be machined with an external gear cutting tool (see Figure III.1c). In both cases, the tooth ratio u is negative ($u < 0$). In the first case (Figure III.1b), the negative

* From the perspective of the *DG/K*-based approach of surface generation [125, 136, 138, 143, 153], the radius of the curvature of a convex cross section of a surface is positive, whereas that of a concave cross section has a negative value. An external gear machining mesh features two external (convex) axodes. Therefore, the radii r_g and r_c themselves, as well as their ratio $u = r_c/r_g \equiv \omega_g/\omega_c$, have positive values. In contrast, for an internal gear machining mesh, one of the radii, either r_g or r_c, is of negative value. This results in a negative value for the tooth ratio u ($u < 0$).

sign of u is attributed to $r_c < 0$ (whereas $r_g > 0$). In the second case (Figure III.1c), the negative sign of u is attributed to $r_g < 0$ (whereas $r_c > 0$).

For an external gear machining mesh, the vector $\boldsymbol{\omega}_{pl}$ of instant rotation is applied at a point within the straight-line segment $C_{g/c}$. In contrast, for an internal gear machining mesh, the vector $\boldsymbol{\omega}_{pl}$ of instant rotation is applied at a point outside the straight-line segment $C_{g/c}$. What is between these two cases? Or, in other words, which type of gear machining mesh corresponds to the case(s) for which the vector $\boldsymbol{\omega}_{pl}$ of instant rotation is applied at one of two ends of the straight-line segment $C_{g/c}$?

The vector diagram for this case, which corresponds to the rotating work gear ($\boldsymbol{\omega}_g$) and translating gear cutting tool ($\mathbf{V}_c$), is schematically illustrated in Figure III.1d. Pitch point P is at distance r_g from the work gear axis O_g. Because the rotation vector $\boldsymbol{\omega}_{pl}$ passes through pitch point P, this means that the cutting tool axis O_c is remote to infinity ($r_c \to \infty$). Since $r_c \to \infty$, this results in $\boldsymbol{\omega}_c = 0$ and the relative motion can be expressed in terms of the linear velocity $\mathbf{V}_c$.

The vector diagram for the case that is inverse to that discussed above, which corresponds to the translating work gear ($\mathbf{V}_g$) and rotating gear cutting tool ($\boldsymbol{\omega}_c$), is schematically illustrated in Figure III.1e. Pitch point P is at distance r_c from the cutting tool axis O_c. Because the rotation vector $\boldsymbol{\omega}_{pl}$ passes through pitch point P, this means that the work gear axis O_g is remote to infinity ($r_g \to \infty$). Because $r_g \to \infty$, this results in $\boldsymbol{\omega}_g = 0$ and the relative motion can be expressed in terms of the linear velocity $\mathbf{V}_g$.

A gear cutting tool can be designed based on each of the vector diagrams shown in Figure III.1. Various designs of gear cutting tools featuring the parallel-axis work gear to cutting tool mesh can be developed. It is convenient to begin this discussion by focusing on the design of a gear cutting tool featuring the parallel-axis gear machining mesh shown in Figure III.1d.

9

Rack Cutters for Planing of Gears

Spur and helical gears may be planed with a rack cutter. Rack cutters are also suitable for cutting sector gears. The generating action in the gear planing operation is similar to rolling of a gear along a mating rack. For profiling of rack cutters as well as for design purposes, the generation surface of the rack cutter must be determined.

9.1 Generating Surface of a Rack Cutter

Analysis of the kinematics of machining gears with rack cutters reveals that generation of the gear tooth flank can be interpreted as the enveloping surface to successive positions of the rack when the pitch surface of the rack is rolling with no sliding over the pitch cylinder of the gear being machined. The kinematics of the gear machining operation in this case corresponds to the *gear machining mesh* (Figure III.1d).

The generated surface of the rack cutter can be viewed as the enveloping surface to consecutive positions of the gear tooth when the pitch cylinder of the gear being machined is rolling with no sliding over the pitch plane of the rack cutter. In practice, a rack cutter can be designed based on the corresponding phantom rack that is engaged in proper meshing with the work gear.

However, in order to enhance the capabilities of the tool designer, representation of the generating surface of the rack cutter in terms of the design parameters of the work gear and the kinematics of the gear machining operation is strongly recommended.

Equation for the generating surface of the rack cutter. To derive an equation for the generating surface T of the rack cutter, consider a left-hand–oriented Cartesian coordinate system $X_g Y_g Z_g$ associated with the work gear as shown in Figure 9.1. The axis Z_g of the coordinate system $X_g Y_g Z_g$ is aligned with axis of rotation O_g of the work gear. In Figure 9.1, the pitch diameter of the gear is denoted by $d_{w.g}$. In the gear machining mesh, the pitch diameter exceeds the base diameter of the gear ($d_{w.g} \geq d_{b.g}$), where $d_{b.g}$ denotes the base diameter of the gear. On the other hand, the pitch diameter $d_{w.g}$ does not exceed a certain limit value $[d_{g.o}]$, under which either pointing of the rack cutter teeth is observed or the actual length of the top cutting edge is insufficiently short ($d_{w.g} < [d_{g.o}]$). To summarize, one can conclude that the pitch diameter of the work gear in the gear machining mesh is within the interval

$$d_{b.g} \leq d_{w.g} < [d_{g.o}] \tag{9.1}$$

In Figure 9.1, the pitch plane of the rack cutter is designated as W_c. Pitch plane W_c is at the distance $r_{w.g} = 0.5 d_{w.g}$ from the gear axis O_g. When designing a rack cutter, the tool designer is allowed to vary the distance $r_{w.g}$ in the range of

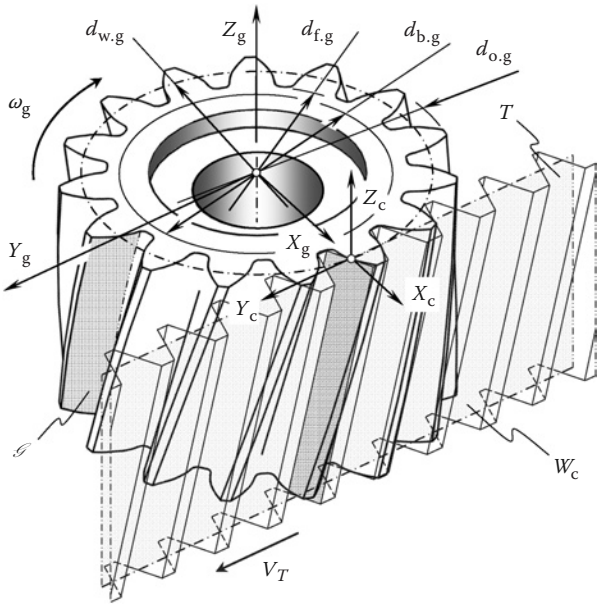

FIGURE 9.1
Determination of the generating surface T of the rack cutter.

$$0.5d_{b.g} \le r_{w.g} < 0.5[d_{g.o}] \tag{9.2}$$

At this point, the generated surface T is not determined yet. Therefore, the motion of a certain reference system with respect to the coordinate system $X_gY_gZ_g$—and not the motion of the rack cutter with respect to the work gear—is considered. For this purpose, a left-hand–oriented Cartesian coordinate system $X_cY_cZ_c$ is implemented. The reference system is somehow associated with the pitch plane W_c. The tool designer is free to make his/her decision on how the pitch plane W_c is represented in $X_cY_cZ_c$. Convenience of the analytical representation of pitch plane W_c in the reference system $X_cY_cZ_c$ is the only criterion for the selection of the desired configuration of the coordinate system $X_cY_cZ_c$ with respect to the pitch plane W_c. For convenience, at the beginning the reference system $X_cY_cZ_c$ is oriented so that it is just shifted along the X_g axis at the distance $r_{w.g}$ as shown in Figure 9.1.

After it has been derived, the generating surface T of the rack cutter will be represented in the reference system $X_cY_cZ_c$.

When machining, the work gear is rotating ω_g about its axis O_g. The rack cutter is tangentially reciprocating to the work gear tooth flank, and is moving forward with a certain velocity V_T.

The reciprocation of the rack cutter causes the generating surface T to slide over it. Because of this, the reciprocation does not affect the shape of the generating surface T. Therefore, this motion can be omitted from the analysis.

The straight motion of the rack cutter V_T is timed with the rotation ω_g of the work gear. When the reference system of the gear $X_gY_gZ_g$ turns about the Z_g axis through a certain angle $\varphi_g = \omega_g t$, the coordinate system $X_cY_cZ_c$ translates along the Y_g axis at a distance $l_{yc} = V_T t$, where t denotes time. Because the equality $V_T = \omega_g r_{w.g}$ is valid, for the computation of the displacement l_{yc}, the expression $l_{yc} = \varphi_g r_{w.g}$ can be used.

To derive an equation for the generating surface of the rack cutter, an expression that analytically describes the tooth flank of the gear in a current location of the work gear with respect to the reference system $X_cY_cZ_c$ is necessary. The equation for the involute gear tooth flank surface [Equation (1.3)]

$$\mathbf{r}_g(U_g, V_g) = \begin{bmatrix} r_{b.g}\cos V_g + U_g \cos\lambda_{b.g}\sin V_g \\ r_{b.g}\sin V_g - U_g \sin\lambda_{b.g}\sin V_g \\ r_{b.g}\tan\lambda_{b.g} - U_g \sin\lambda_{b.g} \\ 1 \end{bmatrix} \quad \begin{matrix} V_g^{(l)} \le V_g \le V_g^{(a)} \\ 0 \le U_g \le [U_g] \end{matrix} \tag{9.3}$$

can be applied for this purpose.

Equation (9.3) describes the gear tooth flank surface $\mathcal{G}$ in the reference system $X_gY_gZ_g$ associated with the work gear itself. Implementation of operators of linear transformations is helpful for the transition from the coordinate system $X_gY_gZ_g$ to the coordinate system $X_cY_cZ_c$.

During time t, the work gear, together with the reference system $X_gY_gZ_g$, turns about the Z_g axis through a certain angle φ_g. Transition from the coordinate system $X_gY_gZ_g$ to the reference system $X_g^*Y_g^*Z_g^*$ in the initial position of the work gear can be described by the operator of rotation $\mathbf{Rt}(-\varphi_g, Z_g)$. For the analytical description of the transition from the coordinate system $X_g^*Y_g^*Z_g^*$ to the reference system $X_c^*Y_c^*Z_c^*$, the operator of translation $\mathbf{Tr}(-r_{w.g}, X_g^*)$ is used. Here, the coordinate system corresponding to the initial position of the rack cutter is designated as $X_c^*Y_c^*Z_c^*$. Ultimately, the operator of translation $\mathbf{Tr}(-l_{yc}, Y_c^*)$ can be used for the transition from the coordinate system $X_c^*Y_c^*Z_c^*$ to the rack cutter coordinate system $X_cY_cZ_c$. Taking into account the equality $l_{yc} = \varphi_g r_{w.g}$, the operator of translation $\mathbf{Tr}(-l_{yc}, Y_c^*)$ can be represented in the form $\mathbf{Tr}(-\varphi_g r_{w.g}, Y_c^*)$.

Gear tooth flank surface $\mathcal{G}$ is described in the form of a function of two parameters: U_g and V_g [see Equation (9.3)]. Operators of linear transformations are functions of the angle φ_g through which the gear turns about its axis of rotation O_g. Therefore, an expression for the gear tooth flank $\mathcal{G}$ in the coordinate system $X_cY_cZ_c$ will be presented in the form of a function of three independent parameters: Gaussian coordinates U_g and V_g and angle φ_g.

Finally, the expression

$$\mathbf{r}_g(U_g, V_g, \varphi_g) = \mathbf{Tr}(-\varphi_g r_{w.g}, Y_c^*)\cdot\mathbf{Tr}(-r_{w.g}, X_g^*)\cdot\mathbf{Rt}(-\boldsymbol{\varphi}_g, Z_g)\cdot\mathbf{r}_g(U_g, V_g) \tag{9.4}$$

can be derived for the gear tooth flank surface $\mathcal{G}$, which is represented in the reference system $X_cY_cZ_c$ associated with the rack cutter.

The equation for the generating surface of the rack cutter can be derived as the solution to the set of two equations

$$\begin{cases} \mathbf{r}_g = \mathbf{r}_g(U_g, V_g, \varphi_g) \\ \dfrac{\partial}{\partial\varphi_g}\mathbf{r}_g(U_g, V_g, \varphi_g) = 0 \end{cases} \tag{9.5}$$

After the second equation is solved with respect to φ_g and the solution is substituted into the first equation in Equation (9.5), an expression for position vector $\mathbf{r}_c$ of a point of the generating surface T can be presented as

$$\mathbf{r}_c = \mathbf{r}_c(U_c, V_c) \tag{9.6}$$

Without going into details of the derivation, the generating surface T of the rack cutter can be expressed in terms of the design parameters of the gear to be machined

$$\mathbf{r}_c(U_c, V_c) = \begin{bmatrix} U_c \\ \left(U_c \cot\phi_{w.g} + r_{w.g} \tan\phi_{w.g} \pm \dfrac{n_c p_{b.g}}{\cos\phi_{w.g}}\right) \cos\psi_{w.g} - V_c \sin\psi_{w.g} \\ \left(U_c \cot\phi_{w.g} + r_{w.g} \tan\phi_{w.g} \pm \dfrac{n_c p_{b.g}}{\cos\phi_{w.g}}\right) \sin\psi_{w.g} + V_c \cos\psi_{w.g} \\ 1 \end{bmatrix} \tag{9.7}$$

Tooth flanks of the generating surface T are shaped in the form of two families of planes. They form the teeth of the phantom rack. The number of the current tooth of the rack is denoted by n_c.

The planes of one family are parallel to one another. The distance between every two neighboring planes is equal to the base pitch $p_{b.g}$ of the work gear teeth.

Lines of intersection of the planes by $X_g Y_g$ coordinate plane form a certain profile angle $\phi_{w.g}$ with the X_g axis. The angle $\phi_{w.g}$ is equal to the transverse profile angle of the work gear tooth at the pitch cylinder of radius $r_{w.g}$.

Lines of intersection of the planes by $Y_g Z_g$ coordinate plane form a certain helix angle $\psi_{w.g}$ with the Z_g axis. The angle $\psi_{w.g}$ is equal to the helix angle at the pitch cylinder of radius $r_{w.g}$ of the gear.

The planes of another family of planes are also parallel to one another. The only difference between the planes of the two families is in the sign of the profile angle. For the second family of parallel planes, this angle is not equal to $\phi_{w.g}$, but is equal to $-\phi_{w.g}$ instead.

The configuration of these two families of parallel planes relative to each other is an important consideration. Tooth thickness and space width at the pitch cylinder of a standard gear are equal to each other. When a standard gear is machined with a standard rack cutter, this uniquely specifies the configuration of one family of planes relative to the other family. When a standard gear is machined with a nonstandard rack cutter, tooth thickness and space width are not equal to each other. Moreover, these two parameters are getting dependent on the number of teeth of the work gear. Therefore, in this particular case, for the purpose of specifying the configuration of two families of parallel surfaces, the rolling motion of pitch surfaces should be considered. The tooth thickness of the generating surface T at the pitch plane must be equal to the corresponding space width of the work gear teeth at the pitch cylinder of radius $r_{w.g}$. Similarly, the space width of the generating surface T at the pitch plane must be equal to the corresponding tooth thickness of the work gear pitch cylinder of radius $r_{w.g}$. The same approach is applicable when nonstandard gears are required to be machined with a rack cutter.

Equation (9.7) describes the tooth flank surface of a rack cutter for machining of a helical gear. Substitution of the helix angle $\psi_{w.g} = 0°$ reduces Equation (9.7) to a simpler case, which corresponds to the tooth flank surface of a rack cutter for machining of a spur gear.

Because the tooth flank surfaces of the generating surface of the rack cutter are planes, this eliminates the necessity of analyzing the intrinsic geometry of the generating surface T.

In a particular case of gear machining, the variables that are to be entered into Equation (9.7)—base pitch $p_{b.g}$, profile angle $\phi_{w.g}$, and helix angle $\psi_{w.g}$ on the pitch cylinder of radius $r_{w.g}$—can be expressed in terms of tooth number N_g, normal pitch $P_{n.g}$, normal pressure angle ϕ_n, and pitch helix angle ψ_g. For this purpose, the engineering formulae listed in Appendix A are helpful.

A clear understanding of the geometry and the kinematics of the gear machining mesh is of critical importance to a gear cutting tool designer.

9.2 On the Variety of Feasible Tooth Profiles of Rack Cutters

The actual tooth profile of the generating surface of the rack cutter strongly depends on the type of timing of the work gear rotation and the translation of a reference system associated with the rack cutter. Because the pitch plane of the rack cutter rolls over the pitch cylinder of the work gear with no sliding, the linear velocity of the rotational motion of points on the pitch cylinder $\omega_g r_{w.g}$ is equal to the velocity of the translational motion of the rack cutter V_T, that is, the equality $\omega_g r_{w.g} = V_T$ is observed. This equality immediately yields an expression for radius $r_{w.g}$ of the pitch cylinder of the work gear when it is cutting with the rack cutter

$$r_{w.g} = \frac{V_T}{\omega_g} \tag{9.8}$$

Equation (9.8) shows that variation in the ratio V_T/ω_g causes corresponding alterations in the radius of the pitch cylinder of the work gear in the gear machining process. Ultimately, the alterations result in corresponding changes in the parameters of the tooth profile of rack T.

Figure 9.2 illustrates the impact of the radius of the pitch cylinder $r_{w.g}$ of the work gear (in other words, impact of the ratio V_T/ω_g) on the shape of the tooth profile of the generating surface T of the rack cutter.

For the minimum feasible radius $r_{w.g}$ of the pitch cylinder, the equality $r_{w.g} = r_{b.g}$ is observed (Figure 9.2a). The profile angle of the rack cutter tooth is equal to the pressure angle of the work gear at a point on the pitch cylinder ($\phi_c = \phi_{w.g}$). Because the equality $r_{w.g} = r_{b.g}$ is observed, the profile angle ϕ_n of the rack cutter is equal to zero under such a scenario ($\phi_n = 0°$).

The helix angle of the generating surface of the rack cutter is equal to the helix angle $\psi_{w.g}$ of the pitch cylinder of the gear being machined ($\psi_c = \psi_{w.g}$). Again, because the equality $r_{w.g} = r_{b.g}$ is observed, the helix angle ψ_c of the generating surface T of the rack cutter in the case under consideration is equal to base helix angle of the work gear ($\psi_c = \psi_{b.g}$).

The width of the top land t_o of rack T having a zero profile angle $\phi_n = 0°$ is the maximal possible. The base pitch of the tooth flank surfaces of the rack cutter is designated as p_b. It must be identical to the base pitch of the gear to be machined ($p_{b.g} \equiv p_{b.c} \equiv p_b$). Because of this, no additional subscripts are used in the designation of base pitch p_b.

When the tooth profile angle is equal to zero, the tooth addendum vanishes ($a = 0$) and the tooth dedendum b becomes equal to the whole tooth height ($b = h_t$).

For a larger V_T/ω_g ratio (Figure 9.2b), which corresponds to a larger radius $r_{w.g}$ of the pitch cylinder of the work gear, the profile angle of the rack cutter ϕ_c is also larger, and the width of the top land t_o is also smaller. The base pitch p_b, however, remains the same,

and is equal to the base pitch of the gear to be machined—this is the rule. For a larger V_T/ω_g ratio, the expression $\phi_c = \phi_{w.g}$ for the cutter tooth profile angle and the expression $\psi_c = \psi_{w.g}$ for the cutter helix angle are still valid. The tooth addendum a of rack T and the tooth dedendum b are of a certain value. The whole tooth height is equal to $h_t = a + b$.

The tooth thickness of the generating surface T measured within the pitch line is equal to the arc width of the tooth space of the work gear measured on the pitch circle. In both

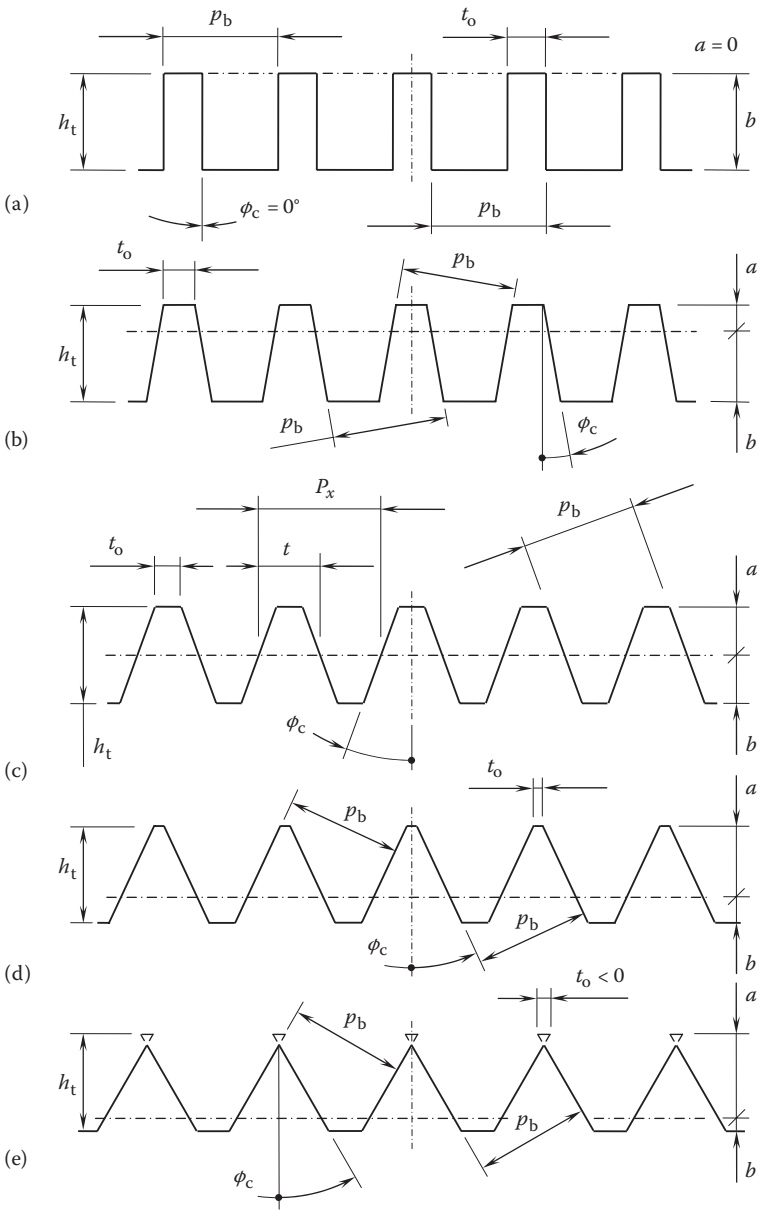

FIGURE 9.2
Various generating surfaces T of a rack cutter can make proper mesh with the work gear.

cases described above, tooth thickness of the rack and width of space between adjacent teeth are not equal to each other.

In a particular case of gear machining, the radius of the pitch cylinder of the gear can be of a certain value when the tooth thickness of rack T is equal to the width of the tooth space (Figure 9.2c).

Although the major relationships for the generating surface T of the rack cutter remain valid ($p_{b.g} \equiv p_{b.c} \equiv p_b$, $\phi_c = \phi_{w.g}$, $\psi_c = \psi_{w.g}$, etc.), this particular case features an important advantage for the practical use of rack cutters. The equality between tooth thickness of the rack cutter and tooth space width makes the rack cutter interchangeable—the same rack cutter can be used for machining gears with different tooth numbers.

There are no physical constraints for further increase of the ratio V_T/ω_g as shown in Figure 9.2d. However, at some point, tooth pointing of the generating surface T of the rack cutter is observed. Physically, a rack cutter having teeth with pointing can exist but this is impractical. Geometrically, the ratio V_T/ω_g can be increased beyond the value of the radius $r_{w.g}$ when tooth pointing occurs (Figure 9.2e). Under such a scenario, the top land of the rack cutter vanishes. Analytically, it can be expressed in negative values. However, the practicality of the rack cutter is at best doubtful.

The following conclusions can be drawn from the preceding discussion:

- Variation in the kinematical parameters of the gear machining operation provides a possibility to control the major design parameters of the rack cutter.
- The actual tooth profile angle of the rack cutter and the actual helix angle of the rack cutter are equal to the corresponding design parameters of the gear to be machined as measured on its pitch cylinder.
- The particular value of the ratio V_T/ω_g under which tooth thickness of the rack cutter is equal to tooth space width is of practical importance. In this particular case, the same rack cutter can be used for machining of gears with different number of teeth.
- The width of the rack cutter top land is under control and reaches its maximum value when the tooth profile angle of the rack is equal to zero.
- The width of the rack cutter top land can be reduced to undesirably small values or tooth pointing can even be observed when the rack cutter tooth profile angle exceeds a certain allowable value.

The features listed above are among the important issues that a tool designer has to keep in mind when aiming to design a high-performance gear cutting tool.

9.3 Cutting Edges of the Rack Cutter

Generating surface is a key element in designing a rack cutter for machining of a work gear.

Each tooth of the rack cutter has three cutting edges. The top cutting edge is shaped in the form of a straight-line segment. The bottom land of the tooth space of the work gear is machined by this cutting edge. The gear tooth profile is generated by two lateral cutting

edges. Lateral cutting edges of the rack cutter are straight. The last is a solid advantage of the gear cutting tool of this type.

Cutting edges of a rack cutter for machining gears are commonly interpreted as the line of intersection of the generating surface of the gear cutting tool by the rake surface.

9.3.1 Rake Surface of a Rack Cutter

Initially, rack cutters were designed with the rake surface shaped in the form of a plane. The rake plane R_s is at a certain rake angle with respect to the perpendicular to the top land of the generating surface T of the rack cutter. This angle is referred to as *rake angle* γ_o, whose value could either be positive ($\gamma_o > 0°$) or negative ($\gamma_o < 0°$). It could also be equal to zero.

Two different configurations of the rake plane R_s are used in the design of rack cutters. One of them is used in designing rack cutters for machining of both spur and helical gears. The other one is used in designing rack cutters for machining of helical gears alone. The latter features the rake plane that forms the pitch helix angle ψ_g with the generating surface of the rack cutter. Here, ψ_g denotes the pitch helix angle of the helical gear to be machined.

The rake plane is perpendicular to the generating straight lines of surface T. Consider the cutting edges of the rack cutter teeth when the rake plane is perpendicular to the generating surface (Figure 9.3).

The generating surface T of the rack cutter is depicted in the system of planes of projections $\pi_1\pi_2\pi_3$ as shown in Figure 9.3. The shape of the generating surface T is specified by a set of design parameters. For this purpose, conventional design parameters—base pitch p_b,

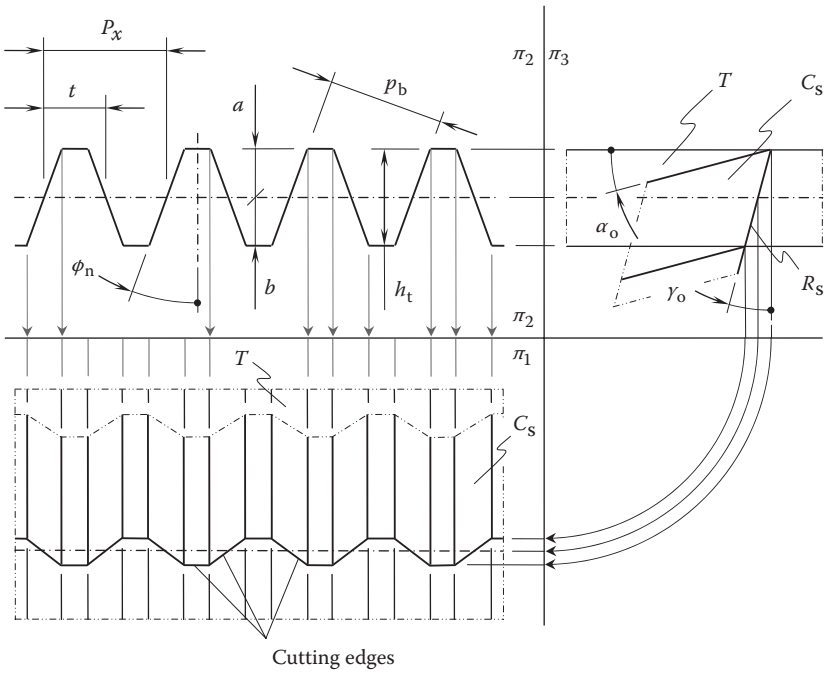

FIGURE 9.3
Configuration of working surfaces of a rack cutter tooth.

tooth profile angle ϕ_n, transverse diametral pitch P_x, tooth thickness t, tooth addendum a, tooth dedendum b, and whole tooth height h_t—can be used.

For the generating surface T of the given orientation and location in the system of planes of projections $\pi_1\pi_2\pi_3$, the rake plane R_s is a projective plane onto the plane of projections π_3. Because of this, the rake plane R_s in π_3 is shown as the trace of this plane. The trace forms the rake angle γ_o with the perpendicular to the top land of the generating surface T. The actual value of the rake angle γ_o has to be known.

Once the rake plane is constructed in π_3, projections of the rake plane R_s onto the planes of projections π_1 and π_2 can be constructed following well-known rules, which are developed in descriptive geometry (*DG*) (Figure 9.3).

The rake plane is at the helix angle to the generating straight lines of surface T. Rack cutters can be used for the purpose of machining gears with shoulders, for example, when machining a cluster gear. For this particular case, rack cutters are designed with the rake plane at the helix angle to the generating lines of surface T.

In Figure 9.4, the generating surface T of the rack cutter is depicted in the system of planes of projections $\pi_1\pi_2\pi_3$. Here, surface T is identical to that shown in Figure 9.3. By definition, the rake plane R_s is at the helix angle ψ_g relative to the generating surface T. At that same time, the rake plane forms rake angle γ_o with the perpendicular to the top land of the generating surface T.

An additional plane of projections π_4 is constructed so that the rake plane R_s occupies the position of a projective plane onto this plane of projections. Therefore, in π_4 the rake plane R_s is shown as the trace, and the rake angle γ_o can be easily constructed. The actual value of the rake angle γ_o has to be known.

Once the rake plane is constructed in π_4, projections of the rake plane R_s onto the planes of projections π_1 and π_2 can be constructed following well-known rules, which are developed in *DG* (Figure 9.4).

Designs of rack cutters often feature one of the various modifications of the rake plane R_s. These modifications are aimed to improve the cutting performance of the rack cutter. Several types of modifications of the rake surface are discussed in this chapter.

Cutting edges of the rack cutter are considered in this text from the standpoint of the kinematic geometry of surface machining [125, 136, 138, 143, 153]. This means that cutting edges CE are viewed as the line of intersection of the generating surface T by the rake plane R_s.

9.3.2 Clearance Surface of a Rack Cutter

Rack cutters are designed with the clearance surface C_s that is shaped in the form of a plane. The clearance plane through the top cutting edge is at the clearance angle α_o relative to the generating surface T of the rack cutter (Figures 9.3 and 9.4).

Clearance planes C_s through the lateral cutting edges of the rack cutter tooth form a certain clearance angle α_{cl} with the generating surface T. The clearance angle α_{cl} correlates to the clearance angle α_o of the top cutting edge of the rack cutter. To clarify the correlation between the clearance angles α_{cl} and α_o, consider the cross section of the clearance surface through the top cutting edge of the rack cutter tooth by a plane, which is perpendicular to the top land of the generating surface T. This plane is perpendicular to the top cutting edge in the case shown in Figure 9.3. For the case shown in Figure 9.4, the cross section forms the helix angle ψ_g with the top cutting edge. In both cases, the line of intersection of the clearance plane C_s is at the clearance angle α_o with respect to the top land of the generating surface T.

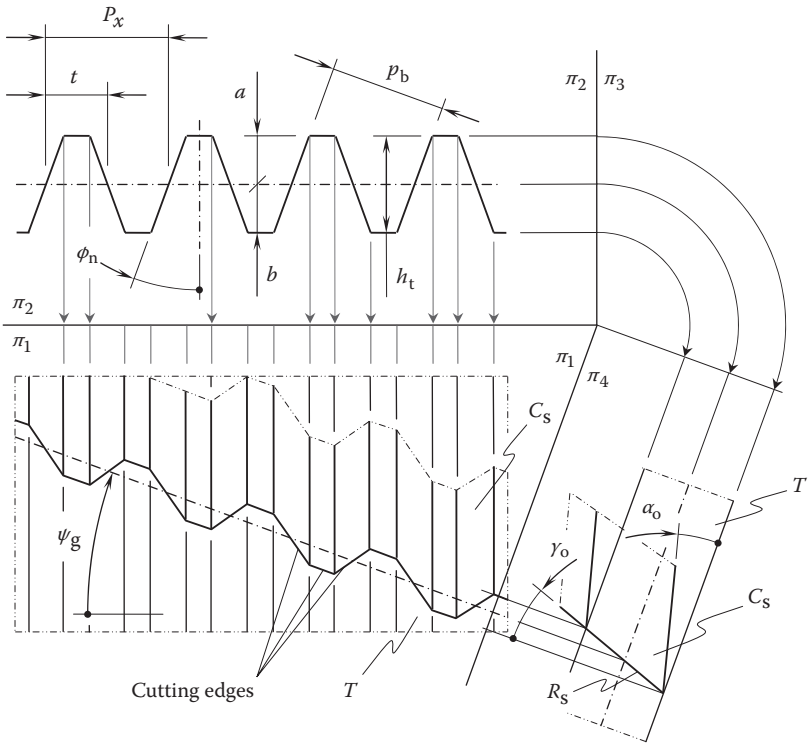

FIGURE 9.4
Configuration of working surfaces of a helical rack cutter tooth.

Furthermore, consider the cross section of the clearance surface through the lateral cutting edge of the rack cutter tooth. The cross section plane is parallel to that just considered. The line of intersection of the clearance surface by the plane forms an angle with respect to the top land of the generating surface *T*. This angle is equal to the clearance angle α_o.

For such a configuration of clearance surfaces through the top cutting edge and through the lateral cutting edges of the rack cutter, normal clearance angles at the cutting edges correlate with each other. The considered configuration of the clearance surfaces resembles the configuration of the clearance surfaces of a cutting tool with relieved clearance surfaces.

Clearance surfaces are the surfaces through the cutting edges CE of the rack cutter teeth.

9.4 Profiling of Rack Cutters

For profiling of rack cutters for machining of gears, both *DG*-based methods and analytical methods of profiling are used. The purpose of profiling of rack cutters is twofold. It is used to determine the rack cutter tooth profile (1) within the rake plane and (2) in the normal cross section of the clearance surface of the rack cutter teeth.

Implementation of both *DG*-based methods and analytical methods of profiling of rack cutters is discussed below.

9.4.1 Profiling of Rack Cutters Using *DG*-Based Methods

It is convenient to begin this discussion by focusing on the profiling of a rack cutter for machining of spur gears. For the purpose of profiling, the generating surface T of the rack cutter is depicted in the system of planes of projections $\pi_2\pi_3$ so that all planes of the generating surface T are projective planes onto the plane π_2 (Figure 9.5). Under such a scenario, the rake plane R_s and the normal cross section of the clearance surface C_s are the projective planes onto the plane of projections π_3. Use of conventional methods developed in *DG* immediately yields the rake plane profile of the rack cutter tooth as well as the normal cross section of the clearance surface C_s (Figure 9.5).

For profiling of a helical rack cutter, the generating surface T is depicted in the system of planes of projections $\pi_1\pi_2\pi_3$ so that all planes of the generating surface T are projective planes onto the plane π_2 (Figure 9.6). The process of profiling of a rack cutter for machining a helical gear having a shoulder additionally features the determination of the generating surface T in a particular plane of projections. This plane of projections is labeled π_4. The axis of projections π_1/π_4 is perpendicular to the rake plane R_s. As a consequence, the rake plane R_s and the normal cross section are the projective planes onto the plane of projections π_4. After the rake plane R_s and the normal cross section are constructed in π_4, the rake face profile of the rack cutter tooth as well as the normal cross section of the clearance surface can be easily constructed within the plane of projections π_1 (Figure 9.6).

It is recommended to perform profiling of a rack cutter using the *DG*-based methods before profiling them analytically. This results in the elimination of rough errors of profiling.

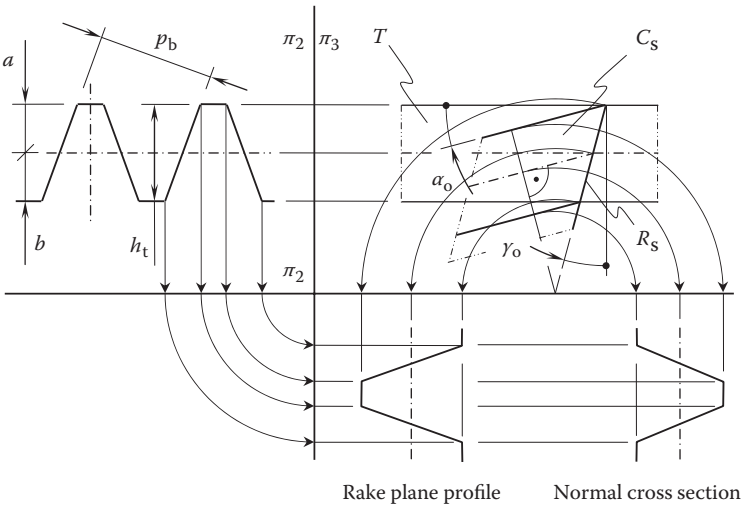

FIGURE 9.5
Profiling of a spur rack cutter using the *DG*-based method.

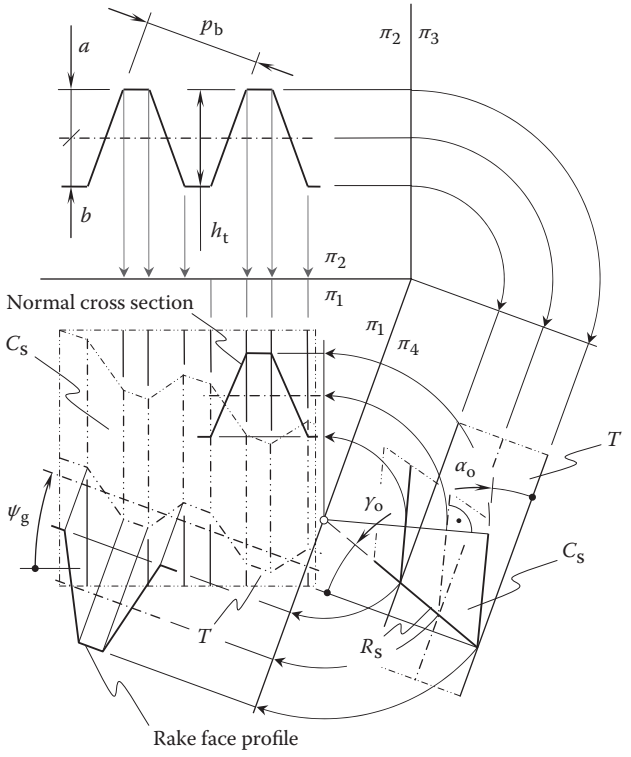

FIGURE 9.6
Profiling of a helical rack cutter using the *DG*-based method.

9.4.2 Analytical Profiling of Rack Cutters

Analytical methods of profiling of rack cutters are used to attain high accuracy. The required equations for the computation of coordinates of points of the tooth profile can be drawn from the graphical solution derived on the basis of the implementation of *DG*-based methods of profiling. Without going into details of elementary derivation, resultant formulae for the computations are given below.

Consider a rack cutter for machining a spur gear (Figure 9.7). The current point of the tooth profile of the generating surface T is at a certain distance τ_y from the tooth centerline. Parameter τ_y is referred to as the width coordinate of the rack tooth profile. For a given value of the width coordinate τ_y, the corresponding height coordinate h_y is either known or can be computed.

For the same width coordinate τ_y, the corresponding height coordinate h_y^{rs} within the rake plane R_s of the rack cutter tooth can be computed as

$$h_y^{rs} = \frac{h_y}{\cos \gamma_o} \tag{9.9}$$

The rack cutter tooth profile angle is designated as ϕ_n. The actual value of this angle is commonly known. The corresponding tooth profile angle ϕ_{rs} within the rake plane is equal to

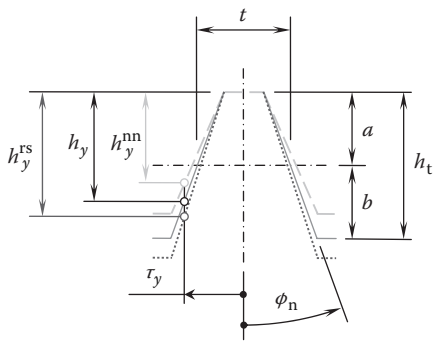

FIGURE 9.7
Correspondence between the design parameters of the rack cutter tooth profile measured in different cross sections of the generating surface *T*.

$$\phi_{rs} = \tan^{-1}(\tan\phi_n \cos\gamma_o) \tag{9.10}$$

Similarly, equations for the height coordinate h_y^{nn} and the profile angle ϕ_{nn} in the normal cross section of the clearance surface C_s

$$h_y^{nn} = h_y \cdot \frac{\cos(\alpha_o + \gamma_o)}{\cos\gamma_o} \tag{9.11}$$

$$\phi_{nn} = \tan^{-1}\left[\frac{\cos\gamma_o}{\cos(\alpha_o + \gamma_o)} \cdot \tan\phi_n\right] \tag{9.12}$$

can be derived. The last two formulae are valid for both spur rack cutters and helical rack cutters.

The preceding discussion reveals that profiling of rack cutters for machining involute gears is easy to perform. These simple examples are helpful for a better understanding of the complex problems of profiling considered in the following chapters.

9.5 Cutting Edge Geometry of the Rack Cutter

Rack cutters for roughing of gears are often designed with rake angle γ_o at the top cutting edge, which is equal to 6°30′. The clearance angle α_o at the top cutting edge of the rack cutters of this design is equal to 5°30′. The geometry of the top cutting edges of rack cutters for finishing gears is slightly different. For finishing rack cutters, the rake angle γ_o is 4° and the clearance angle α_o is 6°52′.

Consider a rack cutter having a standard normal profile angle $\phi_n = 20°$. When the geometry of the top cutting edge of the rack cutter is specified by the angles $\gamma_n = 6°30'$ and $\alpha_o = 5°30'$, the profile angle within the rake plane of the rack cutter is equal to $\phi_{rs} = 19°25'54''$. The profile angle of the normal cross section of the clearance surface in this case is $\phi_{nn} = 20°17'25''$.

9.5.1 Computation of the Cutting Edge Geometry for Lateral Cutting Edges

When the angles γ_o, α_o, and ϕ_n are given, the geometry of the lateral cutting edges of the rack cutter tooth can be analytically determined.

First, let us determine the actual value of the inclination angle λ of the lateral cutting edge of the rack cutter.

Consider the rack cutter tooth depicted in Figure 9.8. A Cartesian coordinate system XYZ is associated with the rack cutter tooth as shown in Figure 9.8. To derive the equation for the inclination angle λ, it is convenient to apply the vector method of analysis.* For this purpose, three vectors, **a**, **B**, and **C**, which are associated with the lateral cutting edge, are constructed.

The inclination angle λ is measured within the surface of cut [136, 138, 143]. The surface of cut is designated in Figure 9.8 as A–A.

The vector **a** is a unit vector. This vector is pointed along the top cutting edge. In the reference system XYZ, the following expression

$$\mathbf{a} = \mathbf{i} \tag{9.13}$$

is valid for the unit vector **a**.

The vector **B** is aligned with the line of intersection of the rake plane R_s by the coordinate plane YZ. To solve the problem under consideration, only the direction of vector **B** is important. The length of vector **B** is out of current interests. Because of this, the vector **B** of the length for which projection of the vector onto the Y axis is equal to unit ($\text{pr}_y\mathbf{B} = 1$) can be applied. Under such a scenario, vector **B** can be described by

$$\mathbf{B} = \mathbf{j} + \mathbf{k} \cdot \tan \gamma_o \tag{9.14}$$

The vector **C** is along the lateral cutting edge CE of the rack cutter. The following expression

$$\mathbf{C} = -\mathbf{i} \cdot \sin \phi_n + \mathbf{j} \cdot \cos \phi_n + \mathbf{k} \cdot \tan \lambda \tag{9.15}$$

is valid for the representation of vector **C** in terms of its projections onto the axes of the reference system XYZ.

As follows from the analysis in Equation (9.15), in the case under consideration the vector **C** chosen so for which length of projection of the vector **C** onto the coordinate plane XY is equal to unit, that is, $\text{pr}_{xy}\mathbf{C} = 1$.

By construction, vectors **a**, **B**, and **C** comprise a set of three coplanar vectors. All three are within the rake plane R_s of the rack cutter. The triple scalar product of coplanar vectors is identical to zero $\mathbf{a} \times \mathbf{B} \cdot \mathbf{C} \equiv 0$. Therefore,

$$\mathbf{a} \times \mathbf{B} \cdot \mathbf{C} \equiv \begin{vmatrix} 1 & 0 & 0 \\ 0 & 1 & \tan \gamma_o \\ -\sin \phi_n & \cos \phi_n & \tan \lambda \end{vmatrix} = 0 \tag{9.16}$$

* Implementation of the vector method for the computation of the cutting edge geometry can be traced back to the mid-1940s and should be attributed to Mozhayev [46].

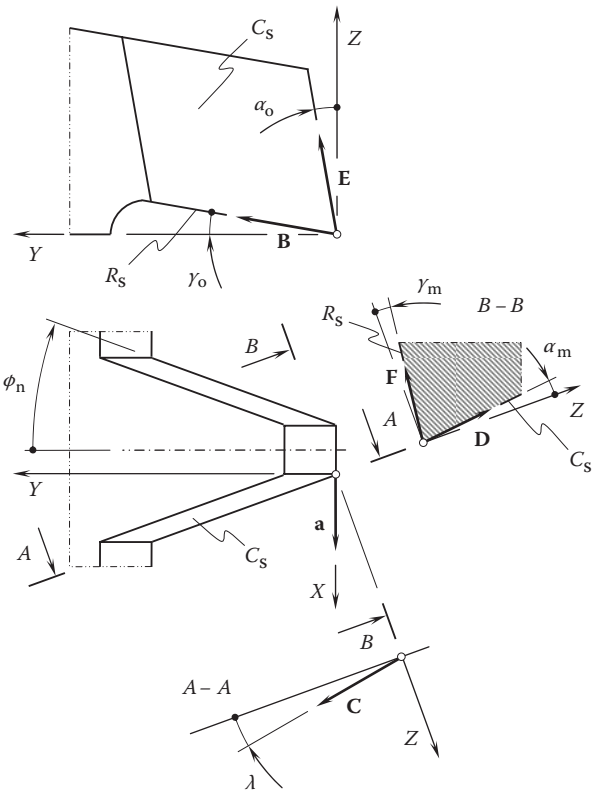

FIGURE 9.8
Cutting edge geometry for the lateral cutting edges of a rack cutter.

This expression [see Equation (9.16)] casts into the formula

$$\lambda = \tan^{-1}(\tan\gamma_o \cos\phi_n) \tag{9.17}$$

for the computation of the angle of inclination λ of the lateral cutting edge of the rack cutter tooth.

Second, an equation can be derived to compute for the actual value of the rake angle γ_m [136, 138, 143]. The angle γ_m is measured within the major section plane of the lateral cutting wedge of the rack cutter. For this purpose, a method similar to that just implemented for the derivation of Equation (9.17) can be used.

Consider the straight line of intersection of the rake plane R_s by the major section plane. (See Figure D.3 in Appendix D for details on the major section plane P_{ms}.) In Figure 9.8, the major section plane P_{ms} is designated as *B–B*. Vector **D** is aligned with this straight line (Figure 9.8).

The length of vector **D** is chosen so for which the projection of **D** onto the coordinate plane. *XY* is equal to unit, that is, $\text{pr}_{xy}\mathbf{D} = 1$. This yields an expression

$$\mathbf{D} = \mathbf{i}\cdot\cos\phi_n + \mathbf{j}\cdot\sin\phi_n + \mathbf{k}\cdot\tan\gamma_m \tag{9.18}$$

for the vector **D**.

By construction, the vectors **a**, **B**, and **D** comprise a set of coplanar vectors. Therefore, the scalar triple product of the vectors is equal to unit. Because of this, the expression $\mathbf{a} \times \mathbf{B} \cdot \mathbf{C} \equiv 0$ is valid. This expression yields representation in the form

$$\mathbf{a} \times \mathbf{B} \cdot \mathbf{D} \equiv \begin{vmatrix} 1 & 0 & 0 \\ 0 & 1 & \tan\gamma_o \\ \cos\phi_n & \sin\phi_n & \tan\gamma_m \end{vmatrix} = 0 \tag{9.19}$$

Equation (9.19) casts into the formula

$$\gamma_m = \tan^{-1}(\tan\gamma_o \sin\phi_n) \tag{9.20}$$

for the computation of the rake angle γ_m in the cross section of the lateral cutting edge of the rack cutter tooth by the major section plane P_{ms}.

Third, consider three vectors, **C**, **E**, and **F**, all of which are within the clearance surface C_s of the lateral cutting edge of the rack cutter tooth (Figure 9.8).

The vector **E** is along the line of intersection of the clearance plane C_s by the coordinate plane *YZ*. Vector **E** is of a length for which projection of **E** onto the *Z* axis is equal to unit ($\text{pr}_z\mathbf{E} = 1$). Because of this, in the coordinate system *XYZ* the following expression

$$\mathbf{E} = \mathbf{j} \cdot \tan\alpha_m + \mathbf{k} \tag{9.21}$$

is valid for vector **E**. Here, α_m denotes the clearance angle that is measured within the major section plane P_{ms} of the lateral cutting wedge of the rack cutter tooth [136, 138, 143].

The vector **F** is along the line of intersection of the clearance surface C_s by the major section plane P_{ms}. The magnitude of the vector **F** is chosen so for which projection of the vector **F** onto the coordinate plane *XY* is equal to unit, that is, $\text{pr}_{xy}\mathbf{F} = 1$. For the vector **F**, the expression

$$\mathbf{F} = \mathbf{i} \cdot \cos\phi_n + \mathbf{j} \cdot \sin\phi_n + \mathbf{k} \cdot \cot\alpha_m \tag{9.22}$$

can be easily composed.

By construction, three vectors, **C**, **E**, and **F**, are located within a common plane. Because of this, the identity $\mathbf{C} \times \mathbf{E} \cdot \mathbf{F} \equiv 0$ takes place. The identity yields representation in the form

$$\mathbf{C} \times \mathbf{E} \cdot \mathbf{F} \equiv \begin{vmatrix} -\sin\phi_n & \cos\phi_n & \tan\lambda \\ 0 & \tan\alpha_o & 1 \\ \cos\phi_n & \sin\phi_n & \cot\alpha_m \end{vmatrix} = 0 \tag{9.23}$$

Ultimately, to compute for the clearance angle α_m, the following formula

$$\alpha_m = \tan^{-1}\left[\frac{\sin\phi_n}{\cot\alpha_o - \tan\gamma_o \cos^2\phi_n}\right] \tag{9.24}$$

can be derived from Equation (9.23).

9.5.2 Possible Improvements in the Geometry of Lateral Cutting Edges

The derived equations make it possible to compute for the geometrical parameters of the cutting edges of rack cutters. The computations reveal that, for example, when the rake angle γ_o and the clearance angle α_o are in the range of 5–6°, the corresponding geometrical parameters γ_m and α_m measured in the major section are in the range of 2° or so. These values of angles γ_m and α_m are insufficient for high-performance gear cutting tools. Because of this, numerous modifications in the working surfaces of rack cutters are proposed to improve the geometry of lateral cutting edges.

Modifications of the rake surface. Improvement in the cutting edge geometry is the major purpose of rake surface modifications. To create favorable conditions for cutting, it is necessary to increase the rake angle γ_m at the lateral cutting edge of the rack cutter. For this purpose, round groves are ground along the lateral cutting edges CE of the coarse pitch rack cutters (for the rack cutters of module $m \geq 10$ mm) as shown in Figure 9.9. In this manner, an increased rake angle γ^* is created in the cross section of the lateral cutting edge by a plane that is perpendicular to the grinding wheel axis of rotation. The actual value of the rake angle γ^* depends on the diameter d_{gw} and the setup parameters of the grinding wheel. When the width of the ground grove is equal to a certain value a_{gr}, the rake angle γ^* of the value (Figure 9.10a)

$$\gamma^* = \sin^{-1}\left(\frac{a_{gr}}{d_{gw}}\right) \tag{9.25}$$

is created at the lateral cutting edge of the rack cutter.

For the modification of the rake surface R_s of rack cutters of module in the range of m = 10–24 mm, grinding wheels of diameters d_{gw} = 35–70 mm are usually suited. Width a_{gr} of the round grove is in the range of 7–15 mm. Under such a scenario, a rake angle γ^* in the range of 11°30′–12°30′ is created.

To eliminate distortions of the rack cutter tooth profile, a narrow land with a width of about 0.05 mm is retained along the lateral cutting edge CE of the rack cutter.

Fine pitch rack cutters could have entirely modified the rake surface R_s (Figure 9.10b). For this purpose, a cylindrical grinding wheel is used. Axis of rotation of the grinding wheel is at a certain angle with respect to the rake plane R_s. For this purpose, it is common

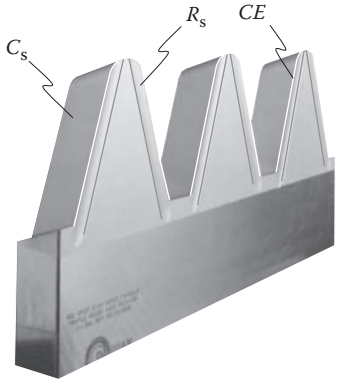

FIGURE 9.9
Modification to the rake surface R_s of the coarse pitch rack cutter for machining of spur gears.

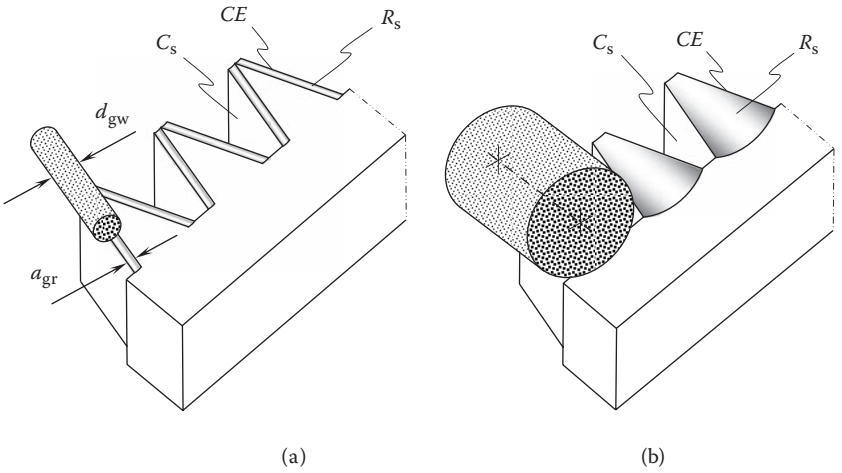

FIGURE 9.10
Parameters of the modification to the rake surface R_s of a rack cutter.

practice to use grinding wheels of diameter $d_{gw} = 8m$ mm. The axis of rotation of the grinding wheel is inclined at the angle of 4°10′ with respect to the rake plane R_s.

Because it is formed in this manner, the rake angle γ^* is not constant within the lateral cutting edge CE of the rack cutter. It is of minimal value in the vicinity of the top cutting edge, and of maximal value at the bottom of the rack cutter tooth. The width of the narrow land is also not constant along the lateral cutting edge.

Rack cutters for machining of helical gears with shoulders feature an increased positive rake angle $\gamma_m > 0°$ at one side of the tooth profile and negative rake angle $\gamma_m < 0°$ at the other side (Figure 9.11). For high-performance rack cutters of this type, modification of the rake surface is a must. The required modification is performed by grinding additional portions of the rake surface R_s (Figure 9.12). These portions are located close to the lateral cutting edges CE and have a favorable rake angle γ_m value.

Modifications of the clearance surface. Insufficient geometry of the clearance surface is among the major reasons cited for the limited cutting performance of rack cutters. Clearance angle α_o at the top cutting edge is usually in the range of 5–6°. Clearance angles α_m at the lateral cutting edge are commonly in the range of 2°. These ranges of clearance angle values are insufficient if high cutting performance of gear cutting tools is

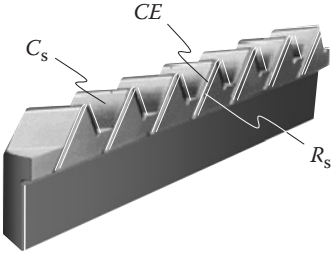

FIGURE 9.11
Rack cutter for machining helical gears with a shoulder.

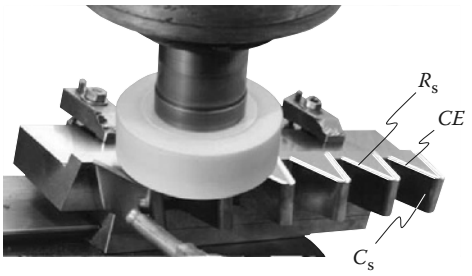

FIGURE 9.12
Grinding of the modified rake surface R_s of the rack cutter shown in Figure 9.11.

required. Considerable improvements in the cutting performance can be achieved with an appropriate modification of the clearance surfaces of rack cutters.

In the design of a standard rack cutter, clearance angle α_o at the top cutting edge CE and clearance angle α_m at the lateral cutting edge correlate to each other [see Equation (9.24)]. The desired increase in the clearance angle α_m requires a corresponding increase in the clearance angle α_o, which is often undesired.

A rack cutter shown in Figure 9.13 features the combined clearance surface through the top cutting edge. Clearance surfaces through the lateral cutting edges of the rack cutter tooth are designed so as to have an increased clearance angle α_m. For this purpose, the clearance angle α_o is increased in accordance with Equation (9.24). To eliminate the negative impact of the increased clearance angle α_o, an auxiliary clearance surface through the top cutting edge is designed. Clearance angle α_o^{eff} at this portion of the clearance surface is smaller than the clearance angle α_o, and the inequality $\alpha_o^{eff} < \alpha_o$ is observed. In this way, the clearance angles α_o and α_m are independent of each other. This makes it possible to assign actual values of the clearance angles α_o and α_m close to their optimal values. Ultimately, the cutting performance of the rack cutter (Figure 9.13) is higher compared to that of rack cutters of standard design.

An increased clearance angle α_m at the lateral cutting edges of the rack cutters makes it possible to cut gears with a modified tooth profile. For this purpose, the rack cutter tooth profile is also required to be modified. It is common practice to make the corresponding modification to the clearance surface of the rack cutter tooth. However, that same problem can be resolved by a corresponding alteration of the shape of the rake surface. In particular cases of gear machining, this option is preferred.

Figure 9.14 illustrates the tooth design of a rack cutter for machining gears having a modified tooth profile. Originally, the entire gear tooth profile is shaped in the form of an involute curve with a certain normal profile angle ϕ_n. A relatively short portion of the gear tooth profile next to the top land is modified. It is shaped in the form of an involute curve but with a slightly bigger profile angle $\phi_n^m > \phi_n$. For machining of a work gear having this type of modification in the tooth profile, it is possible to apply a rack cutter having the combined rake surface R_s [63]. For this purpose, it is necessary to determine the desired value of the rake angle γ_o^m. When the clearance angle α_m is increased, use of the rack cutter having the combined rake surface makes it possible to machine the modified gear tooth profile.

Consider the determination of the desired rake angle γ_o^m of the additional portion of the rake surface of the rack cutter tooth. It is assumed below that the nominal profile angle ϕ_n, the modified profile angle ϕ_n^m, the nominal rake angle γ_o, and the nominal clearance angle

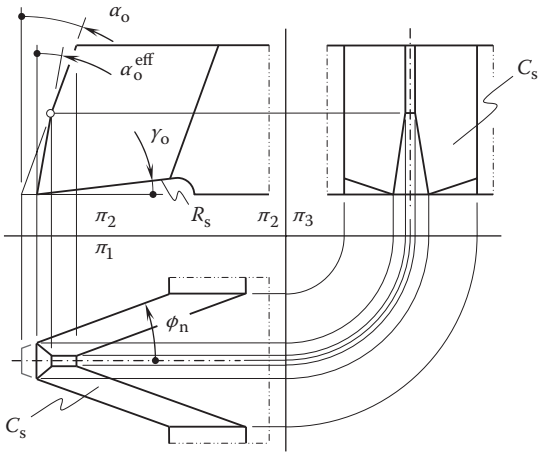

FIGURE 9.13
A rack cutter having an increased clearance angle at the lateral cutting edges.

α_o are known. It is necessary to express the desired rake angle γ_o^m of the auxiliary portion of the rake surface in terms of these design parameters of the rack cutter tooth.

For this purpose, it is convenient to construct three vectors, **A**, **b**, and **C**, as shown in Figure 9.14.

The vector **A** is along the major portion of the lateral cutting edge of the rack cutter tooth. It can be assumed that projection of the vector $\vec{\mathbf{A}}$ onto the coordinate plane XZ is equal to unit ($pr_{xz}\mathbf{A} = 1$). If so, vector **A** can be represented in the coordinate system XYZ associated with the rack cutter tooth in the form

$$\mathbf{A} = \mathbf{i} \cdot \tan \phi_n - \mathbf{j} \cdot \tan \gamma_o + \mathbf{k} \tag{9.26}$$

The unit vector **b** is along the line of intersection of the clearance surface of the rack cutter tooth by the major section plane P_{ms} (see Appendix D). Vector **b** can be expressed in terms of the clearance angle α_o as

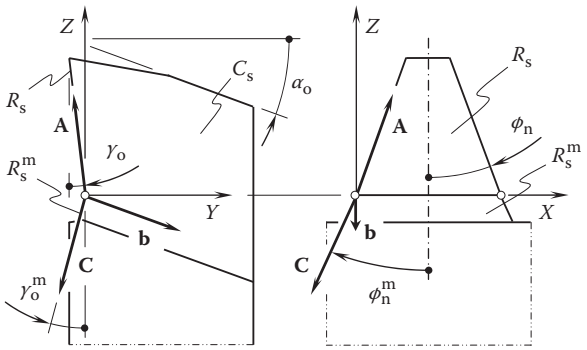

FIGURE 9.14
A rack cutter for machining of gears with modified tooth profile.

$$\mathbf{b} = \mathbf{j} \cdot \cos\alpha_o - \mathbf{k} \cdot \sin\alpha_o \tag{9.27}$$

The vector **C** is along the auxiliary portion of the lateral cutting edge of the rack cutter tooth. The auxiliary lateral cutting edge generates the modified portion of the work gear tooth. It is assumed below that projection of the vector **C** onto the coordinate plane *XZ* is equal to unit ($pr_{xz}\mathbf{C} = 1$). For the analytical representation of vector **C**, the following expression

$$\mathbf{C} = -\mathbf{i} \cdot \tan\phi_n^m - \mathbf{j} \cdot \tan\gamma_o^m - \mathbf{k} \tag{9.28}$$

can be composed.

By construction, vectors **A**, **b**, and **C** comprise a set of coplanar vectors. All are within the clearance plane of the lateral side profile of the rack cutter tooth. Consequently, the scalar triple product of the vectors is identical to zero ($\mathbf{A} \times \mathbf{b} \cdot \mathbf{C} \equiv 0$). The identity yields the expression

$$\mathbf{A} \times \mathbf{b} \cdot \mathbf{C} \equiv \begin{vmatrix} \tan\phi_n & -\tan\gamma_o & 1 \\ 0 & \cos\alpha_o & -\sin\alpha_o \\ -\tan\phi_n^m & -\tan\gamma_o^m & -1 \end{vmatrix} = 0 \tag{9.29}$$

To compute the desired value of the auxiliary rake angle γ_o^m, Equation (9.29) can be cast into

$$\gamma_o^m = \tan^{-1}\left[\frac{(1 - \tan\gamma_o \tan\alpha_o)k_m - 1}{\tan\alpha_o}\right] \tag{9.30}$$

where the coefficient of the tooth profile modification k_m is equal to $k_m = \tan\phi_n^m / \tan\phi_n$.

Equation (9.30) reveals that the greater the angles γ_o and α_o, the more easily the required modification of the rack cutter tooth profile can be achieved. This is the reason why it is recommended to use the modified rake surface (Figure 9.14) in the design of rack cutters having an increased clearance angle α_o.

9.6 Chip Thickness Cut by Cutting Edges of the Rack Cutter Tooth

Cutting of a work gear with the rack cutter is a type of a continuously indexing method of gear machining. When shaping a gear with the rack cutter (Figure 9.15), the work gear is rotating about its axis of rotation O_g. Rotation of the work is denoted in Figure 9.15 as ω_g.

The rack cutter is reciprocating in the direction that is tangent to the flank surface $\mathscr{G}$ of the gear tooth. The direction of the reciprocation $\mathbf{V}_{cut}$ of the rack cutter is parallel to the axis O_g when shaping spur gears. When machining helical gears, the direction of the reciprocation $\mathbf{V}_{cut}$ of the rack cutter is at the pitch helix angle ψ_g relative to the axis of rotation O_g of the work gear.

In addition to the reciprocation $\mathbf{V}_{cut}$, the rack cutter travels tangentially to the work gear. This translation motion $\mathbf{V}_c$ of the rack cutter, together with the rotation ω_g of the work gear, yields interpretation in the form of rolling with no sliding of the pitch plane of the rack

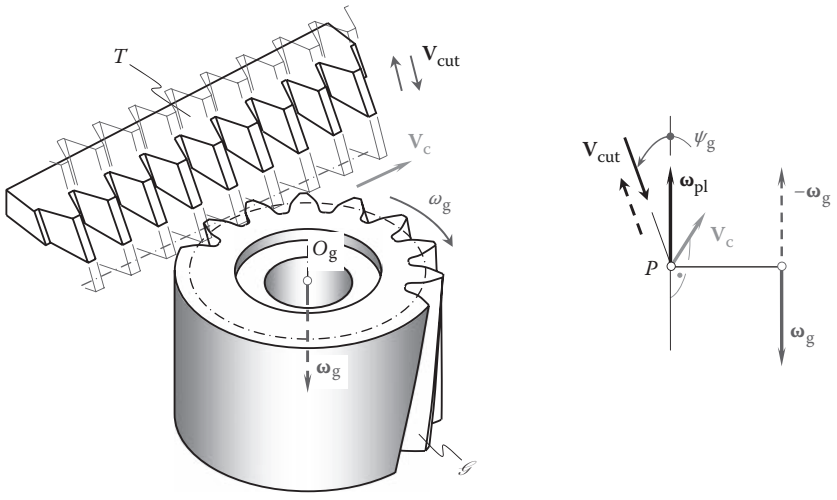

FIGURE 9.15
Machining of a helical gear with the rack cutter.

cutter over the pitch cylinder of the work gear. The rolling motion of the pitch surfaces of the rack cutter and the work gear affects the actual value of the chip thickness cut by cutting edges of the rack cutter.

For machining of work gear teeth, two motions must be performed in the gear machining process: (1) motion of cut and (2) feed motion.

Reciprocation of the rack cutter serves as the cutting motion $\mathbf{V}_{cut}$ in the gear machining operation (Figure 9.15). It provides the necessary speed of cut. Speed of cut is equal to the speed $\mathbf{V}_{cut}$ of the reciprocation of the rack cutter.

Feed motion in gear shaping is attributable to rolling of the pitch plane of the rack cutter over the pitch cylinder of the work gear. When the work gear is rotating about its axis O_g with the rotation ω_g, the rack cutter travels with a linear velocity $\mathbf{V}_c$ (Figure 9.16). No sliding is observed in the rolling motion of pitch surfaces.

Rolling of pitch surfaces can be interpreted as the instant rotation of the generating surface T of the rack cutter about pitch point P. Speed of instant rotation ω_{rl} can be expressed in terms of speed of translational motion $V_c = |\mathbf{V}_c|$ and radius of the pitch cylinder $R_{w.g}$ of the work gear

$$\boldsymbol{\omega}_{rl} = \frac{V_c}{R_{w.g}} \tag{9.31}$$

Because the equality $V_c = \omega_g R_{w.g}$ is observed, the speed of instant rotation is equal to the speed of work gear rotation ($\omega_{rl} = \omega_g$).

Speed of feed motion $F_c = |\mathbf{F}_c|$ is equal to speed of linear motion of the cutting edge of the rack cutter tooth when it is performing the instant rotation ω_{rl}

$$F_c = \boldsymbol{\omega}_{rl} R_{rl} \tag{9.32}$$

where R_{rl} denotes the distance of a point of interest m within the cutting edge CE of the rack cutter tooth from pitch point P. The point of interest can be located within any of the three cutting edges of the rack cutter tooth.

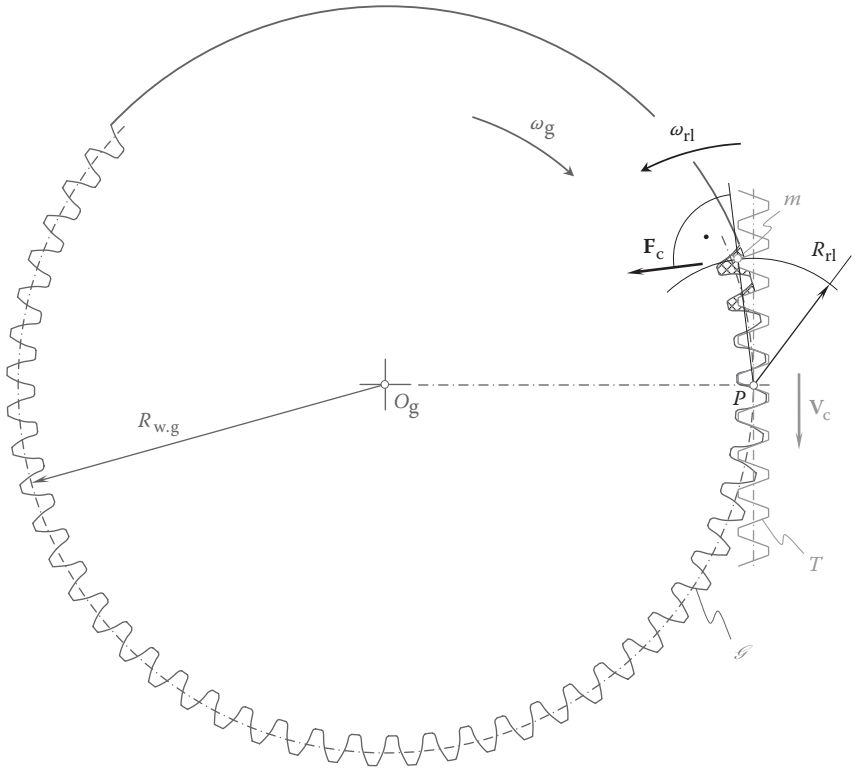

FIGURE 9.16
Feed motion F_c when machining a spur gear with the rack cutter.

When machining a work gear with the rack cutter, instant rotation occurs with a constant speed ω_{rl}. This means that the equality $\omega_{rl} = const$ takes place.

Different points of the cutting edge of the rack cutter are remote at different distances from pitch point *P*, that is, the equality $R_{rl} = \text{var}$ is valid. This means that the magnitude of the instant feed motion F_c depends on the coordinates of the point of interest *m* within the cutting edge of the rack cutter tooth. Moreover, orientation of the position vector $\mathbf{r}_m$ of the point of interest is a function of the coordinates of point *m*. Because the direction of the instant feed motion F_c is perpendicular to the position vector $\mathbf{r}_m$, the direction of the motion $\mathbf{F}_c$ at different points of the cutting edge is also different. To determine the direction of the feed rate motion $\mathbf{F}_c$, use of the equality

$$\mathbf{F}_c = \boldsymbol{\omega}_{rl} \times \mathbf{r}_m \tag{9.33}$$

is helpful.

Next, parameters of a portion of the stock cut out by the rack cutter tooth per one stroke can be computed. For this purpose, the implementation of the approach proposed by Shishkov [186] is important.

To compute for the thickness of cut, it is convenient to consider two consequent locations of the rack cutter. Location of the rack cutter in its initial position can be specified by the configuration of a Cartesian coordinate system $X_gY_gZ_g$ associated with the work gear (Figure 9.17). During one of the reciprocation strokes of the rack cutter, the work gear turns

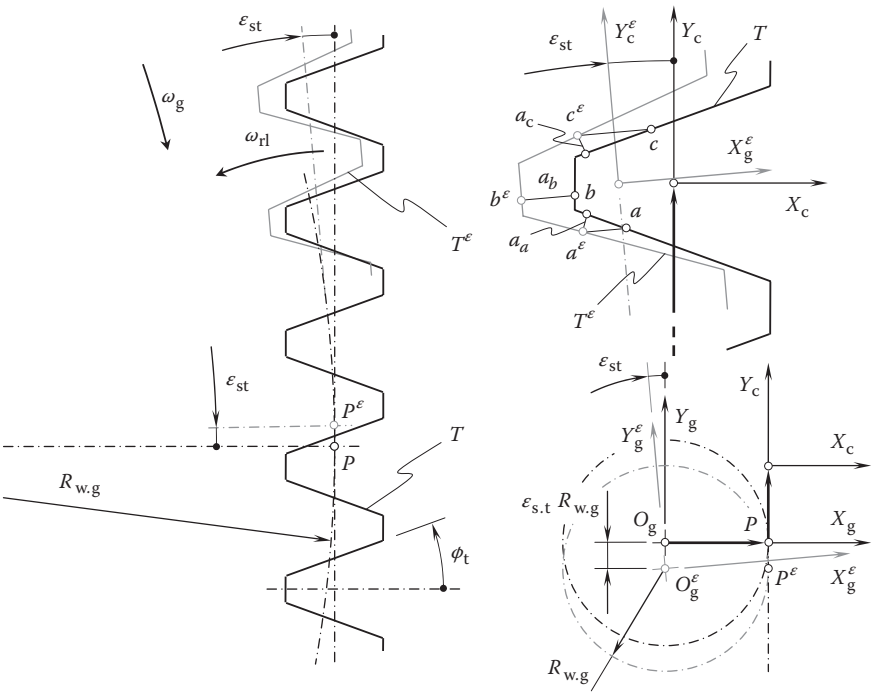

FIGURE 9.17
Thickness of cut when machining a spur work gear with the rack cutter.

about its axis of rotation O_g through a certain angle ε_{st}. The angle ε_{st} is a portion of the roll angle ε. In other words, the angle ε_{st} can be interpreted as a roll angle per stroke of the rack cutter. The actual value of the angle ε_{st} depends on the difference $(\varepsilon_o - \varepsilon_l)$ between the roll angle ε_o at the outer diameter of the gear tooth profile and the roll angle ε_l at the inner diameter of the gear tooth. It also depends on the number of strokes of the rack cutter n_{st} that is required for machining of the entire tooth flank surface

$$\varepsilon_{st} = \frac{\varepsilon_o - \varepsilon_l}{n_{st}} \tag{9.34}$$

Angle ε_{st} is small and its value is in the range of $\varepsilon_{st} \cong 1°$ or so. It can vary depending on the requirements of the particular gear planing operation.

When rotating, the work gear is traveling along the pitch line. Because rolling with no sliding of the pitch surfaces is observed, the travel distance of the gear axis of rotation from the initial position O_g to its current position O_g^ε is equal to $\varepsilon_{st}R_{w.g}$, where $R_{w.g}$ denotes the pitch radius of the work gear in the gear machining operation.

For the analytical description of the translation of the coordinate system at the distance $\varepsilon_{st}R_{w.g}$, the operator of translation $\mathbf{Tr}(\varepsilon_{st}R_{w.g}, Y_g)$ can be used. Accordingly, the operator of the rotation $\mathbf{Rt}(\varepsilon_{st}, Z_g)$ can be implemented for the analytical description of the rotation of the coordinate system through the angle ε_{st}. The resultant linear transformation in the case under consideration can be analytically described by two operators of the linear transformations $\mathbf{Tr}(\varepsilon_{st}R_{w.g}, Y_g)$ and $\mathbf{Rt}(\varepsilon_{st}, Z_g)$. For simplification, only one operator of rolling*

* See Chapter 4 for details on the operators of rolling.

$\mathbf{Rl}_y(\varepsilon_{st}, Z_g)$—and not both operators—is used (Figure 9.17). Ultimately, use of the operator of rolling $\mathbf{Rl}_y(\varepsilon_{st}, Z_g)$ allows for transformation from the coordinate system $X_gY_gZ_g$ in its initial location to the same coordinate system in its current location. The last is designated as $X_g^{\varepsilon}Y_g^{\varepsilon}Z_g^{\varepsilon}$.

Furthermore, consider a point of interest within the cutting edge of the rack cutter tooth. This might be a point a within the lateral cutting edge of the rack cutter tooth, or a point b within the top cutting edge, or a point c within the lateral cutting edge of the opposite side of the tooth profile (Figure 9.17). To specify the coordinates of the point of interest, use of the local coordinate system $X_cY_cZ_c$ is often helpful.

The position vector $\mathbf{r}_a$ of the point of interest a for a certain configuration of the generating surface T is known. (The same is valid with respect to any other point of interest.) Equation (9.7) allows for computation of the unit normal vector $\mathbf{n}_{T.a}$ to the surface T at point a. When cutting a work gear with the rack cutter, the pitch plane of the rack T rolls with no sliding over the pitch cylinder of the gear. For the consequent stroke of cutting, the rack cutter turns through the roll angle ε_{st} and travels through the distance $\varepsilon_{st}R_{w.g}$. In the new position, the generating surface of the rack cutter is designated as T^{ε}. During the rolling, the point of interest a moves to the position a^{ε}. The position vector $\mathbf{r}_a^{\varepsilon}$ of the point of interest in the new location of the rack cutter can be expressed in terms of the position vector $\mathbf{r}_a$ and the operator of rolling $\mathbf{Rl}_y(\varepsilon_{st}, Z_g)$ in the following manner

$$\mathbf{r}_a^{\varepsilon} = \mathbf{Rl}_y(\varepsilon_{st}, Z_g) \cdot \mathbf{r}_a \tag{9.35}$$

Similarly, the following expression

$$\mathbf{n}_{T.a}^{\varepsilon} = \mathbf{Rl}_y(\varepsilon_{st}, Z_g) \cdot \mathbf{n}_{T.a} \tag{9.36}$$

is valid for the unit normal vector $\mathbf{n}^{\varepsilon}{}_{T.a}$ to the generating surface T^{ε} through point a^{ε}.

The direction along which thickness of cut is measured is perpendicular to the machined surface of the work gear. The direction varies within the cutting edge of the rack cutter. At point a^{ε}, thickness of cut is denoted as a_a. Corresponding designations a_b and a_c are used to denote the thickness of cut at points b^{ε} and c^{ε}, respectively.

Thickness of cut a_a is equal to the length of the straight-line segment between point a^{ε} and surface T. The point of interception of the straight line $\mathbf{a}_a(t)$ through point a^{ε} along the unit normal vector $\mathbf{n}_{T.a}^{\varepsilon}$

$$\mathbf{a}_a(t) = \mathbf{r}_a^{\varepsilon} + t \cdot \mathbf{n}_{T.a}^{\varepsilon} \tag{9.37}$$

is shown (but is not labeled) in Figure 9.17. Here, t denotes the parameter of the straight line.

The equation for the generating surface T of the rack cutter [Equation (9.7) describes only one lateral flank of the surface T; a similar equation is valid for the opposite flank of the tooth of the surface T; and the equation for the top land of surface T is a trivial one], together with Equation (9.37), returns the position vector $\hat{\mathbf{r}}_a^{\varepsilon}$ of the point of interception of the straight line $\mathbf{a}_a(t)$ with the generating surface T. This immediately yields a formula

$$a_a = |\mathbf{r}_a^{\varepsilon} - \hat{\mathbf{r}}_a^{\varepsilon}| \tag{9.38}$$

for the computation of thickness of cut at the point of interest m within the cutting edge of the rack cutter tooth.

Equation (9.38), used for the computation of the thickness of cut at a point of interest of the cutting edge of the rack cutter, is derived with no simplifications, and it is an accurate one. It can be used when the point of interest is a far remote point from the pitch point in a gear shaping operation and the chip to be cut is thick. It is also valid when the point of interest is close to the pitch point and the cutting edge—cut thin chip—when the chip thickness is in the range close to the roundness of the cutting edge.

For approximate computations, simpler equations are known. However, the equations are applicable for remote portions of the cutting edges and thus, are not applicable for portions of the cutting edges close to the pitch point or, alternatively, they are applicable for points of the cutting edge close to the pitch point, and are therefore not applicable for remote portions of the cutting edges of the rack cutter.

Equation (9.38) can be used to compute all the other parameters of the portion of the stock that has been removed by a cutting edge of the rack cutter: shape of the cross section of the portion of the stock, its area, etc.

Thickness of cut is important because it significantly affects tooth wear of the rack cutter.

Cutting edges of the rack cutter teeth cut chips of varying thickness.

First, thickness of cut depends on the distance between the point of interest and the pitch point. The greater the distance, the larger the cut thickness becomes.

Second, different cutting edges of the rack cutter tooth cut chips of varying thickness. The top cutting edge cuts the thickest chip. Thickness of chip that is cut by the lateral cutting edge of the entering side of the tooth profile is larger rather than that of the recessing side of the rack cutter tooth profile.

Lateral cutting edges of the rack cutter teeth cut the stock mostly within the distance between the pitch point and the point where the cutting begins. A small amount of the stock is also cut beyond the pitch point. The top land cutting edge does not cut the stock beyond the pitch point.

A detailed analysis of chip thickness is beyond the scope of the book. This issue requires discussion in a separate book.

9.7 Accuracy of the Machined Gear

Accuracy of the machined gear is discussed here from the standpoint of the kinematic geometry of surface generation.

When cutting a work gear with the rack cutter of conventional design, most of the conditions of proper part surface generation (*PSG*) can be easily satisfied. Usually, it is not necessary to verify whether all of them are satisfied or if some of then are violated. In particular cases of gear machining with the rack cutter, only the fifth and sixth conditions of proper *PSG* are required to be satisfied in more careful analyses (see Appendix B for details on conditions of proper *PSG*).

9.7.1 Satisfaction of the Fifth Condition of Proper *PSG*

To satisfy the fifth condition of proper *PSG*, no intersection of the adjacent portions of the tooth profile of the generating surface T of the rack cutter has to be observed. When machining a work gear with the rack cutter, the pitch plane of the rack cutter is rolling

with no sliding over the pitch cylinder of the work gear. Violation of the fifth condition of proper *PSG* occurs mostly because the pitch surfaces roll over each other.

Teeth of the gear to be machined can be considered as a certain number N_g of portions of the circular cylinder surface (root lands as well as top lands), and the same number N_g of the right-hand–oriented and left-hand–oriented screw involute flank surfaces $\mathscr{G}$. Therefore, the generating surface T of the rack cutter is composed of N_c portions of the plane surface (root lands and top lands) and that same number N_c of pairs of lateral planes T. When machining a work gear, the lateral surface makes contact with the different portions of the gear tooth surface $\mathscr{G}$.

Various relative configurations of adjacent portions of the tooth profile of the generating surface T of the rack cutter can be observed. The adjacent portions of the tooth profile of the surface T can

(1) Share no common points, that is, they can be apart from each other

(2) Be connected to each other at the endpoints

(3) Intersect each other

In items (1) and (2), no violation of the fifth condition of proper *PSG* occurs. In item (3), intersection of the adjacent portions of the rack cutter tooth profile is observed. Due to the intersection, the fifth necessary condition of proper *PSG* is violated. Ultimately, violation of the fifth condition of proper *PSG* results in the occurrence of transient curves on the gear tooth.

For example, for the generation of the involute gear tooth profile, the generating surface T of the rack cutter having a transverse profile angle ϕ_t is used. The desired tooth profile of the surface T is composed of three straight-line segments (Figure 9.18): left-side lateral straight-line segment $a_l^* b_l^*$, top land straight-line segment $a_l^{**} a_r^{**}$, and right-side lateral straight-line segment $a_r^* b_r^*$. The straight-line segments intersect each other at points f_l^* and f_r^* as shown in Figure 9.18. Therefore, the portions $a_l^* b_l^*$ and $a_l^{**} f_l^*$ as well as the portions $a_r^* f_r^*$ and $a_r^{**} f_r^*$ of the rack cutter tooth profile do not exist physically. This results in the portions $a_l c_l$ and $a_r c_r$ of the gear tooth profiles $a_l b_l$ and $a_r b_r$ (Figure 9.18) being substituted with the transient curves $c_l d_l$ and $c_r d_r$ that form the fillets.* For the same reason, the portions $a_l d_l$ and $a_r d_r$ of the cylinder root land are also replaced with the transient curves $c_l d_l$ and $c_r d_r$.

To satisfy the fifth condition of proper *PSG*, it is required to keep the transient curve between the circle of root diameter $d_{f.g}$ and the circle of limit diameter $d_{l.g}$. This criterion can be stated analytically as

$$[\Delta] \le 0.5 (d_{l.g} - d_{f.g}) \tag{9.39}$$

When the inequality (9.39) is satisfied, the fifth condition of proper *PSG* is satisfied as well, and thus, the work gear can be machined with the rack cutter in compliance with the blueprint specification. Therefore, expression (9.39) is vital for the computation of the desired design parameters of the rack cutter.

The inequality (9.39) can also be used for the determination and graphical interpretation of a zone of variation (a) of the rack cutter profile angle ϕ_t and (b) of the work gear tooth number N_g, within which the fifth condition of proper *PSG* is satisfied.

* Reminder: The start of active profile (*SAP*) is the intersection of the limit diameter and the involute profile (Figure 9.18). Points c_l and c_r within the circle of limit diameter $d_{l.g}$ are the points of *SAP*.

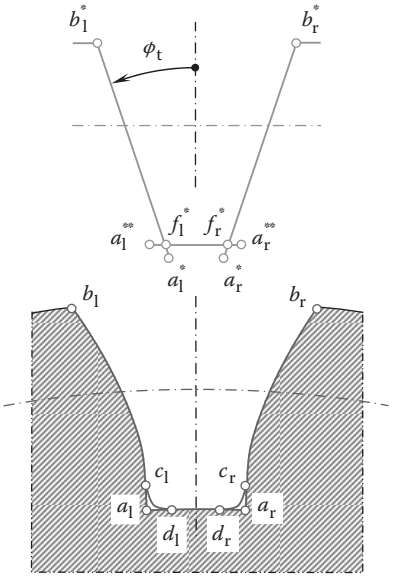

FIGURE 9.18
Intersection of the adjacent cutting edges of the rack cutter tooth results in the occurrence of transient curves.

Consider the generation of a gear tooth profile with a rack cutter (Figure 9.19). The left-hand side of the work gear tooth profile is generated along the active portion of the left-hand side line of action LA_l. Similarly, the right-hand side of the gear tooth profile is generated within the active portion of the right-hand side line of action LA_r. The tooth profile of the rack cutter does not project beyond the work gear root circle of diameter $d_{f.g}$. Because of this, portions of the active lines of action LA_l and LA_r cannot be represented in the gear machining operation. Therefore, within these portions of lines of action, the generation of the transient curves of a certain height Δ is unavoidable.

An equation can be derived for the computation of the height of the transient curve.

Analysis of the *gear-to-rack cutter* meshing diagram (Figure 9.19) allows us to compose two equations for the lines of action LA_l and LA_r, as well as an equation for the root circle of diameter $d_{f.g}$. These equations yield the formula

$$\Delta = 0.5\left(\sqrt{\left(d_{f.g} - \frac{d_{b.g}}{\cos\phi_t}\right)^2 \cot^2\phi_t + d_{f.g}^2} - d_{f.g}\right) \tag{9.40}$$

for the computation of the actual value of the deviation Δ.

Analysis of the gear-to-rack cutter meshing diagram also allows for a convenient graphical interpretation of a zone within which the fifth condition of proper *PSG* in gear planing operation is satisfied.

The maximum value of the deviation Δ is limited to its maximal allowed value $[\Delta]$. This means that the interval $0 \le \Delta \le [\Delta]$ is the permissible interval for the deviation Δ. The last inequality can be expressed in terms of the design parameters of the rack cutter and of the work gear.

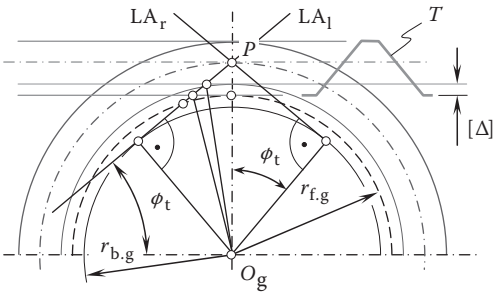

FIGURE 9.19
Gear-to-rack cutter meshing diagram.

To keep the deviation Δ within the allowed range $0 \le \Delta \le [\Delta]$, the transversal profile angle of the rack cutter teeth has to satisfy the inequality (Figure 9.19):

$$\frac{d_{f.g}d_{b.g} - A_c}{(d_{f.g} + 2[\Delta])^2} \le \cos\phi_t \le \frac{d_{f.g}d_{b.g} + A_c}{(d_{f.g} + 2[\Delta])^2} \tag{9.41}$$

where $A_c = \sqrt{d_{f.g}^2 d_{b.g}^2 - (d_{f.g} + 2[\Delta])^2 (d_{b.g}^2 - 4d_{f.g}[\Delta] - 4[\Delta]^2)}$.

As an example, consider planing of a spur involute gear of modulus $m = 10$ mm having normal pressure angle $\phi_g = 20°$, tooth number $N_g = 75$, and radial clearance $c = 0.25$ m. The rest of the design parameters of the gear can be computed: pitch diameter $d_{w.g} = mN_g = 750$ mm, outer diameter $d_{a.g} = d_{w.g} + 2m = 770$ mm, root diameter $d_{f.g} = d_{w.g} - 2 \cdot 1.25m = 725$ mm, base diameter $d_{b.g} = d_{w.g}\cos\phi_g = 704.769$ mm. For machining of the spur involute gear, use of expression (9.41) allows for the computation of the following permissible interval for the rack cutter transverse pressure angle $8.398° \le \phi_t \le 21.817°$. Machining of the work gear with the rack cutter having a transverse pressure angle within the computed interval $8.398° \le \phi_t \le 21.817°$ results in a deviation Δ that is within the radial clearance $\Delta < c$.

Similar computations can be performed for the case of machining of a gear with a different tooth number N_g. Results of computations can be interpreted graphically in the form of the allowed zone within which the fifth condition of proper *PSG* is satisfied. Figure 9.20 illustrates an example of the allowed zone. The allowed zone in Figure 9.20 is computed for the case of machining of a spur involute gear having a profile angle $\phi_g = 20°$ and cut with the rack cutter having tooth profile angle ϕ_t. The deviation Δ of the gear tooth is within the tolerance $0 \le \Delta \le [\Delta] = 0.25m$. A similar allowed zone can be constructed for the case of machining of spur and/or helical gear of any design.

Application of the rack cutter, design parameters of which correspond with the design parameters of the work gear [see inequality (9.41)], results in an increased accuracy of the machined gear.

9.7.2 Satisfaction of the Sixth Condition of Proper *PSG*

When machining a work gear with the rack cutter, a discrete type of generation of the gear tooth flank is observed. The machined gear tooth flank is shaped in the form of numerous straight cuts, each of which is tangent to the desired involute tooth form. Cusps on the machined gear tooth flanks are unavoidable when a gear is cut with the rack cutter.

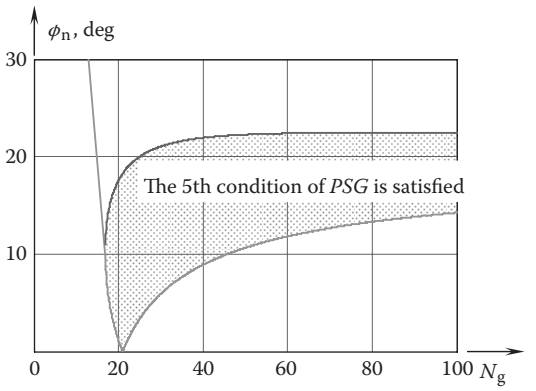

FIGURE 9.20
Zones of satisfaction and violation of the fifth condition of proper *PSG* in a gear planing operation.

For satisfaction of the sixth condition of proper *PSG* (see Appendix B), cusp height on the machined gear tooth flank must be within the allowable range for accuracy on the tooth flank. The cusp height can also be interpreted as the deviation of the actual gear tooth surface from the desired tooth surface. From this standpoint, cusps cause the low accuracy of the machined gear.

To verify whether the sixth condition of proper *PSG* is satisfied, determination of the actual cusp height is required.

Consider the tooth of the gear being machined (Figure 9.21). At an arbitrary point of the gear tooth profile, say at point *i*, the cutting edge of the rack cutter is tangent to the involute profile of the gear tooth. On the next stroke, the cutting edge of the rack cutter is tangent to the gear tooth profile at the adjacent point $(i + 1)$. Perpendiculars to the involute tooth profile at points *i* and $(i + 1)$ form the angle that is equal to the roll angle per stroke ε_{st} of the rack cutter. Ultimately, when the machining process is over, the desired smooth involute gear tooth profile is substituted with a polygonal shape. Deviation of the actual gear tooth profile with respect to the desired tooth profile is denoted by h_{ss}. The deviation h_{ss} is measured along the perpendicular to the desired gear tooth surface that passes through the point of intersection of the *i*th and $(i + 1)$-th cuts.

For the computation of the deviation h_{ss}, it is convenient to implement the straight-line segment through points *i* and $(i + 1)$. Actually, only the length of the straight-line segment is of importance if we are about to solve the problem under consideration.

Position vector of point *i* is designated as $\mathbf{R}_i$. Analytically, the vector $\mathbf{R}_i$ can be expressed as

$$\mathbf{R}_i = \mathbf{r}_{b.i} \cdot r_{b.g} + \mathbf{t}_{b.i} \cdot r_{b.g} \varepsilon_i \tag{9.42}$$

where $\mathbf{r}_{b.i}$ and $\mathbf{t}_{b.i}$ denote the unit vectors in the corresponding directions.

In projections onto coordinate axes of the reference system $X_g Y_g Z_g$, Equation (9.42) casts into

$$\mathbf{R}_i = \mathbf{i} \cdot r_{b.g}(\sin \varepsilon_i - \cos \varepsilon_i) + \mathbf{j} \cdot r_{b.g}(\sin \varepsilon_i + \cos \varepsilon_i) \tag{9.43}$$

Similarly, for the position vector $\mathbf{R}(i+1)$ of the point $(i+1)$, the following expression

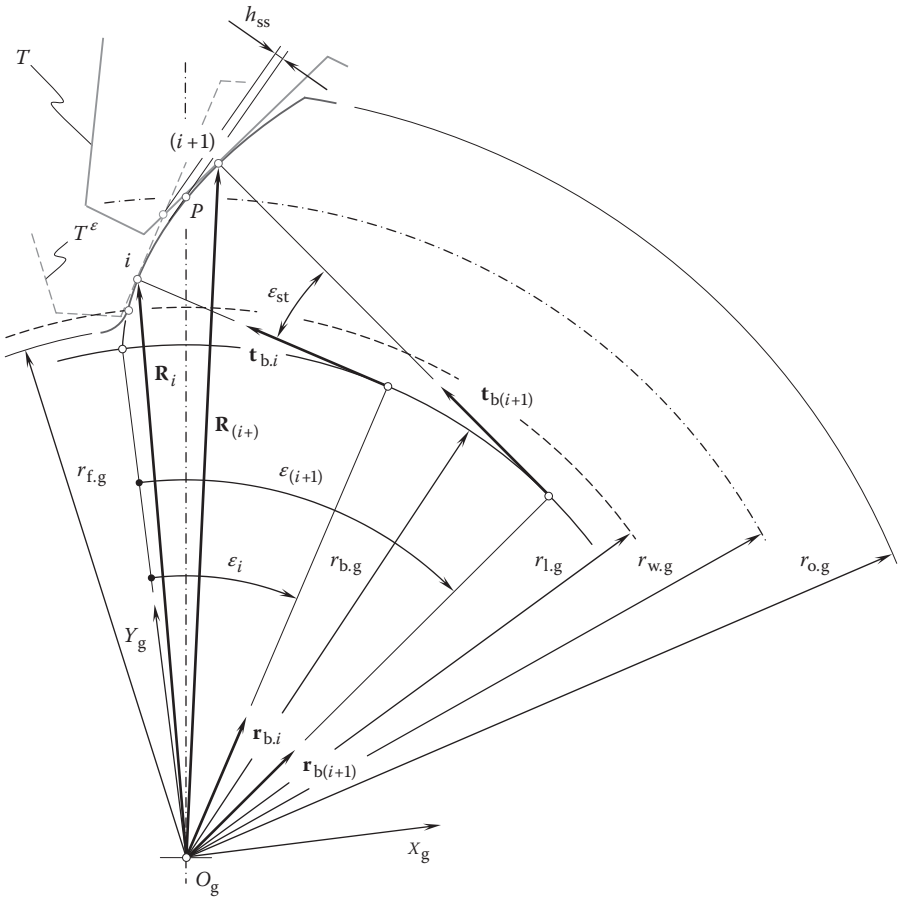

FIGURE 9.21
Major parameters of the discrete generation of the gear tooth profile with the rack cutter.

$$\mathbf{R}_{(i+1)} = \mathbf{i} \cdot r_{b.g}[\sin \varepsilon_{(i+1)} - \cos \varepsilon_{(i+1)}] + \mathbf{j} \cdot r_{b.g}[\sin \varepsilon_{(i+1)} + \cos \varepsilon_{(i+1)}] \tag{9.44}$$

can be composed.

Distance between the points i and $(i+1)$ is equal to $|\Delta\mathbf{R}_i|$ (Figure 9.22). Here, the equality

$$|\Delta\mathbf{R}_i| = |\mathbf{R}_i - \mathbf{R}_{(i+1)}| \tag{9.45}$$

is valid.

Once the distance $|\Delta\mathbf{R}_i|$ is computed, an expression

$$h_{ss} = 0.5\sqrt{r_{b.g}^2[\varepsilon_i + \varepsilon_{(i+1)}]^2 \sin^2(0.5\varepsilon_{st}) - |\Delta\mathbf{R}_i|^2} \tag{9.46}$$

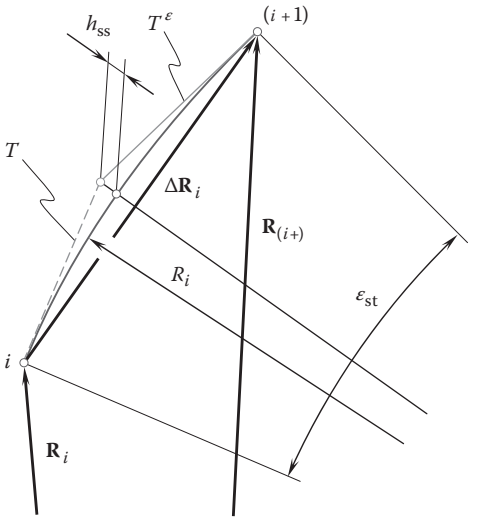

FIGURE 9.22
Geometry of an elementary cusp on the machined gear tooth profile.

for the computation of cusp height h_{ss} immediately follows from the analysis in Figure 9.22.

The sixth condition of *PSG* is satisfied if and only if the inequality

$$h_{ss} \leq [h_{ss}] \tag{9.47}$$

is valid.

9.8 Application of Rack Cutters

The rack cutter, mounted in a clapper box, reciprocates while the gear rolls past its cutting field. Cutting generally takes place during the downstroke, and the clapper box clears the tool from the work on the upstroke (see Figure 9.15).

Rack cutters of three types are used: (1) rough rack cutters, (2) finish rack cutters, and (3) pregrind rack cutters. To compute for the design parameters of rack cutters, the following expressions (Figure 9.23)

$$\frac{t_{finish} - t_{rough}}{2} = 0.2\sqrt{m} \tag{9.48}$$

$$\frac{t_{finish} - t_{grind}}{2} = 0.1\sqrt{m} \tag{9.49}$$

are commonly used.

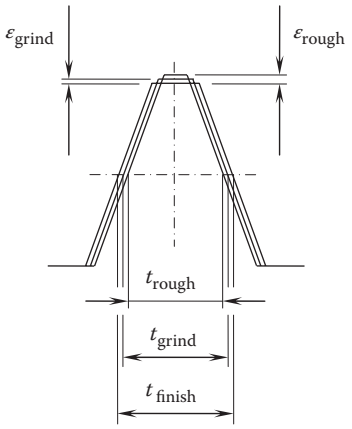

FIGURE 9.23
Tooth profiles of rough rack cutters, finish rack cutters, and pregrind rack cutters.

An increase in tooth height for roughing rack cutters is $\varepsilon_{\text{rough}} = 0.2\sqrt{m}$ mm, and for grind rack cutters it is $\varepsilon_{\text{grind}} = 0.1\sqrt{m}$ mm.

Use of rack cutters makes it possible to machine any gear with continuous indexing and with no interruption of the machining process. For this purpose, at the end of every stroke of the rack cutter it is necessary to turn the work gear about its axis through an angle that corresponds to one tooth of the work gear. This additional discrete indexing is superposed with the original continuous indexing.

A rack shaper cuts only a few teeth in one generating cycle, then indexes to pick up the next teeth. The number of teeth per generation, the number of strokes per tooth (feed), and the stroking speed are all individually variable.

The most common use for rack shapers is for coarse pitches, high hardness material, and narrow-gap double helical gears. It is also ideal for cutting segments, since only the toothed portion must be rolled past the tool. The rack shaper can also machine two- and three-lobe rotors, as a result of the large tool size and the large number of strokes per tooth.

The indexing time varies from about 0.08 min on small machines to about 1.0 min on large machines. When finishing high-precision gears, the machines are indexed once per tooth so that the same tool finishes all the gear teeth, thereby preventing tool pitch errors or mounting errors from being transferred to the gear. In roughing, more teeth may be cut per index, depending on the gear diameter and tooth size.

The fewer the strokes, the larger the generating marks on the given tooth. Gears of 100 to 200 teeth have almost straight-line profiles, whereas smaller numbers of teeth have more profile curvature. For this reason, it is necessary to use more strokes per tooth when finishing gears having small numbers of teeth. In fine pitches, the roughing cuts do not remove too much metal. This makes it possible to use fewer strokes per tooth in roughing than in finishing. In coarse pitches, however, a substantial amount of metal has to be removed in roughing. This makes it necessary to use more strokes per tooth in roughing than in finishing. With heavy-duty machines, however, coarse pitch "gashing" is usually carried out with step-type plunge cutters, which can remove a large volume of material with fewer strokes per tooth.

9.9 Potential Methods of Gear Cutting and Designs of Rack-Type Gear Cutting Tools

Investigation of the kinematics of the parallel-axis gear machining mesh is the key for the development of novel methods of gear machining, and novel designs of gear cutting tools for these methods. A particular case of gear machining mesh that is schematically depicted in Figure III.1d is discussed above. By adding a cutting motion, this simple gear machining mesh is enhanced to a corresponding kinematics of a gear machining process. More opportunities are available there for a gear engineer, especially when considering the cutting motion that is represented by a translation vector, a rotation vector, or combinations of these two vectors. Depending on the actual configuration of the vector of cutting motion, various methods of gear cutting and various designs of gear cutting tools for these methods can be developed. As shown in Figure 9.15, even the simplest case of cutting a gear with a rack cutter allows for significant improvements. A method of gear cutting on G-TRAC generator, created by Gleason Works, is a perfect example in this concern [15]. Rack-type cutting tools mounted on an endless chain are used in this method of gear machining. The gear being cut rolls in mesh with the passing rack teeth assembled in the chain. The method is intended for high volume production, low tool cost, and high accuracy of machining. It is possible, though, to use the method effectively for small production. In this last case, a single row of cutting tools is used, and one tooth slot is formed at a time.

In a conventional gear planing operation, the reciprocation of the rack cutter is utilized as the cutting motion. Work gears having a narrow face width can be generated with round rack cutters or with gang milling cutter, as schematically shown in Figure 9.24. In this case, it is not the reciprocation of the cutting tool, but the rotation $\boldsymbol{\omega}_{cut}$ that is used as the primary motion. Vector representation of the kinematics of the gear machining operation (Figure 9.24a), the work gear in mesh with the gear cutting tool (Figure 9.24b), as well as the gear cutting tool itself (Figure 9.24c), are illustrated in this figure. Gear cutting tools of this type have limited application for machining of gears under specific manufacturing conditions. However, an operation featuring the kinematics of the gear machining opera-

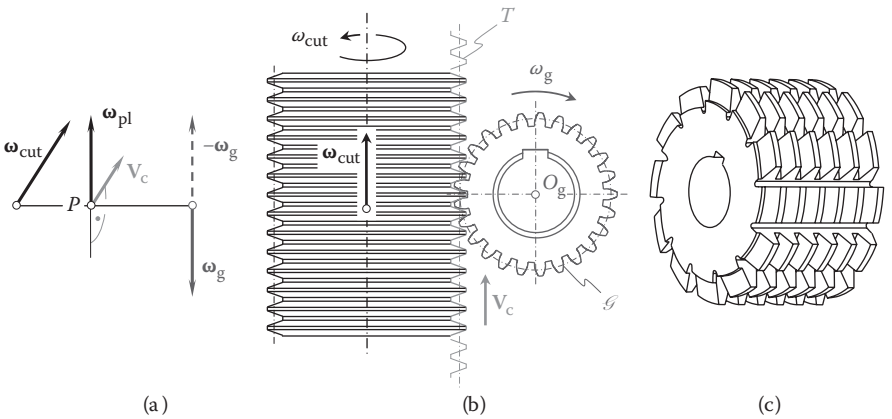

FIGURE 9.24
Kinematics of milling/grinding of a work gear having a narrow face.

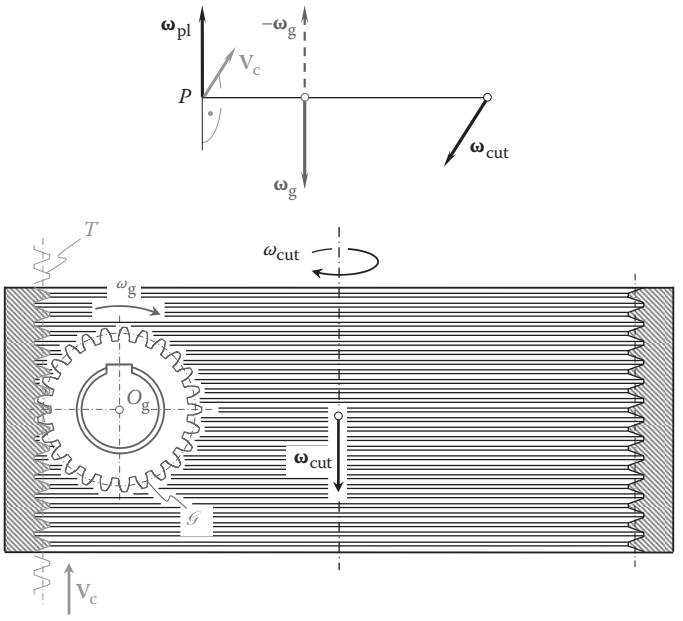

FIGURE 9.25
Kinematics of milling/grinding of a work gear with an enveloping gear cutting tool.

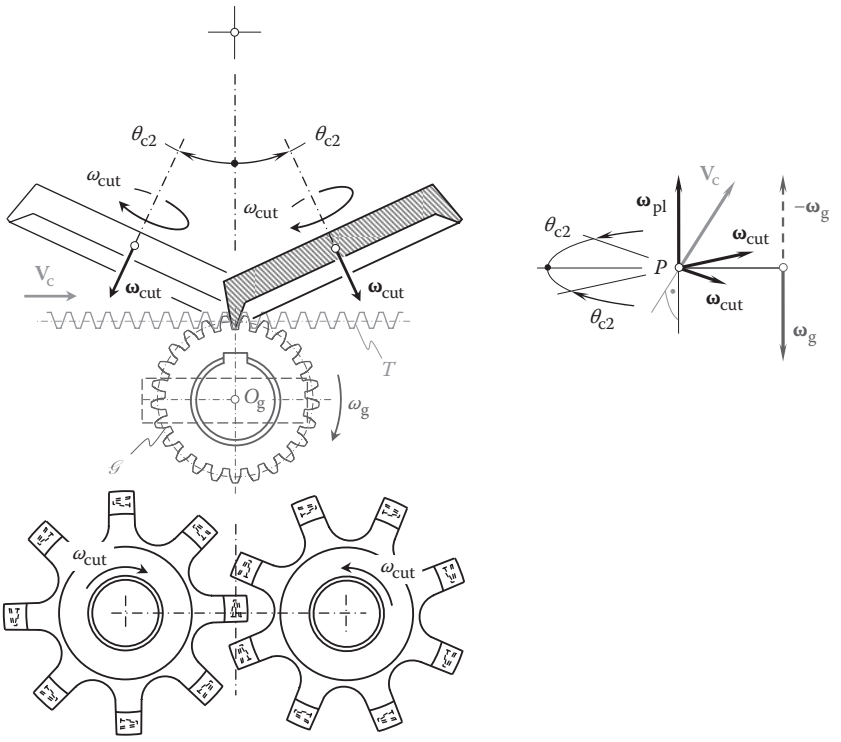

FIGURE 9.26
Kinematics of the generation of a work gear with two tilted disk-type gear cutting tools.

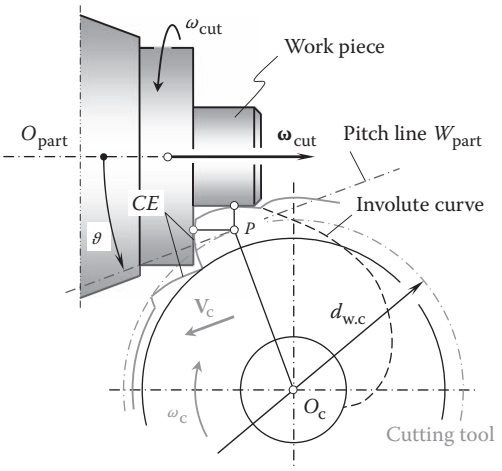

FIGURE 9.27
Machining of a surface of revolution with the generating rotary cutting tool.

tion that is an inverse one to that shown in Figure 9.24 is used for cutting of a round rack with the gear shaper cutter.

Another configuration of the rotation vector $\boldsymbol{\omega}_{cut}$ of the primary motion (Figure 9.25) with respect to that same gear machining mesh corresponds to generation of gears with the enveloping round rack cutter. The alteration of configuration of the vectors $\boldsymbol{\omega}_g$, $\mathbf{V}_c$, and $\boldsymbol{\omega}_{cut}$ in the vector representation of the kinematics of the gear machining operation makes possible the novel method of gear cutting process and novel design of the gear cutting tool for this purpose.

More examples in this concern can be developed using not just one cutting tool, but two cutting tools simultaneously instead. Modification of vector representation of the kinematics of the gear machining process allows for a method of the generation of the cylindrical gear with two milling cutters (or with two grinding wheels instead). In this method, axes of rotation of the gear cutting tools intersect each other at a certain angle $2\theta_{c2}$ (Figure 9.26). The angle θ_{c2} is within the interval $0° \le \theta_{c2} \le \phi_n$. (In a particular case of gear machining, axes of the cutting tool rotation can be parallel to each other.)

Vector representation of the kinematics of the gear machining operation can be designed so that the vectors $\mathbf{V}_c$ and $\boldsymbol{\omega}_{cut}$ are at a certain angle $(180° - \vartheta)$ to each other. An example is illustrated in Figure 9.27. Despite the fact that kinematics of this type is not of great interest for gear manufacturers, it is used for other purposes, for example, for turning of surfaces of revolution on a lathe.

The considered examples clearly illustrate the extensive opportunities that the kinematics of gear machining processes can offer to a gear cutting tool designer.

10

Gear Shaper Cutters I: External Gear Machining Mesh

Gear shaper cutters are mostly used for cutting spur and helical gears, both having either external or internal teeth. In addition, gear shaper cutters, which are often referred to as *pinion cutters*, may be used for machining of face gears and involute worms as well as for rough relieving of hobs.

Designing of shaper cutter begins with the determination of the generating surface of the cutting tool. For this purpose, kinematics of gear shaping operation is utilized.

10.1 Kinematics of Gear Shaping Operation

The generating surface of a gear shaper cutter is a conjugate surface to the work gear tooth surface. When machining the work gear, the generating surface T of the shaper cutter and the gear to be machined are in proper mesh with each other.

Kinematics of gear generation is the critical factor in the determination of the generating surface T of the shaper cutter. When shaping a work gear with the shaper cutter, the work gear and the shaper cutter rotate $\boldsymbol{\omega}_g$ and $\boldsymbol{\omega}_c$ about their axes of rotation O_g and O_c (Figure 10.1). The axes O_g and O_c of the rotations are parallel to each other ($O_g \parallel O_c$). The rotations ω_g and ω_c are timed with one another in compliance with the formula*

$$\frac{\omega_g}{\omega_c} = \frac{N_c}{N_g} \tag{10.1}$$

where N_g denotes the tooth number of the work gear and N_c denotes the tooth number of the shaper cutter.

The shaper cutter reciprocates in its axial direction simultaneously with the rotations ω_g and ω_c. Speed of the reciprocation is designated as $\mathbf{V}_{cut}$. The reciprocation of the shaper cutter is required for stock removal. In the case of a helical work gear, the rotation of the shaper cutter $\boldsymbol{\omega}_{cut}$ is performed in addition to the reciprocation $\mathbf{V}_{cut}$. Timing of the motions $\mathbf{V}_{cut}$ and $\boldsymbol{\omega}_{cut}$ depends on the hand of the tooth helix of the work gear. The resultant screw motion that is composed of the motions $\mathbf{V}_{cut}$ and $\boldsymbol{\omega}_{cut}$ is a screw cutting motion of the

* It is instructive to point out here that that same kinematics of the gear machining mesh is featured in another gear machining process—*parallel axis shaving*. In this application [15, 194], the shaving cutter and the work gear are rotating in mesh with the axes parallel. Without the benefit of the crossed-axis angle, there is no helical sliding of tooth flanks of the shaving cutter and the work gear. Therefore, a reciprocating motion must be induced at a comparatively high frequency. This requires a special machine. The tool cuts only on its face, as it is rotating in one direction and then the other, as the reciprocation is taking place. It is generally applied to internal shaving. This method is not commonly used.

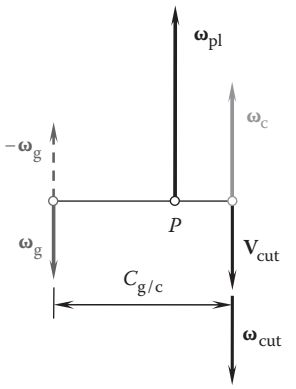

FIGURE 10.1
Vector diagram of the kinematics of the machining process of an external gear with the shaper cutter.

shaper cutter. This screw motion does not correlate to the rotations $\boldsymbol{\omega}_g$ and $\boldsymbol{\omega}_c$, and is independent of the rotations $\boldsymbol{\omega}_g$ and $\boldsymbol{\omega}_c$. The parameter of the screw motion is identical to the screw parameter of the work gear helix. The vector of the screw cutting motion can be pointed either in the same direction as or in the opposite direction of the vector $\boldsymbol{\omega}_c$.

The distance $C_{g/c}$ between the axes O_g and O_c of the rotations changes when the shaper cutter reciprocates back and forth (Figure 10.2). When the shaper cutter moves down and when it cuts the stock, the distance $C_{g/c}$ is equal to the nominal center distance in the virtual gear machining meshing, that is, it is equal to the distance between the axis of rotation of the work gear and the axis of rotation of the generating surface T of the shaper cutter.

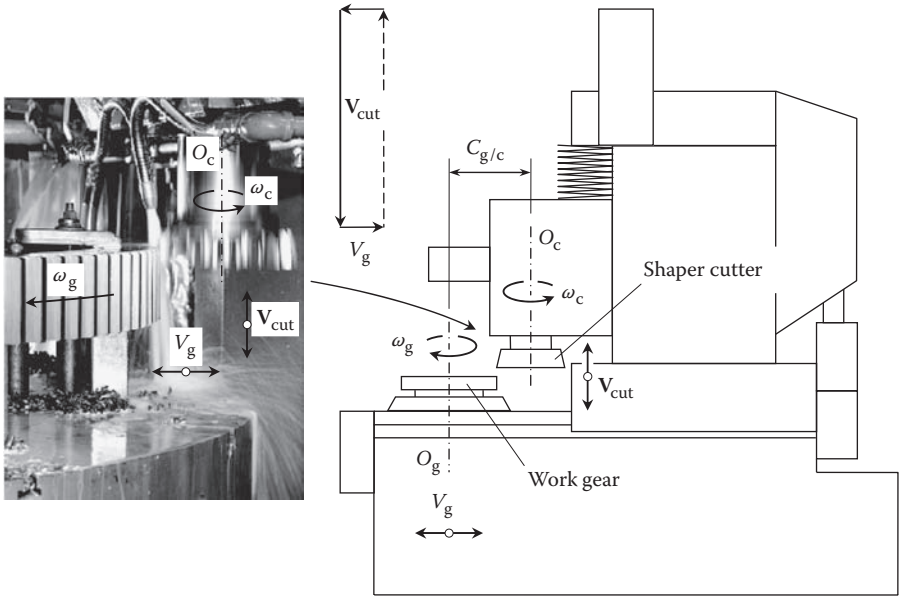

FIGURE 10.2
Principal elements of the kinematics of gear shaping operation.

When the shaper cutter moves back, the distance between the axes O_g and O_c is increased to a certain value. For this purpose, in most designs of gear-shaping machines the worktable with the gear reciprocates in the direction that is perpendicular to the axis of rotation O_g of the work gear. Speed of this reciprocation is designated as V_g. The reciprocation of the work gear is necessary to eliminate the contact between the clearance surface of the shaper cutter teeth and the machined surface of the work gear. In this manner, the tool life of the shaper cutter is increased.

Several types of in-feed motion of the shaper cutter are used in practice. The conventional method of gear shaping features either intermittent radial feed of the shaper cutter with continuous rotary feed or radial feed without rotary feed. Continuous radial and rotary feeds are available in gear-shaping machines of modern design. Numerous other types of in-feed motion of the shaper cutter are also known.

10.2 Generating Surface of a Gear Shaper Cutter

Not all of the motions of the work gear and the shaper cutter discussed above are necessarily considered when determining the generating surface of the gear shaper cutter. Only those motions that actually affect the meshing of the gear to be machined and the virtual gear represented by the generating surface of the shaper cutter are required to be considered.

Once the kinematics of the gear machining process is identified (Figure 10.1), an equation for the gear tooth surface to be machined is the only required input for determining the generating surface of the shaper cutter. As an example, consider the machining of a helical gear. The case of machining of a spur gear can be drawn from the above case as the simplification under the assumption that the pitch helix angle of the gear is equal to zero ($\psi_g = 0°$). The set of reference systems in both cases is similar.

Consider the shaping of a helical gear using the shaper cutter (Figure 10.3). In the Cartesian coordinate system $X_gY_gZ_g$ associated with the gear, tooth flank surface $\mathcal{G}$ of the gear can be analytically described by [see Equation (1.3)]

$$\mathbf{r}_g(U_g, V_g) = \begin{bmatrix} r_{b.g}\cos V_g + U_g \cos\lambda_{b.g}\sin V_g \\ r_{b.g}\sin V_g - U_g \sin\lambda_{b.g}\sin V_g \\ r_{b.g}\tan\lambda_{b.g} - U_g \sin\lambda_{b.g} \\ 1 \end{bmatrix} \tag{10.2}$$

where the position vector of a point $\mathbf{r}_g$ of the work gear tooth flank $\mathcal{G}$ is expressed in terms of Gaussian coordinates U_g and V_g and the design parameters $r_{b.g}$ and $\lambda_{b.g}$ of the work gear.

The kinematic method can be implemented to derive an equation for the tooth flank surface of the generating surface T of the shaper cutter. Following this method, it is necessary to represent the work gear tooth flank $\mathcal{G}$ in the coordinate system $X_cY_cZ_c$ associated with the shaper cutter. Position vector of a point $\mathbf{r}_g^{(c)}$ of the tooth flank surface $\mathcal{G}$ of the work gear allows for representation in the form

$$\mathbf{r}_g^{(c)}(U_g, V_g, \varphi_g, \varphi_c) = \mathbf{Rt}(\varphi_c, Z_c)\cdot\mathbf{Tr}(C_{g/c}, Y_g^*)\cdot\mathbf{Rt}(\varphi_g, Z_g)\cdot\mathbf{r}_g(U_g, V_g) \tag{10.3}$$

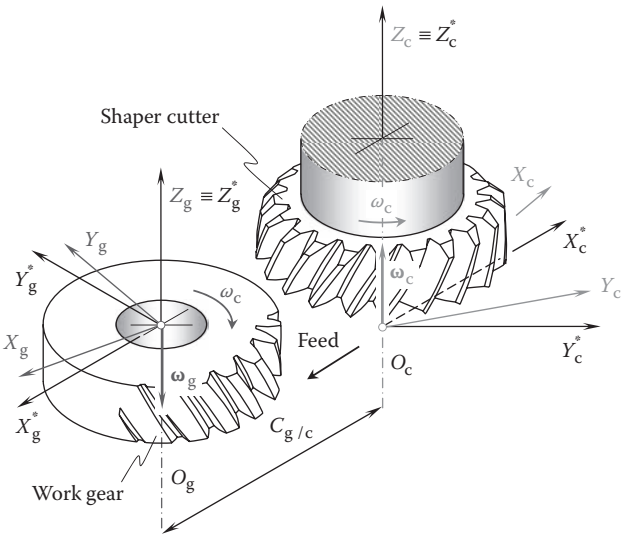

FIGURE 10.3
The applied coordinate systems.

where

φ_g = Angle through which the coordinate system $X_gY_gZ_g$ turns relative to the stationary coordinate system $X_g^*Y_g^*Z_g^*$. Initially, before the rotation starts, axes of the coordinate system $X_gY_gZ_g$ aligns to the corresponding axes of the coordinate system $X_g^*Y_g^*Z_g^*$.

φ_c = Angle through which the coordinate system $X_cY_cZ_c$ turns relative to the stationary coordinate system $X_c^*Y_c^*Z_c^*$. Initially, before the rotation starts, axes of the coordinate system $X_cY_cZ_c$ aligns to the corresponding axes of the coordinate system $X_c^*Y_c^*Z_c^*$.

$C_{g/c}$ = Center distance between the axis of rotation O_g of the work gear and the axis of rotation O_c the shaper cutter.

The angle φ_g may be measured between the coordinate axes X_g and X_g^* (Figure 10.3). Similarly, the angle φ_c may be measured between the coordinate axes X_c and X_c^*.

Of the two angles, φ_g and φ_c, one may be considered an independent parameter, whereas the other is dependent on the current value of the first one. The correlation between the angles φ_g and φ_c can be expressed by the ratio

$$\frac{\varphi_g}{\varphi_c} = \frac{N_c}{N_g} \tag{10.4}$$

Ultimately, Equation (10.3) reduces to the form

$$\mathbf{r}_g^{(c)} = \mathbf{r}_g^{(c)}(U_g, V_g, \varphi_g) \tag{10.5}$$

Equation (10.5) describes the position vector of a point $\mathbf{r}_g^{(c)}$ of the gear tooth flank surface $\mathcal{G}$ in its current position with respect to the shaper cutter coordinate system $X_cY_cZ_c$. The parameter φ_g serves as the parameter of motion.

To come up with the equation for the tooth surface T, it is necessary to eliminate the parameter φ_g from Equation (10.5).

At a certain instant of time, not all points of the tooth flank $\mathscr{G}$ make contact with the tooth flank surface of the generating surface T. Only certain points of the tooth flank $\mathscr{G}$ make contact at which the condition of contact

$$\mathbf{n}_g^{(c)} \cdot \mathbf{V}_{g-c} = 0 \tag{10.6}$$

is satisfied. In this equation, $\mathbf{r}_g^{(c)}$ denotes the unit normal vector to the surface and $\mathbf{V}_{g-c}$ is a vector of speed of the relative motion of the gear relative to the coordinate system $X_cY_cZ_c$.

It should be pointed out that Equation (10.6) is commonly referred to as Shishkov's *equation of contact* [186].

The vector $\mathbf{V}_{g-c}$ of speed of the relative motion may be represented in the form of summa of two vectors: (1) $\mathbf{V}_g$, which is the vector of linear speed of the rotation of a point of the work gear tooth flank about the axis of rotation of the work gear; and (2) $\mathbf{V}_{pl}$, which is the vector of linear speed of rotation of the gear axis of rotation O_g about the axis of rotation O_c of the coordinate system $X_cY_cZ_c$. Ultimately, the equality $\mathbf{V}_{g-c} = \mathbf{V}_g + \mathbf{V}_{pl}$ is valid. Note that only the direction of the vector $\mathbf{V}_{g-c}$ is of importance for further consideration. Magnitude of the vector $\mathbf{V}_{g-c}$ is not important when the equation of contact is used. This is because the dot product in Equation (10.6) is equal to zero.

Both vectors $\mathbf{n}_g^{(c)}$ and $\mathbf{V}_{g-c}$ are functions of coordinates of a point of the moving surface $\mathbf{r}_g^{(c)}$. In other words, the dot product $\mathbf{n}_g^{(c)} \cdot \mathbf{V}_{g-c}$ allows for interpretation in the form of a function of the parameters U_g, V_g, and φ_g. After solving the function with respect to the parameter of motion φ_g, the derived expression for φ_g is substituted into Equation (10.5). This yields an equation for the tooth flank surface T of the generating surface of the shaper cutter. Ultimately, in the coordinate system $X_cY_cZ_c$, the derived equation for the surface T can be presented in vector form

$$\mathbf{r}_c = \mathbf{r}_c(U_c, V_c) \tag{10.7}$$

In a particular case of shaping of a helical involute gear, Equation (10.7) casts into the expression in matrix form

$$\mathbf{r}_c(U_c, V_c) = \begin{bmatrix} r_{b.c}\cos V_c + U_c \cos\lambda_{b.c}\sin V_c \\ r_{b.c}\sin V_c - U_c \sin\lambda_{b.c}\sin V_c \\ r_{b.c}\tan\lambda_{b.c} - U_c \sin\lambda_{b.c} \\ 1 \end{bmatrix} \tag{10.8}$$

where

$r_{b.c}$ = radius of the base cylinder of the generating surface T of the shaper cutter

$\lambda_{b.c}$ = base lead angle of the generating surface T of the shaper cutter

Equation (10.8) is very similar to Equation (10.2). This is a common occurrence because a screw involute surface can be properly meshed only with another screw involute surface.

Equation (10.8) can be expressed in terms of the design parameters of the shaper cutter. For this purpose, engineering formulae listed in Appendix A can be used.

The normal profile angle $\phi_{n.c}$ on the pitch cylinder of the shaper cutter is equal to the normal profile angle $\phi_{n.g}$ in a gear shaping operation ($\phi_{n.c} = \phi_{n.g} = \phi_n$). Therefore, this angle is designated as ϕ_n.

Similarly, the pitch helix angle ψ_c of the shaper cutter is equal to $-\psi_g$, where ψ_g is the pitch helix angle of the work gear.

The above-mentioned correlation between the normal profile angles of the shaper cutter and the work gear, as well as between the pitch helix angles ψ_c and ψ_g gives the cutting tool designer the chance to alter the design parameters of the shaper cutter. The possibility of altering the design parameters can be used to improve the cutting performance of the shaper cutter. Equality of the base pitch of the shaper cutter $p_{b.c}$ to base pitch of the work gear $p_{b.g}$ is a must ($p_{b.c} \equiv p_{b.g}$).

Features of profiling of shaper cutters for machining noninvolute shapes. Shaper cutters are also used for machining of noninvolute profiles. For profiling of shaper cutters intended for machining noninvolute profiles, use of the kinematic method of profiling of generating tools is recommended.

When shaping parts having a noninvolute tooth profile, the kinematics of part surface generation (*PSG*) is similar to that when machining involute tooth profiles. The pitch cylinder of the radius R_{wg} of the gear to be machined is rolling without sliding over the pitch cylinder of radius R_{wc} of the shaper cutter as shown in Figure 10.4. An orthogonal Cartesian coordinate system $X_gY_gZ_g$ is associated with the work gear and is rotating with it with a certain rotation ω_g. The initial position of the coordinate system $X_gY_gZ_g$ is designated as $X_{gs}Y_{gs}Z_{gs}$. Another Cartesian coordinate system $X_cY_cZ_c$ is the cutting tool reference system with which the shaper cutter will be associated after it has been designed. This reference system is rotating with the rotation ω_c. The rotations ω_g and ω_c are timed with each other so that the ratio $\omega_g R_g = \omega_c R_c$ is observed. When the work gear turns about its axis of rotation O_g through a certain angle φ_g, the shaper cutter turns about its axis of rotation O_c through the angle $\varphi_c = \varphi_g(R_g/R_c)$.

Shishkov's equation of contact $\mathbf{n}_g^{(m)} \cdot \mathbf{V}_\Sigma^{(m)} = 0$ is used for the purpose of profiling of the shaper cutter for the machining of the work gear having a noninvolute tooth profile. To compose the equation of contact, an analytical representation of the vector of relative motion $\mathbf{V}_\Sigma^{(m)}$ of a point of interest within the gear tooth profile is required. It is also necessary to compute a unit normal vector $\mathbf{n}_g^{(m)}$ to the gear tooth profile at that same point of interest.

A point of interest m is chosen within the work gear tooth profile ab. In the motionless coordinate system $X_{gs}Y_{gs}Z_{gs}$, the unit normal vector $\mathbf{n}_g^{(m)}$ to the gear tooth profile at m can be described by

$$\mathbf{n}_g^{(m)} = -\mathbf{i} \cdot \tan(\vartheta_g + \varphi_g) + \mathbf{j} \tag{10.9}$$

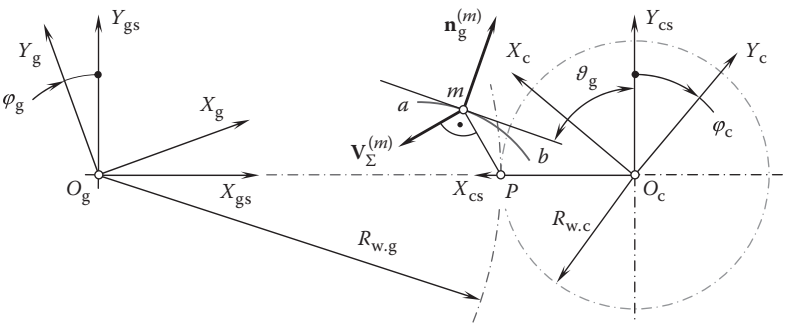

FIGURE 10.4
Schematic of implementation of the kinematic method of profiling of generating cutting tools for profiling of the shaper cutter for machining a gear with noninvolute tooth profile.

Here and below, only the direction of the relative motion as well the direction of the normal vector are of importance.

In Equation (10.9), angle ϑ_g designates the angle that the tangent to the tooth profile *ab* at the point of interest *m* makes with the Y_g axis of the reference system $X_gY_gZ_g$.

Vector of linear motion of the instant rotation of point *m* about pitch point *P* is designated as $\mathbf{V}_{\Sigma}^{(m)}$. This allows for the representation of the vector $\mathbf{V}_{\Sigma}^{(m)}$ in the form of a vector equation

$$\mathbf{V}_{\Sigma}^{(m)} = \mathbf{i} \cdot Y_{gs} - \mathbf{j} \cdot X_{gs} \tag{10.10}$$

Substituting Equations (10.9) and (10.10) into the equation of contact $\mathbf{n}_g^{(m)} \cdot \mathbf{V}_{\Sigma}^{(m)} = 0$, the particular form of the equation of contact

$$\sin(\vartheta_g + \varphi_g) = \frac{X_g \cos\vartheta_g + Y_g \sin\vartheta_g}{R_{wg}} \tag{10.11}$$

can be derived.

Equation (10.11) yields computation of the angle φ_g at which a given point of the gear tooth profile makes contact with the corresponding point of the shaper cutter tooth profile point. Furthermore, coordinates of the point of the shaper cutter tooth profile are computed using operators of linear transformations.

10.3 Cutting Edges of the Shaper Cutter

When designing a shaper cutter the cutting edges CE are commonly viewed as the lines of intersection of the generating surface *T* by the rake surface R_s of the shaper cutter. Furthermore, the clearance surface C_s is designed so as to pass through the cutting edge at a desired clearance angle with respect to the generating surface *T*.

Another way of creating the cutting edges of the shaper cutter is also possible. In compliance with this second approach, the cutting edges CE are created as lines of intersection of the generating surface *T* by the clearance surface C_s of the shaper cutter. After that, the rake surface R_s is designed so as to pass through the cutting edge at a desired rake angle with respect to the perpendicular to the generating surface *T*.

In both cases, there are three surfaces—(1) generating surface *T* of the shaper cutter, (2) rake surface R_s, and (3) clearance surface C_s—through the cutting edge CE of the shaper cutter. Only the rake surface R_s and the clearance surface C_s exist physically. The generating surface *T* of the shaper cutter is a phantom surface, which does not exist physically. However, surface *T* imposes a restriction onto the required location of the cutting edges CE.

10.3.1 Rake Surface of a Shaper Cutter

It is reasonable to distinguish the difference between the geometry of the rake surfaces of (a) shaper cutters for machining of spur gears from (b) those used for machining of helical gears.

Geometry of rake surface of a spur shaper cutter. The rake surface of a spur shaper cutter is shaped in the form of one of three surfaces. In reality, the rake surface R_s is shaped in the form of (1) a plane that is perpendicular to the axis of rotation of the shaper cutter, or (2) an internal cone of revolution, or (3) in particular cases, a surface of revolution of more complex geometry.

Spur shaper cutters having a rake surface shaped in the form of plane that is perpendicular to the axis of rotation of the shaper cutter have zero rake angle ($\gamma_o = 0°$). The rake surface R_s of this geometry satisfies the equation $Z_c = 0$ (Figure 10.5a). For profiling of the shaper cutter, it is preferred to use the matrix representation of the surface $Z_c = 0$

$$\mathbf{r}_{rs}(U_c, V_c) = \begin{bmatrix} U_c \\ V_c \\ 0 \\ 1 \end{bmatrix} \tag{10.12}$$

where

$\mathbf{r}_{rs}$ = position vector of a point of the rake plane R_s
U_c, V_c = Gaussian coordinates of the rake plane R_s

Convenience of application is the only criterion for selecting Gaussian coordinates U_c and V_c of the rake plane R_s for a particular design of shaper cutters. For example, Gaussian coordinates U_c and V_c could be equal to the corresponding Cartesian coordinates X_c and Y_c of the rack plane R_s, that is, $U_c = X_c$ and $V_c = Y_c$.

The cutting performance of the shaper cutter can be significantly enhanced when the rake surface forms a certain desired rake angle with the perpendicular to the generating surface T of the shaper cutter. For this purpose, the conical rake surface R_s is commonly used in the design of shaper cutters (Figure 10.5b). Conical rake surface can be analytically described by the matrix equation

$$\mathbf{r}_{rs}(Z_c, V_c) = \begin{bmatrix} Z_c \tan\gamma_o \cos V_c \\ Z_c \tan\gamma_o \sin V_c \\ Z_c \\ 1 \end{bmatrix} \tag{10.13}$$

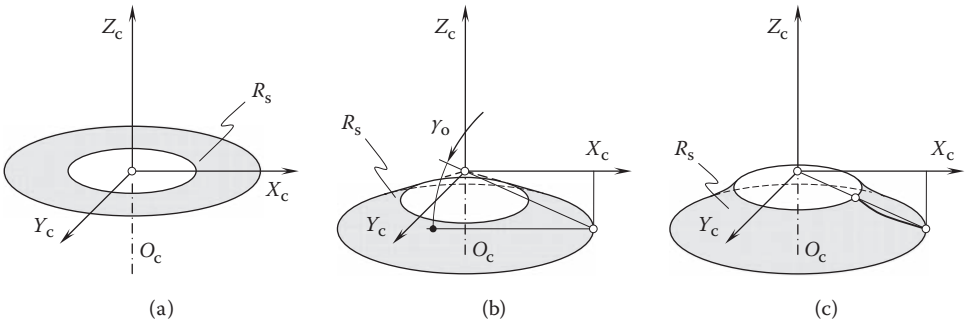

FIGURE 10.5
Practical types of rake surfaces R_s of shaper cutters for machining spur gears.

In special cases, for precision shaper cutters implementation of a rake surface that is shaped in the form of a surface of revolution of more complex geometry is known (Figure 10.5c). In this case, for the analytical description of the rake surface R_s, use of matrix equation

$$\mathbf{r}_{rs}(U_c, V_c) = \begin{bmatrix} r_{rs}(U_c)\cos U_c \cos V_c \\ r_{rs}(U_c)\cos U_c \sin V_c \\ r_{rs}(U_c)\sin U_c \\ 1 \end{bmatrix} \tag{10.14}$$

has proven to be convenient. Here, the equality $r_{rs} = |\mathbf{r}_{rs}|$ is valid.

In all three cases considered above, only one common surface (a plane, or an internal cone of revolution, or a surface of revolution) serves as the rake surface for all shaper cutter teeth. Local modifications of the rake surface within the narrow strip along the cutting edge are not considered here.

Geometry of the rake surface of a helical shaper cutter. Helical shaper cutters having a reasonably small pitch helix angle ψ_c are manufactured with a rake plane R_s similar to that shown in Figure 10.5a. Helical shaper cutters of this design have one common rake plane R_s for all shaper cutter teeth.

Helical shaper cutters with a larger helix angle are designed so that each tooth has an individual rake plane R_s (Figure 10.6). This is mostly because the impact of the pitch helix angle onto the rake angle of the lateral cutting edges of the shaper cutter tooth cannot be neglected in this case.

Figure 10.6 gives an insight on the derivation of equation for the rake plane R_s of the helical shaper cutter

$$\mathbf{r}_{rs}(X_c, Y_c) = \begin{bmatrix} X_c \\ Y_c \\ Y_c \tan \psi_c \\ 1 \end{bmatrix} \tag{10.15}$$

The shaper cutter teeth are turned relative to each other about the axis of rotation of the cutting tool through a certain angle. The actual value of this angle θ_{cn} is equal to

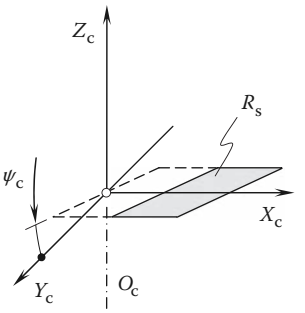

FIGURE 10.6
Rake plane R_s of a helical shaper cutter tooth.

$\theta_{cn} = 2\pi n/N_c$. Here, n denotes the number of the tooth counting from the tooth for which Equation (10.15) is derived. Use of the operator of rotation $\mathbf{Rt}(\theta_{cn}, Z_c)$ yields an expression

$$\mathbf{r}_{rs}^{(n)}(X_c, Y_c) = \mathbf{Rt}(\theta_{cn}, Z_c) \cdot \mathbf{r}_{rs}(X_c, Y_c) \tag{10.16}$$

for the rake plane of the shaper cutter tooth that is numbered with n.

10.3.2 Clearance Surface of a Shaper Cutter Tooth

A screw surface through the cutting edge can be utilized as the desired clearance surface of a shaper cutter tooth. For this purpose, the screw surface C_s has to have an appropriate pitch.

When the equation for the generating surface T of the shaper cutter [Equation (10.8)] is considered together with the equation for the rake surface R_s [see Equations (10.12) through Equation (10.16)], the points satisfying both equations simultaneously specify the cutting edge CE of the shaper cutter tooth. Generally speaking, the cutting edge of the shaper cutter tooth can be viewed as a spatial curve of intersection of the generating surface T by the rake surface R_s.

To derive an equation for the cutting edge CE of the shaper cutter tooth, the surfaces T and R_s must be properly parameterized. Often, a reparameterization of one of the surfaces is required to be carried out for this purpose (see Appendix C on details of reparameterization of a surface). After the reparameterization is performed, both the surfaces T and R_s are expressed in terms of common parameters U and V. In other words, the equation for the generating surface T [Equation (10.8)] and a corresponding equation of the rake surface R_s [see Equations (10.12) through (10.16)] are represented in the form $\mathbf{r}_c = \mathbf{r}_c(U,V)$ and $\mathbf{r}_{rs} = \mathbf{r}_{rs}(U,V)$, respectively. One of the parameters (either U or V) can be eliminated from the set of two equations, $\mathbf{r}_c = \mathbf{r}_c(U,V)$ and $\mathbf{r}_{rs} = \mathbf{r}_{rs}(U,V)$. Ultimately, this yields an equation for the cutting edge CE of the shaper cutter tooth in the form $\mathbf{r}_{ce} = \mathbf{r}_{ce}(t_{ce})$, where t_{ce} is a parameter of the cutting edge CE.

For construction of the clearance surface C_s of the shaper cutter tooth, a screw motion of the cutting edge CE is considered. When the cutting edge is performing an appropriate screw motion, the clearance surface C_s is generated as the set of successive positions of the cutting edge. To derive the desired clearance surface C_s of the shaper cutter tooth, it is sufficient to derive an equation for the cutting edge CE in its current location and orientation while performing the screw motion. Use of the operator of screw motion is helpful when deriving the equation for the desired clearance surface C_s (see Section 4.1.5). Ultimately, position vector $\mathbf{r}_{cs}$ of a point of the desired clearance surface C_s of the shaper cutter tooth yields vector interpretation in the form

$$\mathbf{r}_{cs}(t_{ce}, \varphi_z) = \mathbf{Sc}_z(\varphi_z, p_z) \cdot \mathbf{r}_{ce}(t_{ce}) \tag{10.17}$$

In this equation, position vector $\mathbf{r}_{cs}$ of a point of the clearance surface C_s is expressed in terms of two parameters: t_{ce} and φ_z.

Reduced pitch p_z of the clearance surface C_s can be expressed in terms of two parameters: (1) clearance angle α_m in the main cross section of the cutting edge and (2) pitch diameter $d_{w.c}$ of the shaper cutter. Finally, the following expression

$$p_z = 2\pi \cot \alpha_m \tag{10.18}$$

is derived for the computation of the reduced pitch p_z of the clearance surface C_s of the shaper cutter tooth.

Unfortunately, the desired clearance surface C_s of the shaper cutter tooth [see Equation (10.17)] is not convenient for grinding. This is the major reason for why in practice, the desired clearance surface C_s of the gear shaper cutter tooth is approximated by a screw surface that is more convenient for grinding.

10.4 Profiling of Gear Shaper Cutters

Gear shaper cutters are round cutting tools. The pitch diameter of a shaper cutter becomes progressively smaller after each resharpening of the worn tool. Because of the change in pitch diameter, the shape of the cutting edges of a new shaper cutter and its shape after resharpening are not identical. This factor must be taken into account when designing a gear shaper cutter.

The following discussion is largely based on the analysis of meshing of a partially ground gear shaper cutter with the auxiliary phantom rack $\mathscr{R}_T$.

In the case under consideration, the generating surface T of the gear shaper cutter is formed as the enveloping surface to successive positions of a phantom rack surface. The phantom rack surface $\mathscr{R}_T$ serves as the auxiliary generating surface of the shaper cutter. The rack surface $\mathscr{R}_T$ properly meshes with the gear to be machined as well as the generating surface T of the shaper cutter. Application of the second approach of forming of the generating surface T of the gear shaper cutter is convenient from the standpoint of the reduction of diameters after every resharpening of the shaper cutter.

Consider an example of meshing of the auxiliary rack surface $\mathscr{R}_T$ with the generating surface T of the gear shaper cutter (Figure 10.7). The example is used to illustrate how different portions of the generating surface T have to change their relative orientation when the pitch diameter of the shaper cutter becomes increasingly smaller after every resharpening of the gear cutting tool. The geometry of the portions of the generating surface remains the same as it is for the new gear shaper cutter. It has been proven convenient to use the auxiliary rack surface $\mathscr{R}_T$ for illustrative purposes.

Consider the cross-sectional view of the rack by a plane that is perpendicular to the axis of rotation O_c of the gear shaper cutter. When the surface T is generating, the pitch line w of the auxiliary rack rolls without sliding over the pitch circle of the diameter $d_{w.c}$. The involute tooth profile of the generating surface T is shaped in the form of the enveloping surface to successive positions of the auxiliary rack $\mathscr{R}_T$ when the pitch line w rolls over the pitch circle.

To be capable of cutting the stock, a positive clearance angle is necessary at all cutting edges of the tooth of the gear shaper cutter. The practical way to create the required clearance angles at all cutting edges of the shaper cutter tooth is to design the shaper cutter in such a way that the clearance angle α_o at the top cutting edge corresponds to the clearance angles at the lateral cutting edges. To do this, the configuration of portions of the generating surface T through the lateral sides of the tooth profile should have to be changed as the outer diameter of the gear shaper cutter keeps getting smaller. In this way, the clearance angles of a certain value can be obtained on the lateral cutting edges of the shaper cutter.

Let us assume that the nominal cross section of the generating surface T aligns with the cross section by the plane through points A and B. The plane of the nominal cross section

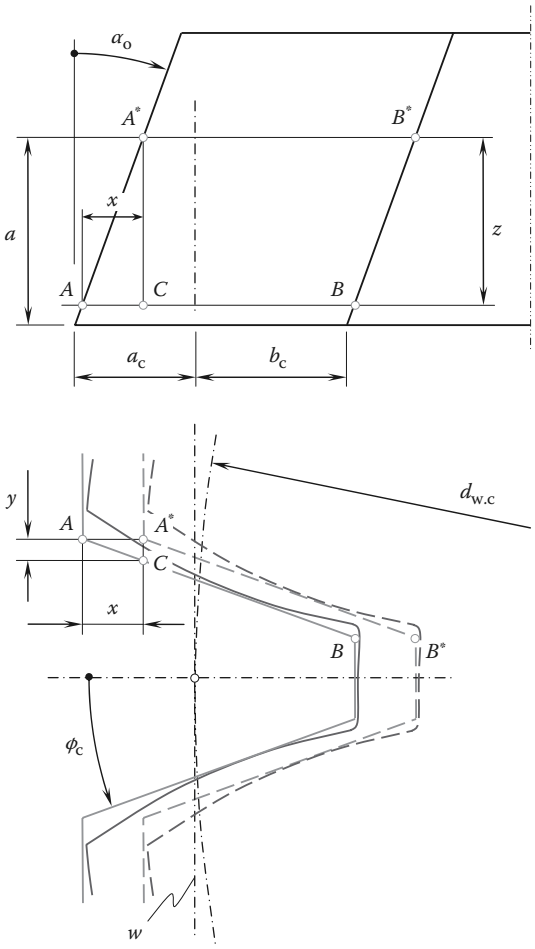

FIGURE 10.7
Schematic of meshing of the auxiliary rack surface $\mathscr{R}_T$ with the generating surface T of the gear shaper cutter.

is perpendicular to the axis of rotation O_c. The ordinary involute tooth profile of the generating surface T is formed in the nominal cross section. Calculations of most of the design parameters of the gear shaper cutter are usually performed for the nominal cross section.

In the nominal cross section, the tooth profile of the gear shaper cutter can be specified in terms of the following design parameters: addendum $a_c = 1.25m$ [mm] (here and below, the shaper cutter module is denoted by m), dedendum $b_c = 1.25m$ [mm], pitch diameter $d_{w.c} = mN_c$ (where the shaper cutter tooth number is denoted by N_c), nominal circular tooth thickness $t_n = \pi m/2$ [mm]; the circular space width is equal to the circular tooth thickness. The actual value of the circular tooth thickness exceeds its nominal value:

$$t = t_n + 0.5B, \text{ mm} \tag{10.19}$$

where B designates backlash in the gear transmission that comprises two gears in mesh.

The cross section by the plane through points A^* and B^* is an arbitrary normal cross section of the generating surface T (Figure 10.7). The arbitrary normal cross section is at a

certain distance z from the nominal normal cross section. Within the arbitrary normal cross section, the tooth profile of the generating surface T of the gear shaper cutter can be generated by the auxiliary rack that is identical to the auxiliary rack $\mathscr{R}_T$. However, in this cross section, the auxiliary rack $\mathscr{R}_T$ is closer to the axis of rotation O_c of the shaper cutter. The distance x at which the auxiliary rack $\mathscr{R}_T$ within the arbitrary normal cross section is shifted toward the axis O_c relative to its initial position can be computed from the formula

$$x = z \tan \alpha_o \tag{10.20}$$

where α_o is the desired clearance angle at the top cutting edge of the gear shaper cutter tooth.

After it has been shifted, the auxiliary rack $\mathscr{R}_T$ generates the corresponding tooth profile of the generating surface T. The profile shift correction coefficient ξ_c in this case is

$$\xi_c = \frac{x}{m} = \frac{z \tan \alpha_o}{m} \tag{10.21}$$

It is critically important to point out that the coefficient of correction ξ_c is a function of the z coordinate [$\xi_c = \xi_c(z)$].

The parameters of rolling motion of the auxiliary rack $\mathscr{R}_T$ remain the same for both initial normal cross section and any arbitrary normal cross section. Therefore, the pitch diameter $d_{w.c}$ of the gear shaper cutter when it is meshing with the auxiliary rack $\mathscr{R}_T$ also retains its original value. The pitch circle of the diameter $d_{w.c}$ is the circle at which the circular pitch P_c of the shaper cutter teeth is equal to the pitch of the auxiliary rack $\mathscr{R}_T$ teeth ($P_c = \pi m$).

The base diameter $d_{b.c}$ of the gear shaper cutter can be computed from the formula

$$d_{b.c} = d_{w.c} \cos \phi_c \tag{10.22}$$

where ϕ_c is the profile angle of the auxiliary rack $\mathscr{R}_T$.

As follows from Equation (10.22), the base diameter at any arbitrary normal cross section has the same value as that in the nominal normal cross section.

The rest of the design parameters of the gear shaper cutter tooth in the arbitrary normal cross section can be expressed in terms of the corresponding design parameters measured in the nominal normal cross section of the shaper cutter. For example, the shaper cutter tooth addendum a_c^* is equal to

$$a_c^* = a_c + z \tan \alpha_o = 1.25m + z \tan \alpha_o, \text{ mm} \tag{10.23}$$

To compute for the gear shaper cutter tooth dedendum b_c^*, the formula

$$b_c^* = b_c - z \tan \alpha_o = 1.25m - z \tan \alpha_o, \text{ mm} \tag{10.24}$$

can be used.

Whole depth $h_{t.c}$ remains the same

$$h_{t.c} = a_c + b_c = a_c^* + b_c^* = 2.25m, \text{ mm} \tag{10.25}$$

Tooth thickness of the gear shaper cutter requires special treatment. In an arbitrary normal cross section, tooth thickness t^* can be expressed in terms of the design parameters of the gear cutting tool. For this purpose, the expression

$$t^* = \frac{\pi m}{2} + B + 2z \tan \alpha_o, \text{ mm} \tag{10.26}$$

is derived.

The involute tooth profile within an arbitrary normal cross section of the generating surface T of the gear shaper cutter is constructed from the same base circle of diameter $d_{b.c}$ as the involute profile within the nominal normal cross section. This means that the same involute curve is used for the tooth profile both in the nominal as well as in the arbitrary normal cross section. However, the two tooth profiles differ from each other. This is because different segments of the same involute curve are used in these two cases.

An angular displacement of the involute tooth profile in the arbitrary normal cross section with respect to the tooth profile within the nominal cross section is observed. To compute for the current value of the angular displacement ε of the tooth profiles, the following formula

$$\varepsilon = \frac{t^* - t}{d_{w.c}} = \frac{\tan \alpha_o \tan \phi_c}{d_{w.c}} \cdot z \tag{10.27}$$

can be used.

As follows from Equation (10.27), the angular displacement ε is a linear function of the z coordinate. Consequently, the locus of successive positions of the involute tooth profile in various locations of the arbitrary normal cross section when it moves along the axis of rotation O_c of the gear shaper cutter is within a screw surface of constant axial pitch. The axial pitch P_x of the surface is equal to

$$P_x = \frac{\pi d_{w.c}}{\tan \alpha_o \tan \phi_c} \tag{10.28}$$

Equation (10.28) immediately follows from Equation (10.27) when the angle of 2π is substituted instead of an arbitrary value of the angular displacement ε. Under such a scenario, the equality $z = P_x$ is observed.

10.5 Critical Distance to the Nominal Cross Section of the Gear Shaper Cutter

A cross section of the generating surface T of the gear shaper cutter for which the design parameters of the cutting tool are computed is commonly referred to as the nominal cross section of the shaper cutter.

Parameters of the tooth profile of the gear shaper cutter that has been resharpened differ, for many reasons, from that of the new shaper cutter. It is practical to design a shaper cutter so that deviations of the tooth profile of the new shaper cutter are of maximal permissible values. After every resharpening of the gear shaper cutter, the tooth profile deviations are becoming smaller. At a certain cross section, the tooth profile deviations of the gear shaper cutter are equal to zero. Further resharpenings cause progressively larger deviations of the gear shaper cutter tooth profile. The sign of the deviations is opposite to

the sign of the deviations of the new shaper cutter. Ultimately, at a certain cross section, the deviations reach values of the corresponding tolerances. The distance in the axial direction of the gear shaper cutter between the initial cross section of the generating surface T and the cross section that corresponds to the completely worn out shaper cutter is of critical importance to the cutting tool designer. It specifies the location of the nominal cross section of the gear shaper cutter.

The nominal cross section of the gear shaper cutter is at a distance a in the axial direction from the corresponding cross section of the new shaper cutter. Distance a is half a distance between the cross sections of the new and the worn-out gear shaper cutter.

It is desirable to design a shaper cutter with the greatest possible distance a. The greater the distance a, the larger the number of resharpenings of the gear shaper cutter allowed. This means that a larger number of gears can be machined during the life span of the given shaper cutter. In this way, the cost of the gear shaper cutter per machined gear can be significantly reduced.

The maximal length of distance a is limited by two major factors.

First, distance a affects the length of the top cutting edge of the gear shaper cutter. The greater the distance a, the shorter the top cutting edge becomes. If the shaper cutter is inappropriately designed, then either the length of the top cutting edge is insufficiently short or a shaper cutter tooth pointing may be occurring. The life span of a gear shaper cutter having a short top cutting edge is shorter compared to the life span of a gear properly designed shaper cutter.

Second, distance a also affects the parameters of the transient profile that connects the bottom land and the involute tooth profile of the cut gear. When distance a exceeds a certain allowed value, the transient profile can spread out beyond the allowed limits.

It has been proven in practice that the distance a for which the length of the top cutting edge is sufficient also satisfies the requirements imposed by the parameters of the transient profile. Therefore, the optimal value of distance a can be computed from the condition of sufficient length of the top cutting edge of the gear shaper cutter.

The length of the top cutting edge $t_{o.c}$ must not be shorter than a specific allowed value, $t_{o.c} \le [t_{o.c}]$. The shortest allowed length $[t_{o.c}]$ of the top cutting edge depends on module m of the shaper cutter. It can be computed from the empirical formula

$$[t_{o.c}] = \sqrt{0.2594m - 0.0375} \tag{10.29}$$

To compute for the actual length of the top cutting edge $t_{o.c}$ of the gear shaper cutter, the following equation can be used (Figure 10.8)

$$t_{o.c} = 0.5 d_{o.c} \upsilon \tag{10.30}$$

where υ denotes the central angle that the top cutting edge spans over and $d_{o.c}$ is the outer diameter of the gear shaper cutter.

Figure 10.8 shows that for computation of the angle υ, the following formula is valid

$$\upsilon = \frac{2t_{w.c}}{d_{w.c}} - 2(\text{inv}\,\phi_o - \text{inv}\,\phi_w) \tag{10.31}$$

where ϕ_o denotes the profile angle at the outer diameter $d_{o.c}$ of the generating surface T of the gear shaper cutter and ϕ_w is the profile angle at the pitch diameter $d_{w.c}$ of the generating surface T.

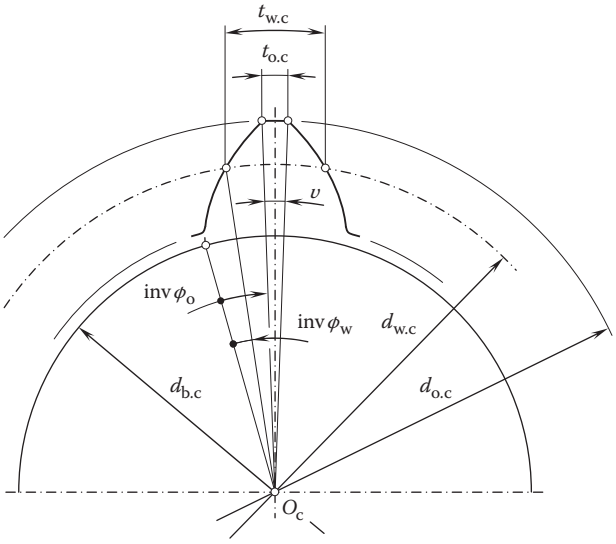

FIGURE 10.8
Design parameters of the gear shaper cutter affecting the actual length $t_{o.c}$ of the top cutting edge.

Equation (10.31) can be substituted into Equation (10.30). This yields an expression

$$t_{o.c} = d_{o.c}\left(\frac{t_{w.c}}{d_{w.c}} - \text{inv}\,\phi_o + \text{inv}\,\phi_w\right) \tag{10.32}$$

for the computation of the length of the top cutting edge of the shaper cutter.

The parameters that will be entered in Equation (10.32) can be expressed in terms of the design parameters of the gear shaper cutter:

$$d_{o.c} = d_{w.c} + 2.5m + 2a\tan\alpha_o \tag{10.33}$$

$$t_{w.c} = \frac{\pi m}{2} + B + 2a\tan\alpha_o\tan\phi_w \tag{10.34}$$

$$\phi_o = \cos^{-1}\frac{d_{w.c}\cos\phi_w}{d_{o.c}} \tag{10.35}$$

To compute for the length of the top cutting edge $t_{o.c}$ of the gear shaper cutter, use of commercial software (e.g., of MathCAD) has proven to be convenient.

Another approach in determining the length of the top cutting edge $t_{o.c}$ of the gear shaper cutter is used in practice. The shortest allowed length $[t_{o.c}]$ of the top cutting edge can be computed from Equation (10.29). Moreover, the desired distance a can be determined by using the corresponding value of the profile shift correction coefficient ξ_c.

In the nominal cross section, addendum of standard gear shaper cutters is equal to $1.25m$. Figure 10.9 illustrates the function of the reduced length of the top cutting edge $t_{o.c}/m$ of the new gear shaper cutter versus the profile shift correction coefficient ξ_c for standard gear

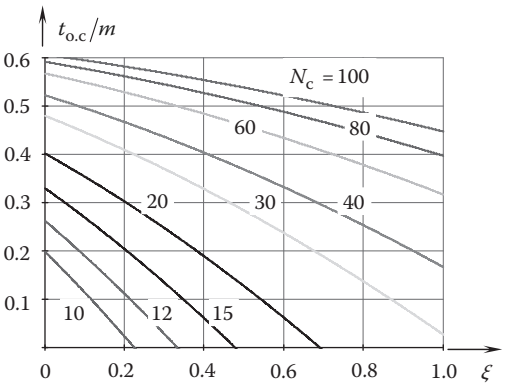

FIGURE 10.9
Graphical interpretation of the function of the reduced length of the top cutting edge $t_{o.c}/m$ of the new gear shaper cutter versus profile shift correction coefficient ξ_c for standard gear shaper cutters having different tooth number N_c.

shaper cutters having a different tooth number N_c. When computing for the coordinates of points of the curves in Figure 10.9, it is assumed that the backlash is equal to $B = 0.01m$.

The graph shown in Figure 10.9 allows for a reasonable determination of an approximate value of the profile shift correction coefficient ξ_c. Thus, the required distance a can be computed from the expression

$$a = \frac{\xi_c}{\tan \alpha_o} \cdot m \tag{10.36}$$

After the desired distance a is computed, the parameters of the cross section of the generating surface T of the gear shaper cutter are as follows

$$\text{Tooth addendum} \quad \Rightarrow \quad a_c = 1.25m + a \tan \alpha_o \tag{10.37}$$

$$\text{Tooth dedendum} \quad \Rightarrow \quad b_c = 1.25m - a \tan \alpha_o \tag{10.38}$$

To compute for the circular tooth thickness $t_{w.c}$, Equation (10.34) can be used.

Ultimately, verification of the absence of interference of the designed gear shaper cutter with the gear teeth must be performed.

10.6 Cutting Edge Geometry of a Gear Shaper Cutter Tooth

Shaper cutters for machining involute gears feature small values of the major geometrical parameters of cutting edges. Because of this, even small deviations in the geometrical parameters of cutting edges from the corresponding computed values can significantly affect the gear shaper cutter tool life and the accuracy of the machined gears. Therefore, rigorous control over the geometry of the cutting edges of gear shaper cutters tooth is advantageous.

Standard gear shaper cutters are designed so as to have the rake angle $\gamma_o = 5°$ at the top cutting edge and with the clearance angle $\alpha_o = 6°$. The inclination angle of the top cutting edge is $\lambda_o = 0°$. The values of angles γ_o, α_o, and λ_o do not change within the top cutting edge. Thus, they do not require further investigation.

Special care should be given to the lateral cutting edges of the gear shaper cutter.

10.6.1 Angle of Inclination of the Lateral Cutting Edge

For the computation of the actual value of the angle of the inclination at the current point of interest within the cutting edge, use of elements of vector algebra is helpful.

The local Cartesian coordinate system $x_m y_m z_m$ is associated with the cutting edge of the gear shaper cutter as shown in Figure 10.10. Origin of the coordinate system $x_m y_m z_m$ is at the current point of interest m of the cutting edge. In reality, a Cartesian coordinate system having an arbitrary orientation of the coordinate axes can be implemented. However, for the reader's convenience, the axes are oriented as shown in Figure 10.10.

To derive the equation for the angle of inclination λ_y at point m, the following three vectors are used.

(1) Vector **A** is the vector along the line of intersection of the rake surface R_s of the gear shaper cutter by the axial cross section through point m. The magnitude of vector **A** is chosen such that projection of vector **A** onto the coordinate plane $x_m y_m$ is equal to unit ($\text{pr}_{xy}\mathbf{A} = 1$). The following expression

$$\mathbf{A} = \mathbf{i} + \mathbf{k} \cdot \tan \gamma_o \tag{10.39}$$

is valid for the analytical description of vector **A**.

(2) Vector **B** is tangent to the cutting edge of the gear shaper cutter. The magnitude of vector **B** is chosen such that the projection of vector **B** onto the coordinate plane $x_m y_m$ is equal to unit ($\text{pr}_{xy}\mathbf{B} = 1$). For the analytical representation of vector **B**, the following expression

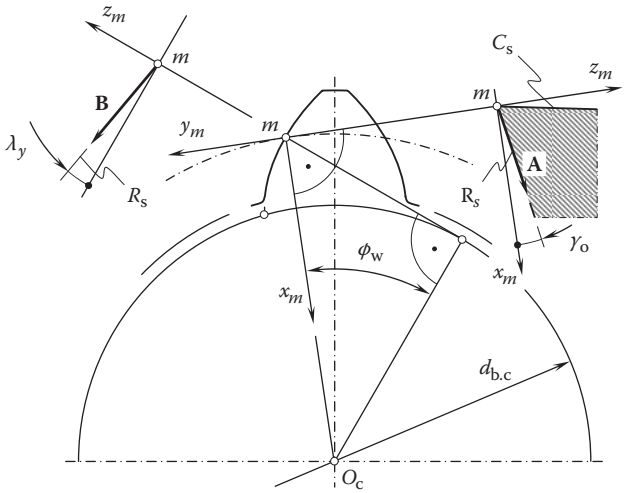

FIGURE 10.10
Cutting edge geometry of the involute gear shaper cutter tooth: angle of inclination λ of the cutting edge.

$$\mathbf{B} = \mathbf{i} \cdot \cos\phi_{y.c} - \mathbf{j} \cdot \sin\phi_{y.c} + \mathbf{k} \cdot \tan\lambda_y \tag{10.40}$$

can be composed.

(3) For solving the problem under consideration, the unit vector **j** is used.

By construction, vectors **A**, **B**, and **j** are located within a common plane. At point m within the cutting edge, this plane is tangent to the rake surface R_s of the gear shaper cutter tooth. Because vectors **A**, **B**, and **j** comprise a set of three coplanar vectors, their scalar triple product is identical to zero ($\mathbf{A} \times \mathbf{B} \cdot \mathbf{j} \equiv 0$). An expanded expression for the scalar triple product can be represented in the form of a determinant

$$\mathbf{A} \times \mathbf{B} \cdot \mathbf{j} \equiv \begin{vmatrix} 0 & 1 & 0 \\ 1 & 0 & \tan\gamma_o \\ \cos\phi_{y.c} & -\sin\phi_{y.c} & \tan\lambda_y \end{vmatrix} = 0 \tag{10.41}$$

A formula

$$\lambda_y = \tan^{-1}(\tan\gamma_o \cos\phi_{y.c}) \tag{10.42}$$

for the computation of the inclination angle λ_y immediately follows from Equation (10.41).

Analysis of Equation (10.42) reveals that a very limited variation in the angle of inclination within the lateral cutting edge of the gear shaper cutter is observed. This variation can be neglected when designing a gear shaper cutter.

10.6.2 Rake Angle of the Lateral Cutting Edge

The normal rake angle at the lateral cutting edge of the gear shaper cutter tooth is measured within a cross section of the cutting wedge by a plane that is perpendicular to the cutting edge at the point of interest.

The rake surface R_s of a standard gear shaper cutter is shaped in the form of a cone of revolution. The axis of rotation of the cone of revolution aligns with the axis of the shaper cutter.

To determine the normal rake angle γ_N, a local Cartesian coordinate system $x_m y_m z_m$ is used. Origin of the coordinate system $x_m y_m z_m$ is at the point of interest within the lateral cutting edge. Coordinate axes are oriented as shown in Figure 10.11.

Three vectors are used to derive the equation for the normal rake angle γ_N of the involute gear shaper cutter.

(1) The earlier derived vector **B** [see Equation (10.40)] is used to derive the equation for the rake angle γ_N.

(2) Vector **C** is along the line of intersection of the rake surface R_s by the plane that is tangent to the base cylinder of the gear shaper cutter. The magnitude of vector **C** is chosen so that the projection of vector **C** onto the coordinate plane $x_m y_m$ is equal to unit ($\text{pr}_{xy}\mathbf{C} = 1$). This yields the following expression for the analytical representation of vector **C** in the local coordinate system $x_m y_m z_m$

$$\mathbf{C} = \mathbf{i} \cdot \sin\phi_{y.c} + \mathbf{j} \cdot \cos\phi_{y.c} + \mathbf{k} \cdot \tan\gamma_m \tag{10.43}$$

where γ_m denotes the rake angle in the major section plane.

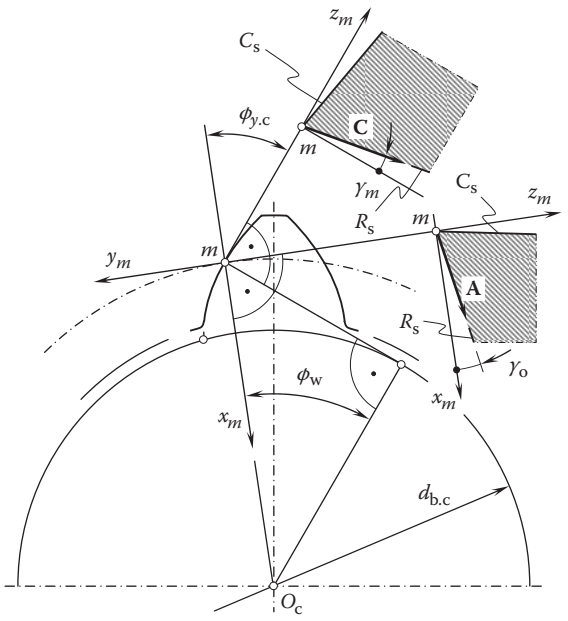

FIGURE 10.11
Cutting edge geometry of the involute gear shaper cutter tooth: normal rake angle γ_N of the cutting edge.

The third vector is the unit vector **j** along the y_m axis.

By construction, vectors **A**, **C**, and **j** are located within a common plane. At point m within the cutting edge, this plane is tangent to the rake surface R_s of the gear shaper cutter tooth. Because vectors **A**, **C**, and **j** comprise a set of three coplanar vectors, their scalar triple product is identical to zero ($\mathbf{A} \times \mathbf{C} \cdot \mathbf{j} \equiv 0$). The scalar triple product $\mathbf{A} \times \mathbf{C} \cdot \mathbf{j} \equiv 0$ can be expressed in the form of determinant

$$\mathbf{A} \times \mathbf{C} \cdot \mathbf{j} \equiv \begin{vmatrix} 0 & 1 & 0 \\ 1 & 0 & \tan\gamma_o \\ \sin\phi_{y.c} & \cos\phi_{y.c} & \tan\gamma_m \end{vmatrix} = 0 \tag{10.44}$$

Equation (10.44) casts into the formula

$$\gamma_m = \tan^{-1}(\tan\gamma_o \sin\phi_{y.c}) \tag{10.45}$$

for the computation of the rake angle γ_m at the point of interest within the lateral cutting edge of the gear shaper cutter tooth.

The normal rake angle γ_N can be expressed in terms of (a) the rake angle γ_m and (b) the angle of inclination γ_y. For this purpose, the formula

$$\gamma_N = \tan^{-1}(\tan\gamma_m \cos\lambda_y) \tag{10.46}$$

can be used. This formula is known from many advanced sources (e.g., [136, 138, 143]).

Ultimately, after Equations (10.42) and (10.45) are substituted into Equation (10.46), the following formula

$$\gamma_{\mathrm{N}} = \tan^{-1}\left(\frac{\tan\gamma_{\mathrm{o}}\sin\phi_{y.\mathrm{c}}}{\sqrt{1+\tan^2\gamma_{\mathrm{o}}\cos^2\phi_{y.\mathrm{c}}}}\right) \tag{10.47}$$

can be obtained for the computation of the normal rake angle γ_{N} of the gear shaper cutter.

10.6.3 Clearance Angle of the Lateral Cutting Edge

A screw involute surface through the lateral cutting edge serves as the clearance surface of the shaper cutter tooth. In the cross section of the generating surface T by a cylinder that is coaxial with the gear shaper cutter, the surface T and the clearance surface C_{s} form the clearance angle α_{f}. The value of the clearance angle α_{f} is equal to the lead angle of the helix within the intersecting cylinder. Thus, the following formula can be used to compute for the angle α_{f}

$$\alpha_{\mathrm{f}} = \tan^{-1}\left(\frac{d_{y.\mathrm{c}}}{d_{\mathrm{w.c}}}\cdot\tan\alpha_{\mathrm{o}}\tan\phi_{\mathrm{w}}\right) \tag{10.48}$$

where $d_{y.\mathrm{c}}$ denotes the diameter of the intersecting cylinder through the point of interest m within the lateral cutting edge.

For the computation of the clearance angle α_{f} at the pitch diameter of the gear shaper cutter, Equation (10.48) simplifies to

$$\alpha_{\mathrm{f}} = \tan^{-1}(\tan\alpha_{\mathrm{o}}\tan\phi_{\mathrm{w}}) \tag{10.49}$$

When the clearance angle α_{f} is known, the normal clearance angle α_{N} can be computed. The clearance angle α_{N} is measured within the cross section of the cutting wedge by a plane that is perpendicular to the cutting edge at the point of interest.

To derive the equation for the normal clearance angle α_{N} of the gear shaper cutter for machining involute gears, it is convenient to use the method that is based on vector algebra.

Origin of a local Cartesian coordinate system $x_m y_m z_m$ is located at the point of interest m within the lateral cutting edge of the gear shaper cutter tooth. Axes of the coordinate system $x_m y_m z_m$ are directed as shown in Figure 10.12.

The vector **D** in Figure 10.12 is constructed so that it is tangent to the line of intersection of the clearance surface C_{s} by a plane that is tangent to the base cylinder of the gear shaper cutter. In the coordinate system $x_m y_m z_m$, the vector **D** can be analytically expressed as

$$\mathbf{D} = \mathbf{i}\cdot\tan\alpha_m + \mathbf{k} \tag{10.50}$$

where α_{m} denotes the clearance angle that is measured in the major cross section of the cutting wedge.

The vector **E** through the point of interest m is constructed so that it is tangent to the helix within the intersecting cylinder. This allows the following expression

$$\mathbf{E} = \mathbf{i}\cdot\tan\alpha_{\mathrm{f}}\cos\phi_{y.\mathrm{c}} - \mathbf{j}\cdot\tan\alpha_{\mathrm{f}}\sin\phi_{y.\mathrm{c}} + \mathbf{k} \tag{10.51}$$

for vector **E**.

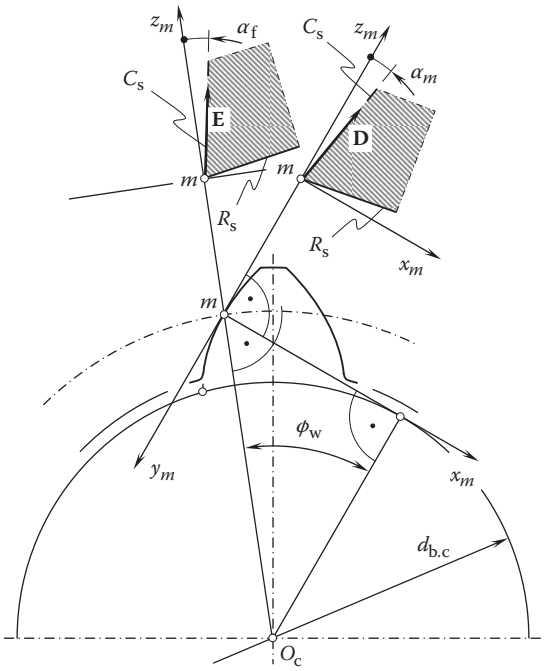

FIGURE 10.12
Cutting edge geometry of the involute gear shaper cutter tooth: normal clearance angle α_N of the cutting edge.

Vectors **D**, **E**, and **j** are tangent to the clearance surface C_s of the gear shaper cutter tooth. They comprise a set of coplanar vectors for which the identity $\mathbf{D} \times \mathbf{E} \cdot \mathbf{j} \equiv 0$ is valid. The identity can be expressed in the form of determinant

$$\mathbf{D} \times \mathbf{E} \cdot \mathbf{j} \equiv \begin{vmatrix} 0 & 1 & 0 \\ \tan\alpha_m & 0 & 1 \\ \tan\alpha_f \cos\phi_{y.c} & -\tan\alpha_f \sin\phi_{y.c} & 1 \end{vmatrix} = 0 \tag{10.52}$$

Taking Equation (10.49) into account allows us to cast Equation (10.52) into the formula

$$\alpha_m = \tan^{-1}(\tan\alpha_o \sin\phi_w) \tag{10.53}$$

for the computation of the clearance angle α_m.

An analysis of Equation (10.53) shows that the value of clearance angle α_m does not change within the lateral cutting edge of the gear shaper cutter tooth.

The normal clearance angle α_N can be expressed in terms of (a) the clearance angle α_m and (b) the angle of inclination λ_y. For this purpose, the formula

$$\alpha_N = \cot^{-1}(\cot\alpha_m \cos\lambda_y) \tag{10.54}$$

can be used. This formula is known from many advanced sources (e.g., [136, 138, 143]).

Ultimately, after Equations (10.42) and (10.53) are substituted into Equation (10.54), the following formula

$$\alpha_N = \tan^{-1}\left(\tan\alpha_o \sin\phi_w \sqrt{1+\tan^2\gamma_o \cos^2\phi_w}\right) \tag{10.55}$$

can be obtained for the computation of the normal clearance angle of the gear shaper cutter.

As follows from Equation (10.55), the value of the normal clearance angle α_N at a point of interest within the lateral cutting edge of the gear shaper cutter depends on the rake angle γ_o.

The following values of the design parameters are common for standard shaper cutters: (a) clearance angle $\alpha_o = 6°$ and (b) profile angle $\phi_w = 20°$. Under such a scenario, the normal clearance angle is $\alpha_N \cong 2°10'$.

10.6.4 Improvement in the Geometry of Lateral Cutting Edges

The actual values of the geometrical parameters of the cutting edge of the gear shaper cutter are insufficient and are significantly far from the optimum values.

The profile angle of the gear shaper cutter tooth $\phi_{y.c}$ varies within the lateral cutting edge. Its value is smallest at the end of active profile diameter $d_{l.c}$ and largest at the outer diameter $d_{o.c}$. Variation in the angle $\phi_{y.c}$ depends on the tooth number N_c of the shaper cutter. The cutting edge geometry of the gear shaper cutter is significantly affected by the variation in the tooth profile angle.

Enhancement of the geometry of the rake surface of the gear shaper cutter tooth. For the standard shaper cutter with a rake angle $\gamma_o = 5°$, the smallest value of the normal rake angle γ_N can be as small as $\gamma_N = 0°$. This occurs when the base diameter $d_{b.c}$ is equal to the end of the active profile diameter $d_{l.c}$ of the shaper cutter. The largest normal rake angle $\gamma_N = 2–3°$ is observed at the outer diameter of the gear shaper cutter. Evidently, the normal rake angle in the range of $\gamma_N = 0–3°$ is too small. Cutting performance can be enhanced if the rake angle γ_N of the cutting tool is increased.

The normal rake angle γ_N can be increased when the rake angle γ_o at the outer diameter of the gear shaper cutter is larger [see Equation (10.47)]. Improving the cutting performance of the shaper cutter in this manner, however, is not promising for two reasons.

First, a significant increase in the rake angle γ_o is required for a reasonable increase in the normal rake angle γ_N. Second, the accuracy of the shaper cutter is significantly affected by the increased rake angle γ_o. The larger the rake angle γ_o, the larger the deviations of the actual tooth profile of the machined gears from the desired tooth profile. For these reasons, improvement of the cutting performance of the gear shaper cutter using this approach is impractical.

For particular cases of gear shaping, shaper cutters with modified rake surfaces can be implemented.

An example of the modified rake surface R_s of the coarse pitch gear shaper cutter is depicted in Figure 10.13. The portion of the rake surface R_s^o at the outer cylinder of the shaper cutter is formed by a cylindrical grinding wheel. The grinding wheel of diameter d_{gw} is used for this purpose. Portions of the rake surface R_s^f close to the lateral cutting edges are generated with a conical grinding wheel. Design parameters of the grinding wheel, for example, the outer diameter d_{gw} and the profile angle θ_{gw}, as well as the setup parameters—(a) the angle φ_{gw} that the grinding wheel axis of rotation O_{gw} makes with the centerline of the shaper cutter tooth, (b) location of the grinding wheel apex A_{gw} in radial

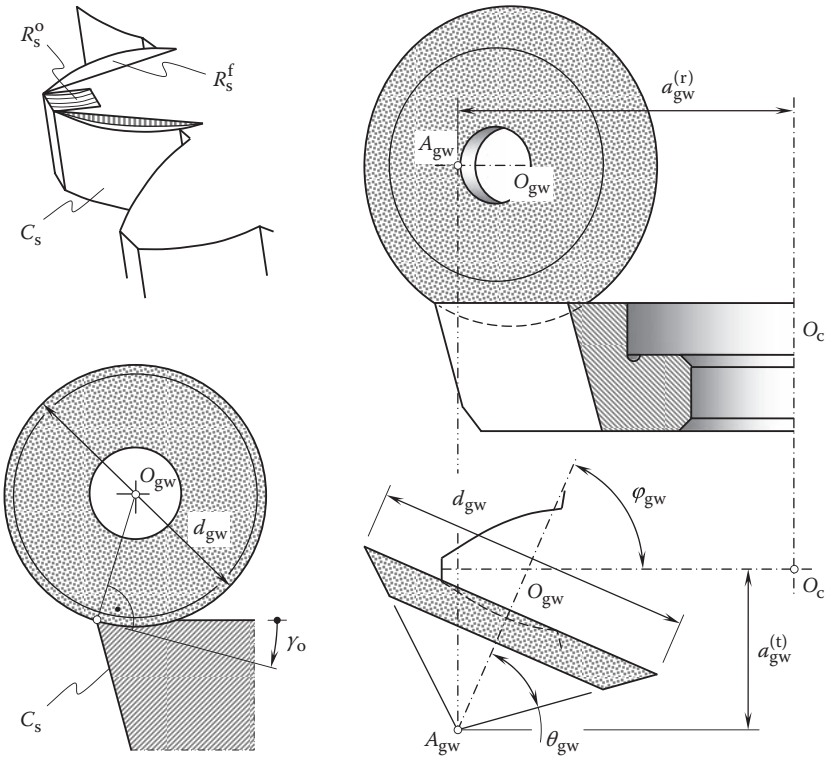

FIGURE 10.13
A type of modification of the rake surface R_s of the coarse pitch gear shaper cutter.

direction $a_{gw}^{(r)}$, and (c) location of the grinding wheel apex A_{gw} in tangential direction $a_{gw}^{(t)}$- are computed for the shaper cutter of a given design. In Figure 10.13, the modification of the rake surface of the gear shaper cutter makes it possible to design a gear cutting tool with the optimal values of the normal rake angle γ_N. In this way, the cutting performance of the shaper cutter can be significantly enhanced. Use of modification of this type (Figure 10.13) is practical for gear shaper cutters having a large outer diameter ($d_{o.c} \geq 360$ mm).

Rake surfaces of each tooth of gear shaper cutters of smaller outer diameter can be ground using either double-conical grinding wheel or the form cutting tool as shown in Figure 10.14. The shape of the generating surface T_{gw} of the form grinding wheel is designed so as to enable the lateral cutting edges of the ground gear shaper cutter to be identical to that of the new one. The outer diameter of the grinding wheel d_{gw} and the distance a_{gw} between the axis of rotation O_{gw} of the grinding wheel and the axis of rotation O_c of the shaper cutter, as well as length b_{gw} of the grinding wheel top land, are computed so as to enable a design of the gear shaper cutter with an optimal normal rake angle γ_N value.

Shaping of coarse pitch spur gears having a large tooth number N_g is an appropriate area for the implementation of a gear shaper cutter with a modified rake surface. The modification of the rake surface of the shaper cutter tooth becomes more practical when the tool life of the shaper cutter has to be sufficient for machining at least one gear of large diameter.

Enhancement of the geometry of the clearance surface of the gear shaper cutter tooth. The normal clearance angle of the shaper cutter is also very far from the optimal value for this parameter of the cutting edge geometry. Both spur and helical gear shaper cutters have

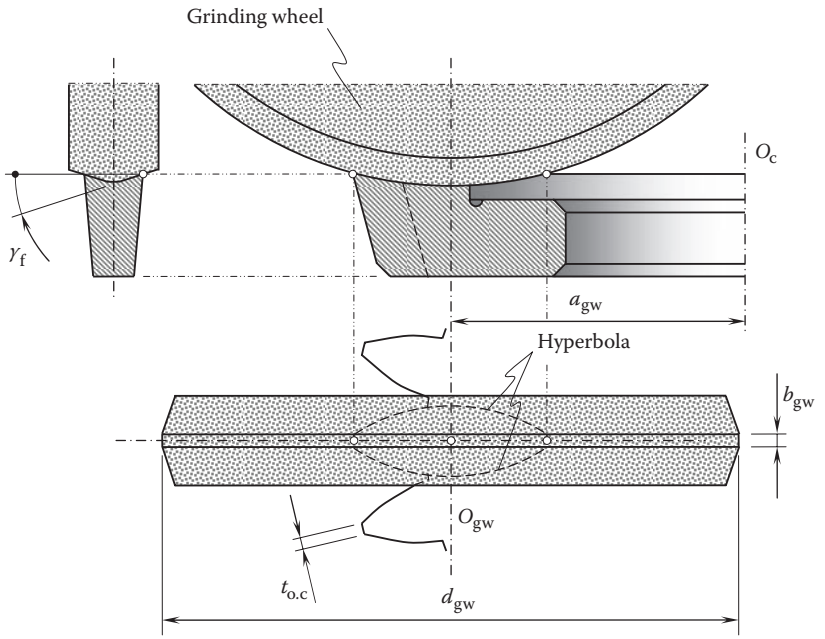

FIGURE 10.14
An example of modification of the rake surface R_s of the medium-size gear shaper cutter.

undesirably small normal clearance angle α_N. It is much more difficult to improve the geometry of the clearance surface of the gear shaper cutter. However, such possibilities are feasible and they can be determined. As an example, consider the helical gear shaper cutter [68] for machining of involute gears (Figure 10.15).

The generating surface of the helical shaper cutter is shaped in the form of a screw involute surface *T*. Theoretically, any line within the surface *T* can serve as a cutting edge of the gear shaper cutter. The screw involute surface can be generated by the straight line that is performing the screw motion. There are no principal constraints on using the straight generating line as the lateral cutting edge CE of the shaper cutter.

A plane that is tangent to the generating surface *T* is a plane T_{pl} through the straight generating line. In the lower portion of Figure 10.15, the particular cutting edge CE that is aligned with the straight generating line of the surface *T* is projected into the point CE. In this illustration, the tangent plane is projected into the line T_{pl}.

Because the lateral cutting edge CE is straight, the plane can be chosen as the clearance surface C_s (another plane can also be chosen as the rake surface R_s) of the shaper cutter tooth. The plane C_s is a plane through the cutting edge CE. It can be constructed so as to pass at the optimal normal clearance angle α_N^{opt} relative to the tangent plane T_{pl}. This means that the normal clearance angle of the gear shaper cutter is (1) of constant value within the lateral cutting edge and (2) it could be of optimal value at every point of the lateral cutting edge. Use of gear shaper cutters having an optimal value of the normal clearance angle extends the tool life of the shaper cutter and enhances the accuracy of the machined gears.

The same is true with respect to the rake surface. The rake surface R_s is a plane through the cutting edge CE. It can be designed so as to form an optimal normal rake angle γ_N^{opt}

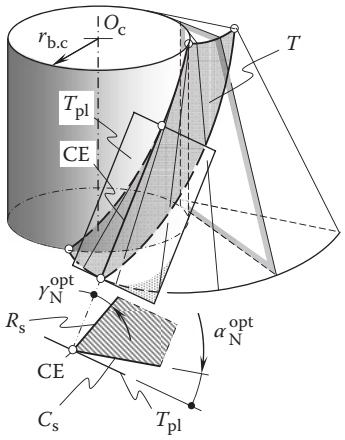

FIGURE 10.15
Possibility of optimization of the cutting edge geometry of a helical gear shaper cutter.

with respect to a perpendicular to the tangent plane T_{pl}. Again, the normal rake angle is of constant value within the lateral cutting edge, and the value of the rake angle γ_N^{opt} could be optimal at every point of the lateral cutting edge. Use of gear shaper cutters having an optimal value of the normal rake angle extends the tool life of the shaper cutter and enhances the accuracy of the machined gears.

Similar improvements are feasible for the lateral cutting edge of the opposite side of the shaper cutter tooth profile. The design of the helical gear shaper cutter was first proposed by Radzevich [68] and later investigated in another work [154]. There is plenty of room for improvements using this concept.

10.7 Desired Corrections to the Gear Shaper Cutter Tooth Profile

Working surfaces formed by the cutting wedge of the gear shaper cutter tooth are shaped in the form of (1) a cone of revolution for the rake surface, (2) a cone of revolution for the clearance surface at the top cutting edges, or (3) a screw involute surface for the clearance surface at the lateral cutting edges of the gear shaper cutter tooth. The lines of intersection of the clearance surfaces by the rake surface are within the corresponding portions of the generating surface of the shaper cutter. Otherwise, deviations of the actual cutting edges of the shaper cutter from its generating surface are all but unavoidable.

Resharpening of standard gear shaper cutters is performed over the conical rake face. The addendum modification coefficient changes after each resharpening of the shaper cutter. However, it is known that the same involute gear can be properly machined with shaper cutters having a different addendum modification coefficient value. This means that use of a screw involute surface as the clearance surface of the lateral tooth profiles of the gear shaper cutter tooth is reasonable.

Because the rake angle exceeds zero ($\gamma_o > 0°$), the projection of the actual lateral cutting edge onto the plane perpendicular to the axis of rotation of the gear shaper cutter deviates from

the true involute curve. The deviations of the gear shaper cutter tooth are transferred to the machined gear. Actual values of the deviations strongly depend on the value of the rake angle γ_o and the value of the clearance angle α_o. This is the major reason for why standard shaper cutters are designed with very small values of these geometrical parameters of the cutting wedge ($\gamma_o = 5°$ and $\alpha_o = 6°$). No practical possibilities are available that would result in an increase of the values of angles γ_o and α_o for gear shaper cutters of standard design.

The impact of the cutting edge geometry onto the accuracy of the gear shaper cutter tooth profile can be evaluated. For this purpose, it is convenient to determine the value of the tooth profile angle of the rack that can be generated by the projection of the lateral cutting edge onto the plane perpendicular to the shaper cutter axis of rotation.

Consider a point m that is located at the intersection of the cutting edge and the circle of pitch diameter of the gear shaper cutter. A local Cartesian coordinate system $x_m y_m z_m$ is associated with the shaper cutter. Origin of the coordinate system $x_m y_m z_m$ is located at point m. The z_m axis is aligned with the axis of rotation O_c of the shaper cutter. The rest of the coordinate axes are oriented as shown in Figure 10.16.

Vectors **A**, **B**, and **C** through point m are constructed so that all three of them are within a common tangent plane to the clearance surface C_s.

Vector **A** is within the plane that is perpendicular to the axis of rotation of the gear shaper cutter. This vector is tangent to the clearance surface of the shaper cutter tooth. In the coordinate system $x_m y_m z_m$, vector **A** can be analytically described by the formula

$$\mathbf{A} = \mathbf{i} + \mathbf{j} \cdot \tan \phi_w \tag{10.56}$$

Vector **B** is tangent to the helix of intersection of the clearance surface C_s by the pitch cylinder of the gear shaper cutter. This vector forms the clearance angle α_f with the axis of rotation O_c of the shaper cutter. For vector **B**, the following expression

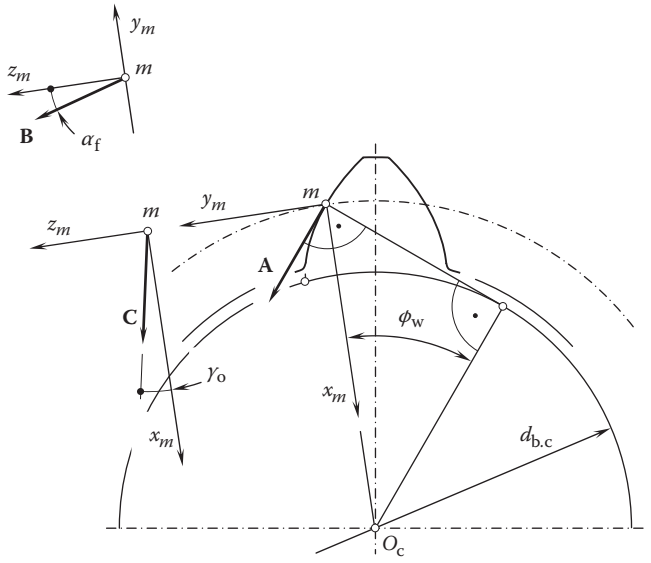

FIGURE 10.16
Computation of the desired correction to the profile angle ϕ_w of the gear shaper cutter tooth.

$$\mathbf{B} = -\mathbf{j} \cdot \tan \alpha_{\mathrm{f}} + \mathbf{k} \tag{10.57}$$

is valid.

Taking into account Equation (10.48) for the clearance angle α_{f}, this expression for vector **B** can be represented in the form

$$\mathbf{B} = -\mathbf{j} \cdot \tan \alpha_{\mathrm{o}} \tan \phi_{\mathrm{w}} + \mathbf{k} \tag{10.58}$$

Vector **C** is tangent to the cutting edge. Therefore, in the coordinate system $x_m y_m z_m$, it can be analytically represented by the expression

$$\mathbf{C} = \mathbf{i} + \mathbf{j} \cdot \tan \phi_{\mathrm{ce}} + \mathbf{k} \cdot \tan \gamma_{\mathrm{o}} \tag{10.59}$$

where ϕ_{ce} denotes the tooth profile angle of the auxiliary rack for the projection of the lateral cutting edge.

Because vectors **A**, **B**, and **C** comprise a set of coplanar vectors, the identity

$$\mathbf{A} \times \mathbf{B} \cdot \mathbf{C} \equiv 0 \tag{10.60}$$

is observed.

Equation (10.60) can be represented in the form

$$\mathbf{A} \times \mathbf{B} \cdot \mathbf{C} \equiv \begin{vmatrix} 1 & \tan \phi_{\mathrm{w}} & 0 \\ 0 & -\tan \alpha_{\mathrm{o}} \tan \phi_{\mathrm{w}} & 1 \\ 1 & \tan \phi_{\mathrm{ce}} & \tan \gamma_{\mathrm{o}} \end{vmatrix} = 0 \tag{10.61}$$

Ultimately, Equation (10.61) casts into a formula

$$\phi_{\mathrm{ce}} = \tan^{-1}\left[\tan \phi_{\mathrm{w}} (1 - \tan \alpha_{\mathrm{o}} \tan \gamma_{\mathrm{o}})\right] \tag{10.62}$$

for the computation of the corrected tooth profile angle ϕ_{ce}.

Computations in compliance with Equation (10.62) indicate that, for the gear shaper cutter having a profile angle $\phi_{\mathrm{c}} = 20°$, a rake angle $\gamma_{\mathrm{o}} = 5°$, and a clearance angle $\alpha_{\mathrm{o}} = 6°$, the profile angle ϕ_{ce} is equal to $\phi_{\mathrm{ce}} = 20°10'$.

It is recommended to generate the clearance surface of the lateral sides of the tooth profile of standard shaper cutters with the auxiliary rack having a modified tooth profile. Then, the pitch diameter of the base cylinder of the clearance surfaces can be computed as

$$d^{*}_{\mathrm{w.c}} = d_{\mathrm{w.c}} \cos \phi_{\mathrm{ce}} = mN_{\mathrm{c}} \cdot \cos \phi_{\mathrm{ce}} \tag{10.63}$$

Special care is required to avoid confusion between the different base cylinders of the shaper cutter, that is, between the base cylinder of the generating surface T of the shaper cutter and the base cylinder of the clearance surface of the lateral cutting edge of the gear shaper cutter tooth. Because the generating surface T and the clearance surface C_{s} are two different screw involute surfaces, it is evident that they are constructed from different base cylinders.

10.8 Thickness of Chip Cut by Gear Shaper Cutter Tooth

Gear shaping operation is a type of continuously indexing method of gear machining. The kinematics of the machining process of a work gear with a gear shaper cutter is illustrated in Figure 10.1. When shaping a gear using the gear shaper cutter, the work gear is rotating about its axis of rotation O_g. The shaper cutter is rotating about its axis of rotation O_c. Rotation of the gear ω_g is timed with the rotation of the shaper cutter ω_c so that the ratio $\omega_g/\omega_c = N_c/N_g$ is valid.

Two motions are required for machining of a work gear with the shaper cutter: primary motion (the motion of cut) and feed motion.

Reciprocation of the gear shaper cutter is used here as the primary motion. The reciprocation of the shaper cutter provides the necessary speed of cut $\mathbf{V}_{cut}$. Speed of cut is equal to the speed of the shaper cutter reciprocation V_{rc}.

Rotations of the work gear ω_g and the gear shaper cutter ω_c cause the feed rate motion F_c. Rolling of the pitch surfaces of the work gear and the shaper cutter about their axes of rotation allows for interpretation in the form of instant rotation of the gear shaper cutter pitch cylinder about pitch point. Speed of the instant rotation ω_{rl} can be expressed in terms of the rotations ω_g and ω_c, and the design parameters of the gear and the gear shaper cutter. Ultimately, speed of the feed motion F_c is equal to the speed of linear motion of the cutting edge of the shaper cutter tooth in its instant rotation

$$F_c = \omega_{rl} R_{rl} \tag{10.64}$$

where R_{rl} is the distance of a point of interest m of the shaper cutter cutting edge from pitch point P. The point of interest m can be chosen within any of three cutting edges of the shaper cutter tooth.

For a particular gear shaping operation, instant rotation ω_{rl} has a constant value (ω_{rl} = const). The distance R_{rl} depends on the coordinates of the point of interest m within the cutting edge of the gear shaper cutter. This can be specified by the position vector $\mathbf{r}_m$. Two vectors, $\boldsymbol{\omega}_{rl}$ and $\mathbf{r}_m$, allow for an expression

$$\mathbf{F}_c = \boldsymbol{\omega}_{rl} \times \mathbf{r}_m \tag{10.65}$$

for the computation of vector $\mathbf{F}_c$ of the feed motion.

To compute for the parameters of a portion of stock cut out by the gear shaper cutter tooth per stroke, the approach proposed by Shishkov [186] can be used.

Two consequent locations of the shaper cutter tooth are considered for the computation of thickness of cut. The initial position of the gear shaper cutter can be defined by a Cartesian coordinate system $X_gY_gZ_g$ that is embedded to the work gear (Figure 10.17). When machining, the work gear turns about its axis O_g through a certain portion ε_{st} of the roll angle ε. The angle ε_{st} is viewed as a roll angle per stroke of the shaper cutter. The actual value of the angle ε_{st} can be expressed in terms of: (1) the roll angle ε_o for the tooth profile point at the outer diameter of the gear tooth profile, (2) the roll angle ε_l for the tooth profile point at the inner diameter of the gear tooth profile, and (3) the number of strokes n_{st} of the gear shaper cutter necessary for shaping the whole tooth flank surface

$$\varepsilon_{st} = \frac{\varepsilon_o - \varepsilon_l}{n_{st}} \tag{10.66}$$

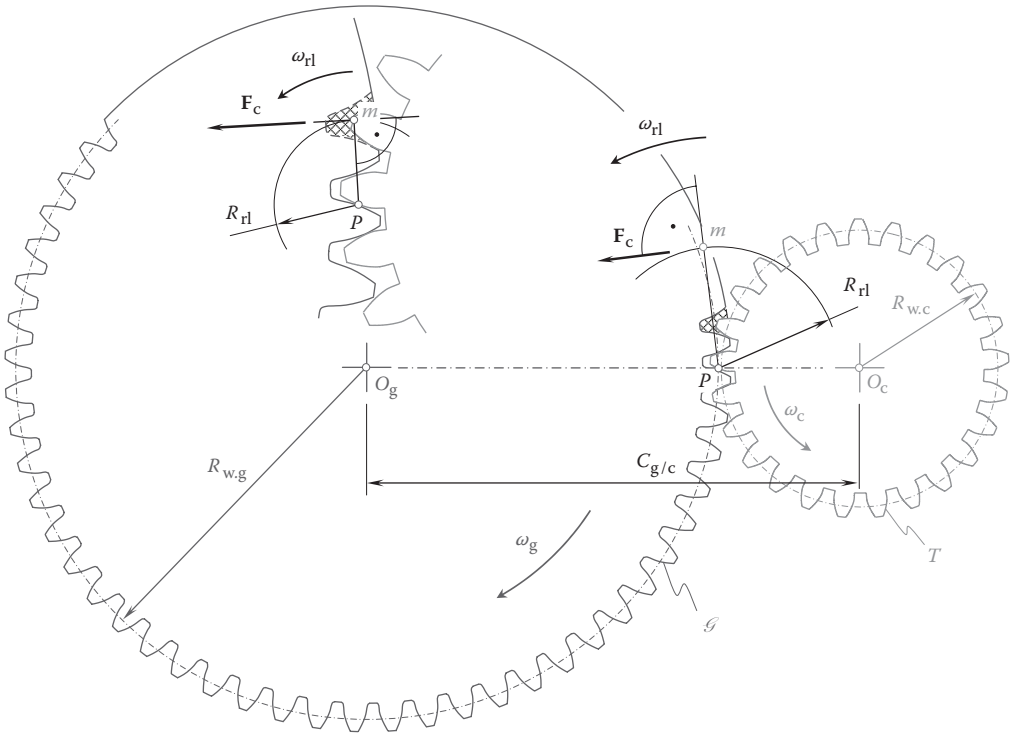

FIGURE 10.17
Feed motion F_c in shaping of a spur gear with the gear shaper cutter.

Usually, the value of the angle ε_{st} is in the range of $\varepsilon_{st} \cong 1°$ or so. It can vary depending on the requirements of a particular gear shaping operation.

Rotation of the shaper cutter ω_c is timed with the rotation of the work gear ω_g. The rotations ω_g and ω_c are timed so that the ratio

$$\frac{\omega_g}{\omega_c} = \frac{N_g}{N_c} \tag{10.67}$$

is observed.

Tooth ratio N_g/N_c is designated below as u. The angle of rotation of the cutter $\varepsilon_{st}^{(c)}$ can be expressed in terms of the angle of rotation of the work gear ε_{st} and the tooth ratio u

$$\varepsilon_{st}^{(c)} = \frac{\varepsilon_{st}}{u} \tag{10.68}$$

When the work gear turns about its axis O_g through the angle ε_{st}, the shaper cutter turns about its axis of rotation O_c through the corresponding angle $\varepsilon_{st}^{(c)}$. Moreover, in the relative motion of the gear shaper cutter with respect to the stationary work gear, the axis of rotation O_c turns about the axis of rotation O_g through the angle ε_{st}.

The operator of rotation $\mathbf{Rt}[\varepsilon_{st}^{(c)}, Z_c]$ can be used for the analytical description of the rotation of the gear shaper cutter about the axis O_c. Then, for the analytical description of the

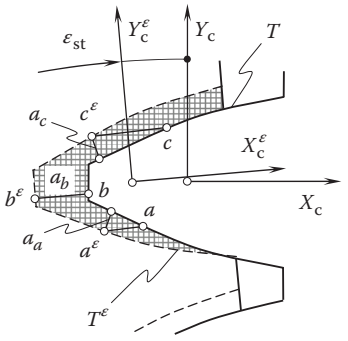

FIGURE 10.18
Thickness of cut when shaping a spur gear with the gear shaper cutter.

rotation of the shaper cutter about the axis O_g through the angle ε_{st}, the operator of rotation $\mathbf{Rt}(\varepsilon_{st}^{(c)}, Z_c)$ is used. Ultimately, translation at the center distance $C_{g/c}$ along the X_g axis can be analytically described by the operator of translation $\mathbf{Tr}(C, X_g)$.

In the case under consideration, the resultant linear transformation can be analytically described by three operators of elementary transformations: $\mathbf{Rt}[\varepsilon_{st}^{(c)}, Z_c]$, $\mathbf{Rt}(\varepsilon_{st}, Z_g)$, and $\mathbf{Tr}(C, X_g)$. To simplify the derivation of the required equations, it is not necessary to use all three operators of linear transformations ($\mathbf{Rt}[\varepsilon_{st}^{(c)}, Z_c]$, $\mathbf{Rt}(\varepsilon_{st}, Z_g)$, and $\mathbf{Tr}(C, X_g)$); instead, only the operator of rolling* $\mathbf{Rr}_u(\varepsilon_{st}, Z_g)$ is used (Figure 10.18). Ultimately, use of the operator of rolling $\mathbf{Rr}_u(\varepsilon_{st}, Z_g)$ enables the transition from the coordinate system $X_cY_cZ_c$ in its initial location to that same coordinate system in its current location, which is designated as $X_cY_cZ_c$.

Consider a point of interest within the cutting edge of the gear shaper cutter tooth. This might be a point a within the lateral cutting edge of the shaper cutter tooth, or a point b within the top cutting edge, or a point c within the lateral cutting edge of the opposite side of the tooth profile (Figure 10.18). To specify the coordinates of the point of interest, use of the local coordinate system $X_cY_cZ_c$ is often helpful.

For a given configuration of the generating surface T of the gear shaper cutter, position vector $\mathbf{r}_a$ of the point of interest a is known. (The same is valid with respect to any other point of interest within the cutting edge.) Equation (10.8) allows for computation of the unit normal vector $\mathbf{n}_{T.a}$ to the surface T at point a. When shaping a gear with the gear shaper cutter, the pitch cylinder of the shaper cutter rolls without sliding over the pitch cylinder of the work gear. For the consequent stroke of cutting, the work gear turns about its axis of rotation through the roll angle ε_{st} and the shaper cutter turns about its axis of rotation through the corresponding roll angle $\varepsilon_{st}^{(c)}$.

The new position of the gear shaper cutter is designated as T^{ε} in Figure 10.18. Under the rolling motion of the pitch cylinders, the point of interest a moves to the position a^{ε}. The position vector $\mathbf{r}_a^{\varepsilon}$ of the point of interest in the new location of the shaper cutter can be expressed in terms of the position vector $\mathbf{r}_a$ and the operator of rolling $\mathbf{Rr}_u(\varepsilon_{st}, Z_g)$ as follows

$$\mathbf{r}_a^{\varepsilon} = \mathbf{Rr}_u(\varepsilon_{st}, Z_g) \cdot \mathbf{r}_a \tag{10.69}$$

Similarly, the following expression

* See Chapter 4 for details on the operator of rolling $\mathbf{Rr}_u(\varepsilon_{st}, Z_g)$ as well as operators of rolling along and about other axes of a reference system.

$$\mathbf{n}^{\varepsilon}_{T.a} = \mathbf{R}\mathbf{r}_u(\varepsilon_{\text{st}}, Z_{\text{g}}) \cdot \mathbf{n}_{T.a} \tag{10.70}$$

is valid for the unit normal vector $\mathbf{n}^{\varepsilon}_{T.a}$ to the generating surface T^{ε} through point a^{ε}.

Thickness of cut is measured in the direction perpendicular to the machined surface of the work gear. Its value varies within the cutting edge of the gear shaper cutter. At point a^{ε}, the thickness of cut is denoted by a_a. Corresponding designations a_b and a_c are used to denote thickness of cut at points b^{ε} and c^{ε}, respectively. Thickness of cut a_a is equal to the length of the straight-line segment between point a^{ε} and surface T. The point of interception of the straight line $\mathbf{a}_a(t)$ through the point a^{ε} along the unit normal vector $\mathbf{n}_{T.a}$ (shown but not labeled in Figure 10.18) is computed as

$$\mathbf{a}_a(t) = \mathbf{r}^{\varepsilon}_a + t \cdot \mathbf{n}^{\varepsilon}_{T.a} \tag{10.71}$$

where t is a parameter of the straight line.

Solving the equation for the generating surface T of the gear shaper cutter [note that Equation (10.8) describes only one lateral flank of the surface T; a similar equation is valid for the opposite flank of the tooth of the surface T; and the equation for the top land of surface T is a trivial one], together with Equation (10.71), returns the position vector $\hat{\mathbf{r}}^{\varepsilon}_a$ of the point of interception of the straight line $\mathbf{a}_a(t)$ with the generating surface T. This immediately yields a formula

$$a_a = |\, \mathbf{r}^{\varepsilon}_a - \hat{\mathbf{r}}^{\varepsilon}_a \,| \tag{10.72}$$

for the computation of thickness of cut at the point of interest within the cutting edge of the gear shaper cutter tooth.

Equation (10.72), used to compute for the thickness of cut at a point of interest within the cutting edge of a shaper cutter, is derived with no simplifications, and it is an accurate one. It can be used when the point of interest is a far remote point from the pitch point in a gear shaping operation. In this case, the chip thickness is greater. The equation is also valid when the point of interest is close to the pitch point. In this second case, the cutting edge cuts thin chips. The chip thickness can be in the range of or close to the roundness of the cutting edge.

For approximate computations, simpler equations are known. However, the simplified equations are applicable either for remote portions of the cutting edges and thus, are not applicable for the cutting edges close to the pitch point, or alternatively, they are applicable for the points of the cutting edges close to the pitch point and are therefore not applicable for the remote portions of the cutting edges of the shaper cutter.

Equation (10.72) can be used to compute for all the other parameters of the portion of the stock that has been removed by a cutting edge of the gear shaper cutter: shape of the cross section of the portion of the stock, its area, etc.

Thickness of cut is an important issue for gear manufacturers because it significantly affects the wear of the shaper cutter teeth.

Cutting edges of the gear shaper cutter teeth cut chips of varying thickness.

First, thickness of cut depends on the distance between the point of interest and the pitch point. The greater the distance between these points, the larger the thickness of cut.

Second, different cutting edges of the gear shaper cutter tooth cut chips of varying thickness. The top cutting edge cuts the thickest chips. Thickness of chip that is cut by the

lateral cutting edge of the entering side of the tooth profile is larger than that of the recessing side of the gear shaper cutter tooth profile.

Lateral cutting edges of the gear shaper cutter teeth cut the stock mostly within the distance between the pitch point in the gear machining mesh and the point where the cutting begins. A small amount of the stock is also cut beyond the pitch point. The top cutting edge does not cut the stock beyond the pitch point.

A detailed analysis of thickness of cut is beyond the scope of this book and can be discussed separately.

10.9 Accuracy of Gears Cut with the Gear Shaper Cutter

The accuracy of gears cut with the shaper cutter is discussed here from the standpoint of satisfaction/violation of the necessary conditions of proper *PSG*. Satisfaction of the necessary conditions of proper *PSG* is a must when machining gears with the gear shaper cutter. (See Appendix B for details on conditions of proper *PSG*.)

When shaping a gear with a gear shaper cutter of conventional design, most of the conditions of proper *PSG* are satisfied, and usually it is not necessary to verify whether they are satisfied. In particular cases of gear machining, only the fifth and sixth conditions of proper *PSG* are required to be satisfied in a more careful analysis.

10.9.1 Satisfaction of the Fifth Condition of Proper *PSG*

To satisfy the fifth condition of proper *PSG*, no intersection of the adjacent portions of the tooth profile of the generating surface T of the gear shaper cutter must be observed. When shaping a gear with the shaper cutter, the pitch cylinder of the shaper cutter is rolling without sliding over the pitch cylinder of the work gear. In such kinematics of gear machining, violation of the fifth conditions of proper *PSG* may occur.

Teeth of the gear to be machined can be considered as a certain number N_g of portions of circular cylinder surface (root lands as well as top lands), and the corresponding number of pairs N_g of screw involute flank surfaces $\mathscr{G}$ for each of the gear teeth. Therefore, the generating surface T of the gear shaper cutter is composed of portions of the circular cylinders (N_c root lands and N_c top lands) and the corresponding number of the screw involute surfaces. When shaping the gear, the surface T makes contact with different portions of the gear tooth surface $\mathscr{G}$.

Various configurations of adjacent portions of the tooth profile of the generating surface of the gear shaper cutter are feasible. Adjacent portions of the generating surface T of the shaper cutter tooth profile can:

1. Share no common points with each other, that is, they can be apart from each other
2. Be connected to one another at the endpoints
3. Intersect each other

The first two items are not of interest from the perspective of satisfaction/violation of the fifth condition of proper *PSG*. No violation of the fifth condition of proper *PSG* occurs in items (1) and (2). In item (3), adjacent portions of the gear shaper cutter tooth profile

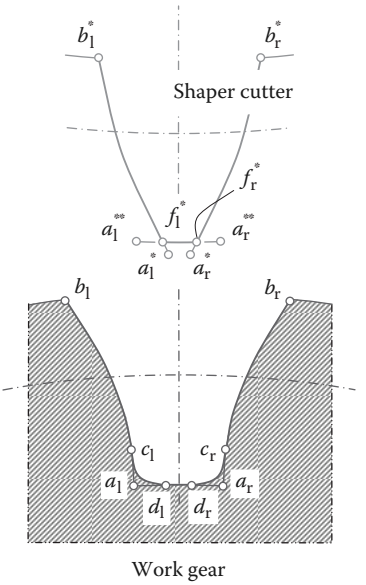

FIGURE 10.19
Violation of the fifth necessary condition of proper *PSG* in gear machining with the gear shaper cutter (transition curves are observed).

intersect each other. Because of the intersection, the fifth condition of proper *PSG* is violated. Ultimately, the transient curves on the gear tooth profile are observed as a result.

For example, for generation of the involute gear tooth profile, the generating surface T of the gear shaper cutter is used. The desired tooth profile of the surface T is composed of three arc segments (Figure 10.19): (1) left-side lateral arc segment $a_l^*b_l^*$, (2) top land circular arc segment $a_l^{**}b_r^{**}$, and (3) right-side lateral arc segment $a_r^*b_r^*$. The arc segments intersect each other as shown in Figure 10.19, and the points f_l^* and f_r^* are the points of the intersection. Therefore, the portions $a_l^*b_l^*$ and $a_l^{**}f_l^*$, as well as the portions $a_r^*f_r^*$ and $a_r^{**}f_r^*$ of the gear shaper cutter tooth profile do not exist physically. As a consequence, the portions a_lc_l and a_rc_r of the gear tooth profiles a_lb_l and a_rb_r (Figure 10.19) are substituted with the transient curves c_ld_l and c_rd_r, which form the fillets.* For the same reason, the portions a_ld_l and a_rd_r of the cylinder root land are also replaced with the transient curves c_ld_l and c_rd_r.

To satisfy the fifth condition of proper *PSG*, it is required to keep the transient curve within the space between the circle of root diameter $d_{f.g}$ and the circle of limit diameter $d_{l.g}$. This criterion can be stated analytically as

$$\Delta \le 0.5(d_{l.g} - d_{f.g}) = [\Delta] \tag{10.73}$$

When the inequality (10.73) is satisfied, the fifth condition of proper *PSG* is satisfied as well, and thus the gear can be machined with the gear shaper cutter in compliance with the blueprint specification. Therefore, satisfaction of expression (10.73) is vital for the computation of the desired design parameters of the shaper cutter.

* Reminder: The Start of Active Profile (*SAP*) is the intersection of the limit diameter and the involute profile (Figure 10.20). The points c_l and c_r within the circle of limit diameter $d_{l.g}$ are the points of *SAP*.

The inequality (10.73) can also be used for the determination and graphical interpretation of a zone of variation of the gear shaper cutter profile angle ϕ_t, that is, the zone within which satisfaction of the fifth condition of proper *PSG* is guaranteed.

Consider the generation of the tooth profile of the work gear with the gear shaper cutter (Figure 10.20). The left-hand side of the work gear tooth profile is generating along the active portion of the left-hand side line of action LA_l. Similarly, the right-hand side of the gear tooth profile is generating within the active potion of the right-hand side line of action LA_r. The tooth profile of the shaper cutter does not project beyond the root circle of diameter $d_{f.g}$ of the work gear. Because of this, certain portions of the active lines of action LA_l and LA_r cannot be represented physically in the gear machining operation. Therefore, within these portions of lines of action, transient curves of a certain height Δ are generated.

For the computation of the height of the transient curve, a corresponding equation can be derived.

Analysis of the *gear-to-shaper cutter* meshing diagram (Figure 10.20) allows us to compose equations for the lines of action LA_l and LA_r, as well as an equation for the root circle of diameter $d_{f.g}$. To compute for the actual value of deviation Δ, these equations yield the formula

$$\Delta = 0.5\left(\sqrt{d_{o.c}^2 + 4C_{g/c}^2 - 8d_{o.c}C_{g/c}\cos(\text{inv}\,\phi_{t.o})} - d_{f.g}\right) \tag{10.74}$$

where

$d_{o.c}$ = outside diameter of the gear shaper cutter
$C_{g/c}$ = center distance in the *work gear-to-shaper cutter* mesh
$\phi_{t.o}$ = transverse tooth profile angle at the outer diameter ($d_{o.c}$) of the shape cutter [$\phi_{t.o} = \cos^{-1}(d_{b.c} / d_{o.c})$]
$d_{b.c}$ = base diameter of the gear shaper cutter
$d_{f.g}$ = root diameter of the work gear

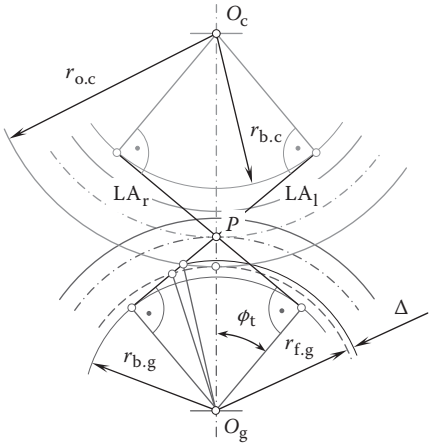

FIGURE 10.20
Gear-to-shaper cutter meshing diagram.

Informative graphical interpretation of the fifth condition of proper *PSG* in gear shaping operation can be drawn from the analysis of the work gear–to–shaper cutter meshing diagram.

The maximum value of the deviation Δ is limited to its maximal allowed value $[\Delta]$. This means that the interval $0 \leq \Delta \leq [\Delta]$ for the allowed value of the deviation Δ can be established. This inequality can be expressed in terms of the design parameters of the gear shaper cutter and the design parameters of the work gear.

To keep the deviation Δ within the allowed interval $0 \leq \Delta \leq [\Delta]$, the transversal pitch profile angle $\phi_{t.c}$ of the shaper cutter teeth has to satisfy the inequality (Figure 10.20):

$$\phi_{t.c}^{\min} \leq \phi_{t.c} \leq \phi_{t.c}^{\max} \tag{10.75}$$

Consideration of the inequality $0 \leq \Delta \leq [\Delta]$ together with Equations (10.74) and (10.75) allows for a graphical interpretation of the allowed zone, within which the fifth condition of proper *PSG* is satisfied (similar to the allowed zone shown in Figure 9.21 that is constructed for the case of planing gears with the rack cutter). The allowed zone can be constructed for the shaping of spur and/or helical gear of any design.

The satisfaction of the fifth condition of proper *PSG* must be verified for three cases:

- New gear shaper cutter (when the distance a to the nominal cross section of the shaper cutter is of maximal value $a = a_{\max} > 0$)
- Partially worn gear shaper cutter (when the distance a to the nominal cross section of the shaper cutter is equal to a $\cong 0$)
- Completely worn gear shaper cutter (when the distance a to the nominal cross section of the shaper cutter is minimal $a = a_{\min} < 0$)

Accuracy of the shaped gear can be increased if the design parameters of the shaper cutter correlate with the corresponding design parameters of the work gear. This is a way to satisfy the fifth condition of proper *PSG*.

10.9.2 Satisfaction of the Sixth Condition of Proper *PSG*

When machining a gear with a gear shaper cutter, the discrete type of generation of the gear tooth flank is observed. The machined gear tooth flank is shaped in the form of numerous curved cuts, each of which is tangent to the desired involute tooth form. Cusps are unavoidable on the gear tooth surface that is machined with the gear shaper cutter.

The cusp height on the machined gear tooth surface must be kept within the tolerance for accuracy of the tooth flank in order to satisfy the sixth condition of proper *PSG* (see Appendix B). Cusp height can also be interpreted as the deviation of the actual gear tooth surface from the desired tooth surface. From this perspective, the cusps result in low accuracy of the machined gear.

To conclude whether the sixth condition of proper *PSG* is satisfied, determination of the actual cusp height is required.

Consider a tooth of the work gear being machined with the gear shaper cutter (Figure 10.21). At an arbitrary point of the gear tooth profile, say at point i, the cutting edge of the shaper cutter is tangent to the involute profile of the gear tooth. On the consequent stroke, the cutting edge of the gear shaper cutter is tangent to the gear tooth profile at the adjacent point $(i + 1)$. The perpendiculars to the involute tooth profile at points i and $(i + 1)$ form the angle

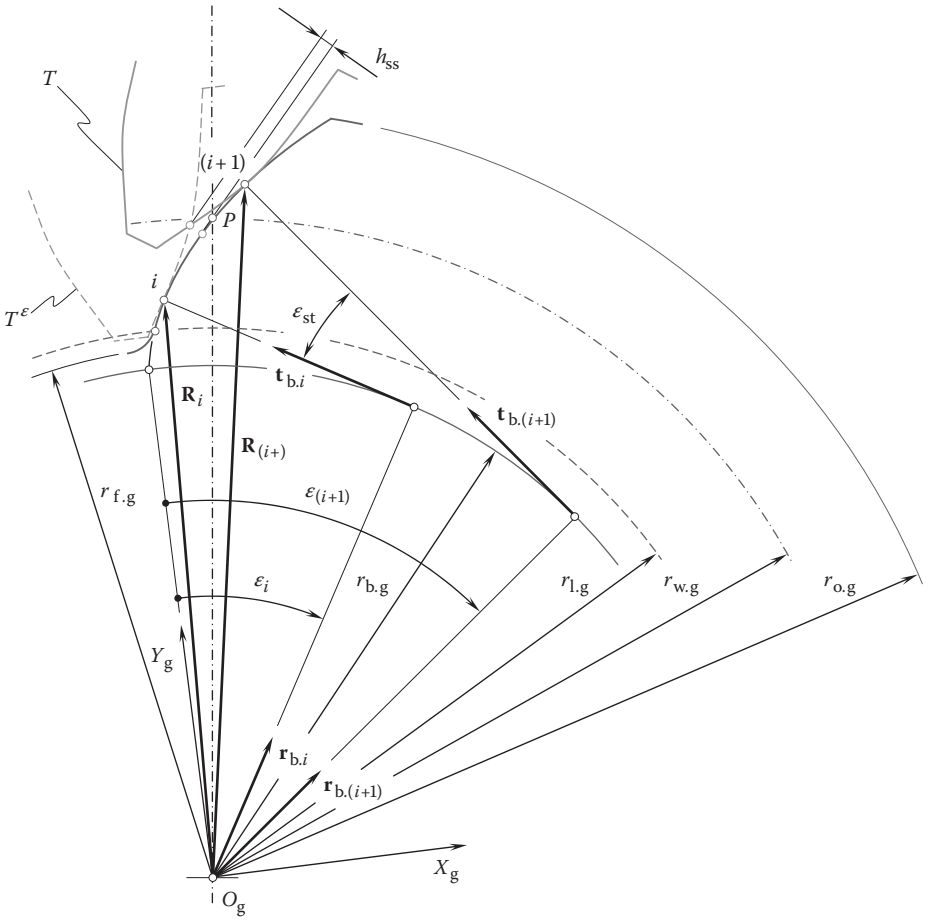

FIGURE 10.21
Principal elements of the discrete generation of the gear tooth profile with the gear shaper cutter.

that is equal to the roll angle per stroke ε_{st} of the gear shaper cutter. Ultimately, the desired smooth involute gear tooth profile is substituted with a polygonal shape having curved cusps on its profile. Deviation of the actual gear tooth profile from the desired tooth profile is denoted by h_{ss}. The deviation h_{ss} is measured along the perpendicular to the desired gear tooth surface that passes through the point of intersection of the ith and the $(i + 1)$-th cuts.

To compute for the deviation h_{ss}, it is convenient to consider the circular arc segments through points i and $(i + 1)$. Actually, only the length of the circular arc segment is of importance from the standpoint of solving the problem under consideration.

To compute for deviation h_{ss}, Equation (8.14) from [143] (Figure 10.22)

$$h_{ss} \cong \frac{\varepsilon_{st}}{r_i^{(c)}} \cdot R_i[R_i - r_i^{(c)}] \tag{10.76}$$

can be applied.

In Equation (10.76), current value of the radius of curvature R_i of the gear tooth profile is computed from the equation

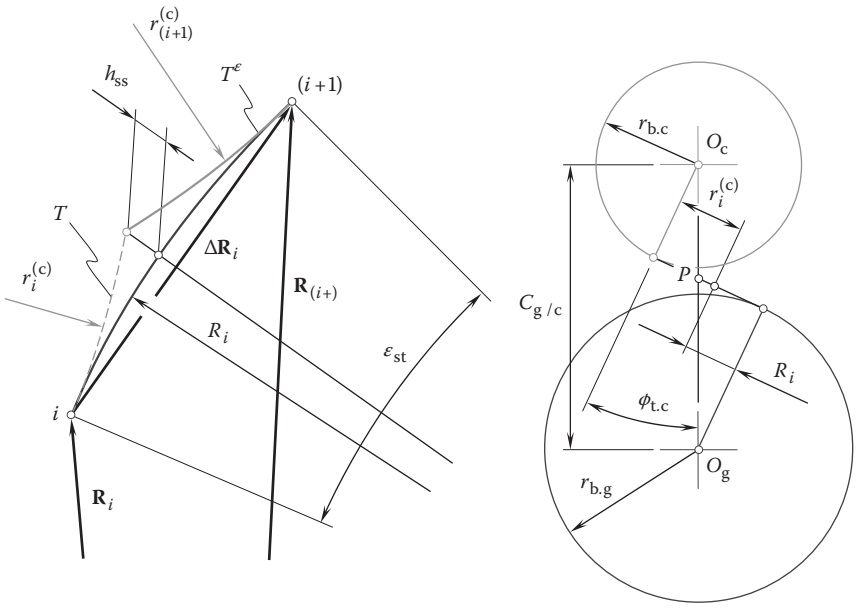

FIGURE 10.22
Geometry of an elementary cusp on the machined gear tooth profile.

$$R_i = \frac{\varepsilon_i + \varepsilon_{i+1}}{2} \cdot r_{b.g} \tag{10.77}$$

To compute for the corresponding radius of curvature $r_i^{(c)}$ of the gear shaper cutter tooth profile, the equation (Figure 10.22)

$$r_i^{(c)} \cong (r_{b.g} + r_{b.c}) \tan \phi_{t.c} - R_i \tag{10.78}$$

can be used.

The sixth condition of *PSG* is satisfied if and only if the inequality

$$h_{ss} \le [h_{ss}] \tag{10.79}$$

is valid.

10.10 Application of Gear Shaper Cutters

Cylindrical gears of any design can be cut with the gear shaper cutter. In particular, shaper cutters are used for machining of shoulder gears, cluster gears, etc. Machining of the cylindrical gear of small modules, having a large tooth number, a narrow face width, and a big helix angle, is especially efficient when using gear shaper cutters.

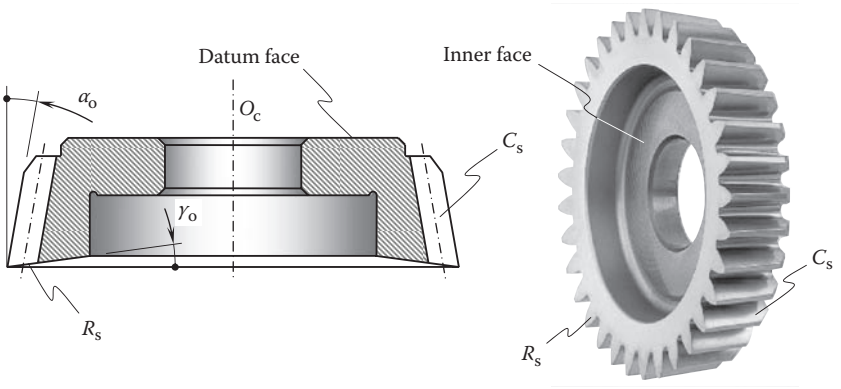

FIGURE 10.23
A typical disk-type gear shaper cutter.

10.10.1 Design of Shaper Cutters

Various types and sizes of gear shaper cutters are available in the market. Commonly, two basic designs of shaper cutters are used for machining of external gears: (1) disk type and (2) deep counterbore type.

Disk-type gear shaper cutters are the most commonly used cutters for machining of external gears and splines. Figure 10.23 shows a typical disk-type shaper cutter. This is the common type and it is normally installed directly on the cutter spindle (Figure 10.24). Disk-type shapers are also used on adapters, especially when the required size is between a disk and taper shank cutter.

Deep counterbore-type gear shaper cutters are similar to disk-type ones, except that the blank thickness is increased to position the cutter holding nut or screw above the cutter's lifeline (Figure 10.25). Deep counterbore-type cutters are normally used for cutting shoulder gears and cluster gears, as well as for machining of cluster gears (Figure 10.26).

Shaper cutters are made of high speed steels (HSS) containing molybdenum and tungsten. They are heat treated to a Rockwell C hardness of 64 to 65. A nitriding surface treatment further improves their wear resistance.

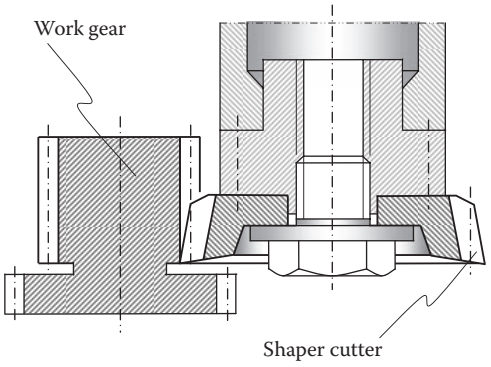

FIGURE 10.24
Shaping of a spur gear with the disk-type gear shaper cutter.

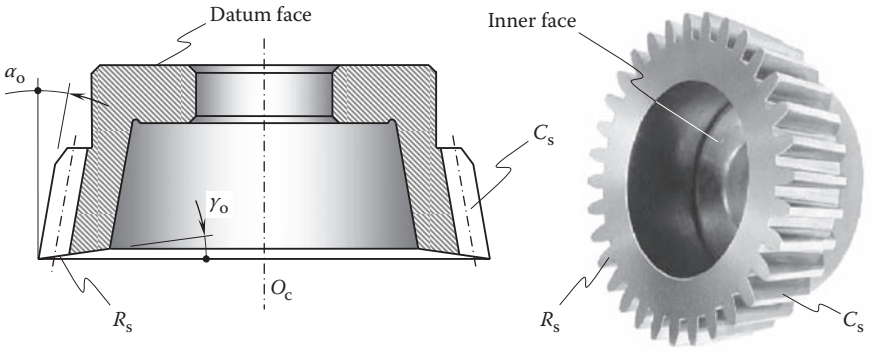

FIGURE 10.25
A typical counterbore-type gear shaper cutter.

Titanium nitride (TiN) coating is often applied to increase permissible feeds and speeds on modern shaping machines. Shaper cutters coated with TiN increase productivity by as much as 30% without reducing tool life.

It is common to assign the rake angle at the top cutting edge of the shaper cutter equal to $\gamma_o = 5°$. Roughing shaper cutters sometimes have a rake angle as high as $\gamma_o = 10°$.

The clearance angle at the top cutting edge of the gear shaper cutter is commonly equal to $\alpha_o = 6°$. The sides of the cutter have a side clearance of about $\alpha_f = 2°$.

The rake angle γ_o and the clearance angles α_o and α_f are all necessary to make the shaper cutter an efficient metal-cutting tool.

Commercial-quality gear shaper cutters for spur gears with $\phi = 20°$ profile angle are usually available from stock. High-accuracy precision ground cutters for finishing operations and ground cutters for preshaving, pregrinding, and roughing operations are made per special order. Gear shaper cutters are made in two quality classes: class A cutters for finishing and preshaving and class B for roughing and pregrinding. Shaper cutters for finishing work are usually manufactured to a very high degree of precision.

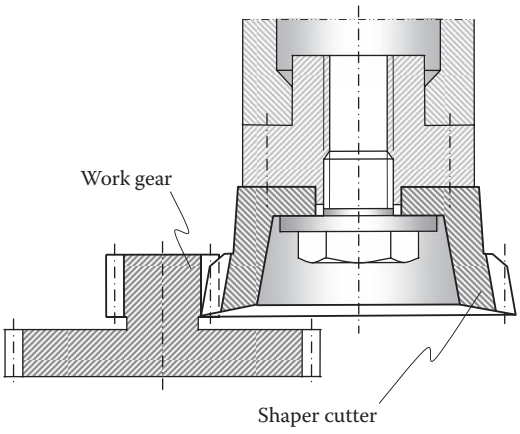

FIGURE 10.26
Shaping of a spur gear with the counterbore-type gear shaper cutter.

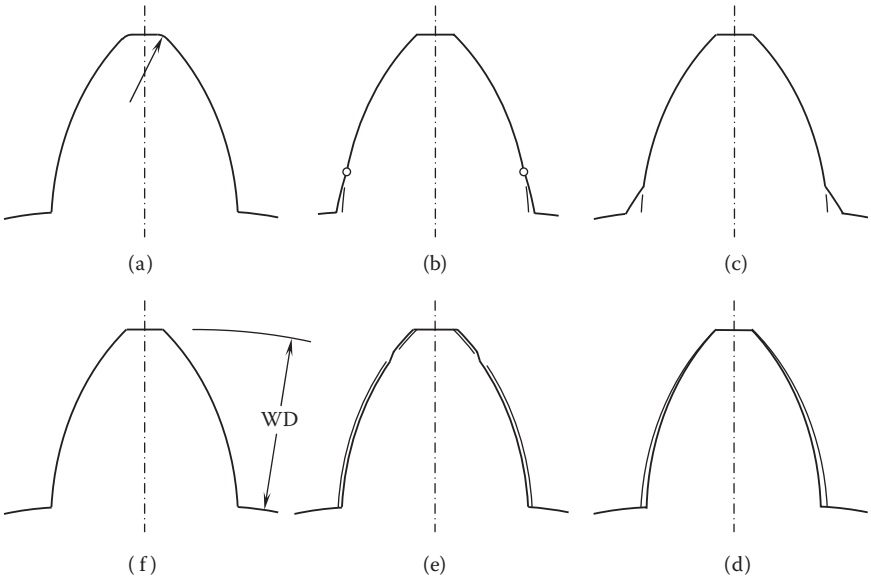

FIGURE 10.27
Special features of the gear shaper cutter tooth profile.

In many high-production jobs, it is desirable to design the gear shaper cutter for a particular gear so that the cutter will do exactly what is wanted throughout its life. This is particularly true when cutters are used to preshave-cut a gear and leave an undercut. The position of the undercut must remain constant within close limits to tie in with the gear shaving cutter design.

10.10.2 Special Features of the Shaper Cutter Tooth Profile

Standard gear shaper cutters are designed to produce a true involute without modifications to the tooth profile. Often, gear design mandates the use of modified profiles to improve performance. Shaper cutters can be ordered with various profile modifications.

A variety of special features can be provided—and are frequently needed—in gear shaper cutter teeth. Figure 10.27 illustrates six different special features.

(1) *Root fillet*. Root fillet radius modification consists of blending the corners of the tool tip with a radius that produces a controlled fillet in the root corners of the generated teeth (Figure 10.27a). A root fillet increases bending strength of the gear teeth and improves fatigue life. Tool wear of the gear shaper cutter is also improved, as a sharp corner would chip off very quickly.

(2) *Tip relief*. Tip relief cutters remove slightly more material near the top of the gear tooth (Figure 10.27b). Tip relief compensates for interference between mating profiles and usually results in reduced gear noise. In high-speed gears, it is often desirable to minimize noise and tip bearing resulting from tooth deflection under heavy loads. For the tooth profile modification of this type, implementation of the method proposed by Radzevich [63] can be helpful.

(3) *Semitopping (or chamfer)*. The root area of semitopping shaper cutters is modified at an angle to create a chamfer at the tip of the generated gear teeth (Figure 10.27c).

Root of cutter is filled in to generate a sharp corner break of chamfer on the tips of the gear. It minimizes tip buildup during heat treatment due to nicks incurred during handling. This feature is very helpful in minimizing damage due to nicks and burrs during part handling. These nicks and burrs could result in gear noise.

(4) *Protuberance*. The shaper cutter tooth profile is built up on the cutter tip to provide an undercut near the root of the gear being generated (Figure 10.27d). The undercut in the gear root area acts as a clearance. The undercut is intended to facilitate subsequent finishing operations. Protuberance cutters are frequently applied for gears that are finished by shaving or grinding.

(5) *Modified pressure angle*. The gear shaper cutter tooth profile is ground to a slightly lower pressure angle to provide for a constantly increasing amount of stock from root to tip of the gear generated (Figure 10.27e). The tooth profile modification provides relief for subsequent finishing operations.

(6) *Full topping*. The gear shaper cutter tooth is ground equal to the whole depth of the gear tooth (Figure 10.27f). The outside diameter of the gear is "topped" to size when the teeth are cut. Modification of this type is used more frequently for fine pitch gearing.

In particular cases of gear machining, customized tooth profile modifications can also be used.

10.10.3 Shaper Cutters for Machining of Helical and Herringbone Gears

Helical gears can be cut with helical shaper cutters (Figure 10.28), provided that the cutter has an appropriate helix angle and the shaping machine has a helical guide of appropriate lead to twist the cutter as it strokes back and forth. Each helix angle requires its own special helical guide. A helical shaper cutter and its guide form a set of tooling required to cut a specific helical gear. Two helical cutters and two guides are required to cut a pair of meshing helical gears (left- and right-hand gears).

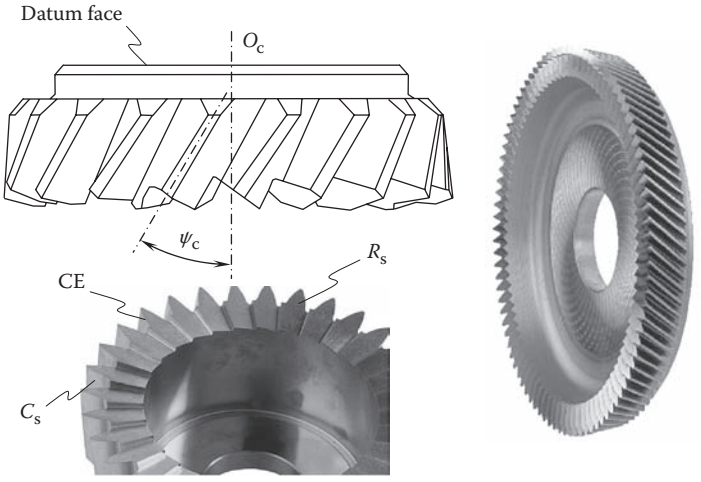

FIGURE 10.28
Design of a helical gear shaper cutter.

The helix angle that a shaper cutter produces depends on both the lead of the guide and the number of cutter teeth. The helix of the cutter must also agree with the helix angle being cut or else serious "cutter rub" will occur. The formula for the relation of cutter teeth to lead of guide is

$$\frac{\text{No. of teeth in cutter}}{\text{Lead of guide}} = \frac{\text{No. of teeth in gear}}{\text{Lead of gear}} \tag{10.80}$$

Ordinarily, helical gears are cut with shaper cutters having a rake face normal to the helix of the cutter tooth. If the helix angle is low, the transverse section could serve as the rake face of the shaper tooth.

Helical shaper cutters generally require a wider recess at the bottom of the cut for full cutter runout.

Gear shaper cutters do not usually cut the same whole depth throughout their life. A shaper cutter can be designed with a front clearance angle that has such a relation to the side clearance angle that a certain number of teeth may be cut to an exact depth and thickness for the cutter. However, if this cutter is used to cut gear of substantially larger or smaller numbers of teeth, the whole depth cut will vary slightly from the design value. If a shaper cutter designed to cut an external gear is used to cut an internal gear of the same tooth thickness, the discrepancy in whole depth may be quite appreciable. In many cases, a designer of a shaper cutter does not know all the numbers of teeth that the cutter may have to cut during its life. This leads the designer to make the front clearance angle large enough so that the cutter usually cuts a little extra on the whole depth. It is usually reasoned that the problem of a little extra depth is less than the problem of having the depth too shallow.

Herringbone gears of the continuous-tooth type must be cut with a pair of gear shaper cutters working together. To make the cutting match from both sides, it is necessary to use a cutter with the top face ground normal to the cutter axis. This makes the top face angle $\gamma_o = 0°$ and it makes one side of the cutter tooth have an acute angle and the other side an obtuse angle. These features do not aid the cutting action of the tool, but they are necessary to produce the continuous tooth. A special sharpening technique has produced a good cutting edge even on the obtuse-angle side.

10.10.4 Special Designs of Gear Shaper Cutters

Possible designs of gear shaper cutters are not limited to just disk-type shaper cutters and deep counterbore-type shaper cutters discussed above. Many other designs of shaper cutters are developed for industrial applications. In this section, only a few designs of gear shaper cutters are briefly discussed. Moreover, they could be of importance for practical application—those chosen to be considered for designs of shaper cutters are interesting from the scientific prospective.

Shaper cutters having an improved cutting edge geometry. The investigation into the geometry of the rake surface of gear shaper cutters has been carried out by Kau [27] and Ngok [47]. These research activities resulted in a novel design of a shaper cutter having an optimal value of the rake angle γ_o^{opt} (Figure 10.29). The shaper cutter features the rake surface R_s^{cmb} of a combined geometry.

The proposed shaper cutter design is developed on the premise of its conventional design. The rake surface R_s and the clearance surface C_s form the cutting wedge of the

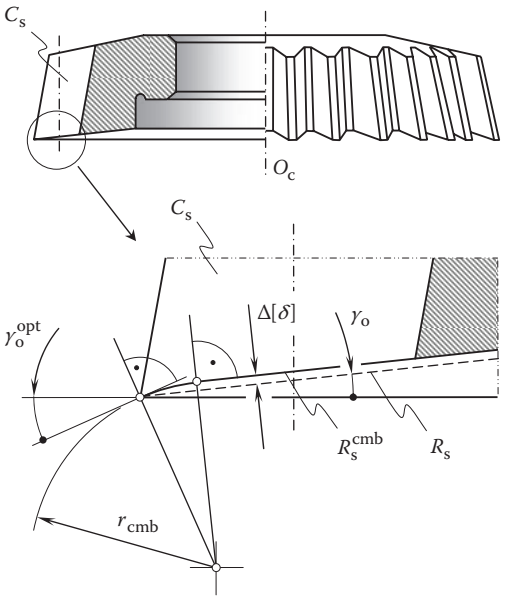

FIGURE 10.29
Gear shaper cutter having a rake surface of a combined geometry.

shaper cutter of conventional design. The rake angle of the shaper cutter is designated as γ_o. The actual value of the rake angle γ_o is small and is too far from the optimal value γ_o^{opt}. Because the inequality $\gamma_o \ll \gamma_o^{opt}$ occurs, the tool life of the shaper cutter of conventional design is far from optimal.

The proposed improvements in the design of the shaper cutter incorporate the tolerance $[\delta]$ on the accuracy of the rake face R_s of the shaper cutter. Any and all deviations in the shape of the surface R_s within the tolerance $[\delta]$ are feasible and are allowed.

In particular cases, the tolerance $[\delta]$ can be tightened to a certain value $[\delta^*] < [\delta]$. This enables a considerable improvement in the geometry of the rake surface. The available portion $\Delta[\delta] = [\delta] - [\delta^*]$ of the tolerance $[\delta]$ can be used for controllable deviation of the actual rake surface from its initial form R_s. The modified rake surface is referred to as the *combined rake surface* of the shaper cutter and designated as R_s^{cmb}.

The rake surface R_s^{cmb} is composed of the conical portion blended with the portion of torus surface. The torus surface is generated by a circle of certain radius r_{cmb}. If the available portion $\Delta[\delta]$ of the tolerance $[\delta]$ is known, the value of the radius r_{cmb} can be expressed in terms of the optimal rake angle γ_o^{opt} and the portion $\Delta[\delta]$ of the tolerance $[\delta]$

$$r_{cmb} = \frac{\Delta[\delta]}{1 - \cos \gamma_o^{opt}} \tag{10.81}$$

Reasonable corrections to the computed value of the radius r_{cmb} can be made.

The cutting performance and tool life of the shaper cutter having an optimal value of the rake angle are significantly higher compared to that of shaper cutters of conventional design.

Improvements in the geometry of the clearance surface of the shaper cutter are constrained more significantly.

The insufficiently small clearance angle α_f is among the few major factors that significantly limit the cutting performance of shaper cutters. Analysis of the kinematics of a gear shaping operation [160] reveals that an opportunity for the improvement of the geometry of the clearance surface is available. First of all, it is desirable to increase the clearance angle α_f at the entering side of the shaper cutter tooth profile. For this purpose, the clearance surfaces of the shaper cutter teeth are constructed from different base cylinders. In this way, the clearance angle α_f at the entering cutting edge is slightly increased; however, the clearance angle α_f at the opposite cutting edge is slightly reduced. Ultimately, reasonable changes (i.e., redistribution) in clearance angles at the lateral cutting edges result in an improved cutting performance of the shaper cutter. It should be pointed out that no changes occur in the base cylinder of the generating surface of the gear shaper cutter. It retains its original value before the recommended changes are implemented in the geometry of the clearance surfaces.

The cutting performance of the shaper cutter can be significantly increased if the design allows for the elimination of interference of chip flows from the adjacent cutting edges of the shaper cutter tooth. Use of sets of two gear shaper cutters set up on a common spindle is a perfect example in this concern [103]. Chip removal is performed by the top cutting edges of one of the two shaper cutters (lateral cutting edges of this shaper cutter do not cut the material) while the second one generates the tooth profile of the work gear by the lateral cutting edges (top cutting edges of this second shaper cutter do not cut the material).

Extremely small values of the clearance angle α_f at the lateral cutting edges represent one of the critical factors limiting the cutting performance and tool life of the gear shaper cutters of conventional design. Clearance surfaces of the set of two shaper cutters shown in Figure 10.30 are designed so as to make it possible to increase the clearance angle α_f at one side of the tooth profile of one of the shaper cutters, and an increased clearance angle α_f at the opposite side of the tooth profile of the other shaper cutter. Ultimately, the working cutting edges of both lateral sides of the tooth profile of the shaper cutter set have an increased clearance angle α_f [101].

The top cutting edges and lateral cutting edges of one side of the tooth profile of the lower shaper cutter cut the stock. Similarly, the top cutting edges and lateral cutting edges of the opposite side of the tooth profile of the upper shaper cutter cut the rest of the stock. A greater clearance angle α_f at the lateral cutting edges results in a significant increase in the productivity rate of machining of gears with the set of two shaper cutters compared to that when cutting gears with shaper cutters of conventional design.

To perform regrinding, the worn set of two shaper cutters must first be disassembled. Next, each of the shaper cutters can be ground separately. Either the rake faces R_s (conventional approach) or the clearance surfaces C_s can be ground. In regrinding of gear shaper cutters, grinding of clearance surfaces require less material to be removed. This process causes less reduction of tooth width compared to grinding over the rake face. In certain cases, grinding of clearance surfaces of the shaper cutters is preferred.

After being reground, the gear shaper cutters should be assembled on the common spindle. Because the teeth of reground shaper cutters have become narrower, this in turn requires the shaper cutters to be at a certain angle with respect to each other. In the design of a set of two gear shaper cutters shown in Figure 10.30, the required rotation of the shaper cutters with respect to each other is performed by using specially designed key ways.

Key slots on the upper gear shaper cutter are made at a certain angle φ to each other. Circumferentially, the key slots can be distributed evenly. Key slots on the lower shaper

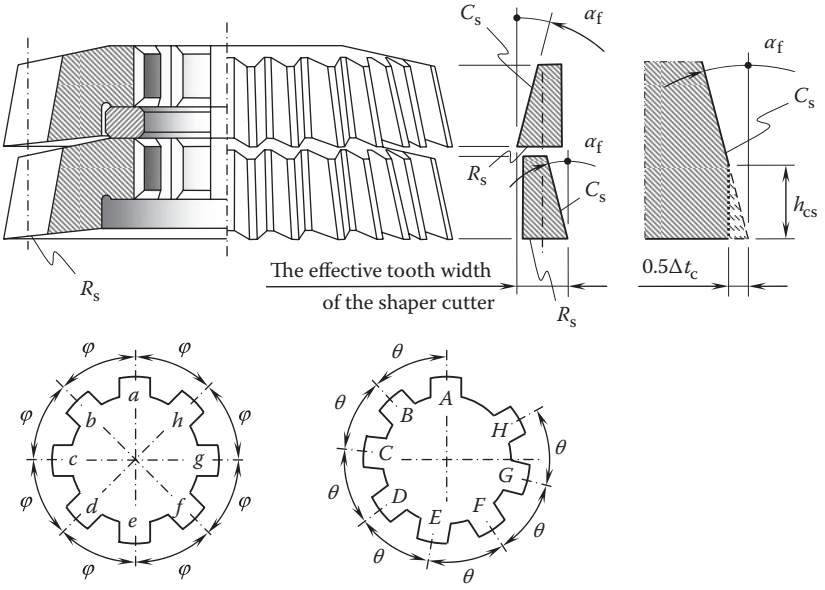

FIGURE 10.30
A set of two gear shaper cutters: design I. (From Radzevich, S.P., USSR Patent 1039657, Int. Cl. B23F 21/10, March 16, 1982.)

cutter are at a certain angle θ to each other. The angular pitches φ and θ are different. The difference between the angular pitches is computed as follows

$$\varphi - \theta = 2\sin^{-1}\left(\frac{\Delta t_c}{d_c}\right) \tag{10.82}$$

where Δt_c denotes the reduction of tooth thickness of the gear shaper cutter (Figure 10.30) and d_c is the pitch diameter of the shaper cutter.

First, the key slots labeled "a" and "A" are used for assembling the shaper cutter. After regrinding of the worn gear cutting tool, the slots "b" and "B" are used for assembling the gear shaper cutter, and so on. Because of the difference $(\varphi - \theta)$ between the angular pitches of the key slots, the upper and lower portions of the two gear shaper cutter sets turn relative to each other through the angle $\varphi - \theta$.

A result similar to that discussed above can be achieved by implementation of the set of two gear shaper cutters shown in Figure 10.31. The upper portion of the gear cutting tool has only one key slot [103]. The lower portion of the gear cutting tool is designed with multiple key slots. The key slots of the lower portion of the gear cutting tool are at a certain angular pitch φ. The angle φ is a function of the angular pitch $2\pi / N_c$ of the shaper cutter teeth

$$\varphi - 2n\pi / N_c = 4\cos\frac{\varphi}{2} \tag{10.83}$$

where n denotes a reasonable integer number.

The gear cutting tool determined in this manner enables precise turns of the upper portion of the gear shaper cutter relative to its lower portion through the angle

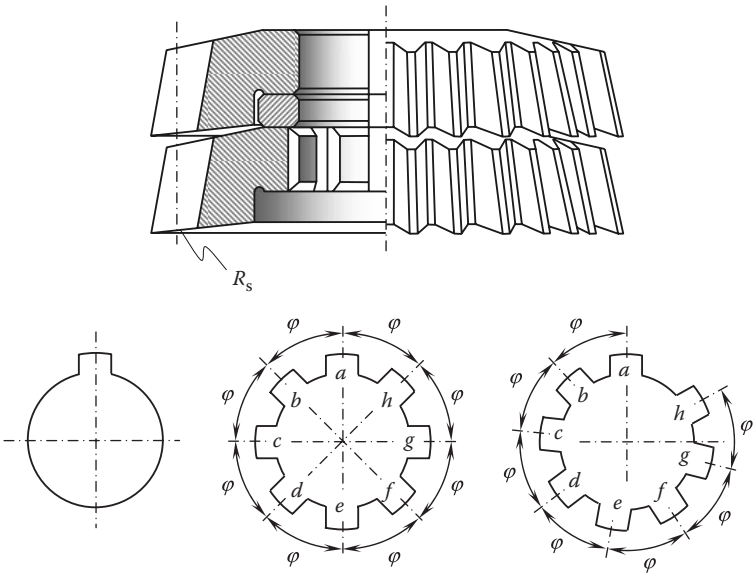

FIGURE 10.31
A set of two gear shaper cutters: Design II. (From Radzevich, S.P., USSR Patent 1172660, Int. Cl. B23F 21/10, Feb. 13, 1984.)

$$\sigma = \frac{4h_{cs}}{d_c} \cdot \tan \alpha_f \tag{10.84}$$

Sufficiency in just one key slot at the upper portion is an advantage of the gear cutting tool over the one shown in Figure 10.30. However, timing of the angular pitches φ and $2\pi / N_c$ can be a challenge.

Implementations of gear cutting tools (Figures 10.30 and 10.31), which are composed of two gear shaper cutters, make it possible to apply the modified gear cutting diagram that eliminates the interference of chip flows from the adjacent cutting edges of the shaper cutter of conventional design.

Precision gear shaper cutters. Possibilities of increasing accuracy are strongly restricted by the allowed values of the rest of the design parameters of the gear shaper cutter. As a result, any attempt to remedy this problem is especially valuable.

A design of precision shaper cutter can be developed on the premise of the implementation of the rake surface R_s that is generated via rotation of the lateral cutting edge CE of a corresponding geometry. This is constructed not as the line of intersection of the generating surface T of the gear shaper cutter by the rake surface R_s, but as the line of intersection of the generating surface T of the shaper cutter by the actual clearance surface C_s. The cutting edge CE that is constructed as the line of intersection of the surfaces T and C_s is rotated about the shaper cutter axis O_c. Ultimately, the rake surface R_s is shaped in the form of a surface of revolution, which is generated with the help of the cutting edge CE.

In compliance with this concept, a design of precision gear shaper cutter is developed [48]. The shaper cutter is illustrated in Figure 10.32. The generating profile of the rake surface R_s

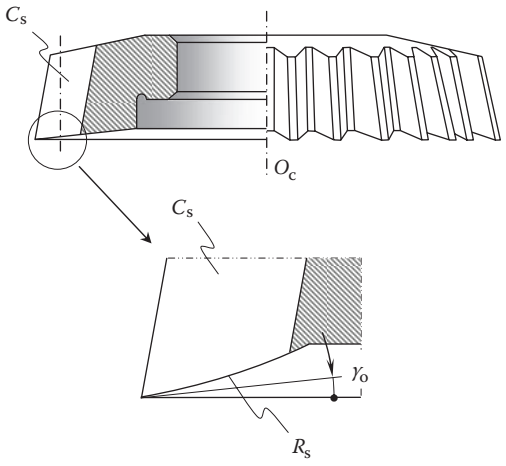

FIGURE 10.32
A design of precision gear shaper cutter having a modified rake surface R_s.

is convex for shaper cutters with a positive rake angle γ_o. When the rake angle has a negative value, the generating profile of the rake surface R_s becomes concave.

The disclosed concept can be implemented to increase the accuracy of spur gear shaper cutters alone and is not applicable with respect to helical shaper cutters. For helical shaper cutters, another approach [68] can be implemented to improve their accuracy.

The helical gear shaper cutter [68] has straight lateral cutting edges as shown in Figure 10.33. The cutting edges CE are aligned with the straight lines tangent to the base helices of the generating surface T of the helical shaper cutter. Therefore, the lateral cutting edges cross the axis of rotation O_c of the shaper cutter at the base helix angle $\psi_{b.c}$. Tangency of the lateral cutting edges to the base helices of the gear shaper cutter is the essence of the helical shaper cutter design under consideration. For the configuration of the lateral cutting edges that is shown in Figure 10.33, the cutting edges are within a common plane that serves as the rake plane R_s of the gear shaper cutter tooth. However, this is not a must. The lateral cutting edges can align with a pair of skew straight lines if this happens to be of importance for a particular application. Numerous designs of precision gear shaper cutters can be developed on the premise of this concept.

The concept of the precision helical shaper cutter having straight lateral cutting edges can be enhanced to the area of verification of accuracy of the clearance surfaces of the gear shaper cutter [90].

Shaper cutters for machining hardened gears. Shaping of hardened gears is a challenging problem for gear manufacturers. The high level of hardness of tooth flanks of hardened gears is the major reason for why gear manufacturers are faced with significant difficulties in sharpening of hardened gears. This mostly explains why shaping of hardened gears has limited applications in industry to date.

Carbide gear shaper cutters are rarely used in normal gear production. The advantages of carbide tools cannot be fully exploited for gear shapers because machines are limited in terms of the maximum reciprocating speed of the cutter spindle. As opposed to hobbing, where the hob material limits the permissible cutting speed, the limiting factor in shapers is the maximum speed of the reciprocating mechanism of the cutter spindle.

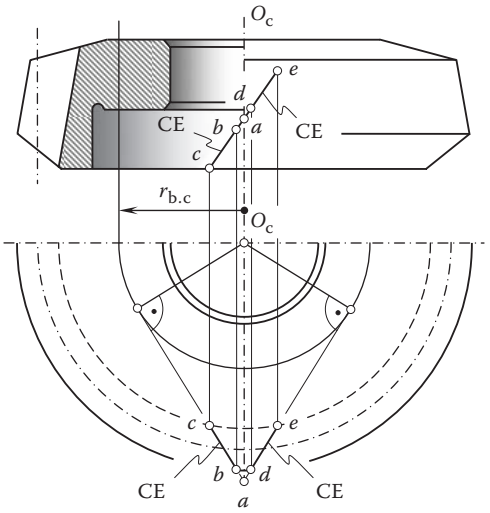

FIGURE 10.33
Concept of precision helical gear shaper cutter having straight lateral cutting edges. (From Radzevich, S.P., USSR Patent 956187, Int. Cl. B24B 3/34, Jan. 12, 1988).

Carbide gear shaper cutters are used when it is necessary to machine gears made of hard steel. Design and the cutting edge geometry of the carbide shaper cutters are very similar to those used for shaper cutters made of HSS.

For particular cases of semifinishing and/or finishing of hardened gears, carbide shaper cutters of special designs are developed. An example of carbide shaper cutter for semifinishing of hardened gears is depicted in Figure 10.34. Except for the geometry of the rake face R_s, the carbide shaper cutter is very similar to the shaper cutter of conventional

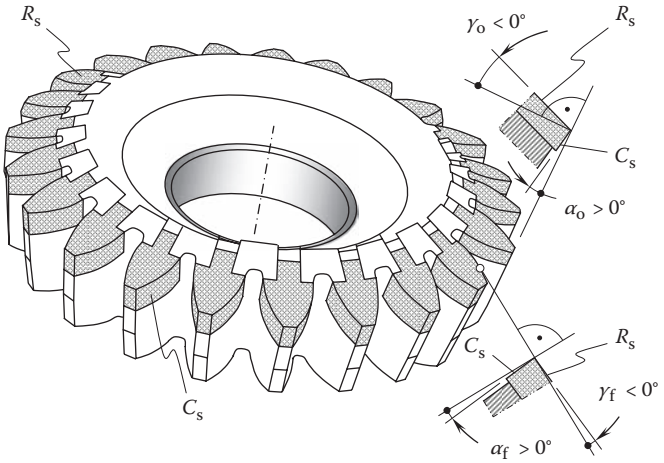

FIGURE 10.34
Carbide gear shaper cutter of special design for semifinishing and/or finishing of hardened gears.

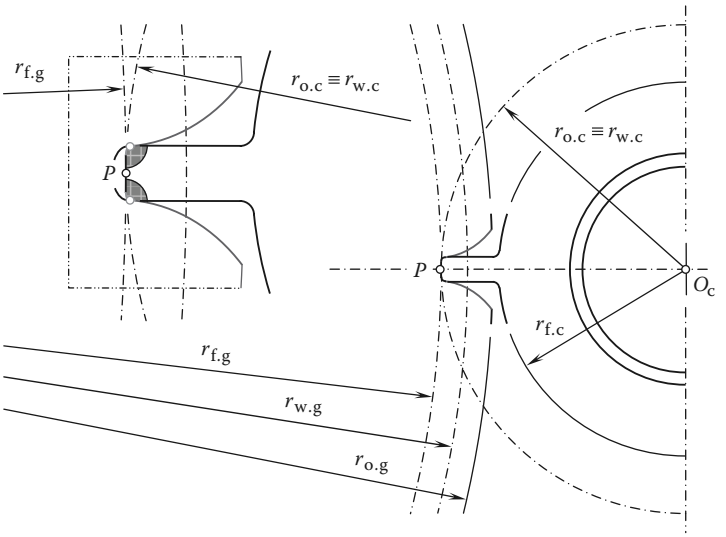

FIGURE 10.35
Concept of the finishing gear shaper cutter having shortened cutting edges.

design. The rake surface R_s of the semifinishing gear shaper cutter is shaped either in the form of a round cone surface or an individual plane R_s (facet) for each tooth of the shaper cutter.

The rake surface R_s of the semifinishing shaper cutter is at a negative rake angle γ_o = –10 to –25°. Due to the negative rake angle $\gamma_o < 0°$, the negative rake angles $\gamma_f < 0°$ of corresponding values are created at the lateral cutting edges. These make the shaper cutter teeth capable of withholding high loads when shaping hardened gears.

Use of cutting elements made of superhard materials (borazon etc.) proved to be useful for machining of hardened surfaces. It is natural to assume that use of cutting elements made of superhard materials can solve numerous problems relating to machining of gears with shaper cutters. Unfortunately, dimensions of the cutting elements are often too small to span over the entire lateral cutting edge of the gear shaper cutter. Small dimensions of the cutting elements impose strong constraints in the implementation of cutting elements made of superhard materials (borazon etc.) in the design of gear shaper cutters. This particular problem can be resolved by using shaper cutters [102] specifically designed so that the pitch diameter and outer diameter of the shaper cutter are equal to each other (Figure 10.35). When the equality $r_{w.c} = r_{o.c}$ is observed, the lateral cutting edge shrinks to a point [102]. In reality, the generating surface of the shaper cutter is reduced to the set of straight lines through the corners of the top cutting edge. All of the straight lines are parallel to the axis of rotation O_c of the shaper cutter. This makes it possible to place a cutting element of small size into that point. In such a case, the shaper cutter (Figure 10.36) can be used for machining of a gear of any coarse pitch.

In reality, the gear tooth profile that is machined with the shaper cutter (Figure 10.36) is shaped in the form of an epicycloid when machining external gears, and in the form of a hypocycloid when machining internal gears. However, reasonable approximation of the desired involute tooth profile with a cycloidal curve is possible.

One more advantage of the gear shaper cutter design depicted in Figure 10.36 stems from the fact that its cutting edge geometry does not depend on the gear tooth profile to

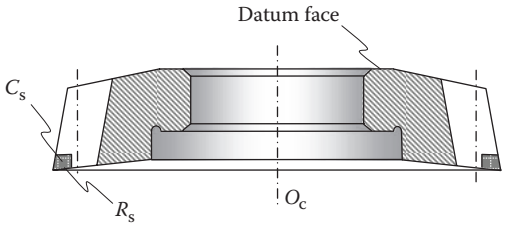

FIGURE 10.36
Schematic of the finishing gear shaper cutter with cutting elements made of a superhard material.

be machined. Because of this, the shaper cutter can be designed with the optimal values of the rake angle and the clearance angle. The design of the gear shaper cutter (Figure 10.36) does not entail problems with the kinematics of grinding of the rake surface R_s and the clearance surface C_s.

10.10.5 Typical Gear Shaping Operations

Spur and helical gears can be cut with a pinion-type gear shaper cutter. Either internal or external gears can be cut. Parts ranging from less than 1 to more than 300 mm (1/16 to more than 120 in.) may be shaped. Relatively wide face widths may be cut, but in certain cases shaping will not handle as much face width as the hobbing process.

Furthermore, with the advent of the modern cutter spindle back-off type of machines, it is not uncommon to see stroking rates of 1000 strokes/min for face widths 25 mm (1 in.) or smaller. In fact, for narrow face widths of 6 mm (1/4 in.), high-speed shapers capable of stroking rates of more than 2000 strokes/min are in use.

Gear shaping is quite advantageous for parts with narrow face width. In hobbing, it takes time for the hob to travel into and out of the cut. For helical gears, the hob travel must be increased proportionally. In shaping, there is a minimum of overtravel for spur gears, and this overtravel does not increase for helical gears.

Length of stroke in gear shaping can be calculated as the summa of (1) the gear face width, (2) the length of approach, and (3) the overrun length. The gear face width is a value that is read directly from the part blueprint. Approach and overrun are only required to ensure safe cutting conditions. As a rule of thumb, 15% should be added to the face width to account for approach and overrun distance (Figure 10.37).

In designing gears to be shaped, it is necessary to machine a groove as deep as the gear tooth at the end of the face width for overrun of the cutter. Shaper cutters need only a small amount of cutter-overrun clearance at the end of the cut or stroke. Shaped teeth may be located close to shoulders.

A cluster gear can be readily shaper-cut where it may be impossible to hob because of insufficient hob-overrun clearance. One NC shaper could conceivably cut a cluster gear in one setup, depending on gear data. Double helical gears can be cut with very narrow gaps between helices. In fact, one design of shaper cutter can actually produce a "continuous" double helical tooth.

Several types of gear shaping are practically used in industry for machining of cluster gears [16].

Combination shaping. Two gears with the same number of teeth can be cut simultaneously with two shaper cutters mounted on the same arbor (Figure 10.38a). The tooth forms may

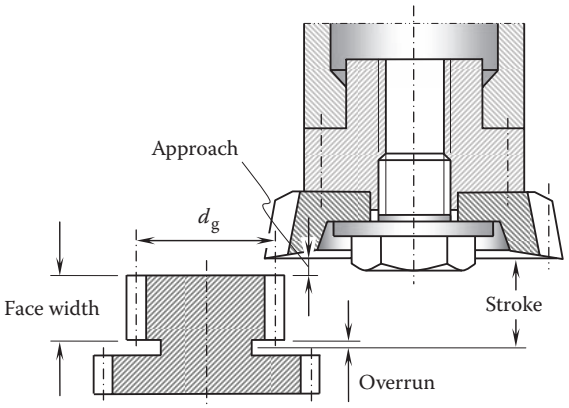

FIGURE 10.37
Length of stroke in a shaping operation.

differ in pressure angle or tooth thickness, but must have the same number of teeth. This setup requires only half the stroke length of a single cutter operation. Machining time is, therefore, reduced by 50%.

Cutting of two gears with similar diametral pitch. This a typical NC shaping operation where two gears with the same diametral pitch and pressure angle are cut in sequence during the same cycle (Figure 10.38b). The machining parameters are automatically adjusted for each gear by NC control so that both gears are produced under optimum cutting conditions. It is essential for this application that one shaper cutter design is suitable for gears.

Cutting of two gears with different diametral pitch. When the gears have different diametral pitches, the same cutter obviously cannot be used. The solution is to mount two cutters on the same arbor as shown in Figure 10.38c.

Cutting two gears with up and down shaping. The cluster gear shown in Figure 10.38d can be cut in one cycle by mounting two shaper cutters back to back on the same arbor. The upper gear is cut with downstroke, whereas the lower gear is cut with upstroke.

The special drives resulted in the development of a new cutting method, sometimes referred to as the *spiral infeed*. This cutting method tends to improve chip loading conditions and more evenly distributes tool wear around the cutter.

10.10.6 Grinding of Shaper Cutters

Rake surfaces as well as clearance surfaces of gear shaper cutter teeth are ground.

Grinding of clearance surfaces. Clearance surfaces are commonly ground in the production of gear shaper cutters. For grinding, the shaper cutter is set up on the grinder as schematically depicted in Figure 10.39. The grinding wheel is rotating ω_{gw} about its axis O_{gw}. When grinding the clearance surfaces C_s, both the shaper cutter and the grinding wheel roll over each other. The relative rolling motion is a superposition of the reciprocation $\mathbf{F}_{rl}$ of the grinding wheel and the rotation ω_{rl} of the shaper cutter. In addition, either the grinding wheel or the gear shaper cutter reciprocates $\mathbf{F}_c$ in the lengthwise direction of the shaper cutter tooth. In this way, the entire clearance surface C_s of the shaper cutter tooth is ground. The relative rolling motion ($\mathbf{F}_{rl}$ and ω_{rl}) and the reciprocation ($\mathbf{F}_c$) should be properly timed with each other in order to avoid nonground patches on the clearance surface C_s.

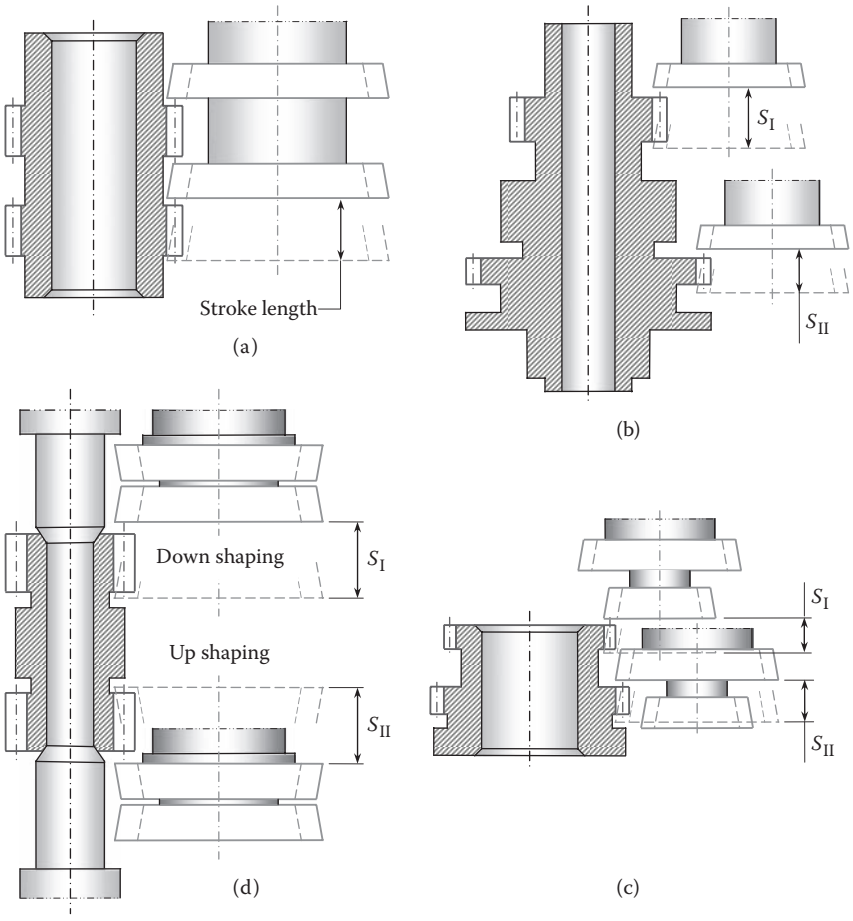

FIGURE 10.38
Consecutive cutting of two gears.

The grinding wheel is gradually fed ($\mathbf{F}_{gw}$) toward the shaper cutter axis O_c.

Grinding of rake surfaces. Wear of the cutting wedge is usually observed over the clearance surface of the shaper cutter teeth. When the extent of the worn or rubbed areas on the cutter tooth tips or flanks reach about 0.010–0.015 in. (0.25–0.40 mm), they should be resharpened to remove the worn surface by grinding material off the front face. It is preferred to grind the worn shaper cutter on clearance surfaces of its teeth. Because of the absence of grinders with appropriate capabilities, regrinding of worn shaper cutters on face surface is widely implemented.

Grinding of spur gear shaper cutters is performed either on specially designed grinders or conventional grinders.

When grinding (Figure 10.40), the shaper cutter is rotating about its axis O_c. The rotation ω_c of the shaper cutter serves as the feed motion. The grinding wheel axis of rotation O_{gw} makes an obtuse angle ($90° - y_o$) with the shaper cutter axis of rotation O_c. The rotation ω_{gw} of the grinding wheel creates the primary motion of cutting. When capabilities of the actual grinder allow, it is recommended to reciprocate ($\mathbf{F}_c$) the grinding wheel along the straight generating line of the conical rake surface R_s.

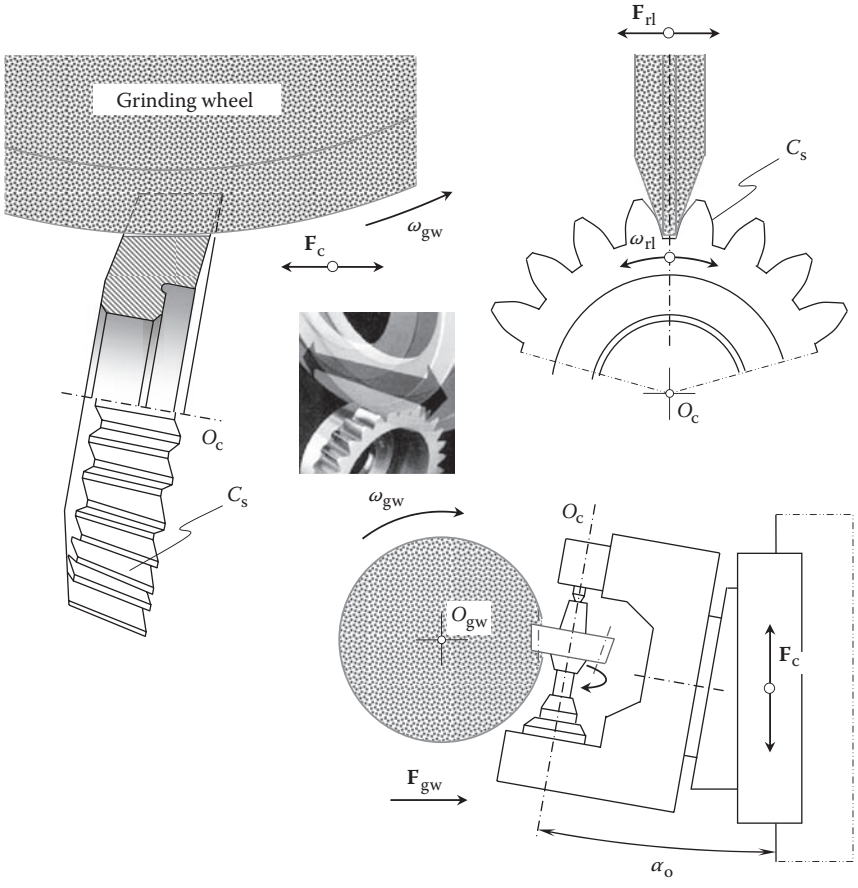

FIGURE 10.39
Grinding of the clearance surface C_s of a shape cutter.

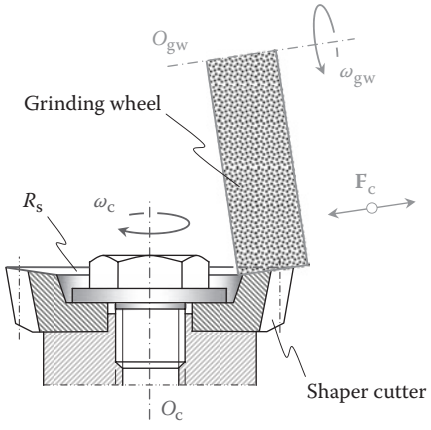

FIGURE 10.40
Kinematics of sharpening of a standard shaper cutter.

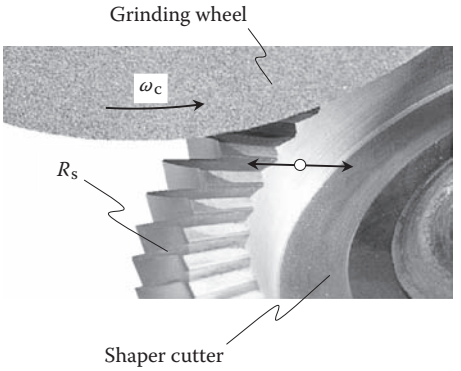

FIGURE 10.41
Schematic of sharpening of a helical shaper cutter.

Because the rake angle y_o at the top cutting edges of standard shaper cutters is small ($y_o \cong 6°$), no violation of the third necessary condition of proper *PSG* generation is observed when grinding shaper cutters on the rake surface. However, this problem could become critical when grinding shaper cutters of special design, for example, when grinding precision shaper cutters shown in Figure 10.32.

Depending on the features of the design, two approaches are used for sharpening of helical gear shaper cutters. The first approach is applicable for grinding shaper cutters for machining of helical gears. For grinding of shaper cutters for machining of herringbone gears, the second approach is implemented.

Each rake plane R_s of the helical shaper cutter of conventional design can be ground separately (Figure 10.41). Indexing of the shaper cutter after grinding of the rake plane is accomplished is required in this method. Accumulated wear of the grinding wheel reduces the accuracy of the ground helical shaper cutter.

To eliminate the negative impact of the accumulated wear of the grinding wheel onto the accuracy of the gear shaper cutter, a continuously indexing method of resharpening of helical shaper cutters is developed. When sharpening, the helical shaper cutter is rotating about its axis of rotation O_c (Figure 10.42). Continuous rotation of the shaper cutter ω_c makes it possible to transfer from sharpening the rake plane of the shaper cutter tooth to sharpening of the rake plane of the next tooth of the shaper cutter [57].

For sharpening, the grinding wheel with plane working surface is used. At the instant of generation of the rake plane R_s, the working surface of the grinding wheel is congruent to the rake plane R_s. The grinding wheel is rotating about its axis of rotation O_{gw}. The rotation of the grinding wheel serves as the primary (cutting) motion.

Simultaneously with the rotation of the shaper cutter, the grinding wheel reciprocates toward the rake surface to be ground and in backward direction. It is recommended to keep the reciprocation distance of the shortest possible length. However, it must be sufficient for free rotation of the shaper cutter when the grinding wheel is far away from it.

The grinding wheel slowly approaches the shaper cutter. Then, at a very short instant of time, it makes contact with the rake plane. After that, it moves backward. Speed of this last motion is much greater than the speed of approach of the shaper cutter toward the grinding wheel.

Between each two consequent contacts of the shaper cutter tooth and the grinding wheel, the shaper cutter turns about its axis O_c through a whole number of teeth for indexing.

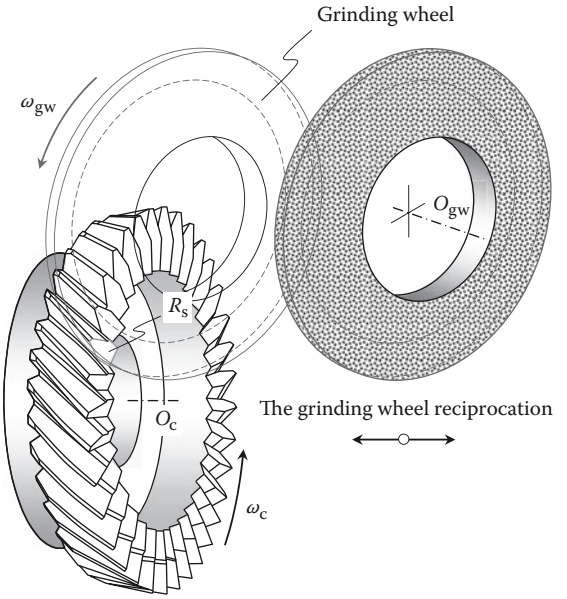

FIGURE 10.42
Schematic of the continuously indexing method of sharpening of helical shaper cutters. (From Radzevich, S.P., USSR Patent 1604567, Int. Cl. B23F 21/10, Sept. 9, 1980.)

There must be no common multipliers between the whole number of teeth and the shaper cutter tooth number.

When grinding helical shaper cutters in compliance to the method shown in Figure 10.43, the impact of the grinding wheel wear onto the accuracy of the ground shaper cutter is much smaller. Productivity rate of grinding is significantly higher. This is mostly because the indexing is continuous.

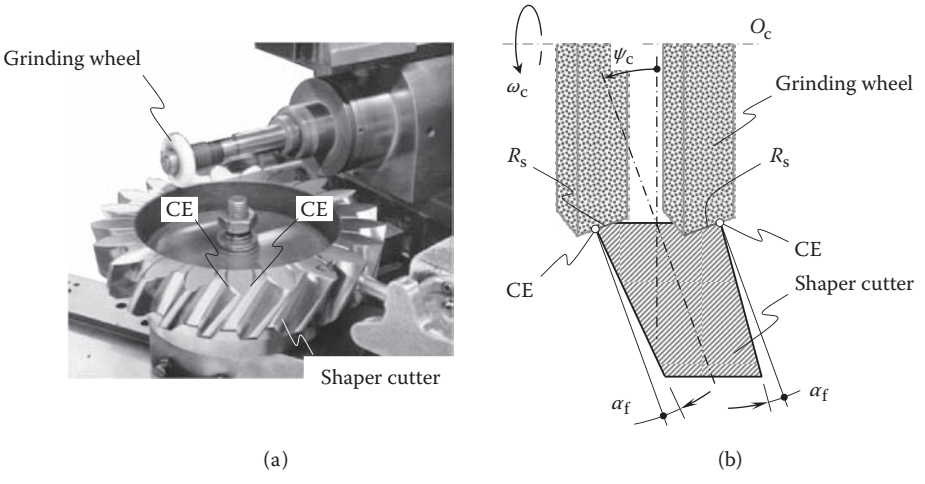

FIGURE 10.43
Sharpening of a helical shaper cutter for machining herringbone gears.

Herringbone gears of the continuous tooth type usually cut with a pair of shaper cutters working together. To make the cutting match from both sides, it is necessary to use a cutter with the top face ground normal to the gear axis. This makes the top rake angle 0°, and it results in one side of the cutter tooth having an acute flank rake angle ($\gamma_f < 90°$) angle and the other side having an obtuse angle ($\gamma_f > 90°$). These features do not aid the cutting action of the tool, but they are necessary to produce the continuous tooth.

When sharpening shaper cutters for machining of herringbone gears, special care is required. The sharpening is performed with grinding wheels of small outer diameter (Figure 10.43a). Making a groove from one side of the shaper cutter tooth profile and making a corresponding chamfer from the opposite side of the shaper cutter tooth profile produce optimal values of the rake angles γ_f at both sides of the cutter tooth profile (Figure 10.43b).

11

Gear Shaper Cutters II: Internal Gear Machining Mesh

The gear shaper cutter is the primary type of gear cutting tool for machining of internal spur and helical gears. Before designing a shaper cutter for machining of a given internal gear, the generating surface of the gear cutting tool should be determined. To determine the generating surface of the shaper cutter, the internal gear machining mesh is used. The internal gear machining mesh is one of the many possible types of gear machining meshes classified in Figure 3.8.

11.1 Kinematics of Shaping Operation of an Internal Gear

The internal gear machining mesh, together with a primary motion (cutting motion) of the gear cutting tool, comprises the kinematics of the shaping operation of an internal gear.

In the internal gear machining mesh, the rotation vectors of the work gear $\boldsymbol{\omega}_g$ and the gear cutting tool $\boldsymbol{\omega}_c$ are at a center distance $C_{g/c}$ from each other, and are parallel to each other. In this type of gear machining mesh, the vectors $\boldsymbol{\omega}_g$ and $\boldsymbol{\omega}_c$ are pointed in the same direction. Under such a scenario, pitch point P of the gear machining mesh is located not within the center distance $C_{g/c}$, but outside of it.* The vector of instant rotation $\boldsymbol{\omega}_{pl}$ is a vector through pitch point P and parallel to vectors $\boldsymbol{\omega}_g$ and $\boldsymbol{\omega}_c$. An example of the configuration of rotation vectors $\boldsymbol{\omega}_g$, $\boldsymbol{\omega}_c$, and $\boldsymbol{\omega}_{pl}$ is illustrated in Figure 11.1.

Because the gear shaping operation of the pitch point takes place outside the center distance $C_{g/c}$, the rotation vectors $\boldsymbol{\omega}_g$ and $\boldsymbol{\omega}_c$ are not allowed to be of the same magnitude. Therefore, satisfaction of the inequality $\omega_g \neq \omega_c$ is a must for gear shaping operations of this type. Here, ω_g and ω_c denote the magnitudes of the rotation vectors $\boldsymbol{\omega}_g$ and $\boldsymbol{\omega}_c$, that is, $\omega_g = |\boldsymbol{\omega}_g|$ and $\omega_c = |\boldsymbol{\omega}_c|$, respectively.

To satisfy the inequality $\omega_g \neq \omega_c$, either rotation ω_c must exceed rotation ω_g, or rotation ω_g must exceed rotation ω_c. In the first case, the inequality $\omega_g < \omega_c$ is valid, whereas in the second case the inequality $\omega_g > \omega_c$ is observed. The first case ($\omega_g < \omega_c$) corresponds to the operation of machining an internal gear using the shaper cutter. Shaping of an internal work gear with the shaper cutter is schematically illustrated in Figure 11.2.

The inequality $\omega_g \neq \omega_c$ is not the only constraint in the ratio between the rotations ω_g and ω_c. One more constraint is attributed to the numbers of teeth of the work gear N_g and the shaper cutter N_c, under which no interference of the gear teeth and the shaper cutter teeth is observed *before* teeth are engaged in the mesh and *after* they are disengaged from the mesh. This issue needs to be discussed as a separate topic.

* It should be noted here that the same kinematics of the gear machining mesh is featured in another gear machining process—*parallel axis shaving* [15, 194].

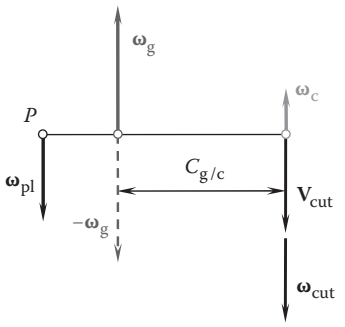

FIGURE 11.1
Vector diagram of the kinematics of the machining process of an internal gear with the shaper cutter.

The generating surface of a gear shaper cutter is conjugate to the work gear tooth surface. When shaping the work gear, the generating surface T of the shaper cutter and the gear to be machined are in proper tight mesh with each other.

The kinematics of gear generation is of critical importance for the determination of the generating surface T of the shaper cutter. When shaping an internal gear with a shaper cutter, the work gear and the shaper cutter rotate $\boldsymbol{\omega}_g$ and $\boldsymbol{\omega}_c$ about their axes of rotation O_g and O_c (Figure 11.1). The axes O_g and O_c of the rotations are parallel to each other ($O_g \parallel O_c$). The rotations ω_g and ω_c are timed with each other in such a way that the ratio

$$\frac{\omega_g}{\omega_c} = \frac{N_c}{N_g} \tag{11.1}$$

is valid.

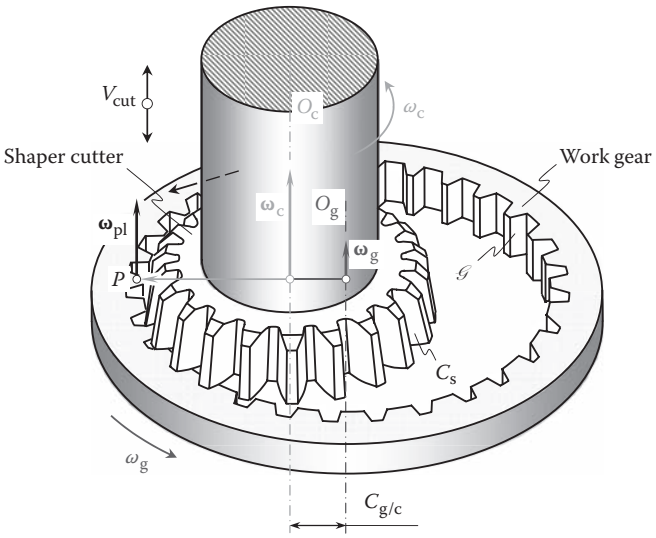

FIGURE 11.2
Shaping of an internal work gear with the shaper cutter.

The shaper cutter is reciprocating in its axial direction simultaneously with the rotations ω_g and ω_c. Speed of reciprocation is designated as $\mathbf{V}_{cut}$. Reciprocation of the shaper cutter is necessary for stock removal.

When shaping a helical work gear, the rotation of the shaper cutter $\boldsymbol{\omega}_{cut}$ is performed in addition to the reciprocation $\mathbf{V}_{cut}$. Timing of the motions $\mathbf{V}_{cut}$ and $\boldsymbol{\omega}_{cut}$ depends on the hand of the tooth helix of the work gear. The resultant screw motion that is composed by the translation $\mathbf{V}_{cut}$ and the rotation $\boldsymbol{\omega}_{cut}$ is a screw cutting motion of the shaper cutter along and about its axis. This screw motion does not correlate to rotations $\boldsymbol{\omega}_g$ and $\boldsymbol{\omega}_c$, and is independent of rotations $\boldsymbol{\omega}_g$ and $\boldsymbol{\omega}_c$. The parameter of the screw motion is identical to the screw parameter of the work gear helix. The vector of the screw cutting motion can be pointed either in the same direction or in the opposite direction of the rotation vector $\boldsymbol{\omega}_c$.

The distance between the axes O_g and O_c of the rotations changes when the shaper cutter reciprocates back and forth, similar to that shown in Figure 10.2.

11.2 Design of Shaper Cutters

A detailed discussion of the design of shaper cutters reproducing an external gear machining mesh (see Chapter 10 for details) makes it easier to form a concise analysis of the design of gear shaper cutters engaged in an internal gear machining mesh when shaping gears.

11.2.1 Generating Surface of Gear Shaper Cutters

Most of the internal gears machined with shaper cutters are spur gears. However, internal gears having helical teeth can also be machined with shaper cutters.

The generating surface of a shaper cutter for machining internal gears is similar to that used for machining of external gears. Therefore, without going into details of the analysis, Equation (10.8)

$$\mathbf{r}_c(U_c, V_c) = \begin{bmatrix} r_{b.c}\cos V_c + U_c \cos\lambda_{b.c}\sin V_c \\ r_{b.c}\sin V_c - U_c \cos\lambda_{b.c}\sin V_c \\ r_{b.c}\tan\lambda_{b.c} - U_c \sin\lambda_{b.c} \\ 1 \end{bmatrix} \tag{11.2}$$

can be used for the analytical description of the generating surface T of the shaper cutter for machining of internal gears.

Equation (11.2) is applicable for both helical shaper and spur shaper cutters. In the latter, it is required to make the base lead angle $\lambda_{b.c}$ of the surface T equal to 90°.

11.2.2 Profiling of Gear Shaper Cutters

When profiling a gear shaper cutter, it is necessary to satisfy the condition under which three surfaces are passing through a common line: (1) generating surface of the shaper cutter T, (2) rake surface R_s, and (3) clearance surface C_s. These surfaces have to pass through the common line, that is, through the cutting edge CE of the shaper cutter tooth.

There are three methods of transforming the generating body of the cutting tool* into a workable edge cutting tool [43]:

1. Intersect the generating surface T by the rake suface R_s. Then, the clearance surface C_s is a surface at a clearance angle α through the cutting edge CE.
2. Intersect the generating surface T by the clearance surface C_s. Then, the rake surface R_s is a surface at a rake angle γ through the cutting edge CE.
3. Construct on the generating surface T the cutting edge having optimal the inclination angle λ. Then, the rake surface R_s, and the clearance surface C_s are surfaces through the cutting edge CE.

In the first method, considered the most practical option for this particular case, the generating surface T of the shaper cutter is intersected by the rake surface R_s. The cutting edge CE of the shaper cutter is viewed here as the line of intersection of the surfaces T and R_s.

The generating surface of the shaper cutter is defined above [see Equation (11.2)]. An internal cone of revolution or a plane (that is orthogonal to the shaper cutter axis of rotation) is used as the rake surface R_s of the shaper cutter tooth (see Figure 10.5). For helical shaper cutters, the plane that is orthogonal to the pitch helix of the shaper cutter tooth (see Figure 10.6) can be used as the rake surface as well. Coordinates of points of the cutting edge CE satisfy both the equation for the generating surface T of the shaper cutter and the equation for the rake surface R_s. Next, the clearance surface C_s is specifically constructed so as to pass through the cutting edge CE. For the convenience of the manufacturer of shaper cutters, the desired clearance surface is approximated with a screw involute surface. Clearance surface C_s of the chosen geometry is not exactly passing through the cutting edge CE. Because of the approximation, deviations of the actual location of the cutting edges from their desired location are unavoidable. To minimize the deviations, certain corrections can be introduced in the shaper cutter tooth profile. Determination of the critical distance to the nominal cross section is also a critical issue when designing the shaper cutter.

For internal gears, it is frequently necessary to use small cutters when the disk-type construction cannot be used. The smallest cutters are usually made shank type. When the cutters are small in diameter for the tooth size, they are made integral with a shank. If the face width to be cut is wide, the shank has to be rather long and sturdy.

Two basic designs of shaper cutters for machining of internal gears have been developed: (1) the shank-type shaper cutter and (2) the deep counterbore shaper cutter that is assembled on a special adapter.

Figure 11.3 shows a shank-type shaper cutter and its nomenclature. Shaper cutters of this type are generally used in cutting small pitch diameter internal parts. The cutter length below the taper must by adequate to accommodate the face width of the gear to be cut plus the required overtravel at the bottom of the machine stroke and available life of the cutter. The work-holding fixture or a recess of the gear teeth in the blank may require extra length. Taper shank-type cutters are available in four taper sizes (measured at the large end of the taper).

* A body that is made of the cutting material and bounded by the generating surface T of the cutting tool is referred to as the *generating body of the cutting tool*.

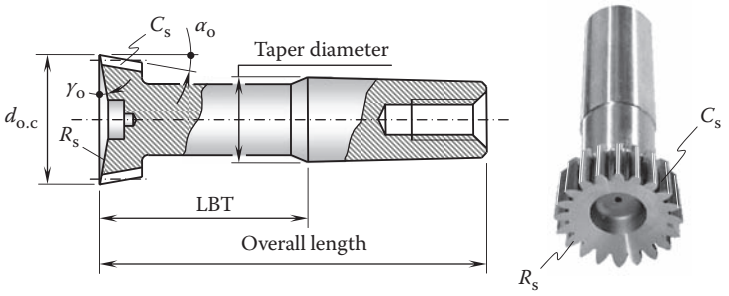

FIGURE 11.3
Design of a shank-type shaper cutter.

TABLE 11.1

Taper Sizes for Shank-Type Shaper Cutters

Taper Diameter (in.)	Taper Type
1.0625	0.6235 in tpf
0.700	#2 Morse
0.475	#1 Morse
0.250	#2 Jarno

The pitch diameter of the cutter should approximate the diameter of the taper. Flutes can be added to long cutters of small pitch diameter to minimize deflection when cutting.

Taper shank cutters, which come in various sizes, normally cut small internal gears or splines. The taper fits directly into the machine spindle or indirectly with a reduction taper bushing.

The cutter has external teeth and must be small enough to avoid damaging the corners of the internal teeth.

Shaper cutters frequently have small enough numbers of teeth to cause the base circle to come high on the tooth flank. The region below the base circle may be left as a simple radial flank or it may be filled in. The filled-in design can be used to break the top corner of the gear tooth being cut. Shaper cutters can be made with a protuberance at the tip. The protuberance cuts an undercut at the root of the gear tooth. This provides a desirable relief for a shaving tool. The protuberance design is also used in some cases to permit the sides of gear teeth to be ground without having to grind the root fillet.

A small disk-type shaper cutter with a deep counterbore mounted on a special adapter is shown in Figure 11.4. Shaper cutters of this design are also often used for cutting of internal gear teeth.

11.2.3 Cutting Edge Geometry of Gear Shaper Cutters

The rake angles γ_o and γ_f at the top and lateral cutting edges, respectively, as well as the clearance angles α_o and α_f and are all necessary to make the shaper cutter an efficient metal-cutting tool.

The geometry of three major surfaces, T, R_s, and C_s, in shaper cutters for machining gears in the internal gear machining mesh is similar to the geometry of the same major surfaces

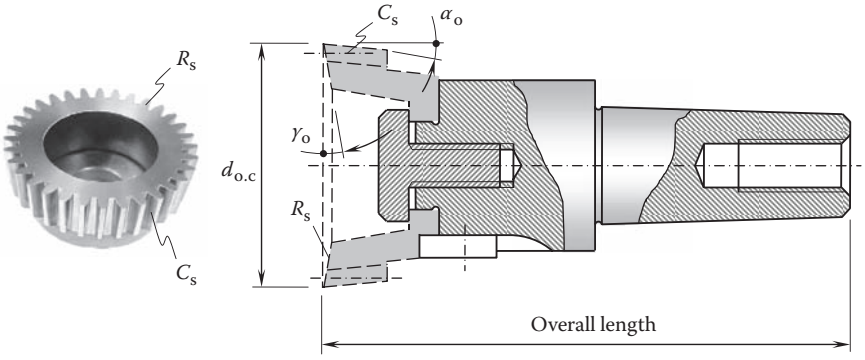

FIGURE 11.4
Small disk-type shaper cutter with deep counterbore mounted on a special adapter.

in shaper cutters for machining gears in the external gear machining mesh. Thus, for the computation of (a) angle of inclination λ, (b) rake angles γ_o and γ_f, and (c) clearance angles α_o and α_f, the formulae developed earlier are applicable.

It is common practice to make the rake angle at the top cutting edge of the shaper cutter equal to 5°. Occasionally, roughing shaper cutters have a rake angle as high as $\gamma_o = 10°$. The clearance angle at the top cutting edge of the shaper cutter is usually equal to $\alpha_o = 6°$. The sides of the cutter have a side clearance of about $\alpha_f = 2°$.

Because of the smaller tooth number, changes in the rake angle γ_f and the clearance angle α_f within the lateral cutting edges of shank-type shaper cutters and small-diameter disk-type shaper cutter with deep counterbore exceed changes in the corresponding angles γ_f and α_f for shaper cutters of conventional design.

11.3 Thickness of Chip Cut by the Gear Shaper Cutter Tooth

Thickness of cut is an important consideration because it significantly affects the wear of shaper cutter teeth. Computation is the most preferred means of determining the thickness of cut.

The kinematics of the gear shaping operation features continuous indexing of rotations of the work gear and the shaper cutter. When shaping an internal gear with the gear shaper cutter (Figure 11.1), the work gear is rotating about its axis of rotation O_g. The shaper cutter is rotating about its axis of rotation O_c. In the case under consideration, vectors of both rotations $\boldsymbol{\omega}_g$ and $\boldsymbol{\omega}_c$, as well as the vector $\boldsymbol{\omega}_{pl}$ of instant relative rotation, are pointed in the same direction. Thus, the equality $\boldsymbol{\omega}_{pl} = \boldsymbol{\omega}_c - \boldsymbol{\omega}_g$ is observed when shaping an internal gear. Rotation of the gear ω_g is timed with the rotation of the shaper cutter ω_c so that the ratio $\omega_g/\omega_c = N_c/N_g$ is valid.

Two motions are necessary for machining of a work gear with the shaper cutter: (1) motion of cut and (2) feed motion.

Reciprocation of the shaper cutter serves as the primary motion (motion of cut). Reciprocation of the shaper cutter provides the necessary speed of cutting. Speed of cutting is equal to the speed V_{rc} of the shaper cutter reciprocation.

The feed motion F_c is attributed to the instant relative rotation $\boldsymbol{\omega}_{pl}$ of the shaper cutter with respect to the work gear, that is, to rotation $\boldsymbol{\omega}_g$ of the work gear and rotation $\boldsymbol{\omega}_c$ of the shaper cutter. Rolling of the pitch surfaces of the work gear and the shaper cutter about their axes of rotation allows for interpretation in the form of instant rotation of the shaper cutter pitch cylinder about the pitch line. Speed of the instant rotation ω_{pl} can be expressed in terms of the rotations ω_g and ω_c, and in terms of the design parameters of the gear and the gear shaper cutter. Ultimately, speed of the feed motion F_c allows for interpretation in the form of product of the speed of linear motion of the elementary portion of the cutting edge of the shaper cutter tooth in its instant relative rotation

$$F_c = \omega_{pl} R_{rl} \tag{11.3}$$

where

ω_{pl} = instant relative rotation of the shaper cutter
R_{rl} = distance of a point of interest m within the shaper cutter cutting edge (the point of interest m can be chosen among the three cutting edges of the shaper cutter tooth)

For a given gear shaping operation, the value of the instant rotation ω_{pl} is constant (ω_{pl} = const). The distance R_{rl} depends on the coordinates of the point of interest m of the shaper cutter cutting edge. This can be specified by the position vector $\mathbf{r}_m$. This yields a formula

$$\mathbf{F}_c = \boldsymbol{\omega}_{pl} \times \mathbf{r}_m \tag{11.4}$$

for the computation of the vector $\mathbf{F}_c$ of the feed motion. This formula reveals that both the magnitude and direction of the feed motion depend on the location of the chosen point of interest within the cutting edge.

The approach proposed by Shishkov [186] can be used to compute for the parameters of a portion of stock cut out per stroke by the shaper cutter tooth.

Two consequent locations of the shaper cutter tooth are considered for the computation of thickness of cut. The initial position of the shaper cutter tooth is defined by a Cartesian coordinate system $X_g Y_g Z_g$ associated with the work gear (Figure 11.5). Similar to Equation (10.66), the angle per stroke ε_{st} of the shaper cutter can be expressed in terms of (1) the roll angle ε_o at the outer diameter of the gear tooth profile, (2) the roll angle ε_l at the inner diameter of the gear tooth profile, and (3) the number or strokes n_{st} of the shaper cutter necessary for shaping the whole tooth flank surface

$$\varepsilon_{st} = \frac{\varepsilon_o - \varepsilon_l}{n_{st}} \tag{11.5}$$

Usually, the value of the angle ε_{st} is in the range of $\varepsilon_{st} \cong 1°$ or so. However, when shaping internal gears, it can exceed the corresponding value computed during the shaping of external gears. This is mostly because the convex tooth profile of the shaper cutter is making contact with the concave tooth profile of the gear, rather then two convex tooth profiles making contact when machining external gears with a shaper cutter of standard design.

Rotation of the shaper cutter ω_c is timed with the rotation of the work gear ω_g so that the ratio

$$\frac{\omega_g}{\omega_c} = \frac{N_c}{N_g} \tag{11.6}$$

is observed.

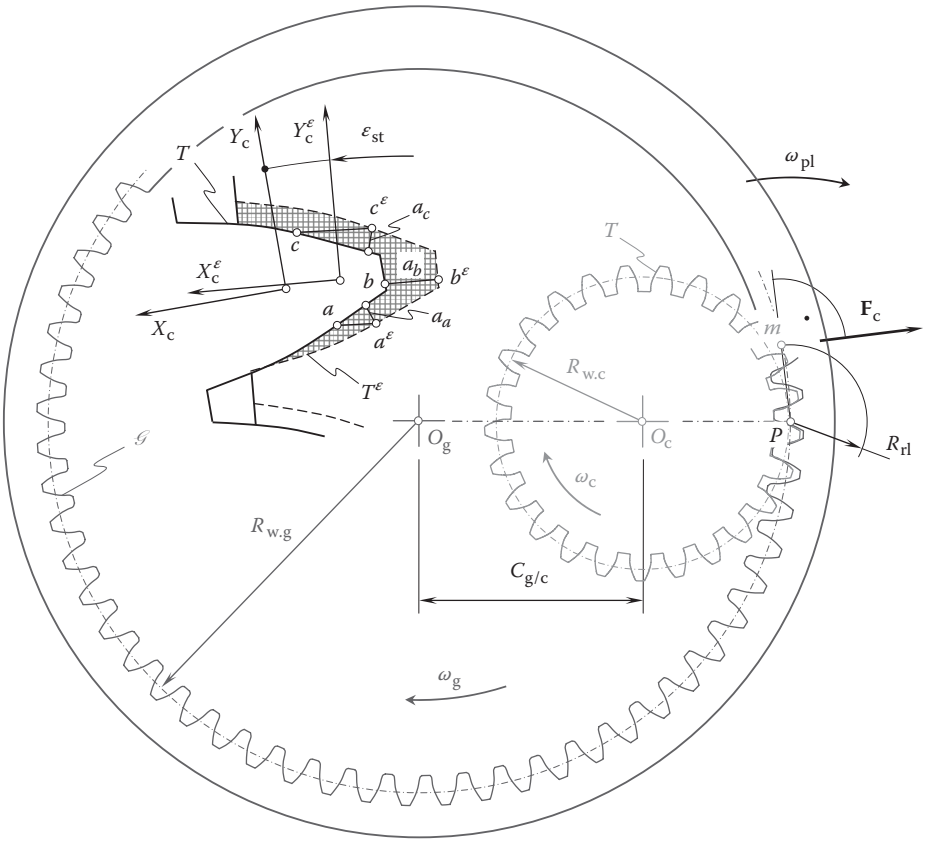

FIGURE 11.5
Determination of thickness of cut when shaping an internal spur gear with the shaper cutter.

In this test, the tooth ratio N_c/N_g is denoted by u. The angle of rotation of the cutter $\varepsilon_{st}^{(c)}$ can be expressed in terms of the angle of rotation of the work gear ε_{st} and the tooth ratio u by the expression

$$\varepsilon_{st}^{(c)} = \frac{\varepsilon_{st}}{u} \tag{11.7}$$

When the work gear turns about its axis O_g through a certain angle ε_{st}, the shaper cutter turns about its axis of rotation O_c through the corresponding angle $\varepsilon_{st}^{(c)}$. In addition, as this relative motion takes place, the axis of rotation O_c turns about the axis of rotation O_g through the angle ε_{st}. Under rotations ω_g and ω_c, the pitch cylinder of the shaper cutter is rolling with no sliding over the pitch cylinder of the work gear. The relative motion of the coordinate system of the shaper cutter with respect to the coordinate system of the work gear is the result of rolling of pitch cylinders. The Cartesian coordinate system associated with the gear shaper cutter in its initial position is designated as $X_cY_cZ_c$. In the current configuration of the shaper cutter relative to the work gear, that same coordinate system is designated as $X^\varepsilon{}_cY^\varepsilon{}_cZ^\varepsilon{}_c$.

The resultant linear transformation from the coordinate system $X_cY_cZ_c$ to the coordinate system $X^\varepsilon{}_cY^\varepsilon{}_cZ^\varepsilon{}_c$ can be analytically expressed by the operator of rolling $\mathbf{Rr}_u(\varepsilon_{st}, Z_g)$

(Figure 11.5). The operator of rolling $\mathbf{Rr}_u(\varepsilon_{st}, Z_g)$ can be viewed as a type of superposition of three consequent operators of elementary transformations: operator of rotation $\mathbf{Rt}[\varepsilon_{st}^{(c)}, Z_c]$, operator of rotation $\mathbf{Rt}(\varepsilon_{st}, Z_g)$, and operator of translation $\mathbf{Tr}(C_{g/c}, X_g)$. See Chapter 4 for details on the operator of rolling $\mathbf{Rr}_u(\varepsilon_{st}, Z_g)$.

Consider a point of interest within the cutting edge of the shaper cutter tooth. This may be a point a within the lateral cutting edge of the shaper cutter tooth, or a point b within the top cutting edge, or a point c within the lateral cutting edge of the opposite side of the tooth profile (Figure 11.5). For the specific coordinates of the point of interest, use of the local coordinate system $X_cY_cZ_c$ is often helpful.

For a given location of the generating surface T of the shaper cutter position vector $\mathbf{r}_a$ of the point of interest a is known (the same is valid with respect to any other point of interest within the cutting edge). The unit normal vector $\mathbf{n}_{T.a}$ to the surface T at point a can be computed using Equation (11.2).

In the new position of the shaper cutter, its generating surface is designated as T^{ε} (Figure 11.5). Under the rolling of pitch cylinders, the point of interest a moves to position a^{ε}. The position vector $\mathbf{r}^{\varepsilon}{}_a$ of the point of interest in the new location of the shaper cutter can be expressed in terms of the position vector $\mathbf{r}_a$ and the operator of rolling $\mathbf{Rr}_u(\varepsilon_{st}, Z_g)$ in the following manner

$$\mathbf{r}_a^{\varepsilon} = \mathbf{Rr}_u(\varepsilon_{st}, Z_g) \cdot \mathbf{r}_a \tag{11.8}$$

Similarly, the following expression

$$\mathbf{n}_{T.a}^{\varepsilon} = \mathbf{Rr}_u(\varepsilon_{st}, Z_g) \cdot \mathbf{n}_{T.a} \tag{11.9}$$

is valid for the unit normal vector $\mathbf{n}_{T.a}$ to the generating surface T^{ε} through point a^{ε}.

Thickness of cut is measured perpendicular to the machined surface of the work gear. Its value varies within the cutting edge of the shaper cutter. At point a^{ε}, the thickness of cut is denoted by a_a. Parameters a_b and a_c are implemented for the thickness of cut at points b^{ε} and c^{ε}, respectively.

Thickness of cut a_a is equal to the length of the straight-line segment between point a^{ε} and surface T. The point of interception of the straight line $\mathbf{a}_a(t)$ through point a^{ε} along the unit normal vector $\mathbf{n}^{\varepsilon}{}_{T.a}$ (shown, but not labeled, in Figure 11.5) is obtained as follows

$$\mathbf{a}_a(t) = \mathbf{r}_a^{\varepsilon} + t \cdot \mathbf{n}_{T.a}^{\varepsilon} \tag{11.10}$$

where t is a parameter of the straight line.

Solving the equation for the generating surface T of the shaper cutter [note that (a) Equation (11.2) describes only one lateral flank of the surface T; a similar equation is valid for the opposite flank of the tooth of the surface T; and (b) equation for the top land of surface T is a trivial one], together with Equation (11.10), returns the position vector $\hat{\mathbf{r}}^{\varepsilon}{}_a$ of the point of interception of the straight line $\mathbf{a}_a(t)$ with the generating surface T. This immediately yields a formula

$$a_a = |\mathbf{r}_a^{\varepsilon} - \hat{\mathbf{r}}_a^{\varepsilon}| \tag{11.11}$$

for the computation of thickness of cut at the point of interest within the cutting edge of the shaper cutter tooth.

Equation (11.11), used to compute for thickness of cut at a point of interest within the cutting edge of the shaper cutter, is derived with no assumptions or simplifications. It is an accurate one. It can be used for cases when the point of interest is a far remote point from the pitch point of the gear machining mesh in a gear shaping operation and the cutting edge—cut thick chip. It is also valid when the point of interest is close to the pitch point and the cutting edge—cut thin chip whose thickness is in a range close to the roundness of the cutting edge.

For approximate computations, simpler equations are known. However, known equations are applicable for remote portions of the cutting edges and thus, are not applicable for portions of the cutting edges close to the pitch point, or alternatively, they are applicable for the points of the cutting edge close to the pitch point and are therefore not applicable to the remote portions of the cutting edges of the shaper cutter.

Equation (11.11) can be used to compute for the other parameters of the portion of stock that has been removed by the cutting edge of a shaper cutter: shape of the cross section of the portion of stock, its area, etc.

The analysis reveals that cutting edges of the shaper cutter teeth cut chips of varying thickness.

First, thickness of cut depends on the distance between the point of interest and the pitch point of the gear machining mesh. The greater the distance between these points, the larger the thickness of cut.

Second, the different cutting edges of the shaper cutter tooth cut chips of varying thickness. The chip that is cut by the top cutting edge is the thickest one. The thickness of chip that is cut by the lateral cutting edge of the entering side of the tooth profile is greater than that of the recessing side of the shaper cutter tooth profile.

Lateral cutting edges of the gear shaper cutter teeth cut the stock mostly within the distance between the pitch point and the point where the cutting begins. A small amount of the stock is also cut beyond the pitch point. The top land cutting edge does not cut the stock beyond the pitch point.

A detailed analysis of the thickness of cut is beyond the scope of the book, and should be discussed as a separate topic.

11.4 Accuracy of Shaped Internal Gears

Accuracy of the internal gears machined with shaper cutters is discussed from the perspective of satisfying a set of required conditions for proper part surface generation (*PSG*).

Satisfaction of the conditions of proper *PSG* is a must when machining gears using the shaper cutter (see Appendix D for details on conditions of proper *PSG*). When shaping an internal gear with a shaper cutter of conventional design, the pitch surface of the work gear is shaped in the form of an inner cylinder of revolution, whereas pitch surface of the shaper cutter is shaped in the form of an external cylinder of revolution.

Because pitch cylinders form an inner tangency with each other, the importance of the fifth condition of proper *PSG* is not as critical as when shaping external gears. Only in very special cases of gear machining does it become necessary to verify whether the fifth condition of proper *PSG* is satisfied.

Similarly, when machining an internal gear with a shaper cutter of conventional design, the convex tooth profile of the shaper cutter is interacting with the concave tooth profile

of the work gear. Tangency of this type significantly reduces the cusp height. Therefore, the sixth condition of proper *PSG* is also not essential for the practical needs of gear manufacturers.

When machining an internal gear with a conventional shaper cutter, most of the conditions of proper *PSG* are satisfied, and usually there is no need for their verification. Violation of the conditions of proper *PSG* may occur when the difference between the number of teeth of the internal work gear and the shaper cutter is small. Under such a scenario, interference of the work gear teeth and shaper cutter teeth is likely to be observed. The last should not be allowed to occur.

Elimination of interference of the internal work gear and shaper cutter teeth. Interference of the internal work gear and shaper cutter teeth can be caused by contact with noninvolute portions of the tooth flank. As internal gears are usually machined with pinion-type cutters, special attention has to be paid to the length of involute tooth flanks.

Where the difference between the number of work gear and shaper cutter teeth is very small, tip interference could occur due to the collision between the tooth tips of the gear and shaper cutter beyond the line of action [34]. This is caused by the special geometry of engagement of internal gears and is not connected with the choice of the shaper cutter. To remedy this type of interference, it is necessary to change the geometrical layout of the pair of gears in the gear machining mesh. In particular, an adequately large working pressure angle is recommended.

The following shaper cutter data are required to check for interference:

N_c—tooth number of the shaper cutter

$d_{b.c}$—shaper cutter base diameter

x_c—addendum modification coefficient in reground condition of the shaper cutter (where applicable)

$d_{o.c}$—outer diameter of the shaper cutter in reground condition (where applicable)

The pressure angle $\phi_{o.c}$ at the shaper cutter tooth tip is given by

$$\phi_{o.c} = \cos^{-1}\left(\frac{d_{b.c}}{d_{o.c}}\right) \tag{11.12}$$

The generating pressure angle usually differs from the nominal pressure angle when an internal gear is cut by a shaper cutter. When the shaper cutter reaches the full theoretical tooth depth on the internal gear, the transverse generating pressure angle is given by [34]

$$\text{inv}\phi_{gt} = \text{inv}\phi_t + 2\frac{(x_g - x_c)}{N_g - N_c}\cdot\tan\phi_n \tag{11.13}$$

The center distance between the gear and the shaper cutter becomes

$$C_{g/c} = \frac{d_{b.g} - d_{b.c}}{2\cos\phi_{gt}} \tag{11.14}$$

The interference between an internal gear and the shaper cutter with very small difference in the number of teeth occurs if the number of teeth of the internal gear and the shaper cutter differs only by a few teeth. Whether such interference occurs can be analytically

verified. Note that results of the computations are very sensitive to small changes in center distance. Therefore, it is recommended to verify the upper and lower limits of the center distance.

To prevent interference between an internal gear and the shaper cutter having a small difference in their number of teeth, the following inequality [34]

$$\frac{d_{\mathrm{b.c}}}{2}(\mathrm{inv}\phi_{\mathrm{o.c}} - \mathrm{inv}\phi^* + \mathrm{arc}\delta_{\mathrm{c}}) - \frac{d_{\mathrm{b.g}}}{2}(\mathrm{inv}\phi_{\mathrm{o.g}} - \mathrm{inv}\phi^* + \mathrm{arc}\delta_{\mathrm{g}}) > 0 \tag{11.15}$$

has to be satisfied.

The design parameters of the internal gear and the shaper cutter that will be entered in Equation (11.14) can be computed from the following formulae

$$\phi^* = \cos^{-1}\left(\frac{d_{\mathrm{b.g}} - d_{\mathrm{b.c}}}{2C_{\mathrm{g/c}}}\right) \tag{11.16}$$

$$\phi_{\mathrm{o.c}} = \cos^{-1}\left(\frac{d_{\mathrm{b.c}}}{d_{\mathrm{o.c}}}\right) \tag{11.17}$$

$$\delta_{\mathrm{c}} = \cos^{-1}\left[\left(1 + \frac{d_{\mathrm{o.g}}}{d_{\mathrm{o.c}}}\right)\cdot\frac{d_{\mathrm{o.g}} - d_{\mathrm{o.c}}}{4C_{\mathrm{g/c}}} - \frac{C_{\mathrm{g/c}}}{d_{\mathrm{o.c}}}\right] \tag{11.18}$$

$$\phi_{\mathrm{o.g}} = \cos^{-1}\left(\frac{d_{\mathrm{b.g}}}{d_{\mathrm{o.g}}}\right) \tag{11.19}$$

$$\delta_{\mathrm{g}} = \cos^{-1}\left[\left(1 + \frac{d_{\mathrm{o.c}}}{d_{\mathrm{o.g}}}\right)\cdot\frac{d_{\mathrm{o.g}} - d_{\mathrm{o.c}}}{4C_{\mathrm{g/c}}} - \frac{C_{\mathrm{g/c}}}{d_{\mathrm{o.g}}}\right] \tag{11.20}$$

When the shaper cutter tooth number N_c is too small, cutter interference at the tips of the teeth of the machined internal gear may occur. This results in loss of a portion of the involute profile. This trimming of the involute profile results in a smaller transverse contact ratio. Provided the transverse contact ratio is still greater than 1, it will not affect the transmission of motion but will reduce the load-carrying capacity of the mating gears.

To prevent this from happening, the shaper cutter tooth number N_{c} should be greater than the required minimum number of teeth, as given by following formula [34]

$$N_{\mathrm{c}} \geq N_{\mathrm{g}}\left(1 - \frac{\tan\phi_{\mathrm{o.g}}}{\tan\phi_{\mathrm{gt}}}\right) \tag{11.21}$$

In this expression, the value of angle $\phi_{\mathrm{o.g}}$ is computed from Equation (11.19) and the value of angle ϕ_{gt} is computed from Equation (11.13).

11.5 Enveloping Gear Shaper Cutters

Shaping of external gears with an enveloping shaper cutter is another example of the implementation of the internal gear machining mesh. This kinematics corresponds to the case when rotation of the work gear ω_g exceeds the rotation of the shaper cutter ($\omega_g > \omega_c$). A vector diagram of the kinematics of the machining process of an external gear with the enveloping shaper cutter is illustrated in Figure 11.6. Again, the rotation vectors $\boldsymbol{\omega}_g$ and $\boldsymbol{\omega}_c$ are parallel to each other and are pointed in the same direction. The vector of instant rotation $\boldsymbol{\omega}_{pl}$ is parallel to the rotation vectors $\boldsymbol{\omega}_g$ and $\boldsymbol{\omega}_c$, and pointed in the same direction as the rotation vectors.

Enveloping shaper cutters are used for machining of spur gears. The generating surface of an enveloping shaper cutter is shaped in the form of the corresponding spur gear. Enveloping shaper cutters can be also designed and manufactured for machining of helical gears. No physical constraints exist in this concern. The reason why helical enveloping shaper cutters are not used in industry is attributed to difficulties in grinding of internal screw involute clearance surfaces.

The principal steps of designing an enveloping shaper cutter for machining of external gears are the same as those for the external shaper cutter for machining of internal gears. A close-up view of the enveloping shaper cutter is shown in Figure 11.7. This type of cutter may be used in the production of external gears where it is impractical to use a normal external disk cutter—for example, because of lack of space between the external teeth of the component and some protrusion in the component. Often, a shank-type cutter is used to perform the task, although this may have to be of a very small diameter and contain very few teeth. The internal cutter is fully generated to provide excellent tool life and much higher rates of productivity compared to a small shank.

11.6 Application of Gear Shaper Cutters

Shaper cutters are made up of high-speed steels containing molybdenum and tungsten. They are heat-treated to a Rockwell C hardness of 64 to 65. A nitriding surface treatment further improves their wear resistance.

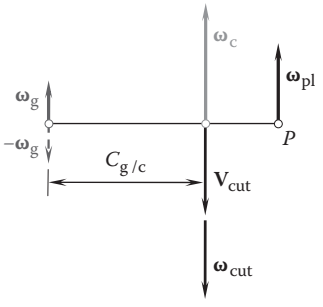

FIGURE 11.6
Vector diagram of the kinematics of the machining process of an external gear with the enveloping shaper cutter.

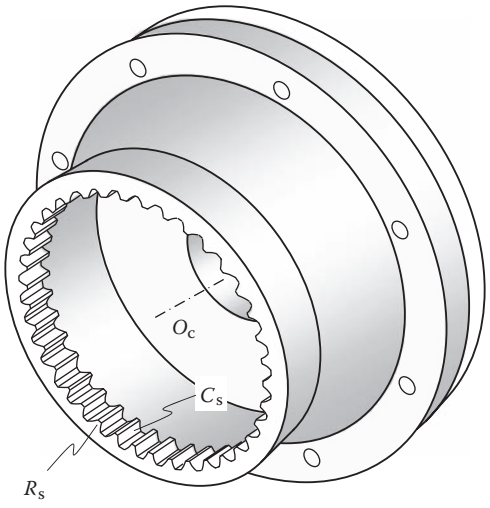

FIGURE 11.7
An enveloping shaper cutter.

Titanium nitride (TiN) coating is often applied to increase permissible feeds and speeds on modern shaping machines. Shaper cutters coated with TiN increase productivity by as much as 30% without decreasing tool life.

Kinematic schemes of machining of gear teeth featuring parallel rotation vectors of the same direction are used mostly for shaping of internal gears. An additional advantage of using this schematic of gear machining can be attained when shaping an internal gear with a shoulder as depicted in Figure 11.8.

An internal gear and an external gear can be cut in the same cycle by mounting an internal and an external shaper cutter on the same arbor (Figure 11.9). Machining parameters for each cut are performed in the numerical control. Machining of the cluster gear in a single setup is economical because it saves time in remounting of the shaper cutters.

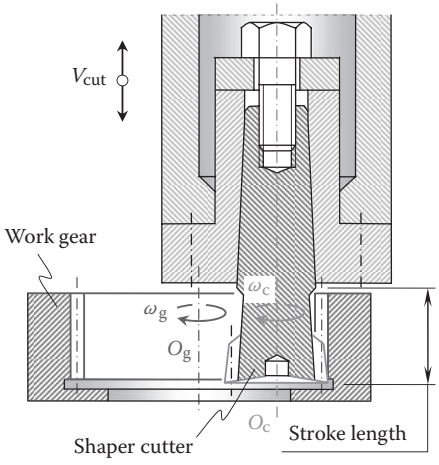

FIGURE 11.8
Shank-type shaper cutter for machining of small-diameter internal gears with a shoulder.

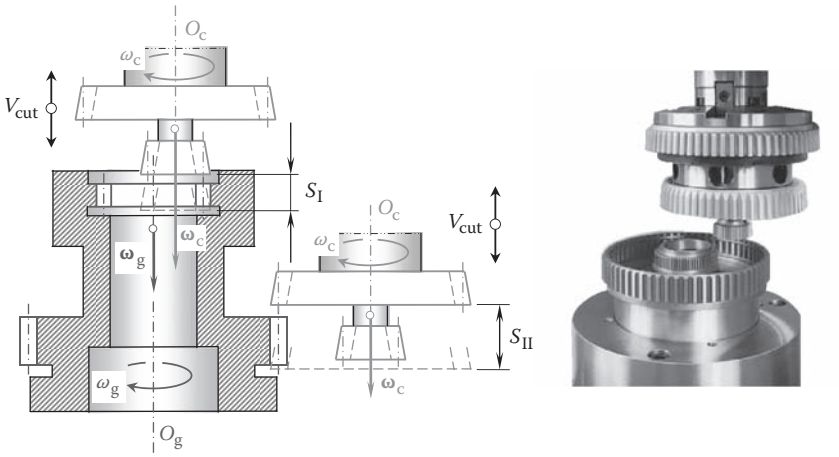

FIGURE 11.9
Consecutive cutting of an internal gear and an external gear in the same machine cycle.

In the gear shaping operation, cutting is accomplished by feeding the shaper cutter radially into the annulus and the number of cuts required is controlled by the material, the size of the work gear, and the quality expected. It is common practice to finish with a light finishing cut and this may range from about 0.002 to 0.010 in. (0.05–0.25 mm) deep. Internal gears tend to distort easily unless their thickness is substantial. For epicyclic (planetary) gear units, some flexibility in the annulus is beneficial, but during cutting it is necessary to prevent radial deflection by whatever means is most suitable.

Shaping of external gears with enveloping shaper cutters is not often used (Figure 11.10). However, in some particular cases of gear machining enveloping shaper cutters can be substituted with no gear cutting tool of any other design instead. High cost is the major reason for the limited use of enveloping shaper cutters.

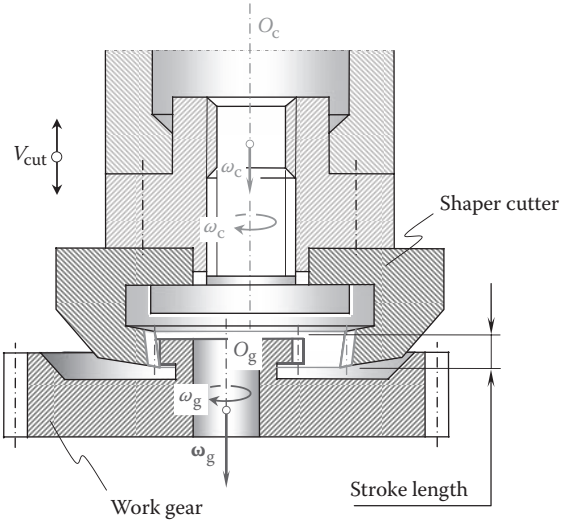

FIGURE 11.10
An enveloping shaper cutter for machining an external gear.

Section IV

Cutting Tools for Gear Generating: Intersecting-Axis Gear Machining Mesh

Intersecting-axis gear machining mesh is another example of planar gear machining meshes. Gear cutting tools that work based on the generating principle can be designed on the premise of the intersecting-axis gear machining mesh. When machining a work gear with a generating gear cutting tool, rolling with no sliding of the axode of the work gear over the axode of the gear cutting tool is always observed.

For convenience, this review of designs of gear cutting tools begins with an analysis of the kinematics of the intersecting-axis gear machining mesh.

Kinematics of the Intersecting-Axis Gear Machining Mesh

Intersecting-axis gear machining mesh can be schematically depicted by two rotation vectors, $\boldsymbol{\omega}_g$ and $\boldsymbol{\omega}_c$, lines of action of which intersect each other. These vectors are the rotation vector $\boldsymbol{\omega}_g$ of the work gear and rotation vector $\boldsymbol{\omega}_c$ of the gear cutting tool.

The rotation vectors $\boldsymbol{\omega}_g$ and $\boldsymbol{\omega}_c$ form a certain angle Σ. They are along the axes O_g and O_c of rotation of the work gear and the gear cutting tool, respectively. Commonly, vectors $\boldsymbol{\omega}_g$ and $\boldsymbol{\omega}_c$ are applied at the point of intersection of the axes O_g and O_c. This point is referred to as the *apex*, as shown in Figure IV.1. However, because vectors $\boldsymbol{\omega}_g$ and $\boldsymbol{\omega}_c$ are a type of sliding vectors, in particular cases for convenience they can be applied at other points within the corresponding axis of rotation.

Because rotation vectors $\boldsymbol{\omega}_g$ and $\boldsymbol{\omega}_c$ intersect each other, the vector of instant rotation $\boldsymbol{\omega}_{pl} = \boldsymbol{\omega}_c - \boldsymbol{\omega}_g$ is also within the plane through these vectors. The vector $\boldsymbol{\omega}_{pl}$ of instant rotation is applied at the same point P of intersection of the axes O_g and O_c.

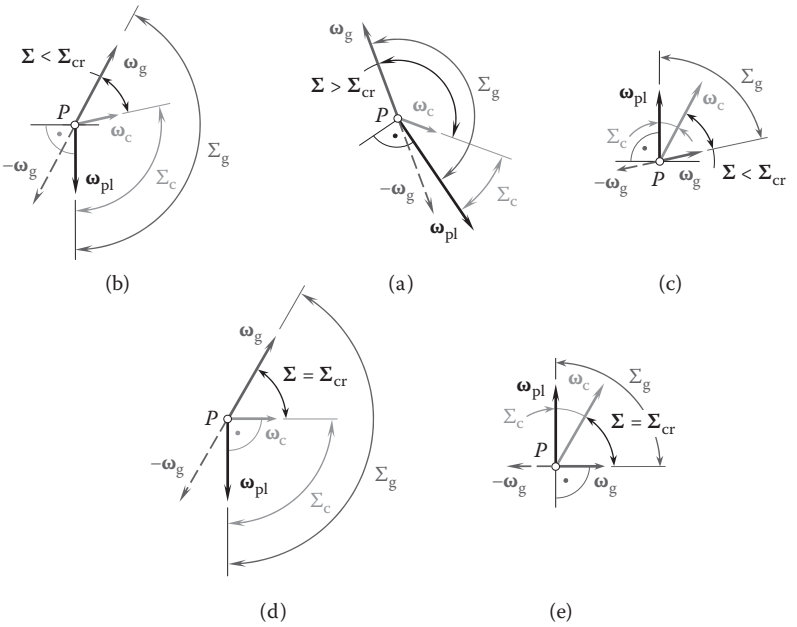

FIGURE IV.1
Types of intersecting-axis gear machining meshes.

The rotation vector of the work gear $\boldsymbol{\omega}_g$ and the vector of instant rotation $\boldsymbol{\omega}_{pl}$ form an angle that is denoted by Σ_g. Similarly, the angle formed by the rotation vector of the gear cutting tool $\boldsymbol{\omega}_c$ and the vector of instant rotation $\boldsymbol{\omega}_{pl}$ is denoted by Σ_c. A simple correlation is observed between magnitudes ω_g and ω_c of the rotation vectors $\boldsymbol{\omega}_g$ and $\boldsymbol{\omega}_c$, and between the angles Σ_g and Σ_c [see Equation (3.15)]

$$-\frac{\sin \Sigma_g}{\sin \Sigma_c} = \frac{\omega_c}{\omega_g} \tag{IV.1}$$

The actual configuration of the vector of instant rotation $\boldsymbol{\omega}_{pl}$ within the plane through the rotation vectors $\boldsymbol{\omega}_g$ and $\boldsymbol{\omega}_c$ depends on the ratio ω_g/ω_c. This ratio is commonly referred to as the tooth ratio (u) of the gear machining mesh. For the computation of u, the expression $u = \omega_g/\omega_c$ is valid.

In Figure IV.1a, the vector diagram corresponds to an external *work gear to cutting tool mesh*. For an external work gear to cutting tool mesh, the tooth ratio u is positive ($u > 0$). In this particular case, the rotation vectors $\boldsymbol{\omega}_g$ and $\boldsymbol{\omega}_c$ form an obtuse angle Σ. Any alteration in the ratio $u = \omega_g/\omega_c$ immediately entails a corresponding change in the configuration of the vector of instant rotation $\boldsymbol{\omega}_{pl}$.

If Σ is an acute angle, the corresponding vector diagram corresponds to an internal gear machining mesh. Two types of internal gear machining meshes are recognized.

First, an external work gear can be machined with an enveloping gear cutting tool. A vector diagram for this particular case of gear machining is shown in Figure IV.1b. Second, an internal work gear can be machined with an external gear cutting tool. A vector diagram for this case of gear machining is shown in Figure IV.1c. In both cases, the tooth ratio u

is negative ($u < 0$). In the first case (Figure IV.1b), the negative sign of u is attributed to $\Sigma_c < 0$ (whereas $\Sigma_g > 0$). In the second case (Figure IV.1c), the negative sign of u is attributable to $\Sigma_g < 0$ (whereas $\Sigma_c > 0$).

For an external gear machining mesh, the angle Σ is obtuse. In contrast, for an internal gear machining mesh the angle Σ is acute. What is between these two cases? Or, in other words, what type of gear machining mesh corresponds to the case(s), which separates an external intersecting-axis gear machining mesh from an internal intersecting-axis gear machining mesh?

A vector diagram for this case shows that either the rotation vector of the gear cutting tool $\boldsymbol{\omega}_c$ is perpendicular to the vector of instant rotation $\boldsymbol{\omega}_{pl}$ (Figure IV.1d) or the rotation vector of the work gear $\boldsymbol{\omega}_g$ is perpendicular to the vector of instant rotation $\boldsymbol{\omega}_{pl}$ (Figure IV.1e).

In the first case (Figure IV.1d), the cutting tool transforms into a round rack. Because the vector of instant rotation $\boldsymbol{\omega}_{pl}$ is specified as the difference ($\boldsymbol{\omega}_{pl} = \boldsymbol{\omega}_c - \boldsymbol{\omega}_g$) between the rotation vectors $\boldsymbol{\omega}_g$ and $\boldsymbol{\omega}_c$, this immediately yields an analytical expression

$$(\boldsymbol{\omega}_c - \boldsymbol{\omega}_g) \cdot \boldsymbol{\omega}_c = 0 \tag{IV.2}$$

that makes it possible to identify a gear machining mesh of this type.

In the second case (Figure IV.1e), the work gear degenerates into a round rack. The expression

$$(\boldsymbol{\omega}_c - \boldsymbol{\omega}_g) \cdot \boldsymbol{\omega}_g = 0 \tag{IV.3}$$

can be used to identify a gear machining mesh of this type.

The derived analytical criteria [Equations (IV.2) and (IV.3)] allows for the corresponding expressions

$$(\boldsymbol{\omega}_c - \boldsymbol{\omega}_g) \cdot \boldsymbol{\omega}_g < 0 \tag{IV.4}$$

$$(\boldsymbol{\omega}_c - \boldsymbol{\omega}_g) \cdot \boldsymbol{\omega}_c < 0 \tag{IV.5}$$

which are valid for an external gear machining mesh, as well as the expressions

$$(\boldsymbol{\omega}_c - \boldsymbol{\omega}_g) \cdot \boldsymbol{\omega}_g > 0 \tag{IV.6}$$

$$(\boldsymbol{\omega}_c - \boldsymbol{\omega}_g) \cdot \boldsymbol{\omega}_c > 0 \tag{IV.7}$$

which are valid for an internal gear machining mesh.

A gear cutting tool can be designed based on each of the vector diagrams shown in Figure IV.1. Various designs of gear cutting tools featuring the intersecting-axis work gear to cutting tool mesh can be developed. It is convenient to begin this discussion by focusing on the design of a gear cutting tool featuring the intersecting-axis gear machining mesh shown in Figure IV.1b.

12

Gear Shapers with a Tilted Axis of Rotation

The classification of all possible types of gear machining meshes (see Figure 3.8) offers several advantages: (1) systematization of all known designs of gear cutting tools as well as known methods of gear cutting and (2) development of novel designs of gear cutting tools and novel methods of gear machining. Numerous designs of gear cutting tools utilizing the advantages of the planar intersecting-axis gear machining mesh are used in industry today. One good example of these tools is the gear shaper with a tilted axis of rotation.

12.1 Kinematics of Gear Shaper Operation with the Shaper Cutters Having a Tilted Axis of Rotation

Consider the two rotations about intersecting axes O_g and O_c. In Figure 12.1, the vector of one of the rotations is designated as $\boldsymbol{\omega}_g$. This vector is along the axis O_g of rotation of the gear to be machined. The vector of another rotation, designated as $\boldsymbol{\omega}_c$ in Figure 12.1, is along the axis O_c of the gear shaper cutter to be designed. The rotation vectors $\boldsymbol{\omega}_g$ and $\boldsymbol{\omega}_c$ are at a certain shaft angle Σ. The vector of instant rotation $\boldsymbol{\omega}_{pl}$ of the gear cutting tool relative the work gear ($\boldsymbol{\omega}_{pl} = \boldsymbol{\omega}_c - \boldsymbol{\omega}_g$) is within the plane through the rotation vectors $\boldsymbol{\omega}_g$ and $\boldsymbol{\omega}_c$.

The rotation vector of the work gear $\boldsymbol{\omega}_g$ is at a certain angle Σ_g with respect to the vector of instant rotation $\boldsymbol{\omega}_{pl}$. For an external gear machining mesh, $\Sigma_g = 180° - \gamma_g$, where γ_g denotes the pitch angle of the work gear. The rotation vector of the gear cutting tool $\boldsymbol{\omega}_c$ forms a certain angle Σ_c with the vector of instant rotation $\boldsymbol{\omega}_{pl}$. This angle is equal to the pitch angle of the gear cutting tool ($\Sigma_c = \gamma_c$).

In the case under consideration (Figure 12.1), the following relationship

$$\gamma_g + \gamma_c = \pi - \Sigma \tag{12.1}$$

is valid.

When the equality [see Equation (IV.1)] is known, the following ratio

$$\frac{\sin\gamma_g}{\sin\gamma_c} = \frac{\omega_c}{\omega_g} \tag{12.2}$$

can be used for the computation of the cone angles γ_g and γ_c.

The ratio can be expressed in terms of the tooth numbers of the gear (N_g) and the gear cutting tool (N_c)

$$\frac{\sin\gamma_g}{\sin\gamma_c} = \frac{N_g}{N_c} \tag{12.3}$$

Rotations $\boldsymbol{\omega}_g$ and $\boldsymbol{\omega}_c$, which are synchronized with each other in a properly timed manner, result in the generating action of the gear cutting tool. To make the material removal

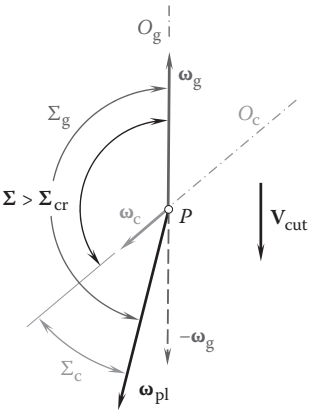

FIGURE 12.1
Kinematics of the gear shaping operation using a shaper cutter with a tilted axis of rotation.

possible when machining a work gear, a corresponding primary motion $\mathbf{V}_{cut}$ (motion of cut) is required to be performed. Usually, a plurality of solutions to the problem of selecting the primary motion is available. For this purpose, it is convenient to investigate any and all possible motions of the reference system $X_cY_cZ_c$ associated with a gear cutting tool relative to the coordinate system $X_gY_gZ_g$ associated with the work gear. When analyzing a possible candidate for the primary motion $\mathbf{V}_{cut}$, one should consider the restrictions imposed by the rolling motion in the gear machining mesh onto the feasible additional relative motion $\mathbf{V}_{cut}$ of the work gear and the gear cutting tool.

When no restrictions are imposed onto the additional relative motion, the coordinate system $X_cY_cZ_c$ of the gear cutting tool can perform three elementary translations ($\mathbf{V}_x$, $\mathbf{V}_y$, and $\mathbf{V}_z$) along the coordinate axes, and three elementary rotations ($\boldsymbol{\omega}_x$, $\boldsymbol{\omega}_y$, and $\boldsymbol{\omega}_z$) about the coordinate axis of the reference system $X_gY_gZ_g$. Consider all six possible elementary motions and all of their possible combinations by 1, 2, … , 6. Various values of the speed ratio of elementary motions need to be considered. Not all relative motions and their combinations are feasible for machining of a given gear. The motions that are not feasible should be omitted from further analysis. In this way, a suitable primary motion(s) can be determined.

As an example, let us assume that the reference system $X_cY_cZ_c$ of the gear cutting tool is performing a straight motion of cut $\mathbf{V}_{cut}$ that is parallel to the work gear axis of rotation O_g. Such configuration of the primary motion is illustrated in Figure 12.2. For the reader's convenience, in addition to the rotation vectors $\boldsymbol{\omega}_g$, $\boldsymbol{\omega}_c$, and $\boldsymbol{\omega}_{pl}$, the axodes $\mathscr{A}_g$ and $\mathscr{A}_c$ as well as pitch surfaces $\mathscr{P}_{sg}$ and $\mathscr{P}_{sc}$ of the work gear and of the gear cutting tool, respectively, are shown in Figure 12.2.

A method of shaping a spur gear using the shaper cutter with a tilted axis of rotation is based on the kinematics of machining shown in Figure 12.2. In this method,* the work gear is rotating about its axis of rotation O_g, as shown in Figure 12.3. Vector of rotation $\boldsymbol{\omega}_g$ of the

* To the author's best knowledge, the concept of shaping of spur gears with a shaper cutter having a tilted axis of rotation should be attributed to Prof. Ye.M. Khaimovich of the Kiev Polytechnic Institute (Ukraine). In the 1930s, he was granted a USSR patent on an invention entitled "Gear Shaping Machine." In accordance with the description of this invention, the gear shaping machine featured the spindle of the gear shaper that is tilted at an angle to the work-gear arbor. Reciprocation of the shaper is performed in the direction that is parallel to the axis of rotation of the work gear. Since the time the patent was issued, much research has been carried out on the method of gear machining as well as on the design of the gear shaper cutters.

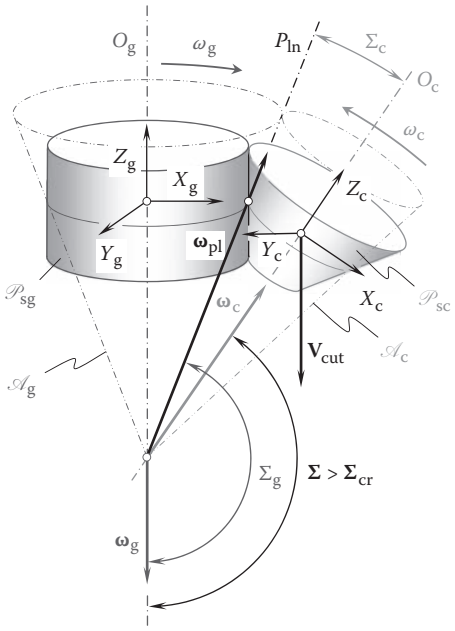

FIGURE 12.2
Straight primary motion $\mathbf{V}_{cut}$ in the kinematics of machining of a spur gear using a gear shaper cutter with a tilted axis of rotation.

work gear is aligned with the gear axis O_g. The gear shaper cutter is rotating about its axis of rotation O_c. The rotation vector $\boldsymbol{\omega}_c$ is aligned with the shaper axis O_c. The shaper cutter axis of rotation O_c is at a certain angle with respect to the axis of rotation O_g of the work gear. This angle is equal to the clearance angle α_o at the top cutting edge of the shaper.

In addition to the rotations $\boldsymbol{\omega}_g$ and $\boldsymbol{\omega}_c$, either the shaper cutter or the work gear reciprocates along the axis of rotation of the work gear. The speed of reciprocation is equal to the speed of the primary motion $\mathbf{V}_{cut}$.

The rake surface R_s of the shaper cutter teeth is shaped in the form of a cone of revolution. The kinematics of the gear machining used in the method of shaping of spur gears

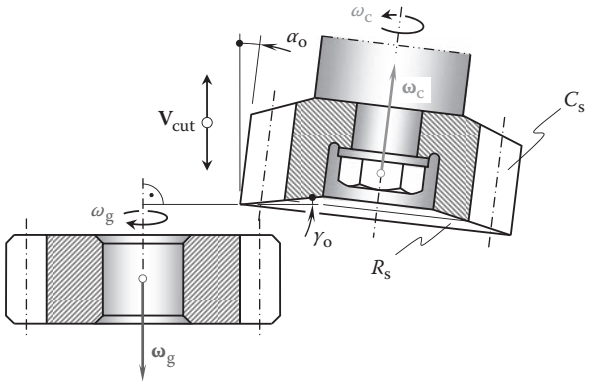

FIGURE 12.3
A method of shaping of spur gears using the shaper cutter with a tilted axis of rotation.

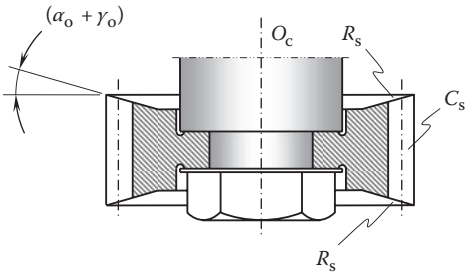

FIGURE 12.4
Design of a shaper cutter having rake surfaces at opposite ends.

(Figure 12.3) makes it possible to implement the clearance surfaces C_s, which are shaped in the form of involute cylinders. Because of this feature, the shaper cutter has two strong advantages over shaper cutters of conventional design. First, the accuracy of the shaper cutter with the tilted axis of rotation does not depend on the number of its regrindings. Second, the shaper cutter can be designed so as to have two rake surfaces R_s, which are located on opposite ends of the shaper cutter (Figure 12.4). This makes it possible to use the rake surface at one face, and after it has been worn out, to use the rake surface of the opposite side of the shaper cutter. This doubles the time interval between two consequent regrindings of the shaper cutter.

12.2 Determination of the Generating Surface of a Gear Shaper Cutter Having a Tilted Axis of Rotation

To determine the generating surface of a gear shaper cutter having a tilted axis of rotation, the kinematic method for the determination of enveloping surfaces can be used.* Three Cartesian reference systems are used for the purpose to derive an equation for the generating surface T of the shaper (Figure 12.5).

A left-hand–oriented coordinate system $X_gY_gZ_g$ that is associated with the gear is the first reference system. The Z_g axis of this coordinate system is aligned with the rotation vector $\boldsymbol{\omega}_g$ of the work gear. The coordinate system $X_gY_gZ_g$ is rotating together with the work gear.

* The kinematic method for the determination of enveloping surfaces was developed by A.V. Shishkov in the late 1940s, whose concept he summarized in a monograph [186]. The method uses the so-called equation of contact $\mathbf{n}_g \cdot \mathbf{V}_\Sigma = 0$, where $\mathbf{n}_g$ is the (unit) vector to the gear tooth flank and $\mathbf{V}_\Sigma$ is the vector of the relative motion of the cutting tool relative to the gear to be machined at the point of their contact. Often, the gear tooth flank is of relatively simple geometry and allows for the determination of the vector $\mathbf{n}_g$ without the necessity of using the derivatives of the position vector of a point with respect to the surface parameters. The kinematics of the relative motion of the gear cutting tool is also often simple, which makes it possible to determine the vector $\mathbf{V}_\Sigma$ without the necessity of using the derivatives of the position vector of a point with respect to the parameter of the relative motion. Ultimately, equations for vectors $\mathbf{n}_g$ and $\mathbf{V}_\Sigma$ can be derived directly from the geometry of the gear tooth flank and from the kinematics of meshing. Because no derivatives are required, this results in a significant simplification when determining an enveloping surface. No advantages can be obtained from the use of the kinematic method if derivatives are used for the computation of the vectors $\mathbf{n}_g$ and $\mathbf{V}_\Sigma$. Under such a scenario, the kinematic method reduces to the conventional method known from the theory of enveloping surfaces.

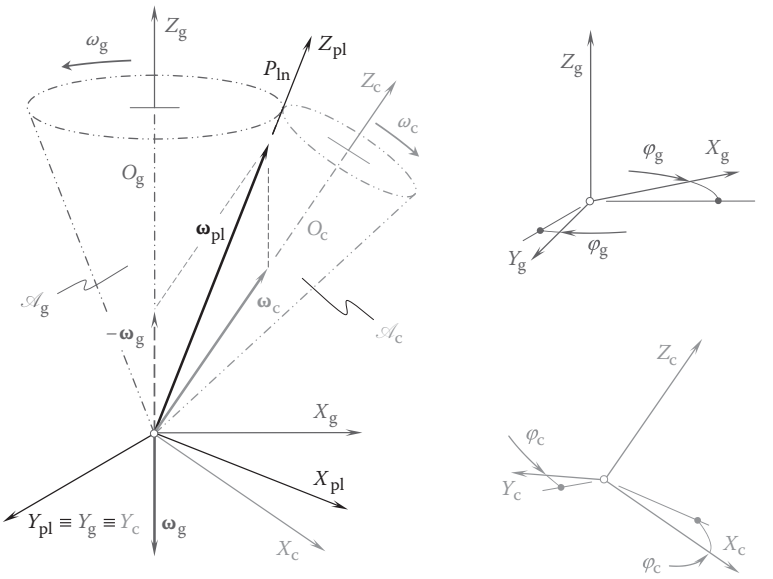

FIGURE 12.5
Reference systems used for the determination of the generating surface of the gear shaper cutter with a tilted axis of rotation.

A left-hand–oriented coordinate system $X_cY_cZ_c$ that is associated with the shaper cutter is the second reference system. The Z_c axis of this coordinate system is aligned with the rotation vector of the gear shaper cutter. The coordinate system $X_cY_cZ_c$ is rotating together with the shaper cutter.

A stationary left-hand–oriented coordinate system $X_{pl}Y_{pl}Z_{pl}$ is the third reference system to be used. The Z_{pl} axis of this coordinate system is aligned with the vector of the instant rotation $\boldsymbol{\omega}_{pl}$.

Origins of the coordinate systems $X_gY_gZ_g$, $X_cY_cZ_c$, and $X_{pl}Y_{pl}Z_{pl}$ are snapped together at the point of intersection of the axes of rotation O_g, O_c, and P_{ln}.

The coordinate axes Z_g, Z_c, and Z_{pl} are within a common plane. Let us assume that initially the axes Y_g, Y_c, and Y_{pl} align with each other as shown in Figure 12.5.

When the coordinate system $X_gY_gZ_g$ is turned about the gear axis O_g through a certain angle φ_g, the coordinate system $X_cY_cZ_c$ is turned about the shaper axis O_c through the corresponding angle φ_c. The ratio of the angles of rotations φ_g and φ_c satisfies the proportion

$$\frac{\varphi_g}{\varphi_c} = \frac{\sin\gamma_c}{\sin\gamma_g} \tag{12.4}$$

The generating surface of the shaper cutter T allows for interpretation in the form of an enveloping surface to successive positions of the gear tooth flank surface $\mathscr{G}$ in the relative motion of the gear and the shaper cutter. To use this concept, the following operators of the coordinate system transformations must be composed for the derivation of the equation for the generating surface T.

First, the operator $\mathbf{Rs}(\mathrm{pl} \mapsto \mathrm{g})$ of the transition from the coordinate system $X_gY_gZ_g$ that is rotating together with the gear to the motionless coordinate system $X_{pl}Y_{pl}Z_{pl}$ is required to be composed. Without going into details of the derivation, an expression for the operator $\mathbf{Rs}(\mathrm{g} \mapsto \mathrm{pl})$ can be represented in matrix form

$$\mathbf{Rs}(\mathrm{g} \mapsto \mathrm{pl}) = \begin{bmatrix} \sin\varphi_g \cos\gamma_g & \cos\varphi_g \cos\gamma_g & -\sin\gamma_g & 0 \\ \cos\varphi_g & -\sin\varphi_g & 0 & 0 \\ \sin\varphi_g \sin\gamma_g & \cos\varphi_g \sin\gamma_g & \cos\gamma_g & 0 \\ 0 & 0 & 0 & 1 \end{bmatrix} \tag{12.5}$$

For the inverse transformation of the operator $\mathbf{Rs}(\mathrm{pl} \mapsto \mathrm{g}) = \mathbf{Rs}^{-1}(\mathrm{g} \mapsto \mathrm{pl})$ can be used.

Similarly, the operator $\mathbf{Rs}(\mathrm{c} \mapsto \mathrm{pl})$ of transition from the coordinate system $X_cY_cZ_c$ that is rotating together with the shaper cutter to the motionless coordinate system $X_{pl}Y_{pl}Z_{pl}$ is also required to be composed. Without going into details of the derivation, an expression for the operator $\mathbf{Rs}(\mathrm{c} \mapsto \mathrm{pl})$ can be represented in matrix form

$$\mathbf{Rs}(\mathrm{c} \mapsto \mathrm{pl}) = \begin{bmatrix} -\sin\varphi_c \cos\gamma_c & \cos\varphi_c \cos\gamma_c & \sin\gamma_c & 0 \\ \cos\varphi_c & \sin\varphi_c & 0 & 0 \\ \sin\varphi_c \sin\gamma_c & -\cos\varphi_c \sin\gamma_c & \cos\gamma_c & 0 \\ 0 & 0 & 0 & 1 \end{bmatrix} \tag{12.6}$$

For the inverse coordinate system transformation, the operator $\mathbf{Rs}(\mathrm{pl} \mapsto \mathrm{c}) = \mathbf{Rs}^{-1}(\mathrm{c} \mapsto \mathrm{pl})$ can be used.

The operators of the coordinate system transformations, $\mathbf{Rs}(\mathrm{g} \mapsto \mathrm{pl})$ and $\mathbf{Rs}(\mathrm{pl} \mapsto \mathrm{c})$, allow for the derivation of an expression

$$\mathbf{Rs}(\mathrm{g} \to \mathrm{c}) = \mathbf{Rs}(\mathrm{pl} \to \mathrm{c}) \cdot \mathbf{Rs}(\mathrm{g} \to \mathrm{pl}) \tag{12.7}$$

for the operator $\mathbf{Rs}(\mathrm{g} \mapsto \mathrm{c})$ of the direct resultant transition from the work gear coordinate system $X_gY_gZ_g$ to the shaper cutter coordinate system $X_cY_cZ_c$. The operator $\mathbf{Rs}(\mathrm{g} \mapsto \mathrm{c})$ yields matrix representation

$$\mathbf{Rs}(\mathrm{g} \to \mathrm{c}) = \begin{bmatrix} \cos\varphi_g \sin\varphi_c + & \cos\varphi_g \cos\varphi_c \cos(\gamma_g + \gamma_c) - & -\cos\varphi_c \sin(\gamma_g + \gamma_c) & 0 \\ +\sin\varphi_g \cos\varphi_c \cos(\gamma_g + \gamma_c) & -\sin\varphi_g \sin\varphi_c & & \\ \cos\varphi_g \cos\varphi_c - & -\sin\varphi_g \cos\varphi_c - & \sin\varphi_c \sin(\gamma_g + \gamma_c) & 0 \\ -\sin\varphi_g \sin\varphi_c \cos(\gamma_g + \gamma_c) & -\cos\varphi_g \sin\varphi_c \cos(\gamma_g + \gamma_c) & & \\ \sin\varphi_g \sin(\gamma_g + \gamma_c) & \cos\varphi_g \sin(\gamma_g + \gamma_c) & \cos(\gamma_g + \gamma_c) & 0 \\ 0 & 0 & 0 & 1 \end{bmatrix} \tag{12.8}$$

Suppose that the gear tooth profile is given analytically in the coordinate plane X_gY_g by the vector equation

$$\mathbf{r}_{g.pr} = \mathbf{r}_{g.pr}(t) \tag{12.9}$$

where t is a parameter of the tooth profile $\mathbf{r}_{g.pr}$.

Equation (12.9) allows for the computation of the unit tangent vector $\mathbf{t}_{g.pr}(t)$

$$\mathbf{T}_{g.pr}(t) = \frac{\partial \mathbf{r}_{g.pr}(t)}{\partial t} \tag{12.10}$$

$$\mathbf{t}_{\text{g.pr}}(t) = \frac{\mathbf{T}_{\text{g.pr}}(t)}{\left|\mathbf{T}_{\text{g.pr}}(t)\right|} \tag{12.11}$$

as well as the unit normal vector $\mathbf{n}_{\text{g.pr}}(t)$

$$\mathbf{N}_{\text{g.pr}}(t) = \frac{\partial \mathbf{r}^2_{\text{g.pr}}(t)}{\partial t^2} \tag{12.12}$$

$$\mathbf{n}_{\text{g.pr}}(t) = \frac{\mathbf{N}_{\text{g.pr}}(t)}{\left|\mathbf{N}_{\text{g.pr}}(t)\right|} \tag{12.13}$$

at a current point of the gear tooth profile.

Equation for the unit normal vector $\mathbf{n}_{\text{g.pr}}$ can be presented in the form

$$\mathbf{n}_{\text{g.pr}} = \mathbf{i} \cdot \sin\vartheta + \mathbf{j} \cdot \cos\vartheta \tag{12.14}$$

where ϑ denotes the angle that the unit tangent vector $\mathbf{t}_{\text{g.pr}}$ makes with the X_{g} axis.

The unit normal vector $\mathbf{n}_{\text{g.pr}}$ can be represented in the stationary reference system $X_{\text{pl}}Y_{\text{pl}}Z_{\text{pl}}$. For this purpose, the operator $\mathbf{Rs}(\text{g} \mapsto \text{pl})$ of the coordinate system transformation is used

$$\mathbf{n}^{\text{pl}}_{\text{g.pr}} = \mathbf{Rs}(\text{g} \mapsto \text{pl}) \cdot \mathbf{n}_{\text{g.pr}} \tag{12.15}$$

In the instant rotation of the work gear relative to the shaper cutter, the linear speed of the rotation can be expressed as

$$\mathbf{V}_{\text{g/c}} = \boldsymbol{\omega}_{\text{pl}} \times \mathbf{r}_{\text{g.pr}} \tag{12.16}$$

Substituting Equations (12.15) and (12.16) into the equation of contact [186] ($\mathbf{n}^{\text{pl}}_{\text{g.pr}} \cdot \mathbf{V}_{\text{g/c}} = 0$), the following equation can be derived for the computation of the angle ϑ

$$\cos(\vartheta + \varphi_{\text{g}}) = 2 \cdot \frac{X\cos\vartheta - Y\sin\vartheta}{d_{\text{g}}} \tag{12.17}$$

Equation (12.17) allows for the selection of points of the gear tooth profile $\mathbf{r}_{\text{g.pr}}$ that make contact with the shaper tooth profile at the given angle of rotation φ_{g}.

Coordinates of points within the tooth profile of the generating surface T of the gear shaper cutter for machining a given gear are determined in the following order:

1. At a point within the tooth profile of the gear to be machined, the unit tangent vector $\mathbf{t}_{\text{g.pr}}$ is computed. This immediately yields the current value of the angle of inclination ϑ of the unit vector $\mathbf{t}_{\text{g.pr}}$.
2. From the equation of contact [see Equation (12.17)], a corresponding rotation angle φ_{g} of the gear can be determined. This angle corresponds to the instant of time when the chosen point within the gear tooth profile makes contact with the shaper tooth profile.

3. Coordinates of the chosen point within the gear tooth profile along with the computed value of the rotation angle φ_g can be used to compute the coordinates of the corresponding point in the shaper tooth profile.

It is practical to approximate a desired tooth profile of the shaper by a smooth regular curve. The approximation of the shaper tooth profile by an involute curve is advantageous because the involute tooth profile is easier for machining. Under such a scenario, the shaper tooth flanks would be identical to the tooth flanks of a corresponding spur gear.

Let us determine an involute profile that is tangent to the shaper tooth profile on the pitch cylinder.

As shown in Figure 12.6a, point m of tangency of the tooth profiles is located on the axode of the work gear. The actual location of point m within the face width of the work gear affects the actual value of the profile shift correction coefficient $\xi_c = x/m$. It is recommended to design the shaper with a zero profile shift coefficient ($\xi_c = 0$). Consequently, point m is located in the middle of the gear face width F_g.

Point m is remote from the axis of rotation of the work gear O_g at a distance $0.5d_g$. The corresponding diameter of the shaper cutter is designated as d_c.

A local reference system xyz is associated with the cutting edge of the shaper cutter. Origin of the coordinate system xyz is at point m. Axes of the coordinate system xyz are parallel to the corresponding axes of the coordinate system $X_gY_gZ_g$ associated with the work gear.

Consider a plane through point m that is tangent to the gear tooth profile. This plane is a projecting plane onto the transverse plane of the work gear and forms a profile angle ϕ_g

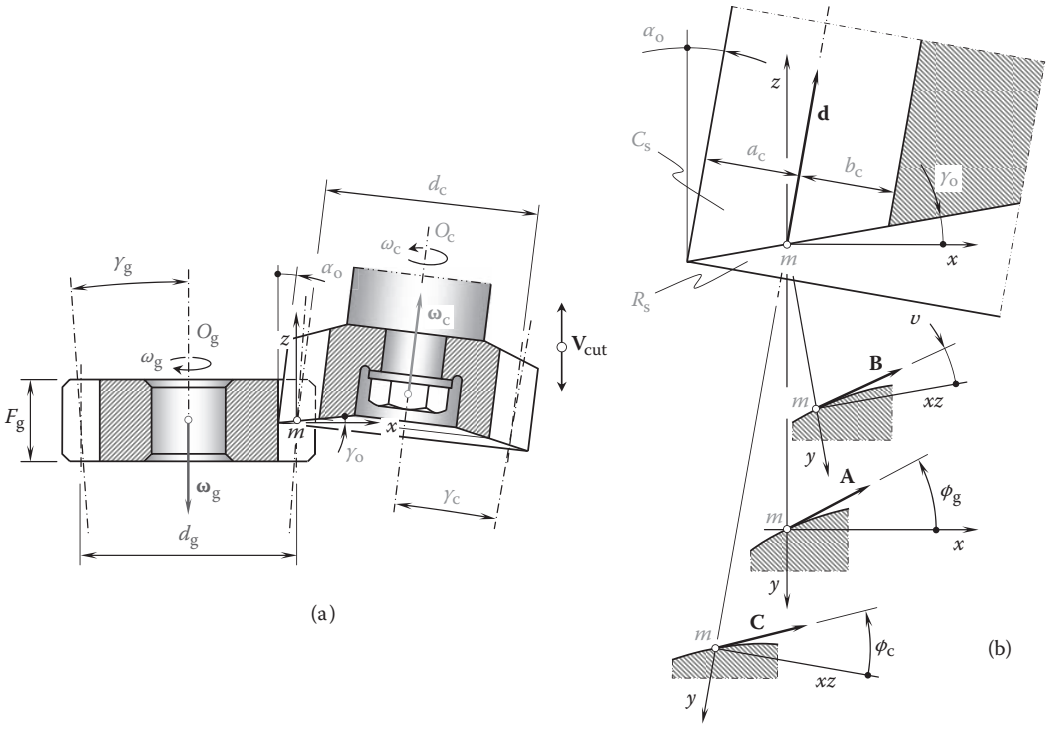

FIGURE 12.6
Determination of an involute profile of the shaper cutter for machining of an involute gear.

with the x axis (Figure 12.6b). The plane is also tangent to the generating surface T of the shaper cutter.

Vector **A** is constructed so that it is tangent to the generating surface T and located within the xy plane. The following expression

$$\mathbf{A} = \mathbf{i} - \mathbf{j} \cdot \tan \phi_g \tag{12.18}$$

is valid for vector **A**.

Vector **B** is tangent to the cutting edge of the shaper cutter. It can be analytically expressed as

$$\mathbf{B} = \mathbf{i} \cdot \cos \gamma_o - \mathbf{j} \cdot \tan \upsilon + \mathbf{k} \cdot \sin \gamma_o \tag{12.19}$$

where υ denotes the angle that the tangent line to the cutting edge makes with the xz plane and **k** is the unit vector along the z axis.

Vectors **A**, **B**, and **k** comprise a set of coplanar vectors, and are within the plane that is tangent to the gear tooth flank surface. Therefore, the triple scalar product of these vectors is identical to zero ($\mathbf{A} \times \mathbf{B} \cdot \mathbf{k} \equiv 0$) and can be represented in the form of a determinant

$$\mathbf{A} \times \mathbf{B} \cdot \mathbf{k} \equiv \begin{vmatrix} 1 & -\tan \phi_g & 0 \\ \cos \gamma_o & -\tan \upsilon & \sin \gamma_o \\ 0 & 0 & 1 \end{vmatrix} = 0 \tag{12.20}$$

A formula for the computation of the angle υ

$$\upsilon = \tan^{-1}(\tan \phi_g \cos \gamma_o) \tag{12.21}$$

immediately follows from Equation (12.12).

Vector **C** is constructed so that it is within the plane that is perpendicular to the shaper cutter axis O_c. For vector **C**, the expression

$$\mathbf{C} = \mathbf{i} \cdot \cos(\gamma_g + \gamma_c) - \mathbf{j} \cdot \tan \phi_c - \mathbf{k} \cdot \sin(\gamma_g + \gamma_c) \tag{12.22}$$

is valid.

Unit vector **d** is along the generating line of the clearance surface C_s of the shaper cutter tooth. Vector **d** can be expressed in terms of its projections onto the axes of the reference system xyz

$$\mathbf{d} = \mathbf{i} \cdot \sin(\gamma_g + \gamma_c) + \mathbf{k} \cdot \cos(\gamma_g + \gamma_c) \tag{12.23}$$

Again, vectors **B**, **C**, and **d** comprise a set of coplanar vectors, and their triple scalar product is identical to zero ($\mathbf{B} \times \mathbf{C} \cdot \mathbf{d} \equiv 0$). This identity allows the expression

$$\mathbf{B} \times \mathbf{C} \cdot \mathbf{d} \equiv \begin{vmatrix} \cos \gamma_o & -\tan \upsilon & \sin \gamma_o \\ \cos(\gamma_g + \gamma_c) & -\tan \phi_c & -\sin(\gamma_g + \gamma_c) \\ \sin(\gamma_g + \gamma_c) & 0 & \cos(\gamma_g + \gamma_c) \end{vmatrix} = 0 \tag{12.24}$$

from which the formula for ϕ_c

$$\phi_c = \tan^{-1}\left(\frac{\tan \upsilon}{\cos(\gamma_o + \gamma_g + \gamma_c)}\right) \tag{12.25}$$

is derived.

Substituting Equation (12.21) into Equation (12.25), the formula

$$\phi_c = \tan^{-1}\left(\frac{\tan \phi_g \cos \gamma_o}{\cos(\gamma_o + \gamma_g + \gamma_c)}\right) \tag{12.26}$$

can be derived for the computation of the shaper cutter profile angle ϕ_c.

The base diameter of the shaper cutter can be computed from the equation

$$d_{b.c} = d_c \cos \phi_c \tag{12.27}$$

Tooth thickness on the pitch diameter d_c of the shaper cutter is equal to space width on the pitch diameter d_g of the gear to be machined. Addendum a_c and dedendum b_c of the shaper tooth are assumed to be equal to each other, and can be computed by using the formula

$$a_c = b_c = 1.25m \cdot \frac{\cos(\gamma_o + \gamma_g + \gamma_c)}{\cos \gamma_o} \tag{12.28}$$

The rest of the design parameters of the shaper cutter with a tilted axis of rotation can be determined in the same way as the corresponding design parameters of conventional shaper cutter.

Shaper cutters having a tilted axis of rotation can also be used for machining of racks as schematically illustrated in Figure 12.7. In this case, the rack is viewed as the work gear having an infinite tooth number. The axis of rotation O_c of the shaper cutter is tilted at the clearance angle α_o relative to the pitch plane of the rack. The direction of reciprocation $\mathbf{V}_{cut}$ is parallel to the pitch plane of the rack.

When the tilt angle is zero, the equations derived for the shaper cutter with a tilted axis of rotation reduce to the case of shaper cutter of conventional design.

Shaper cutters with a tilted axis of rotation are easier in production. This is mostly because the straight generating lines of the cylindrical clearance surface are parallel to the axis of rotation of the shaper cutter. The design of the shaper cutters makes it possible to increase the rake angle γ_o and—more importantly—the clearance angle α_o. The improved cutting

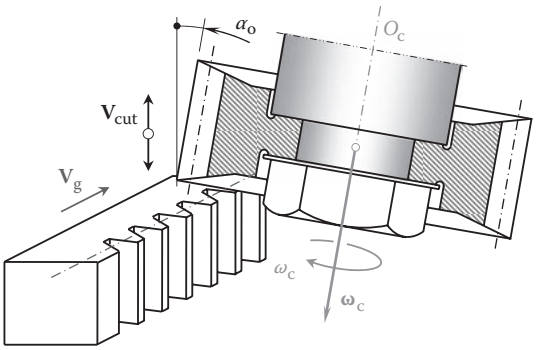

FIGURE 12.7
Shaping of a rack using the shaper cutter having a tilted axis of its rotation.

edge geometry results in a better cutting performance of the shaper cutter. The accuracy of the shaper cutter does not depend on the number of resharpenings and remains the same throughout the tool's life span. If accuracy is a critical issue, it can be improved by implementing a specially designed curved generating profile of the shaper cutter rake surface R_s. However, use of shaper cutters with a tilted axis of rotation requires specially designed gear shaping machines that are capable of handling the tilted axis of the shaper cutter spindle.

12.3 Illustration of Capabilities of the External Intersecting-Axis Gear Machining Mesh

The potential capabilities of the external intersecting-axis gear machining mesh (Figure IV.1a) are not just limited to the discussed gear shaping operation (Figure 12.3). Other combinations of translations and of rotations of the reference system $X_cY_cZ_c$ associated with the gear cutting tool relative to the work gear are feasible. As an example, two more practical methods of gear machining are discussed in the following subjections.

12.3.1 Shaping of Conical Involute Gears

Conical involute gears are used in helicopter transmissions as well as in other applications. More examples of industrial applications of conical involute gears are reported elsewhere (e.g., [9, 42]). Tapered splines are often used in synchronizer and coupler designs to prevent jumping out of gears. A tapered tooth form also compensates for heat treatment distortions and unequal shrinkage [6].

The kinematic scheme shown in Figure 12.8 can be used in designing a gear cutting tool for machining of conical involute gears. The kinematic scheme is composed of two rotations, $\boldsymbol{\omega}_g$ and $\boldsymbol{\omega}_c$. The shaft angle is denoted by Σ. The primary motion (motion of cut $\mathbf{V}_{cut}$) is along the axis of rotation O_c of the shaper cutter.

Conical involute gears (or, a tapered tooth form) can be produced by tilting the axis of the shaper cutter as shown in Figure 12.9 or by tilting the axis of rotation O_g of the work gear. The work gear and the shaper cutter are rotating about their axes of rotation O_g and O_c in a properly timed manner. The direction of the primary motion $\mathbf{V}_{cut}$ is at a certain angle with respect to the gear axis of rotation O_g. This angle is equal to the pitch cone angle of the conical involute gear.

Evidently, the concept of gear machining using the shaper cutter with a tilted axis of rotation (see Figure 12.3) can be enhanced for machining of conical involute gears.

12.3.2 Shaping of Face Gears

Face gear drives are widely used in industry [3]. Examples of their applications can be easily found out in the aerospace industry (helicopter transmissions), in the design of automobile differentials, etc. Shaping is the easiest way to machine teeth of face (crown) gears.

The kinematics of machining of a face gear with the shaper cutter can be composed based on the gear machining mesh shown in Figure IV.1a. Standard shaper cutters can be used in this operation. Either conventional or special gear shaper machines can be used for machining of crown gears. Special attachment is required in the first case to enable the rotations of the work gear and the shaper cutter about the axes, which are intersecting at a right angle.

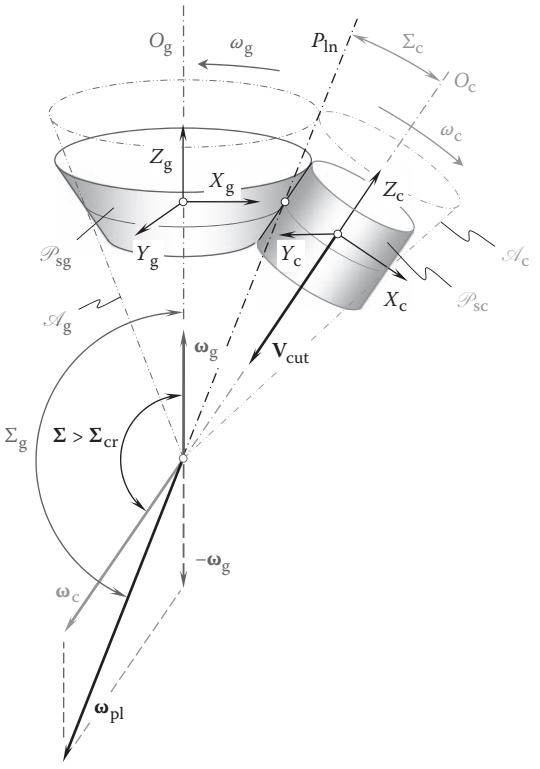

FIGURE 12.8
Kinematics of shaping of a conical involute gear (a tapered tooth form of the gear) using the shaper cutter of conventional design. (Straight primary motion $\mathbf{V}_{cut}$ is along the axis of the shaper.)

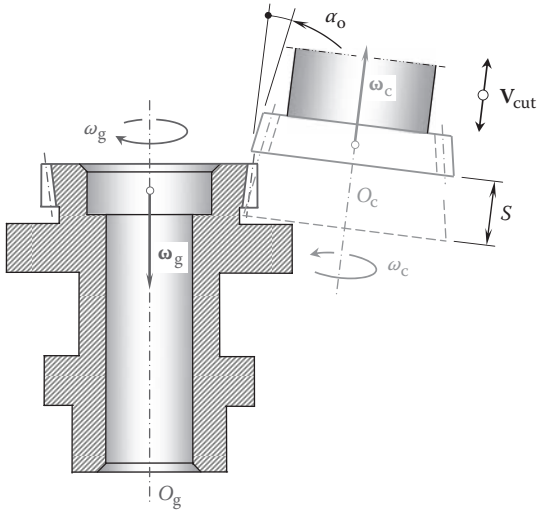

FIGURE 12.9
Shaping of a conical involute gear using a shaper cutter of conventional design.

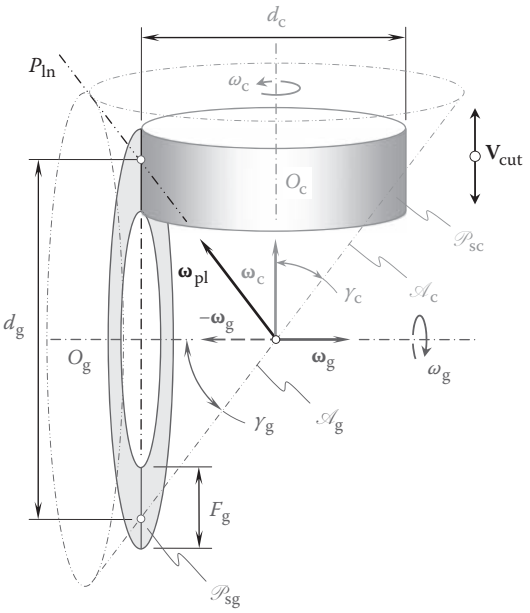

FIGURE 12.10
Straight primary motion (the motion of cut $\mathbf{V}_{cut}$) when shaping a face gear with the standard shaper cutter.

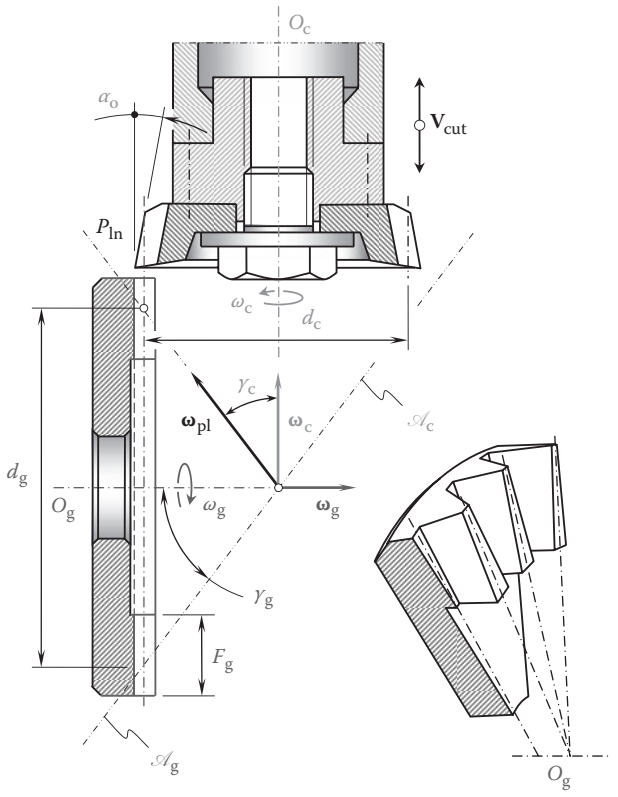

FIGURE 12.11
Shaping of a face gear (a crown gear) using a shaper cutter of conventional design.

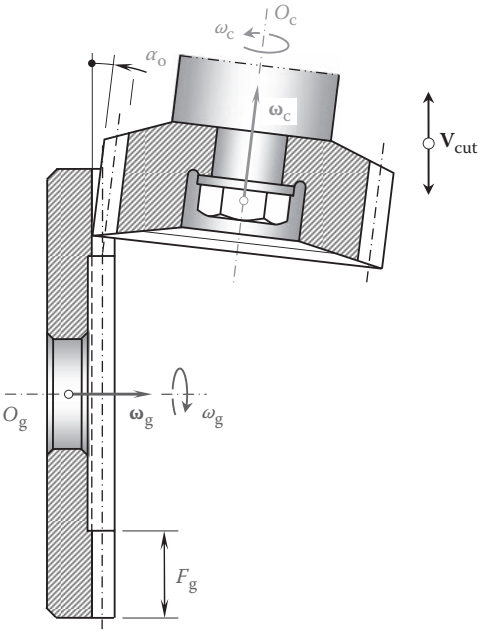

FIGURE 12.12
Shaping of a face gear (a crown gear) using a shaper cutter having a tilted axis of rotation.

Figure 12.10 illustrates the kinematics of shaping a conventional face gear with the standard shaper cutter. When shaping the face gear, the rotation vectors of the work gear $\boldsymbol{\omega}_g$ and the shaper $\boldsymbol{\omega}_c$ are at right angle. In the relative motion, the shaper cutter is performing an instant rotation $\boldsymbol{\omega}_{pl}$ about the axis P_{ln} of the instant rotation.

The direction of the primary motion (of the reciprocation of the shaper cutter $\mathbf{V}_{cut}$) is orthogonal to the face gear axis of rotation O_g. The diameter of the operating pitch circle of the gear is designated as d_g and the corresponding diameter of the operating pitch cylinder of the shaper cutter is denoted by d_c.

When shaping the face gear (Figure 12.11), the work gear and the shaper cutter are rotating about their axes of rotations O_g and O_c, respectively. The rotations ω_g and ω_c are timed so that the relation $\omega_g N_g = \omega_c N_c$ is observed. Here, N_g is the tooth number of the face gear and N_c is the tooth number of the shaper cutter. The shaper cutter is reciprocating in the direction toward the axis O_g of the work gear and back. Proper face gear tooth flank generation is feasible within a reasonable face width F_g. The feasibility of proper tooth generation strongly depends on tooth pointing at the outer diameter of the face gear and on tooth undercutting at the inner diameter of the shaper cutter as shown in Figure 12.11.

The concept of gear shaping using the shaper cutter having a tilted axis of rotation (see Figure 12.3) discussed above can be enhanced for machining of face gears as well. A schematic diagram of this concept is illustrated in Figure 12.12.

To date, the kinematic scheme of gear generation (Figure 12.11) has not been investigated thoroughly. Analysis of the feasibility of other combinations of translations and rotations of the reference system associated with the gear cutting tool with respect to the work gear reference system could reveal novel methods of gear generating as well as new design concepts for gear cutting tools of novel designs. There remains a considerable amount of research to be conducted in this field.

13

Gear Cutting Tools for Machining Bevel Gears

Two rotation vectors—one of which is associated with the work gear and the other with the gear cutting tool—uniquely determine the vector of instant rotation of the gear cutting tool relative to the work gear. The latter makes possible the classification of various types of gear machining meshes (Figure 3.8). The actual configuration of the vector of instant rotation $\boldsymbol{\omega}_{pl}$ depends on the rotation vectors $\boldsymbol{\omega}_g$ and $\boldsymbol{\omega}_c$. The angle $\angle(\boldsymbol{\omega}_g, \boldsymbol{\omega}_c)$ that is measured between the rotation vectors $\boldsymbol{\omega}_g$ and $\boldsymbol{\omega}_c$ along with magnitudes ω_g and ω_c of the vectors $\boldsymbol{\omega}_g$ and $\boldsymbol{\omega}_c$ uniquely determine the angles $\angle(\boldsymbol{\omega}_{pl}, \boldsymbol{\omega}_g)$ and $\angle(\boldsymbol{\omega}_{pl}, \boldsymbol{\omega}_c)$, which the rotation vectors $\boldsymbol{\omega}_g$ and $\boldsymbol{\omega}_c$ form with the vector of instant rotation $\boldsymbol{\omega}_{pl}$.

Depending on the rotation vectors $\boldsymbol{\omega}_g$ and $\boldsymbol{\omega}_c$, each of the angles $\angle(\boldsymbol{\omega}_{pl}, \boldsymbol{\omega}_g)$ and $\angle(\boldsymbol{\omega}_{pl}, \boldsymbol{\omega}_c)$ can either be obtuse or acute. In a particular case, one of these angles is equal to a right angle (either $\angle(\boldsymbol{\omega}_{pl}, \boldsymbol{\omega}_g) = 90°$ or $\angle(\boldsymbol{\omega}_{pl}, \boldsymbol{\omega}_c) = 90°$).

The first case ($\boldsymbol{\omega}_{pl} \perp \boldsymbol{\omega}_g$) relates to the intersecting-axis gear machining mesh, whose vector diagram is shown in Figure IV.1e. Additional details of this gear machining mesh are shown in Figure 13.1. Here, in addition to the vector diagram (Figure 13.1a), axodes of the work gear $\mathscr{A}_g$ and the gear cutting tool $\mathscr{A}_c$ are also depicted (Figure 13.1b). To date, this type of gear machining mesh has not been thoroughly investigated. To fully utilize its potential in the industry, an extensive investigation of its capabilities must be carried out. Because of the limited amount of available research results, it will not be discussed further in this work.

The second case ($\boldsymbol{\omega}_{pl} \perp \boldsymbol{\omega}_c$) relates to the intersecting-axis gear machining mesh, whose vector diagram is shown in Figure IV.1d. Additional details of this gear machining mesh are illustrated in Figure 13.2. Here, in addition to the vector diagram (Figure 13.2a), axodes of the work gear $\mathscr{A}_g$ and the gear cutting tool $\mathscr{A}_c$ are also depicted (Figure 13.2b). This type of gear machining mesh is extensively used in industry. Numerous gear cutting tool designs as well gear machining methods are developed based on the gear machining mesh schematically shown in Figure 13.2. The analysis performed in this chapter is focused on the application of the intersecting-axis gear machining mesh, for which the condition ($\boldsymbol{\omega}_{pl} \perp \boldsymbol{\omega}_c$) is observed. Gear cutting tools of various designs for machining bevel gears can be designed based on gear machining mesh of this type. However, capabilities of the gear machining mesh (Figure 13.2) are not limited to the design of gear cutting tools for cutting bevel gears; gear cutting tools for other types of machining gears can also be designed on the premise of this gear machining mesh.

13.1 Principal Elements of the Kinematics of Bevel Gear Generation

For generation of a bevel gear, an intersecting-axis gear machining mesh is used (Figure 13.2). The rotation vectors $\boldsymbol{\omega}_g$ and $\boldsymbol{\omega}_c$ are along the corresponding axes of rotations O_g and O_c. The rotation vectors $\boldsymbol{\omega}_g$ and $\boldsymbol{\omega}_c$ are at a certain shaft angle Σ relative to each

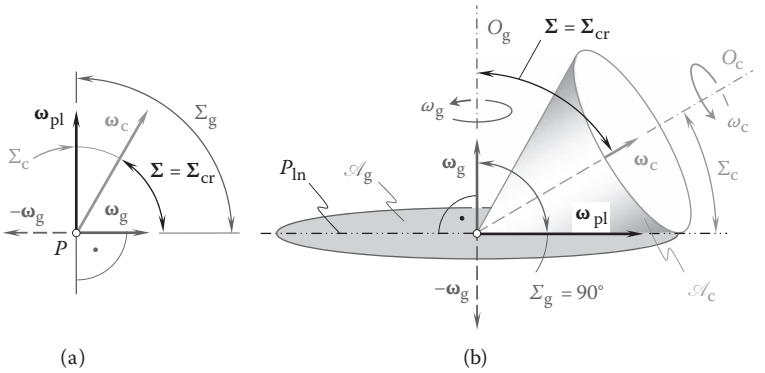

FIGURE 13.1
Vector representation of the intersecting-axis gear machining mesh for machining a round rack.

other. For this particular case, the shaft angle Σ is equal to its critical value Σ_{cr}, that is, the equality $\Sigma = \Sigma_{cr}$ is observed. This occurs because the condition $\boldsymbol{\omega}_{pl} \perp \boldsymbol{\omega}_c$ is observed. By definition, the critical value of the shaft angle Σ_{cr} is that for which the rotation vector of the gear cutting tool $\boldsymbol{\omega}_c$ is perpendicular to the vector of instant rotation $\boldsymbol{\omega}_{pl}$.

For readers who prefer to visualize the gear machining mesh, two axodes* can be associated with the rotation vectors $\boldsymbol{\omega}_g$ and $\boldsymbol{\omega}_c$. The axode $\mathscr{A}_g$ is associated with the rotation vector $\boldsymbol{\omega}_g$, whereas the axode $\mathscr{A}_c$ is associated with the rotation vector $\boldsymbol{\omega}_c$. Generally speaking, both axodes are shaped in the form of two cones of revolution.

Parameters of the axodes $\mathscr{A}_g$ and $\mathscr{A}_c$ can be specified in terms of the pitch angles γ_g and γ_c. In the case under consideration, the pitch angle $\gamma_c = \pi/2$. This means that the axode of the gear cutting tool is transformed into plane $\mathscr{A}_c$ that is rotating about the axis O_c. The axis of rotation O_c is perpendicular to the plane $\mathscr{A}_c$. An advantage of the planar axode $\mathscr{A}_c$ is used when designing a gear cutting tool for machining bevel gears, that is, those bevel gears having (a) straight teeth, (b) skew teeth, or (c) circular arc teeth, etc.

When the shaft angle Σ is given, for the computation of the pitch angle γ_g of the axode of the work gear, the formula $\gamma_g = \pi/2 - \Sigma$ can be used.

To compute for the pitch angle γ_g, the following formula

$$\gamma_g = \sin^{-1}\left(\frac{\omega_c}{\omega_g}\right) \tag{13.1}$$

can be used.

The formula for pitch angle γ_g can be expressed in terms of tooth numbers of the work gear (N_g) and of the generating surface of the gear cutting tool (N_c)

$$\gamma_g = \sin^{-1}\left(\frac{N_g}{N_c}\right) \tag{13.2}$$

Pitch line P_{ln} is aligned with the vector $\boldsymbol{\omega}_{pl}$ of the instant rotation of axodes $\mathscr{A}_g$ and $\mathscr{A}_c$.

* The axodes themselves are not the main focus in this book. Any and all results here can be derived without applying the concept of axodes. In some illustrations, the axodes are shown only for readers who have special preferences.

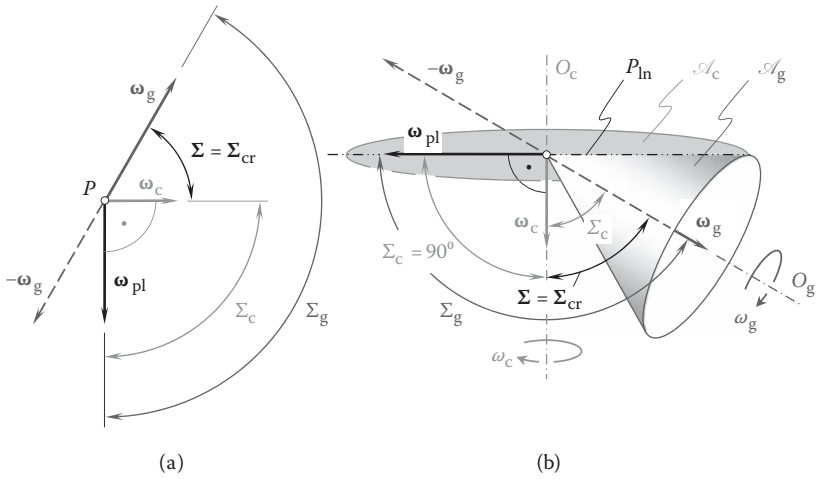

FIGURE 13.2
Vector representation of the rack-type intersecting-axis gear machining mesh.

When machining a work gear with the gear cutting tool that is designed in compliance with the gear machining mesh (Figure 13.2), cone $\mathscr{A}_g$ is rolling over plane $\mathscr{A}_c$ with no sliding between them. The relative motion of axode $\mathscr{A}_c$ of the gear cutter with respect to axode $\mathscr{A}_g$ of the work gear allows for interpretation in the form of instant rotation $\boldsymbol{\omega}_{pl}$ about the pitch line P_{ln}.

The generating action of the gear cutting tool is the result of the two rotations, $\boldsymbol{\omega}_g$ and $\boldsymbol{\omega}_c$. The rotations are synchronized with each other in a timely manner. To make the material removal possible, the corresponding primary motion (motion of cut) is required when machining the gear. A plurality of solutions is available when determining the primary motion. Any and all feasible motions of a reference system $X_cY_cZ_c$ associated with the gear cutting tool relative to the coordinate system $X_gY_gZ_g$ associated with the work gear are considered when selecting an appropriate motion of cut. When performing the analysis, one should bear in mind the restrictions imposed by the rolling motion of the axodes onto the feasible relative motion of the work gear and the gear cutting tool.

When no restrictions are imposed, the relative motion of the coordinate system $X_cY_cZ_c$ of the gear cutting tool can be reduced to not more then three elementary translations ($\mathbf{V}_x$, $\mathbf{V}_y$, and $\mathbf{V}_z$) along the coordinate axes, and not more then three elementary rotations ($\boldsymbol{\omega}_x$, $\boldsymbol{\omega}_y$, and $\boldsymbol{\omega}_z$) about the coordinate axis of the reference system $X_cY_cZ_c$.

Consider all six possible elementary motions and all of their possible combinations by 1, 2, … , 6. Various ratios of speed of the elementary motions need to be accounted for. Not all relative motions and their combinations are feasible when machining a given gear. Motions that are not feasible for implementation in cutting gears should be omitted from further analysis. In this way, all feasible motion(s) of cut can be determined.

13.2 Geometry of Interacting Tooth Surfaces

The gear machining mesh that is schematically depicted in Figure 13.2 is used in industry for the design of gear cutting tools used for machining of straight bevel gears as well as

bevel gears having skew teeth. Gear cutting tools used in these machining processes and gear machining methods are good illustrations of the classification of possible types of gear machining meshes (Figure 3.8).

To design a cutting tool for machining of a given bevel gear, a comprehensive analysis of the geometry of the tooth flank of the work gear should be carried out.

13.2.1 Principal Elements of the Geometry of the Involute Straight Bevel Gear Tooth Flank

Figure 13.3 illustrates the shape of a straight tooth of a bevel gear. Major design parameters of the bevel gear are also indicated in the figure. Generally speaking, tooth flank $\mathcal{G}$ of a straight bevel gear is shaped in the form of a conical surface. The apex of the cone surface coincides with the pitch cone apex. The tooth profile serves as the directing line of the conical surface $\mathcal{G}$. This means that the tooth flank can be interpreted as a locus of straight lines through a point of the tooth profile and the pitch cone apex. Therefore, the straight bevel gear tooth flank $\mathcal{G}$ is a type of developable surface.

The straight bevel gear tooth flank can be analytically described by Equation (1.27)

$$\mathbf{r}_g(U_g, \varphi_g) = \begin{bmatrix} U_g \tan\theta_g \sin\varphi_g - \varphi_g U_g \tan\theta_g \cos\varphi_g \\ U_g \tan\theta_g \cos\varphi_g + \varphi_g U_g \tan\theta_g \sin\varphi_g \\ -U_g \\ 1 \end{bmatrix} \tag{13.3}$$

The generating surface of a gear cutting tool is conjugate to the bevel gear tooth flank given by Equation (13.3).

The geometry and generation of the straight bevel gear tooth flank were more extensively investigated by Kolchin [29]. It has been shown that the tooth flank $\mathcal{G}$ of a straight bevel gear is a surface of complex geometry. This surface significantly differs from that of a spur gear. The profile of a straight bevel gear tooth can be constructed on a sphere having a

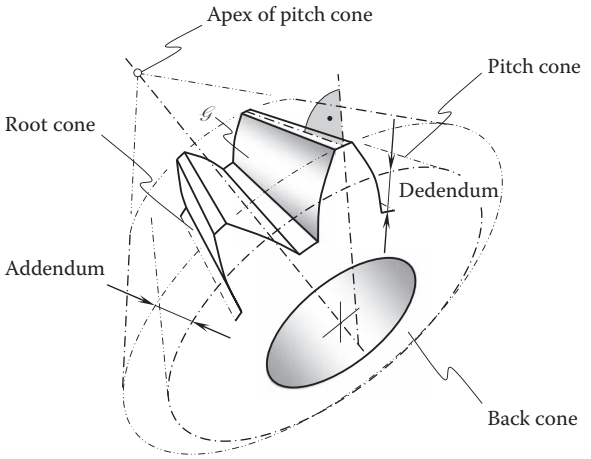

FIGURE 13.3
Geometry of the tooth flank and the major design parameters of a straight bevel gear.

center coincident with the apex of the pitch cone of the bevel gear. The actual tooth profile of a straight tooth bevel gear is commonly referred to as the *octoidal profile*.

13.2.2 Generating Surface of the Gear Cutting Tool

In the gear machining mesh (Figure 13.2), the axis of rotation O_c of the generating surface of a cutter is perpendicular to the vector of instant rotation $\boldsymbol{\omega}_{pl}$. The generating straight line of the cutting tool axode $\mathscr{A}_c$ is aligned to the vector $\boldsymbol{\omega}_{pl}$. In the case under consideration, the generating surface T of a gear cutting tool can be viewed as a surface of a straight bevel gear having a pitch cone angle $\gamma_c = 90°$.

The geometry of an involute straight bevel gear having pitch cone angle $\gamma_c = 90°$ has been investigated earlier by Kolchin [29] as well as by other researchers. A bevel gear of this geometry is often referred to as *round rack*. Tooth flanks of the round rack (of the crown gear, in other terms) have an octoidal profile (Figure 13.4). A tooth profile of this type is often viewed as an involute curve constructed on a sphere of the corresponding diameter. The tooth profile features a point of inflection that is located within the axode $\mathscr{A}_c$.

A bevel round involute rack with a tooth form (shown in Figure 13.4) can be engaged in proper mesh with the straight bevel involute gear to be machined as shown in Figure 13.5. Potentially, a round rack of such design can be used as the generating surface of the gear cutting tool for machining of bevel involute gears. However, use of the bevel round involute rack for this purpose is inconvenient. First, although proportions remain the same, dimensions of the tooth profile of the round rack reduce toward the axis of rotation of the rack. The cutting edge of the gear cutting tool is not capable of changing its shape in response to the change in the dimensions of the round rack tooth profile. Second, in order to avoid interference of the cutting edge beneath the bottom land of the bevel gear, the direction of the primary motion $\mathbf{V}_{cut}$ of the cutting tool has to be pointed at the dedendum

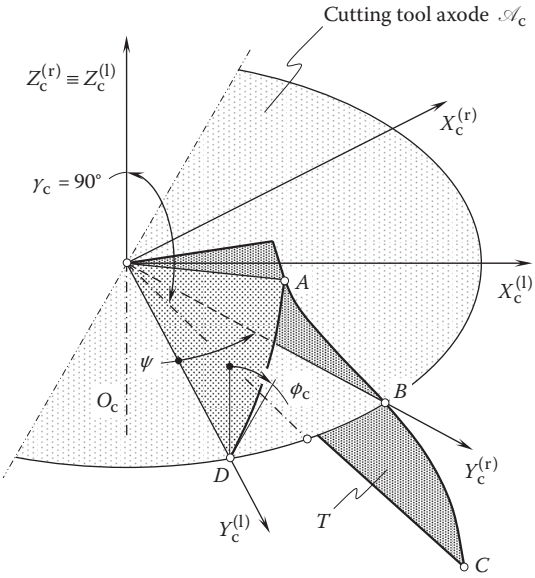

FIGURE 13.4
Generating surface T of a gear cutting tool for machining a straight involute (octoidal) bevel gear tooth form.

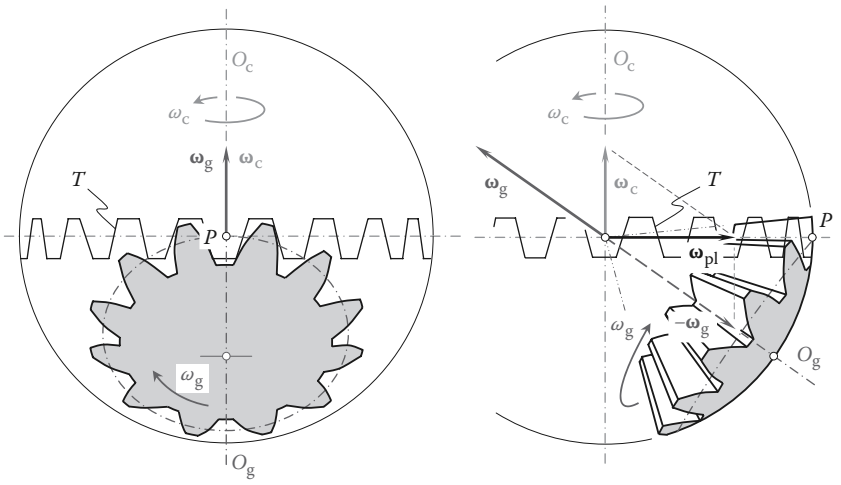

FIGURE 13.5
A bevel gear to be machined in mesh with the bevel round involute rack.

angle γ_b relative to the vector of instant rotation $\boldsymbol{\omega}_{pl}$ (Figure 13.6). Under such a scenario, the rotation vector of the cutting tool $\boldsymbol{\omega}_c$ is perpendicular to the vector of instant rotation $\boldsymbol{\omega}_{pl}$, whereas the vector of the primary motion $\mathbf{V}_{cut}$ is not orthogonal to the rotation vector of the gear cutting tool $\boldsymbol{\omega}_c$.

Fortunately, the curvature of the tooth profile above and below axode $\mathscr{A}_c$ is small enough. Figure 13.7 provides an insight on the actual shape of the spherical mapping of the round rack having a mean cone distance A_m = 200 mm. This makes it possible to substitute the curved cutting edge with a straight one. The approximation of the curved cutting edge with the straight one could be reasonable in many practical cases of bevel gear design and manufacture. The straight cutting edge does not need to change its shape when the cutting tool moves toward the axis of rotation of the cutting tool. This is an important advantage of the approximation.

Moreover, in most practical cases of bevel gear design and manufacture, the actual value of the dedendum angle γ_b is small compared to the pitch cone angle. Because of that the

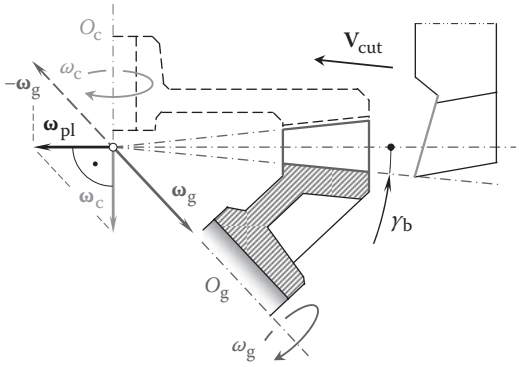

FIGURE 13.6
The desired direction of the primary motion $\mathbf{V}_{cut}$ is not perpendicular to the rotation vector $\boldsymbol{\omega}_c$.

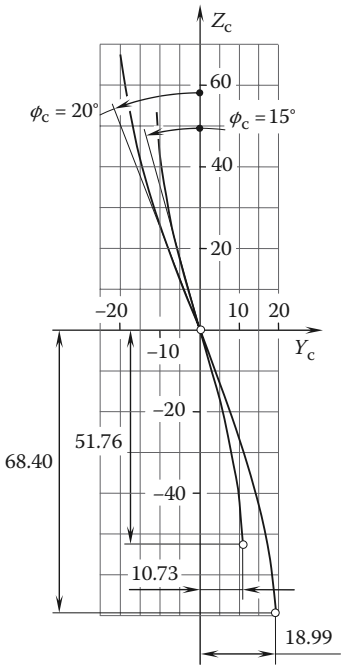

FIGURE 13.7
Spherical mapping of tooth profiles of the bevel round involute rack.

direction of the primary motion $\mathbf{V}_{cut}$ is practically pointed along the vector of instant rotation $\boldsymbol{\omega}_{pl}$ as shown in Figure 13.8. As a result, the rotation vector $\boldsymbol{\omega}_c$ of the gear cutting tool is not perpendicular to the vector of instant rotation $\boldsymbol{\omega}_{pl}$. Under such a condition, the pitch surface of the round rack is no longer a plane. It reverts to a cone having the cone angle γ_c, whose magnitude is close to right angle ($\gamma_c \approx 90°$). This particular design of the round rack is referred to as the planar top land (PTL) rack. PTL rack is a type of practical approximation to the desired bevel round involute rack.

Two simplifications—(1) approximation of the curved cutting edge of the gear cutting tool with straight cutting edge and (2) substitution of the bevel round involute rack with

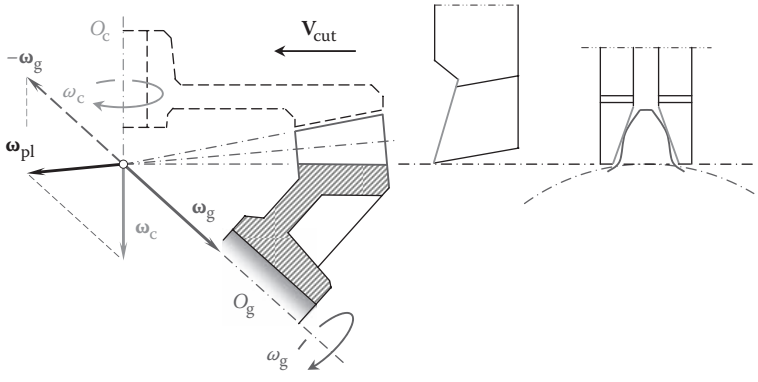

FIGURE 13.8
The actual direction of the primary motion $\mathbf{V}_{cut}$ is perpendicular to the rotation vector $\boldsymbol{\omega}_c$.

the PTL rack—affect the accuracy of the machined bevel gears. However, in most practical cases of bevel gear machining both simplifications are reasonable and allowable.

Tooth flanks of the PTL rack are not conjugate to the bevel involute gear tooth flanks $\mathcal{G}$. Therefore, the PTL rack can be considered as a type of approximation T_a of the desired generating surface T of the cutting tool. Thus, straight bevel gears—and not the desired bevel involute gears—can be generated with the surface T_a. In reality, the generated straight bevel gear is a type of approximation of the desired bevel involute gear.

Generation of straight bevel gear teeth illustrates a perfect example when the generating surface T is not the enveloping surface to successive positions of the desired bevel involute gear tooth flanks, which is given by the blueprint. Instead, the approximate generating surface T_a is considered the given surface. For such a case, the straight bevel gear tooth flank $\mathcal{G}_a$ can be interpreted as an approximation of the desired tooth flank $\mathcal{G}$.

Under such a scenario, an equation for the approximate generating surface of the gear cutting tool is derived not in the same way as it has often been done above. Tooth flanks of the approximate generating surface T_a (namely, of the PTL rack) are shaped in the form of planes through the apex of the pitch cone of the rack, and they form the profile angle ϕ_c with the rotation vector $\boldsymbol{\omega}_c$ of the cutting tool. This makes it possible to derive an equation for the surface T_a of the desired bevel involute gear $\mathcal{G}$ independently of Equation (13.3). To derive the equation of the approximate generating surface T_a, only the design parameters of the bevel gear to be machined are used as input parameters.

Figure 13.9 shows a Cartesian coordinate system $X_cY_cZ_c$ with which the gear cutting tool will be associated after it has been designed. In the coordinate system $X_cY_cZ_c$, a plane T_a^* is the plane through the X_c axis. The plane T_a^* is at the profile angle ϕ_c with respect to the Z_c axis. This immediately yields an equation

$$\mathbf{r}_{ta}^* = \begin{bmatrix} X_c \\ -Y_c \\ Y_c \cot\phi_c \\ 1 \end{bmatrix} \tag{13.4}$$

for the position vector $\mathbf{r}_{ta}^*$ of a point of the plane T_a^*.

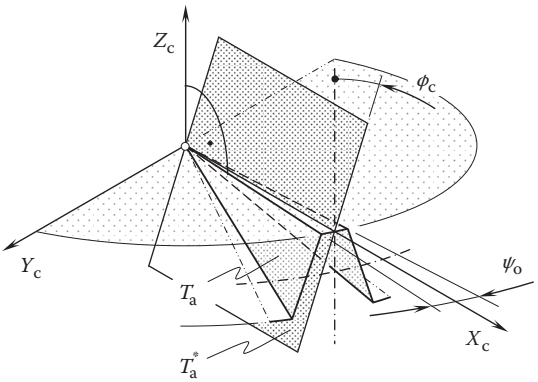

FIGURE 13.9
Determination of the configuration of the lateral tooth flank of the PTL rack.

Let us turn the plane T_a^* about the Z_c axis through the angle $0.5\psi_o$. Here, ψ_o denotes the angle over which the top land of the generating surface T_a spans (Figure 13.9). After it has been turned, the plane T_a^* occupies the position of the lateral plane of the generating surface T_a of the gear cutting tool. Therefore, the equation for the position vector $\mathbf{r}_{ta}$ of a point of the lateral plane T_a can take the form

$$\mathbf{r}_{ta} = \mathbf{Rt}(0.5\psi_o, Z_c) \cdot \mathbf{r}_{ta}^* \tag{13.5}$$

It is important to stress here that the plane T_a is a plane through the apex of the PTL rack.

Similarly, an equation for the opposite tooth flank of the PTL rack can be composed. The opposite tooth flank is also a plane through the apex of the PTL rack.

13.2.3 Geometry of Tooth Flanks of the Generated Gear

An analytical description for the generated tooth flank $\mathscr{G}_a$ of the straight bevel gear can be derived using the kinematic method of generation of enveloping surfaces. For this purpose, it is necessary (1) to represent the lateral plane T_a in its current location and orientation in the reference system $X_gY_gZ_g$ associated with the work gear and (2) to find out in the coordinate system $X_gY_gZ_g$ the loci of lines of contact of the known plane T_a with the straight bevel gear tooth flank $\mathscr{G}_a$ to be determined.

Figure 13.10 illustrates the way the coordinate systems $X_gY_gZ_g$ and $X_cY_cZ_c$ are embedded to the work gear and gear cutting tool, respectively. For convenience, origins of booth reference systems are snapped together at the apex of the pitch cone of the work gear and of the gear cutting tool. The selected configuration of the reference systems makes it easier to compose the operator $\mathbf{Rs}(c \mapsto g)$ of the resultant coordinate system transformation, namely, the transition from the cutting tool coordinate system $X_cY_cZ_c$ to the coordinate system $X_gY_gZ_g$ of the straight bevel gear. The operator $\mathbf{Rs}(c \mapsto g)$ is equal to the product of the corresponding operators of elementary transformations discussed in Chapter 4.

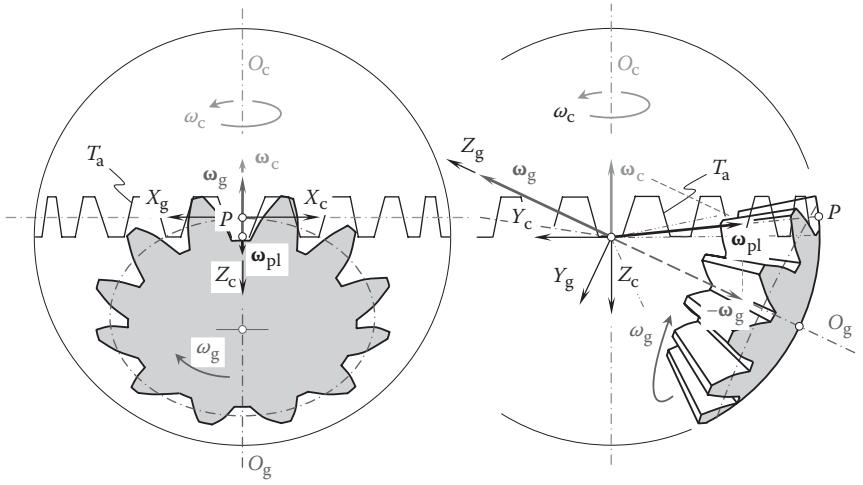

FIGURE 13.10
Determination of the generated tooth flank $\mathscr{G}_a$ of the straight bevel gear.

The current location and orientation of the lateral plane T_a in the reference system $X_gY_gZ_g$ can be analytically expressed in terms of the position vector $\mathbf{r}_{ta}$ of a point of the lateral plane T_a [see Equation (13.5)] and the operator of coordinate system transformation $\mathbf{Rs}(c \mapsto g)$. For position vector of a point $\mathbf{r}_{ta}^{(g)}$ of the lateral plane T_a in the reference system $X_gY_gZ_g$, the following expression

$$\mathbf{r}_{ta}^{(g)}(\varphi_g) = \mathbf{Rs}(c \mapsto g) \cdot \mathbf{r}_{ta} \tag{13.6}$$

is valid.

It should be stressed here that position vector $\mathbf{r}_{ta}^{(g)}$ is a function of the angle of rotation φ_g of the gear. This is because the operator of the resultant coordinate system transformation $\mathbf{Rs}(c \mapsto g)$ depends on the current value of the angle φ_g.

Next, it is necessary to compose the equation of contact for the plane T_a in its motion relative to the reference system $X_gY_gZ_g$. The equation can be represented in the form of dot product [186]

$$\mathbf{n}_{ta}^{(g)} \cdot \mathbf{v}_{c/g}^{(g)} = 0 \tag{13.7}$$

where $\mathbf{n}_{ta}^{(g)}$ designates the unit normal vector to the lateral plane T_a and $\mathbf{v}_{c/g}^{(g)}$ is the vector of the relative motion of the plane T_a. Note that both vectors have to be represented in the common coordinate system $X_gY_gZ_g$.

Equation (13.4) yields

$$\mathbf{n}_{ta} = \frac{Y_c}{\cos\phi_c} \cdot \mathbf{Rt}(0.5\psi_o, Z_c) \cdot \begin{bmatrix} X_c \\ Y_c \\ Y_c \tan\phi_c \\ 1 \end{bmatrix} \tag{13.8}$$

for the unit normal vector $\mathbf{n}_{ta}$ to the lateral plane T_a in $X_cY_cZ_c$. Next, the unit normal vector $\mathbf{n}_{ta}^{(g)}$ can be computed as

$$\mathbf{n}_{ta}^{(g)}(\varphi_g) = \mathbf{Rs}(c \mapsto g) \cdot \mathbf{n}_{ta} \tag{13.9}$$

It is convenient to compose an expression for the vector $\mathbf{v}_{c/g}^{(g)}$ of relative motion of the plane T_a using, for this purpose, vector $\mathbf{v}_{c/g}$ of the linear speed of the plane T_a in $X_cY_cZ_c$.

In the case under consideration, vector $\boldsymbol{\omega}_c$ is the rotation vector of the plane T_a. This immediately yields the formula

$$\mathbf{v}_{c/g} = \boldsymbol{\omega}_c \times \mathbf{r}_{ta} \tag{13.10}$$

for the computation of $\mathbf{v}_{c/g}$.

In this equation, position vector $\mathbf{r}_{ta}$ is given by Equation (13.5). The rotation vector $\boldsymbol{\omega}_c$ is equal to the product

$$\boldsymbol{\omega}_c = \omega_c \cdot \mathbf{k}_c \tag{13.11}$$

where ω_c is the magnitude of the rotation and $\mathbf{k}_c$ is the unit vector along the Z_c axis.

Vector $\mathbf{v}_{c/g}^{(g)}$ of the relative motion of the plane T_a can be expressed in terms of the vector $\mathbf{v}_{c/g}$ and the operator $\mathbf{Rs}(c \mapsto g)$ of the resultant coordinate system transformation

$$\mathbf{v}_{c/g}^{(g)}(\varphi_g) = \mathbf{Rs}(c \mapsto g) \cdot \mathbf{v}_{c/g} \tag{13.12}$$

Substitution of vectors $\mathbf{n}_{ta}^{(g)}$ and $\mathbf{v}_{c/g}^{(g)}$ into Equation (13.7) yields the equation of contact in the form

$$\mathbf{n}_{ta}^{(g)}(\varphi_g) \cdot \mathbf{v}_{c/g}^{(g)}(\varphi_g) = 0 \tag{13.13}$$

Furthermore, we are required to solve the last equation [Equation (13.13)] with respect to angle of rotation φ_g. The expression for φ_g derived in this manner is then substituted into Equation (13.6), which makes it possible to eliminate the angle φ_g from the expression for position vector $\mathbf{r}_{ta}^{(g)}(\varphi_g)$. Position vector $\mathbf{r}_{ta}^{(g)}$ is no longer dependent on the angle φ_g, and in its current form it describes points of the tooth flank $\mathcal{G}_a$ of the generated straight bevel gear.

The generated tooth flank $\mathcal{G}_a$ of the straight bevel gear deviates from the corresponding tooth flank $\mathcal{G}$ of the involute straight bevel gear. At a current point i of the tooth flank $\mathcal{G}$, the deviation δ_i of surface $\mathcal{G}_a$ from surface $\mathcal{G}$ is measured along the perpendicular to the tooth flank $\mathcal{G}$. The deviation δ_i can be expressed in terms of the parameters of the geometry of the tooth flanks $\mathcal{G}$ and $\mathcal{G}_a$.

The position vector of a point within the tooth flank $\mathcal{G}$ of the gear is designated as $\mathbf{r}_g^{(i)}$ [see Equation (13.3)]. The unit normal vector $\mathbf{n}_g^{(i)}$ to the tooth flank $\mathcal{G}$ at point i can be computed on the premise of Equation (13.3)

$$\mathbf{N}_g(U_g, \varphi_g)\Big|_i = \frac{\partial \mathbf{r}_g}{\partial U_g} \times \frac{\partial \mathbf{r}_g}{\partial \varphi_g}\Bigg|_i \tag{13.14}$$

$$\mathbf{n}_g(U_g, \varphi_g)\Big|_i = \frac{\mathbf{N}_g(U_g, \varphi_g)}{\left|\mathbf{N}_g(U_g, \varphi_g)\right|}\Bigg|_i \tag{13.15}$$

The straight line along the unit normal vector $\mathbf{n}_g^{(i)}$ intersects the tooth flank $\mathcal{G}_a$ of the straight bevel gear at a point whose position vector is denoted by $\mathbf{r}_{ga}^{(i)}$. The deviation δ_i can be expressed in terms of vectors $\mathbf{r}_g^{(i)}$ and $\mathbf{r}_{ga}^{(i)}$. For this purpose, the formula

$$\delta_i = \left| \mathbf{r}_{ga}^{(i)} - \mathbf{r}_g^{(i)} \right| \tag{13.16}$$

can be used.

At some point i within the tooth flank $\mathcal{G}$, the deviation δ_i reaches its maximum value δ_{max}. The deviation δ_{max} determined in this manner is equal to the maximal deviation of the tooth flank surface $\mathcal{G}_a$ from the tooth flank surface $\mathcal{G}$.

13.3 Peculiarities of Generation of Straight Bevel Gears with Offset Teeth

Bevel gears can be designed not just with straight teeth, but with helical teeth as well (Figure 1.15). Bevel gears of this type are also referred to as bevel gears with offset teeth (and also bevel gears with skew teeth).

13.3.1 Generating Surface of the Gear Cutting Tool

As has been shown above, the following expression [see Equation (1.33)]

$$\mathbf{r}_g(U_g, \varphi_g) = \begin{bmatrix} (\sin\varphi_g - 2\varphi_g \tan\psi_{b.g} \sin\theta_g \sin\varphi_g)U_g \tan\theta_g \\ [\cos\varphi_g + 2\varphi_g \sin\varphi_g - \tan\psi_{b.g} \sin\theta_g \cos\varphi_g(\tan\theta_g - \varphi_g)]U_g \tan\theta_g \\ -U_g \\ 1 \end{bmatrix} \tag{13.17}$$

is valid for the position vector $\mathbf{r}_g$ of a point of tooth flank $\mathcal{G}$ of a helical bevel gear.

Equation (13.17) allows for the computation of all principal elements of the geometry of the involute straight bevel gear tooth flank $\mathcal{G}$ having offset teeth.

Without going into details of the analysis here, it should be noted that helical bevel gears having a tooth flank geometry described by Equation (13.17) are inconvenient for manufacturing purposes. As a result, the tooth flanks $\mathcal{G}$ with the desired geometry are approximated by tooth flanks $\mathcal{G}_a$, which are more convenient for manufacturers. Straight bevel gears with offset teeth are a practical example of approximation of such type.

Straight bevel gears with offset teeth can be generated using the same process used for the generation of straight bevel gears. The principal kinematics of the generation of the bevel helical gear tooth flanks is similar to that used for the generation of conventional straight bevel gear tooth flanks.

13.3.2 Generating Surface of the Gear Cutting Tool

Generating surface must be predetermined before designing a gear cutting tool for machining of straight bevel gears with offset teeth. The generating surface of a gear cutting tool is a type of virtual surface that is in proper mesh with the gear to be machined. Finishing cutting edges of the gear cutting tool are within the generating surface.

Similar to generation of ordinary straight bevel gears, the actual generating surface T_a for generation of straight bevel gears with offset teeth is not an enveloping surface to successive positions of the desired tooth flank surface $\mathcal{G}_a$, which is given by Equation (13.17). Instead, the surface T_a can be considered as a type of approximation to the desired generating surface T.

The generating surface T_a for the generation of straight bevel gears with offset teeth is depicted in Figure 13.11. In the case under consideration, the surface T_a is shaped in the form of a crown rack. The diameter of the midsection of the face of the crown rack is denoted by d_c and the diameter of the concentric circle specifying the value of the offset is denoted by d_{ot}. Because of the offset, at points within the midsection, teeth of the crown rack T_a are at a spiral angle θ with respect to the corresponding radial direction. Once the diameters d_c and d_{ot} are known, the value of the spiral angle θ can be computed from the formula $\theta = \sin^{-1}(d_{ot}/d_c)$.

In the auxiliary reference system $X_{ot}Y_{ot}Z_{ot}$ (Figure 13.11), the generating surface T_a can be analytically described by an equation that is identical to Equation (13.5). To represent the surface T_a in the coordinate system $X_cY_cZ_c$ associated with the gear cutting tool, a corresponding operator of the coordinate system transformation $\mathbf{Rs}(\mathrm{ot} \mapsto \mathrm{g})$ needs to be composed. The coordinate system transformation can be significantly simplified if the reference systems are selected properly. For example (Figure 13.12), in the coordinate system $X_c^{(s)}Y_c^{(s)}Z_c^{(s)}$ the generating surface T_a can be analytically described by an equation that is

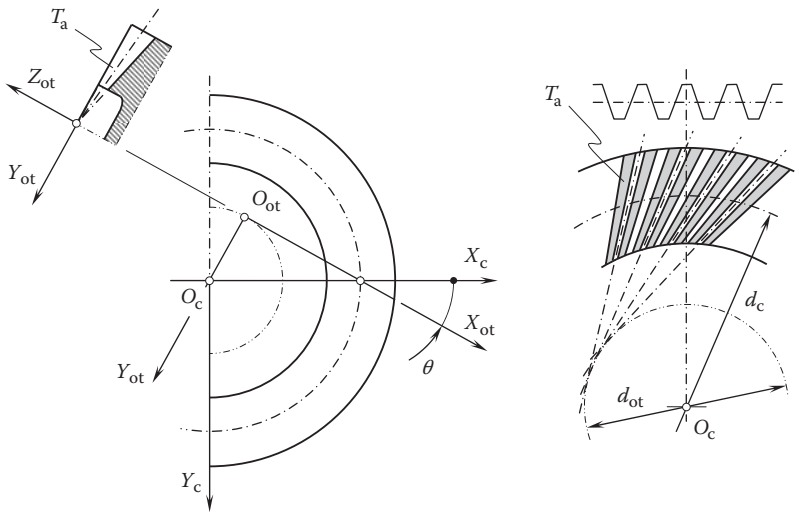

FIGURE 13.11
Design parameters of the generating surface T_a for generation of straight bevel gears with offset teeth.

identical to Equation (13.5). Because the configuration of $X_c^{(s)}Y_c^{(s)}Z_c^{(s)}$ with respect to $X_cY_cZ_c$ is convenient, the resultant coordinate system transformation can be described by the operator of elementary translation $\mathbf{Tr}[-0.5d_{ot}, Y_c^{(s)}]$.

Equation (13.5) and the operator of elementary translation $\mathbf{Tr}[-0.5d_{ot}, Y_c^{(s)}]$ yield the expression

$$\mathbf{r}_{ta}^{(s)} = \mathbf{Tr}[-0.5d_{ot}, Y_c^{(s)}] \cdot \mathbf{r}_{ta} \tag{13.18}$$

for the position vector of a point $\mathbf{r}_{ta}^{(s)}$ of the generating surface T_a for the generation of straight bevel gears with offset teeth.

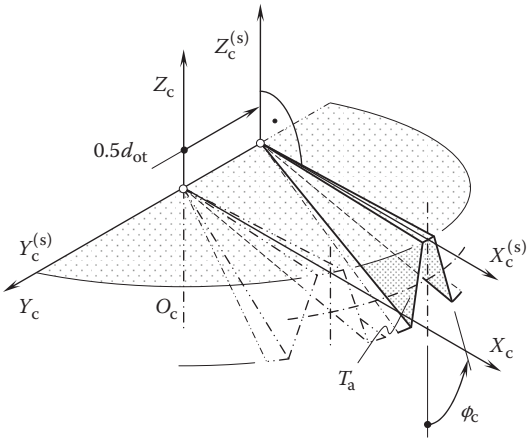

FIGURE 13.12
Analytical representation of the generating surface T_a for generation of straight bevel gears having offset teeth.

Equation (13.18) is used to derive the equation for the tooth flanks $\mathcal{G}_a$ of the generated straight bevel gears with offset teeth. It is also important for the computation of the actual tooth flank surface $\mathcal{G}_a$ from the desired tooth flank $\mathcal{G}$ [see Equation (13.17)].

13.4 Generation of Straight Bevel Gear Teeth

The approximate generating surface of the gear cutting tool is required to be reproduced by cutting edges of the tool when machining straight bevel gears. It is shown above that tooth flank of the approximate generating surface T_a is shaped in the form of a plane surface in both cases of gear machining: (1) when machining straight bevel gears of conventional design [see Equation (13.5)] and (2) when machining straight bevel gears with offset teeth [see Equation (13.18)].

The straight cutting edge of the gear cutting tool is the simplest shape of the cutting edges to be used in the reproduction of the plane T_a. The straight motion of the cutting edge and its rotation are the two easiest motions to reproduce. The straight motion is performed in the direction that is parallel to the plane T_a. The rotation is performed about the axis of rotation, which is perpendicular to the plane T_a. Other possibilities of reproducing the plane T_a exist. However, not all of them are as simple as the two just mentioned.

13.4.1 Generation of the Plane T_a by Straight Motion of the Cutting Edge

Reciprocation of the straight cutting edge C_e toward the axis of rotation O_c of the generation surface T_a, as shown in Figure 13.13, is the most reasonable means of reproducing the approximate generating surface T_a. Other directions of the reciprocation motion $\mathbf{V}_{cut}$ are theoretically feasible. However, they are too far to be of practical importance to the designer of gear cutting tools. Under such a scenario, the plane T_a is reproduced as the loci

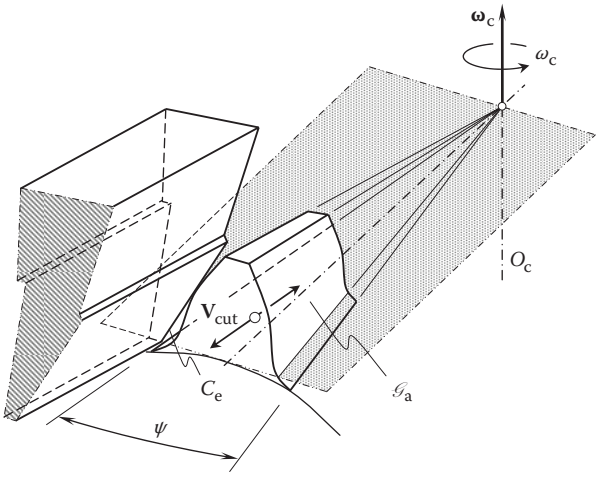

FIGURE 13.13
Generation of the plane T_a by a straight cutting edge C_e moving toward the axis of rotation O_c of the cutting tool.

of consequent positions of the straight cutting edge C_e when it is reciprocating toward the axis O_c of the rotation $\boldsymbol{\omega}_c$.

13.4.2 Machining of Straight Bevel Gears

The principles governing the generation of bevel gears are analogous to the case of spur and helical gears; the difference lies in the fact that whereas spur and helical gears are generated by tools representing the teeth of the basic rack, the cutters used for bevel gear generation represent the teeth of the basic crown wheel. This is commonly called the generating surface of the gear cutting tool. The motions resulting in generation are therefore those of rolling pitch cones instead of rolling pitch cylinders.

The cutters themselves must be given a form and motion that cause them to sweep out the surface of the basic crown wheel T_a, and the work is then given, relative to the cutters—the rolling motion that the finished gear would have when engaging with the crown wheel, which the cutters represent. Two distinct cases arise: (1) that in which each of a pair of gears (both of which are to be generated) is conjugate to the same side of the surface of the imaginary crown wheel (which must therefore be symmetrical) and (2) that in which the mating gears are conjugate to opposite sides of the same basic crown wheel. The first case finds application in the cutting of bevel gears having straight (and "uncorrected") teeth, and the second in spiral bevel gears. Considering the generation of either of a pair of gears individually, however, both cases reduce to the same thing, the only difference being in the setting of the cutters.

Figure 13.14 illustrates the process diagrammatically for the case of straight bevel gears. Two cutters, which have straight-side cutting edges CE, are arranged to reciprocate $\mathbf{V}_{cut}$

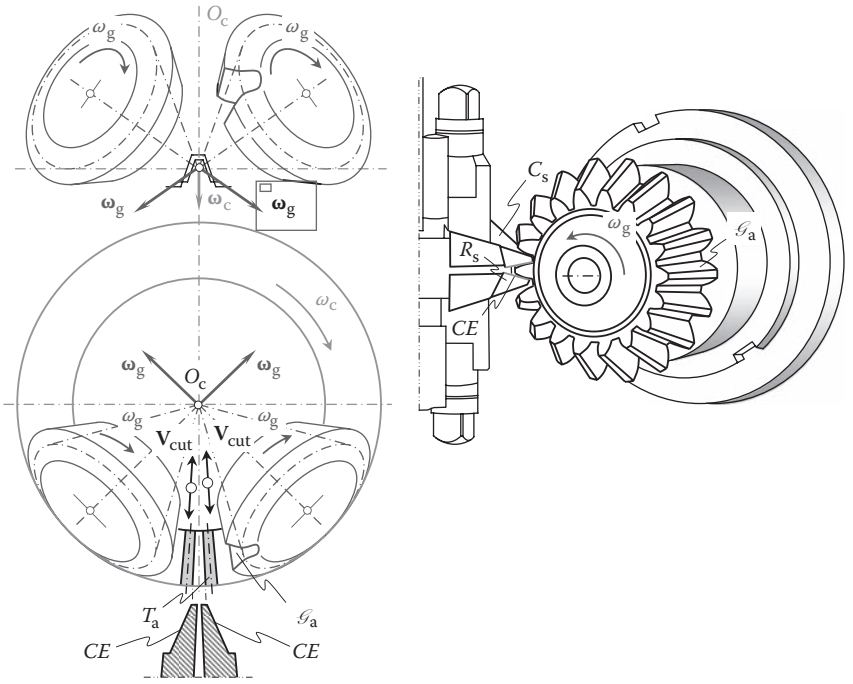

FIGURE 13.14
Diagrammatic representation of straight bevel gear generation.

along radial lines, sweeping out the surfaces T_a of the teeth of the imaginary crown wheel having its center at O_c. The cutting edge CE is viewed here as the line of intersection of the rake surface R_s and the clearance surface C_s of the gear cutting tool.

The work gear is arranged with its axis O_g passing through O_c and with its pitch cone in contact with the pitch plane of the crown wheel T_a. It is then given a rotation $\boldsymbol{\omega}_g$ about its own axis, together with a rotation of the axis bodily about the axis O_c of the crown wheel T_a, so related that the pitch cone of the work rolls over the pitch plane of the crown wheel. In passing through the zone in which the cutters operate, therefore, material is removed, and the result is a generated profile $\mathscr{G}_a$ conjugate with that of the basic crown wheel. It may be observed that in practice the component motions are rearranged as a matter of practical convenience, the work and the cutter each having only rotational motion about their respective axes.

13.4.3 Gear Cutting Tools for Machining Straight Bevel Gears

Typical cutting tools for machining straight bevel gears are shown in Figure 13.15. Both roughing tools (Figure 13.15a) and finishing tools (Figure 13.15b) are specified by diametral pitch and profile angle. They are mounted in holders that are attached to the front of reciprocating slides on the face of the cradle. Each tool can be adjusted relative to the holder so that the end of the tool is in the gear root plane and so that the tool edge travels along a line that intersects the cradle axis. This tool positioning is checked via gauging fixtures that are set on a proof block. The position of the tool holder on the face of the tool slide is adjusted to accommodate the cone distance of the work, and the length of stroke is adjusted so that the tool overtravels the face width by a small amount.

Major design parameters of the cutting tool for machining of straight bevel gears. A close-up view of a cutting tool for machining straight bevel gears of both designs—gears of regular design as well as gears with offset teeth—is shown in Figure 13.16. In addition to the major design parameters labeled in Figure 13.16, it is noteworthy that the required clearance angle is due to the appropriate setup of the cutting tool.

Sharp corners of the tooth profile are usually rounded. The practical value of the radius r of the roundness is in the range of $r \approx 0.03m$. Here, module is denoted by m.

Tooth height h (Figure 13.16) must be sufficient for the purposes of the whole tooth height of the straight bevel gear. It is common practice to assign $h = 2.5m$. Width a of the top land must exceed half of the root land width at the heel side of the gear, and must not exceed root land width at the toe side of the gear. It is practical to assign $a \approx 0.4m$.

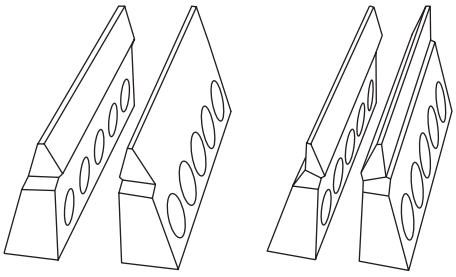

FIGURE 13.15
(a) Roughing tools and (b) finishing tools for machining bevel gears with straight teeth.

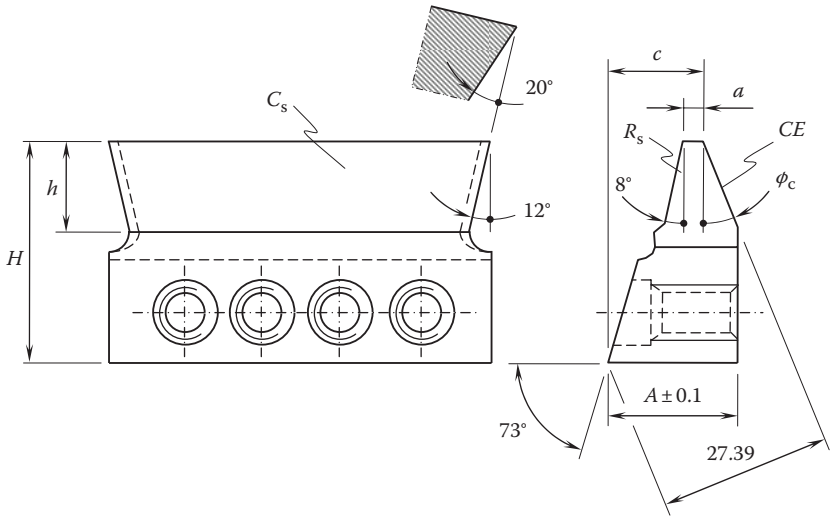

FIGURE 13.16
Design parameters of the cutting tool for machining of bevel gears with straight teeth.

Cutting tools for machining straight bevel gears can be designed so as to have two working ends from the opposite ends of the tool. After cutting edges of the first working portion of the tool have been worn out, the tool setup is changed and the opposite working portion of the tool takes its turn to cut the stock. This makes it possible to use one rake face for planing bevel gears, and after it is worn out, to use the rake surface of the opposite end of the gear cutting tool, thereby doubling the time interval between two consequent regrindings of the shaper cutter.

Special duplet tools are used. These tools have two cutting edges in tandem—one edge roughs and the other finishes the bevel gear tooth flanks.

Cutting tool geometry. Cutting tools for machining straight bevel gears are designed so that the rake angle is in the range of $\gamma = 10–25°$ depending on the work material. Standard gear cutting tools have a rake angle $\gamma = 20°$. Lateral cutting edge is at the set angle $\beta = 12°$. Its orientation is also defined by the profile angle ϕ_c of the cutting tool. Because the set angle $\beta = 12°$, an appropriate clearance angle is created. Clearance angle at the top cutting edge is equal to $\alpha_o \equiv \beta = 12°$.

The tilted orientation of the cutting tool makes it possible to create positive clearance angles at the top cutting edge ($\alpha_o > 0°$). However, clearance angle α_f at the lateral cutting edge is significantly smaller than the angle α_o. The actual value of the clearance angle α_f can be expressed in terms of the clearance angle α_o and the design parameters of the cutting tool.

Because of the tilted orientation of the cutting tool, the inclination angle λ at the lateral cutting edge is equal to zero ($\lambda = 0°$). Therefore, it is necessary to measure the clearance angle α_f in the cross section that is perpendicular to the cutting edge C_e (Figure 13.17).

Vector **A** through a point *m* of interest within the lateral cutting edge CE is aligned with the line of intersection of the clearance surface C_s by normal cross section. In the coordinate system $X_cY_cZ_c$, the following expression can be composed for vector **A**

$$\mathbf{A} = \mathbf{i} \cdot \sin\alpha_f \cos\phi_c^* + \mathbf{j} \cdot \sin\alpha_f \sin\phi_c^* - \mathbf{k} \cdot \cos\alpha_f \tag{13.19}$$

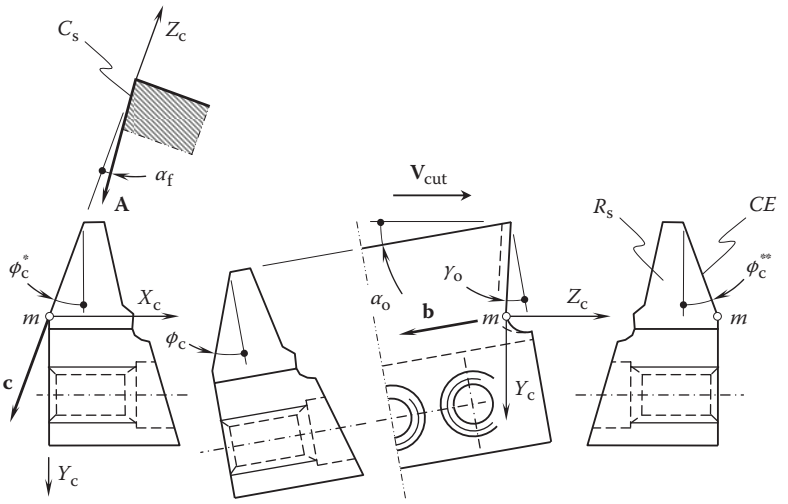

FIGURE 13.17
Computation of the geometry of the cutting edge of the gear cutting tool for machining straight bevel gears.

where ϕ_c^* denotes the profile angle that is measured in the cross section that is perpendicular to the vector $\mathbf{V}_{cut}$ (Figure 13.17). It can be shown that for computation of the angle ϕ_c^*, the following expression

$$\phi_c^* = \tan^{-1}(\tan\phi_c \cos\alpha_o) \tag{13.20}$$

is valid.

For the computation of the tooth profile angle in the cross section that is perpendicular to the generating straight line of the pitch cone, we can derive the following formula

$$\phi_c^{**} = \tan^{-1}(\tan\phi_c \cos\alpha_o \cos\delta_g) \tag{13.21}$$

where δ_g denotes the gear dedendum angle.

Unit vector **b** is aligned with the line of intersection of the clearance surface C_s by a plane that is parallel to vector $\mathbf{V}_{cut}$. This vector is entirely within the plane shown in Figure 13.17. The unit vector **b** can be expressed in terms of its projections onto the axes of the coordinate system $X_cY_cZ_c$

$$\mathbf{b} = \mathbf{j} \cdot \sin\alpha_o - \mathbf{k} \cdot \cos\alpha_o \tag{13.22}$$

Ultimately, unit vector **c** is along the lateral cutting edge. This vector can be expressed analytically as follows

$$\mathbf{c} = -\mathbf{i} \cdot \sin\phi_c^* + \mathbf{j} \cdot \cos\phi_c^* \tag{13.23}$$

Vectors **A**, **b**, and **c** are constructed so that they comprise a set of coplanar vectors, all of which are within the clearance plane C_s. Consequently, their triple scalar product is identical to zero ($\mathbf{A} \times \mathbf{b} \cdot \mathbf{c} \equiv 0$). This yields an expression

$$\mathbf{A}\times\mathbf{b}\cdot\mathbf{c}\equiv\begin{vmatrix}\sin\alpha_f\cos\phi_c^* & \sin\alpha_f\sin\phi_c^* & -\cos\alpha_f\\ 0 & \sin\alpha_o & -\cos\alpha_o\\ -\sin\phi_c^* & \cos\phi_c^* & 0\end{vmatrix}=0 \tag{13.24}$$

Equation (13.24) immediately casts into the formula

$$\alpha_f=\tan^{-1}(\tan\alpha_o\sin\phi_c^*) \tag{13.25}$$

for the computation of the clearance angle α_f.

Computations reveal that the clearance angle α_f for standard cutting tools is approximately equal to $\alpha_f\cong 4^o$. Because angle α_f is obtained by tilting to cutting tool, the rake angle is reduced in the corresponding value.

13.5 Peculiarities of Straight Bevel Gear Cutting

Production methods for straight bevel gears have received much attention largely because of the substantial number required by the automotive industry. In principle, the methods normally used for cutting spur and helical gears apply, but the generating process is modified to suit the rolling motions of two pitch cones instead of pitch cylinders. The important difference between conical and cylindrical gears is that teeth on the latter are generated by tools that simulate or are derived from the basic rack, whereas bevel gear teeth are produced by cutters representing the basic crown wheel (round rack). With this difference borne in mind, the numerous methods of cutting bevel gears bear considerable similarity to one another.

Straight bevel teeth are produced by a generating machine that reciprocates a cutting tool in a motion somewhat like that of a shaper cutter. The tools used do not resemble a pinion or a segment of a rack. The peculiar geometry of the bevel gear makes use of a special tool to cut each side of the bevel gear tooth. These tools each have a single inclined cutting edge that generates the bevel gear tooth on one side or the other. The machines achieve a generating motion by rolling the work gear and the cutter head at a slow rate, whereas the cutters reciprocate rapidly back and forth.

In the production of straight bevel gears by planing, the cutters are straight sided and they sweep out the surfaces of the basic crown wheel teeth, whereas the work gear is given the appropriate rolling motion.

A typical example of this method of cutting straight bevel gears features two straight-sided cutting tools that reciprocate across the face of a blank. The cutters are secured to the cradle of the machine that rolls in correct relationship to the work gear. The blank rolls about the center of the crown wheel. Each cutter advances in turn as the combined rolling takes place and they remove material to form tooth space in a manner similar to that followed in planing a spur gear. Indexing is intermittent and takes place on the completion of each tooth space.

This type of bevel gear generating machine is useful for cutting straddle mounted pinions since the length of the cutting stroke can be limited so that generation over the full face can be completed without causing damage to the bearing seating. Another advantage is

that during the cutting stroke, an additional motion is imparted to the work that produces a small amount of heel and toe end relief, thereby giving a barreled effect to the teeth. By providing a slightly excessive generating roll, tip and root easing are also obtained, and hard contact in the root and at the tip of gears meshing at their correct cone distance is prevented.

The latest models of straight bevel gear generators have a design feature that permits the tooth to be cut with a slight amount of crown. A cam can be set so that the cutting tool will remove a little extra metal at each end of the tooth. This makes it possible to secure a localized tooth bearing in the center of the face width.

In a few cases, cemented carbide cutters have been used to make gears instead of high-speed cutters. Much higher cutting speeds can be used with carbides, provided that the machine is rugged enough and powerful enough to drive the carbide cutter.

13.6 Milling of Straight Bevel Gears

Milling of straight bevel gears features a rotational primary motion (motion of cut). For the generation of the bevel gear tooth flank, the lateral tooth surface of the generating surface T_a should be reproduced. In bevel gear planing operations, the reproduction of the lateral tooth surface T_a is achieved by reciprocating of the cutting tool in the radial direction of the generating surface. Reciprocation in the direction that is perpendicular to that just mentioned is geometrically feasible; however, it is extremely inconvenient for practical use. Rotation about an axis that is perpendicular to the plane T_a is the ultimate possibility to reproduce the lateral tooth surface of the virtual crown gear. Milling cutters for machining of bevel gears are designed based on this concept.

13.6.1 Peculiarities of the Gear Machining Operation

A productive type of straight bevel generation is that which uses a pair of interlocking disk-mill cutters having a multiplicity of blades that cut on two sides of a tooth space [190]. Interlocking arrangement of the cutters allows a complete cutting process. The two interlocking cutters have to be adjusted independently during setup, which is complicated and time consuming.

Figure 13.18 shows a close-up view of a finished bevel gear and two interlocking milling cutters. The profile angle ϕ_c of the gears being cut is obtained via machine settings. The disk cutters rotate on axes O_c, which are inclined to the face of the cradle. The cutting edges CE sweep out slightly internal conical surfaces.

The motions between work gear ω_g and cutting tools V_{rol} are combined to give the minimum amount of rolling movement necessary to obtain fully generated teeth. No longitudinal traverse is provided and the cutters feed into the work in a direction normal to the pitch cone. As a result, the tooth roots are slightly concave, but the tooth flanks could be slightly modified to give tip and root easing. Indexing takes place after each tooth space has been completed and the machine is fully automatic in its motions. When a gear has been completed the machine stops, the cutters withdraw, and the work gear can be changed with little delay.

In nearly all cases, gears cut in accordance to this method are completed from the solid blank in one operation that combines the roughing and finishing cuts. The method features

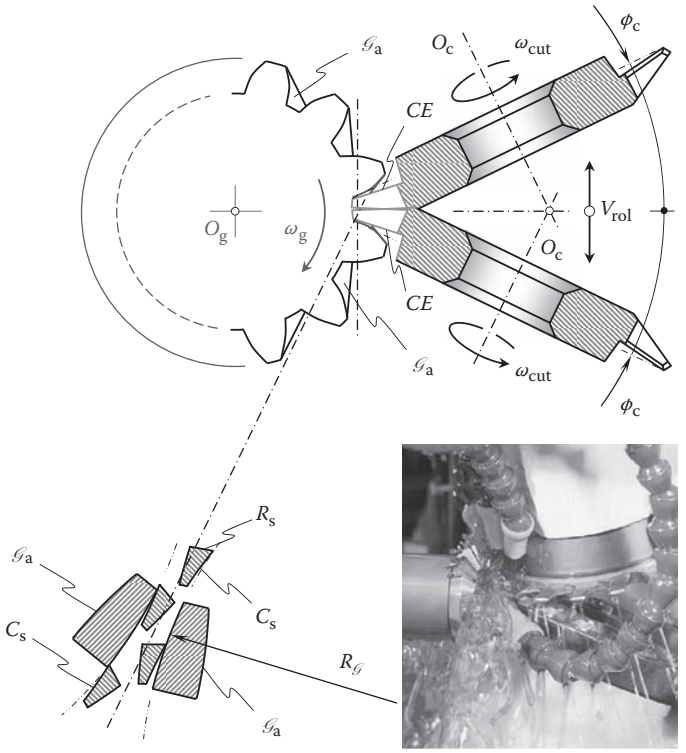

FIGURE 13.18
A close-up view of a finished straight bevel gear and the interlocking milling cutters.

high productivity of straight bevel gear machining. The productivity is as much as four to five times greater than that for the gear planing process.

13.6.2 Design of Milling Cutters

Straight bevel gears are cut with a circular milling cutter having a circumferential blade arrangement. As with other straight bevel gear generators, the tools form the blanks of a tooth simulating the basic crown wheel. Tooth flanks of the generating surface T_a are identical to that used for planing of straight bevel gears [see Equations (13.5) and (13.18)]. Cutter teeth are intermeshing and the disks are inclined to one another at the required pressure angle, which is usually $\phi_c = 20°$.

Milling cutters of two different designs are used for the machining of straight bevel gears.

First, lateral cutting edges of the milling cutter could be located within a plane that is perpendicular to the axis of rotation of the milling cutter. Milling cutters of this design are used in the production of straight bevel gear of conventional design having no modification of the tooth flanks.

Second, lateral cutting edges of the milling cutter could make a certain angle δ with respect to the perpendicular to the axis of rotation of the milling cutter. Commonly, the angle δ is assigned in the range of $\delta = 1–5°$. (Bevel gears having coarser teeth are machined with the milling cutters having a smaller angle δ.)

Shown in Figure 13.19 is a disk-type milling cutter consisting of a body having slots. Cutting blades are bolted in the slots in the cutting tool body. The top of the cutting blade is wider than the width of the slots. This provides reliable fixturing of the blades in the cutting tool body. The cutting blades height h exceeds the height of the gear tooth. It is practically equal to $h = 2.5m$. Similar to bevel gear planing, width of the top land of the cutting blades is assigned the value $a = 0.4m$.

Rake angle γ_f at the lateral cutting edge is commonly equal to $\gamma_f = 20°$. Clearance angle α_c at the top cutting edge is usually equal to $\alpha_o = 10–12°$.

Standard milling cutters are available in two outer diameters $d_{o.c}$. Milling cutters with $d_{o.c} = 150$ mm are used for machining of bevel gears of small module (up to $m = 2$ mm). For machining of bevel gears of coarse module (up to $m = 8$ mm), disk-type milling cutters having $d_{o.c} = 275$ mm are commonly used. Custom-size milling cutters are also available.

The blades of *Coniflex* cutters are relief ground when manufactured and thus require sharpening only on the front face. Blade-to-blade spacing and cutter diameter, as well as angle and surface finish of the front face, must be closely controlled in sharpening. Special-purpose sharpeners, offered by the gear machine manufacturers, are recommended to assure consistency in sharpening as well as the longest (cutter) tool life.

13.6.3 Specific Features of the Shape of Finished Bevel Gear Flanks

Two cutters generate a combination of profile and length crowning in the flank surfaces of the bevel gear. A side effect of the cutter arrangement is a curved root line, depending on the cutter diameter. Slightly concave root land surfaces are produced because the cutters are not stroked in the direction of the teeth. The curvedness of the root line can be evaluated by the parameter Δh (Figure 13.20)

$$\Delta h = \frac{d_{o.c}\cos\phi_c - \sqrt{d_{o.c}^2\cos^2\phi_c - b^2}}{2} \tag{13.26}$$

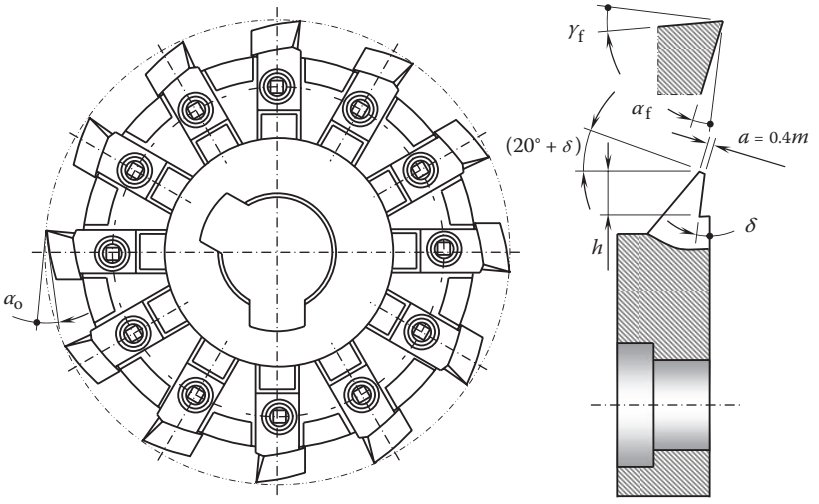

FIGURE 13.19
Milling cutter for machining of straight bevel gear.

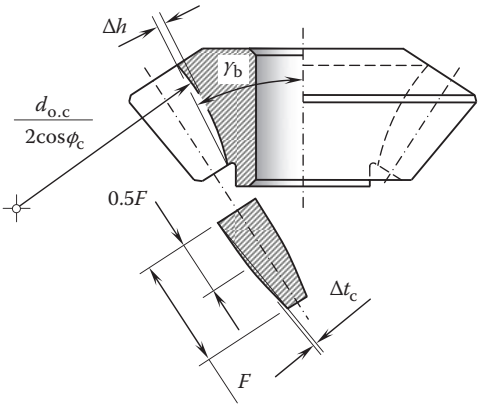

FIGURE 13.20
Specific features of shape of the finished bevel gear flanks.

When the milling cutter rotates, the cutting edges generate a conical surface. Milling cutters of this design are used in the production of bevel gears having longitudinal modification of their teeth. The value of the longitudinal modification Δt_c depends on: (1) the outer diameter $d_{o.c}$ of the milling cutter, (2) the cutting edge angle δ, and (3) face width F of the bevel gear (Figure 13.20)

$$\Delta t_c = \frac{F^2 \sin\delta}{4d_{o.c}} \tag{13.27}$$

The effect of the inner cone surface in connection with curved cutter blades is used to produce the crowning effect in straight bevel gears. As noted before, a pair of cutters is always required, one left-hand and one right-hand cutter, to realize the interlocking arrangement in the cutting machine in order to cut both flanks of a slot at the same time.

Again, milling of straight bevel gears with two milling cutters produces not the desired tooth flank surface $\mathcal{G}$ but a practical, suitable type of its approximation $\mathcal{G}_a$.

13.7 Machining of Bevel Gears with Curved Teeth

More opportunities in designing of gear cutting tools appear due to the variety of feasible orientation of rotation vector of the primary motion (motion of cut). For example, rotation vector $\boldsymbol{\omega}_{cut}$ can be pointed so that it is parallel to the axis of rotation O_c of the generating surface of the cutting tool as shown in Figure 13.21. In this way, bevel gears with curved teeth having a certain spiral angle ψ_g could be produced. Suitable spiral angles lie between about $\psi_g = 15$ and 35° but are usually chosen between $\psi_g = 30$ and 35° to provide adequate overlap, and it is normal practice to make spiral bevel gears with about 35% overlap.

When machining a bevel gear with curved teeth, the cutter is rotating about its axis with a certain angular velocity ω_{cut}. The work gear and the generating surface T_a roll over each other. For this purpose, the rotations of the work gear ω_g and of the generating surface of the gear cutting tool ω_c are synchronized with each other in a properly timed manner.

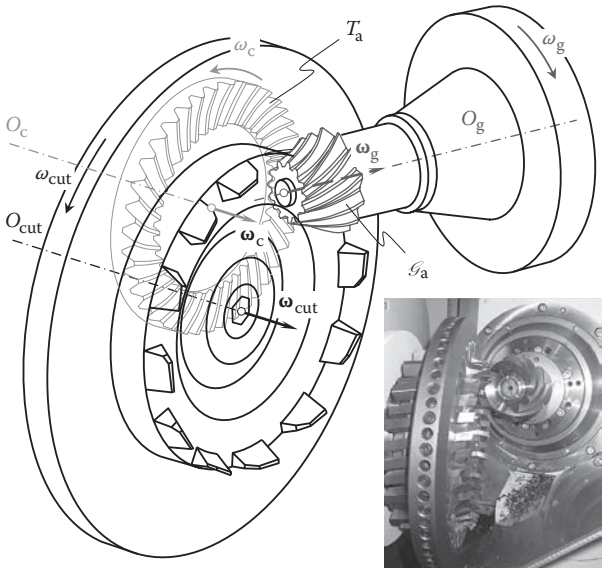

FIGURE 13.21
Representation of the generating surface T_a with the face-mill cutter.

The generation of spiral bevel gears follows the same principle, and the only difference between the numerous types of spiral bevel gear lies in the motion of the cutter in relation to the work.

13.7.1 Peculiarities of the Gear Machining Operation

In the method of generating curved tooth bevel gears, the tooth spirals take the form of circular arcs. The straight-sided cutting tools represent the flanks of the basic crown wheel teeth and the combined motions of the generating cutter and the work sweep out the surface of the imaginary crown wheel teeth (round rack teeth). Generation of the tooth profiles is obtained by giving the work a rolling motion relative to the cutter, similar to that which the finished gear would have when engaging with the crown wheel.

The tool-holder is rotating to cause a cutting action while the work slowly rotates with the tool-holder. The rotation of the work gear with respect to the tool-holder causes a generating action to occur. After one tooth space is finished, the machine goes through an indexing motion to bring the cutter into the next tooth slot.

Pinions are cut as the reverse of wheels insofar as they are assumed to engage with the opposite side of the basic crown wheel surface. In practice, the axes of the generating cutter and the work gear are not inclined at the theoretical angle; the axes are arranged to accommodate the tapering depth of the tooth and also to provide deflection allowance in the tooth spirals.

In operation, the cutter is given a rotation speed and feed suitable for the material of the work gear and is fed into the full depth required while cutter and work gear roll together. A copious supply of cutting oil is fed to the cutting zone to act as lubricant and coolant. It is normal to expect a minimum of 100 gears to be cut between cutter sharpenings. As soon as a tooth space has been completed, the work and cutter roll out of engagement, the work gear is indexed to the next tooth space, and the cutting process continues.

Teeth are usually rough cut and finish cut as two separate operations and if the quantities are sufficiently large, it is usual to carry out rough cutting on one machine and retain the second machine solely for finishing. Wheels being rough cut may be produced without tooth generation and that refinement is deferred until the finish cutting operation. Pinions are invariably fully generated and if they are intended to be run with form cut wheel, the full shape is applied to the pinion profiles only.

Gears that demand a high quality are always provided with fully generated teeth on both the wheel and pinion.

To machine a bevel gear having a prescribed spiral angle ψ_g at the central point *C*, the setup parameters of the cutting tool should satisfy the values that are computed from the formulae (Figure 13.22)

$$H = L - R_C \sin \psi_g \tag{13.28}$$

$$V = R_C \cos \psi_g \tag{13.29}$$

Bevel gear generators are often designed so that they require setup parameters expressed in polar coordinates. The polar angle σ and the offset distance OP = *U* can be computed from the expressions

$$U = \sqrt{H^2 + V^2} \tag{13.30}$$

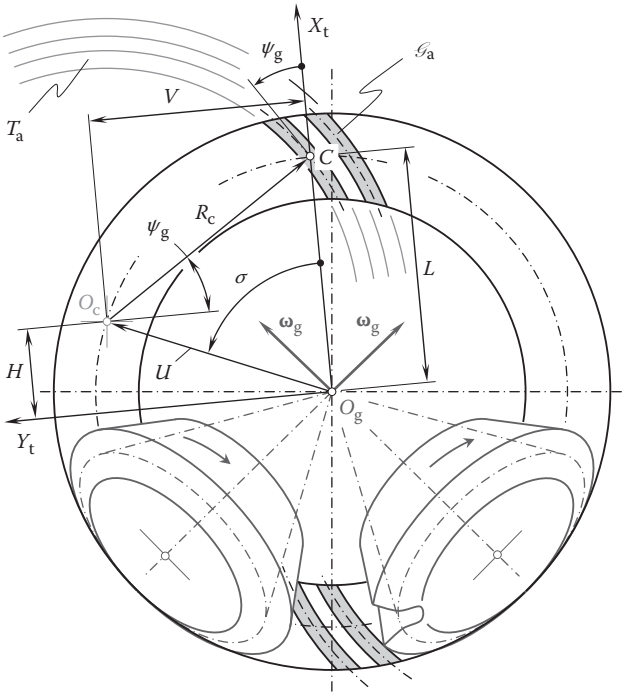

FIGURE 13.22
Diagrammatic arrangement of spiral bevel gear generation.

$$\sigma = \tan^{-1}\left(\frac{V}{H}\right) \tag{13.31}$$

In a rolling motion, the values of coordinates H and V change. However, the radial offset U remains constant when the polar angle σ varies.

13.7.2 Design of Cutters

For machining of bevel gears with circular arc teeth, the generating surface of the cutting tool is chosen in the form of two cones of revolution having a common axis of rotation (Figure 13.23). Equation of the generating surface T_a can be derived from Figure 13.23.

The position vector of a point $\mathbf{r}_a^{(i)}$ for the inner portion $T_a^{(i)}$ of the generating surface can be expressed in the form

$$\mathbf{r}_a^{(i)}(\varphi_c, \theta_c) = \frac{(d_c - t_c)}{2} \cdot \begin{bmatrix} \cos\varphi_c \cos\theta_c \\ \cos\varphi_c \sin\theta_c \\ \sin\varphi_c \\ 1 \end{bmatrix} \cdot \frac{\cos\phi_c}{\cos(\varphi_c - \phi_c)} \tag{13.32}$$

Similarly, for the outer portion $T_a^{(o)}$ of the generating surface for the position vector of a point $\mathbf{r}_a^{(o)}$, the following formula

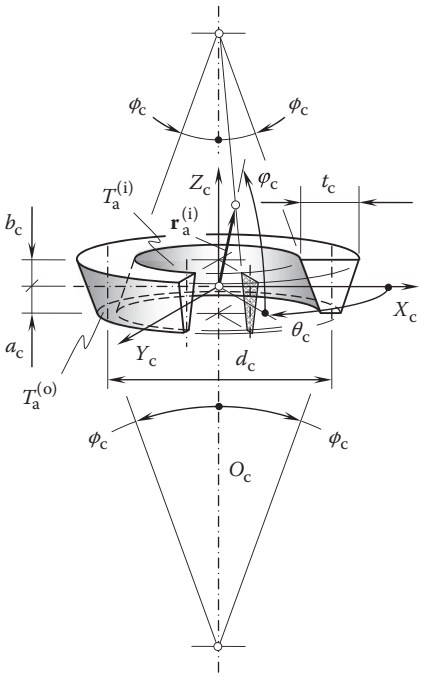

FIGURE 13.23
Design parameters of the generating surface T_a of the face-mill cutter.

$$\mathbf{r}_a^{(o)}(\varphi_c, \theta_c) = \frac{(d_c - t_c)}{2} \cdot \begin{bmatrix} \cos\varphi_c \cos\theta_c \\ \cos\varphi_c \sin\theta_c \\ -\sin\varphi_c \\ 1 \end{bmatrix} \cdot \frac{\cos\phi_c}{\cos(\varphi_c - \phi_c)} \tag{13.33}$$

can be derived.

Lateral cutting edges CE of the face-mill cutter are within the surfaces $T_a^{(i)}$ and $T_a^{(o)}$ [Equations (13.32) and (13.33)]. In this way, the straight-sided cutting tools represent the flanks of the basic crown wheel teeth.

Cutting tools of small diameter (up to 50 mm) are made solid. Cutting tools of larger diameter are often made assembled. They consist of a tool body and a plurality of cutting blades bolted into the tool body (Figure 13.24). The cutter blades themselves are bolted in slots in the body of the cutter and are arranged so that each flank of a tooth space is cut by alternate blades.

Cutting tools of small diameter have two cutting blades, whereas cutting tools of larger diameter usually have up to 32 cutting blades.

For roughing of coarse teeth, roughing face-mill cutters are used. Finishing of bevel gears is performed with the finishing face-mill cutters.

It can be shown that the profile angle $\phi_c^{(o)}$ of the outer cutting blades is smaller than its nominal value ϕ_c, whereas the profile angle $\phi_c^{(i)}$ of the inner cutting blades exceeds its nominal value ϕ_c. Because of this, the cutting blades are designed with an asymmetrical tooth profile. The profile angles are as follows:

$$\phi_c^{(o)} = \phi_c - \Delta\phi_c \tag{13.34}$$

$$\phi_c^{(i)} = \phi_c + \Delta\phi_c \tag{13.35}$$

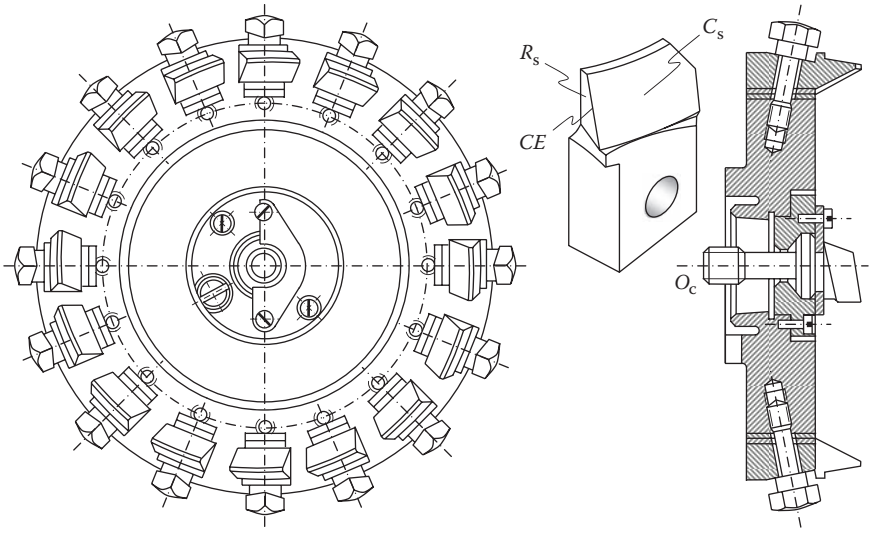

FIGURE 13.24
Face-mill cutter for machining of bevel gears with curved teeth.

where

$$\Delta\phi_c = \frac{\phi_{fr} + \phi_{fl}}{2} \cdot \sin\psi_g \tag{13.36}$$

where ϕ_{fr} and ϕ_{fl} denote the root profile angles and ψ_g is the spiral angle at the central point *C*.

Equations (13.34) through (13.36) are approximate. Computations return the result of the computation within 2–3%.

The normal rake angle range from γ_o = 10–15° to γ_o = 22–27°. For standard cutting tools, γ_o = 20°.

Clearance angle α_o = 11–13° and α_f = 2–5°. Most designs of the cutting tools make it possible to increase the value of α_f.

14

Gear Shaper Cutters Having a Tilted Axis of Rotation: Internal Gear Machining Mesh

Gear machining operations featuring intersecting axes of rotation of the work gear and cutting tool can be executed when an internal gear machining mesh is reproduced when machining the gear. Under such a scenario, either internal gears (ring gears) can be cut with gear cutting tools having an external generating surface, or external gears can be machined with enveloping gear cutting tools.

14.1 Principal Kinematics of Internal Gear Machining Mesh

Principal kinematics of the internal gear machining mesh can be illustrated by two rotation vectors. One of the rotation vectors, $\boldsymbol{\omega}_g$, represents rotation of the work gear, whereas another rotation vector, $\boldsymbol{\omega}_c$, represents the corresponding rotation of the cutting tool. The vectors $\boldsymbol{\omega}_g$ and $\boldsymbol{\omega}_c$ of the rotations align with the intersecting axes of rotations O_g and O_c of the work gear and cutting tool. Moreover, the vectors $\boldsymbol{\omega}_g$ and $\boldsymbol{\omega}_c$ originate from the point of intersection of the axes O_g and O_c, as shown in Figure 14.1.

The internal gear machining mesh under consideration features the shaft angle Σ that is smaller than its critical value Σ_{cr} (i.e., the inequality $\Sigma < \Sigma_{cr}$ is observed for the internal gear machining mesh).

Only the relative motion of the gear cutting tool and work gear is of importance for consideration.

The rotation of the cutter ω_c can exceed the rotation of the work gear ω_g. Such a configuration of the rotation vectors $\boldsymbol{\omega}_g$ and $\boldsymbol{\omega}_c$ is schematically depicted in Figure 14.1a, where the inequality $\omega_c > \omega_g$ is observed. In this case, vector $\boldsymbol{\omega}_{pl}$ of the cutter's instant rotation can be constructed in compliance with the equality $\boldsymbol{\omega}_{pl} = \boldsymbol{\omega}_c - \boldsymbol{\omega}_g$. For this purpose, it is convenient to construct the rotation vector $-\boldsymbol{\omega}_g$, which is pointed opposite from the rotation vector $\boldsymbol{\omega}_g$. After the rotation vector $-\boldsymbol{\omega}_g$ is applied to both the work gear and the gear cutting tool, then the work gear becomes motionless ($\boldsymbol{\omega}_g - \boldsymbol{\omega}_g = 0$). Instant rotation of the cutting tool relative to the work is represented by the rotation vector $-\boldsymbol{\omega}_{pl}$.

For illustration purposes, axodes $\mathscr{A}_g$ and $\mathscr{A}_c$ can be associated with the rotation vectors $\boldsymbol{\omega}_g$ and $\boldsymbol{\omega}_c$ (Figure 14.1b). The relative motion of the gear cutting tool with respect to the work gear allows for interpretation in the form of rolling, with no sliding of the axodes $\mathscr{A}_c$ of the gear cutting tool over the axode $\mathscr{A}_g$ of the work gear. Pitch line P_{ln} serves as the axis of the instant rotation $\boldsymbol{\omega}_{pl}$.

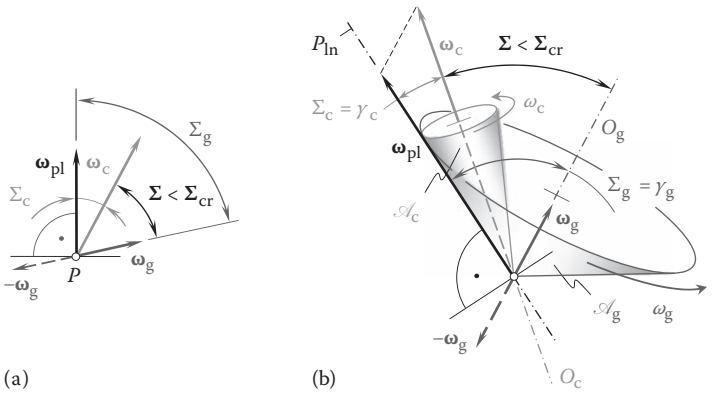

FIGURE 14.1
Vector representation of the internal intersecting-axis gear machining mesh for cutting an internal gear.

14.2 Peculiarities of the Gear Cutting Tool Design

Derivation of the generating surface of a gear cutting tool is one of the major purposes of the kinematics of the gear machining mesh. Then when the gear cutting tool is designed, the gear machining mesh can be complemented with a primary motion of the cutting tool ($\mathbf{V}_{cut}$). Ultimately, kinematics of the gear machining process is composed in this manner.

14.2.1 Shaping of Internal Gear

A shaper for machining an internal gear can be designed on the premise of the internal gear machining mesh. For design purpose, a Cartesian coordinate system $X_cY_cZ_c$ is associated with the gear cutting tool to be designed, as shown in Figure 14.2. The rotation vectors $\boldsymbol{\omega}_g$ and $\boldsymbol{\omega}_c$ are at a certain shaft angle $\boldsymbol{\Sigma}$. They are synchronized with each other in a timely proper manner.

The cutting tool reference system $X_cY_cZ_c$ can perform a certain motion with respect to the coordinate system $X_gY_gZ_g$. This relative motion can be employed as the primary motion (motion of cut). The motion of cut can be represented as superposition of the elementary translations along axes of the coordinate system $X_cY_cZ_c$, and the elementary rotations about axes of that same coordinate system. The number of elementary motions of the cutting tool is limited to a total of six. The elementary motions of the cutting tool can be considered separately, as well as the combinations of the elementary motions by two, three, four, five, and six. In this way, all possible relative motions of the cutting tool with respect to the work gear can be encompassed.

At this point, let us simplify the problem to be solved, and as an example let us consider not an arbitrary relative motion of cut, but a particular type of this motion instead. Let us assume that the motion of cut is a straight motion parallel to the axis of O_g. This means that the motion of cut $\mathbf{V}_{cut}$ can be represented in the form of vector summa $\mathbf{V}_{cut} = \mathbf{V}_x + \mathbf{V}_z$. Here, $\mathbf{V}_x$ and $\mathbf{V}_z$ designate projections of the vector $\mathbf{V}_{cut}$ onto the axes of the coordinate system $X_cY_cZ_c$.

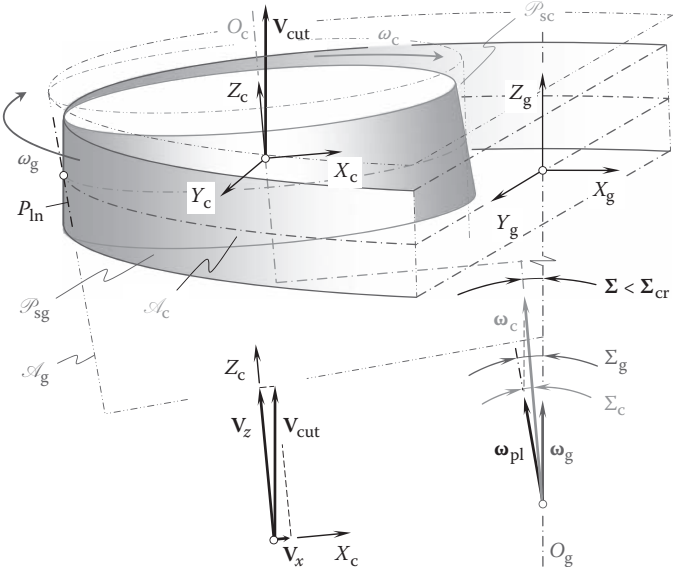

FIGURE 14.2
Kinematics of the gear machining operation that features the primary motion (motion of cut $\mathbf{V}_{cut}$) parallel to the axis of rotation O_g of the work gear.

Axodes $\mathscr{A}_g$ and $\mathscr{A}_c$ can be associated with the work gear and the cutting tool. When machining a gear, the axodes $\mathscr{A}_g$ and $\mathscr{A}_c$ are rolling over each other with no sliding between the rolling surfaces.

The actual shape of the operating pitch surfaces $\mathscr{P}_{sg}$ and $\mathscr{P}_{sc}$ of the work gear and cutting tool, respectively, depends on the chosen kind and direction of the primary motion. For the straight motion of cut $\mathbf{V}_{cut}$, the pitch surface of the work gear $\mathscr{P}_{sg}$ is shaped in the form of a cylinder of revolution. The pitch surface of the cutting tool $\mathscr{P}_{sc}$ is shaped in the form of the corresponding cone of revolution.

The kinematics of the gear-machining operation depicted in Figure 14.2 features the motion of cut $\mathbf{V}_{cut}$ parallel to the axis of rotation O_g of the work gear. Such a kinematics can be used for the purpose of designing a shaper for machining an internal gear. Shaping the internal gear with the external shaper is illustrated in Figure 14.3.

The work gear rotates about its axis O_g. The shaper cutter rotates about its axis of rotation O_c. Rotation of the work gear ω_g and rotation of the shaper cutter ω_c are properly timed with each other. The rotation vectors $\boldsymbol{\omega}_g$ and $\boldsymbol{\omega}_c$ are aligned with the corresponding axes of rotations O_g and O_c. The vectors $\boldsymbol{\omega}_g$ and $\boldsymbol{\omega}_c$ make a certain angle, which in the case under consideration is equal to the clearance angle α_o at the top cutting edge of the shaper cutter. This makes it possible to shape the clearance surfaces C_s in the form of nearly involute cylinders. Straight generating lines of the involute cylinders are parallel to the axis of rotation O_c of the shaper cutter. Finishing grinding of the clearance surfaces C_s in this case is much easier.

Rake surface R_s of the shaper cutter teeth is shaped in the form of a cone of revolution. This cone is coaxial with the axis of rotation of the shaper cutter. As shown in Figure 14.3, parameters of the conical rake surface R_s can be expressed in terms of the rake angle γ_o and of the clearance angle α_o at the top cutting edge of the shaper cutter teeth.

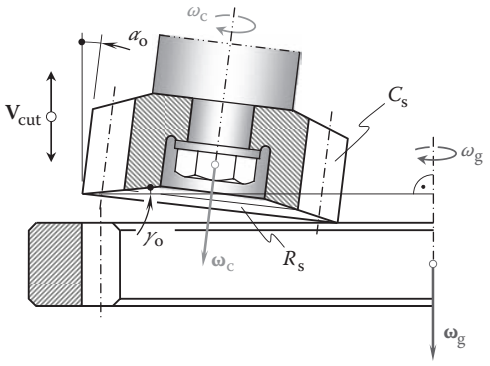

FIGURE 14.3
Schematic of shaping of an internal gear with the shaper cutter having a tilted axis of its rotation.

Direction of the motion of cut $\mathbf{V}_{cut}$ is parallel to the axis of rotation O_g of the work gear. It is easy to show that the motion of cut $\mathbf{V}_{cut}$ allows for representation in the form of vector summa $\mathbf{V}_{cut} = \mathbf{V}_x + \mathbf{V}_z$.

14.2.2 Shaping a Spur Gear with Enveloping Shaper Cutter

Similar to machining of the internal gear with the shaper cutter (see Figure 14.3), machining of an external gear with the enveloping shaper cutter can be performed as well. Vector representation of the internal intersecting-axis gear machining mesh for cutting an external gear with an enveloping shaper cutter is schematically depicted in Figure 14.4. The

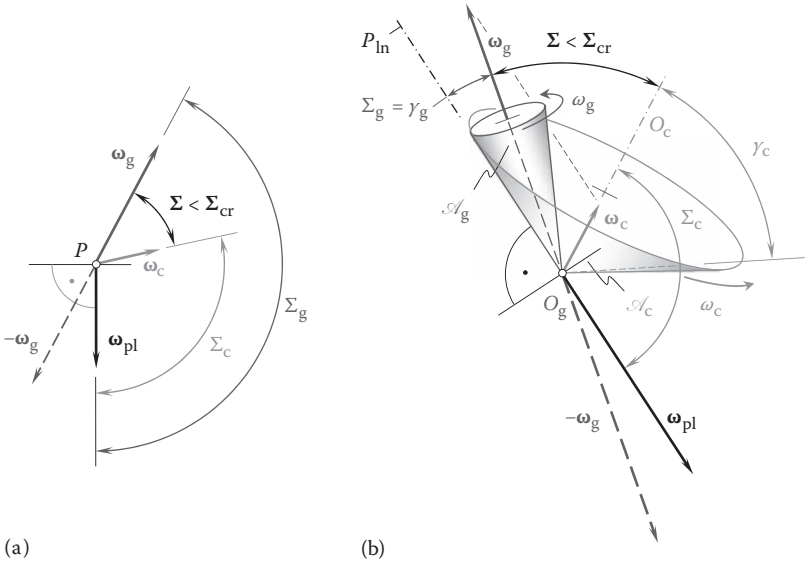

FIGURE 14.4
Vector representation of the internal intersecting-axis gear machining mesh for cutting an external gear with an enveloping shaper cutter.

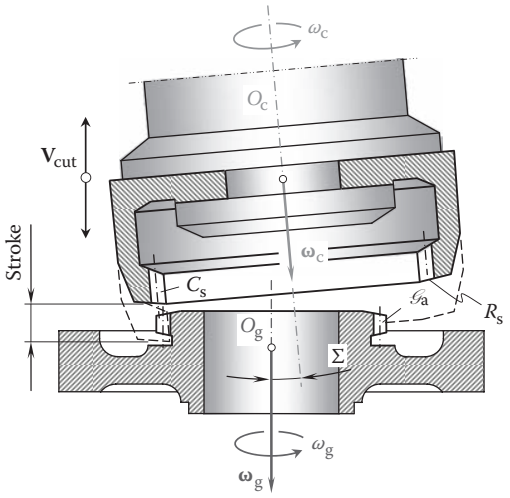

FIGURE 14.5
Machining of a spur gear with the enveloping shaper cutter.

vector diagram is constructed on the premises of the two rotation vectors $\boldsymbol{\omega}_g$ and $\boldsymbol{\omega}_c$ of the work gear and the gear cutting tool. Vector $\boldsymbol{\omega}_{pl}$ of the instant rotation of the gear shaper cutter is constructed in the way similar to that illustrated in Figure 14.1. Again, for convenience, the rotation vector $-\boldsymbol{\omega}_g$ is applied to both the work gear and the gear cutting tool.

A schematic of the machining process of a spur gear with the enveloping shaper cutter is shown in Figure 14.5. The work gear and the shaper cutter are rotating about their axes O_g and O_c. The rotations ω_g and ω_c are properly timed with each other. The rotation vectors $\boldsymbol{\omega}_g$ and $\boldsymbol{\omega}_c$ are aligned with the corresponding axes of rotations O_g and O_c. The vectors $\boldsymbol{\omega}_g$ and $\boldsymbol{\omega}_c$ make a certain angle. In the case under consideration, this angle is equal to the clearance angle α_o at the top cutting edge of the shaper cutter. This makes it possible to shape the clearance surfaces C_s in the form of nearly involute cylinders. Straight generating lines of the involute cylinders are parallel to the axis of rotation O_c of the shaper. Finishing grinding of the clearance surfaces C_s of the gear shaper cutter in this case is much easier.

The rake surface R_s of the shaper cutter teeth is shaped in the form of a cone of revolution that is coaxial with the shaper cutter axis of rotation. Parameters of the conical rake surface R_s can be expressed in terms of the rake angle γ_o and of the clearance angle α_o at the top cutting edges of the shaper cutter teeth.

The direction of the primary motion (motion of cut $\mathbf{V}_{cut}$) is pointed parallel to the axis of rotation O_g of the work gear. It is easy to show that the motion of cut $\mathbf{V}_{cut}$ allows representation in the form of vector summa $\mathbf{V}_{cut} = \mathbf{V}_x + \mathbf{V}_z$.

14.2.3 Shaping of External Recessed Tooth Forms with Enveloping Shaper Cutter

Implementation of the kinematic scheme of gear generating shown in Figure 14.4 can be extended to machining of external recessed tooth forms with an enveloping shaper cutter. Gears of this kind are commonly referred to as *beveloids*. A perfect example of implementation of gears of such a design can be found in [16].

The gear shown in Figure 14.6 has an external spline tooth that is recessed below the rim face of the gear.

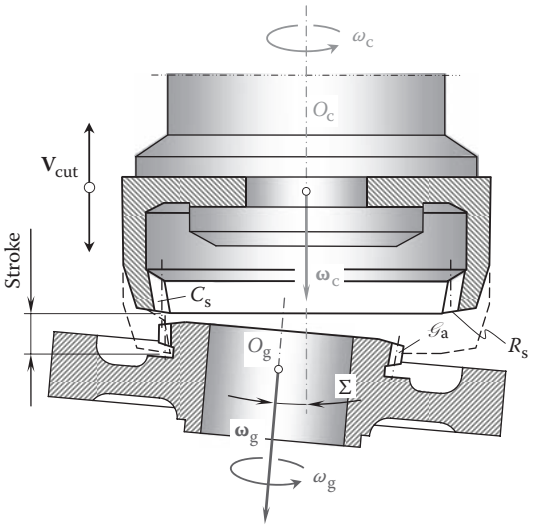

FIGURE 14.6
Shaping of a recessed tooth form with an enveloping gear shaper cutter. The tooth form is tapered by tilting the axis of the work gear relative to the axis of the gear shaper cutter.

The work gear and the shaper cutter rotate about their axes of rotations O_g and O_c. The rotations ω_g and ω_c are properly timed with each other. The rotation vectors $\boldsymbol{\omega}_g$ and $\boldsymbol{\omega}_c$ align with the corresponding axes of rotations O_g and O_c. The vectors $\boldsymbol{\omega}_g$ and $\boldsymbol{\omega}_c$ make a certain angle. In the case under consideration, this angle is equal to the angle of the recessed teeth.

The rake surface R_s of the shaper cutter teeth is shaped in the form of a cone of revolution that is coaxial with the shaper cutter axis of rotation. Parameters of the conical rake surface R_s can be expressed in terms of the rake angle γ_o and of the clearance angle α_o at the top cutting edges of the shaper cutter teeth.

The direction of the motion of cut $\mathbf{V}_{cut}$ is parallel to the axis of rotation O_g of the work gear. It is easy to show that the motion of cut $\mathbf{V}_{cut}$ allows for representation in the form of vector summa $\mathbf{V}_{cut} = \mathbf{V}_x + \mathbf{V}_z$.

With an external shaper cutter, the cutter diameter would be limited to maximum 1.00 in. (25.4 mm) resulting in low generating feeds, multiple passes, long cycle times, and low cutter life. Tool life can be increased, and cycle time reduced, by using an enveloping shaper cutter with internal teeth [16]. The spline teeth can be cut straight or with a back-taper, as shown in Figure 14.6 on a tilting table mechanism. The accuracy of an enveloping cutter is inherently less because of the large manufacturing tolerances required for the internal teeth.

Along with machining of external beveloid teeth, shaping of internal gears having recessed tooth forms is feasible as well. For this purpose, shaper cutters of conventional design can be implemented.

In addition to motion of cut that is parallel either to the axis of rotation of the work gear or to the axis of rotation of the shaper cutter, motions of cut of other types are also feasible. To discover all feasible motions of cut, it is necessary to investigate a possibility of implementation for this purpose of (a) all elementary translation motions $\mathbf{V}_x$, $\mathbf{V}_y$, and $\mathbf{V}_z$; (b) all elementary rotation motions $\boldsymbol{\omega}_x$, $\boldsymbol{\omega}_y$, and $\boldsymbol{\omega}_z$; and (c) all possible combinations of

elementary translations and elementary rotations by one, two, three, four, five, and six. The ratio of magnitudes of the elementary motions in every combination should be put into consideration.

Potential capabilities of the kinematic scheme of gear generation (see Figures 14.1 and 14.4) from the standpoint of gear cutting tool design have not been profoundly investigated yet. There is much room for research and development in this area of gear engineering. Novel methods of gear machining and gear cutting tools of novel designs can be developed on the premise of the analysis of the kinematic scheme shown in Figures 14.1 and 14.4.

Section V

Cutting Tools for Gear Generating: Spatial Gear Machining Mesh

Spatial gear machining mesh is observed in the most general cases of gear generation. Continuously indexing gear cutting tools are used in gear machining processes of this kind. Hobs, shaver cutters, as well as gear cutting tools of other designs work on this principle.

Depending on the parameters, spatial gear machining meshes could be either the external or internal type. Another possible type of spatial gear machining meshes exists between the external and the internal gear machining meshes. Gear machining meshes of this particular type are referred to as *quasi-planar gear machining meshes*.

It is convenient to consider the design of gear cutting tools separately depending on the type of gear machining mesh that is simulated in a particular gear machining process. Therefore, discussion of the continuously indexing gear cutting tools design will be split into three sections below, each of which is devoted to (a) external gear machining mesh, (b) quasi-planar gear machining mesh, and (c) internal gear machining mesh.

Section V-A: Design of Gear Cutting Tools: External Gear Machining Mesh

Continuously indexing gear cutting tools of various types are designed on the premise of external spatial gear machining mesh. This group of gear cutting tools is the most common in industry. The similarity of the kinematics of the gear machining process together with the similarity of the geometry of the generating surfaces of gear cutting tools make it reasonable to consider them in a common section.

15

Generating Surface of the Gear Cutting Tool

The geometry of the tooth shape to be machined along with the kinematics of the gear machining operation are the two components that are of critical importance for the creation of generating surface of the gear cutting tool.

Tooth flank geometry of the work gear is specified by the blueprint of the gear. It can also be described analytically, for example, by Equations (1.2), (1.3), (1.27), (1.33), and others. Once the design parameters of a gear to be machined are known from the blueprint, then the corresponding analytical description for tooth flanks can be derived from this data.

The kinematics of spatial motion of the gear cutting tool relative to the work gear is complex in nature. It deserves to be analyzed in greater detail.

15.1 Kinematics of External Spatial Gear Machining Mesh

External spatial gear machining mesh is comprised of two rotations about crossing axes. One of the rotations, $\boldsymbol{\omega}_g$, is the rotation of the work gear, and another, $\boldsymbol{\omega}_c$, is the rotation of the cutting tool to be designed. The rotations $\boldsymbol{\omega}_g$ and $\boldsymbol{\omega}_c$ are synchronized with each other in a timely proper manner so that when the cutting tool completes one full rotation about its axis O_c, the work gear turns about the axis O_g through the angle $2\pi(N_c/N_g)$. Here, N_g and N_c denote the tooth number of the gear to be machined, and the tooth number (number of starts) of the gear cutting tool correspondingly.

An example of vector representation of the external spatial gear machining mesh is shown in Figure 15.1. The vector diagram is specified in terms of (a) two rotation vectors $\boldsymbol{\omega}_g$ and $\boldsymbol{\omega}_c$, (b) crossed-axis angle Σ, and (c) center distance $C_{g/c}$. The gear machining mesh shown in Figure 15.1 is one of three possible types of spatial gear machining meshes classified in Figure 3.8.

In Figure 15.1a, the rotation vectors $\boldsymbol{\omega}_g$ and $\boldsymbol{\omega}_c$ are constructed so that they are parallel to the horizontal plane of projections π_1. Such a configuration of the rotation vectors $\boldsymbol{\omega}_g$ and $\boldsymbol{\omega}_c$ is advantageous for two reasons. First, the actual value of the crossed-axis angle Σ can be measured within the plane π_1, and second, the actual value of the center distance $C_{g/c}$ can be measured within the vertical plane of projections π_2.

Let us suppose the axode of the work gear is motionless and the axode of the gear cutting tool is free to roll over the axode of the work gear. For this purpose it is sufficient to assume that both the work gear and the gear cutting tool are given an additional rotation $-\boldsymbol{\omega}_g$. Due to the additional rotation $-\boldsymbol{\omega}_g$, the work gear becomes stationary $[\boldsymbol{\omega}_g + (-\boldsymbol{\omega}_g) = 0]$, while the gear cutting tool will be subjected to two rotations simultaneously, namely, it performs (a) the initial rotation $\boldsymbol{\omega}_c$ and (b) the additional rotation $-\boldsymbol{\omega}_g$. Two rotations ω_c and $-\boldsymbol{\omega}_g$ together result in the instant rotation $\boldsymbol{\omega}_{pl} = \boldsymbol{\omega}_c - \boldsymbol{\omega}_g$ of the gear cutting tool about the axis of instant rotation P_{ln} (pitch line). Vector ω_{pl} of the instant rotation is applied at a certain point within the center distance $C_{g/c}$.

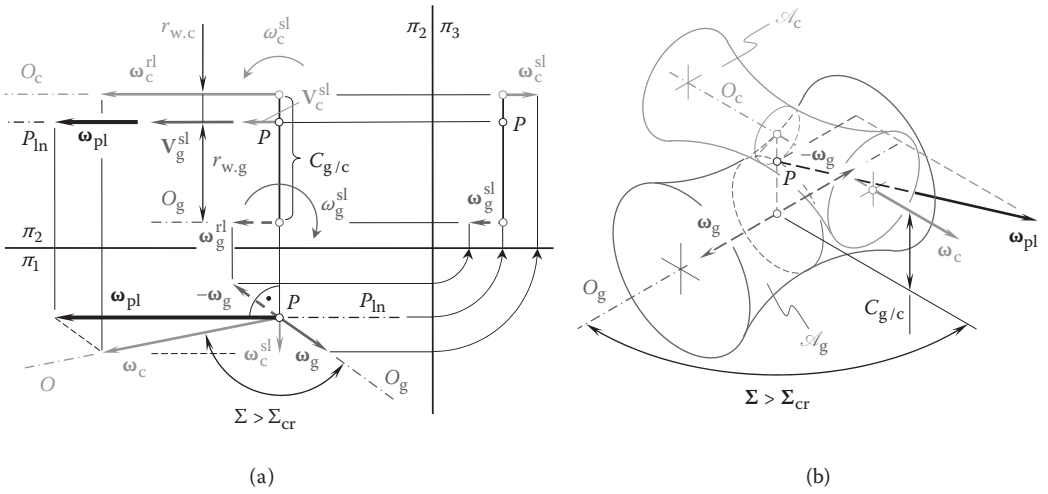

FIGURE 15.1
Vector diagram of an external spatial gear machining mesh.

The rotation vector $\boldsymbol{\omega}_{pl}$ is parallel to the horizontal plane π_1. Projections of the rotation vectors $\boldsymbol{\omega}_g$ and $\boldsymbol{\omega}_c$ onto the vertical plane of projections π_2 are denoted as $\boldsymbol{\omega}_g^{rl}$ and $\boldsymbol{\omega}_c^{rl}$, respectively. The components $\boldsymbol{\omega}_g^{rl}$ and $\boldsymbol{\omega}_c^{rl}$ are parallel to the axis P_{ln} of instant rotation $\boldsymbol{\omega}_{pl}$. The components $\boldsymbol{\omega}_g^{rl}$ and $\boldsymbol{\omega}_c^{rl}$ result in pure rolling of the axodes $\mathscr{A}_g$ of the work gear and $\mathscr{A}_c$ of the gear cutting tool (Figure 15.1b). For the magnitudes $\omega_g^{rl} = |\boldsymbol{\omega}_g^{rl}|$ and $\omega_c^{rl} = |\boldsymbol{\omega}_c^{rl}|$, the following ratio is valid

$$\frac{r_{w.g}}{\omega_c \cos \Sigma_c} = \frac{C_{g/c}}{\omega_{pl}} = \frac{r_{w.c}}{\omega_g \cos \Sigma_g} \tag{15.1}$$

where $r_{w.g}$ denotes the distance from point P to the axis of rotation O_g of the work gear. Similarly, the distance from that same point P to the axis of rotation O_c of the gear cutting tool is designated as $r_{w.c}$.

The angles Σ_g and Σ_c can be expressed in terms of the rotation vectors $\boldsymbol{\omega}_g$, $\boldsymbol{\omega}_c$, and $\boldsymbol{\omega}_{pl}$. For this purpose the formulas $\Sigma_g = \angle(\boldsymbol{\omega}_g, \boldsymbol{\omega}_{pl})$ and $\Sigma_c = \angle(\boldsymbol{\omega}_c, \boldsymbol{\omega}_{pl})$ can be employed.

Evidently, the equality

$$r_{w.g} + r_{w.c} = C_{g/c} \tag{15.2}$$

is observed. This equality can be utilized for the purpose of determining the exact location of point P within the center distance $C_{g/c}$. The condition of pure rolling is helpful for solving this problem.

The condition of pure rolling of the axodes can be employed for the purpose of determining the exact location of point P within center distance $C_{g/c}$. The following ratio

$$\frac{r_{w.g}}{r_{w.c}} = \frac{\omega_c^{rl}}{\omega_g^{rl}} \tag{15.3}$$

immediately follows from the condition of pure rolling of the axodes $\mathscr{A}_g$ and $\mathscr{A}_c$. Here, in Equation (15.3) is designated $\omega_g^{rl} = |\boldsymbol{\omega}_g^{rl}|$ and $\omega_c^{rl} = |\boldsymbol{\omega}_c^{rl}|$.

Generally speaking, magnitudes ω_g^{rl} and ω_c^{rl} of the vectors of pure rolling $\boldsymbol{\omega}_g^{rl}$ and $\boldsymbol{\omega}_c^{rl}$ are not equal to each other. The inequality $\omega_g^{rl} < \omega_c^{rl}$ is commonly observed. The equality $\omega_g^{rl} = \omega_c^{rl}$ is observed only in particular cases when the tooth number of the work gear N_g and the tooth number of the cutting tool N_c are equal to each other. In particular cases, N_c could also mean the number of threads/starts of the worm-type cutting tool.

The equality $r_{w.g} = C_{g/c} - r_{w.c}$ immediately follows from Equation (15.2). Substituting this value of $r_{w.g}$ into Equation (15.3), the formula

$$r_{w.c} = \frac{\omega_g^{rl}}{\omega_c^{rl} + \omega_g^{rl}} \cdot C_{g/c} \tag{15.4}$$

for the computation of $r_{w.c}$ can be derived.

Then, the distance $r_{w.g}$ can be computed from the above formula $r_{w.g} = C_{g/c} - r_{w.c}$. This expression for $r_{w.g}$ casts into

$$r_{w.g} = \frac{\omega_c^{rl}}{\omega_c^{rl} + \omega_g^{rl}} \cdot C_{g/c} \tag{15.5}$$

In the case under consideration, point P is located within the center distance $C_{g/c}$.

The other two components $\boldsymbol{\omega}_g^{sl}$ and $\boldsymbol{\omega}_c^{sl}$ of the rotation vectors $\boldsymbol{\omega}_g$ and $\boldsymbol{\omega}_c$ are perpendicular to the axis P_{ln} of the instant rotation $\boldsymbol{\omega}_{pl}$. With no distortion these components are projected onto the frontal plane of projections π_3.

The rotation vectors $\boldsymbol{\omega}_g^{sl}$ and $\boldsymbol{\omega}_c^{sl}$ are of the same magnitude and are directed opposite from each other ($\boldsymbol{\omega}_g^{sl} = -\boldsymbol{\omega}_c^{sl}$). The rotations $\boldsymbol{\omega}_g^{sl}$ and $\boldsymbol{\omega}_c^{sl}$ result in pure sliding of the axodes of the work gear and the gear cutting tool.

One of two components, $\mathbf{V}_g^{sl}$, of the vector of the linear velocity of the sliding of the axodes (i.e., owing to the rotation of the work gear) is equal to

$$\mathbf{V}_g^{sl} = r_{w.g} \cdot \boldsymbol{\omega}_g^{sl} \tag{15.6}$$

Another component, $\mathbf{V}_c^{sl}$, of the vector of the linear velocity of the sliding of the axodes (i.e., due to the rotation of the gear cutting tool) can be computed from the formula

$$\mathbf{V}_c^{sl} = r_{w.c} \cdot \boldsymbol{\omega}_c^{sl} \tag{15.7}$$

Commonly, the inequality $r_{w.g} > r_{w.c}$ is observed in the gear machining operation. Therefore, the component $\mathbf{V}_g^{sl}$ always exceeds the component $\mathbf{V}_c^{sl}$ (i.e., the inequality $|\mathbf{V}_g^{sl}| > |\mathbf{V}_c^{sl}|$ is valid). This is because the magnitudes of the rotations $\boldsymbol{\omega}_g^{sl}$ and $\boldsymbol{\omega}_c^{sl}$ are equal to each other ($|\boldsymbol{\omega}_g^{sl}| = |\boldsymbol{\omega}_c^{sl}|$).

The vectors $\mathbf{V}_g^{sl}$ and $\mathbf{V}_c^{sl}$ of the linear velocities of sliding are pointed opposite from each other. Therefore, vector $\mathbf{V}_{g-c}^{sl}$ of the linear velocity of the resultant sliding of the axode of the work gear relative to the axode of the gear cutting tool can be computed as the difference

$$\mathbf{V}_{g-c}^{sl} = \mathbf{V}_g^{sl} - \mathbf{V}_c^{sl} \tag{15.8}$$

The opposite-directed vector $\mathbf{V}_{c-g}^{sl}$ of the resultant linear velocity of the sliding of the axode of the gear-cutting tool with respect to the axode of the work gear can be computed from the equation

$$\mathbf{V}_{c-g}^{sl} = -\mathbf{V}_{g-c}^{sl} = \mathbf{V}_{c}^{sl} - \mathbf{V}_{g}^{sl} \tag{15.9}$$

In the case under consideration, the magnitude $\mathbf{V}_{\Sigma}^{sl}$ of the linear speed of the sliding of the axodes can be determined as the summa

$$V_{\Sigma}^{sl} = V_{g}^{sl} + V_{c}^{sl} \tag{15.10}$$

The component vectors $\boldsymbol{\omega}_{g}^{sl}$ and $\boldsymbol{\omega}_{c}^{sl}$ comprise a pair of rotations. This is because the vectors $\boldsymbol{\omega}_{g}^{sl}$ and $\boldsymbol{\omega}_{c}^{sl}$ are of the same magnitude and are pointed opposite from each other. A pair of rotations is equivalent to a translation with a linear velocity $\mathbf{V}_{sc}$. The vector of linear velocity $\mathbf{V}_{sc}$ of the translation is parallel to the vector of instant rotation $\boldsymbol{\omega}_{pl}$. The magnitude V_{sc} of the vector $\mathbf{V}_{sc}$ is equal to

$$V_{sc} = |\mathbf{V}_{sc}| = C_{g/c}\omega_{g} \sin \Sigma_{g} = C_{g/c}\omega_{c} \sin \Sigma_{c} \tag{15.11}$$

It is important to point out here that the linear velocities $\mathbf{V}_{\Sigma}^{sl}$ and $\mathbf{V}_{sc}$ are of the same magnitude ($\mathbf{V}_{\Sigma}^{sl} = V_{sc}$).

Two motions, namely, (a) the instant rotation $\boldsymbol{\omega}_{pl}$, and (b) the translation $\mathbf{V}_{sc}$, are performing simultaneously. For the computation of parameter p_{sc} of the resultant instant screw motion, the following formula can be used

$$p_{sc} = \frac{V_{sc}}{\omega_{pl}} = \frac{C_{g/c}\omega_{g} \sin \Sigma_{g}}{\omega_{pl}} = \frac{C_{g/c}\omega_{c} \sin \Sigma_{c}}{\omega_{pl}} \tag{15.12}$$

where $\omega_{pl} = |\boldsymbol{\omega}_{pl}|$.

Equation (15.1) yields an expression

$$\omega_{pl} = \frac{C_{g/c}\omega_{g} \cos \Sigma_{g}}{r_{w.c}} = \frac{C_{g/c}\omega_{c} \cos \Sigma_{c}}{r_{w.g}} \tag{15.13}$$

for the computation of magnitude ω_{pl} of the instant rotation $\boldsymbol{\omega}_{pl}$.

Therefore, the following expression

$$p_{sc} = r_{w.g} \tan \Sigma_{p} = r_{w.p} \tan \Sigma_{g} \tag{15.14}$$

is valid. This immediately yields the ratio

$$\frac{r_{w.g}}{r_{w.c}} = \frac{\tan \Sigma_{c}}{\tan \Sigma_{g}} \tag{15.15}$$

Ultimately, in the case under consideration, two rotations $\boldsymbol{\omega}_{g}$ and $\boldsymbol{\omega}_{c}$ about the skew axes result in instant screw motion. The resultant motion can be interpreted as rolling with the sliding of the hyperboloid $\mathscr{A}_{c}$ of the gear cutting tool over the motionless hyperboloid $\mathscr{A}_{g}$

of the work gear. The axode of the gear cutting tool $\mathscr{A}_c$ is represented as loci of successive positions of the axis P_{ln} in its rotation about the axis of rotation O_c of the gear cutting tool. The stationary axode of the work gear $\mathscr{A}_g$ is represented as loci of successive positions of the axis P_{ln} in its rotation about the axis of rotation O_g of the work gear. Rolling and sliding occur about and along a straight generating line when the lines align with each other at a certain instance of time.

Configuration of the rotation vectors $\boldsymbol{\omega}_g$ and $\boldsymbol{\omega}_c$ relative the axodes of the gear $\mathscr{A}_g$ and the gear cutting tool $\mathscr{A}_c$ is illustrated in Figure 15.1b. Here, we stress one more time that axodes $\mathscr{A}_g$ and $\mathscr{A}_c$ themselves are not of prime importance and are not used in this text for the analysis of the kinematics of the gear machining operation. The vector diagrams are self-consistent and are preferred for the analysis of the kinematics of the gear machining processes.

15.2 Auxiliary Generating Surface of the Gear Cutting Tool

The auxiliary generating surface of the gear cutting tool is utilized in cases when the first Olivier principle [49] is used for the purpose of determining the generating surface of the gear cutting tool.

The resultant motion of the gear cutting tool with respect to the work gear is decomposed into two elementary components. The auxiliary generating surface is an enveloping surface to successive positions of the gear tooth flank when the gear performs one of the two component motions. Then, the generating surface is obtained as an enveloping surface to successive positions of the auxiliary generating surface when the auxiliary surface performs the second of two elementary component motions.

For generation of the auxiliary generating surface of the gear cutting tool, consider a gear to be machined that is performing a certain motion relative to a reference system $X_rY_rZ_r$. After being generated, the auxiliary generating surface $\mathscr{R}_T$ will be associated with this reference system $X_rY_rZ_r$.

In order to determine all possible types of auxiliary surfaces $\mathscr{R}_T$, it is necessary to consider all possible motions of the gear tooth flank surface $\mathscr{G}$ with respect to the coordinate system $X_rY_rZ_r$. Then an analysis is performed, which targets the determination of whether an enveloping surface to successive positions of the tooth flank $\mathscr{G}$ is feasible. If the enveloping surface exists, then it can be utilized as an auxiliary generating surface of the gear cutting tool. Actually, not only tooth flank $\mathscr{G}$ should be considered, but the surfaces those forming the top land and bottom land of the gear tooth should be considered as well. Tooth flank surface $\mathscr{G}$ is taken into consideration here only as a representative example.

Consider tooth flank $\mathscr{G}$ of a gear that is given by Equation (1.3)

$$\mathbf{r}_g(U_g, V_g) = \begin{bmatrix} r_{b.g}\cos V_g + U_g \cos\lambda_{b.g}\sin V_g \\ r_{b.g}\sin V_g - U_g \sin\lambda_{b.g}\sin V_g \\ r_{b.g}\tan\lambda_{b.g} - U_g\sin\lambda_{b.g} \\ 1 \end{bmatrix} \quad \begin{matrix} V_g^{(l)} \le V_g \le V_g^{(a)} \\ 0 \le U_g \le [U_g] \end{matrix} \tag{15.16}$$

The surface $\mathscr{G}$ is used for the derivation of an equation of the auxiliary phantom rack $\mathscr{R}_T$ of the gear cutting tool. The rack $\mathscr{R}_T$ is conjugate to the gear tooth surface $\mathscr{G}$.

The rack surface $\mathscr{R}_T$ can be generated as the envelope of the consecutive positions of the gear teeth surface $\mathscr{G}$ in its motion relative to the coordinate system $X_rY_rZ_r$.

As shown in Figure 15.2a, the gear to be machined rotates about its axis of rotation O_g with a certain angular velocity $\boldsymbol{\omega}_g$. Simultaneously, the gear performs a straight motion with a certain velocity $V_g = |\mathbf{V}_g|$.

The relative motion of the work gear and the reference system $X_rY_rZ_r$ can be interpreted as rolling of the gear pitch cylinder of diameter $d_{w.g} = 2R_{w.g}$ over the pitch plane W_r associated with the reference system $X_rY_rZ_r$. The auxiliary rack $\mathscr{R}_T$ (Figure 15.2b) can be determined as the envelope of consecutive positions of the gear tooth surface $\mathscr{G}$ when the pitch plane W_r rolls without sliding over the pitch cylinder of diameter $d_{w.g}$. Velocity V_g of the translational motion depends on the rotation ω_g. It can be computed from the equation $V_g = 0.5\omega_g d_{w.g}$.

For the derivation of an equation of the auxiliary generating surfaces $\mathscr{R}_T$ of the gear cutting tool, the following main coordinate systems are used (Figure 15.3): (a) the coordinate system $X_gY_gZ_g$ associated with the gear being machined, and (b) the coordinate system $X_rY_rZ_r$, with which the auxiliary generating rack $\mathscr{R}_T$ will be associated. A few more intermediate reference systems were used as well.

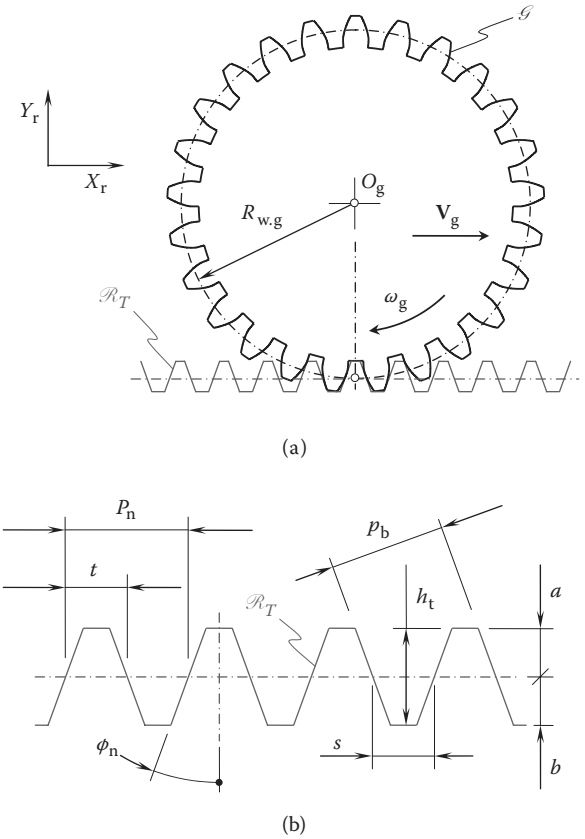

FIGURE 15.2
An auxiliary generating surface $\mathscr{R}_T$ of a gear cutting tool that is shaped in the form of a straight rack.

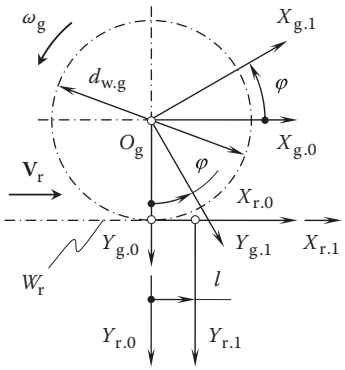

FIGURE 15.3
The coordinate systems applied for the derivation of an equation of the auxiliary generating surfaces $\mathscr{R}_T$ of a gear cutting tool. (From Radzevich, S.P., *ASME Journal of Mechanical Design*, 129, 334–345, 2007. With permission.)

For further analysis, it is necessary to represent the tooth flank surface $\mathscr{G}$ in the coordinate system $X_rY_rZ_r$. In this coordinate system, the position vector of point $\mathbf{r}_g^{(r)}$ can be expressed in terms of the position vector of that same point $\mathbf{r}_g$ in the original reference system $X_gY_gZ_g$, and in terms of the operator $\mathbf{Rs}(\mathscr{G} \mapsto \mathscr{R}_T)$ of transition from the coordinate system $X_gY_gZ_g$ associated with the work gear to the coordinate system $X_rY_rZ_r$ [138, 143]. The following expression

$$\mathbf{r}_g^{(r)}(U_g, V_g) = \mathbf{Rs}(\mathscr{G} \mapsto \mathscr{R}_T) \cdot \mathbf{r}_g(U_g, V_g) \tag{15.17}$$

is valid for the position vector of point $\mathbf{r}_g^{(r)}$.

The transformation operator $\mathbf{Rs}(\mathscr{G} \mapsto \mathscr{R}_T)$ analytically describes the resultant coordinate system transformation.

In the case under consideration, the resultant coordinate system transformation can be analytically represented as a superposition of several consequent elementary coordinate system transformations (Figure 15.3). The required elementary linear transformations are described analytically by (a) the operator $\mathbf{Rt}(\varphi, Z_g)$ of the rotation about the Z_g axis through an angle φ, (b) the operator $\mathbf{Tr}(-0.5d_{w.g}, Y_r)$ of the translation along the Y_r axis at a distance $-0.5d_{w.g}$, and (c) the operator $\mathbf{Tr}(-l, X_r)$ of the translation along the X_r axis at a distance $-l$. The above-mentioned operators of the elementary coordinate system transformations yield an expression for the operator $\mathbf{Rs}(\mathscr{G} \mapsto \mathscr{R}_T)$ of the resultant coordinate system transformation

$$\mathbf{Rs}(\mathscr{G} \mapsto \mathscr{R}_T) = \mathbf{Tr}(-l, X_r) \cdot \mathbf{Tr}(-0.5d_{w.g}, Y_r) \cdot \mathbf{Rt}(\varphi, Z_g) \tag{15.18}$$

The value of the angle φ can be computed from the formula $\varphi = \omega_g t$, and the distance l is equal to $l = |\mathbf{V}_r| \cdot t$. Here time is denoted as t.

In the relative motion, the gear tooth flank surface $\mathbf{r}_g^{(r)}$ occupies various positions consequently. Equation (15.16) can be employed for the purpose of analytical representation of the screw involute surface $\mathbf{r}_{g,t}^{(r)}$ in its current location $\mathbf{r}_{g,t}^{(r)} = \mathbf{r}_{g,t}^{(r)}(U_g, V_g, t)$ (here, time is designated as t). To eliminate time, equation $\mathbf{r}_{g,t}^{(r)} = \mathbf{r}_{g,t}^{(r)}(U_g, V_g, t)$ should be considered together with Shishkov's equation of contact $\mathbf{n}_g \cdot \mathbf{V}_{g-r} = 0$ [186]. The solution to the set of two equations

$$\begin{cases} \mathbf{r}_{g.t}^{(r)} = \mathbf{r}_{g.t}^{(r)}(U_g, V_g, t) \\ \mathbf{n}_g \cdot \mathbf{V}_{g-r} = 0 \end{cases} \tag{15.19}$$

returns the equation of the tooth surface of the auxiliary rack $\mathscr{R}_T$. Here, the unit normal vector to the gear tooth flank $\mathscr{G}_r$ (i.e., in the coordinate system $X_rY_rZ_r$) is designated as $\mathbf{n}_g$, and $\mathbf{V}_{g-r}$ is the vector of speed of the motion of the gear tooth flank surface $\mathscr{G}$ relative to the coordinate system $X_rY_rZ_r$.

Expanding Equation (15.19) and eliminating the enveloping parameter, one can come up with an equation of the lateral tooth surface of the auxiliary generating surface $\mathscr{R}_T$ in matrix representation

$$\mathbf{r}_r(U_r, V_r) = \begin{bmatrix} X_r(U_r, V_r) \\ Y_r(U_r, V_r) \\ Z_r(U_r, V_r) \\ 1 \end{bmatrix} \tag{15.20}$$

Eventually, the solution to Equation (15.19) reveals that (a) the rack tooth flank surface $\mathscr{R}_T$ is a plane, (b) this plane makes the base lead angle $\lambda_{b.g}$ with the gear axis of rotation O_g, and (c) the plane makes the pressure angle ϕ_r with the pitch plane W_r (Figure 15.2b).

One tooth flank of the auxiliary rack generates just one tooth flank of the work gear. A corresponding number of planes $\mathscr{R}_T$ is required for simultaneous machining of several tooth flanks of the work gear. All of these planes are parallel to each other. Every two neighboring planes are at a distance that is equal to the base pitch p_b of the gear. The distance is measured along perpendicular to the planes $\mathscr{R}_T$. The same is true for the opposite side of the tooth profile of the gear, and of the auxiliary rack $\mathscr{R}_T$.

Hence, the auxiliary rack $\mathscr{R}_T$ of a gear cutting tool for the machining of involute gears has straight-line tooth profile. The profile angle ϕ_r of the rack $\mathscr{R}_T$ is identical to the profile angle $\phi_{w.g}$, which is measured on the gear pitch diameter ($\phi_r \equiv \phi_{w.g}$).

It is proven analytically [130] that for the machining purposes the actual value of the gear pitch diameter $d_{w.g}$ can be chosen within a certain interval $d_{b.g} \le d_{w.g} \le d^*_{w.g}$. Here, $d^*_{w.g}$ designates the maximum feasible pitch diameter of the gear, for which tooth pointing of the auxiliary rack $\mathscr{R}_{y.T}$ is avoided, and moreover, the width of the top land of teeth of the rack exceeds a certain minimum allowed value. The diameter $d^*_{w.g}$ can be determined on the basis of an analysis of the satisfaction of the set of necessary conditions of proper part surface generation [128, 138, 143] (see Appendix B). For different values $d_{y.g}$ of the gear pitch diameter, the conjugate rack surface $\mathscr{R}_{y.T}$ has the corresponding value of the profile angle $\phi_{y.r}$. The actual values of the pitch $P_{y.x}$ and helix angle $\psi_{y.r}$ of the rack $\mathscr{R}_{y.T}$ also depends on the diameter $d_{y.g}$. Therefore, variation in the gear pitch diameter $d_{y.g}$ results in corresponding alterations in (a) profile angle $\phi_{y.r}$, (b) pitch $P_{y.x}$, and (c) helix angle $\psi_{y.r}$ of the auxiliary rack $\mathscr{R}_{y.T}$ as shown in Figure 15.4. All the feasible auxiliary phantom racks $\mathscr{R}_{y.T}$ are always conjugate to the gear being machined.

A gear can be interpreted as a certain number of the tooth-flank surfaces $\mathscr{G}$ that are evenly distributed around the gear pitch cylinder. Therefore, the auxiliary rack $\mathscr{R}_{y.T}$ can be considered as two sets of planes evenly distributed within the pitch plane W_r. The planes in each set are parallel to one another. The distance between every two neighboring planes of the rack $\mathscr{R}_{y.T}$ (or, which is the same, the distance between every two neighboring straight-

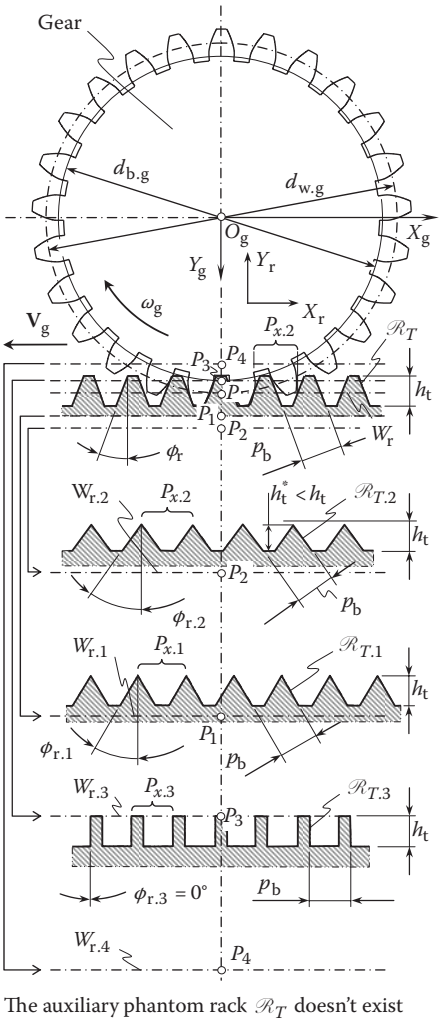

FIGURE 15.4
Generation of the auxiliary phantom racks $\mathscr{R}_T$ with a different profile angle ϕ_r. (From Radzevich, S.P., *ASME Journal of Mechanical Design*, 129, 438–444, 2007. With permission.)

line profiles) is measured along the pitch line. This distance is equal to the gear pitch $P_{y.x} = \pi d_{w.g}/N_g$, which is measured on the pitch circle of the gear.

Thus, a variety of the auxiliary racks with different design parameters can be generated [132]. It is of critical importance to stress here that the base pitch p_b for all feasible auxiliary racks $\mathscr{R}_{y.T}$ is of the same value and is equal to the gear base pitch.

Variation of the pitch diameter $d_{y.g}$ within the interval $d_{b.g} \le d_{w.g} \le d^*_{w.g}$ results in variation of the gear pitch helix within the corresponding interval $\psi^*_{w.g} \le \psi_{y.g} \le \psi_{f.g}$.

The pitch diameter $d_{w.g}$ of the gear should not be too small; its actual value should not be less than the gear base diameter $d_{b.g}$ (Figure 15.4); that is, the inequality $d_{w.g} \ge d_{b.g}$ has to be observed.

When the gear pitch diameter $d_{w.g}$ is smaller than the gear base diameter (when $d_{w.g} < d_{b.g}$), then the corresponding auxiliary rack $\mathscr{R}_T$ does not exist; no envelope can be generated for the consecutive positions of the gear tooth flank surface $\mathscr{G}$. This indicates that under such a scenario the first necessary condition of proper generation of the gear tooth surface is violated [128, 138, 143]. Therefore, in the event $d_{w.g} < d_{b.g}$ no auxiliary rack $\mathscr{R}_T$ can be generated.

The actual value of the profile angle ϕ_r of the auxiliary rack $\mathscr{R}_T$ depends on actual timing of the rotation ω_g and the translation V_g (Figure 15.2a). Two constraints are imposed on the actual value of the profile angle ϕ_r.

First, the profile angle cannot be too small. Theoretically, the smallest permissible value of the profile angle is $\phi_r = 0°$. Due to the necessity of creating an appropriate value of the normal clearance angle at the lateral cutting edges of the gear cutting tool, the minimum value of the profile angle is commonly set to $\phi_r \cong 10°$.

Second, the profile angle ϕ_r cannot be too big. A large profile angle ϕ_r results in a shorter top cutting edge of the gear cutting tool. Because of violation of the fifth necessary condition of proper part surface generation [128, 138, 143], a large profile angle may even cause pointing of the top cutting edge (Figure 15.4). The maximum allowed value of the profile angle ϕ_r is restricted by the inequality $\phi_r \le [\phi_r]$, where $[\phi_r]$ designates the limit value of the tooth profile angle, for which width of the top land of the auxiliary rack tooth does not exceed a certain critical value. The critical value of the length of the top land corresponds to the shortest allowed length of the top cutting edge of the gear cutting tool.

The minimal required face width F_r of the auxiliary rack $\mathscr{R}_T$ is equal to face width F_g of the work gear.

As shown in Figure 15.5, a tooth of the auxiliary rack $\mathscr{R}_T$ contacts the gear tooth flank $\mathscr{G}$ along the straight line. This straight line is commonly referred to as *characteristic line* E_g. The characteristic line E_g (i.e., $E_g \mapsto AB$) is in tangency with the base cylinder of the work gear and with the gear base helix (not shown in Figure 15.5). It is instructive to compare the gear tooth shown in Figure 15.5, with the screw involute surface depicted in Figure 1.13. The family of straight lines within the screw involute surface $\mathscr{G}$ in Figure 1.13 represents various configurations of the characteristic line E_g when the gear is rolling relative to the reference system $X_rY_rZ_r$. At a certain instant of time, the characteristic E_g is aligned with

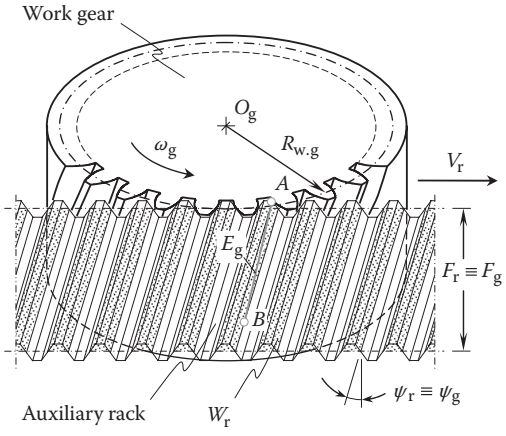

FIGURE 15.5
The auxiliary phantom rack $\mathscr{R}_T$ in mesh with a work gear. (From Radzevich, S.P., *ASME Journal of Mechanical Design*, 124, 772–786, 2002. With permission.)

the vector **C**. The ruled tooth flank surface $\mathscr{G}$ is generated as the family of consecutive positions of the characteristic E_g.

In order to make sure the generation of the work gear tooth flanks is completed, the minimum face width F_r of the auxiliary rack $\mathscr{R}_T$ must be represented in full by the gear cutting tool in the gear machining operation. For this purpose, the travel distance of the gear cutting tool in axial direction of the work gear must exceed the work gear face width.

It is important to stress here that the lateral plane of the auxiliary rack tooth is generated as an envelope to the consecutive positions of the gear tooth screw involute surface $\mathscr{G}$. This statement is evident and well known. It will be helpful below for derivation of an equation of the generating surface of the gear cutting tool.

15.3 Examples of Possible Types of Auxiliary Generating Surfaces of Gear Cutting Tools

The auxiliary generating surface $\mathscr{R}_T$ of the gear cutting tool that is generated when the gear rotates ω_g about its axis of rotation, and simultaneously it is translating V_g in the direction that is parallel to X_r axis of the Cartesian coordinate system $X_rY_rZ_r$ (Figure 15.2a) is the simplest example of the auxiliary generating surfaces. More examples of the auxiliary generating surfaces $\mathscr{R}_T$ can be derived on the premise of other types of kinematics of relative motion of the gear to be machined and of the reference system $X_rY_rZ_r$.

The gear to be machined can perform not just one translation in the direction that is parallel to the X_r axis, but two translations. The second translation can be performed along the Y_r axis of the coordinate system $X_rY_rZ_r$. In this case the resultant translation V_g is at an angle θ_r as depicted in Figure 15.6a.

For machining of gears with a different profile angle at the opposite sides of the tooth profile, the auxiliary generating rack $\mathscr{R}_T$ also features different profile angles $\phi_{r.1}$ and $\phi_{r.2}$ at the opposite sides of its tooth profile (Figure 15.6b). The base pitch for the opposite sides of the tooth profiles of the rack $\mathscr{R}_T$ is not of the same value. This is because the teeth flank pitch that is measured within the pitch plane is the same for both opposite sides of the tooth profile, while the profile angles $\phi_{r.1}$ and $\phi_{r.2}$ are not equal to each other.

Simultaneously with the rotation ω_g, the gear to be machined can perform an additional rotation ω_r with respect to the reference system $X_rY_rZ_r$. Depending on the parameters of the additional rotation ω_g, the auxiliary generating rack $\mathscr{R}_T$ is shaped in the form either of an internal gear sector (Figure 15.6c) or an external gear sector (Figure 15.6d). The radius of the pitch cylinder R_r of the auxiliary rack $\mathscr{R}_T$ is negative ($R_r < 0$) in the first case (Figure 15.6c), and positive ($R_r > 0$) in the second case (Figure 15.6d). Appropriate portions of the circular sectors can be employed as the auxiliary generating surfaces of the gear cutting tools.

15.4 Generation of Generating Surface of a Gear Cutting Tool

The generating surface of a gear cutting tool is an envelope to successive positions of the auxiliary generating surface in its motion relative to a reference system. After being

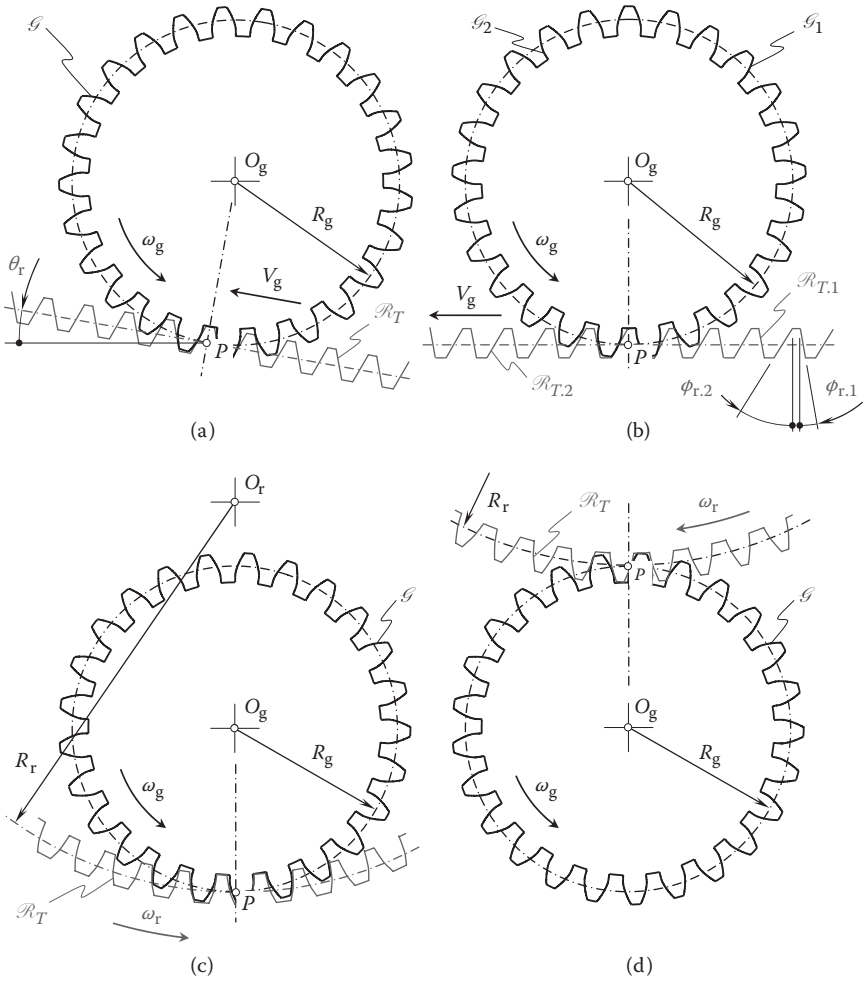

FIGURE 15.6
Examples of possible kinds of auxiliary generating surfaces $\mathscr{R}_T$ of a gear cutting tool.

designed, the gear cutting tool will be associated with this reference system. Such an approach for determining the generating surface of a gear cutting tool is aligned with the first Olivier principle [49] of the generation of enveloping surfaces.

For the specific case of a gear cutting tool, the following definition for the generating surface T can be derived from [128, 138, 143]:

Definition 15.1

The generating surface of a gear cutting tool is a screw surface that is conjugate to the gear tooth flank surface being machined.

Following the definition, corresponding formulae for computation of the major design parameters of the generating surface of the gear cutting tool can be derived.

15.4.1 Design Parameters of the Generating Surface of the Gear Cutting Tool

For the purpose of the creation of generating surface of the gear cutting tool an auxiliary generating rack $\mathscr{R}_T$ is used. The generating surface is an envelope to successive positions of the auxiliary rack $\mathscr{R}_T$ in its motion with respect to the gear cutting tool. At this point the generating surface is not constructed yet, so a Cartesian coordinate system $X_cY_cZ_c$ with which the gear cutting tool will be associated is considered instead.

Feasible motion of the auxiliary generating surface $\mathscr{R}_T$ relative to the reference system $X_cY_cZ_c$ strongly depends on the geometry of the actual surface $\mathscr{R}_T$. For the auxiliary generating surfaces that are shaped in the form of straight rack $\mathscr{R}_T$ (see Figures 15.2a and 15.6a and b), a screw motion of the rack $\mathscr{R}_T$ about the axis of rotation O_c of the gear cutting tool is feasible. For the auxiliary generating surfaces that are shaped in the form of a round rack $\mathscr{R}_T$ (see Figure 15.6c and d), a complex motion of the rack $\mathscr{R}_T$ about the axis of rotation O_c of the gear cutting tool could be feasible. This motion can be interpreted as superposition of the rotation $\boldsymbol{\omega}_r$ of the rack $\mathscr{R}_T$ about its axis of rotation O_r, and of the rotation $\boldsymbol{\omega}_c$ of the rack $\mathscr{R}_T$ about the axis of rotation O_c of the gear cutting tool. The resultant motion $\boldsymbol{\omega}_{scr} = \boldsymbol{\omega}_c + \boldsymbol{\omega}_r$ is feasible when the rotations $\boldsymbol{\omega}_r$ and $\boldsymbol{\omega}_c$ are synchronized with each other in timely proper manner.

The scenario when a straight rack $\mathscr{R}_T$ is performing a screw motion about axis O_c (see Figure 15.2a) is the simplest and most common one. In the screw motion the lateral planes of the rack $\mathscr{R}_T$ teeth generate envelopes that are conjugate to corresponding tooth flanks $\mathscr{G}$ of the gear. For further analysis it is convenient to investigate the geometry of an envelope to successive positions of a plane that is performing a screw motion.

Envelope to successive positions of a plane with a screw motion. Consider a plane $\mathscr{R}_T$ that is performing a screw motion. The plane $\mathscr{R}_T$ makes a certain angle τ_b with the X_0 axis of a Cartesian coordinate system $X_0Y_0Z_0$. The reduced pitch p of the screw motion is given. Axis X_0 is the axis of the screw motion.

The auxiliary coordinate system X_1Y_1 is rigidly connected to the plane $\mathscr{R}_T$ (Figure 15.7).

The equation of the plane $\mathscr{R}_T$ can be represented in the form

$$Y_1 = X_1 \tan \tau_b \tag{15.21}$$

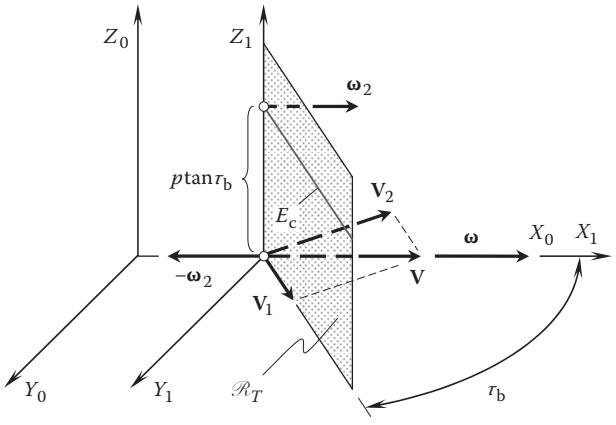

FIGURE 15.7
Generation of a screw involute surface as an envelope to successive positions of a plane that is performing a screw motion.

The auxiliary coordinate system $X_1Y_1Z_1$ performs the screw motion together with the plane $\mathscr{R}_T$. The screw motion is performing with respect to the motionless coordinate system $X_0Y_0Z_0$. In the coordinate system $X_1Y_1Z_1$, unit normal vector $\mathbf{n}_T$ to the plane $\mathscr{R}_T$ can be analytically expressed as

$$\mathbf{n}_T = \begin{bmatrix} 1 \\ -\tan\tau_b \\ 0 \\ 1 \end{bmatrix} \tag{15.22}$$

Position vector $\mathbf{r}_T$ of arbitrary point m of the plane $\mathscr{R}_T$

$$\mathbf{r}_T = \begin{bmatrix} X_T \\ Y_T \\ Z_T \\ 1 \end{bmatrix} \tag{15.23}$$

Speed of point m in the screw motion

$$\mathbf{v}_m = \mathbf{v} + [\boldsymbol{\omega} \times \mathbf{R}] \tag{15.24}$$

where

$\mathbf{v}$ = speed of translation
$\boldsymbol{\omega}$ = speed of rotation
$\mathbf{R}$ = position vector of the point m with respect to the axis of the screw motion (magnitude of the vector $\mathbf{R}$ is equal to the distance of the point m from the X_0 axis, and the vector $\mathbf{R}$ is pointed from the axis X_0 to the point m)

The direction of the vector $\mathbf{v}_m$ is of importance for determining the characteristic line E_c, while the magnitude of the vector $\mathbf{v}_m$ is out of interest (it is important to stress here that as shown in Figure 15.7 the characteristic line E_c and the characteristic line E_g in Figure 15.5 are two different characteristics). Because of this, it can be assumed that magnitude of the rotation vector $\boldsymbol{\omega}$ is equal $\omega = |\boldsymbol{\omega}| = 1$. Therefore

$$\boldsymbol{\omega} = \mathbf{i}, \quad \mathbf{v} = \mathbf{i} \cdot p \tag{15.25}$$

This yields

$$\mathbf{v}_M = \mathbf{i} \cdot p + \begin{vmatrix} \mathbf{i} & \mathbf{j} & \mathbf{k} \\ 1 & 0 & 0 \\ X_1 & Y_1 & Z_1 \end{vmatrix} \tag{15.26}$$

and

$$\mathbf{v}_M = \mathbf{i} \cdot p - \mathbf{j} \cdot Y_1 + \mathbf{k} \cdot Z_1 \tag{15.27}$$

The dot product of the unit normal vector $\mathbf{n}_T$ and of the speed $\mathbf{v}_m$ is equal to

$$\mathbf{n}_T \cdot \mathbf{v}_M = p \tan \tau_b - Z_1 = 0 \tag{15.28}$$

Thus, the equation of contact can be represented in the form

$$Z_1 = p \tan \tau_b \tag{15.29}$$

The equation for the position vector of a point of the characteristic line E_c

$$\mathbf{r}_E(t) = \begin{bmatrix} y \\ t \tan \tau_b \\ p \tan \tau_b \\ 1 \end{bmatrix} \tag{15.30}$$

is derived on the premise of simultaneous consideration of the equation of contact together with the equation that describes the plane $\mathscr{R}_T$ in its current configuration with respect to the axis of the screw motion.

In Equation (15.30), $\mathbf{r}_E$ designates the position vector of a point of the characteristic line E_c, and the parameter of the characteristic line E_c is denoted as t.

In the case under consideration, the characteristic E_c is the straight line of intersection of two planes. The plane $\mathscr{R}_T$ is the first of two planes. Another plane is parallel to the coordinate plane X_1Z_1 and is remote at the distance $p \tan\tau_b$.

For a given screw motion, the location of the characteristic line E_c within the plane $\mathscr{R}_T$ in the initial coordinate system $X_0Y_0Z_0$ remains the same.

The angle of rotation of the coordinate system $X_1Y_1Z_1$ about the X_0 axis is designated as ε. The translation of the coordinate system $X_1Y_1Z_1$ with respect to $X_0Y_0Z_0$ that corresponds to the angle ε is equal to $p\varepsilon$. This makes it possible for composing the operator $\mathbf{Rs}(1 \mapsto 0)$ of the resultant coordinate system transformation

$$\mathbf{Rs}(1 \mapsto 0) = \begin{bmatrix} 1 & 0 & 0 & p\varepsilon \\ 0 & \cos\varepsilon & \sin\varepsilon & 0 \\ 0 & -\sin\varepsilon & \cos\varepsilon & 0 \\ 0 & 0 & 0 & 1 \end{bmatrix} \tag{15.31}$$

In order to represent analytically the enveloping surface P, the equation $\mathbf{r}_E(t)$ of the characteristic E_c should be considered together with the operator $\mathbf{Rs}(1 \mapsto 0)$ of coordinate system transformation

$$\mathbf{r}_P(X_1, \varepsilon) = \mathbf{Rs}(1 \mapsto 0) \cdot \mathbf{r}_E(t) = \begin{bmatrix} X_1 + p\varepsilon \\ X_1 \tan \tau_b \cos\varepsilon + p \tan \tau_b \sin\varepsilon \\ -X_1 \tan \tau_b \sin\varepsilon + p \tan \tau_b \cos\varepsilon \\ 1 \end{bmatrix} \tag{15.32}$$

Consider the intersection of the enveloping surface P by the plane $X_0 = X_1 + p = 0$. The last equation yields representation in the form $X_1 = -p$. Therefore

$$\mathbf{r}_{X_0}(\varepsilon) = \begin{bmatrix} 0 \\ p\tan\tau_b(\sin\varepsilon - p\varepsilon\cos\varepsilon) \\ p\tan\tau_b(\cos\varepsilon + p\varepsilon\sin\varepsilon) \\ 1 \end{bmatrix} \tag{15.33}$$

Equation (15.33) describes the involute of a circle.

The radius of the base circle of the involute curve

$$r_b = p\tan\tau_b \tag{15.34}$$

Therefore, a screw involute surface allows for interpretation in the form of the envelope to successive positions of a plane $\mathcal{R}_T$ with a screw motion. The reduced pitch of the involute screw surface is equal to p, and the radius of the base cylinder is equal to $r_b = p\tan\tau_b$. The screw involute surface shares common points with the base cylinder. These points are within a helix. The tangent to the helix makes the angle ω_b with the axis of screw motion [1, 2]

$$\tan\omega_b = \frac{r_b}{p} \tag{15.35}$$

From this, one may conclude that $\tan\omega_b = \tan\tau_b$, and $\omega_b = \tau_b$. The straight characteristic E_c is tangent to the base helix of the enveloping surface P. This means that (a) if a plane A is tangent to the base cylinder, (b) a straight line E_c within the plane A makes the angle τ_b with the axis of the screw motion, and (c) the plane A rolls over the base cylinder without sliding, then the enveloping surface P can be represented as a locus of successive positions of the straight line E_c that rolls without sliding over the base cylinder together with the plane A. The enveloping surface is a screw involute surface.

The obtained screw involute surface (Figure 15.7) is that shown in Figure 1.13 and which is analytically described by Equation (15.16).

Another solution to the problem of determining the envelope of a plane with a screw motion is given by Cormac [13].

Principal elements of the geometry of the generating surface of the gear cutting tool. Figure 15.8 shows that the Cartesian coordinate system $X_cY_cZ_c$ is the reference system with which the gear cutting tool will be associated after it is designed.

In the coordinate system $X_cY_cZ_c$, relative motion of the auxiliary generating rack $\mathcal{R}_T$ can be represented as superposition of two motions. The rotation ω_c about the axis O_c of the gear cutting tool is the first of two motions. The translation of the rack $\mathcal{R}_T$ is the second motion. The speed of the translation is denoted as $\mathbf{V}_{\Sigma T}$.

Speed $\mathbf{V}_{\Sigma T}$ of the translation can be decomposed onto two components (Figure 15.8)

$$\mathbf{V}_{\sum T} = \mathbf{V}_T + \mathbf{V}_{\mathrm{sl}.T} \tag{15.36}$$

The first component $\mathbf{V}_T$ is pointed along the axis O_c of the gear cutting tool. Magnitude $V_T = |\mathbf{V}_T|$ of this component is equal to

$$V_T = \frac{V_{\sum T}}{\cos\zeta_c} \tag{15.37}$$

where ζ_c denotes the setting angle of the gear cutting tool.

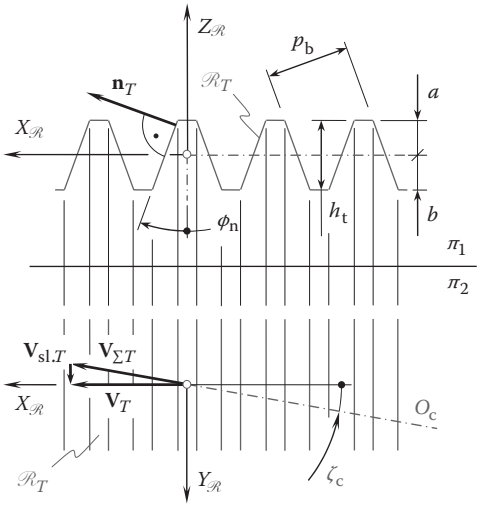

FIGURE 15.8
A screw motion of the auxiliary generating rack $\mathscr{R}_T$ about the axis O_c.

The second component $\mathbf{V}_{sl.T}$ is along the straight generating line of the auxiliary rack $\mathscr{R}_T$. Sliding of the rack $\mathscr{R}_T$ over itself is caused by this motion. Due to the sliding, this motion does not affect the shape of the envelope, and thus it can be omitted from further consideration. Eventually, the resultant motion of the auxiliary generating rack $\mathscr{R}_T$ relative to the reference system $X_cY_cZ_c$ is a kind of screw motion. Axis O_c is the axis of the screw motion. The parameter of the screw motion p_c is equal to

$$p_c = \frac{V_T}{\omega_c} = \frac{V_{\Sigma T}}{\omega_c \cos\zeta_c} = \frac{\omega_g}{\omega_c} \cdot \frac{r_{w.g}}{\cos\zeta_c} \tag{15.38}$$

Owing to the ratio

$$\frac{\omega_c}{\omega_g} = \frac{N_g}{N_c} \tag{15.39}$$

the following expression

$$p_c = \frac{N_c r_{w.g}}{N_g \cos\zeta_c} \tag{15.40}$$

can be used for the computation of parameter of the screw motion p_c.

A screw involute surface is the envelope to successive positions of the lateral plane of the auxiliary rack $\mathscr{R}_T$ in its screw motion about the axis O_c. The radius of base cylinder $r_{b.c}$ of this screw involute surface is equal

$$r_{b.c} = p_c \tan\varphi \tag{15.41}$$

where φ denotes the angle that the axis O_c makes with the lateral plane of the auxiliary rack tooth.

In the case under consideration, the characteristic line E_c is a line within the lateral plane of the rack tooth at which perpendicular $\mathbf{n}_T$ to the plane $\mathscr{R}_T$ makes certain angle ε with the axis O_c of the screw motion. The value of the angle ε can be computed from Ball's formula [1, 2]

$$\varepsilon = \tan^{-1}\left(\frac{\varphi}{r_i}\right) \tag{15.42}$$

where r_i is the shortest distance of approach of the straight line along $\mathbf{n}_T$ and the axis O_c of the screw motion.

When a plane performs a screw motion, the characteristic is the straight line at a distance r_i from the axis O_c of the screw motion. The characteristic makes an angle φ with the axis O_c. The value of the angle φ can be determined analytically. For this purpose, unit normal vector $\mathbf{n}_T$ to the lateral plane of the auxiliary rack tooth surface $\mathscr{R}_T$ is utilized. Consider a Cartesian coordinate system $X_{\mathscr{R}}Y_{\mathscr{R}}Z_{\mathscr{R}}$ associated with the auxiliary rack $\mathscr{R}_T$ as shown in Figure 15.8. In the reference system $X_{\mathscr{R}}Y_{\mathscr{R}}Z_{\mathscr{R}}$, unit normal vector $\mathbf{n}_T$ can be analytically expressed in the form

$$\mathbf{n}_T = \mathbf{i}\cdot\cos\phi_n + \mathbf{k}\cdot\sin\phi_n \tag{15.43}$$

Unit vector $\mathbf{a}$ is a vector along the axis O_c. (The unit vector $\mathbf{a}$ is aligned with the vector $\mathbf{V}_{\Sigma T}$.) It can be analytically represented in the form

$$\mathbf{a} = \mathbf{i}\cdot\cos\zeta_c - \mathbf{j}\cdot\sin\zeta_c \tag{15.44}$$

Because the vectors $\mathbf{n}_T$ and $\mathbf{a}$ are of unit length, then the equality $\cos(90° - \varphi) = \mathbf{n}_T \cdot \mathbf{a}$ is observed. This expression casts into the formula

$$\varphi = \sin^{-1}(\cos\phi_n \cos\zeta_c) \tag{15.45}$$

for the computation of the angle φ.

Equation (15.45) allows for an expression

$$d_{b.c} = \frac{d_{w.g}N_c\cos\phi_n}{N_g\sqrt{1-\cos^2\phi_n\cos^2\zeta_c}} \tag{15.46}$$

for the computation of base diameter $d_{b.c}$ of the generating surface of the gear cutting tool.

For gear cutting tools with a standard tooth profile (for which tooth thickness t and space width w on the pitch diameter are equal to each other), Equation (15.46) reduces to

$$d_{b.c} = \frac{mN_c\cos\phi_n}{\sqrt{1-\cos^2\phi_n\cos^2\zeta_c}} \tag{15.47}$$

The axial pitch of the screw involute surface can be computed from the formula

$$P_{x.c} = \frac{\pi d_{w.g}}{N_g \cos \zeta_c} \tag{15.48}$$

For the computation of base pitch $p_{b.c}$ of the gear cutting tool, the formula

$$p_{b.c} = P_{x.c} \sin \varphi = \frac{\pi d_{w.g} \cos \phi_n \cos \zeta_c}{N_g \cos \zeta_c} = \frac{\pi d_{b.g}}{N_g} \equiv p_{b.g} \tag{15.49}$$

can be used.

The above equations are used for the derivation of equations for the computation of the design parameter of involute hobs and other gear cutting tools.

Within the characteristic line E_c a perpendicular $\mathbf{n}_T$ is orthogonal to the vector of speed $\mathbf{V}_T$ of the linear motion.

15.4.2 Equation of the Generating Surface of the Gear Cutting Tool

Lateral cutting edges of a precision gear cutting tool (e.g., of a precision involute hob) are within the generating surface *T*. Any displacements of the lateral cutting edges out of the generating surface *T* cause the gear cutting tool errors. Generating surface *T* of the gear cutting tool serves as the only reliable reference surface for computation of deviations of the actual machining surface T_m of the gear cutting tool from its desired shape *T*.

For the derivation of an equation of the generating surface *T*, consider an auxiliary generating surface $\mathscr{R}_T$ (Figure 15.9). The auxiliary rack $\mathscr{R}_T$ is associated with a left-hand–oriented Cartesian coordinate system $X_rY_rZ_r$. The pitch plane of the rack is at a distance $0.5d_{w.c}$ from the Z_r axis, and it is parallel to the X_rZ_r coordinate plane. Here, $d_{w.c}$ denotes the pitch diameter of the gear cutting tool. In the coordinate system $X_rY_rZ_r$, the equation of the lateral tooth surface of the auxiliary rack $\mathscr{R}_T$ yields matrix representation

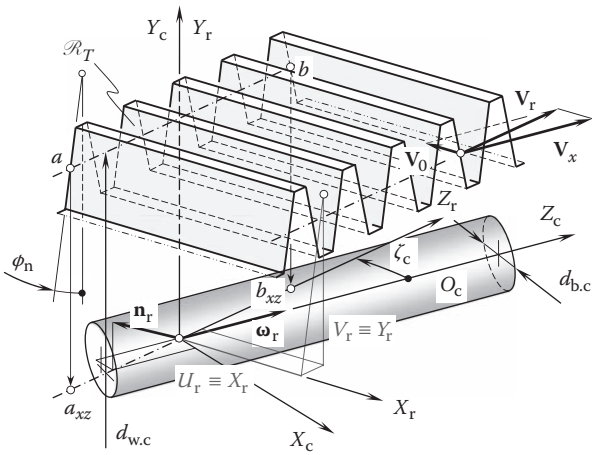

FIGURE 15.9
Configuration of the auxiliary generating rack $\mathscr{R}_T$ with respect to the axis of rotation O_c of a gear cutting tool.

$$\mathbf{r}_{\mathrm{r}}(U_{\mathrm{r}}, V_{\mathrm{r}}) = \begin{bmatrix} U_{\mathrm{r}} \\ V_{\mathrm{r}} \\ V_{\mathrm{r}} \tan\phi_{\mathrm{n}} \\ 1 \end{bmatrix} \tag{15.50}$$

It is assumed in Equation (15.50) that $U_{\mathrm{r}} = X_{\mathrm{r}}$ and $V_{\mathrm{r}} = Y_{\mathrm{r}}$. Therefore the equality $V_{\mathrm{r}}\tan\varphi_{\mathrm{n}} = Z_{\mathrm{r}}$ is observed.

In order to generate the generating surface T of the gear cutting tool, it is necessary to represent Equation (15.50) in the left-hand–oriented Cartesian coordinate system $X_{\mathrm{c}}Y_{\mathrm{c}}Z_{\mathrm{c}}$ that is associated with the gear cutting tool. The reference systems $X_{\mathrm{r}}Y_{\mathrm{r}}Z_{\mathrm{r}}$ and $X_{\mathrm{c}}Y_{\mathrm{c}}Z_{\mathrm{c}}$ share common axis $Y_{\mathrm{r}} \equiv Y_{\mathrm{c}}$. They are turned about this axis through the setting angle ζ_{c}. Therefore, in the coordinate system $X_{\mathrm{c}}Y_{\mathrm{c}}Z_{\mathrm{c}}$, the expression for the position vector $\mathbf{r}_{\mathrm{r}}^{(\mathrm{c})}$ of a point of the auxiliary rack $\mathscr{R}_T$ can be represented in the form

$$\mathbf{r}_{\mathrm{r}}^{(\mathrm{c})}(U_{\mathrm{r}}, V_{\mathrm{r}}) = \mathbf{Rt}(\zeta_{\mathrm{c}}, Y_{\mathrm{r}}) \cdot \mathbf{r}_{\mathrm{r}}(U_{\mathrm{r}}, V_{\mathrm{r}}) \tag{15.51}$$

Furthermore, consider a screw motion that the auxiliary rack $\mathscr{R}_T$ performs about the Z_{c} axis. The reduced pitch (parameter) of the screw motion is denoted as p_{c}.

The screw motion of the auxiliary generating rack $\mathscr{R}_T$ can be decomposed on two elementary motions. The translation along the Z_{c} axis is the first of two elementary motions. The translation of the rack $\mathscr{R}_T$ along Z_{c} axis through a certain distance a_z is caused by this elementary motion. The coordinate system transformation due to the translation can be described analytically by the operator of translation $\mathbf{Tr}(a_Z, Z_{\mathrm{c}})$. Rotation about the Z_{c} axis is the second of two elementary motions. This elementary motion causes rotation of the auxiliary rack $\mathscr{R}_T$ about the Z_{c} axis through a certain angle θ_z. The coordinate system transformation due to the rotation can be described analytically by the operator of rotation $\mathbf{Rt}(\theta_z, Z_{\mathrm{c}})$. Here, the actual values of the translation a_z and the rotation θ_z are not important. Only the ratio a_z/θ_z is of critical importance for the analysis that follows. The ratio a_z/θ_z is equal to the reduced pitch p_{c} of the screw motion of the auxiliary rack $\mathscr{R}_T$ in the case under consideration ($a_z/\theta_z = p_{\mathrm{c}}$).

The coordinate system transformation due to the screw motion of the auxiliary generating rack $\mathscr{R}_T$ can be analytically described by the operator of the resultant coordinate system transformation $\mathbf{Rs}(\mathscr{R} \mapsto \mathrm{c})$. The operator yields representation in the form of product

$$\mathbf{Rs}(\mathscr{R} \mapsto \mathrm{c}) = \mathbf{Rt}(\theta_z, Z_{\mathrm{c}}) \cdot \mathbf{Tr}(a_z, Z_{\mathrm{c}}) \tag{15.52}$$

The auxiliary rack $\mathscr{R}_T$ in its current location in the screw motion is described by the matrix equation

$$\bar{\mathbf{r}}_{\mathrm{r}}^{(\mathrm{c})}(U_{\mathrm{r}}, V_{\mathrm{r}}, \theta_z) = \mathbf{Rs}(\mathscr{R} \mapsto \mathrm{c}) \cdot \mathbf{r}_{\mathrm{r}}^{(\mathrm{c})}(U_{\mathrm{r}}, V_{\mathrm{r}}) \tag{15.53}$$

In Equation (15.53), the position vector $\bar{\mathbf{r}}_{\mathrm{r}}^{(\mathrm{c})}$ of a point depends on the rotation angle θ_z. Due to the equality ($a_z/\theta_z = p_{\mathrm{c}}$) being observed, position vector $\bar{\mathbf{r}}_{\mathrm{r}}^{(\mathrm{c})}$ can be expressed not in terms of the rotation angle θ_z, but in terms of the translation a_z instead.

Further, consider the family of the auxiliary rack tooth surfaces $\bar{\mathbf{r}}_{\mathrm{r}}^{(\mathrm{c})}$ along with the equation of contact $\mathbf{n}_T \cdot \mathbf{V}_{\mathrm{r-c}} = 0$. In the last equation, the unit normal vector of the rack tooth

surface $\bar{\mathbf{r}}_r^{(c)}$ is designated as $\mathbf{n}_T$, and $\mathbf{V}_{r-c}$ denotes the relative screw motion of the auxiliary rack with respect to the reference system $X_cY_cZ_c$.

The generating surface T of the gear cutting tool can be analytically described by Equation (15.53) together with the equation of contact. Omitting bulky formulae transformation, the generating surface of the gear cutting tool T is represented in matrix form by the following equation

$$\left.\begin{array}{l}\text{Generating surface } T\\ \text{of a gear cutting tool}\end{array}\right| \quad \Rightarrow \quad \mathbf{r}_c(U_c, V_c) = \begin{bmatrix} 0.5d_{b.c}\sin V_c - U_c \sin\psi_{b.c}\cos V_c \\ 0.5d_{b.c}\cos V_c + U_c \sin\psi_{b.c}\sin V_c \\ p_{b.c}V_c - U_c\cos\psi_{b.c} \\ 1 \end{bmatrix} \tag{15.54}$$

where

U_c, V_c = curvilinear (Gauss) coordinates of a point of the generating surface T
$d_{b.c}$ = base diameter of the screw involute surface T
$p_{b.c}$ = base pitch of the screw involute surface T
$\psi_{b.c}$ = base helix angle of the generating surface T

In the case under consideration, the generating surface T is a kind of screw involute surface that is conjugate to the gear tooth flanks $\mathscr{G}$. Figure 15.10 illustrates an example of the generating surface T of the gear cutting tool.

Equation (15.54) can be expressed in terms of the design parameters of the gear cutting tool. For this purpose, the set of engineering gear equations is used (see Appendix A).

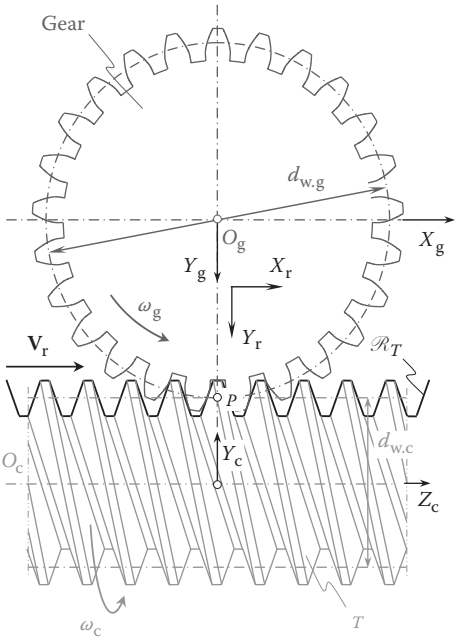

FIGURE 15.10
Generating surface T of a cylindrical gear cutting tool. (From Radzevich, S.P., *ASME Journal of Mechanical Design*, 129, 334–345, 2007. With permission.)

Equation (15.54) immediately allows for an analytical representation of a perpendicular to the generating surface T of the gear cutting tool. The unit normal vector $\mathbf{n}_c$ can be computed from Equation (15.54) as cross product $\mathbf{n}_c = \mathbf{u}_c \times \mathbf{v}_c$ of the two unit vectors $\mathbf{u}_c$ and $\mathbf{v}_c$. The unit vector $\mathbf{u}_c$ is aligned with the coordinate line U_c on the generating surface T. The unit vector $\mathbf{v}_c$ is tangent to the coordinate curve V_c on the surface T. Unit vectors $\mathbf{u}_c$ and $\mathbf{v}_c$ are equal to $\mathbf{u}_c = \mathbf{U}_c/|\mathbf{U}_c|$ and $\mathbf{v}_c = \mathbf{V}_c/|\mathbf{V}_c|$ correspondingly. Here, $\mathbf{U}_c = \partial \mathbf{r}_c/\partial U_c$ and $\mathbf{V}_c = \partial \mathbf{r}_c/\partial V_c$.

For the case under consideration, unit normal vector $\mathbf{n}_c$ is equal to

$$\mathbf{n}_c = \begin{bmatrix} \sin\psi_{b.c} \sin V_c \\ \sin\psi_{b.c} \cos V_c \\ \cos\psi_{b.c} \\ 1 \end{bmatrix} \tag{15.55}$$

Equation (15.54) allows for computation of the rest of the design parameters of generating surface of the gear cutting tool as well.

15.4.3 Setting Angle of the Gear Cutting Tool

The orientation of the auxiliary generating rack $\mathscr{R}_T$ with respect to the axis of rotation O_c is an important consideration. In the case considered above (Figures 15.9 and 15.10), the axis of rotation O_c is parallel to the pitch plane W_r of the auxiliary rack. In this way a cylindrical generating surface T of the gear cutting tool is obtained. However, the axis O_c can occupy various configurations while within the pitch plane W_r. This variation of orientation of the auxiliary rack $\mathscr{R}_T$ with respect to the axis O_c is illustrated in Figure 15.11.

The auxiliary generating rack makes a certain angle ψ_r with the axis of rotation O_g of the gear. Commonly, this angle is referred to as *helix angle* of the auxiliary rack $\mathscr{R}_T$. The axis of rotation O_c of the gear cutting tool is passing through the center distance $C_{g/c}$. In Figure 15.11, the center distance is depicted as a point $C_{g/c}$ of intersection of the center distance itself and the pitch plane W_r of the auxiliary generating rack $\mathscr{R}_T$.

The straight line ${}^0O_c$ (which is parallel to the pitch plane W_r) through the point $C_{g/c}$ is orthogonal to the line along the tooth of the auxiliary rack $\mathscr{R}_T$. For a spur gear, the line ${}^0O_c$ is parallel to the gear face. The axis of rotation of the gear cutting tool makes a certain angle with the straight line ${}^0O_c$. The axis of rotation of the gear cutting tool with a configuration that is denoted as ${}^+O_c$ makes a positive angle $\zeta_c > 0°$ with the straight line ${}^0O_c$. The axis of rotation of the gear cutting tool with a configuration that is designated as ${}^-O_c$

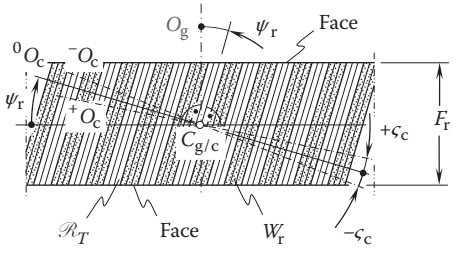

FIGURE 15.11
Setting angle ζ_c of a gear cutting tool. (From Radzevich, S.P., *ASME Journal of Mechanical Design*, 124, 772–786, 2002. With permission.)

makes a negative angle $\zeta_c < 0°$ with the same straight line ${}^0O_c$. It is convenient to use the designation $+\zeta_c$ for positive ($\zeta_c > 0°$) inclination of the axis of rotation of the gear cutting tool, and it is convenient to use the designation $-\zeta_c$ for negative ($\zeta_c < 0°$) inclination of the axis of rotation of the gear cutting tool. Commonly, the angle ζ_c is referred to as the *setting angle* of the gear cutting tool ([112, 146] and others). It is important to stress here that setting angle ζ_c is a *design parameter* of the gear cutting tool. Its value is not mandatory equal to the helix angle ψ_c of the gear cutting tool.

The actual value of the setting angle ζ_c is usually close or equal to the corresponding pitch helix angle ψ_c of the gear cutting tool. This is the major reason for why the angles ζ_c and ψ_c are often not distinguished from each other. However, they are the angles of completely different nature.

Setting angle ζ_c. The concept of the setting angle of the gear cutting tool has been introduced and discussed in detail earlier ([112, 146] and others).

Definition 15.2

Setting angle ζ_c of the gear cutting tool is the angle that complements (adds to 90°) the angle between (a) the projection of the axis of rotation of the gear cutting tool onto the pitch plane W_r of the auxiliary generating surface $\mathscr{R}_T$, and (b) the perpendicular to the auxiliary rack $\mathscr{R}_T$ tooth, which is constructed within the pitch plane W_r of the auxiliary rack $\mathscr{R}_T$.

For a given gear cutting tool, the cutting tool setting angle ζ_c has a particular constant value ($\zeta_c = \text{const}$). The value of the cutting tool setting angle ζ_c does not depend on the current pitch diameter $d_{w.c}$ of the gear cutting tool, while helix angle ψ_c of the gear cutting tool is a function of the diameter $d_{w.c}$ (i.e., a relationship $\psi_c = \psi_c(d_{w.c}, ...)$ is observed). Comparison of the equations $\zeta_c = const$ and $\psi_c = \psi_c(d_{w.c}, ...)$ makes evident the difference between the angles ζ_c and ψ_c.

Pitch diameter $d_{w.c}$ changes after each resharpening of the gear cutting tool. For example, its value reduces after each regrinding of a gear hob. Its value also reduces after each re-dressing of the grinding worm. For gear cutting tools with an enveloping generating surface *T*, an increase of the pitch diameter $d_{w.c}$ is observed after each resharpening or re-dressing of the gear cutting tool.

A clear understanding of the difference between the gear cutting tool setting angle ζ_c and the pitch helix angle ψ_c is of critical importance for the designer of gear cutting tools. In order to emphasize the difference between the design parameters ζ_c and ψ_c, it is instructive to compute the actual value of the helix angle ψ_c for a gear hob with a zero value of the setting angle ($\zeta_c = 0°$). This computation is performed below for a single-start FETTE gear hob (DIN8002A, Cat. No. 2022, Ident. No. 1202055) of module $m = 10$mm, outer diameter $d_{o.c} = 140$mm, and normal pressure angle $\phi_n = 20°$ [17]. The computations [132] reveal that the helix angle for the gear hob with a setting angle $\zeta_c = 0°$ is equal to $\psi_c = 2.490°$. It is evident that the pitch helix angle $\psi_c = 2.490°$ is not identical to the setting angle $\zeta_c = 0°$. The difference $\delta = |\zeta_c - \psi_c| = 2.490°$ of values between the angles ζ_c and ψ_c is of significant value and cannot be neglected when computing the design parameters of a precision gear hob.

Let us assume that that same involute hob is designed not with a zero setting angle, but with the setting angle of value $\zeta_c = 2.490°$. Computations of the helix angle ψ_c for the involute hob with this set of the design parameters return $\psi_c = 2.492°$ [132]. The difference $\delta = |\zeta_h - \psi_c| = 0.002°$ in this case is negligibly small.

The consideration above makes it clear that the angles ζ_c and ψ_c are two different design parameters of the gear cutting tool. Moreover, it is shown below that the gear cutting tool setting angle ζ_c is the major design parameter, while pitch helix angle ψ_c of the gear cutting tool is a design parameter of secondary importance, the actual value of which can be expressed in terms of the angle ζ_c. In the gear machining operation, the crossed-axis angle Σ is equal to the difference $\Sigma = 90° - \zeta_c$, regardless of the actual value of the helix angle ψ_c on the pitch cylinder of the gear cutting tool.

15.4.4 Complementary Equations

The parameter (the reduced pitch) of the screw motion is

$$p_c = d_{w.g}\omega_g/2\omega_c \cos\zeta_c \tag{15.56}$$

For single-start involute hobs of conventional design, this equation reduces to

$$p_c = d_{w.g}/2N_c \cos\zeta_c \tag{15.57}$$

where the number of starts of the gear cutting tool is denoted by N_c.

When the axis of the screw motion O_c is parallel to the pitch plane W_r of the auxiliary generating rack $\mathscr{R}_T$, the generating surface T is shaped in the form of a cylindrical involute worm (Figure 15.9). In the screw motion, the plane surfaces of the top land of the auxiliary rack $\mathscr{R}_T$, and the planes of the root land generate two coaxial surfaces of circular cylinders (Figure 15.10). The first one is the inner cylinder of the gear cutting tool, and the second one is the outer cylinder of the gear cutting tool.

The envelope to successive positions of the lateral plane surfaces of the auxiliary rack $\mathscr{R}_T$ are shaped in the form of screw involute surfaces.

Equation (15.54) describes the generating surface T of the involute gear cutting tool. The position vector of a point $\mathbf{r}_c$ is expressed here in terms of curvilinear (Gauss') U_c and V_c coordinates. It is easy to verify that cross-section of the surface T by a plane $Z_c = const$ is an involute curve having a base circle of radius $r_{b.c}$.

Equation (15.54) yields the formula for the computation of the base diameter $d_{b.c}$ of the generating surface T

$$d_{b.c} = 2r_{b.c} = \frac{mN_c \cos\phi_n}{\sqrt{1 - \cos^2\phi_n \cos^2\zeta_c}} \tag{15.58}$$

where m is the module of the gear cutting tool.

Equation (15.58) indicates that the base diameter depends only on module m of the gear cutting tool, the number of its starts Z_c, the normal profile angle ϕ_n of the auxiliary generating rack $\mathscr{R}_T$, and finally on the setting angle ζ_c of the gear cutting tool.

The base diameter of generating surface of the gear cutting tool can be expressed in terms of the pitch P_c of the surface T. Taking into account that the equality $m = 25.4/P_c$ is observed, then Equation (15.58) casts into the form

$$d_{b.c} = \frac{25.4N_c \cos\phi_n}{P_c\sqrt{1 - \cos^2\phi_n \cos^2\zeta_c}} \tag{15.59}$$

Helix angle ψ_c of the gear cutting tool often (but not mandatorily) is approximately equal to the setting angle ζ_c of the gear cutting tool (i.e., the approximate equality $\psi_c \cong \zeta_c$ is commonly observed). Under the assumption that the equality $\psi_c \cong \zeta_c$ is valid, Equation (15.59) can be simplified to the form

$$d_{b.c} \cong \frac{25.4N_c \cos\phi_n}{P_c\sqrt{1-\cos^2\phi_n \cos^2\psi_c}} \tag{15.60}$$

Equation (15.54) also yields the formula for the computation of base helix angle $\psi_{b.c}$ of generating surface T of the gear cutting tool

$$\psi_{b.c} = \tan^{-1}\left(\frac{\sqrt{\sin^2\phi_n + \tan^2\zeta_c}}{\cos\phi_n}\right) \tag{15.61}$$

It is important to stress here that setting angle ζ_c of the gear cutting tool is incorporated into Equation (15.61).

Equation (15.61) is equivalent to the equation

$$\psi_{b.c} = \cos^{-1}(\cos\phi_n \cos\zeta_c) \tag{15.62}$$

for the computation of the base helix angle $\psi_{b.c}$ that is proposed by Radzevich [130].

Equations (15.61) and (15.62) are used for the computation of

(1) The axial pitch $P_{x.c}$ of the gear cutting tool

$$P_{x.c} = \pi d_{b.c} \tan\psi_{b.c} \tag{15.63}$$

(2) The base pitch of the gear cutting tool

$$p_{b.c} = P_{x.c} \cos\phi_n \cos\zeta_c \tag{15.64}$$

as well as many other design parameters of the gear cutting tool.

The formula used for computation of the setting angle of the gear cutting tool can also be derived from Equation (15.54)

$$\zeta_c = \tan^{-1}\left(\frac{mN_c}{\sqrt{(d_{o.c} - 2.5m - \Delta d_{o.c})^2 - m^2Z_c^2}}\right) \tag{15.65}$$

where

$d_{o.c}$ = outer diameter of the gear cutting tool
$\Delta d_{o.c}$ = decrease of the outer diameter of the gear cutting tool; it is equal to $\Delta d_{o.c} = (d_{o.c}^{(n)} - d_{o.c}^{(w)})/2$
$d_{o.c}^{(n)}$ = outer diameter of the new gear cutting tool
$d_{o.c}^{(w)}$ = outer diameter of the completely worn gear cutting tool

The following statements [112, 146, 158] immediately follow from the analysis of Equation (15.54):

- The curvature of the involute profile of the generating surface T at all points at the base cylinder (i.e., at the start points of the screw involute surface) is equal to infinity, and it is equal to zero at infinity.
- The principal curvatures of the involute generating surface of the gear cutting tool at the points within the base helix are equal to $k_{1.c} \to \infty$ and $k_{2.c} = 0$ correspondingly.
- There is an infinite number of points at which the expressions $k_{1.c} \to \infty$ and $k_{2.c} = 0$ are valid.
- The first principal curvature of the generating surface of the gear cutting tool is equal to zero ($k_{1.c} = 0$) at points within the straight generating line of the surface T, while the second principal curvature is equal to infinity ($k_{2.c} \to \infty$) at points within the base helix.
- The straight generating line (i.e., the straight-line element of the involute generating surface of the gear cutting tool) is tangent to the helix on the base cylinder. Normal vectors to the involute surface—those along the straight-line element of the generating surface of the involute gear cutting tool—do not change their orientation; they are located within a common plane.

The above-listed statements are based on implementation of the formulae for the computation of fundamental magnitudes of the first and second order (see Chapter 1) of the generating surface T of the gear cutting tool.

15.5 Use of the *DG*-Based Methods for Determining the Design Parameters of the Generating Surfaces of the Gear Cutting Tools

In order to get an all-inclusive understanding of the geometry of the generating surface T of the gear cutting tool, in addition to the analytical investigation performed above, it is helpful to consider a *DG*-based (i.e., a descriptive-geometry-based) approach for investigating the geometry of the involute screw surface. Use of the *DG*-based approach provides a fruitful insight to the development and validation of the results of implementation of the *DG/K*-based approach. Usually, results of implementation of the *DG*-based methods serve as the perfect "filter" for the eliminating of rough errors of the analysis. Both approaches, namely the *DG*-based, as well as *DG/K*-based approach complement one another. Together, they provide the user with a profound understanding of the geometry of the generating surface of the gear cutting tool ([11, 92–94, 112, 130, 146], and others). As an example, the base helix angle and base diameter of the generating surface of the gear cutting tool are determined below using the *DG*-based approach of the analysis.

15.5.1 Base Helix Angle $\psi_{b.c}$ of the Generating Surface of the Gear Cutting Tool

For solving the problem of determining the base helix angle $\psi_{b.c}$, the actual values of the normal pressure angle ϕ_n as well as of the setting angle ζ_c of the gear cutting tool must be given.

Base helix angle $\psi_{b.c}$ can be constructed in a system of planes of projections $\pi_1\pi_2\pi_3$. In case of necessity, additional auxiliary plane(s) of projections can be constructed as well.

At the beginning, it is necessary to construct the lateral tooth surface of the auxiliary generating rack $\mathscr{R}_T$. A possible way for the construction of the lateral plane of the auxiliary generating rack $\mathscr{R}_T$ is as follows.

Consider an arbitrary plane A that is perpendicular to the axis of projections π_1/π_2 (Figure 15.12). The plane A is specified by the traces A_1 and A_2 onto the horizontal π_1 and the vertical π_2 planes of projections. Next, turn the plane A about the trace A_2 through the setting angle ζ_c of the gear cutting tool to the position Q. The plane Q is specified by the traces Q_1 and Q_2, the second of which is aligned with the trace A_2 of the plane A. After that, the plane Q is turned about the trace Q_1 through the normal profile angle ϕ_n of the gear cutting tool. In this final location, the plane is designated as $\mathscr{R}_T$. It is specified by the traces $\mathscr{R}_{T.1}$ and $\mathscr{R}_{T.2}$, respectively.

In order to construct base helix angle $\psi_{b.c}$ for this particular configuration (location and orientation) of the plane $\mathscr{R}_T$, an auxiliary plane of projections π_4 is constructed so that the axis of projections π_1/π_4 is perpendicular to the trace $\mathscr{R}_{T.1}$.

Base helix angle $\psi_{b.c}$ of the gear cutting tool is the angle that the lateral rack surface $\mathscr{R}_T$ makes with a plane, which is (a) orthogonal to the horizontal plane of projections π_1, and (b) orthogonal to the trace $\mathscr{R}_{T.4}$. Use of conventional rules—those developed in descriptive geometry—allows for construction of base helix angle $\psi_{b.c}$ of the gear cutting tool, as well as of base lead angle $\lambda_{b.c}$ of the generating surface of the gear cutting tool. The latter complements base helix angle $\psi_{b.c}$ to the right angle (Figure 15.12).

The derived *DG*-based solution to the problem of determining base helix angle $\psi_{b.c}$ gives an insight into how the expressions [see Equations (15.61 and 15.62)] can be derived analytically. It also serves as a perfect tool for verification of the results of the analytical solution to the problem.

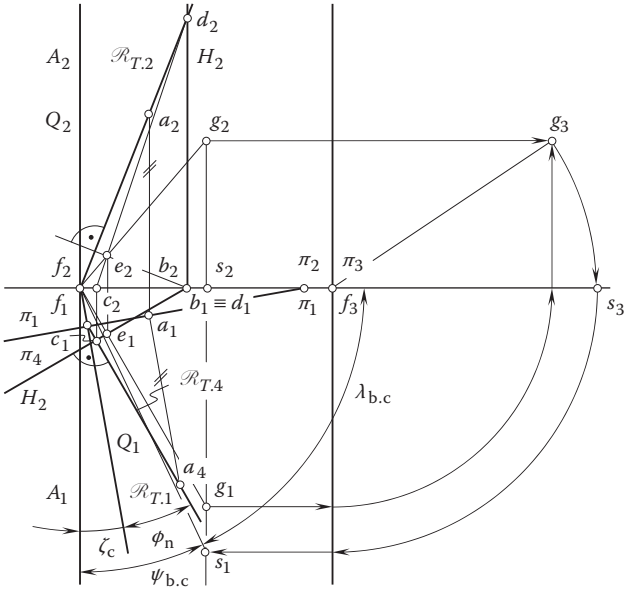

FIGURE 15.12
Determination of base helix angle $\psi_{b.c}$ of generating surface T of an involute gear cutting tool. (From Radzevich, S.P., *ASME Journal of Mechanical Design*, 129, 334–345, 2007. With permission.)

15.5.2 Base Diameter $d_{b.c}$ of the Generating Surface of the Gear Cutting Tool

Let us again begin with the analysis of the property in accordance to which generating surface T of the gear cutting tool can be represented as an enveloping surface to successive positions of the lateral plane of the tooth of the auxiliary generating surface $\mathscr{R}_T$.

Consider the plane $\mathscr{R}_T$, configuration of which (location and orientation) is specified in a system of planes of projections $\pi_1\pi_2\pi_3$, as shown in Figure 15.13. The plane $\mathscr{R}_T$ performs a translation along the π_1/π_2 axis of projections. The velocity of the translation is designated as $\mathbf{V}_r$. Simultaneously, the plane $\mathscr{R}_T$ rotates about that same axis π_1/π_2 with an angular velocity ω_r.

The base diameter $d_{b.c}$ of the gear cutting tool is equal to the shortest distance of approach between the characteristic line E_c and the axis π_1/π_2 of the screw motion. In order to determine the characteristic line E_c, it is necessary to select those points within the plane $\mathscr{R}_T$, the resultant velocity of which is perpendicular to the normal vector $\mathbf{n}_r$ to the plane $\mathscr{R}_T$ itself. To do that, velocity $\mathbf{V}_r$ of the translation is required to be considered together with linear velocity of the rotation $\boldsymbol{\omega}_r$. Those points within the plane $\mathscr{R}_T$, the resultant velocity $\mathbf{V}^{\Sigma}$ of which is perpendicular to the normal vector $\mathbf{n}_r$, are the points of the characteristic line E_c. In the case under consideration, the characteristic line E_c is the straight line at a distance $d_{b.c}/2$ from the axis of rotation π_1/π_2 of the gear cutting tool. The characteristic line E_c crosses the axis π_1/π_2 at the base helix angle $\psi_{b.c}$.

The *DG*-based solution to the problem of the determining of base diameter $d_{b.c}$ is depicted in Figure 15.13. The derived solution to the problem of determining base diameter $d_{b.c}$ of the generating surface T of the gear cutting tool is insightful for the derivation of Equations (15.58) through (15.60).

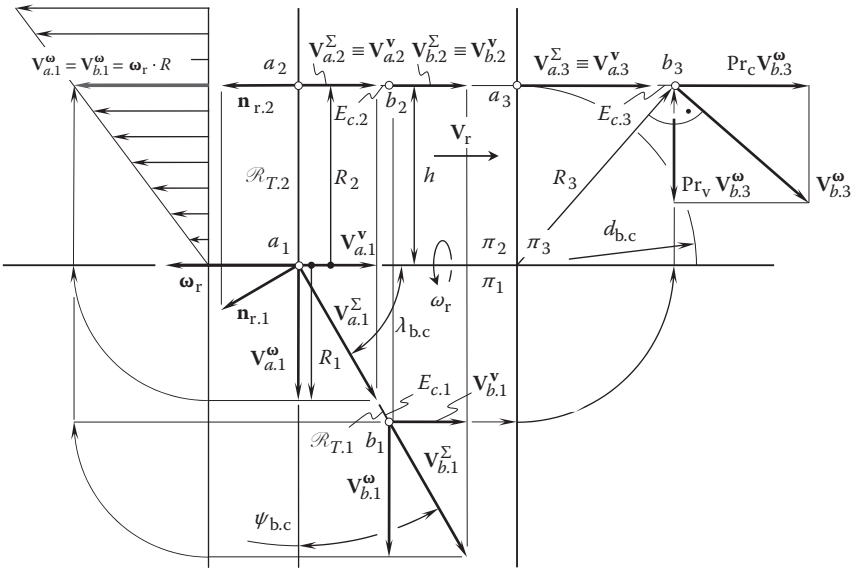

FIGURE 15.13
Determination of base diameter $d_{b.c}$ of generating surface T of an involute gear cutting tool. (From Radzevich, S.P., *ASME Journal of Mechanical Design*, 129, 334–345, 2007. With permission.)

Many other design parameters of the generating surface of the gear cutting tool, as well as the design parameters of the gear cutting tool itself can be determined using the *DG*-based method.

15.6 Possible Types of Generating Surfaces of Gear Cutting Tools

The generating surface of a gear cutting tool is an envelope to consecutive positions of the auxiliary generating surface in its motion relative to a coordinates system, with which the surface T will be associated. Numerous types of the auxiliary generating surface $\mathscr{R}_T$ are depicted in Figures 15.2, 15.4, and 15.6. All of these, as well as auxiliary generating surfaces of those not shown above, can be utilized for the purposes of the generation of generating surface of the gear cutting tool. The relative motion of the auxiliary surface $\mathscr{R}_T$ relative to the reference system $X_cY_cZ_c$ should be appropriate in order for the surface T to exist.

When the auxiliary generating rack $\mathscr{R}_T$ is performing a screw motion about the Z_c axis, and the axis is parallel to the pitch plane W_r of the rack $\mathscr{R}_T$, the generating surface T can be generated if and only if velocity of the translation $\mathbf{V}_r$ and velocity of the rotation $\boldsymbol{\omega}_g$ are timed with each other so that when the rack $\mathscr{R}_T$ turns through the angle of 2π, it is simultaneously translated at a distance of nP_x. Here, n designates an integer number (which actually is the number of starts of the generating surface $\mathscr{R}_T$), and the pitch of the rack's $\mathscr{R}_T$ teeth in the direction of the Z_c axis is denoted as P_x. Ultimately, proper combination of the motions $\mathbf{V}_r$ and $\boldsymbol{\omega}_g$ results in generation of the cylindrical surface T, shown in Figure 15.10.

15.6.1 Generating Surface of the Gear Cutting Tool with a Zero Profile Angle

In a particular case, a gear cutting tool can be designed with a zero normal profile angle ϕ_n. An example of the auxiliary generating surface $\mathscr{R}_T$ with a zero profile angle is shown at the bottom of Figure 15.4 (the third case). The generating surface of the gear cutting tool is subject to significant changes in the event when the equality $\phi_n = 0°$ is observed. Besides the reduced normal profile angle itself, enormous increase of base diameter $d_{b.c}$ of the gear cutting tool occurs in this case. Following Equation (15.58), the base diameter is equal to

$$d_{b.c} = \frac{mN_c}{\sqrt{1 - \cos^2 \zeta_c}} \tag{15.66}$$

when the equality $\phi_n = 0°$ is observed.

Taking into account that practical values of setting angle ζ_c of the gear cutting tool are in the range of just a few angular degrees, the reduction of normal profile angle to $\phi_n = 0°$ results in that base diameter $d_{b.c}$ in this case exceeds not just outer diameter $d_{o.c}$ of the gear cutting tool, but it exceeds any reasonable values. Moreover, in the case of a zero setting angle ($\zeta_c = 0°$), the base diameter of the gear cutting tool approaches infinity ($d_{b.c} \to \infty$). No screw involute surface is feasible under this scenario, when the inequality $d_{o.c} < d_{b.c}$ is valid.

When normal profile angle is zero, both the tooth addendum a_c as well as the tooth dedendum b_c of the auxiliary generating rack $\mathscr{R}_T$ shrink to zero ($a_c = 0$ and $b_c = 0$). The tooth profile of the gear cutting tool is shrunk to a point—to the corner point of the auxiliary rack $\mathscr{R}_T$. Because of this feature, the work gear tooth profile is generated not by the

corresponding conjugate profile of the gear cutting tool (which does not exist for gear cutting tools with a zero profile angle), but by the corner point of the rack $\mathscr{R}_T$. This makes it possible to design a gear cutting tool of coarse pitch with cutting edges made of superhard materials such as manmade diamond, borazon, and so forth.

Tooth height $h_{t.c}$ of the rack $\mathscr{R}_T$ is not equal to $h_{t.c} \neq a_c + b_c$. Instead, it is approximately equal to tooth height $h_{t.g}$ of the gear to be machined ($h_{t.c} \approx h_{t.g}$).

However, it does not mean that a gear cutting tool with a zero normal profile angle cannot be designed for machining an involute gear. The gear cutting tool can be designed, using for this purpose a generating surface T that is reduced in the case under consideration to two helices, which are within the outer cylinder of the cutting tool (Figure 15.14). For the computation of axial pitch P_{hx} of the helices, the formula

$$P_{hx} = p_{b.c} \frac{N_c}{\cos \zeta_c} \tag{15.67}$$

can be used.

When machining an involute gear, the gear cutting tool should be set up to allow the straight generating line W_c of the outer cylinder of the gear cutting tool be tangent to base cylinder of the gear to be machined.

For machining of involute gears with a low tooth count (for which the inequality $d_{l.g} \leq d_{b.g}$ is observed), helical generating line T is within just one portion of the outer cylinder. For machining of involute gears with a greater tooth count (for which the inequality $d_{l.g} >$

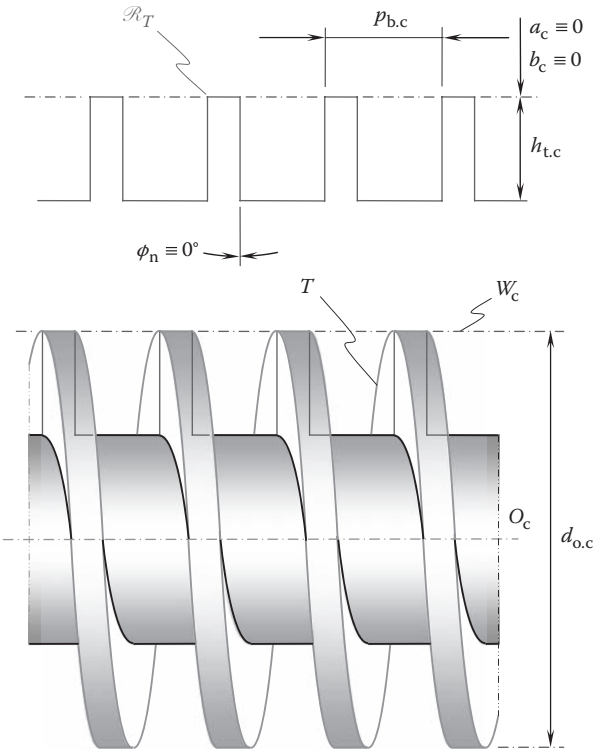

FIGURE 15.14
Generating surface of a gear cutting tool T with a zero normal profile angle ϕ_n.

$d_{b.g}$ is observed), two portions of the helical generating line are required. The helices are located separately on two coaxial outer cylinders.

15.6.2 Conical Generating Surface of the Gear Cutting Tool

Possible shapes of generating surfaces of the gear cutting tools are not limited only to cylindrical surfaces *T*. Other geometries of the surface *T* are feasible as well.

Auxiliary generating rack $\mathscr{R}_T$ of a conical gear cutting tool is tilted with respect to the axis of rotation O_c of the gear cutting tool. The angle that the axis O_c makes with pitch plane W_r of the auxiliary rack $\mathscr{R}_T$ is designated as θ_r (Figure 15.6a). The straight motion of the auxiliary generating surface $\mathscr{R}_T$ can be performed in a direction parallel to the pitch plane W_r of the auxiliary generating rack $\mathscr{R}_T$. When the angles θ_r and ϕ_r correlate to each other properly (i.e., when the inequality $-\phi_r < \theta_r < \phi_r$ is observed), then a conical generating surface *T* of the gear cutting tool can be generated (Figure 15.15).

That same auxiliary generating rack shown in Figure 15.2b can be used for the generation of conical generating surface of the gear cutting tool. When the rack $\mathscr{R}_T$ is traveling at an angle θ_r relative to the axis O_c, then generating surface *T* is shaped in the form of a conical worm. Envelopes to successive positions of top lands and bottom lands of the auxiliary rack $\mathscr{R}_T$ are cones of revolution. Axes of the cones of revolution are aligned with axis O_c.

The straight motion of the auxiliary rack should be investigated in more detail in order to get proper understanding on geometry of the lateral surfaces of the conical generating surface *T*.

When generating the surface *T* of the conical gear cutting tool, the direction of the straight motion $\mathbf{V}_{\mathscr{R}}$ of the auxiliary rack $\mathscr{R}_T$ is perpendicular to the axis of rotation O_g of the gear being machined. It is convenient to decompose the straight motion $\mathbf{V}_{\mathscr{R}}$ of the auxiliary rack

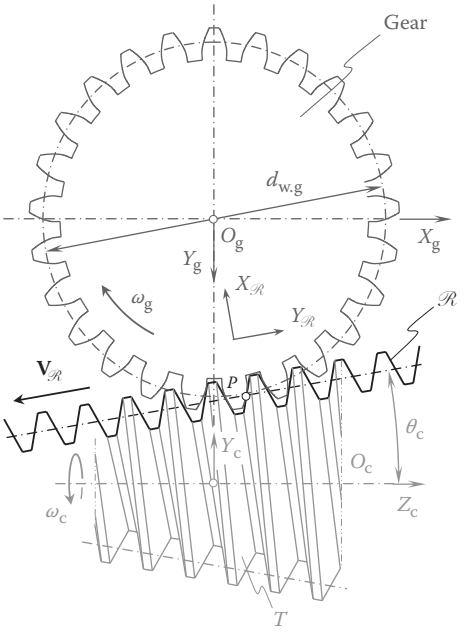

FIGURE 15.15
Generation of conical generating surface of a gear cutting tool.

$\mathscr{R}_T$ onto two components as shown in Figure 15.16. The first component $\mathbf{V}_{\text{sl}}$ is within the lateral plane of the auxiliary rack $\mathscr{R}_T$ tooth. The second component $\mathbf{V}_T$ is parallel to the axis of rotation O_{c} of the gear cutting tool. Subscript 1 is assigned to the projections of the vectors $\mathbf{V}_{\mathscr{R}}$, $\mathbf{V}_T$, and $\mathbf{V}_{\text{sl}}$ onto the horizontal plane of projections π_1, and subscript 2 is assigned to the projections of those same vectors onto the vertical plane of projections π_2.

The equality

$$\mathbf{V}_{\mathscr{R}} = \mathbf{V}_T + \mathbf{V}_{\text{sl}} \tag{15.68}$$

is valid.

The translation $\mathbf{V}_{\text{sl}}$ results in the lateral plane of the auxiliary rack $\mathscr{R}_T$ tooth moving over itself. This motion does not affect shape of the envelope to successive positions of the auxiliary rack in its motion with respect to the cutting tool reference system $X_{\text{c}}Y_{\text{c}}Z_{\text{c}}$. Therefore, the component $\mathbf{V}_{\text{sl}}$ can be neglected when determining conical generating surface T of the gear cutting tool.

The lateral plane travels along the axis O_{c} with a certain speed V_T. Simultaneously with the translation V_T, the rack $\mathscr{R}_T$ rotates about the O_{c} axis with the rotation ω_{r}. The ratio

$$\frac{V_T}{\omega_{\text{r}}} = \frac{P_{x.\text{c}}}{2\pi} \tag{15.69}$$

is valid. Here, in Equation (15.69), the axial pitch of the screw surface is denoted as $P_{x.\text{c}}$.

Ultimately, the lateral surface of the conical generating surface T can be interpreted as the envelope to consecutive positions of the lateral plane of the auxiliary rack $\mathscr{R}_T$ that is performing a screw motion. The screw motion is composed of the rotation $\boldsymbol{\omega}_{\text{r}}$ of the rack

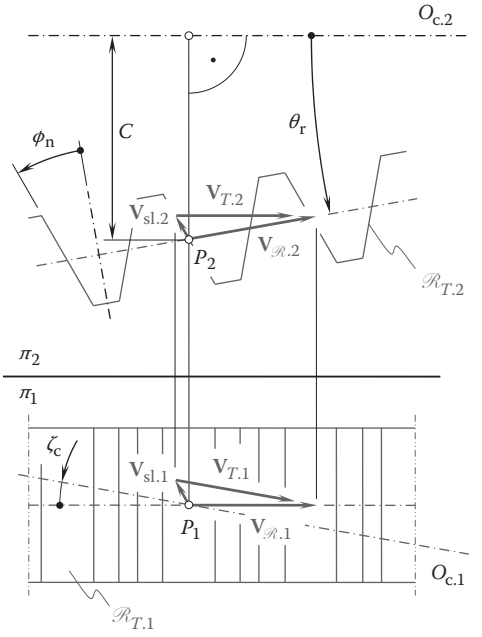

FIGURE 15.16
Generation of generating surface T of a conical gear cutting tool for machining of cylindrical gears.

$\mathscr{R}_T$ about the axis of rotation O_c of the gear cutting tool, and of the translation $\mathbf{V}_T$ along the O_c axis. When the velocity $V_{\mathscr{R}} = |\mathbf{V}_{\mathscr{R}}|$ is known, then the velocity $V_T = |\mathbf{V}_T|$ can be computed from the equation

$$V_T = V_{\mathscr{R}} \cdot \frac{\cos\phi_n}{\cos\zeta_c \cos(\phi_n \pm \theta_r)} \tag{15.70}$$

Owing to the fact that the generating surface is shaped in the form of a conical worm and not a cylindrical worm, two ways are possible for the specification of configuration of the auxiliary generating rack $\mathscr{R}_T$ relative to the axis O_c.

First, for the specification of a configuration of the rack $\mathscr{R}_T$ relative to the axis O_c, the setting angle ζ_c of the gear cutting tool can be utilized. The setting angle ζ_c complements to 90° the angle between the axis O_c and the straight generating lines of the rack $\mathscr{R}_T$. In Equation (15.70), velocity V_T is expressed in terms of setting angle ζ_c of the gear cutting tools.

Second, an angle that complements to 90° the angle between the axes O_g and O_c can be used for the specification of configuration of the auxiliary generating rack $\mathscr{R}_T$ relative to the axis O_c. This angle is denoted as ζ_c^*. The angle ζ_c^* is not equal to the setting angle ζ_c of the gear cutting tool ($\zeta_c^* \neq \zeta_c$). However, the angle ζ_c^* can be expressed in terms of the setting angle ζ_c and vice versa.

When the angle ζ_c^* is used for the specification of configuration of the auxiliary generating rack $\mathscr{R}_T$ relative to the axis O_c, then magnitude of the component $\mathbf{V}_T$ can be computed from the equation

$$V_T = \frac{\sin\theta \tan(\theta + \phi_n) + \cos\theta}{\cos\zeta_c^*} V_{\mathscr{R}} \tag{15.71}$$

This makes possible the conclusion that the lateral plane of the rack tooth performs a screw motion; axis O_c is the axis of the screw motion, and the parameter of the screw motion is equal

$$p_{sc.1} = \frac{V_T}{\omega_r} = \frac{V_{\mathscr{R}}}{\omega_r} \cdot \underbrace{\frac{\sin\theta \tan(\theta + \phi_n) + \cos\theta}{\cos\zeta_c^*}}_{a_1} = \frac{P_{x.c}}{2\pi} \cdot a_1 \tag{15.72}$$

It is assumed there that $\omega_{\mathscr{R}} = 1$, and $V_T = P_{x.c}$.

As already shown (see Figure 15.7), the envelope to consecutive positions of the plane that performs a screw motion is a screw involute surface. By definition, parameter p_c (the reduced pitch) of the screw involute surface is equal

$$p_c = \frac{\mathbf{V}_T}{\omega_r} \tag{15.73}$$

where $\omega_r = |\boldsymbol{\omega}_r|$.

Due to the lateral planes of the opposite sides of the auxiliary generating rack $\mathscr{R}_T$, tooth profiles are at different angles with respect to the axis of rotation O_c, and the gear cutting tool features not one, but two base cylinders instead. One is the base cylinder of the screw involute surface of one side of the gear cutting tool tooth profile, while the other is the base cylinder of the screw involute surface of the opposite side of the gear cutting tool tooth profile. Schematically, the base cylinders of the opposite sides of the tooth profile of the gear cutting tool are depicted in Figure 15.17.

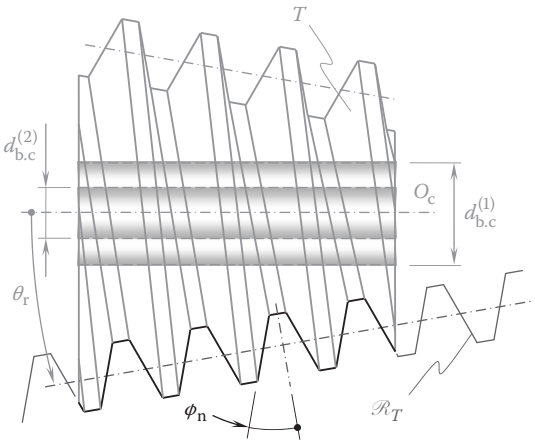

FIGURE 15.17
Conical generating surface of the gear cutting tool *T* for the machining of cylindrical gears.

For the purpose of determining the base diameters of conical generating surface *T,* it is convenient to consider a Cartesian coordinate system $X_{\mathscr{R}}Y_{\mathscr{R}}Z_{\mathscr{R}}$ associated with the auxiliary generating rack $\mathscr{R}_T$ as shown in Figure 15.16. The origin of the reference system $X_{\mathscr{R}}Y_{\mathscr{R}}Z_{\mathscr{R}}$ is at a distance *C* from the axis O_c. Another reference system $X_cY_cZ_c$ is associated with the gear cutting tool.

The transition from the reference system $X_{\mathscr{R}}Y_{\mathscr{R}}Z_{\mathscr{R}}$ to the reference system $X_cY_cZ_c$ can be analytically described by the operator $\mathbf{Rs}(\mathscr{R} \mapsto c)$ of the result coordinate system transformation. In the case under consideration the operator $\mathbf{Rs}(\mathscr{R} \mapsto c)$ allows for matrix representation

$$\mathbf{Rs}(\mathscr{R} \mapsto c) = \begin{bmatrix} 0 & \sin\theta & \cos\theta & -C_{g/c} \\ \cos\zeta_c^* & \sin\zeta_c^* \cos\theta & -\sin\zeta_c^* \sin\theta & 0 \\ -\sin\zeta_c^* & \cos\zeta_c^* \cos\theta & -\cos\zeta_c^* \sin\theta & 0 \\ 0 & 0 & 0 & 1 \end{bmatrix} \tag{15.74}$$

For the transition from the reference system $X_cY_cZ_c$ to the reference system $X_{\mathscr{R}}Y_{\mathscr{R}}Z_{\mathscr{R}}$, the operator $\mathbf{Rs}(c \mapsto \mathscr{R})$ of the inverse transformation can be used $[\mathbf{Rs}(c \mapsto \mathscr{R}) = \mathbf{Rs}^{-1}(\mathscr{R} \mapsto c)]$.

In the coordinate system $X_{\mathscr{R}}Y_{\mathscr{R}}Z_{\mathscr{R}}$, the lateral plane of tooth of the auxiliary rack $\mathscr{R}_T$ can be analytically described by the equation $Y_{\mathscr{R}} = -Z_{\mathscr{R}} \tan\phi_n$. Implementation of the operator $\mathbf{Rs}(\mathscr{R} \mapsto c)$ of the linear transformation allows for an expression for the position vector of point $\mathbf{r}_{\mathscr{R}}$ of that same plane represented in the coordinate system $X_cY_cZ_c$. Ultimately, for the computation of perpendicular $\mathbf{n}_{\mathscr{R}}$ to the lateral plane of the auxiliary rack $\mathbf{r}_{\mathscr{R}}$, the following expression

$$\mathbf{n}_{\mathscr{R}} = \begin{bmatrix} \sin\zeta_c^* \\ \cos\zeta_c^* \\ \tan(\theta + \phi_n) \\ 1 \end{bmatrix} \tag{15.75}$$

can be derived.

Let us determine speed $\mathbf{V}_m$ of an arbitrary point m within the lateral plane of the rack $\mathscr{R}_T$

$$\mathbf{V}_m = \mathbf{i} \cdot Z_c + \mathbf{j} \cdot p_{sc} - \mathbf{k} \cdot X_c \tag{15.76}$$

Substituting $\mathbf{n}_{\mathscr{R}}$ [see Equation (15.75)] and $\mathbf{V}_m$ [see Equation (15.76)] into Shishkov's equation of contact $\mathbf{n}_{\mathscr{R}} \cdot \mathbf{V}_m = 0$ and considering it with the expression for the lateral plane in an arbitrary configuration of the auxiliary rack $\mathscr{R}_T$ allows for an equation

$$d_{b.c}^{(1)} = 2 \frac{p_{sc.1} \cos \zeta_c^*}{\sqrt{\sin^2 \zeta_c^* + \tan^2(\theta - \phi_n)}} \tag{15.77}$$

for the base diameter of the screw involute generating surface T.

An equation

$$d_{b.c}^{(2)} = 2 \frac{p_{sc.1} \cos \zeta_c^*}{\sqrt{\sin^2 \zeta_c^* + \tan^2(\theta + \phi_n)}} \tag{15.78}$$

similar to Equation (15.77) is valid for the opposite side of tooth profile of the rack $\mathscr{R}_T$.

Base diameters of a conical gear cutting tool can also be expressed in terms of setting angle ζ_c

$$d_{b.c} = \frac{mN_c \cos(\phi_n \pm \theta_r)}{\sqrt{1 - \cos^2(\phi_n \pm \theta_r) \cos^2 \zeta_c}} \tag{15.79}$$

When $\theta = 0°$, then Equations (15.77)–(15.79) are valid for cylindrical gear cutting tools.

It is important to recall here that by definition the setting angle of the gear cutting tool is measured within the pitch plane W_c (see Definition 15.1). Following from this statement, the setting angle ζ_c of the conical gear cutting tool does not complement to 90° the angle between the axes O_g and O_c. However, the angle $\bar{\zeta}_c$ that complements to 90° the angle between the axis O_g of the work gear and the axis O_c of the gear cutting tool can be expressed in terms of the angles ζ_c and θ_r.

The angle that the axis of rotation O_g of the work gear makes with the axis of rotation O_c of the gear cutting tool is denoted as Σ. The crossed-axis angle Σ is equal to $\Sigma = 90° - \bar{\zeta}_c$. For the derivation of a formula for the computation of the crossed-axis angle Σ, the operators of coordinate system transformations can be implemented.

A Cartesian coordinate system $X_cY_cZ_c$ is associated with the generating surface of the conical gear cutting tool as shown in Figure 15.18. Another Cartesian coordinate system $X_rY_rZ_r$ is associated with the auxiliary generating surface $\mathscr{R}_T$ so that (a) the Y_rZ_r–coordinate plane is congruent with the pitch plane W_r of the auxiliary rack $\mathscr{R}_T$, and (b) the Y_r axis is aligned with straight generating line of the auxiliary rack tooth. The cone angle θ_c is the angle between the axis Z_c of the gear cutting tool reference system and between the Z_2 axis of the auxiliary coordinate system $X_2Y_2Z_2$. The setting angle ζ_c of the gear cutting tool is the angle that the axis Y_2 makes with the axis Y_r.

Under such a scenario, the Z_c axis and Z_r axis make the angle $\bar{\zeta}_c$ to be determined (i.e., $\bar{\zeta}_c = \angle(Z_c, Z_r)$.

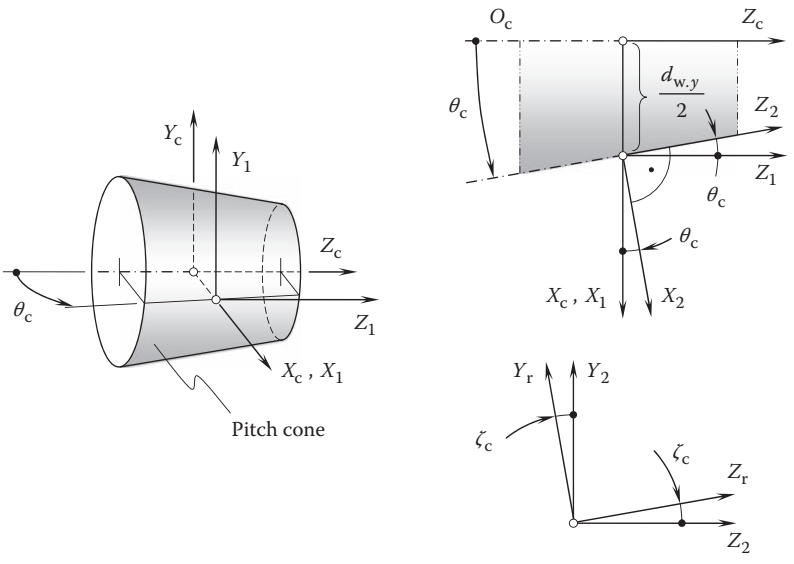

FIGURE 15.18
Crossed-axis angle when machining a cylindrical gear with a conical gear cutting tool.

In order to compute the angle $\bar{\zeta}_c = \angle(Z_c, Z_r)$, both the axes Z_c and Z_r are required to be represented in a common reference system. The required coordinate system transformation can be analytically described by the operators of elementary coordinate system transformations.

For analytical representation of the transition of the reference system $X_cY_cZ_c$ along the X_c axis through the distance $d_{w.y}/2$ to the position of the first auxiliary coordinate system $X_1Y_1Z_1$, the operator of translation $\mathbf{Tr}(d_{w.y}/2, X_c)$ is used. Here, current value of pitch diameter of the conical pitch surface of the gear cutting tool is designated as $d_{w.y}$.

For rotation of the auxiliary reference system $X_1Y_1Z_1$ about the Y_1 axis through the cone angle θ_c to the position of the second auxiliary coordinate system $X_2Y_2Z_2$, the operator of rotation $\mathbf{Rt}(\theta_c, Y_1)$ is implemented.

Ultimately, rotation of the reference system $X_2Y_2Z_2$ about the X_2 axis through the setting angle ζ_c of the gear cutting tool to the position of the coordinate system $X_rY_rZ_r$ can be analytically described by the operator of rotation $\mathbf{Rt}(\zeta_c, X_2)$.

The operators of elementary coordinate system transformations make it possible to compose the operator $\mathbf{Rs}(c \mapsto r)$ of the resultant coordinate system transformations. The following expression

$$\mathbf{Rs}(c \mapsto r) = \mathbf{Rt}(\zeta_c, X_2) \cdot \mathbf{Rt}(\theta_c, Y_1) \cdot \mathbf{Tr}(d_{w.y}/2, X_c) \tag{15.80}$$

can be used for computation of the operator $\mathbf{Rs}(c \mapsto r)$ of the linear transformation.

The operator of translation $\mathbf{Tr}(d_{w.y}/2, X_c)$ does not affect the actual value of the crossed-axis angle Σ. Therefore, this operator can be omitted from further analysis.

Unit vector $\mathbf{k}_c$ along the Z_c axis of the reference system $X_cY_cZ_c$ can be represented in the coordinate system $X_rY_rZ_r$ of the auxiliary generating rack $\mathscr{R}_T$

$$\mathbf{k}_c^{(r)} = \mathbf{Rs}(c \mapsto r) \cdot \mathbf{k}_c \tag{15.81}$$

Equation (15.81) immediately yields an equation for the crossed-axis angle Σ

$$\Sigma = 90^\circ - \tan^{-1}\left(\frac{|\mathbf{k}_r \times \mathbf{k}_c^{(r)}|}{\mathbf{k}_r \cdot \mathbf{k}_c^{(r)}}\right) \tag{15.82}$$

where $\mathbf{k}_r$ denotes the unit vector along the Z_r axis of the reference system $X_rY_rZ_r$.

We stress again the principal difference between the helix angle ψ_c and the setting angle ζ_c of the gear cutting tool: Because pitch diameter $d_{w.c}$ varies within the face width of the conical gear cutting tool, the pitch helix angle ψ_c is also varied within the face width of the gear cutting tool. The value of the setting angle ζ_c of the gear cutting tool remains the same within the face width of the gear cutting tool regardless of which portion of it is currently in mesh with the work gear.

15.6.3 Generating Surface of a Gear Cutting Tool with an Asymmetric Tooth Profile

Gear cutting tools with different profile angles at opposite sides of tooth profile of the auxiliary generating rack are used for machining of spur and helical gears with different tooth profile angles. The auxiliary generating rack $\mathscr{R}_T$ with a corresponding conjugate profile is depicted in Figure 15.6b. In the case under consideration it is convenient to designate the opposite sides of the tooth of the auxiliary generating rack as $\mathscr{R}_{T.1}$ and $\mathscr{R}_{T.2}$.

When the auxiliary rack $\mathscr{R}_T$ is performing a screw motion about the axis O_c, then the generating surface of the gear cutting tool that features an asymmetric tooth profile is generated (Figure 15.19). Again, in the case under consideration it is convenient to designate the screw involute surfaces of the opposite sides of the thread profile as T_1 and T_2. The axial pitch of the opposite sides of the generating surface threads profile is of the same value. The setting angle ζ_c of the gear cutting tool is the same for the opposite sides of the threads profile.

Owing to a different profile angle, namely $\phi_{r.1}$ for one side and $\phi_{r.2}$ for the opposite side of the threads profile, base diameters $d_{b.c}^{(1)}$ and $d_{b.c}^{(2)}$ of the corresponding screw involute surfaces are also of a different value. For the computation of the base diameters, the following formulae

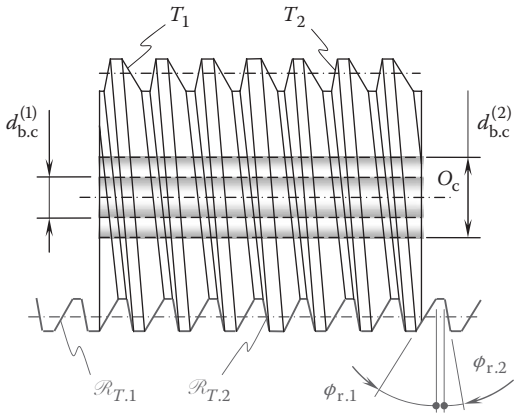

FIGURE 15.19
Generating surface of a gear cutting tool for machining gears with an asymmetric tooth profile.

$$d_{b.c}^{(1)} = \frac{mN_c \cos\phi_{r.1}}{\sqrt{1-\cos^2\phi_{r.1}\cos^2\zeta_c}} \tag{15.83}$$

$$d_{b.c}^{(2)} = \frac{mN_c \cos\phi_{r.2}}{\sqrt{1-\cos^2\phi_{r.2}\cos^2\zeta_c}} \tag{15.84}$$

can be used.

When the inequality $\phi_{r.1} > \phi_{r.2}$ is observed, then the inequality $d_{b.c}^{(1)} < d_{b.c}^{(2)}$ is valid as shown in Figure 15.19.

15.6.4 Generating Surfaces of the Gear Cutting Tools Featuring Torus-Shaped Pitch Surfaces

For the purposes of the generation of generating surfaces of the gear cutting tool, the auxiliary generating surfaces either in the form of an internal gear sector (Figure 15.6c), or an external gear sector (Figure 15.6d) can be implemented. Generating surfaces of this kind have been investigated by Radzevich [5] since 1970th.

When the auxiliary generating rack $\mathscr{R}_T$ rotates $\omega_r^{(1)}$ about its axis of rotation O_r, and when the reference system $X_rY_rZ_r$ simultaneously rotates $\omega_r^{(2)}$ about the axis of rotation of the gear cutting tool O_c, then the generating surface T of the gear cutting tool can be generated if the rotations $\omega_r^{(1)}$ and $\omega_r^{(2)}$ are properly timed with each other. Depending on the configuration of the auxiliary generating rack $\mathscr{R}_T$ and the axis of rotation O_c, and on the timing of the rotations $\omega_r^{(1)}$ and $\omega_r^{(2)}$, either a convex (Figure 15.20a) or a saddle-type (Figure 15.20b) surface T of the gear cutting tool can be generated.

For the derivation of an equation of the generating surface T of the gear cutting tool, the kinematic method [2, 143, 186] can be implemented.

Consider two rotation vectors $\boldsymbol{\omega}_r$ and $\boldsymbol{\omega}_c$ as shown in Figure 15.21. The rotations vectors $\boldsymbol{\omega}_r$ and $\boldsymbol{\omega}_c$ are the vectors, one of which is along the axis of rotation O_r of the auxiliary

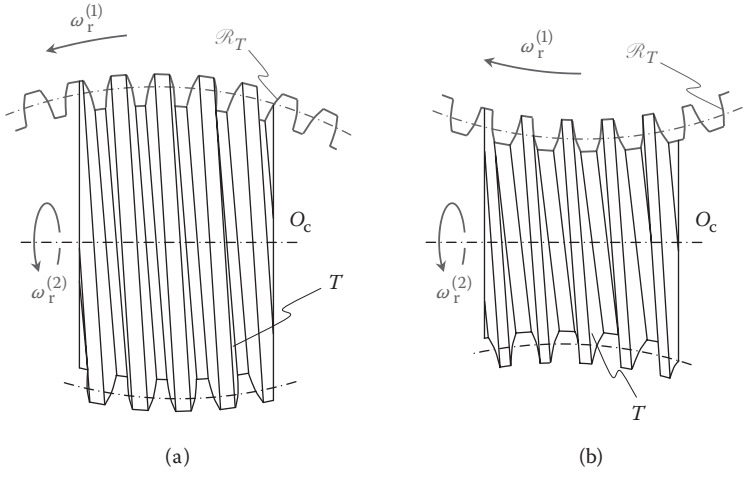

FIGURE 15.20
Generating surface of a gear cutting tool with a torus-shaped pitch surface.

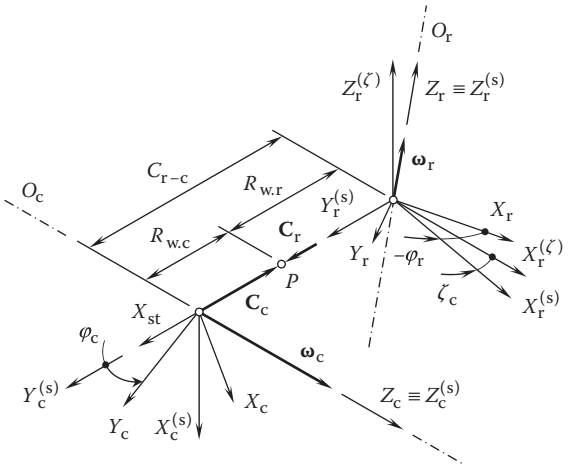

FIGURE 15.21
Instant configuration of the reference systems $X_rY_rZ_r$ and $X_cY_cZ_c$ associated with auxiliary generating rack $\mathscr{R}_T$ and with a gear cutting tool with a torus-shaped pitch surface.

generating rack $\mathscr{R}_T$, while the other is the vector along the axis of rotation O_c of the gear cutting tool, respectively. The axes of rotations O_r and O_c are at a certain center distance C_{r-c}. They cross each other at a certain crossed-axis angle $\Sigma - 90° - \zeta_c$. The center distance C_{r-c} and the setting angle ζ_c of the gear cutting tool are considered as the given design parameters.

Let us suppose that the auxiliary generating rack $\mathscr{R}_T$ of the gear cutting tool is represented in the reference system $X_rY_rZ_r$ by matrix equation

$$\mathbf{r}_r(U_r, V_r) = \begin{bmatrix} X_r(U_r, V_r) \\ Y_r(U_r, V_r) \\ Z_r(U_r, V_r) \\ 1 \end{bmatrix} \tag{15.85}$$

For the derivation of an equation of the generating surface T of the gear cutting tool, it is necessary to compose an equation of the rack $\mathscr{R}_T$ in its current configuration when it is turned through an arbitrary angle of rotation φ_r. Then, it is necessary to represent the equation of the auxiliary rack $\mathscr{R}_T$ when the rack $\mathscr{R}_T$ occupies its current orientation in a reference system $X_cY_cZ_c$ associated with the gear cutting tool. For this purpose, Equation (15.61) should be considered together with the operator $\mathbf{Rs}(r \mapsto c)$ of the resultant coordinate system transformations. The operator $\mathbf{Rs}(r \mapsto c)$ of the linear transformation can be expressed in terms of the operators of elementary coordinate system transformations

$$\mathbf{Rs}(r \mapsto c) = \mathbf{Rt}(\varphi_c, Y_c^{(s)}) \cdot \mathbf{Tr}(-C_{c-r}, Y_r^{(s)}) \cdot \mathbf{Rt}(-\zeta_c, Y_r^{(s)}) \cdot \mathbf{Rt}(-\varphi_r, Z_r) \tag{15.86}$$

All the applied intermediate coordinate systems are depicted in Figure 15.21. Here, in Equation (15.86) the rotation angle φ_r of the auxiliary generating rack $\mathscr{R}_T$, and the rotation angle φ_c of the gear cutting tool correlate to each other in compliance with the ratio

$\varphi_r N_r = \varphi_c N_c$, where N_r and N_c denote the number of teeth of the auxiliary rack $\mathscr{R}_T$ and the number of starts of the gear cutting tool correspondingly.

After the operator $\mathbf{Rs}(r \mapsto c)$ of the resultant linear transformation is composed, then the auxiliary generating rack $\mathscr{R}_T$ in its current configuration with respect to the reference system $X_c Y_c Z_c$ can be analytically described by the equation

$$\mathbf{r}_r^{(c)}(U_r, V_r, \varphi_r) = \mathbf{Rs}(r \mapsto c) \cdot \mathbf{r}_r(U_r, V_r) \tag{15.87}$$

Using Equation (15.87) together with Shishkov's equation of contact, the following set of two equations is composed

$$\begin{cases} \mathbf{r}_r^{(c)} = \mathbf{r}_r^{(c)}(U_r, V_r, \varphi_r) \\ \mathbf{n}_r^{(c)} \cdot \mathbf{V}_{r-c}^{(c)} = 0 \end{cases} \tag{15.88}$$

where $\mathbf{n}_r^{(c)}$ denotes unit normal vector to the auxiliary rack surface $\mathscr{R}_T$ and $\mathbf{V}_{r-c}^{(c)}$ denotes the vector of the resultant motion of the generating rack $\mathscr{R}_T$ with respect to the coordinate system $X_c Y_c Z_c$. Both vectors $\mathbf{n}_r^{(c)}$ and $\mathbf{V}_{r-c}^{(c)}$ should be represented in the coordinate system $X_c Y_c Z_c$, with which the gear cutting tool will be associated after it is designed.

A solution to the set of Equation (15.88) returns an expression for the position vector of a point $\mathbf{r}_c = \mathbf{r}_c(U_c, V_c)$ of the generating surface T of the gear cutting tool.

It is important to stress here that the setting angle ζ_c of the gear cutting tool remains of constant value regardless of which portion of the threads of the surface T are currently meshing with the work gear. This is one more evidence of the difference between the setting angle ζ_c and the helix angle ψ_c of the gear cutting tool.

For further analysis, it is convenient to introduce a stationary reference system $X_{st} Y_{st} Z_{st}$. The origin of the reference system $X_{st} Y_{st} Z_{st}$ is located at the pitch point P of the mesh of the auxiliary rack $\mathscr{R}_T$ and the generating surface T of the gear cutting tool. Due to lack of space, only the X_{st} axis of the newly introduced reference system $X_{st} Y_{st} Z_{st}$ is shown Figure 15.21. The axes Y_{st} and Z_{st} are not shown.

Similar to the vectors $\mathbf{C}_g$ and $\mathbf{C}_c$ shown in Figure 3.6, the analogous vectors $\mathbf{C}_r$ and $\mathbf{C}_c$ are depicted in Figure 15.21. The vectors $\mathbf{C}_r$ and $\mathbf{C}_c$ can be expressed in terms of unit vector $\mathbf{c}$ along the X_{st} axis, and in terms of radii $R_{w.r}$ and $R_{w.c}$ of pitch surfaces of the auxiliary generating rack $\mathscr{R}_T$, and of the gear cutting tool: $\mathbf{C}_r = \mathbf{c} \cdot R_{w.r}$ and $\mathbf{C}_c = -\mathbf{c} \cdot R_{w.c}$. Depending on the actual values and configurations of (a) the rotations vectors $\boldsymbol{\omega}_r$ and $\boldsymbol{\omega}_c$, and (b) the vectors $\mathbf{C}_r$ and $\mathbf{C}_c$, either a convex (barrel-type) or saddle-type generating surface of the gear cutting tool is generated (Figure 15.20).

For gear cutting tools with a pitch surface in the form of torus surface, the specification of setting angle ζ_c^* as the angle between the axes O_g and O_c is the only possible way for the specification of configuration of the gear cutting tool relative to the work gear to work.

15.7 Constraints on the Design Parameters of the Generating Surface of a Gear Cutting Tool

For machining of an involute gear, gear cutting tools featuring the generating surface T in the form of a screw involute surface are used. The base cylinder is one of the main features

of the screw involute surface. The screw involute surface exists within the exterior of the base cylinder, not within the interior. The latter point imposes certain constraints onto values of the design parameters of the generating surfaces of the gear cutting tools.

Practically, the outer diameter of the gear cutting tool is restricted by design parameters of the gear generator at which the gear cutting tool is applied. This means that actual outer diameter of the gear cutting tool $d_{o.c}$ does not exceed the maximal allowed its value $[d_{o.c}]$ (i.e., the inequality $d_{o.c} \le [d_{o.c}]$ is always observed). The working depth of threads h_k of the generating surface T is equal to the summa of the addendum a_c and the dedendum b_c of the threads ($h_k = a_c + b_c$). Thus, the inner diameter of the gear cutting tool $d_{f.c}$ does not exceed the value of

$$d_{f.c} \le [d_{o.c}] - 2h_k \tag{15.89}$$

From another side, inner diameter of the gear cutting tool $d_{f.c}$ is equal to or exceeds the base diameter $d_{b.c}$ (i.e., the inequality $d_{f.c} \ge d_{b.c}$ is required to be satisfied). In the most critical case, the last inequality reduces to the equality $d_{f.c} = d_{b.c}$.

For a gear cutting tool of the given module m and number of starts N_c, base diameter $d_{b.c}$ depends only on the normal profile angle ϕ_n and on setting angle ζ_c of the gear cutting tool. Equation (15.58) yields a graphical interpretation of the function $d_{b.c}(\phi_n, \zeta_c)$. For a single-start gear cutting tool ($N_c = 1$) with a normalized module ($m = 1$), an example of the function $d_{b.c}(\phi_n, \zeta_c)$ is plotted in Figure 15.22. As it immediately follows from Figure 15.22, base diameter $d_{b.c}$ approaches infinity ($d_{b.c} \to \infty$) when profile angle ϕ_n and setting angle ζ_c of the gear cutting tool approach zero ($\phi_n \to 0°$, $\zeta_c \to 0°$). The last point makes possible a conclusion that when certain constraints are imposed on actual values of diameters of the gear cutting tool (outer diameter and inner root diameter), this immediately restricts the minimal value of the profile angle of the generating surface of the gear cutting tool. The above-mentioned inequality $d_{f.c} \ge d_{b.c}$ along with Equation (15.58)

$$d_{b.c} = \frac{mN_c \cos\phi_n}{\sqrt{1 - \cos^2\phi_n \cos^2\zeta_c}} \tag{15.90}$$

for the computation of the base diameter allow an expression

$$\phi_n \le [\phi_n] = \cos^{-1}\left(\frac{d_{f.c}}{\sqrt{m^2N_c^2 + d_{f.c}^2\cos^2\zeta_c}}\right) \tag{15.91}$$

for the computation of the minimal allowed value of normal pressure angle ϕ_n of the gear cutting tool.

If normal profile angle ϕ_n exceeds the maximal allowed its value $[\phi_n]$, then a corresponding portion of the generating surface T of the gear cutting tool cannot be reproduced by cutting edges. Ultimately, this results in violation of the conditions of proper part surface generation [128, 138, 143]. When conditions of proper part surface generation are not fulfilled, then the gear cannot be machined in compliance with the blueprint specification. Therefore, an accurate gear cutting tool for machining of involute gears cannot be designed under a scenario when the base helix angle $\psi_{b.c}$ [see Equation (15.62)] approaches zero ($\psi_{b.c} \to 0°$), or its actual values is less than the minimal allowed value $|\psi_{b.c}|$.

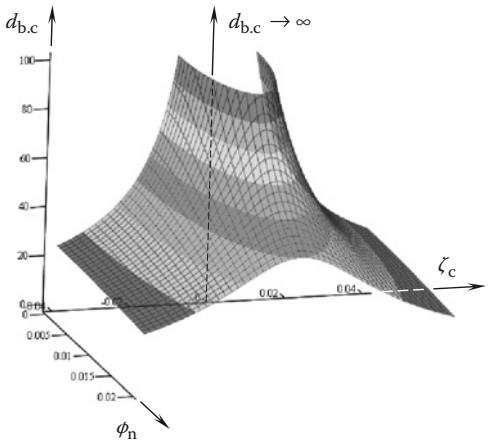

FIGURE 15.22
Impact of the normal profile angle ϕ_n, and of the setting angle ζ_c on the value of the base diameter of a gear cutting tool.

How is the last statement correlated with the case depicted in Figure 15.4? Under a scenario when the auxiliary generating rack $\mathscr{R}_{T.3}$ features a zero profile angle and setting angle ζ_c of a small value, then the screw involute surface cannot practically be generated.

However, the last point does not mean that gear cutting tools featuring a zero profile angle $\phi_n = 0°$ are not feasible. They are feasible. However, in this particular case, the cutting edges of the gear cutting tools are located along the helix line on the outer cylinder of the gear cutting tool.

16

Hobs for Machining Gears

Hobs are widely used for machining gears. Hobbing is usually and justifiably regarded as the accurate method of gear production and more thought and mechanical skill have been expended on hobbing machines and their correct functioning than on any other type of gear cutting machine. The process lends itself to the production of all types of gear, including those based on cones that constitute a special application, and it is unlikely to be superseded in the foreseeable future, particularly when large externally toothed cylindrical gears of high accuracy are required.

16.1 Transformation of the Generating Surface into a Workable Gear Cutting Tool

Consider a body that is made up of a cutting material. The body is bounded by the generating surface of the gear cutting tool. The body can be referred to as the *generating body* of the gear cutting tool.

In order to transform the generating body into the gear cutting tool it is necessary to make the body capable of removing the stock. Two ways to do that are considered below.

First, the generating surface of the gear cutting tool can be entirely generated by cutting elements (e.g., by cutting edges). This is the easiest way to transform the generating body into a workable gear cutting tool. Following this method, grinding worms for machining gears can be designed.

As an example, consider a process of finishing of a helical gear with the grinding worm as shown in Figure 16.1. The work gear rotates about its axis of rotation O_g, and the grinding worm rotates about its axis of rotation O_c. The grinding worm is feeding in axial direction of the work gear with a feed F_c. Conversely, the work gear could be feeding in its axial direction. In the sense of surface generation, only relative motions of the work gear and of the gear cutting tool are of importance.

The rotations of the work gear ω_g and the grinding worm ω_c, as well as the feed F_c, are properly timed with each other in compliance with the design parameters of the work gear (namely, with the tooth number N_g, pitch helix angle ψ_g, and the helix hand), as well as with the design parameters of the grinding wheel (namely, with the starts number N_c, pitch helix angle ψ_c, and the helix hand).

The motions shown in Figure 16.1 are the same as those shown in Figure 3.8. The only difference is the feed motion F_c. The necessity of the feed motion F_c is solely due to the fact that the generating surface T of the gear cutting tool makes point contact with the gear tooth flank surface $\mathscr{G}_g$. The characteristic line E_g (for the gear tooth flank surface $\mathscr{G}_g$ and the auxiliary generating surface $\mathscr{R}_T$) and the characteristic line E_c (for the auxiliary generating surface $\mathscr{R}_T$ and the generating surface T of the gear cutting tool) intersect at the point of contact of the surfaces $\mathscr{G}_g$ and T. In rolling motion the point of contact traces the involute

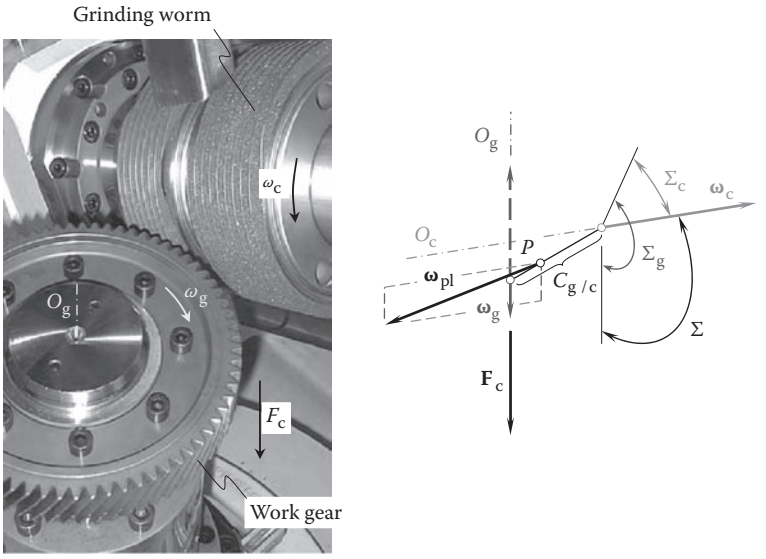

FIGURE 16.1
Grinding a helical gear with the grinding worm.

tooth profile of the work gear. In order to spread the generated involute tooth profile along the face width of the work gear*, the feed motion $\mathbf{F}_c$ is required.

As such, the kinematics of part surface generation is practical to use for semifinishing and for finishing of gears. However, fine pitch gears can be ground up from a solid blank—under such a scenario gear grinding becomes not just a finishing operation, but it also works as a roughing operation.

There are several possible ways to incorporate the feed motion $\mathbf{F}_c$ into the kinematic scheme of the gear machining operation.

A helical gear can perform a screw motion $\mathbf{S}_{cr}^{(g)}$ under which tooth flank surface $\mathscr{G}_g$ of the helical gear tooth moves over itself. The screw motion $\mathbf{S}_{cr}^{(g)}$ is the result of superposition of a rotation $\boldsymbol{\omega}_g^{(a)}$ and of a translation $\mathbf{V}_g^{(a)}$ of the work gear. These motions are timed with each other so that the ratio $|\mathbf{V}_g^{(a)}|/|\boldsymbol{\omega}_g^{(a)}|$ is equal to the reduced pitch p_g of the tooth flank surface $\mathscr{G}_g$ (Figure 16.2). The hand of the screw motion $\mathbf{S}_{cr}^{(g)}$ goes in the same direction as the direction of the hand of the gear tooth flank $\mathscr{G}_g$. For right-hand helical surface $\mathscr{G}_g$ the vectors of the rotation $\boldsymbol{\omega}_g^{(a)}$ and the translation $\mathbf{V}_g^{(a)}$ go in the same direction (Figure 16.3a and b). They can be pointed either in the same direction as the main rotation vector $\boldsymbol{\omega}_g$ of the work gear (Figure 16.3a), or they can be pointed in the opposite direction of the vector $\boldsymbol{\omega}_g$ (Figure 16.3b). Here, vector $\boldsymbol{\omega}_g$ of the main rotation that is considered together with vector $\boldsymbol{\omega}_c$ of the main rotation of the gear cutting tool result in rolling of the axodes of the work gear and the gear cutting tool.

* Only in a particular case when (a) the cutting edge is congruent to the characteristic line E_c, (b) the characteristic line E_c is congruent to the characteristic line E_g, and (c) the characteristic line $E_c \equiv E_g$ performs rolling motion about the axis O_g of the work gear, then the feed motion F_c can be eliminated from the kinematics of the gear machining operation.

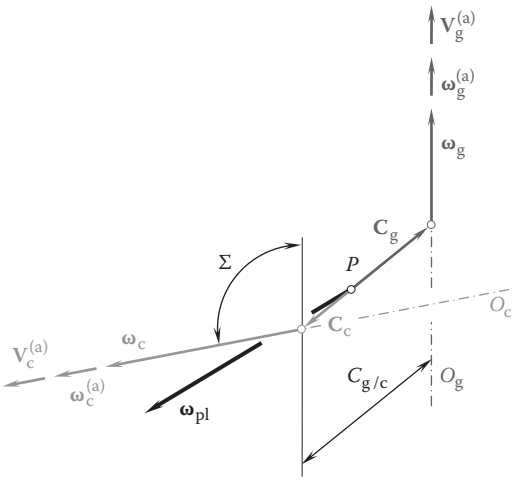

FIGURE 16.2
Configuration of the motion vectors for the operation of gear machining that features the point contact of the gear tooth flank surface $\mathscr{G}_g$ and the generating surface T of the gear cutting tool.

For a left-hand-oriented helical surface $\mathscr{G}_g$ the vectors $\boldsymbol{\omega}_g^{(a)}$ and $\mathbf{V}_g^{(a)}$ are pointed in the opposite directions (Figure 16.3c and d). While pointing in the opposite directions, the rotation vector $\boldsymbol{\omega}_g^{(a)}$ can be either pointing in the same direction as the main rotation vector $\boldsymbol{\omega}_g$ of the work gear (Figure 16.3c), or it can be pointed in the opposite direction of the vector $\boldsymbol{\omega}_g$ (Figure 16.3d).

Possible configurations of the vectors $\boldsymbol{\omega}_g^{(a)}$ and $\mathbf{V}_g^{(a)}$ with respect to each other, as well as with respect to vector $\boldsymbol{\omega}_g$ of the main rotation of the work gear (Figure 16.3), encompass both right-hand-oriented helices $\mathscr{G}_g$ and left-hand-oriented helices $\mathscr{G}_g$ as well. They also encompass conventional methods of gear machining (e.g., conventional gear hobbing operations), and climb methods of gear machining (e.g., climb gear hobbing operations).

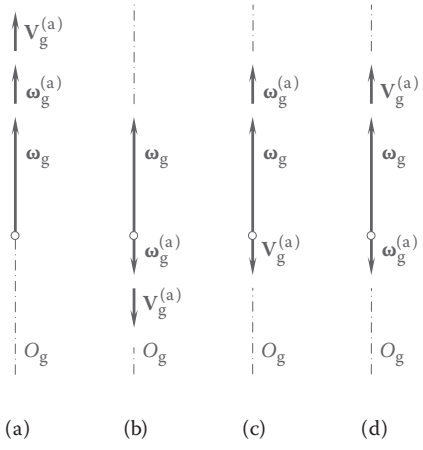

FIGURE 16.3
Possible configurations of the rotation vector $\boldsymbol{\omega}_g^{(a)}$ and the translation vector $\mathbf{V}_g^{(a)}$ with respect to the main rotation vector $\boldsymbol{\omega}_g$ of the work gear.

In a specific case of gear machining either the rotation or translation degenerates to zero; namely, either the equality $\boldsymbol{\omega}_g^{(a)} = 0$ or $\mathbf{V}_g^{(a)} = 0$ is observed. The first case corresponds to machining of spur gears, while the second case corresponds to machining of round racks.

A screw motion $\mathbf{S}_{cr}^{(g)}$ similar to the screw motion $\mathbf{S}_{cr}^{(g)}$ that was just considered can also be performed by the gear cutting tool. When performing the screw motion $\mathbf{S}_{cr}^{(c)}$, the generating surface T of the gear cutting tool moves over itself. In the case under consideration, the screw motion $\mathbf{S}_{cr}^{(c)}$ is a kind of superposition of a rotation $\boldsymbol{\omega}_c^{(a)}$ and a translation $\mathbf{V}_c^{(a)}$ of the gear cutting tool. The rotation $\boldsymbol{\omega}_c^{(a)}$ and the translation $\mathbf{V}_c^{(a)}$ are timed so that the ratio $|\mathbf{V}_c^{(a)}|/|\boldsymbol{\omega}_c^{(a)}|$ is equal to the reduced pitch p_c of the generating surface T of the gear cutting tool. The hand of the screw motion $\mathbf{S}_{cr}^{(c)}$ is going in the same direction as the hand of the generating surface T. For right-hand helical surface T the vectors of the rotation $\boldsymbol{\omega}_c^{(a)}$ and the translation $\mathbf{V}_c^{(a)}$ are going in the same direction. They can be pointed either in the same direction as the main rotation vector $\boldsymbol{\omega}_c$ of the gear cutting tool, or they can be pointed in the opposite direction of the vector $\boldsymbol{\omega}_c$.

Feasible configurations of the vectors $\boldsymbol{\omega}_c^{(a)}$ and $\mathbf{V}_c^{(a)}$ with respect to each other, as well as with respect to vector $\boldsymbol{\omega}_c$ of the main rotation of the gear cutting tool encompass both right-hand-oriented helices T and left-hand-oriented helices T as well. A screw motion $\mathbf{S}_{cr}^{(c)}$ of the gear cutting tool is employed, for example, (a) when hobbing worm gears, (b) in the operation of diagonal hobbing of gears, (c) in three main methods of gear shaving operation, and so forth.

Tools for grinding gears reproduce generating surface T, which actually is a discontinuous surface. However, due to the large number of abrasive grains involved it can be interpreted as the continuous surface.

Reproduction of a continuous generating surface T by cutting elements (e.g., by abrasive grains) of the gear grinding tool is not the only feasible way for transforming the generating body into a workable gear cutting tool. The surface T can also be reproduced discretely. In this way, hobs for machining gears and gear cutting tools of other designs can be designed. As illustrated in Figure 16.4, the generating surface T of the gear cutting tool can be reproduced by a certain number of discrete cutting edges CE. Geometrically,

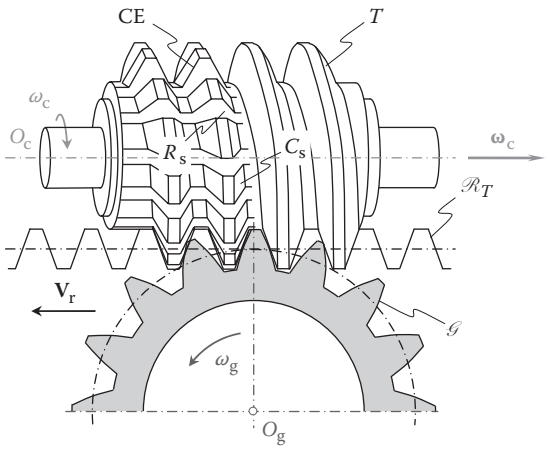

FIGURE 16.4
Discrete reproduction of the generating surface of a gear cutting tool.

cutting edge can be viewed as the line of intersection of the generating surface T by the rake surface R_s. Gashes are cut up in the generating body of the gear cutting tool in order to form the rake surfaces R_s. After the cutting edges CE and the rake surfaces R_s are formed, then the clearance surfaces C_s are created in order to pass through the cutting edges at a certain clearance angle α with respect to the surface T. More details on the methods of transforming the generating bogy into a workable gear cutting tool can be found in [138, 143], as well as from other sources.

It is of critical importance to stress here that all cutting edges, namely the cutting edges of both sides of the tooth profile of the gear cutting tool as well as the top cutting edges, are within the corresponding portions of the generating surface of the gear cutting tool. Any displacement of the cutting edge from the generating surface causes deviations of the actually machined gear tooth surface from the desired gear tooth surface. The complexity of the problem is mostly due to three surfaces: the generating surface T of the gear cutting tool, the rake surface R_s, and the clearance surface C_s; all three should pass through the corresponding cutting edge CE. In practical terms, it is often difficult to ensure that the three surfaces pass through a cutting edge (i.e., guarantee that the three surfaces pass through a common line).

Rake surfaces R_s and clearance surfaces C_s of various geometries are used in the design of a gear cutting tool. For the generation of the surfaces R_s and C_s, numerous methods are used in industry. Methods of roughing (i.e., methods of machining with edge cutting tools), and finishing methods (i.e., methods of machining with grinding wheels) are distinguished. The ultimate geometry of both the rake surfaces and the clearance surfaces is produced on finishing operations. This book is focused on a detailed investigation of geometrical and kinematical aspects of the finishing of the surfaces R_s and C_s.

16.2 Geometry and Generation of Rake Surface of a Gear Hob

The cut chip flows out of the machined part surface over the rake surface of the hob tooth. The surface R_s is one of the surfaces bounding the hob gashes. Often, the rake surface R_s is orthogonal to the helix of the threads on the pitch cylinder of the generating surface T of the hob.

16.2.1 Geometry of the Rake Surface

Surfaces of various geometries can be implemented as the rake surface of a gear hob. A screw rake surface R_s that features an assigned value of helix angle ψ_{rs} is considered below as a representative example of rake surfaces. An example of generation of rake surface R_s of a precision involute hob is schematically depicted in Figure 16.5.

Involute hobs with a small helix angle may have straight gashes. Rake angle γ_o at the top cutting edge of the hob is often equal to zero $\gamma_o = 0°$. However, for roughing of gears as well as for machining of low accuracy gears, involute hobs with positive rake angle $\gamma_o > 0°$ are often used. For semifinishing and/or for finishing of hardened gear hobs with an increased negative rake angle, $\gamma_o << 0°$ are used as well.

The rake surface is represented here as a family of successive positions of a straight-line generator, G_{rs}, which performs a screw motion about the hob axis O_c. In the Cartesian

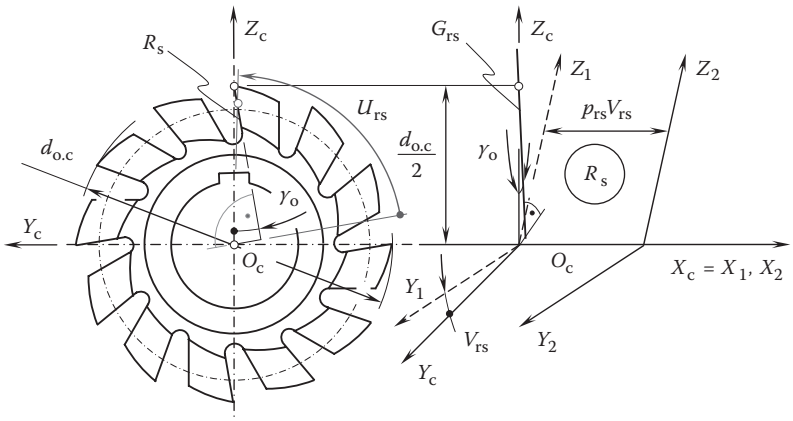

FIGURE 16.5
Generation of the rake surface R_s of an involute hob. (From Radzevich, S.P., *SME Journal of Manufacturing Processes*, 9(2), 121–136, 2007. With permission.)

coordinate system $X_cY_cZ_c$ associated with the gear cutting tool the straight-line generator G_{rs} makes the rake angle γ_o with the Z_c axis. Position vector $\mathbf{r}_{rg}$ of a point of the straight-line G_{rs} is located within the Y_cZ_c coordinate plane as shown in Figure 16.6. The equation of the straight-line G_{rs} yields vector representation in the form $\mathbf{r}_{rg} = \mathbf{r}_{rg}(U_{rs})$, where U_{rs} denotes the parameter of the straight-line G_{rs}. For an involute hob with a rake angle of a certain value γ_o, the straight-line generator G_{rs} is at the distance p_{rg} away from the axis $O_c \equiv X_c$. As it is clear from Figure 16.6, for the hob with an outer diameter $d_{o.c}$, the parameter p_{rg} can be computed from the formula

$$p_{rg} = 0.5d_{o.c} \sin \gamma_o \tag{16.1}$$

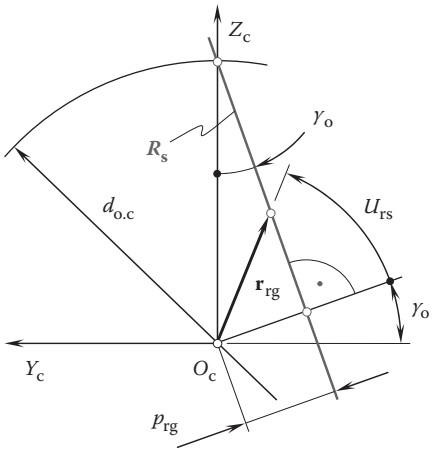

FIGURE 16.6
On deriving an equation of the straight-line generator G_{rs} of the helical rake surface R_s of the hob. (From Radzevich, S.P., *SME Journal of Manufacturing Processes*, 9(2), 121–136, 2007. With permission.)

The position vector of a point $\mathbf{r}_{rg}$ of the straight-line G_{rs} makes the certain angle U_{rs} with the shortest distance of approach of the generator G_{rs} and X_c axis. Therefore, the position vector $\mathbf{r}_{rg}$ of a point of the straight-line G_{rs} yields matrix representation in the form [149]

$$\mathbf{r}_{rg}(U_{rs}) = \begin{bmatrix} 0 \\ p_{rg} \cdot \dfrac{\sin\gamma_o \cos(\gamma_o + U_{rs})}{\cos U_{rs}} \\ p_{rg} \cdot \dfrac{\sin\gamma_o \sin(\gamma_o + U_{rs})}{\cos U_{rs}} \\ 1 \end{bmatrix} \tag{16.2}$$

The generating line G_{rs} performs a screw motion about the hob axis of rotation O_c. The parameter of the screw motion is designated as p_{rs}.

To make the analysis clear, two auxiliary reference systems $X_1Y_1Z_1$ and $X_2Y_2Z_2$ are introduced as shown in Figure 16.5. The reference system $X_1Y_1Z_1$ rotates about the hob axis of rotation O_c, while the reference system $X_2Y_2Z_2$ travels along the axis O_c.

The screw motion of the generating line G_{rs} can be decomposed onto the rotation together with the reference system $X_1Y_1Z_1$ about the X_c axis, and onto the translation together with the coordinate system $X_2Y_2Z_2$ along the X_c axis. The rotation and the translation are timed with each other according to the parameter of the screw motion p_{rs}.

For the derivation of an equation for the screw rake surface R_s of the hob tooth, the operator $\mathbf{Rs}(2 \mapsto c)$ of the resultant coordinate system transformation, say of the transition from the coordinate system $X_2Y_2Z_2$ to the gear hob coordinate system $X_cY_cZ_c$, is used. An analysis of Figure 16.5 reveals that the operator $\mathbf{Rs}(2 \mapsto c)$ can be expressed in terms of the operator of rotation, $\mathbf{Rt}(V_{rs}, Z_c)$, and of the operator of translation, $\mathbf{Tr}(p_{rs}V_{rs} \mapsto X_c)$, say

$$\mathbf{Rs}(2 \mapsto c) = \mathbf{Tr}(p_{rs}V_{rs} \mapsto X_c) \cdot \mathbf{Rt}(V_{rs}, Z_c) \tag{16.3}$$

Position vector of a point $\mathbf{r}_{rs}$ of the rake surface R_s, therefore, can be expressed by the equation

$$\mathbf{r}_{rs}(U_{rs}, V_{rs}) = \mathbf{Rs}(2 \mapsto c) \cdot \mathbf{r}_{rg}(U_{rs}) \tag{16.4}$$

Equations (16.2) through (16.4) yield a matrix representation for equation of the screw rake surface R_s of an involute hob [149]

$$\mathbf{r}_{rs}(U_{rs}, V_{rs}) = \begin{bmatrix} p_{rs}V_{rs} \\ \dfrac{\sqrt{2}p_{rg}\sin\gamma_o \cos(\gamma_o + U_{rs})}{\cos U_{rs}} \cdot \sin\left(\dfrac{\pi}{4} + V_{rs}\right) \\ \dfrac{\sqrt{2}p_{rg}\sin\gamma_o \sin(\gamma_o + U_{rs})}{\cos U_{rs}} \cdot \cos\left(\dfrac{\pi}{4} + V_{rs}\right) \\ 1 \end{bmatrix} \tag{16.5}$$

The parameters of the rake surface R_s can be expressed in terms of the corresponding design parameters of the hob (see Appendix A).

The performed analysis of feasible geometries of rake surfaces of gear hobs [149] reveals that all feasible types of rake surfaces can be interpreted as a specific case of the convolute surface (Figure 16.7), and therefore an equation for each of them could be derived from Equation (16.5).

Gear hobs of conventional design feature the rake surface in the form of an Archimedean helicoid, which is a specific case of a convolute surface with a zero rake angle ($\gamma_o = 0°$). For this particular case of gear hob design, an equation of the rake surface can be represented in matrix form

$$\mathbf{r}_{rs}(Z_c, V_{rs}) = \begin{bmatrix} p_{rs} V_{rs} \\ Z_c \sin V_{rs} \\ Z_c \cos V_{rs} \\ 1 \end{bmatrix} \tag{16.6}$$

The case of a gear hob with a zero rake angle $\gamma_o = 0°$ is a degenerated one. This is due to the distance p_{rg} reducing to zero ($p_{rg} = 0$).

For gear hobs with negligibly small pitch lead angle λ_{rs} of the rake surface R_s, the rake surface is often shaped in the form of a plane. In this particular case of gear hob design, the equation of the rake surface can be described in matrix form

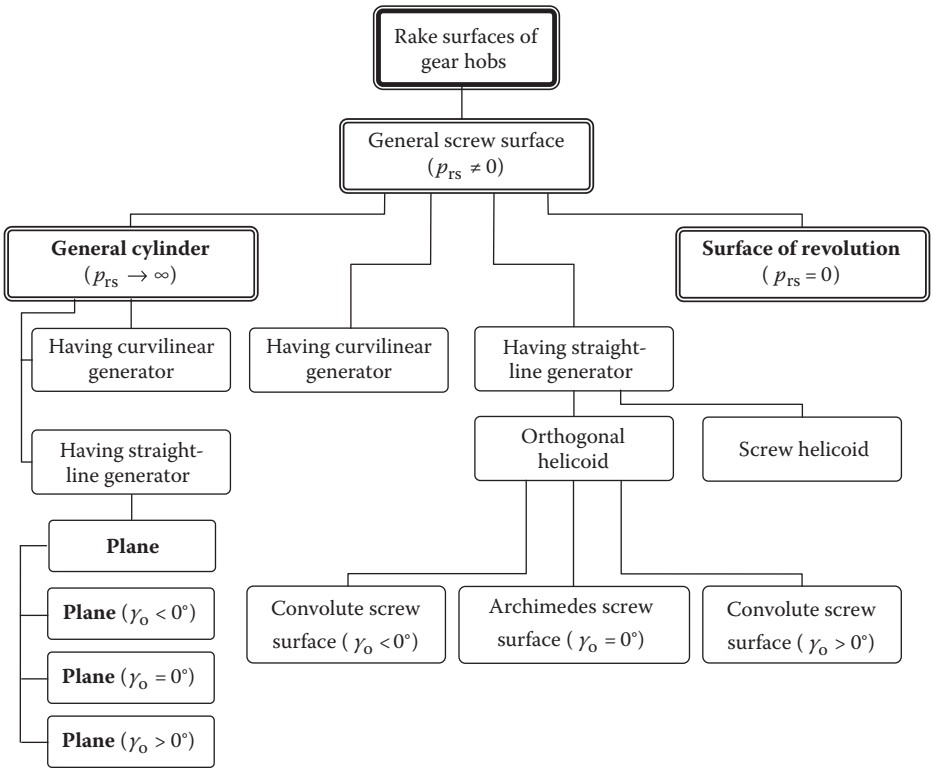

FIGURE 16.7
Possible kinds of rake surfaces of a gear hob. (From Radzevich, S.P., *SME Journal of Manufacturing Processes*, 9(2), 121–136, 2007. With permission.)

$$\mathbf{r}_{rs}(U_{rs}, X_c) = \begin{bmatrix} X_c \\ \dfrac{\sin\gamma_o \cos(\gamma_o + U_{rs})}{\cos U_{rs}} \\ \dfrac{\sin\gamma_o \sin(\gamma_o + U_{rs})}{\cos U_{rs}} \\ 1 \end{bmatrix} \tag{16.7}$$

The case considered above is also a degenerated one. This is because the screw parameter of the plane approaches infinity ($p_{rs} \to \infty$).

Ultimately, the rake angle γ_o of the hob with a rake surface R_s shaped in the form of a plane can also be of zero value ($\gamma_o = 0°$). This yields further simplification of the equation of the rake surface

$$\mathbf{r}_{rs}(U_{rs}, X_c) = \begin{bmatrix} X_c \\ 0 \\ Z_c \\ 1 \end{bmatrix} \tag{16.8}$$

It is important to note that the equation of the rake surface R_s of any feasible geometry allows for representation in the form $\mathbf{r}_{rs} = \mathbf{r}_{rs}(U_{rs}, X_c)$. This form of representation of the rake surfaces is proven convenient for performing the analysis of geometry of gear hobs.

16.2.2 Generation of the Rake Surface

Depending on the geometry of the actual rake surface of a hob, several methods for the generation of the surface R_s are used. A comprehensive investigation of methods for generation of screw surfaces is not a subject of this monograph. Therefore, only a few practical methods of generation of the rake surfaces are considered below as examples. The methods of the rake surface generation are considered from the kinematic and geometric perspective.

16.2.2.1 Generation of a Rake Surface in the Form of a Plane

The rake surface of the simplest geometry of the hob tooth is shaped in the form of a plane. The plane can be generated by means of another plane, which is congruent to the plane R_s as depicted in Figure 16.8. Generation of the rake plane R_s of the hob tooth is performed with the grinding wheel. The grinding wheel rotates ω_{gw} about its axis of rotation O_{gw}. The working plane T_{gw} of the grinding wheel (in other words, the generating surface T_{gw} of the grinding wheel) is perpendicular to the axis of rotation O_{gw}. The setup parameters of the grinding wheel are assigned so as to make the generating plane T_{gw} congruent to the rake plane R_s. While rotating, the grinding wheel is reciprocating $\mathbf{F}_{gw}$ in the axial direction of the hob being ground. In this way the rake plane R_s of the hob teeth is generated. The method is suitable for grinding hobs with a positive ($\gamma_o > 0°$) and negative ($\gamma_o < 0°$) rake angle γ_o, as well as for grinding hobs with a zero rake angle ($\gamma_o = 0°$).

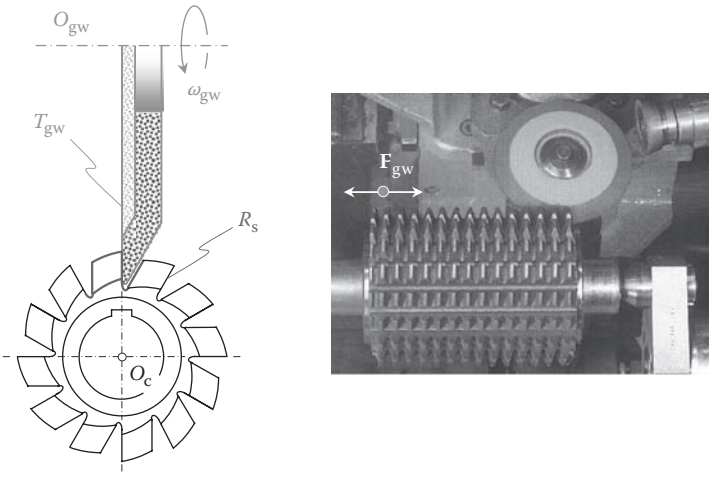

FIGURE 16.8
Generation of the rake plane R_s of a gear hob with a planar generating surface T_{gw} of the grinding wheel.

Geometrically, generation of the rake plane R_s can be performed with a narrow strip of generating surface T_{gw} of the grinding wheel (Figure 16.9). Width F_{gw} of the working portion of the generating surface T_{gw} is significantly smaller compared to height of the hob tooth. This particular method of rake plane generation is used for grinding hobs featuring cutting elements made up of carbide alloys, ceramics, superhard alloys, and so forth.

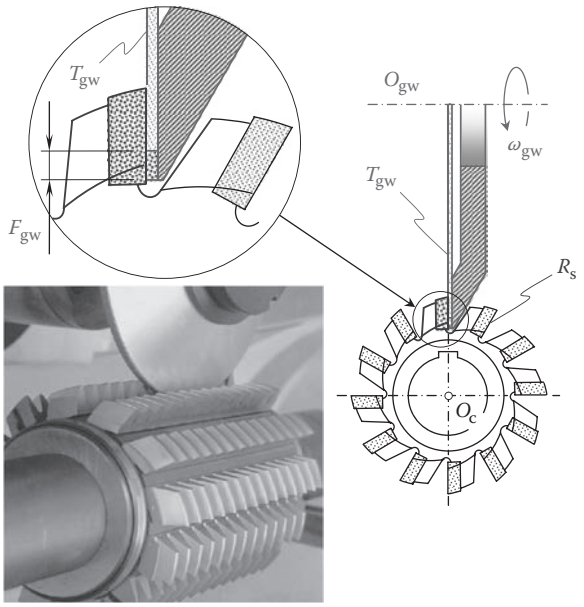

FIGURE 16.9
Generation of the rake plane R_s with a narrow portion of the plane of the generating surface T_{gw} of the grinding wheel.

16.2.2.2 Generation of a Screw Rake Surface

For the purposes of generation of a screw rake surface of a gear hob, a grinding wheel with a conical generating surface T_{gw} is commonly used. The grinding wheel rotates ω_{gw} about its axis of rotation O_{gw} (Figure 16.10). The setup parameters of the grinding wheel are assigned so to make the straight generating line of the conical generating surface T_{gw} aligned to the straight generating line of the screw rake surface R_s. While rotating, the grinding wheel is reciprocating in the axial direction of the hob being ground. (The reciprocation of the grinding wheel is not shown in Figure 16.10.) The hob is spinning about its axis O_c. The reciprocation of the grinding wheel is timed with the spinning of the hob. In this way the screw rake surface R_s of the hob teeth is generated.

In order to satisfy the set of necessary conditions of proper part surface generation [128, 138, 143], the setup parameters of the grinding wheel should be of appropriate values. This particular problem can be solved using the descriptive geometry–based method (*DG*-based method). Then, on the premise of the derived *DG*-based solution to the problem, corresponding analytical expressions can be derived to determine the setup parameters of the grinding wheel.

Consider a screw rake surface R_s of the hob having an outer diameter $d_{o.c}$. In Figure 16.11, the screw rake surface R_s is depicted in the system of planes of projections $\pi_1\pi_2\pi_3$. Assume that, in general, the surface R_s is not an orthogonal helicoid, but a skew helicoid, which features the straight generating line L at the $\psi_{r.s}$ with respect to the axis O_c. For the generation of the screw rake surface R_s, a conical grinding wheel of diameter D_{gw} is used. The generating surface T_{gw} of the grinding wheel features cone angle θ_{gw}. It is necessary to determine the crossing angle δ_{gw} of the axis of rotation O_{gw} of the grinding wheel, and the axis of rotation O_c of the hob.

All straight-generating lines of the rake surface R_s are offset from the axis O_c at a distance r_γ that is equal

$$r_\gamma = \frac{d_{o.c}}{2} \cdot \sin \gamma_o \tag{16.9}$$

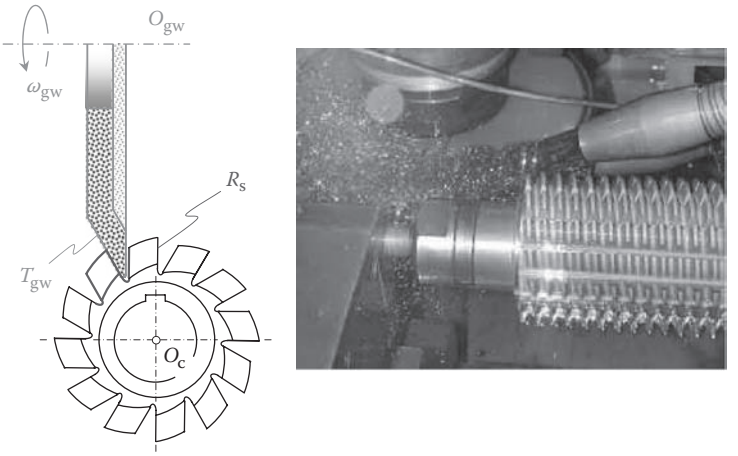

FIGURE 16.10
Generation of a screw rake R_s of the gear hob with a conical generating surface T_{gw} of the grinding wheel.

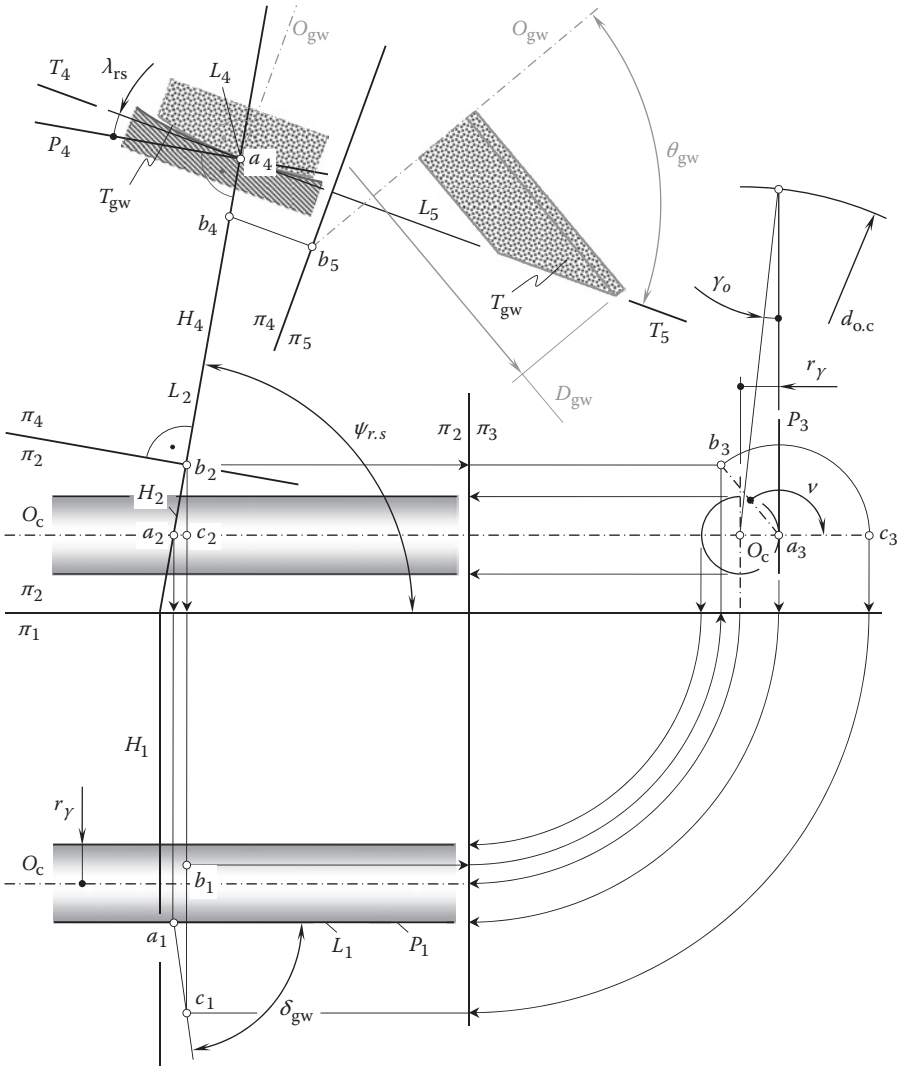

FIGURE 16.11
Determination of the setup parameters of the conical grinding wheel for the generating of a screw rake R_s of the gear hob.

This means that all straight-generating lines of the rake surface R_s are tangent to the round cylinder of radius r_γ. The cylinder is shown in Figure 16.11.

A plane P is tangent to the cylinder of radius r_γ. For convenience, the plane P is chosen so that it is parallel to the plane of projections π_2. An arbitrary point a is located within the line of tangency of the cylinder and of the plane P. The straight-generating line L of the rake surface R_s is the line through the point a, which is located within the plane P.

A plane H passes through the straight line L, and is perpendicular to the plane of projections π_2. It makes the angle $\psi_{r.s}$ with hob axis of rotation O_c. The auxiliary axis of projections π_2/π_4 is perpendicular to the trace H_2 of the plane H. A plane T is constructed so that it passes through the straight line L, and it makes an angle λ_{rs} with the plane P.

On the plane of projections π_4 the plane T is projected into the trace T_4. This allows for construction of the actual value of the angle λ_{rs}, and in this way for constructing the trace T_4.

The auxiliary axis of projections π_4/π_5 is constructed so that it is perpendicular to the trace T_4. Onto the plane of projections π_4 the straight line L is projected into point L_4, while onto the plane of projections π_5 the straight line L is projected with no distortion. In π_5 the projections L_5 aligns with the trace T_5.

Within the plane of projections π_5 actual value of the cone angle θ_{gw} can be constructed. In this way configuration of the axis of rotation O_{gw} of the grinding wheel is determined. The axis O_{gw} intersects the axis of projections π_4/π_5 at point b. The point b is necessary to specify the configuration of the axis O_{gw} within the rest of the planes of projections.

Ultimately, spinning the projection a_3b_3 about the axis O_c through the angle ν, the actual value of the crossing angle δ_{gw} can be constructed within the horizontal plane of projections π_1.

In most practical cases of generation of the screw rake surface of the gear hob, the angle $\psi_{r.s}$ is equal to the right angle. The determination of the crossing angle δ_{gw} is simplified under a scenario when the equality $\psi_{r.s} = 90°$ is valid.

The method of generation of the screw rake surface with a conical grinding wheel is suitable for grinding of hobs with a positive ($\gamma_o > 0°$), and negative ($\gamma_o < 0°$) rake angle γ_o, as well as for grinding of hobs with a zero rake angle ($\gamma_o = 0°$).

16.2.2.3 Peculiarities of Generation of a Screw Rake Surface of a Multistart Hob

Grinding wheels with a conical generating surface T_{gw} can be used for generation of a screw rake surface of gear hobs either when the lead angle of the rake surface R_s is reasonably small or if the accuracy of the gear hob is not a critical issue (e.g., as it is observed for roughing gear hobs). This is due to the fact that the conical generating surface of the grinding wheel is capable of generating the screw rake surface of the hob

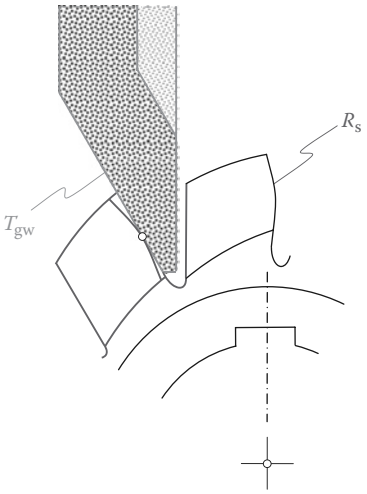

FIGURE 16.12
Deviation of the transverse profile of a screw rake R_s surface of a multistart hob.

only approximately. Therefore, the actually generated screw rake surface features not a straight-generating line, but a curved generating line instead (Figure 16.12). The proof can be found in [130]. For this purpose *DG*-based methods of analysis are used. After being generated with the conical generating surface T_{gw}, the profile of transverse cross-section of the screw rake surface R_s gets convex. The convexity of the transverse cross-section of the rake surface R_s is mostly due to the fact that the surfaces R_s and T_{gw} make line contact. The line of contact of the surfaces R_s and T_{gw} is not a planar curve, but a spatial 3-D curve. Ultimately, the peculiarities of the geometry of the line of contact result in the deviations of the actually generated surface R_s from the desired screw rake surface of the hob.

Deviations of the actual parameters of the screw rake surface R_s from its desired shape and geometry cause the corresponding deviations in tooth profile of the gear, of which the hob is used for machining.

When grinding a precision gear hob, especially when grinding a multistart gear hob, deviations of the actually ground rake surface from the desired screw surface R_s could exceed the tolerance for its shape and geometry. This particular source of the inaccuracies can be eliminated if generation of the screw rake surface of the gear hob teeth is performed with the grinding wheel having a form axial profile (Figure 16.13). For a specific hob design, the generating surface of the form grinding wheel T_{gw} can be found out as an envelope to successive positions of the desired screw rake surface R_s in its rotation about the axis of rotation of the grinding wheel. For the derivation of an equation of the generating surface T_{gw} of the form grinding wheel, the kinematic method for determining enveloping surfaces can be used [186].

Then the desired axial profile of the form grinding wheel can be derived as the axial cross-section of the surface T_{gw}. The axial profile can be used for dressing of the form grinding wheel.

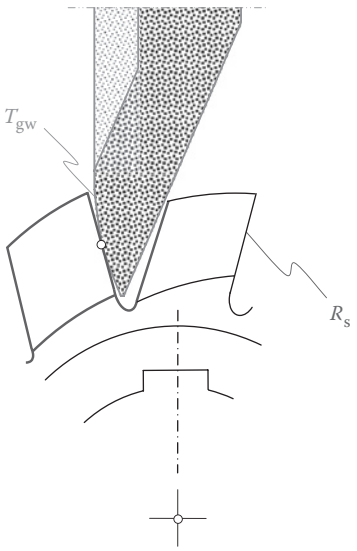

FIGURE 16.13
Generation of a screw rake R_s of a multistart hob with a form grinding wheel.

16.2.2.4 Methods for Generation of an Intermittent Rake Surface of the Special-Purpose Gear Hob

The considered methods of generation of rake surfaces are applicable in cases when the rake surface of each tooth within a gash of the gear hob is within a continuous surface. The last can be shaped either in the form of a common plane, or in the form of a common screw surface. The rake surfaces of more complex geometry are used in design of gear hobs as well.

Special-purpose gear hobs may have rake surfaces, which do not belong to a common continuous surface. Instead, rake surface of each tooth can be shifted with respect to each other along pitch helix of the hob. Rake surfaces of this type are referred to as *intermittent rake surface* of the gear hob. Special methods are developed for grinding of the special-purpose gear hobs featuring intermittent rake surfaces. The methods make it possible to grind separately the rake plane of every single tooth of the gear hob.

As an example, kinematics of a method [81] for generation of an intermittent rake surface R_s of the special-purpose gear hob is schematically illustrated in Figure 16.14. The hob to be ground features the rake surfaces of each tooth that are shifted along the pitch helix with respect to one another at a certain distance. Because of this, the rake surfaces that belong to a common gash of the hob are not within a common continuous surface, but represent the intermittent surface. When grinding, the hob rotates about its axis of rotation O_c as shown in Figure 16.14. The grinding wheel with generating plane T_{gw} is used for grinding the hob. The grinding wheel rotates ω_{gw} about its axis of rotation O_{gw}. Configuration of the axis of rotation O_{gw} with respect to the gear hob is specified by two angles, ξ_{gw} and ξ^*_{gw}.

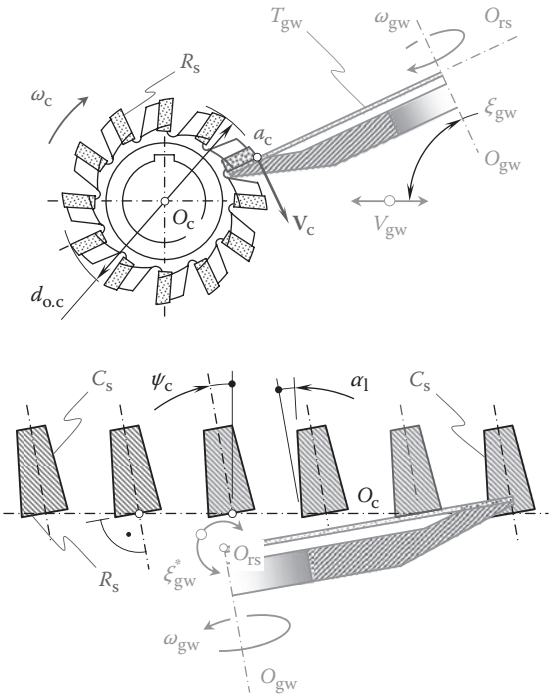

FIGURE 16.14
Generation of an intermittent rake surface R_s of a special-purpose gear hob.

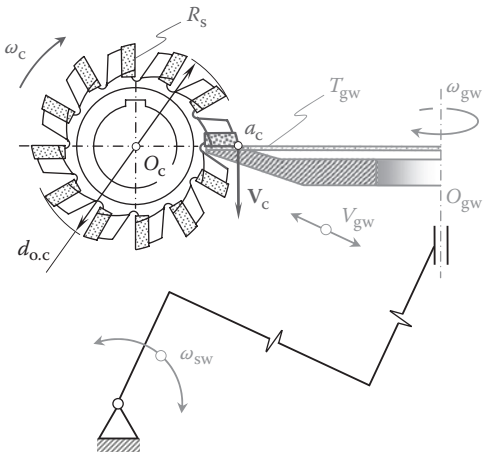

FIGURE 16.15
Method of generating the intermittent rake surface R_s of a special-purpose gear hob that features swivel motion ω_{sw} of the grinding wheel.

When grinding a rake plane R_s, the hob rotates with constant angular velocity ω_c. The grinding wheel reciprocates back and forth with respect to the hob. The grinding wheel reciprocation features (a) a slow approach to the hob, (b) instant interaction of the surfaces R_s and T_{gw}, and (c) fast departure of the grinding wheel from the hob. In order to avoid the collision of the grinding wheel with the hob, the speed of the departure V_{gw} and the angle ξ_{gw} have to be chosen so as to fulfill the inequality (Figure 16.14)

$$V_{gw} \geq |\mathbf{V}_c| = 0.5\omega_c d_{o.c} \cos\xi_{gw} \tag{16.10}$$

where

$\mathbf{V}_c$ = Vector of linear velocity of rotation of the point a_c about the hob axis of rotation
$d_{o.c}$ = Outer diameter of the hob
ξ_{gw} = An angle at which the axis of the grinding wheel is tilted in transverse cross-section of the hob

In addition to the tilt angle ξ_{gw}, the axis of rotation of the grinding wheel O_{gw} is turned about the axis O_{rs} through an angle ξ^*_{gw}. The axis O_{rs} is perpendicular to the hob axis of rotation O_{gw}, and it is located within the rake plane R_s of the hob tooth. In particular, the angle ξ^*_{gw} could be of the value $\xi^*_{gw} = \psi_c$ under which the rake plane is perpendicular to pitch helix of the hob. Here ψ_c denotes the pitch helix angle of the hob.

A method of grinding of gear hobs similar to that discussed above is disclosed in [173]. The method features not the reciprocating motion but swivel motion ω_{sw} of the grinding wheel instead. The method of rake surface generation is illustrated in Figure 16.15. The setup parameters of the grinding wheel and the motions ω_c and ω_{sw} are determined so as to satisfy the inequality $|\mathbf{V}_c| \leq pr_{\mathbf{V}_c} V_{gw}$, where $pr_{\mathbf{V}_c} V_{gw}$ designates projection of the vector V_{gw} onto direction of the vector $\mathbf{V}_c$.

Much room is available for further improvements in the area of grinding hobs that feature continuous as well as intermittent rake surfaces.

16.3 Geometry and Generation of Clearance Surfaces of Gear Hobs

Once the rake surface of the hob is generated, then the clearance surface of the hob tooth can be generated as well. As illustrated in Figure 16.16, the rake surface R_s intersects the generating surface T of the hob. Geometrically, the cutting edge is considered here as the line of intersection of the surface T by the surface R_s. The desired clearance surface C_s is a surface through the cutting edge CE, which makes clearance angle α of the required value with the surface of the cut.

Implementation of the surface of the cut is inconvenient for the analysis below. Generating surface T of the hob is a practically reasonable approximation to the surface of the cut in the vicinity of the cutting edge CE. Therefore, approximately (however, with sufficient degree of accuracy) the surface of the cut is substituted with the generating surface of the hob. Ultimately, the clearance surface C_s is interpreted as a surface through the cutting edge CE, which makes clearance angle α of the required value with the generating surface T. In the ideal case, cutting edge CE is the line of intersection of three surfaces, namely the surfaces T, R_s, and C_s. It is of critical importance to notice here that the last requirement is vital for new hobs as well as for reground hobs.

16.3.1 Equation of the Desired Clearance Surface of the Hob Tooth

Three methods for transforming the generating body of the cutting tool into a workable cutting tool are known [138, 143]. Below, the most common method is followed. This approach features the clearance surface that passes through the cutting edge at the desired clearance angle. The cutting edge CE is considered here as the line of intersection of generating surface T of the hob by the rake surface R_s. Then for the derivation of an equation of the clearance surface C_s, a motion of the cutting edge CE with respect to the generating surface T is considered. The direction of this motion makes the desired clearance angle α with the surface T. Ultimately, the clearance surface of the hob tooth is represented as the set of successive positions of the cutting edge CE when it performs the motion described above.

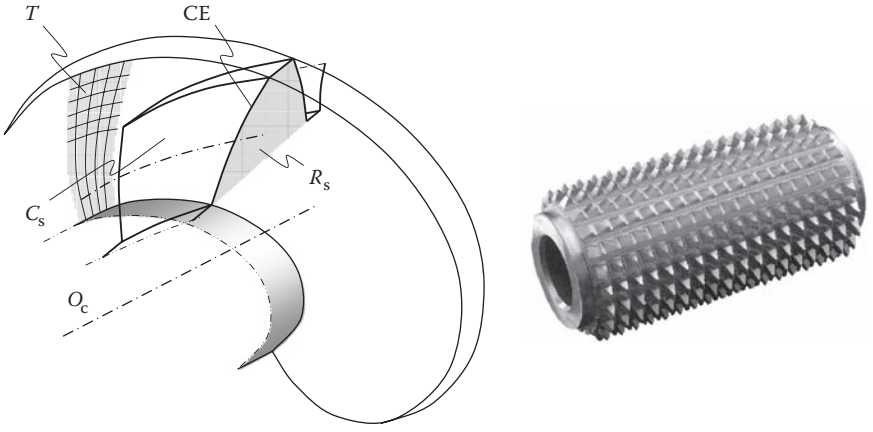

FIGURE 16.16
Clearance surface C_s of the hob tooth passing through the cutting edge CE. (The latter is interpreted as the line of intersection of the generating surface T of the hob by the rake surface R_s.)

The geometry of the desired clearance surface C_s of the involute hob tooth is illustrated in Figure 16.17. It is assumed below that the generating surface T of the hob is determined, and the rake surface R_s is given. For simplicity, but without loss of generality of the consideration, the rake plane R_s through the axis of rotation O_c is considered as an example.

The rake plane R_s of the new hob intersects the generating surface T of the hob. In Figure 16.17, the line of the intersection is denoted as N. The line N starts at a point n within the base cylinder of diameter $d_{b.c}$ of the hob and goes outward toward the hob axis of rotation O_c. It intersects (a) the cylinder of outer diameter $d^n_{o.c}$, (b) the pitch cylinder of diameter d^n_c, and (c) the cylinder of limit diameter $d^n_{l.c}$, of the new hob at the points a, b, and c correspondingly. The arc $\widehat{abc}$ of the intersection curve N is chosen as the cutting edge CE^n of the new hob.

Each time after the hob is reground, the diameters of the hob get smaller and smaller. This is due to the necessity in the clearance angle for good cutting performance of the hob. Ultimately, after the last regrind, the diameters of the fully worn hob are designated in Figure 16.17 as $d^w_{o.c}$, d^w_c, and $d^w_{l.c}$. These diameters correspond to the diameters $d^n_{o.c}$, d^n_c, and $d^n_{l.c}$ of the new hob before it has been reground.

The rake plane R_s of the worn hob intersects the generating surface T of the hob. In Figure 16.17, the line of the intersection is denoted as W. The line W starts at a point w within the base cylinder of diameter $d_{b.c}$ of the hob and goes outward toward the hob axis of rotation O_c. It intersects (a) the cylinder of outer diameter $d^w_{o.c}$, (b) the pitch cylinder of diameter d^w_c, and (c) the cylinder of limit diameter $d^w_{l.c}$, of the worn hob at the points d, e, and f correspondingly. The arc $\widehat{def}$ of the intersection curve W is chosen as the cutting edge CE^w of the worn hob.

Similar to the method above, any and all intermediate locations of the cutting edge CE of the partially worn involute hob can be determined. The family of all of them is within the desired clearance surface of the involute hob.

The schematic discussed above (Figure 16.17) can be employed for the purpose of deriving an equation of the clearance surface C_s of the hob tooth.

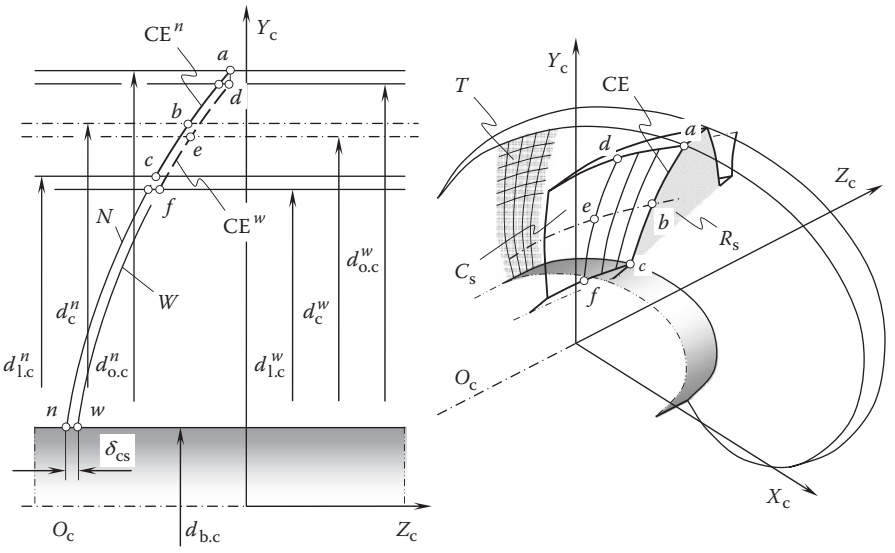

FIGURE 16.17
Geometry of the desired clearance surface C_s of the hob for machining involute gears.

Consider the equation [see Equation (16.54)]

$$\left.\begin{array}{l}\text{Generating surface } T\\ \text{of the involute hob}\end{array}\right| \quad \Rightarrow \quad \mathbf{r}_c(U_c, V_c) = \begin{bmatrix} 0.5d_{w.c}\sin V_c - U_c \sin\psi_{b.c}\cos V_c \\ 0.5d_{w.c}\cos V_c + U_c \sin\psi_{b.c}\sin V_c \\ p_{b.c}V_c - U_c\cos\psi_{b.c} \\ 1 \end{bmatrix} \tag{16.11}$$

of the generating surface T of the gear hob together with the equation

$$\left.\begin{array}{l}\text{The screw rake surface } R_s\\ \text{of the involute hob}\end{array}\right| \quad \Rightarrow \quad \mathbf{r}_{rs}(U_{rs}, V_{rs}) = \begin{bmatrix} p_{rs}V_{rs} \\ \dfrac{\sqrt{2}p_{rg}\sin\gamma_o\cos(\gamma_o + U_{rs})}{\cos U_{rs}}\cdot\sin\left(\dfrac{\pi}{4}+V_{rs}\right) \\ \dfrac{\sqrt{2}p_{rg}\sin\gamma_o\sin(\gamma_o + U_{rs})}{\cos U_{rs}}\cdot\cos\left(\dfrac{\pi}{4}+V_{rs}\right) \\ 1 \end{bmatrix} \tag{16.12}$$

of the screw rake surface R_s of the involute hob [see Equation (16.5)].

The position vector of a point of the cutting edge $\mathbf{r}_{ce} = \mathbf{r}_{ce}(U_{ce})$ satisfies both Equations (16.11) and (16.12) simultaneously. Two equations, Equations (16.11) and (16.12), cast into an expression of the form

$$\mathbf{r}_{ce}(U_{ce}) = \begin{bmatrix} X_{ce}(U_{ce}) \\ Y_{ce}(U_{ce}) \\ Z_{ce}(U_{ce}) \\ 1 \end{bmatrix} \tag{16.13}$$

which can be derived for the computation of the position vector $\mathbf{r}_{ce}$.

For the derivation of an equation of the desired clearance surface C_s of the hob tooth a screw motion of the cutting edge $\mathbf{r}_{ce}$ is considered. The reduced pitch of the screw motion of the cutting edge depends on (a) reduced pitch p_x of threads of generating surface T of the hob, and (b) value of the clearance angle α at the lateral cutting edges of the hob tooth. The reduced pitch p_x of threads of the generating surface T is a signed value. It is positive for the right-handed involute hobs, and it is negative for the left-handed involute hobs. In the case under consideration, it is convenient to treat the rake angle α as a signed value as well. The clearance angle α is positive for the clearance surface of the hob tooth when it increases the reduced pitch of the clearance surface (i.e., it is added with the pitch helix angle ψ_c). The clearance angle α is negative for the clearance surface of the hob tooth when it makes the reduced pitch of the clearance surface smaller (i.e., it is subtracted from the pitch helix angle ψ_c).

For further analysis it is convenient to refer to Figure 16.18 where cross-section of a hob thread by the pitch cylinder of diameter d_c is depicted. As shown in Figure 16.18, the cross-section of the hob tooth is bounded by the rake surface R_s and by two clearance surfaces C_s. The clearance surface that has the bigger reduced pitch ${}^{+}p_{cs} > p_x$ is designated as ${}^{+}C_s$. The

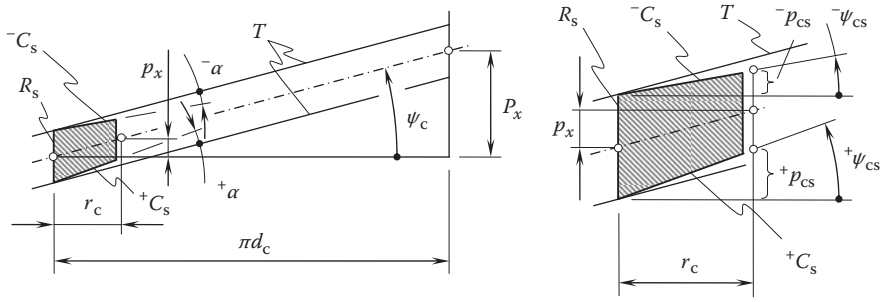

FIGURE 16.18
Cross section of a thread of an involute hob by the pitch cylinder of diameter d_c.

opposite clearance surface that features the smaller reduced pitch $-p_{cs} < p_x$ is designated as $-C_s$.

The actual value of the reduced pitch p_x for the involute hob with a given axial pitch P_x of threads can be computed from the following formula

$$p_x = \frac{P_x}{2\pi} \tag{16.14}$$

Pitch helix angle ψ_c can be expressed in terms of the axial pitch P_x, and of pitch diameter d_c of the hob

$$\psi_c = \tan^{-1}\left(\frac{P_x}{\pi d_c}\right) \tag{16.15}$$

For the clearance surface $^{+}C_s$ the corresponding helix angle $^{+}\psi_{cs}$ is equal

$$^{+}\psi_{cs} = \psi_c + \alpha \tag{16.16}$$

Once the helix angle $^{+}\psi_{cs}$ is computed, then for the computation of the reduced pitch $^{+}p_{cs}$ the following expression

$$^{+}p_{cs} = 0.5 d_c \tan {}^{+}\psi_{cs} \tag{16.17}$$

can be used.

Similarly, for the computation of the reduced pitch $-p_{cs}$ of the clearance surface $-C_s$ of the opposite side of the hob tooth profile the formula

$$^{-}p_{cs} = 0.5 d_c \tan {}^{-}\psi_{cs} \tag{16.18}$$

is valid. Here, for the computation of the helix angle $-\psi_{cs}$ the formula

$$^{-}\psi_{cs} = \psi_c - \alpha \tag{16.19}$$

can be used.

Clearance surface ${}^{+}C_s$ can be represented as a loci of successive positions of the cutting edge CE [see Equation (16.13)] when it performs the screw motion. The Z_c axis of the coordinate system $X_cY_cZ_c$ associated with the hob is the axis of the screw motion, and ${}^{+}p_{cs}$ is the parameter of the screw motion. Use of the operator of the linear transformation $\mathbf{Sc}_z(\varphi_{ce}, {}^{+}p_{cs})$ that analytically describes the screw motion (see Chapter 4)

$$\mathbf{Sc}_z(\varphi_{ce}, {}^{+}p_{cs}) = \begin{bmatrix} \cos\varphi_{ce} & \sin\varphi_{ce} & 0 & 0 \\ -\sin\varphi_{ce} & \cos\varphi_{ce} & 0 & 0 \\ 0 & 0 & 1 & {}^{+}p_{cs}\varphi_{ce} \\ 0 & 0 & 0 & 1 \end{bmatrix} \tag{16.20}$$

makes possible the following expression for the position vector ${}^{+}\mathbf{r}_{cs}$ of a point of the clearance surface ${}^{+}C_s$

$${}^{+}\mathbf{r}_{cs}(\varphi_{ce}, U_{ce}) = \mathbf{Sc}_z(\varphi_{ce}, {}^{+}p_{cs}) \cdot \mathbf{r}_{ce}(U_{ce}) \tag{16.21}$$

An equation for the position vector of a point ${}^{-}\mathbf{r}_{cs}$ of the clearance surface ${}^{-}C_s$ can be derived in a similar manner to how Equation (16.21) is derived.

In practice, for many reasons, the actual clearance surface C_s of the hob tooth deviates from the desired clearance surface. The desired clearance surface [see Equation (16.21)] serves as the reference surface for the computation of the deviations of the actual clearance surface from the desired clearance surface of the hob tooth.

16.3.2 Generation of the Clearance Surface of the Hob Tooth

Clearance surfaces of the hob teeth commonly are machined on a specific operation, which is often referred to as a *tooth relieving operation*. Relieving of the hob teeth is executed in the green (soft) stage of the hob and in the hard stage after heat treatment of the hob. Edge cutting tools are used in the first case, and grinding wheels are used in the second case.

16.3.2.1 Cutting of the Relieved Clearance Surfaces of the Hob Teeth

The relieved clearance surface is a practical type of approximation of the desired clearance surface of the hob tooth. A properly relieved hob (a) features a positive clearance angle, which is more or less close to the optimal value, and (b) has cutting edges the accuracy of which is within the tolerance for the accuracy of the hob.

Cutting of the relieved clearance surfaces of the hob teeth is used in two cases: (a) as a preliminary roughing operation of machining of the clearance surfaces, and/or (b) as a finishing operation of machining of the hob teeth. Basic methods of cutting of the relieved clearance surface of the hob tooth are depicted in Figure 16.19.

When cutting the clearance surface C_s, the hob rotates ω_c about its axis of rotation O_c. The direction of the rotation is chosen so that the rake surface R_s faces toward the rotation ω_c. The form cutter is reciprocating toward the axis of rotation O_c. In Figure 16.19 reciprocation motion of the cutter is denoted as $\mathbf{V}_{rc}$. In addition to the reciprocation motion $\mathbf{V}_{rc}$ the cutter travels $\mathbf{V}_{sc}$ in the axial direction of the hob. This motion $\mathbf{V}_{sc}$, together with the rotation ω_c, provide the screw motion of the cutter with respect to the clearance surface C_s to be cut.

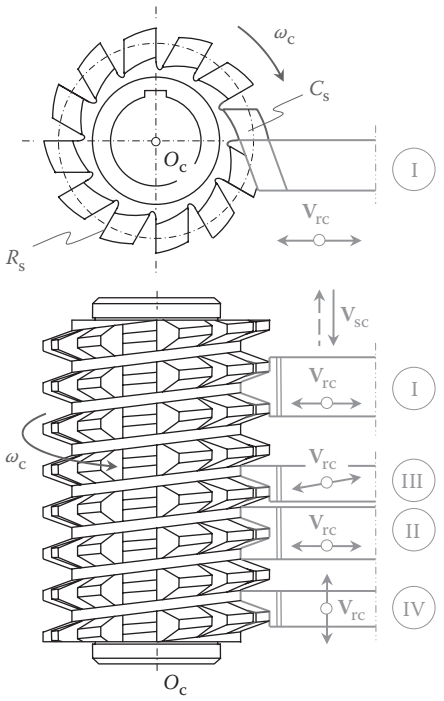

FIGURE 16.19
Basic methods of cutting the relieved clearance surface C_s of the hob tooth.

The form cutter is designed so that it is capable of cutting either space between two adjacent hob teeth (case I in Fig. 16.19), or it is cutting the clearance surfaces of the opposite sides of the hob tooth (case II in Fig. 16.19).

In production of coarse pitch hobs, two more methods of cutting the clearance surfaces of the hob teeth are used as well. The first method features the reciprocation motion $\mathbf{V}_{rc}$ of the form cutter pointed at a certain angle with respect to the axis of rotation O_c of the hob. A schematic of the method is illustrated in Figure 16.19 (case III). The reciprocation motion $\mathbf{V}_{rc}$ in the second method of cutting the surfaces C_s is parallel to the axis of rotation O_c of the hob (case IV in Figure 16.19).

When the second method of cutting the relieved surfaces of the hob teeth is implemented, the hob manufacturer is often faced with the necessity of solving two problems.

The first problem is mostly due to the limited room between the adjacent teeth of the hob for the form cutter to be used.

The second problem is owed to the following: The top land of the hob tooth is machined by the bottom land cutting edge of the form cutter, and the bottom land of the hob tooth is machined by the top land cutting edge of the form cutter. The distance between the top land cutting edge and the bottom land cutting edge of the form cutter must be chosen to be equal to half of the difference between the outer diameter $d^n_{o.c}$ of the new hob and the smallest inner diameter $d^{min}_{f.c}$ of the hob. This means that the tooth height within the rake surface of the form cutter must be equal to $h_{fc} = (d^n_{o.c} - d^{min}_{f.c})/2$.

Elements of the cutting edge geometry (the clearance surface of the relieved hob tooth). Normal clearance angle α_n and the clearance angle α_o that is measured in cross-section of the cutting edge by a plane that is perpendicular to the axis of rotation of the hob are the two

major elements of the cutting edge geometry that depend on the geometry and the configuration of the clearance surface C_s of the relieved hob tooth.

Without going into details of derivation, for hobs clearance surface of which is shaped with the help of Archimedean spiral, Figure 16.20 yields an expression

$$\alpha_o = \tan^{-1}\left(\frac{K_{cs} Z_{gashes}}{2\pi R_{o.c}}\right) \tag{16.22}$$

for the computation of the clearance angle α_o.

Equation (16.22) reveals that actual value of the clearance angle α_o depends on

(1) Outer diameter of the hob ($d_{o.c} = 2R_{o.c}$)

(2) Number of gashes Z_{gashes} (For hobs featuring straight gashes the parameter Z_{gashes} is expressed in integer numbers; for hobs with helical gashes the parameter Z_{gashes} is expressed in numbers with fractions.)

(3) The parameter K_{cs} of relieving (see Figure 16.20)

In practice, the computations performed in the inverse order are of importance. Instead of the computation of the clearance angle α_o, computation of the required value of the parameter K_{cs} of relieving are performed

$$K_{cs} = \frac{\pi d_{o.c}}{Z_{gashes}} \cdot \tan\alpha_o \tag{16.23}$$

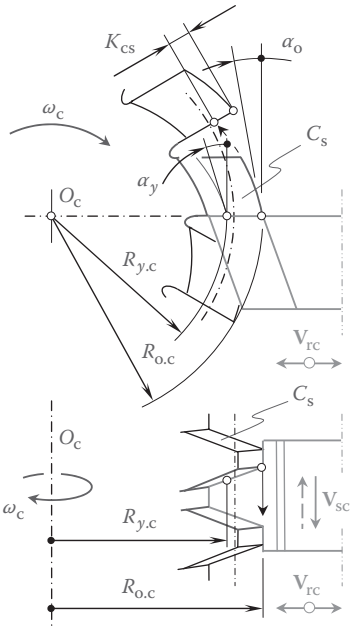

FIGURE 16.20
Determining the major parameters of the relieving operation in terms of the clearance angle α_o at the top cutting edge of a hob.

In this latter case, value of the clearance angle α_o should be given. For solid gear hobs (i.e., for those made up of one piece of cutting material), the practically reasonable values of the clearance angle are within the interval $\alpha_o = 10 \ldots 12°$.

Normal clearance angle α_n at the lateral cutting edge of the hob tooth depends on clearance angle α_o at the top cutting edge of the hob. This feature is inherited to relieved hobs of all designs. The actual value of the normal clearance angle α_n of involute hobs with a zero rake angle γ_o can be computed from the following formula

$$\alpha_n = \tan^{-1}\left(\tan\alpha_o \sin\phi_{rs}\right) \tag{16.24}$$

Here, in Equation (16.24), ϕ_{rs} denotes a profile angle that is measured within the rake surface of the hob tooth.

Hobs for machining of involute gears feature the clearance angle α_o, the actual value of which is almost constant within the lateral cutting edge ($\alpha_o \cong$ const). Only for coarse pitch, hobs of small diameter variation of the clearance angle α_o within the lateral cutting edge could be of importance. For the computation of the clearance angle α_y at an arbitrary point within the lateral cutting edge of the hob the formula

$$\alpha_y = \tan^{-1}\left(\frac{R_{o.c}}{R_{y.c}} \cdot \tan\alpha_o\right) \tag{16.25}$$

is commonly used. Here, in Equation (16.25), the radius of a cylinder through the arbitrary point m of the lateral cutting edge is denoted as $R_{y.c}$ (see Figure 16.20).

Considered together, Equations (16.24) and (16.25) allow for an expression

$$\alpha_{n.y} = \tan^{-1}\left(\frac{R_{o.c}}{R_{y.c}} \cdot \tan\alpha_o \sin\phi_{rs}\right) \tag{16.26}$$

for the computation of normal clearance angle $\alpha_{n.y}$ at an arbitrary point m within the lateral cutting edge of the hob.

While variation of the profile angle ϕ_{rs} within lateral cutting edge of the hob for machining of involute gear is negligibly small and thus can be neglected, variation of the angle ϕ_{rs} is of critical importance for hobs for machining splines and hobs for machining form profiles. In this latter case, the angle ϕ_{rs} is measured within the rake plane of the hob tooth (it is assumed here that the equality $\gamma_o = 0°$ is valid) between tangent through the point of interest m of the cutting edge and between the perpendicular to the hob axis of rotation O_c.

Gear hobs with a clearance angle $\alpha_o = 10 \ldots 12°$ feature very small normal clearance angles α_n. It is common practice that the normal clearance angle at the lateral cutting edge of the hob tooth is in the interval $\alpha_n = 2 \ldots 4°$. Cutting performance of the gear hobs can be significantly improved due to increased normal clearance angles α_n.

The method for relieving a gear hob that features the reciprocation motion $\mathbf{V}_{rc}$ of the form cutter pointed at a certain angle with respect to the axis of rotation O_c of the hob (see Figure 16.19, case III) is a powerful remedy for the purpose of an increase of normal clearance angle α_n. When the reciprocation motion $\mathbf{V}_{rc}$ is at a certain angle ϑ_{rc} as shown in Figure 16.21, then the normal clearance angle $\alpha_{n.y}$ can be computed from the formula

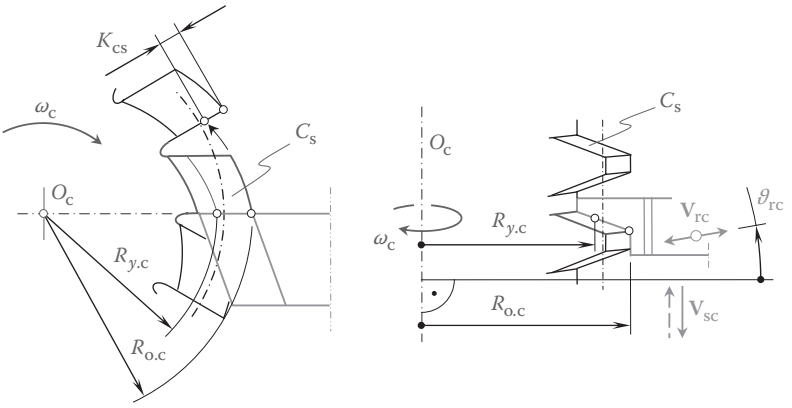

FIGURE 16.21
More elements of the cutting edge geometry of a relieved hob tooth.

$$\alpha_{n.y} = \frac{K_{cs} Z_{gashes}}{2\pi R_{y.c}} \cdot \sin(\phi_{rs} + \vartheta_{rc}) \tag{16.27}$$

When hobbing splines and/or when machining parts with a form profile, it is of critical importance to compute a reasonable value of the angle ϑ_{rc}. A practical method for this is as follows.

Two points a and b can be chosen within the lateral cutting edge CE. Normal clearance angles $\alpha_{n.a}$ and $\alpha_{n.b}$ at the points a and b are equal to their critical values. They should not be less then $\alpha_{n.y} \geq 2 \ldots 4°$. When the critical (the minimal) values $[\alpha_{n.a}]$ and $[\alpha_{n.b}]$ of the angles $\alpha_{n.a}$ and $\alpha_{n.b}$ are known, then a set of two equations

$$\alpha_{n.a} = \frac{K_{cs} Z_{gashes}}{2\pi R_{a.c}} \cdot \sin(\phi_{rs.a} + \vartheta_{rc}) \tag{16.28}$$

$$\alpha_{n.b} = \frac{K_{cs} Z_{gashes}}{2\pi R_{b.c}} \cdot \sin(\phi_{rs.b} + \vartheta_{rc}) \tag{16.29}$$

can be composed.

The solution to the set of Equations (16.28) and (16.29) returns a formula

$$\vartheta_{rc} = \tan^{-1}\left(\frac{R_{a.c} \tan\alpha_{n.a} \sin\phi_{rs.b} - R_{b.c} \tan\alpha_{n.b} \sin\phi_{rs.a}}{R_{b.c} \tan\alpha_{n.b} \cos\phi_{rs.a} - R_{a.c} \tan\alpha_{n.a} \cos\phi_{rs.b}} \right) \tag{16.30}$$

for the computation of the angle ϑ_{rc}.

The corresponding value of the parameter K_{cs} of relieving can be computed from the expression

$$K_{cs} = \frac{2\pi R_{a.c} \tan\alpha_{n.a}}{Z_{gashes} \sin(\phi_{rs.a} + \vartheta_{rc})} = \frac{2\pi R_{b.c} \tan\alpha_{n.b}}{Z_{gashes} \sin(\phi_{rs.b} + \vartheta_{rc})} \tag{16.31}$$

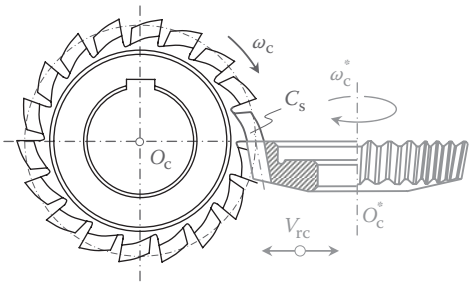

FIGURE 16.22
Relieving a coarse pitch hob with a shaper cutter (SU Pat No 155718).

In particular, the angles $\alpha_{n.a}$ and $\alpha_{n.b}$ can be equal to each other ($\alpha_{n.a} = \alpha_{n.b}$). This significantly simplifies Equations (16.30) and (16.31).

The equations derived above are valid when the reciprocation motion $\mathbf{V}_{rc}$ is parallel to the axis of rotation of the hob to be relieved (see Figure 6.19, case IV). In this latter case the angle ϑ_{rc} is equal to the right angle ($\vartheta_{rc} = 90°$).

When deriving Equations (16.22) through (16.31), the impact of the translational motion V_{sc} onto the elements of geometry of the hob cutting edge is neglected.

Advanced methods for the hob relieving operation. In addition to the basic methods (Figure 16.19), a few more methods of cutting the relieved clearance surface C_s of the hob tooth are used.

Numerous methods of relieving coarse pitch hobs with shaper cutters are developed.

A schematic of a method of relieving of coarse pitch hob with shaper cutter is depicted in Figure 16.22. In this method, the hob to be relieved rotates ω_c about its axis of rotation O_c [52]. The shaper cutter rotates ω_c^* about its axis of rotation O_c^*. The shaper cutter is also performing the reciprocation motion V_{rc} towards the axis of rotation of the hob. Simultaneously with the reciprocation V_{rc}, the shaper cutter travels V_{sc} in the axial direction of the hob (this motion is not shown in Figure 16.22). The rotations ω_c and ω_c^*, as well as the translation V_{sc}, are timed with each other, making it possible to relieve all teeth of the coarse pitch hob in just one path of the shaper cutter along the axis of the hob. No multiple paths of the shaper cutter along the O_c axis are necessary when the method (Figure 16.22) is used. In this way the machining time is significantly reduced.

In another method for relieving coarse pitch hob with shaper cutter the reciprocation motion is tangential with respect to the clearance surface C_s to be cut (Figure 16.23). In this method, the hob to be relieved rotates ω_c about its axis of rotation O_c [77]. The shaper cutter rotates ω_c^* about its axis of rotation O_c^*. The shaper cutter is also performing the reciprocation motion V_{rc}. The direction of the reciprocation V_{rc} is tangential to the clearance surface C_s to be cut. The hob turns through one tooth for each reciprocation V_{rc}.

Simultaneously with the reciprocation V_{rc}, the shaper cutter travels V_{sc} in the axial direction of the hob. (This motion is not shown in Figure 16.23.) The rotations ω_c and ω_c^*, as well as the translation V_{sc} are timed with each other, making it possible to relieve all teeth of the coarse pitch hob just in one path of the shaper cutter along the axis of the hob. No multiple paths of the shaper cutter along the O_c axis are necessary when using this method (Figure 16.23). In this way the machining time is significantly reduced. Better conditions of cutting are another advantage of the method of relieving that is schematically depicted in Figure 16.23. Better conditions of cutting result in longer tool-life of the shaper cutter.

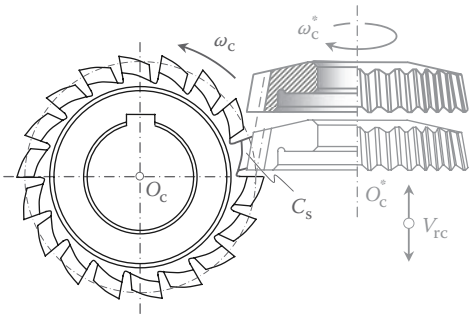

FIGURE 16.23
Method of relieving a coarse pitch hob with a shaper cutter (SU Pat No 751583).

The methods for relieving of hobs shown in Figures 16.22 and 16.23 require implementation of shaper cutters of special design. This is due to the incompatibility of the cutting edge geometry of the top cutting edges of the standard hob and the standard shaper cutter. Clearance angle α_o at the top cutting edge of a standard hob is in the range of $\alpha_o = 10° \ldots 12°$. In specific cases the clearance angle can be increased up to $\alpha_o = 18°$.

Clearance angle α_o^* at the top cutting edge of the standard shaper cutter is equal to $\alpha_o^* = 6°$.

Clearance angle α_o^* at the top cutting edge of a shaper cutter to be used on the relieving operation should exceed that angle α_o of the hob (i.e., satisfaction of the inequality $\alpha_o^* > \alpha_o$ is a must when relieving hobs with shaper cutters). The latter requirement is because the actual clearance angle α_Σ in the relieving operation of the hob is equal to the difference $\alpha_\Sigma = \alpha_o^* - \alpha_o$, which must be positive. This means that implementation of special-purpose shaper cutters is required for machining clearance surfaces C_s of hob teeth. The shaper cutters should feature clearance angle α_o^* that satisfies the inequality $\alpha_o^* > \alpha_o$.

In order to make the relieving operation of standard hobs possible with standard shaper cutters, a method for relieving hobs with the standard shaper cutter was developed. A schematic of the method is illustrated in Figure 16.24 [78]. In this method, the hob to be relieved rotates ω_c about its axis of rotation O_c. It is important to stress the attention here on the direction of the rotation ω_c. The rotation ω_c in the method shown in Figure 16.24 is opposite to the direction of ω_c in the method [52]. The clearance surface of the hob tooth is faced toward the direction of the rotation.

The shaper cutter rotates ω_c^* about its axis of rotation O_c^*. The shaper cutter is also reciprocating V_{rc} toward the axis of the hob rotation. Simultaneously with the reciprocation V_{rc}, the shaper cutter travels V_{sc} in the axial direction of the hob. (This motion is not shown in Figure 6.24.) The rotations ω_c and ω_c^*, as well as the translation V_{sc}, are timed with each other, making it possible to relieve all teeth of the coarse pitch hob just in one path of the shaper cutter along the axis of the hob. No multiple paths of the shaper cutter along the O_c axis are necessary when using this method (Figure 16.24). In this way the machining time is significantly reduced.

Better conditions of cutting are another advantage of the method. The kinematics of the method of relieving results in the actual clearance angle α_Σ being equal not to the difference but to the summa $\alpha_\Sigma = \alpha_o^* + \alpha_o$ of the clearance angles at the top cutting edges of the hob to be relieved and the shaper cutter to be used on the hob relieving operation. Using this method has two important advantages: (a) shaper cutters of standard design can be

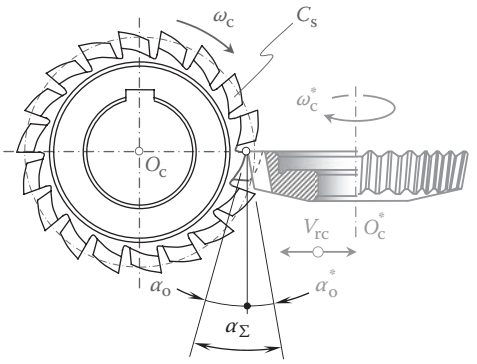

FIGURE 16.24
Method for relieving a coarse pitch hob with a standard shaper cutter. (From Radzevich, S.P., USSR Pat. 1087309, Int. Cl. B24b 3/12, April 23, 1980.)

used on the hob relieving operation, and (b) the increased clearance angle α_Σ allows for better quality of the machined surfaces, as well as longer tool-life of the standard shaper cutter.

Further improvements to the methods of cutting of clearance surfaces of a gear hob are targeting the equalization of clearance angles $\alpha_{c.l}$ at the lateral cutting edges of the opposite sides of the tooth profile of the shaper cutter [79]. A schematic of the method for relieving a coarse pitch hob with the standard shaper cutter is shown in Figure 16.25. The method for hob relieving is similar to the method just discussed (Figure 16.24). The difference between the method shown in Figure 16.25 and the method schematically illustrated in Figure 16.24 is that the axis of rotation of the shaper cutter O_c^* is tilted at the pitch helix angle ψ_c of the hob. This makes it possible to have equal clearance angles $\alpha_{c.l}$ at the lateral cutting edges of the opposite sides of tooth profile of the shaper cutter when relieving the hob.

The above-discussed methods of hob relieving with shaper cutters (Figures 16.22, 16.23, and 16.24) feature that same translation motion V_{sc} of the shaper cutter depicted in Figure 16.25.

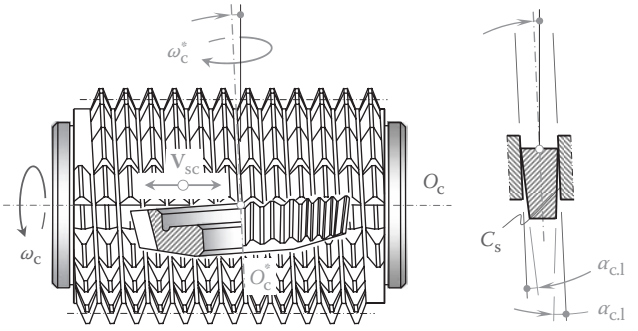

FIGURE 16.25
Method of hob relieving with a standard shaper cutter. (From Radzevich, S.P., USSR Pat. 1240548, Int. Cl. B24b 3/12, Sept. 22, 1984.)

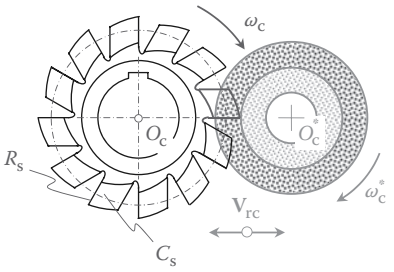

FIGURE 16.26
Basic methods for relief grinding of the clearance surface C_s of the hob tooth.

Much room remains for further improvements to the methods of cutting of clearance surfaces of gear hobs.

16.3.2.2 Grinding of the Relieved Clearance Surfaces of the Hob Teeth

Methods for relief grinding are used for the finishing of the clearance surfaces of the gear hob.

Relief grinding of a solid gear hob. Basic methods for relief grinding of the hob teeth are similar to those used for roughing of clearance surfaces (see Figure 16.19). When grinding (Figure 16.26), the hob rotates ω_c about its axis of rotation O_c. The direction of the rotation is chosen so that the rake surface R_s of the hob tooth faces toward the direction of the rotation. For relief grinding, the grinding wheel of a reasonably small outer diameter is used. The grinding wheel rotates ω_c^* about its axis of rotation O_c^*. The axis O_c^* of the grinding wheel is tilted through a certain angle with respect to the axis of rotation O_c of the hob. The axes O_c and O_c^* are crossing at the angle $(90° - \psi_c)$, where ψ_c denotes pitch helix angle of the hob. The grinding wheel is reciprocating $\mathbf{V}_{rc}$ towards the axis O_c of the hob. In addition to the reciprocation $\mathbf{V}_{rc}$, the grinding wheel travels $\mathbf{V}_{sc}$ in the axial direction of the hob. This motion $\mathbf{V}_{sc}$ together with the rotation ω_c provides the screw motion of the grinding wheel with respect to the clearance surface C_s to be ground. The translation motion $\mathbf{V}_{sc}$ of the grinding wheel is not shown in Figure 16.26.

The form grinding wheel is dressed so that it is capable of grinding either the space between two adjacent hob teeth (similar to case I in Figure 16.19), or it is grinding the clearance surfaces of the opposite sides of the hob tooth (similar to case II in Figure 16.19).

In the production of coarse pitch hobs, other methods for relief grinding featuring reciprocation motion $\mathbf{V}_{rc}$ of the form grinding wheel pointed either (a) at a certain angle with respect to the axis of rotation O_c of the hob (a schematic of the method is similar to that illustrated in Figure 16.19, case III), or (b) in the direction that is parallel to the axis of rotation O_c of the hob (a schematic of the method is similar to that illustrated in Figure 16.19, case IV). The application of the last method is strictly restricted due to the small amount of room for the grinding wheel even in the case when the finger-type grinding wheel is used for this purpose.

A performed analysis of the geometry of contact* of the clearance surface of the hob tooth and of the generating surface of the form grinding wheel revealed an opportunity

* It is the right point to notice here that the *DG/K*-based method of surface generation [84, 138, 143, 153] provides a perfect tool for the analysis of the geometry of contact of the part surface to be machined and of the generating surface of the cutting tool to be applied.

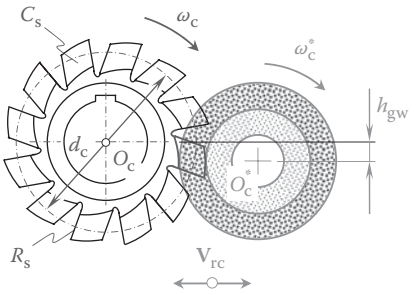

FIGURE 16.27
Method for relief grinding of the gear hob teeth. (From Radzevich, S.P., USSR Pat. 848290, Int. Cl. B24b 3/12, Aug. 6, 1979.)

for improvement to the basic methods of relief grinding. It is proven [84] that the accuracy of the relief ground hob can be significantly increased because the path of reciprocation of the grinding wheel axis of rotation O_c^* is displaced down as shown in Figure 16.27. The recommended value of the displacement h_{gw} depends on pitch diameter of the hob d_c and on clearance angle α_w on the pitch diameter of the hob. The required displacement h_{gw} can be computed from the formula

$$h_{gw} = 0.5 d_c \sin \alpha_w \tag{16.32}$$

Equation (16.25) yields an expression

$$\alpha_w = \tan^{-1}\left(\frac{d_{o.c}}{d_c} \cdot \tan \alpha_o \right) \tag{16.33}$$

for the computation of the clearance angle α_w.

In a relief-grinding process of a gear hob, the clearance surface being ground and the generating surface of the form grinding wheel make line contact. Every point of the line of contact traces a trajectory over the clearance surface C_s of the hob tooth. Lines of this kind are often referred to as *relief lines*.

When the grinding wheel is reciprocating, a point of the line of contact is moving from a point a to a point b within the corresponding relief line. Reduction of pitch diameter from its value $d_{c.a}$ at the point a to the corresponding value $d_{c.b}$ at the point b is observed. Because the pitch diameter $d_{c.a}$ is bigger than the pitch diameter $d_{c.b}$ (the inequality $d_{c.b} > d_{c.b}$ is observed), pitch helix angle ψ_c also changes. Its value $\psi_{c.a}$ at the point a is smaller than that $\psi_{c.b}$ at the point b. In order to compensate for the change of pitch helix angle, an additional swivel motion ω_{rc}^* is performed by the grinding wheel in the method for relief grinding of gear hob teeth [85] as shown in Figure 16.28. The additional swivel motion of the grinding wheel is performed for each tooth of the hob to be relief-ground.

This means that when the grinding wheel approaches the axis of rotation O_c of the hob (reciprocation motion V_{rc}) simultaneously it performs the swivel motion ω_{rc}^* [87]. Due to the swivel motion of the grinding wheel, the crossing angle between the axes O_c and O_c^* changes in time. The crossing angle $\tau_{c.a}^*$ at the point a is smaller than the crossing angle $\tau_{c.b}^*$ at the point b. This is obvious because equalities $\tau_{c.a}^* = \psi_{c.a}$ and $\tau_{c.b}^* = \psi_{c.b}$ are observed.

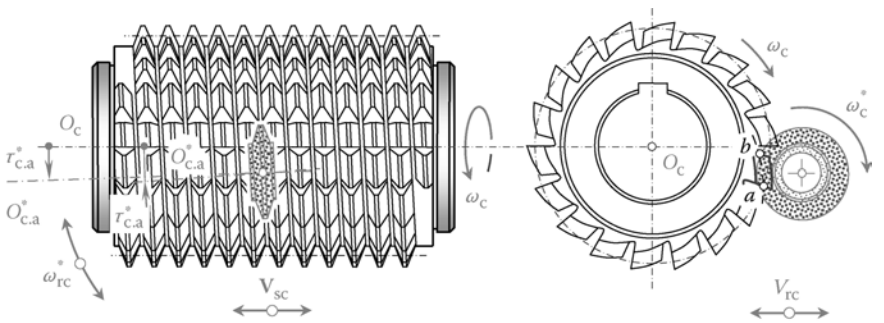

FIGURE 16.28
Method for relief grinding of gear hob teeth that features swivel motion of the grinding wheel. (From Radzevich, S.P., USSR Pat. 1743810, Int. Cl. B24b 3/12, Sept. 13, 1989.)

Because the method for relief grinding [87] features the swivel motion of the grinding wheel, this makes it possible to maintain proper conditions of contact of the clearance surface C_c of the hob tooth and of the generating surface T_{gw} of the form grinding wheel. In this way the accuracy of the ground hob is better.

Reciprocation $\mathbf{V}_{rc}$ of the grinding wheel can be replaced with an additional rotation of the hob being relieved. In the method [86] of relief grinding, the axis of rotation O_c of the grinding wheel is motionless [i.e., the grinding wheel is just rotating ω^*_c about its axis (Figure 16.29)]. The hob being relieved rotates ω_c about its axis of rotation O_c. In addition, the hob rotates ω_e about an axis O_e, which is parallel to the hob axis of rotation O_c (i.e., $O_e \parallel O_c$. The axis O_e is at a distance e_c from the axis O_c [85]. The distance e_c is bigger than the relieving parameter K_{cs} (i.e., inequality $e_c > K_{cs}$ is observed).

The method for relief grinding can be executed when directions of the rotations ω_c and ω_e are inversed. The inversed kinematics of the relief grinding operation is depicted by dashed lines.

Depending on the actual location of the axis O_e of the additional rotation ω_e, both the rotations ω_c and ω_e could be either continuous, or rotation ω_e could be continuous while rotation ω_c is intermittent (i.e., it serves only for indexing purposes).

Elimination of the reciprocation motion $\mathbf{V}_{rc}$ from the kinematics of the relief grinding operation improves the dynamics of the hob relieving process. Due to this the accuracy of the relieved hobs gets better.

Much room remains for further improvements to the methods of relief grinding of gear hobs.

Relief grinding of assembled gear hobs. Assembled gear hobs are relief-ground in one of two ways. First, conventional methods for relief grinding are also applicable to assembled hobs with inserted cutting racks. Second, because hobs are not solid, more opportunities for performing hob relieving operations appear in this concern.

At the beginning, it is necessary to stress that two different configurations of the cutting racks in the body of the assembled hob should be recognized. One of the configurations corresponds to that when the hob is capable of cutting the work gear. This configuration of the cutting racks is referred to as the *working position* of the cutting racks. Another configuration corresponds to that at which clearance surfaces of the hob teeth could be ground. Configuration of the cutting racks in the body of the assembled hob in the working position can differ from their configuration in the position when grinding clearance surfaces. The latter is referred to as the *position for machining* of the cutting rack.

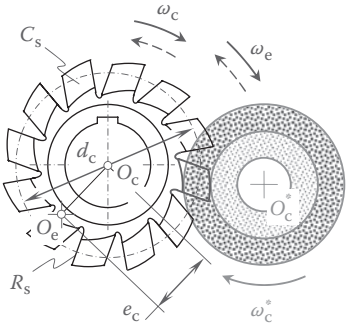

FIGURE 16.29
Method for relief grinding of gear hob teeth. (From Radzevich, S.P., USSR Pat. 1194612, Int. Cl. B24b 3/12, July 20, 1984.)

For example, an assembled gear hob may feature bearing surfaces of the cutting racks shaped in the form of external round cylinders as shown in Figure 16.30. These surfaces of the cutting racks interact with the corresponding internal surfaces in the form of round cylinders in the body of the hob. This makes it possible to turn each cutting rack about its axis O_r through the clearance angle α_o from the working position to their position for machining and vice versa.

When the cutting racks occupy their working positions, then the outer diameter of the hob, pitch diameter, and inner diameter are denoted as $d_{o.c}$, d_c, and $d_{f.c}$ correspondingly. After the cutting racks are turned to the position for machining, the outer diameter and inner diameter are designated as $d^m_{o.c}$ and $d^m_{f.c}$. It is important to notice here that the outer diameter $d_{o.c}$ is bigger then the outer diameter $d^m_{o.c}$, and the difference Δd is equal

$$\Delta d = \frac{d^m_{o.c} - d_{o.c}}{2} \tag{16.34}$$

In the position for machining of the cutting racks, the axis of rotation of the hob O_c and the technological axis O^m_c align with each other. In the working position of the cutting rack

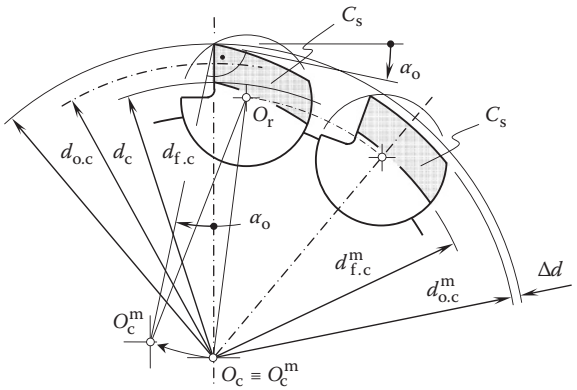

FIGURE 16.30
An assembled gear hob for machining fine pitch gears.

the axes O_c and O_c^m don't align to each other; however, they remain parallel to each other. The location of the technological axis O_c^m in the working position of the cutting racks can be determined as illustrated in Figure 16.30.

When the cutting racks are turned about their axes O_r from the working position to the position for machining, the clearance surfaces C_s of all teeth of all the cutting racks are located within a common screw surface. This is because in the position for machining clearance angle α_o vanishes; it becomes equal to zero. The screw surface can be ground as threads of a worm using for this purpose conventional methods for grinding worms. It is much more convenient to grind worm surfaces rather than to relief-grind clearance surfaces C_s of the hob.

After being ground, the cutting racks turn back to their working position at which clearance angle α_o is positive ($\alpha_o > 0°$).

Implementation of the concept discussed above (Figure 16.30) is practical when designing fine-pitch gear hobs. When cutting fine-pitch gears, the hob with round bearing surfaces is capable of withstanding cutting forces.

Another concept of assembled hobs can be implemented for machining coarse pitch gears.

Assembled gear hobs featuring rectangular-shaped slots for cutting racks can be relief-ground using a method similar to that depicted in Figure 16.30. As it follows from Figure 16.31, clearance surfaces C_s of the hob teeth can be located within a common screw surface when the cutting racks are displaced at a distance h_{cs} from their working position to the position for machining. In these positions of the cutting racks all clearance surfaces C_s can be ground as thread surfaces of the worm. Again, it is much more convenient to grind worm surfaces rather than to relief-grind clearance surfaces C_s of the hob. Moreover, diameters of the cutting racks in their positions for machining can be maintained equal to the corresponding diameters in the working positions of the cutting racks ($d_c^m = d_c$, $d_{o.c}^m = d_{o.c}$, and $d_{f.c}^m = d_{f.c}$). This is because two different bodies are used, one for the purposes of grinding of the clearance surfaces C_s of the hob teeth, and another is the working body of the hob.

Gear hobs can be relief-ground in the hob body that serves two purposes: (a) grinding the clearance surfaces of the hob teeth, and (b) for assembling the hob in the working

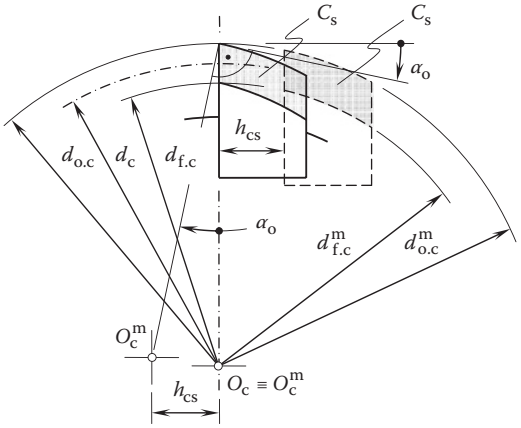

FIGURE 16.31
Location and orientation of the cutting racks in the working position and the position for machining in a special technological body.

positions of the cutting racks. Figure 16.32 reveals that under a certain value of the displacement Δh_{cs} of the centerline of the cutting rack from the centerline of the gear hob, the hob body can be applied for two purposes: (a) for positioning of the cutting racks in their working positions [in such the orientation clearance angle α_o is positive ($\alpha_o > 0°$)], and (b) for positioning the cutting racks for the purposes of grinding of the clearance surfaces [in this case the orientation clearance angle α_o is of zero value ($\alpha_o = 0°$), and clearance surfaces C_s are located within a common screw surface of the so-called *technological worm*]. It is important to notice here that the outer diameter of the hob $d_{o.c}$ is bigger than that of the technological worm $d^m_{o.c}$ [i.e., the inequality $d_{o.c} > d^m_{o.c}$ is observed ($d_{o.c} - d^m_{o.c} = 2\Delta d$)].

For designing assembled gear hobs with a hob body that is capable of serving both purposes simultaneously, a method for determining the location and the orientation of cutting rack slots in the hob body was developed.

Consider a simplified example of an assembled hob with a zero clearance angle $\alpha_o = 0°$. Assume also that the back face of the cutting rack is congruent to the bearing surface of the slot in the body of the hob as shown in Figure 16.33. Point A is chosen at the top cutting edge of the hob tooth. The straight line AB is within the rake plane R_s. Point B is at the outer cylinder of the hob body. Because the clearance angle is equal to zero ($\alpha_o = 0°$), the straight line AB is the line through the axis of rotation O_c of the hob. It is assumed here that the transverse profile of the slot is aligned with the straight line AB.

Point C within the outer cylinder of the hob body is chosen at a distance that is equal to the desired width of the slot. The opposite side of the transverse profile of the slot is through the point C. The straight line CD passes at a distance r_{cs} from the axis O_c of the hob rotation (i.e., the straight line CD is tangent to a circle of radius r_{cs}). The distance r_{cs} is equal

$$r_{cs} = \frac{d_{o.c}}{2} \cdot \sin \alpha_o \tag{16.35}$$

Equation (16.35) occurs because the cutting racks are turned through the angle of 180° from their working positions to the positions for machining of the clearance surfaces.

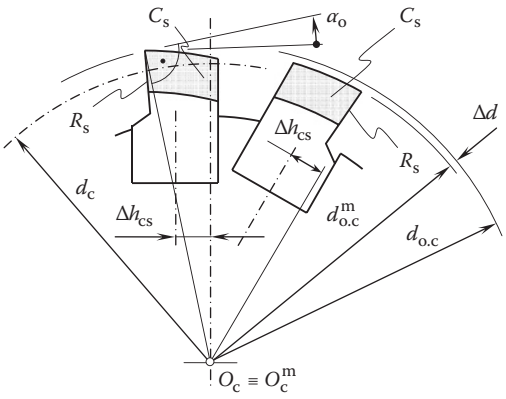

FIGURE 16.32
Illustration of the possibility of implementing a hob body for assembling a hob in working positions of the cutting racks and in their positions for machining purposes.

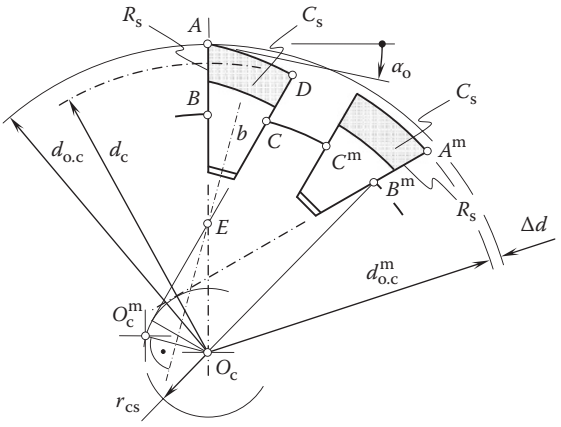

FIGURE 16.33
Method for determining the parameters of the slots in the body of an assembled hob.

In order to turn the cutting racks from working positions to their positions for machining, the racks are turned through the angle of 180° about the bisector b of the angle $\angle BEC$.

Axis O_c^m of the screw clearance surface C_s is the mirror symmetry of the hob axis of rotation O_c. The bisector b serves as the axis of the symmetry.

In the technological position of the cutting racks, superscript m is assigned to all elements of the hob. In the technological position of the clearance surfaces C_s of the cutting rack, teeth are ground as a continuous screw surface. No reciprocation of the grinding wheel is required in this case.

The importance of the disclosed solution to the problem of determining the location and orientation of slots in the hob body (Figure 16.33) is due to the fact that it can be used as a template when solving similar problems, for instance when designing hobs with slots of any desired shape, and so forth. An example is shown in Figure 16.34.

An assembled hob with slots in the hob body of a desired rectangular shape is depicted in Figure 16.34. Values of the rake angle γ_o and of the clearance angle α_o are given. The earlier constructed solution to the similar problem is shown in Figure 16.34 in thin lines. It is used as the reference for the slots of the desired shape. Further, the cutting rack of the desired design is treated together with the cutting rack of the simplified geometry. In this way the desired location and the orientation of the slots are determined.

It is important to notice here that the outer diameter $d_{o.c}$ of the hob exceeds that of the technological worm $d^m_{o.c}$ (i.e., the inequality $d_{o.c} > d^m_{o.c}$ is observed).

In a similar way to that described above, slots of any desired shape in the hob body can be designed. The simplified solution to the problem (see Figure 16.33) works in all cases, and is applicable for hobs of any desired geometry of the cutting edges.

As it follows from the above consideration, the pitch diameter d_c^m of the technological worm (as well as other diameters of threads of the technological worm) is smaller than the pitch diameter d_c (and other corresponding diameters) of the hob. Just as the actual values of the diameters d_c and d_c^m are different, the pitch helix angles ψ_c and ψ_c^m are also of different values ($\psi_c^m > \psi_c$). The difference in pitch helix angles is one of the reasons that reduce the accuracy of assembled hobs. In aiming for high accuracy of the gear hob, it is desirable to have identical pitch diameters of the hob and the technological worm. For this purpose,

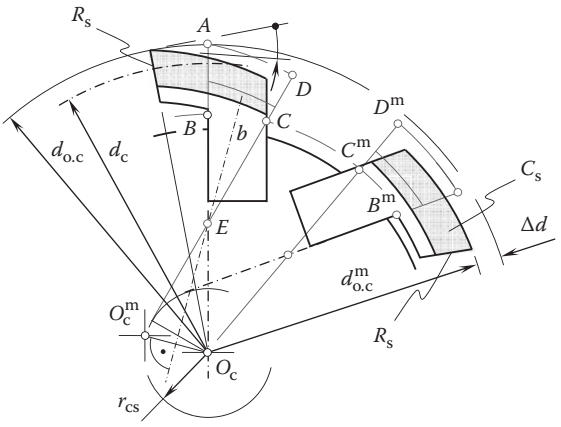

FIGURE 16.34
An example of implementing the method shown in Figure 16.33.

slots in the hob body are shaped so that a ledge is formed at the bottom of every slot [114]. When the cutting rack is in the working position (Figure 16.35), then the ledge surfaces are not interacting with the corresponding surfaces of the cutting rack. After the cutting rack is turned to the position for machining, then the lowest plane of the cutting rack contacts the top or the ledge. In this way the cutting rack shifts outward toward the hob axis of rotation O_c. The ledge height Δh is computed so

$$\Delta h = \frac{d_{o.c} - d^*_{o.c}}{2\cos(0.5\alpha_o)} \tag{16.36}$$

to compensate for the change of diameter of the technological worm.

Slots with a ledge at the bottom allow for elimination of a source of deviations of the relief ground gear hob from the desired geometry [114].

Deviation in angular positions of the slots for cutting racks in the hob body is another source of inaccuracies of assembled gear hobs. The order of location of the cutting racks in the working position is inversed to that in the position for grinding clearance surfaces. If one would decide to numerate the slots and the cutting racks in their working position, for example in a clockwise direction, then the order of the cutting racks in their position for machining would be in the counterclockwise direction. It is clear that in the position for grinding the cutting racks do not occupy their slots in their working positions. Therefore, deviation in the angular position of the slots for cutting racks in the hob body directly affects the hob accuracy.

The desired clearance surface of the hob tooth [see Equation (16.21)] can be approximated with a screw surface. In this case it is possible to grind the clearance surfaces after they are displaced in axial direction of the hob body to align with a screw surface, which in this configuration is common for all of the clearance surfaces [152].

In the working positions of the cutting racks of the assembled gear hob, the pitch helix angle ψ_c is equal (Figure 16.36a)

$$\psi_c = \tan^{-1}\left(\frac{mN_c}{d_c}\right) \tag{16.37}$$

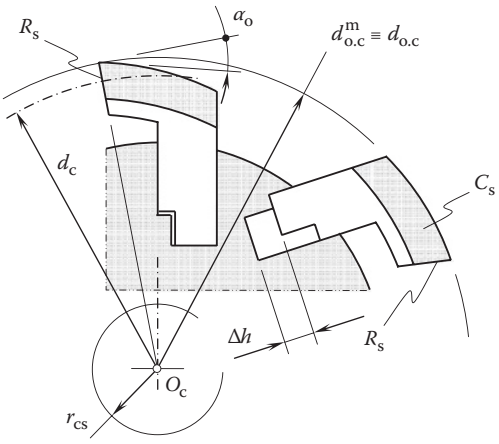

FIGURE 16.35
The working position and the position for machining the cutting rack in a hob body with the slots of a modified profile.

In Equation (16.37), the number of starts of the hob is denoted as N_c (for a single-start hob $N_c = 1$).

The cutting racks can be displaced in the axial direction of the hob body to the positions of machining as illustrated in Figure 16.36b. Maximum displacement δ_{max} of the cutting rack is equal to $\delta_{max} = P_x m_c$, where the axial pitch of the hob is designated as P_x, and m_c is an integer number (usually $m_c = \pm 1$). Axial displacement δ_i of the ith cutting rack depends on its number "i"

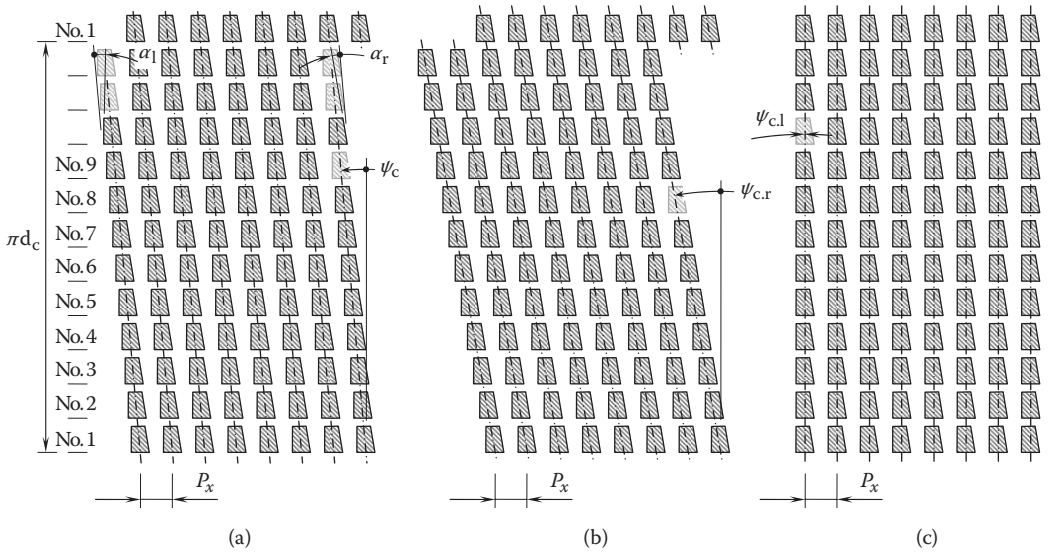

FIGURE 16.36
The working positions and positions for machining the cutting racks in a hob body. (The cutting racks are displaced in the axial direction of the hob.)

$$\delta_i = \frac{P_x m_c}{n_c} \cdot i \tag{16.38}$$

where total number of the cutting racks of the hob is designated as n_c.

In the position of the cutting racks shown in Figure 16.36b, the pitch helix angle $\psi_{c.r}$ of the right-hand side clearance surfaces can be computed from the formula

$$\psi_{c.r} = \tan^{-1}\left[\frac{m(N_c + m_c)}{d_c}\right] \tag{16.39}$$

Under such a scenario, the right-hand side clearance surfaces of the tooth profile of the hob are getting an inclination at the clearance angle α_r

$$\alpha_r = \psi_{c.r} - \psi_c \tag{16.40}$$

Equations similar to those above are valid for the opposite side (i.e., for the left-hand side) of profile of the hob tooth (Figure 16.36c)

$$\psi_{c.l} = \tan^{-1}\left[\frac{m(N_c - m_c)}{d_c}\right] \tag{16.41}$$

$$\alpha_l = -\psi_{c.l} + \psi_c \tag{16.42}$$

Implementation of the method for grinding clearance surfaces of the assembled gear hobs (Figure 16.36) makes possible precision generation of the clearance surfaces of the lateral sides of tooth profile of the hob.

After clearance surfaces through the lateral cutting edges are ground, then simplified methods for relief grinding can be used* for grinding the clearance surfaces through the top cutting edges [159]. Two examples of kinematics of the simplified methods of relief grinding are depicted in Figure 16.37.

For the relief grinding of clearance surfaces through the top cutting edges of the gear hob, standard grinding wheels, either cylindrical (Figure 16.37a) or conical (dish-type) (Figure 16.37b) are commonly used. The hob being relief-ground rotates about its axis of rotation O_c so that the rake surface R_s is faced toward the direction of the hob rotation ω_c. The grinding wheel rotates about its axis of rotation O_c^*. The rotation of the grinding wheel is denoted as ω_c^*. The grinding wheel is reciprocating V_{rc} toward the axis of the hob rotation O_c per each hob tooth being relief-ground. In addition, the grinding wheel travels V_{sc} along the hob axis of rotation O_c. There are no kinematical correlations between the translation V_{sc} of the grinding wheel and the rotation ω_c^* of the hob and its number of starts N_c. Independence of the translation V_{sc} from ω_c^* and N_c makes it possible to assign the desirable

* SU Pat. No. 1335425, *A method of relief grinding of hob teeth*. S.P. Radzevich, V.I. Lempert, Int. Cl. B23f 21/16, Filed: April 24, 1986.

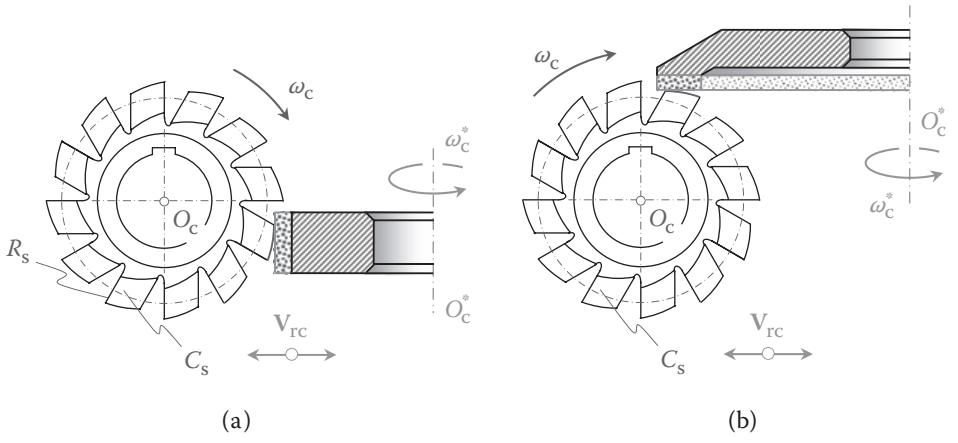

FIGURE 16.37
Method for grinding the top clearance surfaces of the hob. (From Radzevich, S.P. and Lempert, V.I., USSR Pat. 1335425, Int. Cl. B24b 3/12, April 24, 1986.)

speed V_{sc} of the translation of the grinding wheel. The speed V_{sc} can be set so that the relief grinding is performed in just a single path of the grinding wheel along the axis of rotation O_c of the hob.

For relief grinding of assembled hobs, other methods are developed as well (see [88] and others).

16.4 Accuracy of Hobs for Machining of Involute Gears

Accuracy of gear hobs is an important consideration. Inaccuracies of gear hobs directly affect the accuracy of the machined gears. Many efforts have been undertaken in investigating the accuracy of gear hobs, as well as investigating the accuracy of the hobbed gears. However, many of those issues related to the accuracy of the designed and manufactured gear hobs remain not yet properly investigated. The problem of the accuracy of gear hobs deserves to be comprehensively discussed separately in another book. Below a few problems are discussed.

16.4.1 Preliminary Remarks

Absence of the common line of intersection of three surfaces: (a) of the generating surface T of the hob, (b) of the rake surface R_s of the hob tooth, and (c) of the clearance surface C_s of the hob tooth, is the major reason for the deviations of the cutting edges of the hob from their desired geometry and location. A few examples of the deviations of the rake surface R_s from its desired position and geometry, and the corresponding deviations in profile of the hobbed gear tooth caused by the deviations, are illustrated in Figure 16.38.

No deviations of the tooth profile of the cut gear is observed when the rake surface of the hob is located properly (Figure 16.38a).

A slightly positive (Figure 16.38b) or slightly negative (Figure 16.38c) rake angle at the top cutting edge of the hob tooth results in the corresponding reduction of tooth thickness either at the top of the tooth or at the bottom of the tooth of the hobbed gear.

Concavity of the rake surface of the hob (Figure 16.38d) makes the machined gear tooth thicker, while convexity of the rake surface of the hob (Figure 16.38e) makes the machined gear tooth thinner at the top and bottom.

Inaccuracies in angular pitch of the hob teeth (Figure 16.38f) results in bigger height of the residual cusps on the machined surface of the gear tooth. No doubt, more examples of this concern can be provided.

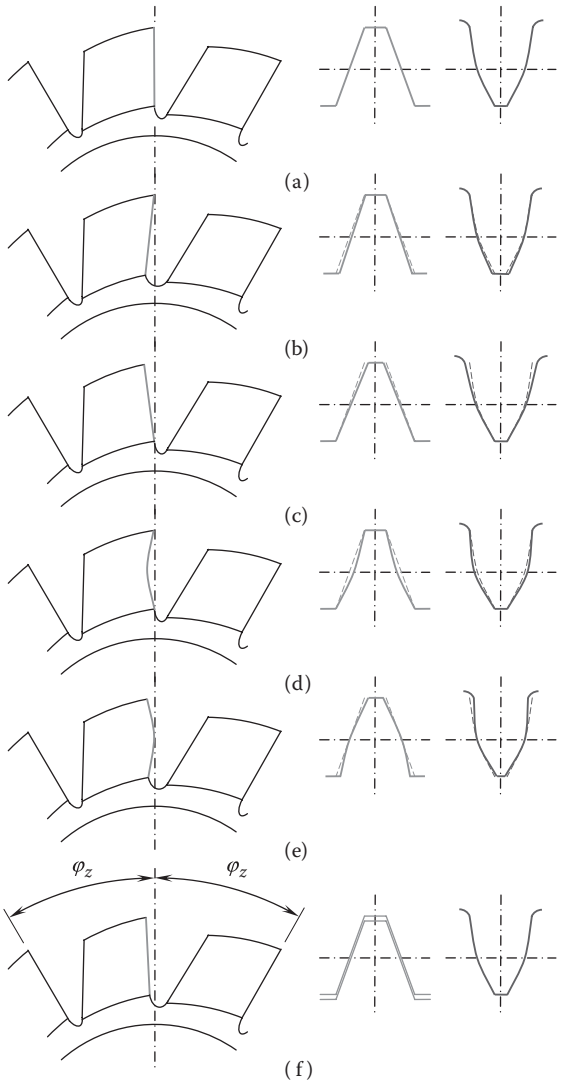

FIGURE 16.38
Examples of deviations of the rake surface from its desired position and geometry, and the corresponding deviations in the profile of the cut tooth of the gear caused by deviations of a hob.

Taking into account the importance of proper shape and correct configuration of the rake surface, the parameters of shape and of the configuration of the rake surface of a hob tooth are carefully inspected for a new hob, as well as after every hob resharpening (Figure 16.39).

Due to clearance surfaces of gear hob teeth are relief-ground, this makes possible a corrective grinding of the hobs. The corrective grinding is aimed at a reduction of the inaccuracies of gear hobs. It is based on the analysis similar to that illustrated in Figure 16.38. More details on the corrective grinding of gear hobs can be found in the paper by Arkhangelskiy in [24].

The preliminary qualitative analysis of the deviations of the gear hob tooth, and their effect on accuracy of the machined gear, makes clear the necessity and importance of more detailed analysis of gear hob accuracy.

16.4.2 Accuracy of an Involute Gear Hob as a Function of Its Design Parameters

Lateral cutting edges CE of an involute hob are understood in this text as lines of intersection of the generating surface T of the hob and the rake surface R_s. The third surface, namely the clearance surface C_s, is required to pass through the cutting edge CE of the hob tooth. Though the lateral cutting edges CE are required within the surface T, actually they are displaced from this surface. An approximation of the desired lateral cutting edges with lines that are convenient in manufacturing of the hob is the chief reason for the displacement. Often, the desired 3-D lateral cutting edges CE of a hob are approximated with a straight line. This results in unavoidable deviations δ_c of the actual machining surface T^m from the desired generating surface T of the involute hob. The deviation δ_c is measured as a distance between the surfaces T^m and T. The distance δ_c is perpendicular to the generating surface T of the hob, and the perpendicular is through a point of interest with the lateral cutting edge of the hob.

For the computation of the deviation δ_c an equation of both the desired and actual lateral cutting edge of the hob tooth are necessary.

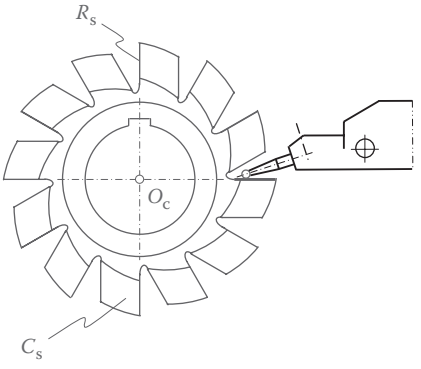

FIGURE 16.39
Inspection of the geometry and configuration of the rake surface of a gear hob.

16.4.2.1 Analytical Description of the Desired Lateral Cutting Edge

For the analytical description of the desired lateral cutting edges CE of the involute hob, equation $\mathbf{r}_c = \mathbf{r}_c(U_c, V_c)$ of the generating surface T of the hob [see Equation (16.110)] together with equation $\mathbf{r}_{rs} = \mathbf{r}_{rs}(U_{rs}, V_{rs})$ of the rake face R_s [see Equations (16.4) through (16.8)] are convenient to employ. On the basis of these equations, the position vector of a point $\mathbf{r}_{ce}$ of the desirable lateral cutting edge CE can be analytically described by matrix equation

$$\mathbf{r}_{ce}(U_{ce}) = \begin{bmatrix} X_{ce}(U_{ce}) \\ Y_{ce}(U_{ce}) \\ Z_{ce}(U_{ce}) \\ 1 \end{bmatrix} \tag{16.43}$$

For the practical needs of designing of an involute hob, not the entire curve [Equation (6.43)] is of interest. The hob designer needs just an arc of the curve $\mathbf{r}_{ce} = \mathbf{r}_{ce}(U_{ce})$. This 3-D arc through the points a, b, and c is located within the outer hob diameter $d_{o.c}$, and the limit hob diameter of the value $d_{l.c}$. It is common practice to assume that $d_{l.c} = d_{o.c} - 2 \cdot 2.25m$ (Figure 16.40). Here m designates the hob module.

The solution to Equation (16.43) under $d_{o.c}$ returns position vector $\mathbf{r}_{a.c}$ of the point $a(X_a, Y_a, Z_a)$. Similarly, the solution to Equation (16.43) under d_c returns position vector $\mathbf{r}_{b.c}$ of the point $b(X_b, Y_b, Z_b)$, while the solution to that same equation [Equation (16.43)] under $d_{l.c}$ returns position vector $\mathbf{r}_{c.c}$ of the point $c(X_c, Y_c, Z_c)$ correspondingly.

16.4.2.2 Analytical Description of the Actual Lateral Cutting Edge

Targeting a simplification of manufacture of involute hobs, the desired lateral cutting edges *abc* are often approximated with a straight-line segment through the points *a* and *b*.

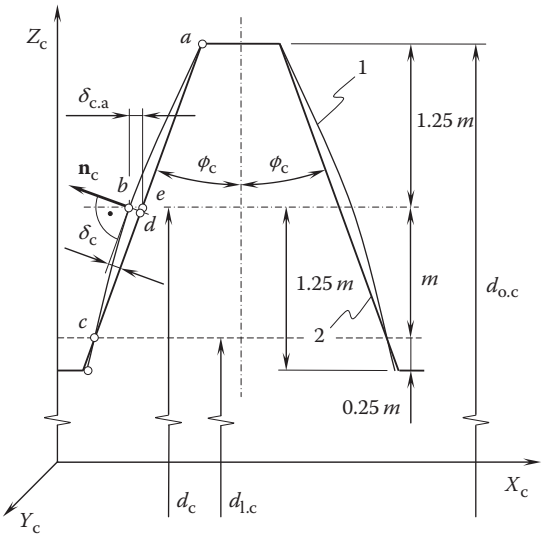

FIGURE 16.40
(1) Desired and (2) actual lateral cutting edges of an involute hob. (From Radzevich, S.P., *SME Journal of Manufacturing Processes*, 9(2), 121–136, 2007. With permission.)

The approximation causes a deviation of the actual lateral cutting edge 2 with respect to the desired lateral cutting edge 1 of the involute hob (Figure 16.40).

For the computation of deviations of the actual machining surface T^{m} from the desired generating surface T of the involute hob, it is necessary to derive an equation of the surface T^{m}. Such an equation can be drawn up on the premise of an equation of the actual lateral cutting edge of the hob.

Because the desired 3-D lateral cutting edge is approximated with a straight-line segment through the points a and b, the equation for the position vector $\tilde{\mathbf{r}}_{\mathrm{ce}}$ of the actual cutting edge of the hob could be represented in the form

$$(\tilde{\mathbf{r}}_{\mathrm{ce}} - \mathbf{r}_{a.\mathrm{c}}) \times (\tilde{\mathbf{r}}_{\mathrm{ce}} - \mathbf{r}_{c.\mathrm{c}}) = 0 \tag{16.44}$$

which immediately yields

$$\tilde{\mathbf{r}}_{\mathrm{ce}}(\tilde{U}_{\mathrm{ce}}) = \mathbf{r}_{a.\mathrm{c}} + \tilde{U}_{\mathrm{ce}}(\mathbf{r}_{c.\mathrm{c}} - \mathbf{r}_{a.\mathrm{c}}) \tag{16.45}$$

where $\tilde{U}_{\mathrm{ce}}$ designates a parameter of the lateral cutting edge $\tilde{\mathbf{r}}_{\mathrm{ce}} = \tilde{\mathbf{r}}_{\mathrm{ce}}(\tilde{U}_{\mathrm{ce}})$.

16.4.2.3 Machining Surface of an Involute Hob

With the equation of the lateral cutting edge $\tilde{\mathbf{r}}_{\mathrm{ce}}$ [see Equation (16.45)], the machining surface T^{m} of the hob can be represented as a set of successive positions of the cutting edge $\tilde{\mathbf{r}}_{\mathrm{ce}}$ that performs a screw motion about the hob axis O_{c}. The parameter of the screw motion of the cutting edge $\tilde{\mathbf{r}}_{\mathrm{ce}}$ is equal to the reduced pitch p_x of the involute hob [see Equation (6.14)]. The schematic of the generation of the hob surface T^{m} resembles what is already done for the derivation of the rake face R_{s} (Figure 16.5). A Cartesian coordinate system $X_3Y_3Z_3$ is associated with the cutting edge $\tilde{\mathbf{r}}_{\mathrm{ce}}$. The cutting edge $\tilde{\mathbf{r}}_{\mathrm{ce}}$ performs the screw motion about the hob axis O_{c} with the parameter of the screw motion p_x. Recall that in Figure 16.5, the hob axis O_{c} is aligned with the X_{c} axis of the coordinate system $X_{\mathrm{c}}Y_{\mathrm{c}}Z_{\mathrm{c}}$. For an analytical description of the screw motion, the operator $\mathbf{Rs}(3 \mapsto \mathrm{c})$ of the resultant coordinate system transformation can be composed.

In the case under consideration, it is convenient to decompose the screw motion of the cutting edge $\tilde{\mathbf{r}}_{\mathrm{ce}}$ onto the rotation about the X_{c} axis [this linear transformation is analytically described by the operator $\mathbf{Rt}(V_{\mathrm{rs}}, X_{\mathrm{c}})$ of rotation], and onto the translation along the X_{c} axis [this linear transformation is analytically described by the operator $\mathbf{Tr}(p_{\mathrm{rs}}V_{\mathrm{rs}} \mapsto X_{\mathrm{c}})$ of translation] [149]. The operators of the elementary coordinate system transformations yield the operator $\mathbf{Rs}(3 \mapsto \mathrm{c})$ of the resultant coordinate system transformation

$$\mathbf{Rs}(3 \mapsto \mathrm{c}) = \mathbf{Rt}(V_{\mathrm{rs}}, X_{\mathrm{c}}) \cdot \mathbf{Tr}(p_{\mathrm{rs}}V_{\mathrm{rs}} \mapsto X_{\mathrm{c}}) \tag{16.46}$$

Skipping routing formulae transformation, an equation of the actual machining surface T^{m} of the involute hob can be represented in the form

$$\left.\begin{array}{l}\text{Machining surface } T^{\mathrm{m}} \\ \text{of an involute hob}\end{array}\right| \quad \Rightarrow \quad \tilde{\mathbf{r}}_{\mathrm{c}} = \mathbf{Rs}(3 \mapsto \mathrm{c}) \cdot \tilde{\mathbf{r}}_{\mathrm{ce}} \tag{16.47}$$

Equation (16.47) can be cast into matrix form:

$$T^{m}: \quad \Rightarrow \quad \tilde{\mathbf{r}}_{c}(\tilde{U}_{c}, \tilde{V}_{c}) = \begin{bmatrix} X_{c}(\tilde{U}_{c}, \tilde{V}_{c}) \\ Y_{c}(\tilde{U}_{c}, \tilde{V}_{c}) \\ Z_{c}(\tilde{U}_{c}, \tilde{V}_{c}) \\ 1 \end{bmatrix} \tag{16.48}$$

Here, $\tilde{U}_{c}$ and $\tilde{V}_{c}$ designate curvilinear (Gaussian) coordinates of a point of the hob surface T^{m}.

16.4.2.4 Deviation of the Actual Machining Surface from the Desired Generating Surface of an Involute Hob

Computation of the deviations of the actual machining surface T^{m} from the desired generating surface T of a precision involute hob is a complex engineering problem. The consideration below is limited just to the computation of maximum deviation δ_{c} of the hob surface T^{m} from the desired surface T of the involute hob.

Definition of the maximum deviation δ_{c} of the hob tooth profile. The maximum deviation δ_{c} is on the hob pitch diameter $d_{o.c}$ (Figure 16.40). The deviation δ_{c} is measured in the direction of the outward unit normal vector $\mathbf{n}_{c}$ to the generating surface T of the hob. The deviation δ_{c} is a signed value. It is positive when it is measured outward the surface T, and it is negative if it is measured in the opposite direction.

An expression for the position vector $\mathbf{r}_{\delta}$ of a point of the straight line through the point b in the direction of $\mathbf{n}_{c}$ can be written in matrix form

$$(\mathbf{r}_{\delta} - \mathbf{r}_{b.c}) \times \mathbf{n}_{c} = 0 \tag{16.49}$$

An equation for $\mathbf{r}_{\delta}(U_{\delta})$ immediately follows from Equation (16.49)

$$\mathbf{r}_{\delta}(U_{\delta}) = \mathbf{r}_{b.c} + U_{\delta} \cdot \mathbf{n}_{c} \tag{16.50}$$

Point d is the point of interception of the straight line $\mathbf{r}_{\delta}(U_{\delta})$ with the machining surface T^{m} of the involute hob (Figure 16.40). Coordinates X_{d}, Y_{d}, and Z_{d} of the point d are computed as a solution to the set of Equations (16.48) and (16.50). Ultimately, the expression

$$\delta_{c} = -|\mathbf{r}_{b.c} - \mathbf{r}_{d.c}| \tag{16.51}$$

can be composed for computation of the deviation δ_{c}. Here $\mathbf{r}_{d.c} = \mathbf{r}_{d.c}(X_{d}, Y_{d}, Z_{d})$.

The deviation δ_{c} of tooth profile is of negative value. This means that the deviation is directed toward the generating surface T. In other words, the deviation δ_{c} is measured in a negative direction of the unit normal vector $\mathbf{n}_{c}$ to the surface T.

It is important to point out perfect correlation between the deviations δ_{c} and $\delta_{c.x}$. (The deviation $\delta_{c.x}$ is measured in the axial direction of the involute hob.) An approximate equality $\delta_{c.x} \cong \delta_{c}/\cos\phi_{n}$ is observed. The accuracy of the approximation is commonly within 5%.

Impact of the rake angle γ_{o} on tooth profile deviation δ_{c}. Deviation δ_{c} of the hob tooth profile depends on rake angle γ_{o} of the involute hob. Numerical examples are convenient to use

to illustrate the function $\delta_c(\gamma_o)$. The major design parameters of the involute hob for the illustrative computations are summarized in Table 16.1.

Analytical expressions for the computation for the deviation δ_c of the tooth profile of the hob in terms of the current value of the rake angle γ_o can be derived from Equation (16.51) for involute hobs with straight gashes that have various values of module m, normal pressure angle ϕ_n, and outer diameter $d_{o.c}$.

A graphical interpretation of the function $\delta_c(\gamma_o)$ for involute hobs with the design parameters (see Table 16.1) is shown in Figure 16.41 [149]. Functions δ_c vs. γ_o for the entering side of the hob tooth profile are plotted in Figure 16.41a. Figure 16.41b illustrates the similar functions δ_c vs. γ_o for the exiting side of the hob tooth profile. The functions $\delta_c = \delta_c(\gamma_o)$ have extrema for both the entering side and the exiting side of the tooth profile The extrema of the function $\delta_c = \delta_c(\gamma_o)$ correspond to the tooth profile deviation that is equal to $\delta_c = 0$. For the entering side of the hob tooth profile, the extremum $\delta_c = 0$ is observed under a positive rake angle $\gamma_o > 0°$, while for the exiting side of the hob tooth profile the extremum $\delta_c = 0$ is observed under a negative rake angle $\gamma_o < 0°$. The extremum value of the rake angle γ_o is equal to $\gamma_o \cong +8.645°$ in the first case, and it is equal to $\gamma_o \cong -8.645°$ in the second case.

It is critical to stress here that the extreme values of the rake angle γ_o are of those values for which the lateral cutting edges of the hob tooth are tangent from the opposite sides to the hob base cylinder of diameter $d_{b.c}$, and to the base helices as well.

The impact of the hob module m onto the hob tooth profile deviation δ_c is illustrated in Figure 16.42 [149]: for the entering side of the hob tooth profile (Figure 16.42a), and for the exiting side of the tooth profile (Figure 16.42b) as well. Here, the hob module is represented as a continuous parameter. This is valid because there are no physical restrictions on the module values with fractions. Following common practice, here module m is understood in $m = 25.4/P$, where diametral pitch is designated as P.

It is natural to expect that involute hobs of a module m have tooth profile deviation δ_c which are of different values for opposite sides of tooth profile of the hub. Actually, they do (Figure 16.42). Under similar initial conditions, the deviations δ_c for the exiting side of the hob tooth profile are smaller in comparison to the deviations δ_c for the entering side of the hob tooth profile. This is due to the additional impact of kinematics of the gear hobbing onto the deviation δ_c.

Two other issues are of critical importance for involute hob designers, as well as for manufacturers of precision gear hobs. They are the impact on the maximum value of the deviation δ_c of (a) the hob outside diameter, $d_{o.c}$, and (b) the hob normal profile angle, ϕ_n.

The bigger the outer diameter d_c of the involute hob the smaller hob tooth profile deviations δ_c for both, for the entering side of the hob tooth (Figure 16.43a) as well as for the exiting side of the hob tooth profile (Figure 16.43b). Similarly, involute hobs with normal profile angle ϕ_n also have tooth profile deviation δ_c for the entering side of the tooth profile (Figure 16.44a) as well as for the exiting side of the hob tooth profile (Figure 16.44b). Again, under

TABLE 16.1

Design Parameters of the Precision Involute Hob

Module	$m = 10\,\text{mm}$
Normal pressure angle	$\phi_n = 20°$
Setting angle of the hob	$\zeta_c = 4°$
Outer diameter	$d_{o.c} = 160\,\text{mm}$
Number of starts	$N_c = 1$

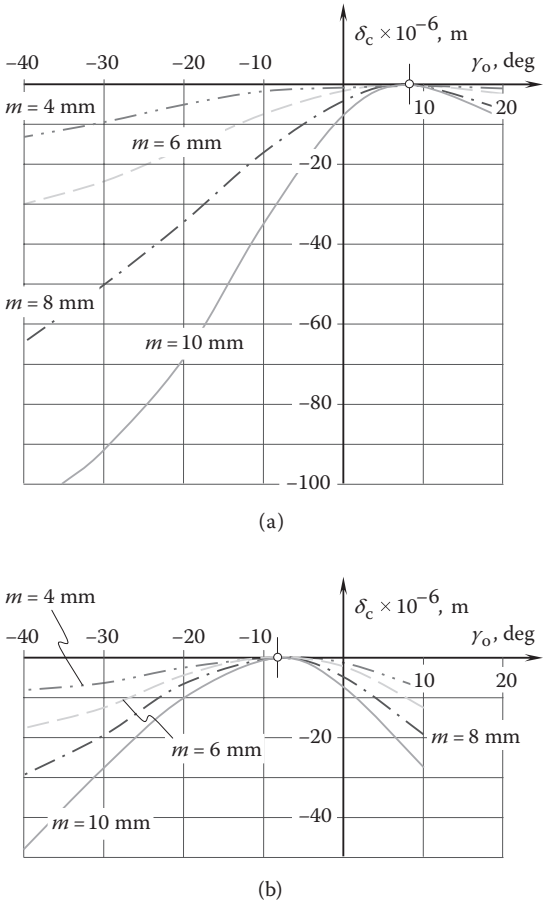

FIGURE 16.41
Impact of the rake angle γ_o on the tooth profile deviation δ_c for involute hobs of various modulus with an outer diameter $d_{o.c} = 160$ mm and normal pressure angle $\phi_n = 20°$: (a) the entering side of the tooth profile and (b) the exiting side of the tooth profile. (From Radzevich, S.P., *SME Journal of Manufacturing Processes*, 9(2), 121–136, 2007. With permission.)

similar initial conditions, the deviations δ_c for the exiting side of the hob tooth profile are smaller in comparison to the deviations δ_c for the entering side of the hob tooth profile. This is owing to the impact of the kinematics of the gear hobbing onto the deviation δ_c.

The impact of the lead angle λ_{rs} of the screw rake surface on the deviation δ_c of tooth profile of an involute hob. Deviation δ_c of the tooth profile of the involute hob depends on lead angle λ_{rs} of the rake surface of the hob. An equation

$$\delta_c = \delta_c(\lambda_{rs}, \zeta_c, \phi_n, d_{b.c}, d_c, t_c) \tag{16.52}$$

for the tooth profile deviation δ_c can be derived. The solution to the equation

$$\frac{\partial \delta_c(\lambda_{rs}, \ldots)}{\partial \lambda_{rs}} = 0 \tag{16.53}$$

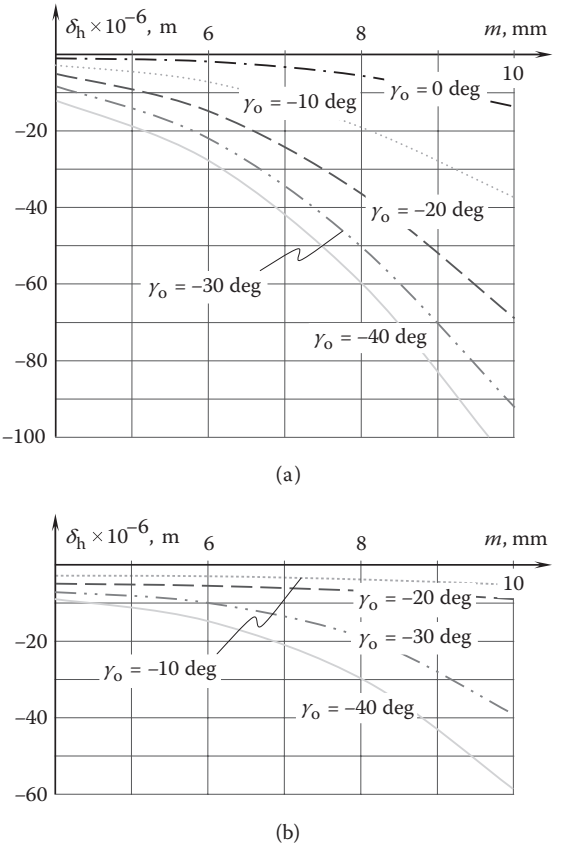

FIGURE 16.42
Impact of the hob modulus m on the tooth profile deviation δ_c for involute hobs with various values of the rake angle γ_o, outer diameter $d_{o.c}$ = 160 mm, and the normal pressure angle $\phi_n = 20°$: (a) the entering side of the tooth profile and (b) the exiting side of the tooth profile. (From Radzevich, S.P., *SME Journal of Manufacturing Processes*, 9(2), 121–136, 2007. With permission.)

returns the formula for the computation of an optimal value, λ_{rs}^{opt}, of the lead angle of the rake surface under which the tooth profile deviation δ_c vanishes.

Without going into the details of derivation, it should be mentioned here that the optimal value λ_{rs}^{opt} of lead angle λ_{rs} of the rake face, under which tooth profile deviation δ_c vanishes, can be computed from the formula [149]

$$\lambda_{rs}^{opt} = -\tan^{-1}\left[\frac{d_{b.c}\cos\zeta_c}{\sqrt{(d_c + t_c\cot\phi_n)^2 - d_{b.c}^2}\tan\phi_n + d_{b.c}\sin\zeta_c}\right] \tag{16.54}$$

The sign "–" in Equation (16.54) indicates that the recommended direction of the hand of the screw rake surface R_s is opposite from the direction of the hand for gear hobs of conventional design. Thus, the hand of the screw rake surface R_s is going in the same direction as the threads of the generating surface T of the hob.

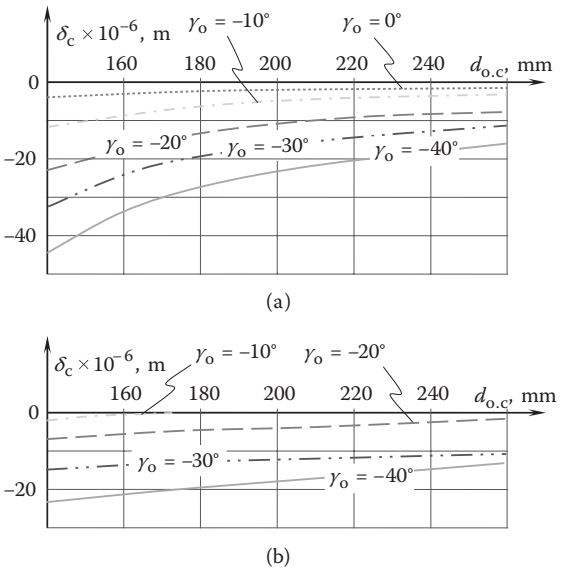

FIGURE 16.43
Impact of the hob outer diameter $d_{o.c}$ on the tooth profile deviation δ_c for involute hobs with various rake angle γ_o and normal pressure angle $\phi_n = 20°$: (a) the entering side of the tooth profile, and (b) the exiting side of the tooth profile. (From Radzevich, S.P., *SME Journal of Manufacturing Processes*, 9(2), 121–136, 2007. With permission.)

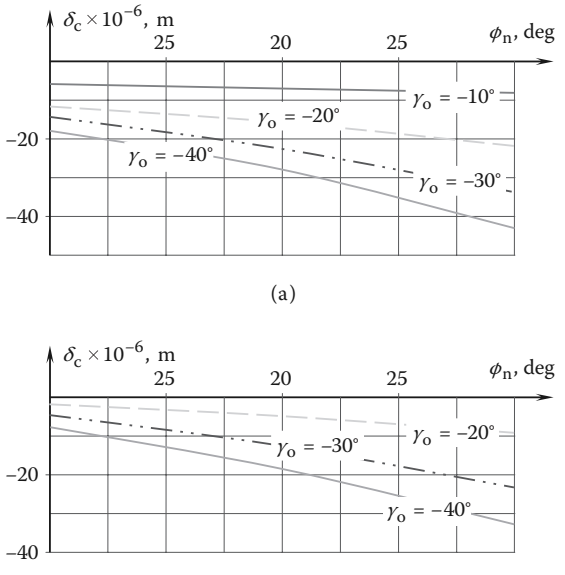

FIGURE 16.44
Impact of the hob pressure angle ϕ_n on tooth profile deviation δ_c for involute hobs having various rake angle γ_o, and outer diameter $d_{o.c} = 160$ mm: (a) entering side of the tooth profile, (b) exiting side of the tooth profile. (From Radzevich, S.P., *SME Journal of Manufacturing Processes*, 9(2), 121–136, 2007. With permission.)

Equation 16.54 allows for the computation of the optimal value λ_{rs}^{opt} of the lead angle λ_{rs} of the rake surface R_s of the involute hob. For the single-start gear hob of module $m = 10\,\text{mm}$, the outside diameter $d_{o.c} = 160\,\text{mm}$, and the profile angle $\phi_n = 20°$, for Archimedean screw surface R_s Equation (16.54) returns $\lambda_{rs}^{opt} = 20.225°$ for the optimal value λ_{rs}^{opt} of the lead angle λ_{rs}.

It is assumed in the computation that the setting angle of the hob $\zeta_c = 3.772°$. The chosen value of the hob-setting angle ζ_c is close to the actual value of the pitch helix angle $\psi_c = 3.699°$ of the hob. The latter is mostly for the purposes of avoiding pointing of the hob tooth.

Usually, the setting angle of the hob ζ_c is either exactly or approximately equal to the hob helix angle $\zeta_c \cong \psi_c$. However, it is not mandatory to keep the equality $\zeta_c \cong \psi_c$. The actual value of the hob-setting angle ζ_c affects pitch helix angle ψ_c of the hob. This is due to the relationship [Equation (15.62)]

$$\psi_{b.c} = \cos^{-1}(\cos\phi_n \cos\zeta_c) \tag{16.55}$$

for the base helix angle $\psi_{b.c}$ is valid [130].

Thickness t_c of the hob tooth can be computed from the equation

$$t_c = \frac{\pi m}{2} \tag{16.56}$$

and in the case under consideration it is equal to $t_c = 15.708\,\text{mm}$.

For the computation of the hob base diameter $d_{b.c}$, Equation (15.58)

$$d_{b.c} = 2r_{b.c} = \frac{mN_c \cos\phi_n}{\sqrt{1 - \cos^2\phi_n \cos^2\zeta_c}} \tag{16.57}$$

is used [91, 112, 130, 135, 138]. In the numerical example, Equation (16.57) returns $d_{b.c} = 27.037\,\text{mm}$.

The computations reveal that deviations of the tooth profile of the involute hob with the above-listed design parameters (Table 16.1) are of zero value ($\delta_c = 0$) for both opposite sides of the tooth profile.

The impact of other design parameters of an involute hob on the tooth profile deviation δ_c. As proven in our earlier work [144], minimum tooth profile deviation δ_c is observed when the hob-setting angle, ζ_c, is exactly equal to the pitch helix angle, ψ_c, of the involute hob. In other words, when the equality $\zeta_c = \psi_c$ is observed, then the condition $\delta_c \mapsto \min$ is satisfied. This statement is derived on the premise of the solution to the equation $\partial\delta_c(\zeta_c, \ldots)/\partial\zeta_c = 0$ [54, 132, 135, 144].

The tooth profile deviation δ_c affects the base pitch of the involute hob.

Due to a difference between the actual base pitch $\tilde{p}_b$ and the desired its value p_b, the base pitch error $\delta p_b = p_{b.c} - \tilde{p}_{b.c}$ becomes unavoidable. The deviation δp_b directly affects the conjugate action of the cut gear and the pinion tooth profiles, causing noise, whine, vibration, and other negative effects.

The results of the analytical investigation of the accuracy can be used for the purposes of increasing the accuracy of the hobbed gears.

Once gear hobs are manufactured with straight lateral cutting edges, this feature of the hob design allows for significant reduction or even for elimination of the deviation δ_c of tooth profile of the hob. Figure 16.41 reveals that the deviation δ_c of tooth profile is the smallest possible under a specific value of the rake angle γ_o. This value of the rake angle γ_o corresponds to the configuration of the lateral cutting edge of the involute hob when it is aligned with the straight line that is tangent to the base helix angle of the hob (Figure 16.45).

When the lateral cutting edge of one side of the tooth profile of a precision involute hob of conventional design is straight, the cutting edge of the opposite side of tooth profile should be curved.

Precision single-start involute hobs featuring straight lateral cutting edges with zero tooth profile deviation, $\delta_c = 0$, can be used for the machining of precision spur and helical gears of nonreversible gear trains (e.g., for machining gears for helicopter transmissions, gear reducers for electric windmill stations, and turbine reducers). Precision involute hobs with a positive rake angle, $\gamma_o > 0°$ (Figure 16.45a), are recommended for hobs made of high-speed steel, while hobs with negative rake angle, $\gamma_o < 0°$ (Figure 16.45b), are recommended for carbide involute hobs. Positive rake angle, $\gamma_o > 0°$, results in a corresponding positive value of the normal rake angle, $\gamma_n > 0°$, at the hob tooth lateral cutting edges, which are suitable for high-speed steel hobs, while negative rake angle, $\gamma_o < 0°$, causes a negative

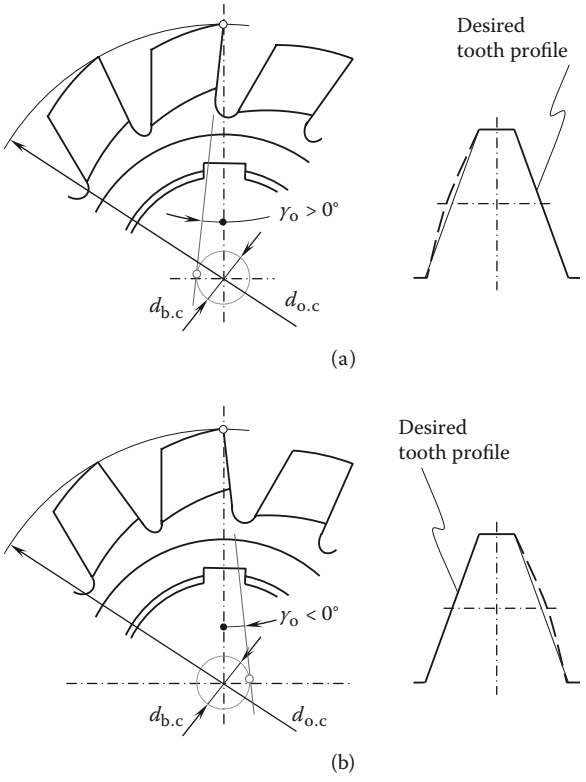

FIGURE 16.45
The required configuration of the straight lateral cutting edge of a precision involute hob with a (a) positive and (b) negative rake angle γ_o. (From Radzevich, S.P., *SME Journal of Manufacturing Processes*, 9(2), 121–136, 2007. With permission.)

value of the normal rake angle, $\gamma_n < 0°$, at the hob tooth lateral cutting edges, which are recommended for carbide hobs. In both cases, for single-start hobs of conventional design, the absolute value of the rake angle γ_o is in the range of $|\gamma_o| \approx 10°$.

Owing to nonzero rake angle γ_o on the top cutting edge of the hob tooth (Figure 16.45), lateral cutting edges of the hob tooth feature a corresponding value of the inclination angle λ_{ce}. The inclination angle λ_{ce} can be either positive ($\lambda_{ce} > 0°$) or negative ($\lambda_{ce} < 0°$) depending on (a) the sign of the rake angle γ_o, and (b) the hand of the hob threads. Usually, the lateral cutting edge geometry is of critical importance for roughing and semiroughing involute hobs. It is of much less importance for finishing and/or semifinishing hobs [138, 142, 143].

The accuracy of precision skiving hobs with a rake angle γ_o up to $\gamma_o = -60°$ [28] can also be improved using the method discussed above. To eliminate the deviation δ_c of the hob tooth profile, it uses not a single-start but multiple-start skiving hobs (Figure 16.46a) [133, 144, 153]. The required number N_c of the hob starts depends on the actual rake angle γ_o of the hob. To ensure the specified negative value of the rake angle γ_o, the precision involute skiving hob must be of a right-hand helix in order to have the entering lateral cutting edges of a straight form (Figure 16.46b), and it must be of a left-hand helix to have the entering lateral cutting edges of a straight form (Figure 16.46c). Therefore, two different hobs are required for the machining of a precision hardened gear. Otherwise, the gear should be hobbed in two setups.

16.4.3 Impact of Pitch Diameter on the Accuracy of a Gear Hob

The kinematics of the relative motion of the work gear and the involute hob depends on the current value of the pitch diameter of the hob. Changes to the kinematics of the relative motion could affect the resultant accuracy of the hobbed gear.

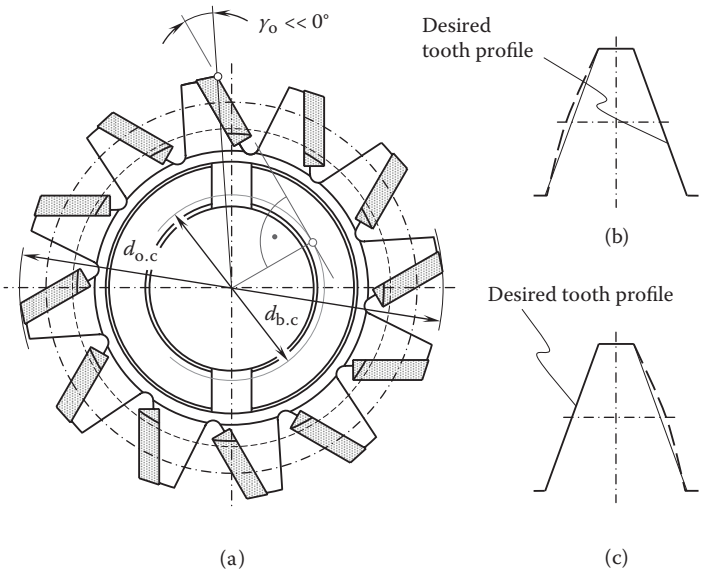

FIGURE 16.46
An example of a precision skiving involute hob with the rake angle γ_o of a prescribed value that features the desired straight lateral cutting edges. (From Radzevich, S.P., *SME Journal of Manufacturing Processes*, 9(2), 121–136, 2007. With permission.)

16.4.3.1 Peculiarities of the Relative Motion of the Work Gear and the Hob

The kinematics of meshing of a work gear and the involute hob includes rotations of the work gear and the hob about their axis of rotation. Simultaneously, the work gear and the hob are traveling relative to each other in the axial direction of the work gear with a feed motion.

The kinematics of meshing of the work gear and the hob resembles the meshing observed in a worm gear set. A comprehensive analysis of the kinematics of worm gearing can be found in [11]. While the kinematics of meshing are similar, the kinematics of the relative motion of the work gear and the involute hob differs from the relative motion of the worm and the worm gear in a conventional worm set. The difference is mainly due to the change in pitch diameter after each regrinding of the gear hob. The reduction of pitch diameter after the hob bas been reground is illustrated in Figure 16.47.

After each regrinding, the clearance surface of the hob tooth remains within a certain central angle σ (Figure 16.47). Practically, a portion of the clearance surface for regrinding of the hob tooth spans over a central angle ~0.6σ. The outer diameter of the new hob is designated as $d_{o.c}$, and the pitch diameter of the hob is denoted as d_c. After being reground, the outer diameter of the hob reduces at a value of $\Delta d_{o.h}$. The maximum reduction $\Delta d_{o.h}$ of the hob outer diameter depends on the clearance angle α_o of the hob tooth (Figure 16.47) and the permissible value of the central angle σ. When the outer diameter $d_{o.c}$ of the hob gets smaller, a corresponding change to pitch diameter d_c of the hob is observed [110, 130].

A change to the hob pitch diameter d_c causes the corresponding change of the pitch helix angle ψ_c of the hob. The pitch helix angle of a new hob can be computed from the formula

$$\psi_c = \sin^{-1}\left(\frac{N_c P_{x.c}}{d_c}\right) \tag{16.58}$$

where $P_{x.c}$ denotes the axial pitch of the involute hob.

After being reground, the pitch diameter d_c of the hob reduces to a certain value $d_{y.c}$, while the hob axial pitch $P_{x.c}$ and number of starts d_c of the hob remain of the same value

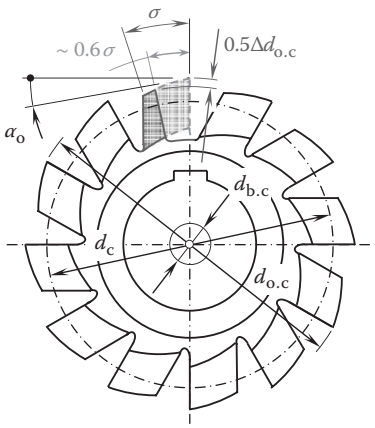

FIGURE 16.47
Change of pitch diameter of an involute gear hob after being reground. (From Radzevich, S.P., *ASME Journal of Mechanical Design*, 124, 772–786, 2002. With permission.)

and are identical to the values of the corresponding parameters of the new hob. Therefore, the pitch helix angle $\psi_{y.c}$ for a partially worn hob increases to

$$\psi_{y.h} = \sin^{-1}\left(\frac{N_h P_{x.h}}{d_{y.h}}\right) > \psi_h \tag{16.59}$$

The pitch helix angle $\psi_{y.c}$ is of the biggest value when the pitch diameter $d_{y.c}$ is the smallest feasible. This means that when the diameter $d_{y.c} = d_c^{min}$ then the angle $\psi_{y.c} = \psi_c^{max}$. The difference $\Delta\psi_c = -(\psi_c - \psi_{y.c})$ can be employed for the evaluation of the range of change to the pitch helix angle ψ_c after each regrinding of the hob.

The difference $\Delta\psi_c$ in the pitch helix angle of the hob strongly depends on the hob clearance angle α_o. The bigger the clearance angle α_o, the bigger the difference $\Delta\psi_c$ is observed and vice versa. Figure 16.48 illustrates the impact of the hob clearance angle α_o on the current value of the deviation $\Delta\psi_c$ for involute hobs with various numbers of starts. It is assumed in Figure 16.48 that the maximum tooth depth at which the hob is reground is equal to the hob module (i.e., the central angle ~0.6σ is equal to ~$0.6\sigma = 2m/d_{o.c}$, and thus, the equality $\sigma \cong 3.3m/d_{o.c}$ is valid). For the computation of the deviation $\Delta\psi_c$ the following formula [110, 130]

$$\Delta\psi_c = \sin^{-1}\left(\frac{mN_c}{d_{o.c} - 2m\tan\alpha_o}\right) - \sin^{-1}\left(\frac{mN_c}{d_{o.c}}\right) \tag{16.60}$$

is used.

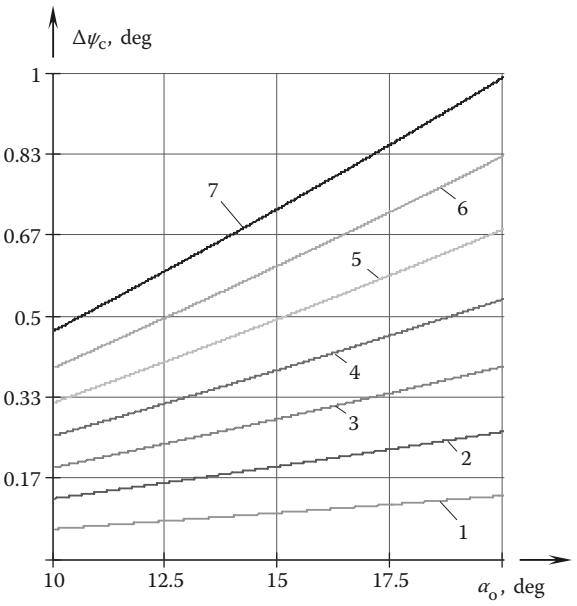

FIGURE 16.48
Impact of the clearance angle α_o of a hob (module m = 10 mm, pitch diameter d_c = 160 mm) on the pitch helix deviation $\Delta\psi_c$ when the number of starts of the hob is (1) $N_c = 1$, (2) $N_c = 2$, (3) $N_c = 3$, (4) $N_c = 4$, (5) $N_c = 5$, (6) $N_c = 6$, and (7) $N_c = 7$. (From Radzevich, S.P., *ASME Journal of Mechanical Design*, 129, 1076–1085, 2007. With permission.)

Figure 16.48 reveals the strong impact of the clearance angle α_o on the deviation of the pitch helix angle $\Delta\psi_c$ of a gear hob. The bigger the number of starts N_c of the hob the sever impact of the clearance angle α_o on value of the deviation $\Delta\psi_c$.

The strong influence of the hob diameter on the resultant accuracy of the hob is well recognized. The average value of pitch diameter $\overline{d}_c$ is commonly used for computation of the design parameters of an involute hob. Here,

$$\overline{d}_c = \frac{d_c - d_c^{\text{worn}}}{2} \tag{16.61}$$

where d_c^{worn} designates pitch diameter of the totally worn involute hob after its last feasible regrinding.

Figure 16.49 illustrates the desired change in value of the hob-setting angle ζ_c versus the current value of the hob pitch diameter $d_{y.c}$. Involute hobs of smaller diameter and hobs with a greater number of starts require even more significant change to the hob-setting angle. It is the right point to stress here that the maximum practical number of starts of an involute hob reaches $N_c = 13$. This means that an appropriate change to the current value of the hob-setting angle is of critical importance for precision multistart involute hobs of small diameter [110, 130].

An unavoidable change $\Delta p_{b.c}$ to base pitch $p_{b.c}$ of the hob is observed if the setting angle of the hob ζ_c changes in the proper manner and no corresponding compensation is made to other design parameters of the hob. The impact of the hob pitch diameter d_c, and the hob number of starts N_c on the deviation $\Delta p_{b.c}$, are illustrated in Figure 16.50. The bigger alteration in the hob pitch diameter $d_{y.c}$, the bigger the deviation $\Delta p_{b.c}$ of the actual base pitch of the hob from it nominal value $p_{b.c}$. Involute hobs with bigger numbers of starts N_c are more vulnerable to the changes to the hob pitch diameter (Figure 16.50). The function $\Delta p_{b.c} = \Delta p_{b.c}(d_{y.c})$ is nonlinear. However, the curves of the nonlinear function $\Delta p_{b.c}(d_{y.c})$ are close to straight lines. This is because the interval of changing of the pitch diameter $d_{y.c}$ is small. In the case under consideration this interval is equal to just $d_{y.c} = (150 - 140) = 10$ mm.

Any changes to base pitch $p_{b.c}$ of the hob are undesirable. The changes $\Delta p_{b.c}$ are allowed only within the corresponding tolerances $[\Delta p_{b.c}]$ for the base pitch $p_{b.c}$ (i.e., fulfillment of the

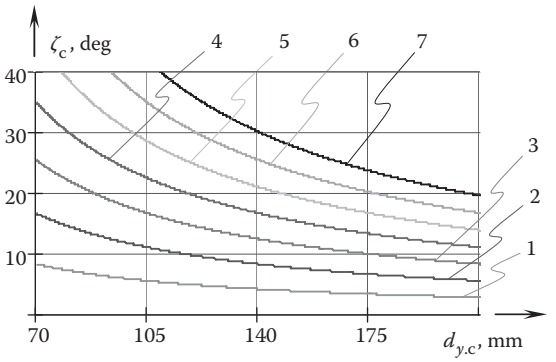

FIGURE 16.49
Impact of the pitch diameter $d_{y.c}$ of a hob of the module $m = 10$ mm on the desirable value of the hob-setting angle ζ_c when the number of starts of the hob is (1) $N_c = 1$, (2) $N_c = 2$, (3) $N_c = 3$, (4) $N_c = 4$, (5) $N_c = 5$, (6) $N_c = 6$, and (7) $N_c = 7$. (From Radzevich, S.P., *ASME Journal of Mechanical Design*, 129, 1076–1085, 2007. With permission.)

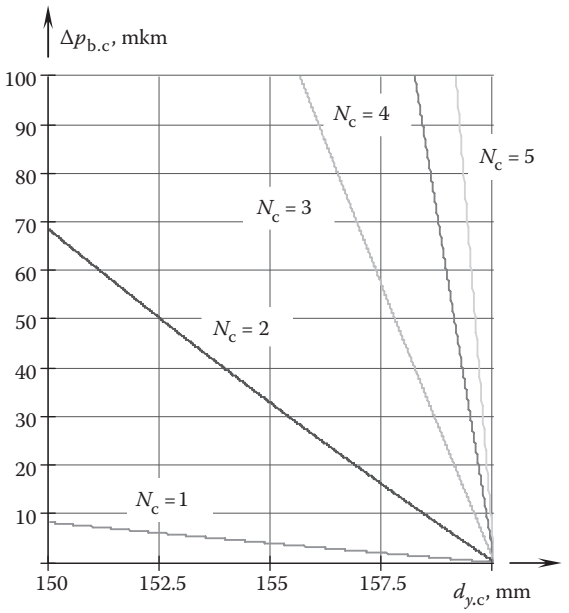

FIGURE 16.50
Impact of the value of the reduction of the hob pitch diameter $d_{y.c}$ on the deviations of the hob base pitch $\Delta p_{b.c}$ for involute hobs with various numbers of starts N_c. (From Radzevich, S.P., *ASME Journal of Mechanical Design*, 129, 1076–1085, 2007. With permission.)

inequality $\Delta p_{b.c} \le [\Delta p_{b.c}]$ is a must). Otherwise, the accuracy of the hobbed involute gears is unacceptably poor.

Evidently, change Δd_c to hob diameter d_c results in a strongly undesirable change to the base pitch of the hob.

16.4.3.2 Principal Design Parameters of an Involute Hob

The following principal design parameters are required to be known prior to designing the involute hob: (a) the hob module m, (b) the normal profile angle ϕ_n, (c) the number of starts N_c of the hob threads, and (d) the desired value of the setting angle of the hob ζ_c. The rest of the important design parameters, namely, (a) the hob outside diameter $d_{o.c}$, (b) the number of gashes, (c) the rake angle γ_o of the hob tooth, and (d) the clearance angle α_o of the hob tooth, are incorporated into the designing process during the later stages of the design process.

The design parameters m and ϕ_n yield immediate computation of the hob base pitch

$$p_{b.c} = \pi m \cos \phi_n \tag{16.62}$$

The axial pitch of the hob threads can be computed by the formula

$$P_{x.c} = \frac{\pi m N_c}{\cos \zeta_c} \tag{16.63}$$

For the computation of base diameter $d_{b.c}$ of the hob, the following equation [54, 130, 144]

$$d_{b.c} = \frac{mN_c \cos\phi_n}{\sqrt{1-\cos^2\phi_n \cos^2\zeta_c}} \tag{16.64}$$

can be used.

Ultimately, the hob base helix angle $\psi_{b.c}$ can be computed from the equation [130, 144]

$$\psi_{b.c} = \cos^{-1}(\cos\phi_n \cos\zeta_c) \tag{16.65}$$

Equation (16.65) also allows for representation in the form

$$\tan\psi_{b.c} = \frac{\sqrt{\sin^2\phi_n + \tan^2\zeta_c}}{\cos\phi_n} \tag{16.66}$$

which had proven to be convenient for some applications.

The base lead angle $\lambda_{b.c}$ is equal to $\lambda_{b.c} = 90° - \psi_{b.c}$.

Further, the base bitch of the hob $p_{b.c}$ can be expressed in terms of the hob axial pitch $P_{x.c}$, of the normal pressure angle ϕ_n, and of the setting angle of the hob ζ_c

$$p_{b.c} = P_{x.c} \cos\phi_n \cos\zeta_c \tag{16.67}$$

This equation is useful when performing an analysis of geometry of the involute hob and the kinematics of meshing.

If the axial pitch of the hob threads $P_{x.c}$ is computed from Equation (16.63), then for the computation of the hob pitch helix ψ_c angle the equation

$$\psi_c = \tan^{-1}\left(\frac{P_{x.c}}{\pi d_c}\right) \tag{16.68}$$

can be employed.

Equation (16.63) yields a simple formula for the computation of the pitch helix angle $\psi_{y.c}$ of the hob

$$\tan\psi_{y.c} = \frac{P_{x.c}}{\pi d_{y.c}} = \frac{\pi m N_c}{\pi d_{y.c}\cos\zeta_c} = \frac{mN_c}{d_{y.c}\cos\zeta_c} \tag{16.69}$$

Equating the setting angle of the hob ζ_c to the pitch helix angle $\psi_{y.c}$ of the hob (i.e., targeting the equality $\zeta_{y.c} = \psi_{y.c}$ be valid), Equation (16.69) yields the expression

$$\tan\zeta_{y.c} = \frac{mN_c}{d_{y.c}\cos\zeta_{y.c}} \tag{16.70}$$

Equation (16.70) reduces to

$$\sin\zeta_{y.c} = \frac{mN_c}{d_{y.c}} \tag{16.71}$$

If the current value of the hob-setting angle $\zeta_{y.c}$ is computed from Equation (16.71), then the equality $\zeta_{y.c} = \psi_{y.c}$ is observed for a new involute hob and for the hob being reground as well.

The above equations are derived based on the following.

Consider the auxiliary generating rack $\mathscr{R}_T$ of the hob. The tooth profile angle of the rack $\mathscr{R}_T$ is designated as ϕ_n, and the base pitch of the rack is designated as $p_{b.\mathscr{R}}$. Other design parameters of the rack $\mathscr{R}_T$ (tooth addendum $a_{\mathscr{R}}$, tooth dedendum $b_{\mathscr{R}}$, whole depth $h_{\mathscr{R}}$, pitch $P_{n.\mathscr{R}}$, tooth thickness $t_{\mathscr{R}}$, space width $w_{\mathscr{R}}$) are also known. Commonly, most of the design parameters of the rack $\mathscr{R}_T$ can be expressed in terms of module m.

Initially, the auxiliary rack $\mathscr{R}_T$ is described analytically in a left-hand-oriented Cartesian coordinate system $X_cY_cZ_c$ (Figure 16.51). The pitch plane of the rack is at a distance $d_c/2$ from the Z_c axis, and is parallel to the coordinate plane X_cZ_c. The axis of rotation O_c of the hob is aligned to the Z_c axis. The rack $\mathscr{R}_T$ is turned through the setting angle of the hob ζ_c with respect to the hob axis O_c.

In the coordinate system $X_cY_cZ_c$, the rack $\mathscr{R}_T$ performs a screw motion about the Z_c axis. The parameter of the screw motion (the reduced pitch) of the rack $\mathscr{R}_T$ is designated as $p_{\mathscr{R}}$.

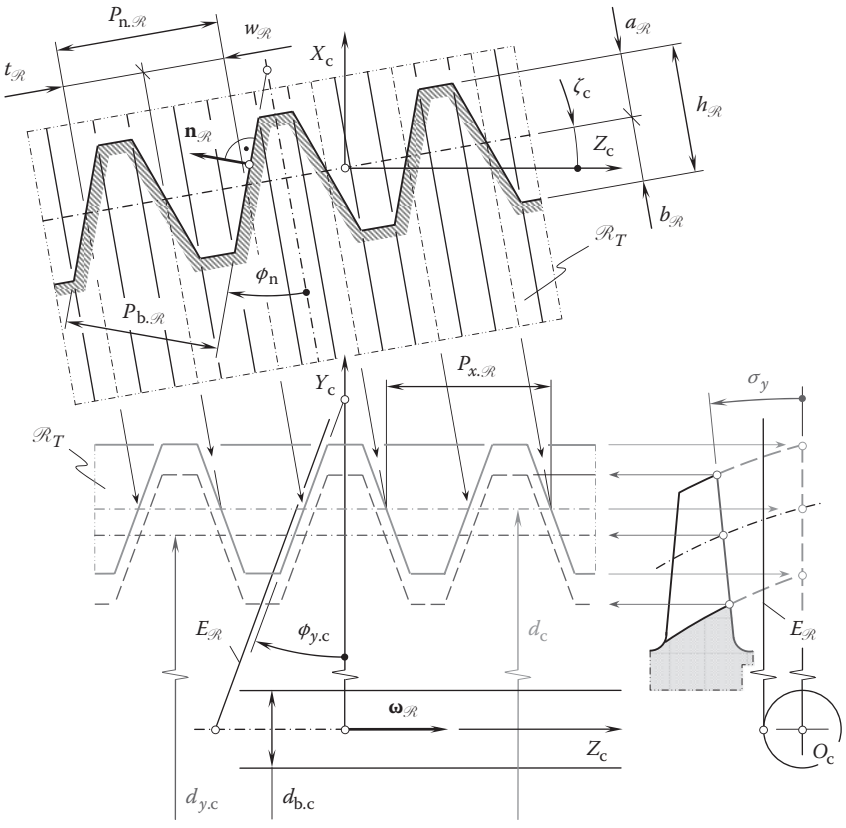

FIGURE 16.51
The computation of the desired changes to the parameters of the kinematic geometry of an involute hob. (From Radzevich, S.P., *ASME Journal of Mechanical Design*, 129, 1076–1085, 2007. With permission.)

The screw motion of the rack $\mathscr{R}_T$ can be decomposed onto two elementary motions, (a) on the rotation $\boldsymbol{\omega}_{\mathscr{R}}$ of the rack $\mathscr{R}_T$ about the Z_c axis, and (b) on the translation $\mathbf{V}_{\mathscr{R}}$ of the rack $\mathscr{R}_T$ along the Z_c axis.

Further, it is convenient to decompose the translation motion $\mathbf{V}_{\mathscr{R}}$ onto two elementary motions $\mathbf{V}_{\mathscr{R}} = \mathbf{V}_z + \mathbf{V}_0$. The translational motion with the speed $\mathbf{V}_z$ is in the direction that is parallel to the Z_c axis. The translational motion $\mathbf{V}_0$ is in the direction of the generating line of the auxiliary rack $\mathscr{R}_T$. The translation $\mathbf{V}_0$ results in sliding of the rack $\mathscr{R}_T$ over itself. This motion does not affect the shape of the enveloping surface T. Therefore, the motion $\mathbf{V}_0$ can be omitted from further analysis.

The magnitude V_z of the speed $\mathbf{V}_z$ is equal to

$$V_z = \frac{|\,\mathbf{V}_{\mathscr{R}}\,|}{\cos\zeta_c} \tag{16.72}$$

Therefore, the parameter of the screw motion of the auxiliary rack $\mathscr{R}_T$ can be computed from the formula

$$p_{\mathscr{R}} = \frac{V_z}{|\,\boldsymbol{\omega}_g\,|} = \frac{d_c\omega_{\mathscr{R}}}{2\,\omega_g\cos\zeta_c} \tag{16.73}$$

For a single-start involute hob, Equation (16.73) reduces to

$$p_{\mathscr{R}} = \frac{d_c}{2\,N_g\cos\zeta_c} \tag{16.74}$$

where N_g denotes number of teeth of the hobbed gear.

The design parameters of generating surface T of the hob can be determined in the following way.

The characteristic line $E_{\mathscr{R}}$ can be interpreted as a locus of points on the auxiliary generating surface $\mathscr{R}_T$, at which perpendicular $\mathbf{n}_{\mathscr{R}}$ to the surface $\mathscr{R}_T$ makes a certain angle ε with the axis of the screw motion O_c. In other words, the characteristic line $E_{\mathscr{R}}$ can be interpreted as a locus of points at which the unit normal vector $\mathbf{n}_{\mathscr{R}}$ is perpendicular to the vector $\mathbf{V}_{\mathscr{R}}$. For the computation of the angle ε, Ball's equation [1, 72]

$$\tan\varepsilon = \frac{p_{\mathscr{R}}}{r_{y.c}} \tag{16.75}$$

is used. Here $r_{y.c}$ denotes the shortest distance of approach of the straight line along the unit normal vector $\mathbf{n}_{\mathscr{R}}$, and of the axis Z_c of the screw motion.

The angle that the tooth flank surface of the auxiliary rack $\mathscr{R}_T$ makes with the axis Z_c of the screw motion is designated as ρ. Thus, unit normal vector $\mathbf{n}_{\mathscr{R}}$ makes the angle $(90° - \rho)$ with the axis Z_c of the screw motion. Owing to this, at points within the characteristic line $E_{\mathscr{R}}$, the following equalities

$$\tan(90° - \rho) = \frac{p_{\mathscr{R}}}{r_{y.h}} \quad \text{or} \quad r_{y.h} = p_{\mathscr{R}}\tan\rho \tag{16.76}$$

are valid.

Equation (16.76) reveals that the characteristic line $E_{\mathscr{R}}$ is the straight line that makes the angle ρ with the Z_c axis, and that is remote from the axis Z_c at a distance $r_{y.c}$.

For further analysis, it is necessary to determine the angle ρ. For this purpose, a unit vector **a** is constructed. The vector **a** is along the axis Z_c of the screw motion. Therefore, in the coordinate system $X_cY_cZ_c$, this vector can be represented in the form

$$\mathbf{a} = \mathbf{k} \tag{16.77}$$

In that same reference system $X_cY_cZ_c$, the unit normal vector $\mathbf{n}_{\mathscr{R}}$ can be represented as

$$\mathbf{n}_{\mathscr{R}} = \mathbf{i} \cdot \cos\phi_n \cos\zeta_c + \mathbf{j} \cdot \sin\phi_n - \mathbf{k} \cdot \cos\phi_n \sin\zeta_c \tag{16.78}$$

The vectors **a** and $\mathbf{n}_{\mathscr{R}}$ make the angle ρ. Therefore, the equality

$$\tan\rho = \frac{\mathbf{a} \cdot \mathbf{n}_{\mathscr{R}}}{|\mathbf{a} \times \mathbf{n}_{\mathscr{R}}|} \tag{16.79}$$

is valid.

After substituting Equations (16.77) and (16.78), Equation (16.79) casts into

$$\tan\rho = \frac{\cos\phi_n}{\sqrt{\sin^2\phi_n + \tan^2\zeta_c}} \tag{16.80}$$

When the actual value of the angle ρ is known, then the base diameter of the hob can be computed from

$$d_{b.c} = 2p_{\mathscr{R}} \tan\rho = \frac{N_c}{N_g} \cdot \frac{d_c \cos\phi_n}{\sqrt{1 - \cos^2\phi_n \cos^2\zeta_c}} \tag{16.81}$$

In a specific case of design of the involute hob for which tooth thickness $t_{\mathscr{R}}$ on the hob pitch diameter is equal to the hob space width $w_{\mathscr{R}}$, Equation (6.81) reduces to

$$d_{b.c} = \frac{mN_c \cos\phi_n}{\sqrt{1 - \cos^2\phi_n \cos^2\zeta_c}} \tag{16.82}$$

In Equation (16.82), the advantage of independence of the hob base diameter $d_{b.c}$ from the hobbed gear tooth number N_g is taken.

The derived equations above yield computation of the hob axial pitch

$$P_{x.c} = 2\pi p_{\mathscr{R}} = \frac{\pi d_c}{N_c \cos\zeta_c} \tag{16.83}$$

Normal pitch is measured on the unfolded base cylinder of the hob. It is equal to

$$p_{b.c} = p_{x.c} \sin\rho = \frac{\pi d_g}{N_g} = p_{b.g} \tag{16.84}$$

The requirement $p_{b.c} = p_{b.g}$ is a must. This means that various hobs with different normal profile angle ϕ_n can be used for hobbing of that same involute gear. However, the base pitch $p_{b.c}$ of all of them must be the same, and also must be equal to the base pitch of the involute gear being hobbed.

The equations derived above allow for the computation of any and all principal design parameters of the involute hob.

16.4.3.3 Elements of Kinematic Geometry of an Involute Hob

The base pitch $p_{b.c}$ of the hob must be exactly equal to the base pitch of the gear $p_{b.g}$. The equality $p_{b.c} = p_{b.g}$ reflects the principal condition of high accuracy of the hobbed gear. Because of the equality $p_{b.c} = p_{b.g}$ should be always observed, the involute hob base pitch $p_{b.c}$ must remain of that same value after regrinding of the hob. However, according to Equations (16.67) and (16.70), change to the hob pitch diameter d_c causes a strongly undesirable change to the hob base pitch $p_{b.c}$. Ultimately, this results in the hob lateral cutting edges shifting from the generating surface *T*. In this way, the shift of the cutting edges causes errors of the hob tooth profile.

The desired change to normal profile angle. In order to maintain high accuracy of the hob, it is desired to keep the setting angle of the hob ζ_c equal to pitch helix angle ψ_c of the hob. This means that fulfillment of the equality $\zeta_c = \psi_c$ is one of the prerequisites of high accuracy of involute hobs [54, 129]. According to Equations (16.67) and (16.70), the following equation for the computation of base pitch $p_{b.c}$ is valid

$$p_{b.c} = \frac{d_c P_{x.c}}{\sqrt{d_c^2 + m^2 N_c^2}} \cdot \cos\phi_n \tag{16.85}$$

where

$p_{b.c}$ = base pitch of the hob
d_c = pitch diameter of the hob
$P_{x.c}$ = axial pitch of the hob
m = hob module
N_c = number of starts of the hob (sometimes this design parameter is incorrectly referred to as *number of threads*)
ϕ_n = normal profile angle of the hob

It is evident that the change to the pitch diameter after regrinding of the hob is unavoidable. The hob diameters, namely, (a) pitch diameter d_c, (b) outer diameter $d_{o.c}$, and (c) limit diameter $d_{l.c}$, are getting smaller and smaller after each regrinding of the hob.

Change to the pitch helix angle indicates that the parameters of the relative motion of the worn hob with respect to the work gear differ from the corresponding parameters of relative motion of the new hob with respect to that same work gear. This means that the kinematics of meshing of the work gear with the new hob differ from the kinematics of meshing of the work gear with the worn hob. This also makes clear that the accuracy of an involute hob does not remain the same after the hob has been reground. The smaller the diameter of the hob, the bigger the deviations of the lateral cutting edges from the generating surface *T* of the hob. In order to accommodate for the deviations, a method for relieving involute hobs was developed [87].

The proposed method for relief grinding of an involute hob [85] is a perfect example of implementation of the *DG/K*-based method of surface generation for solving a problem that pertains to hobbing of involute gears.

The reduction of pitch diameter after regrinding of the hob is unavoidable. Therefore, the negative impact of this change to the hob base pitch must be compensated somehow. The required compensation can be performed by corresponding change to another design parameter of the hob on precalculated values.

Figure 16.51 illustrates configurations of the auxiliary rack of the new hob and of the hob being reground. Configuration of the Cartesian coordinate system $X_cY_cZ_c$ in Figure 16.51 is identical to the configuration of the coordinates system $X_cY_cZ_c$ in Figure 15.9. The major parameters of kinematic geometry of the hob are indicated in Figure 16.51.

The straight-line generator (the characteristic line $E_{\mathscr{R}}$) is tangent to the base cylinder of diameter $d_{b.c}$ of the hob. It also makes the base helix angle $\psi_{b.c}$ with the axis Z_c. Therefore, the characteristic line $E_{\mathscr{R}}$ is tangent to the base helix of the hob. The profile angle of the auxiliary rack $\mathscr{R}_T$ in the axial cross-section of the hob is designated as $\phi_{y.c}$.

An analysis of Equation (16.64) shows that the hob profile angle is the only design parameter that can be helpful for compensation of the unavoidable change of the hob diameter. When the hob pitch diameter gets smaller, the hob profile angle has to be properly changed in a manner that the hob base pitch $p_{b.c}$ remains constant.

An equation for the computation of the required change to the hob profile angle $\phi_{y.c}$ can be derived.

Configuration of the reground hob rake surface R_s with respect to its configuration for the new hob can be expressed in terms of current value of central angle σ_y (Figure 16.51). Here σ_y is within the interval $0.6\sigma \le \sigma_y \le 0°$. Design parameters $d_{y.c}$ and $\phi_{y.c}$ of the hob are functions of σ_y. This means that the equations $d_{y.c} = d_{y.c}(\sigma_y)$ and $\phi_{y.c} = \phi_{y.c}(\sigma_y)$ are valid. The generalized form of these equations needs to be expressed in terms of the design parameters of the hob.

In order to maintain the hob base pitch of constant value (and not changeable after hob regrinding), the equality $\partial p_{b.c}/\partial \sigma_y = 0$ is required to be satisfied. By differentiating Equation (16.72) with respect to σ_y, one can come up with the differential equation

$$\tan \phi_{y.c}\, \partial \phi_{y.c} = \left(\frac{1}{d_{y.c}} - \frac{d_{y.c}}{d_{y.c}^2 + mN_c} \right) \partial d_{y.c} \tag{16.86}$$

Here, in Equation (16.86), the variables [$\phi_{y.c}(\sigma_y)$ and $d_{y.c}(\sigma_y)$] are split. This is mostly due to both being dependant not on σ_y but on $\Delta d_{y.c}$. Therefore, separate integration of the left-hand side and the right-hand side of Equation (16.86) is valid

$$\int_{\phi_n}^{\phi_{y.c}} \tan \phi_{y.c}\, \partial \phi_{y.c} = \int_{d_c}^{d_{y.c}} \left(\frac{1}{d_{y.c}} - \frac{d_{y.c}}{d_{y.c}^2 + mN_c} \right) \partial d_{y.c} \tag{16.87}$$

The intervals of integration (from ϕ_n to $\phi_{y.c}$, and from d_c to $d_{y.c}$) in Equation (16.87) are semiopen.

Ultimately, the equation for the computation of the desirable current value of the profile angle $\phi_{y.c}$ of the hob tooth can be represented in the form

$$\phi_{y.c} = \arccos\left(\frac{d_c}{d_{y.c}} \cdot \sqrt{\frac{d_{y.c}^2 + m^2 N_c^2}{d_c^2 + m^2 N_c^2}} \cdot \cos\phi_n \right) \tag{16.88}$$

A 3-D graph that illustrates the influence of the design parameters of the hob on the desirable value of the hob profile angle $\phi_{y.c}$ is plotted in Figure 16.52. Because the deviations of the hob normal profile angle are small, the 3-D plot in Figure 16.52 represents the visualization only of the function $\Delta\phi_{y.c}$ versus $d_{y.c}$ and N_c (here $\Delta\phi_{y.c} = \phi_n - \phi_{y.c}$). The function $\phi_{y.c}$ vs. $d_{y.c}$ and N_c is not shown in Figure 16.52.

The required alteration $\Delta\phi_n$ of the hob profile angle ϕ_n can be expressed in terms of current value of the pitch diameter $d_{y.c}$ of the hob. The bigger the alterations to the hob pitch diameter $d_{y.c}$, the bigger the precalculated alterations $\Delta\phi_n$ to the hob profile angle are required. Again, for the multistart involute hob, the function $\Delta\phi_n = \Delta\phi_n(d_{y.c})$ is much more vulnerable to the deviations of the actual value of the pitch diameter compared to its nominal value (Figure 16.52). As in the example considered above, the function $\Delta\phi_n = \Delta\phi_n(d_{y.c})$ is a nonlinear one. The curves of the nonlinear function $\Delta\phi_n(d_{y.c})$ are close to straight lines. This is because the interval of alteration of pitch diameter $d_{y.c}$ is small and is only equal to $d_{y.c} = 10$ mm. The increased interval of change of the diameter $d_{y.c}$ makes the nonlinearity of the function $\Delta\phi_n(d_{y.c})$ evident.

The following interpretation of the simultaneous change of profile angle ϕ_n and of the hob-setting angel ζ_c can be given.

Consider a lateral tooth surface of the auxiliary rack $\mathscr{R}_T$. The straight-line generator (the characteristic line $E_{\mathscr{R}}$) of the generating surface T of the hob is located within this plane. Assume then that the lateral plane of the tooth turns through a certain angle about the straight-line generator $E_{\mathscr{R}}$. This turn of the plane results in a corresponding change to

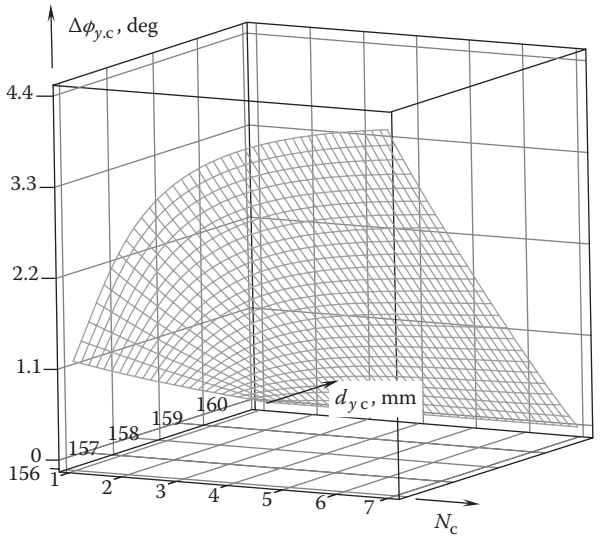

FIGURE 16.52
Impact of the number of starts N_c of a hob and a hob current diameter $d_{y.c}$ on the required precalculated value of the correction $\Delta\phi_{y.c}$ to the hob profile angle ϕ_n. (From Radzevich, S.P., *ASME Journal of Mechanical Design*, 129, 1076–1085, 2007. With permission.)

current value of the normal profile angle ϕ_n, as well as to the setting angle of the hob ζ_c. Current values of the angles ϕ_n and ζ_c are changing in a way that follows the rotation of the lateral plane of the rack $\mathscr{R}_T$ about the straight-line generator $E_{\mathscr{R}}$. However, under such the rotation of the lateral plane of the auxiliary rack $\mathscr{R}_T$ the following design parameters of the hob (a) base diameter $d_{b.c}$, (b) base helix angle $\psi_{b.c}$, as well as (c) base pitch $p_{b.c}$, remain constant.

In order to accommodate for the deviations of the base pitch $p_{b.c}$ due to changes to the pitch diameter of the hob after each regrinding of the hob, a design of the hob is proposed by Radzevich [97]. The hob features the ground relief clearance surfaces through the lateral cutting edges of the hob tooth, the geometry of which allows for fulfillment of the requirements imposed by Equation (16.88).

The clearance surfaces of precision involute hobs of the proposed design can be ground. For this purpose several methods for relief grinding of the hob were developed by Radzevich [82, 83, 179]. Use of the methods makes it possible to keep the tooth profile angle $\phi_{y.c} < \phi_n$ of the hob smaller after each regrinding operation in compliance with Equation (16.88). Reduction of the hob profile angle on the precalculated value retains the constant value of the hob base pitch ($p_{b.c}$ = const). In this way, one of the major sources of the hob errors is eliminated. Ultimately, the hob accuracy is not reduced after regrinding each hob.

The desired value of center-distance in gear hobbing operation. Each regrinding of an involute hob causes a reduction of its diameter. Evidently, this reduction is required to be compensated by the corresponding reduction of center distance in the gear hobbing operation. At first glimpse, the required reduction ΔC of the center distance must be equal to half of the reduction of the hob diameter. However, due to the alteration into the hob normal profile angle, the desired value of the center distance depends on the current value of the hob profile angle $\phi_{y.c}$.

The tooth ratio u_c in the gear hobbing operation is a constant parameter. This parameter is equal $u_c = N_g/N_c$, and it does not depend on how significant the change is to the hob diameter. From a diagram of meshing of the hob and the work gear in the gear hobbing operation, the following formula for computation of $\Delta C(\sigma_y)$ can be derived

$$\Delta C(\sigma_y) = \frac{1}{2}\left[d_c \sigma_y \tan\alpha_o + mN_g\left(1 - \frac{\cos\phi_n}{\cos\phi_{y.c}}\right)\right] \tag{16.89}$$

Analysis of Equation (16.89) reveals that the required reduction $\Delta C(\sigma_y)$ of the center distance C in the gear hobbing operation depends on the tooth number of the work gear. Figure 16.53 illustrates an example of impact of the tooth number of the work gear N_g, and of the hob number of starts N_c on the precalculated desirable value of the correction $\Delta C_y(\sigma_y)$ to the center distance C. Because the changes of $\Delta C_c(\sigma_y)$ caused by the reduction to the hob diameter itself are small compared to the changes caused by reduction of the hob profile angle, the inequality $\Delta C_c(\sigma_y) > \Delta C_y(\sigma_y)$ is observed. Only one portion $\Delta C_y(\sigma_y)$ of $\Delta C(\sigma_y)$ is plotted in Figure 16.53. For this purpose, Equation (16.89) is represented in the form $\Delta C(\sigma_y) = \Delta C_c(\sigma_y) > \Delta C_y(\sigma_y)$:

$$\Delta C(\sigma_y) = \underbrace{\frac{1}{2}\cdot d_c(\sigma_y)\tan\alpha_o}_{\Delta C_c(\sigma_y)} + \underbrace{\frac{mN_g}{2}\left(1 - \frac{\cos\phi_n}{\cos\phi_{y.c}}\right)}_{\Delta C_y(\sigma_y)} \tag{16.90}$$

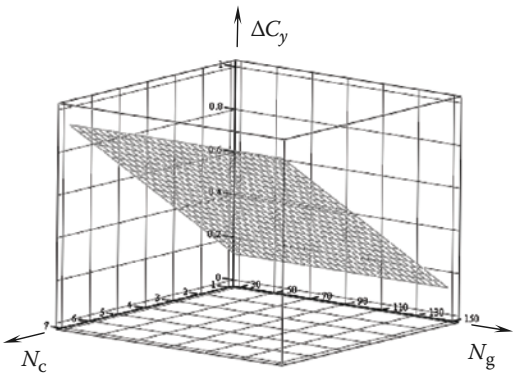

FIGURE 16.53
Impact of the tooth number of the work gear N_g and the number of starts N_c of a hob on the required precalculated value of correction ΔC_y to the center distance C. (From Radzevich, S.P., *ASME Journal of Mechanical Design*, 129, 1076–1085, 2007. With permission.)

The portion $\Delta C_c(\sigma_y)$ depends on reduction of the hob diameter. It does not depend on alteration of profile angle after the hob has been reground.

Work gears with bigger tooth number require a slightly smaller reduction $\Delta C(\sigma_y)$ to the center distance. The impact of the hob number of starts onto the parameter $\Delta C(\sigma_y)$ is the strongest. The bigger reduction $\Delta d_{y.c}$ of the hob diameters causes the bigger required reduction $\Delta C(\sigma_y)$ to the center distance.

The desirable change to the parameters of the kinematic geometry of an involute hob can be achieved in one of two possible methods.

The first method is based on implementation of a precalculated modification of the clearance surface of the hob tooth. The modification of this kind can be achieved on the hob relieving operation. Therefore, the first method for improvement to the hob accuracy can be recommended for manufacturers of involute hobs.

The second method is based on use of precalculated desirable deviations of the rake surface of the hob tooth, and thus it can be used when regrinding the hob. This method for increasing the hob accuracy is briefly considered below.

The desired correction to the configuration of the rake surface of the hob. As an example of application of the discussed approach, a method of corrective regrinding of an involute hob is developed [110, 130].

Consider an involute hob with a plane rake surface that is parallel to the hob axis of rotation O_c. The top cutting edge of the hob tooth has a positive rake angle $\gamma_o > 0°$. The clearance angle of that same cutting edge is equal to α_o. For a certain current value of the hob pitch diameter $d_{y.c}$ a corresponding correction $\Delta\gamma_o$ to the rake angle can be computed on the premise of the function of $\phi_{y.c} = \phi_{y.c}(d_{y.c})$ [see Equation (16.88)]. Without going into details of derivation of equations, the implemented approach can be briefly summarized in the following way.

For the derivation of an equation for the computation of the desired correction $\Delta\gamma_o$, consider three vectors **A**, **B**, and **c** through a point $\mathfrak{M}$ within the lateral cutting edge of the hob after it has been reground (Figure 16.54). The vectors **A**, **B**, and **c** are constructed so that they comprise a set of coplanar vectors. All are located within a certain plane that is tangent to the work gear tooth surface.

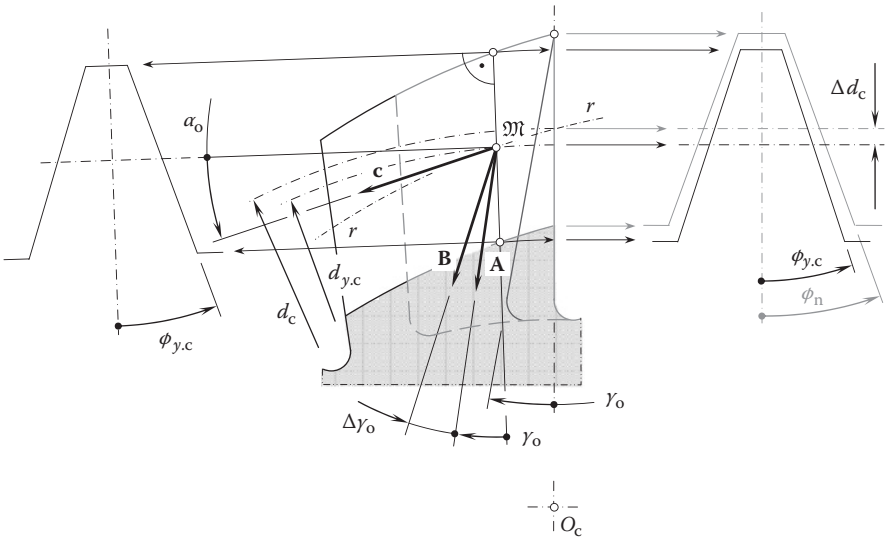

FIGURE 16.54
Computation of the desired correction $\Delta\gamma_o$ to a hob rake angle γ_o. (From Radzevich, S.P., *ASME Journal of Mechanical Design*, 129, 1076–1085, 2007. With permission.)

Three vectors **A**, **B**, and **c** can be expressed analytically as follows

$$\mathbf{A} = -\mathbf{i}\cdot\tan\gamma_o - \mathbf{j}\cdot\cos\phi_n + \mathbf{k}\cdot\sin\phi_n \tag{16.91}$$

$$\mathbf{B} = -\mathbf{i}\cdot\tan(\gamma_o + \Delta\gamma_o) - \mathbf{j}\cdot\cos\phi_{y.c} - \mathbf{k}\cdot\sin\phi_{y.c} \tag{16.92}$$

$$\mathbf{c} = -\mathbf{i}\cdot\cos\alpha_o - \mathbf{j}\cdot\sin\alpha_o \tag{16.93}$$

By construction, the vectors **A**, **B**, and **c** are coplanar. Therefore, triple scalar product of the vectors **A**, **B**, and **c** is identical to zero $\mathbf{A}\times\mathbf{B}\cdot\mathbf{c}\equiv 0$. This yields a determinant

$$\mathbf{A}\times\mathbf{B}\cdot\mathbf{c} = \begin{vmatrix} -\tan\gamma_o & -\cos\phi_n & \sin\phi_n \\ -\tan(\gamma_o+\Delta\gamma_o) & -\cos\phi_{y.c} & -\sin\phi_{y.c} \\ -\cos\alpha_o & -\sin\alpha_o & 0 \end{vmatrix} = 0 \tag{16.94}$$

After being expanded, the determinant casts into the formula for the computation of the desired value of the correction $\Delta\gamma_o$

$$\Delta\gamma_o = \arctan\left(\frac{\sin\phi_{y.c}\tan\gamma_o + \sin(\phi_n - \phi_{y.c})\cot\alpha_o}{\sin\alpha_o}\right) - \gamma_o \tag{16.95}$$

For involute hobs with $\gamma_o = 0°$, Equation (16.95) reduces to

$$\Delta\gamma_o = \arctan\left[\frac{\sin(\phi_n - \phi_{y.c})\cot\alpha_o}{\sin\alpha_o}\right] \tag{16.96}$$

For an angle ϑ of relatively small value, the approximate equality $\tan\vartheta \cong \sin\vartheta \cong \vartheta$ is valid. (Here the angle ϑ is measured in radians.) Taking into consideration the latter equality, Equation (16.95) can be simplified to

$$\Delta\gamma_o = \frac{(\phi_n - \phi_{n.y})}{\sin\phi_n \tan\alpha_o} \tag{16.97}$$

Figure 16.55 illustrates the influence of the current value of the pitch diameter $d_{y.c}$ of the hob, and of the number of starts of the hob N_c on the desired value of correction $\Delta\gamma_o$ to the rake angle γ_o. The bigger the change to the hob pitch diameter, and the bigger the number of starts of the hob, the bigger the precalculated desired value of the correction $\Delta\gamma_o$ to the rake angle γ_o.

Computations show that for the difference in pressure angle of only $(\phi_n < \phi_{y.c}) = 10'$, the required value of the correction $\Delta\gamma_o$ can reach $\Delta\gamma_o = 2.8°$. This numerical example clearly indicates the necessity and importance of implementation of the precomputed corrections to the rake angle γ_o when regrinding precision involute hobs. The bigger the hob clearance angle α_o, the smaller the precalculated value of the deviation $\Delta\gamma_o$ is necessary [110, 130].

Numerical example. Use of the disclosed approach allows for the computation of the desirable change to the parameters of the kinematic geometry of the involute hob with the following design parameters:

TABLE 16.2

Design Parameters of the Involute Hob

Module	$m = 10\,\text{mm}$
Normal profile angle	$\phi_n = 20°$
Pitch diameter	$d_c = 160\,\text{mm}$
Number of starts	$N_c = 3$
Work gear tooth number	$N_g = 100$
Tooth clearance angle	$\alpha_o = 12°$

The computations reveal that in order to maintain the constant value of the base pitch of the hob, the corresponding design parameters of the involute hob have to be changed in accordance with the actual value of wear VB_N of the hob clearance surface. (Here VB_N designates wear of the clearance surface of the hob tooth.) Assume that the wear is equal to $VB_N = 0.6\,\text{mm}$. This value of VB_N requires a reduction of the hob rake angle at $\Delta\gamma_o = 2.703°$, and an additional reduction of the center distance at $\Delta C_c = 0.621\,\text{mm}$. These changes to the parameters of the kinematic geometry of the hob ensure that the

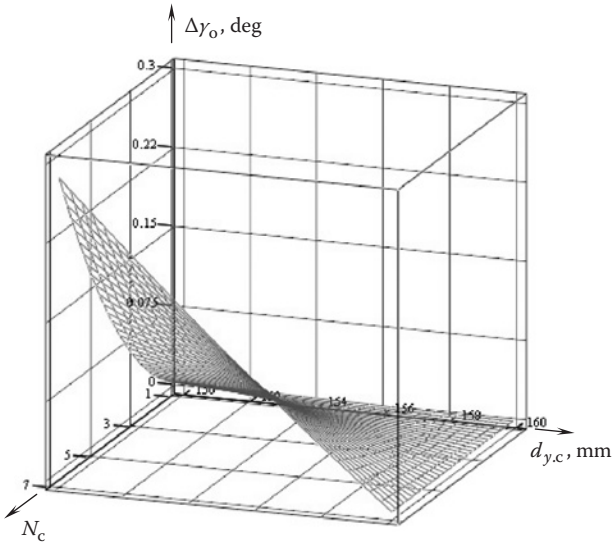

FIGURE 16.55
Impact of the current diameter $d_{y.c}$ of a hob, and of the hob number of starts N_c on the desired precalculated value of the correction $\Delta\gamma_o$ to the hob rake angle γ_o. (From Radzevich, S.P., *ASME Journal of Mechanical Design*, 129, 1076–1085, 2007. With permission.)

base pitch of the hob remains of the same value $p_{b.c} = 29.521$ mm for both the new hob as well as for the hob being reground. The above-mentioned changes to the parameters of the kinematic geometry of the involute hob will also cause the increase of the pitch helix angle of the hob at $\Delta\psi_c = 1.048'$. However, this change to ψ_c does not affect the hob accuracy.

The obtained results of the computations are plotted in Figure 16.56. Here, in Figure 16.56, the following graphs are represented: (a) the desired current value of the correction $\Delta\gamma_o$ vs. VB_N, (b) the desired increase to center distance $\Delta C_c = \Delta C_c(VB_N)$ in meshing of the hob and of the work gear ΔC_c vs. VB_N, and (c) variation $\Delta\psi_c$ of pitch helix angle ψ_c of the hob in terms of the hob wear VB_N.

Use of the method discussed above allows for the complete elimination of deviation of the base pitch of the hob. As it follows from Figure 16.56, base pitch $p_{b.c}$ of the hob does not depend on the hob wear, and thus remains of the same value $p_{b.c} = 29.521$ mm regardless of how many times the hob has been reground. The same is valid with respect to diameter of the base cylinder $d_{b.c}$ of the hob. The base cylinder diameter does not depend on the hob wear, and remains of constant value.

The derived Equation (16.88) has been used for solving numerous gear-related engineering problems in the field of accuracy of hobbed involute gears. Implementation of the obtained results of the research made it possible to develop (a) novel designs of precision involute hobs [123, 148], (b) novel methods for relieving operation of an involute hob [80, 82, 83, 84, 85, 171, 179] (c) novel designs of precision cutting tools for the finishing of involute gears, and (d) novel methods for regrinding precision cutting tools for finishing of involute gears [164 and others].

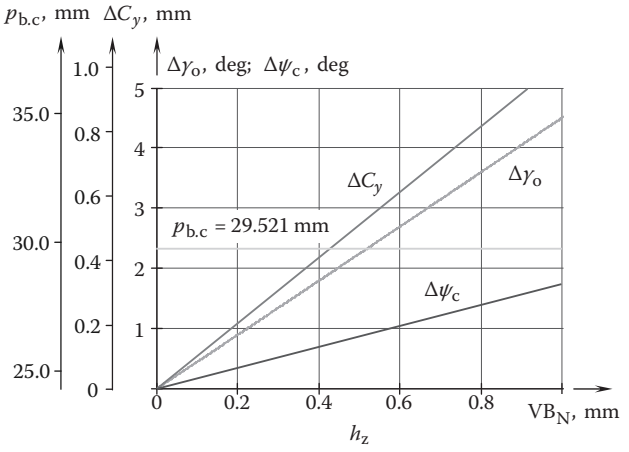

FIGURE 16.56
A diagram for corrective regrinding of the involute hob. (From Radzevich, S.P., *ASME Journal of Mechanical Design*, 129, 1076–1085, 2007. With permission.)

16.5 Design of Gear Hobs

The design of gear hobs is mainly the problem of gear manufacturing organizations and gear-tool companies who handle the design of tools for machine gears. It is common for industry engineers to consider a gear hob as a cylindrical worm converted into a cutting tool. Cutting edges are formed by "gashing" the worm with a number of slots. The slots are usually either parallel with the hob axis of rotation or *perpendicular* to the worm thread. The teeth of the hob are relieved back of the cutting edge to make an efficient cutting tool. The cutting face may be radial, or it may be given a slight "hook" to improve the cutting action.

16.5.1 Design Parameters of a Gear Hob

A closeup of typical shell-type hobs is shown in Figure 16.57. The lateral cutting edges of the hob-tooth are usually made straight. Theoretically, the hob should have a slight

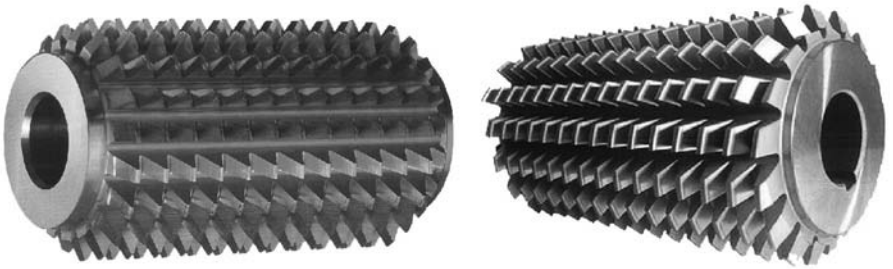

FIGURE 16.57
Typical shell-type gear hobs.

FIGURE 16.58
A hob integral with a hob arbor.

curvature in its profile to cut a true involute gear. The curvature should correspond to that of an involute helicoid. Practically, though, the curvature required is so slight that it is disregarded. Only on multiple-start hobs of coarse pitch does it become necessary to grind an involute curve.

Hobs may be made with straight bores (Figure 16.57), tapered bores, or integral with the hob arbor (Figure 16.58). The shell type of hob with a straight bore is the most commonly used type. Taper bore hobs require more wall thickness than shell hobs. Hobs for machining helical gears require a taper when the gear helix angle exceeds $\psi_g > 30°$. Even below this angle, a taper is helpful if the gear tooth number is over $N_g > 150$. Some companies prefer the taper-bore hob because of the more rigid mounting that the taper provides.

Integral-shank hobs are expensive. They are used when the hob diameter has to be so small that the hole of a big-enough diameter cannot be put through the hob. Very small hob diameters may be required when hob runout space or the gap between the helices is limited. Worm-gear hobs sometimes have to be very small to match the diameter of a small worm (Figure 16.59).

In high-volume production of gears, the use of multistart gear hobs (Figure 16.60) has proven to be effective.

In the last decades of the twentieth century, there have been several important developments in hob design. The three most important developments to the gear industry are:

- Built-up hobs. Special hob blades are attached to a body made of less costly material than the blade material.
- Special roughing hobs. The special roughing hob is a very efficient tool to remove stock, but it does not produce gear teeth intended to run together.
- Skiving hobs [28]. Hobs of this design can finish-cut fully hardened gear teeth.

FIGURE 16.59
A worm-gear hob.

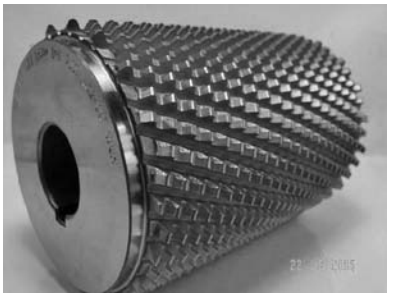

FIGURE 16.60
A multistart hob.

The built-up hobs may have blades brazed to an alloy steel body, or the blades may be mechanically attached. The blade material may be expensive high-speed steel, or it may even be a carbide material. The large sizes of built-up hobs may be rebladed. The built-up hob tends to be less expensive (in large sizes) because the body material is not nearly as costly as the blade material.

The special roughing hobs cut very efficiently. They remove large chips, and the chips tend to cut and break away in an efficient manner. The *K-Kut Rouging Hob* is a perfect example of roughing hobs of this design. The design is developed by *Barber & Colman* (USA).

The skiving hob uses a special carbide blade and a negative rake angle of $\gamma_o = 30°$ (Figure 16.61). Skiving hobs are used for finish-cutting a fully hardened gear that was finish-hobbed before hardening with a protuberance type of hob [28, 129, 133, 144]. It is a remarkable achievement, of course, to be able to finish a case-hardened gear by hobbing instead of grinding. In the case where very high accuracy and smooth finish are needed, the hard gear—finished by skiving—may be given a further honing operation of a very light final grinding. When a final grinding is used, the skiving serves to remove the bulk of the heat-treat distortion, and to remove it in a quicker and more efficient manner than grinding.

The design parameters of a shell-type hob are schematically shown in Figure 16.62. The set of the design parameters of a shell-type gear hob includes but is not limited to (a) pitch diameter d_c, (b) outer diameter $d_{o.c}$, and (c) length L. The diameter of the hob bore is designated as d_{sh}. The hob features two cylindrical surfaces of diameter d_l and length l from both

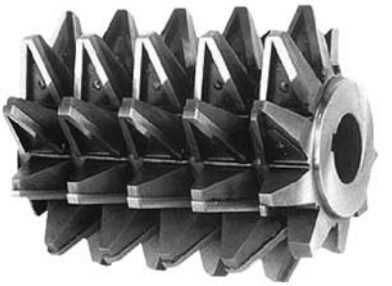

FIGURE 16.61
A skiving hob.

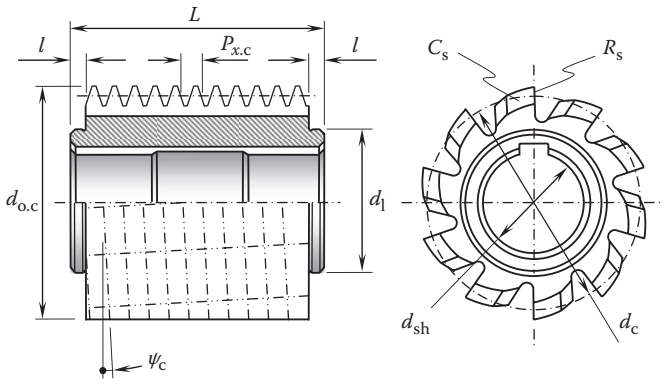

FIGURE 16.62
Design parameters of a shell-type hob.

sides of the hob. They are used for checking the hob run-out. The axial pitch of the hob threads and pitch helix angle are denoted in Figure 16.62 as $P_{x.c}$ and ψ_c correspondingly.

16.5.2 Tooth Profile of the Gear Hob

The tooth profile of the hob correlates, but is not identical to, the tooth profile of the gear to be machined. As it follows from Figure 16.63, some of the design parameters of the gear hob could be identical to the corresponding design parameters of the gear, while others could not. The feasible difference between the design parameters of the hob and the gear is strongly restricted by the equality of the base pitch of the hob $p_{b.c}$ to the base pitch of the gear $p_{b.g}$. Fulfillment of the condition $p_{b.c} = p_{b.g} = p_b$ is the mandatory requirement for machining gears properly. In most practical cases of gear hob design the profile angle $\phi_{n.c}$ of the hob tooth and axial pitch of the hob threads $P_{x.c}$ are equal to the profile angle ϕ_n of the gear tooth and the axial pitch P_x of the basic rack of the gear, respectively. When the equalities $\phi_{n.c} = \phi_n$ and $P_{x.c} = P_x$ are observed, then the hob tooth addendum a_c is equal to the gear tooth dedendum b; the hob tooth dedendum b_c is equal to the summa of the gear tooth addendum a and the hob clearance c_c (i.e., the equality $b_c = a + c_c$ is satisfied).

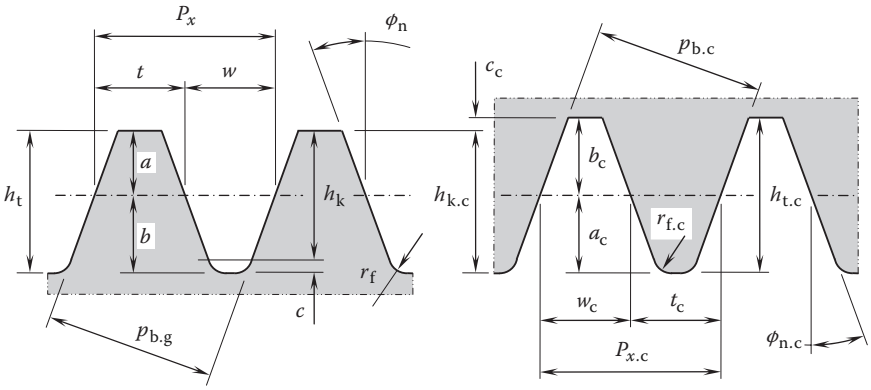

FIGURE 16.63
Correlation between design parameters of a gear hob and design parameters of a work gear.

The whole depth of the gear tooth h_t is equal to $h_t = a + b$, and the working depth of the gear tooth can be computed from the formula $h_k = h_t - c$, where c designates clearance. Similar formulae are valid for the hob tooth. The whole depth $h_{t.c}$ of the hob tooth is equal to $h_{t.c} = a + b$, while the working depth of the hob tooth can be computed from $h_{k.c} = h_t$. For the computation of the whole depth $h_{t.c}$ of the hob tooth, an equality $h_{t.c} = h_{t.c} + c_c$ is valid as well.

The normal tooth thickness t and the space width w are equal to each other ($t = w$) for gears with a standard tooth profile. The corresponding design parameters of the hob tooth correlate to the gear design parameters as follows: $t_c = w$ and $w_c = t$. The basic rack of the gear features a fillet of the radius r_f at the bottom land. The basic rack of the hob features a similar roundness $r_{f.c}$ at the top land of the tooth.

The cutting racks of an assembled gear hob (Figure 16.64) have similar design parameters of the tooth profile as that of solid hobs.

One more for reason that the hob tooth profile differs from the corresponding tooth profile of the gear to be machined is due to the necessity of backlash B_n when the machined gears are assembled in the housing. In order to provide the gear pair with backlash, the gear teeth are machined thinner, and the gear space widths are machined wider compared to the corresponding parameters specified by the basic rack (Figure 16.63).

Hobs with a modified tooth profile are used as well, with the aim of improving cutting conditions. A few examples of the modified hob tooth profiles are schematically depicted in Figure 16.65. The modification of the hob tooth profile includes but is not limited to (a) sharp corner tooth profile (Figure 16.65a), (b) chamfered corner tooth profile (Figure 16.65b), (c) rounded corner tooth profile (Figure 16.65c), (d) full round (full capped) tooth profile (Figure 16.65d), and so forth. Another reason for using hobs with a modified tooth profile is that they leave extra stock around the pitch line of the preshaved hobs. In this case a special hob with slight tooth hollow is implemented.

When designing a gear hob, much attention should be focused on increasing the cutting performance of the cutting tool. For this purpose, wear on the hob tooth should be minimized by all means.

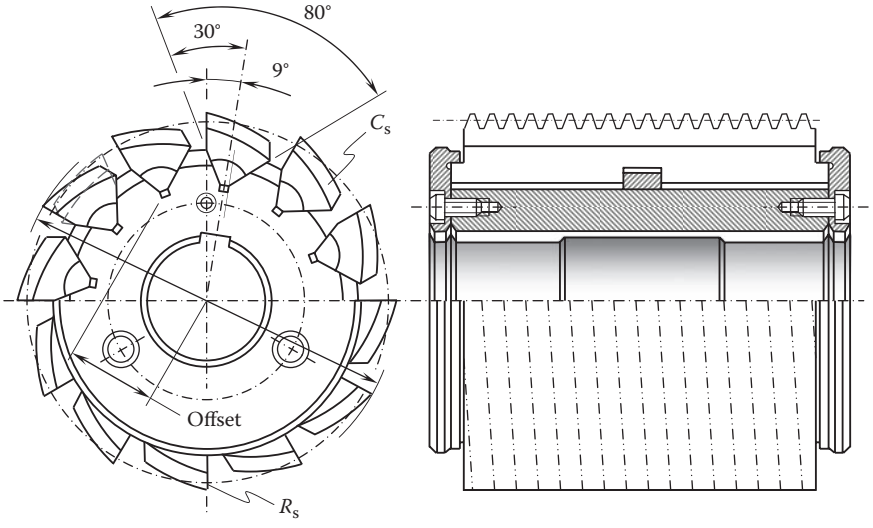

FIGURE 16.64
An assembled gear hob with inserted cutting racks.

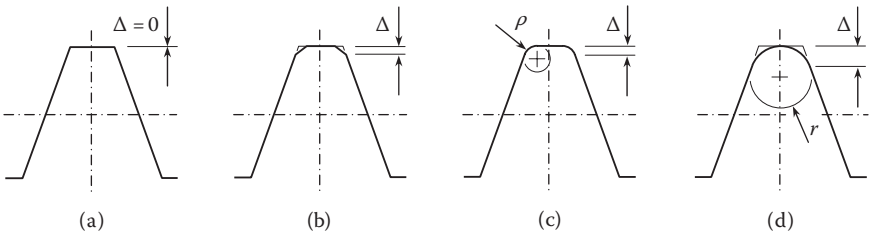

FIGURE 16.65
Possible kinds of modification of the tooth profile of a gear hob. (From Radzevich, S.P., *ASME Journal of Mechanical Design*, 128(4), 803–811, 2006. With permission.)

Figure 16.66a illustrates regular wear of the hob tooth. However, improper cutting conditions could result in intensive wear of hob teeth. The interference of chip flows from adjacent cutting edges is the major reason for catastrophic wear of the gear hob. Chip flows from the top cutting edge interact with chip flows from lateral cutting edges (Figure 16.66b). The impact of the chip flows' interference onto the cutting performance of the hob becomes greater for coarser pitch hobs. Possible types of wear of the hob tooth are summarized in Figure 16.66c. In practice, not all of the possible types of tooth wear are observed simultaneously; only one or two dominate.

In order to avoid catastrophic wear of the hob tooth (Figure 16.66d), various cutting diagrams for improving cutting performance of the hob are implemented in practice. The cutting diagrams eliminate the interference of chip flow from adjacent cutting edges. They

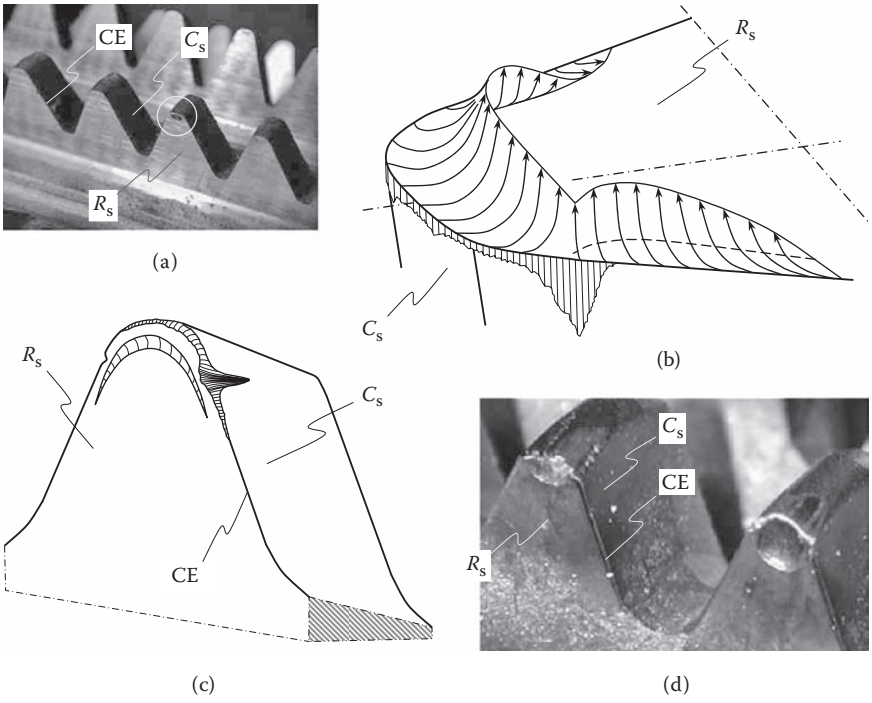

FIGURE 16.66
Kinds of wear on a hob tooth.

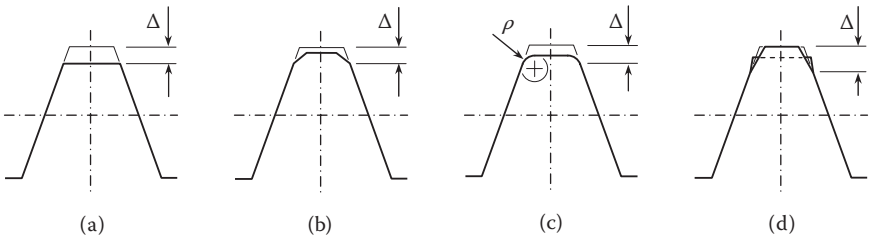

FIGURE 16.67
Kinds of tooth profile modification of involute hobs. (From Radzevich, S.P., *ASME Journal of Mechanical Design*, 128(4), 803–811, 2006. With permission.)

also result in corresponding modification of the hob tooth profile. Some practical examples of tooth modification are shown in Figure 16.67. Many patents for inventions are issued on designs of gear cutting hobs that feature improved cutting diagrams. The gear hobs in [161, 162] detail just a few of them.

The issue is investigated in depth by Medveditskov [38]. More recent results of the research are available from Medveditskov et al. [39], Radzevich [144], Smirnov [187], and others [195].

16.5.3 Precision Involute Hobs with Straight Lateral Cutting Edges

As proven in the previous chapters, for machining of high-accuracy gears, the lateral cutting edges of the hob should be within the generating surface, which is shaped in the form of an involute worm. The lateral cutting edges of the hob teeth align with the line of intersection of the generating surface T of a gear hob by the rake surface R_s of the hob tooth. These lines are a type of curved lines. For manufacturing purposes, the desirable curved lateral cutting edges of the hob teeth usually are approximated with the straight-line lateral cutting edges. Linear approximation of the lateral cutting edges of the hob tooth is the major source of gear tooth deviations. Deviations of this kind are unavoidable for gear hobs of conventional design.

The lateral portions of the generating surface of an involute hob are screw involute surfaces. A screw involute surface with any combination of the design parameters features a straight generating line that is entirely located within the surface T. This property of the screw involute surface is well known. It is often used, for example, for dressing grinding worms for grinding of precision involute gears.

A grinding worm for finishing precision involute gears (Figure 16.68) can be properly dressed if the dressing diamond reciprocates back and forth along the straight generating line. Two generating lines E_l and E_r for the opposite sides of the thread profile of the grinding worm are the straight lines through points *ab* and *de*. The generating lines E_l and E_r are entirely located within the screw involute surfaces of the corresponding side of the thread profile. At points *c* and *f*, the generating lines E_l and E_r are tangent to the base cylinder of diameter $d_{b.c}$ of the grinding worm. Using the portions *ab* and *de* of the straight generating lines E_l and E_r for dressing the grinding worm makes the dressing operation much easier to perform.

The property of a screw involute surface that makes possible the precise generation of the surface with the straight line is utilized in many designs of gear finishing tools [198–200]

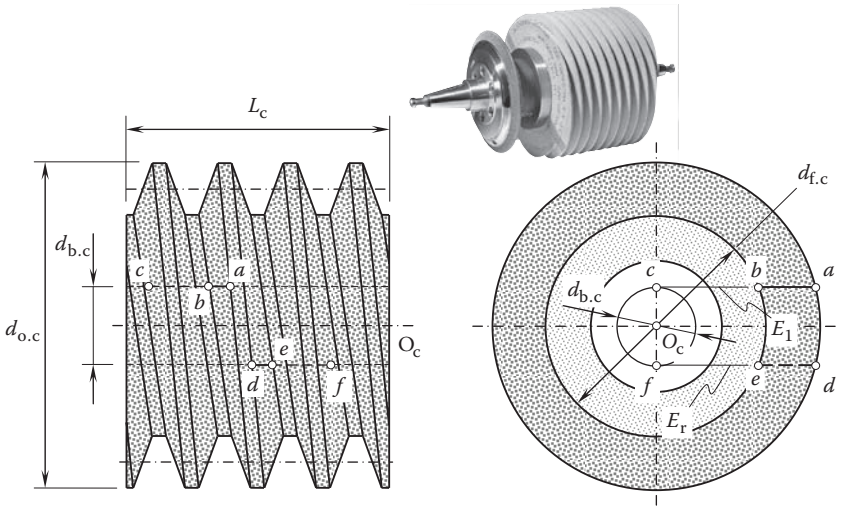

FIGURE 16.68
Straight generating lines E_r and E_l within the screw involute surfaces of the opposite sides of the thread profile of generating surface T of a grinding worm.

and so forth. It can be enhanced and implemented for improving the design of a hob for machining involute gears.

The straight line segments, similar to the straight line segments *ab* and *de*, can be used as the cutting edges of the lateral sides of the tooth profile of the precision gear hob. The possibility for increasing the accuracy of involute hobs is briefly discussed above (see Figure 16.45). However, for the manufacturer of precision involute hobs, as well as for the manufacturer of involute gears, it is much more convenient to have both lateral cutting edges of the hob tooth within a common rake plane. The possibility of designing precision involute hobs with straight lateral cutting edges is discussed below.

It is assumed below that the generating surface T of the involute hob is described analytically by Equation (15.54)

$$T: \quad \Rightarrow \quad \mathbf{r}_c(U_c, V_c) = \begin{bmatrix} 0.5d_{b.c}\sin V_c - U_c \sin\psi_{b.c}\cos V_c \\ 0.5d_{b.c}\cos V_c + U_c \sin\psi_{b.c}\sin V_c \\ p_c V_c - U_c\cos\psi_{b.c} \\ 1 \end{bmatrix} \tag{16.98}$$

For the computation of the hob base diameter $d_{b.c}$ and the hob base helix angle $\psi_{b.c}$, engineering formulae available in Appendix A can be used.

Equation (16.98) is of particular importance for developing the design of a precision gear hob with straight lateral cutting edges. This is mostly owing to the important features of the geometry of the generating surface T. It is easy to verify that for a specific value of the V_c parameter, Equation (16.98) describes a straight generating line E_r (or E_l) within the surface T. Further, the lateral cutting edge of the involute hob will be aligned with the straight-line characteristics E_r and E_l. The straight-line characteristic lines E_r and E_l serve as a vital link between the geometry of generating surface T of the involute hob and the principal features of its design.

16.5.3.1 Principal Design Parameters of the Precision Involute Hob

The proposed concept of the design of the precision involute hob with straight lateral cutting edges is based on the following considerations [98]:

(1) The lateral cutting edges of one side of the tooth profile of an involute hob are located within the corresponding screw involute surface, say for the screw involute surface T_r
(2) The lateral cutting edges of the opposite side of tooth profile of the involute hob are located within the screw involute surface of the opposite side of the thread profile, say for the screw involute surface T_l
(3) The screw involute surfaces T_r and T_l of the opposite sides of the tooth profile of the involute hob intersect each other, and the line of the intersection is a helix
(4) Two characteristics E_r and E_l pass through every point of the helix
(5) Two characteristics E_r and E_l through the common point of the helix intersect each other at that point, and thus they specify a plane through the straight lines E_r and E_l
(6) The plane through the straight lines E_r and E_l is implemented as the rake surface R_s of the cutting teeth of the precision involute hob

Steps (1) through (6) listed above allow for determining the desirable configuration of the rake surface of the precision involute hob teeth.

The DG*-based approach for the determination of the desirable configuration of the rake plane.* The *DG*-based solution to the problem of determining the desirable configuration of the rake plane R_s of the precision involute hob teeth is illustrated in Figure 16.69.

Prior to beginning to solve the problem of determining the desirable configuration of the rake plane of the hob tooth, the following design parameters of the hob are required to be known: modulus m of the hob tooth, normal profile angle ϕ_n, the setting angle of the hob ζ_c, the number of starts of the hob N_c, the hob outer diameter $d_{o.c}$, and base diameter $d_{b.c}$ of the hob.

The solution to the problem of determining the desirable configuration of the rake plane of the hob tooth is represented in the system of three planes of projections π_1, π_2, and π_3, respectively. Two auxiliary planes of projections, say π_4 and π_5, are also used. The auxiliary axis of projections π_1/π_4 makes the angle ζ_c with the axis of projections π_1/π_2. The axis of projections π_1/π_5 is parallel to the axis π_1/π_4. Use of the plane of projections π_5 allows for significant reduction of the size of Figure 16.69.

In the system of planes of projections π_1, π_2, and π_3, the hob to be designed is oriented so that the hob axis of rotation O_c is parallel to the axis π_1/π_2 (Figure 16.69).

The normal plane section of the auxiliary generating rack $\mathscr{R}_T$ is shown in the plane of projections π_4.

Consideration of images of the hob elements in the planes of projections π_4 and π_3 (that are connected to one another through the planes of projections π_1 and π_2) allows for the determination of the location of point A within the plane π_3. Two straight lines through point A_3 that are tangent from the opposite sides to the base cylinder of diameter $d_{b.c}$ of the hob represent straight lines with which the lateral cutting edges of the hob will align. The rake plane of the hob tooth is the plane through these two straight lines. Conventional methods developed in descriptive geometry are used for the construction of the rest of the projections of these two straight lines that initially are constructed in the plane of projections π_3.

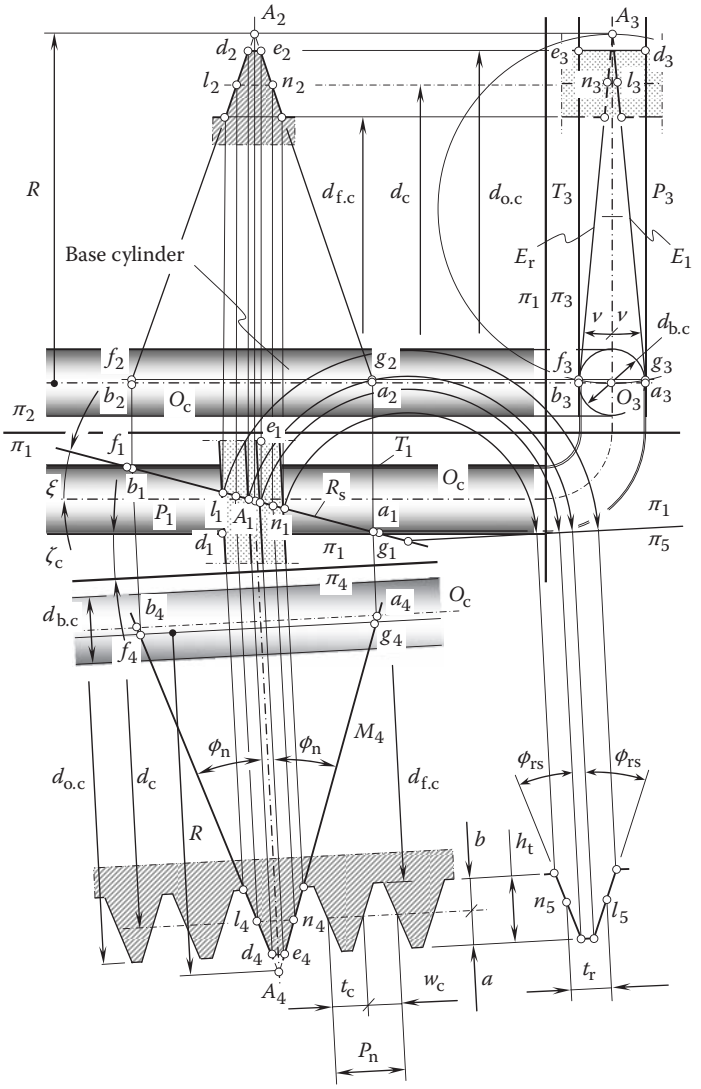

FIGURE 16.69
An example of implementation of the *DG*-based approach for determining the desirable configuration of the rake plane R_s of precision involute hob teeth. (From Radzevich, S.P., *ASME Journal of Mechanical Design*, 129, 334–345, 2007. With permission.)

Angle ξ that the rake plane makes with the axis of rotation O_c of the hob is constructed in the plane of projections π_1. A profile of the hob tooth within the rake plane is constructed in the plane of projections π_5.

Analytical determination of the desirable configuration of the rake plane. Figure 16.69 provides clear understanding of geometry of the precision involute gear hob with straight lateral cutting edges. The derived *DG*-based solution to the problem is helpful for deriving the corresponding formulae for the computation of the design parameters of the gear hob.

The lateral surfaces of the auxiliary rack $\mathscr{R}_T$ tooth intersect each other. The line of the intersection is the straight line through point A (Figure 16.70). This straight line is at a distance R from the axis of rotation O_c of the hob. For the distance R Figure 16.71 yields

$$R = 0.5(d_c + t_c \cot \phi_n) \tag{16.99}$$

The angle ϕ_{rs} between the lateral cutting edges is measured within the rake plane of the hob tooth. Prior to deriving an equation for the computation of the angle ϕ_{rs}, it is convenient to derive an equation for the computation of the projection ν of the angle ϕ_{rs} onto the coordinate plane X_cY_c.

Projections of the lateral cutting edges of the involute hob onto the coordinate plane X_cY_c make a certain angle ν. The actual value of the angle ν can be computed from the formula

$$\nu = \tan^{-1}\left(\frac{d_{b.c}}{\sqrt{4R^2 - d_{b.c}^2}}\right) \tag{16.100}$$

Then, consider three unit vectors **a**, **b**, and **c** (see Figures 16.70 and 16.71). The vector **a** is along the line of intersection of the tooth flanks of the auxiliary generating rack $\mathscr{R}_T$. The vector **b** is aligned with the lateral cutting edge of the involute hob. The vector **c** is along the tooth profile of the auxiliary generating rack $\mathscr{R}_T$.

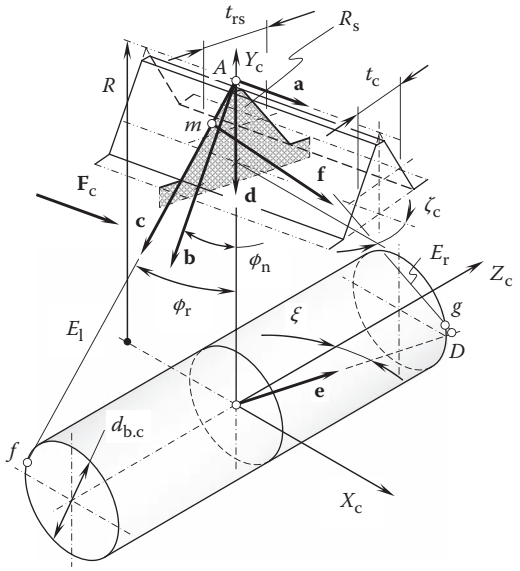

FIGURE 16.70
The desirable orientation of the rake plane of a precision involute hob. (From Radzevich, S.P., *ASME Journal of Mechanical Design*, 129, 334–345, 2007. With permission.)

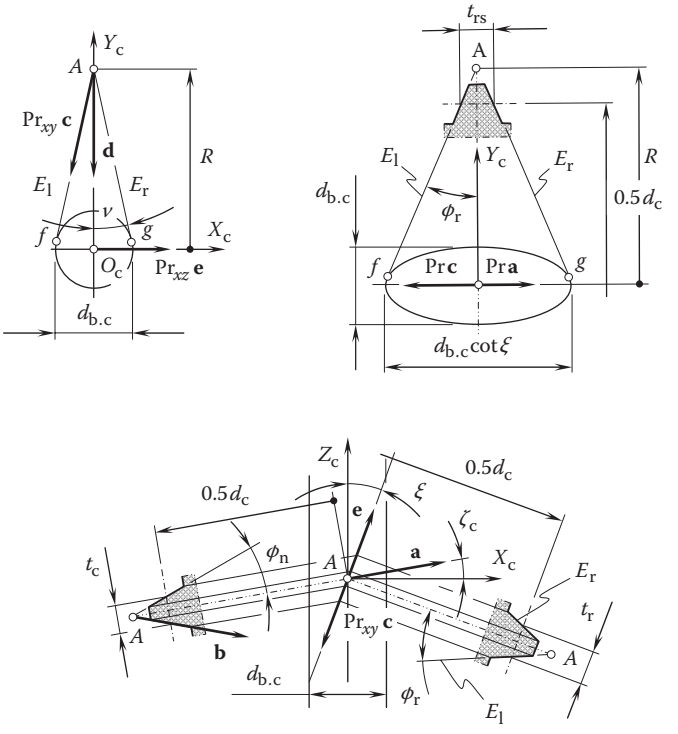

FIGURE 16.71
The employed characteristic vectors. (From Radzevich, S.P., *ASME Journal of Mechanical Design*, 129, 334–345, 2007. With permission.)

The vectors **a**, **b**, and **c** allow for analytical representation in the form

$$\mathbf{a} = \mathbf{i} \cdot \cos\zeta_c + \mathbf{k} \cdot \sin\zeta_c \tag{16.101}$$

$$\mathbf{b} = \mathbf{i} \cdot \sin\phi_n \sin\zeta_c - \mathbf{j} \cdot \cos\phi_n - \mathbf{k} \cdot \sin\phi_n \cos\zeta_c \tag{16.102}$$

$$\mathbf{c} = -\mathbf{i} \cdot \cos\phi_{rs} \tan\nu - \mathbf{j} \cdot \cos\phi_{rs} - \mathbf{k} \cdot \sin\phi_{rs} \cos\xi \tag{16.103}$$

where ζ_c denotes the setting angle of the precision involute hob.

The actual value of the setting angle ζ_c can be chosen by a designer of the gear hob. Usually, it is recommended to assign the actual value of the setting angle ζ_c equal to the pitch helix angle ψ_c of the involute hob. In order to satisfy the equality $\zeta_c = \psi_c$ (this condition is the best possible), the actual value of the setting angle of the hob is required to be computed from the equation [54, 129]

$$\zeta_c = \tan^{-1}\left(\frac{mN_c}{\sqrt{(d_{o.c} - 2 \cdot 1.25m - \Delta d_{o.c})^2 - m^2N_c^2}}\right) \tag{16.104}$$

where $\Delta d_{o.c}$ designates the reduction of the outer diameter $d_{o.c}$ of the hob due to resharpening of the worn gear hob (Figure 16.47).

As the vectors **a**, **b**, and **c** are located within the common lateral tooth flank of the auxiliary rack $\mathscr{R}_T$, therefore the triple scalar product of the vectors is identical to zero, and thus, the following identity $\mathbf{a} \times \mathbf{b} \cdot \mathbf{c} \equiv 0$ is observed. The last expression yields a determinant

$$\mathbf{a} \times \mathbf{b} \cdot \mathbf{c} = \begin{vmatrix} \cos\zeta_c & 0 & \sin\zeta_c \\ \sin\phi_n \sin\zeta_c & -\cos\phi_n & -\sin\phi_n \cos\zeta_c \\ -\cos\phi_{rs} \tan\nu & -\cos\phi_{rs} & -\sin\phi_{rs} \cos\xi \end{vmatrix} \equiv 0 \tag{16.105}$$

Equation (16.105) casts into the equation of two unknowns, namely ϕ_{rs} and ξ.

The rake plane R_s of the involute hob is inclined with respect to the hob axis O_c at a certain angle ξ. In order to determine the required value of the angle ξ, two more unit vectors, **d** and **e**, are constructed. The vector **d** is along the Y_c axis. The vector **e** is located within the rake plane R_s and is perpendicular to the axis Y_c (Figure 16.71).

For the vectors **d** and **e**, the following expressions

$$\mathbf{d} = -\mathbf{j} \tag{16.106}$$

$$\mathbf{e} = \mathbf{i} \cdot \sin\xi + \mathbf{k} \cdot \cos\xi \tag{16.107}$$

are valid.

As the vectors **c**, **d**, and **e** are located within the rake plane R_s of the hob tooth, therefore the triple scalar product of the vectors is identical to zero, and thus, the following identity $\mathbf{c} \times \mathbf{d} \cdot \mathbf{e} \equiv 0$ is observed. This yields the determinant

$$\mathbf{c} \times \mathbf{d} \cdot \mathbf{e} = \begin{vmatrix} -\cos\phi_{rs} \tan\nu & -\cos\phi_{rs} & -\sin\phi_r \cos\xi \\ 0 & -1 & 0 \\ \sin\xi & 0 & \cos\xi \end{vmatrix} \equiv 0 \tag{16.108}$$

Equation (16.108) casts into the equation of two unknowns, namely ϕ_{rs} and ξ.

Further, consider the set of two equations, say of Equations (16.105) and (16.108) of the two unknowns ϕ_{rs} and ξ. The solution to the set of the above equations can be represented in the form

$$\xi = \tan^{-1}\left(\frac{\cos\zeta_c \tan\nu}{\tan\phi_n + \sin\zeta_c \tan\nu}\right) \tag{16.109}$$

$$\phi_{rs} = \tan^{-1}\left(\frac{\tan\nu}{\sin\xi}\right) \tag{16.110}$$

The setting angle ζ_c specifies inclination of the axis of rotation O_c of the involute hob with respect to the auxiliary generating rack $\mathscr{R}_T$. It is necessary to point out here that the setting angle ζ_c is a design parameter of the gear hob, and it is not a parameter of the gear hobbing operation.

Equations (16.109) and (16.110) return the required values of the angles ϕ_{rs} and ξ. These angles are indicated in the involute hob blueprint.

The precision involute hob of the discussed design [98] (a) features straight lateral cutting edges, and (b) is free of the major source of the tooth profile deviations. The concept of this design is enhanced to other designs of precision hobs for the machining of involute gears: two more modifications of the gear hob design [99, 100] are developed as well. More details on the concept are available from [92–94, 96] and others.

Example of the computation. A single-start involute hob with module m = 10 mm, outer diameter $d_{o.c}$ = 180 mm, and normal pressure angle $\phi_n = 20°$ is used as an example for the computation of the design parameters of the precision involute hob with straight lateral cutting edges.

The results of the computation are collected in Table 16.3.

For accurate computation of the design parameters of the precision involute hob pitch diameter, neither the new hob nor the completely worn hob can be entered into the

TABLE 16.3

Results of the Computation of the Design Parameters of the Involute Hob with Straight Lateral Cutting Edges

Design Parameter of the Hob	Equation	Computation	Result of the Computation
Normal pitch	$P_n = \pi m$	$P_n = \pi \cdot 10$	P_n = 31.4159 mm
Setting angle of the hob	16.104	$\zeta_c = \tan^{-1}\left(\frac{10 \cdot 1}{\sqrt{(180 - 2 \cdot 1.25 \cdot 10 - 3)^2 - 10^2 \cdot 1^2}}\right)$	ζ_c = 3.772 deg
The hob base diameter	15.58	$d_{b.c} = \frac{10 \cdot 1 \cdot \cos 20°}{\sqrt{1 - \cos^2 20° \cos^2 3.772°}}$	$d_{b.c}$ = 27.037 mm
The hob base helix angle	15.62	$\psi_{b.c} = \cos^{-1}(\cos 20° \cos 3.772°)$	$\psi_{b.c}$ = 20.338 deg
Axial pitch	$P_x = \frac{P_n}{\cos \zeta_c}$	$P_x = \frac{31.4159}{\cos 3.772°}$	P_x = 31.484 mm
Pitch diameter	$d_c = d_{o.c} - 2 \cdot 1.25m$	$d_c = 180 - 2 \cdot 1.25 \cdot 10$	d_c = 155 mm
The hob pitch helix angle	$\tan \psi_c = \frac{P_x N_c}{\pi d_c}$	$\psi_c = \tan^{-1}\left(\frac{31.484 \cdot 1}{\pi \cdot 155}\right)$	ψ_c = 3.699 deg
Tooth thickness	$t_c = \frac{P_n}{2}$	$t_c = \frac{31.4159}{2}$	t_c = 15.708 mm
The auxiliary parameter R	16.99	$R = 0.5(155 + 15.708 \cot 20°)$	R = 99.079 mm
Transverse projection of half of the angle that makes lateral cutting edges	16.100	$\nu = \tan^{-1}\left(\frac{27.037}{\sqrt{4 \cdot 99.709 - 27.037^2}}\right)$	ν = 7.842 deg
The angle that makes the rake face and the gear axis	16.109	$\xi = \tan^{-1}\left(\frac{\cos 3.772° \tan 7.842°}{\tan 20° + \sin 3.772° \tan 7.842°}\right)$	ξ = 20.225 deg
Rake face pressure angle	16.110	$\phi_{rs} = \tan^{-1}\left(\frac{\tan 7.842°}{\sin 20.225°}\right)$	ϕ_{rs} = 21.723 deg

equations. For accurate computations, it is recommended to use the pitch diameter of the partly worn hob that correlates with the outer diameter of the cutting tool. The outer diameter of the new gear hob is equal to $d_{o.c}$ (Figure 16.47), while the outer diameter of the completely worn hob could be computed from the equation $(d_{o.c} - \Delta d_{o.c})$. For the computation of the reduction $\Delta d_{o.c}$ of the outer diameter $d_{o.c}$, the following approximate equation

$$\Delta d_{o.c} \cong 2L \tan \alpha_o = 5.585 \cdot \frac{\tan \alpha_o}{n_c} \tag{16.111}$$

can be used. Here it is designated that L is a distance between two neighboring hob teeth that is measured along the helix on the outer cylinder of the hob (Figure 16.47), α_o is the clearance angle at the top cutting edge of the hob tooth, and n_c is the effective number of the hob teeth.

For involute hobs featuring straight slots, n_c is always an integer number, and it is always equal to the actual hob tooth number $n_c^{(a)}$, which is usually in the range of $n_c^{(a)} = 8\sim16$. This immediately yields a formula

$$\cup L = \frac{\pi d_{o.c}}{n_c^{(a)}} \tag{16.112}$$

for the computation of the distance L.

For hobs with helical slots, the effective hob teeth number n_c is always a number with fractions. Moreover, the actual value of n_c depends on the hand of helix of the slots. This is due to the fact that in the last case the distance L is computed from equation in [129, 130, 138] and others:

$$\cup L = \frac{\pi d_{o.c}}{n_c^{(a)}} + P_{x.c} N_c \cos \lambda_{rs} \sin \lambda_{rs} \tag{16.113}$$

where $d_{o.c}$ is the outside diameter of the hob, $P_{x.c}$ is the axial pitch of the hob, N_c is the hob starts number, and λ_{rs} is the lead angle of the hob rake surface R_s (λ_{rs} is the signed value).

Equation (16.111) is a type of approximation that returns reasonably accurate results of the computation.

It is important to point out here the direction at which the angle ξ of the rake plane orientation is measured. The angle ξ is measured in the direction of positive pitch helix ψ_c of the precision involute hob. The direction to measure the angle ξ is the same as the direction to measure the angle ψ_c, thus the angle ξ affects the cutting edge geometry of the lateral cutting edges of the precision involute hob.

Figure 16.72 illustrates a closeup of the precision involute hob with straight lateral cutting edges. For the reader's convenience, designation of most design parameters in Figure 16.72 are identical to those in Figures 16.70 and 16.71.

Analysis of the impact of the design parameters of the precision involute hob onto the value of the angle ξ of the orientation of the rake surface reveals that a reduction of the angle ξ is observed when

(1) The number of starts N_c of the hob is smaller, as illustrated in Figure 16.73

(2) The profile angle ϕ_n of the hob tooth is greater, as shown in Figure 16.74

(3) The setting angle of the hob ζ_c is greater (Figure 16.75)

(4) The hob pitch diameter d_c is greater (Figures 16.73 through 16.75)

The rake planes of the involute hob teeth (Figure 16.72) are not coplanar to each other. Figure 16.76a illustrates that the rake planes R_s of each of the two neighboring teeth make a step. The precision involute hob can be designed so that the rake planes R_s of all the teeth in each row in the axial direction of the hob could be located in a common plane, as shown in Figure 16.76b. Such an arrangement of the rake planes provides an insight of a practical type of approximation of the rake planes of the hob teeth within a common row.

An approximation of the rake plane of the involute hob by a surface that features convenient geometry is possible For example, the set of the rake planes R_s can be approximated by a screw surface of the same hand as the hand of the generating surface T of the involute hob. Under such a scenario, the rake surface is shaped in the form of the Archimedean screw surface. The helix angle ψ_{rs} of the screw rake surface R_s is equal to the angle ξ, and thus the equality $\psi_{rs} = \xi$ is observed.

The involute hob with the approximated rake surface features a zero rake angle at the top cutting edge ($\gamma_o = 0°$). The inclination angle λ_o of the top cutting edge is approximately equal to the angle ξ.

16.5.3.2 A Method for Resharpening the Precision Involute Hob

After an involute hob becomes worn, either the rake surface R_s or the clearance surface C_s of the hob teeth could be reground in order to restore the cutting performance of the hob. For the purposes of resharpening of the worn precision involute hob, a method [78] of the hob regrinding can be employed. A machine tool of conventional design for relief grinding of the cutting tools can be used for the purpose of grinding the clearance surfaces of the worn involute hob.

In the method shown in Figure 16.77, the hob rotates about its axis of rotation O_c with steady rotation ω_c [78]. The clearance surface of the hob tooth is faced toward the direction

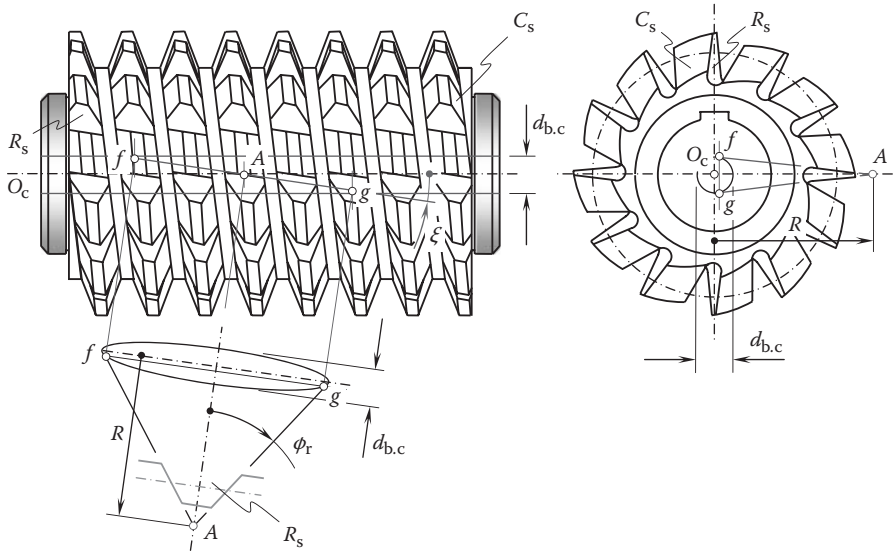

FIGURE 16.72
A close-up view of the precision involute hob with straight lateral cutting edges. (From Radzevich, S.P., USSR Patent 990445, Int. Cl. B24b 3/12, October 8, 1981.)

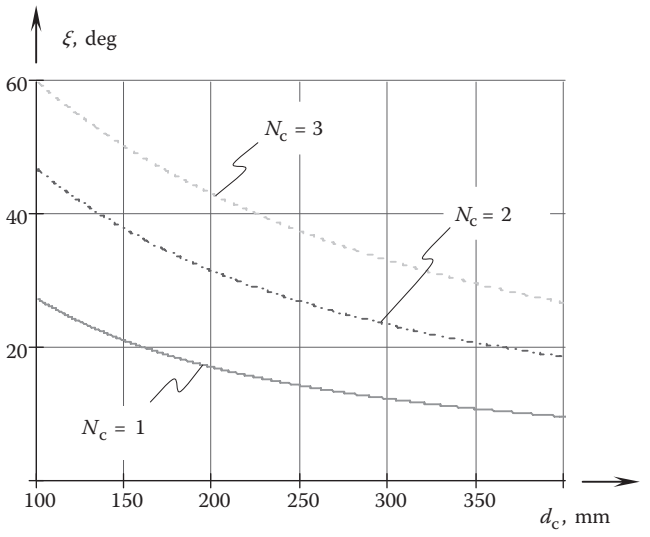

FIGURE 16.73
Impact of the number of starts N_c of an involute hob on the actual orientation of the rake plane specified by the angle ξ ($m = 10$ mm, $\phi_n = 20°$, $\zeta_c = 3°$, $n_h = 10$, $\alpha_o = 12°$). (From Radzevich, S.P., *ASME Journal of Mechanical Design*, 129, 334–345, 2007. With permission.)

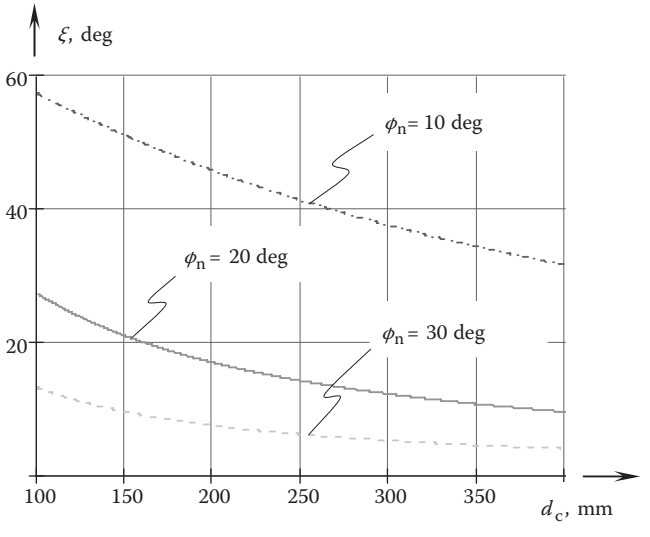

FIGURE 16.74
Impact of the normal profile angle ϕ_n of an involute hob on the actual orientation of the rake plane specified by the angle ξ ($m = 10$ mm, $N_c = 1$, $\zeta_c = 3°$, $n_c = 10$, $\alpha_o = 12°$). (From Radzevich, S.P., *ASME Journal of Mechanical Design*, 129, 334–345, 2007. With permission.)

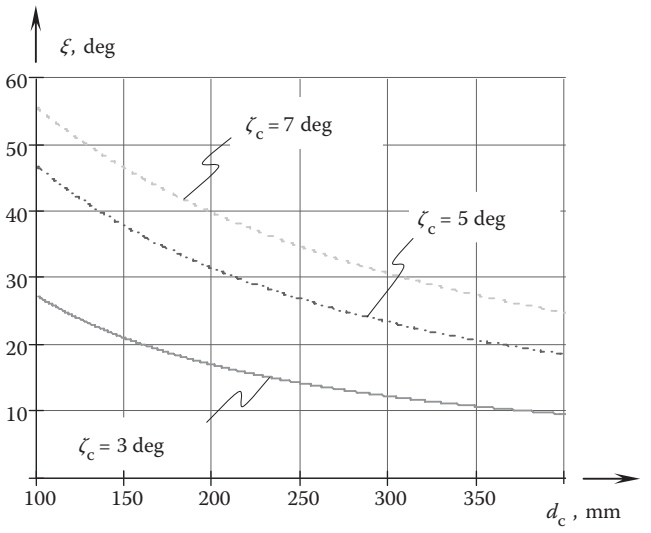

FIGURE 16.75
Impact of the setting angle ζ_c of a hob onto the actual orientation of the rake plane specified by the angle ξ (m = 10 mm, $\phi_n = 20°$, $N_c = 1$, $n_c = 10$, $\alpha_o = 12°$). (From Radzevich, S.P., *ASME Journal of Mechanical Design*, 129, 334–345, 2007. With permission.)

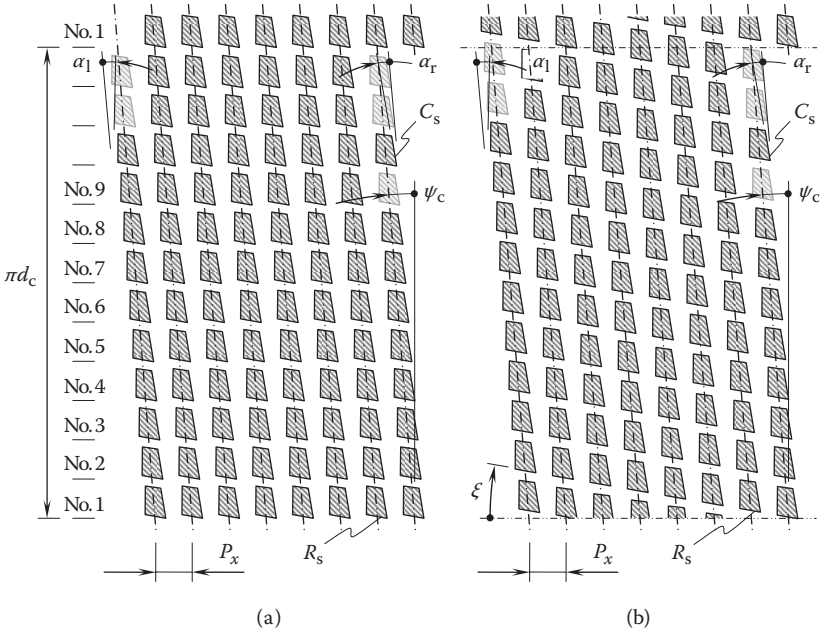

FIGURE 16.76
The arrangement of rake planes R_s of a precision involute hob with straight lateral cutting edges so that they are located within a common plane. (From Radzevich, S.P., USSR Patent 990445, Int. Cl. B24b 3/12, October 8, 1981.)

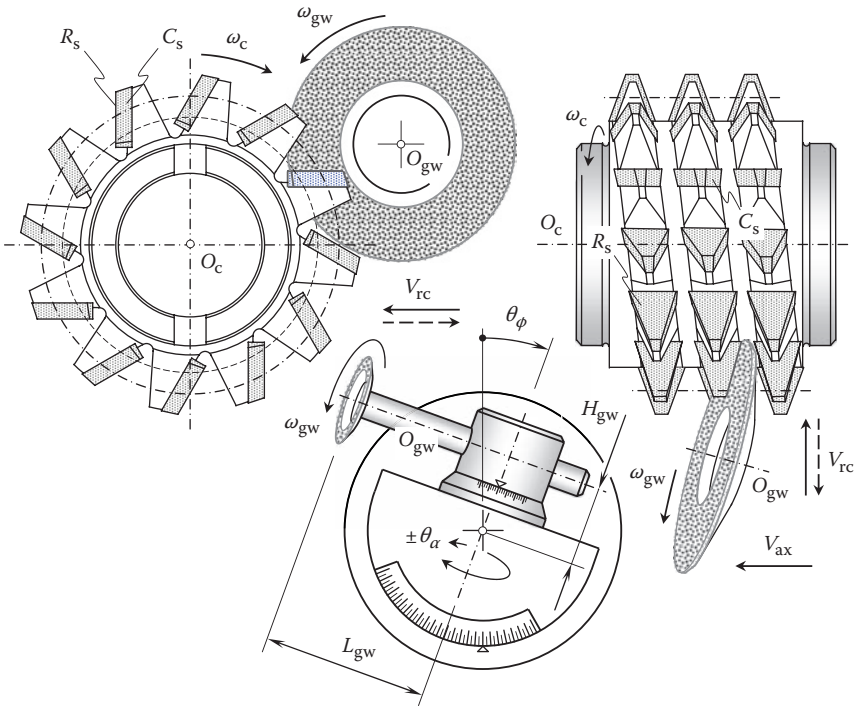

FIGURE 16.77
Method for resharpening built-up involute hobs. (From Radzevich, S.P., USSR Patent 1087309, Int. Cl. B24b 3/12, April 23, 1980.)

of the rotation ω_c. A dish-type grinding wheel is used in the hob resharpening operation. The grinding wheel rotates about its axis of rotation O_{gw}. The rotation of the grinding wheel is denoted as ω_{gw}. Two angles θ_ϕ and θ_α together with two linear displacements L_{gw} and H_{gw} are the main setup parameters of the grinding wheel. The angles θ_ϕ and θ_α depend mainly on the normal profile angle ϕ_n of the hob and the clearance angle α_l at the lateral cutting edge of the hob tooth. The displacement H_{gw} is specified by the design of the machine tool. Ultimately, the displacement L_{gw} is a relatively free parameter, which makes possible the optimization of the hob regrinding operation. The setup parameters θ_ϕ, θ_α, and L_{gw} can be expressed in terms of the design parameters of the involute hob to be reground.

When resharpening an involute hob, the grinding wheel reciprocates toward the hob axis and in the opposite direction. The grinding wheel slowly approaches the hob. At a certain instant of time the grinding plane of the grinding wheel touches the clearance surface of the hob tooth, and after that it immediately moves outward toward the hob. The speed of the last motion is significantly higher then the speed of approach of the grinding wheel toward the hob. Simultaneously with the rotation ω_c of the hob, the grinding wheel travels V_{ax} in an axial direction of the hob.

The clearance surfaces C_s of the hob teeth after resharpening are shaped in the form of planes. The use of this method makes possible increased clearance angles α_l at the lateral cutting edges of the hob. Normally, the method allows the clearance angles up to $\alpha_l = 6 \ldots 8°$ against $\alpha_l = 2 \ldots 4°$ for the relief-ground hobs. The increased clearance angle α_l results in a significantly higher cutting performance of the involute hob.

Initially the method [78] was developed [130] for the purpose of resharpening of semi-finishing and finishing built-up *Azumi* hobs (Japan). However, the method can also be used for resharpening of the precision involute hobs.

16.5.3.3 An Involute Hob for Machining Gear with a Modified Tooth Profile

The concept of the precision involute hob with straight lateral cutting edges can be extended to a hob design for machining gears with a modified tooth profile. Such a possibility becomes clear from the analysis of Figure 16.78.

The straight lateral cutting edge of the precision involute hob aligns with the straight line E_c, which is located within the generating surface T of the hob. In searching for a possible approach to design a hob with a modified tooth profile, it sounds promising to turn attention to the possibility of angular displacement of the characteristic E_c (and the lateral cutting edge of the gear hob as well) through a certain angle φ about the point K on the pitch line of the auxiliary generating rack $\mathscr{R}_T$ of the hob. Due to the angular displacement of the straight line E_c, the lateral profile of the tooth of the auxiliary rack $\mathscr{R}_T^m$ becomes curved.* If the angular displacement φ is determined properly, then a gear hob for the machining gears with a modified tooth profile can be designed [100]. A design of the gear hob is proposed for this purpose.

For the derivation of a formula for the computation of the required value of the angular displacement φ, the use of Euler's formula

$$R_T(\varphi) = \left(\frac{\cos^2 \varphi}{R_{1.T}} + \frac{\sin^2 \varphi}{R_{2.T}} \right)^{-1} \tag{16.114}$$

is helpful.

Here, the principal radii of curvature $R_{1.T}$ and $R_{2.T}$ of the nonmodified generating surface T are equal to [138, 158]

$$R_{1.T} = \frac{\sqrt{d_c^2 - d_{b.c}^2}\, \cos \psi_{b.c}}{2 \sin^2 \psi_{b.c}} \quad \text{and} \quad R_{2.T} \to \infty \tag{16.115}$$

The approximate equation

$$\varphi \cong \cos^{-1} \sqrt{\frac{R_{1.T}}{R_T}} \tag{16.116}$$

for the computation of the desired value of the angular displacement φ immediately follows from the consideration of Equation (16.114) together with Equation (16.115).

* In order to clarify the transition from the auxiliary rack $\mathscr{R}_T$ with a straight-line tooth profile to the auxiliary rack $\mathscr{R}_T^m$ with a curved tooth profile, the following analogy can be considered. When a straight-line rotates about an axis that is parallel to the line, a surface of circular cylinder is generated. Then consider the straight line that crosses the axis of rotation. Consecutive positions of the straight line in the second case form a surface of a single-sheet hyperboloid of revolution.

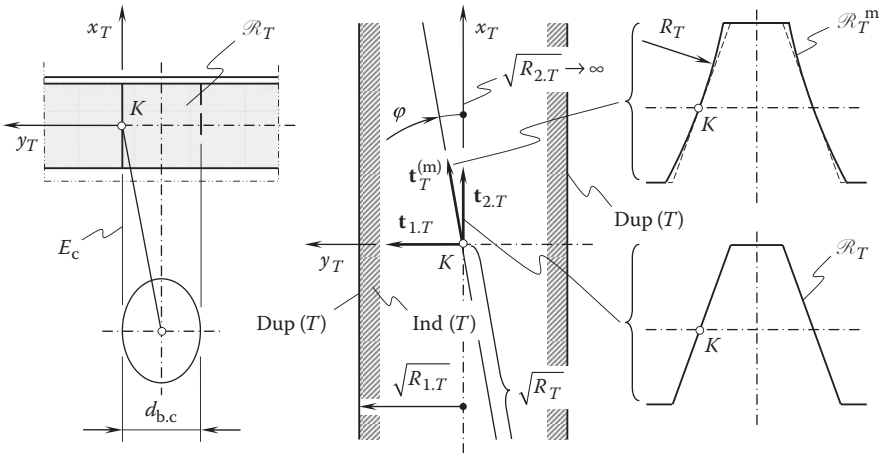

FIGURE 16.78
The design concept of an involute hob for machining gears with a modified tooth profile (RU Pat. No. 2040376). (From Radzevich, S.P., *ASME Journal of Mechanical Design*, 129, 334–345, 2007. With permission.)

Equation (16.116) is approximate because all points within the modified generating surface of the hob are of the hyperbolic type rather than the parabolic type, as observed for all points within the generating surface of the nonmodified hob.

To illustrate a feasibility of modification of the hob tooth profile, using the characteristic curves, namely of the $\mathscr{An}_R(T)$-indicatrix of the first kind and the $\mathscr{An}_k(T)$-indicatrix of the second kind, is helpful [95, 142].

The position vector $\mathbf{r}_{iR}$ of a point on the $\mathscr{An}_R(T)$-indicatrix of the first kind is given by the matrix equation

$$\mathscr{An}_R(T) \quad \Rightarrow \quad \mathbf{r}_{iR}(\varphi) = \begin{bmatrix} R_T(\varphi)\cos\varphi \\ R_T(\varphi)\sin\varphi \\ 0 \\ 1 \end{bmatrix} \tag{16.117}$$

This characteristic curve illustrates the alteration of normal radii of curvature $R_T(\varphi)$ of the generating surface T of the gear hob in differential vicinity of the point K (Figure 16.79).

For position vector $\mathbf{r}_{ik}$ of a point on the $\mathscr{An}_k(T)$-indicatrix of the second kind, the following matrix equation

$$\mathscr{An}_k(T) \quad \Rightarrow \quad \mathbf{r}_{ik}(\varphi) = \begin{bmatrix} k_T(\varphi)\cos\varphi \\ k_T(\varphi)\sin\varphi \\ 0 \\ 1 \end{bmatrix} \tag{16.118}$$

is known from [95, 138].

This characteristic curve illustrates the alteration of normal curvature $k_T(\varphi)$ within the differential vicinity of the point K of the generating surface T of the hob (Figure 16.79).

Figure 16.79 reveals that any desirable value of the hob tooth modification (R_T) is feasible [100].

Another way to illustrate the feasibility of the modification of the involute gear tooth profile with the help of the angular displacement of the lateral cutting edges is based on the following consideration. The well-known equation $R_T = \Phi_{1.T}/\Phi_{2.T}$ for the computation of radii of normal curvature can be rewritten in expended form. Let us designate the ratio dV_T/dU_T as $\upsilon = dV_T/dU_T$. Then, the expressions for $R_T(\varphi)$ and $k_T(\varphi)$ could be replaced with the similar expressions $R_T(\upsilon)$ and $k_T(\upsilon)$ in terms of the υ parameter

$$R_T(\upsilon) = \frac{E_c + 2F_c\upsilon + G_c\upsilon^2}{L_c + 2M_c\upsilon + N_c\upsilon^2} \quad \text{and/or} \quad k_T(\upsilon) = R_T^{-1}(\upsilon) \tag{16.119}$$

The extreme values $R_{1.T}$ and $R_{2.T}$, as well as $k_{1.T}$ and $k_{2.T}$, occur at roots υ_1 and υ_2 of

$$\det\begin{bmatrix} \upsilon^2 & -\upsilon & 1 \\ E_c & F_c & G_c \\ L_c & M_c & N_c \end{bmatrix} = 0 \tag{16.120}$$

where E_c, F_c, and G_c designate Gaussian coefficients of the first fundamental form $\Phi_{1.T}$ of the generating surface T of the involute hob (see Chapter 1).

Gaussian coefficients of the second fundamental form $\Phi_{2.T}$ of the generating surface T of the involute hob are designated as L_c, M_c, and N_c (see Chapter 1).

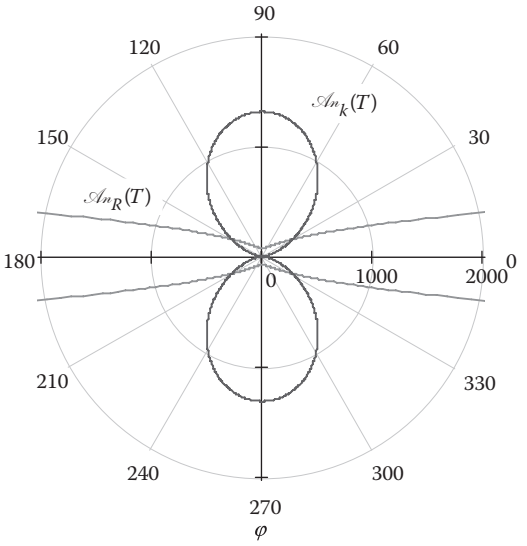

FIGURE 16.79
Alteration of the normal curvature $k_T = k_T(\varphi)$ and normal radii of curvature $R_T = R_T(\varphi)$ in the differential vicinity of a point on the generating surface T of an involute hob. (From Radzevich, S.P., *ASME Journal of Mechanical Design*, 129, 334–345, 2007. With permission.)

Both the characteristic curves $R_T = R_T(\upsilon)$ and $k_T = k_T(\upsilon)$ are a kind of graphical interpretation of the alteration of the radii of normal curvature as well as normal curvatures themselves in a differential vicinity of a point within the generating surface of the involute hob (Figure 16.80). They perfectly correlate with the $\mathscr{A}_{n_R}(T)$-indicatrix of the first kind and the $\mathscr{A}_{n_k}(T)$-indicatrix of the second kind (Figure 16.79) of the generating surface T.

Computation of the design parameters of the involute hob with a modified tooth profile is similar to that of the hob with a nonmodified tooth profile. The major difference occurs in the computation of the parameter R_{m} and the distance d_{m}. The parameter R_{m} for the hob with a modified tooth profile differs from the corresponding parameter R [see Equation (16.99)], and the distance d_{m} is not equal to the base diameter $d_{\mathrm{b.c}}$ of the hob.

The desirable value of R_{m} is required to be expressed in terms of modification R_T of the hob tooth. For this purpose, it is convenient to solve an elementary geometrical problem, namely to determine coordinates of a certain point S of the intersection of the circular arc of the radius R_T (Figure 16.78) with the centerline of the modified tooth profile. (Point S is not shown in Figure 16.78.) Then, the parameter R_{m} can be determined as a distance of point S to the axis of rotation O_{c} of the hob. Following the routine outlined above, the equation

$$R_{\mathrm{m}} = \frac{R_T \sin\phi_{\mathrm{n}} - t_{\mathrm{r}} + 0.5d_{\mathrm{c}} - \sqrt{R_T^2 \sin^2\phi_{\mathrm{n}} - R_T t_{\mathrm{r}} \cos\phi_{\mathrm{n}} - t_{\mathrm{r}}^2}}{4R_T t_{\mathrm{r}} \cos\phi_{\mathrm{n}} + t_{\mathrm{r}}^2} \tag{16.121}$$

for the computation of the parameter R_{m} is derived.

The corresponding equation for the distance d_{m} can be represented in the form

$$d_{\mathrm{m}} = d_{\mathrm{c}} \cdot \frac{\sin(\theta - \varphi)}{\cos\theta \cos\zeta_{\mathrm{c}}} \tag{16.122}$$

where for the computation of the angle θ the earlier derived formula

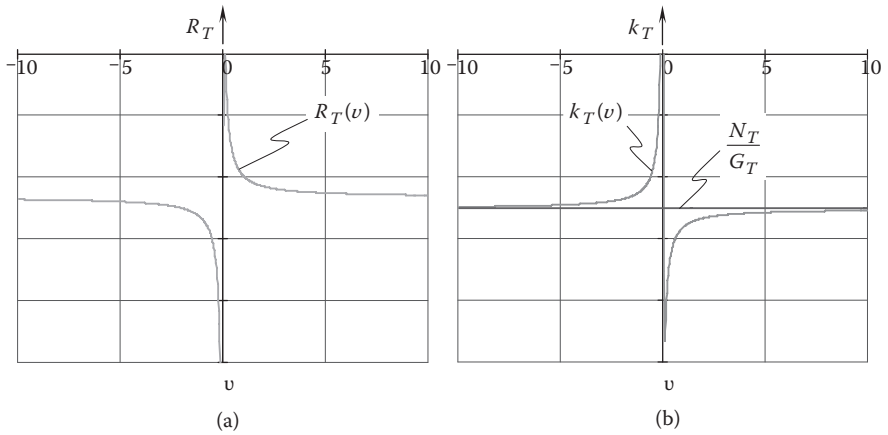

FIGURE 16.80
(a) Alteration of the radii of normal radii $R_T(\upsilon)$ and (b) normal curvature $k_T(\upsilon)$ of the generating surface T of an involute hob versus $\upsilon = \mathrm{d}VT/\mathrm{d}UT$. (From Radzevich, S.P., *ASME Journal of Mechanical Design*, 129, 334–345, 2007. With permission.)

$$\theta = \tan^{-1}\left(\frac{d_{\text{b.c}}}{d_{\text{c}}} \cdot \cos\psi_{\text{b.c}}\right) \tag{16.123}$$

is used.

The generating surface T_{m} of the gear hob with a modified tooth profile is different from the generating surface T of the hob for machining nonmodified gears. However, it is of critical importance to stress here that the tooth profile angle ϕ_{n} and the setting angle of the hob ζ_{c} do not change their values, and for the modified surface T_{m} they are of the same value as for the generating surface T.

Actually, the involute hob [100] provides a hyperbolic modification of the tooth profile of the hobbed gear. The hyperbolic modification enhances known types of modification of the gear tooth profile, namely of (a) circular modification, (b) parabolic modification, (c) topological modification, and so forth.

An illustrative example of the computation. Consider a single-start involute hob with a module $m = 10$ mm, outer diameter $d_{\text{o.c}} = 180$ mm, and normal profile angle $\phi_{\text{n}} = 20°$. The desired modified tooth profile is a hyperbola through three points a_3, a_k, and a_4. The hyperbolic tooth profile is approximated with a circular arc through the same three points a_3, a_k, and a_4. It is assumed that the approximation is reasonable, and it insignificantly affects the accuracy of the hobbed gear.

The initial tooth profile of the hob is not modified. It is the straight line segment through points $a_1(x_1,y_1)$, $a_k(x_k, y_k)$, and $a_2(x_2, y_2)$ (Figure 16.81). Actually, for the involute hob under consideration, the coordinates of points a_1, a_k, and a_2 are as follows: $x_1 = 0$ mm, $y_1 = 0$ mm; $x_k = 3.64$ mm, $y_k = 10$ mm; and $x_2 = 8.189$ mm, $y_2 = 22.5$ mm.

The hob tooth profile has a modification of 0.127 mm. This allows for the computation of coordinates of points a_3 and a_4, which are as follows: $x_3 = -0.127$ mm, $y_3 = 0$ mm and $x_4 = 8.062$ mm, $y_4 = 22.5$ mm.

In order to provide the tooth of the involute hob with the modification of the range of 0.127 mm, the tooth profile radius of curvature R_T has to be equal to

$$R_T = \sqrt{\frac{B^2 + C^2}{4A^2} - \frac{D}{A}} = 593.625\,\text{mm} \tag{16.124}$$

where all the parameters A, B, C, and D are of constant value. They are computed from the formulae immediately following:

$$A = \begin{vmatrix} x_3 & y_3 & 1 \\ x_k & y_k & 1 \\ x_4 & y_4 & 1 \end{vmatrix} = 2.858 \tag{16.125}$$

$$B = -\begin{vmatrix} x_3^2 + y_3^2 & y_3 & 1 \\ x_k^2 + y_k^2 & y_k & 1 \\ x_4^2 + y_4^2 & y_4 & 1 \end{vmatrix} = 3.165 \times 10^3 \tag{16.126}$$

$$C = \begin{vmatrix} x_3^2 + y_3^2 & x_3 & 1 \\ x_k^2 + y_k^2 & x_k & 1 \\ x_4^2 + y_4^2 & x_4 & 1 \end{vmatrix} = -1.224 \times 10^3 \tag{16.127}$$

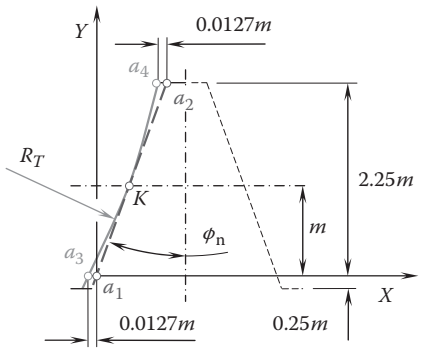

FIGURE 16.81
Computation of the desirable value of the radius of the normal curvature R_T of the generating surface T of a hob with a modified tooth profile. (From Radzevich, S.P., *ASME Journal of Mechanical Design*, 129, 334–345, 2007. With permission.)

$$D = -\begin{vmatrix} x_3^2 + y_3^2 & x_3 & y_3 \\ x_k^2 + y_k^2 & x_k & y_k \\ x_4^2 + y_4^2 & x_4 & y_4 \end{vmatrix} = 401.864 \tag{16.128}$$

The first principal radius of curvature $R_{1.T}$ of the generating surface T of the hob [Equation (16.115)

$$R_{1.T} = \frac{\sqrt{155^2 - 27.037^2}\cos 20.338^\circ}{2\sin^2 20.338^\circ} = 592.357\ \text{mm} \tag{16.129}$$

The required value of the angular displacement φ [Equation (16.116)]

$$\varphi = \cos^{-1}\left(\sqrt{\frac{592.357\ \text{mm}}{593.625\ \text{mm}}}\right) = 3.746\ \text{deg} \tag{16.130}$$

The projection of the lateral cutting edge onto the X_cY_c coordinate plane makes the angle ν_m with the centerline (Figure 16.82). This angle is of the value of $\nu_m = 3.835$ deg.

The above-computed design parameters of the precision involute hob yield computation of the radius $R_m = 123.175$ mm and the displacement $d_m = 16.478$ mm. These values are obtained from the solution of the triangles shown in Figure 16.82.

Finally, Equation (16.109) yields for ξ_m

$$\xi_m = \arctan\frac{\cos 3.772^\circ \tan 3.835^\circ}{\tan 20^\circ + \sin 3.772^\circ \tan 3.835^\circ} = 10.292^\circ \tag{16.131}$$

For computation of ϕ_{rs}^{m}

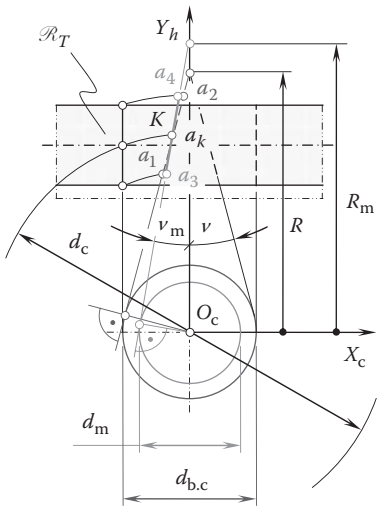

FIGURE 16.82
On the computation of the parameters $d^*_{b.c}$ and R^* of the precision involute hob having modified tooth profile. (From Radzevich, S.P., *ASME Journal of Mechanical Design*, 129, 334–346, 2007. With permission.)

$$\phi^{m}_{rs} = \arctan\frac{\tan 3.835^\circ}{\sin 10.292^\circ} = 21.466^\circ \tag{16.132}$$

Equation (16.110) was used.

The computed design parameters allow for designing of the precision involute hob with a desired modification of the tooth profile.

16.5.4 Examples of Nonstandard Designs of Involute Hobs

Although involute hobs of standard design are the most common cutting tools for machining gears, in many specific cases of gear machining, hobs of improved designs are used as well.

16.5.4.1 Cylindrical Hobs of Nonstandard Design

Numerous designs of cylindrical hobs are developed that target the improvement of cutting performance, gaining a capability of cutting of hard stock, and so forth.

A gear hob for smooth roughing of coarse pitch gears. An example of a standard involute hob for the machining of coarse pitch gears is depicted in Figure 16.83a. Without going into details of description of the hob design, it is of interest to turn the reader's attention here to the configuration of hob teeth within each row (i.e., in the direction of the slot).

The slots in the body of the hob are machined so that the rake faces are orthogonal to the pitch helix through the centerline of each tooth (Figure 16.83b). This teeth arrangement equalizes the cutting edge geometry of the lateral cutting edges of the opposite sides of the hob tooth profile: the corresponding parameters of the cutting edge geometry of the opposite lateral cutting edges are equal to each other. Gear hobs of standard design feature the pitch helix angle ψ_c identical to the lead angle λ_{rs} of the screw rake surface R_s.

For standard gear hobs the identity $\psi_c \equiv \lambda_{rs}$ is observed. In standard gear hobs the setting angle ζ_c is equal to the pitch helix angle ψ_c, so the hob teeth of each row of teeth start the stock removal simultaneously (or almost simultaneously). They also exit from cutting the stock simultaneously (or almost simultaneously). Under such a scenario, vibrations are observed. The vibrations negatively affect the gear machining process, which is especially critical when hobbing coarse pitch gears.

This particular problem of gear hob design is eliminated in the design of the gear hob that is developed mostly for the purpose of roughing coarse pitch gears [71].

The frequency of the vibrations depends on the period of time between the instant of time when the cutting edges enter the stock and the instant of time when the cutting edges exit the stock. For gear hobs of a certain pitch diameter d_c, this period of time t can be expressed in the form

$$t = \frac{l_{rs}}{V_c} = \frac{2l_{rs}}{\omega_c d_c} \tag{16.133}$$

where

l_{rs} = distance between every two consequent teeth along thread of the hob
V_c = linear velocity of rotation of the cutting edge point at the pitch diameter of the hob
ω_c = hob rotation

For a given hob design, the distance l_{rs} is of constant value, and it cannot be changed. The distance l_{rs} can be expressed in terms of design parameters of the hob (Figure 16.84)

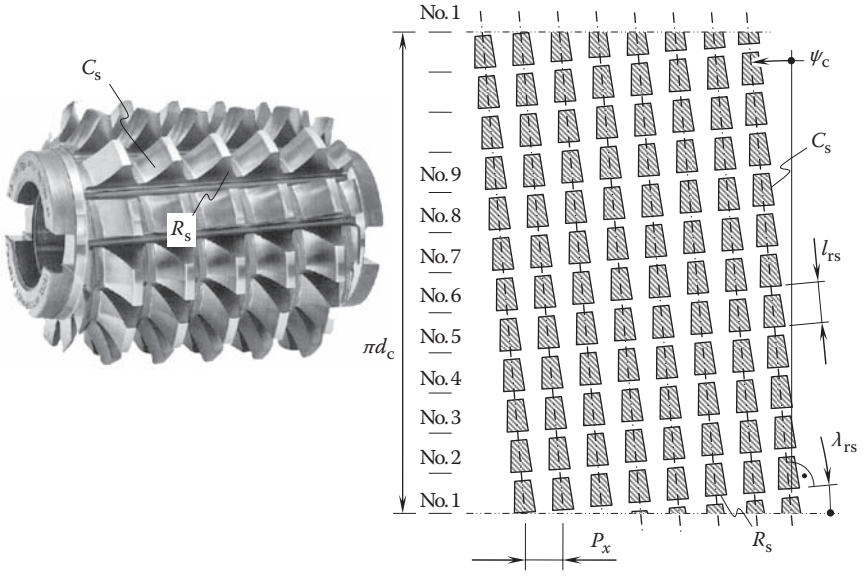

FIGURE 16.83
An example of an unfolded cross section of standard involute hob teeth by the pitch cylinder.

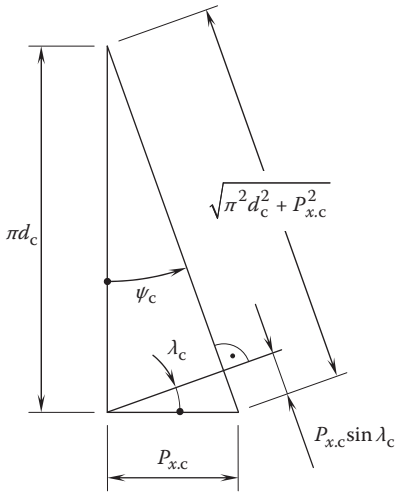

FIGURE 16.84
Computation of the distance l_{rs} between every two rake surfaces R_s of a gear hob of standard design.

$$l_{rs} = \frac{\sqrt{\pi^2 d_c^2 + P_{x.c}^2} - P_{x.c}\sin\lambda_{rs}}{n_c} \tag{16.134}$$

where $P_{x.c}$ denotes the axial pitch of the hob threads ($P_{x.c} = \pi m N_c$), N_c is number of starts of the hob (sometimes this design parameter of the hob is referred to as the *number of hob threads*, which is not recommended), λ_{rs} is lead angle of the hob rake surface R_s, and number of teeth of the hob is designated as n_c.

When hobbing a gear, each cutting edge is heavily loaded because the length of the distance l_{rs} is relatively large. This results in every row of the hob teeth becoming loaded heavily as well. Alteration of the cutting load with the low frequency t^{-1} causes undesirable vibrations.

Shown in the hob in Figure 16.85 [71] are rake surfaces R_s, which are shifted at a certain distance δ_{rs} in the direction of the hob threads. After being shifted at the distance δ_{rs} the rake planes R_s of the hob teeth align with a helix on the pitch cylinder of the hob. The helix angle that specifies the actual location of the rake planes is designated as ξ_{rs}.

The shift distance δ_{rs} can be either positive (in this case the angle ξ_{rs} is greater than the lead angle λ_{rs} as shown in Figure 16.85a)—or it can be negative (in this case $\xi_{rs} < \lambda_{rs}$), as depicted in Figure 16.85b. In a specific case the angle ξ_{rs} can be of zero value ($\xi_{rs} = 0°$). The latter makes possible the design and manufacture of assembled gear hobs.

Each tooth of the hob (Figure 16.85) withholds the cutting load of that same range as the standard gear hob does. A significant reduction of vibration is observed because the cutting teeth are entering into and exiting from the chip removal process not simultaneously, but consequently. The negative effect of the vibrations is eliminated mostly because of significant reduction of the variation of the cutting load, and due to frequency of the vibrations it becomes higher.

For manufacturing of hobs for smooth roughing of the coarse pitch gears (Figure 16.85) [71], the methods of hob grinding discussed above (see Figures 16.14 through 16.77) can be used [78, 81, 129, 130, 133, 144, 159, 173, and others].

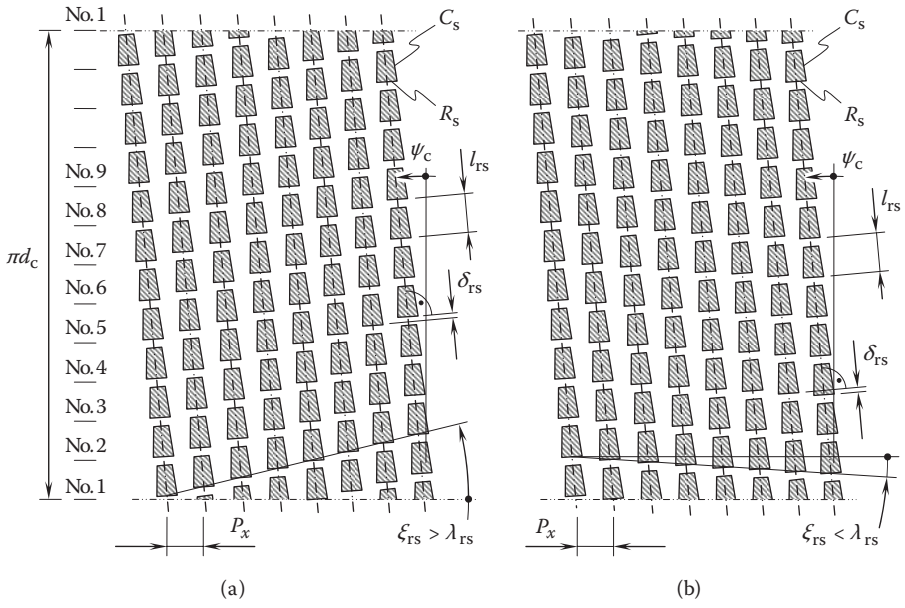

FIGURE 16.85
The unfolded cross section (by the pitch cylinder) of a hob for the roughing of coarse pitch gears. (From Radzevich, S.P., USSR Patent 944828, Int. Cl. B24b 3/12, Sept. 4, 1980.)

A hob for finishing hardened (Rockwell hardness up to HR_C 62) gears. Hardened gears with surface hardness up to HR_C 62 are used in the design of turbine reducers, helicopter transmissions, and so forth. For high productive semifinishing and/or finishing of hardened gears, special-purpose hobs are proposed [129, 133].

Chip removal from a hardened gear tooth surface is feasible if a built-up hob with cutting edges made of superhard materials (borazon, man-made diamond, etc.) is used for this purpose. Due to unavoidable limitations imposed by the synthesizing process of superhard materials, cutting elements of only a small size can be obtained. The available size of cutting elements is insufficient for implementation in the standard design of gear hobs of medium and/or coarse pitch. In order to make possible the use of superhard materials in the design of gear cutting tools, a special-purpose gear hob design is proposed* (Figure 16.86).

The profile angle ϕ_n of the auxiliary generating rack $\mathscr{R}_T$ of the hob is equal to zero ($\phi_n = 0°$). The pitch line of the auxiliary rack $\mathscr{R}_T$ is tangent to the base cylinder $d_{b.g}$ of the gear being machined. When hobbing, the base cylinder $d_{b.g}$ serves as the pitch cylinder $d_{w.g}$ of the gear; therefore the equality $d_{w.g} = d_{b.g}$ is observed in the gear hobbing process.

The hob is comprised of two semihobs. The semihobs are separated from each other by the spacer (by the distance ring).

The total length L of the active portion of the line of action is equal

$$L = \sqrt{d_{o.g}^2 - d_{b.g}^2} \tag{16.135}$$

* In 1970, an extensive research on design and implementation of special purpose hobs for cutting hardened gears was undertaken by Dr. Oleg I. Moiseyenko (Kiev, Ukraine).

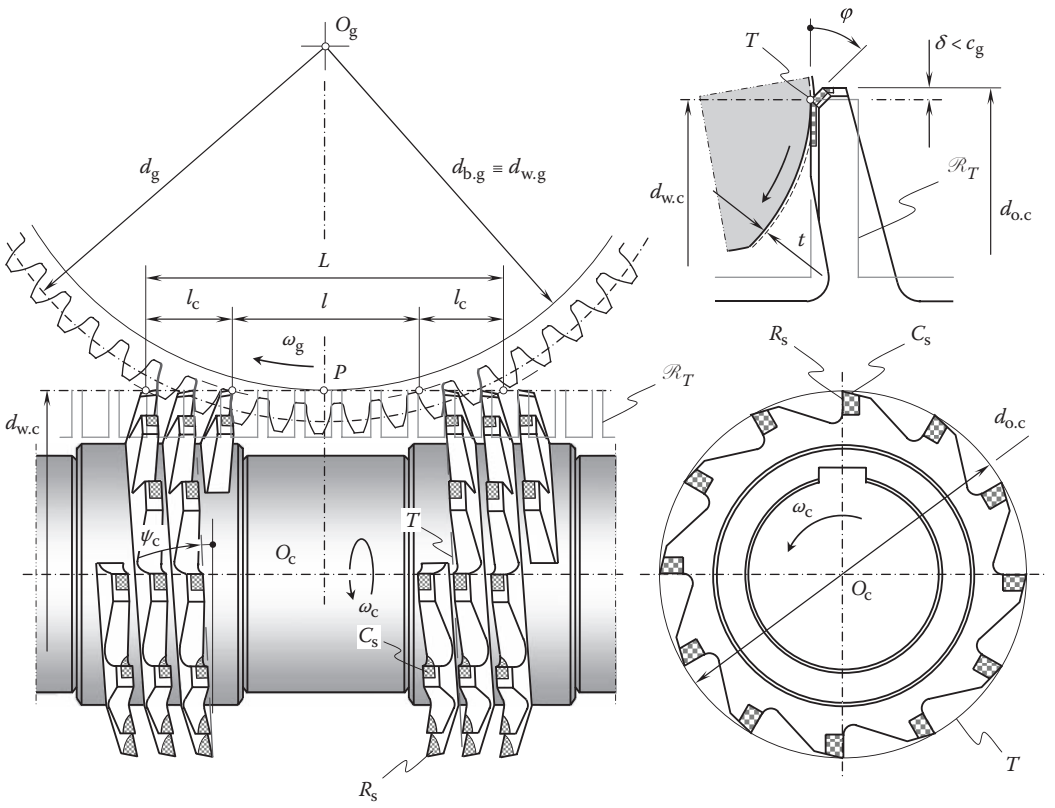

FIGURE 16.86
A special-purpose hob for finishing and/or semifinishing of hardened (Rockwell hardness up to HR_c 62) gears.

The similar expression

$$l = \sqrt{d_{l.g}^2 - d_{b.g}^2} \tag{16.136}$$

is valid for the inner portion l of the line of action (Figure 16.86).

Here, in Equations (16.135) and (16.136), the outer diameter of the gear is designated as $d_{o.g}$, the base diameter of the gear is designated as $d_{b.g}$, and the limit diameter of the gear is designated as $d_{l.g}$.

Equations (16.135) and (16.136) allow for a formula

$$l_c = \frac{L - l}{2} \tag{16.137}$$

for the computation of the length l_c of the active part of the hob.

The pitch helix angle ψ_c of the hob can be specified in two ways.

First, the angle ψ_c is equal (Figure 16.87)

$$\psi_c = \tan^{-1}\left(\frac{P_{x.c}}{\pi d_{w.c}}\right) \tag{16.138}$$

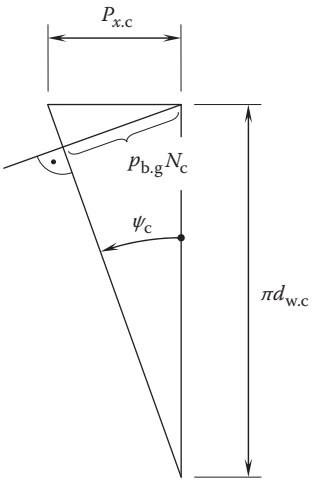

FIGURE 16.87
Computation of the axial pitch $P_{x.c}$ and pitch helix ψ_c of the hob shown in Figure 16.86.

Second, that same angle ψ_c can be expressed in terms of other design parameters of the hob and the gear to be machined (Figure 16.87)

$$\psi_c = \cos^{-1}\left(\frac{p_{b.g}}{P_{x.c}}\right) \tag{16.139}$$

Equations (16.138 and (16.139) specify that same pitch helix angle ψ_c. The equations allow for a formula

$$P_{x.c} = \frac{\pi p_{b.g} d_{w.c}}{\sqrt{\pi^2 d_{w.c}^2 - p_{b.g}^2}} \tag{16.140}$$

for the computation of the axial pitch $P_{x.c}$ of the hob helix.

Then Equation (16.138) considered together with Equation (16.140) allow for an expression

$$\psi_c = \tan^{-1}\left(\frac{p_{b.g}}{\sqrt{\pi^2 d_{w.c}^2 - p_{b.g}^2}}\right) \tag{16.141}$$

for the computation of the pitch helix angle ψ_c.

Because the hob profile angle is zero ($\phi_n = 0°$), in the case under consideration the setting angle of the hob ζ_c is equal to the pitch helix angle ψ_c. This statement correlates with Equation (15.62).

The design of the gear hob makes possible the use of cutting elements with short cutting edges for hobbing gears of any desired coarse pitch. Another advantage is that the cutting edge geometry is independent from the kinematics of meshing. Due to that, the gear hob

can be designed with optimal cutting edge geometry. Taken as a whole, the use of the hob (Figure 16.86) allows for high productive machining of hardened gears.

16.5.4.2 Conical Gear Hobs

Conical hobs can be used for machining of spur and helical gears. Conical gear hobs are designed on the premise of the generating surface T, which is shaped in the form of a conical worm conjugate to the gear being machined (Figure 15.15). An example of a conical hob for machining spur and helical gears is schematically illustrated in Figure 16.88.

The profile angle of the auxiliary generating rack $\mathscr{R}_T$ tooth is designated in Figure 16.88 as ϕ_c. Due to the cone angle θ_c, the tooth flanks of the opposite sides of the tooth profile of the auxiliary rack $\mathscr{R}_T$ are at different angles relative to the axis of rotation O_c of the hob. The angle that the right-hand flank makes with the axis O_c is greater, and is equal to $(\phi_c + \theta_c)$. The angle that the left-hand flank makes with the axis O_c is smaller, and is equal to $(\phi_c - \theta_c)$, accordingly.

Because the lateral tooth flanks of the auxiliary rack $\mathscr{R}_T$ have additional inclination through the cone angle θ_c (Figures 15.15 and 15.17), the conical hobs for machining spur and helical involute gears feature not one, but two base cylinders. The diameters of the base cylinders are designated as $d_{b.c}^{(r)}$ and $d_{b.c}^{(l)}$. The base cylinder of a bigger diameter $d_{b.c}^{(r)}$ corresponds to the hob tooth side with a smaller angle $(\phi_c - \theta_c)$, and the base cylinder of a smaller diameter $d_{b.c}^{(l)}$ corresponds to the hob tooth side with a bigger angle $(\phi_c - \theta_c)$.

Numerous designs of conical tools for machining cylindrical (spur and helical) gears are known from [55, 99] and others. Methods for relief grinding, as well as for the sharpening of conical gear cutting tools are developed [82, 83, and others]. Comprehensive research in the field of design and implementation of conical hobs for machining cylindrical gears has been carried out in [12].

The researchers and users were particularly interested in conical hobs for the machining of spur and helical gears, mainly for two reasons.

First, the use of conical hobs makes it possible to optimize the parameters of the *work gear to cutting tool* penetration curve (further, the GT-penetration curve).

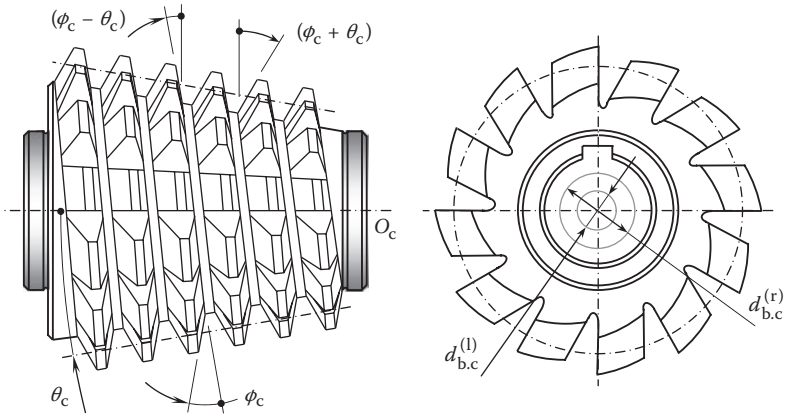

FIGURE 16.88
A conical hob for machining spur and helical gears.

The cutter's entering and exiting sides are distinguished when hobbing gears. Roughly speaking, the cutter's entering and exiting sides are separated from each other by the closest distance of approach of the work gear axis of rotation and the hob axis of rotation. The precutting zone of the hob is located mostly at the entering side of the hob, while the profile generating zone is located on both sides of the hob.

The shape of the precutting zone depends on the external shape of the hob (Figure 16.89). In the work gear/cutting tool penetration, the GT-penetration curve can be understood as a spatial line of intersection of the cylindrical outer surface of the work gear with the outer surface of the hob. The shape and position of the G/C_{pc} curve depends on (a) the crossing angle of the two axes, (b) the size of the hob, and (c) a type of the outer surface of the hob. It is clear from Figure 16.89 that when machining a work gear with the cylindrical hob (Figure 16.89a), the shape and parameters of the GT-penetration curve differs from that when machining a work gear with a conical hob (Figure 16.89b). The use of conical hobs makes it possible to optimize the parameters of the entering and the exiting zones in a gear hobbing operation.

Second, a work gear can be machined with two conical hobs simultaneously. The hobs should be appropriately arranged on a common arbor as shown in Figure 16.90. Such an arrangement of a pair of conical tools for machining cylindrical gears is known from [44, 56] and from other sources.

For machining involute gears with different values of the profile angle ϕ_c at the left-hand and right-hand side of the tooth profile, cylindrical hobs of a special design are used. The

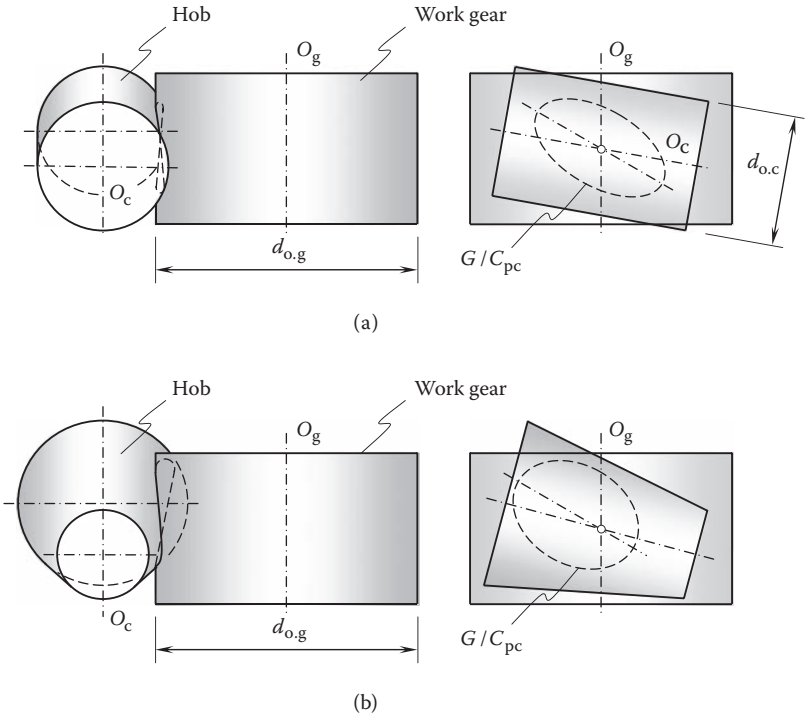

FIGURE 16.89
Work gear to cutting tool penetration curve G/C_{pc} for (a) case machining a gear with the cylindrical hob and (b) machining of that same gear with a conical hob.

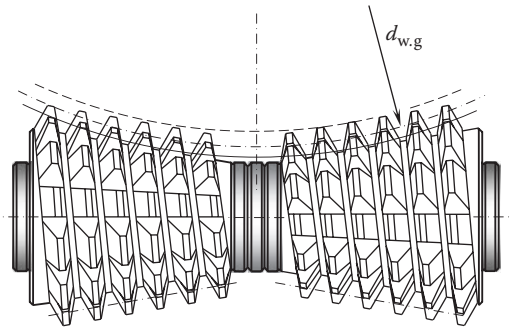

FIGURE 16.90
A set of two conical hobs arranged on a common arbor for machining a cylindrical gear.

hob features different values of profile angle ϕ_c at the left-hand side $\phi_{c.l}$ and at the right-hand side $\phi_{c.r}$ of the hob tooth (Figure 6.91). Due to this design feature, two base cylinders of different diameters $d_{b.c}^{(l)}$ and $d_{b.c}^{(r)}$ are used to construct the screw involute surfaces T_l and T_r of the opposite sides of thread profile of the generating surface T. The base cylinder of the bigger diameter $d_{b.c}^{(l)}$ corresponds to the generating surface T_l with a smaller profile angle $\phi_{c.l}$. Accordingly, the base cylinder of the smaller diameter $d_{b.c}^{(r)}$ corresponds to the generating surface T_r that features a bigger profile angle $\phi_{c.r}$.

The geometry of the generating surfaces T_l and T_r is identical to the geometry of corresponding surfaces of a conical hob for machining cylindrical gears (see Figure 16.88). This is the reason that the cylindrical hob shown in Figure 16.91 is discussed together with conical hobs. The difference between the cylindrical hob (Figure 16.91) and the conical hob (Figure 16.88) is mainly because the first features the outer cylinder of diameter $d_{o.c}$ and the inner cylinder of diameter $d_{f.c}$, while the second features the corresponding cone surface instead.

The pitch line of the cylindrical hob (Figure 16.91) is parallel to the axis of rotation O_c of the hob.

In a specific case, the pitch cone angle θ_r could be equal to the right angle ($\theta_r = 90°$). Under such a scenario, the conical hob degenerates to a disk-type gear cutting tool that is often

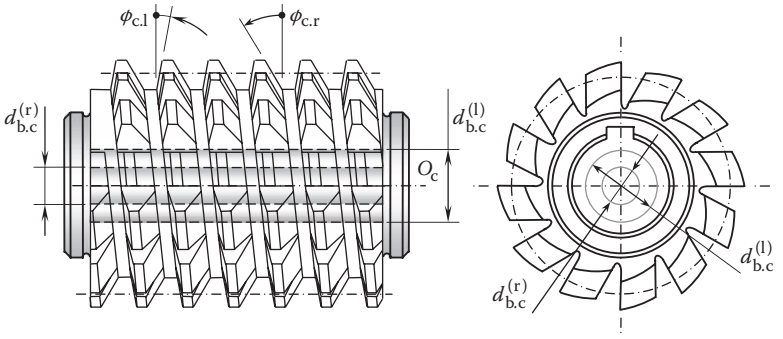

FIGURE 16.91
A hob with different values of profile angle at the left-hand side $\phi_{c.l}$ and the right-hand side $\phi_{c.r}$ of the hob tooth.

referred to as *face hob*. *Butt-end hob* is another name for hobs of this design (Figure 16.92) [96]. The conical pitch surface of the butt-end hob is converted to the pitch plane. The pitch plane is perpendicular to the axis O_c of rotation of the hob. Under such a scenario, the pitch helix lines transform to the corresponding pitch spiral lines, which are planar curves within the pitch plane.

The generating surfaces T_l and T_r of the face hob are constructed from two base cylinders of the diameters $d_{b.c}^{(r)}$ and $d_{b.c}^{(l)}$. In the event that the tooth profile of the auxiliary generating rack $\mathscr{R}_T$ is symmetrical with respect to it center-line, the base cylinders become congruent to each other. Elementary analysis reveals that formally the diameters of the base cylinders can be interpreted as having opposite signs: the diameter of one of the base cylinders is of positive value, while diameter of another is of negative value.

Spur and helical gears can be machined either with one or with two face hobs simultaneously, as shown in Figure 16.93 [165].

When machining a gear, the work gear rotates about its axis of rotation O_g. The rotation of the work gear is denoted in Figure 16.93 as ω_g. The face hob rotates about its axis of rotation O_c. The rotation of the hob is denoted as ω_c. The axes O_g and O_c of the rotations ω_g and ω_c are at a certain center distance $C_{g/c}$.

The rotations ω_g and ω_c are timed so that the equality $\omega_g N_g = \omega_c N_c$ is observed. Here, N_g denotes the tooth number of the work gear, and the number of starts of the hob is denoted as N_c. In order to fulfill the required ratio between the rotations ω_g and ω_c and between the tooth numbers N_g and N_c, both of the face hobs have to be of the same hand of threads.

The in-feed motions of two kinds are feasible.

First, after the work gear is set up at the desired center-distance $C_{g/c}$, both face hobs travel in their axial direction toward the work gear with the axial feed $F_c^{(a)}$. Before all the

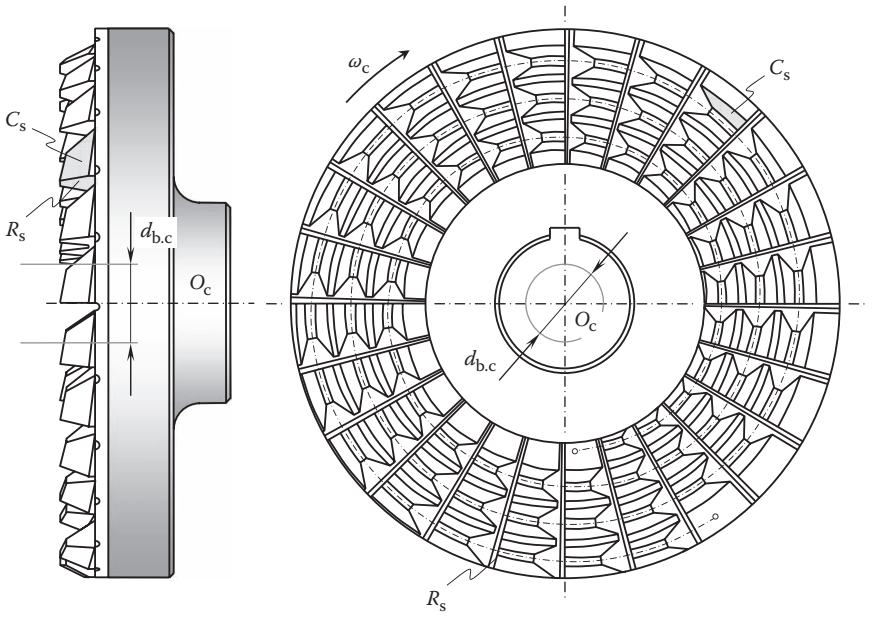

FIGURE 16.92
A conical hob that features a cone angle of the value $\theta_c = 90°$, the so-called *face hob* or *butt-end hob*. (From Radzevich, S.P., USSR Patent 1038122, Int. Cl. B23f 21/04, May 4, 1981.)

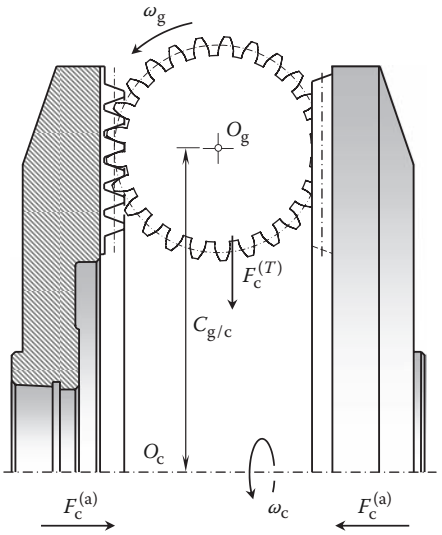

FIGURE 16.93
Kinematics of machining of spur and helical gears with two face hobs. (From Radzevich, S.P. and Palaguta, V.A., USSR Patent 1328042, Int. Cl. B21h 5/00, Dec. 3, 1985.)

teeth of the work gear are hobbed, the work gear should make more than one full rotation about its axis O_g (when machining is performed only with one face hob). When two face hobs are used for machining a gear, then the rotation of the work gear through an angle over 180° is required.

Second, the face hobs are set at the desired distance between their pitch planes and do not move in the axial direction. Instead, the work gear travels in its tangential direction with the tangential feed $F_c^{(T)}$. In the second case, proper timing between the tangential feed $F_c^{(T)}$ and the rotations of the face hobs is vital: for the in-feed period of time the face hobs are rotating in the same directions, but with different angular velocities in order to make the feed motion $F_c^{(T)}$ feasible.

Using the face tools for the machining of spur and helical gears makes it possible to machine not only one work gear, but multiple work gears simultaneously as well.

16.5.4.3 Toroidal Gear Hobs

Toroidal hobs can be used for machining spur and helical gears. Gear hobs of this design feature the generating surface T shown in Figure 15.20b. The concept of toroidal tools for machining spur and helical gears is known from [109]. An example of a toroidal hob is depicted in Figure 16.94.

When machining a spur or helical gear, the work gear rotates about its axis of rotation O_g. The hob rotates about its axis O_c. The axes O_g and O_c of the rotations ω_g and ω_c cross with each other at a certain crossed-axis angle. The rotation of the work gear ω_g and the toroidal hob ω_c are timed so as to fulfill the equality $\omega_g N_g = \omega_c N_c$.

Toroidal hobs feature concave lateral cutting edges. This is because the pitch surface of the toroidal hob is a portion of a torus surface. Because the lateral cutting edges are concave, this reduces the height of the cusps on the tooth flanks of the machined gear. Ultimately, when radius $R_{w.\mathscr{R}}$ of the pitch surface of the auxiliary generating rack $\mathscr{R}_T$ becomes equal

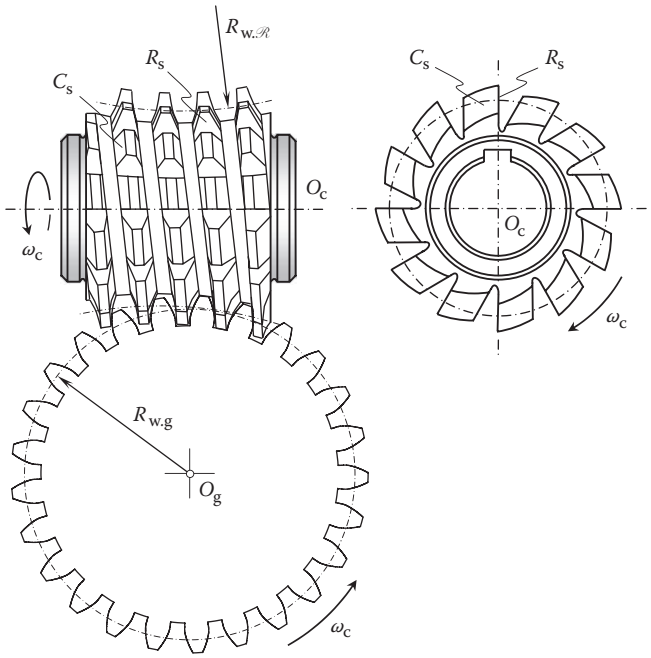

FIGURE 16.94
A hob for machining spur and helical gears that features toroidal pitch surface. (From Radzevich, S.P., USSR Patent 965582, Int. Cl. B21h 5/00, Oct. 2, 1980.)

to the pitch radius $R_{w.g} = d_g/2$ (i.e., when the equality $R_{w.\mathscr{R}} = R_{w.g}$ is observed), then the rack $\mathscr{R}_T$ becomes congruent to the gear surface $\mathscr{G}$. In this particular case cusps are vanished, and true involute tooth profile can be machined. The waviness of the tooth flanks of the machined gear remains the only source of deviations, of concern if the consideration is limited only to the geometry and kinematics of gear machining.

For hobbing of an internal gear, a special-purpose hob can be designed using for this purpose the toroidal generating surface T schematically shown in Figure 15.20a. Actually, a hob designed in this way is capable of cutting external gears as well. However, in the case of machining the external gears' cusp height on the tooth flanks of the cut gear is significantly greater.

16.6 The Cutting Edge Geometry of a Gear Hob Tooth

The cutting edge geometry of a gear hob tooth can be specified in terms of the rake angle, the clearance angle, the angle of inclination, and so forth. The specification of the cutting edge geometry follows the requirements of the Standard ISO 3002.*

* Standard ISO 3002. Basic Quantities in Cutting and Grinding—Part 1: Geometry of the Active Part of Cutting Tools—General Terms, Reference Systems, Tool and Working Angles, Chip Breakers, 1982, 52 pp. The ISO 3002 standard has much room for improvement.

A certain correlation between the parameters of the cutting edge geometry of the lateral and the top cutting edges of a hob tooth commonly is observed. This is mostly due to the methods applied for the generation of the clearance surfaces of the hob teeth, as well as of the rake surfaces of the hob teeth.

It is proven [7, 8, 21, 25, 26, 36, 38, 40, 41, 50, 182, 183, 188, 189, 191, 192, 196, 197 and others], that there exists an optimal combination of parameters of the cutting edge geometry for cutting tool of any and all designs. This means that an optimal combination of parameters of the cutting edge geometry for a gear hob tooth exists and it can be determined.

The nature of the optimal geometry of the cutting edge of a gear hob is not discussed here. At this point it is sufficient just to realize that the optimal values of the cutting edge geometry can be determined somehow, and they are known. The optimal tool geometry for a given application is a matter of experimental finding. Figure 16.95 illustrates an example of existence of the optimal value of clearance angle α. The maximum hob performance is observed when the clearance angle α is equal to its optimal value α_{opt}. When clearance angle α is either greater ($\alpha > \alpha_{opt}$) or smaller ($\alpha < \alpha_{opt}$) than the optimal value α_{opt}, the hob performance becomes smaller. The same is true with respect to other parameters of the cutting edge geometry of the gear hob tooth.

It is of critical importance for the hob designer to express the desirable optimal geometry of the cutting edge in terms of the design parameters of the involute hob. The problem is not that easy to understand from the first glimpse.

In practice, the value of the clearance angle at the top cutting edge of the hob tooth is close to the optimal of its value. The value of the clearance angle at the lateral cutting edge of the hob tooth depends on the value of the clearance angle at the top cutting edge. It is often desired to increase the clearance angle at the lateral cutting edge. However, the desired increase entails a strongly unwanted increase of the clearance angle at the top cutting edge. There is a trade-off between the clearance angles at the top and at the lateral cutting edges of the hob tooth.

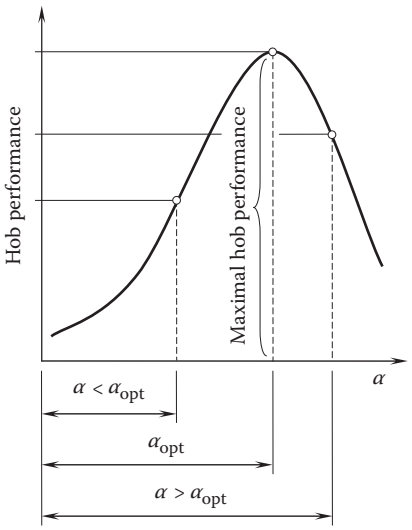

FIGURE 16.95
Qualitative relation of a gear hob performance versus the clearance angle α.

16.6.1 The Penetration Curve and the Machining Zone in a Gear Hobbing Operation

The machining zone is a zone within which the hob interacts with the work gear. The stock removal and the gear tooth profile generation are observed only within the machining zone. The machining zone is bounded by the penetration curve. The penetration curve is an important consideration in hobbing of gears. It was briefly mentioned above and is depicted in Figure 16.89.

The relative motion of the work gear and the hob in the gear hobbing process is of a complex nature. The relative motion is comprised of the elementary motions performed by the work gear and the hob. The work gear rotates about its axis O_g with a certain angular velocity ω_g (Figure 16.96). The hob rotates about its axis O_c with the angular velocity ω_c. The axes of rotations O_g and O_c are at a certain center distance $C_{g/c}$. They are crossed at a crossed-axis angle Σ. The rotations ω_g and ω_c are timed with each other so that the ratio $\omega_g/\omega_c = N_c/N_g$ is always satisfied. The hob travels along the work gear axis with feed-rate F_c. In a climb hobbing operation (Figure 16.96), the gear hob travels upward. In a conventional hobbing operation, the direction of the gear hob traveling is opposite to the direction of F_c shown in Figure 16.96.

Not all of the hob teeth are involved in the stock removal process simultaneously. Only a few of the hob teeth that pass through the machining zone remove chips and generate the gear tooth profile.

The machining zone is bounded by the gear to hob *penetration curve* G/H_{pc}. Therefore, in the tool-in-use reference system, the cutting edge geometry of the hob tooth can be determined only when a certain tooth of the hob is within the penetration curve G/H_{pc}. Otherwise, determining the cutting edge geometry loses any sense. Because of the above-mentioned issue, determining the penetration curve G/H_{pc} is necessary prior to exploring the cutting edge geometry of the hob teeth.

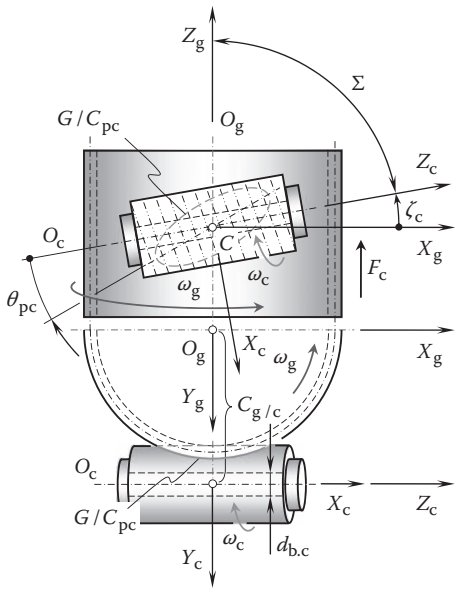

FIGURE 16.96
The "gear to hob" penetration curve G/H_{pc}. (From Radzevich, S.P., *ASME Journal of Manufacturing, Science and Engineering*, 129(8), 750–759, 2007. With permission.)

16.6.1.1 Parameters of the G/H_{pc} Penetration Curve

Referring to Figure 16.96, the penetration curve G/H_{pc} is understood as the line of intersection of the outer cylinder of the work gear ($d_{o.g}$) and the outer cylinder of the hob ($d_{o.c}$). The penetration curve G/H_{pc} is a type of spatial curve.

Targeting derivation of an equation of the penetration curve, consider two cylinders of the diameters $d_{o.g}$ and $d_{o.c}$. The axes O_g and O_c of the cylinders are at a center distance $C_{g/c}$, and the axes make the crossed-axis angle Σ.

In the coordinate system $X_gY_gZ_g$ associated with the work gear, the position vector of point $\mathbf{r}_{o.g}(\varphi_g, U_g)$ of the outer cylinder of the work gear can be expressed in the form of a column matrix

$$\mathbf{r}_{o.g}(\varphi_g, U_g) = \begin{bmatrix} 0.5d_{o.g}\cos\varphi_g \\ 0.5d_{o.g}\sin\varphi_g \\ U_g \\ 1 \end{bmatrix} \tag{16.142}$$

where φ_g and U_g designate curvilinear (Gaussian) coordinates on the surface $\mathbf{r}_{o.g}$.

In the coordinate system $X_cY_cZ_c$ embedded to the hob, an expression

$$\mathbf{r}_{o.c}(\varphi_c, U_c)_c = \begin{bmatrix} 0.5d_{o.c}\cos\varphi_c \\ 0.5d_{o.c}\sin\varphi_c \\ U_c \\ 1 \end{bmatrix}_c \tag{16.143}$$

for the position vector $\mathbf{r}_{o.c}(\varphi_c, U_c)_c$ of a point of the outer cylinder of the hob is similar to Equation (16.142).

Here φ_c and U_c designate curvilinear (Gaussian) coordinates on the surface $\mathbf{r}_{o.c}$.

For the purposes of derivation of an equation of the penetration curve G/H_{pc}, it is necessary to represent both the surfaces $\mathbf{r}_{o.g}$ and $\mathbf{r}_{o.c}$ in a common reference system. In the specific case under consideration, it is convenient to employ the coordinate system $X_gY_gZ_g$ and to represent the hob surface $\mathbf{r}_{o.c}$ in the reference system associated with the work gear. For the coordinate system transformation, the operator $\mathbf{Rs}(c \rightarrow g)$ of the resultant coordinate system transformation

$$\mathbf{Rs}(c \rightarrow g) = \begin{bmatrix} \cos\Sigma & 0 & -\sin\Sigma & 0 \\ 0 & 1 & 0 & C_{g/c} \\ \sin\Sigma & 0 & \cos\Sigma & 0 \\ 0 & 0 & 0 & 1 \end{bmatrix} \tag{16.144}$$

is composed.

Use of the operator $\mathbf{Rs}(c \rightarrow g)$ allows for the representation of Equation (16.143) of the outer cylinder of the hob in the coordinate system $X_gY_gZ_g$ (recall that initially $\mathbf{r}_{o.c}$ is represented in the hob coordinate system $X_cY_cZ_c$)

$$\mathbf{r}_{o.c}(\varphi_c, U_c)_g = \mathbf{Rs}(c \rightarrow g) \cdot \mathbf{r}_{o.c}(\varphi_c, U_c)_c \tag{16.145}$$

Ultimately, the following expression

$$\text{The } GT_{\text{pc}}\text{-Penetration Curve} \quad \Rightarrow \quad \begin{cases} \mathbf{r}_{\text{o.g}}(\varphi_{\text{g}}, U_{\text{g}}) = \begin{bmatrix} 0.5d_{\text{o.g}} \cos\varphi_{\text{g}} \\ 0.5d_{\text{o.g}} \sin\varphi_{\text{g}} \\ U_{\text{g}} \\ 1 \end{bmatrix} \\ \mathbf{r}_{\text{o.c}}(\varphi_{\text{c}}, U_{\text{c}})_{\text{g}} = \mathbf{Rs}(\text{c} \rightarrow \text{g}) \cdot \mathbf{r}_{\text{o.c}}(\varphi_{\text{c}}, U_{\text{c}})_{\text{c}} \end{cases} \tag{16.146}$$

for the penetration curve can be obtained.

Equation (16.146) casts into the form of a column matrix

$$G / H_{\text{pc}} \quad \Rightarrow \quad \mathbf{r}_{\text{p.c.}}(\varphi_{\text{g}}) = \begin{bmatrix} 0.5d_{\text{o.g}} \cos\varphi_{\text{g}} \\ 0.5d_{\text{o.g}} \sin\varphi_{\text{g}} \\ \dfrac{\sqrt{d_{\text{o.c}}^2 - (d_{\text{o.g}} \sin\varphi_{\text{g}} - 2C_{\text{g/c}})^2} - d_{\text{o.g}} \cos\varphi_{\text{g}} \cos\Sigma}{2\sin\Sigma} \\ 1 \end{bmatrix} \tag{16.147}$$

In the expanded form, Equation (16.147) is bulky. It is preferred to compose a corresponding computer code for the computations rather than the straightforward use of Equation (16.147).

As seen in Figure 16.96, the direction of the view of the penetration curve is from the hob toward the work gear along the closest distance of approach $C_{\text{g/c}}$ of the axes O_{g} and O_{c}. The two cylinders $\mathbf{r}_{\text{o.g}}$ and $\mathbf{r}_{\text{o.c}}$ penetrate into each other at a depth that is equivalent to the depth of the machining zone. The intersecting line between the two surfaces $\mathbf{r}_{\text{o.g}}$ and $\mathbf{r}_{\text{o.c}}$ is a 3-D curve, which follows both on the work gear and the hob cylinders.

For further analysis, projection of the penetration curve G/H_{pc} onto the plane through the pitch point is of importance. This reference plane is perpendicular to the shortest distance of approach $C_{\text{g/c}}$ of the axes O_{g} and O_{c}. Where a reference is made below to the penetration curve, the projection of the intersecting line G/H_{pc} onto the above-mentioned plane is understood. An equation of the projection of the penetration curve onto the plane through the pitch point (i.e., the projection onto the plane that is parallel to $X_{\text{g}}Z_{\text{g}}$) could be derived from Equation (16.147)

$$\mathbf{Pr}_{xz}[\mathbf{r}_{\text{p.c.}}(\varphi_{\text{g}})] = \begin{bmatrix} X_{\text{g}}(\varphi_{\text{g}}) \\ 0.5d_{\text{g}} \\ Z_{\text{g}}(\varphi_{\text{g}}) \\ 1 \end{bmatrix} \tag{16.148}$$

where d_{g} designates the pitch diameter of the work gear.

The shape and parameters of the penetration curve depend on (a) the work gear outer diameter $d_{\text{o.g}}$, (b) the hob outer diameter $d_{\text{o.c}}$, (c) the crossed-axis angle Σ, and (d) the center distance $C_{\text{g/c}}$ in the gear hobbing process.

All the hob teeth not passing through the machining zone during the hob rotation (Figure 16.96) do not make contact with the work gear. They are not, therefore, involved in the chip removal process. The cutting edge geometry of the hob teeth located outside the area bounded by the penetration curve cannot be identified.

A distinction must be drawn in hobbing between the precutting zone and the profile-generating zone. The greater portion of material from tooth space of the work gear is removed in the precutting (roughing) zone. The precutting zone is at the end of the hob, which first enters the body of the work gear during the gear hobbing. The hob must be positioned until it completely covers the precutting zone.

16.6.1.2 Partitioning of the Machining Zone

Not all of the hob teeth cut chips even when they are located within the machining zone. For a better understanding of the cutting edge geometry of the hob teeth, differentiation between the approach side and the recessing side of the hob teeth is required. The approaching side and the recessing side of the hob teeth are identical to the similar terms that are common for conventional gearing.

Differentiation between the roughing sector and the gear tooth profile generating sector is required as well. For the differentiation, implementation of the concept of the hob base cylinder is vital. The diameter of the base cylinder of the involute hob is computed from Equation (15.58)

$$d_{b.c} = \frac{mN_c \cos\phi_n}{\sqrt{1 - \cos^2\phi_n \cos^2\zeta_c}} \tag{16.149}$$

The characteristic line E of the generating surface T of the involute hob is a straight line that is tangent to the hob base cylinder of diameter $d_{b.c}$. The characteristic line E is at the base helix angle to the hob axis of rotation. The base helix angle could be computed from Equation (15.62)

$$\psi_{b.c} = \cos^{-1}(\cos\phi_n \cos\zeta_c) \tag{16.150}$$

Equations similar to that above are also valid for the involute tooth surface $\mathscr{G}$ of the gear being machined.

Three sides of the tooth profile of the involute hob are distinguished. They are (a) the entering cutting edge, (b) the recessing cutting edge, and (c) the top cutting edge. Because of these, three corresponding areas of the machining zone are recognized. They are as follows:

(1) The area of cutting by the entering edges (roughing and profiling)

(2) The area of cutting by the recessing edges (just profiling)

(3) The area of cutting by the top edges of the involute hob (Figure 16.97)

The areas (a) through (c) are separated from each other by planes that are perpendicular to the plane of the drawing in Figure 16.97.

The area (a) of machining by the entering cutting edge is bounded by the plane though *ab* at the bottom, and by the vertical plane through *b* at the far left. The tilted bounding plane though *ab* is tangent to the hob base cylinder at the top, and the vertical bounding plane through *b* passes though the most remote left point of the entering line of action in the gear hobbing operation.

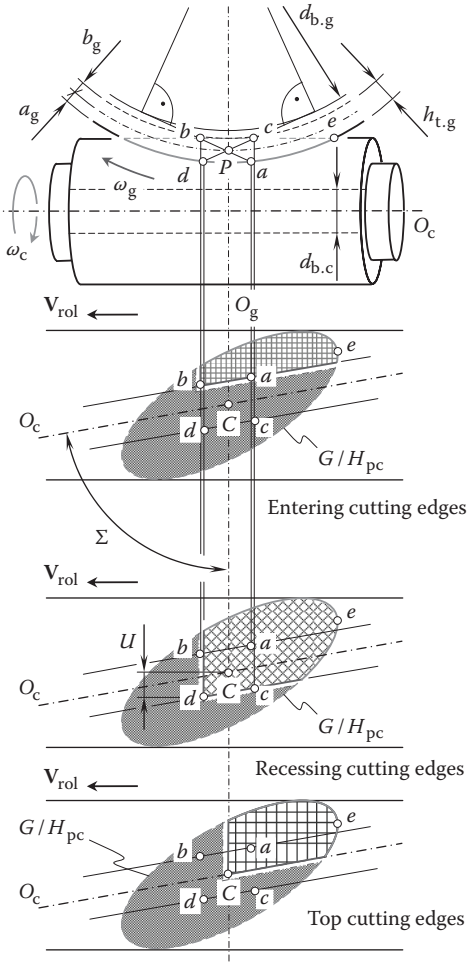

FIGURE 16.97
Three areas within the machining zone in hobbing an involute gear. (From Radzevich, S.P., *ASME Journal of Manufacturing, Science and Engineering*, 129(8), 750–759, 2007. With permission.)

The area (b) of machining by the recessing cutting edge is bounded by the plane through *cd* at the bottom, and by the vertical plane through *d* at the far left. The tilted bounding plane through *cd* is tangent to the hob base cylinder at the bottom, and the vertical bounding plane through *d* passes through the most remote left point of the recessing line of action in the gear hobbing operation. In particular, the vertical bounding planes for the entering and recessing cutting edges could be coincidental with one another.

The area (c) of machining by the top cutting edge is bounded by the plane through the gear hob axis of rotation at the bottom, and by the vertical bounding plane though *C* at the far left. Point *C* is the crossing point of the axes O_g and O_c.

Actually, all three tilted bounding planes are shifted down in the direction of the feed-rate $\mathbf{F}_c$ at a distance that is equal to half of the axial feed-rate per revolution $0.5F_c$ of the work gear.

Point *e* of the penetration curve is the far right point of the machining zone where entering cutting edges of the gear hob start cutting the stock.

The actual shape of the entering cutting edge area, as well as the recessing cutting edge area, strongly depends on the location of the pitch point in the gear hobbing operation [142].

The investigation of the cutting edge geometry of an involute hob makes sense only within the corresponding area of the machining zone (Figure 16.97). This is because in the tool-in-use reference system, no cutting edge geometry can be determined outside of the machining zone. (The surface of the cut, which is the main reference surface, does not exist outside the machining zone.)

16.6.2 The Cutting Edge Geometry of a Hob Tooth in the Tool-in-Use Reference System

Two major reference systems are commonly used for determining the cutting edge geometry of cutting tools. The *tool-in-hand* reference system is one of them, and the *tool-in-use* reference systems is the other. The tool-in-use reference system is used for analysis of the cutting edge geometry of the active part of the hob tooth.

The interested reader is referred to Appendix D for the definitions and details on the basics of the cutting edge geometry.

16.6.2.1 The Tool-in-Use Reference System in a Gear Hobbing Operation

For the analysis of a gear hobbing process, it is convenient to place the origin of the tool-in-use reference system at a point of interest *m* within the cutting edge of the hob tooth. Three vectors are used for the purpose of constructing the tool-in-use reference system. These vectors are as follows [138]: (a) the unit normal vector $\mathbf{n}_c$ to the surface of the cut, (b) the vector $\mathbf{V}_\Sigma$ of the speed of the resultant motion of the cutting edge relative to the surface of the cut, and (c) the unit vector $\mathbf{c}_e$ that is tangent to the cutting edge at a point *m*. In addition to the vectors $\mathbf{n}_c$, $\mathbf{V}_\Sigma$, and $\mathbf{c}_e$, a few complementary vectors are applied as well.

Unit normal vector to the surface of the cut. The surface of the cut in a gear hobbing operation could be represented as a set of successive positions of the cutting edge of the hob tooth that travels with respect to the work gear. Three different cutting edges of the hob tooth, namely the entering cutting edge, the recessing cutting edge, and the top cutting edge, generate three different surfaces of the cut.

The resultant motion of the hob cutting edges is complex in nature. It could be represented as a superposition of three partial motions. These partial motions are created by (a) rotation of the work gear, (b) rotation of the gear hob, and (c) by the feed motion of the hob. Ultimately, the complex resultant motion of the cutting edges results in complex and bulky equations for each of three surfaces of the cut. However, a reasonable simplification of the equations is possible. The simplification utilizes the property of the generating surface *T* of the involute hob according to which the surface *T* is tangent to the surface of the cut. This geometrical property of the surface *T* allows a feasible conclusion: The unit normal vector $\mathbf{n}_c$ to the surface of the cut is aligned with the unit normal vector $\mathbf{n}_T$ to the generating surface *T* (i.e., it is assumed that the identity $\mathbf{n}_c \equiv \mathbf{n}_T$ is observed).

The unit normal vector $\mathbf{n}_c$ to the surface *T* can be computed from the equation $\mathbf{n}_c = \mathbf{u}_T \times \mathbf{v}_T$, where it is designated: $\mathbf{u}_T = \mathbf{U}_T/|\mathbf{U}_T|$, $\mathbf{v}_T = \mathbf{V}_T/|\mathbf{V}_T|$, and $\mathbf{U}_T = \partial \mathbf{r}_T/\partial U_c$, $\mathbf{V}_T = \partial \mathbf{r}_T/\partial V_c$. For computation of the derivatives, Equation (15.54)

$$T: \quad \Rightarrow \quad \mathbf{r}_T(U_c, V_c) = \begin{bmatrix} 0.5d_{b.c}\sin V_c - U_c \sin\psi_{b.c}\cos V_c \\ 0.5d_{b.c}\cos V_c + U_c \sin\psi_{b.c}\sin V_c \\ p_c V_c - U_c \cos s\,\psi_{b.c} \\ 1 \end{bmatrix} \tag{16.151}$$

of the generating surface T is employed. In this equation, the negligible impact of the feed onto the parameters of the unit normal vector $\mathbf{n}_c$ is ignored.

The resultant motion of a point of interest within the cutting edge. The following three motions are performed simultaneously when hobbing an involute gear: (a) a rotation of the work gear ω_g, (b) a rotation of the hob ω_c, and (c) a feed-rate F_c (Figure 16.98). Figure 16.99 illustrates the important details on the kinematics of the gear hobbing process These three elementary motions cause the resultant speed of motion $\mathbf{V}_\Sigma$ of the cutting edge with respect to the surface of cut. Evidently, the vector $\mathbf{V}_\Sigma$ could be expressed in terms of the elementary motions ω_g, ω_c, and F_c.

First, it is convenient to express the vector $\mathbf{V}_\Sigma$ as a summa of

$$\mathbf{V}_\Sigma = \mathbf{r}_{i.c} \times \boldsymbol{\omega}_c + \mathbf{V}_{rol} + \mathbf{F}_c \tag{16.152}$$

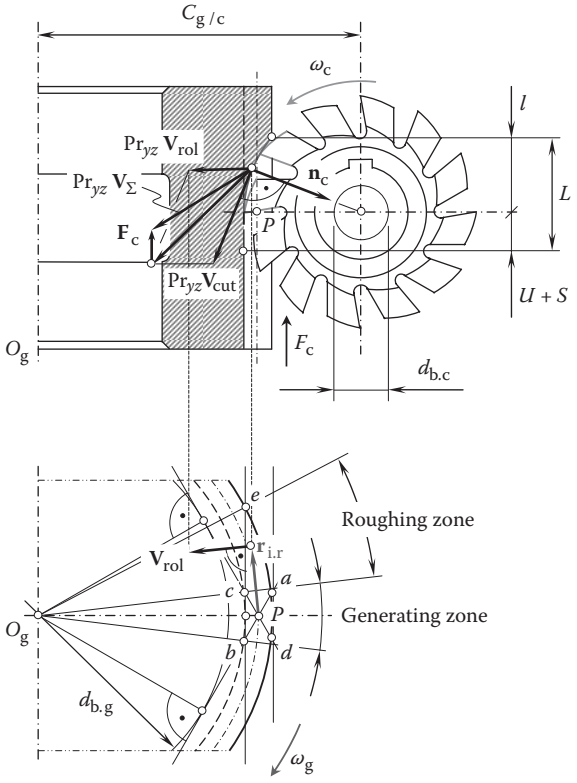

FIGURE 16.98
The resultant speed in the gear hobbing process. (From Radzevich, S.P., *ASME Journal of Manufacturing, Science and Engineering*, 129(8), 750–759, 2007. With permission.)

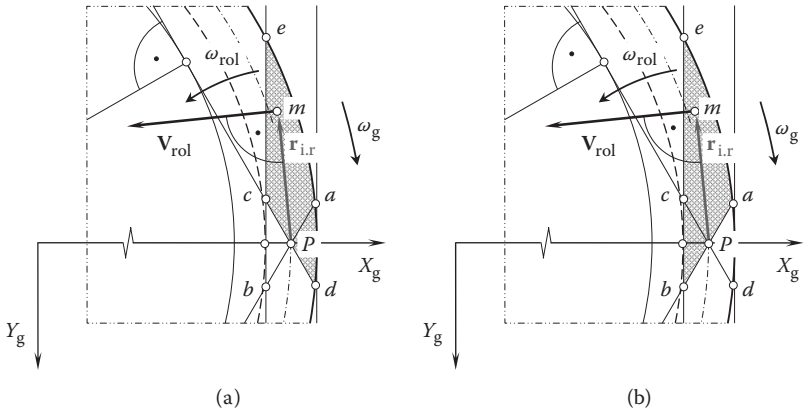

FIGURE 16.99
Rolling motion for (a) the entering side of a hob tooth profile and (b) the recessing side of a hob tooth profile. (From Radzevich, S.P., *ASME Journal of Manufacturing, Science and Engineering*, 129(8), 750–759, 2007. With permission.)

where, $\mathbf{r}_{i.c}$ designates a vector that is pointed from the axis of rotation O_c of the involute hob to the point of interest m within the given cutting edge at the specified angular position of the hob. (The vector $\mathbf{r}_{i.c}$ is orthogonal to the hob axis of rotation O_c; i.e., $\mathbf{r}_{i.c} \perp O_c$.) This vector could be also interpreted as the projection of a position vector of a point of interest m onto the X_cY_c coordinate plane. The vector of the hob rotation is designated as $\boldsymbol{\omega}_c$. The rolling motion $\mathbf{V}_{rol}$ in the gear hobbing operation can be expressed as the cross product $\mathbf{V}_{rol} = \boldsymbol{\omega}_{rol} \times \mathbf{r}_{i.rol}$. Here $\boldsymbol{\omega}_{rol}$ is the vector of the rolling of the hob pitch plane over the work pitch cylinder, and $\mathbf{r}_{i.rol}$ designates the projection of the position vector of the cutting edge point of interest onto the X_gY_g coordinate plane. The vector $\mathbf{F}_c$ is a vector of the hob feed-rate.

Figure 16.96 reveals that the following expressions for the vectors $\mathbf{r}_{i.c}$, $\boldsymbol{\omega}_c$, $\mathbf{V}_{rol}$, and $\mathbf{F}_c$ are valid

$$\mathbf{r}_{i.c} = \mathbf{i} \cdot |\, \mathbf{r}_{i.c} \,| \cdot \cos\varepsilon + \mathbf{k} \cdot |\, \mathbf{r}_{i.c} \,| \cdot \sin\varepsilon \tag{16.153}$$

$$\boldsymbol{\omega}_c = \mathbf{j} \cdot |\boldsymbol{\omega}_c| \tag{16.154}$$

$$\mathbf{V}_{rol} = \mathbf{i} \cdot |\mathbf{V}_{rol}| \cos\kappa + \div \mathbf{j} \cdot |\mathbf{V}_{rol}| \sin\kappa \tag{16.155}$$

$$\mathbf{F}_c = -\mathbf{i} \cdot |\, \mathbf{F}_c \,| \cdot \cos\zeta_c + \mathbf{k} \cdot |\, \mathbf{F}_c \,| \cdot \sin\zeta_c \tag{16.156}$$

Angle κ is the angle that the vector of the rolling motion $\mathbf{V}_{rol}$ makes with the positive direction of the X_g axis. (Angle κ is not shown in Figure 16.96.)

Angle ε in Equation (16.153) defines the current angular position of the cutting edge point of interest of the rotating hob. The angle ε can be computed from the equation $\varepsilon = |\boldsymbol{\omega}_c| \cdot t$, where t designates time.

Second, all the vectors in Equation (16.152) require being represented in a common coordinate system. For this purpose, a left-handed local coordinate system xyz with the origin at the point of interest m on the cutting edge is used. The axis z of the coordinate system xyz is aligned with the unit normal vector $\mathbf{n}_c$ to the surface of the cut. This vector is pointed outward toward the bodily side to the void side of the work gear tooth. The axis y is directed along the vector $\mathbf{V}_\Sigma$ of the speed of the resultant motion of the cutting edge. The axis x complements the axes y and z to the left-hand-oriented Cartesian coordinate system xyz.

Unit tangent vector to the cutting edge. The lateral cutting edge of the precision involute hob is aligned with the line of intersection of the generating surface T of the hob by the rake surface of the hob tooth. There is not much room to vary the parameters of the surface T. However, there is much room for variation of the shape and the parameters of the rake surface R_s of the hob tooth. Because of this, the unit tangent vector $\mathbf{c}$ to the cutting edge at the point of interest m can be specified only for the hob of a given design. As an illustrative example, let us determine the unit tangent vector $\mathbf{c}_e$ for the precision involute hob, the design of which is proposed by the author [98].

The lateral cutting edge is aligned with the straight-line characteristic E. The characteristic line E and the hob axis of rotation are crossed at the hob base helix angle $\psi_{b.c}$ [see Equation (16.150)], and are at a distance $0.5d_{b.c}$ [see Equation (16.149) and Figure 16.70]. This yields an equation

$$\mathbf{c}_e = \frac{\mathbf{C}_e}{|\mathbf{C}_e|} \tag{16.157}$$

for the unit vector $\mathbf{c}_e$, where

$$\mathbf{C}_e = -\mathbf{i} \cdot \cos\phi_{rs} \tan\nu - \mathbf{j} \cdot \cos\phi_{rs} - \mathbf{k} \cdot \sin\phi_{rs} \cos\xi \tag{16.158}$$

and the angles ν, ξ, and ϕ_{rs} are computed from Equations (16.100), (16.109), and (16.110), correspondingly.

The parameter t_c designates the tooth thickness within pitch plane of the auxiliary rake $\mathscr{R}_T$ of the hob. In common practice the equality $t_c = 0.5\pi m$ is observed.

Here ζ_c designates the setting angle of the hob. The angle ζ_c is measured within the pitch plane of the auxiliary rack $\mathscr{R}_T$. The required value of the hob-setting angle ζ_c can be chosen by the designer of the hob. Usually (but not mandatory), it is recommended to assign the actual value of the setting angle of the hob ζ_c equal to the pitch helix angle ψ_c of the hob. The setting angle of the value $\zeta_c = \psi_c$ is preferred from many perspectives.

The derived equations for three vectors $\mathbf{n}_c$ (here $\mathbf{n}_c = \mathbf{u}_T \times \mathbf{v}_T$), $\mathbf{V}_\Sigma$ [Equation (16.152)] and $\mathbf{c}$ (Equation (16.157)] comprise a trihedron of the tool-in-use reference system. In this reference system, the cutting edge geometry of the hob tooth can be determined.

16.6.2.2 Geometrical Parameters of the Hob Cutting Edge in the Tool-in-Use Reference System

After all three main vectors $\mathbf{n}_c$, $\mathbf{V}_\Sigma$, and $\mathbf{c}$ are represented in a common coordinate system, the analysis of the cutting edge geometry of the hob tooth can be performed analytically.

The total number of geometrical parameters of the cutting edges of the hob is limited by the specific features of the design of the involute hob. Ultimately, the following geometrical parameters of the cutting edge are considered:

(1) Rake angle
(2) Clearance angle
(3) Angle of the cutting edge inclination
(4) Cutting wedge angle
(5) Angle of cutting
(6) Cutting edge roundness
(7) Cutting edge curvature

In special cases, the cutting edge torsion could also be involved in the analysis of the cutting edge geometry. All of the above-listed geometrical parameters could be computed for each of the three cutting edges of every tooth of the hob at any instant of the gear hobbing operation [138, 140, 141, 153]. For illustrative purposes, only the first three of the above-listed geometrical parameters of the cutting edge of the gear hob are discussed below in detail.

Rake angle of the cutting edge of the hob tooth. The rake angle γ is used to specify the inclination of the rake surface of the hob tooth with respect to the surface of the cut. For the analysis of the material removal process in the gear hobbing process, it is convenient to specify the inclination of the rake surface (a) by normal rake angle γ_N that is measured in the normal cross-section of the cutting edge, (b) by the rake angle γ_v that is measured in the cross-section of the cutting edge by main section plane, and (c) by the rake angle γ_{cf} that is measured in the cross-section of the cutting edge by the plane of chip flow.

The normal rake angle γ_N of the hob cutting edge is specified in the reference plane that is orthogonal to the hob cutting edge at the point of interest m. It is natural that this reference plane is perpendicular to the surface of the cut so it passes through the unit normal vector $\mathbf{n}_c$. The normal rake angle γ_N is specified as the angle that complements to 90° the angle between the vectors $\mathbf{n}_c$ and $\mathbf{n}_{rs}$ [i.e., by definition, the normal rake angle is equal to $\gamma_N = 90° - \angle(\mathbf{n}_c, \mathbf{n}_{rs})$]. Here $\mathbf{n}_{rs}$ designates the unit normal vector to the rake surface of the hob tooth at the point of interest.

For the computation of the normal rake angle γ_N, the equation

$$\gamma_N = 90° - \tan^{-1}\left(\frac{|\mathbf{n}_c \times \mathbf{n}_{rs}|}{\mathbf{n}_c \cdot \mathbf{n}_{rs}}\right) = \tan^{-1}\left(\frac{\mathbf{n}_c \cdot \mathbf{n}_{rs}}{|\mathbf{n}_c \times \mathbf{n}_{rs}|}\right) \tag{16.159}$$

can be used.

The rake angle γ_v is measured in the direction of the resultant motion $\mathbf{V}_\Sigma$ of the cutting edge with respect to the surface of the cut. This reference plane is perpendicular to the surface of the cut as well. It also passes through the unit normal vector $\mathbf{n}_c$. The rake angle γ_v is specified as the angle between the vectors $\mathbf{n}_c$ and $\mathbf{b}$ [i.e., the normal rake angle γ_v is equal to $\gamma_v = \angle(\mathbf{n}_c, \mathbf{b})$]. Here $\mathbf{b}$ designates the unit vector that is tangent to the rake surface R_s of the hob tooth. The vector $\mathbf{b}$ is located within the plane through the vectors $\mathbf{n}_c$ and V_Σ.

For computation of the rake angle γ_v, the equation

$$\gamma_{\mathrm{v}} = \tan^{-1}\left(\frac{|\,\mathbf{n}_{\mathrm{c}} \times \mathbf{b}\,|}{\mathbf{n}_{\mathrm{c}} \cdot \mathbf{b}}\right) \tag{16.160}$$

can be used.

The rake angle γ_{cf} is measured in the plane of the chip flow over the rake face R_{s}. The chip-flow reference plane is the plane through the vectors $\mathbf{V}_{\Sigma}$ and $\mathbf{V}_{\mathrm{cf}}$. The vector $\mathbf{V}_{\mathrm{cf}}$ is within the rake surface. The vector $\mathbf{V}_{\mathrm{cf}}$ is at the angle η with respect to the unit normal vector $\mathbf{n}_{\mathrm{ce}}$ to the cutting edge. For involute hobs featuring the angle of inclination $\lambda \le 45°$, the approximate equality $\eta \cong \lambda$ is commonly observed. For involute hobs of special design, for example, for skiving gear hobs [129, 130] when the angle of inclination $\lambda > 45°$ (and it can even reach the value of $\lambda = 60°$), the angle η could slightly deviate from λ. It is proven experimentally that for most cases of metal cutting, the deviation $\delta_h = \lambda - \eta$ does not exceed 5° … 10° [138, 188].

The rake angle γ_{cf} is defined as $\gamma_{\mathrm{cf}} = \angle(\mathbf{V}_{\Sigma}, \mathbf{V}_{\mathrm{cf}}) - 90°$. It is computed from the equation

$$\gamma_{\mathrm{cf}} = \tan^{-1}\left(\frac{|\,\mathbf{V}_{\Sigma} \times \mathbf{V}_{\mathrm{cf}}\,|}{\mathbf{V}_{\Sigma} \cdot \mathbf{V}_{\mathrm{cf}}}\right) - 90° = \tan^{-1}\left(\frac{\mathbf{V}_{\Sigma} \cdot \mathbf{V}_{\mathrm{cf}}}{|\,\mathbf{V}_{\Sigma} \times \mathbf{V}_{\mathrm{cf}}\,|}\right) \tag{16.161}$$

All the above-discussed rake angles γ_{N}, γ_{v}, and γ_{cf} could be either of positive or negative value. In specific cases they could be equal to zero as well.

Clearance angle of the cutting edge of the hob tooth. Clearance angles are usually specified in two reference planes, say in planes within which the rake angles γ_{N} and γ_{v} are specified.

The normal clearance angle α_{N} is defined as an angle that complements to 180° the angle between the unit normal vectors $\mathbf{n}_{\mathrm{c}}$ and $\mathbf{n}_{\mathrm{cs}}$. Here $\mathbf{n}_{\mathrm{cs}}$ designates the unit normal vector to the clearance surface at the point of interest within the cutting edge. Therefore, the following equality is observed: $\alpha_{\mathrm{N}} = 180° - \angle(\mathbf{n}_{\mathrm{c}}, \mathbf{n}_{\mathrm{cs}})$. This immediately yields an equation for computation of the normal clearance angle

$$\alpha_{\mathrm{N}} = 180° - \tan^{-1}\left(\frac{|\,\mathbf{n}_{\mathrm{c}} \times \mathbf{n}_{\mathrm{cs}}\,|}{\mathbf{n}_{\mathrm{c}} \cdot \mathbf{n}_{\mathrm{cs}}}\right) = -\tan^{-1}\left(\frac{|\,\mathbf{n}_{\mathrm{c}} \times \mathbf{n}_{\mathrm{cs}}\,|}{\mathbf{n}_{\mathrm{c}} \cdot \mathbf{n}_{\mathrm{cs}}}\right) \tag{16.162}$$

The clearance angle α_{v} is defined as an angle that the unit normal vector $\mathbf{n}_{\mathrm{c}}$ makes with the vector $\mathbf{c}_{\mathrm{s}}$. Here $\mathbf{c}_{\mathrm{s}}$ designates a unit tangent vector to the clearance surface of the cutting tool. The vector $\mathbf{c}$ is within the reference plane through the vectors $\mathbf{n}_{\mathrm{c}}$ and $\mathbf{V}_{\Sigma}$. Therefore, the equality $\alpha_{\mathrm{v}} = \angle(\mathbf{n}_{\mathrm{c}}, \mathbf{c}_{\mathrm{s}})$ is observed. Ultimately, the equation

$$\alpha_{\mathrm{v}} = \tan^{-1}\left(\frac{|\,\mathbf{n}_{\mathrm{c}} \times \mathbf{c}_{\mathrm{s}}\,|}{\mathbf{n}_{\mathrm{c}} \cdot \mathbf{c}_{\mathrm{s}}}\right) \tag{16.163}$$

is valid for computation of the clearance angle α_{v}.

Both the clearance angles α_{N} and α_{v} are positive. In specific cases, within a narrow chamfer along the cutting edge, they could be equal to zero or even of a certain negative value.

Angle of inclination of the cutting edge of the hob tooth. The inclination angle λ is measured within the plane that is tangent to the surface of the cut at the point of interest m of the cutting edge. The angle λ complements to 90° the angle between the vectors $\mathbf{V}_{\Sigma}$ and $\mathbf{c}_{\mathrm{e}}$ (i.e., $\lambda = \angle(\mathbf{V}_{\Sigma}, \mathbf{c}_{\mathrm{e}}) - 90°$). Here $\mathbf{c}_{\mathrm{e}}$ designates the unit vector that is tangent to the cutting edge. The vector $\mathbf{c}_{\mathrm{e}}$ is within the plane that is tangent to the surface of the cut. Angle λ is positive

when the rotation from $\mathbf{c}_e$ to $\mathbf{V}_\Sigma$ through a smaller angle is performed in a counterclockwise direction (looking from the far end of the unit normal vector $\mathbf{c}_e$ toward the surface of the cut). Otherwise, the angle λ is of negative value. The following equation

$$\lambda = \tan^{-1}\left(\frac{|\,\mathbf{c}_e \times \mathbf{V}_\Sigma\,|}{\mathbf{c}_e \cdot \mathbf{V}_\Sigma}\right) - 90^\circ = \tan^{-1}\left(\frac{\mathbf{c}_e \cdot \mathbf{V}_\Sigma}{|\,\mathbf{c}_e \times \mathbf{V}_\Sigma\,|}\right) \tag{16.164}$$

can be used for computation of the inclination angle λ.

The cutting wedge angle β can be computed from the known formula $\beta = 90°-(\alpha + \gamma)$. In this equation, all the angles must be taken in a common reference plane. The derived Equations (16.159) and (16.162) reveal the impact of the design parameters of the hob onto the current value of the cutting wedge angle β.

The angle of cutting δ can be computed from the known formula $\delta = 90°- \gamma$. In this equation, all the angles must be taken in a common reference plane. The derived Equation (16.159) makes evident the influence of the design parameters of the hob onto the current value of the angle of cutting δ.

The effective angle of cutting δ_{cf} is the angle that the inverse direction of the vector $\mathbf{V}_\Sigma$ makes with the vector $\mathbf{V}_{cf}$ of the chip flow over the rake surface R_s of the involute hob tooth ($\delta_{cf} = 180°- \angle(\vec{\mathbf{V}}_\Sigma, \vec{\mathbf{V}}_{cf})$). For free oblique cutting, the effective angle of cutting δ_{cf} can be expressed in terms of the inclination angle λ_{sc}, and of the angle η of the chip flow over the rake surface [138]

$$\delta_{cf} = \cos^{-1}(\cos\lambda\cos\eta\cos\delta_v + \sin\lambda\sin\eta) \tag{16.165}$$

where δ_v designates the angle of cutting that is measured in the main reference plane.

This formula reveals that when the angle of inclination λ and the angle of the chip flow η decrease, then the effective angle of cutting δ_{cf} decreases as well. This relationship is in good correspondence with the results of experiments in [189].

The computed effective angle of the cutting wedge can be used in a classic Merchant's formula

$$\tan\varphi = \frac{\xi\cos\gamma_{cf}}{1-\xi\sin\gamma_{cf}} \tag{16.166}$$

for the computation of the effective shear angle φ. Here ξ designates the chip thickness ratio $\xi = t_p/t_c$.

Further, the chip compression ratio ζ also depends on the effective rake angle γ_{cf}

$$\zeta = \frac{L_p}{L_c} = \frac{\cos(\varphi - \gamma_{cf})}{\sin\varphi} \tag{16.167}$$

The cutting edge roundness ρ is of limited importance for a gear hobbing operation, as well as for wear of the working surfaces of the hob teeth. The hob cutting edge is usually subject to wear mostly of the clearance surface and the rake surface (crater wear of the rake face), as shown in Figure 16.66. The cutting edge roundness ρ is of prime importance concerning the wear of the involute hobs.

The curvature of the cutting edge k_{ce} is almost out of control in a gear hobbing operation. The curvature cannot be changed because of the following: any change to curvature k_{ce}

immediately affects conditions of the meshing of the hob and the work gear. Because of this, the hobbed gear accuracy would drop down drastically.

In a similar manner, any other required geometrical parameter of the cutting edge of a gear hob can be computed.

Examples of the computation of the parameters of the cutting edge geometry of the involute hob. The discussed approach for the computation of the cutting edge geometry is applicable for a hob of any design. As an illustrative example, computation of the geometrical parameters of the precision gear hob shown in Figure 16.72 is considered below.

Computation of the inclination angle λ of the lateral cutting edges. A hob of conventional design features zero the inclination angle at the lateral cutting edges. In specific cases, the inclination angle could be only of a few angular degrees. In order to develop a design of a precision involute hob, alterations to the orientation of the rake surface with respect to the hob axis of rotation have been introduced. These result in that the lateral cutting edges of the precision gear hob (Figure 16.72) [92, 98] do not pass through the hob axis of rotation, and therefore they are inclined relative to the vector $\mathbf{V}_\Sigma$. For the case under consideration, Equation (16.164) together with Equation (16.149) for $d_{b.c}$ allows for derivation of an expanded expression for the computation of the inclination angle λ_y at a point of interest m within the cutting edge of the hob tooth

$$\lambda_y = -\arcsin \frac{mN_c \sin\phi_n \cos\phi_n}{d_{y.c}\sqrt{1-\cos^2\phi_n \cos^2\zeta_c}} \tag{16.168}$$

A diameter of the hob cylinder through the point of interest m of the hob cutting edge is designated as $d_{y.c}$. Actually, the diameter $d_{y.c}$ is within the interval $d_{f.c} \le d_{y.c} \le d_{o.c}$, where $d_{o.c}$ and $d_{f.c}$ are the outer diameter and the inner diameter of the hob correspondingly.

Computations reveal that the inclination angle λ is of opposite signs for the left-side and right-side profiles of the gear hob teeth (Figure 16.100a). The magnitude of the angle of inclination is in the range of $|\lambda| \cong 15° \div 20°$. The magnitude $|\Delta\lambda|$ of variation of λ within the hob tooth height does not exceed $|\Delta\lambda| \le 5°$.

Computation of the normal rake angle γ_N of the lateral cutting edges. Equation (16.159) allows for derivation of an expanded expression for the computation of the normal rake angle γ_N. It is instructive to mention here that in the specific case under consideration, an equation for the computation of the normal rake angle γ_N can be derived in a way that is easier than the straightforward approach, which is based on Equation (16.159).

Consider three unit vectors **d**, **e**, and **f** (Figure 16.70).

The unit vector **d** is aligned with the centerline of the hob tooth profile within the rake surface R_s. The equation for the vector **d** can be represented in the form

$$\mathbf{d} = -\mathbf{j} \tag{16.169}$$

The unit vector **e** is located within the plane that is congruent to the rake surface R_s. The vector **e** can be expressed by the equation

$$\mathbf{e} = \mathbf{i} \cdot \sin\xi + \mathbf{k} \cdot \cos\xi \tag{16.170}$$

Finally, vector **f** is directed orthogonally to the cutting edge at the point of interest m, and it is located within the rake surface R_s. The equation for the vector **f** could be represented in terms of the unknown yet normal rake angle γ_N

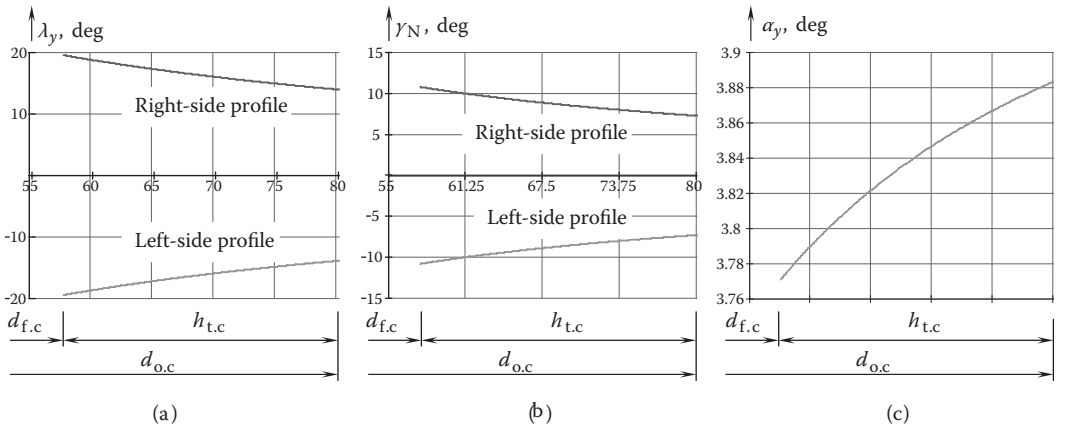

FIGURE 16.100
Actual value of the inclination angle λ_y (a) of the normal rake angle γ_N (b) and the clearance angle α_y at the left-side cutting edge (c) at different points within the cutting edge of the hob shown in Figure 16.72. (From Radzevich, S.P., *ASME Journal of Manufacturing, Science and Engineering*, 129(8), 750–759, 2007. With permission.)

$$\mathbf{f}(\gamma_N) = \mathbf{i} \cdot \left|\mathbf{f}(\gamma_N)\right|_x + \mathbf{j} \cdot \left|\mathbf{f}(\gamma_N)\right|_y + \mathbf{k} \cdot \left|\mathbf{f}(\gamma_N)\right|_z \tag{6.171}$$

By construction, the vectors **d**, **e**, and **f** are within the rake surface R_s of the hob tooth. These vectors comprise a set of coplanar vectors. Because of this, a triple scalar product of the vectors **d**, **e**, and **f** is identical to zero (i.e., the identity $\mathbf{d} \times \mathbf{e} \cdot \mathbf{f} \equiv 0$ occurs). This immediately yields an expression

$$\mathbf{d} \times \mathbf{e} \cdot \mathbf{f} = \begin{vmatrix} 0 & -1 & 0 \\ \sin\xi & 0 & \cos\xi \\ |\mathbf{f}(\gamma_N)|_x & |\mathbf{f}(\gamma_N)|_y & |\mathbf{f}(\gamma_N)|_z \end{vmatrix} \equiv 0 \tag{16.172}$$

After the determinant [see Equation (16.172)] has been expended, and after the necessary formulae transformations are accomplished, an equation for the computation of the normal rake angle γ_N at the hob cutting edge point of interest* can be derived.

The function γ_N vs. $h_{t.c}$ is plotted in Figure 16.100b. The computations reveal that the normal rake angle γ_N is of opposite signs for the left-side and right-side profiles of the gear hob teeth (Figure 16.100b). The magnitude of the normal rake angle γ_N is in the range of $|\gamma_N| \cong 7 \div 11°$. The magnitude $|\Delta\gamma_N| \cong$ of variation of γ_N within the hob tooth height does not exceed $|\Delta\gamma_N| \leq 4°$.

Computation of the clearance angle α at the lateral cutting edges. Following the method discussed above, an equation for the computation of the normal clearance angle α_y in the reference plane through the vectors $\mathbf{n}_c$ and $\mathbf{V}_\Sigma$ can be derived. Omitting the routing formulae transformation, the results illustrated in Figure 16.100c are obtained. Clearance angle α_y is positive for both sides of the gear hob teeth. The magnitude of the clearance angle is in the range of $|\alpha_y| \cong 4°$. The magnitude $|\Delta\alpha_y|$ of variation of α_y within the hob tooth height does not exceed $|\Delta\alpha_y| \leq 1.5°$. The variation $\Delta\alpha_y$ of the clearance angle for the opposite cutting edges

* This equation is not represented here as it is bulky.

of the hob tooth is not shown in Figure 16.100c because this curve is almost congruent to the one depicted in Figure 16.100c.

Slightly modified equations could also be applied for computation of the cutting edge geometry of the precision gear hobs [99, 100], as well for of the hobs of the similar designs.

The examples discussed above illustrate the possibility of computation of the cutting edge geometry of an involute hob that aims for further optimization of the hob tooth design. The derived equations make possible an optimization of all the geometrical parameters of the hob cutting edges.

16.6.2.3 The Possibility of Improving a Hob Design on the Premise of the Results of Investigating the Cutting Edge Geometry

Optimization of the cutting edge geometry of the gear hob tooth is a reliable way to improve the cutting performance of hobs for machining gears. It is strongly desired to develop a hob design that features optimal values of all cutting angles at every point of the cutting edge. Such a possibility is illustrated below with the improvement of the design of a hob for skiving of hardened gears.

The geometry of the active part of skiving hobs for finishing and/or semifinishing of hardened gears significantly differs from that of hobs of conventional design. Only lateral cutting edges of the hob teeth remove the stock—the top edges do not cut the work material [69, 129, 130, 133, 143, 144]. This is an important feature of skiving hobs. The negative rake angle γ_o at the top edge of the hob tooth is commonly within the interval $\gamma_o = (-30° \div -60°)$.

Owing to the great negative rake angle γ_o at the top edge of the skiving hob, the inclination angle λ at the lateral cutting edges varies greatly. The estimation of the range of the variation of the inclination angle λ can be derived from Figure 16.101a. It is evident that the inequality $\gamma_{o.a} < \gamma_{o.b} < \gamma_{o.c}$ is observed. The difference between values of the inclination angle λ that are measured at the outer diameter of the hob $d_{o.c}$ and at the limit diameter of the hob $d_{l.c}$ is in the range up to $\Delta\lambda \cong 30°$. It is known from many sources that deviation of the inclination angle of the cutting tool only on $\Delta\lambda \cong 5°$ from its optimal value could cause a double reduction of the cutting tool life. This means that the design of a skiving hob could be significantly improved if the inclination angle of the hob cutting edges would be of constant value within the cutting edge, and the angle of inclination would be of optimal value at every point of the cutting edge of the hob.

For this purpose it is recommended [69] to shape the rake surface R_s with the help of a convex segment of logarithmic spiral curve with a pole at the hob axis of rotation O_c as shown in Figure 16.101b. (For hobs with a positive rake angle γ_o, a concave segment of the logarithmic spiral curve is used.)

An equation of the generating curve of the hob rake surface can be derived on the premise of the differential equation for isogonal trajectories

$$\left(\frac{\partial\varphi}{\partial x}\cos\theta - \frac{\partial\varphi}{\partial y}\sin\theta\right)dx + \left(\frac{\partial\varphi}{\partial x}\sin\theta + \frac{\partial\varphi}{\partial y}\cos\theta\right)dy = 0 \tag{16.173}$$

In the case under consideration, the solution to Equation (16.173) returns an equation of the logarithmic spiral curve

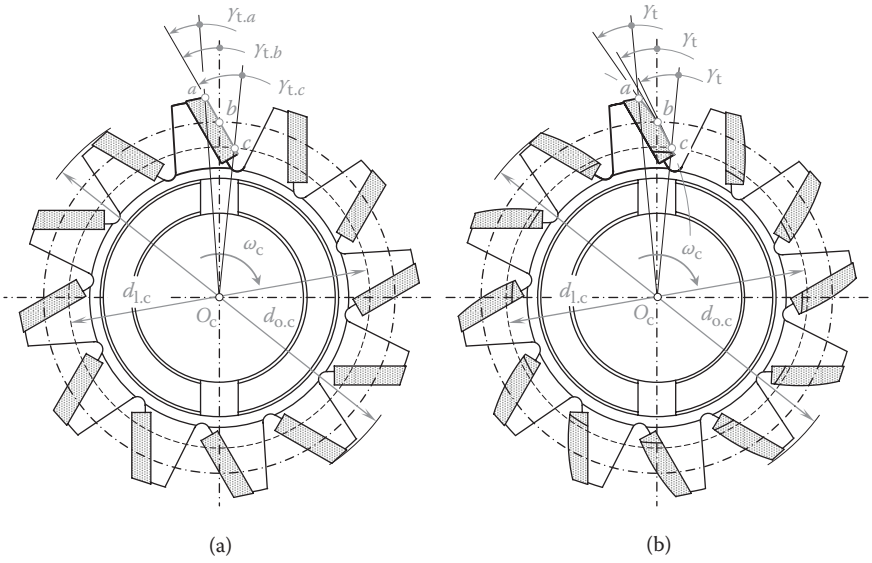

FIGURE 16.101
Elements of the geometry of the active part of a skiving hob with (a) the rake angle at the top edge $\gamma_{o.a} < \gamma_{o.b} < \gamma_{o.c}$ (From Kimura, K. and Ainoura, M., U.S. Patent No. 3.786.719, 1974) and (b) the skiving hob with γ_o = Const. (From Radzevich, S.P., USSR Patent 1114543, Int. Cl. B23f 21/16, Sept. 7, 1982.)

$$\rho = \rho_0 e^{\varphi \tan \lambda_{opt}} \tag{16.174}$$

Actually, Equation (16.174) describes a curve that is a reasonably good approximation to the profile for which the requirement λ_{opt} = Const is fulfilled. This is because the actual value of the inclination angle λ is measured not in the transverse cross-section of the hob, but within the surface of the cut. However, it is proven that the derived solution [see Equation (16.174)] is practical.

The logarithmic spiral curve (see Equation (16.174)] has many applications in the field of gear cutting tool design. Application of this curve includes but is not limited to the use (a) for the purposes of relief grinding of gear hobs, (b) for the purposes of dressing of form grinding wheels, (c) for inspection of form cutting tools, and so forth [60, 61, 115–122, 156, 157, 174, 175, 193, and others].

Modification of the rake surface of the hob teeth makes possible [69] the hobbing of the modified gear tooth profiles [63], and so forth. There is much room for improvement of hob design on the premise of in-depth analysis of the cutting edge geometry of the hob tooth.

16.7 Constraints on the Parameters of Modification of the Hob Tooth Profile

Involute hobs featuring a modified tooth profile are used for many purposes [91]. While modification is aimed at an increase of the hob cutting performance, modification of an

involute hob tooth addendum often results in violation of the fifth necessary condition* of proper part surface generation (further, conditions of proper *PSG*) (see Appendix B). The violation of the fifth condition of proper *PSG* can cause a significant reduction of the accuracy of the hobbed gears.

No modification is observed on the tooth profile of a standard gear hob (Figure 16.65a). Finishing and semifinishing involute hobs (e.g., the involute hobs for machining of hardened (up to HRC 60 … 62) gears have shortened on Δ height of the tooth addendum (Figure 16.67a) [28, 133, 144]. A similar tooth profile modification is used in the design of disk-type milling cutters (Figure 7.17c). The length of the lateral cutting edges of a hob with a chamfered tooth profile (Figure 16.65b) is shortened compared to that for hobs with a standard tooth profile. Owing to shorter lateral cutting edges, generation of a gear tooth profile with a hob with a chamfered hob tooth profile (Figure 16.65b) is similar to that performed with the hob with a reduced addendum (Figure 16.67a). The addendum reduction (Figure 16.67a) can be combined with the chamfered hob tooth profile (Figure 16.65b). This results in the modified hob tooth addendum (Figure 16.67b).

The lateral cutting edges of the hob tooth also become shorter due to (a) the rounded (ρ) corners as shown in Figure 16.65c, and (b) the full rounded r cap (Figure 16.65d). The roundness ρ, as well as the full roundness r affect the hob tooth profile similar to how the shortened one on the Δ height of the addendum (Figure 16.67a) does. The rounded hob tooth profile (Figure 16.65c) can be combined with the shortened tooth addendum (Figure 16.67a). This type of tooth modification results in the combined modification of the involute hob tooth profile depicted in Figure 16.67c. A tooth profile modification of a complex nature, for example as shown in Figure 16.67d, also can entail violation of the fifth condition of proper *PSG*. Numerous other designs of the hob tooth modification are known [38, 39, 64, 65, 133, 144, 161, 187, 195, and many others].

Modification of the hob tooth profile could be the dominant factor that limits the accuracy of the hobbed gear. It is strongly desired to maintain a proper correspondence between the parameters of tooth profile modification of the hob and between the parameters of the work gear. The problem of the computation of the min/max allowed value Δ of the tooth profile modification in terms of the tooth normal profile angle ϕ_c for machining of an involute gear with prespecified tooth number is discussed below [91].

In order to compute the constraints on the parameters of modification of the tooth profile, corresponding reference systems used for analytical description of the geometry and kinematics of the gear hobbing process are required to be established.

16.7.1 The Applied Reference Systems

When hobbing a gear, the work gear rotates $\boldsymbol{\omega}_g$ about its axis O_g (Figure 16.102). The hob rotates about its axis O_g with a certain angular velocity $\boldsymbol{\omega}_c$. The axes of rotations O_g and O_c are at a certain distance $C_{g/c}$ from each other. The gear and the hob rotate in a time-coordinated manner. Rotations $\boldsymbol{\omega}_g$ and $\boldsymbol{\omega}_c$ are timed with each other in a way for which the ratio $\omega_g/\omega_c = N_c/N_g$ is valid. Here N_c designates the number of starts of the hob, and N_g is the teeth number of the gear being hobbed. The hob climbs in an axial direction of the gear (i.e., it travels up along the axis O_g with a certain feed-rate $\mathbf{F}_c$). In a conventional gear hobbing operation, the gear hob travels down in the direction that is opposite to the direction of the gear hob climbing.

* In order to satisfy the fifth necessary condition of proper part surface generation, the intersection of adjacent portions of the generating surface T of a cutting tool is required to be eliminated.

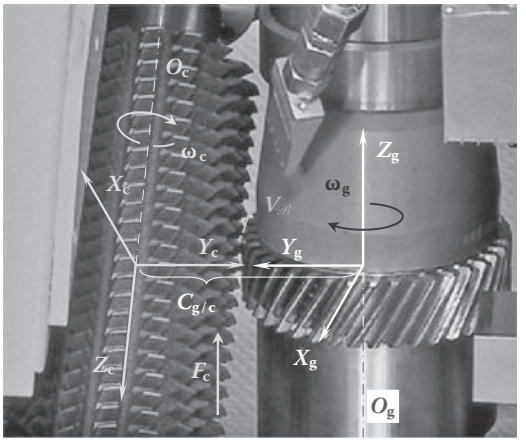

FIGURE 16.102
The applied coordinate systems. (From Radzevich, S.P., *ASME Journal of Mechanical Design*, 128(4), 803–811, 2006. With permission.)

The coordinate system $X_gY_gZ_g$ is associated with the work gear as shown in Figure 16.102. This reference system rotates ($\boldsymbol{\omega}_g$) together with the work gear. The coordinate system $X_cY_cZ_c$ is associated with the hob. This reference system rotates ($\boldsymbol{\omega}_c$) and travels ($\mathbf{F}_c$) together with the hob. Numerous auxiliary reference systems are used in addition to the coordinate systems $X_gY_gZ_g$ and $X_cY_cZ_c$. They are not depicted in Figure 16.102.

16.7.2 Kinematics of the Elementary Gear Drive

An elementary gear drive is comprised of two gears and a housing; for example, it is comprised of pinion 1 and gear 2 (Figure 16.103), which are assembled in the housing (not shown in Figure 16.103). Pinion 1 and gear 2 rotate about the axes $O_{g.1}$ and $O_{g.2}$. The axes $O_{g.1}$ and $O_{g.2}$ of rotation are at a certain operating center distance.

The following two diameters are recognized for the pinion and the mating gear.

Limit diameter is considered as the diameter of a gear at which the line of action intersects the maximum addendum circle of the mating gear. This is sometimes referred to as the start or end of contact of profile (start of active profile, *SAP*). The limit diameter ($d_{l.g}$) is the lowest portion of a tooth that can actually come in contact with teeth of a mating gear. It is a calculated value and is not to be confused with form diameter. It is the boundary between the active profile and the fillet area of the tooth.

Form diameter is considered as the diameter of a circle, at which the transition curve produced by the tooling intersects, or joins, the involute or specified profile. This diameter cannot be less than the base circle diameter. Form diameter is a specified diameter on the gear, above which the transverse profile is to be in accordance with drawing specifications on profile. It is an inspection and should be placed at a somewhat smaller radius than the limit diameter to allow for shop tolerances.

In order to generate the desired involute tooth profile between the outer diameter circle, and between the limit diameter circle, the actual modification of the involute hob tooth profile must not exceed the maximum allowed value [Δ]. It is necessary to determine the maximum allowed value of [Δ] in the way that provides the gear clearance *c*. The latter is often equal to 0.25*m* (here *m* designates modulus of the involute hob).

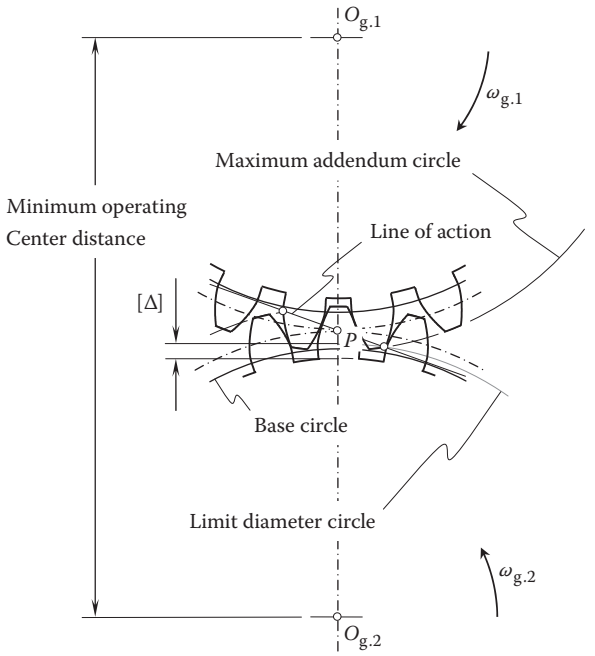

FIGURE 16.103
Limit diameter and the maximum allowed value [Δ] of modification of a gear tooth profile. (From Radzevich, S.P., *ASME Journal of Mechanical Design*, 128(4), 803–811, 2006. With permission.)

Computation of the maximum allowed value of [Δ] is a critical issue for designing of a special-purpose involute hob.

16.7.3 Computation of the Maximum Allowed Value of the Modification of the Tooth Profile of an Involute Hob

A convenient analytical approach for the computation of the maximum allowed value of [Δ] is based on analysis of satisfaction (or violation) of the fifth necessary condition of proper part surface generation (*PSG*). This condition requires avoiding intersecting the neighboring segments of the tooth profile of the generating surface *T* of the hob.

A gear can be interpreted as (a) the set of N_g portions of circular cylinder surface formed top lands of the gear teeth, (b) the set of N_g portions of circular cylinder surface formed root lands of the gear teeth, and the set of N_g pairs of screw involute surfaces $\mathcal{G}^{(des)}$ through both sides of the gear tooth profile. Because of this, the generating surface *T* of the involute hob is composed of N_c number of portions of circular cylinder surfaces (root lands as well as top lands), and that same number N_c of pairs of the screw involute surfaces through both sides of the hob tooth profile. When hobbing a gear, the surfaces composed of the generating surface of the hob make contact with the corresponding portions of the gear tooth surface $\mathcal{G}^{(des)}$.

In order to make a conclusion whether the fifth necessary condition of *PSG* is satisfied or is violated in a gear hobbing process, it is necessary to investigate the relative disposition of the neighboring portions of the generating surface *T* of the gear hob.

In reality, three different kinds of relative disposition of the neighboring portions of the generating surface T of the hob are physically possible. The neighboring portions of the generating surface of a hob (a) can share no common points (i.e., they can be apart from each other), (b) can be connected to each other at the end-points, and (c) can intersect each other.

In cases (a) and (b), no violation of the fifth necessary condition of proper *PSG* occurs. The corresponding dispositions of the neighboring portions of the generating surface of the hob are of interest from the perspective of satisfaction or violation of the fifth necessary condition of proper *PSG*.

When neighboring portions of the involute hob tooth profile intersect each other as observed in case (c), then violation of the fifth necessary condition of proper *PSG* occurs. As a result, the desired involute tooth profile is not generated in the bottom of the tooth space of the gear tooth profile, but a transition curve is generated instead.

Consider an example of the generation of an involute profile of the work gear tooth space. The work gear tooth space is generated by a corresponding tooth of the auxiliary generating rack $\mathscr{R}_T$ of the hob. One side of the work gear tooth space is generated by the left-side tooth profile $a_l^* b_l^*$ of the hob tooth (Figure 16.104a). The opposite side of the gear tooth space is generated by the right-side tooth profile $a_r^* b_r^*$ of the hob tooth. The opposite sides $a_l^* b_l^*$ and $a_r^* b_r^*$ of the tooth profile of the auxiliary rack $\mathscr{R}_T$ make a certain profile angle ϕ_c with the centerline of the rack tooth. The bottom land of the gear tooth space is generated by top land $a_l^{**} a_r^{**}$ of the hob tooth.

The neighboring portions of tooth profile of the auxiliary rack $\mathscr{R}_T$ intersect each other. Point f_l^* is the point of intersection of the straight-line segments $a_l^* b_l^*$ and $a_l^{**} a_r^{**}$. Similarly, point f_r^* is the point of intersection of the straight-line segments $a_r^* b_r^*$ and $a_l^{**} a_r^{**}$. Due to the intersections, the portions $a_l^* f_l^*$ and $a_l^{**} f_l^*$ at one corner of the hob tooth, as well as the portions $a_r^* f_r^*$ and $a_r^{**} f_r^*$ at the opposite corner of the hob tooth, physically cannot exist. Instead of the absent portions $a_r^* f_r^*$ and $a_r^{**} f_r^*$ of the hob tooth profile, only corners f_l^* and f_r^* physically exist in reality.

Because of the absence of portions of the hob tooth profile, corresponding portions of the work gear tooth space profile cannot be properly generated. Referring to Figure 16.105, the segments $a_l c_l$ and $a_r c_r$ of the involute profiles $a_l b_l$, and $a_r b_r$ of the gear tooth space, which should be generated by the absent portions $a_l^* f_l^*$ and $a_r^* f_r^*$ of the hob tooth profile, as well as the segments $a_l d_l$ and $a_r d_r$, which should be generated by the absent segments $a_l^{**} f_l^*$ and $a_r^{**} f_r^*$, actually are generated by the corners f_l^* and f_r^*. The corners f_l^* and f_r^* generate not the desired portions $a_l c_l$ and $a_r c_r$ of the involute profiles, and not the portions $a_l d_l$ and $a_r d_r$ of the bottom land, but transient curves $c_l d_l$, and $c_r d_r$ instead. The transient curves are often referred to as fillets.*

By proper selection of the design parameters of the hob tooth, the dimensions of the transient curves can be reduced to fit the tolerance. Moreover, the transient curves can be eliminated altogether (Figure 16.104b).

Aiming for elimination of the transient curves $c_l d_l$, and $c_r d_r$, the corresponding reduction of the normal profile angle of the hob ϕ_c is necessary. When the hob normal profile angle ϕ_c is reduced to the value of $\phi_c^{(1)} = \phi_{l.g}$ (here $\phi_{l.g}$ designates the tooth profile angle on the limit diameter of the gear), then the transient curve vanishes. Under such a scenario, the tooth profile of the hobbed gear is shaped exactly in the form of true involute curves $a_l b_l$, and $a_r b_r$, while the root land is shaped in the form of the arc $a_l a_r$ of a circle.

---

* Reminder: The start of active profile (*SAP*) is the intersection of the limit diameter and the involute profile (Figure 16.105). Points c_l and c_r are the points of *SAP*.

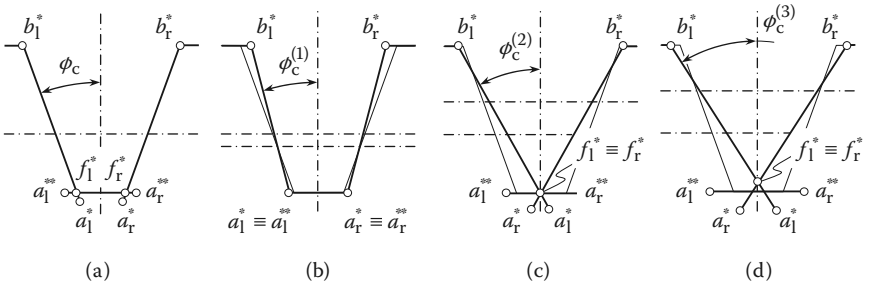

FIGURE 16.104
Examples of violation of the fifth necessary condition of proper part surface generation. (From Radzevich, S.P., *ASME Journal of Mechanical Design*, 128(4), 803–811, 2006. With permission.)

Two more examples of intersection of the adjacent segments of the tooth profile of the gear hob are depicted in Figure 16.104c and d. The corresponding transient curves are shown in Figure 16.105.

At a certain value of the normal profile angle $\phi_c^{(2)} > \phi_c$, the point of intersection $f_l^* \equiv f_r^*$ of the lateral sides $a_l^* b_l^*$ and $a_r^* b_r^*$ of the hob tooth profile is located within the top land profile $a_l^{**} a_r^{**}$ (Figure 16.104c). In this specific case two transient curves $c_l d_l$, and $c_r d_r$ degenerate to a common continuous transient curve $e_l f_l (\equiv f_r) e_r$. The transient curve $e_l f_l (\equiv f_r) e_r$ (a) shares a common point $f_l \equiv f_r$ with the gear root land, and (b) it could spread above the limit circle of diameter $d_{l.g}$ (Figure 16.105).

When the point $f_l^* \equiv f_r^*$ of intersection of the lateral sides $a_l^* b_l^*$ and $a_r^* b_r^*$ of the hob tooth profile is shifted from the top land profile $a_l^{**} b_r^{**}$ toward the pitch line of the hob (Figure 16.104d), then the transient curve in the tooth space of the hobbed gear has no common point with the bottom land, and the transient curve could spread far beyond the limit circle of diameter $d_{l.g}$ (Figure 16.105).

In the cases shown in Figure 16.104c and d, the deviations of the desired profile of the gear tooth could exceed the tolerance for accuracy of the hobbed tooth profile.

Other types of the relative disposition of the neighboring portions of the generating surface T of a hob are possible in specific cases of gear hobbing. However, all of them can

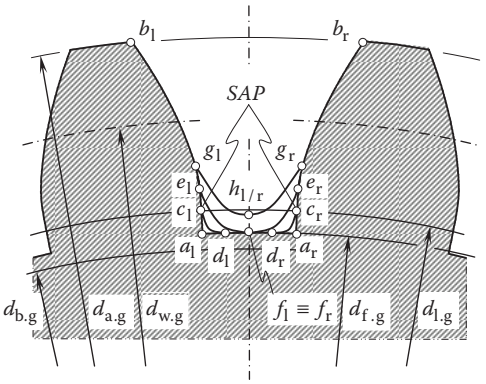

FIGURE 16.105
The transient curves in the bottom of the tooth space of a hobbed gear. (From Radzevich, S.P., *ASME Journal of Mechanical Design*, 128(4), 803–811, 2006. With permission.)

be interpreted as degenerated cases of the three major types of the relative dispositions listed above.

If we are about to prevent the impact of modification of the hob tooth profile onto the accuracy of the hobbed gear, the transient curve must be located within the narrow strip between the circle of root diameter $d_{f.g}$ and the circle of limit diameter $d_{l.g}$. This criterion can be stated analytically as:

$$[\Delta] \le 0.5(d_{l.g} - d_{f.g}) \tag{16.175}$$

The fifth necessary condition of proper *PSG* is satisfied if and only if the inequality (16.175) is fulfilled. In this case, a work gear can be hobbed in full accordance with the blueprint specification on the gear tooth profile. Otherwise, deviations of the actual gear tooth profile from the desired tooth profile are unavoidable.

The inequality (16.175) can be expressed in terms of the design parameters of the gear to be machined and of the gear hob. For this purpose consider the generation of a gear tooth profile with an involute hob (Figure 16.106).

The left-hand side of the gear tooth profile* generates along the left-hand side line of action LA_l, or to be more exact, within portion *DE* of it. The involute hob tooth profile does not exceed the gear root circle of diameter $d_{f.g}$. The hob tooth profile is bounded by the straight-line-segment *AC*. Because of this, the portion *AD* of the line of action LA_l cannot be reproduced in the gear hobbing operation. Therefore, within the portion *AB* of the gear tooth height that is overlapped in the gear hobbing operation by the portion *AD* of the line of action LA_l, the transient curve of the height $AB = \Delta$ is observed. The parameter Δ can be analytically determined in the following way

$$\Delta = AO_g - BO_g = AO_g - CO_g \tag{16.176}$$

The equation of the line of action LA_l can be represented in the form

$$\text{The Line of Action L A}_l \quad \Rightarrow \quad Y_g = X_g \tan\phi_c + \frac{d_{b.g}}{2\cos\phi_c} \tag{16.177}$$

The Y_A coordinate of the point of intersection *A* of the line of action AL_l with the circle of radius $r_{f.g}$ (Figure 16.106) is equal $Y_A = 0.5d_{f.g}$. This result makes possible the computation X_A coordinate of the point of *A*. Equation (16.177) returns

$$X_A = 0.5\left(d_{f.g} - \frac{d_{b.g}}{\cos\phi_c}\right)\cot\phi_c \tag{16.178}$$

Ultimately, Equation (16.176) casts into

$$\Delta = 0.5\left(\sqrt{\left(d_{f.g} - \frac{d_{b.g}}{\cos\phi_c}\right)^2 \cot^2\phi_c + d_{f.g}^2} - d_{f.g}\right) \tag{16.179}$$

* That same approach is applicable for the line of action LA_r the right-hand side of the tooth profile.

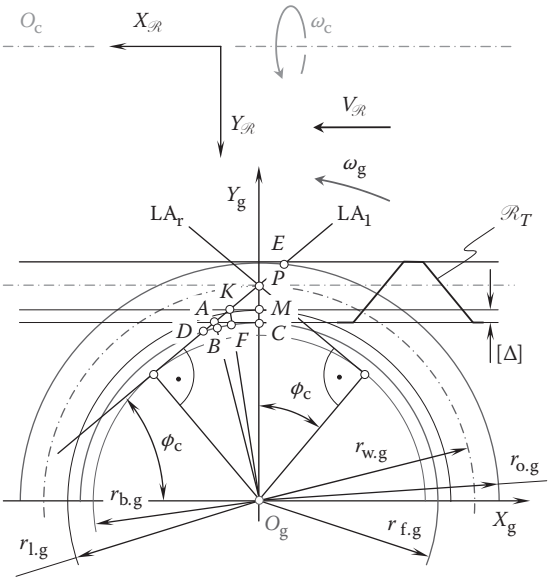

FIGURE 16.106
Gear-to-hob diagram of meshing. (From Radzevich, S.P., *ASME Journal of Mechanical Design*, 128(4), 803–811, 2006. With permission.)

The design parameters of standard gears satisfy the equalities

$$d_{b.g} = d_{w.g}\cos\phi_g = mN_g\cos\phi_g \tag{16.180}$$

$$d_{f.g} = d_{w.g} - 2\cdot 1.25m = m(N_g - 2.5) \tag{16.181}$$

For the specific case of hobbing of a standard gear, Equation (16.179) can be represented in the form

$$\Delta = \frac{m}{2}\left\{\sqrt{\left[(N_g - 2.5) - N_g\cdot\frac{\cos\phi_g}{\cos\phi_c}\right]^2\cot^2\phi_c + (N_g - 2.5)^2} - (N_g - 2.5)\right\} \tag{16.182}$$

The last equation yields computation of the actual value of the parameter Δ of the transition curve in the tooth space of an involute gear.

16.7.4 Normalized Deviation Δ_m of the Tooth Profile of the Hobbed Gear

In specific cases of exploration of the impact of the design parameters of a hob onto the parameters of the transient curve, it is convenient to use not the deviation Δ, but the ratio of the deviation Δ to the gear modulus m instead. For this purpose it is sufficient only to divide both sides of the expression (16.182) by the modulus m. The ratio Δ/m is referred to as a normalized deviation, and it is designated as Δ_m.

As it follows from Equation (16.182), the normalized deviation Δ_m depends on the current value of normal profile angle ϕ_c of the hob. The function $\Delta_m = \Delta_m(\phi_c)$ features an extremum (Figure 16.107a). This indicates that under certain conditions, say for a certain combination of the design parameters of the hob, the deviation Δ_m can be minimized, and the accuracy of the hobbed gear can be improved.

The normalized deviation Δ_m also depends on tooth number N_g of the gear to be machined. The function $\Delta_m = \Delta_m(N_g)$ also features an extremum (Figure 16.107b). The minimum normalized value of the deviation Δ_m for a hobbed gear with a given tooth number occurs when machining is executed with the gear hob with a certain value of normal pressure angle ϕ_c.

The above results of the analysis make possible a convenient graphical interpretation of the area within which the fifth necessary condition of proper *PSG* in the gear hobbing process is satisfied, and it is violated outside of the area.

The maximum allowed value of the deviation Δ is designated as $[\Delta]$ (i.e., $\Delta \le [\Delta]$). The undesired increase of the deviation Δ beyond the tolerance $[\Delta]$ can be compensated by corresponding alteration to the normal profile angle ϕ_c of the gear hob. In order to keep the deviation Δ within the tolerance $[\Delta]$, the normal profile angle ϕ_c of the hob tooth should be within the interval (Figure 16.106):

$$\cos^{-1}\left(\frac{d_{f.g}d_{b.g} + A_c}{(d_{f.g} + 2[\Delta])^2}\right) \le \phi_c \le \cos^{-1}\left(\frac{d_{f.g}d_{b.g} - A_c}{(d_{f.g} + 2[\Delta])^2}\right) \tag{16.183}$$

where $A_c = \sqrt{d_{f.g}^2 d_{b.g}^2 - (d_{f.g} + 2[\Delta])^2 (d_{b.g}^2 - 4d_{f.g}[\Delta] - 4[\Delta]^2)}$.

As an example, a zone within which the fifth necessary condition of proper *PSG* is satisfied is depicted in Figure 16.108. A spur involute gear with a profile angle $\phi_g = 20°$ can be hobbed with the gear hob with a corresponding normal profile angle ϕ_c. The deviation Δ is within the tolerance $0 \le \Delta \le [\Delta] = 0.25m$. A similar boundary can be plotted for the spur and/or helical gear of any desirable design.

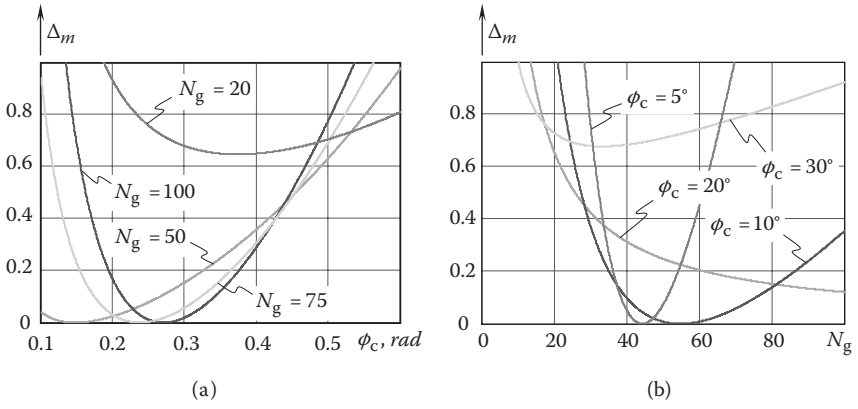

FIGURE 16.107
Impact of (a) hob normal profile angle ϕ_c and (b) gear tooth number N_g on the actual value of the normalized deviation Δ_m of the work gear tooth profile. (From Radzevich, S.P., *ASME Journal of Mechanical Design*, 128(4), 803–811, 2006. With permission.)

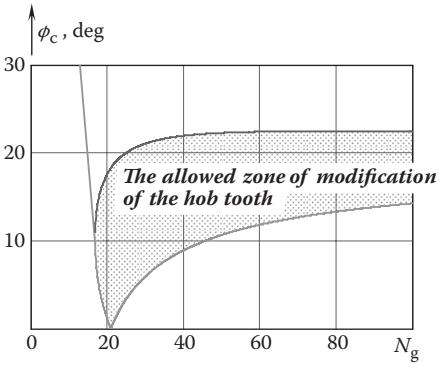

FIGURE 16.108
Zone of satisfaction of the fifth necessary condition of proper *PSG* for the hobbing process of an involute gear. (From Radzevich, S.P., *ASME Journal of Mechanical Design*, 128(4), 803–811, 2006. With permission.)

The application of gear hobs, design parameters of which correlate with the design parameters of the gear being machined (see inequality (16.183)] results in an increase of accuracy of the hobbed gear.

16.7.5 Peculiarities of Involute Hobs with Reduced Addendum

For avoiding an interaction of the top edge of the hob tooth with the completely finished bottom land of the precut gear, involute hobs with shortened addendum (δ) are commonly used (Figure 16.109). Finishing and semifinishing skiving hobs *Azumi* (Figure 16.101), which feature the reduced addendum (δ) either combined with the rounded (ρ) corners or not, are a good example in this situation [28, 133, 144]. Both the addendum reduction and the rounded corner cause the deviation Δ.

In order to make possible an accurate hobbing of the gears with hobs with either reduced tooth addendum and/or with rounded corners, the design parameters of the hob should fit the design parameters of the gear to be machined.

Referring to Figure 16.106, an expression

$$Y_g = X_g \tan\phi_c + \frac{d_{b.g}}{2\cos\phi_c} \tag{16.184}$$

for the Y_g coordinate can derived.

For point K, at which the line of action intercepts the outer diameter of the hob, Equation (16.184) yields expressions for the X_K and Y_K coordinates

$$Y_K = 0.5d_{f.g} + \delta \tag{16.185}$$

$$X_K = 0.5\left(d_{f.g} - \frac{d_{b.g}}{\cos\phi_c} + \delta\right)\cot\phi_c \tag{16.186}$$

Therefore, the deviation Δ can be computed from the formula

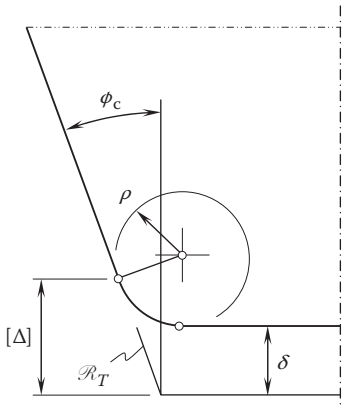

FIGURE 16.109
Tooth profile of a finishing involute hob with the reduced (δ) addendum. (From Radzevich, S.P., *ASME Journal of Mechanical Design*, 128(4), 803–811, 2006. With permission.)

$$\Delta = 0.5\left(\sqrt{\left(d_{f.g} - \frac{d_{b.g}}{\cos\phi_c} + \delta\right)^2 \cot^2\phi_c + (d_{f.g} + \delta)^2} - d_{f.g}\right) \tag{16.187}$$

On solving Equation (16.187), the inequality

$$\delta \le [\Delta] = 0.5\left(d_{b.g}\cos\phi_c + \sqrt{(d_{f.g} + 2[\Delta])^2 - d_{b.g}^2}\sin\phi_c - d_{f.g}\right) \tag{16.188}$$

can be obtained.

In order to satisfy the fifth condition of proper *PSG*, the reduction of the involute hob tooth addendum must not exceed the maximum allowed value of [Δ]. In the case under consideration, analytical representation of the fifth necessary condition of proper *PSG* for the gear hobbing process casts into the inequality

$$d_{b.g}\cos\phi_c + \sqrt{(d_{f.g} + 2[\Delta])^2 - d_{b.g}^2}\sin\phi_c - d_{f.g} - 2\delta \ge 0 \tag{16.189}$$

In the particular case of hobbing of standard gears [for which the conditions of Equations (16.180) and (16.181) are satisfied), the above inequality (16.188) casts into the form [91]

$$\delta \le [\Delta] = \left[N_g\cos\phi_c\cos\phi_g + \sqrt{(N_g + 3)^2 - N_g^2\cos^2\phi_g}\sin\phi_c - (N_g + 2.5)\right] \tag{16.190}$$

Examples of the functions $\delta = \delta(\phi_c)$, and $\delta = \delta(N_g)$ are plotted in Figure 16.110. All curves of the function $\delta = \delta(\phi_c)$ feature a maximum. This indicates that an increase of the allowed value of δ can be achieved by choosing a proper value of the normal profile angle ϕ_c (Figure 16.110a). A similar relationship is observed for the function $\delta = \delta(N_g)$ (Figure 16.110b).

Equation (16.187) yields an analytical expression for the min/max boundary curves, which bound the area within which the fifth necessary condition of proper *PSG* is satisfied

$$\phi_c = \cos^{-1}\left(\frac{(d_{f.g}d_{b.g} + 2\delta d_{b.g}) \pm \sqrt{(d_{f.g}d_{b.g} + 2\delta d_{b.g})^2 + (d_{f.g} + [\Delta])^2\{(2d_{f.g} + \delta + 2[\Delta])(2\Delta - \delta) - d_{b.g}^2\}}}{(d_{f.g} + [\Delta])^2} \right) \tag{16.191}$$

For a specific case of hobbing, a standard involute gear [$\phi_g = 20°$, and when the conditions of Equations (16.180) and (16.181) are satisfied], when δ is assumed to be that in Equation (16.191) casts into

$$\cos\phi_c = \frac{(N_g - 2.4)N_g\cos\phi_g \pm \sqrt{(N_g - 2.4)^2 N_g^2\cos^2\phi_g + (N_g - 2)^2(0.9N_g - N_g^2\cos^2\phi_g - 1.9975)}}{(N_g - 2)^2} \tag{16.192}$$

It is assumed here in Equation (16.192) that the reduction δ of the tooth addendum of the hob is equal to $\delta = 0.05m$ (i.e., $\delta = 0.1(0.05m)$).

The area for feasible combinations of the normal profile angle ϕ_c of the hob tooth and the tooth number N_g of the gear to be machined is plotted in Figure 16.111 (the inner contour). The outer contour in Figure 16.111 corresponds to the case when no reduction (δ) of the tooth addendum of the hob is observed.

Referring to Figure 16.111, the reduction of the hob tooth addendum (δ) considerably narrows the zone within which the fifth necessary condition of proper *PSG* is satisfied.

When the tolerance [Δ] is known, the reduction of the hob tooth addendum by the value $\delta < [\Delta]$ is permissible. Within the remaining portion ([Δ] − δ) the hob tooth can be either chamfered or rounded. For the computation of the maximum allowed radius ρ of rounding of the involute hob tooth, the formulae

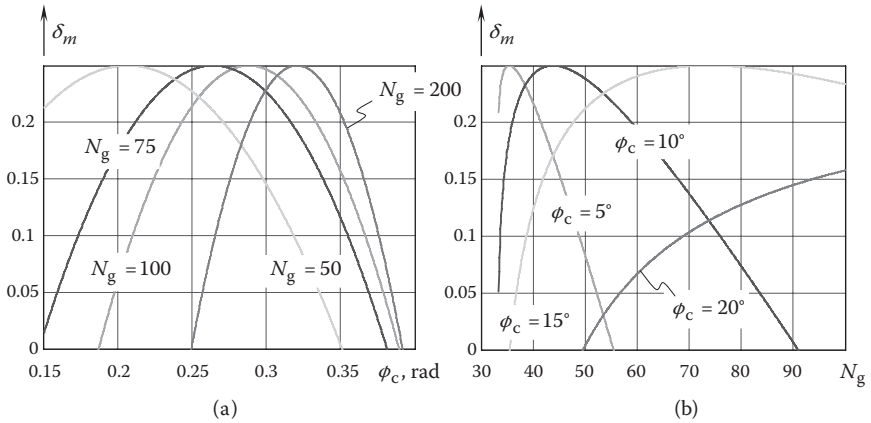

FIGURE 16.110
Impact of (a) hob normal profile angle ϕ_c and (b) work gear tooth number N_g on the allowed value of reduction of the tooth addendum of a hob. (From Radzevich, S.P., *ASME Journal of Mechanical Design*, 128(4), 803–811, 2006. With permission.)

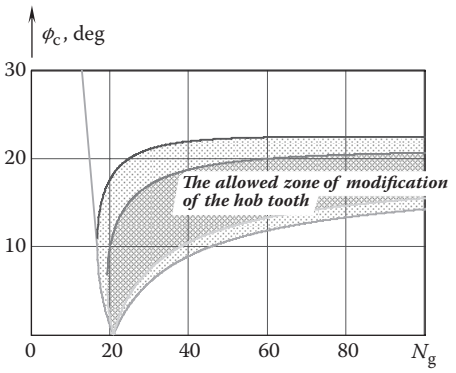

FIGURE 16.111
Zone of satisfaction of the fifth necessary condition of proper *PSG* in a gear hobbing operation with application of an involute hob with a reduced tooth addendum. (From Radzevich, S.P., *ASME Journal of Mechanical Design*, 128(4), 803–811, 2006. With permission.)

$$\rho - \rho \sin \phi_c = [\Delta] - \delta \quad \Rightarrow \quad \rho \le \frac{[\Delta] - \delta}{1 - \sin \phi_c} \tag{16.193}$$

are derived.

An analysis similar to that above can be done for hobbing helical gears as well.

16.7.6 Illustrative Examples of the Computation

The following examples illustrate the capabilities of the approach discussed above for computation of the parameters of the modification of the tooth profile of the precision involute hob.

Computation of the actual value of the deviation Δ. Consider hobbing of a spur involute gear with a modulus $m = 10\,\text{mm}$, normal profile angle $\phi_g = 20°$, tooth number $N_g = 75$, and clearance $c = 0.25m$. For the given involute gear the rest of the design parameters, namely the pitch diameter $d_{w.g} = mN_g = 750\,\text{mm}$, the outer diameter $d_{a.g} = d_{w.g} + 2m = 770\,\text{mm}$, the root diameter $d_{f.g} = d_{w.g} \times 2 \cdot 1.25m = 725\,\text{mm}$, and the base diameter $d_{b.g} = d_{w.g}\cos\phi_g = 704.769\,\text{mm}$ can be computed (see Appendix A).

The gear is machined with a single-start $N_c = 1$ involute hob with a normal profile angle $\phi_c = 25°$. On solving Equation (16.182), the actual value of the deviation $\Delta = 4.366\,\text{mm}$ is computed.

Comparison of the actual deviation $\Delta = 4.366\,\text{mm}$ with the tolerance $[\Delta] \equiv c = 0.25m = 2.5\,\text{mm}$ [$\Delta(= 4.366\,\text{mm}) > c\ (= 2.5\,\text{mm})$] makes possible the conclusion that the given gear cannot be properly hobbed with the hob with a normal profile angle $\phi_c = 25°$. In order to reduce the actual value of the deviation Δ, an appropriate correction to the hob normal profile angle is required.

Computation of the allowed interval for the hob normal profile angle. For machining of the spur involute gear of the same design as above, the expression in Equation (16.183) yields the following permissible interval for the involute hob normal profile angle $8.398° \le \phi_c \le 21.817°$. The computed interval for the normal profile angle ϕ_c perfectly correlates with what is shown in Figure 16.108. Machining of the gear with the involute hob with a normal

profile angle within the computed interval results in the deviation $\Delta < c$ being within the tolerance.

Computation of the allowed rounding of an involute hob tooth corner. Feasibility of the reduction of the hob tooth addendum is proven above. Based on these results, as well as on the above results discussed in the previous two examples of the computations, for the gear hob with a normal profile angle $\phi_c = 25°$ the computed radius of the rounding of the hob tooth corner must not exceed $\rho \leq 2.598\,\text{mm}$. Here $[\Delta] = c = 2.5\,\text{mm}$, $\delta = 0.1\,m = 1\,\text{mm}$, and $\phi_c = 25°$. Equation (16.193) is used for computation of ρ.

16.8 Application of Hobs for Machining Gears

Spur, helical, and worm gears can be produced by hobbing. Double-helical and herringbone gears can be hobbed as well. The hobbing of gears differs by type.

16.8.1 Peculiarities of a Gear Hobbing Operation

Gears can be finished by setting the hob to full depth and making only one cut. Where the highest accuracy is desired, it is customary to make a *roughing* and *finishing* cut. Coarse pitch gears customarily are roughed (Figure 16.112) prior to the finishing cut. The roughing cut removes almost all the stock from the tooth space. Medium and fine pitch gears can do the finishing cut in one step (Figure 16.113). The finishing cut may remove from 0.25 to 1.0 mm (0.010 to 0.040 in.) of tooth thickness, depending on the size of the tooth.

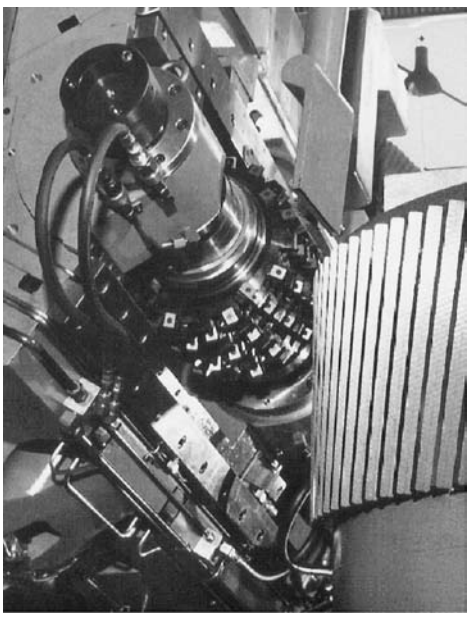

FIGURE 16.112
Roughing of a coarse pitch helical gear.

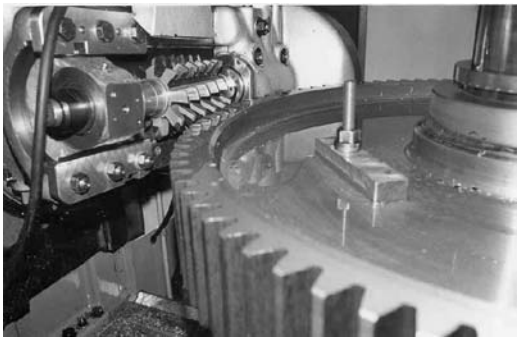

FIGURE 16.113
Hobbing of a spur gear.

The hobbing process is quite advantageous in cutting gears with wide face widths or gears that have a toothed section that is integral with a long shaft. A high degree of tooth-spacing accuracy can be obtained with hobbing. High-speed marine and industrial gears with pitch-line speeds in the range of 15 to 100 m/s (3000 to 20,000 fpm) and diameters up to 5m (200 in.) are often cut by hobbing (Figure 16.114). A few large mill gears up to 10m (400 in.) in diameter are hobbed.

When machining a gear, the generating surface *T* of the hob will make contact with the teeth on the work in a series of points as the cutting proceeds. The points, in fact, become shallow elliptical slices in the metal being cut as each hob tooth makes contact with the work. Figure 16.115 shows the generation of a tooth space by the action of the succeeding hob teeth. The envelope of the points or elliptical flecks approximates to an involute curve, and the extent to which the generated curve approaches a true involute theoretically

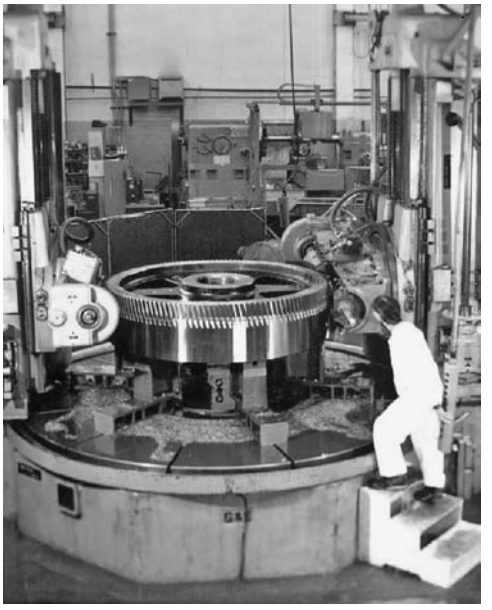

FIGURE 16.114
Hobbing of a large-scale gear.

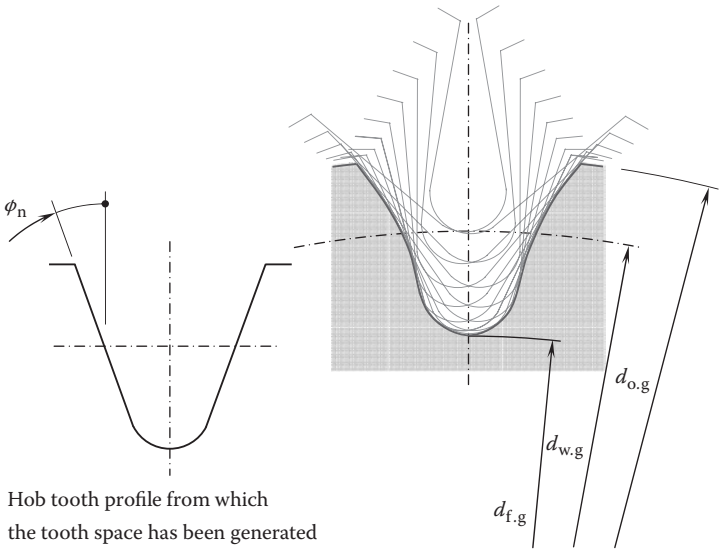

FIGURE 16.115
Tooth space in 24 toothed spur gear generated by a hobbing process.

depends on the number of teeth or gashes in the hob thread and the feed of distance the hob traverses across the face of the blank with each revolution of the work. In practice it is not easy to generate a true involute tooth form by hobbing but the continuous rolling of the gear being cut with the cutting teeth of the hob ensures that every tooth on the work is progressively generated.

The hobbing of a worm gear is illustrated in Figure 16.116. Hobs that are integral with the hob arbor (Figure 16.59) are used for this purpose.

All gears except worm gears are cut by feeding the hob across the face width of the gear. Referring to Figure 16.117, the feed motion is along the axis of rotation of the gear O_g. This axial feed motion is designated as $\mathbf{F}_{ag}$. Either the work gear travels along its axis of rotation, or the hob travels along the axis of rotation O_g of the work gear in the opposite direction. The latter depends on the design peculiarities of a particular gear hobber.

The positive direction of the feed motion $\mathbf{F}_{ag}$ corresponds to the positive direction of the rotation vector $\boldsymbol{\omega}_g$ of the work gear. The method of hobbing of gears that features the positive direction of the feed motion $\mathbf{F}_{ag}$ is customarily referred to as *climb hobbing*. Otherwise, when the direction of the feed motion $\mathbf{F}_{ag}$ is negative, the method of gear hobbing is often referred to as *conventional hobbing*.

The two possible methods of combining the direction of rotation of the hob $\boldsymbol{\omega}_c$ with the direction of the hob saddle feed $\mathbf{F}_{ag}$ are illustrated in Figure 16.118. In the first, the two motions $\boldsymbol{\omega}_c$ and $\mathbf{F}_{ag}$ are in the same direction, and in the second, the direction of feed $\mathbf{F}_{ag}$ is opposite to the rotation of the hob $\boldsymbol{\omega}_c$. The shapes of the chip produced by the two methods are also schematically shown in Figure 16.118.

It has been found that "climb" cutting has the beneficial effect on extending life of a hob between grinds. This probably results from the hob teeth taking a maximum bite f_{ag} at the commencement of the cut, which gradually diminishes in thickness as the cut proceeds, and there is consequently less rubbing at the tip. In the "conventional" method of cutting, however, the cutter does not cut cleanly until the pressure between the cutter and the work is sufficient to bite into the metal. The cutter tends to rub before actually making chips.

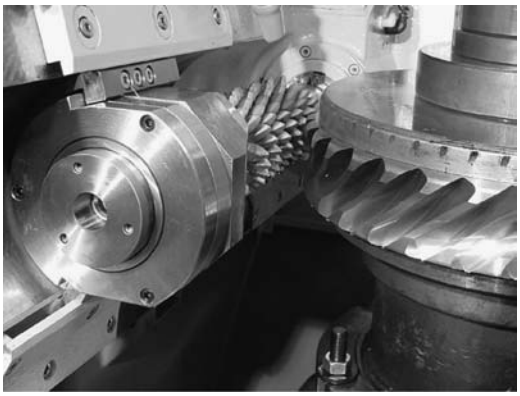

FIGURE 16.116
Hobbing of a worm gear.

Another advantage incidental to climb hobbing is that when cutting a double-helical gear and driving on the same flanks of the table worm wheel, it is possible to feed the hob downwards on both helices. This results in a better surface finish on the teeth because the swarf can be washed away and does not fall back onto the work to produce scratches; in one direction climb cutting is necessary. If possible, it is an advantage to rough hob precision gears on machines other than those used for finishing and to retain the highest precision machines for finish hobbing only.

When helical gears are being hobbed, the relative motions of the hob and work are not quite the same as those applied to cutting spur gears because it is necessary to compensate for the advancement or regression that the hob would have moved owing to the helix angle, had it been meshing with a stationary gear.

When cutting a right-hand helix, it is necessary to use a right-hand hob and similarly, a left-hand hob should be used to cut a left-hand helix. This maintains a positive drive with the direction of loading on the master table driving gear teeth always in the same direction. When a left-hand helix is cut by a right-hand hob there is a tendency for the hob to control the work by pulling it away from the table drive. As a result, the tooth profile accuracy, pitch, and surface finish suffer in quality.

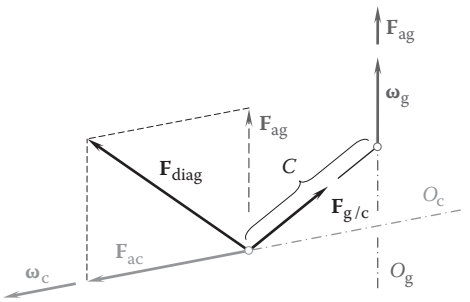

FIGURE 16.117
Feed motions in a gear hobbing process.

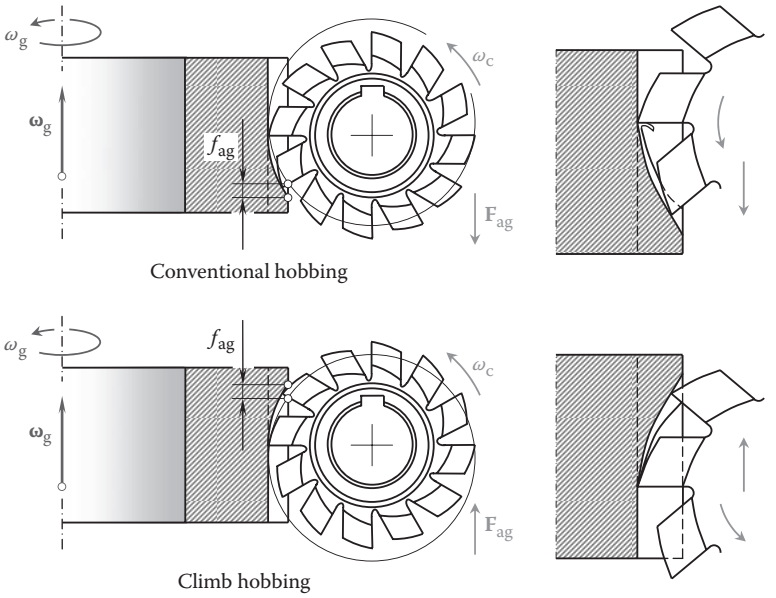

FIGURE 16.118
The difference between climb gear hobbing ($\mathbf{F}_{ag} > 0$) and conventional gear hobbing ($\mathbf{F}_{ag} < 0$) processes.

In the past it has been quite customary to use single-thread hobs for finishing and single- or double-thread hobs for roughing. Single-thread hobs give the best surface finish and tooth accuracy. In many cases, though, multiple-thread hobs are used for both roughing and finishing. When gears are shaved or lapped after hobbing, the surface finish in hobbing is not quite so important. If the gear has enough teeth and they are not an even multiple of the number of hob threads, hobs with as many as five or seven threads may be quite profitably used. For best results there should be about 30 gear teeth for each hob thread. This would mean that a five-thread hob would not be used to cut fewer than 151 gear teeth. For commercial work of moderate accuracy, the number of gear teeth may be as low as 15 per hob thread.

Worm gears are normally produced by hobbing (Figure 16.116) and the process is basically the same as that used for cutting spur or helical gears. For that reason, worm gears may be cut in a standard gear hobbing machine. In the case of worm gears, the hob is fed either *tangentially* past the blank or *radially* into the blank (Figure 16.117).

In the first case the hob travels along its axis of rotation O_c. The axial feed motion of this kind is designated as $\mathbf{F}_{ac}$. It is positive when the vector $\mathbf{F}_{ac}$ is pointed in the same direction as the rotation vector $\boldsymbol{\omega}_c$ of the hob. The feed motion is negative when the vector $\mathbf{F}_{ac}$ is pointed opposite to the direction of the rotation vector $\boldsymbol{\omega}_c$.

In the second case the hob travels toward the axis of rotation O_g of the work gear. This feed motion is designated as $\mathbf{F}_{g/c}$. It is positive when the vector $\mathbf{F}_{g/c}$ is pointed toward the axis of rotation of the work gear, and negative when the vector $\mathbf{F}_{g/c}$ is pointed outward toward the axis O_g.

With the introduction of tangential feed $\mathbf{F}_{ac}$, the process is slightly more complicated but has compensatory advantages. Simultaneously with the infeed the hob is given additional feed in the direction of its axis, or, as an important cutting refinement to improve contact

conditions, the axes of the hob and worm gear are at an angle that differs slightly from the axes of the worm and the worm gear. This process is known as "swing" hobbing. The hob is made a bit larger in diameter than the worm but of the same normal pitch and pressure angle. The worm makes correct contact with the worm wheel though the helix angles of the worm and hob differ by the amount of the swing.

When the tangential feed $\mathbf{F}_{ac}$ is applied, the hob should preferably move in a direction opposite to the rotation of the work so that backlash is taken up and there is no tendency for the hob to pull the wheel around. The rotary motions of the hob and the work gear are geared to the hob traversing motion to impart to the hob one more revolution than would be required by the ratio. This must operate at the same time that the hob is traversed one lead, to compensate for axial movement of the hob equal to the lead.

When the number of gashes in the hob is fewer than six or seven, the tangential feed $\mathbf{F}_{ac}$ should be applied in order to impart a satisfactory finish to the worm-wheel tooth profiles. This principle also applies when a fly hob is used to cut a worm wheel.

An important point to watch for when using radial infeed $\mathbf{F}_{g/c}$ for cutting worm gears by means of multistart hobs is to ensure that the number of starts and gashes in the hob do not contain a common factor greater than unity. When there is no common factor between the number of starts and gashes, all the teeth are effective in cutting the profile, which is then a much smoother curve.

A sharp hob is essential for cutting worm-wheel teeth to the required profile. Too often a poor tooth form is obtained because the hob has been rubbing instead of cutting during the finishing pass. This defect can be rectified by using a really sharp hob for the final cut and the practice has grown of employing separate hobs for roughing and finishing, particularly in quantity production. The fully relieved rounding hob is used to remove the bulk of the material, leaving about 0.005 in. (0.12 mm) per flank for finishing hob, often a serrated type made from case-hardened steel. When tungsten carbide is used for the hob material, a considerable increase in hob life between grindings is obtained, amounting to about 15-fold, and as a result, the quality of the work is improved.

In a specific case a gear hobber is capable of performing two simultaneous feed motions, namely of the axial feed $\mathbf{F}_{ag}$ along the axis of rotation of the work gear simultaneously with the axial feed motion $\mathbf{F}_{ac}$ along the axis of rotation of the hob, as shown in Figure 16.119. Combinations of the axial feed motions $\mathbf{F}_{ag}$ and $\mathbf{F}_{ac}$ result in the so-called *diagonal hobbing*

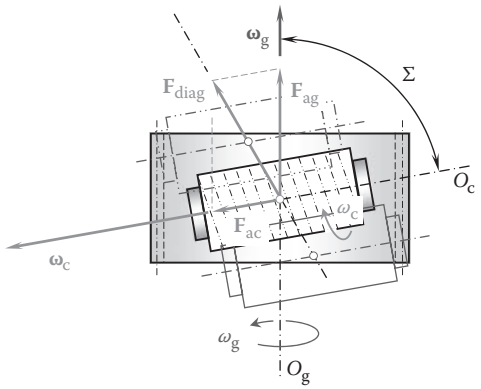

FIGURE 16.119
Combining two feed motions $\mathbf{F}_{ag}$ and $\mathbf{F}_{ac}$ performing simultaneous results in the *diagonal* method of a gear hobbing process.

of gears. Diagonal hobbing of gears can be specified by the resultant feed motion that is designated as $\mathbf{F}_{diag}$. The vector $\mathbf{F}_{diag}$ is equal

$$\mathbf{F}_{diag} = \mathbf{F}_{ag} + \mathbf{F}_{ac} \tag{16.194}$$

The tool-life of hobs in diagonal hobbing process is usually longer. In addition, use of the diagonal hobbing makes it possible to hob more accurate gears.

16.8.2 Cycles of Gear Hobbing Operations

Numerous types of cycles of gear hobbing used in practice have been developed.

In the simplest case of hobbing of a spur and/or a helical gear (Figure 16.120a), during the cutting operation the hob is carried on a spindle, the axis of which is oriented at such an angle to the work gear axis that its thread meshes with the teeth of the gear being cut. The work gear and hob are then caused to rotate with uniform motion and with relative rotational speeds in inverse ratio to the number of teeth required in the work and the threads in the hob.

The total travel distance of the hob is composed of an approach distance E, of the face width of the gear F_g, and the idle distance U. The clearance E at the beginning of the cut is necessary to run-in the hob into the stock to be cut. The clearance U is required to run-out the hob at the end of the cut.

In the method depicted in Figure 16.120a, the hob is set up at the nominal center distance $C_{g/c}$ from the work gear. Under such a scenario the hob approach distance E is greater than the idle distance U (the inequality $E > U$ is observed). The axial feed motion $\mathbf{F}_{ag}$ serves for

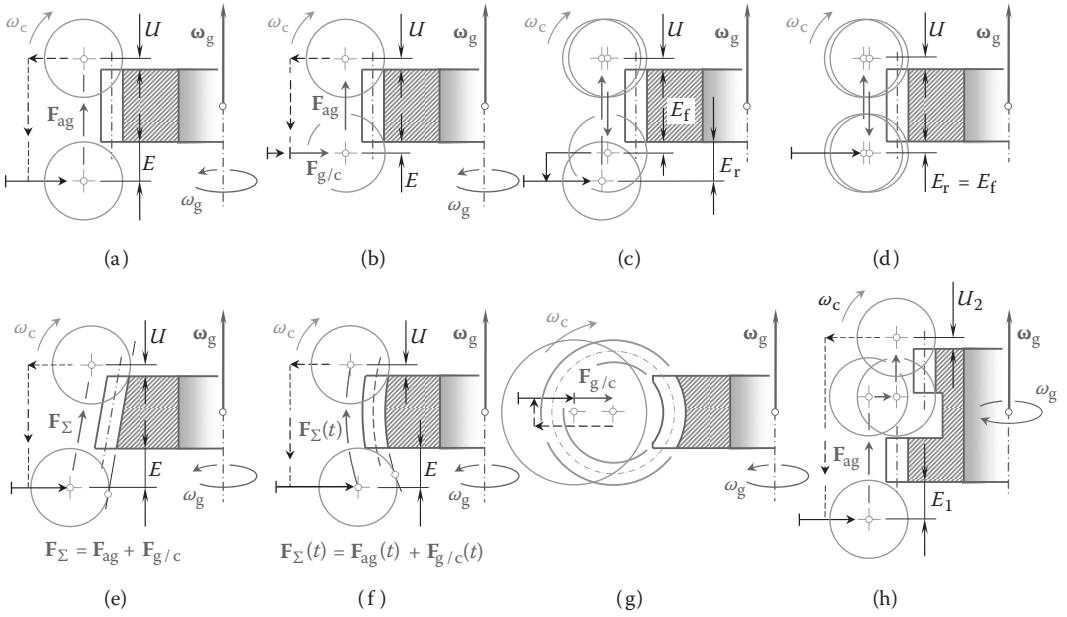

FIGURE 16.120
Examples of the cycles of a gear hobbing process.

two purposes, (a) as the infeed motion, and (b) the feed motion when the hob is generating tooth flanks of the gear.

Aiming at an increase of the productivity rate of a gear hobbing operation, it is possible to reduce the hob approach distance E, and make it equal to the hob idle distance U (Figure 16.120b). In order to make the equality $E = U$ possible, two feed motions are applied. The feed motion $\mathbf{F}_{g/c}$ is applied to infeed the hob into the stock to be cut, and the feed motion $\mathbf{F}_{ag}$ is applied for generating tooth flanks of the gear.

Precision gears and coarse pitch gears are often cut in two paths. When a gear is cut in two paths, the first and second paths could be either a combination of the cycle shown in Figure 16.120a and b, or it can be a doubled cycle that is depicted in Figure 16.120b. Figure 16.120c illustrates the first case, while the second case is illustrated in Figure 16.120d.

The axial feed $\mathbf{F}_{ag}$ can be combined with the continuous feed $\mathbf{F}_{g/c}$ in the direction of the closest distance of approach $C_{g/c}$ of the axes of rotation O_g and O_c. The resultant feed motion $\mathbf{F}_\Sigma$ in this case is equal to the vector summa

$$\mathbf{F}_\Sigma = \mathbf{F}_{ag} + \mathbf{F}_{g/c} \tag{16.195}$$

The combined feed motion $\mathbf{F}_\Sigma$ makes possible the hobbing of the so-called *beveloids* depicted in Figure 16.120e. For hobbing beveloid gears, hobbers of a special design are required.

There is one more advantage to hobbing gears in two separate paths. When roughing a gear, productivity of the material removal process is a critical issue. The accuracy of the machining is an issue of secondary importance in the roughing process. In order to increase the productivity rate of the roughing of the work gear it is recommended [37] to set the crossed-axis angle Σ_r a bit bigger compared to its nominal value Σ. It is proven that a significant increase in the productivity rate of roughing of the gears can be achieved when the crossed-axis angle on the roughing path Σ_r is set up in the range of

$$\Sigma_r = \Sigma + (0.5^\circ \ldots 3.0^\circ) \tag{16.196}$$

On the finishing path the crossed-axis angle is equal to it nominal value of Σ.

The axial feed $\mathbf{F}_{ag}$, as well as the feed motion $\mathbf{F}_{g/c}$, cannot be of constant value, but can be functions of time t [i.e., $\mathbf{F}_{ag}(t)$ and/or $\mathbf{F}_{g/c}(t)$]. Under such a scenario, the resultant feed motion $\mathbf{F}_\Sigma$ also depends on time [$\mathbf{F}_\Sigma(t)$]

$$\mathbf{F}_\Sigma(t) = \mathbf{F}_{ag}(t) + \mathbf{F}_{g/c}(t) \tag{16.197}$$

If the feed motions $\mathbf{F}_{ag}$ and $\mathbf{F}_{g/c}$ are properly timed with one another, this makes it possible to hob gears featuring a toroidal pitch surface. The possibility of hobbing a gear with a toroidal pitch surface is illustrated in Figure 16.120f.

A worm gear can be completely hobbed either when the feed motion $\mathbf{F}_{g/c}$ is applied (Figure 16.120g), or axial feed $\mathbf{F}_{ac}$ is used instead (not shown in Figure 16.120).

In designing gears to be hobbed, especially in designing cluster gears, a number of things must be considered. Because a hob needs in a clearance to "run in" at the beginning of the cut and a clearance to "run out" at the end of the cut, if the gear teeth come too close to a shoulder or other obstruction, it may be impossible to cut the part by hobbing (Figure 16.120f). If the gear is double-helical, a gap must be left between the helices for hob run-out.

The optimal cycle of hobbing of a particular gear can be developed by varying values of the feed motions $\mathbf{F}_{ag}$, $\mathbf{F}_{ac}$, and $\mathbf{F}_{g/c}$. In addition, an appropriate variation of the crossed-axis angle can be implemented when the gear is hobbed in two or more paths.

16.8.3 Minimum Hob Travel Distance

The cutter's total travel distance is an important parameter in a gear hobbing operation. The cutter's total travel distance $L = AD$ (Figure 16.121) is equal to sum of the hob approach distance E, of the gear to be machined's face width F_g, and of the hob's idle distance (or hob overrun) U

$$L = E + F_g + U \tag{16.198}$$

The hob approach $E = AB$ is the distance that the hob should travel parallel to the gear axis, from the point of initial contact between the hob and the work to the point where the center distance reaches the first gear face (at point B).

The gear face width is indicated on the part blueprint. When more than one blank per load are to be hobbed, the total face width of all the blanks must be considered.

The hob's idle distance $U = CD$ is the linear hob carriage travel beyond the second gear face C that is required to complete generation of the teeth.

There are two substantial reasons making the hob total travel distance of importance for the development of an efficient gear hobbing process. They are (a) the hobbing time and (b) the axial size of a hobbed cluster gear. The smaller the approach distance and the hob overrun, the larger the productivity rate of the gear hobbing operation. It is necessary to compute an exact value of the required total hob travel distance.

16.8.3.1 Hobbing Time as a Function of the Hob Total Travel Distance

The actual computation connected with finding the time that is required to hob a given part is relatively simple. The expression for hobbing time T is [19, 190]

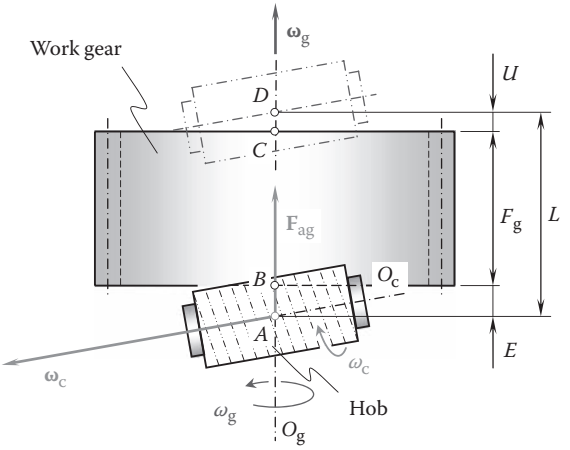

FIGURE 16.121
Hob total travel distance in climb hobbing of a cylindrical gear.

$$t = \frac{N_g L}{N_c \omega_c F_{ag}}, \text{ min} \tag{16.199}$$

where
N_g = tooth number of the work gear
L = total hob travel distance, mm
N_c = number of starts (threads) on the hob
ω_c = rotation of the hob, min^{-1}
F_{ag} = axial feed, mm per revolution, of the work gear

Equation (16.199) returns the time t required for cutting the part. It can be easily shown that hobbing time t can be represented as a function $t = t(E, F_g, U)$.

16.8.3.2 Impact of the Hob's Idle Distance on the Minimal Neck Width of the Hobbed Cluster Gear

Two distances E and U [see Equation (16.197)] make the total travel distance L greater than the gear face width F_g.

Referring to Figure 16.122, the length of the hob approach distance E can be specified as the height of the highest point B_1 on the penetration curve G/H_{pc} above the horizontal plane through the center distance—through the crossing point of the axis of rotation of the work gear O_g and the axis of rotation of the hob O_c.

When the hob is away from the upper face of the gear, the penetration curve G/H_{pc} intersects the upper face at points C_1 and C_2. Because of the intersection, it is evident that in the climb hobbing of cylindrical gears the hob's approach distance is greater than the hob's idle distance ($E > U$). In specific cases of gear hobbing the equality $E = U$ could be observed. However, under no circumstances does the hob idle distance exceed the hob approach distance.

In order to make the neck width of the cluster gear the shortest possible, hobbing of the cluster gear usually starts from the open end (where there is enough space for hob approach distance) and finishes at the opposite end (where there is lack of space for the

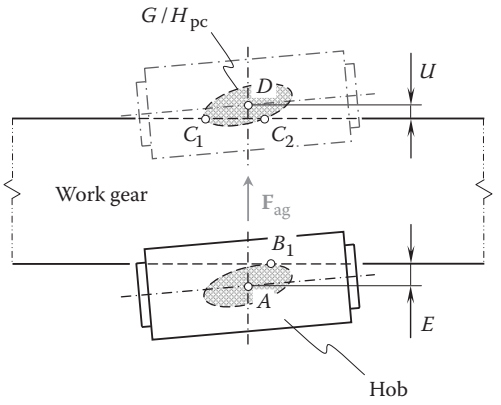

FIGURE 16.122
Comparison of the hob approach distance E and the hob idle distance U in climb hobbing of a cylindrical gear. (From Radzevich, S.P., *ASME Journal of Mechanical Design*, 124, 772–786, 2002. With permission.)

hob). This is because the minimum neck width of the cluster gear depends on the hob's idle distance U. The greater the idle distance U is required, the wider the neck width l_{min} of the cluster gear and vice versa (Figure 16.123).

The hob's idle distance must be the shortest possible to cut the time of gear hobbing and to minimize the neck width of a cluster gear. At that same time, the length of the hob idle distance U must be sufficient for the completion of the generation of the gear tooth flanks. The lack of length ΔU of the hob's idle distance U causes the deviation f_{max} of the actual tooth flank $\mathcal{G}^{(a)}$ from the desired shape $\mathcal{G}$ (Figure 16.124).

It is important to point out here that the length of the distance ΔU depends only on the relative location of the hob in the axial direction of the gear to be machined. It does not depend on the hob's outer diameter, while the maximal deviation f_{max} of the actual gear tooth flank $\mathcal{G}^{(a)}$ from the nominal gear tooth surface $\mathcal{G}$ does.

16.8.3.3 Selection of a Proper Value of the Setting Angle of the Hob

The selection of the setting angle of the hob is of critical importance when hobbing a cluster gear. The importance of proper selection of the setting angle of the hob is conveniently illustrated with the case of the hobbing of a spur gear (Figure 16.125).

A hob of conventional design features a positive ($\zeta_c > 0°$) setting angle as shown in Figure 16.125a. In this particular case, the axis of rotation of the hob is designated as ${}^{+}O_c$. It is customary to assign a value of the setting angle ζ_c of the hob equal to (or at least approximately equal to) the pitch angle ψ_c of the hob. In this case, the crossed-axis angle is obtuse ($\Sigma = 90° + \zeta_c$ is greater than 90°, i.e., $\Sigma > 90°$).

Hobs with a zero setting angle $\zeta_c = 0°$ have been known for a long time. In Figure 16.125b, the axis of rotation of the hob in this case is designated as ${}^{0}O_c$. Under such a scenario, the axis of rotation of the work gear O_g and the cutter axis of rotation ${}^{0}O_c$ cross at right angle ($\Sigma = 90°$).

Ultimately, that same spur gear can be machined with a hob that features a negative setting angle ($\zeta_c < 0°$) as shown in Figure 16.125c. In this particular case, the axis of rotation of the hob is designated in Figure 16.125c as ${}^{-}O_c$. In this case, the crossed-axis angle is acute ($\Sigma = 90° - \zeta_c$ is smaller than 90°, i.e., $\Sigma < 90°$).

A different minimum idle distance is required when hobbing a gear with hobs featuring a different setting angle. For climb hobbing of a spur gear, an impact of the setting angle ζ_c of the hob onto the required hob idle distance U_{min} is illustrated in Figure 16.126.

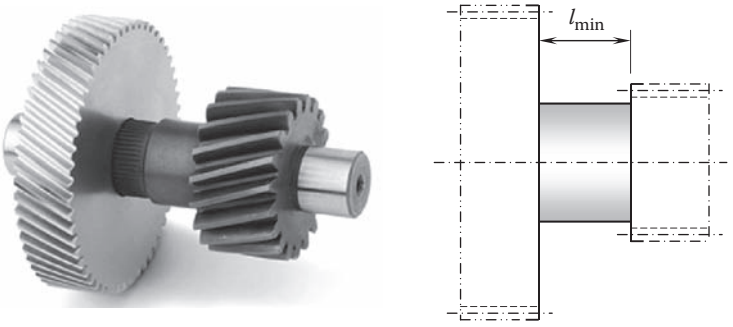

FIGURE 16.123
Minimal neck width l_{min} of a cluster gear.

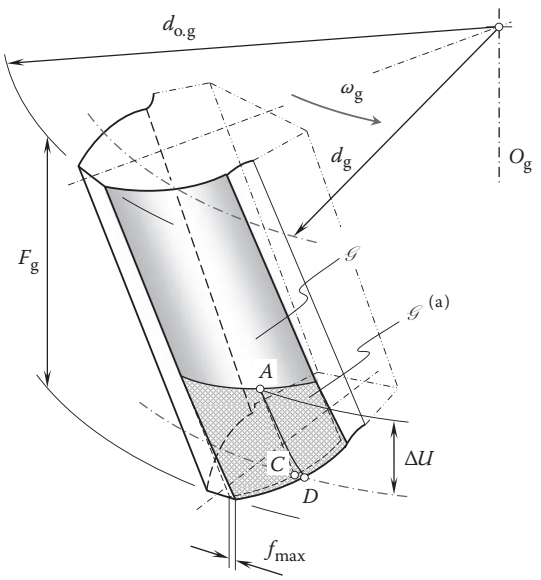

FIGURE 16.124
Lack of the hob idle distance ΔU causes deviation f_{max} of the actual gear tooth flank $\mathscr{G}^{(a)}$ from the desired gear tooth surface $\mathscr{G}$. (From Radzevich, S.P., *Gear Technology*, 20(4), 44–50, 2003. With permission.)

The simplest possible configuration of the work gear and the hob is depicted in Figure 16.126a. In this degenerated case of gear hobbing, the hob setting angle is reduced to zero ($\zeta_c = 0°$), the crossed-axis angle is equal to $\Sigma = 90°$, and the hob idle distance is equal to half the base diameter of the hob ($U = 0.5d_{b.c}$).

Generating the gear tooth flanks with the hob begins at the instant of time when the straight generating $E_1^{(t)}$ of the recessing flank of the hob thread profile in its horizontal position reaches the lower face of the work (Figure 16.126b). When the hob travel distance exceeds the length of $l_1 = d_{b.c}$, the opposite flank of the hob tooth profile begins generating the opposite side of the gear tooth profile. From this moment on, both flanks of the gear teeth are generating simultaneously.

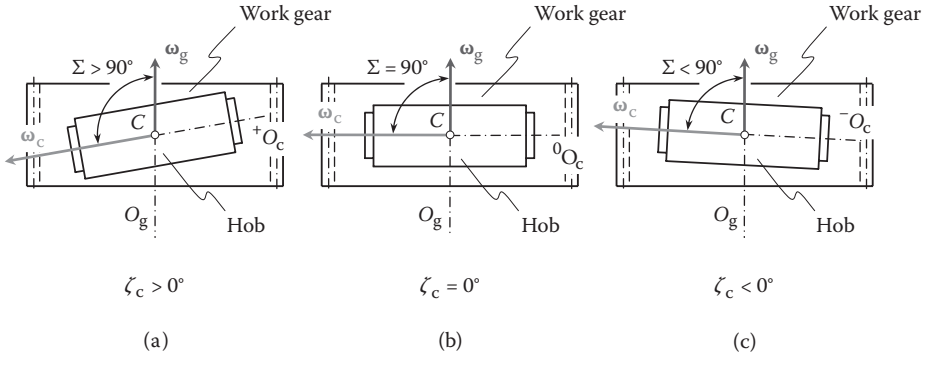

FIGURE 16.125
Configuration of a hob and a work gear when hobbing a spur gear with the hob having (a) a positive $\zeta_c > 0°$, (b) a zero $\zeta_c = 0°$, and (c) a negative $\zeta_c < 0°$ setting angle ζ_c. (From Radzevich, S.P., *ASME Journal of Mechanical Design*, 124, 772–786, 2002. With permission.)

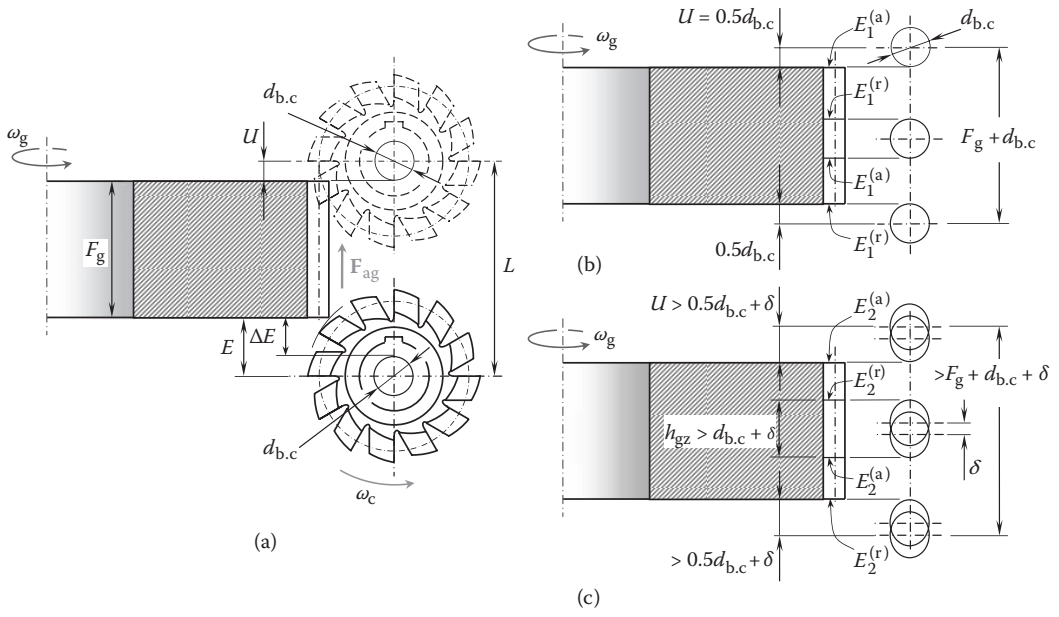

FIGURE 16.126
Impact of the setting angle ζ_c of a hob on the hob idle distance U in climb hobbing of a spur involute gear. (From Radzevich, S.P., *ASME Journal of Mechanical Design*, 124, 772–787, 2002. With permission.)

Generating the gear tooth flanks is accomplished at the instant of time when the straight generating lines $E_1^{(a)}$ of the opposite (of the approaching) flank of the hob thread profile in its horizontal position reaches the upper face of the work (Figure 16.126b). In the case under consideration, the hob's idle distance U is equal to half of the base diameter of the hob ($U = 0.5d_{b.c}$) and is the shortest feasible. To accomplish generation of the gear tooth flanks, the cutter's total travel distance must be equal to or exceed the length of $L \geq F_g + d_{b.c}$. It is of critical importance to stress here that the shortest feasible hob idle distance cannot be less than $0.5d_{b.c}$ (i.e., the inequality $U_{min} \geq 0.5d_{b.c}$ is always observed).

The above discussion can be enhanced to the case when the setting angle of the hob is not equal to zero.

Referring to Figure 16.126c, consider the configuration when the setting angle of a hob is not equal to zero and, for example, this angle is positive. In this particular case of gear hobbing the straight generating lines $E_2^{(a)}$ and $E_2^{(r)}$, which are similar to the straight generating lines $E_1^{(a)}$ and $E_1^{(r)}$ in Figure 16.126b, are additionally shifted through a certain distance δ relative to each other along the axis of rotation O_g of the work gear. The actual value of the shift δ depends on (a) the actual length of the generating zone of the gear tooth profile, and (b) the setting angle ζ_c of the hob. This question is under consideration below in greater detail. Distance δ increases the length of the hob's idle distance U and the total hob's travel distance, which is necessary to accomplish generation of the gear tooth profile.

16.8.3.4 Computation of the Shortest Allowed Hob Idle Distance

The discussion above returns only qualitatively an understanding of the impact of the setting angle of the hob onto the shortest allowed hob idle distance (Figure 16.126c). Determination of the minimum permissible hob idle distance in quantities is the next step

to be undertaken if we are to solve the problem under consideration. A conceptual solution to the problem under consideration that is accompanied with a workable formula for the computation of $U_{\min}$ has been derived by Radzevich as early as 1987 [201].

It is convenient to begin the consideration from the determination of the hob's idle distance in the case of hobbing of a spur gear.

The shortest allowed hob idle distance when hobbing a spur gear. For development of an analytical solution to the problem under consideration, the use of methods developed in descriptive geometry (*DG*-based methods) is helpful.

Consider a gear to be machined that is specified by the following set of design parameters: (a) the outer diameter $d_{o.g}$, (b) the pitch diameter d_g, (c) the root diameter d_f, (d) the tooth addendum a_g, (e) the tooth dedendum b_g, and (f) the whole height h_t of the tooth as shown in (Figure 16.127).

The auxiliary generating rack $\mathscr{R}_T$ is conjugate to the gear being machined. The auxiliary rack $\mathscr{R}_T$ is specified by (a) the tooth addendum $a_{\mathscr{R}} = b_g$, (b) the tooth dedendum $b_{\mathscr{R}} = a_g$, (c) the whole tooth height h_t, and (d) the profile angle $\phi_{\mathscr{R}}$ that is equal to the profile angle of the gear tooth on the pitch cylinder (i.e., $\phi_{\mathscr{R}} = \phi_g = \phi_n$).

The rack $\mathscr{R}_T$ performs a straight steady motion with linear velocity $V_{\mathscr{R}}$. The straight motion $V_{\mathscr{R}}$ of the generating rack $\mathscr{R}_T$ is timed with the rotation ω_g of the gear.

The axis of rotation O_c of the hob is remote at a center distance $C_{g/c}$ relative to the axis of rotation O_g of the gear. The axis O_c makes the crossed-axis angle Σ with the gear axis O_g. The crossed-axis angle Σ is equal to $\Sigma = 90° - \zeta_c$. The rotation of the hob ω_c is synchronized with rotation of the gear ω_g.

It is customary to assign subscript 1 to projections of all elements (namely, of all points, of all lines, etc.) onto the horizontal plane of projections π_1. Subscript 2 is assigned to the projections of the corresponding points, lines, and so forth onto the vertical plane of projections π_2.

The tooth profile of the gear to be machined and tooth profile of the auxiliary generating rack are conjugate to each other. In their relative motion, the line of action of the approaching side of the teeth profile is designated as $l_{LA}^{(a)}$. The line of action of the recessing side of the teeth profile is designated as $l_{LA}^{(r)}$. The lines of action $l_{LA}^{(a)}$ and $l_{LA}^{(r)}$ intersect each other at the pitch point *P*. Projections of these elements onto the horizontal plane of projections π_1 are denoted as P_1, $l_{LA}^{(a)} = a_1b_1$, and $l_{LA}^{(r)} = c_1d_1$ (Figure 16.127). Point *a* is the point of intersection of the approaching portion of the line of action $l_{LA}^{(a)}$ with the hob outer diameter $d_{o.c}$. It corresponds to the beginning of the generation zone. Point *d* is the point of intersection of the recessing portion of the line of action $l_{LA}^{(a)}$ with the hob outer diameter $d_{o.c}$. It corresponds to the end of the generation zone. At that same time, point *a* indicates the end of the roughing zone. The beginning of the roughing zone is denoted as $\mathfrak{R}$. This point is located at the intersection of the outer diameter $d_{o.g}$ of the gear with the outer diameter $d_{o.c}$ of the hob.

At the beginning of the generation of the gear tooth profile, the straight generating line *ae* of the generating surface of the gear hob (i.e., the characteristic line $E^{(a)}$ is in tangency with the hob base cylinder of diameter $d_{b.c}$ at point *e*). The characteristic line $E^{(a)}$ remains orthogonal to the corresponding line of action $l_{LA}^{(r)}$ through the period of the tooth profile generation. At the end of the generating zone, the straight generating line *df* of the generating surface of the gear hob (i.e., the characteristic line $E^{(r)}$) is in tangency with the hob base cylinder at point *f*. The characteristic line $E^{(r)}$ retains perpendicular to the corresponding line of action $l_{LA}^{(r)}$ through all the period of the tooth profile generation.

Figure 16.127 is helpful for a clear understanding of what the generating zone is in nature.

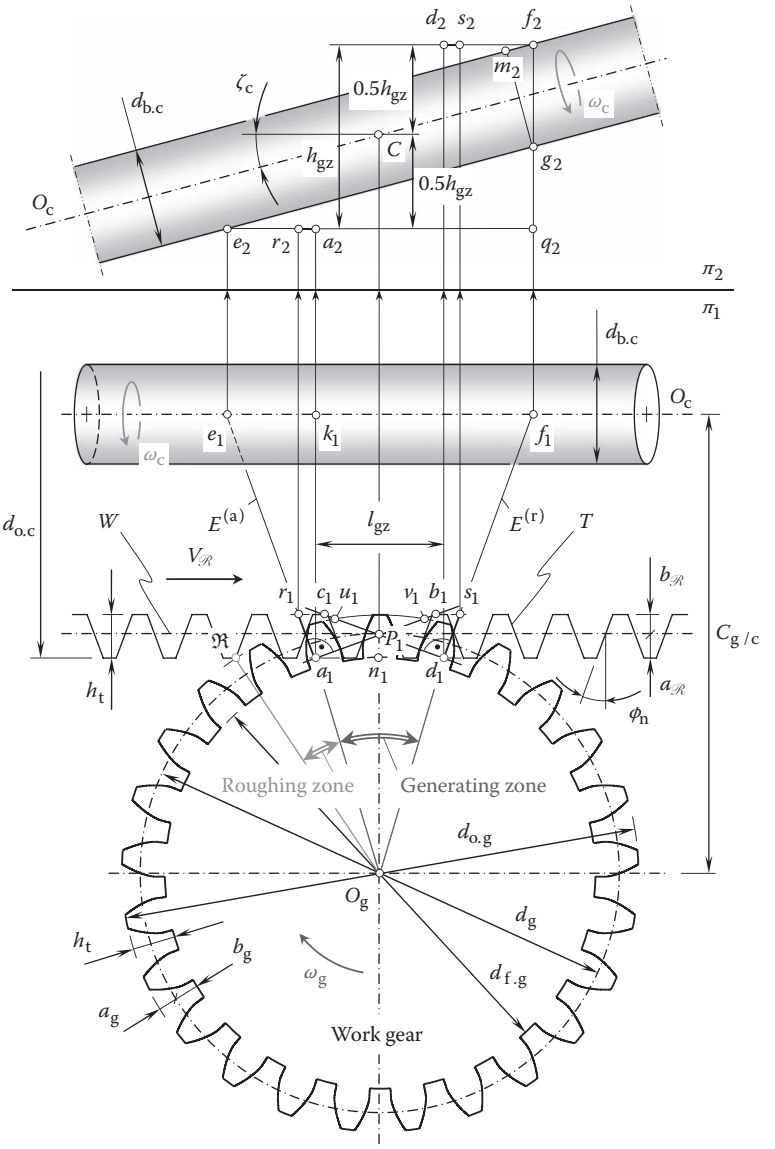

FIGURE 16.127
Determination of the shortest permissible hob idle distance in hobbing of a spur involute gear. (From Radzevich, S.P., *ASME Journal of Mechanical Design*, 124, 772–788, 2002. With permission.)

The height h_{gz} of the generating zone is equal to $h_{gz} = f_2q_2 = f_2g_2 + g_2q_2$. Here $f_2g_2 = d_{o.c}/\cos\zeta_c$, and, therefore $h_{gz} = d_{b.c}/\cos\zeta_c + g_2q_2$. The length of the straight-line segment g_2q_2 can be determined from the $\Delta e_2g_2q_2$. In this triangle $e_2q_2 = e_1f_1$, and therefore $g_2q_2 = e_2q_2 \tan\zeta_c = e_1f_1\tan\zeta_c$. Ultimately, the length of the straight-line segment e_1f_1 can be represented as the summa $e_1f_1 = l_{gz} + 2e_1k_1$.

The length of the generating zone can be computed from the simplified formula $l_{gz} = 2a_1n_1 = 2a_r/\tan\phi_n$ that is evident from Figure 16.127. This simplified formula has been derived under the assumption that the gear tooth number is equal to infinity ($N_g = \infty$). The

simplified formula is in wide use for performing an approximate computation. For more accurate computation, the formula [112]

$$l_{gz} = d_{o.g}\cos(\phi_n + \alpha) = \left(\sqrt{d_{o.g}^2 - d_g^2\cos^2\phi_n} - d_{o.g}\sin\phi_n\right)\cos\phi_n \tag{16.200}$$

should be used instead. Figure 16.128 was used for the derivation of Equation (16.200) [112].

The length of the straight-line segment e_1k_1 is equal to $e_1k_1 = 0.5d_{o.c}\tan\phi_n$ (see $\Delta a_1e_1k_1$). Ultimately this yields the formula

$$U = \frac{1}{2}h_{gz} = \frac{1}{2}\left(l_{gz} + d_{o.c}\tan\phi_n\right) = \frac{1}{2}\left[\left(\sqrt{d_{o.g}^2 - d_g^2\cos^2\phi_n} - d_g\sin\phi_n\right)\cos\phi_n + d_{o.c}\tan\phi_n\right] \tag{16.201}$$

for the computation of the hob's idle distance when machining a spur gear.

In a specific case of hobbing of gears with a standard tooth profile (i.e., when $a_g = m$, and $b_g = 1.25m$), Equation (16.201) casts into

$$U = \frac{1}{2}\left[\frac{mN_c\cos\phi_n}{\sqrt{1-\cos^2\phi_n\cos^2\zeta_c}\cos\zeta_c} + \left(d_{o.c}\tan\phi_n + 2.25m\cot\phi_n\right)\tan\zeta_c\right] \tag{16.202}$$

Other types of representation of Equation (16.201) are known as well.

The shortest allowable hob idle distance when hobbing a helical gear. The crossed-axis angle Σ is equal to $\Sigma = 90° - \zeta_c - \psi_g$ when hobbing a helical gear (Figure 16.129). Because of that, the height of the generating zone h_{gz} exceeds the length of the straight-line segment f_4q_4 that is similar to the straight-line segment f_3q_3 shown in Figure 16.127. The length of the straight-line segment q_4u_4 can be computed by the formula (Figure 16.129)

$$q_4u_4 = e_4u_4\sin\psi_g = e_1f_1\sin\psi_g \tag{16.203}$$

Here the length of the straight-line segment e_1f_1 has been defined above.

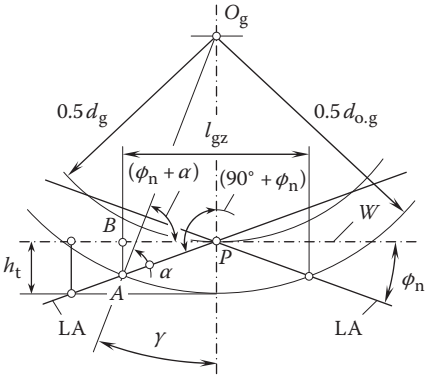

FIGURE 16.128
Length of the generating zone in hobbing of an involute gear. (From Radzevich, S.P., *ASME Journal of Mechanical Design*, 124, 772–789, 2002. With permission.)

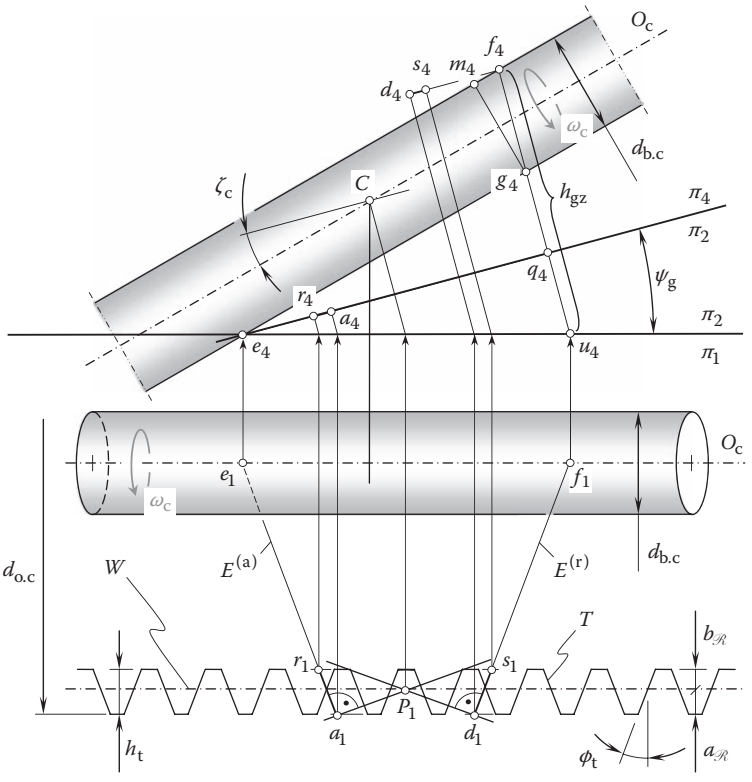

FIGURE 16.129
Determining the shortest permissible hob idle distance in hobbing of a helical involute gear. (From Radzevich, S.P., *ASME Journal of Mechanical Design*, 124, 772–790, 2002. With permission.)

A formula for the computation of the hob's idle distance when machining a helical gear can be represented in the form

$$\begin{aligned} U &= 0.5\,h_{gz} = 0.5[l_{gz} + d_{o.c}\tan\phi_n + (l_{gz} + d_o\tan\phi_n)\sin\psi_g] = \\ &= 0.5\left\{\left(\sqrt{d_{o.g}^2 - d_g^2\cos^2\phi_n} - d_g\sin\phi_n\right)\cos\phi_n + d_{o.c}\tan\phi_n + \right. \\ &\left. + \left[\left(\sqrt{d_{o.g}^2 - d_g^2\cos^2\phi_n} - d_g\sin\phi_n\right)\cos\phi_n + d_{o.c}\tan\phi_n\right]\sin\psi_g\right\} \end{aligned} \tag{16.204}$$

When the pitch helix angle ψ_g of the work gear is zero ($\psi_n = 0°$), then Equation (16.204) reduces to Equation (16.201).

In the specific case of hobbing of gears with a standard tooth profile (i.e., when $a_g = m$, and $b_g = 1.25\,m$), Equation (16.204) casts into

$$U = \frac{1}{2}\left[\frac{m\,N_c\cos\phi_n}{\sqrt{1-\cos^2\phi_n\cos^2\zeta_c}\,\cos\zeta_c} + (d_{o.c}\tan\phi_n + 2.25\,m\cot\phi_n)\tan\zeta_c \pm 1.25\,m\tan\psi_g\cot\phi_n\right] \tag{16.205}$$

Other types of representation of the formula in Equation (16.204) are known as well.

Examination of Equations (16.201) and (16.204) reveals that the hob's idle distance U does not depend on the outer diameter $d_{o.c}$ of the hob when the gear is hobbed with the hob with a zero setting angle $\zeta_c = 0°$. In cases when the setting angle of the hob is not equal to zero ($\zeta_c \neq 0°$), the hob's idle distance U depends on the hob's outer diameter.

16.8.3.5 Impact of Tolerance onto the Shortest Possible Hob Idle Distance

The generation of tooth flanks of both sides of the gear tooth is complete if and only if the hob passes beyond the upper face of the work gear at a distance that is equal to or exceeds the hob's idle distance U. In cases when this requirement is not fulfilled and the actual hob's idle distance $U^{(act)}$ is shorter at a certain distance ΔU than the nominal hob's idle distance U (i.e., $U^{(act)} = U - \Delta U$), the actual profile AD in the longitudinal direction of the gear tooth deviates from the desired profile AC (Figure 16.130). The maximum deviation is observed at point D at which deviation is equal to δ (the maximum deviation is designated as f_{max} if measured in transverse plane, and is equal to $f_{max} = CD$). The maximum allowable deviation δ must not exceed the tolerance $[\delta]$ for accuracy of the gear tooth flank.

Because of the tolerance $[\delta]$, the hob's idle distance can be considerably reduced. Referring to Figure 16.130, the reduction ΔU of the minimum allowable hob idle distance U can be expressed in terms of the tolerance $[\delta]$ [146]

$$\Delta U(\delta) = \frac{-[\delta]\cos\phi_n \tan\psi_g + \sqrt{[\delta]^2 \cos^2\phi_n \tan^2\psi_g - \left[[\delta]^2 \dfrac{\cos^2\phi_n}{\cos^2\psi_g} - 2R_g[\delta]\right]}}{\cos\psi_g} \tag{16.206}$$

For engineering application, a simplified approximated formula

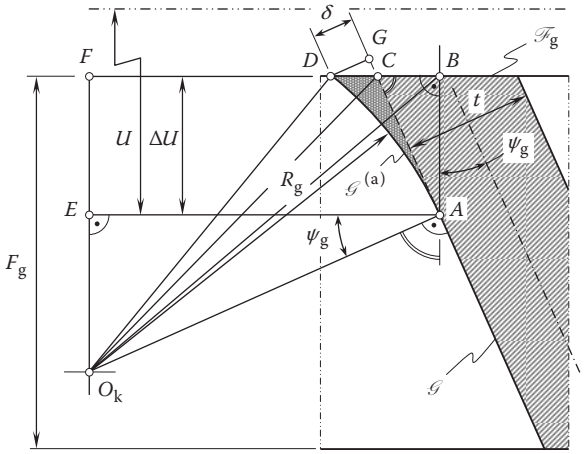

FIGURE 16.130
The desired $\mathcal{G}$ and actual $\mathcal{G}^{(a)}$ tooth flanks of a hobbed gear. (From Radzevich, S.P., *Gear Technology*, 20(4), 44–50, 2003. With permission.)

$$\Delta U(\delta) \cong \frac{\sqrt{2R_g[\delta]}}{\cos\psi_g} \tag{16.207}$$

for the computation of the distance $\Delta U(\delta)$ can be used.

It is assumed here in Equation (16.207) that the radius R_g is equal to $R_g \cong R_{l.c}$, where $R_{l.c}$ denotes the first principle radius of curvature of the generating surface T of the hob.

The first principal radius of curvature $R_{l.c}$ can be computed from the expression (see Equation (16.115) that is also available from Appendix A

$$R_{1.c} = \frac{\sqrt{d^2 - d_{b.c}^2}}{2\sin\psi_c \sin\phi_n} \tan\psi_{b.c} \tag{16.208}$$

The derivation of Equation (16.208) can be found in [158].

For the computation of the base helix angle $\psi_{b.c}$, Equation (16.61) and/or Equation (16.66)

$$\psi_{b.c} = \tan^{-1}\left(\frac{\sqrt{\sin^2\phi_n + \tan^2\zeta_c}}{\cos\phi_n}\right) \tag{16.209}$$

can be used. The expression for $\psi_{b.c}$ is also available in Appendix A.

An example of graphical interpretation of the function $\Delta U = \Delta U(\delta)$ is depicted in Figure 16.131. This graph indicates that incorporation of deviation δ even of a small value makes possible a significant reduction ΔU of the hob's idle distance U. The bigger the outer diameter $d_{o.c}$ of the hob, the bigger the allowable distance ΔU and vice versa.

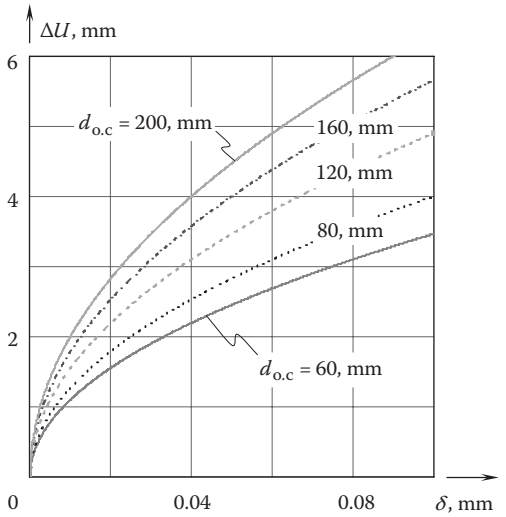

FIGURE 16.131
Impact of the deviation δ on the length ΔU (for cutting gears with hobs of different outer diameters $d_{o.c}$). (From Radzevich, S.P., *ASME Journal of Mechanical Design*, 124, 772–786, 2002. With permission.)

As shown by Radzevich [146], the neck width reduction up to 20% or so can be achieved by the appropriate computation of the hob's idle distance U. A reduction of the neck width of a cluster gear entails the corresponding reduction of size and weight of a cluster gear as well as the weight reduction of the shafts and the housing.

The results of the computation of the hob's idle distance can be entered into Equation (16.199) for the computation of hobbing time.

Computation of $l_{\min}$ of when $d_{o.g}^{(2)} >> d_{o.g}^{(1)}$. Consider computation of the shortest allowable neck width of a cluster gear that features considerable difference between the outer diameter $d_{o.g}^{(1)}$ of the smaller gear and the outer diameter $d_{o.g}^{(2)}$ of the bigger gear, as shown in Figure 16.132.

In the case under consideration, the collision of the hob of a certain outer diameter $d_{o.c}$ and of the upper face of the bigger gear at a point a could occur. The minimum allowable neck width $l_{\min}^{(1)}$ of the cluster gear must be sufficient to avoid the collision while hobbing the smaller gear.

The minimum allowable neck width $l_{\min}^{(1)}$ of the cluster gear can be represented as the summa of the straight-line segment bd, and of the projections of the straight-line segments cd and ac onto the axis O_g of the cluster gear. The length of the straight-line segment bd is equal to half of the hob's idle distance U. Projection of the straight-line segment cd onto the cluster gear axis is equal to $0.5l_{gz}\cos\Sigma$. In addition, projection of the straight-line seg-

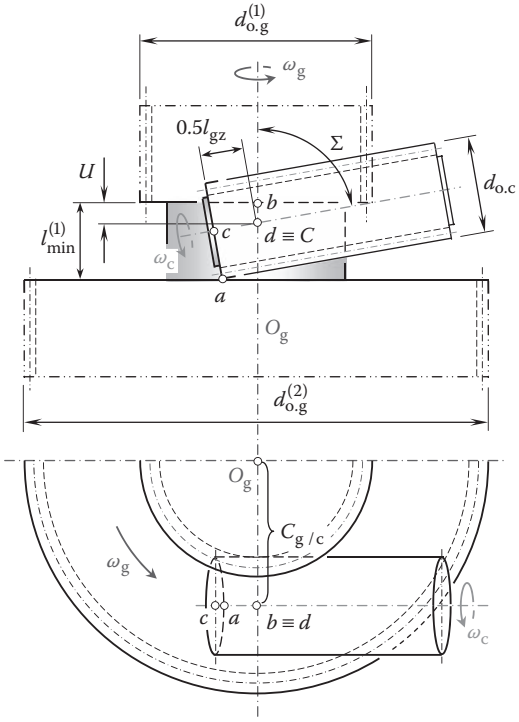

FIGURE 16.132
Determining the shortest allowed neck width $l_{\min}^{(1)}$ of a cluster gear that features considerable difference between the outer diameter $d_{o.g}^{(1)}$ of a smaller gear and the outer diameter $d_{o.g}^{(2)}$ of a bigger gear. (From Radzevich, S.P., *ASME Journal of Mechanical Design*, 124, 772–787, 2002. With permission.)

ment *ac* onto the same axis is equal to $0.5d_o \sin\Sigma$. The consideration immediately yields the formula

$$l_{min}^{(1)} = 0.5(l_{gz}\cos\Sigma + d_{o.c}\sin\Sigma + U) \tag{16.210}$$

for computation of the minimum allowable neck width $l_{min}^{(1)}$ of the cluster gear.

For a cluster gear of a given design, the shortest hob idle distance U, computed from Equation (16.201), allows for the shortest minimum allowable neck width $l_{min}^{(1)}$. As such, the cluster gear is shorter in its axial direction and its weight is lighter. It can be assembled with a shorter shaft that also is shorter in its axial direction and its weight is smaller. The gear train that is composed of such cluster gears needs smaller housing that is lighter as well.

Computation of l_{min} when $d_{o.g}^{(2)}$ and $d_{o.g}^{(1)}$ are of comparable value. Consider computation of the permissible shortest neck width of a cluster gear that features no considerable difference between the outer diameter $d_{o.g}^{(1)}$ of the smaller gear and the outer diameter $d_{o.g}^{(2)}$ of the bigger gear, as shown in Figure 16.133.

In the case under consideration, the collision of the hob with an outer diameter $d_{o.c}$ and of the upper face of the bigger gear at point *e* could occur. The minimum allowable neck

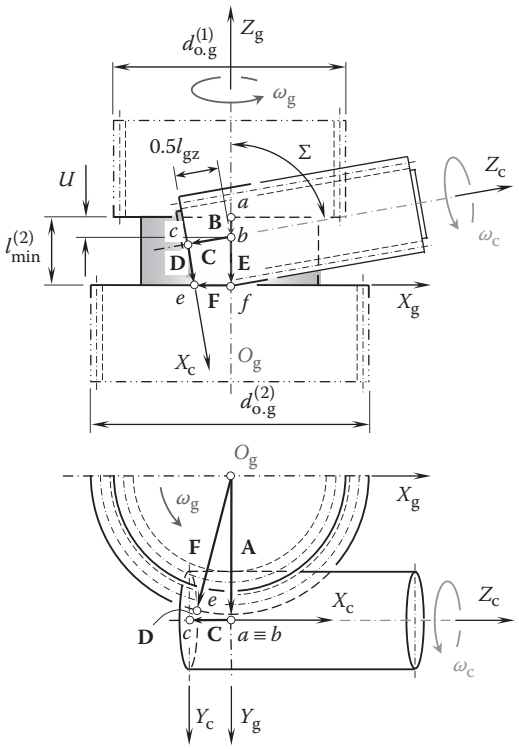

FIGURE 16.133
Determining the shortest allowed neck width $l_{min}^{(2)}$ of a cluster gear that feature a comparable the outer diameter $d_{o.g}^{(1)}$ of a smaller gear and the outer diameter $d_{o.g}^{(2)}$ of a bigger gear. (From Radzevich, S.P., *ASME Journal of Mechanical Design*, 124, 772–788, 2002. With permission.)

width $l^{(2)}_{\min}$ of the cluster gear must be sufficient to avoid the collision while hobbing the smaller gear.

To determine the minimum allowable neck width $l^{(2)}_{\min}$ of a cluster gear, it is convenient to construct four vectors **A**, **B**, **C**, and **D** shown in Figure 16.133. The vector **A** is located within the lower face of the smaller gear and is pointed out from its axis O_g parallel to the direction of the center distance $C_{g/c}$. The vector **B** is pointed out from the end *a* of the vector **A**. It is parallel to the axis of rotation O_g of the cluster gear. The length of the vector **B** is equal to the hob's idle distance U to be determined. The vector **C** is pointed out from the end *b* of the vector **B**. It is directed along the hob axis of rotation O_c toward point *c*. The length of the vector **B** is equal to the distance between the center distance $C_{g/c}$ and the closest hob face *c*. Finally, the vector **D** is pointed out from the end *c* of the vector **C**. It is directed along the hob face radius toward point *e* of contact of the upper face edge of a bigger gear and the edge of the closest face of the hob (see Figure 16.133).

The minimum allowable neck width $l^{(2)}_{\min}$ of the cluster gear can be represented as the projection of summa of the vectors (**A** + **B** + **C** + **D**) onto the axis of rotation O_g of the cluster gear $l^{(2)}_{\min} = \mathrm{Pr}_{Og}(\mathbf{A} + \mathbf{B} + \mathbf{C} + \mathbf{D})$. In this equation, the equality $|\mathbf{B}| = U$ takes place.

In order to complement the set of the vectors **A**, **B**, **C**, and **D** to a close loop of vectors, two complementary vectors **E** and **F** are constructed. The vectors **E** and **F** make possible the equality (**A** + **B** + **C** + **D**) = (**E** + **F**). The last equality can be solved with respect to U (remember that $|\mathbf{B}| = U$). In this way the smallest allowable hob idle distance for the machining of a given cluster gear with a given hob can be determined [112].

Another approach for the computation of the minimum allowable neck width $l^{(2)}_{\min}$ of a cluster gear is based on the following consideration.

The round edge of the left-hand face of the hob is colliding with the round edge of the upper face of the larger gear at point *e* (Figure 16.133). Once coordinates of the point *e* are expressed in terms of the minimum allowable neck width $l^{(2)}_{\min}$ of a cluster gear, then the neck width can be computed as a solution to a set of two equations. These equations analytically describe (a) the round edge of the upper face of the bigger gear, and (b) the round edge of the left-hand face of the hob. It is important to point out here that both of the equations should be represented in a common reference system.

Consider a Cartesian coordinate system $X_gY_gZ_g$, associated with the cluster gear as shown in Figure 16.133.

In the reference system $X_gY_gZ_g$ equation, the round edge of the upper face of the larger gear allows for representation in matrix form

$$\mathbf{r}_{eg}(\varphi_g) = 0.5\, d_{o.g} \begin{bmatrix} \cos\varphi_g \\ \sin\varphi_g \\ 0 \\ 1 \end{bmatrix} \tag{16.211}$$

where

$\mathbf{r}_{eg}$ = position vector of a point of the round edge of the upper face of the larger gear
φ_g = angular parameter of the round edge of the upper face of the larger gear
$d_{o.g}$ = outer diameter of the bigger gear

Similarly, a Cartesian coordinate system $X_cY_cZ_c$, associated with the hob is shown in Figure 16.133.

In the reference system $X_cY_cZ_c$, the round edge of the left-hand face of the hob allows matrix representation

$$\mathbf{r}_{ec}(\varphi_c) = 0.5\, d_{o.c} \begin{bmatrix} \cos\varphi_c \\ \sin\varphi_c \\ 0 \\ 1 \end{bmatrix} \tag{16.212}$$

where

$\mathbf{r}_{ec}$ = position vector of a point of the round edge of the left-hand face of the hob
φ_c = angular parameter of the round edge of the left-hand face of the hob
$d_{o.c}$ = outer diameter of the hob

The set of two equations, that is, of Equations (16.211) and (16.212), can be solved if both are represented in a common coordinate system. For example, the equations can be represented in the coordinate system $X_gY_gZ_g$. In such a case, Equation (16.212) requires being rewritten in the coordinate system $X_gY_gZ_g$.

The transition from the coordinate system $X_cY_cZ_c$ to the coordinate system $X_gY_gZ_g$ can be performed as a set of consequent translations along and rotations about the corresponding axis of coordinates.

First, the operator of translation $\mathbf{Tr}\,(0.5l_{gz}, Z_c)$ is used for the analytical description of the translation of the coordinate system $X_cY_cZ_c$ along the positive Z_c axis at the distance $0.5l_{gz}$

$$\mathbf{Tr}\,(0.5l_{gz}, Z_c) = \begin{bmatrix} 1 & 0 & 0 & 0 \\ 0 & 1 & 0 & 0 \\ 0 & 0 & 1 & -0.5l_{gz} \\ 0 & 0 & 0 & 1 \end{bmatrix} \tag{16.213}$$

The new position of the coordinate system $X_cY_cZ_c$ is denoted as $X_1Y_1Z_1$.

Second, for the analytical description of the rotation of the intermediate reference system $X_1Y_1Z_1$ about the Y_1 axis through the crossed-axis angle Σ in the counterclockwise direction to the position, which is denoted as $X_2Y_2Z_2$, the operator of rotation $\mathbf{Rt}(\Sigma, Y_1)$ is used

$$\mathbf{Rt}\,(\Sigma, Y_1) = \begin{bmatrix} \cos\Sigma & 0 & \sin\Sigma & 0 \\ 0 & 1 & 0 & 0 \\ \sin\Sigma & 0 & -\cos\Sigma & 0 \\ 0 & 0 & 0 & 1 \end{bmatrix} \tag{16.214}$$

Third, the operator of translation $\mathbf{Tr}\{-[l_{min}^{(2)} - U], Z_2\}$ is implemented for the analytical description of the translation of the intermediate coordinate system $X_2Y_2Z_2$ at the distance $-[l_{min}^{(2)} - U]$ along negative axis Z_2 to the position in which the axes of the reference system $X_2Y_2Z_2$ align with the corresponding axes of the reference system $X_gY_gZ_g$

$$\mathbf{Tr}\{-[l_{\min}^{(2)} - U], Z_2\} = \begin{bmatrix} 1 & 0 & 0 & 0 \\ 0 & 1 & 0 & 0 \\ 0 & 0 & 1 & -[l_{\min}^{(2)} - U] \\ 0 & 0 & 0 & 1 \end{bmatrix} \tag{16.215}$$

The intermediate reference systems $X_1Y_1Z_1$ and $X_2Y_2Z_2$ are not shown in Figure 16.133.

The operator **Rs**(c → g) of the resultant coordinate system transformation (i.e., of the transition from the coordinate system $X_cY_cZ_c$ to the coordinate system $X_gY_gZ_g$) can be computed as

$$\mathbf{Rs}(\mathrm{c} \rightarrow \mathrm{g}) = \mathbf{Tr}\{-[l_{\min}^{(2)} - U], Z_2\} \cdot \mathbf{Rt}(\Sigma, Y_1) \cdot \mathbf{Tr}(0.5l_{gz}, Z_c) \tag{16.216}$$

The use of the derived operator **Rs**(c → g) of the resultant coordinate system transformation makes possible the analytical representation of the position vector of point $\mathbf{r}_{ec}^{(g)}$ of the round edge of the left-hand face of the hob [see Equation (16.212)] in the coordinate system $X_gY_gZ_g$

$$\mathbf{r}_{ec}^{(g)}(\varphi_c) = \mathbf{Rs}(\mathrm{c} \rightarrow \mathrm{g}) \cdot \mathbf{r}_{ec}(\varphi_c) \tag{16.217}$$

(Remember that initially the position vector of point $\mathbf{r}_{ec}$ of the round edge of the left-hand face of the hob is specified in the reference system $X_cY_cZ_c$).

Ultimately, Equation (16.217) for the position vector $\mathbf{r}_{ec}^{(g)}$ casts into matrix equation

$$\mathbf{r}_{ec}^{(g)}(\varphi_c) = 0.5d_o \begin{bmatrix} \cos\Sigma\cos\varphi_c \\ \sin\varphi_c \\ \sin\Sigma\cos\varphi_c - 0.5l_{gz} + l_{\min}^{(2)} - U \\ 1 \end{bmatrix} \tag{16.218}$$

The round edge $\mathbf{r}_{ec}$ of the upper face of the larger gear [see Equation (16.211)] and the round edge $\mathbf{r}_{ec}^{(g)}$ of the left-hand face of the hob [see Equation (16.218)] meet each other at point *e*. At point *e* the equality

$$\mathbf{r}_{eg}(\varphi_g)\Big|_e = \mathbf{r}_{ec}^{(g)}(\varphi_c)\Big|_e \tag{16.219}$$

is observed.

The set of three equations of three unknowns; that is, φ_c, φ_g, and $l_{\min}^{(2)}$

$$0.5d_{o.c}\cos\Sigma\cos\varphi_c = 0.5d_{o.g}\cos\varphi_g \tag{16.220}$$

$$0.5d_{o.c}\sin\varphi_c = 0.5d_{o.g}\sin\varphi_g \tag{16.221}$$

$$0.5\,d_{o.c}\sin\Sigma\cos\varphi_c - 0.5\,l_{gz} + l_{min}^{(2)} - U = 0 \tag{16.222}$$

can be derived from Equation (16.219).

The solution to the set of Equations (16.220) through (16.222) returns the shortest neck width $l_{min}^{(2)}$ of a cluster gear that features not a considerable difference between the outer diameter $d_{o.g}^{(1)}$ of the smaller gear and the outer diameter $d_{o.g}^{(2)}$ of the bigger gear.

The computed shortest neck width allows for the shortest possible axial size of the cluster gear. In this case the cluster gear becomes smaller and lighter. It can be assembled with a shorter shaft that is also lighter. The gear train composed of such cluster gears requires smaller housing and is lighter as well.

16.8.3.6 Computation of the Shortest Allowable Approach Distance of the Hob

The solution to the problem of the computation of the shortest allowable approach distance of the hob is given by E. Buckingham (see pages 167–169 in [11]). The problem to be solved is formulated by E. Buckingham as follows:

> Given the proportions of a helical involute gear and the setting of the hob of given proportions, to determine the minimum distance of the center of the hob from the face of the gear before the hob starts to cut.

Referring to Figure 16.134, when

$r_{o.g}$ = outside radius of gear
$r_{o.c}$ = outside radius of hob
$C_{g/c}$ = center distance between centers of hob and gear
Σ = angle of axis of hob with face of gear
ε_g = angle on gear to point on intersection line
ε_c = angle on hob to point on intersection line

We first determine the projection of the form of the intersection of the outside cylinder of the hob with the outside cylinder of the work gear, on a plane parallel to the axes of the gear and the hob. We use the intersection of these axes on the reference plane as the origin of the coordinate system, as shown in Figure 16.134.

When x denotes abscissa of projection of intersection form
y denotes the ordinate of projection of intersection form

we have the following from the conditions shown in Figure 16.134:

$$x = r_{o.g}\sin\varepsilon_g \tag{16.223}$$

from

$$\sin\varepsilon_g = \frac{x}{r_{o.g}} \tag{16.224}$$

$$y = x\tan\Sigma + \frac{r_{o.c}\sin\varepsilon_c}{\cos\Sigma} \tag{16.225}$$

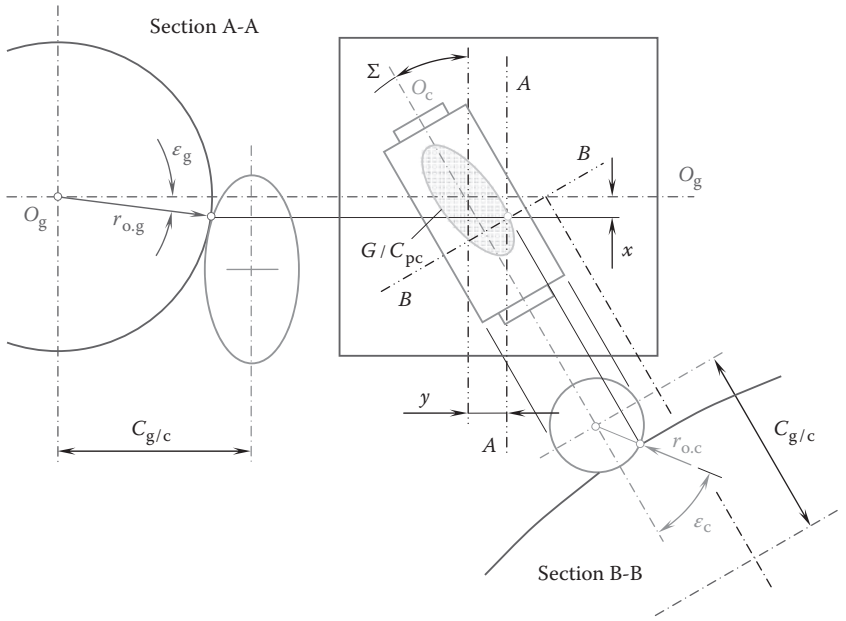

FIGURE 16.134
Computation of the shortest permissible approach distance *E* of a hob. (After Buckingham, E., *Analytical Mechanics of Gears*, New York, NY: Dover Publications, Inc., 1988, 546 pp.)

$$C_{g/c} = r_{o.g} \cos \varepsilon_g + r_{o.c} \cos \varepsilon_c \tag{16.226}$$

Rearranging and combining these equations so as to solve for values of y in terms of x and the other known values, we obtain

$$\cos \varepsilon_g = \sqrt{1 - \sin^2 \varepsilon_g} = \frac{\sqrt{r_{o.g}^2 - x^2}}{r_{o.g}} \tag{16.227}$$

$$C_{g/c} = r_{o.c} \cos \varepsilon_c + \sqrt{r_{o.g}^2 - x^2} \tag{16.228}$$

from

$$\cos \varepsilon_c = \frac{C_{g/c} - \sqrt{r_{o.g}^2 - x^2}}{r_{o.c}} \tag{16.229}$$

$$\sin \varepsilon_c = \sqrt{1 - \cos^2 \varepsilon_c} = \frac{\sqrt{r_{o.c}^2 - \left(C_{g/c} - \sqrt{r_{o.g}^2 - x^2}\right)^2}}{r_{o.c}} \tag{16.230}$$

Substituting this value of sin ε_c into the equation for y, we obtain

$$y = \frac{x \tan \Sigma + \sqrt{r_{o.c}^2 - \left(C_{g/c} - \sqrt{r_{o.g}^2 - x^2}\right)^2}}{\cos \Sigma} \tag{16.231}$$

This equation will give the coordinates of the projection of the intersection G/C_{pc} of two cylinders on a plane parallel to their axes. The maximum value of y, that is, y_m, will be the minimum distance of the center of the hob from the face of the gear before the hob starts to cut, unless the hob is too short to cover the full intersection.

An examination of Equation (16.231) shows that the maximum value of x (i.e., x_m), will be reached when

$$C_{g/c} - \sqrt{r_{o.g}^2 - x_m^2} = r_{o.c} \tag{16.232}$$

because the expression under the radical in Equation (16.231) becomes minus and imaginary when the value of x is greater than that given by this relationship. Solving this expression for x_m

$$x_m = \sqrt{r_{o.g}^2 - (C_{g/c} - r_{o.c})^2} \tag{16.233}$$

The value of y when x is equal to zero (i.e., y_0), is given by the following:

$$y_0 = \frac{\sqrt{r_{o.c}^2 - (C_{g/c} - r_{o.g})^2}}{\cos \Sigma} \tag{16.234}$$

The value of x when the value of y is a maximum (i.e., x_1), is given very closely by the following equation

$$x_1 = \frac{x_m^2 \tan \Sigma}{\sqrt{y_0^2 + x_m^2 \tan^2 \Sigma}} \tag{16.235}$$

Then

$$y_m = x_1 \tan \Sigma + \frac{\sqrt{r_{o.c}^2 - \left(C_{g/c} - \sqrt{r_{o.g}^2 - x_1^2}\right)^2}}{\cos \Sigma} \tag{16.236}$$

If the length of the hob is shorter than the distance to x_1, then the value of x_1 for use in Equation (16.236) will be given very closely by the following:
When x_c is the extension of the end of hob,

$$x_1 = x_c \cos \Sigma \tag{16.237}$$

For the computation of the shortest allowable approach distance of the hob, a corresponding computer code can be developed.

16.8.3.7 Designing a Hob Featuring a Prescribed Value of the Setting Angle

The results discussed above of the investigation of the impact of design parameters of a hob onto the minimum allowable hob idle distance make it possible to design a special-purpose hob [201] with a prescribed value of the setting angle. Hobbing of a cluster gear with a minimum allowable neck width is the main purpose of implementation of the hob of this design [132].

For hobbing of a cluster gear with a minimum allowable neck width, use of hobs with the setting angle ζ_c equal to $\zeta_c = -\psi_g$ is preferred. Hobs with the prescribed setting angle ζ_c are referred to as ζ_c–hobs [132]. In a specific case of hobbing of a spur gear, the use of ζ_c–hobs featuring a zero setting angle ($\zeta_c = 0°$) is recommended (Figure 16.125b).

For computation of the design parameters of a ζ_c–hob, a desired value of setting angle ζ_c of the hob should be known. Furthermore, the design parameters of the hob listed below: (a) module m, (b) normal profile angle $\phi_n = \phi_{\mathscr{R}}$, (c) pitch diameter $d_{w.c}$ of the hob, and (d) number of the hob starts (threads) N_c, should be given as well.

Once the principal design parameters of the ζ_c–hob are computed, then determination of the rest of the design parameters of the hob turns becomes trivial.

Two issues are of critical importance when designing a ζ_c–hob. First, the crossed-axis angle Σ should be equal to $\Sigma = 90°$. Second, the base diameter of the hob should be the smallest possible.

When hobbing a gear, the equality $\Sigma = \psi_g + \psi_c$ is observed for the crossed-axis angle Σ. In order to keep the crossed-axis angle orthogonal ($\Sigma = 90°$), the pitch helix angle of the hob ψ_c (and, thus the setting angle ζ_c of the hob) should be equal to

$$\zeta_c = \psi_c = 90° - \psi_g \tag{16.238}$$

when designing a ζ_c–hob.

Furthermore, the expression [see Equation (15.62)]

$$\psi_{b.c} = \cos^{-1}(\cos\phi_n \cos\zeta_c) \tag{16.239}$$

allows for computation of the base helix angle $\psi_{b.c}$ of the ζ_c–hob. Ultimately, Equation (15.58) returns the desired value of the base diameter $d_{b.c}$ of the ζ_c–hob.

The approximate value of the required number of starts N_c of the ζ_c–hob can be computed from Equation (15.58), which in the case under consideration casts into

$$N_c = \frac{d_{b.c} N_g \sqrt{1 - \cos^2\phi_n \cos^2\zeta_c}}{d_{w.g}\cos\phi_n} \tag{16.240}$$

Equation (16.240) returns a value $N_c^{(c)}$ of the desired number of starts N_c of the ζ_c–hob, which commonly is a number with fractions. The computed value of $N_c^{(c)}$ should be rounded to the nearest integer number N_c.

Two options are available at this point. First, the computed value $N_c^{(c)}$ of the number of starts N_c of the hob is rounded to N_c^{max}, which is the nearest integer number that exceeds the computed value of $N_c^{(c)}$. In this case the inequality $N_c^{(c)} < N_c^{max}$ is observed. Second, the computed value $N_c^{(c)}$ of the hob number of starts N_c is rounded to N_c^{min}, which is the nearest

integer number that is smaller than the computed value of $N_c^{(c)}$. In this case the inequality $N_c^{(c)} > N_c^{min}$ is observed. Further computations are split in two separate paths.

If the first option is chosen, the computations of the minimum allowable neck width l_{min} should be accomplished for N_c^{min}. When the second option is chosen, the computations of the minimum allowable neck width l_{min} should be accomplished for N_c^{min}. Practically, the solution for l_{min} under N_c^{min} often makes the shorter minimum allowable neck width l_{min} possible.

Aiming for minimization of the critical neck width of the hobbed cluster gear, it is strongly recommended to use a hob with the smallest possible outer diameter $d_{o.c}$ as well as the smallest possible base diameter $d_{b.c}$. The minimum outer diameter of the hob $d_{o.c}$ is limited to

$$d_{o.c} = d_{b.c} + 2h_c \tag{16.241}$$

where h_c designates the effective total height of the hob tooth ($h_c = a_{\mathscr{R}} - b_{\mathscr{R}}$).

For hobbing a cluster gear, it is recommended designing ζ_c–hobs with the smallest possible outer diameter $d_{o.c}$. This recommendation perfectly correlates with the earlier reported results of the research by the author [112].

The problem of minimization of the critical neck width l_{min} of the hobbed cluster gear is reduced at this point to the problem of minimization of the function $l = l(\phi_n, \zeta_c, N_c) \Rightarrow$ min. This problem is trivial in nature. The computed values of the parameters ϕ_n, ζ_c, and N_c are used on further steps for the computations of the design parameters of a particular ζ_c–hob.

When making a final decision on values of the design parameters of a ζ_c–hob, it is important to bear in mind that both the normal profile angle ϕ_n as well as the setting angle ζ_c of the hob affect the width of the top land $t_{o.c}$ of the auxiliary generating rack $\mathscr{R}_T$ of the ζ_c–hob. It is desired to keep the length of the top cutting edge of the hob the longest possible. Therefore, the width of the top land $t_{o.c}$ of the auxiliary rack $\mathscr{R}_T$ should also be the widest possible.

Examples of the function ϕ_n vs. $t_{o.c}$ are plotted in Figure 16.135. The maximum width $t_{o.c\ max}$ of the top land $t_{o.c}$ is observed when $\phi_n = \phi_{l.g}$ [132]. Here $\phi_{l.g}$ denotes the profile angle of the gear tooth at the limit diameter $d_{l.g}$.

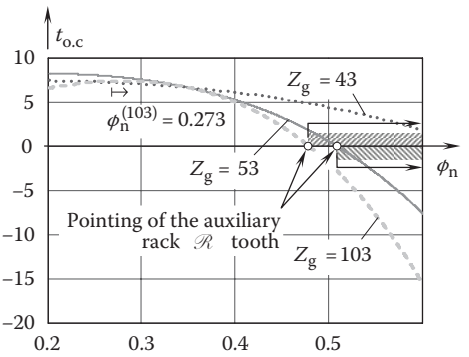

FIGURE 16.135
Impact of the normal profile angle ϕ_n on the width of the top land $t_{o.c}$ of the auxiliary generating rack $\mathscr{R}_T$ of a ζ_c–hob. (From Radzevich, S.P., *ASME Journal of Mechanical Design*, 129, 438–444, 2007. With permission.)

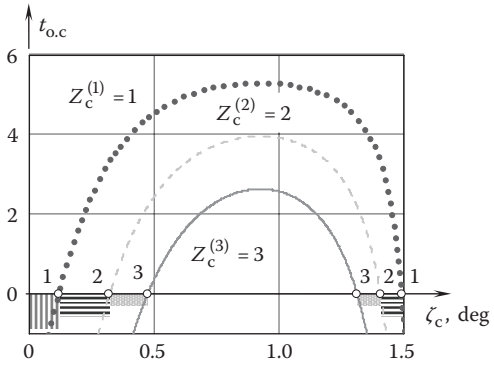

FIGURE 16.136
Impact of the setting angle ζ_c on the width of the top land $t_{o.c}$ of the auxiliary generating rack $\mathscr{R}_T$ of a ζ_c hob. (From Radzevich, S.P., *ASME Journal of Mechanical Design*, 129, 438–444, 2007. With permission.)

A graphical interpretation of the impact of the setting angle ζ_c of the ζ_c–hob onto width $t_{o.c}$ of the top land is illustrated in Figure 16.136 [132]. Functions $t_{o.c}$ vs. ζ_c have extremes. This means that there exists a combination of the principal design parameters of a particular design of the ζ_c–hob under which width $t_{o.c}$ of the hob tooth top land is maximal $t_{o.c}^{max}$.

An example of the computation of the design parameters of a ζ_c–hob. It is assumed that the design parameters of the gear to be machined are as follows: module $m = 10$ mm, normal profile angle $\phi_n = 20°$, pitch helix angle $\psi_g = 15°$, tooth number $N_g = 28$, pitch diameter $d_{w.g} = 280$ mm, outer diameter $d_{o.g} = 300$ mm, root diameter $d_{f.g} = 255$ mm, and face width $F_g = 24$ mm.

For the two-start ζ_c–hob, Equation (16.58) returns $d_{b.c} = 44.782$ mm for the base diameter of the hob. The use of the engineering formulae for the specification of the gear tooth flank (Appendix A) allows for computation of the hob pitch diameter $d_c = 70$ mm, the hob outer diameter $d_{o.c} = 95$ mm, and the pitch helix $\psi_c = 15.993°$.

The difference $\Delta\psi = \psi_c - \psi_g = 0.993°$ is negligibly small for the case under consideration.

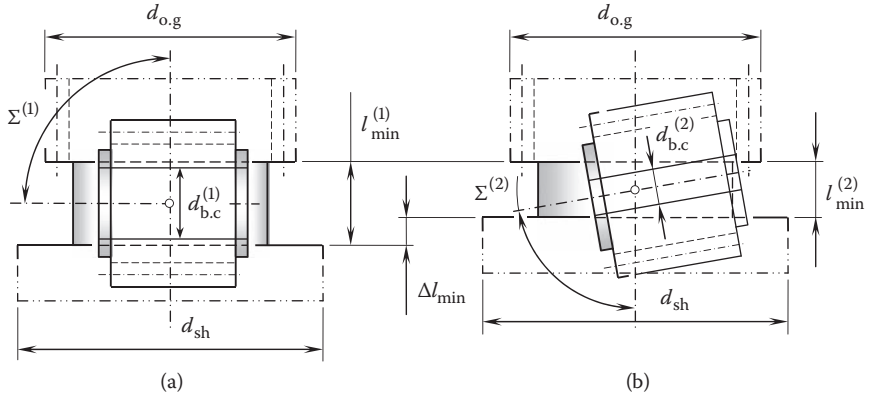

FIGURE 16.137
One more problem that relates to designing ζ_c–hobs.

The implementation of the two-start ζ_c–hob with the computed design parameters makes it possible to hob a cluster gear with the neck width in the range of $l_{min} \cong 70\,mm$.

In a specific case of hobbing of a cluster gear, a problem, the nature of which is similar to that discussed above, could arise. The problem is illustrated in Figure 16.137. When special constraints are applied, it could be necessary to answer the questions (a) whether it is preferred to hob the cluster gear when the setting angle ζ_c of the ζ_c–hob is exactly equal to $\zeta_c = -\psi_g$, but the number of the hob starts is greater, and hence, the base diameter of the hob is bigger as well (Figure 16.137a), or (b) it is preferred to sacrifice the exact equality $\zeta_c = -\psi_g$, to use a hob with a slightly smaller setting angle, and, instead, a smaller base diameter as shown in Figure 16.137b. This problem can be easily solved using for this purpose the approach just disclosed.

The disclosed approach can be enhanced to design hobs for machining gears with a noninvolute tooth profile, for example, for hobbing Novikov gears, as well as for hobbing splines, ratchets, sprockets, and so forth.

17

Gear Shaving Cutters

Although many gears are satisfactorily produced by hobbing or gear shaping without subsequent gear finishing operations, finishing operations become a necessity when high load-carrying capacities, high speeds, long wear life, or quiet operation make surface finish and tooth accuracy of major design importance. Shaving cutters are used for finishing gear tooth flanks.

17.1 Transforming the Generating Surface into a Workable Gear Shaving Cutter

The kinematics of a rotary shaving operation* is similar to that shown in Figure 16.2. Referring to Figure 17.1, the axis of rotation of the work gear O_g and the axis of rotation of the shaving cutter O_c are shown at a certain center distance $C_{g/c}$. They are crossed with each other at a certain crossed-axis angle Σ. The rotation of the work gear ω_g and the rotation of the shaving cutter ω_c are properly timed with each other. In addition to the rotations either the work gear or the shaving cutter reciprocates across the face of the shaving cutter in a transverse direction, and up-feed an increment into the cutter with each stroke of the table. The direction of the reciprocation $\mathbf{F}_c$ is perpendicular to the center distance $C_{g/c}$ between the work gear and the shaving cutter. While perpendicular to the center distance $C_{g/c}$, the actual direction of the reciprocation $\mathbf{F}_c$ with respect to the axes of rotation of the shaving cutter and of the work gear can vary. Ultimately, different kinds of gear shaving processes are recognized.

The up-feed motion $\mathbf{F}_{up}$ reduces the center distance and removes metal from the work gear tooth surfaces in the form of minute, hairlike chips. The up-feed motion $\mathbf{F}_{up}$ serves only for roughing purposes. If the motion $\mathbf{F}_{up}$ is assigned properly it does not affect the shape and geometry of the machined tooth flank $\mathcal{G}$ of the shaved gear.†

17.1.1 Generating Surface of a Shaving Cutter

Due to the similarity in the kinematics of surface generation, the equation of the generating surface of a shaving cutter for machining of an involute gear resembles that of a hob

* The rotary gear shaving process was introduced to industry by *National Broach & Machine Division* (USA) in 1932. Originally the shaving process was applied (as early as 1911) to worm wheels when serrated hobs were first used for finishing worm-wheel teeth, and the principle used then was applied to shaving in general. After generation by a full hob in a normal manner, a serrated hob removes fine shavings of metal from the flanks of the teeth and imparts a smooth finish to the flanks of the worm-wheel teeth, which then conforms to the serrated hob shape.

† It should be mentioned here that the kinematics which are almost identical to the kinematics in the rotary shaving process, are also used in generating the honing (abrasive sharing, in other words) of gears.

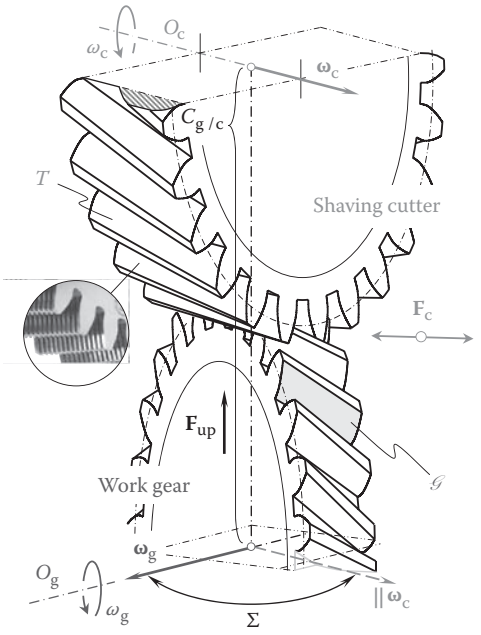

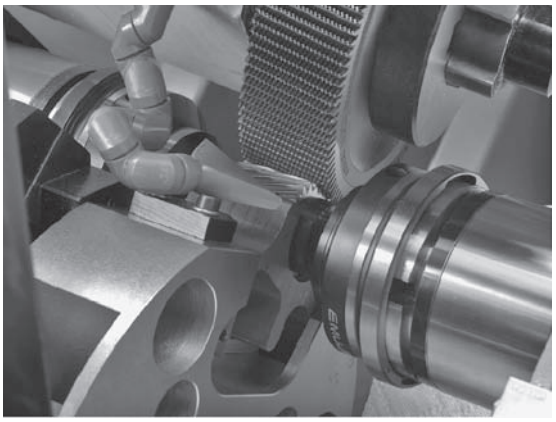

FIGURE 17.1
Configuration of the work gear and the shaving cutter in the rotary shaving process.

for machining of that same involute gear. Omitting bulky derivation, an equation of the generating surface T of a shaving cutter for machining an involute gear can be represented in matrix form [see Equation (17.54)].

$$\left.\begin{array}{l}\text{Generating surface } T\\ \text{of a gear shaving cutter}\end{array}\right| \Rightarrow \mathbf{r}_c(U_c, V_c) = \begin{bmatrix} 0.5d_{b.c}\sin V_c - U_c \sin\psi_{b.c}\cos V_c \\ 0.5d_{b.c}\cos V_c + U_c \sin\psi_{b.c}\sin V_c \\ p_{b.c}V_c - U_c\cos\psi_{b.c} \\ 1 \end{bmatrix} \tag{17.1}$$

The generation surfaces for both a hob and a shaving cutter are analytically described by similar equations, so the difference between them is mostly due to the different values of the base diameter $d_{b.c}$ as well as of other design parameters of these gear cutting tools.

17.1.2 Rake Surface of the Cutting Teeth of a Shaving Cutter

Cutting edges are made of all the shaving cutter teeth across every flank (Figure 17.2a). A slotting process is used for this purpose. After the slotting is complete, each flank of the shaving cutter tooth is grooved by serrations [6]. In this way every cutting tooth is provided with planar rake surfaces R_s. Wedges of intersection of the rake plane R_s with the generating surface T of the shaving cutter form the cutting edge CE (Figure 17.2b). Under such a scenario the cutting edges feature a zero ($\gamma_c = 0°$) or nearly zero ($\gamma_c \cong 0°$) rake angle (Figure 17.2b).

We mention here again that the chips to be removed in the gear shaving process are minute and hairlike. In practice the uncut chip thickness t is significantly below the

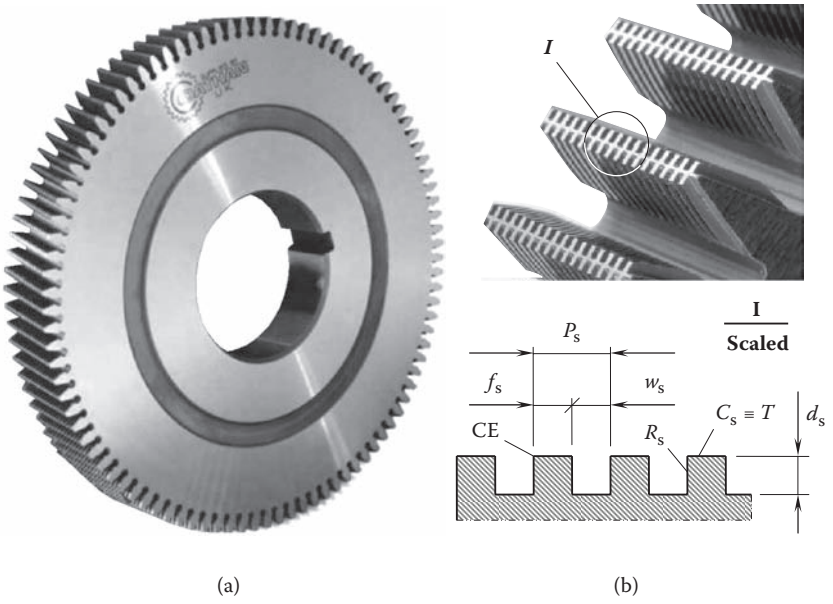

FIGURE 17.2
Closeup of a shaving cutter (a) and serrations in a shaving cutter tooth (b). (From Radzevich, S.P., *ASME Journal of Mechanical Design*, 129(9), 969–980, 2007. With permission.)

roundness ρ_c of the shaving cutter cutting edge ($t << \rho_c$). This fact is illustrated in Figure 17.3. Because the inequality $t << \rho_c$ is observed, the actual value of the rake angle γ_c does not affect the performance of the shaving process or the tool life of the shaving cutter. Regardless of the actual value of the rake angle (it can be either reasonably positive $\gamma_c > 0°$ or reasonably negative $\gamma_c < 0°$), the cutting performance of the gear shaving cutter practically remains in the same range. The cutting performance of a shaving cutter depends on the roundness ρ_c of the cutting edge of the shaving cutter rather than on the rake angle γ_c.

Because the design parameters of a shaving cutter are not restricted against the negative rake angle ($\gamma_c < 0°$), this makes it possible to design the serration with a trapezoidal profile, as shown in Figure 17.3.

There is a significant advantage of the feasibility of the negative rake angle ($\gamma_c < 0°$). Slotting cutters of conventional design feature a zero clearance angle ($\alpha_{sc} < 0°$). The cutting performance of the slotting cutters with zero clearance angles is low. It can be increased if the positive clearance angle can be created at the lateral cutting edges of the slotting cutter. If a shaving cutter is designed with a negative rake angle ($\gamma_c < 0°$), then slotting cutters with a positive clearance angle ($\alpha_{sc} < 2 \div 4°$) at the lateral cutting edges can be used in the production of the shaving cutter. Slotting of the serrations with the slotting cutter with a positive clearance angle ($\alpha_{sc} > 0°$) is preferred; cutting conditions in this case are significantly smoother.

A trapezoidal serration profile also entails a variation of width of the serration land. This effect can be used to control contact pressure in the *work gear to shaving cutter mesh*, and in that way to compensate for the variation of the contact pressure caused by the variation of the number of teeth in contact in the mesh. This issue has not yet been comprehensively investigated.

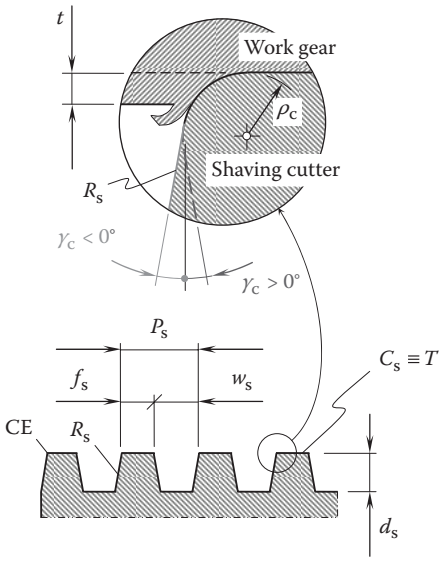

FIGURE 17.3
Serrations in shaving cutter tooth flanks with a modified profile. (From Radzevich, S.P., *ASME Journal of Mechanical Design*, 129(9), 969–980, 2007. With permission.)

17.1.3 Clearance Surface of the Cutting Teeth of a Shaving Cutter

Shaving cutters of most known designs feature a clearance surface C_s, which is congruent with the generating surface of the shaving tool (Figure 17.2b). The clearance surface C_s is shaped in the form of a screw involute surface that is conjugate to tooth flank $\mathscr{G}$ of the gear being machined. Because the surfaces C_s and T are congruent to one another, a zero clearance angle $\alpha_c = 0°$ at the cutting edges of the shaving cutter teeth is observed as the result.

17.1.4 Inclination Angle of the Cutting Edges of a Shaving Cutter

Since a shaving cutter is a finishing cutting tool, it is recommended to design it with a greater inclination angle λ of the cutting edges. It is proven by many researchers and by practice that when thin chips are being cut off, the use of cutting tools with an increased inclination angle λ is preferred.

At a point of interest m within the cutting edge of a shaving cutter, the angle of inclination λ is measured within the plane of cut P_{cv} (see Appendix D). The plane of cut P_{cv} through the point of interest m is tangent to the generating surface T of the shaving cutter. The plane of cut P_{cv} can also be specified as the plane that is perpendicular to the unit normal vector $\mathbf{n}_c$ to the surface T at point m.

The inclination angle λ is the angle that the unit normal vector $\mathbf{n}_{ce}$ to the cutting edge CE makes with the vector of resultant motion $\mathbf{V}_\Sigma$ of the cutting edge relative to the surface of the cut [$\lambda = (\mathbf{n}_{ce}, \mathbf{V}_\Sigma)$]. Computation is the only reasonable way to determine the inclination angle λ at a point of interest of the cutting edge of the shaving cutter tooth at a given instant of time. In the meantime, no special equipment for this particular purpose is available on the market.

Two vectors should be determined prior to computation of the angle of inclination λ of the cutting edge of a shaving cutter tooth. They are (a) the unit normal vector $\mathbf{n}_{ce}$, and (b) the vector of the resultant motion $\mathbf{V}_{\Sigma}$ of the cutting edge relative to the surface of the cut. Both vectors are required to be determined at the point of interest m within the cutting edge. In addition, both should be represented in a common reference system.

Referring to Figure 17.4, the unit normal vector $\mathbf{n}_{ce}$ to the cutting edge can be expressed in terms of the unit normal vector $\mathbf{n}_c$ to the generating surface T of the shaving cutter and the unit vector $\mathbf{c}_e$ that is tangent to the cutting edge ($\mathbf{n}_{ce} = \mathbf{c}_e \times \mathbf{n}_c$). The earlier derived Equation (17.55)

$$\mathbf{n}_c(V_c) = \begin{bmatrix} \sin\psi_{b.c} \sin V_c \\ \sin\psi_{b.c} \cos V_c \\ \cos\psi_{b.c} \\ 1 \end{bmatrix} \tag{17.2}$$

is valid for the unit normal vector $\mathbf{n}_c$.

The order of the multipliers in $\mathbf{n}_{ce} = \mathbf{c}_e \times \mathbf{n}_c$ is of importance when determining the unit vector $\mathbf{n}_{ce}$.

An analytical expression for the unit vector $\mathbf{c}_e$ can be derived for a shaving cutter of a given design. Consider the rake plane R_s of a shaving cutter that is perpendicular to the axis of rotation of the shaving cutter. The unit vector $\mathbf{c}_e$ is tangent to the involute profile of the shaving cutter tooth. It is located within the X_cY_c coordinate plane, and thus can be expressed only as a function of two X_c and Y_c parameters. Otherwise, if the rake plane R_s is not perpendicular to the axis of rotation of the shaving cutter, the third Z_c parameter is required to be incorporated into an expression for the unit tangent vector $\mathbf{c}_e$.

In a coordinate system $X_cY_cZ_c$ associated with the shaving cutter equation for the unit vector $\mathbf{c}_e$, the general case can be expressed in matrix form

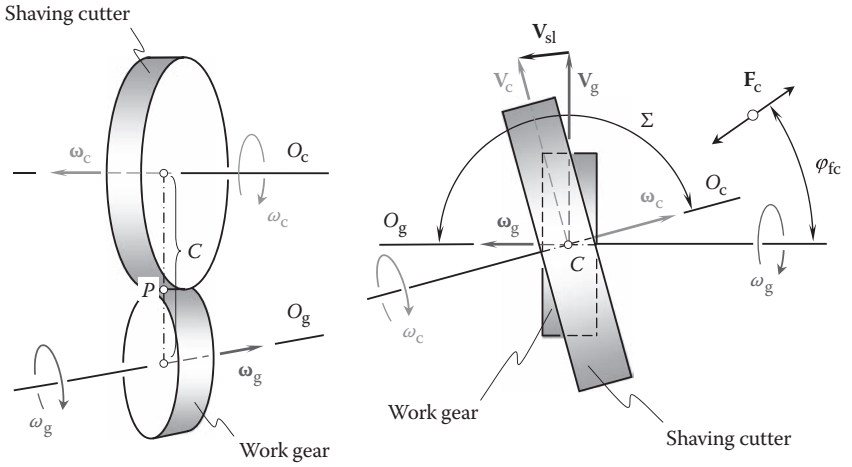

FIGURE 17.4
Schematic of the gear shaving process.

$$\mathbf{c}_e(t_{ce}) = \begin{bmatrix} X_c(t_{ce}) \\ Y_c(t_{ce}) \\ Z_c(t_{ce}) \\ 1 \end{bmatrix} \tag{17.3}$$

where t_{ce} designates the parameter of the cutting edge.

The cross product of the unit vector $\mathbf{n}_c$ [see Equation (17.2)] and the unit vector $\mathbf{c}_e$ [see Equation (17.3)] returns the required expression for the unit normal vector $\mathbf{n}_{ce} = \mathbf{c}_e \times \mathbf{n}_c$.

Vector $\mathbf{V}_\Sigma$ is also within the plane of cut P_{cv}. This vector can be represented as superposition

$$\mathbf{V}_\Sigma = \mathbf{V}_{sl} + \mathbf{V}_{pr} + \mathbf{V}(\mathbf{F}_c) \tag{17.4}$$

of three vectors, namely of (a) the vector $\mathbf{V}_{sl}$ of the sliding velocity in the lengthwise direction of the work gear tooth, (b) the vector $\mathbf{V}_{pr}$ of the profile sliding, and (c) the vector $\mathbf{V}(\mathbf{F}_c)$ due to the reciprocation motion.

Determining the vector $\mathbf{V}_\Sigma$ of the resultant motion of the shaving cutter tooth relative the work gear is a bit more complicated than determining the unit vector $\mathbf{n}_{ce}$. For this purpose, refer to Figure 17.5 in which a schematic of a gear shaving process is depicted.

The work gear rotates ω_g about its axis O_g. At the pitch point P the vector $\mathbf{V}_g$ of the linear velocity of the rotation can be expressed in terms of the rotation vector $\boldsymbol{\omega}_g$ and radius $\mathbf{R}_g$ of the work gear pitch cylinder

$$\mathbf{V}_g = \boldsymbol{\omega}_g \times \mathbf{R}_g \tag{17.5}$$

Here, the vector $\mathbf{R}_g$ can be computed from the formula $\mathbf{R}_g = \mathbf{k}_g(d_g/2)$. It is assumed here that the Z_g axis of the reference system $X_gY_gZ_g$ associated with the work gear is aligned with the shortest distance of approach $C_{g/c}$ of the axes O_g and O_c. This axis is pointed from the work gear axis toward the shaving cutter axis of rotation.

The shaving cutter rotates ω_g about its axis O_c. At the pitch point P the vector $\mathbf{V}_c$ of the linear velocity of the rotation can be expressed in terms of the rotation vector $\boldsymbol{\omega}_c$ and radius $\mathbf{R}_c$ of the shaving cutter pitch cylinder

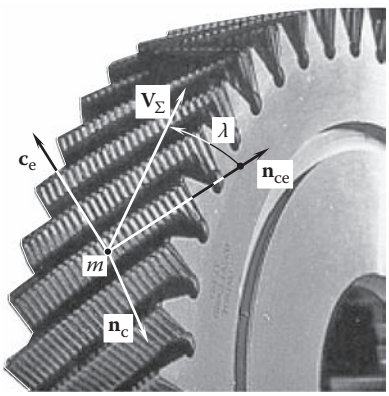

FIGURE 17.5
Angle of inclination λ of the cutting edge of a gear shaving cutter.

$$\mathbf{V}_c = \boldsymbol{\omega}_c \times \mathbf{R}_c \tag{17.6}$$

Similar to the process above, for computing the vector $\mathbf{R}_c$ the formula $\mathbf{R}_c = \mathbf{k}_c(d_c/2)$ can be used. It is assumed in the case under consideration that the Z_g axis of the reference system $X_cY_cZ_c$ associated with the shaving cutter is aligned with the shortest distance of approach $C_{g/c}$ of the axes O_g and O_c. This axis is pointed from the shaving cutter axis toward the work gear axis of rotation.

As the work gear axis O_g and the shaving cutter axis O_c are crossed at a certain crossed-axis angle Σ, the velocity vectors $\mathbf{V}_g$ and $\mathbf{V}_c$ do not align with each other, and they make a certain angle. The angle between the vectors $\mathbf{V}_g$ and $\mathbf{V}_c$ is exactly equal to the crossed-axis angle Σ (Figure 17.5).

The sliding velocity vector $\mathbf{V}_{sl}$ is the difference between the vectors $\mathbf{V}_g$ and $\mathbf{V}_c$

$$\mathbf{V}_{sl} = \mathbf{V}_c - \mathbf{V}_g \tag{17.7}$$

Both the vectors $\mathbf{V}_g$ and $\mathbf{V}_c$ in Equation (17.7) should be expressed in a common reference system.

It can be shown that for the magnitude $V_{sl} = |\mathbf{V}_{sl}|$ Equation (17.7) yields the formula

$$V_{sl} = 0.5(\omega_g d_g \sin\psi_g + \omega_c d_c \sin\psi_c) \tag{17.8}$$

where

ω_g = rotation of the work gear
ω_c = rotation of the shaving cutter
d_g = pitch diameter of the work gear
d_c = pitch diameter of the shaving cutter
ψ_g = pitch helix diameter of the work gear
ψ_g = pitch helix diameter of the shaving cutter

Note that in Equation (17.8), pitch helix angles ψ_g and ψ_c are signed values.

The profile sliding $\mathbf{V}_{pr}$ of the shaving cutter tooth relative to the work gear tooth also contributes to the speed $\mathbf{V}_\Sigma$ of the resultant motion. This contribution becomes more significant when the tooth number of the work gear and/or tooth number of the shaving cutter gets smaller. A zero profile sliding is observed at the pitch point, and it becomes greater toward the top and bottom of the work gear teeth.

The feed motion $\mathbf{F}_c$ of the shaving cutter is pointed at an angle φ_{fc} with respect to the axis O_g of the work gear (Figure 17.5). The actual value of the angle φ_{fc}, as well as magnitude of the feed motion $\mathbf{F}_c$, is known. This makes possible the derivation of an expression for the vector $\mathbf{F}_c$ in a reference system that is common for the work gear and the shaving cutter.

The components of Equation (17.4) are not discussed in detail here. Analytical expressions for the components $\mathbf{V}_{sl}$, $\mathbf{V}_{pr}$ and $\mathbf{V}(\mathbf{F}_c)$ are derived below. The only issue of critical importance at this point is that (a) the vector $\mathbf{V}_\Sigma$ is within the plane of cut P_{cv}, and (b) the vector $\mathbf{V}_\Sigma$ can be expressed in terms of (i) the design parameters of the work gear and the shaving cutter, (ii) their configuration, and (iii) their relative motion in the gear shaving process.

The magnitude of the vector of up-feed motion $\mathbf{F}_{up}$ is negligibly small compared to the vectors $\mathbf{V}_{sl}$, $\mathbf{V}_{pr}$ and $\mathbf{V}(\mathbf{F}_c)$. Therefore the vector $\mathbf{F}_{up}$ can be ignored when computing the inclination angle λ.

After the vector $\mathbf{V}_\Sigma$ is described analytically, it can be represented in matrix form as

$$\mathbf{V}_\Sigma = \begin{bmatrix} V_{\Sigma x} \\ V_{\Sigma y} \\ V_{\Sigma z} \\ 1 \end{bmatrix} \tag{17.9}$$

where $V_{\Sigma x}$, $V_{\Sigma x}$, and $V_{\Sigma x}$ are Cartesian components of the vector $\mathbf{V}_\Sigma$ of resultant motion of the cutting edge CE relative to the surface of cut P_{cv}.

Having the unit normal vector $\mathbf{n}_{ce}$ along with the vector $\mathbf{V}_\Sigma$ of the resultant motion of the cutting edge expressed in a common coordinate system, computation of the inclination angle λ becomes trivial

$$\lambda = \tan^{-1}\left(\frac{|\,\mathbf{n}_{ce} \times \mathbf{V}_\Sigma\,|}{\mathbf{n}_{ce} \cdot \mathbf{V}_\Sigma}\right) \tag{17.10}$$

The inclination angle λ is not constant but it varies within the cutting edge of a shaving cutter.

17.2 Design of the Gear Shaving Cutters

The rotary shaving cutters (Figure 17.6) are high-precision generating gear cutting tools. They have ground tooth flanks and are held to Class A and AA tolerances in all principle

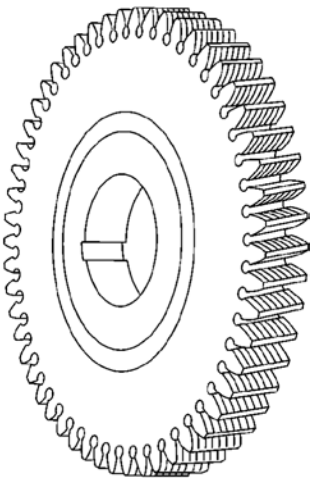

FIGURE 17.6
Closeup of a shaving cutter for rotary shaving of gears.

elements. Precision shaving cutters are utilized for finishing gears by a rotary shaving process.

Shaving cutters are almost invariably made of high-speed steel. A hardness of 63 HRC minimum after tempering is considered satisfactory.

17.2.1 Design Parameters of a Shaving Cutter

Just as the generating body of a gear shaving cutter is identical to the corresponding helical gear, many similarities are observed in the design of a gear shaving cutter and the helical gear.

The shaving cutter must have the same base pitch as the work gear it is intended to shave. To fulfill this critically important requirement, the normal diametral pitch and normal profile angle of the shaving cutter should be the same as those of the gears to be shaved [6]. However, the mandatory equality of the base pitches of the shaving cutter and the work gear can be achieved under another combination of normal diametral pitch and normal pressure angles.

It is normal for a particular shaving cutter to shave a range of gears of the same base pitch. Unlike a hob, however, it is preferable to design a shaving cutter for a restricted range of gears, and if it is economically justified, a shaving cutter designed for shaving one particular gear can be expected to give the best results.

The average recommended shaving cutter pitch diameter is 8 in. for most external gears. A 9-in. pitch diameter shaving cutter is frequently used for low tooth numbers in the work gear.

The face widths of the shaving cutters vary from 1 to 4 in., depending on the requirements and type of application. Fine-pitch shaving cutters are furnished with a face width of 3/8 to 5/8 in. and with a diameter of 3 to 4 in.

Helix angle is chosen so as to give a desired crossed-axes angle between the work gear and shaving cutter.

The shaving cutter tooth addendum is always calculated so that the shaving cutter will finish the gear profile slightly below the lowest point of contact with the mating gear. This addendum may be varied to suit fillet (root radius, conditions of undercut, protuberance) and the size of the mating gear.

Better results are obtained from shaving cutters that have no common ratio between the numbers of teeth in the shaving cutter and the work gear. Therefore, a rotary shaving cutter is usually designed with a prime number of teeth. This "hunting-tooth" condition further refines spacing errors and increases the accuracy of the shaved gear. It is also beneficial in distributing small errors that may occur in the shaving cutter.

The dedendum area of the shaving cutter is supplemented with a drilled hole to form an undercut to allow the serrating tool to clear itself during manufacturing. The hole is the run-out clearance for the serrating tool.

Holes are drilled between and at the base of the teeth of the shaving cutters to provide clearance for chips formed by the shaving operation. An unrestricted flow of coolant passes through the serrations and holes to keep the shaving cutter clean of these chips. The circle within which the holes are located is often referred to as the *hole circle*. Its diameter is chosen so as to allow for clearance between the tips of the gear teeth being shaved and the point of intersection between the shaving cutter profile and oil hole.

The holes are drilled at an angle ~1° smaller than the pitch helix angle of the shaving cutter. This is because the helix angle of a shaving cutter can vary within the tooth height, and gets smaller toward the axis of the shaving cutter.

17.2.2 Serrations on the Tooth Flanks of a Shaving Cutter

The tooth flanks of a rotary shaving cutter are serrated with multiple gashes (Figure 17.7a). The gashes (serrations) extend from top to bottom of the tooth, terminating in a clearance space at the bottom. These clearance spaces also provide unrestricted channels for constant flow of coolant to promptly dispose of chips.

There is still considerable indecision about the most suitable shape of the serrations. Commonly the serrations are shaped so that the cutting edges are located within a plane that is either perpendicular to the shaving cutter axis (Figure 17.7b) or perpendicular to the line of the tooth (Figure 17.7c). When the serrations are perpendicular to the line of the tooth as shown in Figure 17.7c, then the width of the end lands is not constant within the tooth height. In a specific case the serrations could be designed with a trapezoidal profile (Figure 17.7d). Fine-pitch shaving cutters are usually made with the serrations cut through the teeth. These tend to be rather more fragile than when the teeth support the serrations (Figure 17.7e). In this last case, the serrations with a trapezoidal profile are commonly used.

It is common practice to cut the serrations with a straight bottom that does not follow the tooth flank involute profile (Figure 17.8a). The serrations therefore do not have a constant depth d_s along the whole tooth height. This peculiarity is not due to bad conditions

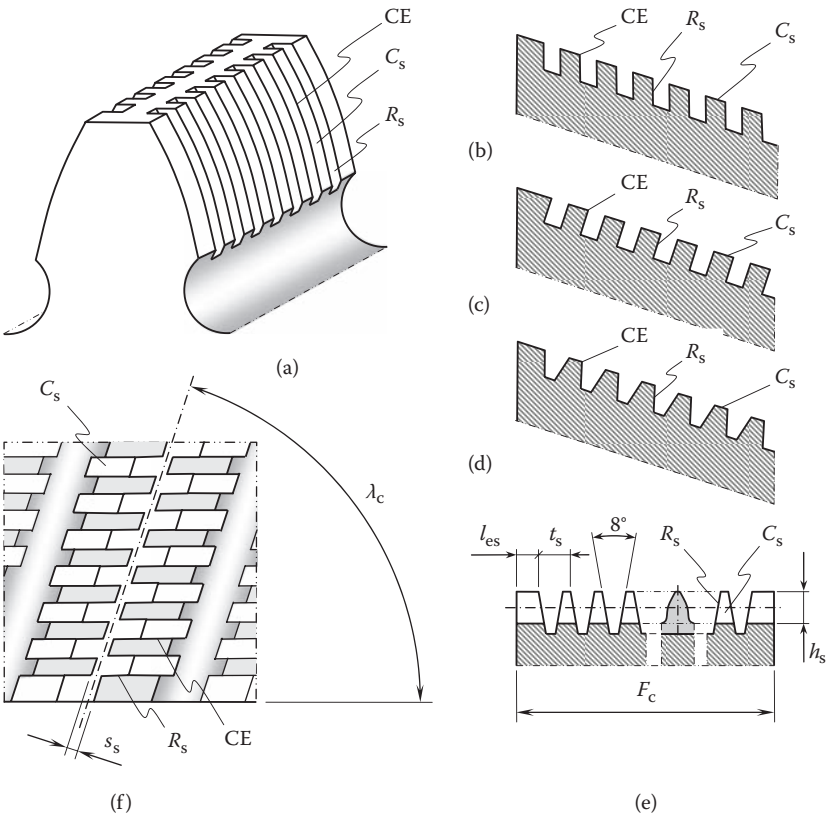

FIGURE 17.7
Practical designs of serrations in a shaving cutter tooth flank.

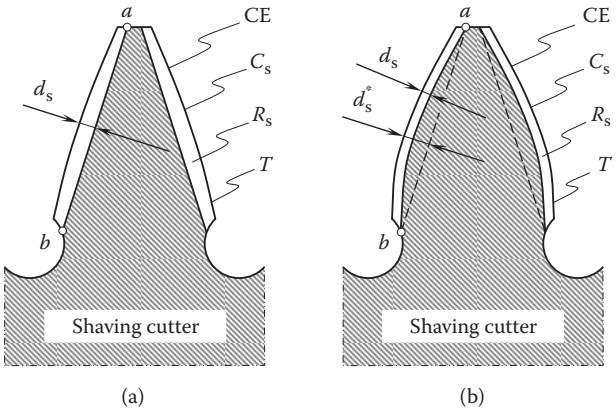

FIGURE 17.8
Serrations of two types of shaving cutter tooth flanks.

of cutting when machining the serrations, but mostly due to the complexity of the kinematics of machining of the serrations that feature equal the serration depth. Most slotting machines available on the market are capable of providing the slotting cutter with a rectilinear motion. In order to follow the involute profile, the machine kinematics would be greatly complicated without granting the shaving cutter a real advantage in performance.

However, in a specific case of producing shaving cutters with a low tooth number, the convexity (d_s^*) of the shaving cutter tooth profile cannot be neglected. It is not allowed to approximate the bottom of the serrations with a straight line segment *ab*. Therefore, the serrations have an involute form and a constant depth throughout (Figure 17.8b).

The serrations in the shaving cutter tooth flank (Figure 17.2b) can be specified by (a) the serration pitch P_s, (b) the serration land width f_s, (c) the serration space width w_s, and (d) the serration depth d_s.

The serration pitch and the division between the land and space mainly depend on the module and the stock removal. The gashes are usually a little wider than the lands on a new shaving cutter. For standard shaving cutters the serration pitch P_s is in the range of $P_s = 1.80\,\text{mm} \div 2.20\,\text{mm}$. For these values of the serrations pitch, the width of the land serration f_s is in the range of $f_s = 1.05 \div 1.20\,\text{mm}$, and the serration space w_s is normally in the range of $w_s = 0.75 \div 1.00\,\text{mm}$.

The serration depth value d_s depends on the module and the profile angle of the shaving cutter. It is determined by the strength requirements, also taking into account an allowance for resharpening the shaving cutter. The serration depth is in the range of $d_s = 0.6 \ldots 1.0\,\text{mm}$.

The lands could be tapered on one side for strength and to facilitate washing the chips out.

The serrations in tooth flanks of opposite sides of the shaving cutter tooth profile must not interfere with one another.

A portion of the top land s_s of the shaving cutter tooth within which no serrations occur must not be less than $s_s \geq 0.1\,\text{mm}$ (Figure 17.7f)

$$s_s = t_{oc} - 2 \cdot \frac{d_s}{\cos\phi_{t.o.c} \cos\psi_{o.c}} \tag{17.11}$$

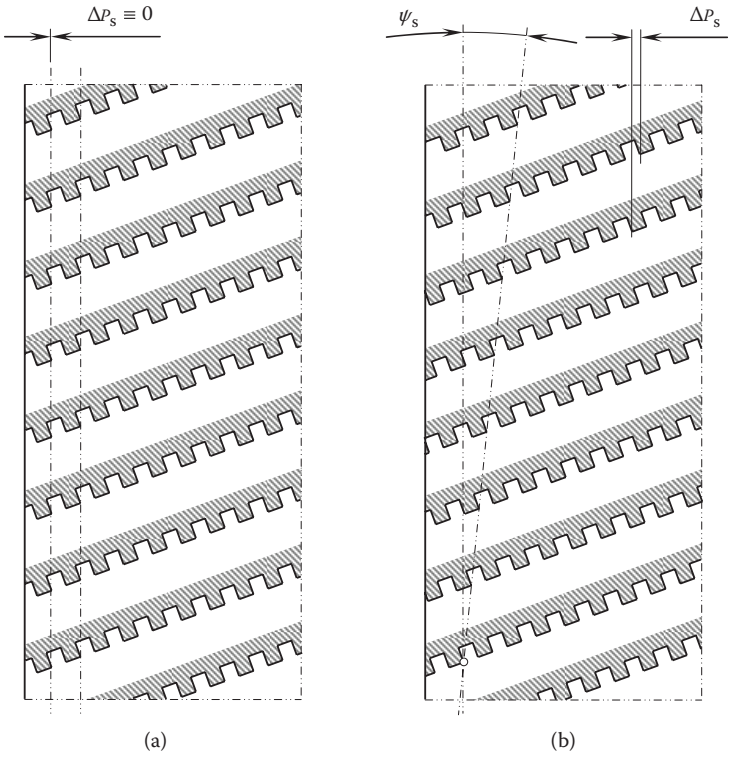

FIGURE 17.9
Annular (a) and staggered (b) pattern of the serrations in tooth flanks of a shaving cutter. (From Radzevich, S.P., *ASME Journal of Mechanical Design*, 129(9), 969–980, 2007. With permission.)

The width of the top land t_{oc} of the shaving cutter can be computed from the formula

$$t_{oc} = d_{o.c}\left(\frac{t_c}{d_c} + \text{inv}\phi_{t.c} - \text{inv}\phi_{t.o.c}\right) \tag{17.12}$$

where the profile angle at the outer diameter of the shaving cutter is denoted as $\phi_{t.c.o}$.

The end lands are designed to be wider than the inner serrating lands as shown in Figure 17.7a and f.

Shaving cutters are sometimes made with one flank unserrated so that only one flank of the work is shaved. This feature may be useful for nonreversible gears driving in one direction only.

Depending on the type of shaving, whether transverse, modified underpass, or full underpass, the serrations will be annular or with a staggered pattern. The annular serration (Figure 17.9a) is used for transverse or modified underpass methods of shaving. The staggered type of serration* (Figure 17.9b) for full underpass shaving compensates for the

* The staggered types of serrations are often referred to as *differential serrations*.

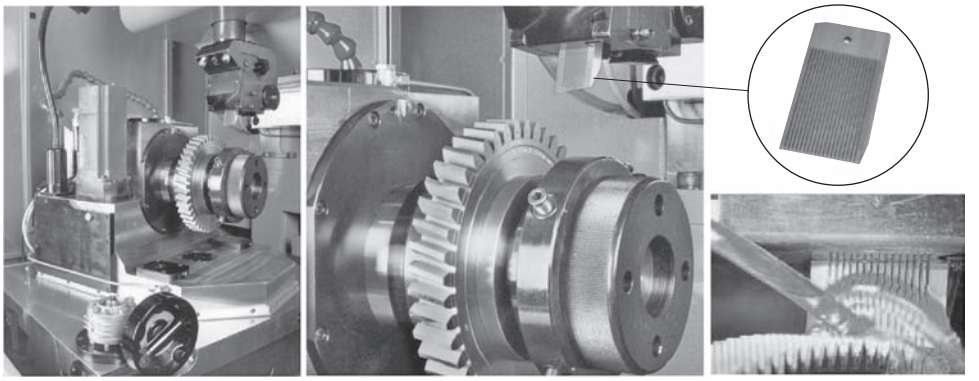

FIGURE 17.10
Process of slotting the serrations in the tooth flank of a shaving cutter.

reduced axial sliding and prevents the tracking of serration lands on the tooth flank of the shaved part. Therefore, the action of the cutting edges tends to be nearly continuous.

The serrations are slotted (Figure 17.10) by a serrating tool reciprocated vertically while the shaving cutter is rolled with its axis horizontal. In this way the shaving cutter tooth profile follows the desired involute curve.

The most convenient way to cut the serrations is to make them lie in planes perpendicular to the shaving cutter axis and to follow approximately the involute profile. The serrations are made nearly parallel to the side faces of the shaving cutter with a small angular relief to facilitate cutting them. Unfortunately, they are not finished after hardening, apart from vapor blasting to remove deposits of hardening salt or light scale, and as a result, the edges of the lands lying between the serrations may not be ideally true.

17.2.3 Resharpening of a Shaving Cutter

The shaving cutter, upon dulling, will react in a manner to warn that a tool change is needed. Keeping shaving cutters sharp is of critical importance for finishing high-quality gears. It is recommended to regrind the shaving cutter before using it for finishing gears.

Shaving cutters are sharpened on their flanks, which are screw involute surfaces. This makes the shaving cutter change quite appreciably in the outside diameter during its life. Shaving cutters do not produce the same thickness on the work gear tooth throughout their lives. If the thickness of the work gear tooth is held constant, the depth that the shaving cutter is fed into the work gear will vary.

The shaving cutter throughout its life is designed to maintain the same "true form diameter" on the part. This is accomplished by retaining the correct proportions of tooth addendum and tooth thickness. The tooth thickness of the shaving cutter is decreased with each resharpening of the shaving cutter. This causes a reduction in the operating center distance and the consequent change in operating pressure angle. The addendum must be decreased to contact at the original *true involute form* (TIF) diameter [15]. This does not change in the same proportion as the change in center distance.

In practice, the base diameter is constant and remains so throughout the life of the shaving cutter. The cross-axis angle decreases slightly with each resharpening.

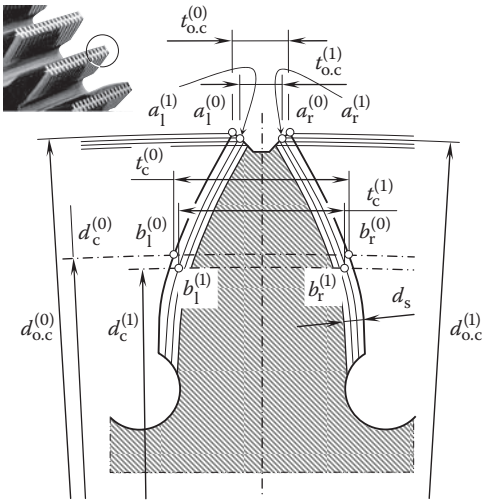

FIGURE 17.11
A gear shaving cutter with a grooved top land. (From Radzevich, S.P. and Palaguta, V.A., USSR Patent 1632662, Int. Cl. B23f 21/28, March 30, 1989.)

The tendency of the shaving cutter to cut a deeper depth as the teeth become thinner from sharpening may be controlled by reducing the shaving cutter's outside diameter an appropriate amount each time it is sharpened [15]. Various techniques can be used for this purpose.

Grinding the shaving cutter's outer diameter is inconvenient for the user of the shaving cutter. This undesired process can be eliminated by using a gear shaving cutter with the design proposed by Radzevich and Palaguta [163].

The principal features of the gear shaving cutter of this proposed design are illustrated in Figure 17.11.

Referring to Figure 17.11, a new shaving cutter can be specified by the set of the design parameters, namely by (a) pitch diameter $d_c^{(0)}$, (b) tooth thickness $t_c^{(0)}$, (c) outer diameter $d_{o.c}^{(0)}$, (d) width of the top land $t_{o.c}^{(0)}$, and others. The profile of the tooth addendum of the new shaving cutter is designated as $a_l^{(0)}b_l^{(0)}$ for the left side and $a_r^{(0)}b_r^{(0)}$ the right side of the tooth profile.

After being reground for the first time, the pitch diameter of the shaving cutter becomes smaller and is designated as $d_c^{(1)}$. The tooth thickness of the resharpened shaving cutter $t_c^{(1)}$ differs from that of $t_c^{(0)}$ for the new one. The reduction of the pitch diameter entails the need in the corresponding reduction of the outer diameter of the shaving cutter from the value of $d_{o.c}^{(0)}$ to the value of $d_{o.c}^{(1)}$. The corresponding width of the top land $t_{o.c}^{(1)}$ can be computed for the given values of the design parameters of the resharpened shaving cutter. In this way the addendum profile $a_l^{(i)}\,b_l^{(i)}$ for the left side and $a_r^{(1)}\,b_r^{(1)}$ the right side of the tooth of the resharpened shaving cutter can be determined.

These computations are performed for a variety of different pitch diameters of the shaving cutter depending on the number of its resharpenings. Ultimately, in addition to points $a_l^{(0)}$, $a_l^{(1)}$, and $a_r^{(0)}$, $a_r^{(1)}$, more points $a_l^{(i)}$ and $a_r^{(i)}$ can be determined. The set of points $a_l^{(0)}$, $a_l^{(1)}$, … , $a_l^{(i)}$ specifies the left-side profile and the set of the points $a_r^{(0)}$, $a_r^{(1)}$, and $a_r^{(i)}$ specifies the right-side profile of the groove along the top land of the shaving cutter tooth.

The shaving cutter that features grooves along the top lands of its teeth does not need regrinding over the outer cylinder after every resharpening [163], as is commonly practiced.

When resharpening a shaving cutter, the fifth necessary condition of proper *PSG* must be satisfied. For the resharpened shaving cutter as well as for the new cutter, zones of satisfaction of the fifth necessary condition of the proper *PSG* can be drawn similar to that for the gear hobs (see Figures 16.108 and 16.111).

The duration of a shaving cutter life depends primarily on the depth of the serration. This varies with the pitch.

The teeth are finished by a final profile grinding and honing and this tends to leave no feathering on the edges of the lands that may remain during the operative life of the shaving cutter.

Because the shaving cutter is designed for finishing gears it is of critical importance to maintain a high accuracy throughout its lifetime. In other words, after the shaving cutter has been reground, it is highly desirable that it is capable of shaving gears with the same accuracy as before. For this purpose a method of resharpening shaving cutters is proposed by Radzevich and Palaguta [164]. The method of resharpening shaving cutters utilizes the concept of the constant base pitch of the new $[p_{b.c}^{(0)}]$ and resharpened $[p_{b.c}^{(i)}]$ shaving cutter. In other words, using this method makes it possible to maintain the base pitch of the shaving cutter constant ($p_{b.c}$ = Const) regardless of how many times (i) the shaving cutter is resharpened and how much its pitch diameter (d_c) is reduced due to resharpening. The base pitch of a shaving cutter $p_{b.c}$ must be (a) of constant value throughout the lifetime of the shaving cutter, and (b) it must be equal to the base pitch of the gear $p_{b.g}$ intended to be shaved. Fulfillment of the equality $p_{b.c} = p_{b.g}$ is a prerequisite to achieving high quality of the gear being shaved.

A schematic of the method of resharpening the gear shaving cutter is illustrated in Figure 17.12.

The generation of the shaving cutter tooth flank is performed by a plane. For this purpose a dish-type grinding wheel can be used. The grinding wheel is rotated about its axis with a certain rotation ω_{gw}. The rotation ω_{gw} serves as the primary motion of cutting in the shaving cutter grinding process.

In the relative motion of the shaving cutter and the grinding wheel the swivel $\pm\omega_c$ of the shaving cutter and the reciprocation $\pm V_{gw}$ of the grinding wheel are timed so that the shaving cutter pitch cylinder ($d_c^{(0)}$) rolls without sliding over the pitch plane $W_{gw}^{(0)}$ associated with the rotating grinding wheel, as shown in Figure 17.12. The pitch point in such a rolling motion is designated as $P^{(0)}$.

In an arbitrary configuration of the grinding wheel with respect to the shaving cutter, perpendicular to the generating surface $T_{gw}^{(0)}$ of the grinding wheel through the point of contact $k^{(0)}$ of the plane $T_{gw}^{(0)}$ and the tooth flank is tangent to the base cylinder of the shaving cutter ($d_{b.c}^{(0)}$) at the corresponding point $a^{(0)}$. Under such a scenario the shaving cutter with a profile angle $\phi_c^{(0)}$ is ground.

The shaving cutter needs in to be resharpened after it gets dull. When the shaving cutter is resharpened for the i–time, its pitch diameter reduces to $d_c^{(i)} < d_c^{(0)}$. If no special action is taken, the reduction of the pitch diameter entails the corresponding changes in the other design parameters of the shaving cutter as well as in the shaving cutter base pitch. The latter is not permitted as it violates the accuracy requirements.

The base pitch of the shaving cutter $p_{b.c}$ can be expressed in terms of axial pitch $P_{x.c}$, pitch helix angle ψ_c, and normal profile angle ϕ_g of the shaving cutter [10]

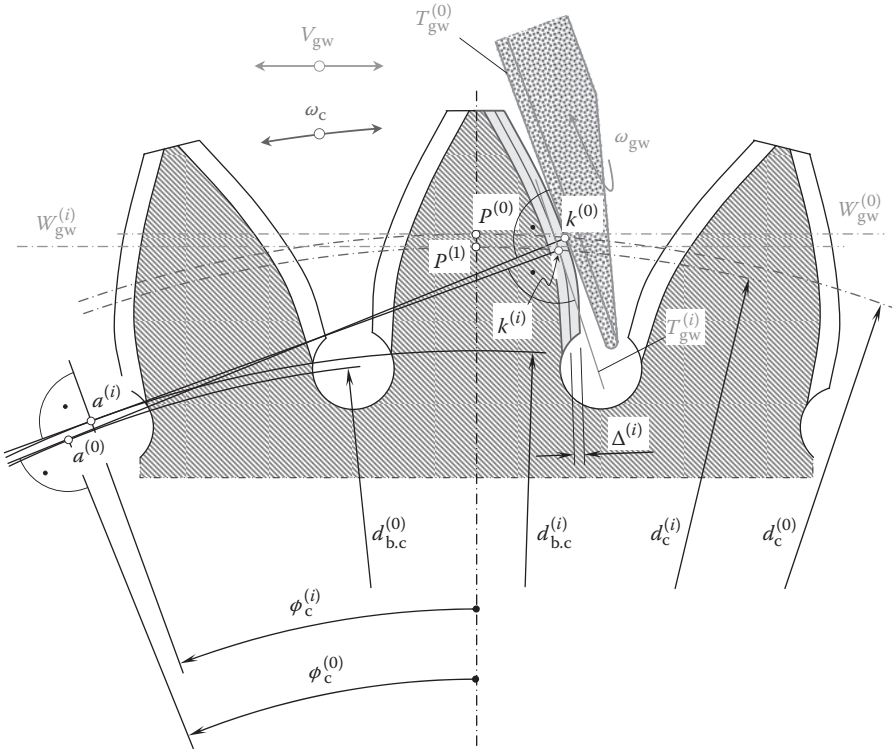

FIGURE 17.12
Schematic of the method of resharpening a gear shaving cutter. (From Radzevich, S.P. and Palaguta, V.A., USSR Patent 1646725, Int. Cl. B23f 21/28, Dec. 13, 1988; Radzevich, S.P., *ASME Journal of Manufacturing, Science and Engineering*, 127(4), 819–828, 2005. With permission.)

$$p_{b.c} = P_{x.c} \sin\psi_c \cos\phi_c \tag{17.13}$$

By using the engineering formulae for specification of the gear tooth flank (see Appendix A), Equation (17.13) can be cast into an equivalent form

$$p_{b.c} = \frac{P_{x.c}\pi d_c \cos\phi_c}{\sqrt{P_{x.c}^2 + \pi^2 d_c^2}} \tag{17.14}$$

Equation (17.14) unveils that in the conventional methods of resharpening shaving cutters, the base pitch $p_{b.c}$ is a function of pitch diameter d_c of the shaving cutter [i.e., dependence $p_{b.c} = p_{b.c}(d_c)$ is observed]. The pitch diameter of the shaving cutter reduces from $d_c^{(0)}$ to $d_c^{(i)} < d_c^{(0)}$ after each resharpening of the shaving cutter. Therefore, corresponding alterations to the base pitch $p_{b.c}$ after resharpening the shaving cutter are unavoidable.

Any alterations to the base pitch of a shaving cutter are strongly undesirable due to accuracy requirements. As alterations to diametral dimensions of the shaving cutter after

resharpening are unavoidable, their impact on the base pitch $p_{b.c}$ can be compensated by corresponding changes to other design parameters of the shaving cutter. Ultimately, in this way it is possible to resharpen a shaving cutter so as to make it base-pitch insensitive to the unavoidable reduction of the pitch diameter.

The base pitch of a shaving cutter is not affected by any alterations to the pitch diameter if and only if the equality

$$\frac{\partial p_{b.c}(d_c)}{\partial d_c} = 0 \tag{17.15}$$

is fulfilled. Equation (17.15) states that any and all alterations to the design parameters of the shaving cutter are allowed as long as the equality [see Equation (17.15)] is satisfied.

After substituting Equation (17.14) in Equation (17.15), the latter casts into a formula for the computation of profile angle $\phi_c^{(i)}$ of the shaving cutter after being resharpened i times

$$\phi_c^{(i)} = \cos^{-1}\left(C \cdot \frac{P_{x.c}^2 + \pi^2 [d_c^{(i)}]^2}{\pi^2 [d_c^{(i)}]^2} \right) \tag{17.16}$$

where C is the coefficient, which is computed from the equation

$$C = \frac{P_{x.c}^2 + \pi^2 [d_c^{(0)}]^2}{\pi^2 [d_c^{(0)}]^2} \cdot \cos \phi_c^{(0)} \tag{17.17}$$

Example. Design parameters of a new shaving cutter are collected in Table 17.1.

Equation (17.17) allows for computation of the coefficient $C = 0.06295$.

In the case under consideration the stock $\Delta^{(i)}$ for resharpening the shaving cutter is equal to $\Delta^{(i)} = 0.05\,\text{mm}$.

The set of the design parameters of a new shaving cutter (Table 17.1) along with the computed value of the coefficient C and the given value for the stock $\Delta^{(i)}$ to be reground allows for computation of the desired profile angle $\phi_c^{(i)}$ of the resharpened shaving cutter. Equation (17.16) returns $\phi_c^{(i)} = 19°38'$ [164].

In order to obtain the desired profile angle $\phi_c^{(i)} = 19°38'$ base diameter for the resharpened shaving cutter, $d_{b.c}^{(i)}$ is required to increase from $d_{b.c}^{(0)} = 208.288\,\text{mm}$ to $d_{b.c}^{(i)} = 209.390\,\text{mm}$ [164].

The recommended alterations to the design parameters of the resharpened shaving cutter compared to the corresponding design parameters of the new shaving cutter result in increased accuracy of the finished gears.

TABLE 17.1

Design Parameters of a New Shaving Cutter

Module	$m = 5\,\text{mm}$
Tooth number	$N_c = 43$
Pitch diameter	$d_c^{(0)} = 222.584\,\text{mm}$
Normal profile angle	$\phi_c^{(0)} = 20°$
Pitch helix angle	$\psi_c^{(0)} = 15°$
Base diameter	$d_{b.c}^{(0)} = 208.288\,\text{mm}$
Axial pitch	$P_{x.c} = 2608.373\,\text{mm}$

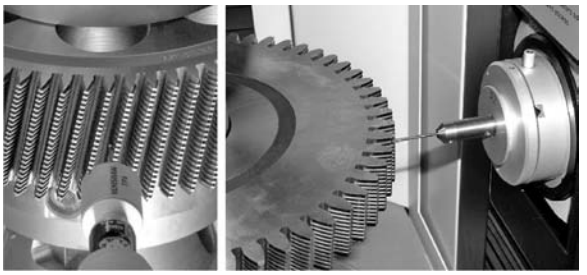

FIGURE 17.13
Inspection of a shaving cutter tooth profile after being resharpened.

Accuracy of the resharpened tooth profile of the shaving cutter is inspected (Figure 17.13). For this purpose CMM is commonly used.

17.3 Axial Method of the Gear Shaving Process

The axial* method of the gear shaving process is one of four basic methods of rotary shaving of the external spur and helical gears. This method of shaving gears is widely used in low- and medium-production operations. It is the most economical method for shaving wide face width gears.

17.3.1 Kinematics of the Axial Method of the Gear Shaving Process

When the axial method of gear shaving is used, the work gear and the shaving cutter are meshed in a crossed-axis relationship (Figure 17.14). The crossing axes of the work gear O_g and the shaving cutter O_c are at a certain center distance $C_{g/c}$ apart of one another.

The shaving cutter is rotated in both directions during the work cycle. The work gear spindle and the shaving cutter spindle are driven in timed relation to each other by CNC-controlled motors. When a non-CNC machine is used, the rotation of the work gear spindle is not timed with that of the shaving cutter spindle. In Figure 17.14, the rotation of the work gear about its axis O_g is designated as $\boldsymbol{\omega}_g$. The rotation of the shaving cutter about it axis O_c is designated as $\boldsymbol{\omega}_c$. The rotations $\boldsymbol{\omega}_g$ and $\boldsymbol{\omega}_c$ are properly timed with one another ($\omega_g N_g = \omega_c N_c$, here N_g and N_c denote the tooth number of the work gear and the shaving cutter, respectively, and the equalities $\omega_g = |\boldsymbol{\omega}_g|$ and $\omega_c = |\boldsymbol{\omega}_c|$ are observed). The rotation vectors $\boldsymbol{\omega}_g$ and $\boldsymbol{\omega}_c$ are at the angle $\Sigma = \angle(\boldsymbol{\omega}_g, \boldsymbol{\omega}_c)$. The angle $\bar{\Sigma}$ of crossing of the axes O_g and O_c complements the angle Σ to 180° (i.e., $\bar{\Sigma} = \pi - \Sigma$).

In addition to the rotations $\boldsymbol{\omega}_g$ and $\boldsymbol{\omega}_c$, the work gear is reciprocated $\mathbf{F}_c$ in a path parallel to the work gear axis of rotation. It is customary to move the work gear past the shaving cutter by means of the feed slide. On some of the larger shaving machines, for obvious reasons, the shaving cutter is mounted on a feed slide. In the consideration below, the *relative motion* of the work gear and the shaving cutter is considered regardless of whether the work-table or the shaving cutter is actually reciprocated.

* The axial method of the gear shaving process is also referred to as either the *conventional* or *traverse* method of rotary shaving of the gears.

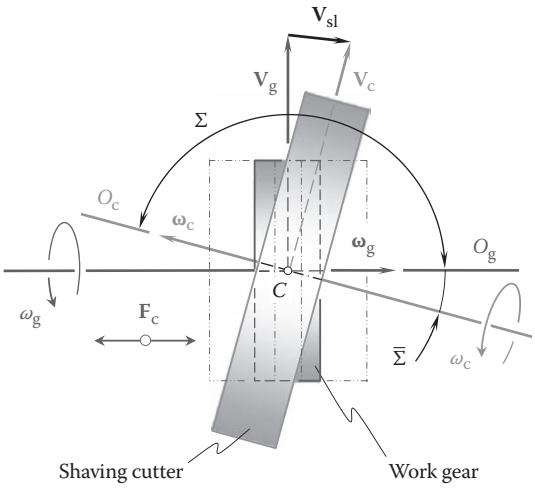

FIGURE 17.14
Schematic of an axial method of the gear shaving process.

The length of traverse is determined by the face width of the work gear. In practice [190], for best results the length of traverse should be approximately 1.6 mm (1/16 in.) greater than the face width of the work gear, allowing for minimum overtravel at each end of the work gear face. In Figure 17.14, the left-end position and the right-end position of the reciprocating work gear is shown by dashed lines. The length of the reciprocating path depends on (a) the face width of the work gear, (b) the face width of the shaving cutter, and (c) the crossed-axis angle Σ.

During the work cycle the center distance is being reduced in small controlled increments. In order to gradually reduce the center distance the shaving cutter is fed into the work gear to give the required radial tooth loading, and the machine is then run with

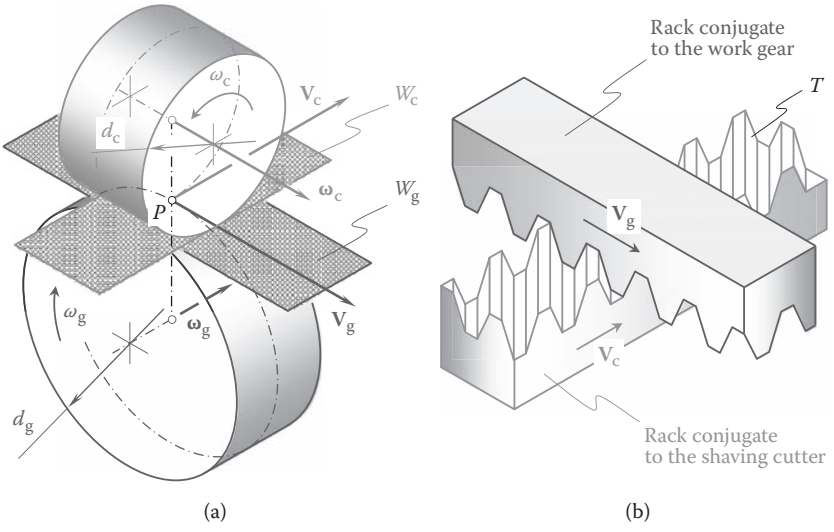

FIGURE 17.15
The nature of the action between the work gear and the shaving cutter in the gear shaving process.

the shaving cutter and the work gear in mesh for a predetermined number of passes. The automatic infeed of 0.001 to 0.002 in. (0.025–0.050 mm) is applied at each end of the shaving cutter traverse.

In the axial method of shaving, the traverse path is along the axis of the work gear. The number of strokes may vary due to the amount of stock to be removed. In this way the desired tooth form, thickness, and finish are produced.

17.3.2 Cutting Speed in the Axial Method of Rotary Shaving of the Gear

The speed of cutting in the gear shaving process is created in a peculiar manner, which significantly differs from that, for example, in the turning or milling process. This issue was already briefly discussed in Section 17.1.4.

The speed of the primary motion $\mathbf{V}_{cut}$ in the rotary shaving of the gears is equal to the speed of the resultant sliding $\mathbf{V}_{\Sigma}$ of the shaving cutter tooth flank with respect to the work gear tooth flank. As the teeth of the shaving cutter move across face width of the work gear, the fine chips are shaved up from flanks of the work gear teeth.

The nature of sliding of the shaving cutter tooth flanks relative the work gear tooth flanks is the same as observed, for example, in the gear hobbing process. However, in rotary shaving the flank sliding is not that evident as it is when hobbing gears.

The speed of cut $\mathbf{V}_{cut}$ can be expressed in terms (a) of the sliding velocity $\mathbf{V}_{sl}$ in the lengthwise direction of the work gear tooth, (b) of the velocity $\mathbf{V}_{pr}$ of the profile sliding, and (c) of the velocity of sliding that is caused by the reciprocation motion $\mathbf{F}_c$. Equation (17.4) reflects this functionality. Understanding the nature of the tooth flank sliding is the clue to determining the cutting speed in the rotary shaving of the gears. For this purpose it is helpful to use the results of investigation of the geometry and kinematics of crossed axes involute gearing [11].

17.3.2.1 Impact of the Crossed-Axis Angle

When the axes O_g and O_c are not parallel to each other (Figure 17.15a)—say they are at a certain crossing angle $\bar{\Sigma}$—the pitch plane of the work gear W_g travels ($\mathbf{V}_g$) in the direction that is perpendicular to both the work gear axis O_g and the line along the closest distance of approach $C_{g/c}$. Similarly, the pitch plane of the shaving cutter W_c travels ($\mathbf{V}_c$) in the direction that is perpendicular to both the shaving cutter axis O_c and the line along the closest distance of approach $C_{g/c}$.

The pitch cylinder of the work gear is driven by the pitch cylinder of the shaving cutter, while its own pitch plane is screwed along and engages the pitch cylinder of the shaving cutter, as indicated in Figure 17.15a.

Thus we have a closed circuit of action on the work gear and the shaving cutter. To summarize, we have the following: The helix of the shaving cutter screws its pitch plane W_c along its line of travel. This pitch plane is always tangent to the pitch cylinder of the work gear and causes it to rotate. The rotation of the work gear screws its pitch plane W_g along its path, and this pitch plane is always tangent to the pitch cylinder of the shaving cutter. The rate of travel of this pitch plane must be the same as that of the circumference of the pitch cylinder of the shaving cutter. This completes the closed circuit.

The auxiliary generating surface T is zero thickness film-shaped in the form of the basic rack. The body of the rack that is conjugate to the gear being machined is located on one side of the surface T, while the body of the rack that is conjugate to the shaving cutter is located on the opposite side of the surface T.

The forms of the conjugate racks of the work gear and the shaving cutter match each other as indicated in Figure 17.15b. When the rack of the shaving cutter is moved in the direction of motion of the pitch plane W_g of the work gear, it acts as a cam on the rack of the work gear, and forces it to move in the direction of the motion of the pitch cylinder of the work gear, as indicated in Figure 17.15b. Two intermediate conclusions follow from this consideration.

First, as the velocity vectors $\mathbf{V}_g$ and $\mathbf{V}_c$ do not align with each other, this results in sliding velocity $\mathbf{V}_{sl} = \mathbf{V}_c - \mathbf{V}_g$ [see Equation (17.77)]. The sliding velocity $\mathbf{V}_{sl}$ is a component that most significantly benefits the speed of cut $\mathbf{V}_{cut}$ compared to that by the rest of the components in Equation (17.4).

Second, because each of the velocity vectors $\mathbf{V}_g$ and $\mathbf{V}_c$ are constant, then the sliding velocity vector $\mathbf{V}_{sl}$ is also constant, and it does not alternate within the tooth height either of the work gear or within the tooth height of the shaving cutter.

Increasing the angle between the shaving cutter and work gear axes increases the cutting action ($\mathbf{V}_{cut}$), but as this reduces the width of the contact zone, the guiding action is sacrificed. Practically no cutting occurs at zero angle $\overline{\Sigma}$. Conversely, the guiding action can be increased by reducing the angle of the crossed axes but at the expense of the cutting action.

17.3.2.2 Impact of the Traverse Motion

In the axial shaving of the gears, the direction of the traverse is parallel to the axis of rotation of the work gear. As the traverse motion is not tangent to the flank of the work gear tooth (except in the case of shaving the spur gear), the reciprocation speed affects the cutting speed in two ways.

Let us assume that the shaving cutter is not rotating, and it is just reciprocating in the axial direction of the work gear. Under such a scenario, the straight reciprocation $\mathbf{F}_c$ of the shaving cutter is at an angle to the work gear tooth flank, as indicated in Figure 17.16. Within the pitch plane this angle is equal to the work gear pitch helix angle ψ_g.

The traverse motion $\mathbf{F}_c$ can be decomposed on two directions. One component $\mathbf{F}_c^{sl}$ is in the direction tangent to the tooth flank of the work gear. The magnitude of this component is equal

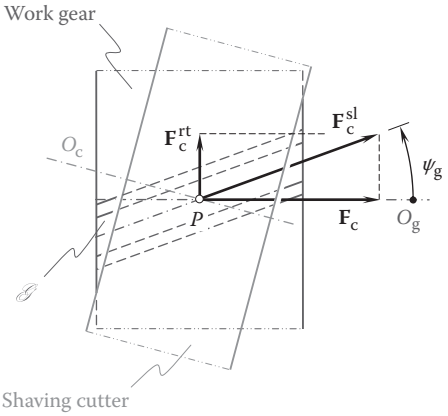

FIGURE 17.16
Impact of the traverse motion on the cutting speed $\mathbf{V}_{cut}$ in the axial shaving of gears.

$$F_c^{sl} = |\mathbf{F}_c^{sl}| = \frac{|\mathbf{F}_c|}{\cos\psi_g} = \frac{F_c}{\cos\psi_g} \tag{17.18}$$

The component $\mathbf{F}_c^{sl}$ represents the pure sliding of the tooth flanks of the work gear and the shaving cutter.

It is important to point out here that the vector $\mathbf{F}_c^{sl}$ of the sliding is constant, and it does not alternate within the tooth height either of the work gear or within the tooth height of the shaving cutter.

Another component $\mathbf{F}_c^{rt}$ of the reciprocation $\mathbf{F}_c$ is within the pitch plane, and it is perpendicular to the axis of rotation of the work gear. For the computation of magnitude F_c^{rt} of the component $\mathbf{F}_c^{rt}$, the formula

$$F_c^{rt} = F_c \tan\psi_g \tag{17.19}$$

can be used. The actual direction of the vector $\mathbf{F}_c^{rt}$ depends on the hand of the pitch helix angle ψ_g.

The component $\mathbf{F}_c^{rt}$ adds to the rotation of the work gear. This additional rotation ω_g^{ad} is equal

$$\omega_g^{ad} = \frac{2F_c \tan\psi_g}{d_g} \tag{17.20}$$

The rotation vector $\boldsymbol{\omega}_g^{ad}$ is aligned with the rotation vector $\boldsymbol{\omega}_g$. Depending on (a) the rotation of the shaving cutter $\boldsymbol{\omega}_c$, (b) the direction of the hand and the value of the helix angle ψ_g, and (c) the actual direction of the reciprocation $\mathbf{F}_c$, the rotation vector $\boldsymbol{\omega}_g^{ad}$ is pointed either in the same direction as the rotation vector $\boldsymbol{\omega}_g$, or opposite of $\boldsymbol{\omega}_g$. In the first case the rotation $\boldsymbol{\omega}_g^{ad}$ adds to the rotation $\boldsymbol{\omega}_g$. In the second case it subtracts from the rotation $\boldsymbol{\omega}_g$.

Because the additional rotation ω_g^{ad} of the work gear depends on the pitch helix angle, the greater the pitch helix angle ψ_g of the work gear, the greater the impact of the reciprocation motion $\mathbf{F}_c$ of the shaving cutter on the cutting speed $\mathbf{V}_{cut}$.

17.3.2.3 Impact of Profile Sliding

Sliding the shaving cutter tooth flank relative to the work gear tooth flank always occurs in the rotary shaving of the gears. The speed of tooth profile sliding also contributes to the speed of the cut in the shaving process.

The *work gear to shaving cutter* meshing is a kind of spatial meshing of the cogged wheels. Implementation of 3-D analysis is required for the purpose of investigating the axial method of the gear shaving process in order to determine the sliding component of the speed of the cut.

Prior to undertaking a comprehensive investigation of the work gear to shaving cutter meshing in 3-D, a preliminary 2-D consideration is helpful. In this case it is an advantage that frequently the crossed-axis angle in the rotary shaving process is reasonably small and does not exceed $\bar{\Sigma} \leq 15 \div 20°$. This means that the results of the investigation of the work gear to shaving cutter meshing in 2-D could be a good approximation of the accurate results of the investigation in 3-D.

For the purposes of the preliminary analysis, consider the work gear to shaving cutter mesh that features the parallel axes O_g and O_c of the rotation as shown in Figure 17.17 [150].

The base diameter of the work gear is designated as $d_{b.g}$, and the base diameter of the shaving cutter is designated as $d_{b.c}$.

The rolling action between the work gear and the shaving cutter is transmitted along the line of action. The sliding action between the work gear and the shaving cutter is observed in the direction perpendicular to the line of action.

The line of action in the work gear to the shaving cutter mesh is tangent from the opposite sides of the base cylinders of the work gear ($d_{o.g}$) and the shaving cutter ($d_{o.c}$). In Figure 17.17, the work gear and the shaving cutter are depicted in a position at which the line of action N^gN^c is horizontal. Points P^g and P^c within the line of action correspond to the points of intersection of the line of action by the outer cylinder of the gear ($d_{o.g}$), and by the outer cylinder of the shaving cutter ($d_{o.c}$), respectively. The segment P^gP^c of the line of action represents the active portion of the line of action.

The pitch cylinders of the work gear and the shaving cutter pass through the pitch point *P*. Due to lack of space, the pitch cylinders are not shown in Figure 17.17.

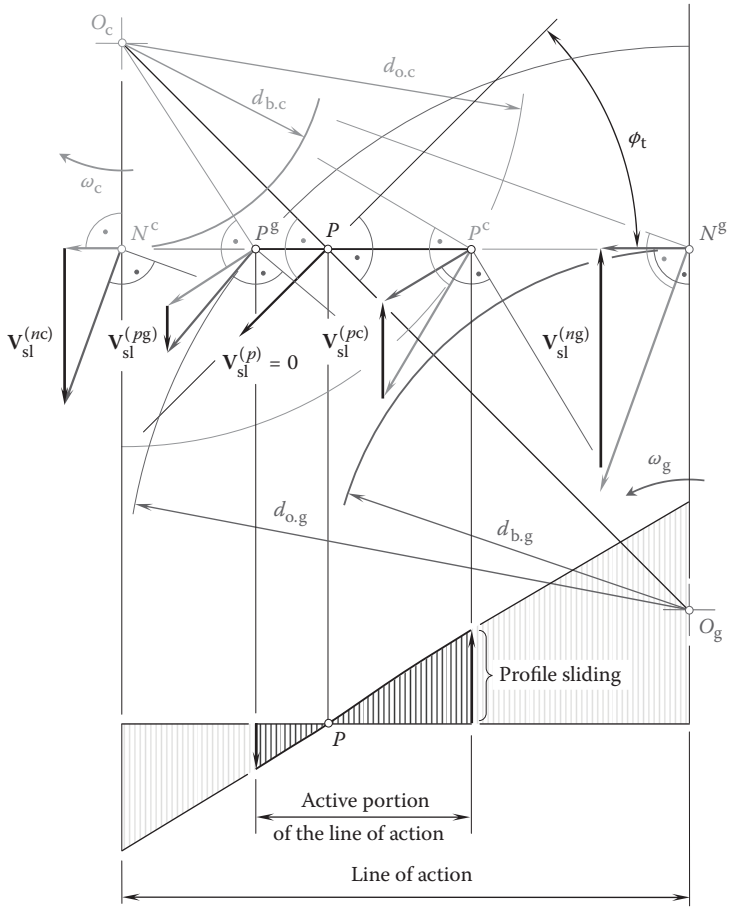

FIGURE 17.17
An approximate 2-*D* interpretation of the *work gear to shaving cutter* mesh in the rotary shaving of gears: Axes of the rotations of the work gear O_g and the shaving cutter O_c are parallel to each other. (After Radzevich, S.P., *AGMA Technical Paper* 06FTM11, 2006, 22 pp.)

The points N^g, P^c, P, P^g, and N^c within the line of action N^gN^c correspond to different instances of phases of meshing. For each of the points, the corresponding vector of linear velocity of the work gear $\mathbf{V}_g^{(i)}$ and the shaving cutter $\mathbf{V}_c^{(i)}$ are depicted in Figure 17.17. Each of the vectors $\mathbf{V}_g^{(i)}$ is perpendicular to the radius of the corresponding point N^g, P^c, P, P^g, and N^c from the gear axis O_g. Similarly, each of the vectors $\mathbf{V}_c^{(i)}$ is perpendicular to the radius to the corresponding point N^g, P^c, P, P^g drawn from the shaving cutter axis O_c. The vectors $\mathbf{V}_g^{(i)}$ and $\mathbf{V}_c^{(i)}$ are not labeled in Figure 17.17 due to lack of space.

The magnitude of the vector $\mathbf{V}_g^{(i)}$ is equal to $V_g^{(i)} = \left|\mathbf{V}_g^{(i)}\right| = \omega_g R_g^{(i)}$. Here, the radius of the cylinder at which the ith point of contact is located is designated as $R_g^{(i)}$. For computing the magnitude of the vector $\mathbf{V}_c^{(i)}$, the similar formula $V_c^{(i)} = \left|\mathbf{V}_c^{(i)}\right| = \omega_c R_c^{(i)}$ is valid. In this expression, $R_c^{(i)}$ denotes radius of the cylinder at which the ith point of contact is located.

Once the velocity vectors $\mathbf{V}_g^{(i)}$ and $\mathbf{V}_c^{(i)}$ are expressed in a common reference system, the vector of the sliding velocity $\mathbf{V}_{sl}^{(i)}$ is equal to the difference

$$\mathbf{V}_{sl}^{(i)} = \mathbf{V}_c^{(i)} - \mathbf{V}_g^{(i)} \tag{17.21}$$

In this equation, the velocity vectors $\mathbf{V}_g^{(i)}$ and $\mathbf{V}_c^{(i)}$ can be expressed in terms of the rotations $\boldsymbol{\omega}_g$ and $\boldsymbol{\omega}_c$, and of distances $\mathbf{R}_g^{(i)}$ and $\mathbf{R}_c^{(i)}$ of the point of contact at a current instant of time:

$$\mathbf{V}_g^{(i)} = \boldsymbol{\omega}_g \times \mathbf{R}_g^{(i)} \tag{17.22}$$

$$\mathbf{V}_c^{(i)} = \boldsymbol{\omega}_c \times \mathbf{R}_c^{(i)} \tag{17.23}$$

After being represented in a common coordinate system, the velocity vectors $\mathbf{V}_g^{(i)}$ and $\mathbf{V}_c^{(i)}$ can be entered into Equation (17.21) for computing the sliding velocity $\mathbf{V}_{sl}^{(i)}$

$$V_{sl}^{(i)} = 0.5\left(\omega_c\sqrt{d_{y.c}^2 - d_{b.c}^2} - \omega_g\sqrt{d_{y.g}^2 - d_{b.g}^2}\right) \tag{17.24}$$

where $d_{y.g}$ and $d_{y.c}$ are the diameters of the circles of the work gear and the shaving cutter passing through the ith point of contact, respectively.

The vector of the sliding velocity $\mathbf{V}_{sl}^{(i)}$ is always perpendicular to the line of action. Its magnitude $V_{sl}^{(i)} = \left|\mathbf{V}_{sl}^{(i)}\right|$ varies within the tooth height of the work gear as well as within the tooth height of the shaving cutter. The bigger the distance of the ith point of contact from the pitch point P, the bigger the sliding velocity $V_{sl}^{(i)}$ and vice versa. No sliding occurs at the pitch point P (i.e., the equality $\mathbf{V}_{sl}^{(p)} = 0$ is always valid at the pitch point P).

Because the vectors $\mathbf{V}_g^{(i)}$ and $\mathbf{V}_c^{(i)}$ of the linear velocity are not constant within the tooth height, the vector $\mathbf{V}_{sl}^{(i)}$ of the profile sliding varies within the tooth height of both the work gear and the shaving cutter teeth.

Because the schematic in Figure 17.17 features parallel axes of rotation O_g and O_c of the work gear and the shaving cutter, the results of the analysis obtained on the premise of Figure 17.17 are an approximation. However, the approximation is practically reasonable because of three reasons. First, the crossing angle $\bar{\Sigma}$ between the axes O_g and O_c is relatively small. Commonly it does not exceed $\bar{\Sigma} \le 20°$. Second, the speed of the profile sliding $\mathbf{V}_{sl}^{(i)}$ contributes less significantly to the cutting speed. Only for work gears and/or shaving cutters with a low number of teeth does the component $\mathbf{V}_{sl}^{(i)}$ become more significant, while in the pitch point P it remains of zero value [$\mathbf{V}_{sl}^{(p)} = 0$] regardless of the tooth numbers. Third, there is no necessity of absolutely accurate determination of the speed of the profile

sliding. However, if necessary, an accurate computation of the component $\mathbf{V}_{sl}^{(i)}$ can be performed as well.

For the purpose of accurately determining the speed of the profile sliding that is not planar (two-dimensional) but spatial (three-dimensional), the mesh of the work gear and the shaving cutter must be considered. In this way it is possible to construct for the 3-D mesh a diagram similar to that constructed for the 2-D mesh (Figure 17.17).

The disposition and relative orientation of the base cylinder of the work gear and the base cylinder of the shaving cutter is illustrated in Figure 17.18.

The shaving cutter interacts with the work gear along the line of action LA. The line of action LA can be interpreted as the line of intersection of two planes, τ_g and τ_c. Plane τ_g is passing through the pitch point *P*. This plane is tangent to the base cylinder of the work gear. The plane τ_c also passes through the pitch point *P*. This plane is tangent to the base cylinder of the shaving cutter. The line of action LA is the straight line of intersection of the planes τ_g and τ_c. It crosses each of the axes O_g and O_c at the base helix angle. The line of action is tangent to both of the base cylinders. A straight line segment between the points of tangency of the line of action LA and the base cylinders represents the entire line of action. Its active portion is terminated by the points of intersection of the straight line LA with the outer cylinder of the work gear and the outer cylinder of the shaving cutter.

Further, due to the axes of rotation O_g and O_c crossing each other at a certain angle $\bar{\Sigma}$, the equivalent base diameter $d_{b.g}^*$ of the work gear and the equivalent base diameter $d_{b.c}^*$ of the shaving cutter differ from that applied in the two-dimensional case.

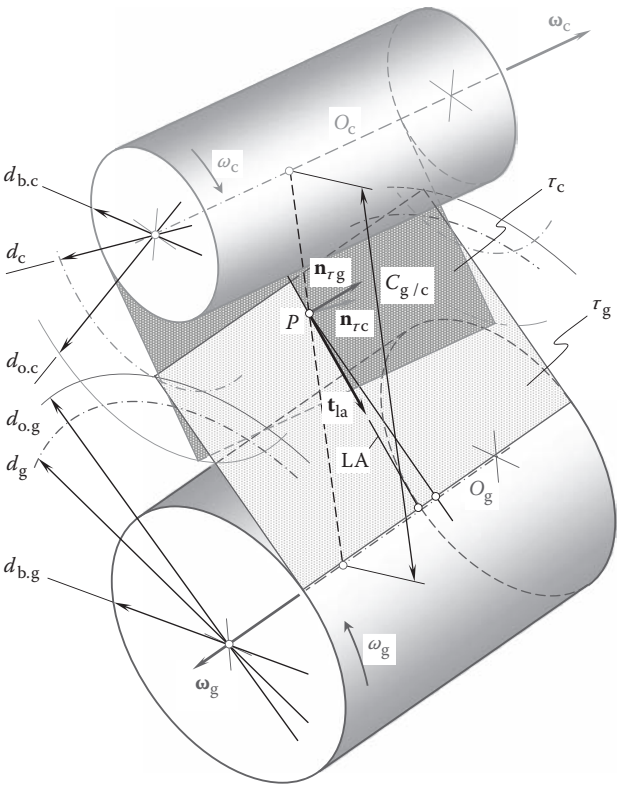

FIGURE 17.18
Three-dimensional schematic of the work gear to shaving cutter mesh.

Ultimately only three design parameters are required for the construction of the 3-D mesh diagram. They are (a) the entire line of action LA measured between the points of tangency of the straight line of action with the base cylinders, (b) the equivalent base diameter $d^*_{b.g}$ of the work gear, and (c) the equivalent base diameter $d^*_{b.c}$ of the shaving cutter.

Line of action. Consider the tangent plane τ_g shown in Figure 17.19. In the coordinate system $X_gY_gZ_g$ associated with the work gear, the position vector $\mathbf{r}_{\tau g}$ of a point of the plane τ_g can be expressed in matrix form as

$$\mathbf{r}_{\tau g}(X_g, Z_g) = \begin{bmatrix} X_g \\ 0.5d_{b.g} \\ Z_g \\ 1 \end{bmatrix} \tag{17.25}$$

Similarly, in the coordinate system $X_cY_cZ_c$ associated with the shaving cutter, the position vector $\mathbf{r}_{\tau c}$ of a point of the plane τ_c can be expressed by the equation

$$\mathbf{r}_{\tau c}(X_c, Z_c) = \begin{bmatrix} X_c \\ -0.5d_{b.c} \\ Z_c \\ 1 \end{bmatrix} \tag{17.26}$$

In order to be treated together, both of the position vectors $\mathbf{r}_{\tau g}$ and $\mathbf{r}_{\tau c}$ should be represented in a common reference system. Neither the coordinate system $X_gY_gZ_g$ associated with the work gear nor the coordinate system $X_cY_cZ_c$ associated with the shaving cutter is convenient to serve as the common reference system. Therefore, an intermediate reference system is used in the case under consideration as the common reference system.

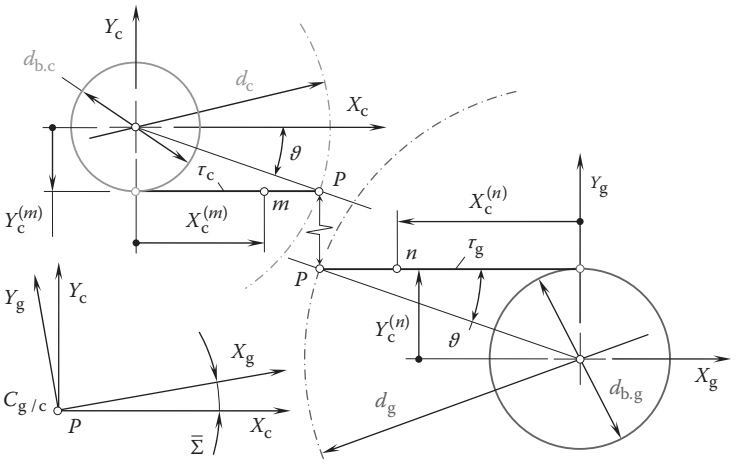

FIGURE 17.19
The planes τ_g and τ_c through the pitch point P tangent to the base cylinders of a work gear and a shaving cutter.

The required coordinate system transformation can be performed in four consequent steps:

(1) The rotation of the shaving cutter reference system $X_cY_cZ_c$ about the Z_c axis through the angle ϑ. This angle can be computed from the expression $\vartheta = \sin^{-1}(d_{b.c}/d_c)$. This linear transformation is analytically described by the operator of rotation $\mathbf{Rt}(\vartheta, Z_c)$.

(2) The translation along the X_c axis at the center distance $C_{g/c}$. Analytically this linear transformation is described by the operator of translation $\mathbf{Tr}(C_{g/c}, X)$.

(3) The rotation about the X_c axis through the crossed-axis angle $\bar{\Sigma}$. For this purpose the operator of rotation $\mathbf{Rt}(\bar{\Sigma}, X)$ is used.

(4) The rotation of the work gear coordinate system $X_gY_gZ_g$ about the Z_g axis through the angle $\vartheta = \sin^{-1}(d_{b.g}/d_g)$, which is equal to the angle ϑ used in the first step (a). This linear transformation is analytically described by the operator of rotation $\mathbf{Rt}(\vartheta, Z_g)$.

Steps (1) through (3) relate to transformations of the shaving cutter coordinate system $X_cY_cZ_c$ to the common coordinate system. In the last step (4), the work gear reference system $X_gY_gZ_g$ is transformed into the common coordinate system.

In the common reference system, the position vector $\hat{\mathbf{r}}_{\tau g}$ of a point of the plane τ_g can be expressed in terms of the position vector $\mathbf{r}_{\tau g}$ and the operator of rotation $\mathbf{Rt}(\vartheta, Z_g)$

$$\hat{\mathbf{r}}_{\tau g} = \mathbf{Rt}(\vartheta, Z_g) \cdot \mathbf{r}_{\tau g} \tag{17.27}$$

In that same reference system, the position vector $\hat{\mathbf{r}}_{\tau c}$ of a point of the plane τ_c can be expressed by the equation

$$\hat{\mathbf{r}}_{\tau c} = \mathbf{Rt}(\bar{\Sigma}, X) \cdot \mathbf{Tr}(C_{g/c}, X) \cdot \mathbf{Rt}(\vartheta, Z_c) \cdot \mathbf{r}_{\tau c} \tag{17.28}$$

Equations (17.27) and (17.28) allow for the computation of unit normal vectors $\mathbf{n}_{\tau g}$ and $\mathbf{n}_{\tau c}$ to the planes τ_g and τ_c, respectively. It is a routing procedure to compute the unit normal vectors $\mathbf{n}_{\tau g}$ and $\mathbf{n}_{\tau c}$. Ultimately, the equation of the line of action LA can be represented in the form

$$\text{LA} \quad \Rightarrow \quad \mathbf{r}_{la}(\lambda) = \mathbf{r}_P + \lambda \cdot \mathbf{t}_{la} \tag{17.29}$$

where $\mathbf{t}_{la}$ designates a unit vector along the line of action LA, and λ is the parameter of the line of action.

Once the equation of the line of contact is derived, the following formula can be used for the computation of length of the entire line of action.

$$\text{LA} = \frac{d_{b.g}}{2} \frac{\tan \phi_{ot.g}}{\sin \psi_{b.g}} + \frac{d_{b.c}}{2} \frac{\tan \phi_{ot.c}}{\sin \psi_{b.c}} \tag{17.30}$$

where

$d_{b.g}$ = base diameter of the work gear
$d_{b.c}$ = base diameter of the shaving cutter
$\phi_{ot.g}$ = transverse profile angle at the outer diameter of the work gear

$\phi_{ot.c}$ = transverse profile angle at the outer diameter of the shaving cutter
$\psi_{b.g}$ = base helix angle of the work gear
$\psi_{b.c}$ = base helix angle of the shaving cutter

Equation (17.30) returns an accurate value for the length of the line of action, which can be used for determining the accurate value of the speed of the profile sliding in the rotary shaving of gears.

For the specification of the location of the pitch point P within the line of action, the tooth ratio $m_{g/c}$ can be used. By definition, the tooth ratio is equal to $m_{g/c} = \omega_g/\omega_c$. The ratio of linear velocities V_g and V_c can be expressed in terms of the pitch helix angles ψ_g and ψ_c (Figure 17.14)

$$\frac{V_g}{V_c} = \frac{\cos\psi_c}{\cos\psi_g} \tag{17.31}$$

With that stated, the expression

$$m_{g/c} = \frac{\omega_g}{\omega_c} = \frac{d_c \cos\psi_c}{d_g \cos\psi_g} \tag{17.32}$$

is valid for the computation of the tooth ratio $m_{g/c}$.

For given diameters $d_{y.g}$ and $d_{y.c}$ of the circles of the work gear and the shaving cutter passing through the ith point of contact, the respective equivalent diameters $d^*_{y.g}$ and $d^*_{y.c}$ are computed by the formulae

$$d^*_{y.g} = \frac{d_{y.g}}{\cos\psi_{b.g}} \tag{17.33}$$

$$d^*_{y.c} = \frac{d_{y.c}}{\cos\psi_{b.c}} \tag{17.34}$$

Equivalent base diameters. The line of action LA crosses the work gear axis of rotation O_g at the base helix angle $\psi_{b.g}$ of the work gear. Similarly, the crossing angle between the line of action LA and the shaving cutter axis of rotation O_c is equal to the base helix angle $\psi_{b.c}$ of the shaving cutter. At the point of tangency with the line of action, the radius of the normal curvature of the work gear base cylinder is equal to the equivalent base diameter $d^*_{b.g}$ of the work gear. Similarly, at the point of tangency with the line of action, the radius of the normal curvature of the shaving cutter base cylinder is equal to the equivalent base diameter $d^*_{b.c}$ of the shaving cutter. It can be concluded from these statements that the equivalent diameters $d^*_{b.c}$ and $d^*_{b.c}$ are doubled normal curvatures of the base helices of the work gear and the shaving cutter. Therefore, the Euler equation can be used for the computation of the equivalent diameters

$$d^*_{b.g} = \frac{d_{b.g}}{\cos^2\psi_{b.g}} \tag{17.35}$$

$$d^*_{b.c} = \frac{d_{b.c}}{\cos^2\psi_{b.c}} \tag{17.36}$$

Having the parameters $d^*_{y.g}$, $d^*_{y.c}$, $d^*_{b.g}$, and $d^*_{b.c}$ computed [Equations (17.33) through (17.36)] makes it possible to enter them into the equation

$$V_{sl}^{(i)} = 0.5\left[\omega_c\sqrt{(d^*_{y.c})^2 - (d^*_{b.c})^2} - \omega_g\sqrt{(d^*_{y.g})^2 - (d^*_{b.g})^2}\right] \tag{17.37}$$

which is an analogy of Equation (17.24).

17.3.2.4 A Resultant Formula for Cutting Speed in Axial Gear Shaving

It is the right point here to summarize the results of the investigation undertaken in this section, and to put together all the components of the speed of the cut.

First, while the rotation of the shaving cutter remains the same [see Equation (17.6)], the rotation of the work gear is affected by the reciprocation motion. Owing to the reciprocation $\mathbf{F}_c$, an additional component $\boldsymbol{\omega}_g^{ad}$ of the rotation of the work gear [see Equation (17.20)] should be incorporated into Equation (17.5) for computation of the vector $\mathbf{V}_g$

$$\mathbf{V}_g = (\boldsymbol{\omega}_g + \boldsymbol{\omega}_g^{ad}) \times \mathbf{R}_g \tag{17.38}$$

Therefore, the sliding velocity vector $\mathbf{V}_{sl}$ [see Equation (17.7)] is equal

$$\mathbf{V}_{sl} = \underbrace{\boldsymbol{\omega}_c \times \mathbf{R}_c}_{\mathbf{v}_c} - \underbrace{(\boldsymbol{\omega}_g + \boldsymbol{\omega}_g^{ad}) \times \mathbf{R}_g}_{\mathbf{v}_g} \tag{17.39}$$

Second, the speed of the reciprocation $\mathbf{F}_c$ adds a component $\mathbf{F}_c^{sl}$ [see Equation (17.18)] to the cutting speed $\mathbf{V}_{cut}$.

Third, due to the profile sliding, the component $\mathbf{V}_{sl}^{(i)}$ affects the cutting speed $\mathbf{V}_{cut}$ as well [see Equation (17.21)].

Taking into account the results of the analysis disclosed in the previous three sections, Equation (17.4) can be cast into an expression for the cutting speed $\mathbf{V}_{cut}$ in the axial gear shaving process

$$\mathbf{V}_{cut} = \mathbf{V}_{sl} + \mathbf{F}_c^{sl} + \mathbf{V}_{sl}^{(i)} \tag{17.40}$$

It is assumed in Equation (17.40) that all the components are expressed in a common reference system.

Because vector $\mathbf{V}_{sl}^{(i)}$ of the profile sliding varies within the tooth height of the work gear as well as within the tooth height of the shaving cutter, then the resultant vector of the cutting speed varies within the tooth height of the shaving cutter as well.

The vector of the cutting speed $\mathbf{V}_{cut}$ is always within the tangent plane to the work gear tooth flank $\mathscr{G}$ at a point of its contact with the shaving cutter tooth flank.

17.4 Diagonal Method of the Gear Shaving Process

The direction of traverse of the shaving cutter may be obliquely inclined to the work gear axis. In this case the method of rotary shaving of the gears is commonly referred to as

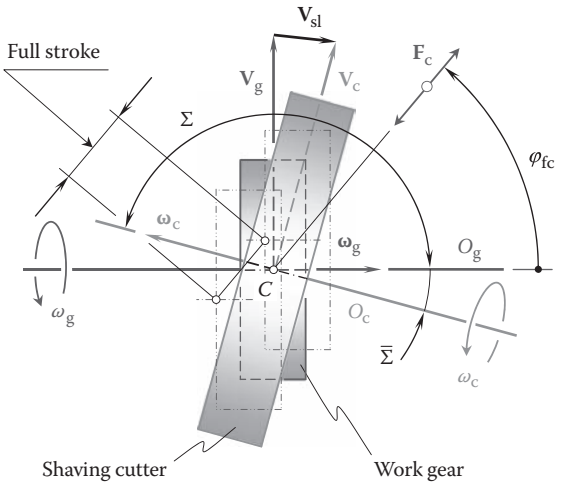

FIGURE 17.20
Schematic of the diagonal method of the gear shaving process.

the *diagonal method* of the gear shaving process.* This is the most widely used method of shaving.

The use of diagonal shaving makes it possible for finishing gears to have a wide range of face widths with the shaving cutter of a given design. It also permits shaving gears with face widths slightly in excess of the shaving cutter width. More even-wear distribution across the face of the shaving cutter can be easily achieved with this method of rotary shaving.

Diagonal shaving is used primarily in medium- and high-production operations. Using this method, shaving times are reduced by as much as 50%. Its production time in shaving is high because of the short stroke of the feed slide. One shaving cycle is usually sufficient to complete the shaving.

Diagonal shaving not only increases production rates substantially but also has other advantages for high-production operations.

17.4.1 Kinematics of the Diagonal Method of the Gear Shaving Process

When the diagonal method of gear shaving is used, the work gear and the shaving cutter are meshed in a crossed-axis relationship (Figure 17.20). The crossing axes of the work gear O_g and the shaving cutter O_c are at a certain center distance $C_{g/c}$.

Referring to Figure 17.20, the rotation of the work gear about it axis O_g is designated as $\boldsymbol{\omega}_g$. The rotation of the shaving cutter about its axis O_c is designated as $\boldsymbol{\omega}_c$. The shaving cutter is rotated in both directions during the work cycle. The rotations $\boldsymbol{\omega}_g$ and $\boldsymbol{\omega}_c$ are properly timed with one another ($\omega_g N_g = \omega_c N_c$; here N_g and N_c denote tooth number of the work gear and the shaving cutter, respectively, and the equalities $\omega_g = |\boldsymbol{\omega}_g|$ and $\omega_c = |\boldsymbol{\omega}_c|$ are observed). The rotation vectors $\boldsymbol{\omega}_g$ and $\boldsymbol{\omega}_c$ are at the angle $\Sigma = \angle(\boldsymbol{\omega}_g, \boldsymbol{\omega}_c)$. The angle $\overline{\Sigma}$ of the crossing of the axes O_g and O_c complements the angle Σ to 180° (i.e., $\overline{\Sigma} = \pi - \Sigma$).

* The diagonal method of the gear shaving process is also referred to as the *modified underpass* or *angular traverse* method of shaving of the gears.

The work gear reciprocates $\mathbf{F}_c$ obliquely in relation to its own axis while the work gear and the shaving cutter are in mesh (Figure 17.20). The traverse angle φ_{fc} is achieved either by positioning the work-piece table obliquely or by interpolating two machine axes. It is customary to move the work gear past the shaving cutter by means of the feed slide. On some of the larger shaving machines, for obvious reasons, the shaving cutter is mounted on a feed slide. In the scenario below, the *relative motion* of the work gear and the shaving cutter is considered regardless of whether the work-table or the shaving cutter actually reciprocates.

The productivity rate of the rotary shaving of the gears directly depends on the length of the traverse path of the work gear. In Figure 17.20, the end positions of the reciprocating work gear are shown with dashed lines. The length of the traverse path in diagonal shaving depends on (a) face width F_g of the work gear, (b) face width F_c of the shaving cutter, (c) angle $\bar{\Sigma}$ between the axis O_g of the work gear and the axis O_c of the shaving cutter, and (d) the traverse angle φ_{fc}. For computation of the length of the traverse path in practice, an approximate formula

$$L \cong \frac{F_g \sin \bar{\Sigma}}{\sin \varphi_{fc}} + m \tag{17.41}$$

is often used [166]. Here, in Equation (17.41), the module is denoted as m.

With diagonal traverse shaving, the centerline of the crossed axes is not restricted to a single position on the cutter as it is in conventional shaving, but is migrated across the shaving cutter face, evening out the wear. Consequently, shaving cutter life is extended.

Multistroke Diagonal Shaving. An automatic up-feed mechanism on the shaving machine materially enlarges the scope of diagonal shaving by also making it available for multistroke operations. This device feeds the work gear into the shaving cutter in a series of small increments, synchronized with table reciprocation.

The removal stock from the work gear in a series of small increments instead of two large increments further increases the shaving cutter life. It also makes the process feasible for gears requiring more stock removal than can be handled on a two-stroke cycle.

17.4.2 Traverse Angle in Diagonal Method of the Rotary Shaving of a Gear

The traverse angle φ_{fc} for diagonal shaving is the angle between the direction of traverse $\mathbf{F}_c$ and the work gear axis O_g. To obtain conditions of cutting speed and work gear quality, in most cases the traverse angle will vary in the range of $\varphi_{fc} = 40 \ldots 70°$.

When shaving cutters with annular serrations are used in diagonal shaving, then the traverse angle φ_{fc} is often limited to approximately $\varphi_{fc} \leq 55°$, unless differential-type serrations (Figure 17.9b) are used. Otherwise, the serrations will track.

When gears are shaved with the shaving cutter traveling at an angle to the axis, the shaving cutter has to be wide enough to shave the whole gear face width in one stroke. The relative face width of the work gear and the shaving cutter has an important relationship with the traverse angle. A wide-faced work gear and a narrow-faced shaving cutter restrict the diagonal traverse to a small angle. Increasing the face width of the shaving cutter permits an increase in traverse angle.

For computation of the maximum permissible traverse angle φ_{fc}, the following formula is recommended [10]

$$\varphi_{fc}^{max} = \tan^{-1}\left(\frac{F_c \sin\bar{\Sigma}}{F_g - F_c \cos\bar{\Sigma}}\right) \tag{17.42}$$

where

F_g = face width of the work gear
F_c = face width of the shaving cutter
$\bar{\Sigma}$ = angle between the axes of rotations O_g and O_c of the work gear and the shaving cutter

The traverse angle φ_{fc} can be expressed in terms of the rotation vector $\boldsymbol{\omega}_g$ of the work gear and the vector $\mathbf{F}_c$ of the reciprocation motion

$$\varphi_{fc} = -\tan^{-1}\left(\frac{|\boldsymbol{\omega}_g \times \mathbf{F}_c|}{\boldsymbol{\omega}_g \cdot \mathbf{F}_c}\right) \tag{17.43}$$

When the shaving cutter face width is increased to slightly greater than the work gear face width, traverse angles up to 90° are permissible. Diagonal shaving that features a large traverse angle is sometimes referred to as *diagonal-underpass shaving*. This shaving method is only an application option but is particularly used in the automotive industry. Since the traverse angle may be very large, this method is also suitable for shaving shoulder gears.

17.4.3 Cutting Speed in the Diagonal Method of the Rotary Shaving of a Gear

Since the shaving cutter is mounted on a shaft that is not parallel to the gear axis, the teeth of the shaving cutter and the teeth of the work gear run together like a pair of *crossed-helical* gears. The choice of crossed-axis angle governs the cutting action of the shaving cutter. In general, the higher the crossed-axis angle, the faster the shaving cutter cuts. The best control over helix angle, though, is gained with a low crossed-axis angle.

A resultant formula for the computation of the cutting speed $\mathbf{V}_{cut}$ in the diagonal shaving of gears is to that [see Equation (17.40)] earlier derived for the case of the axial method of shaving of gears. As in diagonal shaving, the traverse motion $\mathbf{F}_c$ is at the traverse angle φ_{fc} with respect to the work gear axis of rotation, so the impact of the motion $\mathbf{F}_c$ differs from that in the axial method of rotary shaving. Generally speaking, the traverse motion is not tangential to the flank of the work gear tooth. Because of this, the vector of the traverse motion affects the cutting speed in two different ways.

As above (see Figure 17.16), let us assume again that the shaving cutter is not rotating and is only reciprocating at the traverse angle with respect to the work gear axis φ_{fc} as depicted in Figure 17.21. Under such a scenario, vector $\mathbf{F}_c$ of the traverse motion of the shaving cutter is at an angle to the work gear tooth flank. Within the pitch plane, this angle is equal to $(\varphi_{fc} - \psi_g)$. The angle can be expressed in terms of the pitch helix angle ψ_g of the work gear and the pitch helix angle ψ_c of the shaving cutter. In this case the angles ψ_g and ψ_c should be considered as signed values depending of the direction of the hand of the helices.

The traverse motion $\mathbf{F}_c$ can be decomposed on two directions. One component $\mathbf{F}_c^{sl}$ is in the direction tangent to the tooth flank of the work gear. The magnitude of this component is equal

$$F_c^{sl} = |\mathbf{F}_c^{sl}| = \frac{|\mathbf{F}_c| \sin\varphi_{fc}}{\cos\psi_g} = \frac{F_c \sin\varphi_{fc}}{\cos\psi_g} \tag{17.44}$$

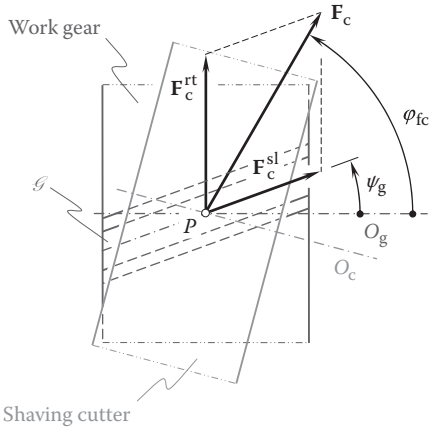

FIGURE 17.21
Impact of the traverse motion on the cutting speed $\mathbf{V}_{cut}$ in the diagonal shaving of gears.

The component $\mathbf{F}_c^{sl}$ represents pure sliding of the tooth flanks of the work gear and the shaving cutter.

It is important to point out here that the sliding vector $\mathbf{F}_c^{sl}$ is of constant magnitude, and it does not alternate within the tooth height either of the work gear or within the tooth height of the shaving cutter.

Another component $\mathbf{F}_c^{rt}$ of the traverse motion $\mathbf{F}_c$ is within the pitch plane and is pointed perpendicular to the axis of rotation of the work gear. For the computation of magnitude F_c^{rt} of the component $\mathbf{F}_c^{rt}$, the formula

$$F_c^{rt} = F_c \frac{\sin(\varphi_{fc} - \psi_g)}{\cos \psi_g} \tag{17.45}$$

can be used. This formula is derived from Figure 17.21 on the premises of the sine law.

The component $\mathbf{F}_c^{rt}$ contributes to the rotation of the work gear. This additional rotation ω_g^{ad} is equal

$$\omega_g^{ad} = F_c \frac{2 \sin(\varphi_{fc} - \psi_g)}{d_g \cos \psi_g} \tag{17.46}$$

The rotation vector $\boldsymbol{\omega}_g^{ad}$ is aligned with the rotation vector $\boldsymbol{\omega}_g$. Depending on (a) the rotation of the shaving cutter $\boldsymbol{\omega}_c$, (b) the direction of the hand and the value of the helix angle ψ_g, and (c) the actual direction of the reciprocation $\mathbf{F}_c$ (the traverse angle φ_{fc}), the rotation vector $\boldsymbol{\omega}_g^{ad}$ is pointed either in the same direction as the rotation vector $\boldsymbol{\omega}_g$, or it is pointed opposite to $\boldsymbol{\omega}_g$. In the first case the rotation $\boldsymbol{\omega}_g^{ad}$ adds to the rotation $\boldsymbol{\omega}_g$. In the second case it subtracts from the rotation $\boldsymbol{\omega}_g$.

Once Equations (17.44) through (17.46) are taken into account, then the resultant formula [see Equation (17.40)] can be used for the computation of cutting speed $\mathbf{V}_{cut}$ in diagonal shaving of the gears.

As the additional rotation ω_g^{ad} of the work gear depends on the pitch helix angle, the greater the pitch helix angle ψ_g of the work gear, the greater the impact of the traverse motion $\mathbf{F}_c$ of the shaving cutter on the cutting speed $\mathbf{V}_{cut}$ and vice versa.

The tangential speed of the work gear is usually about 400 ft/min (2.0 m/s) so that the work speed in

$$\omega_g = \frac{400 \times 12}{d_g \text{ (in.)}} \text{ rev./min.} \tag{17.47}$$

With an angle between the shaving cutter spindle and the work gear spindle in the range of $\bar{\Sigma} \cong 15°$, the cutting speed is about one-quarter of the circumferential speed of the work gear, in this case 110 ft/min. (0.55 m/s).

17.4.4 Optimization of the Kinematics in the Diagonal Method of the Rotary Shaving of a Gear

The design parameters of a shaving cutter as well as the parameters of the kinematics of the diagonal shaving process commonly are chosen empirically. In this way, the choice is made up only on the premise of an accumulated practical experience.

An attempt to develop an analytical solution to the problem of determining the optimal design parameters of the shaving cutter along with the optimal parameters of the kinematics of the diagonal gear shaving process has been undertaken by Radzevich and Palaguta [51, 135, 167]. They have proposed an analytical method for the synthesizing of the optimal gear shaving process. The method is based on an extensive implementation of the *DG/K*-based method of surface generation [59, 136, 138, 143]. Details on the proposed method of synthesis can also be found in [166]. The discussion below encompasses only the preliminary results of the study originally reported in [51, 135 166, 167] and others.

17.4.4.1 The Concept of the Optimization

The rate of metal removal and the surface finish strongly depend on the crossed-axis angle. Figure 17.22a shows diagrammatically the action between a shaving cutter and a helical gear. In Figure 17.22a, the speed of the total sliding motion is denoted as $\mathbf{V}_{sl}^{\Sigma}$. The vector $\mathbf{V}_{sl}^{\Sigma}$ is equal to summa of two components, namely (a) of the vector of sliding $\mathbf{V}_{sl}$, and (b) of the vector $\mathbf{F}_c^{sl}$ caused by the traverse motion $\mathbf{F}_c$. Ultimately, the equality $\mathbf{V}_{sl}^{\Sigma} = \mathbf{V}_{sl} + \mathbf{F}_c^{sl}$

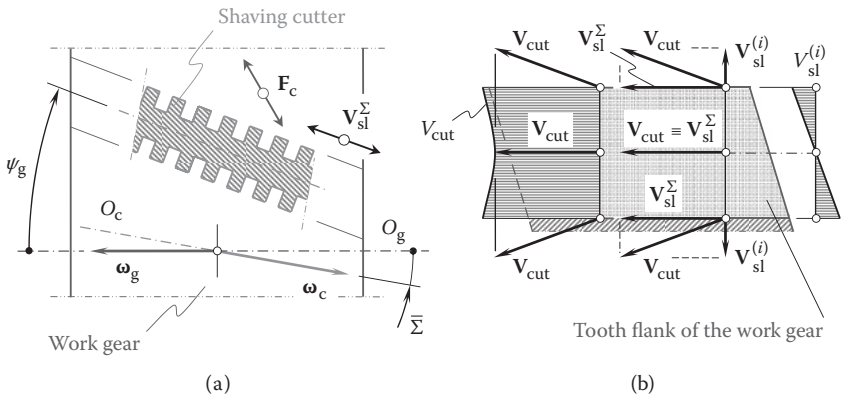

FIGURE 17.22
Variation of the speed cut $\mathbf{V}_{cut}$ within the tooth flank of a work gear.

is observed. The vector $\mathbf{V}_{sl}^{\Sigma}$ is constant at every point of contact of the tooth flank of the shaving cutter and the tooth flank of the work gear (Figure 17.22b).

The smaller the crossed-axis angle $\bar{\Sigma}$, the finer the shavings that are removed. In this way a very good finish can be produced. However burnishing and work hardening of the surface of the work gear teeth may occur unless the cutter is maintained in a very sharp condition.

If the crossed-axis angle is bigger, then shaving action becomes much more positive and it is easy to damage the work tooth surfaces unless light cutter loading is applied. Consequently, the finished surface is of a rather less smooth texture than that produced by a smaller angle.

Since the choice of crossed-axis angle is largely a matter of judgment in weighing different variables, there are no fixed rules [190].

The tooth profile sliding $\mathbf{V}_{sl}^{(i)}$ varies within the tooth flank of the work gear, as illustrated in Figure 17.22b. The vector $\mathbf{V}_{sl}^{(i)}$ affects both the value and the direction of speed of the cut vector $\mathbf{V}_{cut}$. The sliding velocity vector $\mathbf{V}_{sl}^{\Sigma}$ is predominant. However, the impact of the profile sliding velocity $\mathbf{V}_{sl}^{(i)}$ onto the speed of the cut vector $\mathbf{V}_{cut}$ could be significant when the tooth number of the work gear and/or of the shaving cutter is smaller.

Nominal contact between the work gear tooth flank and the shaving cutter tooth flank in diagonal shaving is a point. The point contact of the tooth flanks $\mathscr{G}$ and T can be easily interpreted in the following way. Referring to Figure 17.23a, the work gear tooth flank $\mathscr{G}$ and the auxiliary generating rack tooth flank $\mathscr{R}_T$ contact each other along the characteristic line $\mathscr{E}_g$. The auxiliary rack tooth flank $\mathscr{R}_T$ and the shaving cutter tooth flank T contact one another along the characteristic line $\mathscr{E}_c$. Both the straight lines $\mathscr{E}_g$ and $\mathscr{E}_c$ are located within the plane $\mathscr{R}_T$, and they intersect each other at point K. When the work gear and

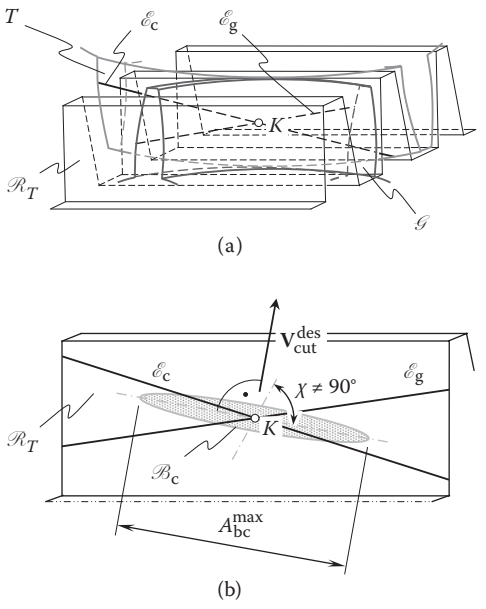

FIGURE 17.23
Contact between the work gear tooth flank and the shaving cutter tooth flank in diagonal shaving process. (From Radzevich, S.P., *International Journal of Advanced Manufacturing Technology*, 32(11–12), 1170–1187. With permission.)

the shaving cutter rotate in tight mesh the point of contact K is traveling from the outer diameter $d_{o.g}$ of the work gear toward it limit diameter $d_{l.g}$ or in the opposite direction depends on the direction of rotation of the work gear and the shaving cutter. In this way a path of contact on the tooth flank $\mathscr{G}$ is generated. When the shaving cutter is traversing, then the path of contact travels across the face width of the work gear. Ultimately, any point of the work gear tooth flank can make contact with the shaving cutter tooth flank.

Under load, the point of contact of the tooth flanks spreads over a certain area that is bounded by an ellipse-like boundary curve as shown in Figure 17.23b. The size and shape of the contact area depends on the pitch helix angle ψ_g of the work gear and the crossed-axis angle Σ (or $\overline{\Sigma}$).

Consider a surface $\mathscr{G}_{[h]}$ that is offset to the pinion tooth surface $\mathscr{G}$. When the offset distance is equal to the tolerance $[h]$ for the surface $\mathscr{G}$ accuracy, then the offset surface is referred to as the *surface of tolerance* $\mathscr{G}_{[h]}$.

When the tooth surface $\mathscr{G}$ of a pinion and the tooth surface T of the shaving cutter make contact at point K, the surface T intersects the surface of tolerance $\mathscr{G}_{[h]}$. The line of the intersection of the surfaces is a certain closed 3-D boundary curve $\mathscr{B}_c$. This curve is often incorrectly referred to as a *contact ellipse*.* The boundary curve $\mathscr{B}_c$ bounds the spot of contact of the pinion and the shaving cutter tooth. The contact area passes over the tooth flank of the work gear and the asperities and protuberances are removed down to a basic smooth surface $\mathscr{G}$ as the shaving cutter rotates in contact with the work gear, and it is traversed $\mathbf{F}_c$ across the face of the work gear at a feed rate.

The following issues are of critical importance for further consideration.

First, gear shaving is a kind of finishing processes. For accuracy reasons, forces that act on the work gear and the shaving cutter must be at the lowest possible range. Low cutting forces cause small deflection of the shaving machine. Surface area that is bounded by the boundary curve $\mathscr{B}_c$ should be as small as possible if we are about achieving low cutting forces.

Second, the path of contact of the work gear tooth flank $\mathscr{G}$ and the shaving cutter tooth flank T should be the widest possible. For this purpose, major axis A_{bc}^{max} of the contact area must be the longest possible. This makes possible a higher productivity rate of the rotary shaving process.

Third, as the productivity of the gear finishing process is of importance, the desired direction of the cutting speed $\mathbf{V}_{cut}^{des}$ must be orthogonal to the major axis A_{bc}^{max} of the boundary curve $\mathscr{B}_c$. It is the right time to point out here that the minor axis A_{bc}^{min} of the boundary curve $\mathscr{B}_c$ (not shown in Figure 17.23b) is not perpendicular to the major axis A_{bc}^{max}. The axes A_{bc}^{max} and A_{bc}^{min} are at a certain angle $\chi \neq 90°$.

Once the above-listed three items are properly understood, then it becomes clear that varying the design parameters of the shaving cutter, and synchronizing the direction and speed of traverse $\mathbf{F}_c$ with the rotation of the work gear ω_g and the shaving cutter ω_c makes it possible to control the shape, size, and orientation of the contact area. The direction of the cutting speed $\mathbf{V}_{cut}$ can also be under control in this way. Ultimately, the accuracy of the finished gears can be increased, and the shaving time reduced if the proper combination of the design parameters of the work gear and the shaving cutter is determined, and all the elementary motions of the rotary shaving process ($\boldsymbol{\omega}_g$, $\boldsymbol{\omega}_c$ and $\mathbf{F}_c$) are properly timed with each other. The crossed-axis angle Σ is not listed here because the rotations of the work gear and the shaving cutter are represented in vector notation.

* The boundary curve $\mathscr{B}_c$ is a type of 3-D curve, while an ellipse is a type of planar curve.

The local topology of the work gear tooth flank $\mathcal{G}$ and the shaving cutter tooth flank T is required to be known for the implementation of *DG/K*-based method of surface generation for the purpose of synthesizing the optimal process of the rotary shaving of gears.

17.4.4.2 Local Topology of the Contacting Tooth Flanks

Investigation of local topology of the tooth flank of both the work gear $\mathcal{G}$ and the shaving cutter T begins with derivation of an equation of the tooth flank that is accomplished with the equation of Dupin indicatrix of the surface. Because the surfaces $\mathcal{G}$ and T are similar, the required equations are considered in detail for the surface $\mathcal{G}$ only. Corresponding equations for the generating surface T of the shaving cutter can be written by an analogy with the equations derived for the tooth flank $\mathcal{G}$.

Equation of tooth flank $\mathcal{G}$ of an involute gear. The equation of the tooth surface $\mathcal{G}$ of the work gear can be represented in the form of a column matrix [see Equation (1.3)]

$$\mathbf{r}_g(U_g, V_g) = \begin{bmatrix} r_{b.g}\cos V_g + U_g \cos\psi_{b.g}\sin V_g \\ r_{b.g}\sin V_g - U_g \sin\psi_{b.g}\sin V_g \\ r_{b.g}\tan\psi_{b.g} - U_g \sin\psi_{b.g} \\ 1 \end{bmatrix} \tag{17.48}$$

where

$r_{b.g}$ = radius of the base cylinder of the work gear
U_g, V_g = curvilinear (Gaussian) coordinates on the tooth flank of the work gear
$\psi_{b.g}$ = base helix angle of the work gear

The first fundamental form of an involute gear tooth surface $\mathcal{G}$. Fundamental magnitudes E_g, F_g, G_g of the first fundamental form $\Phi_{1.g}$ of the work gear tooth flank $\mathcal{G}$ can be computed from Equation (17.48) [138, 143].

$$E_g = 1, \quad F_g = -\frac{r_{b.g}}{\cos\psi_{b.g}}, \quad G_g = \frac{U_g^2\cos^4\psi_{b.g} + r_{b.g}^2}{\cos^2\psi_{b.g}} \tag{17.49}$$

Equation (17.49) yields an expression

$$\boldsymbol{\Phi}_{1.g} \quad \Rightarrow \quad dU_g^2 - 2\frac{r_{b.g}}{\cos\psi_{b.g}}dU_g dV_g + \frac{U_g^2\cos^4\psi_{b.g} + r_{b.g}^2}{\cos^2\psi_{b.g}}dV_g^2 \tag{17.50}$$

for the first fundamental form $\Phi_{1.g}$ of the work gear tooth flank $\mathcal{G}$.

The second fundamental form of an involute gear tooth surface $\mathcal{G}$. Equations (17.48) and (17.49) allow for the computation of fundamental magnitudes L_g, M_g, N_g of the second fundamental form $\Phi_{2.g}$ of the work gear tooth surface $\mathcal{G}$ [138, 143]

$$L_g = 0, \quad M_g = 0, \quad N_g = -U_g \sin\tau_{b.g}\cos\tau_{b.g} \tag{17.51}$$

Equation (17.51) yields an expression

$$\boldsymbol{\Phi}_{2.g} \quad \Rightarrow \quad -U_g \sin\psi_{b.g}\cos\psi_{b.g}dV_g^2 \tag{17.52}$$

for the second fundamental form $\Phi_{2.g}$ of the work gear tooth flank $\mathcal{G}$.

Curvature of an involute gear tooth surface $\mathcal{G}$. Having computed the first $\Phi_{1.g}$ and the second $\Phi_{2.g}$ fundamental forms [see Equations (17.50)–(17.52)], *normal curvature* k_g of the work gear tooth flank $\mathcal{G}$ can be computed from the simple equation $k_g = \Phi_{2.g}/\Phi_{1.g}$. This equation casts into

$$k_g = -\frac{1}{U_g \sin\psi_{b.g} \cos\psi_{b.g}}\lambda^2 + 2\frac{r_{b.g}}{U_g \sin\psi_{b.g} \cos^2\psi_{b.g}}\lambda - \frac{U_g^2 \cos^4\psi_{b.g} + r_{b.g}^2}{U_g \sin\psi_{b.g} \cos^3\psi_{b.g}} \quad (17.53)$$

where λ denotes the ratio $\lambda = dU_g/dV_g$.

The first $k_{1.g}$ and second $k_{2.g}$ *principal curvatures* of the work gear tooth flank $\mathcal{G}$ are equal

$$k_{1.g} = \frac{\tan\psi_{b.g}}{U_g} = \frac{2\sin\psi_{b.g}}{\sqrt{d_{y.g}^2 - d_{b.g}^2}\cos\lambda_{b.g}} = \frac{2\sin\psi_g \sin\phi_n}{\sqrt{d_{y.g}^2 - d_{b.g}^2}\cos\lambda_{b.g}} \quad \text{and} \quad k_{2.g} = 0 \quad (17.54)$$

respectively. It should be pointed out here that the inequality $k_{1.g} > k_{2.g}$ is always observed.*

Dupin indicatrix of an involute gear tooth surface $\mathcal{G}$. As tooth flank $\mathcal{G}$ of the work gear is an involute surface, its local patch in a differential vicinity of a point is a local patch of the parabolic type. In a local orthogonal coordinate system, the equation of the Dupin indicatrix Dup($\mathcal{G}$) is described by equation

$$\text{Dup}(\mathcal{G}) \quad \Rightarrow \quad \frac{U_g \sin\psi_{b.g} \cos^3\psi_{b.g}}{U_g^2 \cos^4\psi_{b.g} + r_{b.g}^2} y_g^2 = \mp 1 \quad (17.55)$$

Equations for the generating surface T of a shaving cutter. A comparison of Equation (17.1) for the generating surface T of a shaving cutter and Equation (17.48) for tooth flank $\mathcal{G}$ of a work gear reveals that the equations are similar to each other in nature. Therefore, once the generating surface of a shaving cutter is represented in a coordinate system $X_cY_cZ_c$ associated with the shaving cutter itself, then equations identical to Equations (17.49) through (17.55) derived above are also valid for the generating surface T of a shaving cutter. To be treated together, Equations (17.1) and (17.48) must be represented in a common reference system.

17.4.4.3 Applied Coordinate Systems

Several reference systems are used for analytical description of the surfaces $\mathcal{G}$ and T, and of their configuration and relative motion. Three of them are of prime importance in the consideration below.

One of the coordinate systems is a left-hand–oriented Cartesian coordinate system $X_gY_gZ_g$ associated with the work gear. Another one is a left-hand–oriented Cartesian coordinate system $X_cY_cZ_c$ connected to the shaving cutter. The third one is a left-hand–oriented local Cartesian coordinate system $x_gy_gz_g$ with the origin at point K of contact of the work gear tooth surface $\mathcal{G}$ and the shaving cutter tooth surface T (Figure 17.24). These three coordinate systems are referred to as main coordinate systems. It is assumed below that configuration of the main reference system is known in a certain common coordinate system, for instance, in a coordinate system $X_{sm}Y_{sm}Z_{sm}$ associated with the shaving machine.

* Remember that algebraic values of the principal curvatures $k_{1.g}$ and $k_{2.g}$ relate to each other as $k_{1.g} > k_{2.g}$.

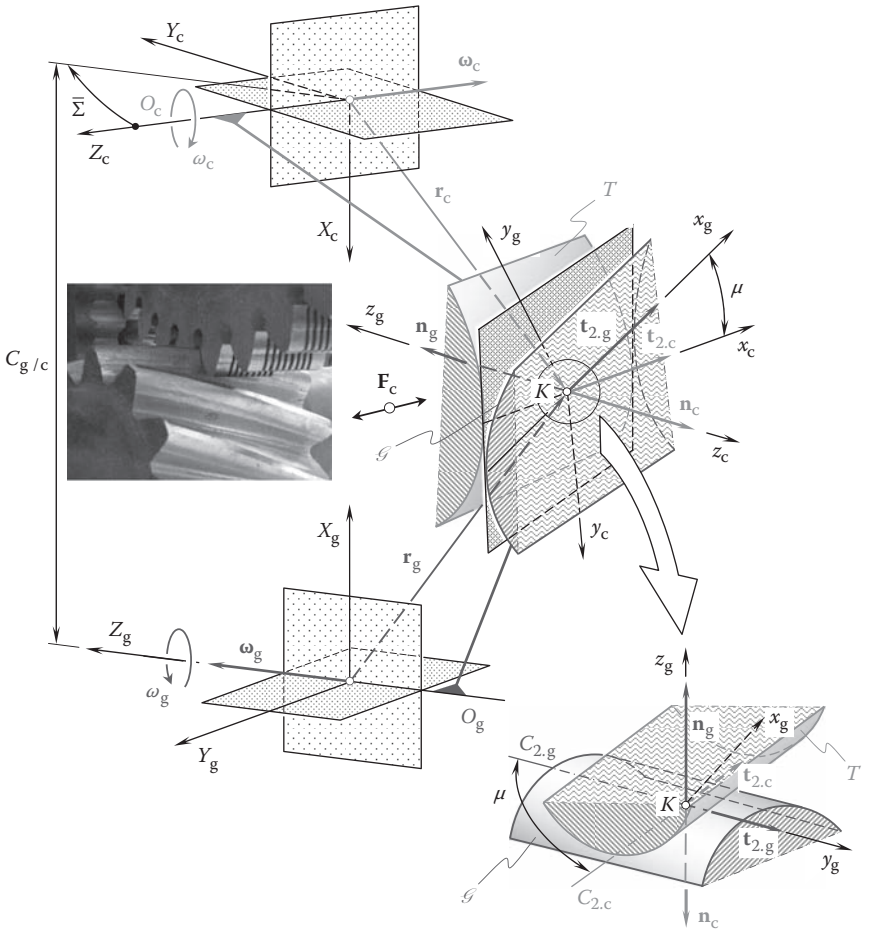

FIGURE 17.24

The coordinate systems associated with the work gear $\mathscr{G}$, with shaving cutter T and current point of contact K. (From Radzevich, S.P., *International Journal of Advanced Manufacturing Technology*, 32(11–12), 1170–1188. With permission.)

Axis Z_g of the reference system $X_gY_gZ_g$ is aligned to the work gear axis O_g, and Z_c axis of the reference system $X_cY_cZ_c$ is aligned with the shaving cutter axis O_c. Axes X_g and X_c are parallel to the common tangent plane to the pitch cylinders of the work gear and the shaving cutter. Ultimately, axes Y_g and Y_c are perpendicular to the common tangent plane to the pitch cylinders of the work gear and the shaving cutter.

A local left-hand–oriented coordinate system $x_gy_gz_g$ is associated with the work gear tooth flank $\mathscr{G}$. Axis x_g is aligned to the unit tangent vector $\mathbf{u}_g = \mathbf{U}_g/|\mathbf{U}_g|$, where $\mathbf{U}_g = \partial\mathbf{r}_g/\partial U_g$ (Figure 17.24); axis Z_p is aligned to the surface $\mathscr{G}$ unit normal $\mathbf{n}_g = \mathbf{u}_g \times \mathbf{v}_g$, where $\mathbf{v}_g = \mathbf{V}_g/|\mathbf{V}_g|$, and $\mathbf{V}_g = \partial\mathbf{r}_g/\partial V_g$; this axis is pointed outward toward the body of the work gear tooth; and axis y_g is aligned to the unit tangent vector $\mathbf{v}_g^* = \mathbf{n}_g \times \mathbf{u}_g$ (under such condition axis y_g is perpendicular to the x_gz_g coordinate plane).

The similar local coordinate system $x_cy_cz_c$ with the origin at point K is associated with the involute tooth surface T of the shaving cutter.

In addition to the above-mentioned coordinate systems, several auxiliary reference systems are also employed.

17.4.4.4 Geometry of Contact of the Tooth Flanks $\mathcal{G}$ and T

The geometry of contact of the tooth flanks $\mathcal{G}$ and T of the work gear and the shaving cutter should be properly described analytically prior to determining the optimal design parameters of a shaving cutter, and the parameters of the kinematics of the rotary shaving operation. Indicatrix of conformity $\mathrm{Cnf}_R(\mathcal{G}/T)$ is used for the purpose of analytical description of the geometry of contact of two smooth regular surfaces $\mathcal{G}$ and T in differential vicinity of point K of their contact.

Principal directions on the contacting tooth flanks $\mathcal{G}$ and T. As tooth flanks $\mathcal{G}$ and T are smooth regular surfaces, two principal directions can be determined on each of the surfaces.

A direction on a work gear tooth flank $\mathcal{G}$ can be uniquely specified by the ratio $\eta_c = dU_c/dV_c$. Those directions $\mathbf{t}_{1.g}$ and $\mathbf{t}_{2.g}$ for which the equality

$$\begin{vmatrix} \eta_g E_g + F_g & \eta_g F_g + G_g \\ \eta_g L_g + M_g & \eta_g M_g + N_g \end{vmatrix} = 0 \tag{17.56}$$

is satisfied are referred to as principal directions on the tooth flank $\mathcal{G}$.

Similarly, two principal directions $\mathbf{t}_{1.c}$ and $\mathbf{t}_{2.c}$ on generating surface T of a shaving cutter can be expressed in terms of the fundamental magnitudes E_c, F_c, G_c and L_c, M_c, N_c, and of the ratio $\eta_g = dU_g/dV_g$.

Local orientation of tooth flanks of a work gear and the shaving cutter. Local orientation of the tooth flanks of a work gear $\mathcal{G}$ and the shaving cutter T can be specified in terms of angle μ of the surfaces $\mathcal{G}$ and T local relative orientation [59, 136, 138, 143]. Angle μ of the surfaces' local relative orientation is the angle that makes unit tangent vectors $\mathbf{t}_{1.g}$ and $\mathbf{t}_{1.c}$ of the first (or, the same, of the second $\mathbf{t}_{2.g}$ and $\mathbf{t}_{2.c}$) principal directions of the surfaces $\mathcal{G}$ and T at point K. Thus, by definition, angle μ of the surfaces' local relative orientation is equal

$$\tan\mu = \frac{|\,\mathbf{t}_{1.g} \times \mathbf{t}_{1.c}\,|}{\mathbf{t}_{1.g} \cdot \mathbf{t}_{1.c}} \equiv \frac{|\,\mathbf{t}_{2.g} \times \mathbf{t}_{2.c}\,|}{\mathbf{t}_{2.g} \cdot \mathbf{t}_{2.c}} \tag{17.57}$$

In the case of the rotary shaving of an involute gear, Equation (17.57) is reduced to

$$\sin\mu = \frac{\sin\phi_n \sin\bar{\Sigma}}{\sqrt{(1-\cos^2\phi_n \sin^2\psi_g)\cdot(1-\cos^2\phi_n \sin^2\psi_c)}} \tag{17.58}$$

where

ϕ_n = normal profile angle in the *work gear to shaving cutter* mesh
ψ_g = pitch helix angle of the work gear
ψ_c = pitch helix angle of the shaving cutter
$\bar{\Sigma}$ = angle between the axes of rotation O_g and O_c of the work gear and the shaving cutter

Indicatrix of conformity $Cnf_R(\mathscr{G}/T)$ of a work gear tooth flank and the tooth flank of a generating surface of the shaving cutter. The indicatrix of conformity* of two smooth regular surfaces [59, 128, 136, 138, 143, 158] is a planar characteristic curve of the fourth order. It possesses the property of central symmetry, and in particular cases, it also possesses the property of mirror symmetry. This characteristic curve quantitatively reflects the rate of conformity of the surfaces, which make contact at a point, or along a curve line. The characteristic curve $\mathrm{Cnf}_R(\mathscr{G}/T)$ can be depicted in a common tangent plane (in the coordinate plane $x_g y_g$ of the local reference system $x_g y_g z_g$).

An equation of indicatrix of conformity $\mathrm{Cnf}_R(\mathscr{G}/T)$ of two smooth regular surfaces can be employed in the case of rotary shaving of an involute gear. For this purpose the expressions for the first $\Phi_{1.g}$, $\Phi_{1.c}$ [see Equation (17.50)], and second $\Phi_{2.g}$, $\Phi_{2.c}$ [see Equation (17.52)], fundamental forms must be represented in a common reference system. The local coordinate system $x_g y_g z_g$ (Figure 17.24) is used as the common reference system in the case under consideration.

For the purposes of transformation of a surface fundamental forms, a formula

$$[\boldsymbol{\Phi}_{1.g}]_K = \mathbf{Rs}^T(g \to K) \cdot [\boldsymbol{\Phi}_{1.g}]_g \cdot \mathbf{Rs}(g \to K) \tag{17.59}$$

$$[\boldsymbol{\Phi}_{2.g}]_K = \mathbf{Rs}^T(g \to K) \cdot [\boldsymbol{\Phi}_{2.g}]_g \cdot \mathbf{Rs}(g \to K) \tag{17.60}$$

is proposed by Radzevich [155]. This formula is also known from other sources [59, 136, 138, 143].

In Equations (17.59) and (17.60), $[\Phi_{1.g}]_g$ and $[\Phi_{2.g}]_g$ denote the first and second fundamental forms of the work gear tooth flank when the surface $\mathscr{G}$ is represented in the coordinate system $X_g Y_g Z_g$; $[\Phi_{1.g}]_K$, and $[\Phi_{2.g}]_K$ denote that same fundamental forms when the equation of the surface $\mathscr{G}$ is transformed to the local reference system $x_g y_g z_g$, and the operator of the resultant coordinate system transformation is designated as $\mathbf{Rs}(g \to K)$.

Equations similar to Equation (17.59) and (17.60) can be composed for the tooth flank T of the generating surface of the shaving cutter.

With the fundamental forms $[\Phi_{1.g}]_K$, $[\Phi_{2.g}]_K$, $[\Phi_{1.c}]_K$ and $[\Phi_{2.c}]_K$ computed, this immediately yields an expression

$$\text{Indicatrix of conformity } \mathrm{Cnf}_R(\mathscr{G}/T) \quad \Rightarrow \quad r_{\mathrm{cnf}}(R_{1.g}, R_{1.c}, \mu, \varphi) = \frac{\sqrt{R_{1.g}}}{\sin\varphi} + \frac{\sqrt{R_{1.c}}}{\sin(\mu - \varphi)} \tag{17.61}$$

for the indicatrix of conformity $\mathrm{Cnf}_R(\mathscr{G}/T)$ of the tooth flanks $\mathscr{G}$ and T. Equation (17.61) is represented in the local coordinate system $x_g y_g z_g$.

Equation (17.61) is represented in polar coordinates with the origin at K. The distance r_{cnf} of a current point of the indicatrix of conformity $\mathrm{Cnf}_R(\mathscr{G}/T)$ is expressed in terms of (a) the first radii of curvature $R_{1.g}$ and $R_{1.c}$ of the contacting surfaces $\mathscr{G}$ and T (here the equalities $R_{1.g} = k_{1.g}^{-1}$ and $R_{1.c} = k_{1.c}^{-1}$ are observed), (b) the angle μ of the tooth flanks' $\mathscr{G}$ and T local relative orientation, and (c) polar angle φ.

---

* An equation of this characteristic curve has been published in (a) SU Pat. No. 1185749, *A Method of Sculptured Surface Machining on Multi-Axis NC Machine.*/S.P. Radzevich, Int. Cl. B23C 3/16, Filed: October 24, 1983, and (b) SU Pat. No. 1249787, *A Method of Sculptured Surface Machining on Multi-Axis NC Machine.*/S.P. Radzevich, Int. Cl. B23C 3/16, Filed: December 27, 1984.

An illustrative example of the characteristic curve $\mathrm{Cnf}_R(\mathscr{G}/T)$ is depicted in Figure 17.25. For convenience, the Dupin indicatrices $\mathrm{Dup}(\mathscr{G})$ and $\mathrm{Dup}(T)$ along with the curvature indicatrices $\mathrm{Ind}(\mathscr{G})$ and $\mathrm{Ind}(T)$ are shown in Figure 17.25 as well.

The rate of conformity of the tooth flank T of the shaving cutter to the tooth flank $\mathscr{G}$ of the work gear at K alternates as a normal cross section of the surfaces $\mathscr{G}$ and T turns about common perpendicular $\mathbf{n}_g$ through the point of contact [135]. In a certain normal cross section of the tooth flanks $\mathscr{G}$ and T, the rate of their conformity reaches the maximum value. This normal cross section $C_{\mathrm{cnf}}^{\max}$ of the surfaces $\mathscr{G}$ and T is referred to as cross section of the *maximum rate of conformity* of the surfaces. The maximum rate of conformity cross section of the surfaces is the cross section through the direction of minimum diameter $d_{\mathrm{cnf}}^{\min}$ of the indicatrix of conformity $\mathrm{Cnf}_R(\mathscr{G}/T)$. Referring to Figure 17.26, this direction is specified by unit tangent vector $\mathbf{t}_{\mathrm{cnf}}^{\max}$.

Equation (17.61) of the indicatrix of conformity $\mathrm{Cnf}_R(\mathscr{G}/T)$ can be expressed in terms of the design parameters of the work gear and the shaving cutter

$$r_{\mathrm{cnf}}(d_{y.g}, d_{y.c}, \varphi, \mu) = \sqrt{\frac{2\sin\psi_g \sin\phi_n}{\sqrt{d_{y.g}^2 - d_{b.g}^2}\cos\lambda_{b.g}\sin^2\varphi}} + \sqrt{\frac{2\sin\psi_c \sin\phi_n}{\sqrt{d_{y.c}^2 - d_{b.c}^2}\cos\lambda_{b.c}\sin^2(\mu-\varphi)}} \quad (17.62)$$

All the information necessary for the computation of the optimal design parameters of the shaving cutter and the optimal parameters of the kinematics of the rotary shaving process of a work gear can be extracted from Equation (17.62).

The lateral tooth plane of the auxiliary generating rack $\mathscr{R}_T$ is tangent at K to both the tooth flank $\mathscr{G}$ of the work gear and the tooth flank T of the shaving cutter. For convenience, in Figure 17.27 the characteristic curve $\mathrm{Cnf}_R(\mathscr{G}/T)$ is depicted in the lateral plane $\mathscr{R}_T$.

The major axis $A_{\mathrm{bc}}^{\max}$ of the *work gear to shaving cutter* contact area is aligned with the direction of the minimum diameter $d_{\mathrm{cnf}}^{\min}$ of the indicatrix of conformity $\mathrm{Cnf}_R(\mathscr{G}/T)$. The axis $A_{\mathrm{bc}}^{\max}$ is within the angle that makes the characteristic lines $\mathscr{E}_g$ of the surface $\mathscr{G}$ and $\mathscr{E}_c$

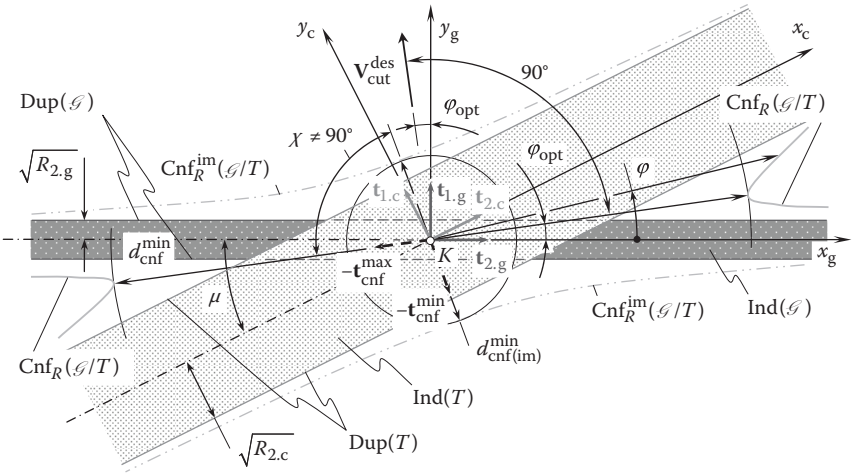

FIGURE 17.25
Indicatrix of conformity $\mathrm{Cnf}_R(\mathscr{G}/T)$ for the contacting tooth flanks $\mathscr{G}$ of the work gear and T of a shaving cutter, which is represented in the local reference system $x_g y_g z_g$. (From Radzevich, S.P., *International Journal of Advanced Manufacturing Technology*, 32(11–12), 1170–1189. With permission.)

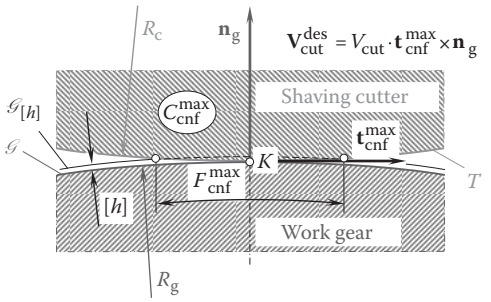

FIGURE 17.26
Normal cross section C_{cnf}^{max} of contacting tooth flanks $\mathscr{G}$ and T, which corresponds to the direction $\mathbf{t}_{cnf}^{max}$ of the maximum rate of conformity of the surfaces $\mathscr{G}$ and T. (From Radzevich, S.P., *International Journal of Advanced Manufacturing Technology*, 32(11–12), 1170–1190. With permission.)

of the surface T. It is important to stress here that the major axis A_{bc}^{max} and the minor axis A_{bc}^{min} of the boundary curve $\mathscr{B}_c$ are not orthogonal to each other (i.e., in the general case angle $\chi \neq 90°$). The desired direction of the speed of the cut $\mathbf{V}_{cut}^{des}$ at K is perpendicular to the minimum diameter d_{cnf}^{min} of the characteristic curve $\mathrm{Cnf}_R(\mathscr{G}/T)$. the direction of the

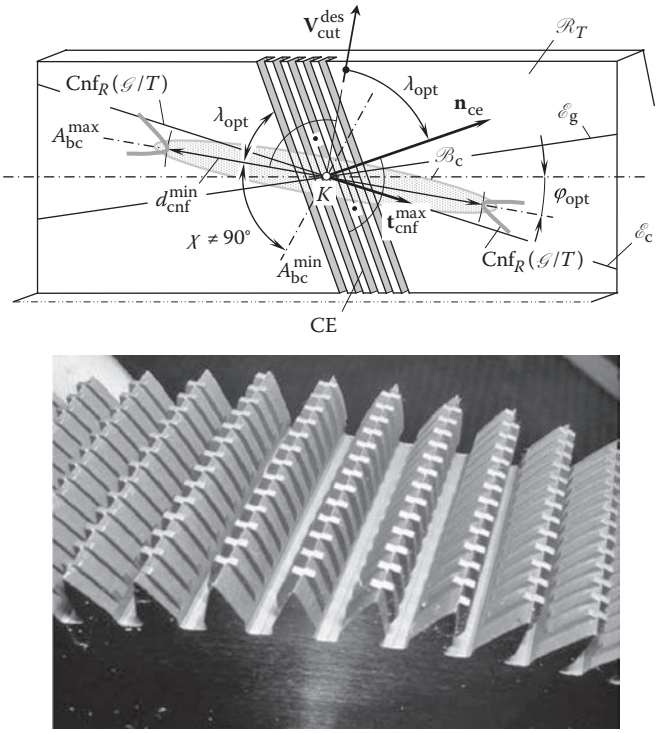

FIGURE 17.27
Location and orientation of the indicatrix of conformity Cnf_R $(\mathscr{G}/T)$ within the tooth flank of auxiliary generating surface $\mathscr{R}_T$. (From Radzevich, S.P., *International Journal of Advanced Manufacturing Technology*, 32(11–12), 1170–1191. With permission.)

minimum diameter is also indicated with unit tangent vector $\mathbf{t}_{cnf}^{max}$ of the direction of the maximum rate of conformity of the tooth flanks $\mathcal{G}$ and T.

The angle of inclination of the cutting edge λ is measured between the cutting speed vector $\mathbf{V}_{cut}^{des}$ and normal unit vector $\mathbf{n}_{ce}$ to the cutting edge CE. The vector $\mathbf{n}_{ce}$ is within the plane $\mathcal{R}_T$ (Figure 17.27). Keeping this in mind, a shaving cutter that features optimal inclination angle λ_{opt} can be designed based on the features of geometry of the indicatrix of conformity $\text{Cnf}_R(\mathcal{G}/T)$.

17.4.4.5 Optimal Design Parameters of a Shaving Cutter and Optimal Parameters of the Kinematics of the Rotary Shaving Operation

At this point, with the indicatrix of conformity $\text{Cnf}_R(\mathcal{G}/T)$ computed, the problem of minimum shaving time can be expressed in terms of the design parameters of the shaving cutter along with the parameters of the kinematics of the rotary shaving process: (a) the rate of conformity of the shaving cutter tooth flank T to the work gear tooth flank $\mathcal{G}$ must be the maximum possible at every point of contact of the surfaces, and (b) an angle that the cutting speed vector $\mathbf{V}_{cut}$ makes with the vector $\mathbf{V}_{cut}^{des}$ of the desired speed of the cut must be the smallest possible.

Necessary and sufficient conditions. Once the geometry of the contact of the tooth flanks $\mathcal{G}$ and T is described analytically by means of indicatrix of conformity $\text{Cnf}_R(\mathcal{G}/T)$, then computation of the optimal design parameters of a shaving cutter and optimal parameters of the kinematics of a rotary shaving process turns to a routing problem.

A set of equations that specifies the necessary conditions for the minimum shaving time and maximum accuracy of the shaved tooth flank of a work gear immediately follows from Equation (17.61) of the indicatrix of conformity $\text{Cnf}_R(\mathcal{G}/T)$.

$$\left.\begin{array}{l}\text{The Necessary Conditions}\\ \text{for}\\ \textit{Minimum Shaving Time}\\ \text{and}\\ \textit{Maximum Accuracy}\\ \text{of the Shaved Gear}\end{array}\right| \Rightarrow \begin{cases} \dfrac{\partial r_{cnf}}{\partial R_{1.c}} = \dfrac{1}{\sqrt{R_{1.c}}\,\sin(\mu-\varphi)} = 0 \\ \dfrac{\partial r_{cnf}}{\partial \mu} = -\dfrac{\cos(\mu-\varphi)}{\sin^2(\mu-\varphi)}\sqrt{R_{1.c}} = 0 \\ \dfrac{\partial r_{cnf}}{\partial \varphi} = -\dfrac{\cos\varphi}{\sin^2\varphi}\sqrt{R_{1.p}} - \dfrac{\cos(\mu-\varphi)}{\sin^2(\mu-\varphi)}\sqrt{R_{1.c}} = 0 \end{cases} \tag{17.63}$$

The *sufficient* conditions for the maximum of function $r_{cnf}(R_{1.c}, \mu, \varphi)$ of three variables in this particular case are also satisfied.

The solution to the set of Equation (17.63) returns optimal values of three parameters, namely of (a) the first radius of curvature $R_{1.c}^{opt}$ of the shaving cutter tooth flank T, (b) the angle μ_{opt} of the relative orientation of the surfaces $\mathcal{G}$ and T, and (c) the angular parameter φ_{opt}. The computed set of the parameters $R_{1.c}^{opt}$, μ_{opt}, and φ_{opt} is optimal for machining a given work gear. Two of the parameters ($R_{1.c}^{opt}$ and μ_{opt}) are sufficient for the computation of optimal values of the rest of the design parameters of a shaving cutter, while the third one (φ_{opt}) determines the desired direction of the cutting speed vector $\mathbf{V}_{cut}^{des}$. Due to the constraints imposed by the design of shaving machines available on the market, the actual values $R_{1.c}^{act}$, μ_{act}, and φ_{act} of the parameters must be as close as possible to their computed values $R_{1.c}^{opt}$, μ_{opt}, and φ_{opt}.

17.5 Tangential Method of the Gear Shaving Process

In the extreme condition a work gear is passed across the face of the shaving cutter at right angles to the work gear axis of rotation. When the traverse is orthogonal to the axis of the work gear, the method of gear shaving is referred to as the *tangential method*. The tangential method is also often referred to as the *underpass method* of gear shaving. Because of the short feed stroke and the one cycle required, the tangential method of shaving is usually the fastest method of shaving. It is used primarily in high-production operations.

17.5.1 Kinematics of the Tangential Method of the Gear Shaving Process

Tangential shaving is basically the same as diagonal shaving but the traverse path of the work gear is perpendicular to its axis (Figure 17.28). With tangential shaving there is no axial reciprocation of the worktable. Instead the work gear reciprocates perpendicularly to its own axis. This method is usually dictated when shaving cluster gears or gears with close adjacent shoulders. The cross-axis angle is usually in the range of 4° to 6° in order to avoid collision of the shaving cutter with the shoulder.

When the tangential method of gear shaving is used, the work gear and the shaving cutter are meshed in crossed-axis relationship (Figure 17.28). The crossing axes of the work gear O_g and the shaving cutter O_c are at a certain center distance $C_{g/c}$.

Referring to Figure 17.28, the rotation of the work gear about it axis O_g is designated as $\boldsymbol{\omega}_g$. The rotation of the shaving cutter about it axis O_c is designated as $\boldsymbol{\omega}_c$. The shaving cutter is rotated in both directions during the work cycle. The rotations $\boldsymbol{\omega}_g$ and $\boldsymbol{\omega}_c$ are properly timed with one another ($\omega_g N_g = \omega_c N_c$; here N_g and N_c denote the tooth number of the work gear and the shaving cutter, respectively, and the equalities $\omega_g = |\boldsymbol{\omega}_g|$ and $\omega_c = |\boldsymbol{\omega}_c|$ are observed). The rotation vectors $\boldsymbol{\omega}_g$ and $\boldsymbol{\omega}_c$ are at the angle $\Sigma = \angle(\boldsymbol{\omega}_g, \boldsymbol{\omega}_c)$. The angle Σ of crossing of the axes O_g and O_c complements the angle Σ to 180° (i.e., $\bar{\Sigma} = \pi - \Sigma$).

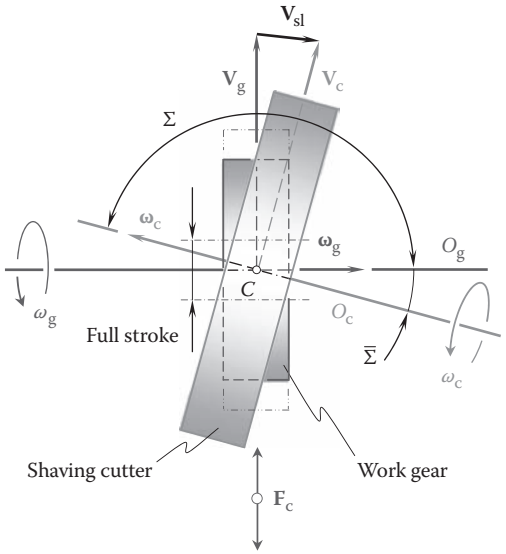

FIGURE 17.28
Schematic of the tangential method of the gear shaving process.

The work gear reciprocates $\mathbf{F}_c$ tangentially in relation to its own axis while the work gear and the shaving cutter are in mesh (Figure 17.28). It is customary to move the work gear past the shaving cutter by means of the feed slide. On some of the larger shaving machines, for obvious reasons, the shaving cutter is mounted on a feed slide. In the consideration below, the *relative motion* of the work gear and the shaving cutter is considered regardless of whether the work-table or the shaving cutter actually reciprocates.

Productivity rate of the rotary shaving of gears directly depends on the length of traverse path of the work gear.

17.5.2 Cutting Speed in the Tangential Method of the Rotary Shaving of a Gear

A resultant formula for the computation of the cutting speed $\mathbf{V}_{cut}$ in the diagonal shaving of gears is similar to that [see Equation (17.40)] earlier derived for the case of the axial method of the shaving of gears. As in tangential shaving, the traverse motion $\mathbf{F}_c$ is perpendicular to the work gear axis of the rotation, so the impact of the motion $\mathbf{F}_c$ differs from that in the diagonal method of rotary shaving. The cutting speed is significantly affected by the transverse motion of the shaving cutter.

Assume again that the shaving cutter is not rotating, and is just reciprocating with respect to the work gear shown in Figure 17.29. Under such a scenario, vector $\mathbf{F}_c$ of the traverse motion of the shaving cutter is perpendicular to the work gear axis O_g.

The component $\mathbf{F}_c^{sl}$ of the vector $\mathbf{F}_c$ of the traverse motion in the direction tangent to the tooth flank of the work gear is equal to zero ($\mathbf{F}_c^{sl} \equiv 0$). Another component $\mathbf{F}_c^{rt}$ of the traverse motion $\mathbf{F}_c$ is within the pitch plane, and it is perpendicular to the axis of the rotation of the work gear ($\mathbf{F}_c^{rt} \equiv \mathbf{F}_c$). The component $\mathbf{F}_c^{rt}$ contributes to the rotation of the work gear. This additional rotation ω_g^{ad} is equal

$$\omega_g^{ad} = \frac{2F_c}{d_g} \tag{17.64}$$

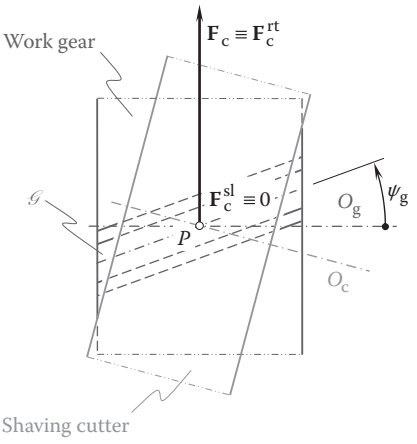

FIGURE 17.29
Impact of the traverse motion on the cutting speed $\mathbf{V}_{cut}$ in the tangential shaving of gears.

The rotation vector $\boldsymbol{\omega}_g^{ad}$ is aligned with the rotation vector $\boldsymbol{\omega}_g$. Depending on (a) the rotation of the shaving cutter $\boldsymbol{\omega}_c$, and (b) the direction of the hand and the value of the helix angle ψ_g, the rotation vector $\boldsymbol{\omega}_g^{ad}$ is pointed either in the same direction as the rotation vector $\boldsymbol{\omega}_g$, or it is pointed opposite to the vector $\boldsymbol{\omega}_g$. In the first case the rotation $\boldsymbol{\omega}_g^{ad}$ adds to the rotation $\boldsymbol{\omega}_g$. In the second case it subtracts from the rotation $\boldsymbol{\omega}_g$.

Once the identity $\mathbf{F}_c^{sl} \equiv 0$ and Equation (17.64) are taken into account, the resultant formula [see Equation (17.40)] can be used for computing the cutting speed $\mathbf{V}_{cut}$ in the tangential shaving of gears.

When the tangential method of gear shaving is applied, the shaving cutter must be wider than the gear to be shaved and its serrations must be placed on a helix in order to produce the relative tooth flank feed. Serrations of this type are shown in Figure 17.9b. Serrations of this type are often referred to as *differential* or *staggered pattern* serrations.

17.5.3 Tangential Shaving of Shoulder Gear: Descriptive Geometry–Based Approach

Gears that are to be shaved should allow room for the shaving cutter to run out. The method of tangential shaving is ideally suited for shaving of close-shoulder gears. We refer to a *shoulder* as to any integral part of a gear that is close enough to the gear face, and diameter d_{sh} of which exceeds outside diameter $d_{o.g}$ of the gear (Figure 16.123). Sometimes, a flange, cam, or the tooling that holds the work-piece, can be the interference. The neck width l_{min} or gap between the gear face and face of the interfering shoulder should always be the minimum obtainable through the tolerance "stack up" of the component part.

It is required to prevent a shaving cutter at crossed-axes from contacting the shoulder face. Therefore, when shaving a shoulder gear the angle between the work gear axis and the shaving cutter axis is often reduced to $\Sigma = 3 \div 5°$. The chief use of a small crossed-axis angle is to operate in a restricted space near a shoulder (Figure 17.30).

The analysis below is based on wide use of the powerful methods developed in descriptive geometry. This approach is referred to as the descriptive-geometry-(*DG*)-based approach.

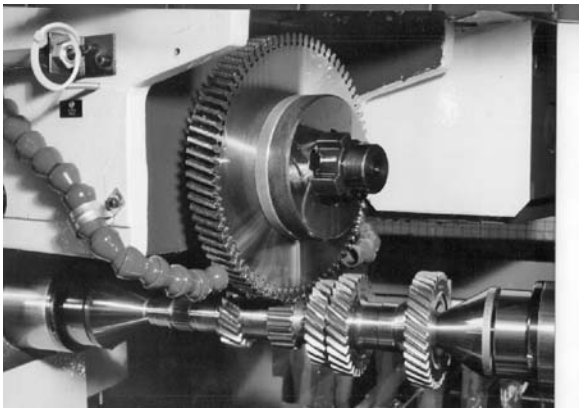

FIGURE 17.30
Shaving of a cluster gear.

17.5.3.1 Maximum Allowed Outer Diameter of a Shaving Cutter

The following design parameters must be known prior to determining a maximum permissible outer diameter of the shaving cutter:* (a) the work gear pitch helix angle ψ_g, (b) the face width of the work gear, (c) the width l_{min} of the shoulder gear neck, and (d) the shaving cutter pitch helix angle ψ_c [59].

A work gear with a shoulder is depicted in two planes of projections, namely in horizontal plane of projections π_1, and in vertical plane of projections π_2 (Figure 17.31) [59]. The work gear axis O_g is at a right angle to the plane π_2.

The vertical plane $\mathscr{T}_c$ coincides with the shaving cutter face in its limit closest location to the shoulder. The vertical plane $\mathscr{T}_{sh}$ coincides with the shoulder face. Because both planes $\mathscr{T}_c$ and $\mathscr{T}_{sh}$ are oriented vertically, in π_1 they are depicted as the straight lines traces $\mathscr{T}_c$ and $\mathscr{T}_{sh}$ (Figure 17.31).

The planes $\mathscr{T}_c$ and $\mathscr{T}_{sh}$ intersect each other along a straight line $\mathscr{A}$. The line $\mathscr{A}$ is oriented vertically.

When the shaving cutter occupies the limit position at which it is closest to the shoulder, and no collision of the shaving cutter and the shoulder occurs, the outer cylinder of the shaving cutter and the shoulder cylinder contact each other at a point. This point is denoted as K. Point K is located within the straight line $\mathscr{A}$. Because point K belongs to a circle of diameter d_{sh}, the vertical projection K_2 of point K is located on the intersection of the vertical projection $\mathscr{A}_2$ of the straight line $\mathscr{A}$ and the vertical projection of the circle of diameter d_{sh}.

An auxiliary plane of projections π_4 is constructed so that it is perpendicular to π_1, and the axis π_1/π_4 makes an angle $\bar{\Sigma}$ with the axis π_1/π_2. An image of the work gear in π_4 is located beyond the shoulder. Thus the work gear is not visible in π_4. However, the work gear is shown in solid lines in π_4 for convenience.

The shaving cutter axis of rotation O_c is at a right angle with respect to the plane of projections π_4. Projection K_4 of point K can be easily found with the help of the appropriate connection lines (Figure 17.31) or by means of the horizontal straight line $\mathscr{B}$. Both projections $\mathscr{B}_2$ and $\mathscr{B}_4$ of the straight line $\mathscr{B}$ are at the same distance $h_{\mathscr{B}}$ from the horizontal plane of projections π_1.

The maximum feasible outer diameter $d_{o.c}^{max}$ of the shaving cutter can be determined in the auxiliary plane of projections π_4. The shaving cutter axis of rotation is located at the closest distance of approach $C_{g/c}$ of the axes O_g and O_c (this straight line passes through C_4). A circle of the maximum outer diameter $d_{o.c}^{max}$ passes through C_4, and through K_4. The straight-line segment C_4K_4 is subdivided onto two equal portions by means of two arc segments of a certain radius $\mathfrak{R}$. The most remote axis of rotation O_c^{max} of the shaving cutter is located within the straight line r–r. Therefore, the center O_c^{max} can be found out as the intersection between the closest distance of approach of the axes O_g and O_c, and between the straight line r–r. Point O_c^{max} specifies the maximum feasible center distance $C_{g/c}^{max}$. The actual shaving cutter outer diameter $d_{o.c}$ should be the largest allowed in its design size class (3.5, 6.0, 8.0, 9.5, or 13.5 in.).

* It is important to point out here that a few more geometrical problems arise in gear shaving of a shoulder gear. Examples are as follow: (a) to determine a maximum permissible neck width l_{min} of the shoulder gear when the shaving cutter outer diameter $d_{o.c}$, the work gear pitch helix angle ψ_g, and the shaving cutter pitch helix angle ψ_c are known, or (b) to determine an appropriate pitch helix angle ψ_c of the shaving cutter when its outer diameter $d_{o.c}$, neck width l_{min} of the shoulder gear, and pitch helix angle ψ_g of the work gear are given. Problems of this type are similar in nature to the problem of determining a maximum permissible outer diameter of the shaving cutter $d_{o.c}$. Solutions to the problems (a), (b), and so forth can be drawn up from the solution to the problem of determining the shaving cutter outer diameter $d_{o.c}$.

The actual shaving cutter axis of rotation O_c^{act} is located within the closest distance of approach of the axes or rotation O_g and O_c, at a distance $R_c^{act} = 0.5d_{o.c}$. After being determined, the shaving cutter's actual outer diameter $d_{o.c}$ allows for the determination of the

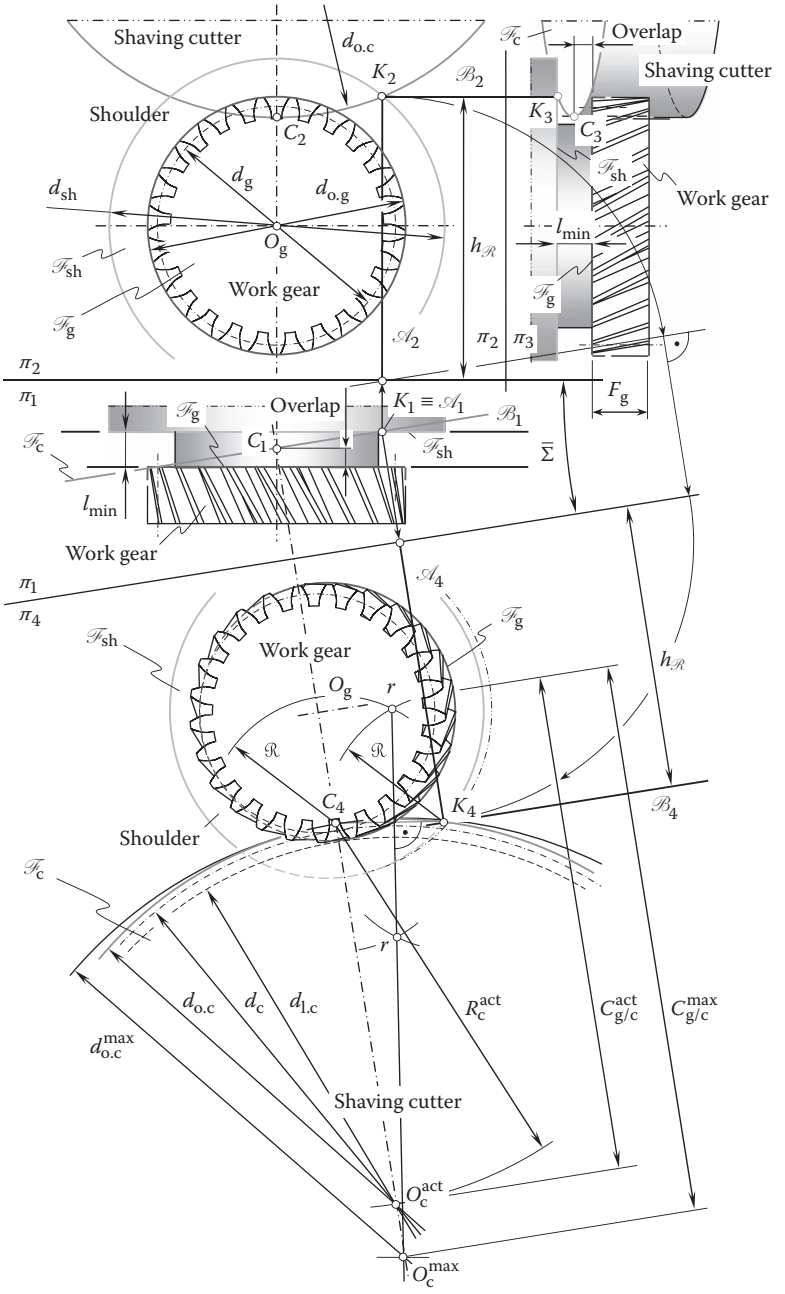

FIGURE 17.31
Determining the maximum permissible outer diameter $d_{o.c}$ of a shaving cutter. (From Radzevich, S.P., *ASME Journal of Manufacturing, Science and Engineering*, 127(4), 893–900, 2005. With permission.)

actual center distance $C^{act}_{g/c}$, as well as the rest of the design parameters of the shaving cutter: base diameter $d_{b.c}$, pitch diameter d_c, limit diameter $d_{l.c}$, and so forth.

17.5.3.2 Minimum Required Overlap of the Work Gear and the Shaving Cutter

While determining the maximum permissible outer diameter of the shaving cutter (Figure 17.31), it has been assumed that the value of the overlap is known. However, usually the minimum required overlap has to be determined. Consideration of (a) the work gear auxiliary generating rack $\mathscr{R}_g$ of the minimum required face width $F_{\mathscr{R}.g}$, and (b) the shaving cutter auxiliary generating rack $\mathscr{R}_c$ of the minimum required face width F_c is a key for determining the overlap.

Minimum permissible width of the auxiliary generating rack $\mathscr{R}_g$, conjugate to the work gear. A work gear with an involute tooth profile is depicted in three planes of projections π_1, π_2, and π_3 as shown in Figure 17.32 [59]. The axis O_g of the work gear is at a right angle to

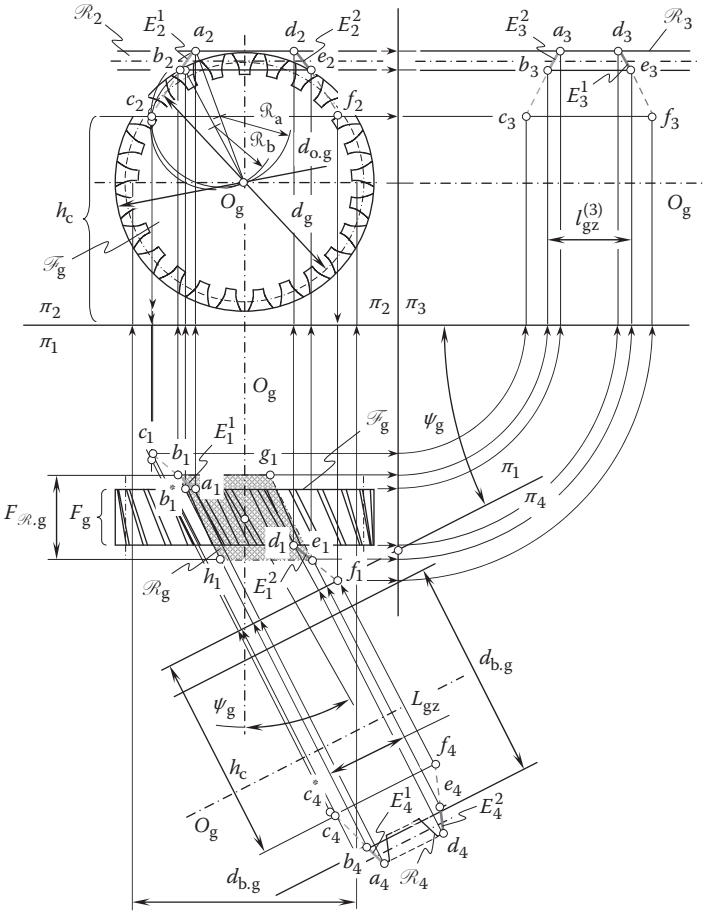

FIGURE 17.32
Determining the minimum permissible width of the auxiliary generating rack $\mathscr{R}_g$, conjugate to a work gear. (From Radzevich, S.P., *ASME Journal of Manufacturing, Science and Engineering*, 127(4), 893–900, 2005. With permission.)

the plane of projections π_2. The vertical auxiliary plane of projections π_4 is at a certain angle with respect to the plane of projections π_2. This angle is equal to the pitch helix angle ψ_g of the work gear. Projection $\mathscr{R}_4$ of the infinitely wide auxiliary generating rack $\mathscr{R}$ is congruent to the cross section of the rack $\mathscr{R}$ by a normal plane. The generation of the screw involute surface of the work gear tooth flank occurs along two characteristic lines. The characteristic lines are labeled as E^1 and E^2. The characteristic lines E^1 and E^2 are located within two planes that are tangent from the opposite sides to the base cylinder of diameter $d_{b.g}$ of the work gear. The active portions of the characteristic lines E^1 and E^2 are bounded with the end-points *a*, *c*, and *d*, *f*, accordingly. The end-points *c* and *f* are within the base cylinder. They are remote from π_1 at a distance h_c. The straight-line segments E^1 and E^2 are tangent to the corresponding base helices of the work gear being shaved. In order to the work gear been completely shaved, not the entire length the characteristics E^1 and E^2 has to be generated in the rotary shaving process. It is sufficient to reproduce only its portions *ab* and *de* (i.e., to reproduce their portions located within the work gear tooth height). Thus, for complete shaving of the work gear it is required to reproduce not the infinite auxiliary generating rack $\mathscr{R}$, but only portion $\mathscr{R}_g$ of it. This portion of the auxiliary generating rack is referred to as *the work gear auxiliary rack*. Within the plane π_1, the portion $\mathscr{R}_g$ of the generating rack $\mathscr{R}$ is shaped in the form of a parallelogram $b_1g_1e_1h_1$. The straight-line segments b_1g_1, and e_1h_1 through points b_1 and e_1 are parallel to the work gear face $\overline{\mathscr{T}}_g$. The straight-line segments b_1h_1 and e_1g_1 align to the corresponding straight-line generatrix of the auxiliary rack $\mathscr{R}$. The minimum face width $F_{\mathscr{R}.g}$ of the auxiliary rack $\mathscr{R}_g$ of the work gear is equal to the length L_{gz} of the generating zone as illustrated in Figure 17.32. It is important to point out here that, first, the straight-line segments a_1b_1 and d_1e_1 are within the tooth flanks of the rack $\mathscr{R}_g$, and, second, the rack $\mathscr{R}_g$ must be of the smallest permissible size in the axial direction of the work gear.

Points *a* and *b* of the auxiliary rack $\mathscr{R}$ tooth are connected to the work gear axis O_g. Both straight line segments aO_g and bO_g were used as a diameter of a circle of the corresponding radius $\mathfrak{R}_a$ and $\mathfrak{R}_b$. The circles of radii $\mathfrak{R}_a$ and $\mathfrak{R}_b$ meet the base cylinder $d_{b.g}$ at points *c* and *c**. Due to lack of space, only the projection c_4^* of point *c** is depicted in Figure 17.32. That point of two points *c* and *c** is chosen for which length l_{gz} of the generating zone is longer (see the projection $l_{gz}^{(3)}$ of this straight line segment).

The similar is true with respect to point *f* of contact of the straight generatrix E^2 and the base cylinder of the work gear.

The auxiliary generating rack $\mathscr{R}_g$ must be as short as possible, and must be the narrowest possible. The length of the parallelogram $b_1g_1e_1h_1$ cannot be shorter than $L_{gz}(\cos\psi_g)^{-1}$ (i.e., the length of the parallelogram is specified by L_{gz} and ψ_g). The required segments *ab*, and *de* of the characteristics E^1 and E^2 must be within the parallelogram. This restricts the shortest width of the parallelogram $b_1g_1e_1h_1$.

Length l_{gz} of the generating zone can be determined from the formula [59]

$$l_{gz} = d_{o.g}\cos(\phi_n + \alpha) = \left(\sqrt{d_{o.g}^2 - d_g^2\cos^2\phi_n} - d_g\sin\phi_n\right)\cos\phi_n \tag{17.65}$$

where

$d_{o.g}$ = outer diameter of the work gear
d_g = pitch diameter of the work gear
ϕ_n = normal profile angle

For the computation of the angle α, an expression $\alpha = \sin^{-1}(d_g/d_{o.g}\cos\phi_n)$ is derived in [59].

The length L_{gz} of the generating zone is equal

$$L_{gz} = l_{gz} + 2\sqrt{(0.5\,d_{o.g})^2 + (0.5\,d_g)^2 + 0.5\,d_{o.g}d_g\cos(\alpha+\phi_n)}\,\frac{\sin^2\phi_n}{\cos\phi_n} \tag{17.66}$$

The minimum required length L_{gz} of the generating zone imposes certain restrictions onto the design parameter of a shaving cutter, as well as onto the parameters of the kinematics of the rotary shaving process.

Minimum permissible width of the auxiliary generating rack $\mathscr{R}_c$, conjugate to the shaving cutter. The characteristics E^1 and E^2 for the work gear tooth flank $\mathscr{G}$ that is conjugated with the auxiliary generating rack $\mathscr{R}_g$ do not align to characteristics $\mathscr{E}^1$ and $\mathscr{E}^2$ for the auxiliary helix (ψ_p) generating rack $\mathscr{R}_c$, that is conjugated to the shaving cutter tooth surface C_c. The characteristics E^1 and $\mathscr{E}^1$ are within lateral tooth surface of the auxiliary generating rack $\mathscr{R}$. They intersect each other at a certain point. The characteristics E^2 and $\mathscr{E}^2$ are within the opposite lateral tooth surface of the auxiliary rack $\mathscr{R}$, and also intersect each other at a certain point.

The tooth flank C_c of the shaving cutter can be generated as an envelope to successive positions of the auxiliary generating helix (ψ_c) rack $\mathscr{R}$ in its rotation about the shaving cutter axis O_c. The minimum required portion of the auxiliary rack $\mathscr{R}$ of the shaving cutter is designated as $\mathscr{R}_c$. The characteristics $\mathscr{E}^1$ and $\mathscr{E}^2$ can be found out in a manner similar to how the characteristics E^1 and E^2 were reconstructed. This particular problem allows for interpretation in the form of the inverse problem to the problem considered above.

The characteristics E^1 and $\mathscr{E}^1$ make a certain angle μ with each other. The characteristics E^2 and $\mathscr{E}^2$ are at that same angle μ relative to each other. The angle μ is the angle of the tooth flanks' $\mathscr{G}$ and C_c local relative orientation. The straight-line characteristic E^1 is aligned with the first principal directions $\mathbf{t}_{1.g}$ of the work gear tooth flank $\mathscr{G}$. The first principal plane $C_{1.g}$ passes through the unit vector $\mathbf{t}_{1.g}$.

The same is observed for the opposite side of the work gear tooth flank and the tooth flank of the auxiliary generating rack $\mathscr{R}$.

In the rotary shaving of an involute gear, the rack surface $\mathscr{R}_g$ is an enveloping surface to consecutive positions of the work gear tooth flank $\mathscr{G}$ in its motion relative to the rack $\mathscr{R}_g$. Referring to Figure 17.33, the straight-line segment a_1b_1 is a portion of the characteristic E^1, and the straight-line segment d_1e_1 is a portion of the characteristic E^2.

The tooth profile of the auxiliary generating rack $\mathscr{R}_c$ is not identical to tooth profile of the auxiliary generating rack $\mathscr{R}_g$. The addendum $a_{\mathscr{R}c}$ exceeds the addendum $a_{\mathscr{R}g}$. The difference ($a_{\mathscr{R}c} - a_{\mathscr{R}g}$) is designated as Δa. For determining the required excess Δa, the fifth necessary condition of proper part surface generation (see Appendix B) can be used [128, 136, 138, 143].

The distance h_{be} at which points b and e are remote from the plane π_5, and the similar distance h_{ad} at which points a and d are remote from the plane π_5 (Figure 17.33) are both equal to the distance at which the corresponding points a, b, d, and e are remote from the plane π_4.

Determination of the characteristics $\mathscr{E}^1$ and $\mathscr{E}^2$ of the auxiliary generating rack $\mathscr{R}$, which is conjugate to the shaving cutter tooth flank C_c, is illustrated in Figure 17.33. Within the plane π_4 the projections E_4^1 and $\mathscr{E}_4^1$, as well as the projections E_4^2 and $\mathscr{E}_4^2$ are congruent to each other. The straight-line segment b_5m_5 is tangent to the shaving cutter base cylinder of diameter $d_{b.c}$. This allows for the construction of point n, and of projections of the

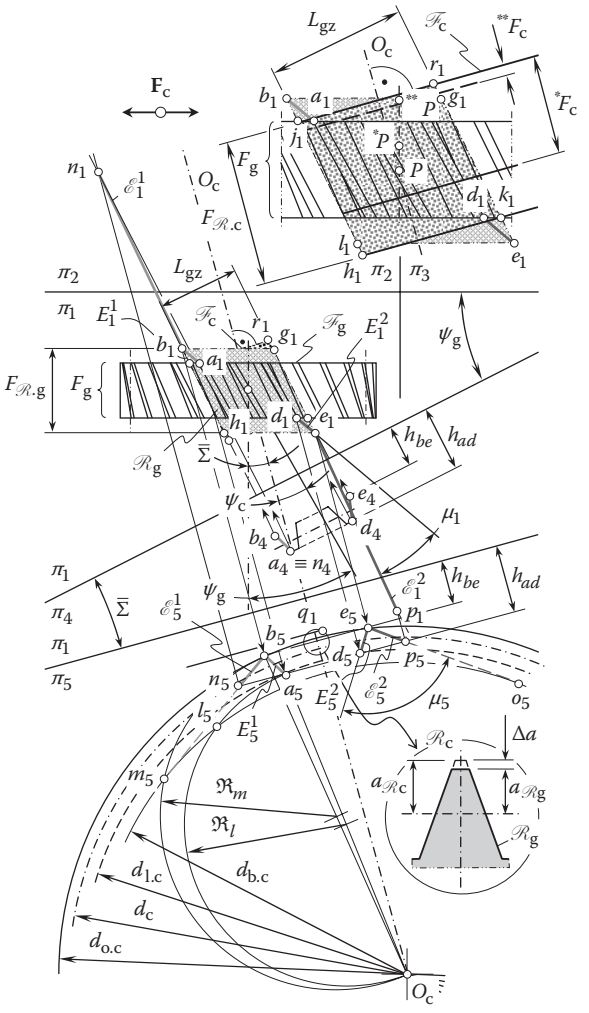

FIGURE 17.33
The minimum required width of the auxiliary generating rack $\mathscr{R}_c$ of a shaving cutter, and the minimum feasible overlap of the work gear and the shaving cutter. (From Radzevich, S.P., *ASME Journal of Manufacturing, Science and Engineering*, 127(4), 893–900, 2005. With permission.)

characteristic $\mathscr{E}^1$ onto all others planes of projections. Similar to that just used, all projections of the characteristic $\mathscr{E}^2$ are constructed as well.

For the purpose of proper selection of one of two points m and l, the semicircles of radii $\mathscr{R}_l$ and $\mathscr{R}_m$ (see the plane π_5 in Figure 17.33) are used. The selection of a point is similar to the selection of a point of two points c and c^* in Figure 17.32.

The length L_{gz} of the auxiliary generating rack $\mathscr{R}_c$ of the shaving cutter is equal to (or exceeds) the length of the auxiliary generating rack $\mathscr{R}_g$ of the work gear. The width of the rack $\mathscr{R}_c$ is specified by two straight lines through points n_1 and p_1. Both of these two straight lines are parallel to the shaving cutter axis of rotation. The width of the auxiliary generating rack $\mathscr{R}_c$ of the shaving cutter is equal to $F_{\mathscr{R}c}$.

Within the plane π_1 the profile of the auxiliary rack $\mathscr{R}_c$ is shaped in the form of a parallelogram $p_1q_1n_1r_1$. The straight-line segments n_1r_1 and p_1q_1 through points n_1 and p_1 are orthogonal to the shaving cutter axis of rotation O_c, and thus, are parallel to the shaving cutter face $\mathscr{F}_c$. The straight-line segments n_1q_1 and r_1p_1 are aligned with the corresponding straight-line generatrix of the auxiliary rack $\mathscr{R}$. The width of the shaving cutter auxiliary rack $\mathscr{R}_c$ is equal to the length of the generating zone L_{gz}. Determination of the length $F_{\mathscr{R}c}$ is shown in Figure 17.33. It is important to point out here that the auxiliary generating rack $\mathscr{R}_c$ of the shaving cutter must be as short as possible, and it must be the narrowest permissible.

17.5.3.3 Minimum Required Face Width of a Shaving Cutter

Determination of the minimum required face width of a shaving cutter is based on the necessity of fulfillment of two following requirements.

First, the entire work gear auxiliary rack $\mathscr{R}_g$ should be generated in the rotary shaving process. Second, the shaving cutter auxiliary rack $\mathscr{R}_c$ must overlap the auxiliary rack $\mathscr{R}_g$.

In order to reproduce the characteristics E^1 and E^2 (see the straight line segments *ab* and *ed*), the corresponding characteristics $\mathscr{E}^1$ and $\mathscr{E}^2$ are required to be reproduced by the shaving cutter in the rotary shaving operation. Two straight lines through j_1 and k_1, which are orthogonal to the shaving cutter axis of rotation O_c, determine the minimum required width $F_{\mathscr{R}c}$ of auxiliary rack $\mathscr{R}_c$ of the shaving cutter. For finishing of the entire tooth flanks of the work gear, the shaving cutter auxiliary rack of the width $F_{\mathscr{R}c}$ (and of length L_{gz}) should be reproduced.

The minimum required width of the shaving cutter for the tangential shaving of a shoulder gear is equal to $F_c = F_{\mathscr{R}c}$.

17.5.4 Tangential Shaving of Shoulder Gear: Analytical Approach

The *DG*-based analysis of tangential shaving of a shoulder gear gives an insight as to how the problem can be solved analytically. On the premise of the derived graphical solution, a corresponding analytical solution to the problem is derived below.

17.5.4.1 Optimal Design Parameters of a Shaving Cutter

The design parameters of a shaving cutter, namely, (a) the greatest outer diameter, and (b) the greatest pitch helix angle under which no collision occurs between the adjacent shoulder and the shaving cutter can be determined analytically. An establishment of appropriate reference systems and the corresponding coordinate system transformations is the starting point for solving the problem under consideration.

Applied reference systems. A left-hand–oriented Cartesian coordinate system $X_gY_gZ_g$ is associated with the work gear. The axis X_g is aligned with the work gear axis of rotation O_g as shown in Figure 17.34. In a gear shaving operation, the axis Y_g is parallel in relation to the closest distance of approach $C_{g/c}$ between the axis O_g of the work gear and the axis O_c of the shaving cutter.

A left-hand–oriented Cartesian coordinate system $X_cY_cZ_c$ is associated with the shaving cutter. The axis X_c is aligned with the shaving cutter axis of rotation O_c. The axis Y_c is aligned with the closest distance of approach $C_{g/c}$ between the axis O_g of the work gear and the axis O_c of the shaving cutter.

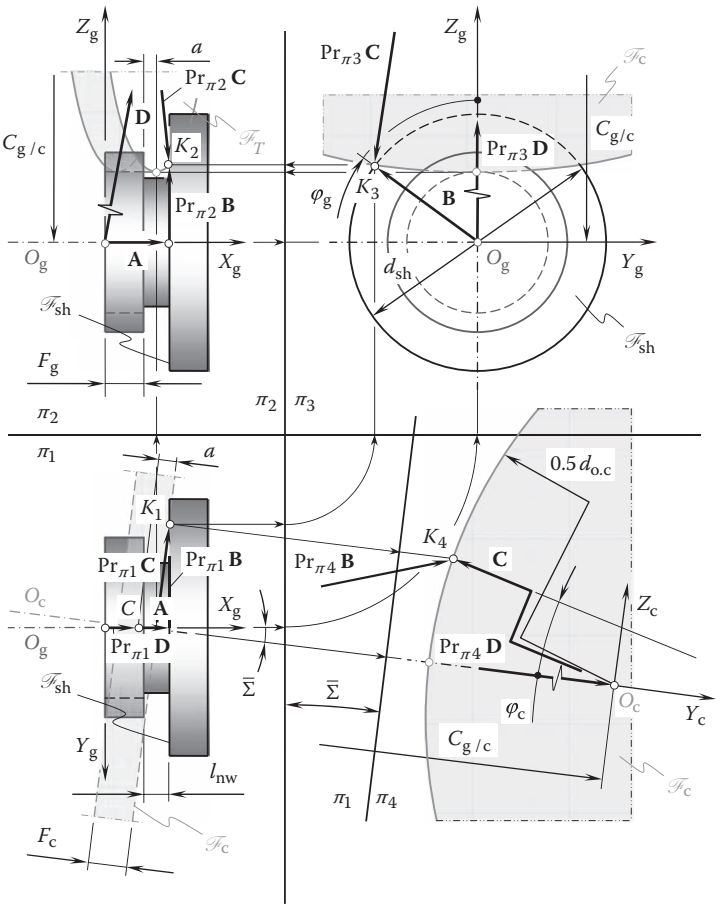

FIGURE 17.34
The applied coordinate systems and the closed vector polygon.

If necessary, auxiliary reference systems can be used in addition to the coordinate systems $X_gY_gZ_g$ and $X_cY_cZ_c$.

Operators of the linear transformations. In order to be treated together, the work gear and the shaving cutter must be represented in a common reference system. The coordinate system $X_gY_gZ_g$ can be used as the common reference system. If the coordinate system $X_gY_gZ_g$ is chosen, then an operator $\mathbf{Rs}(T \rightarrow \mathscr{G})$ of the resultant coordinate system transformation is required to be composed for the conversion of the tooth flank of the shaving cutter to the coordinate system $X_gY_gZ_g$ that is associated with the work gear.

The operator $\mathbf{Rs}(T \rightarrow \mathscr{G})$ of the linear transformation can be computed as a product of the operators of elementary coordinate system transformations, namely of (a) the operator $\mathbf{Tr}[F_g + l_{nw}), X_c]$ of the translation along the X_c axis through the distance $(F_g + l_{nw})$, (b) the operator $\mathbf{Tr}(C_{g/c}, Z_c)$ of the translation along the Z_c axis through the distance $C_{g/c}$, and (c) the operator $\mathbf{Rt}(\bar{\Sigma}, Z_c)$ of the rotation about the Z_c axis through the angle $\bar{\Sigma}$

$$\mathbf{Rs}(T \rightarrow \mathscr{G}) = \mathbf{Tr}[(F_g + l_{nw}), X_c] \cdot \mathbf{Tr}(C, Z_c) \cdot \mathbf{Rt}(\bar{\Sigma}, Z_c) \tag{17.67}$$

where F_g denotes the face width of the gear, l_{nw} is the neck width of the work gear, $C_{g/c}$ denotes the center distance, and $\bar{\Sigma}$ is the angle that make the crossing axes angle O_g and O_c.

A closed vector polygon. In the worst case scenario, the shaving cutter is figured with respect to the shoulder gear so that the shaving cutter face $\mathscr{T}_T$ shares a common point K with the shoulder face $\mathscr{T}_{sh}$ (Figure 17.34).

In the coordinate system $X_gY_gZ_g$, the position vector $\mathbf{R}_K^{(g)}$ of point K can be represented as the summa of two vectors

$$\mathbf{R}_K^{(g)} = \mathbf{A} + \mathbf{B} \tag{17.68}$$

where vector **A** is equal to

$$\mathbf{A} = \begin{bmatrix} (F_g + l_{nw}) \\ 0 \\ 0 \\ 1 \end{bmatrix}_g \tag{17.69}$$

and the vector **B** yields representation in the form

$$\mathbf{B} = \begin{bmatrix} (F_g + l_{nw}) \\ -0.5d_{sh}\sin\varphi_g \\ 0.5d_{sh}\cos\varphi_g \\ 1 \end{bmatrix}_g \tag{17.70}$$

The subscript g at the brackets indicates that the vectors are represented in the coordinate system $X_gY_gZ_g$.

The position vector **D** that specifies origin O_c of the coordinate system $X_gY_gZ_g$ is equal

$$\mathbf{D} = \begin{bmatrix} (F_g + l_{nw}) - (0.5d_{o.c}\sin\varphi_c + a)\cos\bar{\Sigma} \\ 0 \\ C_{g/c} \\ 1 \end{bmatrix}_g \tag{17.71}$$

Ultimately, for the position vector $\mathbf{R}_K^{(c)}$ of point K in the coordinate system $X_cY_cZ_c$, the expression

$$\mathbf{R}_K^{(c)} \quad \Rightarrow \quad \mathbf{C} = \begin{bmatrix} a \\ -0.5d_{o.c}\cos\varphi_c \\ 0.5d_{o.c}\sin\varphi_c \\ 1 \end{bmatrix}_c \tag{17.72}$$

is valid. The subscript c at the brackets indicates that the vector $\mathbf{R}_K^{(c)}$ is represented in the coordinate system $X_cY_cZ_c$.

The closest distance of approach of the shaving cutter to the shoulder in denoted in Equation (17.72) as a (see Figure 17.34).

Equations (17.67), (17.68), and (17.72) yield an expression

$$\mathbf{R}_K^{(g)} - \mathbf{R}_K^{(c)} \cdot \mathbf{Rs}(T \to \mathscr{G}) = (\mathbf{A} + \mathbf{B}) - [\mathbf{Rs}(T \to \mathscr{G}) \cdot \mathbf{C} + \mathbf{D}] \equiv 0 \tag{17.73}$$

for the closed vector polygon [138].

The following column matrix can be obtained

$$\begin{bmatrix} F_g + l_{nw} - a\cos\bar{\Sigma} + 0.5d_{o.c}\sin\bar{\Sigma}\cos\varphi_c - a + (0.5d_{o.c}\sin\varphi_c + a)\cos\bar{\Sigma} \\ -0.5d_{sh}\sin\varphi_g + a\sin\bar{\Sigma} + 0.5d_{o.c}\cos\bar{\Sigma}\cos\varphi_c \\ 0.5d_{sh}\cos\varphi_g - 0.5d_{o.c}\sin\varphi_c - 2C_{g/c} \\ 1 \end{bmatrix} = 0 \tag{17.74}$$

after substituting Equations (17.68) through (17.72) into Equation (17.73).

It is necessary to eliminate two parameters φ_g and φ_c in order to solve Equation (17.74). Once the parameters φ_g and φ_c are eliminated, then Equation (17.74) casts into an implicit equation of the form $F(l_{nw}, \bar{\Sigma}, d_{o.c}) = 0$.

On solving of the equation $F(l_{nw}, \bar{\Sigma}, d_{o.c}) = 0$, a set of optimal design parameters of the shaving cutter for finishing of a given work gear, as well as the closest distance of approach of the shaving cutter to the shoulder face $\mathscr{T}_{sh}$ can be obtained.

17.5.4.2 Influence of the Overlap of a Shaving Cutter over the Work Gear onto the Accuracy of the Finished Tooth Flanks

A minimum required neck width l_{nw} of a shoulder gear can be significantly reduced if the tolerance $[\delta]$ for accuracy of the tooth flank $\mathscr{G}$ of the work gear exceeds the actual deviation δ of a finished gear. Under such a scenario, the difference δ_Δ between the tolerance $[\delta]$ and the actual deviation δ (i.e., $\delta_\Delta = [\delta] - \delta$) allows for the corresponding reduction of the neck width l_{nw}. The reduction of the neck width l_{nw} can be significant as the radii of the normal curvature R_g and R_c of the work gear tooth flank $\mathscr{G}$ and the generating surface T of the shaving cutter are of great value.

The problem of determining the minimum required overlap in rotary shaving of gears is similar in nature to the problem of determining the minimum required hob travel distance discussed above in Section 16.8.3.

In the event the auxiliary rack $\mathscr{R}_c$ of the shaving cutter overlaps the auxiliary rack $\mathscr{R}_g$ of the work gear insufficiently, then a portion of the gear tooth flank $\mathscr{G}$ remains unshaved. Lack of the overlap in the axial direction of the work gear is designated as ΔU. In practice the stock that is not removed from the unshaved portion of the tooth flank $\mathscr{G}$ causes the so-called *tooth bias* [59].

Referring to Figure 17.35, an expression for the function $\delta = \delta(\Delta U)$ can be represented in the form

$$\delta(\Delta U) = \left(R_t\cos\psi_g - \sqrt{R_t^2 - (R_t\sin\psi_g + \Delta U)^2} - \Delta U\tan\psi_g\right)\cos\psi_g \tag{17.75}$$

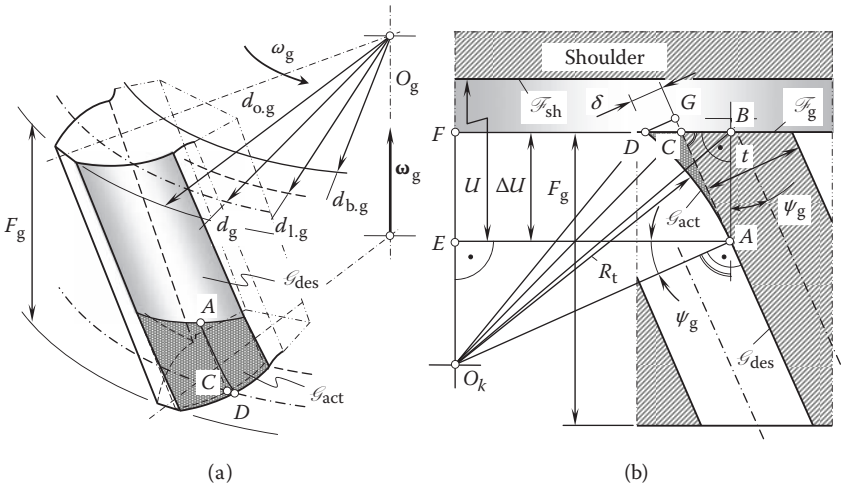

FIGURE 17.35
Impact of the lack of the overlap ΔU on the deviation δ of tooth flank $\mathscr{G}$ of the shaved gear. (From Radzevich, S.P., *Gear Technology*, 20(4), 44–50, 2003. With permission.)

where

R_t = radius of normal curvature of the shaving cutter tooth surface T in a specified direction

ψ_g = pitch helix angle of the work gear

It is important to stress here that angle ψ_g, as well as angle ψ_c below both are a type of signed values.

The radius R_t is measured in the direction of a unit tangent vector $\mathbf{u}_g$ (Figure 17.36). The vector $\mathbf{u}_g$ is within the tooth flank of the auxiliary rack $\mathscr{R}_T$ of the shaving cutter. It makes a certain angle φ with the second principal direction $\mathbf{t}_{2.c}$ on the shaving cutter tooth surface T. The angle φ can be expressed in terms of (a) angle μ of the local relative orientation of the surfaces $\mathscr{G}$ and T, (b) the base helix angle $\psi_{b.g}$ of the work gear, and (c) the base helix angle $\psi_{b.c}$ of the shaving cutter

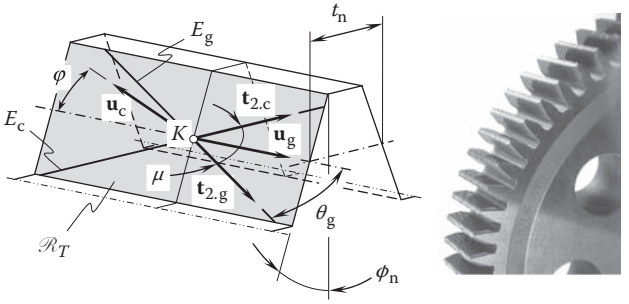

FIGURE 17.36
Radius of normal curvature R_t of a shaving cutter tooth surface T in a prespecified direction.

$$\varphi = \mu - (\psi_{b.g} + \psi_{b.c}) \tag{17.76}$$

For the computation of the angle μ, the formula [167]

$$\sin\mu = \frac{\sin\phi_n \sin\bar{\Sigma}}{\sqrt{(1-\cos^2\phi_n \sin^2\psi_g)(1-\cos^2\phi_n \sin^2\psi_c)}} \tag{17.77}$$

can be used.

Further, Euler's equation is utilized for the derivation of a formula for the computation of the radius of normal curvature R_t

$$R_t = \left[\underbrace{R_{1.c}^{-1}}_{\equiv 0} \sin^2\varphi + R_{2.c}^{-1} \cos^2\varphi \right]^{-1} \tag{17.78}$$

Ultimately, Equation (17.78) casts to

$$R_t = \frac{R_{2.c}}{\cos^2\varphi} \tag{17.79}$$

For the screw involute surface of the shaving cutter, the first principal radius of curvature $R_{1.c}$ is equal to infinity ($R_{1.c} \to \infty$). It is proven [158] that for the computation of the second principal radius of curvature $R_{2.c}$ of the shaving cutter surface T, the formula

$$R_{2.c} = U_c \tan\psi_{b.c} = \frac{1}{2}\sqrt{\frac{d_c^2 - d_{b.c}^2}{1-\sin^2\psi_c \cos^2\phi_n}} \tag{17.80}$$

is valid.

The undertaken examination of the influence of the overlap of a shaving cutter over the face width of the work gear onto the accuracy of the finished tooth flanks is illustrated with the graphical interpretation of the function $\delta = \delta(\Delta U)$ example, which is shown in Figure 17.37a.

Figure 17.37a is important for understanding one of the major reasons for the tooth flank $\mathscr{G}$ bias, which appears when the gear is shaved improperly. The tooth flank $\mathscr{G}$ bias becomes unavoidable when lack of the overlap occurs (e.g., when the work gear is shaved with a shaving cutter with insufficient face width. However, Figure 17.37a also reveals that if a gear can be shaved more accurately than specified by the tolerance $[\delta]$, the difference $\delta_\Delta = [\delta] - \delta$ makes possible a reduction of the minimum required neck width of the shoulder gear. The latter is important for both gear transmission designers as well as manufacturers of gears.

The impact of the radius of the normal curvature R_t of the shaving cutter tooth flank onto the deviation δ of the tooth flank $\mathscr{G}_{act}$ of the shaved gear with respect to the desired true involute surface $\mathscr{G}_{des}$ is illustrated in Figure 17.37b. The radius of normal curvature R_t of the shaving cutter tooth flank T is a function of the shaving cutter tooth number N_c (i.e., $R_t = R_t(N_c)$. The bigger the tooth number N_c, the bigger the radius of the normal curvature R_t, and vice versa. The deviation δ becomes smaller when the radius of the normal curvature R_t is bigger. This immediately allows for a conclusion: Shaving a work gear with the shaving cutter that has a bigger tooth number N_c causes a reduction of the deviation δ of the actual tooth flank $\mathscr{G}_{act}$ with respect to the desired true involute surface $\mathscr{G}_{des}$.

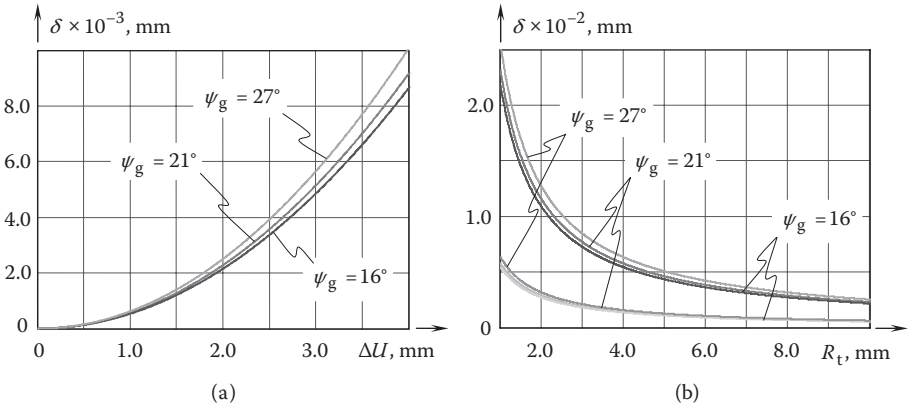

FIGURE 17.37
Work gear tooth flank $\mathscr{G}$ deviation δ versus the parameter ΔU (a), and the deviation δ versus the radius of normal curvature R_t (the upper curves for $\Delta U = 2$ mm, and lower curves for $\Delta U = 1$ mm) (b).

Once the difference $\delta_\Delta = [\delta] - \delta$ is known, then the permissible reduction Δl_{nw} of the neck width can be expressed in terms of δ_Δ

$$\Delta l_{nw} = \sqrt{R_t^2 - (R_t - [\delta])^2} - \sqrt{R_t^2 - (R_t - [\delta] + \delta_\Delta)^2} \tag{17.81}$$

The distance between the face of a shoulder and the corresponding face of the shaving cutter is specified by the parameter a (Figure 17.34). It is desired to keep the parameter a as small as possible [59]. The smaller the distance a, the shorter the width of the neck of the shoulder gear can be achieved. For the minimum deviations of the actual tooth flank of the shaved gear $\mathscr{G}_{act}$ from the desired true screw involute surface $\mathscr{G}_{des}$, the parameter a must satisfy the inequality $a \geq h_{t.\mathscr{R}} \cot\psi_{b.g} \cos\psi_c$ (Figure 17.38). Here $h_{t.\mathscr{R}}$ designates the whole depth of the auxiliary rack $\mathscr{R}$ tooth.

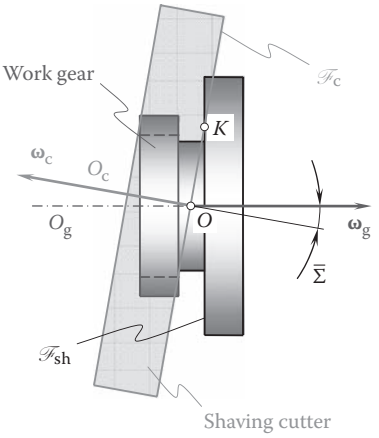

FIGURE 17.38
The desirable posture of a shaving cutter in relation to a shoulder gear ($a \equiv 0$).

17.6 Plunge Method of the Gear Shaving Process

With the plunge method of the gear shaving process there is no worktable translation. Only a radial feed of the work gear against the shaving cutter is performed. Due to very a short cycle time, plunge shaving is used in high-production operations. It is applied to gears, usually of narrow face widths. This method is particularly suited to shaving shoulder gears. The plunge method is not commonly used but is worth mentioning as a possible method.

17.6.1 Kinematics of the Plunge Method of the Gear Shaving Process

In plunge shaving, the work gear and the shaving cutter are meshed in a crossed-axis relationship (Figure 17.39). The crossing axes of the work gear O_g and the shaving cutter O_c are at a certain center distance $C_{g/c}$.

Referring to Figure 17.39, the rotation of the work gear about its axis O_g is designated as $\boldsymbol{\omega}_g$. the rotation of the shaving cutter about its axis O_c is designated as $\boldsymbol{\omega}_c$. The rotations $\boldsymbol{\omega}_g$ and $\boldsymbol{\omega}_c$ are properly timed with each other ($\omega_g N_g = \omega_c N_c$; here N_g and N_c denote the tooth number of the work gear and the shaving cutter, respectively, and the equalities $\omega_g = |\boldsymbol{\omega}_g|$ and $\omega_c = |\boldsymbol{\omega}_c|$ are observed). The rotation vectors $\boldsymbol{\omega}_g$ and $\boldsymbol{\omega}_c$ are at the angle $\Sigma = \angle(\boldsymbol{\omega}_g, \boldsymbol{\omega}_c)$. The angle $\bar{\Sigma}$ of the crossing of the axes O_g and O_c complements the angle Σ to 180°, (i.e., $\bar{\Sigma} = \pi - \Sigma$).

Instead of feed-slide motion, as with the other types of shaving, the plunge method uses strictly an in-feed to obtain the required tooth size of the finished gear. In the plunge method, the work gear travels along the center distance $C_{g/c}$. In this way the work gear is fed $\mathbf{F}_c$ into the shaving cutter with no table reciprocation.

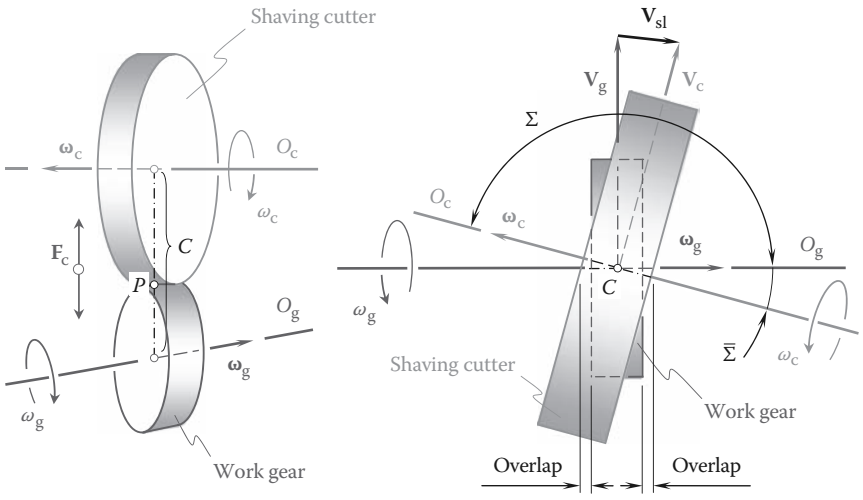

FIGURE 17.39
Schematic of the plunge method of the gear shaving process.

In all cases of plunge shaving, the face width of the shaving cutter must be greater than that of the work gear. The shaving cutter must have the differential-type serrations, otherwise the cutting action will be impaired.

17.6.2 Cutting Speed in the Plunge Method of the Rotary Shaving of a Gear

Since the shaving cutter is mounted on a shaft that is not parallel to the gear axis, the teeth of the shaving cutter and the teeth of the work gear run together like a pair of *crossed-helical* gears. The choice of crossed-axis angle governs the cutting action of the shaving cutter. In general, the higher the crossed-axis angle, the faster the shaving cutter cuts. The best control over helix angle, though, is gained with a low crossed-axis angle.

A formula for the computation of cutting speed $\mathbf{V}_{cut}$ in plunge shaving of gears can be derived from Equation (17.4) under the assumption that $\mathbf{F}_c = 0$

$$\mathbf{V}_{cut} = \mathbf{V}_{sl} + \mathbf{V}_{pr} \tag{17.82}$$

The sliding velocity $\mathbf{V}_{sl} = \mathbf{V}_c - \mathbf{V}_g$ is a component that most significantly contributes to the speed of the cut $\mathbf{V}_{cut}$.

The magnitude $V_{sl} = |\mathbf{V}_{sl}|$ of the sliding velocity $\mathbf{V}_{sl} = \mathbf{V}_c - \mathbf{V}_g$ can be computed from Equation (17.8)

$$V_{sl} = 0.5(\omega_g d_g \sin\psi_g + \omega_c d_c \sin\psi_c) \tag{17.83}$$

The equality $V_{cut} = |\mathbf{V}_{cut}| \cong V_{sl}$ is valid for the computation of the cutting speed in plunge shaving of gears.

17.6.3 Plunge Gear Shaving Process

The kinematics of the plunge gear shaving process is simple (see Figure 17.39). The geometry of the tooth flank $\mathcal{G}$ of the work gear is specified by Equation (1.3)

$$\mathbf{r}_g(U_g, V_g) = \begin{bmatrix} r_{b.g}\cos V_g + U_g \cos\lambda_{b.g}\sin V_g \\ r_{b.g}\sin V_g - U_g \sin\lambda_{b.g}\sin V_g \\ r_{b.g}\tan\lambda_{b.g} - U_g \sin\lambda_{b.g} \\ 1 \end{bmatrix} \quad \begin{matrix} V_g^{(l)} \le V_g \le V_g^{(a)} \\ 0 \le U_g \le [U_g] \end{matrix} \tag{17.84}$$

In the plunge shaving process, the tooth flank $\mathcal{G}$ is rotated about the axis O_g of the work gear, while a reference system $X_g Y_g Z_g$ is rotated about the axis O_c of the shaving cutter. The resultant motion of the work gear in relation to the reference system $X_c Y_c Z_c$ associated with the shaving cutter is referred to as *epicyclical motion*.

The generating surface T of a shaving cutter for the plunge gear shaving process can be determined as an enveloping surface to successive positions of the tooth flank surface $\mathcal{G}$ when the last is performing the epicyclical motion with respect to the reference system $X_c Y_c Z_c$. The kinematic method for determining the generating surfaces of cutting tools, which is based on the equation of contact $\mathbf{n}_g \cdot \mathbf{V}_\Sigma = 0$ [186], can be implemented for solving the problem of profiling the shaving cutter. Ultimately, an equation of the generating surface T of a plunge shaving cutter can be derived using the kinematic method.

The derived equation of the surface T is bulky, and thus it is inconvenient for any practical needs. Therefore, the continuous analytical description of the surface T is not used, but its discrete representation by a set of distinct points within the surface T is used instead when developing a computer code for a numerically controlled (NC) machine.

The similar discrete representation of surfaces is used for determining the tooth flank of a shaving cutter for the shaving of crowned gears, and in the most general case, it is used for shaving gears with topologically modified tooth flanks. From the author's perspective it is reasonable to consider the problem of profiling the shaving cutter for finishing topologically modified gears. Afterwards, the geometry of the tooth flank of a shaving cutter for plunge shaving of crowned gears can be obtained as a reduced case of the geometry of the shaving cutter for shaving topologically modified gears. Ultimately, the geometry of the tooth flanks of the shaving cutter for plunge shaving of nonmodified gears is identical to that for the shaving cutter with topologically modified tooth flanks if it is assumed that the modification is of zero value.

17.6.4 Plunge Shaving of Topologically Modified Gears

It is customary to modify the gear tooth flank to accommodate misalignment and minimize transmission error [155], which is the predominant cause of gear noise.

The problem of determining the geometry of the shaving cutter tooth flank may be informally referred to as: Given a file of a digitized gear tooth flank data, generate the corresponding file for the shaving cutter tooth flank.

17.6.4.1 Geometry of a Topologically Modified Gear Tooth Flank

The desired topologically modified tooth flank is deviated from the nominal tooth surface of the work gear. Screw involute surface $\mathscr{G}$ [see Equation (17.84)] of a nonmodified tooth flank is used as the reference surface for the construction of the topologically modified tooth flank $\mathscr{G}_{\text{mod}}$. For the construction, a grid of points is specified within the tooth flank $\mathscr{G}$. For the construction of the grid, two sets of points are commonly used (Figure 17.40).

The first set of m points is chosen within the gear tooth profile. These m points are evenly distributed either in the radial direction of the gear tooth or in the lengthwise direction of the tooth profile. The second set of n points is chosen within the face width of the work gear. These n points are evenly distributed within the face width of the gear. Ultimately, the gear tooth flank is covered by a grid of $m \times n$ points, each of which is located at a corresponding

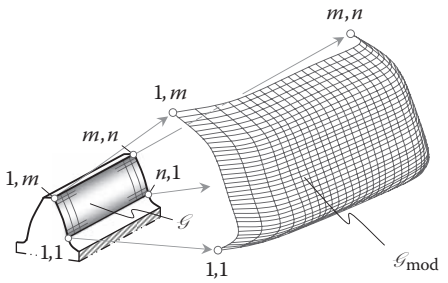

FIGURE 17.40
Nominal screw involute surface $\mathscr{G}$ as the reference surface to the topologically modified tooth flank $\mathscr{G}_{\text{mod}}$ of a work gear.

corner of elementary cells of the grid. For spur gears, the cells feature rectangular shape, and they are shaped in the form of a parallelogram for helical gears [131].

Two numbers $i = 1, 2, \ldots, m$ and $j = 1, 2, \ldots, n$ are assigned to each point of the grid of points. Deviation δ of the surface $\mathscr{G}_{\text{mod}}$ from the screw involute surface $\mathscr{G}$ at a point with the number i,j is denoted as $\delta_{i,j}$ accordingly. The deviation $\delta_{i,j}$ is measured outwards of the work gear tooth body along the perpendicular $\mathbf{n}_{\text{g}}$ to the surface $\mathscr{G}$.

For the particular case of the screw involute surface, an equation for the unit normal vector $\mathbf{n}_{\text{g}}$ can be derived not analytically as a cross-product of the two unit tangent vectors $\mathbf{u}_{\text{g}}$ and $\mathbf{v}_{\text{g}}$ [see Equation (1.6)], but on the premise of two important features of geometry of the screw involute surface $\mathscr{G}$. First, the vector $\mathbf{n}_{\text{g}}$ is aligned to a line that is tangent to the base cylinder of the work gear Second, the line with which the vector $\mathbf{n}_{\text{g}}$ is aligned crosses the gear axis at the angle $(90° - \psi_{\text{b.g}})$. Referring to Figure 1.13, this immediately yields an expression

$$\mathbf{n}_{\text{g}} = \begin{bmatrix} -\cos\psi_{\text{b.g}} \cos V_{\text{g}} \\ \cos\psi_{\text{b.g}} \sin V_{\text{g}} \\ \sin\psi_{\text{b.g}} \\ 0 \end{bmatrix} \tag{17.85}$$

for the unit normal vector $\mathbf{n}_{\text{g}}$.

Usually, the desired deviations $\delta_{i,j}$ are given in matrix form [131]

$$\left[\boldsymbol{\delta}_{\text{g}}^{\text{mod}}\right] = \begin{bmatrix} \delta_{1,1} & \delta_{1,2} & \ldots & \delta_{1,j} & \ldots & \delta_{1,n} \\ \delta_{2,1} & \delta_{2,2} & \ldots & \delta_{2,j} & \ldots & \delta_{2,n} \\ \ldots & \ldots & \ddots & \ldots & \ldots & \ldots \\ \delta_{i,1} & \delta_{i,2} & \ldots & \delta_{i,j} & \ldots & \delta_{i,n} \\ \ldots & \ldots & \ldots & \ldots & \ddots & \ldots \\ \delta_{m,1} & \delta_{m,2} & \ldots & \delta_{m,j} & \ldots & \delta_{m,n} \end{bmatrix} \tag{17.86}$$

The matrix $[\boldsymbol{\delta}_{\text{g}}^{\text{mod}}]$ is referred to as a *gear modification matrix*.

For determining the desired tooth surface $\mathscr{G}_{\text{mod}}$, the screw involute surface $\mathscr{G}$ [see Equation (17.84)] is considered together with the gear modification matrix $[\boldsymbol{\delta}_{\text{g}}^{\text{mod}}]$ [Equation (17.86)]. For further analysis, both the desired tooth surface $\mathscr{G}_{\text{mod}}$ and the gear modification matrix $[\boldsymbol{\delta}_{\text{g}}^{\text{mod}}]$ are required to be represented in a common reference system.

The origin of a local reference system $x_{\text{g}}y_{\text{g}}z_{\text{g}}$ is at point $K_{i,j}$ of the grid of points. The axis z_{g} is aligned with the unit normal vector $\mathbf{n}_{\text{g}}$. This makes it possible for representation of the position vector $\overline{\mathbf{r}}_{\text{g}.i,j}^{\text{mod}}$ of point $K_{i,j}$ in the form of column matrix

$$\overline{\mathbf{r}}_{\text{g}.i,j}^{\text{mod}} = \begin{bmatrix} 0 \\ 0 \\ \delta_{i,j} \\ 1 \end{bmatrix} \tag{17.87}$$

With the operator $\mathbf{Rs}_{i,j}(\text{K}_{i,j} \rightarrow \mathscr{G})$ of the resultant coordinate system transformation composed, the position vector $\mathbf{r}_{\text{g}.i,j}^{\text{mod}}$ of the $K_{i,j}$ point can be represented in the coordinate system $X_{\text{g}}Y_{\text{g}}Z_{\text{g}}$ associated with the work gear [131]

$$\mathbf{r}_{\text{g}.i,j}^{\text{mod}} = \mathbf{Rs}_{i,j}(K_{i,j} \rightarrow \mathscr{G}) \cdot \overline{\mathbf{r}}_{\text{g}.i,j}^{\text{mod}} \tag{17.88}$$

At a certain point $K_{i,j}$, the unit normal vector $\mathbf{n}_{\mathrm{g}}^{\mathrm{mod}}$ to the modified tooth flank $\mathscr{G}_{\mathrm{mod}}$ does not align to the unit normal vector $\mathbf{n}_{\mathrm{g}}$ to the screw involute surface $\mathscr{G}$. For the discretely specified tooth flank $\mathscr{G}_{\mathrm{mod}}$ unit normal vector $\mathbf{n}_{\mathrm{g}}^{\mathrm{mod}}$ can be determined under the assumption that (a) the gear tooth flank $\mathscr{G}_{\mathrm{mod}}$ is smooth, and (b) all the $K_{i,j}$ points are distributed evenly (or at least, almost evenly) within the gear tooth flank. Both assumptions are reasonable.

Equation (17.88) allows for the position vectors $\mathbf{r}_{\mathrm{g}.i,j}^{\mathrm{mod}}$ and $\mathbf{r}_{\mathrm{g}.i,(j+1)}^{\mathrm{mod}}$ of points $K_{i,j}$ and $K_{i,(j+1)}$ (Fig. 17.41). This immediately yields an expression for the vector $\mathbf{t}_{i,(j+1)}$ through point $K_{i,j}$ in the direction of the straight line through points $K_{i,j}$ and $K_{i,(j+1)}$

$$\mathbf{t}_{i,(j+1)} = \mathbf{r}_{\mathrm{g}.i,(j+1)}^{\mathrm{mod}} - \mathbf{r}_{\mathrm{g}.i,j}^{\mathrm{mod}} \tag{17.89}$$

In the same way, an expression

$$\mathbf{t}_{i,(j-1)} = \mathbf{r}_{\mathrm{g}.i,(j-1)}^{\mathrm{mod}} - \mathbf{r}_{\mathrm{g}.i,j}^{\mathrm{mod}} \tag{17.90}$$

for the $\mathbf{t}_{i,(j-1)}$ through point $K_{i,j}$ in the direction of the straight line through points $K_{i,j}$ and $K_{i(j-1)}$ can be derived.

The cross product of the vectors $\mathbf{t}_{i,(j+1)}$ and $\mathbf{t}_{i,(j-1)}$ returns tangent vector $\mathbf{u}_{\mathrm{g}}^{\mathrm{mod}}$ to the modified tooth flank $\mathscr{G}_{\mathrm{mod}}$

$$\mathbf{u}_{\mathrm{g}}^{\mathrm{mod}} = \mathbf{t}_{i,(j+1)} \times \mathbf{t}_{i,(j-1)} \tag{17.91}$$

Similarly, two vectors

$$\mathbf{t}_{(i+1),j} = \mathbf{r}_{\mathrm{g}.(i+1),j}^{\mathrm{mod}} - \mathbf{r}_{\mathrm{g}.i,j}^{\mathrm{mod}} \tag{17.92}$$

$$\mathbf{t}_{(i-1),j} = \mathbf{r}_{\mathrm{g}.(i-1),j}^{\mathrm{mod}} - \mathbf{r}_{\mathrm{g}.i,j}^{\mathrm{mod}} \tag{17.93}$$

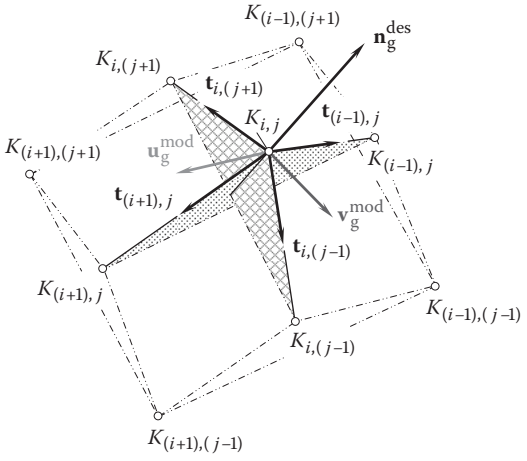

FIGURE 17.41
Unit normal vector $\mathbf{n}_{g}^{\mathrm{mod}}$ to the desirable topologically modified gear tooth flank $\mathscr{G}_{\mathrm{mod}}$. (From Radzevich, S.P., *ASME Journal of Mechanical Design*, 125, 632–639, 2003. With permission.)

through point $K_{i,j}$ (a) in the direction of the straight line through points $K_{i,j}$ and $K_{(i+1),j}$, and (b) in the direction of the straight line through points $K_{i,j}$ and $K_{(i-1),j}$ are computed.

Again, the cross product of the vectors $\mathbf{t}_{(i+1),j}$ and $\mathbf{t}_{(i-1),j}$ returns the tangent vector $\mathbf{v}_{\mathrm{g}}^{\mathrm{mod}}$ to the modified tooth flank $\mathscr{G}_{\mathrm{mod}}$

$$\mathbf{v}_{\mathrm{g}}^{\mathrm{mod}} = \mathbf{t}_{(i+1),j} \times \mathbf{t}_{(i-1),j} \tag{17.94}$$

Ultimately, the cross product of the two tangent vectors $\mathbf{u}_{\mathrm{g}}^{\mathrm{mod}}$ and $\mathbf{v}_{\mathrm{g}}^{\mathrm{mod}}$ allows for an expression [131]

$$\mathbf{n}_{\mathrm{g}}^{\mathrm{mod}} = \mathbf{u}_{\mathrm{g}}^{\mathrm{mod}} \times \mathbf{v}_{\mathrm{g}}^{\mathrm{mod}} \tag{17.95}$$

for the unit normal vector $\mathbf{n}_{\mathrm{g}}^{\mathrm{mod}}$ to the modified tooth flank $\mathscr{G}_{\mathrm{mod}}$ at a given point $K_{i,j}$.

17.6.4.2 Geometry of the Desired Topologically Modified Tooth Flank of a Shaving Cutter

Consider a Cartesian coordinate system $X_{\mathrm{c}}Y_{\mathrm{c}}Z_{\mathrm{c}}$ associated with the shaving cutter. The position vector $\overline{\mathbf{r}}_{\mathrm{g}.i,j}^{\mathrm{mod}}$ of point $K_{i,j}$ of the modified tooth flank $\mathscr{G}_{\mathrm{mod}}$ can be described in the reference system $X_{\mathrm{c}}Y_{\mathrm{c}}Z_{\mathrm{c}}$ by an expression

$$\overline{\mathbf{r}}_{\mathrm{g}.i,j}^{\mathrm{mod}} = \mathbf{Rs}(\mathscr{G} \rightarrow T) \cdot \mathbf{r}_{\mathrm{g}.i,j}^{\mathrm{mod}} \tag{17.96}$$

where the operator of the resultant coordinate system transformation is designated as $\mathbf{Rs}(\mathscr{G} \rightarrow T)$.

The operator $\mathbf{Rs}(\mathscr{G} \rightarrow T)$ can be expressed in terms of the angle of rotation φ_{g} of the work gear and the angle of rotation φ_{c} of the shaving cutter. However, the equality $\varphi_{\mathrm{c}} = \varphi_{\mathrm{g}}(N_{\mathrm{g}}/N_{\mathrm{c}})$ is valid: this is because in the rotary shaving process the work gear and the shaving cutter are in tight mesh, and are rotated about their axis in a properly timed manner. Here the tooth number of the work gear is denoted as N_{g}, and the tooth number of the shaving cutter is denoted as N_{c}. This means that in the coordinate system $X_{\mathrm{c}}Y_{\mathrm{c}}Z_{\mathrm{c}}$, the position vector $\overline{\mathbf{r}}_{\mathrm{g}.i,j}^{\mathrm{mod}}(\varphi_{\mathrm{g}})$ can be interpreted as a function of just one parameter, either φ_{g} or φ_{c}.

The timed rotation of the work gear and the shaving cutter makes it possible to determine a vector $\mathbf{V}_{\Sigma.i,i}$ of the resultant motion of point $K_{i,j}$ of the tooth flank $\mathscr{G}_{\mathrm{mod}}$ relative to the coordinate system $X_{\mathrm{c}}Y_{\mathrm{c}}Z_{\mathrm{c}}$. In the coordinate system $X_{\mathrm{c}}Y_{\mathrm{c}}Z_{\mathrm{c}}$, this vector can be represented as a function of the rotation angle $\mathbf{V}_{\Sigma.i,i}(\varphi_{\mathrm{g}})$.

Ultimately, the position vector $\mathbf{r}_{\mathrm{c}.i,j}^{\mathrm{mod}}$ of a point of the modified tooth flank of the shaving cutter can be determined as the solution to the set of two equations [131]

$$\mathbf{r}_{\mathrm{c}.i,j}^{\mathrm{mod}} \quad \Leftarrow \quad \begin{cases} \overline{\mathbf{r}}_{\mathrm{g}.i,j}^{\mathrm{mod}} = \overline{\mathbf{r}}_{\mathrm{g}.i,j}^{\mathrm{mod}}(\varphi_{\mathrm{g}}) \\ \mathbf{n}_{\mathrm{g}}^{\mathrm{mod}} \cdot \mathbf{V}_{\Sigma.i,i}(\varphi_{\mathrm{g}}) = 0 \end{cases} \tag{17.97}$$

On solving of the set of Equation (17.97) (i.e., after the parameter φ_{g} is excluded from Equation (17.97), an expression for the position vector $\mathbf{r}_{\mathrm{c}.i,j}^{\mathrm{mod}}$ of a point of the modified tooth flank of the shaving cutter can be obtained.

The discretely specified tooth flank of the topologically modified shaving cutter allows for representation in the form of the so-called *shaving cutter modification matrix* [131]

$$\left[\boldsymbol{\delta}_{c}^{\text{mod}}\right] = \begin{bmatrix} \Delta_{1,1} & \Delta_{1,2} & \cdots & \Delta_{1,j} & \cdots & \Delta_{1,n} \\ \Delta_{2,1} & \Delta_{2,2} & \cdots & \Delta_{2,j} & \cdots & \Delta_{2,n} \\ \cdots & \cdots & \ddots & \cdots & \cdots & \cdots \\ \Delta_{i,1} & \Delta_{i,2} & \cdots & \Delta_{i,j} & \cdots & \Delta_{i,n} \\ \cdots & \cdots & \cdots & \cdots & \ddots & \cdots \\ \Delta_{m,1} & \Delta_{m,2} & \cdots & \Delta_{m,j} & \cdots & \Delta_{m,\boldsymbol{n}} \end{bmatrix} \tag{17.98}$$

which is similar to that [see Equation (17.86)] derived for the work gear tooth flank.

The points of the shaving cutter modification matrix [see Equation (17.98)] are in one-to-one correspondence with the points of the gear modification matrix [see Equation (17.86)].

17.6.4.3 Grinding a Topologically Modified Tooth Flank of the Shaving Cutter

The tooth flank of the modified shaving cutter specified by the shaving cutter modification matrix [see Equation (17.98)] is a type of sculptured part surface. For grinding of a sculptured surface, a multiaxis NC machine is used. The tooth flank of the modified shaving cutter can be ground in a multiaxis NC grinder of an appropriate design (Figure 17.42). Under such a scenario, the generating surface of the grinding wheel makes point contact with the modified tooth flank of the shaving cutter. The development of a computer code for a multiaxis NC grinder is a routine procedure that is beyond the scope of this book.

The grinding of the tooth flank of a modified shaving cutter can be also performed with a form grinding wheel that makes line contact with the modified tooth flank being ground. Such a machining process occurs when an NC grinder with a lack of articulation is used.

Precision generation of a topologically modified tooth flank of a shaving cutter is impossible when the grinding wheel and the shaving cutter tooth flank are in line contact. Approximation of the desired generating surface of the grinding wheel with a surface of

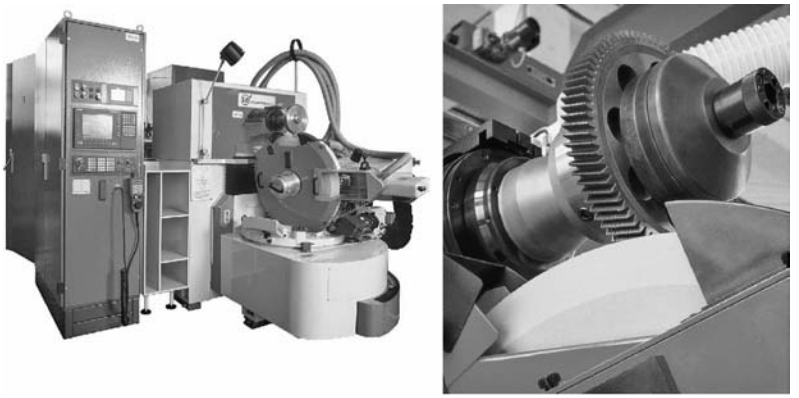

FIGURE 17.42
Grinding the tooth flanks of a shaving cutter.

revolution is unavoidable under such a scenario. The problem of profiling a form grinding wheel for grinding a tooth flank of the topologically modified shaving cutter using an NC grinder that features lack of articulation is important for contemporary gear manufacturers.

Peculiarities of kinematics of NC grinders. For grinding of a topologically modified shaving cutter, an NC grinder featuring a lack of articulation can be used. A typical NC grinder has the following NC axes (Figure 17.43):

X axis: Grinding wheel vertical motion

Y axis: Profile angle setting

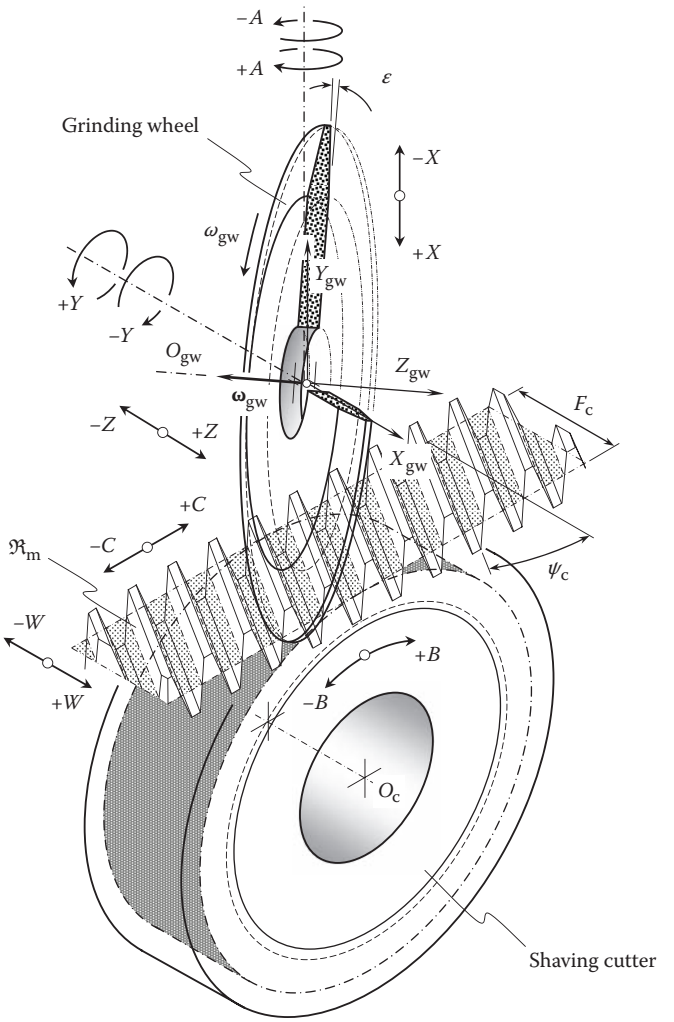

FIGURE 17.43
Kinematics of grinding a shaving cutter with topologically modified tooth flanks. (From Radzevich, S.P., *ASME Journal of Manufacturing, Science and Engineering*, 127(4), 819–828, 2005. With permission.)

Z axis: Grinding wheel motion

A axis: Helix angle setting

B axis: Shaving cutter rotation

C axis: Work-table feed

In addition, the *U* axis and *V* axis are used for the dresser (a) forward/backward, and (b) vertical motion, as well as the *W* axis serves for the shaving cutter positioning.

The kinematics of grinding of the shaving cutter illustrated in Figure 17.43 is implemented, for example, in the design of the Mitsubishi ZA30*CNC* shaving cutter grinder.

The crossing axes of rotation of the shaving cutter O_c and the grinding wheel O_{gw} are at a certain center distance C_{gr}. The shaving cutter swivels about its axis with a certain angular velocity. The swiveling of the shaper cutter is properly timed with the reciprocation of the grinding wheel. In this way the shaving cutter generates the required auxiliary generating rack $\mathfrak{R}_m$. The tooth flank of the auxiliary rack $\mathfrak{R}_m$ is a type of sculptured surface, and it is not a surface of revolution in nature.

Following the way in which the tooth flank $\mathscr{G}_{mod}$ of the shaving cutter is determined [see Equation (17.98)], a similar *auxiliary rack modification matrix* [127, 134, 135, 137, 145]

$$[\boldsymbol{\varepsilon}_{\mathfrak{R}}] = \begin{bmatrix} \varepsilon_{1,1} & \varepsilon_{1,2} & \cdots & \varepsilon_{1,j} & \cdots & \varepsilon_{1,n} \\ \varepsilon_{2,1} & \varepsilon_{2,2} & \cdots & \varepsilon_{2,j} & \cdots & \varepsilon_{2,n} \\ \cdots & \cdots & \ddots & \cdots & \cdots & \cdots \\ \varepsilon_{i,1} & \varepsilon_{i,2} & \cdots & \varepsilon_{i,j} & \cdots & \varepsilon_{i,n} \\ \cdots & \cdots & \cdots & \cdots & \ddots & \cdots \\ \varepsilon_{m,1} & \varepsilon_{m,2} & \cdots & \varepsilon_{m,j} & \cdots & \varepsilon_{m,n} \end{bmatrix} \tag{17.99}$$

can be derived. This matrix specifies a topologically modified tooth flank of the auxiliary generating rack $\mathfrak{R}_m$.

The generating surface of a grinding wheel T_{gw} is a surface of revolution. When grinding a shaving cutter, the grinding wheel must generate the auxiliary rack $\mathfrak{R}_m$. But the sculptured surface $\mathfrak{R}_m$ in no way can be congruent to the surface of revolution T_{gw}. A certain patch of the surface $\mathfrak{R}_m$ can be *almost* congruent to a patch of the surface T_{gw}. This means that approximation of the tooth flank of the generating rack $\mathfrak{R}_m$ with a portion of the surface of revolution is unavoidable. The approximation entails corresponding errors in the tooth shape of the shaving cutter.

Generating surface of a form grinding wheel. The *modification matrix* [see Equation (17.99)] is used for the purposes of transition from the auxiliary generating rack $\mathfrak{R}_m$ to the generating surface T_{gw} of the form grinding wheel.

Consider a Cartesian coordinate system $X_{gw}Y_{gw}Z_{gw}$ associated with the grinding wheel as shown in Figure 17.43. This coordinate system is rigidly connected to the grinding wheel and rotates together with the grinding wheel. Every *i,j*–point of the tooth flank of the generating rack $\mathfrak{R}_m$ traces in $X_{gw}Y_{gw}Z_{gw}$ a circle of the radii $R_{i,j}$. The total number of the circles is equal to the number of points $m \times n$ in the modification matrix [see Equation (17.99)]. The circles intersect an axial plane of the grinding wheel, for example the coordinate plane $X_{gw}Z_{gw}$ of the reference system $X_{gw}Y_{gw}Z_{gw}$. The points of the intersection form a cloud of points within the coordinate plane $X_{gw}Z_{gw}$ (Figure 17.44). The axial profile of the grinding wheel can be derived from the cloud of points [127].

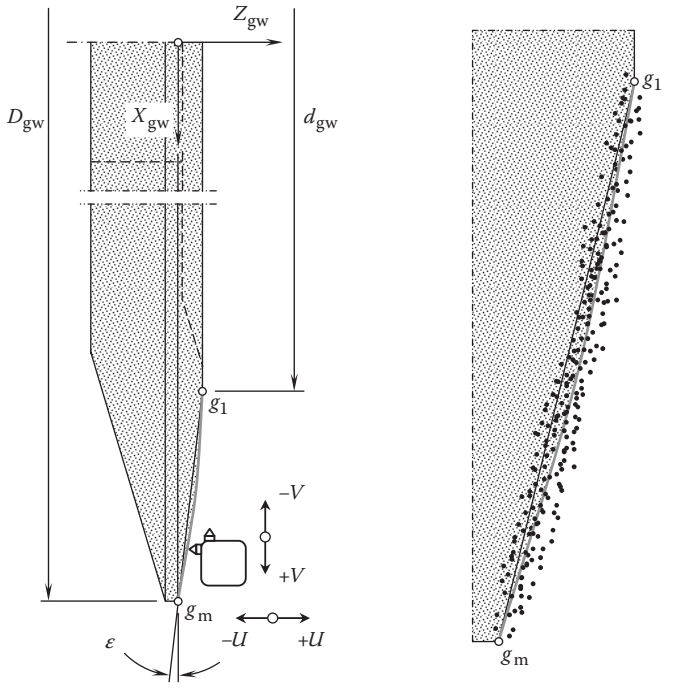

FIGURE 17.44
Geometry of axial profile and kinematics of dressing a form grinding wheel. (From Radzevich, S.P., *ASME Journal of Manufacturing, Science and Engineering*, 127(4), 819–829, 2005. With permission.)

Referring to Figure 17.44, point g_1 of the axial profile of the grinding wheel is located within a circle of the diameter d_{gw}. In the grinding process, point g_1 generates the tooth profile at the outer diameter of the shaving cutter (Figure 17.44). Accordingly, point g_m generates the tooth profile at the inner diameter of the shaving cutter. The shaving cutter can be ground with the grinding wheel with an axial profile shown in Figure 17.45.

Once the axial profile is determined, the generating surface of the grinding wheel is shaped in the form of the surface of revolution with a predetermined axial profile. Further, this makes it possible for computation of deviations due to the approximation of the topologically modified tooth flank $\mathfrak{R}_m$ with a portion of a surface of revolution [127, 134, 135, 137, 145]. Ultimately the predicted deviations of the tooth flank of the shaved gear can be computed as well.

17.6.5 Satisfaction of Conditions of Proper Part Surface Generation When Designing a Shaving Cutter for Plunge Shaving of Gears

When designing a shaving cutter, satisfaction of the set of necessary conditions of proper part surface generation (conditions of proper *PSG*) is a must [128, 136, 138, 143, 153]. Satisfaction of the first and fifth conditions of proper *PSG* is of critical importance when designing a shaving cutter for plunge shaving of both involute helical gear or a gear with topologically modified tooth flanks (see Appendix B). An investigation of this problem was undertaken by Radzevich [147].

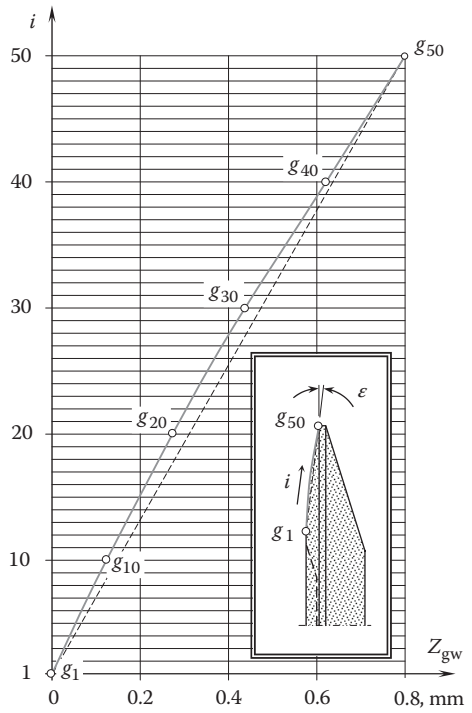

FIGURE 17.45
Example of axial profile of a form grinding wheel for grinding a shaving cutter with a topologically modified tooth flank. (From Radzevich, S.P., *ASME Journal of Manufacturing, Science and Engineering*, 127(4), 819–830, 2005. With permission.)

17.6.5.1 Circular Mapping of Tooth Flanks of a Work Gear and the Shaving Cutter

The *circular mapping* (or simply c–mapping) of the tooth flank $\mathscr{G}$ of the work gear and the tooth flank T of the shaving cutter onto the mapping plane $\mathscr{M}$ [147] is employed in the investigation. The concept of the c–mapping is illustrated in Figure 17.46.

The mapping plane $\mathscr{M}$ is a plane through the shortest distance of approach $C_{g/c}$ of the work gear axis O_g and the shaving cutter axis O_c. At the pitch point P the mapping plane $\mathscr{M}$ is tangent to both the surface $\mathscr{G}$ and the surface T. The unit normal vector $\mathbf{n}_{\mathscr{M}}$ to the mapping plane $\mathscr{M}$ is parallel to the common perpendicular $\mathbf{n}_g$ to the tooth flanks $\mathscr{G}$ and T at the pitch point P.

Consider a plane through an arbitrary point $\mathscr{G}_{ij}$ within the tooth flank $\mathscr{G}$ that is orthogonal to the work gear axis O_g. The circle of a radius R_{ij} with the center at O_g intersects the mapping plane $\mathscr{M}$ at $\mathscr{M}_{ij}$. Point $\mathscr{M}_{ij}$ represents the c–map of point $\mathscr{G}_{ij}$. Similarly, all points of the surface $\mathscr{G}$ can be mapped onto the mapping plane $\mathscr{M}$. In this way, the c–map of the work gear tooth flank $\mathscr{G}$ is constructed. A c–map of the shaving cutter tooth flank can be constructed in the same way as discussed above.

The c-mapping of the tooth flanks $\mathscr{G}$ and T yields an analytical representation. For this purpose it is convenient to introduce a local Cartesian coordinate system $x_p y_p z_p$ with the origin at the pitch point P as shown in Figure 17.46. The axis x_p is aligned with the line

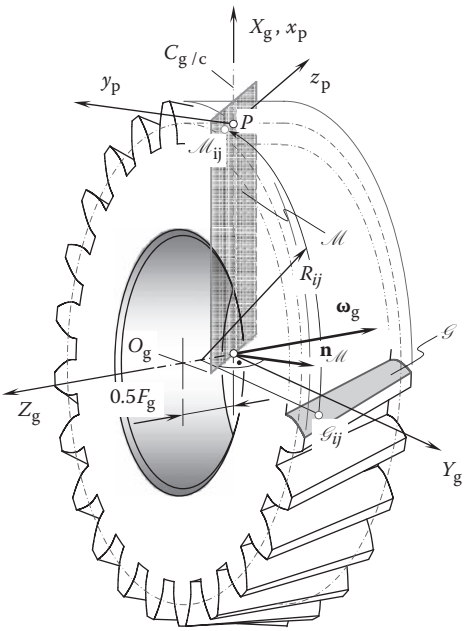

FIGURE 17.46
An example of the c–mapping of the work gear tooth flank $\mathcal{G}$. (From Radzevich, S.P., *ASME Journal of Mechanical Design*, 129(9), 969–980, 2007. With permission.)

through the shortest distance of approach $C_{g/c}$ of the axis O_g of the work gear and O_c of the shaving cutter. The axis y_p is parallel to the unit normal vector $\mathbf{n}_{\mathcal{M}}$ to the mapping plane $\mathcal{M}$. The axis z_p complements the axes x_p and y_p to the left-hand–oriented Cartesian coordinate system $x_p y_p z_p$.

For the computation of the position vector of point $\mathbf{r}_g^{(\mathcal{M})}$ of the c–map of the work gear tooth flank $\mathcal{G}$ in the local reference system $x_p y_p z_p$, the following expression

$$\mathbf{r}_g^{(\mathcal{M})} = \begin{bmatrix} \left(\sqrt{X_g^2 + Y_g^2} - 0.5d_g\right) \\ 0 \\ -\dfrac{Z_g}{\cos\psi_g} \\ 1 \end{bmatrix} \tag{17.100}$$

is valid. For the derivation of Equation (17.100) for the position vector $\mathbf{r}_g^{(\mathcal{M})}$, Equation (17.84) of the work gear tooth flank $\mathcal{G}$ is implemented together with Figure 17.46.

For the purposes of analysis, the position vector $\mathbf{r}_g^{(\mathcal{M})}$ may be normalized by the module m. In this case the equality $\bar{\mathbf{r}}_g^{(\mathcal{M})} = \mathbf{r}_g^{(\mathcal{M})}/m$ specifies the correlation between the position

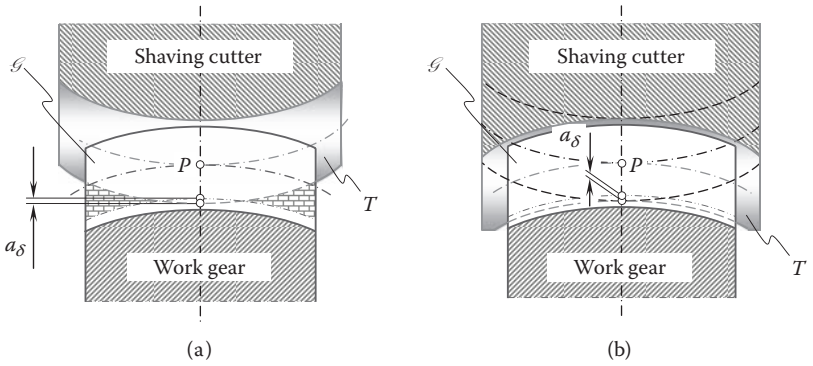

FIGURE 17.47
c–maps of the work gear and shaving cutter tooth flanks. (From Radzevich, S.P., *ASME Journal of Mechanical Design*, 129(9), 969–980, 2007. With permission.)

vector of point $\bar{\mathbf{r}}_g^{(\mathcal{M})}$ of the normalized c–map with the corresponding position vector $\bar{\mathbf{r}}_g^{(\mathcal{M})}$ of the original c–mapping.*

Shown in Figure 17.47a, the c–maps of the tooth flank $\mathcal{G}$ of the work gear and the tooth flank T of the shaving cutter reveal that the entire tooth flank $\mathcal{G}$ of the work gear cannot be finished with a shaving cutter of conventional design. Shadowed portions of the tooth surface $\mathcal{G}$ cannot be reached by the finishing tool, and thus they remain unshaved [168]. This means that a shaving cutter of a special design (Figure 17.47b) is required for the plunge shaving process.

17.6.5.2 Shaving Cutter of a Special Design for Plunge Shaving of Precision Gears

The tooth design of a special-purpose plunge shaving cutter is schematically shown in Figure 17.48. The tooth flanks 1 feature a hollowed geometry. The top land 2 is also hollowed. It is represented with a patch of a surface of revolution. The effective face width of the shaving cutter is denoted as F_c. The total face width of the shaving cutter is designated as F_c^*. The shaving cutter features two side lands, three from both faces. They are necessary to protect the shaving cutter teeth from damage. The face width of the side land is designated as F_s. The bottom land 4 is of a special shape and parameters.

Actually, the design of a plunge shaving cutter is specified in terms of conventional design parameters. Two groups of the design parameters can be distinguished in this concern. The following design parameters

(1) Pitch diameter d_c
(2) Outer diameter $d_{o.c}$
(3) Root diameter $d_{f.c}$
(4) Addendum a_c

* To the best of the author's knowledge, a simplified type of mapping of the tooth flank of a gear is proposed by Gleason Works, Rochester, NY. The mapping plane through the axis of rotation of the helical gear is used in the simplified method of mapping of the tooth flank. This feature significantly limits the capabilities of the simplified type of mapping.

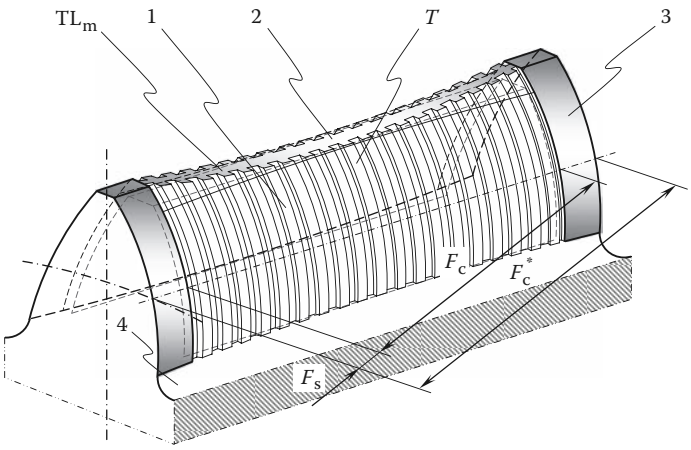

FIGURE 17.48
Tooth design of a special-purpose plunge shaving cutter. (From Radzevich, S.P., *ASME Journal of Mechanical Design*, 129(9), 969–980, 2007. With permission.)

(5) Dedendum b_c
(6) Whole tooth height h_c
(7) Normal profile angle ϕ_n
(8) Pitch helix angle ψ_g
(9) Effective face width F_c

comprise the first group of the design parameters of the shaving cutter.

The second group of the design parameters is comprised by

(1) Extended outer diameter $d_{o.c}^*$
(2) Addendum extension a_c^*
(3) Extended whole tooth height h_c^*
(4) Extended face width F_c^*

All points of the work gear tooth flank $\mathscr{G}$ can be achieved by the shaving cutter tooth due to the addendum extension a_c^*. In this way the accuracy of the shaved work gear teeth is improved.

Fulfillment of two requirements is a must when determining the effective face width F_c of the shaving cutter. First, the c-map of the shaving cutter tooth flank T must overlap the corresponding c-map of the work gear tooth flank $\mathscr{G}$. Second, the effective face width of the plunge shaving cutter must be the narrowest permissible. Following these two requirements, a corresponding expression for the critical value of F_c is derived

$$F_c = F_g + 2 \cdot \frac{a}{\cos \bar{\Sigma}} \tag{17.101}$$

where a designates an excess of the plunge shaving cutter face width in relation to the gear face width F_g [59].

In practice, the effective face width of the plunge shaving cutter can exceed the computed value of it at a reasonable value.

For the computation of the total face width of the plunge shaving cutter F_c^*, the formula

$$F_c^* = F_c + 2F_s \tag{17.102}$$

is valid. Here, in Equation (17.102), the width of the protective side land of the shaving cutter tooth is denoted as F_s.

The c–mapping is useful and can be implemented for determining other design parameters of the shaving cutter tooth, namely of (a) the desired axial profile of the modified top land TL_m, and (b) the desired axial profile of the modified bottom land as proposed in [147].

17.7 Advances in the Design of the Shaving Cutter

The productivity rate of the gear shaving process as well as accuracy of the shaved gears strongly depend on the design of the shaving cutter being applied to the finishing of a given work gear. Consideration in this section is limited only to those opportunities for the improvement of the design of a shaving cutter, which can be drawn up from geometrical and kinematical analyses of a gear shaving process. Implementation of the methods developed in powder metallurgy technology as well as in the production of cutting tools made of carbide alloys, provide the cutting tool designer with more freedom when designing shaving cutters. Ultimately these technologies make it possible for the production of shaving cutters with serrations of complex form.

17.7.1 Elements of the Geometry of the Cutting Edges

A shaving cutter is a type of cutting tool for finishing gears. The cutting edges of a shaving cutter cut thin chips. When chips are thin, the use of cutting tools with a greater inclination angle is highly desired.

A shaving cutter with a near optimal angle of inclination of the cutting edges. The angle of inclination of the cutting edges of a shaving cutter with annular serrations is insufficiently small. This becomes clear from the following consideration.

The tooth of a shaving cutter is depicted in Figure 17.49a. At a point of interest m within the cutting edge CE, three vectors are constructed, namely: unit normal vector $\mathbf{n}_c$ to the generating surface T of the shaving cutter, the cutting speed vector $\mathbf{V}_{cut}$, and the unit normal vector $\mathbf{n}_{ce}$ to the cutting edge CE. The vector $\mathbf{n}_{ce}$ is located within the plane of the cut. For convenience, the vectors $\mathbf{V}_{cut}$ and $\mathbf{n}_{ce}$ are also depicted in Figure 17.49b within the lateral plane of the auxiliary generating plane $\mathscr{R}_T$. By definition (see Appendix D), the inclination angle λ is measured between the vectors $\mathbf{V}_{cut}$ and $\mathbf{n}_{ce}$. The angle of inclination λ is positive when the vector of the cross product $\mathbf{V}_{cut} \times \mathbf{n}_{ce}$ is pointed outward toward the body of the shaving cutter tooth. Figure 17.49b reveals that shaving cutters of conventional design feature the inclination angle of a negligibly small value.

Consider the vectors $\mathbf{V}_{cut}$ and $\mathbf{n}_{ce}$ referring to a certain reference system. The earlier introduced Cartesian coordinate system $X_cY_cZ_c$ (see Figure 17.24) can be employed in this case. The X_c axis is pointed along the shortest distance of approach $C_{g/c}$ of the axes O_g and O_c from the work gear axis O_g toward the shaving cutter axis O_c.

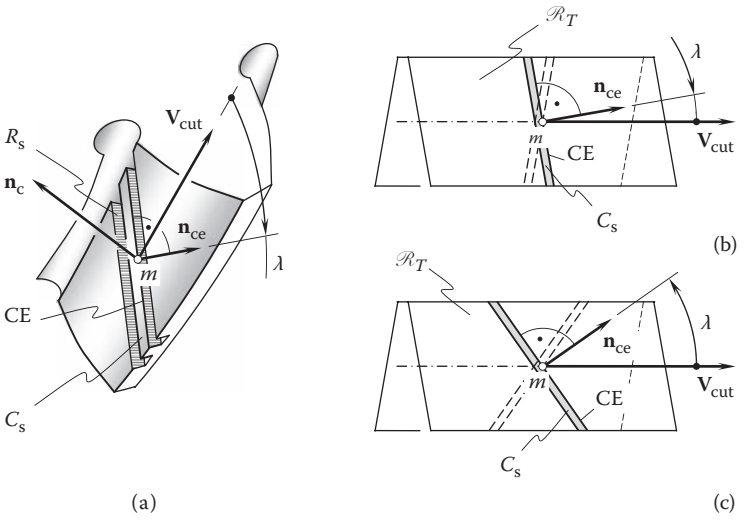

FIGURE 17.49
Tooth design of a shaving cutter with an increased (with the near optimal) angle of inclination λ of the cutting edges.

When the vectors $\mathbf{V}_{cut}$ and $\mathbf{n}_{ce}$ are through the pitch point P, then the following expressions are valid

$$\mathbf{V}_{cut} = \mathbf{j} \mid \mathbf{V}_{cut} \mid \sin \psi_c + \mathbf{k} \mid \mathbf{V}_{cut} \mid \cos \psi_c \tag{17.103}$$

$$\mathbf{n}_{ce} = \mathbf{i} \cos \phi_t - \mathbf{j} \sin \phi_t \tag{17.104}$$

where
ψ_c = pitch helix angle of the shaving cutter
ϕ_t = transverse profile angle in the *work gear to the shaving cutter* mesh

By definition (see Appendix D), for the computation of the angle of inclination, the formula

$$\lambda = \tan^{-1}\left(\frac{\mid \mathbf{V}_{cut} \times \mathbf{n}_{ce} \mid}{\mathbf{V}_{cut} \cdot \mathbf{n}_{ce}} \right) \tag{17.105}$$

is used.

Substituting Equations (17.103) through (17.104) into Equations (17.105), a formula

$$\lambda = \tan^{-1}\left(\sqrt{\frac{1 + \tan^2 \phi_t \cos^2 \psi_c}{(1 + \tan^2 \phi_t) \sin^2 \phi_t \sin^2 \psi_c}} \right) \tag{17.106}$$

for the computation of the inclination angle λ is obtained.

In order to express the inclination angle not in terms of transverse profile angle ϕ_t, but in terms of normal profile angle ϕ_n, an expression (see Appendix A)

$$\phi_t = \tan^{-1}\left(\frac{\tan\phi_n}{\cos\psi_c}\right) \tag{17.107}$$

can be used.

The inclination angle of the cutting edges is significantly increased in the design of a shaving cutter featuring not annular but inclined serrations (Figure 17.49c). In this way the inclination angle λ can be of optimal or near optimal value. The serrations at the opposite side of the shaving cutter tooth profile are inclined oppositely.

A shaving cutter with a constant inclination angle within the cutting edges. Once an optimal value of the inclination angle λ is determined, it is desired to shape the cutting edges so as to have the optimal value λ_{opt} at every point within the cutting edges. This problem is out of critical importance in cases when the tooth number of both the work gear and the shaving cutter is big enough. However, when tooth number either of the work gear or the shaving cutter (or of both) is little, then variation of the direction of the cutting speed $\mathbf{V}_{cut}$ within the cutting edge (see Figure 17.22b) cannot be ignored. Variation of the direction of the cutting speed vector $\mathbf{V}_{cut}$ entails corresponding alterations to the inclination angle λ. Once the inclination angle λ varies within the cutting edge, then it cannot be of optimal value at every point of the cutting edge of the shaving cutter. Ultimately this reduces the cutting performance of the shaving cutter.

The cutting performance of a shaving cutter can be increased if the inclination angle is maintained of optimal value at every point within the cutting edge. For this purpose serrations are made curvilinear in their lengthwise direction. A practical approximation to the desired longitudinal shape of the serrations by a circular arc resolves the issue.

Consider a lateral tooth flank of the auxiliary generating rack $\mathscr{R}_T$ of the shaving cutter as shown in Figure 17.50. Within the plane $\mathscr{R}_T$, the cutting edge is shaped in the form of a circular arc. Center O_{ce} of the circular arc is within a straight line that is aligned with the normal unit vector $\mathbf{n}_{ce}$ to the cutting edge at the pitch point. The radius R_{ce} of the circular arc is computed from the expression

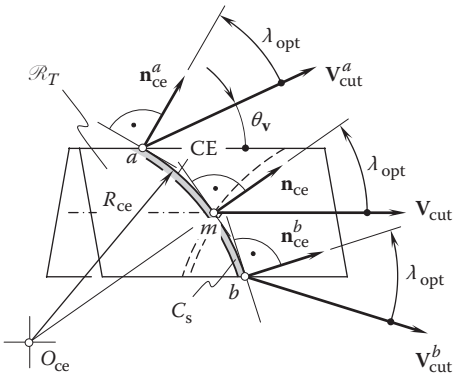

FIGURE 17.50
Tooth design of a shaving cutter with an optimal inclination angle λ_{opt} at every point of the cutting edge.

$$R_{ce} = \frac{a_c}{\sin(\theta_v + \lambda_{opt}) - \sin\lambda_{opt}} \tag{17.108}$$

where

a_c = tooth addendum of the shaving cutter
θ_v = angle within the lateral plane $\mathcal{R}_T$ that the cutting speed vector $\mathbf{V}_{cut}$ at the pitch point makes with the cutting speed vector $\mathbf{V}^a_{cut}$ at the top of the shaving cutter tooth [$\theta_v = \angle(V_{cut}, V^a_{cut})$]
λ_{opt} = desirable value of the inclination angle of the cutting edges of the shaving cutter

After the cutting edge is constructed within the plane $\mathcal{R}_T$, then the plane $\mathcal{R}_T$ is folded over the screw involute surface T of the shaving cutter tooth. Implementation of c–mapping of the circular arc cutting edge is helpful in this case.

Under such a scenario, the inclination angle is of constant value within the cutting edge, and it can be equal to an optimal it value λ_{opt} at every point of the cutting edge. In this way the cutting performance of the shaving cutter can be improved.

The concept of constant inclination angle is also used in the design of the tools for reinforcement of gears with surface plastic deformation [202, 203].

17.7.2 Utilization of Features of the Generating Surface of a Shaving Cutter

The generating surface of a shaving cutter for the machining of involute gears is shaped in the form of a screw involute surface (see Equation 17.1). The screw involute surface is conjugate to the work gear tooth flank. The screw involute surface is a type of developable surface. It can be represented in the form of successive positions of a straight line that is tangent to the base helix of the surface. This immediately allows for a conclusion: a straight line passes through every point of the generating surface T of a shaving cutter. This straight line is often referred to as the straight generating line.

A precision shaving cutter with straight cutting edges. A segment of the straight generating line can be employed as a cutting edge of the shaving cutter. The cutting edges of the precision shaving cutter align to the straight lines, which are tangent to the base helix of the generating surface of the shaving cutter (Figure 17.51) [170].

The cutting speed vector $\mathbf{V}_{cut}$ is located within a plane tangent to the screw involute surface T. At the pitch point the cutting speed vector $\mathbf{V}_{cut}$ is tangent to the pitch cylinder, and it crosses the axis O_c of the shaving cutter at the pitch helix angle ψ_c.

The unit tangent vector $\mathbf{n}_{ce}$ to the cutting edge is pointed opposite of the vector $\mathbf{v}^*_c$. The last vector is one of three direction vectors of the local Cartesian coordinate system. The origin of this reference system is at point of interest m within the cutting edge CE.

Once the cutting speed vector $\mathbf{V}_{cut}$ and either the unit tangent vector $\mathbf{n}_{ce}$ or the direction vector $\mathbf{v}^*_c$ are computed, then the inclination angle λ can be computed from Equation (17.105).

Many advantages are inherent to a precision shaving cutter with straight cutting edges [170]. The feasibility of serrations of constant depth is one of the advantages. Then, the serrations can be designed so that their depth gradually gets bigger either toward the outer diameter or toward the root diameter of the shaving cutter. This feature in combination

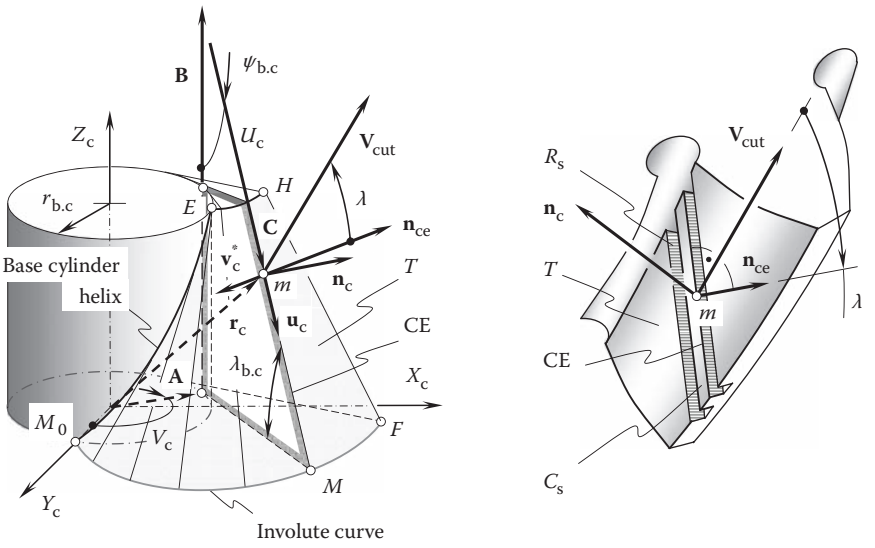

FIGURE 17.51
Tooth design of a precision shaving cutter with straight cutting edges. (From Radzevich, S.P., Palaguta, V.A., Radzevich, A.P., and Tovmasian, M.A., USSR Patent 1537426, Int. Cl. B23f 21/28, Nov. 17, 1986.)

with the trapezoidal shape of the serrations allows for easier control over the width of the serration land.

A precision worm-type shaving cutter can be designed with straight cutting edges as well.

A shaving cutter for a finishing modified work gear tooth flank. Shaving cutters with straight cutting edges can be designed for finishing modified involute gears. As an example, consider a worm-type shaving cutter for a finishing modified work gear tooth flank. The worm-type shaving cutter features straight cutting edges [204]. That same concept for modification of the work gear tooth flanks can be implemented in the design of disk-type shaving cutters as well.

If the cutting edges of the shaving cutter are tangent to the base helix, then the tooth profile of the work gear is shaped in the form of an involute. In this particular case the cutting edge of the shaving cutter is at a distance of $0.5d_{b.c}$ from the axis O_c of the shaving cutter. When cutting edge CE crosses the shaving cutter axis O_c at a distance of $0.5d^*_{b.c}$ that exceeds the distance $0.5d_{b.c}$, then the straight cutting edge is deviated from the generating surface T as shown in Figure 17.52. In this way a modified tooth profile of the work gear is generated in the gear finishing process. For the computation of the desired radius of the curvature R_c of the modified tooth profile, Dupin's indicatrix is implemented.

For a screw involute surface, Dupin's indicatrix Dup(T) of the surface T reduces to a pair of straight lines. These lines are parallel to the direction that is specified by the unit vector $\mathbf{t}_{1.c}$ of the first principal direction of the surface T. For a shaving cutter with given design parameters, the second principal radius of curvature $R_{2.c}$ can be computed [the first principal

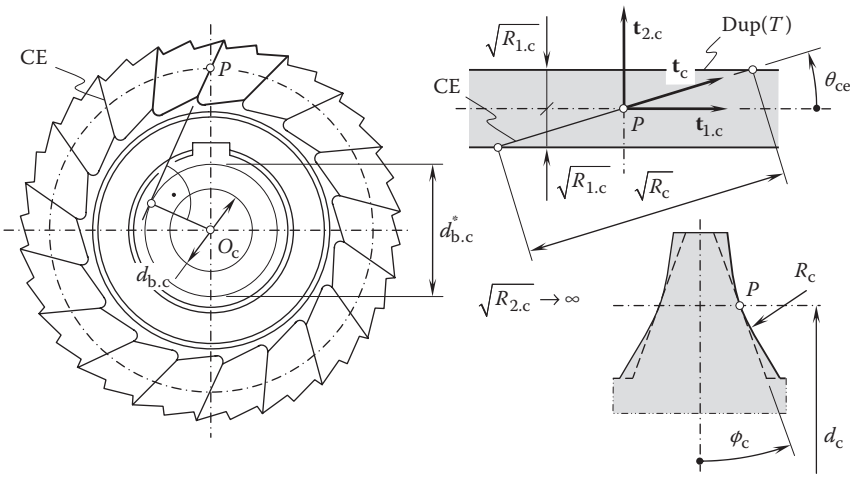

FIGURE 17.52
A precision shaving cutter with straight cutting edges for finishing a modified tooth flank of the work gear. (From Radzevich, S.P., USSR Pat. No. 1683913, Int. Cl. B23f 21/28, Jan. 1, 1989.)

radius of curvature $R_{1.c}$ in the case under consideration is equal to infinity ($R_{1.c} \to \infty$)]. Ultimately, the required angle θ_{ce} can be computed from the equation

$$\theta_{ce} \approx \sin^{-1}\sqrt{\frac{R_{2.c}}{R_c}} \tag{17.109}$$

The direction of the straight cutting edge CE is specified by unit tangent vector $\mathbf{t}_c$. The angle θ_{ce} is the angle that the cutting edge CE makes with the first principal direction $\mathbf{t}_{1.c}$, or in other words, $\theta_{ce} = \angle(\mathbf{t}_{1.c}, \mathbf{t}_c)$.

The illustrated approach in Figure 17.52 for determination of the angle θ_{ce} is a type of approximation. The smaller the angle θ_{ce}, the better the approximation is and vice versa. Actually, the points of the generating surface T of the shaving cutter for finishing modified gears feature negative Gaussian curvature. From this perspective, an exact expression for the computation of angle θ_{ce} can be derived.

Once angle θ_{ce} is computed, then computation of the rest of the design parameters of the shaving cutter is a trivial procedure.

Investigation of (a) the geometry of the cutting edges, (b) the shape and parameters of the generating surface of the shaving cutter, and (c) the kinematics of the gear shaving process, may reveal new opportunities for the improvement of the design of shaving cutters [169].

17.8 Peculiarities of the Gear Shaving Process

Rotary shaving is a low-pressure, free-cutting finishing operation that can be applied to finish preformed, hobbed, or shaped gear teeth before heat treatment. As the shaving

cutter rotates with the work gear in tight mesh, the notches scrape off little shavings of material; hence the name *shaving*.

Gear shaving is the logical remedy for the inaccuracies inherent in gear cutting. It is not, therefore, a "cure-all" but a means of making a good gear better.

17.8.1 Shaving Cutter Selection

The equality of the base pitch of the shaving cutter to the base pitch of the work gear is a requirement of prime importance when selecting a design of a shaving cutter for finishing of a given work gear. The base pitch of the shaving cutter must be equal to the base pitch of the work gear.

Theoretically, one shaving cutter will shave all gears of a given pitch and profile angle regardless of the number of teeth. A slight involute variation due to the difference in sliding action may be noticeable on the gears in the coarser pitches with small numbers of teeth. Therefore, the range of gears that can be shaved with one shaving cutter will depend on the allowable involute tolerances.

Right- and left-hand shaving cutters are usually required for a range of helical gears. However, gears ranging from 5° to 18° helix angle, right- and left-hand, may be shaved with one straight spur shaving cutter. The range of helical angles that one shaving cutter can handle is determined by the crossed-axes angle between the shaving cutter and the work gear axes of rotation. The most desirable range of crossed-axis angles is from 5° to 15°. Thus, one shaving cutter with a 15° helix angle will shave spur gears and opposite-hand helical gears from 0° to 10° helix angle, and from 20° to 30°, approximately.

No particular requirements for the serration design need to be fulfilled when the axial method of shaving is applied. A shaving cutter with either annular serrations or serrations of a differential type can be used in this case. That same is true with respect to a diagonal shaving process with a reasonably small traverse angle. However, it is recommended to apply differential-type serrations in the design of shaving cutters for diagonal (with great traverse angle), tangential, and plunge shaving methods.

In general, it is desired to have a "hunting" ratio between the number of shaving cutter teeth and the number of work gear teeth. This tends to make it desirable to design shaving cutters with *prime* numbers of teeth. A prime number will hunt with all numbers of teeth except itself. Thus numbers of teeth like 37, 41, 43, 47, 53, 59, 61, 67, 73, and so forth, are popular for shaving cutters.

If the gear and the shaving cutter are properly designed, it is possible to improve profile accuracy considerably.

17.8.2 Requirements for Preshaved Work Gear

So much depends on the hobbed tooth form and the desired final shaved tooth form that for the best results, both tools should be regarded as complementary and the shaving cutter designed specifically to modify the hobbed tooth.

Of primary concern to the shaving cutter manufacturer is the fillet produced by the roughing operation. The tips of the shaving cutter teeth must not contact the gear root fillet during the shaving operation. If such contact does occur, excessive wear of the shaving cutter results and the accuracy of the involute profile is affected.

Teeth intended to be shaved are often and preferably cut by a protuberance hob or shaper cutter. Gear cutting tools with protuberance produce a slight undercut or relief near the base of the gear tooth (Figure 17.53). This method assumes a smooth blending of the shaved

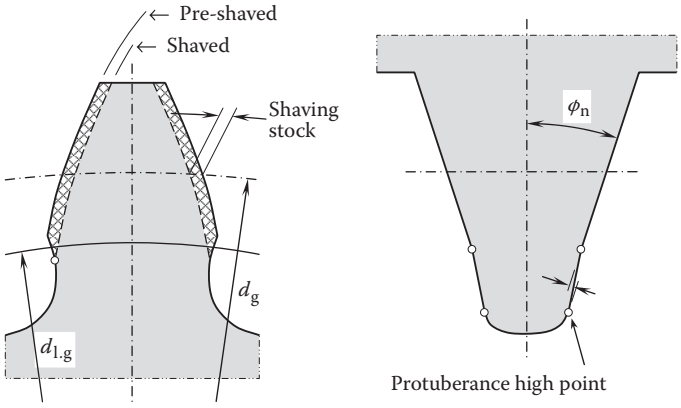

FIGURE 17.53
Tooth of a preshaved work gear and a protuberance-type hob.

tooth profile and the unshaved tooth fillet, and reduces shaving cutter tooth tip wear. The amount of undercut produced by the protuberance-type gear cutting tool should be made for the thin end of the tooth. The position of the undercut should be such that its upper margin meets the involute profile at a point below its limit diameter.

17.8.3 Manufacturing Aspects of Gear Shaving Operation

In rotary shaving of gears the work gear and the shaving cutter rotate in tight mesh. There is no index gearing in the shaving process. Small parts are driven by the cutter that is shaving them, while large parts drive the shaving cutter instead.

The shaving cutter is rotated at high speeds up to 122m (400 and more surface feet) per minute. Feed is fine and the shaving cutter tool contact zone is restricted. Shaving cutter life depends on several factors: operating speed, feed, material and hardness of the work gear, its required tolerances, type of coolant, and the size ratio of shaving cutter to work gear.

The desired range of the crossed-axis angle is from 5° to 15° for spur gears and from 5° to 12° for helical gears. Experience has established these as the most desirable ranges, although in some cases it is permissible to extend them to from 3° to 18°. At the lower end of this extended range, cutting action is reduced and at its upper end, guiding action is somewhat sacrificed.

Shaving is a corrective process. The purpose of gear shaving is to (a) correct eccentricity and errors in index, helix angle, and tooth profile, (b) improve tooth surface finish, (c) maintain tooth size, and (d) eliminate tooth end bearing conditions by producing a crowned tooth form The reason the shaving cutter can produce very high accuracy is that there is an *averaging* action as the shaving cutter rolls with the work. This tends to mask the effect of any slight indexing errors that may have been ground into the cutter.

Tooth-to-tooth spacing is improved by shaving, but accumulated spacing error is not changed by a large amount unless the accumulated error comes mostly from eccentricity effects. On narrow face width gears, helix errors can be controlled by shaving, but a narrow shaving cutter has little or no control on wide-faced gears.

Gears with the smaller numbers of teeth are more critical from a production and sound standpoint than those with greater numbers of teeth. Likewise, spur gears are generally more critical on both scores than helical gears.

Spur pinions with small number of teeth are somewhat more difficult to shave. There are problems with obtaining good involute when shaving pinions with 10 teeth or fewer. It is also difficult to design a suitable shaving cutter for internal gear with fewer than 40 teeth. When internal gears have 25 teeth, it is just about impossible to get a shaving cutter inside that will shave on the crossed-axis principle.

The number of cuts required will depend on the amount of stock left for shaving and the amount taken per cut. Sometimes extra cuts may be needed to secure helix-angle correction. The amount of stock that may be removed in shaving is fairly limited. It is practical to put in only a certain amount of undercut in the preshave cutting. If too much stock is removed, the undercut allowance will be exceeded, and there will be trouble from cutter "bottoming."

In shaving either spur or helical gears by the modified underpass shaving method, there is a choice of direction of feed and rotation. The direction of feed slide should be set to feed in the general direction of the cutter helix. The rotation of the cutter should be in a direction opposing the feed.

The direction of the feed slide should be set to feed in the general direction opposing the helix of the cutter. The rotation of the cutter should be in a direction opposing the feed.

A conical spur or helical gears (tapered tooth gears that mesh on nonparallel axes) can be shaved by the high-speed diagonal shaving method.

17.8.4 Modification of Tooth Form and Shape

Modification of the tooth flank from its theoretical form has been found to have a marked effect on improving gear life and reducing operating sound levels by making allowances for deflection conditions under load. By far the most economical, and often the only way to achieve these important tooth modifications, is to make them by a finishing process.

Shaving cutters are capable of removing 0.0005 in. (0.012 mm) from the tip and root of tooth profiles to provide relief and simultaneously they can remove undulations down a tooth profile.

In axial shaving as well as in diagonal shaving that features a small traverse angle, the rocking machine table is used in order to introduce the lead crown of the work gear teeth. For this purpose the built-in crowning mechanism is used. The table supporting the part being shaved is rocking about a pivot point in timed relation with the feed. In this way end relief, barreling, or crowning to the work gear teeth is imparted.

When traverse angles in diagonal shaving are from 60° to 90°, a shaving cutter with reverse-crowned teeth is utilized to provide the crowned tooth form. The same is observed when the tangential or plunge method of shaving is used. All tooth modifications in this case must be made to the shaving cutter as it will not be possible to realize them through axial movements on the machine. This method uses a shaving cutter with differential serrations and is applied to finish shoulder gears.

17.8.5 Shaving of Worm Gear

The object of worm-wheel shaving is to produce tooth surfaces more closely resembling those resulting from running in when small asperities and departures from the shape conjugate with the worm have been removed by wear or by plastic surface deformation.

In operation the process is quite simple and logical. The lands on a serrated hob are not relieved and when they engages with the surface of wheel teeth that have numerous small projections standing above the general surface level, these are removed in thin shavings.

It is not feasible to take heavy cuts and the closely spaced lands quickly remove the projections and produce a smoother finish on the wheel tooth flanks. If the pressure between the work gear and the hob is then slightly increased either by feeding the hob into the work gear radially or by driving the work gear by the hob against some resistance, the surface is locally elastically deformed. This permits the hob to shave off the surface of the work gear protruding between the lands of the hob and remove the metal surrounding hollows. About 0.005 to 0.010 in. (0.12–0.25 mm) of metal per flank is shaved off when finishing worm wheels.

18

Examples of Implementation of the Classification of the Gear Machining Meshes

Gear cutting tools include, but are not limited to, machining-gear hobs and shaving cutters for finishing gears. Their designs originate from the vector diagram of the external spatial gear machining mesh shown in Figure 15.1. Other novel gear cutting tools and corresponding methods for machining cylindrical and conical gears can be designed based on that same vector diagram of the external spatial gear machining mesh (see Figure 3.8). The following examples of novel designs of gear cutting tools and methods for machining gears demonstrate the applications of gear machining meshes (see Figure 3.8).

18.1 A Hob for Tangential Gear Hobbing

The external spatial gear machining mesh (see Figure 15.1a) can be complemented with the feed rate motion $\mathbf{F}_c$ that is pointed in a tangential direction relative to the work gear. Consequently, the principal kinematics of the tangential method for gear hobbing can be derived (see Figure 18.1). In this kinematic model, the feed rate motion $\mathbf{F}_c$ is perpendicular to the work gear axis O_g.

Both spur and helical gears can be machined using the tangential method for gear hobbing. A hob of extended face width is used in this method as schematically shown in Figure 18.2. The length of the hob and the crossed-axis angle S should be set so as to allow the required overlap of the work gear face by the hob. The approach that is illustrated in Figures 17.127 and 17.129 can be employed for the purpose of determining the required combination of the crossed-axis angle Σ and the hob length. Two straight generating lines $\mathscr{E}_r$ and $\mathscr{E}_l$ of the generating surface T of the hob are tangent to the base cylinder of the hob ($d_{b.c}$), and to the base helices as well. The straight lines $\mathscr{E}_r$ and $\mathscr{E}_l$ are configured so that they are parallel to the faces of the work gear. The crossed-axis angle Σ and the hob length should satisfy the conditions under which the distance F_g^* between the crossing straight generating lines $\mathscr{E}_r$ and $\mathscr{E}_l$ is equal to or exceeds the face width F_g of the work gear ($F_g^* \geq F_g$). The work gear face width must not exceed the distance F_g^*. In such a scenario, the gear hob is traveling tangentially in relation to the work gear. The whole work gear is machined in just one short path of the hob. The travel distance of the hob does not depend upon the face width F_g of the work gear. Hobs for the tangential hobbing of gears are of the same design as conventional hobs and differ only in length.

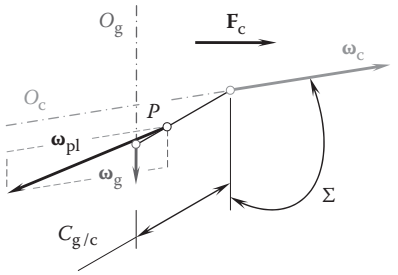

FIGURE 18.1
Kinematics of the tangential method for gear hobbing.

18.2 A Hob for Plunge Gear Hobbing

Another opportunity arises in the event that the feed rate motion $\mathbf{F}_c$ is pointed along the closest distance of approach $C_{g/c}$ of the axes of rotation O_g and O_c of the work gear and of the gear cutting tool, respectively. The principal kinematics of the gear hobbing process is illustrated in Figure 18.3. Because the feed rate motion is pointed toward the work gear O_g, this method of gear hobbing is referred to as the *plunge* method of gear hobbing.

Hourglass-type hobs are used in the plunge gear hobbing method (see Figure 18.4). The auxiliary generating surface $\mathscr{R}_T$ of the hob is congruent to the gear being machined. The length of the hob should be sufficient to overlap the entire face width of the work gear.

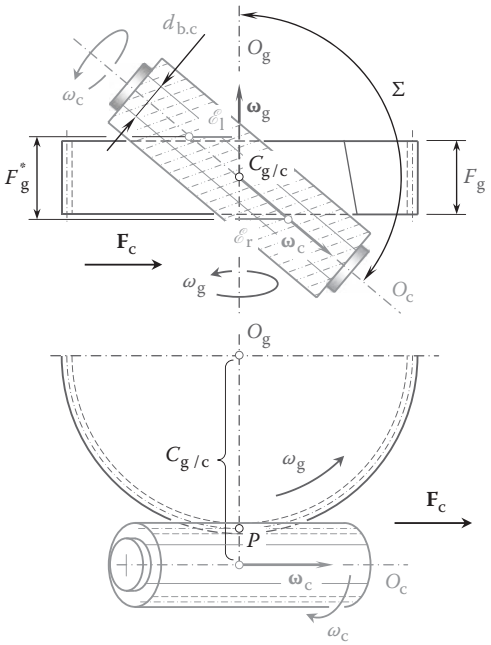

FIGURE 18.2
Configuration of the hob in the tangential method for gear hobbing.

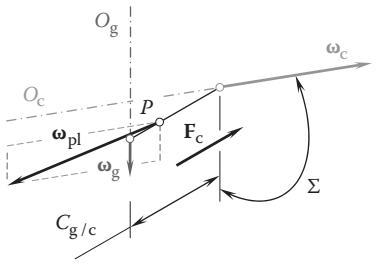

FIGURE 18.3
Kinematics of the plunge method for gear hobbing.

Again, the work cycle is very short—the whole work gear can be machined in one short path of the hob in the radial direction of the work gear. Both spur and helical gears can be machined with the tangential method for gear hobbing.

18.3 Hobbing of a Face Gear

One of the possible directions of the feed rate motion $\mathbf{F}_c$ of the gear cutting tool corresponds to the principal kinematics of cutting a face gear with a standard hob. This possibility is illustrated in Figure 18.5. The work gear and the hob are rotated about their axes O_g and

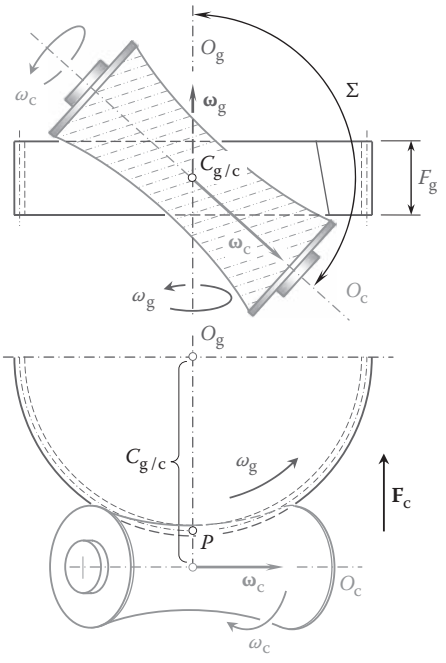

FIGURE 18.4
Relative motions of the hob and of the work gear in the tangential method for gear hobbing.

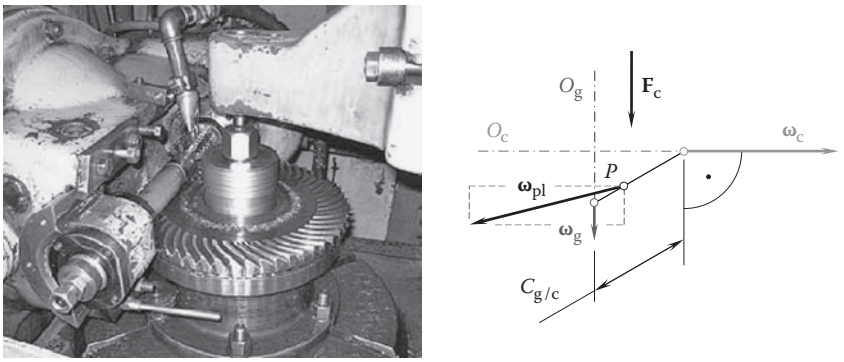

FIGURE 18.5
Kinematics of hobbing of a face gear with the standard hob.

O_c with the axes crossing at a right angle. The rotation of the work gear $\boldsymbol{\omega}_g$ and the rotation of the hob $\boldsymbol{\omega}_c$ are synchronized. The feed rate motion $\mathbf{F}_c$ is pointed toward the work gear. The travel distance of the hob slightly exceeds the depth of the face gear tooth space. Consequently, the cycle time is very short. This method of face-gear hobbing allows for its interpretation as an inversion of the method of gear cutting illustrated in Figure 16.93.

18.4 A Worm-Type Gear Cutting Tool with a Continuous Helix-Spiral Cutting Edge

For most gear cutting tools of common design, the cutting-tool rotation contributes most to the cutting speed. From this standpoint, rests of the elementary motions of the gear cutting tool in relation to the work gear are of minor importance. The parameters of the external spatial gear machining mesh (see Figure 15.1a) can be set up so as to make the rolling motion of the cutting tool the primary motion. In this particular case of special-purpose gear cutting tool design, a minor motion can be the most beneficial. For example, consider a worm-type cutting tool having the continuous helix-spiral cutting edge (HS-cutting edge). This design of gear cutting tool is intended for the finishing of involute gears.

Figure 18.6 depicts an example of a worm-type cutting tool for finishing an involute gear [55, 62, 205–207]. In that case, the gear cutting tool features a zero-normal profile angle ($\phi_n = 0°$). When the normal profile angle is of zero value, then the generating surface T reduces to a helix located within the cylinder of outer diameter $d_{o.c}$. The helix serves as the cutting edge CE of the gear finishing tool.

The rake surface R_s is in the form of a screw surface through the helix CE. It forms the rake angle γ perpendicular to the work gear tooth flank. No restrictions are imposed on the actual value of the rake angle γ. Therefore, it can easily be set to optimal value.

The clearance surface C_s is also a screw surface through the helix CE. It forms the clearance angle α with the cut surface. Again, no restrictions are imposed on the actual value of the clearance angle α; thus, it can be easily set to optimal value.

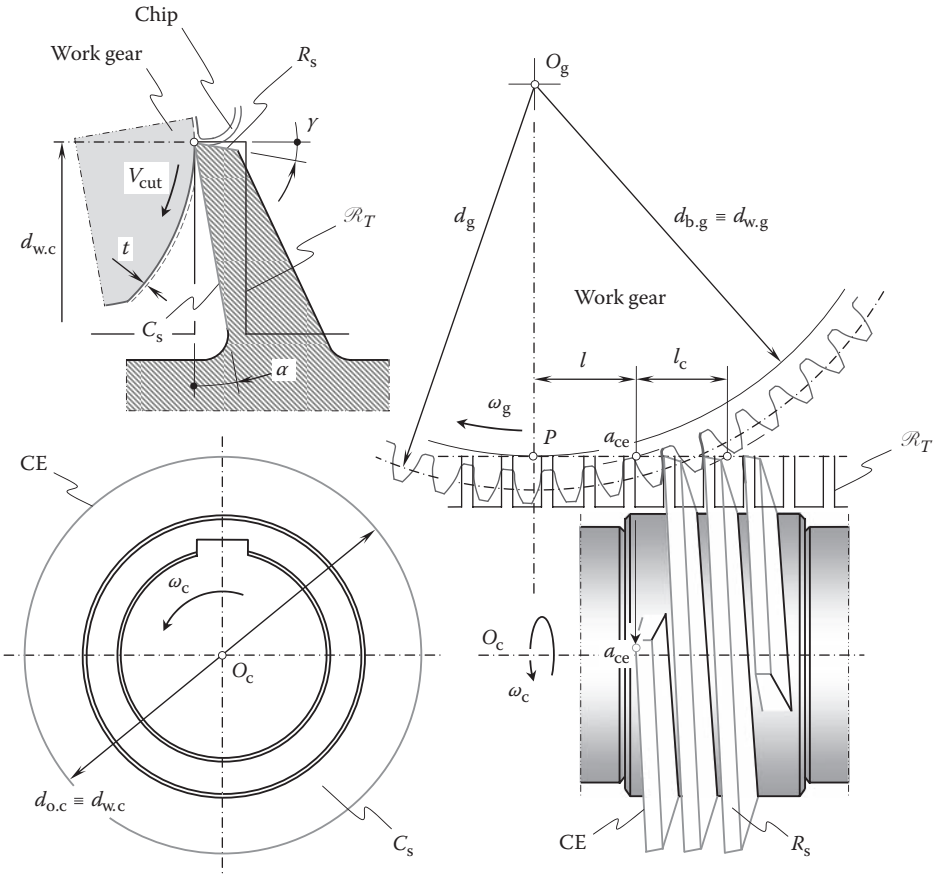

FIGURE 18.6
A worm-type finishing gear cutting tool having the continuous HS-cutting edge.

The inclination angle λ is large. In this case, the actual value of the inclination angle λ strongly depends upon the number of starts of the gear finishing tool. The greater the number of starts, the more reasonable the value of the inclination angle λ, and vice versa.

When machining a work gear, the gear finishing tool is set up so that the line of action is aligned with the top land of the auxiliary generating rack $\mathscr{R}_T$. Consequently, the pitch diameter of the gear finishing tool is equal to its outer diameter $d_{o.c}$.

Generation of the work gear tooth flank begins at a start point a_{ce}. The start point a_{ce} is a certain distance l from the pitch point P. In Figure 18.6, the length of the active portion of the line of action is denoted as l_c. After the design parameters of the work gear are known, then the length of both straight line segments l and l_c can be computed from Figure 18.6.

When finishing, the work gear is rotated (ω_g) about its axis O_g. The gear finishing tool is rotated (ω_c) about its axis O_c. Both rotations are synchronized with each other. Either the work gear or the gear finishing tool is feeding in the axial direction of the work gear. (This motion is not shown in Figure 18.6.) The rolling motion of the gear finishing tool in relation to the work gear is used as the cutting-speed motion V_{cut}. The use of a multistart gear finishing tool is preferable from this standpoint. The reasonable value of stock t can be cut from the work gear tooth flank in one tool path. The chip flows away from the work gear over the rake surface R_s of the gear finishing tool.

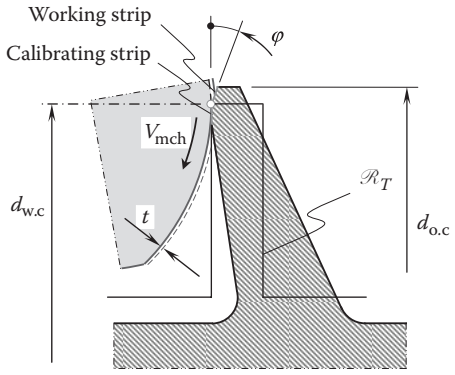

FIGURE 18.7
Schematic of interaction of tooth flank of the work gear with the threads of the worm-type finishing tool for reinforcement of an involute gear. (From Radzevich, S.P., USSR Patent 829280, Int. Cl. B21h 5/00, May 5, 1978.)

High accuracy of the finished gears can be easily achieved due to peculiarities of design of the gear finishing tool. No profile errors are inherent because of profiling of the cutting tool. Sharpening the gear finishing tool does not affect its accuracy; the accuracy of the gear finishing tool remains constant regardless of how many times the tool has been sharpened. The total tool life of the gear finishing tool can be significantly extended because of the theoretically unlimited sharpening allowed. Additionally, the gear finishing tool is easily produced.

Applications of the gear finishing tool (see Figure 18.6) are limited to those involving involute gears with large tooth counts. Only work gears having base diameter $d_{b.g}$ or smaller compared to the form diameter $d_{l.g}$ can be finished with the gear finishing tool ($d_{b.g} < d_{l.g}$). The greater the difference between the diameters $d_{b.g}$ and $d_{l.g}$, the better the conditions for use of the gear finishing tool. This means that work gears having large tooth counts are preferable for finishing with the gear finishing tool.

The continuous HS-cutting edge of the gear finishing tool is in constant contact with the work gear tooth flank at a distinct point. In a rolling motion, this point generates the tooth profile of the work gear. This schematic makes possible the finishing of both external and internal gears with the same gear finishing tool with no changes to the design parameters of the gear finishing tool. In transverse cross section of the work gear by a plane tooth profile is generated by a point—specifically, the point of intersection of the cutting edge with the traverse cross section. The gear finishing tool is capable of finishing only one side of the work gear tooth profile. For finishing the opposite side of the tooth profile, the work gear must be inverted.

The concept of the worm-type gear finishing tool can be traced back to 1978, when a design of a worm-type finishing tool for reinforcement of involute gears was proposed [111]. Gear finishing tools of this design feature a working strip and a calibrating strip as shown in Figure 18.7. The gear finishing tool works in much the same way as other worm-type gear finishing tools (see Figure 18.6). The rolling motion of the gear tool contributes primarily to the machining speed V_{mch}. The working strip deforms the stock while the calibrating strip finishes the work gear tooth flank to the required size. This concept is widely

used in numerous designs of gear finishing tools for the reinforcement of tooth flanks of involute gears [56, 80, 104, 111, 165, 208–219].

In summary, gear finishing tools (see Figure 18.7) can be used for the reinforcement of tooth flanks of work gears having large tooth numbers (the requirement $d_{b.g} < d_{l.g}$ must be fulfilled). The use of multistart gear finishing tools is preferable. These tools are simple to manufacture and a high degree of accuracy in the work gear tooth flank can be achieved with them.

18.5 Cutting Tools for Scudding Gears

The gear scudding process is a continuous cutting operation.* The kinematics of this method of gear machining is based on the vector diagram shown in Figure 15.1a. Two rotation vectors—rotation vector $\boldsymbol{\omega}_g$ of the work gear and rotation vector $\boldsymbol{\omega}_c$ of the gear scudding tool—are at a certain center distance $C_{g/c}$ from each other. The rotation vectors are crossing at a crossed-axis angle $\Sigma = \angle(\boldsymbol{\omega}_g, \boldsymbol{\omega}_c)$. These two rotation vectors are the principal motion vectors in the gear scudding process. Thus, the scudding process has many similarities with processes such as gear hobbing, gear shaving, etc.

18.5.1 Essentials of the Gear Scudding Process

In the scudding of external gears (see Figure 18.8), the cutter feeds directly along the workpiece axis as the cutter and workpiece spin in a synchronized fashion. The feed $\mathbf{F}_{ag}$ is directed parallel to the axis O_g of the work gear. Cutting speed V_{cut} is created due to the axes O_g and O_c of the work gear and the cutter crossing at a certain angle $\bar{\Sigma}$. (The corresponding rotation vectors $\boldsymbol{\omega}_g$ and $\boldsymbol{\omega}_c$ are crossing at angle $\Sigma = 180° - \bar{\Sigma}$.) Profiling of gear scudding tools was investigated by Tsvis [192].

A gear cutting tool of a design similar to a helical shaper cutter is used in scudding. A gear scudding tool can be interpreted as a multistart hob having the same number of starts as the cutter has teeth. In other words, the gear scudding tool has only one cutting tooth at every start. Therefore, cutting tools for scudding can be designed in the same way the multistart gear hobs are designed. However, such an approach to determining the design parameters of the gear scudding tool is applicable only when gears of very low accuracy are to be machined.

18.5.2 A Design Concept of a Precision Cutting Tool for the Gear Scudding Process

The generating surface of a precision gear scudding tool must be determined using an auxiliary generating rack $\mathscr{R}_T$ of the enveloping type as shown in Figure 15.20b. Moreover, the auxiliary rack $\mathscr{R}_T$ must be congruent to the work gear ($R_{w.g} \equiv R_{w.\mathscr{R}}$) similar to that of the gear hob in Figure 16.94. This methodology allows for the determination of the design parameters of the gear scudding tool.

* The technology itself is a current slant on an older hard-gear finishing process developed in Germany called *walzschaelan*, (translated as "hob-peeling"). The elements of hob-peeling are now being used in a different manner, providing the current green process called *scudding*.

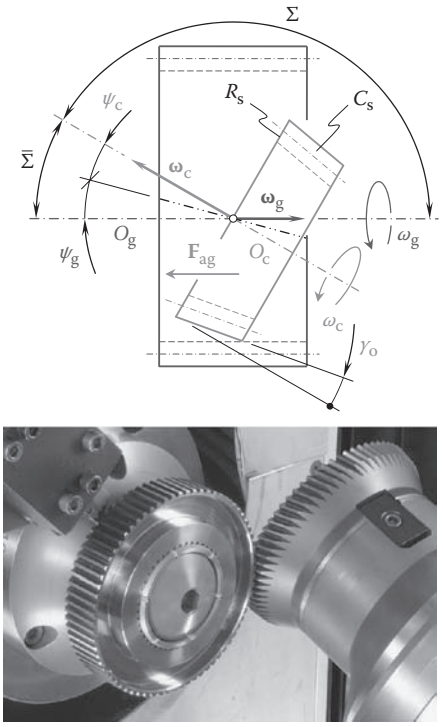

FIGURE 18.8
Schematic of the gear scudding process. (Image courtesy of American Wera, Inc.)

As the auxiliary generating rack $\mathscr{R}_T$ of the gear scudding tool must be congruent to the work gear, the equation of the tooth flank of the involute gear [see Equation (1.3)] is valid for the analytical description of the tooth flank of the auxiliary surface $\mathscr{R}_T$. Therefore, the equation $\mathbf{r}_{\mathscr{R}} = \mathbf{r}_{\mathscr{R}}(U_{\mathscr{R}}, V_{\mathscr{R}})$ of the auxiliary-rack tooth flank is known. This equation is represented in a reference system $X_{\mathscr{R}}Y_{\mathscr{R}}Z_{\mathscr{R}}$ associated with the generating rack $\mathscr{R}_T$. The position vector of a point $\mathbf{r}_{\mathscr{R}}$ of the auxiliary surface $\mathscr{R}_T$ is required to be represented in a reference system $X_cY_cZ_c$ associated with the gear scudding tool. For this purpose, an operator $\mathbf{Rs}\,(\mathscr{R} \mapsto \mathrm{c})$ of the resultant coordinate-system transformation is employed. Ultimately, the following expression

$$\mathbf{r}_{\mathscr{R}}^{(c)} = \mathbf{Rs}\,(\mathscr{R} \mapsto \mathrm{c}) \cdot \mathbf{r}_{\mathscr{R}}(U_{\mathscr{R}}, V_{\mathscr{R}}) \tag{18.1}$$

can be derived for the position vector of a point $\mathbf{r}_{\mathscr{R}}^{(c)}$ of the auxiliary surface $\mathscr{R}_T$ in the coordinate system $X_cY_cZ_c$. The expression for the position vector of a point $\mathbf{r}_{\mathscr{R}}^{(c)}$ of the auxiliary surface $\mathscr{R}_T$ can be finally represented in the form $\mathbf{r}_{\mathscr{R}}^{(c)} = \mathbf{r}_{\mathscr{R}}^{(c)}(U_{\mathscr{R}}, V_{\mathscr{R}}, \varphi_{sc})$. In this expression, φ_{sc} denotes the enveloping parameter because the operator $\mathbf{Rs}\,(\mathscr{R} \mapsto \mathrm{c})$ of the coordinate system transformation is a function of angle φ_{sc}.

Equation (18.1) is considered together with the equation of contact

$$\begin{cases} \mathbf{r}_{\mathscr{R}}^{(c)} = \mathbf{r}_{\mathscr{R}}^{(c)}(U_{\mathscr{R}}, V_{\mathscr{R}}, \varphi_{sc}) \\ \mathbf{n}_{\mathscr{R}} \cdot \mathbf{V}_{\Sigma} = 0 \end{cases} \tag{18.2}$$

where $\mathbf{n}_{\mathscr{R}}$ is the unit-normal vector to the auxiliary generating surface $\mathscr{R}_T$, and $\mathbf{V}_\Sigma$ is the vector of the resultant motion of the generating rack $\mathscr{R}_T$ relative to the coordinate system $X_cY_cZ_c$.

After the enveloping parameter φ_{sc} has been eliminated, the set of Equation (18.2) casts into an expression

$$\mathbf{r}_T = \mathbf{r}_T(U_{\mathscr{R}}, V_{\mathscr{R}}) \tag{18.3}$$

for the position vector of a point $\mathbf{r}_T$ of the generating surface T of the gear cudding tool.

A precision gear scudding tool is a special-purpose gear cutting tool. It is designed for machining a particular work gear. Any alteration to the design parameters of the work gear tooth unavoidably entails alteration to the corresponding design parameters of the gear scudding tool.

18.5.3 Applications of the Gear Scudding Process

The scudding process can be used for a wide range of gear applications, including involute gears like sprocket or ring gears, or on non-involute or non-symmetrical gears, like belt pulleys or straight synchronic gears. It can also hard-finish internal gears with a carbide cutter.

Spur gears ($\psi_g = 0°$), as well as helical gears ($\psi_g \neq 0°$), can be machined with a gear scudding tool. For machining spur gears, cutters with helical teeth ($\psi_c \neq 0°$) are used. Helical work gears can also be machined with gear scudding cutters with straight teeth ($\psi_c = 0°$).

Gear scudding requires the tooth number of the work gear be in the range of $N_g = 80 \ldots 100$ or higher. Scudding of gears having lower tooth numbers cannot be performed on machine tools currently available on the market.

All cutting teeth of the gear scudding tool are loaded evenly. Consequently, the teeth wear evenly. Additionally, the design of the gear scudding tool allows the use of economical high-speed steel and other cutting materials. The gear scudding process can cut a gear in nearly the same time as the hobbing process [23].

18.6 A Shaper Cutter with a Tilted Axis of Rotation for Shaping Cylindrical Gears

The rotation of the cutting tool is the primary motion by which the cutting speed is created in most gear cutting tools. It is not, however, the only type of motion by which the cutting motion can be created; a straight motion of the cutting tool can also be used.

18.6.1 The Kinematics of Shaping a Helical Gear with the Straight-Tooth Shaper Cutter

Consider the kinematics of the gear cutting process, which is based on the vector diagram shown in Figure 15.1a, featuring a straight cutting motion.

Assume that the cutting speed vector $\mathbf{V}_{cut}$ is at a certain angle ϑ_c relative to the rotation vector $\boldsymbol{\omega}_g$ of the work gear. Machining of the work gear is possible if this angle is equal to the pitch helix angle ψ_g of the work gear ($\vartheta_c \cong \psi_g$). Reasonable deviations of the angle

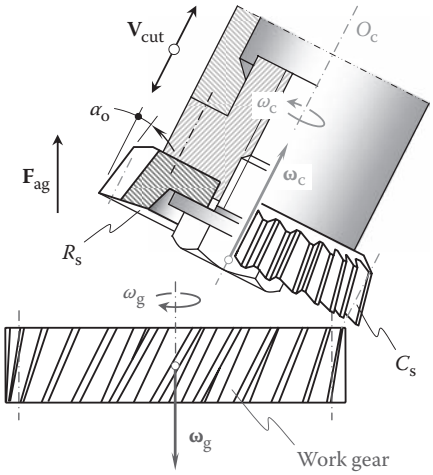

FIGURE 18.9
Schematic of a method of shaping of a cylindrical gear. (From Radzevich, S.P., USSR Patent 1504903, Int. Cl. B23f 5/12, Dec. 2, 1987.)

ϑ_c from the angle ψ_g are permitted in both directions ($\vartheta_c = \psi_g \pm \Delta\vartheta_c$, where reasonable deviation of the angle ϑ_c from the angle ψ_g is designated as $\Delta\vartheta_c$). In the scenario shown in Figure 15.1, a vector diagram of the gear machining operation should be complemented with the cutting speed vector $\mathbf{V}_{cut}$. The vector $\mathbf{V}_{cut}$ makes the angle ϑ_c with axis O_g of the work gear. Ultimately, the kinematics of the gear machining process appears as shown in Figure 18.9. The work gear is fed $\mathbf{F}_{ag}$ in its axial direction. When the pitch helix angle ψ_g of the work gear and the face width of the work gear are reasonably small, the feed motion $\mathbf{F}_{ag}$ could be unimportant.

18.6.2 Principal Elements of Design of the Gear Cutting Tool

The relative motions of the work gear and the reference system in which the gear cutting tool will be represented can be broken down into their elementary components in various ways. One method is to deconstruct the relative motion so that the auxiliary generating surface is shaped in the form of the rack $\mathscr{R}_T$ conjugate to the work gear. The pitch plane of the auxiliary rack $\mathscr{R}_T$ is parallel to the axis of rotation of the gear cutting tool [143].

The auxiliary rack $\mathscr{R}_T$ can then be rolled with no sliding over the pitch cylinder of the gear cutting tool. Under such a scenario, the generating surface of the gear cutting tool T is shaped into a form identical to the generating surface of the standard gear shaper cutter. This means that a standard gear shaper cutter with straight teeth can be used for machining helical gears [143]. Such a possibility is schematically illustrated in Figure 18.9.

18.6.3 A Possible Application for the Gear Shaper Cutter with a Tilted Axis of Rotation

The concept of machining helical gears using a straight-tooth shaper cutter was developed with the goal of equalizing the clearance angles at lateral cutting edges on opposite sides

of the tooth profile of the shaper cutter [89]. In this method of gear cutting, the work gear and the shaper cutter rotate about their axes O_g and O_c (see Figure 18.9) with certain angular velocities ω_g and ω_c [89]. The rotations ω_g and ω_c are synchronized in a timely manner. The shaper-cutter axis O_c is inclined and makes the clearance angle α_o with the axis of the work gear O_g. Inclination of the axis O_c on $\xi_c = 1 \ldots 3°$ equalizes the clearance angle on the opposite flanks of the shaper-cutter tooth. Such an inclination increases the tool life of the shaper cutter. Eventually this concept can be enhanced to include the cutting of helical gears with a shaper cutter that has straight teeth, and features a tilted axis of rotation.

Because the method of shaping helical gears with a straight-teeth shaper cutter (see Figure 18.9) requires a machine tool of special design, use of the method eliminates the necessity of two elements that are critical when cutting helical gears. Neither a helical guide nor a specially designed shaper cutter is necessary for the shaping of helical gears. Additionally, no constraints are imposed on the value of the pitch helix angle. The actual value of the pitch helix angle of the work gear can be assigned any desired (optimal) value [143].

18.7 A Gear Cutting Tool for Machining a Worm in the Continuously Indexing Method

The vector diagram of the gear machining mesh (see Figure 15.1) can be utilized for the purpose of cutting worms. Worms can be cut with the generating form cutters as is shown in Figure 18.10a. The use of generating form tools for cutting worms is particularly advantageous when a long worm is required to be cut in only one path of the cutting tool in relation to the work.

In machining a worm, the work is rotated about its axis O_g with a rotation ω_g, as shown in Figure 18.10a. The generating form cutter is rotating about its axis O_c with the rotation ω_c. Additionally, the cutter is fed $\mathbf{F}_c$ in the axial direction of the work.

The axes O_g and O_c of the rotations ω_g and ω_c are either crossing at a right angle, as shown in Figure 18.10b, or they are crossing at a certain angle (see Figure 18.10c) that is equal, or at least approximately equal, to the helix angle of the worm to be machined.

All of the motions—specifically, the rotation of the work ω_g, the rotation of the cutter ω_c, and the feed rate motion $\mathbf{F}_c$—are synchronized with each other. When the number of starts of the work is denoted as N_g, and the number of teeth of the cutter is designated as N_c, then the rotation of the cutter ω_c^g can be expressed in terms of tooth numbers N_g and N_c, as well as in terms of the rotation of the work, ω_g, by the expression

$$\boldsymbol{\omega}_c^g = \boldsymbol{\omega}_g \frac{N_g}{N_c} \tag{18.4}$$

When the cutter is travelling in the axial direction of the worm with the feed rate $F_c = |\mathbf{F}_c|$, then the cutter should rotate with the rotation ω_c^f that is equal to

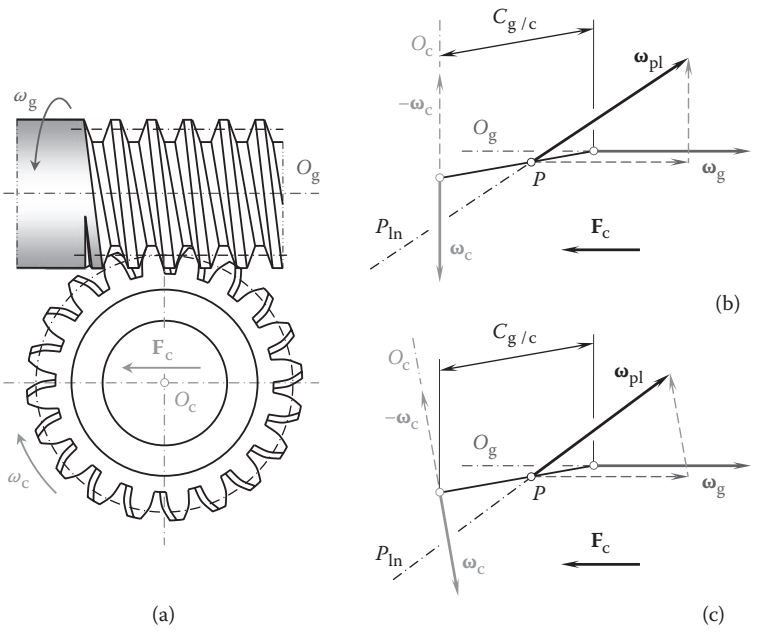

FIGURE 18.10
Schematic and the principal kinematics of a method of cutting of a worm.

$$\omega_c^f = \frac{2F_c}{d_{w.c}}, \tag{18.5}$$

where $d_{w.c}$ denotes pitch diameter of the cutter. The resultant rotation of the cutter, ω_c, can be computed from

$$\omega_c = \omega_g \frac{N_g}{N_c} \pm \frac{2F_c}{d_{w.c}} \cdot \tag{18.6}$$

The choice of sign in Equation (18.6) depends upon two parameters: the direction of the hand of the worm to be cut, and the direction of the feed rate motion $\mathbf{F}_c$. Both single-start and multistart worms, as well as round racks, can be cut in just one path of the cutter regardless of the pitch of the work. A round rack can be interpreted here as a worm having a zero number of starts. The cutting tool and the method of machining are especially efficient when machining long, coarse pitch worms.

18.8 Rack Shaving Cutters

The shaving of gears is commonly performed with a disk-type shaving cutter. The productivity rate of a gear shaving operation depends upon the rate of conformity of the generating surface of the shaving cutter to the tooth flank of the work gear. The higher the

rate of conformity of the surface T to the surface $\mathcal{G}$, the higher the productivity of the gear shaving process and the higher the accuracy of the finished gears.

Examination of Equation (17.63) reveals that the rate of conformity of the generating surface of a gear cutting tool to the tooth surface of the work gear increases as the pitch diameter of the shaving cutter increases. In a gear shaving process, the rate of conformity of the surface T to the surface $\mathcal{G}$ strongly depends upon the tooth number of the shaving cutter.

Assume that the tooth number of a disk-type shaving cutter approaches infinity. Then, the disk-type shaving cutter would transform into a rack-type shaving cutter. If an increase of the productivity rate of a gear shaving process is desired, then a rack shaving cutter is of particular interest: it has the greatest possible number of teeth. External spur and helical gears can be shaved by the rack shaving cutter.

18.8.1 Rack-Type Shaving Cutter

A rack-type shaving cutter can be interpreted as a rack that is conjugate to the work gear. The lateral tooth surfaces of the rack are serrated. The rack-type shaving cutter is assembled from a certain number of teeth that are mounted in the shaving-cutter body. The serration width is equal to 0.8 … 1.0 mm, the serration depth is ~1.0 mm, and the serration pitch is 1.6 … 2.0 mm.

The rack must have a length and stroke longer than the work gear circumference. The length, L_c, of the rack-type shaving cutter is computed from

$$L_c = \frac{\pi m}{\cos \psi_c}(N_g + 2), \tag{18.7}$$

where m represents the module, ψ_c is the pitch helix angle of the shaving cutter, and N_g is the tooth number of the work gear. The length of the shaving cutter that is computed from Equation (18.7) is sufficient for finishing all of the teeth of the work gear.

The rack must be wider that the gear face width. In practice, the face width of the rack-type shaving cutter exceeds the face width of the work gear by three to four times. Therefore, different areas of the shaving-cutter teeth can be involved in the gear finishing process. This extends tool life between re-grindings of the shaving cutter. It is worth noting that rack-type shaving cutters were proposed before disk-type shaving cutters were proposed.

18.8.2 Kinematics of the Rack Shaving Process

In the rack shaving process, the work gear is mounted on the arbor and is free to rotate about its axis O_g (see Figure 18.11). The shaving cutter is mounted on the worktable of the shaving machine. It is engaged in mesh with the work gear. The worktable and the shaving cutter are reciprocated at a certain speed, $\pm V_c$. The work gear is fed up, toward the work gear, after reciprocation of the worktable is complete. The feed of the shaving cutter is in the range of 0.025 … 0.080 mm per reciprocation. Spur gears are shaved with a shaving cutter having helical (inclined) teeth. The straight-tooth shaving cutter can be used for finishing helical gears.

Vector $\mathbf{V}_c$ of the translation motion of the shaving cutter, and rotation vector $\boldsymbol{\omega}_g$, are at a certain angle $\overline{\Sigma}$ to each other. This angle differs from the right angle ($\overline{\Sigma} \neq 90°$). When spur

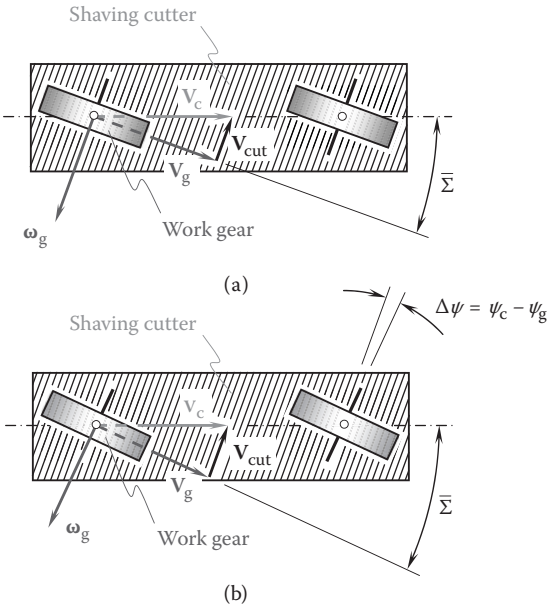

FIGURE 18.11
Schematic of the rack shaving of a gear.

gears are shaved (see Figure 18.11a), the angle $\bar{\Sigma}$ is in the range $\bar{\Sigma} = 20 \ldots 25$. For the shaving of helical gears (Figure 18.11b), the work gear pitch helix angle should be taken into account.

Due to rotation of the work gear, the linear speed of the rotation is observed. This speed is designated as $V_g = |\mathbf{V}_g| = 0.5 d_g \boldsymbol{\omega}_g$. The speed of cut is equal to the difference $\mathbf{V}_{cut} = \mathbf{V}_c - \mathbf{V}_g$. The speed-of-the-cut vector $\mathbf{V}_{cut}$ is always within the tooth flank of the rack-type shaving cutter. The vector diagram of the rack shaving process is illustrated in Figure 18.12. As the work rolls with the reciprocating rack, it is also moved across a portion of the rack so as to equalize wear of the rack. After each stroke of the rack, the gear is fed in a slight amount.

This method of shaving does not lend itself to shaving large parts because the racks used are expensive. The rack shaving process is very rapid, and a large number of parts are obtained per sharpening of the rack. The use of rack shaving is economical in high-production jobs. Rack-type shaving cutters have limited applications in current industry, mostly because of difficulties in their manufacturing and application.

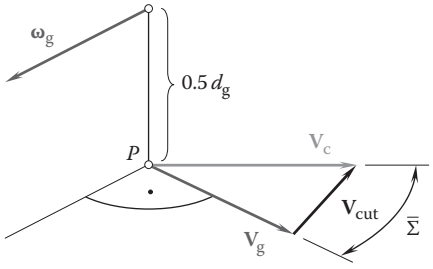

FIGURE 18.12
Vector diagram of the rack shaving process.

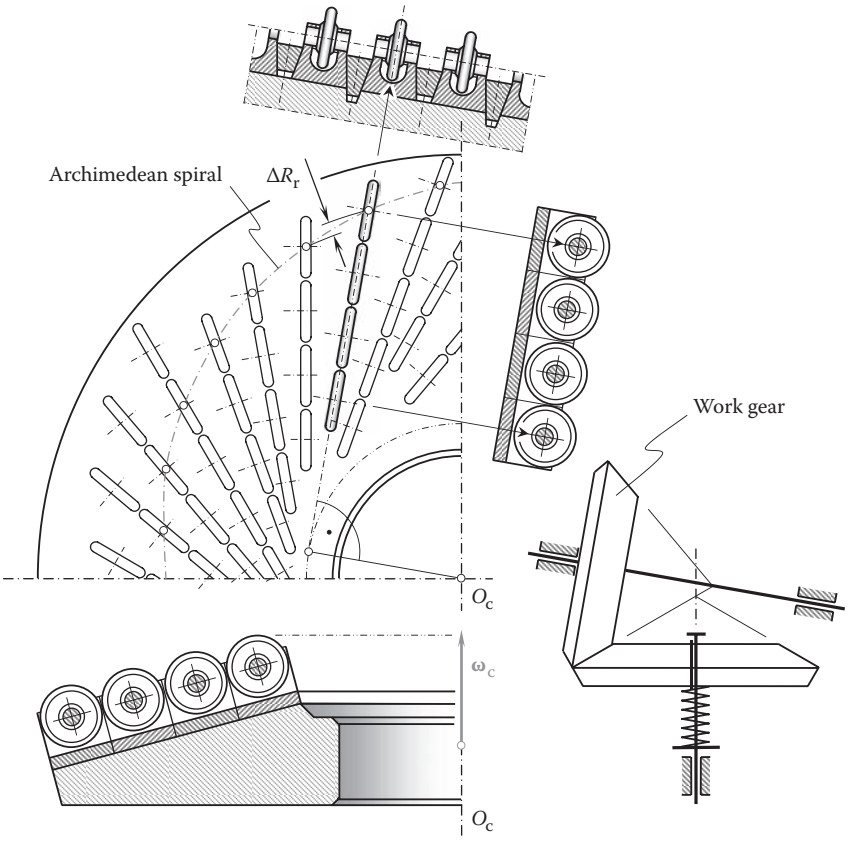

FIGURE 18.13
A tool for reinforcement of conical gears by surface plastic deformation. (From Radzevich, S.P., USSR Patent 846024, Int. Cl. B21h 5/04, Nov. 15, 1978; Radzevich, S.P., USSR Patent 1094659, Int. Cl. B21h 5/04, March 11, 1983; Radzevich, S.P., USSR Patent 1107943, Int. Cl. B21h 5/04, Filed: Feb. 24, 1983.)

It can be shown that there are no physical restrictions on application of the vector diagram (see Figure 18.12) in the inverse manner, such as when the work is reciprocated, while the cutting tool is rotated. Such a schematic corresponds, for example, to the shaving of a rack with a disk-type shaving cutter. With regard to the shaving process, the inverse application of the vector diagram (see Figure 18.12) is only of theoretical importance.

18.9 A Tool for Gear Reinforcement by Surface Plastic Deformation

The sliding motion that is inherent to two rotations about two crossing axes is used for the purpose of designing a tool for reinforcement of gears by plastic deformation. Figure 18.13 shows an example of a finishing tool designed for the reinforcement of fillets—either of bevel gears or of conical gears with skewed teeth [106]. When a tool of this design is used, the work gear and the gear finishing tool are rotated in tight mesh about their axes.

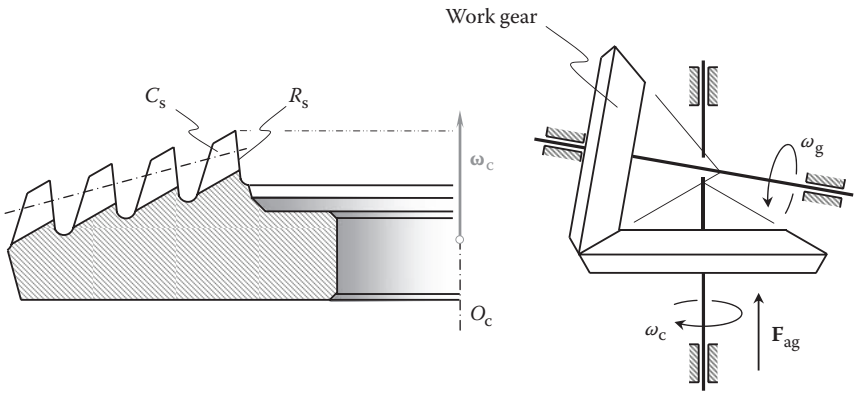

FIGURE 18.14
A tool for cutting a conical gear.

Free-rotating rollers are assembled along the teeth of the generating surface T of the tool. Because of tooth sliding, the rollers roll over the fillet surfaces and deform thin layers of the surface plastic work gear. Every set of rollers is shifted at a distance ΔR_r in the lengthwise direction of the teeth of the generating surface T to overlap traces of the rollers. After having been shifted, the centers of the adjacent rollers are located within an Archimedean spiral curve. No feed motion of the cutting tool is required when using the tool for reinforcement of conical gears by surface plastic deformation. Because lack of space for the rollers is an issue, finding the tooth number for the gear tool (see Figure 18.13) is of critical importance. A few designs of gear finishing tools employ this concept as well [18, 25, 107, 108, 180, 181 and others].

The sliding motion of the tooth flanks of the work gear and the cutting tool can be used for cutting bevel and conical gears, preferably with skewed teeth. This concept of the gear cutting tool is schematically illustrated in Figure 18.14.

Gear cutting tools of this design have not yet been comprehensively investigated. Depending upon the sign and magnitude of the helix of the work gear and the sign and magnitude of the helix of the gear cutting tool, the rake surface R_s of the gear cutting tool is faced either toward axis O_c of the cutter (as shown in Figure 18.14), or in the opposite direction. The direction and magnitude of offset of the work gear teeth, and the direction and magnitude of offset of the cutting-tool teeth can be used instead of the signs and magnitudes of the helices.

18.10 Conical Hob for the Palloid Method of Gear Cutting

A conical hob is used for machining conical gears with spiral teeth. The tooth profile of the machined conical gear is shaped in the form of an involute curve. The lengthwise direction of the gear tooth is also shaped in the form of an involute curve. The angle of the spiral

of the work gear teeth is determined through the selection of the base circle of this second involute curve. A conical hob for the palloid method of gear cutting is an approximate type of gear cutting tool.

18.10.1 Preamble

In most cases, the problem of gear cutting tool design begins with the specification of the tooth flank of the work gear. The generating surface of the gear cutting tool to be designed is determined by the tooth flank of the work gear and of the parameters of the kinematics of the gear machining process. This allows for interpretation of the generating surface of the gear cutting tool as a function of the tooth flank of the work gear and the kinematics of the gear machining operation.

In the palloid method of gear cutting,* a conical hob is given instead of the work gear. The hob is designed independently from the gear to be machined. Afterwards, a gear is cut by the hob and this cut gear is tested and a decision made about whether or not the machined gear satisfies the performance requirements. If it does, the hob is then used for machining gears. If not, certain changes are introduced to the design parameters of the hob and a new gear is cut with a redesigned hob with different design parameters. Ultimately, after several runs, an appropriate set of design parameter for the conical hob can be derived. Therefore, not-generating surface T of the conical hob is determined as a function of the desired work gear tooth flank, but a reasonable tooth flank of the work gear is determined as a function of generating surface T of the conical hob having practical values of it design parameters.

Approximate conical hobs are used primarily for two reasons. First, the desired geometry of the tooth flank of the work gear is complex in nature or not yet known. The generating surface of the conical hob cannot be determined until the tooth-flank geometry is determined. Second, the approximation makes possible the manufacture of conical hobs of the specifically required design.

18.10.2 Design of the Conical Hob

A conical hob is illustrated in Figure 18.15 with a 60° included cone angle θ_c for the basic pitch surface. A handed pair of hobs is needed to cut a pair of gears. The number of gashes is in the range of 8–10. The clearance angle at the top cutting edge is $\alpha_o = 4–6°$ at the hob end having bigger outer diameter, and is $\alpha_o = 15–17°$ at the hob end having a smaller outer diameter. The pitch helix angle ψ_c varies within the face width of the hob. The maximum value of the pitch helix angle $\psi_c = \psi_c^{max}$ is observed at the hob end having a smaller pitch diameter. The minimum value of the pitch helix angle $\psi_c = \psi_c^{min}$ is observed at the opposite end of the hob. The variation of the pitch helix angle is due to the difference between pitch diameters at both ends of the hob. The core design parameters of the conical hob (see Figure 18.15) are similar to those of the conical hob for machining spur and helical gears (see Figure 16.88).

Hob design and manufacture are difficult and costly, which detracts from the usefulness of the system. Owing to the continuous change in the lead angle from one end of the hob to the other with a changing diameter, a conical end-type grinding wheel is used to grind

* The palloid method of gear hobbing was patented by the engineers Schlicht and Preis in the 1920s. This invention was based on application of a conical hob. Use of the palloid method makes it possible to machine a work gear having nearly uniform tooth height along the face-width.

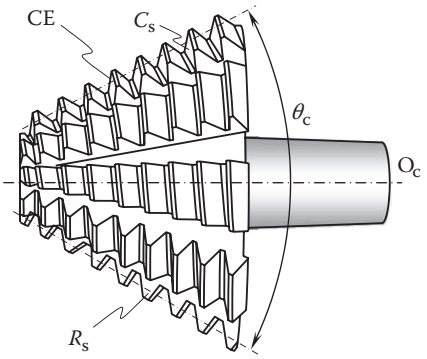

FIGURE 18.15
Klingelnberg spiral bevel hob.

the hob tooth flanks. The use of an end-type grinding wheel is always more difficult than using a disk grinding wheel.

18.10.3 Kinematics of the Palloid Gear Hobbing Process

When machining a conical gear with spiral teeth (see Figure 18.16), the work gear is rotated about its axis O_g. Rotation of the work gear is designated as ω_g. The conical hob with pitch-cone angle θ_c is rotated about its axis O_c. The axes O_g and O_c are a certain center distance $C_{g/c}$ apart from each other (see Figure 18.17), and cross at the crossed-axis angle $\overline{\Sigma}$. The crossing angle $\overline{\Sigma}$ is $\overline{\Sigma} = 180 - \Sigma$, where Σ denotes the crossing angle between the rotation vectors $\boldsymbol{\omega}_g$ and $\boldsymbol{\omega}_c$.

The pitch plane of the auxiliary generating surface $\mathscr{R}_T$ is perpendicular to the straight line that is aligned to the closest distance of approach of the axes O_g and O_c. The generating

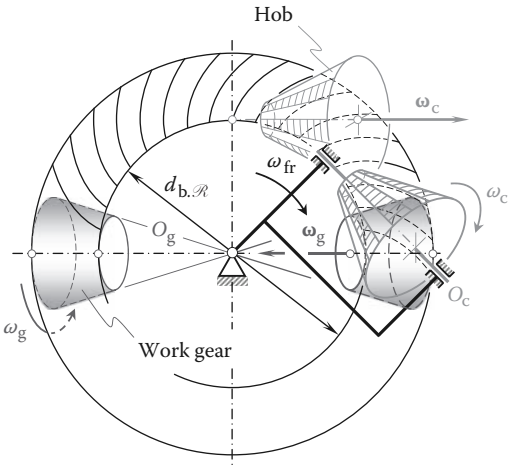

FIGURE 18.16
Schematic of the palloid method of hobbing of a conical gear with spiral teeth.

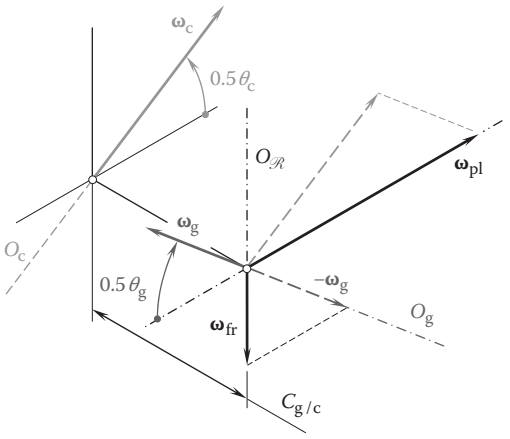

FIGURE 18.17
Vector diagram of the palloid method of hobbing of a conical gear with spiral teeth.

rack $\mathscr{R}_T$ is rotated about the axis $O_{\mathscr{R}}$ through the apex of the pitch cone of the work gear, and it is perpendicular to the pitch plane of the surface $\mathscr{R}_T$.

In addition to the rotations ω_g and ω_c, the hob is rotated about the axis $O_{\mathscr{R}}$. This rotation ω_{fr} is the feeding motion of the hob. The hobbing feed motion is a supplementary rotary movement of the imaginary crown wheel. Ultimately, the resultant motion of the hob relative to the work gear is a kind of planetary (epicyclical) motion that is composed of three rotations: ω_g, ω_c, and ω_{fr}.

Cutting starts at the large end of the hob and finishes at the small end; as generation proceeds, the rotational speed of the hob is progressively increased to provide a more nearly equal peripheral speed for the hob teeth making the finishing cuts. This is achieved due to the rotation vectors $\boldsymbol{\omega}_g$, $\boldsymbol{\omega}_c$, and $\boldsymbol{\omega}_{fr}$ (see Figure 18.17) being synchronized with each other. Because of the tiny slots available for the hob to pass on the small diameter, only very small chip removal magnitudes are achieved.

The tooth profile of the work gear is of involute form in the transverse plane and this is achieved by planetary feeding of the hob around the $O_{\mathscr{R}}$ axis. Indexing is continuous as the work gear and hob rotate and cutting is gradual for all teeth until the full depth of the tooth space has been attained. The depth of the tooth space is constant over the whole face width. The tooth profile from top to root of a portion of the work gear face width is generated by the hob. This is somewhat similar to the hobbing of spur and helical gears by means of tangential feeding.

The tooth spirals are of involute form as shown diagrammatically in Figure 18.16. Consequently, the normal pitch of the teeth is constant for all positions across the face width of a work gear. All gears of a given normal pitch can be cut with a pair of standard hobs of the same pitch. When separate roughing and finishing hobs are utilized, the latter should preferably remove about 0.005 in. (0.12 mm) from each flank in a final cut to produce the best surface finish, taken in the same direction of rotation as that of the blank.

Advantages that even today occasionally lead to the application of the palloid method are to be found in the involute tooth trace (insensibility to displacement), the flaky enveloping lines (smooth rolling and oil-pocket effect), and in the fully rounded root region (no grooving effect).

18.10.4 Peculiarities of Design of a Conical Hob for Machining a Work Gear with Crowned Teeth

Originally, all teeth of the conical hob have the same profile. This is due to the generating surface T of the conical hob being generated by the auxiliary generating rack $\mathscr{R}_T$ having a standard tooth profile (see Figure 16.88). However, for the purpose of cutting a conical gear with a crowned tooth flank, the tooth profile of the conical hob is modified.

Commonly, the modification of the conical hob tooth profile results in the tooth thickness of the hob not being a constant value, but instead being alternated within the face width of the hob. Starting from a certain tooth, the tooth thickness grows larger toward both ends of the hob. The thickness of the thinnest tooth is equal to half of the tooth pitch ($0.5\pi m$). This tooth is at a distance of one-third of the face width of the hob end having a smaller diameter, and it is at a distance of two-thirds of the face width of the larger-diameter hob end. As a result, the thickness of the thickest tooth at the small diameter of the hob is equal to $(0.5\pi + 0.01)m$. Correspondingly, the thickness of the thickest tooth at the opposite end of the conical hob is equal to $0.5\pi + 0.02)m$. Here, the conical hob module is designated as m.

The discussed examples clearly illustrate the capabilities of the gear machining mesh shown in Figure 15.1. If explored properly, this vector diagram is capable of returning more novel designs of gear cutting tools and methods for machining gears.

Section V-B: Design of Gear Cutting Tools: Quasi-Planar Gear Machining Mesh

Gear machining meshes, while spatial, can feature a particular combination of the rotation vectors of the work gear and of the gear cutting tool for which the vector of instant rotation is perpendicular either to the rotation vector of the work gear, or to the rotation vector of the gear cutting tool. The component (either the work gear or the gear cutting tool)—the rotation vector of which is perpendicular to the vector of instant rotation—resembles a planar gear machining mesh. For this reason, gear machining meshes that feature the vector of instant rotation perpendicular to one of the rotation vectors (either that of the work gear or of the gear cutting tool) are referred to as *quasi-planar* gear machining meshes.

In a quasi-planar gear machining mesh pitch, the angle of the generating surface of the gear cutting tool reaches 90°. Under such a scenario, the pitch cone transforms to a plane that is rotating about an axis perpendicular to the plane. The greater the pitch cone angle, the higher the rate of conformity of the generating surface of the gear cutting tool to the tooth flank of the work gear. This statement directly follows from Equation (17.63). This is one of many reasons why a generating surface in the form of a bevel gear having a 90° pitch cone angle is attractive in the design of gear cutting tools.

Kinematics of Quasi-Planar Gear Machining Mesh

A quasi-planar gear machining mesh is a particular case of spatial gear machining meshes. Perpendicularity of either (1) the rotation vector $\boldsymbol{\omega}_g$ of the work gear or (2) the rotation vector $\boldsymbol{\omega}_c$ of the generating surface of the gear cutting tool to the vector $\boldsymbol{\omega}_{pl}$ of instant rotation is the major feature of quasi-planar gear machining meshes. In the first case, the equality $\angle(\boldsymbol{\omega}_g , \boldsymbol{\omega}_{pl}) = 90°$ is observed. Similarly, the equality $\angle(\boldsymbol{\omega}_c, \boldsymbol{\omega}_{pl}) = 90°$ is valid in the second case.

Figure V.1 is a sketch of a vector diagram for a quasi-planar gear machining mesh. In the case shown in Figure V.1, the cutting-tool rotation vector $\boldsymbol{\omega}_c$ is perpendicular to the vector $\boldsymbol{\omega}_{pl}$ of instant rotation ($\boldsymbol{\omega}_c \perp \boldsymbol{\omega}_{pl}$). The pitch cone angle of the generating surface of the gear cutting tool is equal to 90°, and thus the pitch cone is transformed to the pitch plane that is rotated about the O_c axis. The axis O_c is aligned to the rotation vector $\boldsymbol{\omega}_c$. In quasi-planar gear machining meshes the pitch cone of the work gear is rolling over the pitch plane of the generating surface of the gear cutting tool.

Similar to the vector diagram in Figure V.1, a vector diagram for a quasi-planar gear machining mesh can be constructed for the case when the work gear rotation vector $\boldsymbol{\omega}_g$ is perpendicular to the vector $\boldsymbol{\omega}_{pl}$ of instant rotation ($\boldsymbol{\omega}_g \perp \boldsymbol{\omega}_{pl}$). The vector of instant rotation $\boldsymbol{\omega}_{pl}$ of the cutting tool with respect to the work gear is given by $\boldsymbol{\omega}_{pl} = \boldsymbol{\omega}_c - \boldsymbol{\omega}_g$. If the instant rotation of the work gear relative to the cutting tool is considered instead of the relative

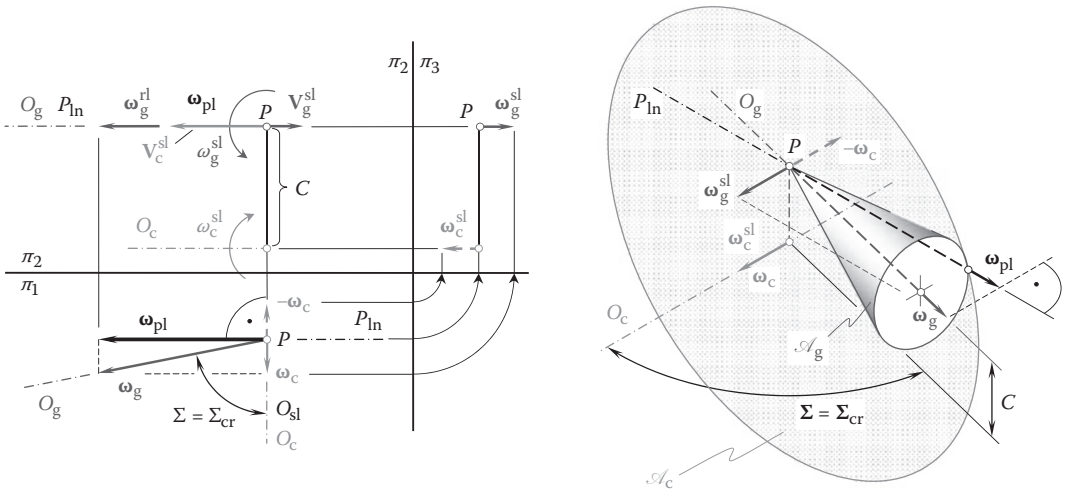

FIGURE V.1
Vector diagram of a quasi-planar gear machining mesh.

rotation of the cutting tool, then the vector of instant rotation is given by $\boldsymbol{\omega}_{pl} = \boldsymbol{\omega}_g - \boldsymbol{\omega}_c$. This equality, along with the known dot product of two vectors, allows for the following expressions that are valid for quasi-planar gear machining meshes:

$$\boldsymbol{\omega}_g \cdot (\boldsymbol{\omega}_g - \boldsymbol{\omega}_c) = 0, \tag{V.1}$$

$$\boldsymbol{\omega}_c \cdot (\boldsymbol{\omega}_c - \boldsymbol{\omega}_g) = 0. \tag{V.2}$$

A gear machining mesh that satisfies either Equation (V.1) or Equation (V.2) can be identified as a quasi-planar spatial mesh and vice versa: all quasi-planar gear machining meshes satisfy either Equation (V.1) or Equation (V.2).

A critical value of the crossed-axis angle Σ corresponds to quasi-planar gear machining mesh ($\Sigma = \Sigma_{cr}$). Within a plane through the closest distance of approach of the axes O_g and O_c, the vector of linear velocity of sliding $\mathbf{V}_g^{sl}$ of the axodes is due exclusively to the component $\boldsymbol{\omega}_g^{sl}$ of the rotation vector $\boldsymbol{\omega}_g$. Irrespective of the component $\boldsymbol{\omega}_c^{sl}$ of the rotation vector, $\boldsymbol{\omega}_c$ is not equal to zero ($\boldsymbol{\omega}_c^{sl} \neq 0$), but the vector of linear velocity of sliding of the axodes $\mathbf{V}_c^{sl}$ is equal to zero ($\mathbf{V}_c^{sl} = 0$). This is because, in the case under consideration, the equality $r_{w.g} = C$ is observed. Therefore, the pitch radius of the generating surface of the cutting tool is zero ($r_{w.c} = 0$). Ultimately, the resulting sliding is given by $V_\Sigma = V_g^{sl}$.

A clear understanding of the vector diagram of quasi-planar gear machining meshes (see Figure V.1) is key to the successful design of gear cutting tools based on this kind of gear machining mesh, as well as to the design of gear cutting tools for machining bevel gears, in particular.

19

Gear Cutting Tools for Machining of Bevel Gears

The sliding of axodes is one of the major features of quasi-planar gear machining meshes. Due to the axodes sliding over one another, the sliding of the tooth flanks of the work gear and of the generating surface of the gear cutting tool in gear machining meshes is unavoidable. The sliding of tooth flanks is similar to that observed in gear-shaving processes. The tooth flank sliding can be employed as the primary (cutting) motion for a gear cutting tool; this is not physically prohibited.

19.1 Design of a Gear Cutting Tool for the Plunge Method of Machining of Bevel Gears

Prior to designing a gear cutting tool, the reader is advised to further study the kinematics of work gear tooth flank generation.

19.1.1 Kinematics

Figure 19.1 is a sketch of the simplest kinematics of generation of a tooth flank of a work gear. The simplest kinematics of the work gear tooth flank generation is composed of just two rotations: a rotation of the work gear, and a rotation of the gear cutting tool. The rotation vector $\boldsymbol{\omega}_g$ of the work gear and the rotation vector $\boldsymbol{\omega}_c$ of generating surface of the gear cutting tool are separated from each other at a center distance $C_{g/c}$, and are crossed at a certain crossed-axis angle Σ. The crossing angle Σ_c of the rotation vector $\boldsymbol{\omega}_c$ and the vector of the instant rotation $\boldsymbol{\omega}_{pl}$ is a right angle. This is because, in a quasi-planar gear machining mesh, the crossed-axis angle Σ is equal to its critical value ($\Sigma = \Sigma_{cr}$).

Rotation of the work gear and of the gear cutting tool about crossing axes O_g and O_c makes it possible to utilize sliding velocity as the velocity of the primary (cutting) motion. No additional motion is required for the generation of a tooth flank of the work gear in this case. For a proper understanding of how the primary motion $\mathbf{V}_{cut}$ is created in the gear machining mesh, the rotation vectors $\boldsymbol{\omega}_g$, $\boldsymbol{\omega}_c$, and $\boldsymbol{\omega}_{pl}$ are projected onto a plane as shown in Figure 19.2. The projection plane is a plane through the pitch point P. It is perpendicular to the closest distance of approach $C_{g/c}$ of the axes O_g and O_c.

At the pitch point P, the linear velocity of a point created by the rotation $\boldsymbol{\omega}_g$ is designated as $\mathbf{V}_g$. The vectors $\boldsymbol{\omega}_g$ and $\mathbf{V}_g$ are perpendicular to each other ($\boldsymbol{\omega}_g \perp \mathbf{V}_g$). Similarly, the linear velocity of a point created by the rotation $\boldsymbol{\omega}_c$ is designated as $\mathbf{V}_c$. Again, the vectors $\boldsymbol{\omega}_c$ and $\mathbf{V}_c$ are perpendicular to each other ($\boldsymbol{\omega}_c \perp \mathbf{V}_c$). Because the rotation axes O_g and O_c are crossed with each other at a certain crossed-axis angle Σ, the vectors $\mathbf{V}_g$ and $\mathbf{V}_c$ make a certain angle. The difference ($\mathbf{V}_c - \mathbf{V}_g$) of the rotations is equal to the vector $\mathbf{V}_{ax}^{sl}$ of axial sliding. When the pitch helix angle of the work gear is equal to ψ_g, then projection of the vector $\mathbf{V}_{ax}^{sl}$ onto the pitch helix through the pitch point P is equal to the speed of sliding of the tooth

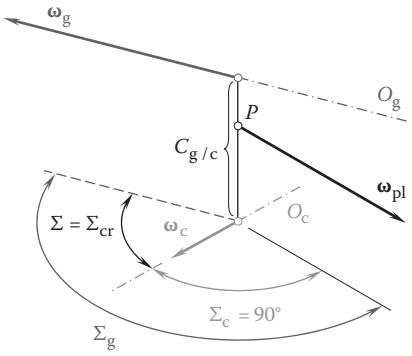

FIGURE 19.1
An example of the quasi-planar gear machining mesh.

flank of the work gear relative to the tooth flank of the cutting tool. The vector $\mathbf{V}_{cut}$ of this component can be used as the vector of primary motion in the gear machining process. For a given work gear, the design parameters (pitch diameter d_g and pitch helix angle ψ_g at P) are of a certain value. They are not allowed to be changed. The crossed-axis angle $\Sigma = \Sigma_{cr}$ also is not allowed to be changed. Therefore, an increase of the sliding velocity requires alteration of design parameters of the gear cutting tool and the gear machining process that will result in an increase of the sliding vector $\boldsymbol{\omega}_g^{sl}$ (see Figure V.1) and increase the distance of the interacting tooth flanks from the pitch point P. This is the only way to control the speed of cut, $\mathbf{V}_{cut}$, in the case under consideration. The greater the sliding vector $\boldsymbol{\omega}_g^{sl}$, and the greater the distance of the interacting tooth flanks from the pitch point P, the greater the speed of cut, $\mathbf{V}_{cut}$.

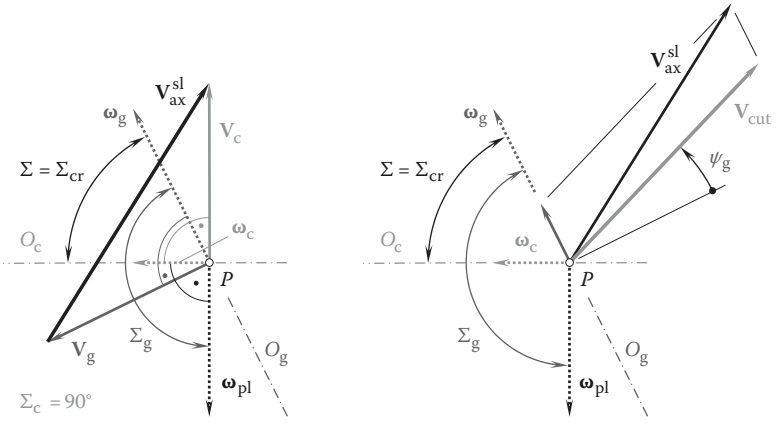

FIGURE 19.2
Primary (cutting) motion $\mathbf{V}_{cut}$ in the plunge method of machining the bevel of a gear.

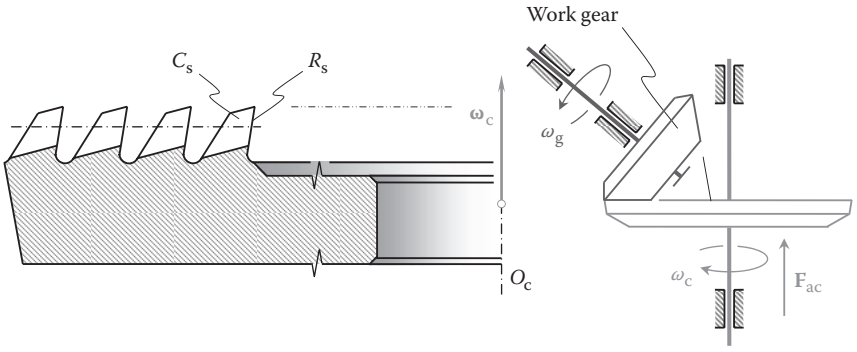

FIGURE 19.3
A schematic of the plunge method of gear machining.

The vector diagram in Figure 19.2 also reveals that the direction of the vector $\mathbf{V}_{cut}$ depends upon the directions of the rotations $\boldsymbol{\omega}_g$ and $\boldsymbol{\omega}_c$. Reversing the rotations $\boldsymbol{\omega}_g$ and $\boldsymbol{\omega}_c$ results in the vector $\mathbf{V}_{cut}$ of the primary motion also being reversed.

19.1.2 Possible Designs of Tools for Machining Bevel Gears

Numerous designs of gear cutting/gear finishing tools can be developed from the simplest kinematics of the work gear tooth flank generation shown in Figure 19.1. Simple kinematics has been employed in the design of the gear cutting tool depicted in Figure 19.3. The pitch angle of the gear cutting tool is given as $\Gamma_c = 90°$. As a result, the pitch cone is transformed to a pitch plane that is perpendicular to the axis O_c.

When machining a bevel gear, the work gear is rotating ω_g about its axis O_g. The cutting tool is rotating ω_c about its axis O_c. The rotations ω_g and ω_c are synchronized with each other in a timed manner. The gear cutting tool is fed (plunged) $\mathbf{F}_{ac}$ in its axial direction toward the work gear. Depending on the directions of the rotations $\boldsymbol{\omega}_g$ and $\boldsymbol{\omega}_c$, rake surface R_s of the gear cutting tool teeth should be faced either toward the axis O_c (as shown in Figure 19.3), or faced oppositely, i.e., outwards from axis O_c.

The sliding vector $\boldsymbol{\omega}_g^{sl}$ and the distance from the pitch point P to the interacting tooth flanks of the work gear and of the gear cutting tool must be sufficient to create a reasonable speed of cut $\mathbf{V}_{cut}$. The gear cutting tool can also be designed for finishing the work gear flanks. In this last case, the cutting teeth can be shaped in a form similar to that shaving cutters feature. Abrasive finishing of the work gear tooth flanks is also possible.

The possibility of machining work gear tooth flanks so that they do not allow for sliding over each other is a strong advantage of gear cutting tools, the design of which is based on the concept under consideration. This means that use of the simplest kinematics of the work gear tooth flank generation (see Figure 19.1) makes possible the machining not only of approximate gears, but also of gears having correct tooth flank geometry.

Tools for the reinforcement of bevel-gear fillets, similar to those previously developed by the author [106, 107, 108], can be designed on the kinematics shown in Figure 19.1.

The simplest kinematics of the work gear tooth flank generation (see Figure 19.1) can be employed in inverse order. Conical gear cutting tools for machining face gears can be

designed on the premise of this kinematics. This opportunity is not discussed in detail here.

19.2 Face Hob for Cutting Bevel Gear

Approximate bevel gears can be cut with face hobs. A face hob can be interpreted as a bevel hob (see Figure 18.15) featuring a pitch angle $\Gamma_c = 90°$. An example of a face hob for cutting bevel gears is schematically illustrated in Figure 19.4. All teeth of the hob within the face width are of the same profile. For this reason, only approximate bevel gears can be cut with a face hob of the design under consideration. A face hob can be designed either as a single-start or as a multiple-start gear cutting tool. Numerous practical applications are based on the concept of the face hob shown in Figure 19.4. Some of the applications are briefly discussed below.

Face-milling cutters for cutting bevel gears by the Gleason method are designed so that the cutter blades cut opposite flanks of the tooth space [194]. The Oerlikon Spiromatic spiral-bevel-gear generation process* bears considerable similarity to the Gleason method. There are, however, significant differences. The cutter blades are arranged in groups of two or three blades. One group, usually of two blades, cuts one tooth space while the next group follows in the next tooth space and so on until the complete gear is cut [194].

Similar to other methods of spiral-bevel-gear generation, the motions of the face hob, work gear, and machine cradle are such that the face hob sweeps out the imaginary crown-wheel tooth flanks with which the work gear is in mesh. The crown wheel is concentric with the axis of rotation of the cradle. Spiral angles range between 30° and 45°, but are usually made to lie between 35° and 40°, and to give adequate overlap. When quiet running is important, it is customary to design to the larger angles.

The Oerlikon method employs continuous indexing. Generation of the tooth profile is achieved by giving the cutter cradle a slow rolling motion while the work gear is given a corresponding roll so that full involute profiles result. The rolling motion of the work gear is superposed on the indexing rotation through a differential. All the teeth are progressively cut in equal increments as generation proceeds. The Oerlikon gear is cut with a constant space width. All the teeth are finish-cut during one rolling motion of the cradle carrying the face hob. Oerlikon spiral-bevel and hypoid-type gears are of high quality and give satisfactory performance in service.

The Fiat spiral bevel-gear generation process is another example of application of the face hob that consists of one complete spiral of cutting blades [194]. Continuous indexing enables the cutter spiral to cut each consecutive tooth space. The tooth profiles are generated by the slow relative rolling between face hob and work gear as in the Oerlikon method of generation. The tooth depth is again constant.

There is much room for improvements in design of cutting tools for generation of bevel gears based on quasi-planar gear machining meshes.

* This is based on a method of producing spiral bevel gears developed by Dr. B. Mammano in Italy in 1936 [194].

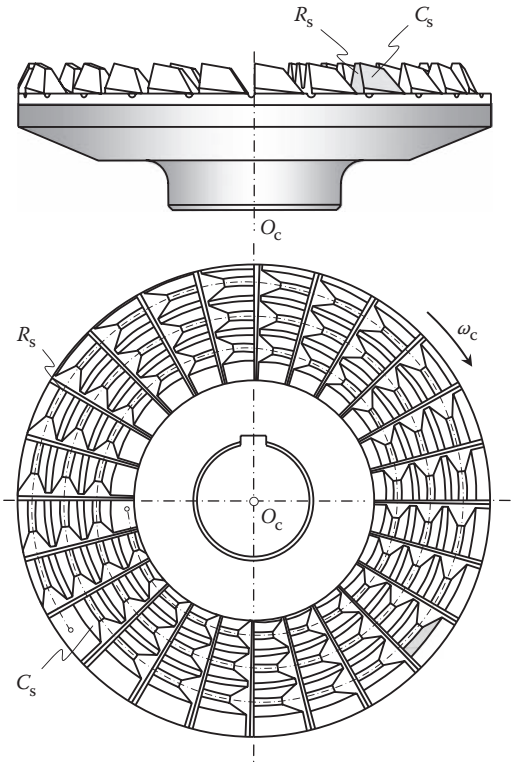

FIGURE 19.4
A conical hob having pitch angle $\Gamma_c = 90°$ (face hob).

19.3 More Possibilities for Designing Gear Cutting Tools Based on Quasi-Planar Gear Machining Meshes

The generating surface of a cutting tool for machining hypoid gears does not allow for sliding over itself. If approximate hypoid gears are machined, then it is practical to reproduce the generating surface by means of a surface of revolution. Rotation of the cutting tool in this case is superposed with the corresponding rolling motion. Ultimately, either one tooth or one tooth space is machined in a single rolling stroke. The schematic of machining is similar in mach to that of machining bevel gears.

Tools for machining bevel gears can also be designed for reinforcement of the gear fillets by means of surface plastic deformation. Numerous gear finishing tools have been developed [105] for this purpose. The gear finishing tool consists of a tool body with circumferentially located rollers (see Figure 19.5). When the gear finishing tool is rotating ω_c about its axis O_c, the rollers are free to rotate ω_{rol} about their axis O_{rol}. Axis O_{rol} of each roller is at a certain distance δ_{rol} from the axis of rotation O_c of the gear finishing tool. For the gear finishing tool of diameter d_c, the offset δ_{rol} is given by $\delta_{rol} = 0.5d_c \sin\psi_c$, where ψ_c denotes the

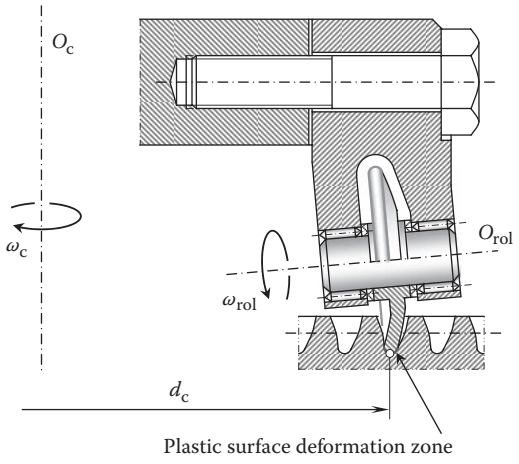

FIGURE 19.5
A finishing tool for reinforcing the fillets of a hypoid gear.

spiral angle of the work gear teeth. When finishing hypoid gears, the rollers are pressed into the fillet and reinforce it by plastic deformation of surface layers of the material.

In addition to gear cutting tools and tools for reinforcing hypoid gears, cutting tools for scudding bevel and hypoid gears can also be developed. No limitation is observed for application of the concept of gear finishing tools featuring a continuous HS-cutting edge similar to that shown in Figure 18.6.

It is important to note that when the tooth number of the face gear approaches infinity, the schematic of the gear machining process transforms to cylindrical gear-to-rack mesh. This kinematics of gear machining is discussed above (see Figure 18.11 and Figure 18.12).

Section V-C: Design of Gear Cutting Tools: Internal Gear Machining Mesh

Internal gear machining mesh is employed either when an internal work gear is cut with an external gear cutting tool or when an external work gear is machined with an internal gear cutting tool. The internal gear machining mesh features an acute crossed-axis angle Σ, the actual value of which is below the critical value Σ_{cr} for this angle ($\Sigma < \Sigma_{cr}$). This means that the inequality $0° < \Sigma < \Sigma_{cr}$ is always observed in internal gear machining mesh. The smaller the crossed-axis angle Σ, the higher the rate of conformity of the generating surface of the gear cutting tool to the tooth flank of the work gear. This statement can be drawn from Equation (17.63). The use of gear cutting tools featuring a higher rate of conformity of their generating surface to the tooth flank of the work gear allows for a higher productivity rate. This is one of many reasons why internal mesh is useful when designing gear cutting tools. Another advantage to an internal gear machining mesh is that there is no waviness observed on tooth flanks of the machined work gear.

Kinematics of Internal Gear Machining Mesh

Internal gear machining mesh is a particular case of spatial mesh. Both the rotation vector of the work gear $\boldsymbol{\omega}_g$, and the rotation vector of the gear cutting tool $\boldsymbol{\omega}_c$ make an acute angle with the vector of instant rotation $\boldsymbol{\omega}_{pl}$. The following inequalities $\angle(\boldsymbol{\omega}_g, \boldsymbol{\omega}_{pl}) < 90°$, $\angle(\boldsymbol{\omega}_c, \boldsymbol{\omega}_{pl}) < 90°$ and $0° < \Sigma < \Sigma_{cr}$ are observed in any and all internal gear machining meshes.

Figure V.2 is a sketch of a vector diagram for an internal gear machining mesh. The case shown in Figure V.2 relates to the machining of an external gear with the cutting tool having an internal type generating surface *T*. The work gear rotation vector $\boldsymbol{\omega}_g$ is at a certain acute angle Σ_g in relation to the vector $\boldsymbol{\omega}_{pl}$ of instant rotation ($0° < \Sigma_g < 90°$). The cutting tool rotation vector $\boldsymbol{\omega}_c$ makes an acute angle Σ_c with the vector $\boldsymbol{\omega}_{pl}$ of instant rotation ($0° < \Sigma_c < 90°$). In the internal gear machining mesh, the external hyperboloid of one sheet associated with the work gear is rolling over the internal hyperboloid of one sheet associated with the generating surface of the gear cutting tool.

Similarly to the illustration in Figure V.2, a vector diagram for an internal gear machining mesh can be constructed for the machining of an internal work gear with a cutting tool having an external generating surface *T*.

The vector of instant rotation $\boldsymbol{\omega}_{pl}$ of the cutting tool with respect to the work gear is equal to $\boldsymbol{\omega}_{pl} = \boldsymbol{\omega}_c - \boldsymbol{\omega}_g$. If not, the instant rotation of the work gear relative to the cutting tool is considered instead and the vector of instant rotation is equal to $\boldsymbol{\omega}_{pl} = \boldsymbol{\omega}_g - \boldsymbol{\omega}_c$. These equalities along with the known property of the product of two vectors allow for the following expressions

$$\boldsymbol{\omega}_g \cdot (\boldsymbol{\omega}_g - \boldsymbol{\omega}_c) > 0 \tag{V.3}$$

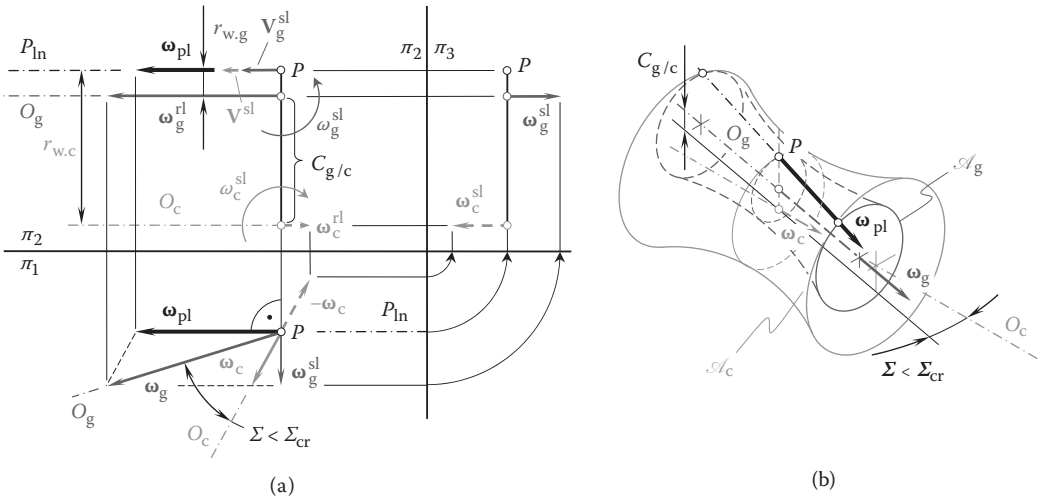

FIGURE V.2
Vector diagram of an internal gear machining mesh.

$$\boldsymbol{\omega}_c \cdot (\boldsymbol{\omega}_c - \boldsymbol{\omega}_g) > 0\,, \tag{V.4}$$

which are valid for internal gear machining mesh. A gear machining mesh that satisfies either Equation (V.3) or Equation (V.4) is an internal spatial mesh and vice versa. All internal gear machining meshes satisfy either Equation (V.3) or Equation (V.4).

Within a plane through the closest distance of approach of the axes O_g and O_c, a vector of the linear velocity of sliding $\mathbf{V}^{sl}$ of the axodes is created by two components $\mathbf{V}_g^{sl}$ and $\mathbf{V}_c^{sl}$. The component $\mathbf{V}_g^{sl}$ is created by the component $\boldsymbol{\omega}_g^{sl}$ of the rotation vector $\boldsymbol{\omega}_g$, while the component $\mathbf{V}_c^{sl}$ is created by the component $\boldsymbol{\omega}_c^{sl}$ of the rotation vector $\boldsymbol{\omega}_c$. Because the components $\boldsymbol{\omega}_g^{sl}$ and $\boldsymbol{\omega}_c^{sl}$ of the rotation vectors are equal to each other, the components $\mathbf{V}_g^{sl}$ and $\mathbf{V}_c^{sl}$ of linear velocity of the sliding motion are not equal to each other. The difference V_Σ between the components V_g^{sl} and V_c^{sl} is due to the difference between the distances of the axes O_g and O_c from the pitch point P. A clear understanding of the vector diagram of internal gear machining mesh (see Figure V.2) is of critical importance when designing gear cutting tools based on this type of gear meshing.

20

Gear Cutting Tools with an Enveloping Generating Surface

The sliding of axodes is one of the major features of internal work gear to cutting tool mesh. Because the axodes slide over each other, the sliding of tooth flanks of the work gear and of the generating surface of the gear cutting tool in gear machining mesh is unavoidable. The sliding of tooth flanks is similar to that observed in the gear shaving process. The tooth flank sliding can be utilized, as the primary (cutting) motion for a gear cutting tool to be designed as this is not physically prohibited.

20.1 Gear Cutting Tools with a Cylindrical Generating Surface

As it is adopted in this book, the determination of the set of design parameters of a work gear is the starting point when designing a gear cutting tool. The design parameters of the work gear are the input, which are of prime importance when designing a high-performance gear cutting tool.

20.1.1 Generating Surface of an Internal Cylindrical Gear Cutting Tool

The kinematics of machining a gear when the gear cutting tool is in internal mesh with the work gear resembles that when the gear cutting tool is in external mesh with the work gear. The geometry of the generating surface of the gear cutting tool in both cases is of the same nature. The location of the body of the gear cutting tool in relation to the generating surface T is the only difference between the cases of external and internal meshing of the work gear and of the gear cutting tool.

For a gear cutting tool that is externally meshed with the work gear (see Figure 15.10), the cutting tool body is located with respect to the generating surface T so that the axis O_c of rotation passes through the bodily side of the cutting tool. In the case of a gear cutting tool that is internally meshed with the work gear (see Figure 20.1), the cutting tool body is located with respect to the generating surface T so that the axis O_c of rotation passes through the void side of the cutting tool. However, the location of the cutting tool body with respect to the generating surface T does not affect the geometry of the generating surface itself. Therefore, without going into the details of derivation, Equation (15.54) for the external generating surface T

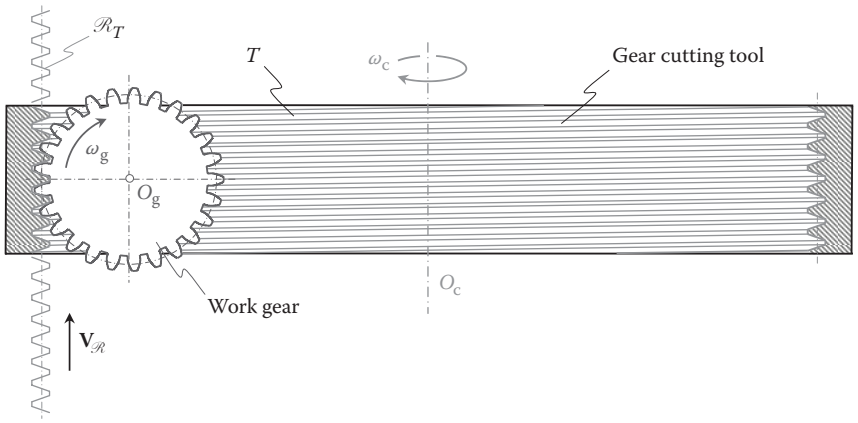

FIGURE 20.1
A gear cutting tool with a cylindrical enveloping generating surface *T*.

$$\left.\begin{array}{l}\text{Generating surface } T\\ \text{of a gear cutting tool}\end{array}\right| \quad \Rightarrow \quad \mathbf{r}_c(U_c, V_c) = \begin{bmatrix} 0.5d_{b.c}\sin V_c - U_c \sin\psi_{b.c}\cos V_c \\ 0.5d_{b.c}\cos V_c + U_c \sin\psi_{b.c}\sin V_c \\ p_{b.c}V_c - U_c\cos\psi_{b.c} \\ 1 \end{bmatrix} \tag{20.1}$$

is also valid for the case of the internal generating surface of the gear cutting tool.

For an internal gear cutting tool for machining spur gears, the preferred design is with a zero setting angle $\zeta_c = 0°$. When helical gears are machined, then it is recommended that the equality $\zeta_c = \psi_g$ be fulfilled, although this is not mandatory. Under such a scenario, the work gear axis O_g and the cutting tool axis O_c are crossed with each other at right angles in both cases.

20.1.2 Solution to the Inverse Problem of Part Surface Generation

When a gear is machined with a gear cutting tool having an internal generating surface, no relative motion of the work gear or the gear cutting tool in the axial direction of the work gear is allowed. Absence of the relative axial motion causes a violation of the conditions for proper part surface generation [125, 128, 136, 138, 143, 153] (see also Appendix B for details on the set of necessary conditions for proper part surface generation). The violation of the conditions for proper part surface generation is inevitable in the case of the application of an internal gear cutting tool for machining a work gear.

For the determination of whether or not a condition of proper part surface generation is violated, the inverse problem of part surface generation is commonly considered. When seeking a solution to the inverse problem of part surface generation for the machining of a work gear with an internal gear cutting tool, consider the given generating surface *T*, which is performing motion relative to a reference system associated with the work gear. The motions are those that the cutting tool is performing relative to the work gear when machining the gear.

Consider a Cartesian coordinate system $X_gY_gZ_g$ associated with the work gear and rotating with it when the work gear is machined. Imagine that a coordinate system $X_cY_cZ_c$ is

embedded in the gear cutting tool. When the cutting tool is rotating, the reference system $X_cY_cZ_c$ is rotating together with the cutting tool. Once the reference systems $X_gY_gZ_g$ and $X_cY_cZ_c$ are chosen, this makes it possible to compose the operator $\mathbf{Rs}(c \mapsto g)$ of the resultant coordinate transformation (see Chapter 4). The operator $\mathbf{Rs}(c \mapsto g)$ allows for representation of the generating surface T of the gear cutting tool in the reference system $X_gY_gZ_g$ associated with the work gear at every instant of time. Therefore, once the generating surface of the gear cutting tool is represented in the form $\mathbf{r}_c = \mathbf{r}_c(U_c, V_c)$ [see Equation (20.3)], the position vector of a point $\mathbf{r}_c^{(g)}$ of the generating surface T, in its current configuration with respect to the work gear, can be computed from the equation

$$\mathbf{r}_c^{(g)}(U_c, V_c, \varphi_c) = \mathbf{Rs}\,(c \mapsto g) \cdot \mathbf{r}_c(U_c, V_c) \tag{20.2}$$

In addition to the parameters U_c and V_c, the position vector of a point $\mathbf{r}_c^{(g)}$ of the surface T in the gear reference system $X_gY_gZ_g$ also depends upon an enveloping parameter. In the case of Equation (20.2), the angle of rotation φ_c of the gear cutting tool serves as the enveloping parameter solely for the purposes of convenience.

Equation (20.2), considered together with Shishkov's equation of contact $\mathbf{n} \cdot \mathbf{V} = 0$, allows for an equation of the machined tooth flank $\mathcal{G}$ of the work gear. Shishkov's equation of contact $\mathbf{n} \cdot \mathbf{V} = 0$ is helpful for the purpose of elimination of the enveloping parameter φ_c from Equation (20.2). The position vector of a point $\mathbf{r}_g^{(a)}$ of the machined tooth flank $\mathcal{G}$ of the work gear can be represented in the form

$$\mathbf{r}_g^{(a)} = \mathbf{r}_g^{(a)}(U_c, V_c) \tag{20.3}$$

At this point, the machined tooth flank of the work gear (see Equation (20.3)] can be compared with the desired tooth flank given by Equation (1.3). To make a consistent comparison, the parameters U_c and V_c in Equation (20.3) must be compatible with the corresponding parameters U_g and V_g in Equation (1.3). Depending on the kind of parameterization of the desired gear tooth flank [see Equation (1.3)], and of the machined tooth flank [see Equation (20.3)], changing the surface parameters (see Appendix C) may be necessary.

After completion, the comparison reveals that the actual tooth flank $\mathcal{G}^{(a)}$ [see Equation (20.3)] differs from the desired tooth flank $\mathcal{G}$ [see Equation (1.3)]. The difference is due to violation of the conditions of proper part surface generation caused by the absence of the axial relative motion of the work gear and of the gear cutting tool in the axial direction of the work gear. If the difference between the actual tooth flank and the desired tooth flank of the work gear is within a reasonable range, then the gear cutting tool can be used for the machining gears.

Practically, the inevitable violation of the conditions of proper part surface generation using enveloping gear cutting tools has disadvantages as well as advantages. Approximate generation of the work gear tooth flank is the major disadvantage of the implementation of enveloping gear cutting tools. However, if the pitch diameter of the enveloping gear cutting tool is large enough, then the deviation of the tooth flank $\mathcal{G}^{(a)}$ from the tooth flank $\mathcal{G}$ can be negligibly small. In this last case, the enveloping gear cutting tool can be used for machining gears.

A large pitch diameter of the enveloping gear cutting tool also results in advantages and disadvantages. Although it is inconvenient to use gear cutting tools with large diameters, the plurality of work gears can be machined simultaneously with gear cutting tools of large diameters, as illustrated in Figure 20.2. In the case under consideration, each work

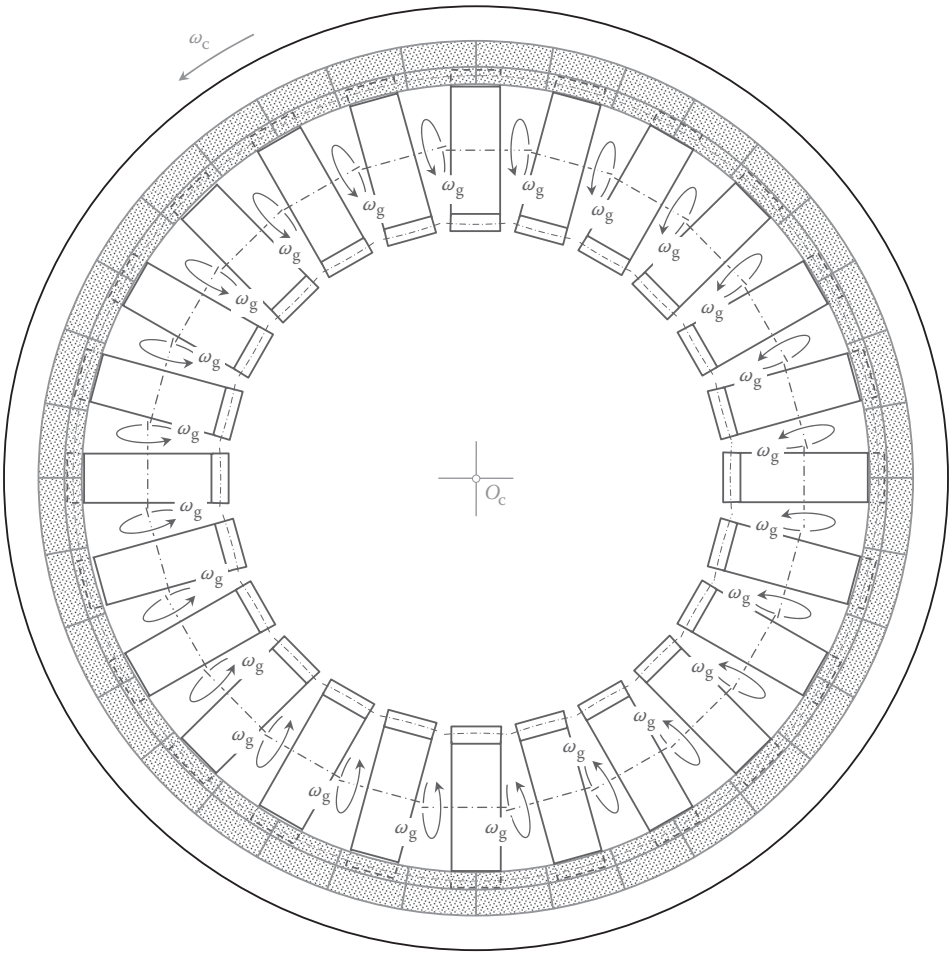

FIGURE 20.2
Machining of multiple work gears simultaneously with an enveloping gear cutting tool.

gear is rotating ω_g about its axis of rotation and the gear cutting tool is rotating ω_c about the axis O_c. Axes of rotation of the work gears are crossed with the gear cutting tool axis O_c at a right angle. This is possible when the equality $\zeta_c = \psi_g$ is observed. While rotating, every work gear is traveling in the axial direction of the gear cutting tool O_c. The rotations ω_g and ω_c, as well as the straight travel motion are synchronized with each other. It is convenient to load the work gears from one end of the gear cutting tool and to unload the machined gears from the opposite end of the gear cutting tool. A gear cutting tool designed on the principle illustrated in Figures 20.1 and 20.2 could be practical in high volume production of gears.

20.1.3 Examples of Gear Cutting Tools with an Enveloping Cylindrical Generating Surface

A vector representation of the kinematics of a gear machining process with a cylindrical enveloping gear cutting tool (see Figure 20.1) is illustrated in Figure 20.3. The rotation

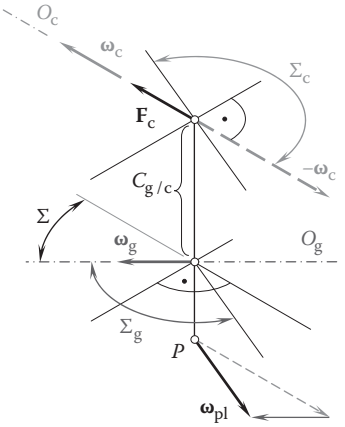

FIGURE 20.3
Vector representation of the kinematics of a gear machining process with a cylindrical enveloping gear cutting tool.

vector of the work gear $\boldsymbol{\omega}_g$ and the rotation vector of the gear cutting tool $\boldsymbol{\omega}_c$ are along the work gear axis O_g and the cutting tool axis O_c, respectively. The ratio $|\boldsymbol{\omega}_g|/|\boldsymbol{\omega}_c|$ depends upon tooth numbers N_g and N_c. The axes of rotation O_g and O_c are at a distance $O_{g/c}$ from each other and they are crossed at the crossed-axis angle Σ. The rotations ω_g and ω_c are synchronized with each other.

The work gear and the gear cutting tool travel $\mathbf{F}_c$ relative to each other in the axial direction of the gear cutting tool. The feed motion $\mathbf{F}_c$ affects the timing of the rotations $\boldsymbol{\omega}_g$ and $\boldsymbol{\omega}_c$. Ultimately, all three motions must be properly timed. No relative motion of the work gear and the gear cutting tool is observed in the axial direction of the work gear.

Because no relative motion of the gear cutting tool in the axial direction of the work gear is observed, then enveloping gear cutting tools featuring cylindrical generating surfaces are perfectly suited for machining gears with crowned teeth. An example of a gear tooth with lengthwise flank modification is schematically depicted in Figure 20.4. The tooth flank modification results in the actual gear tooth flank deviating from the theoretical form. The modification is performed on a precalculated value δ.

Numerous designs of gear cutting tools can be developed based on the concept of an enveloping cylindrical generating surface T, similar to those considered in Chapter 15 for a conventional external generating surface. The possible types of tools for machining gears include, but are not limited to: (a) enveloping hobs, (b) enveloping shaving cutters, (c) enveloping work gear grinding wheels, and (d) gear broaching tools ([58, 72, 73, 76] and others). A special method of hob relieving has been developed for relieving enveloping hobs [171].

In addition to the machining of gear tooth flanks, $\mathcal{G}$, the enveloping gear cutting tools can also be applied to machining chamfered gears. The design of a gear tooth with chamfers is schematically depicted in Figure 20.5. For machining chamfered gears, multiple work gears are set-up within the interior of the enveloping work gear as shown in Figure 20.6. The corresponding face of each work gear is displaced from the axis O_c of the enveloping gear cutting tool at a certain distance H. The actual value of the displacement H depends upon the desired parameters of the chamfers. When machining chamfered gears,

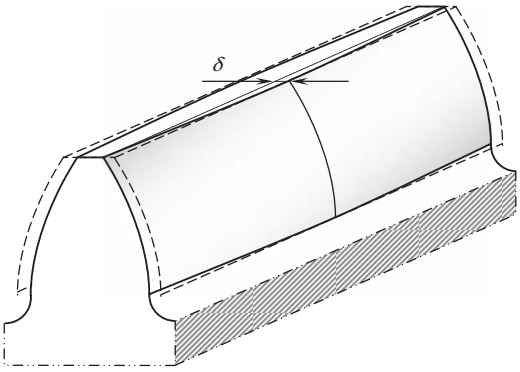

FIGURE 20.4
A work gear tooth featuring lengthwise modification.

the enveloping gear cutting tool is rotating ω_c about its axis O_c. Every work gear is rotating ω_g about its axis O_g. Additionally, all work gears travel along the axis O_c.

The face width of the enveloping gear cutting tool can be expressed in terms of the design parameters of the work gear along with the way the rotations ω_g, ω_c, and the translation F_c are timed with each other. Under any circumstances, the face width of the gear cutting tool must be sufficient for machining all the gear teeth in a single path of the work gear through the gear cutting tool. It is easy to see that the productivity rate of gear chamfering with the enveloping gear cutting tool (see Figure 20.6) will be high.

It is important to note that enveloping gear cutting tools featuring a cylindrical generating surface can also be used for designing (a) enveloping worm grinding wheels, (b) gear cutting tools for scudding gears, (c) finishing gear cutting tools featuring a continuous HS cutting edge (similar to that shown in Figure 18.6), as well as tools for surface reinforcement of gear tooth flanks by surface plastic deformation.

Pitch diameter of the enveloping gear cutting tool increases as the cutting tool tooth number increases. When tooth number approaches infinity, the enveloping gear cutting tool transfers into a rack similar to that discussed in Chapter 18 (see Figure 18.11).

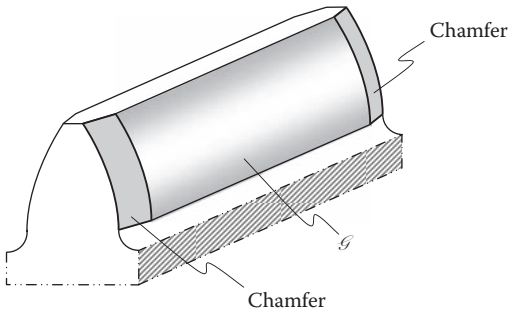

FIGURE 20.5
A gear tooth featuring chamfers.

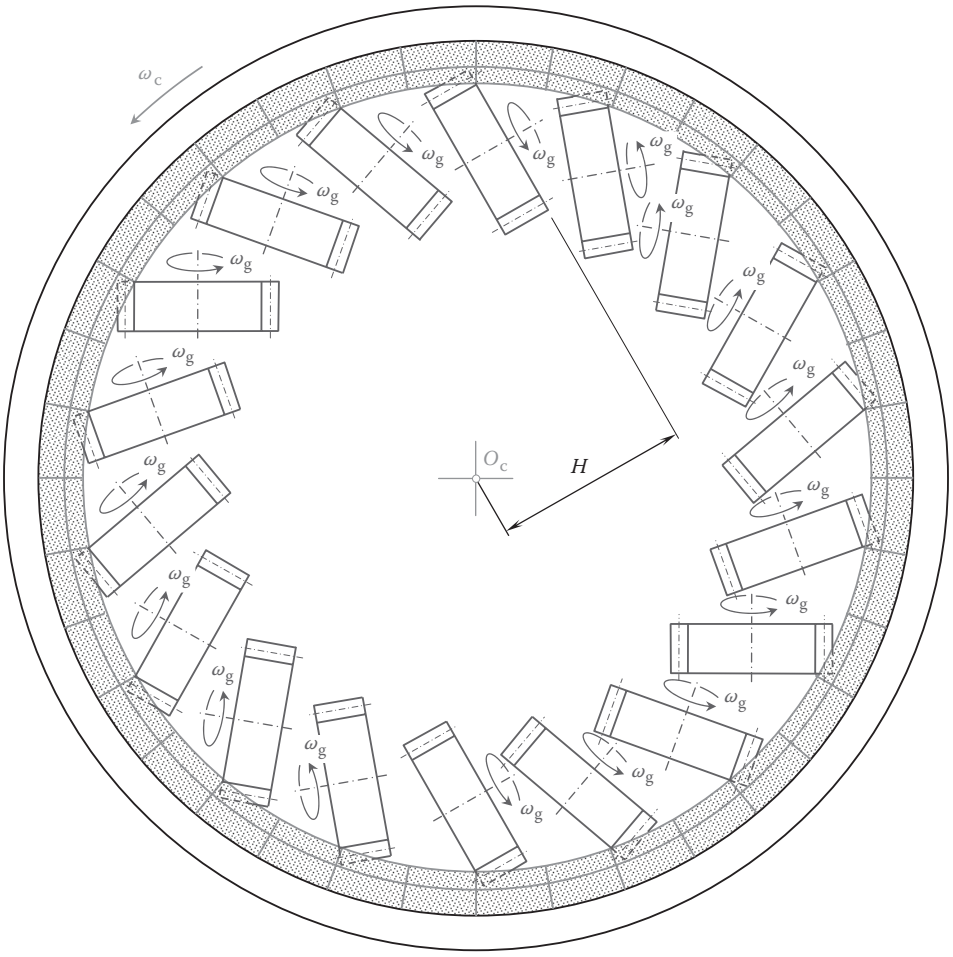

FIGURE 20.6
Schematic of the chamfering of spur and helical gears.

20.2 Gear Cutting Tools with a Conical Generating Surface

An enveloping conical generating surface of a gear cutting tool can be created in a manner similar to the manner in which the external conical generating surface of a gear cutting tool (see Figure 15.15) is created by means of a tilted auxiliary generating surface $\mathscr{R}_T$ (see Figure 15.6a).

20.2.1 Generating Surface of an Enveloping Conical Gear Cutting Tool

The generating surface T of an enveloping conical gear cutting tool can be created as the enveloping surface to successive positions of the auxiliary generating rack. For this purpose, a screw motion of the auxiliary rack $\mathscr{R}_T$ having the axis O_c of rotation of the gear cutting tool as the axis of the screw motion is considered.

The rotation vector of the work gear $\boldsymbol{\omega}_g$ and the rotation vector of the gear cutting tool $\boldsymbol{\omega}_c$ are along the work gear axis O_g and the cutting tool axis O_c, respectively. The axes of rotation O_g and O_c are at a distance $O_{g/c}$ from each other and they are crossed at the crossed-axis angle Σ (see Figure 20.7). The rotations ω_g and ω_c are synchronized with each other.

In the case of a conical gear cutting tool, the pitch plane of the auxiliary rack $\mathscr{R}_T$ is tilted through a certain angle γ_c relative to the axis O_c. Translation $\mathbf{V}_{\mathscr{R}}$ of the auxiliary rack is performed at that same angle γ_c relative to the axis O_c as shown in Figure 20.7. When machining a gear with the conical enveloping gear cutting tool, the feed-rate motion $\mathbf{F}_c$ is performed either in the direction of the translation $\mathbf{V}_{\mathscr{R}}$ or in the direction opposite to $\mathbf{V}_{\mathscr{R}}$.

The work gear and the gear cutting tool travel $\mathbf{F}_c$ in relation to each other in the direction that makes an angle γ_c, relative the axis O_c of the gear cutting tool. The feed motion $\mathbf{F}_c$ affects the timing of the rotations $\boldsymbol{\omega}_g$ and $\boldsymbol{\omega}_c$. All three motions must be properly timed.

The equation of the generating surface of an enveloping conical gear cutting tool can be obtained immediately because of the similarity of generation of the enveloping conical generating surface T to that of the external generating surface (see Chapter 15). The equation for the surface T is identical to Equation (20.1) except for one parameter. Base diameter $d_{b.c}$ for the enveloping conical generating surface T is computed from Equation (15.58)

$$d_{b.c} = \frac{mN_c \cos(\phi_n \pm \gamma_c)}{\sqrt{1 - \cos^2(\phi_n \pm \gamma_c)\cos^2 \zeta_c}} \tag{20.4}$$

The sign + here is valid for a screw involute surface on one side of the tooth profile of the surface T (Figure 20.8), while the sign – is valid for the opposite side of the tooth profile.

20.2.2 Examples of Gear Cutting Tools with an Enveloping Conical Generating Surface

The conical enveloping generating surface T (Figure 20.8) is used for the design of enveloping hobs, grinding worms, shaving cutters, etc., similar to that for which a cylindrical

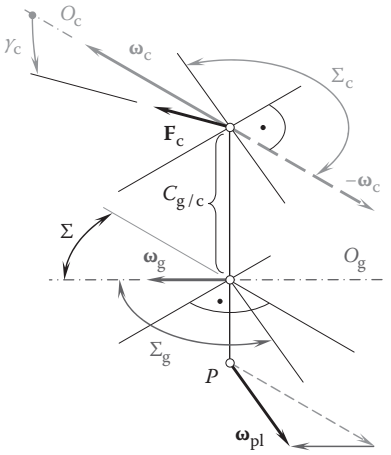

FIGURE 20.7
Vector representation of the kinematics of a gear machining process with a conical enveloping gear cutting tool.

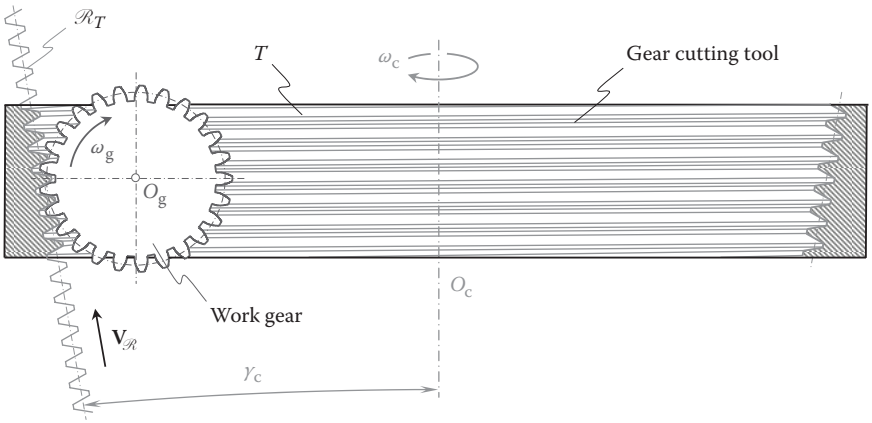

FIGURE 20.8
A gear cutting tool with a conical enveloping generating surface *T*.

enveloping generating surface is used (see Chapter 15). Examples of conical enveloping gear cutting tools are known from many sources [58, 74, 75, 143].

Possible types of tools for machining gears include, but are not limited to: (a) enveloping hobs, (b) enveloping shaving cutters, (c) enveloping worm grinding wheels, (d) tools for scudding gears, (e) gear broaching tools, and (f) finishing gear cutting tools that feature a continuous HS cutting edge (similar to that shown in Figure 18.6), as well as tools for surface reinforcement of gear tooth flanks by surface plastic deformation. As the tooth number of the gear cutting tool increases, the enveloping conical gear cutting tool degenerates into a corresponding rack-type gear cutting tool (see Figure 18.11).

20.3 Gear Cutting Tools with a Toroidal Generating Surface

For purposes of the design of enveloping gear cutting tools, a generating surface with a round auxiliary rack $\mathscr{R}_T$ can be used. Examples of an auxiliary generating rack of this geometry are depicted in Figures 15.6c and d. The use of a round auxiliary rack makes it possible to generate a toroidal enveloping generating surface *T*.

20.3.1 Generating Surface of an Enveloping Toroidal Gear Cutting Tool

The generating surface *T* of an enveloping toroidal gear cutting tool can be created as the enveloping surface to successive positions of the round auxiliary generating rack $\mathscr{R}_T$. For the purpose of generating the surface *T*, the auxiliary rack $\mathscr{R}_T$ performs two motions simultaneously (see Figure 20.9). The motions are the rotation of the rack $\mathscr{R}_T$ about its axis $O_{\mathscr{R}}$ and the rotation of the rack $\mathscr{R}_T$ about the cutting tool axis O_c. The rotations of the round auxiliary rack $\mathscr{R}_T$ are synchronized. After generation, the generating surface of the enveloping toroidal gear cutting tool is shaped in the form of a screw surface on the torus

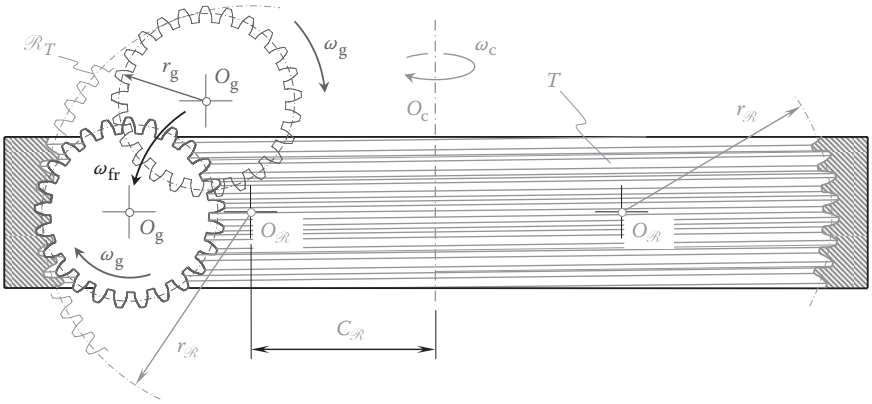

FIGURE 20.9
A gear cutting tool with a toroidal enveloping generating surface *T*.

surface. The torus surface is specified by the radius $r_{\mathscr{R}}$ of the pitch circle of the auxiliary rack $\mathscr{R}_T$, and by the distance $C_{\mathscr{R}}$ of the rack axis $O_{\mathscr{R}}$ from the cutting tool axis O_c. The equation of the generating surface T of the enveloping toroidal gear cutting tool can be derived in the form $\mathbf{r}_c = \mathbf{r}_c(U_c, V_c)$, similar to that derived in Section 15.6.3 for the external toroidal gear cutting tool (see Figure 15.20). An example of the vector representation of the kinematics of a gear machining process with a toroidal enveloping gear cutting tool is schematically illustrated in Figure 20.10.

The rotation vector of the work gear $\boldsymbol{\omega}_g$ and the rotation vector of the gear cutting tool $\boldsymbol{\omega}_c$ are along the work gear axis O_g and the cutting tool axis O_c, respectively. The axes of rotation O_g and O_c are at a distance $O_{g/c}$ from each other and they are crossed at a certain crossed-axis angle Σ (see Figure 20.10). The rotations ω_g and ω_c are synchronized with each other. While rotating, the work gear is fed into the gear cutting tool. The rotation vector $\boldsymbol{\omega}_{fr}$

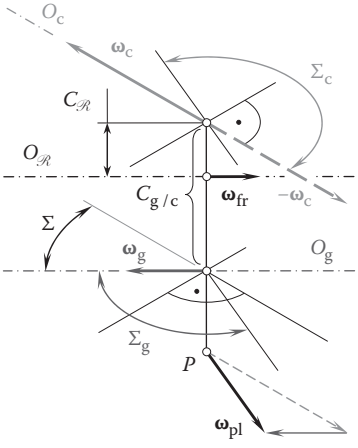

FIGURE 20.10
Vector representation of the kinematics of a gear machining process with a toroidal enveloping gear cutting tool.

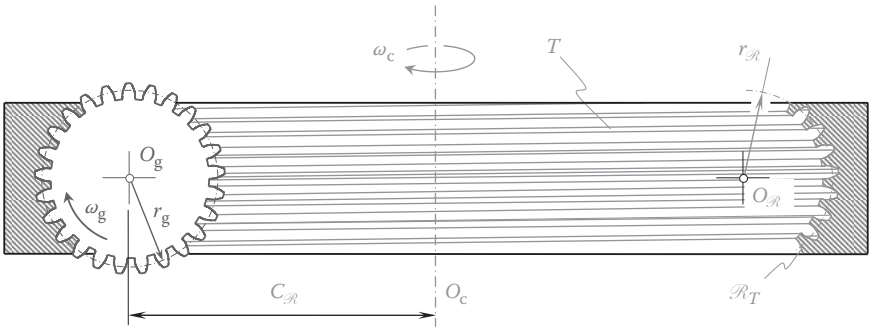

FIGURE 20.11
An example of a conformal toroidal enveloping generating surface *T*.

of the feed-rate motion is along the axis $O_{\mathscr{R}}$. The feed-rate motion $\boldsymbol{\omega}_{fr}$ affects the timing of the rotations $\boldsymbol{\omega}_g$ and $\boldsymbol{\omega}_c$. All three rotations $\boldsymbol{\omega}_g$, $\boldsymbol{\omega}_c$, and $\boldsymbol{\omega}_{fr}$ must be properly timed.

No waviness on tooth flanks of the machined work gear can be observed when an enveloping gear cutting tool of any design (cylindrical, or conical, or toroidal) is used. The actual shape of the machined tooth profile features cusps, which are strongly undesired. No cusps are observe in the lengthwise direction of the machined tooth flank. At every point of the tooth profile of the work gear, the cusps' height depends upon the difference between the radius of curvature R_g of the work gear tooth profile and the corresponding radius of curvature R_c of the generating surface T of the gear cutting tool. The smaller the difference* $(R_g + R_c)$, the smaller the cusp height on the machined tooth flank. If the difference $(R_g + R_c)$ is approaching zero, then the cusps' height approaches zero as well [125, 136, 138, 143, 153]. Cusps practically vanish when the difference $R_g + R_c = 0$.

This concept of the enveloping toroidal generating surface of the gear cutting tool (see Figure 20.9) can be enhanced to a point where it is possible to machine a work gear with no cusps on the tooth flanks. The generating surface T of such geometry is referred to as the *conformal* toroidal enveloping generating surface of the gear cutting tool (Figure 20.11). The equality $r_g = r_{\mathscr{R}}$ of radii of pitch circles is the principal feature of the conformal toroidal generating surface T. Because of the equality $r_g = r_{\mathscr{R}}$ observed, the rotation vector $\boldsymbol{\omega}_{fr}$ of the feed-rate motion is aligned with the rotation vector $\boldsymbol{\omega}_g$ of the work gear. The latter is schematically illustrated in Figure 20.12. No cusps occur on the tooth flank of the work gear that is machined with a gear cutting tool having the conformal toroidal enveloping generating surface T (see Figure 20.11).

In contrast to the gear cutting tools with enveloping toroidal generating surface with a concave auxiliary rack $\mathscr{R}_T$ (see Figure 20.9), enveloping toroidal generating surfaces featuring a convex auxiliary generating rack $\mathscr{R}_T$ can be developed as well. An example is schematically illustrated in Figure 20.13. When a gear cutting tool is designed on the premises of the generating surface T shown in Figure 20.13, it is then possible to cut gears with no longitudinal modification (with no crowning). For this purpose, the setting angle ζ_c must be properly correlated with the crossed-axis angle Σ. It is a trivial engineer-

* Involute tooth profile of an internal gear is concave. Therefore, the corresponding radius of curvature of the tooth profile is always of negative value.

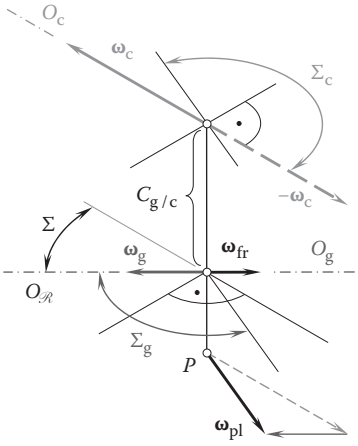

FIGURE 20.12
Vector representation of the kinematics of a gear machining process with the conformal toroidal enveloping gear cutting tool.

ing problem to assign a corresponding value of the setting angle ζ_c of the gear cutting tool.

A vector representation of the kinematics of a gear machining process with the toroidal enveloping gear cutting tool having convex auxiliary rack $\mathscr{R}_T$ is shown in Figure 20.14. Possible types of the enveloping toroidal generating surfaces of gear cutting tools were investigated by Radzevich [139].

20.3.2 Examples of Gear Cutting Tools with an Enveloping Toroidal Generating Surface

Gear cutting tools having an enveloping toroidal generating surface (Figure 20.11 and Figure 20.13) have no wide application in industry yet. An example is known from [62].

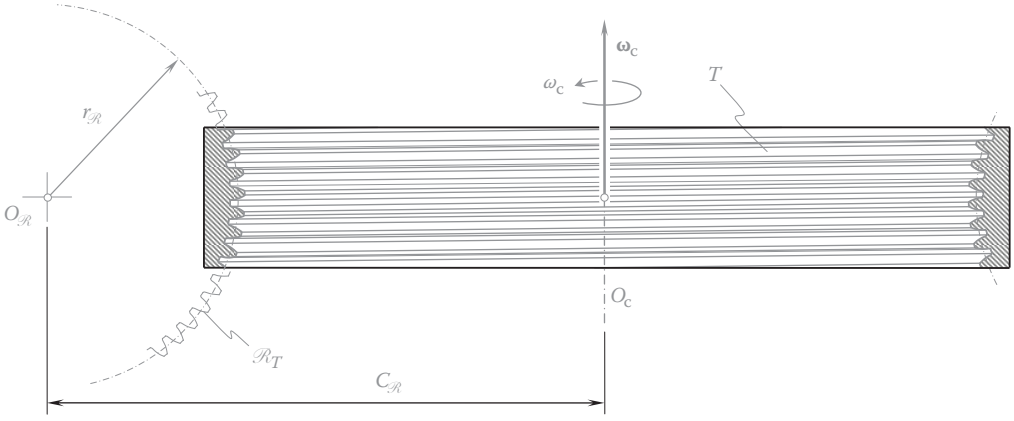

FIGURE 20.13
A gear cutting tool with a toroidal enveloping generating surface T having a convex auxiliary rack $\mathscr{R}_T$.

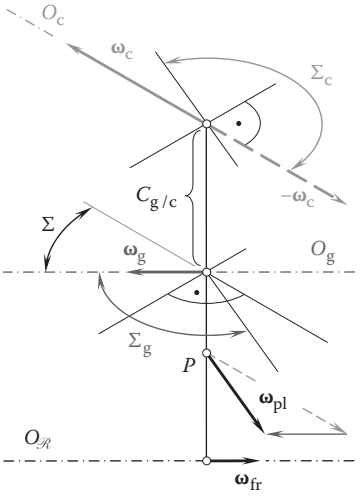

FIGURE 20.14
Vector representation of the kinematics of a gear machining process with a toroidal enveloping gear cutting tool having a convex auxiliary rack $\mathscr{R}_T$.

When machining a work gear, the enveloping toroidal gear cutting tool is rotated ω_c about its axis O_c. The work gear is rotated ω_g about its axis O_g. Simultaneous with the rotation ω_g, the work gear is performing another rotation ω_{fr}. The work gear is fed into the gear cutting tool by the feed-rate rotation ω_{fr}. All three rotations ω_g, ω_c, and ω_{fr} are synchronized with each other. The rotations are timed so that the work gear performs one full rotation while traveling within face width of the gear cutting tool for the complete generation of the tooth flanks of all the work gear teeth.

The gear honing process is a perfect example of the practicality of an application for the enveloping toroidal generating surface with a convex auxiliary rack $\mathscr{R}_T$ shown in Figure 20.13. Gear honing is a hard-finishing method for elimination of the gear errors after the hardening and smoothing of the surface of the gear teeth. Gear honing is also referred to as *shave grinding*. This is due to the fact that the machining kinematics and the tool geometry are similar to gear shaving, while the tool material and cutting speeds are similar to grinding [22].

Gear honing is a continuous, chip-removing, precision machining process and the kinematics is basically analogous to gear shaving. The driven honing tool and the generally non-driven work gear are in rolling contact with a specified radial pressure (see Figure 20.15).

The fact that the axes are crossed at a defined angle (crossed-axis angle) means that the superposition of the feed movements gives a resulting grinding movement in the material-removal region, running diagonally from tip to root and producing a microcutting process with short cutting-point engagement. The large number of grains engaging in the tooth flank at the same time means there is a steady removal of chips, which in turn generates a surface texture on the tooth flank favorable for the gear operation. The module range to be honed is between 0.5 and 8 mm, and the helix angle between 0° and 45°. Gear hardness is generally below HRC 64.

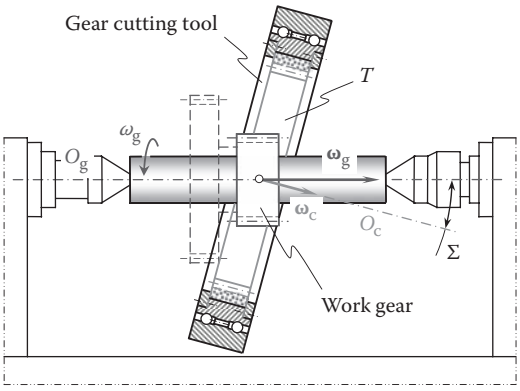

FIGURE 20.15
Schematic of the gear honing (or abrasive shaving) process. (From Neugart, Gear honing, Bethel Park, PA, 2001. www.neugartusa.com/Service/fag/gear_honing.pdf)

Numerous designs of gear cutting tools can be developed on the concept of an enveloping toroidal generating surface T similar to that for conventional external generating surfaces considered in Chapter 15. Possible types of tools for machining gears include, but are not limited to: (a) enveloping hobs, (b) enveloping shaving cutters, (c) enveloping work-grinding wheels, (d) tools for scudding gears, (e) gear broaching tools, and (f) finishing gear cutting tools that feature the continuous HS cutting edge (similar to that shown in Figure 18.6), as well as tools for the surface reinforcement of gear tooth flanks by surface plastic deformation.

21

Gear Cutting Tools for Machining Internal Gears

An internal work gear–to–cutting tool mesh can also be employed for designing a gear cutting tool for machining an internal gear. Such a possibility can be drawn up directly from analysis of Figure V.3 and was investigated by Radzevich [139] as early as 1980.

21.1 Principal Design Parameters of a Gear Cutting Tool for Machining an Internal Gear

As it is adopted in this book, the determination of a set of design parameters of a work gear is the starting point when designing a gear cutting tool.

21.1.1 Geometry of an Internal Gear

An example of an internal gear is illustrated in Figure 1.3. The location of the gear body with respect to the tooth surfaces is the major difference of the geometry of an internal gear from the geometry of an external gear (see Figure 1.4). Therefore, Equation (1.3)

$$\mathbf{r}_{\mathrm{g}}(U_{\mathrm{g}}, V_{\mathrm{g}}) = \begin{bmatrix} r_{\mathrm{b.g}} \cos V_{\mathrm{g}} + U_{\mathrm{g}} \cos \lambda_{\mathrm{b.g}} \sin V_{\mathrm{g}} \\ r_{\mathrm{b.g}} \sin V_{\mathrm{g}} - U_{\mathrm{g}} \sin \lambda_{\mathrm{b.g}} \sin V_{\mathrm{g}} \\ r_{\mathrm{b.g}} \tan \lambda_{\mathrm{b.g}} - U_{\mathrm{g}} \sin \lambda_{\mathrm{b.g}} \\ 1 \end{bmatrix} \quad \begin{matrix} V_{\mathrm{g}}^{(\mathrm{l})} \le V_{\mathrm{g}} \le V_{\mathrm{g}}^{(\mathrm{a})} \\ 0 \le U_{\mathrm{g}} \le [U_{\mathrm{g}}], \end{matrix} \tag{21.1}$$

is valid for the internal gear as well.

The body of an external gear is located within the interior, which is bounded by the surface $\mathscr{G}$. In contrast, the body of an internal gear is located outside the surface $\mathscr{G}$.

21.1.2 Kinematics of Machining an Internal Gear

The internal work gear and the gear cutting tool are rotated about skew axes O_{g} and O_{c}, as depicted in Figure 21.1. The axes O_{g} and O_{c} are at a certain center distance $C_{\mathrm{g/c}}$. The crossed-axis angle Σ is the angle between the rotation vector $\boldsymbol{\omega}_{\mathrm{g}}$ of the work gear and the rotation vector $\boldsymbol{\omega}_{\mathrm{c}}$ of the gear cutting tool, that is, the crossed-axis angle is specified as $\Sigma = \angle(\boldsymbol{\omega}_{\mathrm{g}}, \boldsymbol{\omega}_{\mathrm{c}})$.

Magnitudes ω_{g} and ω_{c} of the vectors $\boldsymbol{\omega}_{\mathrm{g}}$ and $\boldsymbol{\omega}_{\mathrm{c}}$ relate to each other in the same inverse proportion that the corresponding tooth numbers N_{g} and N_{c} relate to each other. When an internal work gear is machined, then the rotation ω_{g} is smaller compared to the cutting tool rotation ω_{c}. However, when the work gear tooth number N_{g} is reduced, the work

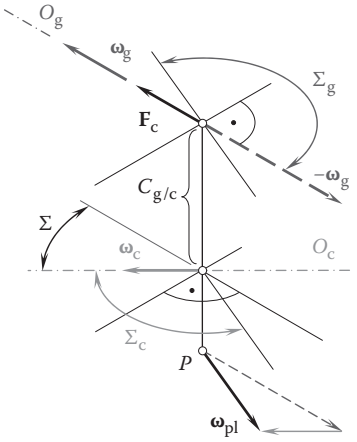

FIGURE 21.1
Vector representation of the kinematics of a machining process of an internal cylindrical work gear with the external gear cutting tool (the feed motion $\mathbf{F}_c$ is pointed along the work gear axis O_g).

gear transforms into an internal worm. Under such a scenario, the rotation ω_g exceeds the rotation ω_c.

The feed motion $\mathbf{F}_c$ of the gear cutting tool is pointed along the work gear axis O_g. Either the work gear or the cutting tool can be fed along axis O_g. This motion affects the resultant motion $\mathbf{V}_\Sigma$ of the work gear relative to the gear cutting tool, and thus it should be taken into account when determining the generating surface of the gear cutting tool.

Another schematic of the machining of an internal gear employs feed motion $\mathbf{F}_c$ pointed along the line $C_{g/c}$, as depicted in Figure 21.2. A feed-rate motion of this type is referred to as plunge feed motion $\mathbf{F}_c$. Plunge feed motion does not affect the resultant motion $\mathbf{V}_\Sigma$ of the work gear relative to the gear cutting tool. Therefore, this motion can be neglected when determining the generating surface T of the gear cutting tool.

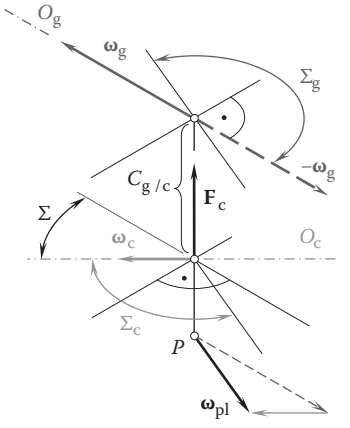

FIGURE 21.2
Schematic of a machining process of an internal cylindrical work gear with the external gear cutting tool that features plunge feed motion $\mathbf{F}_c$.

21.1.3 Determination of the Generating Surface of a Gear Cutting Tool for Machining an Internal Gear

Two main reference systems are used when determining the generating surface of the gear cutting tool for machining an internal gear. In many cases it is convenient to employ the Cartesian coordinate systems $X_g Y_g Z_g$ and $X_c Y_c Z_c$.

The first reference system, $X_g Y_g Z_g$, is associated with the work gear. This coordinate system is rotating with the work gear. The second reference system, $X_c Y_c Z_c$, is the coordinate system with respect to which the gear cutting tool will be analytically described.

The generating surface of the gear cutting tool is represented as a surface that envelopes successive positions of the tooth flank $\mathscr{G}$ when considering the resultant motion of coordinate system $X_g Y_g Z_g$ relative to coordinate system $X_c Y_c Z_c$.

Use of the kinematics, shown in Figure 21.1, of a machining process of an internal cylindrical work gear with the external gear cutting tool allows for composing of the operator $\mathbf{Rs}(g \mapsto c)$ of the resultant coordinate system transformation (see Chapter 4 for details). With the help of the operator $\mathbf{Rs}(g \mapsto c)$, the work gear tooth flank $\mathbf{r}_g$ can be represented in the coordinate system $X_c Y_c Z_c$, which is associated with the gear cutting tool:

$$\mathbf{r}_g^{(c)}(U_g, V_g, \varphi_g) = \mathbf{Rs}(g \mapsto c) \cdot \mathbf{r}_g(U_g, V_g). \tag{21.2}$$

The enveloping parameter $\varphi_g = \omega_g t$ is due to the operator $\mathbf{Rs}(g \mapsto c)$ of the coordinate system transformation. Here, t denotes time.

To derive an equation of the generating surface T, the moving tooth-flank surface $\mathbf{r}_g^{(c)}$ should be considered, together with the equation of contact $\mathbf{n}_g \cdot \mathbf{V}_\Sigma = 0$. Here, in the equation of contact, the unit normal vector to the tooth flank $\mathscr{G}$ is designated as $\mathbf{n}_g$, and $\mathbf{V}_\Sigma$ is the vector of resultant motion of the tooth flank $\mathscr{G}$ with respect to coordinate system $X_c Y_c Z_c$. Considered together, this makes it possible to eliminate the enveloping parameter φ_g from Equation (21.2). Ultimately, the equation of the generating surface T of the gear cutting tool can be represented in the form of vector equation $\mathbf{r}_c = \mathbf{r}_c(U_c, V_c)$.

The generating surface of a gear cutting tool for machining an internal gear is shaped in a form that resembles an external crowned gear.

21.2 Examples of Gear Cutting Tools for Machining an Internal Gear

Hobs for machining internal gears are produced by industry. An example of a hob for cutting internal gears is illustrated in Figure 21.3. The hob design is based on convex auxiliary generating rack $\mathscr{R}_T$. When cutting the work gear, the rack $\mathscr{R}_T$ is properly meshed with the work gear teeth. Rake surface R_s of the hob tooth intersects the corresponding clearance surface C_s. Cutting edges CE of the hob teeth align with the lines of intersection of the surfaces R_s and C_s. Cutting edges of the hob teeth are within the generating surface T of the hob. More examples of designs of hobs for cutting internal gears are known from [70] and from other sources.

The scudding process* can be used for a wide range of internal gear applications. In scudding, the cutter feeds directly through the work gear as the cutter and work gear spin

* The technology itself is a current slant on an older hard-gear finishing process developed in Germany called *walzschaelan* (translated as "hob-peeling"). The elements of hob-peeling are now being used in a different manner, providing the current green process called *scudding.*

FIGURE 21.3
A hob for cutting an internal gear.

in a synchronized fashion. Gear cutting tools for scudding internal gears are a perfect example of cutting tools based on the design of the internal work gear–to–cutting tool mesh. Gear cutting tools for scudding gears are described in [192].

The above considered concept of finishing gear cutting tools having the continuous HS-cutting edge can also be extended to the area of gear cutting tools for finishing internal gears. An example of a gear-finishing tool of this kind is schematically illustrated in Figure 21.4. The gear-finishing tool [104] is designed on the premise of a convex auxiliary generating rack $\mathscr{R}_T$, similar to that from which the hob (Figure 21.3) is designed.

The line of action in the work gear–to–cutting tool is used to construct the continuous HS-cutting edge CE of the gear-finishing tool. When finishing the work gear, an imaginary (phantom) surface of revolution is generated by the line of action when the last gear is rotated about the cutting tool axis O_c. The line of intersection of the generating surface T by the surface of revolution is used as the continuous HS-cutting edge CE of the gear-finishing tool (Figure 21.4).

Due to the peculiarities of the work gear tooth-profile generation by the continuous HS-cutting edge, the gear-finishing tools (see Figures 18.6 and 18.7) designed for finishing external gears can also be used for finishing internal gears. No changes to the design parameters of the gear cutting tool are required in this concern.

Internal gears can be cut with the gear-scudding tools (Figure 21.5). They can also be finished with shaving cutters and/or by a honing method. Internal gears can be shaved on special machines in which the work drives the shaving cutter, or by internal shaving cutter head attachment on external shaving machines.

Because of the crossed-axis relationship between the shaving cutter and the work gear in internal shaving, the shaving cutter requires a slight amount of crown in the teeth to avoid interference with the work gear teeth.

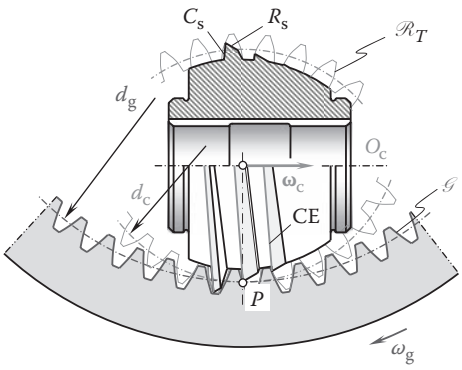

FIGURE 21.4
A gear-finishing tool for internal gears. (From Radzevich, S.P., USSR Patent 880589, Int. Cl. B21h 5/02, Nov. 6, 1979.)

When internal gears are ¾-in. wide or less, or shoulder interferences limit the work gear reciprocation and crossed-axes angle, a plunge shaving method can be applied. Here, the shaving cutter is provided with differential serrations and plunge-fed upward into the work gear. If crowning is desired, a reverse-crowned shaving cutter is used with the plunge-feed shaving process.

When the work gear tooth number approaches infinity ($N_g \to \infty$), then the gear cutting tool transforms into a cutting rack. Gear cutting tools based on the rack-to-gear mesh are discussed above (see, e.g., Figure 18.11). Gear cutting tools for machining bevel gears can also be designed using the work gear–to–cutting tool mesh.

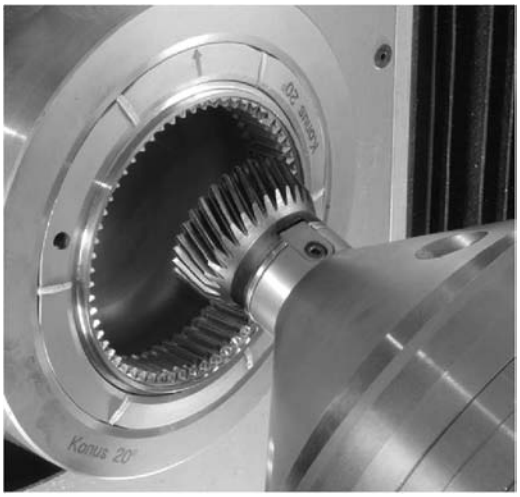

FIGURE 21.5
Scudding of an internal gear. (Courtesy of American Wera, Inc.)

Conclusion

In this work, a novel scientific theory for the design and computation of gear cutting tools is presented. The core of the theory is summarized and outlined below.

First of all, exact and complete information about the gear to be machined is required for the purpose of designing a gear cutting tool. This information includes, but is not limited to, the geometry of tooth flanks of the work gear. The geometry of the tooth flanks can be expressed either in terms of the design parameter of the gear or the parameters that are common in differential geometry of surfaces. Both types of tooth flank specification allow for conversion, that is, the specification of tooth flanks in terms of the parameters of surface geometry (which stems from differential geometry of surfaces) can be converted into the specification in terms of the design parameters of the work gear and vice versa.

Once the geometry of tooth flanks of the gear to be machined is known, the kinematics of the gear machining process should be determined. For this purpose, the scientific classification of all possible types of gear machining meshes (Fig. 3.8) is used. Through this classification, the possibility of machining a given gear in accordance with all kinematics of gear machining meshes is analyzed.

The classification of all possible types of gear machining meshes is the key to solving many major problems relating to gear cutting tool design as well as the development of novel methods of gear machining. The classification, which covers all known and upcoming methods of gear cutting, is a powerful tool for solving many problems relating to gear machining, gear cutting tool design, etc.

Next, one or a few appropriate gear machining meshes are selected for further analysis. The selected gear machining mesh(es) allows for the determination of the generating surface of the gear cutting tool for machining of a given work gear. The generating surface of a gear cutting tool is either conjugate or congruent to the work gear tooth surface. It is also desired (but not required) that generating surfaces allow for sliding over themselves. The predetermined generating surface is the starting point for designing of the gear cutting tool.

Furthermore, each of the gear machining meshes is converted to a corresponding kinematics of the gear machining process. For this purpose, the gear machining mesh is complemented with a primary motion of the cutting tool (i.e., with the cutting motion of the cutting tool) and a feed rate motion of the cutting tool. In many cases, the generating surface of the gear cutting tool allows for sliding over itself. If possible, this motion is preferably used as the primary motion. Otherwise, an additional motion of the gear cutting tool is introduced for this purpose (e.g., broaching of gears, milling of gears with end-type and/or disk-type milling cutters, planing of bevel gears, planing of conical gears having skew teeth, cutting of gears on NC machine).

The presented approach enables the computation of the cutting edge geometry of the gear cutting tool at any instant of time and at any point of interest within the cutting edge. Deviations of the machined gear from its desired geometry can be computed as well.

There is plenty of room for further developments in the field of gear cutting tool design and computation. This book not only summarizes what has already been done in the field, but also outlines areas of potential investigation. The disclosed theory also makes it possible to predict further developments in the field.

Appendix A
Engineering Formulae for the Specification of Gear Tooth

The engineering representation of gear tooth flank can be converted into scientific representation and vice versa. For the conversion, it is convenient to use the so-called "Fundamental Gear Equations" listed below (Table A.1). More useful equations can be found in other sources.

Formulae used for the conversion from the English (pitch) system to the metric system are summarized below (Table A.2)

The formula $P = 25.4/m$ is used to express the diametral pitch P in terms of module m. The expression $m = 25.4/P$ is used for the inverse conversion. For the correspondence between millimeters and inches, the ratio

$$\text{millimeters (mm)} = \frac{\text{inches}}{0.03937} = 25.4 \text{ inches} \tag{A.1}$$

$$\text{inches} = 0.03937 \text{ mm} = \frac{\text{mm}}{25.4} \tag{A.2}$$

is valid.

A brief analysis of the types of gears used in industry, together with the analysis of the local topology of gear tooth flanks to be machined, is necessary for the design of gear cutting tools, especially gear cutting tools for machining/finishing of precision gears.

TABLE A.1

Fundamental Gear Equations

Transverse Diametral Pitch, P_t	$P_t = P_n \cos\psi$
Pitch diameter, D	$D = \frac{N}{P_t}$
Standard addendum, a	$a = \frac{1}{P_n}$
Outside diameter, D_o	$D_o = D + 2a$
Transverse pressure angle, ϕ_t	$\tan\phi_t = \frac{\tan\phi_n}{\cos\psi}$
Base diameter, d_b	$d_b = D\cos\phi_t$
Lead, L	$L = \pi D \cot\psi = \frac{\pi D}{\tan\psi}$ $L = \pi d_b \cos\psi_b$
Normal circular pitch, p_n	$p_n = \frac{\pi}{P_n}$, $p_n = \frac{\pi D\cos\psi}{N}$

TABLE A.1 (CONTINUED)

Transverse Diametral Pitch, P_t	$P_t = P_n \cos\psi$
Standard normal circular thickness, t_n	$t_n = \frac{p_n}{2}$, $t_n = t\cos\psi$
Axial pitch, p_x	$p_x = \frac{\pi}{P_n \sin\psi} = \frac{p_n}{\sin\psi} = \frac{L}{N}$
Transverse circular pitch, p_t	$p_t = \frac{\pi}{P_t} = \frac{p_n}{\cos\psi}$
Helix angle, when the given center distance is standard, ψ	$\cos\psi = \frac{N_p + N_g}{2p_n C}$
Operating pitch diameter (pinion), D_{rp}; with nonstandard center distance, C	$D_{rp} = \frac{2CN_p}{N_p + N_g}$
Operating pressure angle, ϕ_{rt}; with nonstandard center distance C	$\sin\phi_{rt} = \frac{d_{bp} + d_{bg}}{2C}$
Normal diametral pitch, P_n	$P_n = P_t \sec\psi$
Helix angle, ψ	$\cos\psi = \frac{N}{DP_n}$, $\sin\psi = \frac{\pi N}{P_n L}$
Helix angle, ψ_y at any diameter, d_y	$\tan\psi_y = \frac{d_y}{d_1} \cdot \tan\psi_1$
Transverse circular pitch, p_{t2} at any diameter, d_y	$p_{t2} = \frac{\pi d_y}{N}$
Involute function of pressure angle	$\text{inv}\phi = \tan\phi - \breve{\phi}$
Normal pressure angle, ϕ_n	$\tan\phi_n = \tan\phi_t \cos\psi$ $\sin\phi_n = \sin\phi \cos\psi_b$ $\cos\phi_n = \sin\psi_b \csc\psi$
Transverse pressure angle ϕ_{ty}, at any diameter, d_y	$\cos\phi_{ty} = \frac{d_b}{d_y}$
Base helix angle, ψ_b	$\cos\psi_b = \frac{\cos\psi \cos\phi_n}{\cos\phi_t} = \frac{\sin\phi_n}{\sin\phi_t}$ $\sin\psi_b = \sin\psi \cos\phi_n$ $\tan\psi_b = \tan\psi \cos\phi_t$
Base pitch, p_b	$p_b = \frac{\pi d_b}{N} = \frac{\pi D \cos\phi_t}{N}$

TABLE A.2

Formulae for the Conversion from Pitch System to Metric System

Name of the Parameter	English (in.)	Metric (mm)
Pitch diameter, D	$D = \frac{N}{P}$	$D = mN$
Addendum, a	$a = \frac{1}{P}$	$a = m$
Standard outside diameter, D_o	$D_o = D + 2a$	$D_o = D + 2m$
Base diameter, d_b	$d_b = D\cos\phi$	
Circular pitch, p	$p = \frac{\pi}{P}$	$p = \pi m$
Standard circular tooth thickness, t	$t = \frac{p}{2}$	
Average backlash per pair, B	$B = \frac{0.040}{P}$	$B = 0.040m$

Appendix B
Conditions of Proper Part Surface Generation

To make machining of a gear possible, a set of necessary conditions of proper part surface generation (*PSG*) must be satisfied. Satisfaction/violation of the conditions of proper *PSG* significantly depends on the design parameters of the gear cutting tool. Without going into details of the analysis, the set of necessary and sufficient conditions of proper *PSG* is briefly discussed below.

The first condition of proper PSG. In designing a cutting tool for machining of a given gear, the generating surface of the gear cutting tool is required to exist. The generating surface of the gear cutting tool T is viewed as a surface that can be conjugate to the surface of the gear tooth to be machined.

In most cases of gear machining, the generating surface T of the gear cutting tool already exists. However, in particular cases, the existence of the generating surface T could be either questionable or even not feasible. For example, when grinding a gear with dish-type grinding wheel, the generating surface T exists if and only if the pitch diameter in the gear grinding operation exceeds the base diameter of the gear (Figure B.1).

Therefore,

> Existence of the generating surface T of the gear cutting tool is the first and essential condition of part surface machining.

If the first condition of proper *PSG* is violated, the generating surface T of a gear cutting tool does not exist. Thus, a cutting tool for machining of a given gear cannot be designed and therefore the gear cannot be machined.

The second condition of proper PSG. When machining a gear, it is required that the generating surface T of the gear cutting tool makes contact with the gear tooth flank surface $\mathscr{G}$. The contact of the surfaces $\mathscr{G}$ and T has to occur for at least an instant. This requirement can be analytically expressed by the so-called *equation of contact*, that is, by Shishkov's equation $\mathbf{n}_g \cdot \mathbf{V}_\Sigma = 0$, where $\mathbf{n}_g$ denotes the unit normal vector to the surface $\mathscr{G}$ at the point of its contact with the surface T and $\mathbf{V}_\Sigma$ is the vector of the resultant relative motion of the surfaces $\mathscr{G}$ and T. Shishkov's equation of contact ($\mathbf{n}_g \cdot \mathbf{V}_\Sigma = 0$) can serve as an analytical interpretation of the second condition of proper *PSG*. Another form of interpretation of the second condition of proper *PSG* is as follows:

> The unit normal vectors to the given part to be machined and to the generating surface of the cutting tool at each point of their contact must be aligned to each other and be directed oppositely.

The third condition of proper PSG. This condition of proper *PSG* is satisfied if and only if the cutting tool does not penetrate beneath the gear tooth surface $\mathscr{G}$. For this purpose, a proper correspondence between radii of normal curvature of the surfaces $\mathscr{G}$ and T must be observed.

There are many forms of analytical interpretation of the third condition of proper *PSG*. According to one of them, the minimal radius r_{cnf}^{min} of the indicatrix of conformity $\mathrm{Cnf}_R(\mathscr{G}/T)$ has to exceed zero, that is, satisfaction of the inequality $r_{cnf}^{min} \geq 0$ is a must if we are to satisfy the third condition of proper *PSG*.

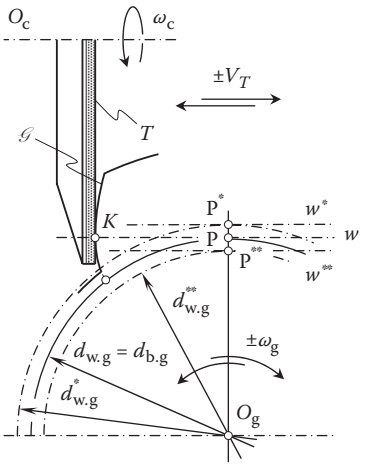

FIGURE B.1
Examples of the satisfaction and violation of the first condition of proper *PSG* in the gear grinding operation. (From Radzevich, S.P., *Computer-Aided Design*, 34(10), 727–740, 2002. With permission.)

This translates the following statement:

> The condition of proper contact of the part surface $\mathscr{G}$ and the generating surface T of a gear cutting tool without their mutual penetration, that is, without their interference in differential vicinity of a point of contact, is the third condition of proper *PSG*.

Satisfaction of the third condition of proper *PSG* is critical for many designs of gear cutting tools.

The fourth condition of proper PSG. When local interference of the surfaces $\mathscr{G}$ and T is eliminated, these surfaces can interfere with each other out of the local vicinity of the point of their contact. To avoid the so-called "global interference" of the surfaces $\mathscr{G}$ and T, the fourth condition of proper *PSG* has to be satisfied. This necessary condition can be formulated as follows:

> The fourth necessary condition of proper *PSG* is satisfied if and only if the global interference of the part surface to be machined and a generating surface of the gear cutting tool does not occur.

The fifth condition of proper PSG. Every gear tooth is bounded by several surfaces: two flank surfaces, two faces, top land surface, fillets, and bottom land surfaces. Most of these surfaces are usually machined in a single setup by the gear cutting tool of an appropriate design.

For machining of a gear tooth, the gear cutting tool has to reproduce corresponding portions of its generating surface. Neighboring portions of the generating surface of the gear cutting tool can occupy various locations relative to each other. To satisfy the fifth condition of proper *PSG*, the neighboring portions of the generating surface of the gear cutting tool must not intersect one another. Otherwise, transition surfaces between the neighboring surfaces of the gear tooth are unavoidable. Therefore,

> The fifth necessary condition of proper *PSG* is satisfied if and only if the neighboring portions of the generating surface of the gear cutting tool do not intersect each other.

In other words, *absence of transition surfaces on the gear tooth* is the fifth condition of proper *PSG*.

The sixth condition of proper PSG. When machining a gear, the so-called *discrete* surface $\mathcal{G}$ generation often occurs. Point contact of the surfaces $\mathcal{G}$ and T, as well as discrete representation of the generating surface T in the form of a set of distinct cutting edges (as the set of lines on the surface T) are the two major reasons for the discrete generation of the gear tooth surfaces.

In a limited period, it is impossible to generate a gear tooth surface $\mathcal{G}$ by a single moving point. Therefore, cusps on the machined gear tooth surface are unavoidable in this case.

The sixth necessary condition of proper *PSG* is formulated as follows:

> Cusp height on the machined gear tooth surface, if any, must be within the tolerance on the surface accuracy.

The maximal height h_Σ of cusps must be less or equal to the tolerance $[h]$ on the gear tooth surface accuracy.

The sixth necessary condition of proper *PSG* is satisfied if and only if the following inequality is satisfied

$$\mathbf{r}_g^{(a)} - \mathbf{r}_g^{(n)} \le \mathbf{n}_g^{(n)} [h] \tag{B.1}$$

where $\mathbf{r}_g^{(n)}$ is the position vector of a point of a nominal tooth flank surface $\mathcal{G}^{(n)}$, $\mathbf{r}_g^{(a)}$ is the position vector of a point of an actual gear tooth surface $\mathcal{G}^{(a)}$, $\mathbf{r}_g^{(t)}$ is the position vector of a point of a surface of tolerance $\mathcal{G}^{(t)}$, and $\mathbf{n}_g^{(n)}$ is the unit normal vector to surface $\mathcal{G}^{(n)}$.

Appendix C
Change of Surface Parameters

When designing a gear cutting tool, it is often necessary to treat two or more surfaces simultaneously. For example, the cutting edge of the cutting tool can be considered as the line of intersection of the generating surface T of the gear cutting tool by the rake surface R_s. The equation for the cutting edge cannot be derived on the premise of the equations for the surfaces T and R_s as long as the initial parameterization of the surfaces is improper.

When two surfaces ($\mathbf{r}_i$ and $\mathbf{r}_j$) are required to be treated simultaneously, it means that they have not been represented in a common reference system, but the parameters U_i and V_i of one of the surfaces, $\mathbf{r}_i = \mathbf{r}_i(U_i, V_i)$, have to be synchronized with the corresponding parameters U_j and V_j of another surface, $\mathbf{r}_j = \mathbf{r}_j(U_j, V_j)$. The procedure of changing of surface parameters is used for this purpose. Use of the procedure allows the representation of one of the surfaces, for example, the surface $\mathbf{r}_j = \mathbf{r}_j(U_j, V_j)$, in terms of the parameters U_i and V_i, say as $\mathbf{r}_j = \mathbf{r}_j(U_i, V_i)$.

If the parameterization of a surface is transformed by the equations $U^* = U^*(U, V)$ and $V^* = V^*(U, V)$, we obtain the new derivatives

$$\frac{\partial \mathbf{r}}{\partial U^*} = \frac{\partial \mathbf{r}}{\partial U} \cdot \frac{\partial U}{\partial U^*} + \frac{\partial \mathbf{r}}{\partial V} \cdot \frac{\partial V}{\partial U^*} \tag{C.1}$$

$$\frac{\partial \mathbf{r}}{\partial V^*} = \frac{\partial \mathbf{r}}{\partial U} \cdot \frac{\partial U}{\partial V^*} + \frac{\partial \mathbf{r}}{\partial V} \cdot \frac{\partial V}{\partial V^*} \tag{C.2}$$

so that

$$\mathbf{A}^* = \left[\frac{\partial \mathbf{r}}{\partial U^*} \middle| \frac{\partial \mathbf{r}}{\partial V^*} \right] = \mathbf{A} \cdot \mathbf{J} \tag{C.3}$$

where

$$\mathbf{J} = \begin{bmatrix} \dfrac{\partial U}{\partial U^*} & \dfrac{\partial U}{\partial V^*} \\ \dfrac{\partial V}{\partial U^*} & \dfrac{\partial V}{\partial V^*} \end{bmatrix} \tag{C.4}$$

is called the *Jacobian matrix* of the transformation.

It can be shown that the new fundamental matrix $\mathbf{G}^*$ is given by

$$\mathbf{G}^* = \mathbf{A}^{*T}\ \mathbf{A}^* = \mathbf{J}^T \mathbf{A}^T \mathbf{A} \mathbf{J} = \mathbf{J}^T \mathbf{G} \mathbf{J} \tag{C.5}$$

From this equation, we see by the properties of the determinants that $|\mathbf{G}^*| = |\mathbf{J}|^2 |\mathbf{G}|$. Using this result and Equation (C.2), we can show that the unit surface normal vector $\mathbf{n}$ is invariant under the transformation, as can be expected.

The transformation of the second fundamental matrix can similarly be shown, as given by

$$\mathbf{D}^* = \mathbf{J}^T \mathbf{D} \mathbf{J} \tag{C.6}$$

by differentiating Equation (C.2) and using the invariance of $\mathbf{n}$. From Equations (C.5) and (C.6), it can be shown that the principal curvatures and directions are invariant under the transformation.

We conclude that the unit normal vector $\mathbf{n}$ and the principal directions and curvatures are independent of the parameters used, and are therefore geometric properties of the surface itself. They should be continuous if the surface is to be tangent and curvature continuous.

Appendix D
Cutting Edge Geometry: Definition of the Major Parameters

The specification of the cutting edge geometry of a gear cutting tool requires a reference system. The corresponding reference system is composed of numerous vectors and planes through the point of interest of the cutting edge. It can be constructed in several steps.

Two main elements for the construction of the reference system are used in this text: the cutting edge and the vector of its resultant motion relative to the work.

Cutting edge. Generally speaking, the cutting edge of the gear cutting tool can be geometrically interpreted as a segment of a spatial curve that features a certain curvature and torsion.

Torsion of the cutting edge is not considered here. Thus, geometrical interpretation of the actual cutting edge is reduced to a segment of a planar curve.

For the analysis of the cutting tool geometry, it is not required to consider the whole cutting edge. In most practical cases, it is sufficient to consider just a segment of infinitesimally short length of the cutting edge. In this work, this infinitesimally short portion of the cutting edge is referred to as the "elementary cutting edge." Geometry of the elementary cutting edge can be specified in terms of its radius of curvature R_{ce} and length dl_{ce}. Curvature of the cutting edge k_{ce} that is reciprocate to its radius of curvature ($k_{ce} = R_{ce}^{-1}$) can be used instead of radius R_{ce}.

In particular cases of the analysis, curvature of the elementary cutting edge could be unimportant. In such simplified cases, the elementary cutting edge reduces to a straight-line segment of length dl_{ce} (Figure D.1). Unit vector $\mathbf{c}_e$ is along the elementary cutting edge CE. The unit vector $\mathbf{c}_e$ is referred to as the "cutting edge vector."

Vector of the resultant motion. The kinematics of a gear machining operation is complex in nature. In general, instant motion of the point of interest *m* within the elementary cutting edge can be interpreted as an "instant screw motion." Parameters of the instant screw motion can be expressed in terms of the resultant translation and the resultant rotation. The resultant speed of relative motion $\mathbf{V}_\Sigma$ of the point of interest of the cutting edge with respect to the surface of cut is equal to the summa of the instant translation and linear speed of the instant rotation (Figure D.1).

The plane of cut. The first reference plane to be introduced is the plane of cut P_{cv}. At the point of interest *m* the plane of cut is the plane through the unit vector $\mathbf{c}_e$ of the cutting edge and the vector $\mathbf{V}_\Sigma$ of the relative motion of the cutting edge. This immediately yields an expression

$$(\mathbf{r}_{cv} - \mathbf{r}_m) \cdot \mathbf{c}_e \times \mathbf{v}_\Sigma = 0 \tag{D.1}$$

for the analytical representation of the plane of cut P_{cv}. It is assumed here that all three vectors—$\mathbf{c}_e$, $\mathbf{V}_\Sigma$, and the position vector of the point of interest $\mathbf{r}_m$—within the cutting edge are given in a certain common Cartesian coordinate system.

The unit normal vector $\mathbf{n}_{cv}$ to the surface of cut can be computed from the equation

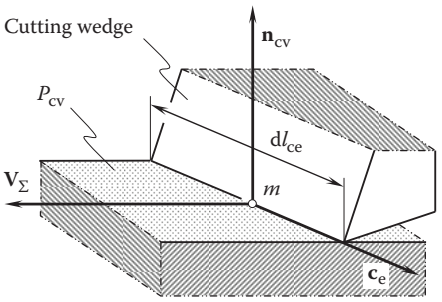

FIGURE D.1
Main elements for the construction of the reference system for the specification of the cutting.

$$\mathbf{n}_{cv} = \mathbf{v}_\Sigma \times \mathbf{c}_e \tag{D.2}$$

where the unit vector of the speed of the relative motion $\mathbf{v}_\Sigma$ is equal to $\mathbf{v}_\Sigma = \mathbf{V}_\Sigma/|\mathbf{V}_\Sigma|$.

The unit normal vector is pointed outward of the bodily side toward the void side of the workpiece. To comply with this requirement, the order of the vectors $\mathbf{c}_e$ and $\mathbf{V}_\Sigma$ in Equation (D.2) is required to be properly chosen.

It is important to point out that at the point of interest within the cutting edge, the plane of cut P_{cv} is tangent to the surface of cut.

Cutting edge geometry in the plane of cut. The angle of inclination of the cutting edge is the only geometrical parameter of the cutting edge that is measured in the plane of cut. This angle specifies the orientation of the cutting edge CE relative to the vector $\mathbf{V}_\Sigma$ of the resultant motion of the cutting edge.

The inclination angle λ is the angle that the vector $\mathbf{V}_\Sigma$ forms with the unit vector $\mathbf{n}_{ce}$. The vector $\mathbf{n}_{ce}$ is orthogonal to the cutting edge (Figure D.2a). If one is observing from the end of the unit normal vector $\mathbf{n}_{cv}$ to the surface of cut P_{cv}, the positive angle λ is measured in a counterclockwise direction, whereas the negative angle λ is measured in a clockwise direction (see Figure D.2b).

When the equality $\lambda = 0°$ is valid, the cutting is referred to as "orthogonal cutting." Otherwise, when $\lambda \neq 0°$, then a more general case of cutting, say the "oblique cutting," is observed.

Major frictions of the cutting tool (e.g., chip deformation, direction of chip flow over the rake surface) depend on the actual value of the angle of inclination λ.

The algebraic value of the angle of inclination λ can be computed from (Figure D.2b):

$$\lambda = \angle(\mathbf{c}_e, \mathbf{v}_\Sigma) - 90° = -\tan^{-1}\left(\frac{\mathbf{c}_e \cdot \mathbf{v}_\Sigma}{|\mathbf{c}_e \times \mathbf{v}_\Sigma|}\right) \tag{D.3}$$

Equation (D.3) returns a signed value of the inclination angle λ.

For gear cutting tools of various designs, the actual value of the angle of inclination λ varies within the interval $\lambda \cong \pm 10°$. In particular cases of gear machining, the inclination angle reaches the value of $\lambda = \pm 80°$. This can be observed in gear shaving operations.

The major section plane. The unit normal vector $\mathbf{n}_{cv}$ to the surface of cut and vector $\mathbf{V}_\Sigma$ of the resultant relative motion of the cutting edge relative to the surface of cut specify a reference plane that is referred to as the *major section plane*. The major section plane is the plane through the vectors $\mathbf{n}_{cv}$ and $\mathbf{V}_\Sigma$ at the point of interest m within the cutting edge. It

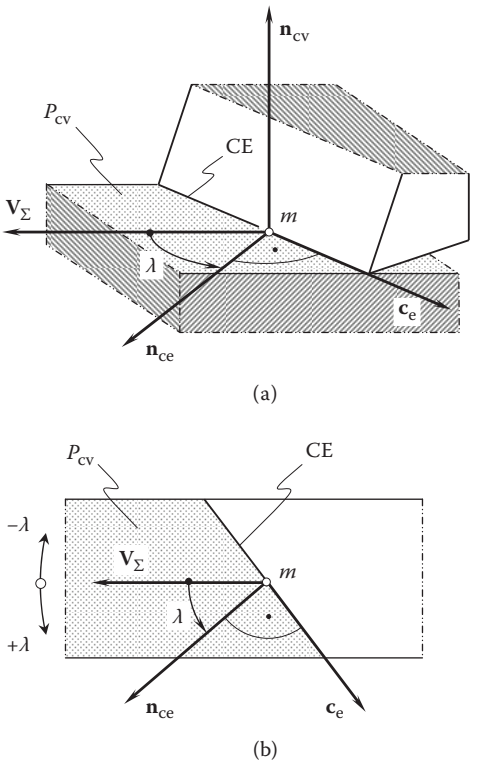

FIGURE D.2
Definition of the angle of inclination λ of the cutting edge geometry of a gear cutting tool.

is designated below as P_{ms} (Figure D.3a). The major section plane is perpendicular to the plane of cut P_{cv}.

The equation for the major section plane P_{ms} in terms of the vectors $\mathbf{v}_\Sigma$ and $\mathbf{n}_{cv}$ yields representation in the form

$$(\mathbf{r}_{ms} - \mathbf{r}_m) \cdot \mathbf{n}_{cv} \times \mathbf{v}_\Sigma = 0 \tag{D.4}$$

where $\mathbf{r}_{ms}$ denotes position vector of a point of the major section plane.

Cutting edge geometry in the major section plane. Four angles are measured within the major section plane of the cutting edge of the gear cutting tool: (1) the rake angle γ_m, (2) the clearance angle α_m, (3) the cutting wedge angle β_m, and (4) the angle of cutting δ_m.

The rake angle γ_m. For the determination of the rake angle γ_m, a unit vector $\mathbf{a}$ is used. Vector $\mathbf{a}$ is tangent to the line of intersection of the rake surface R_s by the major section plane P_{ms} (Figure D.3b). By definition, the rake angle γ_m is equal to the angle between the unit normal vector $\mathbf{n}_{cv}$ to the plane of cut and the unit vector $\mathbf{a}$. Its value can be computed from as follows

$$\gamma_m = \angle(\mathbf{n}_{cv}, \mathbf{a}) = \tan^{-1}\left(\frac{|\mathbf{n}_{cv} \times \mathbf{a}|}{\mathbf{n}_{cv} \cdot \mathbf{a}}\right) \tag{D.5}$$

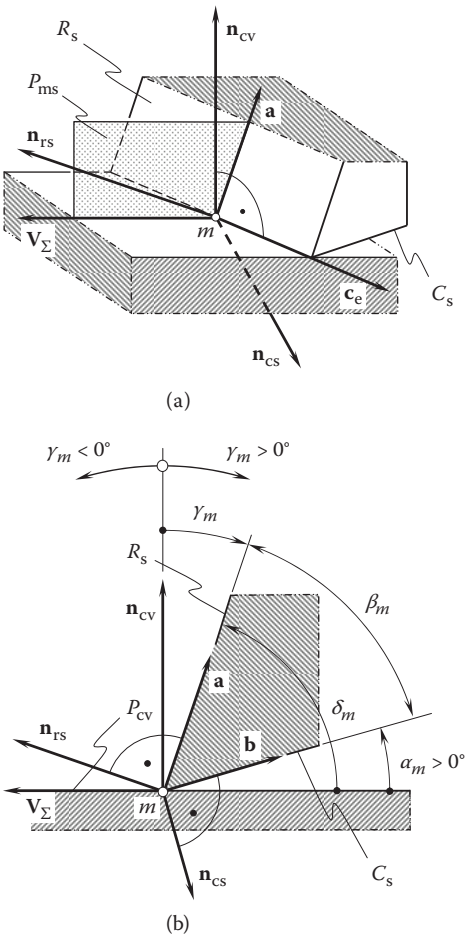

FIGURE D.3
Geometry of the active part of a gear cutting tool in the major section plane P_{ms}.

The rake angle γ_m is positive when the vector $\mathbf{n}_{cv}$ does not pass through the cutting wedge, and negative when it does (Figure D.3b).

The clearance angle α_m. For the determination of the clearance angle α_m, a unit vector $\mathbf{b}$ is used. Vector $\mathbf{b}$ is tangent to the line of intersection of the clearance surface C_s by the major section plane P_{ms} (Figure D.3b). By definition, the clearance angle α_m is the angle that complements to 90° the angle between the unit normal vector $\mathbf{n}_{cs}$ to the clearance surface C_s and the unit vector $\mathbf{b}$. Its value can be computed as (Figure D.3b)

$$\alpha_m = 90° - \angle(\mathbf{n}_{cs}, \mathbf{b}) = \tan^{-1}\left(\frac{\mathbf{n}_{cs} \cdot \mathbf{b}}{|\mathbf{n}_{cs} \times \mathbf{b}|}\right) \tag{D.6}$$

The clearance angle α_m is always positive ($\alpha_m > 0°$).

The cutting wedge angle β_m is the angle that the unit vector $\mathbf{a}$ makes with the unit vector $\mathbf{b}$ (see Figure D.3b):

$$\beta_m = \angle(\mathbf{a}, \mathbf{b}) = \tan^{-1}\left(\frac{|\mathbf{a}\times\mathbf{b}|}{\mathbf{a}\cdot\mathbf{b}}\right) \tag{D.7}$$

The following equality

$$\beta_m = 90° - (\alpha_m + \gamma_m) \tag{D.8}$$

is always observed within the major section plane P_{ms}.

The angle of cutting δ_m is the angle that the unit vector **a** makes with the opposite direction of the vector $\mathbf{V}_\Sigma$ of the resultant motion of the cutting edge relative to the surface of cut (see Figure D.3b)

$$\delta_m = 180° - \angle(\mathbf{V}_\Sigma, \mathbf{a}) = -\tan^{-1}\left(\frac{|\mathbf{v}_\Sigma\times\mathbf{a}|}{\mathbf{v}_\Sigma\cdot\mathbf{a}}\right) \tag{D.9}$$

The equality

$$\delta_m = (90° - \gamma_m) \tag{D.10}$$

is always observed within the major section plane P_{ms}.

Roundness of the cutting edge ρ_m can also be measured within the major section plane P_{ms}.

The normal section plane. Before proceeding with the analysis of the geometry of the elementary cutting edge of the gear cutting tool, let us construct a unit vector $\mathbf{n}_{ce}$ through the point of interest *m* of the cutting edge (Figure D.4a). The vector $\mathbf{n}_{ce}$ is within the plane of cut P_{cv} and is perpendicular to the elementary cutting edge ($\mathbf{n}_{ce} \perp \mathbf{c}_e$). By definition, the normal section plane P_{ns} is the plane through the unit normal vectors $\mathbf{n}_{ce}$ and $\mathbf{n}_{cv}$. Therefore, the position vector of a point $\mathbf{r}_{ns}$ of the normal section plane P_{ns} can be determined from the vector equation

$$(\mathbf{r}_{ns} - \mathbf{r}_m)\cdot\mathbf{n}_{ce}\times\mathbf{n}_{cv} = 0 \tag{D.11}$$

Because the normal section plane P_{ns} is perpendicular to the elementary cutting edge, this yields another expression

$$(\mathbf{r}_{ns} - \mathbf{r}_m)\cdot\mathbf{c}_e = 0 \tag{D.12}$$

for the position vector of a point $\mathbf{r}_{ns}$ of the normal section plane P_{ns}.

Cutting edge geometry in the normal section plane. Four angles are measured within the normal section plane of the cutting edge of the gear cutting tool: (1) the rake angle γ_N, (2) the clearance angle α_N, (3) the cutting wedge angle β_N, and (4) the angle of cutting δ_N.

The normal rake angle. Orientation of the rake surface R_s of the elementary cutting edge relative to the plane of cut P_{cv} can be specified in terms of the normal rake angle. For this purpose, a unit vector **c** through the point of interest *m* of the cutting edge is constructed. Vector **c** is tangent to the line of intersection of the rake surface R_s by the normal section plane P_{ns}.

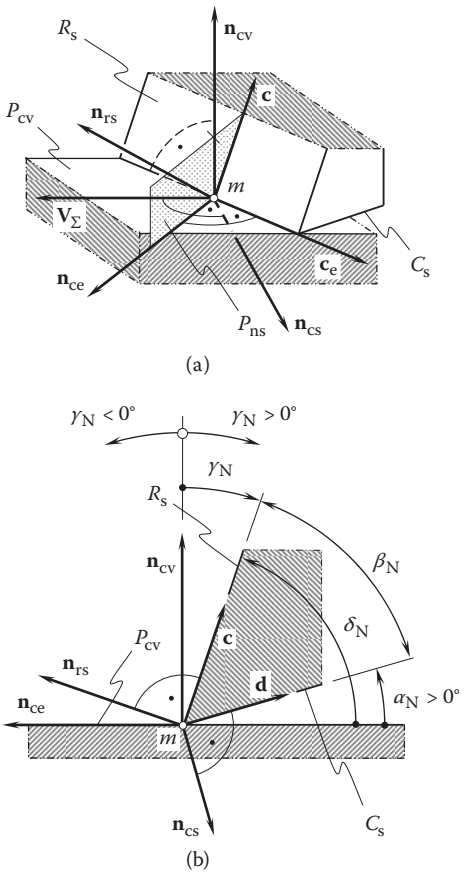

FIGURE D.4
Geometry of the active part of a gear cutting tool in the normal section plane P_{ns}.

The normal rake angle γ_N is the angle that the unit normal vector $\mathbf{n}_{cv}$ to the plane of cut P_{cv} forms with the unit vector $\mathbf{c}$. The value of the angle γ_N is measured from the vector $\mathbf{n}_{cv}$ toward the rake surface R_s. The normal rake angle γ_N is positive when the unit normal vector $\mathbf{n}_{cv}$ does not pass through the cutting wedge of the tool, and negative when it does (Figure D.4b).

It is convenient to define the normal rake angle γ_N as the angle that complements to 90° the angle between the unit normal vectors $\mathbf{n}_{cv}$ and $\mathbf{n}_{rs}$ (see Figure D.4b):

$$\gamma_N = \angle(\mathbf{n}_{cv}, \mathbf{c}) = 90° - \angle(\mathbf{n}_{cv}, \mathbf{n}_{rs}) = \tan^{-1}\left(\frac{\mathbf{n}_{cv} \cdot \mathbf{n}_{rs}}{|\,\mathbf{n}_{cv} \times \mathbf{n}_{rs}\,|}\right) \tag{D.13}$$

Gear cutting tools of various designs feature the normal rake angle γ_N within the interval $\gamma_N = 10–15°$.

The normal clearance angle. Configuration of the clearance surface C_s of the elementary cutting edge with respect to the plane of cut P_{cv} can be specified in terms of the normal clearance angle α_N. To derive a formula for the computation of the normal clearance angle α_N, a unit vector $\mathbf{d}$ through the point of interest m of the cutting edge is constructed. Vector

d is tangent to the line of intersection of the clearance surface C_s by the normal section plane P_{ns}.

The normal clearance angle α_N is the angle that the unit normal vector $-\mathbf{n}_{ce}$ makes with the unit vector **d**. The value of the clearance angle α_N is measured from the plane of cut P_{cv} toward the clearance surface C_s. The normal rake angle α_N is always positive ($\alpha_N > 0°$). Only within a narrow land along the cutting edge can the normal clearance angle α_N be equal to zero or it can even be negative ($\alpha_N \leq 0°$). However, this is not common for standard gear cutting tools. Usually, gear cutting tools feature normal clearance angles α_N of very small value (up to $\alpha_N = 30' \div 2°$).

The normal clearance angle α_N can be defined as the angle that complements to 180° the angle between the unit normal vectors $\mathbf{n}_{cv}$ and $\mathbf{n}_{cs}$ (see Figure D.4b):

$$\alpha_N = \angle(-\mathbf{n}_{ce}, \mathbf{d}) = 180° - \angle(\mathbf{n}_{cv}, \mathbf{n}_{cs}) = -\tan^{-1}\left(\frac{|\mathbf{n}_{cv} \times \mathbf{n}_{cs}|}{\mathbf{n}_{cv} \cdot \mathbf{n}_{cs}}\right) \tag{D.14}$$

For cutting tools of various designs, the optimal value of the normal clearance angle α_N is usually within the interval $\alpha_N = 10–20°$.

The mandatory relationship. For a workable cutting tool, satisfaction of the relationship $\mathbf{n}_{cs} \cdot \mathbf{n}_{cv} < 0°$ is a must (see Figure D.4). Violation of the relationship is allowed only within a narrow land along the cutting wedge.

The normal cutting wedge angle is the angle that the rake plane R_s makes with the clearance plane C_s. The value of the normal cutting wedge angle β_N can be computed from the equation (see Figure D.4b)

$$\beta_N = \angle(\mathbf{c}, \mathbf{d}) = \tan^{-1}\left(\frac{|\mathbf{c} \times \mathbf{d}|}{\mathbf{c} \cdot \mathbf{d}}\right) \tag{D.15}$$

The normal cutting wedge angle β_N can be expressed in terms of the unit normal vector $\mathbf{n}_{rs}$ to the rake surface R_s and $\mathbf{n}_{cs}$ to the clearance surface C_s

$$\beta_N = 180° - \angle(\mathbf{n}_{rs}, \mathbf{n}_{cs}) = -\tan^{-1}\left(\frac{|\mathbf{n}_{rs} \times \mathbf{n}_{cs}|}{\mathbf{n}_{rs} \cdot \mathbf{n}_{cs}}\right) \tag{D.16}$$

The following identity

$$\beta_N = 90° - (\alpha_N + \gamma_N) \tag{D.17}$$

is also valid for the normal cutting wedge angle β_N.

The normal angle of cutting is the angle that the clearance plane C_s makes with the plane of cut P_{cv}. The value of this angle δ_N is given by (see Figure D.4b)

$$\delta_N = \angle(-\mathbf{n}_{ce}, \mathbf{c}) = -\tan^{-1}\left(\frac{|\mathbf{n}_{ce} \times \mathbf{c}|}{\mathbf{n}_{ce} \cdot \mathbf{c}}\right) \tag{D.18}$$

The normal angle of cutting δ_N can be expressed in terms of the unit normal vectors $\mathbf{n}_{cv}$ to the surface of cut P_{cv} and $\mathbf{n}_{rs}$ to the rake surface R_s

$$\delta_N = \angle(\mathbf{n}_{cv}, \mathbf{n}_{rs}) = \tan^{-1}\left(\frac{|\mathbf{n}_{cv} \times \mathbf{n}_{rs}|}{\mathbf{n}_{cv} \cdot \mathbf{n}_{rs}}\right) \tag{D.19}$$

The equality

$$\delta_N = 90° - \gamma_N \tag{D.20}$$

is also observed within the normal section plane P_{ns}.

More equations can be derived for the investigation of the cutting edge geometry of particular designs of gear cutting tools.

Roundness of the cutting edge. The cutting edge of the gear cutting tool is not absolutely sharp. In reality, there exists a transition surface that connects the rake surface R_s and the clearance surface C_s. This transition surface is supposed to have a circular profile of a certain radius that is thought of as the radius ρ_N of the cutting edge roundness (Figure D.5).

Various methods can be used to determine the roundness of the cutting edge. It can be determined experimentally, for example, from etching tests. Roundness of the cutting wedge of a cutting tool made of high speed steel is usually in the range of $\rho_N = 20–50$ μm, whereas that of a cutting tool made of sintered carbide can be as low as $\rho_N = 10–30$ μm. For diamond inserts, roundness drops down up to $\rho_N = 5–8$ μm and can even be reduced to $\rho_N \cong 2$ μm.

The cutting edge roundness ρ_N affects the material removal process in metal cutting. The effect of the cutting edge roundness is more substantial when a thin chip is being removed, especially when the stock to be removed is of the same range as the cutting edge roundness ρ_N. When the stock thickness is about 0.003 mm or less, the rake angle γ_N does not affect the material removal process and can thus be neglected.

When the actual value of roundness ρ_N is known in the normal section plane P_{ns}, the corresponding value of the roundness ρ_m of the cutting edge in the major section plane P_{ms} can be computed using Mensnier's equation

$$\rho_m = \rho_N \cos\lambda \tag{D.21}$$

Special care must be taken when the cutting edge roundness is necessary for finishing gear cutting tools (e.g., shave cutters, gear broach tools).

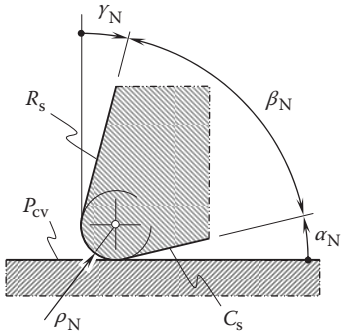

FIGURE D.5
Roundness ρ_N of the cutting edge of the gear cutting tool in the normal plane section P_{ns}.

On correlation of the cutting edge geometry of the gear cutting tool measured within the major section plane and the normal section plane. The geometry of the elementary cutting edge measured in a reference plane correlates with the corresponding geometry of the elementary cutting edge measured in another reference plane. For example, once the geometric parameters of the elementary cutting edge are known in the plane of cut P_{cv} and in the normal section plane P_{ns}, the corresponding geometric parameters can be computed in the major section plane P_{ms} and vice versa.

To demonstrate the correlation, consider the computation of the rake angle γ_m that is measured in the major section plane P_{ms}. It is assumed below that the geometry of the elementary cutting edge in the plane of cut P_{cv} as well as in the normal section plane P_{ns} is known.

For the derivation of equations for the geometry of the active part of cutting tools, implementation of elements of vector calculus is helpful.* For this purpose, a local Cartesian coordinate system $x_m y_m z_m$ is associated with the elementary cutting wedge as shown in Figure D.6.

Vector **A** is constructed so that it is tangent to the line of intersection of the rake surface R_s by the normal section plane P_{ns}. Vector **A** is of a length whose projection onto the $x_m y_m$ coordinate plane is equal to $\mathrm{pr}_{xy}\,\mathbf{A} = 1$. This yields an analytical expression for vector **A** in vector form

$$\mathbf{A} = -\mathbf{i} \cdot \sin\lambda + \mathbf{j} \cdot \cot\gamma_N - \mathbf{k} \cdot \cos\lambda \tag{D.22}$$

The unit vector **b** is constructed so that it is tangent to the line of intersection of the rake surface R_s by the major section plane P_{ms}. In the local coordinate system $x_m y_m z_m$, the unit vector **b** yields representation in the form

$$\mathbf{b} = -\mathbf{j} \cdot \cos\gamma_m + \mathbf{k} \cdot \sin\gamma_m \tag{D.23}$$

Ultimately, the unit vector $\mathbf{c}_e$ is along the elementary cutting edge

$$\mathbf{c}_e = \mathbf{i} \cdot \cos\lambda - \mathbf{j} \cdot \sin\lambda \tag{D.24}$$

By construction, vectors **A**, **b**, and $\mathbf{c}_e$ are within the plane that is tangent to the cutting edge *AB* at the point of interest *m*. Thus, the mixed product of the coplanar vectors **A**, **b**, and $\mathbf{c}_e$ is identical to zero ($\mathbf{A} \times \mathbf{b} \cdot \mathbf{c}_e \equiv 0$). Therefore, the equality

$$\begin{vmatrix} -\sin\lambda & \cot\gamma_N & -\cos\lambda \\ 0 & -\cos\gamma_m & \sin\gamma_m \\ \cos\lambda & 0 & -\sin\lambda \end{vmatrix} = 0 \tag{D.25}$$

is observed.

Equation (D.25) casts into the equation

$$\gamma_m = \cot^{-1}[\cot\gamma_N \cos\lambda] \tag{D.26}$$

for the computation of the rake angle γ_m.

* To the best of the author's knowledge, Mozhayev [46] was the first to use (1948) elements of vector calculus for solving problems relating to the geometry of the active part of a cutting tool.

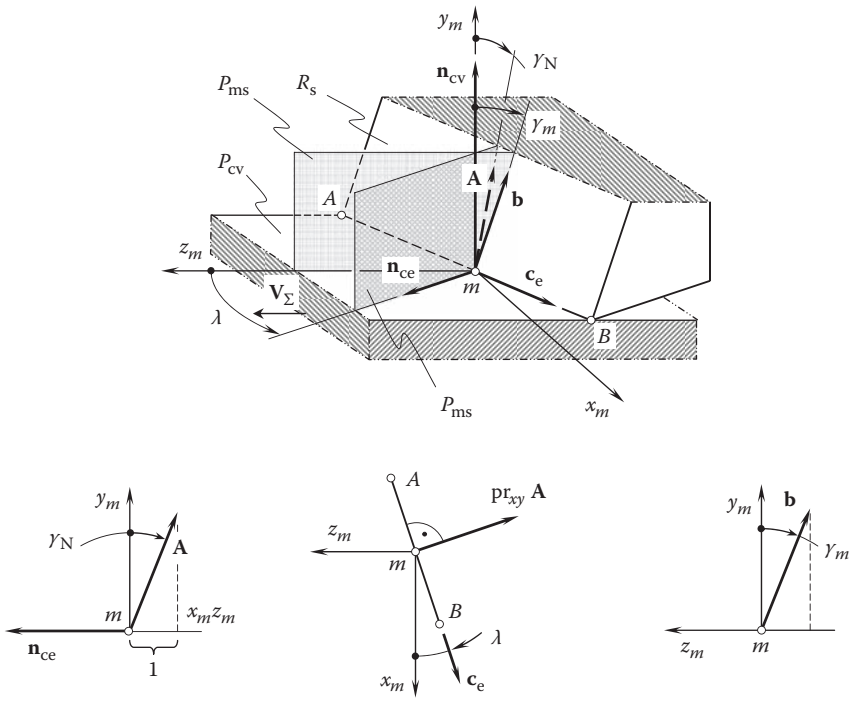

FIGURE D.6
Cutting edge geometry of the gear cutting tool measured within the major section plane P_{ms} and within the normal section plane P_{ns}.

Similarly, the equation

$$\alpha_m = \tan^{-1}(\tan\alpha_N \cos\lambda) \tag{D.27}$$

can be derived for the computation of the clearance angle α_m.

The main reference plane P_{mr} is orthogonal to the vector $\mathbf{V}_\Sigma$ of the resultant motion of the cutting edge with respect to the surface of cut (Figure D.7). Therefore, an expression for position vector of a point $\mathbf{r}_{mr}$ of the main reference plane can be represented in vector form as

$$(\mathbf{r}_{mr} - \mathbf{r}_m) \cdot \mathbf{v}_\Sigma = 0 \tag{D.28}$$

The reference plane P_{mr} can be also defined as a plane through the unit normal vector $\mathbf{n}_{cv}$ to the surface of cut P_{cv} and through the unit vector $\mathbf{m}_{cv}$ that is orthogonal to the vector $\mathbf{V}_\Sigma$

$$(\mathbf{r}_{mr} - \mathbf{r}_m) \cdot \mathbf{n}_{cv} \times \mathbf{m}_{cv} = 0 \tag{D.29}$$

where the unit $\mathbf{m}_{cv}$ is within the surface of cut P_{cv} (Figure D.7a).

Cutting edge geometry in the main reference plane. Three angles are measured within the main reference plane: (1) the major cutting edge approach angle φ_e, (2) the minor cutting edge approach angle φ_{e1}, and (3) tool tip (nose) angle ε_e.

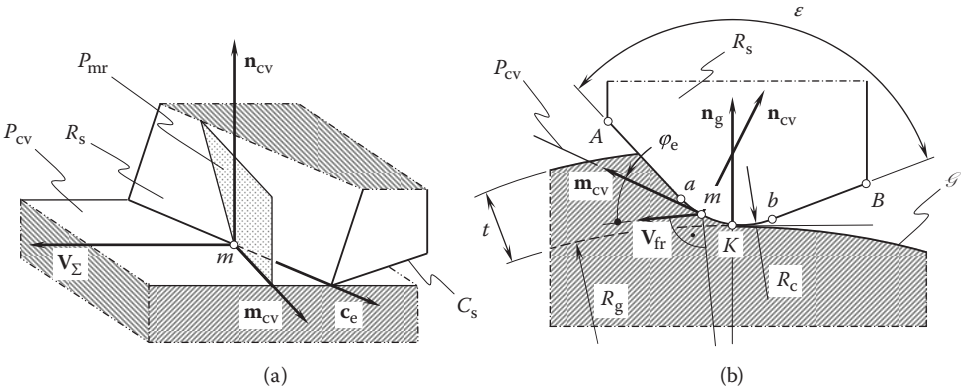

FIGURE D.7
Geometry of the elementary cutting edge within the main reference plane P_{mr}.

The major cutting edge approach angle φ_e is the angle that the vector $\mathbf{V}_{fr}$ of the feed rate motion makes with the unit vector $\mathbf{m}_{cv}$ (Figure D.8). The major cutting edge approach angle φ_e is an acute angle ($0° < \varphi_e \leq 90°$).

For the computation of the major cutting edge approach angle φ_e, the following equation

$$\varphi_e = \angle(\mathbf{V}_{fr}, \mathbf{m}_{cv}) = \tan^{-1}\left(\frac{|\mathbf{V}_{fr} \times \mathbf{m}_{cv}|}{\mathbf{V}_{fr} \cdot \mathbf{m}_{cv}}\right) \tag{D.30}$$

can be used.

The minor cutting edge approach angle. Similarly, the minor cutting edge approach angle φ_{1e} is the angle that the vector $\mathbf{V}^*_{fr}$ makes with the unit vector $\mathbf{m}^*_{cv}$ (Figure D.8). The minor cutting edge approach angle φ_{1e} is also an acute angle ($0° \leq \varphi_{1e} \leq 90°$). Moreover, usually the value of the angle φ_{1e} does not exceed the value of the corresponding angle φ_e.

To compute for the minor cutting edge approach angle φ_{1e}, the following formula can be used

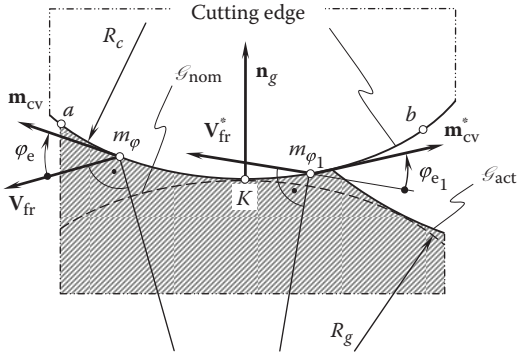

FIGURE D.8
The major φ_e and minor φ_{e1} cutting edge approach angles of the elementary cutting edge.

$$\varphi_{e1} = 180^\circ - \angle(\mathbf{V}^*_{cv}, -\mathbf{m}^*_{cv}) = -\tan^{-1}\left(\frac{|\mathbf{V}^*_{cv} \times \mathbf{m}^*_{cv}|}{\mathbf{V}^*_{cv} \cdot \mathbf{m}^*_{cv}}\right) \tag{D.31}$$

where vector $\mathbf{V}^*_{cv}$ denotes the feed rate at the point $m_{\varphi 1}$ of the cutting edge and vector $\mathbf{m}^*_{cv}$ denotes the unit vector within the plane of cut through the point $m_{\varphi 1}$ of the cutting edge. The unit vector $\mathbf{m}^*_{cv}$ is very similar to the unit vector $\mathbf{m}_{cv}$.

The minor cutting edge approach angle φ_{1e} is computed for the portion of the cutting edge within the residual cusps on the machined gear tooth flank. For the remaining portion of the cutting edge, it does not affect the material removal process.

The tool tip (nose) angle ε can be determined just for the tip of a cutting tool. The angle ε can be computed as

$$\varepsilon = 180^\circ - (\varphi_e + \varphi_{1e}) \tag{D.32}$$

The angle that makes the major and the minor cutting edges of the gear cutting tool is designated as ε^*. This angle is measured within the rake surface R_s. Angle ε^* yields computation of the tool tip angle ε. The tool tip angle ε can be thought of as the projection of the angle ε^* onto to the main reference plane P_{mr}. Conversely, the angle ε^* is the projection of the tool tip angle ε onto the rake face R_s.

The tip of a gear cutting tool coincides with the point of contact K of the generating surface T of the cutting tool and the gear tooth flank surface $\mathscr{G}$ being machined (see Figure D.8). At point K, the tool tip angle $\varepsilon = 180^\circ$.

The reference plane of chip flow. This particular reference plane is of importance for gear cutting tools featuring an increased angle of inclination λ of the cutting edges.

In case of free orthogonal cutting (when the inclination angle $\lambda = 0^\circ$), the vector of chip motion over the rake surface is orthogonal to the cutting edge. Kinematical geometric parameters of the cutting edge are specified in the normal section plane P_{ns}. The correctness of this approach has been comprehensively validated through experiments.

Oblique cutting (when the angle of inclination $\lambda \neq 0^\circ$) is a much more complex phenomenon than orthogonal cutting. This is mostly because the deformation of material does not occur in the major reference plane P_{mr}, but within a certain volume, and thus deformation of material occurs in 3-D space. Inclined cutting is much less understood than orthogonal cutting.

However, the results of the investigation of orthogonal cutting can also be adjusted approximately for implementation in the analysis of oblique cutting.

In an attempt to specify (approximately) the poorly understood oblique cutting, in terms of comprehensively investigated orthogonal cutting, the term *chip-flow reference plane* was introduced. The chip-flow reference plane P_{cf} is the plane through the vectors $\mathbf{V}_\Sigma$ and $\mathbf{V}_{cf}$. Here, $\mathbf{V}_{cf}$ denotes the vector of the chip flow over the rake surface. Vector $\mathbf{V}_{cf}$ is located within the rake plane R_s. It forms the chip-flow angle η with the perpendicular to the cutting edge (Figure D.9). The unit vector $\mathbf{c}$ within the rake plane R_s that is perpendicular to the cutting edge is shown in Figure D.4. Here, the equality $\mathbf{c} = \mathbf{n}_{ce} \times \mathbf{c}_e$ is observed.

Vector $\mathbf{V}_{cf}$ is orthogonal to the unit normal vector $\mathbf{n}_{rs}$ to the rake surface R_s. Therefore, the equality $\mathbf{V}_{cf} \cdot \mathbf{n}_{rs} = 0$ is valid.

At the point of interest, the chip-flow reference plane P_{cf} is the plane through vectors $\mathbf{V}_\Sigma$ and $\mathbf{V}_{cf}$ at point m. This yields

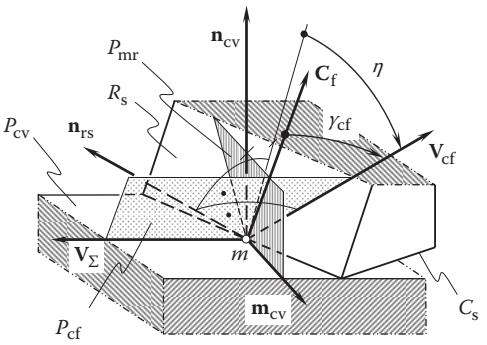

FIGURE D.9
Geometry of the active part of a cutting tool in the chip-flow reference plane P_{cf}.

$$(\mathbf{r}_{cf} - \mathbf{r}_m) \cdot \mathbf{V}_\Sigma \times \mathbf{V}_{cf} = 0 \tag{D.33}$$

where $\mathbf{r}_{cf}$ is the position vector of a point of the chip-flow reference plane P_{cf}.

The chip flow rake angle. For oblique cutting, it is required to specify the rake angle taking into account the direction of chip flow over the rake face.

The chip flow rake angle γ_{cf} is measured within the chip-flow reference plane P_{cf}.

The chip flow rake angle γ_{cf} is the angle that the vector $\mathbf{V}_{cf}$ of chip flow over the rake plane makes with the main reference plane P_{mr} (Figure D.9). This angle is measured within the chip-flow reference plane P_{cf}. Therefore, the rake angle γ_{cf} can be computed as

$$\gamma_{cf} = \angle(\mathbf{V}_\Sigma, \mathbf{V}_{cf}) - 90^\circ = \tan^{-1}\left(\frac{|\mathbf{V}_\Sigma \times \mathbf{V}_{cf}|}{\mathbf{V}_\Sigma \cdot \mathbf{V}_{cf}} - 90^\circ\right) = \tan^{-1}\left(\frac{\mathbf{V}_\Sigma \cdot \mathbf{V}_{cf}}{|\mathbf{V}_\Sigma \times \mathbf{V}_{cf}|}\right) \tag{D.34}$$

Let us assume that the unit vectors $\mathbf{c}_e$, $\mathbf{m}_{cv}$, and $\mathbf{n}_{cv}$ are the direct vectors of the coordinate axes of the local Cartesian coordinate system $x_m y_m z_m$ (not shown in Figure D.9). Thus, for the unit vector $\mathbf{v}_\Sigma = \mathbf{V}_\Sigma / |\mathbf{V}_\Sigma|$, one can derive

$$\mathbf{v}_\Sigma = -\mathbf{i} \cdot \sin\lambda + \mathbf{j} \cdot \cos\lambda \tag{D.35}$$

The vector $\mathbf{v}_{cf}$ is of a length whose projection onto the coordinate plane $y_m z_m$ (i.e., the coordinate plane through the unit vectors $\mathbf{m}_{cv}$ and $\mathbf{n}_{cv}$) is a unit vector. Therefore, the following equality is valid for vector $\mathbf{v}_{cf}$

$$\mathbf{v}_{cf} = \mathbf{i} \cdot \tan\eta - \mathbf{j} \cdot \sin\gamma_N + \mathbf{k} \cdot \cos\gamma_N \tag{D.36}$$

Substituting Equations (D.35) and (D.36) into Equation (D.34), one can come up with the following equation for the computation of the chip flow rake angle γ_{cf}

$$\sin\gamma_{cf} = \sin\eta \sin\lambda + \cos\eta \cos\lambda \sin\gamma_N \tag{D.37}$$

Usually, the angle of inclination does not exceed $\lambda \leq 45°$. Under such a scenario, the approximate equality $\eta \cong \lambda$ is valid. This immediately leads to Stabler's equation for the computation of the rake angle γ_{cf} [188]

$$\sin \gamma_{cf} \cong \sin^2 \lambda + \cos^2 \lambda \sin \gamma_N \cong 1 - \cos^2 \lambda (1 - \sin \gamma_N) \tag{D.38}$$

The derived equations are valid for free oblique cutting. They enable computation of the chip flow rake angle γ_{cf} for any actual value of the inclination angle λ.

Computation of the chip-flow angle η is a challenging problem. A reliable value for the chip-flow angle η can be obtained experimentally.

Notation

$\mathrm{Cnf}_R(\mathscr{G}/T)$	Indicatrix of conformity of the work gear tooth surface $\mathscr{G}$ and the generating surface T of the gear cutting tool at a current contact point K
$C_{1.\mathrm{g}}$, $C_{2.\mathrm{g}}$	The first and second principal plane sections of the gear tooth flank $\mathscr{G}$
$C_{1.T}$, $C_{2.T}$	The first and the second principal plane sections of generation surface T of the gear cutting tool
$\mathscr{E}$	A characteristic line
E_{g}, F_{g}, G_{g}	Fundamental magnitudes of the first order of the gear tooth surface $\mathscr{G}$
E_T, F_T, G_T	Fundamental magnitudes of the first order of generating surface T of the gear cutting tool
$\mathbf{Eu}(\psi,\theta,\varphi)$	Operator of the Eulerian transformation
$\mathscr{G}$	Gear tooth surface
K	Point of contact of the surfaces $\mathscr{G}$ and T (or a point within a line of contact of the surfaces P and T)
L_{g}, M_{g}, $N_{\mathbf{g}}$	Fundamental magnitudes of the second order of the gear tooth surface $\mathscr{G}$
L_T, M_T, N_T	Fundamental magnitudes of the second order of generating surface T of the gear cutting tool
$P_{\mathbf{ln}}$	Pitch line in the gear machining mesh
$\mathbf{Rl}_x(\varphi_y, Y)$	Operator of rolling over a plane (Y axis is the axis of rotation, X axis is the axis of translation)
$\mathbf{Rl}_z(\varphi_y, Y)$	Operator of rolling over a plane (Y axis is the axis of rotation, Z axis is the axis of translation)
$\mathbf{Rl}_y(\varphi_x, X)$	Operator of rolling over a plane (X axis is the axis of rotation, Y axis is the axis of translation)
$\mathbf{Rl}_z(\varphi_x, X)$	Operator of rolling over a plane (X axis is the axis of rotation, Z axis is the axis of translation)
$\mathbf{Rl}_x(\varphi_z, Z)$	Operator of rolling over a plane (Z axis is the axis of rotation, X axis is the axis of translation)
$\mathbf{Rl}_y(\varphi_z, Z)$	Operator of rolling over a plane (Z axis is the axis of rotation, Y axis is the axis of translation)
$\mathbf{Rr}_u(\varphi, Z)$	Operator of rolling of two coordinate systems
$\mathbf{Rs}\,(A \mapsto B)$	Operator of the resultant coordinate system transformation, say from the coordinate system A to the coordinate system B
$\mathbf{Rt}(\varphi_x, X)$	Operator of rotation through an angle φ_x about the X axis
$\mathbf{Rt}(\varphi_y, Y)$	Operator of rotation through an angle φ_y about the Y axis
$\mathbf{Rt}(\varphi_z, Z)$	Operator of rotation through an angle φ_z about the Z axis
$R_{1.\mathbf{g}}$, $R_{2.\mathbf{g}}$	The first and second principal radii of the work gear tooth flank $\mathscr{G}$
$R_{1.T}$, $R_{2.T}$	The first and second principal radii of curvature of generating surface T of the gear cutting tool
$\mathbf{Sc}_x(\varphi_x, p_x)$	Operator of screw motion about the X axis
$\mathbf{Sc}_y(\varphi_y, p_y)$	Operator of screw motion about the Y axis

$\mathbf{Sc}_z(\varphi_z, p_z)$	Operator of screw motion about the Z axis
$\mathbf{Tr}(a_x, X)$	Operator of translation at a distance a_x along the X axis
$\mathbf{Tr}(a_y, Y)$	Operator of translation at a distance a_y along the Y axis
$\mathbf{Tr}(a_z, Z)$	Operator of translation at a distance a_z along the Z axis
U_g, V_g	Curvilinear (Gaussian) coordinates of a point on the work gear tooth flank $\mathscr{G}$
U_T, V_T	Curvilinear (Gaussian) coordinates of a point of generating surface T of the gear cutting tool
$\mathbf{U}_P, \mathbf{V}_P$	Tangent vectors to curvilinear coordinate lines on the work gear tooth flank $\mathscr{G}$
$\mathbf{U}_T, \mathbf{V}_T$	Tangent vectors to curvilinear coordinate lines on generating surface T of the gear cutting tool
$\mathbf{V}_\Sigma$	Vector of the resultant motion of generating surface T of the gear cutting tool in relation to tooth flank $\mathscr{G}$ of the work gear
$k_{1.g}, k_{2.g}$	The first and second principal curvatures of the work gear tooth flank $\mathscr{G}$
$k_{1.T}, k_{2.T}$	The first and second principal curvatures of generating surface T of the gear cutting tool
$\mathbf{n_g}$	Unit normal vector to the work gear tooth flank $\mathscr{G}$
$\mathbf{n_T}$	Unit normal vector to generating surface T of the gear cutting tool
r_{cnf}	Position vector of a point of the indicatrix of conformity Cnf_R $(\mathscr{G}/T)$
$\mathbf{r}_g$	Position vector of a point of the work gear tooth flank $\mathscr{G}$
$\mathbf{t}_{1.g}, \mathbf{t}_{2.g}$	Unit tangent vectors of principal directions on the work gear tooth flank $\mathscr{G}$
$\mathbf{t}_{1.T}, \mathbf{t}_{2.T}$	Unit tangent vectors of principal directions on generating surface T of the gear cutting tool
$\mathbf{u}_g, \mathbf{v}_g$	Unit tangent vectors to curvilinear coordinate lines on the work gear tooth flank $\mathscr{G}$
$\mathbf{u}_T, \mathbf{v}_T$	Unit tangent vectors to curvilinear coordinate lines on generating surface T of the gear cutting tool
$x_P y_P z_P$	Local Cartesian coordinate system having origin at the point of contact of the surfaces $\mathscr{G}$ and T

Greek Symbols

$\boldsymbol{\Phi}_{1.g}, \boldsymbol{\Phi}_{2.g}$	The first and second fundamental forms of the gear tooth flank surface $\mathscr{G}$
$\boldsymbol{\Phi}_{1.T}, \boldsymbol{\Phi}_{2.T}$	The first and second fundamental forms of generating surface T of the gear cutting tool
Σ	Crossed-axis angle
ϕ_n	Normal profile angle of a gear cutting tool
μ	Angle of the surfaces $\mathscr{G}$ and T local relative orientation
ζ_c	Setting angle of a gear finishing tool
$\boldsymbol{\omega}_c$	Rotation of the gear cutting tool
$\boldsymbol{\omega}_g$	Rotation of the work gear
$\boldsymbol{\omega}_{pl}$	Instant rotation of the gear cutting tool in relation to the work gear

Subscripts

cnf	Conformity
max	Maximum
min	Minimum
opt	Optimal
g	Gear
c	Cutting tool

References

[1] Ball, R.S. *A Treatise on the Theory of Screws*. Cambridge, England: J. and C.P. Clay, at the University Press, 1900, 544 pp.; New York, NY: Cambridge University Press, 1998, 544 pp.

[2] Ball, R.S. *The Theory of Screws*. Dublin: Hodges & Foster, 1876.

[3] Basstein, G. Calculation, manufacturing and applications of *Cylkro* angular face gear transmissions. In *Proceedings of the SME Seminar: Basic Gear Design and Manufacturing*, January 26–27, 2000, Troy (Detroit), 8 pp.

[4] Bazhin, A.A. *Gear Cutting Tools*. Moscow: ONTI NKTP, 1935, 112 pp.

[5] Bianco, G. *Gear Hobbing*. Bologna: Novaprint, 2004, 201 pp.

[6] Bianco, G. *Gear Shaving*. Beijing: Jiuge Beijing, 2000, 200 pp. (2nd ed., Bologna: Novaprint, 2005, 174 pp.).

[7] Bobrov, V.F. *Fundamentals of Metal Cutting*. Moscow: Mashinostroyeniye, 1975, 344 pp.

[8] Bobrov, V.F. *Impact of the Angle of Inclination of the Main Cutting Edge of a Cutting Tool onto the Process of Machining of Metal Parts*. Moscow: Mashgiz, 1962, 152 pp.

[9] Börner, J., Humm, K., and Joachim, F.J. Developments of conical involute gears (beveloids) for vehicle transmissions. *Gear Technology* 22, 2005, 28–35.

[10] Bregi, B.F., Erxleben, R.F., Tersch, R.W. et al., *Modern Methods of Gear Manufacture*, 4th ed. Detroit, MI: National Broach & Machine Division/Lear Siegler, Inc., 1972, 160 pp.

[11] Buckingham, E. *Analytical Mechanics of Gears*. New York, NY: Dover Publications, Inc., 1988, 546 pp.

[12] Chkalova, O.N. Conical hobs for machining cylindrical gears. Ph.D. thesis, Kiev Polytechnic Institute, Kiev, 1969, 26 pp.

[13] Cormac, P. *A Treatise on Screws and Worm Gear, Their Mills and Hobs*. London: Chapman & Hall, 1936, 138 pp.

[14] Denavit, J., and Hartenberg, R.S. A kinematics notation for lower-pair mechanisms based on matrices. *ASME Journal of Applied Mechanics* 77, 1955, 215–221.

[15] Dudley, D.W. *Handbook of Practical Gear Design*, New York, NY: McGraw-Hill, 1984, 656 pp.

[16] Endoy, R. *Gear Hobbing, Shaping and Shaving: A Guide to Cycle Time Estimating and Process Planning, SME*. Dearborn, MI: Publication Development Department, 1990, 181 pp.

[17] *FETTE Gear Cutting Tools: Hobbing, Gear Milling*. Leitz Metalworking Technology Group, 2007.

[18] Frayfeld, I.A. *Continuously Indexing Cutting Tools*. Moscow: Mashgiz, 1948, 252 pp.

[19] *Gear Design: Manufacturing and Inspection Manual*. Warrendale, PA: Society of Automotive Engineers, Inc., 1990, 643 pp.

[20] Granovsky, G.I. *Kinematics of Machining*. Moscow: Mashgiz, 1948, 200 pp.

[21] Granovski, G.I., and Granovski, V.G. *Metal Cutting*. Moscow: Visshaya Shcola, 1985, 304 pp.

[22] Neugart, Gear honing, Bethel Park. PA, 2001. http://www.neugartusa.com/Service/faq/gear_honing.pdf.

[23] Wera Profilator. http://www4.profilator.de/.

[24] *Improvement of Gear Cutting Tools*, Collected papers. Moscow: NIIMASh, 1989, 571 pp.

[25] Inozemtsev, G.G. *Design of Metal Cutting Tools*. Moscow: Mashinostroyeniye, 1984, 272 pp.

[26] Inozemtsev, G.G. *Hobs with Rational Parameters of Design and of the Cutting Edge Geometry*. Saratov: Saratov State University, 1961, 224 pp.

[27] Kau, B.-Sh. Gear shaper cutters having the combined rake surface. Ph.D. thesis, Kiev Polytechnic Institute, Kiev, 1975, 215 pp.

[28] Kimura, K., and Ainoura, M., Hobbing cutter. U.S. Patent No. 3.786.719. 1974.

[29] Kolchin, N.I. *Analytical Computation of Planar and Spatial Gearing: with Application to Profiling of the Gear Cutting Tools and to Computation of the Deviations in Gearing*. Moscow: Mashgiz, 1949, 210 pp.

[30] Lashn'ev, S.I. Fundamentals of the theory of surface generation with disk-type, rack-type and worm-type cutting tools. Dr. Sci. thesis, Tula Polytechnic Institute, Tula, 1968, 268 pp.
[31] Lashn'ev, S.I. *Generation of Cogged Parts with Rack-Type and Worm-Type Cutting Tools*. Moscow: Mashinostroyeniye, 1971, 216 pp.
[32] Lashn'ev, S.I., and Yul'ikov, M.I., *Computation and Design of Metal Cutting Tools*. Moscow: Mashinostroyeniye, 1975, 392 pp.
[33] Lashn'ev, S.I., and Yul'ikov, M.I. *Computerized Design of Cutting Tools*. Moscow: Mashinostroyeniye, 1980, 208 pp.
[34] *MAAG Gear Book: Calculation and Practice of Gears, Gear Drives, Toothed Couplings and Synchronous Clutch Couplings*. Zurich, Switzerland: MAAG Gear Company Ltd., 1990, 440 pp.
[35] Margulis, D.K. *Broaches with Alterative Cutting Diagrams*. Moscow: Mashgiz, 1962, 270 pp.
[36] Mat'ushin, V.M., Fundamentals of gear cutting tool design (for spur and helical gears). Dr. Sci. thesis, Moscow, "Stankin," 1957, 48 pp.
[37] Medveditskov, S.N. A method of multi-paths hobbing of spur and helical gears. Pat. No. 1222442, USSR, Int. Cl. B23f 5/22, Filed: July 26, 1984.
[38] Medveditskov, S.N. *High-Productive Gear Hobbing*. Moscow: Mashinostroyeniye, 1981, 104 pp.
[39] Medveditskov, S.N., Radzevich, S.P., and Smirnov, N.N. Gear hobs with new cutting diagrams, *Mashinostroitel*, 1, 1985, 22–25.
[40] Merchant, M.E. Basic mechanics of metal-cutting process. *Journal of Applied Mechanics* 11, 1944, A168–A175.
[41] Merchant, M.E. Mechanics of the metal cutting process: II. Plasticity conditions in orthogonal cutting. *Journal of Applied Mechanics* 16, 1945, 267–318.
[42] Merritt, H.E. *Gear Engineering*. London: Pitman Publishing, 1971, 489 pp.
[43] Michalec, G.W. *Precision Gearing: Theory and Practice*. New York, NY: John Wiley & Sons, 1966, 620 pp.
[44] Misevich, V.S. A method for hobbing cylindrical gears with radially fed hob. *Stanki i Instrument* 1, 1964, 16–18.
[45] Mozhayev, S.S. A generalized theory of cutting tools. Dr. Sci. thesis, Leningrad Polytechnic Institute, Leningrad, 1953, 295 pp.
[46] Mozhayev, S.S. *Analytical Theory of Twist Drills*. Moscow: Mashgiz, 1948, 136 pp.
[47] Ngok, L.-M. Investigation of the geometry of the rake surface of shaper cutters. Ph.D. thesis, Kiev Polytechnic Institute, Kiev, 1972, 166 pp.
[48] Oliphirenko, M.I. Development and investigation of the methods to improve the accuracy of gear shaper cutters. Ph.D. thesis, Kiev Polytechnic Institute, Kiev, 1980, 358 pp.
[49] Olivier, T. *Theorie Geometrique des Engrenages*. Paris: Bachelier, 1842.
[50] Oxley, P.L.B. *Mechanics of Machining. An Analytical Approach to Assessing Machinability*. Chichester, Ellis Horwood Ltd., 1989, 242 pp.
[51] Palaguta, V.A. Investigation and improvement of productivity of gear shaving process. Ph.D. thesis, DSTU, Dneprodzerzhinsk, 1995, 220 pp.
[52] Pat. No. 155718 (USSR), A method of relieving of gear hob with the shaper cutter, Int. Cl. D24b 21/16, Filed: 1961.
[53] Petrukhin, S.S. *Fundamentals of Cutting Tool Design*: *Kinematical Theory*. Moscow: Mashgiz, 1960, 163 pp.
[54] Radzevich, A.P. A study on efficient hobbing of cylindrical involute gears. Ph.D. thesis, Kuybishev Polytechnic Institute, Kuybishev, 1988, 300 pp.
[55] Radzevich, S.P. A conical cutting tool for machining cylindrical gears, Pat. No. 1028451, USSR, Int. Cl. B23f 21/16, Filed: April 26, 1982.
[56] Radzevich, S.P. A conical tool for finishing cylindrical gears, Pat. No. 880590, USSR, Int. Cl. B21h 5/02, Filed: November 6, 1979.
[57] Radzevich, S.P., A continuously indexing method of sharpening of shaper cutters, Pat. No. 1604567, USSR, Int. Cl. B24B 3/34, Filed: January 12, 1988.
[58] Radzevich, S.P. A crowning achievement for automotive applications. *Gear Solutions* 2004, 16–25.

[59] Radzevich, S.P. A descriptive geometry-based solution to a geometrical problem in rotary shaving of a shoulder pinion. *ASME Journal of Manufacturing Science and Engineering* 127(4), 2005, 893–900.
[60] Radzevich, S.P. A device for inspection of a form milling cutter, Pat. No. 1629741, USSR, Int. Cl. G01b 5/20, Filed: March 27, 1989.
[61] Radzevich, S.P. A device for inspection of a form milling cutter, Pat. No. 1754352, USSR, Int. Cl. B23c 9/00, Filed: June 29, 1990.
[62] Radzevich, S.P. A gear cutting tool, Pat. No. 933316, USSR, Int. Cl. B23f 21/00, Filed: October 18, 1979.
[63] Radzevich, S.P. A gear cutting tool, Pat. No. 1017444, USSR, Int. Cl. B 23 f 21/16, Filed: April 26, 1982.
[64] Radzevich, S.P. A gear hob, Pat. No. 1009661, USSR, Int. Cl. B23f 21/16, Filed: October 21, 1981.
[65] Radzevich, S.P. A gear hob, Pat. No. 1537425, USSR, Int. Cl. B23f 21/16, Filed: June 2, 1987.
[66] Radzevich, S.P. A generalized analytical form of the conditions of proper part surface generation. Part 1. In: *Improvement of Efficiency of Metal Cutting*. Volgograd: VolgPI, 1987, pp. 70–79.
[67] Radzevich, S.P. A generalized analytical form of the conditions of proper part surface generation. Part 2. In: *Improvement of Efficiency of Metal Cutting*. Volgograd: VolgPI, 1988, pp. 56–73.
[68] Radzevich, S.P. A helical gear shaper cutter, Pat. No. 956187, USSR, Int. Cl. B23F 21/10, Filed: September 26, 1980.
[69] Radzevich, S.P. A hob, Pat. No. 1114543, USSR, Int. Cl. B23f 21/16, Filed: September 7, 1982.
[70] Radzevich, S.P. A hob for machining internal gear, Pat. No. 946833, USSR, Int. Cl. B23f 21/16, Filed: June 6, 1980.
[71] Radzevich, S.P. A hob for roughing gears, Pat. No. 944828, USSR, Int. Cl. B23f 21/16, Filed: September 4, 1980.
[72] Radzevich, S.P. A machine tool for finishing a crowned gear, Pat. No. 921727, USSR, Int. Cl. B23f 19/00, Filed: September 26, 1980.
[73] Radzevich, S.P. A machine tool for finishing a crowned gear, Pat. No. 984744, USSR, Int. Cl. B23f 19/00, Filed: April 16, 1981.
[74] Radzevich, S.P. A machine tool for finishing a crowned gear, Pat. No. 1000186, USSR, Int. Cl. B23f 19/00, Filed: November 6, 1981.
[75] Radzevich, S.P. A machine tool for finishing a crowned gear, Pat. No. 1028450, USSR, Int. Cl. B23f 19/00, Filed: April 26, 1982.
[76] Radzevich, S.P. A machine tool for finishing a crowned gear, Pat. No. 1110566, USSR, Int. Cl. B23f 19/00, Filed: June 7, 1983.
[77] Radzevich, S.P. A method for relieving of gear hob, Pat. No. 751583, USSR, Int. Cl. B24b 3/12, B23b 5/42, Filed: April 4, 1977.
[78] Radzevich, S.P. A method for relieving of gear hob with the standard shaper cutter, Pat. No. 1087309, USSR, Int. Cl. B24b 3/12, Filed: April 23, 1980.
[79] Radzevich, S.P. A method for relieving of gear hob with the standard shaper cutter, Pat. No. 1240548, USSR, Int. Cl. B24b 3/12, Filed: September 22, 1984.
[80] Radzevich, S.P. A method of grinding and re-grinding of a gear finishing tool, Pat. No. 956114, USSR, Int. Cl. B21h 5/00, Filed: March 18, 1980.
[81] Radzevich, S.P. A method of grinding of gear milling cutters, Pat. No. 975339, USSR, Int. Cl. B 24 b 3/12, Filed: October 10, 1980.
[82] Radzevich, S.P. A method of hob relieving, Pat. No. 965728, USSR, Int. Cl. B24b 3/12, Filed: January 21, 1980.
[83] Radzevich, S.P. A method of relief grinding of conical hob for machining cylindrical gears, Pat. No. 1365550, USSR, Int. Cl. B24b 3/12, Filed: April 29, 1986.
[84] Radzevich, S.P. A method of relief grinding of gear hob, Pat. No. 848290, USSR, Int. Cl. B 24 b 3/12, Filed: August 6, 1979.

[85] Radzevich, S.P. A method of relief grinding of gear hob teeth, Pat. No. 1194612, USSR, Int. Cl. B23f 21/16, B24b 3/12, Filed: July 20, 1984.
[86] Radzevich, S.P. A method of relief grinding of gear hob teeth, Pat. No. 1743810, USSR, Int. Cl. B24b 3/12, Filed: September 13, 1989.
[87] Radzevich, S.P. A method of relief grinding of precision gear hob, Pat. No. 965728, USSR, Int. Cl. B24b 3/12, Filed: January 21, 1980.
[88] Radzevich, S.P. A method of relief grinding of teeth of an assembled hob, Pat. No. 961925, USSR, Int. Cl. B24b 3/12, Filed: March 18, 1980.
[89] Radzevich, S.P. A method of shaping of cylindrical gear, Pat. No. 1504903, USSR, USSR, Int. Cl. B23f 5/12, Filed: December 2, 1987.
[90] Radzevich, S.P. A method to control the accuracy of helical shaper cutter, Pat. No. 1710231, USSR, Int. Cl. B23F 21/10, G01B 5/20, Filed: September 13, 1989.
[91] Radzevich, S.P., A novel approach for computation of constraints on parameters of modification of the tooth addendum of precision involute hob. *ASME Journal of Mechanical Design* 128(4), 2006, 803–811.
[92] Radzevich, S.P. A novel design of cylindrical hob for machining of precision involute gears. *ASME Journal of Mechanical Design* 129, 2007, 334–345.
[93] Radzevich, S.P. A novel hob design for precision involute gears: part I. *Gear Solutions* 50, 2007, 34–43.
[94] Radzevich, S.P. A novel hob design for precision involute gears: part II. *Gear Solutions* 50, 2007, 38–43.
[95] Radzevich, S.P. A possibility of application of Plücker's conoid for mathematical modeling of contact of two smooth regular surfaces in the first order of tangency. *Mathematical and Computer Modeling* 42(9–10), 2005, 999–1022.
[96] Radzevich, S.P. A precision gear cutting tool, Pat. No. 1038122, USSR, Int. Cl. B23f 21/04, Filed: May 4, 1981.
[97] Radzevich, S.P. A precision gear hob, Pat. No. 1004029, USSR, Int. Cl. B23f 21/16, Filed: November 6, 1979.
[98] Radzevich, S.P. A precision involute hob, Pat. No. 990445, USSR, Int. Cl. B23f 21/16, Filed: October 8, 1981.
[99] Radzevich, S.P. A precision involute hob, Pat. No. 1114505, USSR, Int. Cl. B23f 21/16, Filed: October 18, 1982.
[100] Radzevich, S.P. A precision involute hob, Pat. No. 2040376, RU, Int. Cl. B23f 21/16, Filed: January 3, 1992.
[101] Radzevich, S.P. A gear shaper cutter, Pat. No. 1039657, USSR, Int. Cl. B23F 21/10, Filed: March 16, 1982.
[102] Radzevich, S.P. A gear shaper cutter, Pat. No. 1174187, USSR, Int. Cl. B23F 21/10, Filed: April 4, 1981.
[103] Radzevich, S.P. A gear shaper cutter, Pat. No. 1172660, USSR, Int. Cl. B23F 21/10, Filed: February 13, 1984.
[104] Radzevich, S.P. A tool for finishing internal gear, Pat. No. 880589, USSR, Int. Cl. B21h 5/02, Filed: November 6, 1979.
[105] Radzevich, S.P. A tool for reinforcement of bevel gears by surface plastic deformation, Pat. No. 721214, USSR, Int. Cl. B21h 5/04, Filed: March 1, 1977.
[106] Radzevich, S.P. A tool for reinforcement of bevel gears by surface plastic deformation, Pat. No. 846024, USSR, Int. Cl. B21h 5/04, Filed: on November 15, 1978.
[107] Radzevich, S.P. A tool for reinforcement of bevel gears by surface plastic deformation, Pat. No. 1094659, USSR, Int. Cl. B21h 5/04, Filed: March 11, 1983.
[108] Radzevich, S.P. A tool for reinforcement of bevel gears by surface plastic deformation, Pat. No. 1107943, USSR, Int. Cl. B21h 5/04, Filed: February 24, 1983.
[109] Radzevich, S.P. A toroidal tool for finishing cylindrical gears, Pat. No. 965582, USSR, Int. Cl. B21h 5/00, Filed: October 2, 1980.

[110] Radzevich, S.P. A way to improve the accuracy of hobbed involute gears. *ASME Journal of Mechanical Design* 129, 2007, 1076–1085.
[111] Radzevich, S.P. A worm-type finishing tool for reinforcement of involute gear by surface plastic deformation, Pat. No. 829280, USSR, Int. Cl. B21h 5/00, Filed: on May 15, 1978.
[112] Radzevich, S.P. About hob idle distance in gear hobbing operation. *ASME Journal of Mechanical Design* 124, 2002, 772–786.
[113] Radzevich, S.P. *An Advanced Technology of Machining of Hardened Gears*. Moscow: VNIITEMR, 1992, 72 pp.
[114] Radzevich, S.P. An assembled gear hob, Pat. No. 1505695, USSR, Int. Cl. B23f 21/16, Filed: March 16, 1987.
[115] Radzevich, S.P. An attachment to a grinding machine for dressing of a form grinding wheel, Pat. No. 1771937, USSR, Int. Cl. B24b 53/085, Filed: June 21, 1990.
[116] Radzevich, S.P. An attachment to a grinding machining for relief grinding of hobs, Pat. No. 869978, USSR, Int. Cl. B23b 5/42, Filed: December 12, 1979.
[117] Radzevich, S.P. An attachment to a grinding machining for relief grinding of hobs, Pat. No. 1009615, USSR, Int. Cl. B23b 5/42, Filed: September 26, 1980.
[118] Radzevich, S.P. An attachment to a grinding machining for relief grinding of hobs, Pat. No. 1077706, USSR, Int. Cl. B23b 5/42, B24b 3/12, Filed: July 5, 1982.
[119] Radzevich, S.P. An attachment to a grinding machining for relief grinding of hobs, Pat. No. 1117127, USSR, Int. Cl. B23b 5/42, B24b 3/12, Filed: June 15, 1983.
[120] Radzevich, S.P. An attachment to a grinding machining for relief grinding of hobs, Pat. No. 1146134, USSR, Int. Cl. B23b 5/42, Filed: June 29, 1983.
[121] Radzevich, S.P. An attachment to a grinding machining for relief grinding of hobs, Pat. No. 1199458, USSR, Int. Cl. B23b 5/42, Filed: May 29, 1984.
[122] Radzevich, S.P. An attachment to a grinding machining for relief grinding of hobs, Pat. No. 1433769, USSR, Int. Cl. B24b 3/12, Filed: April 23, 1987.
[123] Radzevich, S.P. An involute hob, Pat. No. 1004029, USSR, Int. Cl. B23f 21/16, Filed: November 6, 1979.
[124] Radzevich, S.P. Basic conditions of proper part surface generating while machining on conventional machine tool, *The Scientific Journal "Facta Universitatis,"* Series: *Mechanical Engineering* (University of Niš) 1(6), 1998, 637–651.
[125] Radzevich, S.P. *CAD/CAM of Sculptured Surfaces on Multi-Axis NC Machine: The DG/K-Approach*. San Rafael, CA: M&C Publishers, 2008, 113 pp.
[126] Radzevich, S.P. *Classification of Surfaces, Monograph*. Kiev: UkrNIINTI, No. 1440-Uk88, 1988, 185 pp.
[127] Radzevich, S.P. Computation of parameters of a form grinding wheel for grinding of shaving cutter for plunge shaving of topologically modified involute pinion. *ASME Journal of Manufacturing Science and Engineering* 127(4), 2005, 819–828.
[128] Radzevich, S.P. Conditions of proper sculptured surface machining. *Computer-Aided Design* 34(10), 2002, 727–740.
[129] Radzevich, S.P. *Cutting Tools for Machining of Hardened Gears*. Moscow: VNIITEMR, 1992, 60 pp.
[130] Radzevich, S.P. Design and investigation of skiving hobs for finishing of hardened gears. Ph.D. thesis, Kiev Polytechnic Institute, Kiev, 1982, 298 pp.
[131] Radzevich, S.P. Design of shaving cutter for plunge shaving a topologically modified involute pinion. *ASME Journal of Mechanical Design* 125, 2003, 632–639.
[132] Radzevich, S.P. Design of special-purpose hob with prescribed value of the hob-setting angle for machining of cluster gear. *ASME Journal of Mechanical Design* 129, 2007, 438–444.
[133] Radzevich, S.P. Determination of tooth flank geometry of shaving cutter for plunge shaving of precision gears: part 1. *STIN* 10, 2008, 9–13.
[134] Radzevich, S.P. Determination of tooth flank geometry of shaving cutter for plunge shaving of precision gears: part 2. *STIN* 11, 2008, 18–22.

[135] Radzevich, S.P. Diagonal shaving of an involute pinion: optimization of parameters of the pinion finishing operation. *International Journal of Advanced Manufacturing Technology* 32(11–12), 2007, 1170–1187.
[136] Radzevich, S.P. Differential-geometric method of surface generation. Dr. Sci. thesis, Tula Polytechnic Institute, Tula, 1991, 300 pp.
[137] Radzevich, S.P. Finishing precise gears for low noise/noiseless car transmission. In: *Proceedings of the 1st Annual Manufacturing Technology Summit*, August 10–11, 2004, University of Michigan/Dearborn Fairlane Center, SME, 2004, 20 pp.
[138] Radzevich, S.P. *Fundamentals of Surface Generation*, *Monograph*. Kiev: Rastan, 2001, 592 pp.
[139] Radzevich, S.P. Generating surfaces of worm-type gear cutting tools. In: *Advance Processes in Production Technology*. Volgograd: VolgPI, 1985, 64–78.
[140] Radzevich, S.P. Geometry of the active part of cutting tools (in the tool-in-use system). The SME MIDWEST 2005 Manufacturing Excellence through Collaboration Conference, September 13–14, 2005, Rock Financial Showplace, Novi, MI, SME Paper No. TP06PUB36, 12 pp.
[141] Radzevich, S.P. Geometry of the active part of cutting tools (in the tool-in-hand system). The SME Summit Conference: *Where Manufacturers, Technologies and Innovations Connect*, August 3–4, 2005, Olympia Resort and Conference Center, Oconomowoc, Milwaukee, WI. SME Paper No. TP06PUB37, 12 pp.
[142] Radzevich, S.P. Investigation of the tooth geometry of a hob for machining of involute gears (in the tool-in-use reference system). *ASME Journal of Manufacturing Science and Engineering* 129(8), 2007, 750–759.
[143] Radzevich, S.P. *Kinematic Geometry of Surface Machining*. Boca Raton, FL: CRC Press, 2008, 508 pp.
[144] Radzevich, S.P. *Machining of Hardened Gears*. Moscow: VNIITEMR, 1985, 56 pp.
[145] Radzevich, S.P. Modified shaving cutters for low noise. In: Stott, W.R. (ed.), *Software Bits*. *Gear Technology*, January/February 2004, 20–27.
[146] Radzevich, S.P. On a possible way of size and weight reduction of a car transmission. *Gear Technology* 20(4), 2003, 44–50.
[147] Radzevich, S.P. On satisfaction of the fifth necessary condition of proper part surface generation in design of plunge shaving cutter for finishing of precision involute gears. *ASME Journal of Mechanical Design* 129(9), 2007, 969–980.
[148] Radzevich, S.P. On the accuracy of finishing involute hobs. In: *Cutting and Cutting Tools*, Collected Papers, Vol. 24. Kharkov: Vishcha Shkola, 1980, pp. 105–109.
[149] Radzevich, S.P. On the accuracy of precision involute hobs: an analytical approach. *SME Journal of Manufacturing Processes* 9(2), 2007, 121–136.
[150] Radzevich, S.P. On tooth failure analysis in small-teeth-number gearing: an analytical approach. *AGMA Technical Paper* 06FTM11, 2006, 22 pp.
[151] Radzevich, S.P. Part surfaces those allowing sliding over them. In: Radzevich, S.P. (ed.), *Research in the Field of Surface Generation*. Kiev: UkrNIINTI, No. 65-Uk89, 1989, pp. 29–53.
[152] Radzevich, S.P. Relief grinding of assembled gear hobs with diamond grinding wheels. In: *Diamonds and Super-Hard Materials*, Vol. 4. Moscow: NIIMASh, 1979, pp. 13–14.
[153] Radzevich, S.P. *Sculptured Surface Machining on Multi-Axis NC Machine*, *Monograph*. Kiev: Vishcha Schola, 1991, 192 pp.
[154] Radzevich, S.P. Technological implementation of shape peculiarities of involute treads and worms. *Vestnik Mashinostroyeniya* 11, 1984, 48–51.
[155] Radzevich, S.P. Technological methods for noise/vibration reduction in driveline/transmission of trucks and all-wheel-drive vehicle. *International Journal of Vehicle Noise and Vibration* 2(4), 2006, 283–291.
[156] Radzevich, S.P., and Chernishov, M.V. An attachment to a grinding machining for relief grinding of hobs, Pat. No. 1371875, USSR, Int. Cl. B24b 3/12, Filed: April 28, 1988.
[157] Radzevich, S.P., and Dashevskii, A.N. An attachment for inspection of a form milling cutter, Pat. No. 1516738, USSR, Int. Cl. G01b 5/20, Filed: February 17, 1989.

[158] Radzevich, S.P., Goodman, E.D., and Palaguta, V.A. Tooth surface fundamental forms in gear technology. *The Scientific Journal Facta Universitatis*, Series: *Mechanical Engineering* (University of Niš) 1(5), 1998, 515–525.
[159] Radzevich, S.P., and Lempert, V.I. A method of relieving of gear hobs, Pat. No. 1335425, USSR, Int. Cl. B 24 b 3/12, Filed: April 24, 1986.
[160] Radzevich, S.P., and Medveditskov, S.N. A shaper cutter, Pat. No. 1641535, USSR, Int. Cl. B23F 21/10, Filed: June 26, 1988.
[161] Radzevich, S.P., Medveditskov, S.N., Radzevich, A.P., and Smirnov, N.N., A gear hob, Pat. No. 1134318, USSR, Int. Cl. B23f 21/16, Filed: April 7, 1983.
[162] Radzevich, S.P., Medveditskov, S.N., Radzevich, A.P., and Smirnov N.N. A gear hob, Pat. No. 1187936, USSR, Int. Cl. B23f 21/16, Filed: June 28, 1984.
[163] Radzevich, S.P., and Palaguta, V.A. A gear shaving cutter, Pat. No. 1632662, USSR, Int. Cl. B23f 21/28, Filed: March 30, 1989.
[164] Radzevich, S.P., and Palaguta, V.A. A method of re-sharpening of gear shaving cutter, Pat. No. 1646725, USSR, Int. Cl. B23f 21/28, Filed: December 13, 1988.
[165] Radzevich, S.P., and Palaguta, V.A. A tool for finishing cylindrical gears, Pat. No. 1328042, USSR, Int. Cl. B21h 5/00, Filed: December 3, 1985.
[166] Radzevich, S.P., and Palaguta, V.A. *Advanced Methods for Gear Finishing*. Moscow: VNIITEMR, 1988, 52 pp.
[167] Radzevich, S.P., and Palaguta, V.A. Synthesis of optimal gear shaving process. *Vestnik Mashinostroyeniya* 8, 1997, 36–41.
[168] Radzevich, S.P., Palaguta, V.A., and Goodman, E.D. Geometry of helical gear and tool surfaces for plunge shaving of involute gears. Final Data Report, Michigan State University/Chrysler Corp., 1998, 86 pp.
[169] Radzevich, S.P., Palaguta, V.A., Radzevich, A.P., and Bulgakov, V.A. A shaving cutter, Pat. No. 1514516, USSR, Int. Cl. B23f 21/28, Filed: November 27, 1986.
[170] Radzevich, S.P., Palaguta, V.A., Radzevich, A.P., and Tovmasian, M.A. A shaving cutter, Pat. No. 1537426, USSR, Int. Cl. B23f 21/28, Filed: November 17, 1986.
[171] Radzevich, S.P., and Pasechnik, M.F. A method of hob relieving, Pat. No. 1196232, USSR, Int. Cl. B24b 3/00, Filed: August 3, 1984.
[172] Radzevich, S.P., and Petrenko, T.Yu. Part and tool surfaces those allowing sliding over themselves. *Mechanika ta Mashinobuduvann'a* (Kharkiv, Ukraine), 1, 1999, 231–240.
[173] Radzevich, S.P., and Vinokourov, I.V. A method of grinding of gear milling cutters having straight slots, Pat. No. 1627375, USSR, Int. Cl. B 24 b 3/12, Filed: October 17, 1988.
[174] Radzevich, S.P., and Vinokourov, I.V. An attachment to a grinding machine for dressing of a form grinding wheel, Pat. No. 1393527, USSR, Int. Cl. B23b 5/42, Filed: November 18, 1986.
[175] Radzevich, S.P., and Vinokourov, I.V., An attachment to a grinding machine for relief grinding of hobs, Pat. No. 1335426, USSR, Int. Cl. B24b 3/12, Filed: April 14, 1986.
[176] Radzevich, S.P., Vinokourov, I.V., Radzevich, A.P., Androshchuk, G.A., and Smol'nikov, N. Ya. A method of roughing of coarse pitch gears, Pat. No. 1815024, USSR, Int. Cl. B 23 f 5/20, 17/00, Filed: November 11, 1990.
[177] Rodin, P.R. *Fundamentals of Cutting Tool Design*. Moscow: Mashgiz, 1960, 160 pp.
[178] Rodin, P.R. Issues on theory of cutting tool design. Dr. Sci. thesis, Odessa Polytechnic Institute, Odessa, 1961, 373 pp.
[179] Rodin, P.R., and Radzevich, S.P. A method of relief grinding of precision gear hob, Pat. No. 831546, USSR, Int. Cl. B24b 3/00, Filed: February 7, 1979.
[180] Sakharov, G.N. *Continuously Indexing Cutting Tools*. Moscow: Mashinostroyeniye, 1983, 232 pp.
[181] Sakharov, G.N. Issues on theory of continuously indexing cutting tools. Dr. Sci. thesis, Moscow: Stankin, 1974, 320 pp.
[182] Semenchenko, I.I., Mat'ushin, V.M., and Sahharov, G.N. *Design of Metal Cutting Tools*. Moscow: Mashgiz, 1962, 952 pp.
[183] Shaw, M.C. *Metal Cutting Principles*. Oxford: Clarendon Press, 1984.

[184] Shevel'ova, G.I. *Theory of Surface Generation and of Contact of Moving Bodies*. Moscow: Moscow University STANKIN, 1999, 494 pp.
[185] Shevchenko, N.A. *The Geometry of Cutting Edge and the Parameters of Uncut Chip*. Moscow: Mashgiz, 1957, 140 pp.
[186] Shishkov, V.A. *Generation of Surfaces Using Continuously Indexing Methods of Machining*. Moscow: Mashgiz, 1951, 152 pp.
[187] Smirnov, N.N. Multi-thread hob with new cutting diagrams. *Gear Technology* 8(4), 1991, 27–31.
[188] Stabler, G.V. The fundamental geometry of cutting tools. *Proceedings of the Institute of Mechanical Engineers* 165, 1951, 14–21.
[189] Talantov, N.V. *Physical Foundations of Metal Cutting, Wear and Failure of Cutting Tools*. Moscow: Mashinostroyeniye, 1992, 240 pp.
[190] Townsend, D.P. *Dudley's Gear Handbook. The Design, Manufacture, and Application of Gears*, 2nd edn. New York, NY: McGraw Hill, 1992.
[191] Tsepkov, A.V. *Profiling of Gear Cutting Tools that Feature Relieved Clearance Surfaces*. Moscow: Mashinostroyeniye, 1979, 150 pp.
[192] Tsvis, Yu.V. *Profiling of Cutting Tools for Scudding of Gears*. Moscow: Mashgiz, 1961, 156 pp.
[193] Vinokourov, I.V., and Radzevich, S.P. An attachment to a grinding machining for relief grinding of hobs, Pat. No. 2009762, RU, Int. Cl. B23b 5/42, Filed: December 18, 1991.
[194] Watson, H.J. *Modern Gear Production*. New York, NY: Pergamon Press, 1970, 359 pp.
[195] Yu, M., and Mertz, R. An evaluation of Smirnov hob cutter. Technical Data Report, June 1, 1993, GMGC #0112, General Motors Gear Center, Romulus, MI, 1993, 73 pp.
[196] Zorev, N.N. *Metal Cutting Mechanics*. New York, NY: Pergamon Press, 1956.
[197] Zorev, N.N. *Problems of Metal Cutting Mechanics*. Moscow: ZNIITMash, 1956, 367 pp.
[198] Radzevich, S.P. A tool for finishing gears. Pat. No. 963653, USSR, Int. Cl. B21h 5/00, Filed: October 2, 1980.
[199] Radzevich, S.P. A tool for finishing gears. Pat. No. 1466861, USSR, Int. Cl. B21h 5/00, Filed: February 2, 1987.
[200] Radzevich, S.P. A tool for finishing gears. Pat. No. 1754302, USSR, Int. Cl. B21h 5/02, Filed: September 27, 1989.
[201] Radzevich, S.P. A method of hobbing gear. Pat. No. 4278973/08, USSR, Int. Cl. B23f 5/22, Filed: April 25, 1987.
[202] Radzevich, S.P. and Radzevich, A.P. A tool for finishing gears. Pat. No. 1177016, USSR, Int. Cl. B21h 5/02, Filed: July 8, 1983.
[203] Radzevich, S.P. A tool for finishing gears. Pat. No. 1276408, USSR, Int. Cl. B21h 5/02, Filed: December 25, 1984.
[204] Radzevich, S.P. A method of finishing of a modified gear teeth. Pat. No. 1683913, USSR, Int. Cl. B23f 21/28, Filed: January 1, 1989.
[205] Radzevich, S.P. A gear finishing tool. Pat. No. 1004030, USSR, Int. Cl. B23F 21/16, Filed: April 16, 1981.
[206] Radzevich, S.P. A gear finishing tool. Pat. No. 1106609, USSR, Int. Cl. B23F 21/16, Filed: September 27, 1982.
[207] Radzevich, S.P. A gear finishing tool. Pat. No. 1151392, USSR, Int. Cl. B23F 21/16, Filed: February 15, 1982.
[208] Radzevich, S.P. A gear finishing tool. Pat. No. 795677, USSR, Int. Cl. B21H 5/00, Filed: January 15, 1979.
[209] Radzevich, S.P. A gear finishing tool. Pat. No. 795678, USSR, Int. Cl. B21H 5/00, Filed: January 15, 1979.
[210] Radzevich, S.P. A gear finishing tool. Pat. No. 923688, USSR, Int. Cl. B21H 5/02, Filed: August 6, 1979.
[211] Radzevich, S.P. A gear finishing tool. Pat. No. 965582, USSR, Int. Cl. B21H 5/00, Filed: October 2, 1980.

[212] Radzevich, S.P. An attachment to a machine tool for finishing gear. Pat. No. 969395, USSR, Int. Cl. B21H 5/02, Filed: April 16, 1981.
[213] Radzevich, S.P. A conical gear finishing tool. Pat. No. 980905, USSR, Int. Cl. B21H 5/00, Filed: November 24, 1980.
[214] Radzevich, S.P. A gear finishing tool. Pat. No. 996016, USSR, Int. Cl. B21H 5/02, Filed: April 16, 1981.
[215] Radzevich, S.P. A gear finishing tool. Pat. No. 1016004, USSR, Int. Cl. B21H 5/00, Filed: November 10, 1980.
[216] Radzevich, S.P. A gear finishing tool. Pat. No. 1031610, USSR, Int. Cl. B21H 5/00, Filed: April 16, 1981.
[217] Radzevich, S.P. An attachment to a machine tool for finishing gear. Pat. No. 1055578, USSR, Int. Cl. B21H 5/02, Filed: November 6, 1981.
[218] Radzevich, S.P. A gear finishing tool. Pat. No. 1174139, USSR, Int. Cl. B21H 5/00, Filed: October 10, 1983.
[219] Radzevich, S.P. A gear finishing tool. Pat. No. 1230019, USSR, Int. Cl. B21H 5/00, Filed: December 25, 1984.

Index

A

Addendum, 310, 695*t*, 697*t*
Analytical profiling, of rack cutter, 198–199
Angle of inclination, 240–241
Angular pitches, 268
Archimedean screw surface, 62–63
Archimedean worm, machining, 173
Asymmetric tooth profile, 389–90
Auxiliary generating surface, 357–363
  characteristic line E_g, 362
  coordinate systems, 357–359
  coordinate systems transformations, 359
  pitch diameter, 361–362
  profile angle, 362
  rack surface, 357–358
  relative motion of work gear, 358
  tooth flank surface, 359–360
  types of, 363
Auxiliary parameter, 475*t*
Auxiliary rack, 371–372, 608–610
Axial gear shaving, 576–587. *See also* shaving cutters
  coordinate systems transformations, 585
  cutting speed, 578–587
  equivalent base diameters, 586–587
  formula for cutting speed, 587
  impact of crossed-axis angle, 578–579
  impact of profile sliding, 580–587
  impact of traverse motion, 579–580
  kinematics of, 576–578
  line of action, 584
  workgear to shaving cutter meshing, 580, 581*f*, 583*f*
Axial pitch, 475*t*, 696*t*

B

Backlash per pair, 697*t*
Barreled spur gear, 17
Base diameter
  equation, 695*t*, 697*t*
  of generating surface, 380–381
Base diameter of shaper cutter, 310
Base helix angle, 378–379, 696*t*
Base pitch, 696*t*
Bevel gear machining, 315–342
  generating surface of gear cutting tool, 325–328
  geometry of interacting tooth surfaces, 318–325
    generating surface of gear cutting tool, 319–323
    involute straight bevel gear tooth flank, 318–319
    octoidal profile, 319
    tooth flanks of generated gear, 323–325
  kinematics of, 315–317
    axodes, 316
    coordinate systems, 317
    pitch angle, 316
    rotation vectors, 315–316
  straight bevel gear teeth, 328–333
    gear cutting tools, 330–333
    machining of straight bevel gears, 329–330
    plane T_a by straight motion of cutting edge, 328–329
  straight bevel gears with offset teeth, 325–328
Bevel gears, 14–16
  face hob for, 668, 669*f*
  helical, 15–16
  internal round broach, 170–172
  spiral, 337–342
  straight, 14–15
  teeth, broaching, 81–90
  tooth flank, 14–15
Beveloids, 347
Biparametric motion, 16
Broaching, 73–74
  bevel gear teeth, 81–90
  external gears, 73–74
  internal gears, 73
  push-up pot, 74
Built-up hobs, 463–464
Burnishing button, 73
Butt-end hob, 496, 496*f*

C

Carbide gear shaper cutter, 270–273
Cartesian coordinate system, 10*f*, 20–21
  conversion of orientation, 54
  of gear shaper cutters, 225–226
  screw motion, 48–49
Center distance, 26
  zero value, 40

Chamfers, 263–264, 677–678
Characteristic *E*, 115
Chip per tooth, 59, 65–66
Chip removal diagrams, 65–66
Chip-flow rake angle, 717–718
Chip-flow reference plane, 716–717
Circular mapping, 629–631
Circular pitch, 695*t*, 697*t*
Circular tooth thickness, 697*t*
Clearance angle, 710–711
  definition of, 708–709, 710–711
  disk-type gear milling cutters, 144–146
  of hob tooth cutting edge, 510, 515–516
  of lateral cutting edge, 243–248
  normal, 710–711
  of rack cutter, 202
  of rotary breaches, 80
Clearance surface, 64–65
  of disk-type gear milling cutter, 134–136
  of gear hobs, 411–433
    clearance angle, 413, 416–423
    cutting edges, 411
    cutting of relieved clearance surface, 415–423
    equation of desired clearance surface, 411–415
    grinding of relieved clearance surface, 423–433
    helix angle, 414
    operator of linear transformation, 415
    position vector, 413
    rake plane, 413
    reduced pitch, 413
    tooth relieving operation, 415
  grinding of, 274–275
  of rack cutter, 195–196
  of shaper cutter tooth, 232–233
Climb hopping, 530
Cluster gears, 5, 6*f*
Coarse-pitch gears, 120
Combined rake surface, 266
Cone drive, 5
Conical gear cutting tools, 679–681
Conical generating surface, 383–389
Conical hobs, 493–497
  butt-end hob, 496, 496*f*
  design of, 661–662
  face hob, 496, 496*f*
  palloid gear hobbing with, 658–662
    kinematics of, 660–661
    machining with crowned teeth, 662
  work gear to cutting tool penetration curve, 493, 494*f*
Conical involute gears, shaping of, 311, 312*f*
Conical rake surface, 62–63
Conjugate surfaces, rolling of, 23–24
Contact ellipse, 594
Continuously indexing methods, 25–42
  classification of gear machining meshes, 39–42
  configuration of rotation vectors, 37–39
  kinematic relationships for gear machining mesh, 32–37
  kinematics of gear machining, 42
  vector representation of gear machining mesh, 25–32
Conventional hopping, 530
Coordinate axis, rotation about, 46–47
Coordinate systems transformations, 43–56
  conversion of coordinate system orientation, 54
  direct transformation, 45
  direct transformation of surfaces fundamental forms, 55–56
  homogenous coordinate transformation matrices, 44
  homogenous coordinate vectors, 43–44
  opposite transformation, 54
  orientation-preserving transformation, 45
  orientation-reversing transformation, 54
  overview, 43
  resultant, 47–48
  rolling motion of coordinate system, 50–51
  rolling of two coordinate systems, 52–54
  rotation about coordinate axis, 46–47
  screw motions about coordinate axis, 48–49
  translations, 44–45
Coordinate transformation matrices, homogenous, 43–44
Coordinate vectors, homogenous, 43–44
Critical configuration, 38
Crossed-axis angle, 27, 123
  impact of, 578–579
  zero value, 40
Crowned spur gear, 17
Cut per tooth, 65–66
Cutting edge geometry, 705–718
  chip flow rake angle, 717–718
  chip-flow reference plane, 716–717
  clearance angle, 708–709
  correlation measured within major and normal section planes, 713–715
  cutting edge, 705
  of disk-type gear milling cutters, 143–146
    clearance angle, 144–146
    pressure angle, 145–146

profile angle, 144–145
rake angle, 143, 146
of external gear machining meshes, 239–248
gear hobs, 498–515
of gear shaper cutters
external gear machining mesh, 239–248
internal gear machining mesh, 285–286
hobs for machining gears, 498–515
of internal gear machining meshes, 285–286
in major section plane, 707–708
mandatory relationship, 711–712
minor cutting edge approach angle, 715–716
normal clearance angle, 710–711
normal rake angle, 709–710
in normal section plane, 709
in plane of cut, 706
of rack cutters, 199–207
clearance angle, 202
computation, 200–202
inclination angle, 200
for lateral cutting edges, 200–202
modification of clearance surface, 204–207
modification of rake surface, 203–204
roundness of cutting edge, 712
vector of resultant motion, 705
Cutting edge vector, 705
Cutting edges, 705
definition of, 705
end-type gear milling cutters, 101–114
helix angle, 113
rake surface in form of plane, 109–111
rake surface in form of screw surface, 111–114
of gear broach, 61–65
roundness of, 712
Cutting motion, 208
Cutting tools, 1–2
cylindrical, 673–679
direct problem of design, 2
elementary relative motions, 20–21
with enveloping generating surface, 673–686
feasible relative motions, 21–23
for machining bevel gears, 315–342
for machining internal gears, 687–691
Shear-Speed cutting, 74–80
Cylinders, rolling motion over, 53
Cylindrical gear cutting tool, 673–679
examples of, 676–679
gear tooth with chamfers, 677–678
gear tooth with lengthwise modification, *678f*
generating surface of, 673–674
part surface generation, 674–676
vector diagram, *677f*
Cylindrical hobs, 487–93
for finishing hardened gears, 490–493
number of hob threads, 489
for smooth roughing of coarse pitch gears, 487–489
unfolded cross section, 488*f*, 490*f*

D

Deep counterbore-type shaper cutters, 261, 284–285
Descriptive geometry-based methods, 136–138
generating surfaces, 378–381
for rack cutter, 197, 198*f*
tangential shaving, 605–612
Diagonal shaving, 587–602. *See also* shaving cutters
coordinate systems, 596–598
cutting speed, 590–592
diagonal-underpass, 590
geometry of contact of tooth flanks, 598–602
kinematics of, 588–589
local topology of contacting tooth flanks, 595–596
multistroke, 589
optimal kinetic parameters, 602
optimization of kinematics, 592–595
traverse angle, 589–590
Diagonal-underpass shaving, 590
Differential serrations, 605
Direct problem of gear-cutting tool design, 2
Direct transformation, 45
of surface fundamental forms, 55–56
Disk-type gear milling cutters, 123–161. *See also* end-type gear milling cutters
15-gear, 155
accuracy of tooth flanks machined with, 152–154
application of, 154–161
circular saws, 159–160
cutting edge geometry of, 143–146
clearance angle, 144–146
pressure angle, 145–146
profile angle, 144–145
rake angle, 143, 146
cutting edges of, 132–136
clearance surface, 132f, 134–136
rake surface, 132–134, 132*f*
eight-gear, 155
generating surface of, 125–127
elements of intrinsic geometry, 130–132

Disk-type gear milling cutters (*continued*)
equation for machining spur involute gears, 125–127
for machining helical involute gears, 127–130
inclined tooth profile, 155, 156*f*
indexing, 161
kinematics of gear cutting, 123–124
crossed-axis angle, 123
feed motion, 123
pitch helix angle, 123
rotation vector, 123–124
screw feed motion, 124
multiple-tooth, 161
overview, 123
profiling of, 136–143
analytical, 138–143
descriptive geometry-based methods, 136–138
for roughing of gears, 147–152
assembled cutter, 151*f*
clearance angle, 147–148
design parameters, 147*f*
even-numbered teeth, 150
odd-numbered teeth, 150
progressive cutting diagram, 149
rake angle, 147
top-loaded cutting diagram, 150
wavy cutting edges, 151
single parametric motions in design of, 167–168
span measurement, 158*f*
Disk-type gear shaper cutter, 261
Double-enveloping worm gear drive, 5
Double-helical gears, 3, 6*f*
Dupin indicatrix, 596

E

End-type gear milling cutters, 91–122. *See also* disk-type gear milling cutters
application of, 120–122
cutting edges, 101–114
clearance surface, 105–108
geometry of, 108–114
helix angle, 113
pressure angle, 114
rake surface in form of plane, 109–111
rake surface in form of screw surface, 111–114
generating surface of, 92–101
elements of intrinsic geometry, 100–101
equation for machining helical involute gears, 96–100
equation for machining spur involute gears, 92–96
secondary, 92
for helical gears, 120–121
indexing mechanism, 122
kinematics of gear machining, 91, 92*f*
machining gear tooth flanks with, 115–119
characteristic *E*, 115
curvature of helical gear tooth flank, 118
cusps on tooth flanks of helical gear, 117–119
cusps on tooth flanks of spur gear, 115–117
maximal deviation, 117
waviness of tooth flank, 116
overview, 91
single parametric motions in design of, 166–167
for spur gears, 120
Engineering approach, 8
Enveloping generating surface, 673–686
conical, 679–681
cylindrical, 673–679
toroidal, 681–686
Enveloping shaper cutters, 293, 295*f*
shaping external recessed tooth forms with, 347–349
shaping spur gears with, 346–347
Epicyclical motion, 619
Equivalent base diameters, 586–587
External gear machining meshes, 41*f*, 223–279. *See also* internal gear machining meshes
accuracy of gears cut with, 255–260
fifth condition of proper post surface generation, 255–258
gear-to-shaper cutter meshing diagram, 257
application of, 120–122, 260–279
critical distance to nominal cross section, 236–239
circular tooth thickness, 239
length of top cutting edge, 237–238
maximal length of distance, 237
cutting edge geometry of, 239–248
angle of inclination of lateral cutting edge, 240–241
clearance angle of lateral cutting edge, 243–248
improvement in geometry, 245–248, 265–269
rake angle of lateral cutting edge, 241–243
cutting edges of, 229–233
clearance surface of tooth, 232–233
rake surface, 229–232

definition of, 39
design of shaper cutters, 261–263
deep counterbore-type, 261
disk-type, 261
for machining helical and herringbone gears, 264–265
tooth profiles, 263–264
desired corrections to tooth profile, 248–250
generating surface of, 225–229
Cartesian coordinate system, 225–226
for machining involute shapes, 228
pitch helix angle, 228
position vector, 225–226
profile angle, 227
Shishkov's equation of contact, 227–228
geometry of clearance surface, 246–248
grinding of, 274–279
clearance surfaces, 274–275
rake surfaces, 275–279
helical gears for, 120–121
indexing mechanism, 122
kinematics of gear shaping, 223–225
principal elements, 224*f*
reciprocation, 223
screw motion, 223–224
vector diagram, 224*f*
lateral cutting edges
angle of inclination, 240–241
clearance angle, 243–248
rake angle, 241–243
overview, 223–279
profiling of, 233–236
angular displacement of tooth profile, 236
base diameter, 235
circular tooth thickness, 234–235
meshing of auxiliary rack surface, 233–234
profile shift correction coefficient, 235
tooth addendum, 235
tooth dedendum, 235
tooth thickness, 235–236
rake surface of, 229–232
geometry, 230–231
helical, geometry of, 231–232
improvement in geometry, 245–246
special designs of, 265–273
angular pitches, 268
combined rake surface, 266
improved cutting edge geometry, 265–269
for machining hardened gears, 270–272
precision gear, 269–270
two gears, 267–269
spur gears for, 120
thickness of chip cut by, 251–255
feed rate motion, 251
operator of rolling, 253–254
position vector, 253–254
roll angle, 252
speed of instant rotation, 251
tooth ratio, 252
tooth profiles
chamfer, 263–264
full topping, 264
modified pressure angle, 264
protuberance, 264
root fillet, 263
semitopping, 263–264
tip relief, 263
typical gear shaping operations, 273–274
combination operations, 273–274
cutting two gears with different diametral pitch, 274
cutting two gears with similar diametral pitch, 274
cutting two gears with up and down shaping, 274
length of stroke, 273, 274*f*
spiral infeed, 274
External gears, broaching, 73–74
External recessed tooth forms, shaping of, 347–349
External spatial gear machining, kinematics of, 353–357

F

Face angle radius, 62
Face gear milling cutters, 168–169
Face gears, 6, 311–314
Face hob, 496, 496*f*, 668, 669*f*
Feed motion, 28, 123, 208–209
Fiat spiral bevel-gear generation, 668
Finish rack cutter, 218–219
Finishing teeth, 59
of gear broach, 61–64
Archimedean screw surface, 62–63
clearance surface, 64–65
conical, 62–63
face angle radius, 62
gullet, 62
pitch, 62
tooth depth, 62
Form gear cutting tools, 163–181
analytical profiling of, 77–79
classification of, 181
disk-type gear milling cutters, 123–161
end-type gear milling cutters, 91–122
gear broaching tools, 59–90

Form gear cutting tools (*continued*)
grinding involute worm, 178–181
machining involute worm on lathe, 172–175
milling involute worm, 175–177
single parametric motions in design, 166–172
disk-type gear milling cutter, 167–168
end-type gear milling cutter, 166–172
face gear milling cutter, 168–169
internal round broach for cutting spur and helical gears, 169–170
internal round broach for machining bevel gears, 170–172
single parametric motions, plurality of, 163–166
coordinate system, 163–164
position vector, 163–164
rotations, 165
translations, 164–165
thread whirling, 177–178
Form milling cutter, 120
Full topping, 264
Fundamental forms, direct transformation of, 55–56

G

Gear broaching, 72–73
definition of, 72
kinematics of, 59, 60*f*
pull broaches, 73
push broaches, 73
side-shaving section of, 73
Gear broaching tools, 59–90
application of, 72–74
broaching external gears, 73–74
broaching internal gears, 73
bevel gear teeth broaching, 81–90
burnishing button, 73
chip per tooth, 59, 65–66
chip removal diagrams, 65–66
cut per tooth, 65–66
cutting edges, 61–65
finishing teeth, 59
generating surface of, 60–61
for machining involute gears, 70–72
cross section of auxiliary rack, 72
shapes and configurations of cutting edges, 70–71
straight lateral cutting edges, 71–72
pot broaching, 74
rake angle, 68
rake surface of finishing teeth, 61–64
Archimedean screw surface, 62–63
clearance surface, 64–65
conical, 62–63
face angle radius, 62
gullet, 62
pitch, 62
tooth depth, 62
resharpening of, 69*f*
Revacycle process, 81–90
cutting tools, 83–84
kinematics of, 82*f*
principle of, 82–83
profiling of cutter for bevel gear machining, 85–90
tooth space generation, 83*f*
rotary broaches, 80–81
sharpening of, 66–70
generating of rake surface, 68
generating surface of grinding wheel, 66–67
helical gullet, 68
maximal feasible outer diameter of grinding wheel, 67
schematic diagram, 69*f*
support at center, 67
Shear-Speed cutting, 74–80
application, 79–80
principle of, 74
profiling of form tools, 76–79
slater tools, 80–81
Gear cutting tools, 1–2
cylindrical, 673–679
examples of, 676–679
gear tooth with chamfers, 677–678
gear tooth with lengthwise modification, 678*f*
generating surface of, 673–674
part surface generation, 674–676
vector diagram, 677*f*
direct problem of design, 2
elementary relative motions, 20–21
with enveloping generating surface, 673–686
conical generating surface, 679–681
cylindrical generating surface, 673–679
toroidal generating surface, 681–686
feasible relative motions, 21–23
generating body of, 395
inverse problem of design, 2
for machining internal gears, 687–691
examples of, 689–691
generating surface of, 689
geometry of internal gear, 687
kinematics of machining internal gear, 689–690
Shear-Speed cutting, 74–80

Gear cutting tools, for machining bevel gears, 315–342
curved teeth, 337–342
clearance angle, 342
design of cutters, 340–342
diagrammatic arrangement of, 339*f*
gear machining operation, 338–340
profile angle, 341
rake angle, 342
spiral angles, 337
face hob for, 668, 669*f*
generating surface of, 325–328
geometry of interacting tooth surfaces, 318–325
generating surface of gear cutting tool, 319–323
involute straight bevel gear tooth flank, 318–319
octoidal profile, 319
tooth flanks of generated gear, 323–325
kinematics of bevel gear generation, 315–317
axodes, 316
coordinate systems, 317
pitch angle, 316
rotation vectors, 315–316
overview, 315–42
plunge method, 665–668
face hob, 668, 669*f*
kinematics, 665–667
possible designs, 667–668
quasi-planar gear machining meshes, 669–670
straight bevel gear cutting, 333–334
straight bevel gear milling, 334–337
design of milling cutters, 335–336
disk-type milling cutters, 336
lateral cutting edges, 25–26
shape of finished flanks, 336–337
straight bevel gear teeth, 328–333
gear cutting tools, 330–333
machining of straight bevel gears, 329–330
plane T_a by straight motion of cutting edge, 328–329
straight bevel gears with offset teeth, 325–328
Gear hobs, 395–559
accuracy for machining involute gears, 433–462
actual machining surface vs. desired generating surface, 438–445
analytical description of actual lateral cutting edge, 436–437
analytical description of desired lateral cutting edge, 436
deviations of rack surface, 434*f*
as function of design parameters, 435–445
impact of lead angle of screw rake surface on tooth profile deviation, 440–443
impact of pitch diameter, 445–462
impact of rake angle on tooth profile deviation, 438–440
kinematic geometry of involute hob, 454–462
machining surface, 437–438
maximum deviation of hob tooth profile, 438
pitch helix angle, 447
principal design parameters of, 449–454
relative motions of work gear and hob, 446–449
clearance surface of, 411–433
clearance angle, 413, 416–423
cutting edges, 411
cutting of relieved clearance surface, 415–423
equation of desired clearance surface, 411–415
grinding of relieved clearance surface, 423–433
helix angle, 414
operator of linear transformation, 415
position vector, 413
rake plane, 413
reduced pitch, 413
tooth relieving operation, 415
conical hobs, 493–497
butt-end hob, 496, 496*f*
face hob, 496, 496*f*
work gear to cutting tool penetration curve, 493, 495*f*
cutting edge geometry of gear hob tooth, 498–515
clearance angle, 510, 513–514
cutting edge roundness, 511
improvement of hob design, 514–515
inclination angle, 510–512
machining zone, 500, 503–505
penetration curve, 500–503
rake angle, 509–510, 512–513
resultant motion, 506–508
tool-in-use reference system, 505–515
unit normal vector to surface of cut, 505–506
unit tangent vector, 508
cylindrical hobs of nonstandard design, 487–493
for finishing hardened gears, 490–493
number of hob threads, 489

Gear hobs (*continued*)
for smooth roughing of coarse pitch gears, 487–489
unfolded cross section, 488*f*, 490*f*
definition of, 395
design of, 462–498
design parameters, 462–465
tooth profiles, 465–468
for face gear, 645–646
hobbing operations, 528–534
climb hopping, 530
conventional hopping, 530
cycles, 534–536
hob total travel distance, 536–537
hobbing time, 536–537
idle distance and neck width of cluster gear, 538–540
plunge method, 644–645
prescribed value of setting angle, 555–558
setting angle, 538–540
shortest allowable approach distance, 552–554
shortest allowed idle distance, 540–545
tangential method, 643, 644*f*
tolerance and shortest possible idle distance, 545–552
kinematic geometry of involute hob
change to normal profile angle, 454–457
correction to configuration of rake surface, 458–560
value of center-distance in gear hobbing operation, 457–458
multistart, 407–408
precision involute hubs with lateral cutting edges, 468–487
analytical approach to configuration of rake plane, 471–475
computation, 475–477
design parameters, 470–477
DG-based approach to configuration of rake plane, 470–471
modified tooth profile, 481–487
resharpening, 477–481
rake surface of, 399–410
auxiliary axis of projections, 407
auxiliary reference systems, 401
Cartesian coordinate system, 399–400
cone angle, 407
in form of plane, 403–404
generation of, 403–410
geometry, 399–403
intermittent, 409–410
of multistart hob, 407–408
plane of projections, 407
position vectors, 401
rake angle, 403
screw rake surface, 405–407
straight-generating lines, 405–406
straight-line generator, 400
zero rake angle, 402
tool-in-use reference system, 505–515
clearance angle, 510, 513–514
inclination angle, 510–512
rake angle, 509–510, 512–513
tooth profiles, 515–528
actual value of deviation, 527–528
allowed interval for profile angle, 527–528
applied reference systems, 516–517
elementary gear drive, 517–518
form diameter of gear, 517–518
limit diameter of gear, 517
maximum allowed value of modification, 516–522
modification of, 517
normalized deviation, 522–524
reduced addendum, 524–527
toroidal hobs, 497–498
transformation of generating surface into gear tool, 395–399
feed motion, 395–396
grinding worm, 395, 396*f*
screw motion, 396–398
Gear honing, 685–686
Gear machining, 19–24
continuously indexing methods, 25–42
classification of gear machining meshes, 39–42
configuration of rotation vectors, 37–39
kinematic relationships for gear machining mesh, 32–37
kinematics of gear machining, 42
vector representation of gear machining mesh, 25–32
relative motions, 19–23
elementary, 19–23
feasible, 21–23
rolling of conjugate surfaces, 23–24
Gear machining mesh, 39–42
applications of, 643–662
conical hob for palloid gear cutting, 658–662
cutting tool for machining worm in continuously indexing method, 653–654
cutting tools for scudding gears, 649–651
gear reinforcement by surface plastic deformation, 657–658

hob for face gear, 645–646
hob for plunge gear hobbing, 644–645
hob for tangential gear hobbing, 643, 644*f*
rack shaving cutters, 654–657
shaper cutter with tilted axis of rotation, 651–653
worm-type cutting tool with continuous helix-spiral cutting edge, 646–649
center distance, 40
crossed-axis angle, 40
definition of, 25
external, 39–40, 41*f*
internal, 40, 41*f*
kinematics of, 42
kinematics relationships, 32–37
magnitude of rotation vectors, 40
planar, 39–40, 41*f*
vector diagram, 29, 30*f*
vector representation of, 25–32
Gear milling cutters, disk-type, 123–161
15-gear, 155
accuracy of tooth flanks machined with, 152–154
application of, 154–161
circular saws, 159–160
cutting edge geometry of, 143–146
clearance angle, 144–146
pressure angle, 145–146
profile angle, 144–145
rake angle, 143, 146
cutting edges of, 132–136
clearance surface, 132f, 134–136
rake surface, 132–134, 132*f*
eight-gear, 155
generating surface of, 125–127
elements of intrinsic geometry, 130–132
equation for machining spur involute gears, 125–127
for machining helical involute gears, 127–130
inclined tooth profile, 155, 156*f*
indexing, 161
kinematics of gear cutting, 123–124
crossed-axis angle, 123
feed motion, 123
pitch helix angle, 123
rotation vector, 123–124
screw feed motion, 124
multiple-tooth, 161
overview, 123
profiling of, 136–143
analytical, 138–143
descriptive geometry-based methods, 136–138
for roughing of gears, 147–152
assembled cutter, 151*f*
clearance angle, 147–148
design parameters, 147*f*
even-numbered teeth, 150
odd-numbered teeth, 150
progressive cutting diagram, 149
rake angle, 147
top-loaded cutting diagram, 150
wavy cutting edges, 151
single parametric motions in design of, 167–168
span measurement, 158*f*
Gear milling cutters, end-type, 91–122
application of, 120–122
cutting edges, 101–114
clearance surface, 105–108
geometry of, 108–114
helix angle, 113
pressure angle, 114
rake surface in form of plane, 109–111
rake surface in form of screw surface, 111–114
generating surface of, 92–101
elements of intrinsic geometry, 100–101
equation for machining helical involute gears, 96–100
equation for machining spur involute gears, 92–96
secondary, 92
for helical gears, 120–121
indexing mechanism, 122
kinematics of gear machining, 91, 92*f*
machining gear tooth flanks with, 115–119
characteristic *E*, 115
curvature of helical gear tooth flank, 118
cusps on tooth flanks of helical gear, 117–119
cusps on tooth flanks of spur gear, 115–117
maximal deviation, 117
waviness of tooth flank, 116
overview, 91
single parametric motions in design of, 166–167
for spur gears, 120
Gear modification matrix, 622
Gear scudding, 649–651
applications of, 651
cutting tools for, 649–651
design concept for tools, 649–651
Gear shaper cutters, external gear machining mesh, 223–279
accuracy of gears cut with, 255–260

Gear shaper cutters (*continued*)
fifth condition of proper post surface generation, 255–258
gear-to-shaper cutter meshing diagram, 257
sixth condition of proper post surface generation, 258–260
application of, 260–279
critical distance to nominal cross section, 236–239
circular tooth thickness, 239
length of top cutting edge, 237–238
maximal length of distance, 237
cutting edge geometry of, 239–248
angle of inclination of lateral cutting edge, 240–241
clearance angle of lateral cutting edge, 243–248
improvement in geometry, 245–248, 265–269
rake angle of lateral cutting edge, 241–243
cutting edges of, 229–233
clearance surface of tooth, 232–233
rake surface, 229–232
design of shaper cutters, 261–263
deep counterbore-type, 261
disk-type, 261
for machining helical and herringbone gears, 264–265
tooth profiles, 263–264
desired corrections to tooth profile, 248–250
generating surface of, 225–229
Cartesian coordinate system, 225–226
for machining involute shapes, 228
pitch helix angle, 228
position vector, 225–226
profile angle, 227
Shishkov's equation of contact, 227–228
grinding of, 274–279
clearance surfaces, 274–275
rake surfaces, 275–279
improvement in geometry of clearance surface, 246–248
kinematics of gear shaping, 223–225
principal elements, 224*f*
reciprocation, 223
screw motion, 223–224
vector diagram, 224*f*
lateral cutting edges
angle of inclination, 240–241
clearance angle, 243–248
rake angle, 241–243
overview, 223–279
profiling of, 233–236
angular displacement of tooth profile, 236
base diameter, 235
circular tooth thickness, 234–235
meshing of auxiliary rack surface, 233–234
profile shift correction coefficient, 235
tooth addendum, 235
tooth dedendum, 235
tooth thickness, 235–236
rake surface of, 229–232
geometry, 230–231
helical, geometry of, 231–232
improvement in geometry, 245–246
special designs of, 265–273
angular pitches, 268
combined rake surface, 266
improved cutting edge geometry, 265–269
for machining hardened gears, 270–272
precision gear, 269–270
two gears, 267–269
thickness of chip cut by, 251–255
feed rate motion, 251
operator of rolling, 253–254
position vector, 253–254
roll angle, 252
speed of instant rotation, 251
tooth ratio, 252
tooth profiles, 263–264
chamfer, 263–264
full topping, 264
modified pressure angle, 264
protuberance, 264
root fillet, 263
semitopping, 263–264
tip relief, 263
typical gear shaping operations, 273–274
combination operations, 274
cutting two gears with different diametral pitch, 274
cutting two gears with similar diametral pitch, 274
cutting two gears with up and down shaping, 274
length of stroke, 273, 274*f*
spiral infeed, 274
Gear shaper cutters, internal gear machining mesh, 281–295
accuracy of shaped internal gears, 290–292
interference of internal work gear and shaper cutter teeth, 291–292
tooth number, 292
transverse generating pressure angle, 291
application of, 293–295
cutting edge geometry of, 285–286

design of shaper cutters, 283
enveloping shaper cutters, 293
generating surface of, 283
kinematics of shaping operation, 281–283
rotation vector, 281–282
screw motion, 283
materials used in, 293
profiling of shape cutters
deep counterbore-type, 284–285
shank-type, 284–285
profiling of shaper cutters, 283–285
clearance surface, 283–284
generating surface, 283–284
rake surface, 283–284
thickness of chip cut by, 286–290
feed motion, 286
motion of cut, 286
operator of rolling, 288–289
Gear shaper cutters, with tilted axis of rotation, 301–314
capabilities of external intersecting-axis gear machining mesh, 311–314
shaping conical involute gears, 311, 312*f*
shaping of face gears, 311–314
generating surface of, 304–311
addendum, 310
base diameter of shaper cutter, 310
coordinate systems transformations, 306–307
coordinates of points within tooth profile, 307–308
dedendum, 310
left-hand-oriented coordinate system, 304–305
internal gear machining mesh, 343–349
axodes, 345
kinematics of internal gear machining mesh, 343
motion of cut, 344
operating pitch surfaces, 345
rake surface, 345–346
rotation vectors, 345
shaping of external recessed tooth forms, 347–349
shaping of internal gear, 344–346
shaping of spur gear, 346–347
kinematics of shaping operation, 301–304
rake surface, 303–304
reference systems, 302
rotation vector, 301–302
Gear shaving cutters, 559–642
advances in design of, 633–638
constant inclination angle within cutting edges, 635–636
for finishing modified work gear tooth flank, 637–638
near optimal angle of inclination of cutting edges, 633–635
precision cutter with straight cutting edges, 636–637
axial method of shaving process, 576–587
coordinate systems transformations, 585
cutting speed, 578–587
equivalent base diameters, 586–587
formula for cutting speed, 587
impact of crossed-axis angle, 578–579
impact of profile sliding, 580–587
impact of traverse motion, 579–580
kinematics of, 576–578
line of action, 584
workgear to shaving cutter meshing, 580, 581*f*, 583*f*
clearance surface of cutting teeth, 562
design of shaper cutters, 566–576
design parameters, 567, 575*t*
resharpening, 571–576
serrations on tooth flanks, 568–571
diagonal method of shaving process, 587–602
coordinate systems, 596–598
cutting speed, 590–592
diagonal-underpass, 590
geometry of contact of tooth flanks, 598–602
kinematics of, 588–589
local topology of contacting tooth flanks, 595–596
multistroke, 589
optimal kinetic parameters, 602
optimization of kinematics, 592–595
traverse angle, 589–590
generating surface of, 559–560
inclination angle of cutting edges, 564–568
manufacturing aspects of shaving operation, 640–641
modification of tooth form and shape, 641
plunge method of shaving processing, 619–633
circular mapping of tooth flanks, 629–631
cutting speed, 619
design of shaving cutters, 631–633
epicyclical motion in, 619
kinematics of, 619–620
part surface generation, 628–633
topologically modified gears, 621–628
rake surface of cutting teeth, 560–561
requirements for preshaved work gear, 639–640

Gear shaving cutters (*continued*)
selection of, 639
shaving of worm gear, 641–642
tangential method of shaving process, 603–618
analytical approach, 612–618
cutting speed, 604–605
descriptive geometry-based methods, 605–612
kinematics of, 603–604
serrations, 605
tooth flanks, 595–596
curvature of tooth surface, 596
Dupin indicatrix of tooth surface, 596
equation of tooth flank of, 595
first fundamental form of tooth surface, 595
indicatrix of conformity, 599
local orientation, 598
maximum rate of conformity, 600
optimal design parameters, 600
principal directions, 598
second fundamental form of tooth surface, 595
Gear tooth
engineering formula for, 695–697
for surfaces that allow sliding, 16–18
Gear tooth flank surface, natural parameterization of, 13
Gears, 3–18
definition of, 3
tooth flanks, 6–16
types of, 3–6
cluster, 5, 6*f*
double-helical, 3, 6o
face, 6
helical, 3
helical rack, 3
herringbone, 3
spur, 3, 4*f*
straight bevel, 5–6
Generating body, 395
Generating surfaces, 353–394
auxiliary, 357–363
characteristic line E_g, 362
coordinate systems, 357–359
coordinate systems transformations, 359
pitch diameter, 361–362
profile angle, 362
rack surface, 357–358
relative motion of work gear, 358
tooth flank surface, 359–360
types of, 363
base diameter, 380–381
base helix angle, 378–379, 696*t*
of conical gear cutting tools, 679–680
of cylindrical gear cutting tools, 673–674
definition of, 363–378
descriptive geometry-based methods, 378–381
design parameters, 363–371
base diameter of generating surface, 376–378
characteristic line, 367
complementary equations, 376–378
coordinate systems, 365
envelope to successive positions of plane with screw motion, 365–368
helix angle, 377
principal elements of geometry, 368–370
setting angle, 374–376
straight rack, 365
disk-type gear milling cutters, 124–132
for machining helical involute gears, 127–130
for machining spur involute gears, 125–127
equation, 371–374
auxiliary rack, 371–372
screw motion, 372–373
unit normal vector, 374
of gear broach, 60–61
of gear shaper cutters, 283
for machining involute shapes, 228
pitch helix angle, 228
profile angle, 227
Shishkov's equation of contact, 227–228
of grinding wheel, 66–67
kinematics of external spatial gear machining mesh, 353–357
axode of gear cutting tool, 357
center distance, 353
crossed-axis angle, 353
hyperboloid, 356
opposite-directed vector, 356
pure rolling of axodes, 354–355
rotation of cutting tool, 353
rotation of work gear, 353
rotation vectors, 353–354
vector of linear velocity of sliding of axodes, 355
straight bevel gears with offset teeth, 325–328
of toroidal gear cutting tools, 681–686
types of, 364*f*, 381–392
asymmetric tooth profile, 389–390
conical, 383–389
torus-shaped pitch surfaces, 390–392
zero profile angle, 381–383
Gleason method, 668

Grinding, relief, 423–433
of assembled gear hobs, 425–433
position for machining, 425, 431*f*
of solid gear hobs, 423–425
technological worm, 428
working position, 425, 431*f*
Grinding wheel, 66–67
generating surface of, 66–67
maximal feasible outer diameter, 67
Gullet, 62

H

Hardened gears, machining, 270–272
Helical bevel gear, 15–16
Helical gears, 3
disk-type gear milling cutters, 127–130
end-type gear milling cutter, 96–100
gear milling cutter for, 120–121
internal round broach for, 169–170
involute, 10–14
shaper cutters for, 264–265
tooth flanks, 10–14, 15–16
cusps, 117–119
deviation from desired shape, 118–119
normal curvature of, 118
Helical gullet, 68
Helical rack gears, 3
Helical shaper cutters, rake surface of, 231–232
Helix angle, 113
equation, 696*t*
of involute hobs, 476
Herringbone gears, 3, 264–265
High speed steels (HSS), 261, 293
Hob base diameter, 475*t*
Hobs for machining gears, 395–559
accuracy for machining involute gears, 433–462
actual machining surface vs. desired generating surface, 438–445
analytical description of actual lateral cutting edge, 436–437
analytical description of desired lateral cutting edge, 436
deviations of rack surface, 434*f*
as function of design parameters, 435–445
impact of lead angle of screw rake surface on tooth profile deviation, 440–443
impact of pitch diameter, 445–462
impact of rake angle on tooth profile deviation, 438–440
kinematic geometry of involute hob, 454–462
machining surface, 437–438
maximum deviation of hob tooth profile, 438
pitch helix angle, 447
principal design parameters of, 449–454
relative motions of work gear and hob, 446–449
clearance surface of, 411–433
clearance angle, 413, 416–423
cutting edges, 411
cutting of relieved clearance surface, 415–423
equation of desired clearance surface, 411–415
grinding of relieved clearance surface, 423–433
helix angle, 414
operator of linear transformation, 415
position vector, 413
rake plane, 413
reduced pitch, 413
tooth relieving operation, 415
conical hobs, 493–7
butt-end hob, 496, 496*f*
face hob, 496, 496*f*
work gear to cutting tool penetration curve, 493, 494*f*
cutting edge geometry of gear hob tooth, 498–515
clearance angle, 510, 513–514
cutting edge roundness, 511
improvement of hob design, 514–515
inclination angle, 510–512
machining zone, 500, 503–505
penetration curve, 500–503
rake angle, 509–510, 512–513
resultant motion, 506–508
tool-in-use reference system, 505–515
unit normal vector to surface of cut, 505–506
unit tangent vector, 508
cylindrical hobs of nonstandard design, 487–493
for finishing hardened gears, 490–493
number of hob threads, 489
for smooth roughing of coarse pitch gears, 487–*489*
unfolded cross section, 488*f*, 490*f*
definition of, 395
design of, 462–498
design parameters, 462–465
tooth profiles, 465–468
for face gear, 645–646
hobbing operations, 528–534

Hobs for machining gears (*continued*)
climb hopping, 530
conventional hopping, 530
cycles, 534–536
hob total travel distance, 536–537
hobbing time, 536–537
idle distance and neck width of cluster gear, 537–538
prescribed value of setting angle, 555–558
setting angle, 538–540
shortest allowable approach distance, 552–554
shortest allowed idle distance, 540–545
tolerance and shortest possible idle distance, 545–552
kinematic geometry of involute hob
change to normal profile angle, 454–457
correction to configuration of rake surface, 458–560
value of center-distance in gear hobbing operation, 457–458
multistart, 407–408
for plunge gear hobbing, 644–645
precision involute hubs with lateral cutting edges, 468–487
analytical approach to configuration of rake plane, 471–475
computation, 475–477
design parameters, 470–477
DG-based approach to configuration of rake plane, 470–471
modified tooth profile, 481–487
resharpening, 477–481
rake surface of, 399–410
auxiliary axis of projections, 407
auxiliary reference systems, 401
Cartesian coordinate system, 399–400
cone angle, 407
in form of plane, 403–404
generation of, 403–410
geometry, 399–403
intermittent, 409–410
of multistart hob, 407–408
plane of projections, 407
position vectors, 401
rake angle, 403
screw rake surface, 405–407
straight-generating lines, 405–406
straight-line generator, 400
zero rake angle, 402
for tangential gear hobbing, 643, 644*f*
tool-in-use reference system, 505–515
clearance angle, 510, 513–514
inclination angle, 510–512
rake angle, 509–510, 512–513
tooth profiles, 515–528
actual value of deviation, 527–528
allowed interval for profile angle, 527–528
applied reference systems, 516–517
elementary gear drive, 517–518
form diameter of gear, 517–518
limit diameter of gear, 517
maximum allowed value of modification, 516–522
modification of, 517
normalized deviation, 522–524
reduced addendum, 524–527
toroidal hobs, 497–498
transformation of generating surface into gear tool, 395–399
feed motion, 395–396
grinding worm, 395, 396*f*
screw motion, 396–398
Homogenous coordinate transformation matrices, 43–44
Homogenous coordinate vectors, 43–44

I

Inclination angle, 200, 511–513
Indexing, continuous, 25–42
classification of gear machining meshes, 39–42
configuration of rotation vectors, 37–39
kinematic relationships for gear machining mesh, 32–37
kinematics of gear machining, 42
vector representation of gear machining mesh, 25–32
Indicatrix of conformity, 599
Integral-shank hobs, 463
Intermittent rake surface, 409–410
Internal gear machining meshes, 41*f*, 281–295. *See also* external gear machining meshes
accuracy of shaped internal gears, 290–292
interference of internal work gear and shaper cutter teeth, 291–292
tooth number, 292
transverse generating pressure angle, 291
application of, 293–295
cutting edge geometry of, 285–286
definition of, 40
design of shaper cutters, 283
enveloping shaper cutters, 293
gear cutting tools for machining internal gears, 687–691

gear cutting tools with enveloping generating surface, 673–686
conical generating surface, 679–681
cylindrical generating surface, 673–679
toroidal generating surface, 681–686
generating surface of, 283
kinematics of shaping operation, 281–283
rotation vector, 281–282
screw motion, 283
materials used in, 293
profiling of shaper cutters, 283–285
clearance surface, 283–284
deep counterbore-type, 284–285
generating surface, 283–284
rake surface, 283–284
shank-type, 284–285
thickness of chip cut by, 286–290
feed motion, 286
motion of cut, 286
operator of rolling, 288–289
Internal gears, 5*f*, 687–691
broaching, 73
examples of gear cutting tool, 689–691
generating surface of gear cutting tool, 689
geometry of, 687
hob for cutting, 690*f*
kinematics of machining internal gear, 687–688
shaping of, 344–346
Internal round broach
for bevel gears, 170–172
for helical gears, 169–170
for spur gears, 169–170
Intersecting-axis gear machining mesh
gear cutting tools, for machining bevel gears, 315–342
gear shapers with tilted axis of rotation, 301–304, 343–349
Inverse problem of gear-cutting tool design, 2
Involute curve, 10*f*
Involute function of pressure angle, 696*t*
Involute gears
curvature of tooth surface, 596
Dupin indicatrix of tooth surface, 596
equation of tooth flank of, 595
first fundamental form of tooth surface, 595
machining, 70–72
cross section of auxiliary rack, 72
gear broaching tools for, 70–72
gear milling cutter for, 121
helical gears, 96–100
shapes and configurations of cutting edges, 70–71
spur gears, 92–100
straight lateral cutting edges, 71–72
second fundamental form of tooth surface, 595
tooth flanks, 9–14
helical gears, 10–14
spur gears, 9–10
Involute helical gears, tooth flank, 10–14
Involute hobs, 433–462, 468–487
actual machining surface vs. desired generating surface, 438–445
analytical approach to configuration of rake plane, 471–475
analytical description of actual lateral cutting edge, 436–437
analytical description of desired lateral cutting edge, 436
change to normal profile angle, 454–457
computation, 475–477
conical hobs, 493–497
butt-end hob, 496, 496*f*
face hob, 496, 496*f*
work gear to cutting tool penetration curve, 493, 494*f*
correction to configuration of rake surface, 458–560
cylindrical hobs of nonstandard design, 487–493
for finishing hardened gears, 490–493
number of hob threads, 489
for smooth roughing of coarse pitch gears, 487–489
unfolded cross section, 488*f*, 490*f*
design parameters, 470–477
deviations of rack surface, 434*f*
DG-based approach to configuration of rake plane, 470–471
as function of design parameters, 435–445
impact of lead angle of screw rake surface on tooth profile deviation, 440–443
impact of normal profile angle, 478*f*
impact of number of starts, 478*f*
impact of pitch diameter, 445–462
impact of rake angle on tooth profile deviation, 438–440
impact of setting angle, 479*f*
machining surface, 437–438
maximum deviation of hob tooth profile, 438
modified tooth profile, 481–487
pitch helix angle, 447
principal design parameters of, 449–454, 460*t*
relative motions of work gear and hob, 446–449
tooth profiles, 515–528
actual value of deviation, 527–528

Involute hobs (*continued*)
allowed interval for profile angle, 527–528
applied reference systems, 516–517
elementary gear drive, 517–518
form diameter of gear, 517–518
limit diameter of gear, 517
maximum allowed value of modification, 516–522
modification of, 517
normalized deviation, 522–524
reduced addendum, 524–527
toroidal hobs, 497–498
value of center-distance in gear hobbing operation, 457–458
Involute worm, 171–181
grinding, 178–181
machining, 172–175
milling, 175–177

J

Jacobian matrix, 703

K

Kinematics of gear cutting, 123–124
crossed-axis angle, 123
feed motion, 123
gear milling cutters, disk-type, 123–124
pitch helix angle, 123
rotation vector, 123–124
Kinematics of gear machining, 19–24
bevel gears, 315–317
continuously indexing methods, 42
elementary relative motions, 20–21
external spatial gears, 353–357
feasible relative motions, 21–23
gear broaching, 60*f*
gear machining mesh, 42
gear milling cutters, end-type, 91, 92*f*
internal gears, 687–688
invertibility of, 28
rolling of conjugate surfaces, 23–24
Kinematics of gear shaping
external gear machining mesh, 223–225
gear shapers with tilted axis of rotation, 301–304
internal gear machining mesh, 281–283
Kinematics of gear shaving
axial method, 576–578
diagonal method, 588–589
plunge method, 619–620
tangential method, 603–604

L

Lateral cutting edges
analytical descriptions of, 436–437
angle of inclination, 240–241
clearance angle of, 243–248
computation of geometry for, 200–202
of involute hobs, 436–437
rake angle of, 241–243
Lathe, machining worm on, 172–175
Lead, 695*t*
Line of action, 584

M

M-2 high-speed steel, 80
Machining meshes, 25
applications of, 643–662
conical hob for palloid gear cutting, 658–662
cutting tool for machining worm in continuously indexing method, 653–654
cutting tools for scudding gears, 649–651
gear reinforcement by surface plastic deformation, 657–658
hob for face gear, 645–646
hob for plunge gear hobbing, 644–645
hob for tangential gear hobbing, 643, 644*f*
rack shaving cutters, 656–659
shaper cutter with tilted axis of rotation, 651–653
worm-type cutting tool with continuous helix-spiral cutting edge, 646–649
center distance, 40
crossed-axis angle, 40
external, 39–40, 41*f*
internal, 40, 41*f*
kinematics of, 42
kinematics relationships, 32–37
magnitude of rotation vectors, 40
planar, 39–40, 41*f*
spatial gear, 353–357
gear shaving cutters, 559–642
generating surface of gear cutting tool, 353–394
hobs for machining gears, 395–559
kinematics of, 353–357
vector diagram, 29, 30*f*
vector representation of, 25–32
Machining surface, of involute hobs, 437–438
Machining zone, 500, 503–505
Magnitude of rotation vectors, 40
Major section plane, 706–708

Mensnier's formula, 117, 152
Merchant's formula, 511
Metric-to-pitch system conversion, 697*t*
Minor cutting edge approach angle, 715–716
Modified pressure angle, 264
Multistart hobs, 407–408
Multistroke shaving, 589

N

Natural parameterization, 13
NC grinder, 625–627
Nitriding surface treatment, 293
Normal circular pitch, 695*t*
Normal diametral pitch, 696*t*
Normal pitch, 475*t*
Normal pressure angle, 696*t*
Normal rake angle, 709–710
Normal section plane, 709
Normalized velocity, 34

O

Octoidal profile, 319
Oerlikon method, 668
Offset teeth, 325–328
Operating pitch diameter, 696*t*
Operating pressure angle, 696*t*
Operators of reflections, 54
Operators of rolling motion, 50–51
Operators of rotation, 46–47
Operators of screw motion, 48–49
Operators of translation, 44–45
Opposite transformation, 54
Orientation-preserving transformation, 45
Orientation-reversing transformation, 54
Outside diameter, 695*t*, 697*t*

P

Palloid gear hobbing, 658–662
  design of conical hob, 659–660
  kinematics of, 660–661
  machining with crowned teeth, 662
  overview, 659
Parallel-axis gear machining mesh, 183–185
  gear shaper cutters, 223–295
    external gear machining mesh, 223–279
    internal gear machining mesh, 281–295
  rack cutter, 187–222
Part surface generation, 628–633
  conditions for, 699–701
  cylindrical gear cutting tool, 674–676
  plunge shaving, 628–633
Penetration curve, 498–515
Pitch angle, 475*t*
Pitch diameter
  conversion to metric system, 697*t*
  equation, 695*t*
  of involute hobs, 475*t*
Pitch helix angle
  in disk-type milling cutters, 123–124
  in gear broaching, 59
  of gear shaper cutters, 228
Pitch line, 29
Pitch point, 33
Pitch-to-metric system conversion, 697*t*
Planar gear machining mesh, 39–40, 41*f*
Plane of cut, 705–706
Plastic deformation, gear reinforcement by, 657–658
Plunge shaving, 619–33. *See also* shaving cutters
  circular mapping of tooth flanks, 629–631
  cutting speed, 619
  design of shaving cutters, 631–633
  epicyclical motion in, 619
  kinematics of, 619–620
  part surface generation, 628–633
  topologically modified gears, 621–628
    auxiliary rack modification matrix, 627
    gear modification matrix, 622
    generating surface of form grinding wheel, 627–629
    geometry of, 621–624
    grinding of tooth flanks, 625–628
    NC grinder, 625–627
    tooth flanks of shaving cutter, 624–625
PM4 powder metal, 80
Position for machining, relief grinding, 425, 431*f*
Position vector
  of gear shaper cutters, 225–226
  involute tooth profile, 9
  tooth flank of helical bevel gear, 16
  tooth flank of involute spur gear, 9
  tooth flank of work gear, 226–227
Pot broaching, 74
Precision gear shaper cutters, 269–270
  carbide, 270–273
Pregrind rack cutter, 218–219
Pressure angle
  disk-type gear milling cutters, 145–146
  end-type gear milling cutters, 114
  involute function of, 696*t*
  of involute hobs, 475*t*
  normal, 696*t*

Pressure angle (*continued*)
transverse, 696*t*
Profile angle
disk-type gear milling cutters, 144–145
of gear shaper cutters, 227
Profile sliding, 580–587
Progressive cutting diagram, 149
Proper post surface generation
accuracy of gears and, 255–260
fifth condition of, 212–215, 255–258
sixth condition of, 215–218, 255–258
Protuberance, 264
Pull broaches, 73
Pull-up broaching, 74
Push broaches, 73
Push-up pot broaching, 74

Q

Quasi-planar gear machining meshes, 351, 669–670

R

Rack cutters, 187–222
accuracy of machined gear, 212–218
fifth condition of proper post surface generation, 212–215
gear-to-rack cutter meshing diagram, 214–215
sixth condition of proper post surface generation, 215–218
application of, 218–219
chip thickness cut by cutting edges of, 207–212
clearance angle, 202
computation, 200–202
cutting edge geometry of, 199–207
cutting motion, 208
direction of reciprocation, 207–208
feed motion, 208–209
inclination angle, 200
for lateral cutting edges, 200–202
modification of clearance surface, 204–207
modification of rake surface, 203–204
operator of rolling, 211
position vector, 211
translational motion, 208
cutting edges of, 193–196
clearance surface, 195–196
rake surface, 194–195
feasible tooth profiles, 191–193
helix angle, 191
radius of pitch cylinder, 191
tooth profile angle, 191
tooth thickness of generating surface, 192
finish, 218–219
generating surface of, 187–191
equation for, 187–190
indexing time, 219
methods and designs, 220–222
pregrind, 218–219
profiling of, 196–199
analytical, 198–199
descriptive geometry-based, 197, 198*f*
rough, 218–219
tooth profile angle, 198–199
Rack shaving cutters, 654–657
Rake angle, 709–710
chip-flow, 717–718
definition of, 709–710
disk-type gear milling cutters, 143, 146
of gear broach, 68
of hob tooth cutting edge, 509–510, 512–513
of lateral cutting edge, 241–243
normal, 709–710
Rake surface
of gear hobs, 399–410
auxiliary axis of projections, 407
auxiliary reference systems, 401
Cartesian coordinate system, 399–400
cone angle, 407
in form of plane, 403–404
generation of, 403–410
geometry, 399–403
intermittent, 409–410
of multistart hob, 407–408
plane of projections, 407
position vectors, 401
rake angle, 403
screw rake surface, 405–407
straight-generating lines, 405–406
straight-line generator, 400
zero rake angle, 402
of milling cutter for machining involute gears, 132–134
modification of, 203–204
of rack cutter, 194–195
of shaper cutter, 229–232
combined rake surface, 266
geometry, 230–231
grinding, 275–279
helical, geometry of, 231–232
Ratio of translation V_{cut}, 59
Reciprocation, 207–12, 223
Reference plane of chip flow, 716–717
Reinforcement, 657–658

Relief grinding, 423–433
of assembled gear hobs, 425–433
position for machining, 425, 431*f*
of solid gear hobs, 423–425
technological worm, 428
working position, 425, 431*f*
Resharpening
precision involute hobs, 477–481
shaving cutters, 571–576
Resultant coordinate systems transformations, 47–48
Revacycle process, 81–90. *See also* broaching
cutting tools, 83–84
kinematics of, 82*f*
principle of, 82–83
profiling of bevel gear cutter, 85–90
application, 88–90
finishing teeth, 85–88
reference systems, 85*f*
shape of roughing teeth, 88–90
tooth space generation, 83*f*
Ring-type pot broaching tool, 74
Rolling motion, 50–54
of coordinate system, 50–51
over cylinder, 53
operators of, 50–51
over plane, 50
of two coordinate systems, 52–54
Root fillet, 263
Rotary broaches, 80–81
clearance angle, 80
form size, 81
shank axis, 80
tool holder, 81
Rotation
frequencies, 33
inversion of, 29*f*
Rotation vector, 26–29
configuration of, 37–39
critical configuration of, 38
of disk-type milling cutter, 123–124
in gear machining mesh, 32–33
magnitude of, 36, 40–42
superimposition of translation vector and, 36
Rotations, 19
Rough rack cutter, 218–219
Round rack, 319

S

Scientific approach, 8
Screw surface, Archimedean, 62–63
Screw feed motion, 124
Screw involute surface, 10–13, 10*f*, 13*t*
Screw motion, 26
about coordinate axis, 48–49
gear shaper cutters, 223–224
operators of, 48–49
parameter, 36
Screw rake surface, 405–407
Scudding, 651–653
applications of, 651
cutting tools for, 649–651
design concept for tools, 649–651
Secondary generating surface T_2, 92
Semitopping, 263–264
Serrations, 605
Setting angle, 374–376, 475*t*
Shank axis, 80
Shank-type shaper cutters, 284–285, 294*f*
Shaper cutters
cutting edge geometry of, 285–286
deep counterbore-type, 284–285
enveloping, 293, 295*f*, 346–348
interference of internal work gear and shaper cutter teeth, 291–292
profiling of, 283–285
clearance surface, 283–284
generating surface, 283–284
rake surface, 283–284
shank-type, 284–285, 294*f*
with tilted axis of rotation, 651–653
application, 652–653
kinematics of shaping helical gear, 651–652
principal design elements, 652
tooth number, 292
transverse generating pressure angle, 291
Sharpening of gear broaches, 66–70
generating of rake surface, 68
generating surface of grinding wheel, 66–67
helical gullet, 68
maximal feasible outer diameter of grinding wheel, 67
schematic diagram, 69*f*
support at center, 67
Shave grinding, 685
Shaving cutters, 559–642
advances in design of, 635–640
constant inclination angle within cutting edges, 635–636
for finishing modified work gear tooth flank, 637–638
near optimal angle of inclination of cutting edges, 633–635
precision cutter with straight cutting edges, 636–637

Shaving cutters (*continued*)
axial method, 576–587
coordinate systems transformations, 585
cutting speed, 578–587
equivalent base diameters, 586–587
formula for cutting speed, 587
impact of crossed-axis angle, 578–579
impact of profile sliding, 580–587
impact of traverse motion, 579–580
kinematics of, 576–578
line of action, 584
workgear to shaving cutter meshing, 580, 581*f*, 583*f*
clearance surface of cutting teeth, 562
design of shaper cutters, 566–576
design parameters, 567, 575*t*
resharpening, 571–576
serrations on tooth flanks, 568–571
diagonal method, 587–602
coordinate systems, 596–598
cutting speed, 590–592
diagonal-underpass, 590
geometry of contact of tooth flanks, 598–602
kinematics of, 588–589
local topology of contacting tooth flanks, 595–596
multistroke, 589
optimal kinetic parameters, 602
optimization of kinematics, 592–595
traverse angle, 589–590
generating surface of, 559–560
inclination angle of cutting edges, 562–566
manufacturing aspects of shaving operation, 640–641
modification of tooth form and shape, 641
plunge method, 619–633
circular mapping of tooth flanks, 629–631
cutting speed, 619
design of shaving cutters, 631–633
epicyclical motion in, 619
kinematics of, 619–620
part surface generation, 628–633
topologically modified gears, 621–628
rack-type, 654–657
rake surface of cutting teeth, 560–561
requirements for preshaved work gear, 639–640
selection of, 639
shaving of worm gear, 641–642
tangential method of shaving process, 603–618
analytical approach, 612–618
cutting speed, 604–605
descriptive geometry-based methods, 605–612
kinematics of, 603–604
serrations, 605
tooth flanks, 595–596
curvature of tooth surface, 596
Dupin indicatrix of tooth surface, 596
equation of tooth flank of, 595
first fundamental form of tooth surface, 595
indicatrix of conformity, 599
local orientation, 598
maximum rate of conformity, 600
optimal design parameters, 600
principal directions, 598
second fundamental form of tooth surface, 595
Shear-Speed cutting, 74–80
kinematics of, 75*f*
principle of, 74
profiling of form tools for, 76–79
Shell-type gear hobs, 462*f*, 463–464
Shishkov's equation of contact, 227–228
Shoulder gears, tangential shaving of, 605–618
analytical approach, 612–618
closed vector polygon, 614–615
operators of linear transformations, 613–614
optimal design parameters, 612–615
overlap of shaving cutter over work gear, 615–618
reference systems, 612–613
descriptive geometry-based method, 605–612
maximum allowed diameter of cutter, 606–608
minimum permissible width of auxiliary generating rack, 612–614
minimum permissible width of work gear auxiliary rack, 608–610
minimum required face width, 612
minimum required overlap of gear and cutter, 608–612
Single parametric motion, 16
Skiving hobs, 463–464
Slater tools, 80–81
Sliding motion over surfaces, 23–24
Sliding vectors, 26
Spatial gear machining mesh, 353–357. *See also* machining meshes
gear shaving cutters, 559–642
generating surface of gear cutting tool, 353–394
hobs for machining gears, 395–559

kinematics of, 353–357
axode of gear cutting tool, 357
center distance, 353
crossed-axis angle, 353
hyperboloid, 356
opposite-directed vector, 356
pure rolling of axodes, 354–355
rotation of cutting tool, 353
rotation of work gear, 353
rotation vectors, 353–354
vector of linear velocity of sliding of axodes, 355
Special roughing hobs, 463
Spiral bevel gears, 337–342
clearance angle, 342
design of cutters, 340–342
diagrammatic arrangement of, 339*f*
gear machining operation, 338–340
profile angle, 341
rake angle, 342
spiral angles, 337
Spiral gullet, 68
Spiral infeed, 274
Spur gears, 3, 4*f*
barreled, 17
crowned, 17
cusps on tooth flanks, 115–117
disk-type gear milling cutter, 125–127
gear milling cutter for, 120
internal round broach for, 169–170
involute, 9–10
machining, 92–100
modified, 17
shaping of, 346–347
tooth flank, 9–10
Spur rack, 3
Stabler's equation, 718
Staggered pattern serration, 605
Standard circular tooth thickness, 697*t*
Standard normal circular thickness, 696*t*
Standard outside diameter, 697*t*
Start of active profile (*SAP*), 9
Stick-type pot broaching tool, 74
Straight bevel gears, 5–6
cutting, 333–334
gear cutting tools, 330–333
design parameters, 330–331
tool geometry, 331–333
tool height, 330
machining of, 329–330
milling, 334–337
design of milling cutters, 335–336
disk-type milling cutters, 336
lateral cutting edges, 25–26
shape of finished flanks, 336–337
with offset teeth, 325–328
teeth, 328–33
gear cutting tools, 330–333
machining of straight bevel gears, 329–330
plane T_a by straight motion of cutting edge, 328–329
tooth flank, 14–15
Straight feed motion F_c, 123
Straight rack, 365
Surface of tolerance, 594
Surface parameters, 703–704
Surface plastic deformation, gear reinforcement by, 657–658
Surfaces, fundamental forms, 55–56
Surfaces that allow sliding, gear tooth, 16–18

T

Tangential shaving, 603–618. *See also* shaving cutters
analytical approach, 612–618
cutting speed, 604–605
descriptive geometry-based methods, 605–612
kinematics of, 603–604
serrations, 605
Technological worm, 428
Thickness of chip cut, 286–290
feed motion, 286
motion of cut, 286
operator of rolling, 288–289
Thread whirling, 177–178
Tip relief, 263
Titanium nitride coating, 261, 294
Tool-in-use reference system, 505–515
Tooth depth, 62
Tooth flanks, 6–16
of bevel gear, 14–15
circular mapping of, 629–631
of helical gear, 117–119
cusps, 117–119
deviation from desired shape, 118–119
normal curvature, 118
of involute helical gear, 10–14
of involute spur gears, 9–10
serrations, 568–571
of shaving cutters, 568–571, 595–596
curvature of tooth surface, 596
Dupin indicatrix of tooth surface, 596
equation of tooth flank of, 595
first fundamental form of tooth surface, 595

Tooth flanks (*continued*)
indicatrix of conformity, 599
local orientation, 598
maximum rate of conformity, 600
optimal design parameters, 600
principal directions, 598
second fundamental form of tooth surface, 595
specification, engineering approach, 8
specification, scientific approach, 8
of spur gear, 115–117
waviness of, 116
Tooth profiles
asymmetric, 389–390
gear hobs, 465–468, 515–528
gear shaper cutters, 263–264
chamfer, 263–264
full topping, 264
modified pressure angle, 264
protuberance, 264
root fillet, 263
semitopping, 263–264
tip relief, 263
involute hobs, 515–528
rack cutters, 191–193
Tooth relieving operation, clearance surface of, 415
Top-loaded cutting diagram, 150
Topologically modified gears, 621–628
auxiliary rack modification matrix, 627
gear modification matrix, 622
generating surface of form grinding wheel, 629–30
geometry of, 621–624
grinding of tooth flanks, 625–628
NC grinder, 625–627
tooth flanks of shaving cutter, 624–625
Toroidal gear cutting tools, 681–686
Toroidal gear hobs, 497–498
Torus-shaped pitch surfaces, 390–392
Transformation matrices, 44
Transformations, coordinate-system, 43–56
conversion of coordinate system orientation, 54
direct transformation, 45
direct transformation of surfaces fundamental forms, 55–56
homogenous coordinate transformation matrices, 44
homogenous coordinate vectors, 43–44
opposite transformation, 54
orientation-preserving transformation, 45
orientation-reversing transformation, 54
overview, 43
resultant, 47–48
rolling motion of coordinate system, 50–51
rolling of two coordinate systems, 52–54
rotation about coordinate axis, 46–47
screw motions about coordinate axis, 48–49
translations, 44–45
Translation vector, 26
magnitude of speed, 36
superimposition of rotation vector and, 36
Translational motion, 208
Translations, 44–45
Transverse circular pitch, 696*t*
Transverse pressure angle, 696*t*
Traverse angle, 589–590
Traverse motion, 579–580
Triparametric motion, 16

U

Unit normal vector, 374

V

Vector of instant rotation, magnitude of, 34–36

W

Work gear, 20–23
auxiliary rack, 608–610
elementary relative motions, 20–21
feasible relative motions, 21–23
Work gear to cutting tool penetration curve, 493, 494*f*
Work gear to generation surface mesh, 25
Work gear to shaving cutter meshing, 580, 581*f*, 583*f*
Working position, relief grinding, 425, 431*f*
Worm, 5, 7*f*
grinding, 178–181
machining in continuously indexing method, 653–654
machining on lathe, 172–175
milling, 175–177
technological
Worm gear, 7*f*

Z

Zero profile angle, 381–383

GEAR CUTTING TOOLS

FUNDAMENTALS OF DESIGN AND COMPUTATION

STEPHEN P. RADZEVICH

Billions of gears are produced for use in the aerospace, construction, and agricultural machinery industries, yet the cost of gear cutting tools themselves represents more than half the total cost of the gear machining operation. With an improved understanding of gear machining process and tool design, engineers and scientists can potentially streamline the methods involved to dramatically slash production costs and enhance efficiency.

Gear Cutting Tools: Fundamentals of Design and Computation addresses this issue, presenting the DG/K-based method of surface generation, a novel and practical mathematical method for designing gear cutting tools with optimal parameters. The author, an industry leader for the past 30 years, proposes a scientific classification of kinematic schemes of gear machining before discussing the best possible tool designs. This classification makes it possible to consider gear cutting tool designs currently in practice and those expected to be used in the future. This book also facilitates development of scientific predictions, and in most cases it provides optimal designs and solutions in analytical and/or graphical form.

This author elucidates both the scientific basis and practical aspects of gear machining advances. He covers surface generation, offering an excellent context and motivation for exploring the pervasive ties between the geometry of gear cutting tools and the kinematics of gear machining processes.

The book is divided into five sections:

- Basics
- Form Gear Cutting Tools
- Cutting Tools for Gear Generating: Parallel Axis Gear Machining Mesh
- Cutting Tools for Gear Generating: Intersecting Axis Gear Machining Mesh
- Cutting Tools for Gear Generating Spatial Gear Machining Mesh

Because of its generality and lucid style, this classic work will be invaluable not only to specialists in gear cutting tool design but also to those working in general areas of mechanical/manufacturing engineering.

CRC Press
Taylor & Francis Group
an informa business

6000 Broken Sound Parkway, NW
Suite 300, Boca Raton, FL 33487
270 Madison Avenue
New York, NY 10016
2 Park Square, Milton Park
Abingdon, Oxon OX14 4RN, UK

K11035
ISBN: 978-1-4398-1967-8
90000
9 781439 819678
www.crcpress.com